STATIC AXIAL PILE FOUNDATION RESPONSE

USING SEISMIC PIEZOCONE DATA

A Dissertation
Presented to
The Academic Faculty

by

Fawad Sulaman Niazi

In Partial Fulfillment
of the Requirements for the Degree
Doctor of Philosophy in the
School of Civil and Environmental Engineering

Georgia Institute of Technology
May 2014

STATIC AXIAL PILE FOUNDATION RESPONSE

USING SEISMIC PIEZOCONE DATA

Approved by:

Dr. Paul W. Mayne, Advisor
School of Civil & Environmental Engineering
Georgia Institute of Technology

Dr. Robert C. Bachus
Geosyntec Consultants, Inc.
Atlanta, GA

Dr. Glenn J. Rix
Geosyntec Consultants, Inc.
Atlanta, GA

Dr. Yuhang Wang
School of Earth & Atmospheric Sciences
Georgia Institute of Technology

Dr. Susan E. Burns
School of Civil & Environmental Engineering
Georgia Institute of Technology

Date Approved: December 19, 2013

Dedicated to all those who believe in the richness of learning

ACKNOWLEDGEMENTS

While I was pondering on what I would be writing in my acknowledgements, I was sure that it must start with gratitude to Almighty Allah, who gave me the opportunity and strength to undertake this journey of doctoral research studies. He blessed me with good health and unwrapped avenues for me throughout the time of my residency at Georgia Tech that enabled me to honorably sustain and focus on my studies besides accomplishing achievements and receiving many academic honors, for which I cannot be more grateful.

Mentioning about my mentors at Georgia Tech, first I would like to humbly recognize the support, guidance and advices that I always received from my advisor, Professor Paul W. Mayne throughout my Ph.D. studies. I thank him for being an excellent advisor and a lively person, who kept me encouraged through the odds of this journey. I owe him for polishing my analytical and writing skills, which enabled me to put together and/or publish eight peer-reviewed journal papers and ten conference papers in less than five years. Whenever, I needed his time and guidance, he was always available without the compulsion of scheduling a formal meeting. I thank him for making available to me all books, papers and scientific material required for the completion of this dissertation, for being patient in listening to my concerns and viewpoints, and accommodating me during periods of my frustration. Gratitude is also expressed to Dr. Glenn J. Rix, Dr. Robert C. Bachus, Dr. Susan E. Burns, and Dr. Yuhang Wang for their willingness to serve on my advisory committee, and for rendering useful feedback and guidance.

I must also thank Dr. Kimberly E. Kurtis, and Dr. Donald R. Webster, who provided me the opportunities to offer my services in teaching laboratory sections of CEE-3020 (Civil Engineering Materials) class for five semesters and formally instructing and teaching COE-2001 (Engineering Mechanics: Statics) class for four semesters at Georgia Tech. These opportunities allowed me to hone my teaching skills, besides covering my academic expenses.

I would like to acknowledge ConeTec Investigations, especially David Woeller, for their continued financial and technical support of in-situ testing research at Georgia Tech.

I would also like to thank my colleagues who helped me in different ways during my residency at Georgia Tech, specifically Dr. Taeseo Ku and Aditya Bhatt, with whom I shared office during our common four years period of graduate studies.

To my parents, I am appreciative for their continued and sincerest prayers for me. Their moral support during the last six years empowered me in my academic and professional endeavors.

I am truly blessed to have my beloved wife, Irrum Fawad Niazi, who remained on my side at each step of the way. I love her dearly. She has contributed extraordinarily, much beyond my expectations, in her patience, love, and inspirations. Her push for tenacity has been exemplary and her words of encouragement ring in my ears. I owe this achievement to her.

TABLE OF CONTENTS

LIST OF TABLES

Page

LIST OF FIGURES

Page

SUMMARY

Ever since the use of cone penetration testing (CPT) in geotechnical site investigations, efforts have been made to correlate its readings with the components of static axial pile capacity: unit base resistance (q_b) and unit shaft resistance (f_p). Broadly, the pile capacity analysis from CPT data can be accomplished via two main approaches: *rational* (*or indirect*) *methods*, and *direct methods*. The rational methods require a two-step approach, whereby CPT data are first used to provide assessments of geoparameters that are further utilized as input values within a selected analytical framework to enable the evaluation of the pile capacity components. In contrast, direct CPT methods use the measured penetrometer readings by scaling relationships or algorithms in a single-step process to obtain f_p and q_b for full-size piling foundations. The evolution of the CPT from mechanical to electrical to electronic versions and single-channel readings (i.e., measured tip resistance, q_c) to the piezocone penetration test (CPTu), that provides three readings of point stress (q_t), sleeve friction (f_s), and porewater pressure (u_1 or u_2), has resulted in the concurrent development of multiple CPT-based geotechnical pile design methods. It is noted, however, that current CPT-based methods focus only on an estimate of "axial pile capacity", corresponding to a limiting load or force at full mobilization.

A more comprehensive approach is sought herein utilizing the CPT readings towards producing a complete nonlinear load-displacement-capacity (Q-w-Q_{cap}) on axial pile response. In particular, the seismic cone penetration test (SCPT) provides the profile of shear wave velocity (V_s) that determines the fundamental small-strain shear modulus: $G_{max} = \rho_t \cdot V_s^2$, where ρ_t = total mass density of soil. With the penetrometer readings useful in assessing foundation capacity, the stiffness G_{max} finds application within elastic continuum solutions towards evaluating the load-displacement (Q-w) response.

In this study, a concise review of the deep foundation systems is presented, including pile types and characteristics, various arrangements of axial pile load testing in static mode, and interpretations of the load test data. In addition a comprehensive state-of-the-art review of CPT-based *rational* and *direct methods* of pile capacity evaluations is compiled. It is recognized that the direct methods offer more convenience in their straightforward approach in estimation of the pile capacity. The piezocone-based UniCone direct method proposed by Eslami and Fellenius (1997) is selected for further refinements, as it utilizes all three CPT readings in its design formulations. Concerning the analysis of pile deformations under axial loading, a brief review covers designs employing empirical formulations, analytical solutions, load-transfer (τ-z) methods, numerical simulations, variational approaches, and those using hybrid methods. Specifically, the analytical elastic solution by Randolph and Wroth (1978; 1979) is covered in more detail since it is simple and convenient in application with extended applications to uplift and bidirectional O-cell types of loadings. This elastic approach also serves well in modeling a stacked pile solution for layered soil profiles. The last part of the review covers various shear modulus reduction schemes, since evaluation of the applicable stiffnesses is considered to be the most delicate phase in the nonlinear Q-w response analysis of axially loaded piles. It is identified that the most appropriate scheme applicable to static axial loading of pile foundations is the one that can be derived from the back-analyses of actual load tests within the framework of analytical elastic solution.

In order to conduct a comprehensive research study on the axial Q-w-Q_{cap} response of deep foundations from CPT readings, a large database is compiled. This includes 330 case records of pile load tests at 70 sites from 5 continents and 19 different countries of the world, where pile foundations were load tested under top-down compression or top-applied uplift (tension) loading, or both, or by bi-directional Osterberg cell setups. All test sites had been investigated using CPT soundings; in most cases by the preferred SCPTu that provides all four readings from the same sounding: q_t,

f_s, u_2, and V_s. In a few cases, sites were subjected to CPT or CPTu and the profiles of shear wave velocities were obtained by other field geophysical techniques, otherwise by empirical estimations.

Results of the new correlation efforts are offered to derive coefficients C_{se} for shaft component and C_{te} for base component of the axial pile capacity from CPTu data. The UniCone type of soil classification chart is refined by delineating 11 soil sub-zones along with their respective C_{se}, in contrast to the 5 zones originally proposed. The CPT material index, I_c (Robertson, 2009) is then used to establish direct correlations linking C_{se} vs. I_c and C_{te} vs. I_c. Statistical relationships offer continuous functions for estimating the coefficients over a wide range of I_c values, thereby eliminating the need for use of the soil classification chart as well as improving the reliability in the evaluations of f_p and q_b. The effects of the pile loading direction (compression vs. uplift) and loading rate are also incorporated in the proposed design formulations.

New sets of shear stiffness reduction curves are developed from the back-analysis of pile load tests and G_{max} profiles obtained from the SCPT data. Alternative functions formats are provided in terms of hyperbolic tangent expressions or exponential curves, developed as normalized shear stiffness (G/G_{max}) vs. logarithm of percent pseudo-strain (γ_p = w/d, where w = pile displacement and d = pile diameter). These charts offer convenience in the axial Q-w analysis of different pile categories within the framework of analytical elastic solution. The results also account for the plasticity characteristics of the soil formations within the database.

A stacked pile model for Q-w analysis is presented in which certain adaptations are proposed in the elastic continuum solution. These adaptations enable plotting of separate modulus reduction curves (G/G_{max} vs. γ_p) as function of depth for each layer, and treating pile as a stack of smaller pile segments embedded in a multi-layered soil media. The solution can be used to address the question of progressive failure with depth in a multi-layer soil media that exhibits nonlinear soil stiffness response.

Finally, the closed-from analytical elastic pile solution for predicting the Q-w response is decoupled and modified to account for different setup cases and multi-stage loading of bi-directional O-cell tests. The decoupling accounts for separate assessments of the response to axial loading for different segments of pile shaft and different stages of loading, while the modifications include: (1) reduced maximum radius of influence for the upward displacements of the upper shaft segment, and (2) modeling the non-linear ground stiffness from the back-analysis of a well-documented dataset of O-cell load tests.

CHAPTER 1

INTRODUCTION

1.1 Pile Foundations

The history of deep foundations, more commonly known as piling or piles, dates back to the time when man first sought to establish secure dwellings in soft marshy lake shores and to cross rivers by driving wooden stakes or piles in the ground (Fleming et al., 2008). With the advancement of engineering knowledge, considerable innovations and improvements have been made in the piling industry in terms of material, installation methods, load testing, and sizes of these foundation elements. In the recent history of deep foundations technology, the pace of change has been particularly rapid. Until recent past it used to be possible to categorize deep foundations according to their methods of installation as driven piles or drilled shafts (also called bored piles). This, however, does not satisfactorily cope with the many different forms of piles now in use, some of which are a combination of the two or more of the traditional methods (Fleming et al., 2008). The newer pile designs are dictated by various factors that include, but are not limited to: economy, durability, time required for installation, and far greater loads due to the size/scale of modern state-of-the-art civil engineering projects including multi-span bridges, high-rise towers, and offshore structures. Figure 1.1 shows some common applications of deep foundations in the modern times and the basic concept of pile-to-ground load transfer.

The response of deep foundations to axial loading from the super-structure consists of evaluating the load carrying capacity for design (Q_t) and the amounts of load transferred to the pile shaft ($Q_s = f_{pi}\ \pi\ d\ \Delta z_i$) and the base ($Q_b = q_b\ \pi\ d^2/4$), as well as assessing the magnitudes of pile settlements for different loads, traditionally represented in terms of the load-settlement (Q – w) response. For a circular pile with diameter d, f_{pi}

represents the unit side resistance and π d Δz_i is the shaft surface area corresponding to the i^{th} soil layer; whereas, q_b is the unit end bearing resistance and $\pi d^2/4$ represents the toe/base area of the pile. For non-circular piles, an equivalent value of pile diameter is conveniently adopted. Axial load-settlement response for pile compressibility can be accounted for by evaluating the total displacements corresponding to total, shaft, and base loads ($Q_t - w_t$, $Q_s - w_t$, and $Q_b - w_t$, respectively), and base settlements corresponding to base loads ($Q_b - w_b$).

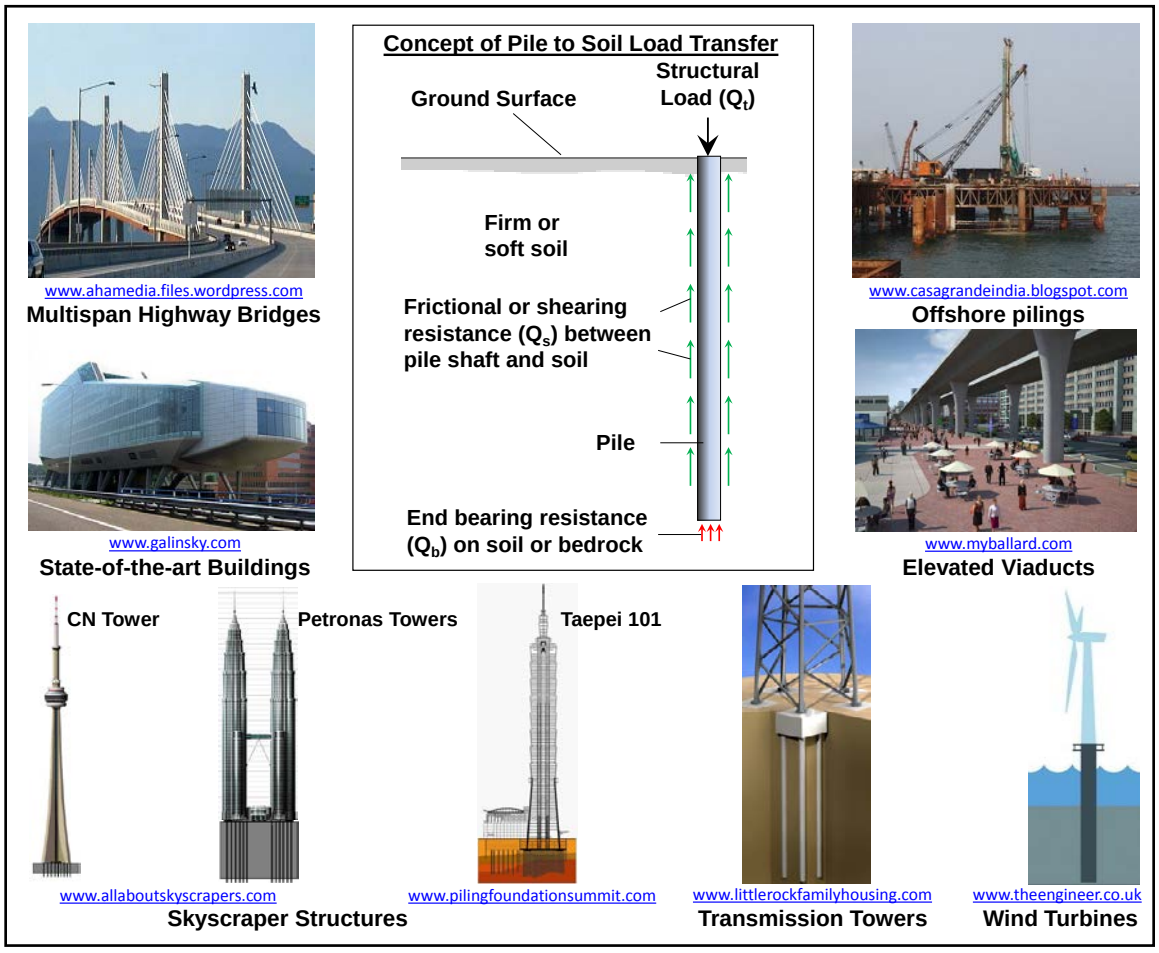

Figure 1.1. Examples of modern applications of pile foundations and the concept of pile–soil load transfer.

1.2 Geotechnical Site Investigations for Deep Foundations

In view of the wide range of methods and equipment now available in the deep foundations industry, thorough geotechnical site investigation has become far more of an essential prerequisite to making learned decisions for the selection of pile design and the choice of appropriate construction methods, both for purposes of reliability as well as economy. Conventional investigation methods for subsurface characterization of soil layers affecting the performance of deep foundations (e.g., boring and sampling) are time consuming, expensive, and tedious. Laboratory tests are conducted either on disturbed samples or more costly undisturbed samples obtained only from selected depths. The results of such investigations are thus highly dependent upon the tools employed in retrieval of the samples from different depths and the skills and expertise of the individual assigned to the task of logging samples.

Cone penetration testing (CPT) is a modern and expedient means of conducting site investigations for exploring subsurface ground for support of civil engineering structures. The CPT soundings can be used either in lieu of or in complement to conventional boring and sampling methods. During CPT, an electronic steel probe is hydraulically pushed into the ground to collect multiple continuous readings throughout the depth of investigation in a much shorter period of time. The data can be simultaneously logged and post-processed in a field computer to evaluate the geostratigraphy and engineering parameters of the geomaterials on-site, thereby offering quick and preliminary conclusions for design parameters and analysis (Mayne, 2007).

The seismic piezocone penetration test (SCPTu), a newer version of CPT, is a hybrid geotechnical-geophysical in-situ method that serves as an expedient, economical and reliable tool for subsurface explorations. The SCPTu provides downhole geophysical measurements of shear wave velocity (V_s) at every 1-m depth interval in addition to the penetration test parameters at 1- to 5-cm depth intervals from a single vertical sounding, specifically: cone tip resistance (q_c) or more proper corrected tip resistance (q_t), sleeve

friction (f_s) or more proper corrected sleeve friction (f_t), and either mid-face porewater pressure (u_1) or shoulder porewater pressure (u_2). Figure 1.2 shows a schematic illustration of implementing SCPTu.

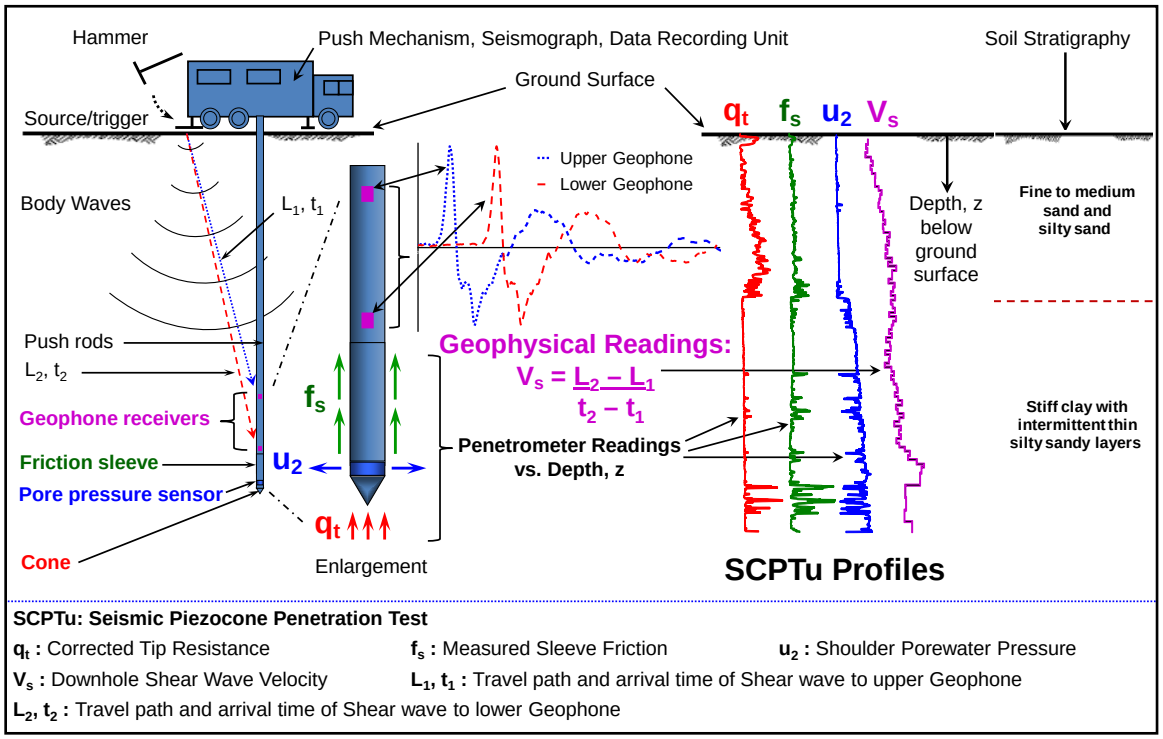

Figure 1.2. A conceptual scheme of acquiring continuous multiple SCPTu readings.

The V_s readings provide direct evaluation of the fundamental small-strain soil stiffness ($G_{max} = \rho_T \cdot V_s^2$, where $\rho_T = \gamma_T / g_a$ = total soil mass density, γ_T being the soil total unit weight and g_a = the gravitational acceleration constant = 9.81 m/s^2), an important parameter required in the soil deformation analysis. On the other hand, the penetrometer readings (q_t, f_s, and u_2) can be used to obtain very detailed stratigraphic information in terms of soil classification type and layering, as well as geotechnical engineering properties (e.g., density, frictional characteristics, strength, stress state, permeability) from well-established relationships. Therefore, a site can be completely

characterized by SCPTu in much less time, effort and expense than a conventional boring, sampling, and laboratory testing program. With better economics and efficiency, the SCPTu thus serves as a better environmental-friendly alternative tool for complete geotechnical site characterization. Figure 1.3 shows an example of an exceptionally deep SCPTu sounding conducted at the newly constructed Golden Ears Bridge site south of Vancouver, BC. Continuous profiles of the penetrometer parameters (q_t, f_s, u_2), as well as downhole V_s at one-m depths, were obtained as deep as 95-m.

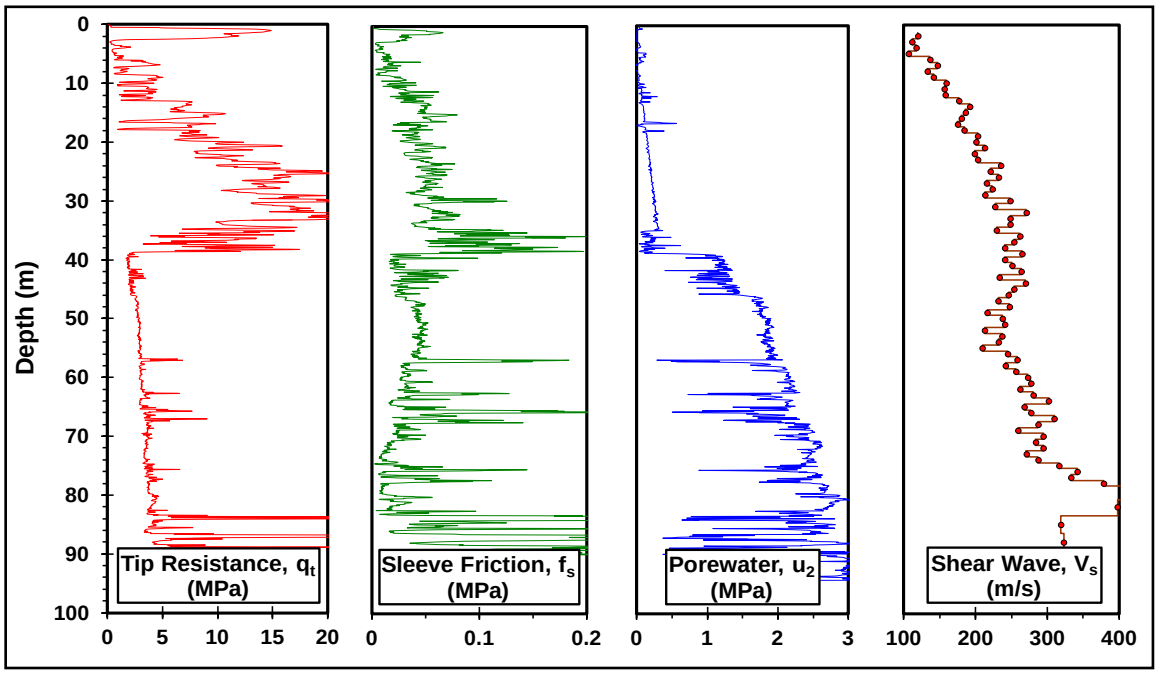

Figure 1.3. SCPTu sounding at Golden Ears Bridge site, Vancouver, BC (Niazi et al., 2010a).

1.3 Alternatives to Interpret Axial Pile Response from Cone Penetration Test Data

The geotechnical design of pile foundations is based on the estimate of their response to anticipated loadings in a soil profile found at any particular site. Soil properties obtained from the site investigation tools are used in either or a combination of more than one of the following interpretive schemes/simulation models to evaluate this

response: (1) empirical; (2) analytical; (3) numerical; and (4) physical measurements via load tests on full-scale pile foundation structures.

Ever since the use of CPT in geotechnical investigations, efforts have been made to correlate its readings with the pile capacity components of q_b and f_p. Such empirical frameworks provide design methods to enable evaluations of pile capacity (Q_t), and load distribution through the pile embedment depth ($Q_s - z$) and to the pile base (Q_b). Herein, the analysis of pile foundations can be performed via rational design methods (or indirect methods, e.g., α- and β-methods for side resistance, and limit plasticity solutions for end bearing resistance), where the geoengineering parameters obtained from CPT-based correlations are used in the evaluation of f_p and q_b. Alternatively, the pile resistances can be determined using direct CPT methods, empirically derived to scale the data from cone penetrometer readings up to full-scale f_p and q_b to allow for the direct capacity evaluations. The evolution of the CPT from mechanical to electrical to electronic versions and single-channel readings (i.e., measured tip resistance, q_c) to the piezocone penetration test (CPTu), that provides three readings of q_t, f_s, and either u_1 or u_2, has resulted in the concurrent development of multiple CPT-based geotechnical pile design methods. Thus, the penetrometer readings facilitate assessment of the peak strength on the stress-strain-strength curve corresponding to the pile capacity.

Analytical frameworks for pile deformation analysis such as those proposed by Randolph and Wroth (1978; 1979), Poulos and Davis (1980), and Mylonakis (2001) are available to estimate the Q – w response for the axial loading of deep foundations. The Randolph-type closed-form elastic pile framework provides a convenient solution that has been applied with reasonable success for evaluating the complete axial load-displacement response for different test piles (e.g., Mayne and Schneider, 2001; Mayne and Elhakim, 2002; Mayne and Woeller, 2008; Mayne and Niazi, 2009; Mayne et al., 2010; Niazi and Mayne, 2010; Niazi et al., 2010a; 2010b; 2010c; Reuter, 2010; Pando et al., 2004). The displacements obtained correspond to different loading ranges starting

from those applicable to nondestructive small strains ($\gamma_s < 10^{-6}$) up to the ultimate pile capacity corresponding to $\gamma_s \rightarrow \infty$. For the initial displacements, corresponding to the small strains, the fundamental stiffness in terms of initial shear modulus (G_{max}) obtained from V_s component of SCPTu is used in the solution. In order to account for the non-linearity of the stress-strain response of soil to loading, appropriate algorithms from the relevant research studies can be applied to obtain the values of operational soil shear stiffness corresponding to different levels of applied load. In addition to the pile top load-displacement evaluation ($Q_t - w_t$), this solution also facilitates estimation of the percent axial load transferred to the pile base (Q_b) for each stage of top loading, thereby enabling derivation of separate load-displacement curves for the shaft component ($Q_s - w_s$) as well for the base ($Q_b - w_b$).

Numerical techniques like the finite element method (FEM) and finite difference method (FDM) are more sophisticated types of simulation to the pile deformation problem (e.g., Ai and Han, 2009; Ellison et al., 1971; Kurian and Shah, 2009; Lee and Long, 2008; Liu et al., 2004; Poulos and Mattes, 1969; Said et al., 2009; Seol et al., 2009; Sheng et al., 2005; Simonini, 1996; Smith, 1980; Tosini et al., 2010; Zhusupbekov and Zhakulin, 2006). Although numerical methods offer a more elaborate means of addressing nonlinear pile response that accounts for wide ranges in strains from near-field to far-field, many researchers still underline the importance of adopting a representative analytical stress-strain-strength model of soil derived from actual measurements (e.g., Berardi and Bovolenta, 2005; Mayne and Poulos, 2001; Burghignoli et al., 1991). A rigorous verified numerical solution is still beyond routine use by practicing engineers.

Field measurements via pile load tests provide yet another alternative to evaluate the pile response to loadings. Geotechnical parameters acquired from analytical and numerical models can be calibrated properly with the recorded performance of full-scale geostructures. Also, statistical or empirical correlations can be developed amongst different test methods. A descriptive illustration is presented in Figure 1.4, where the

measurements from SCPTu are shown to allow various paths to interpretation in the assessment of the full-scale axial response of piling foundations.

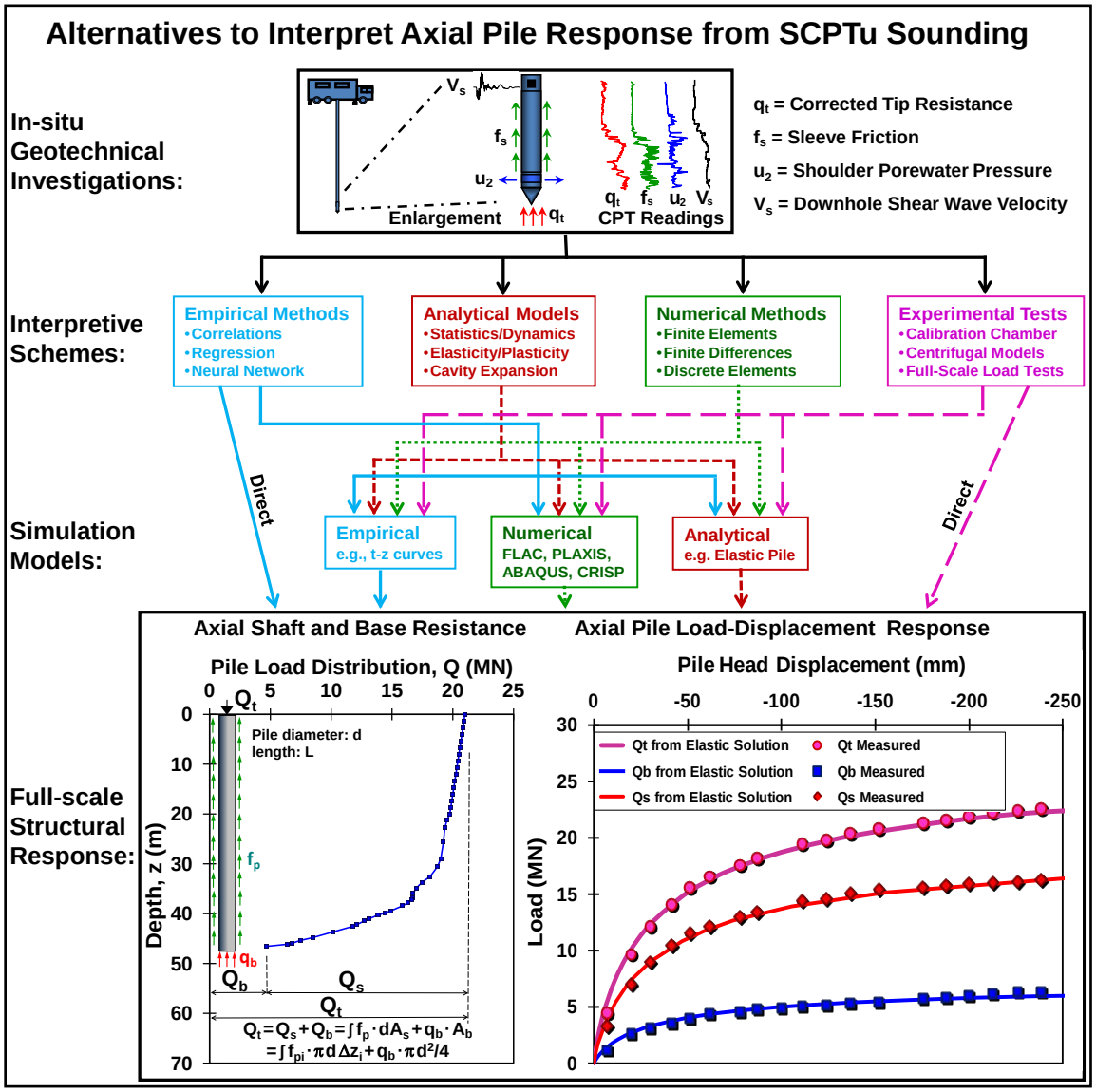

Figure 1.4. Various paths to interpretation of axial pile foundation response from SCPTu (modified from Mayne et al., 2009).

1.4 Performance-based Pile Design and Resulting Database

While multiple methods can be adopted towards the evaluation of pile response to loading, a desired level of confidence in the design achieved via physical measurements of full-scale pile load test cannot be paralleled. Accordingly, the performance-based foundation design is still considered to be the most reliable method. Yet, it is done at considerable cost on large projects, yet not possible on small to medium size projects. This has resulted in a plethora of pile load tests conducted for a variety of large scale civil engineering projects and the allied works executed by state agencies, private contractors, prominent research institutions, and universities at many geotechnical experimentation sites in different parts of the world, alongside in-situ, laboratory, and geophysical measurements of soil parameters. Foundation design and construction industry have also been involved in high cost initiatives to acquire reliable data on the capacity of pile foundations and to understand the failure mechanisms in order to improve foundation design (e.g., Zuidberg and Vergobbi, 1996).

A pile load test can be conducted on either an uninstrumented or instrumented full-scale pile. With technological advancements, the methodologies and instrumentations for pile load testing have continuously remained under refinement. Figure 1.5 shows different pile load test systems currently being used in practice based on: (1) static dead weight, (2) reaction frame setup, (3) statnamic test, and (4) Osterberg load cell or O-cell arrangement. The direction of axial loading in the former two types (i.e., dead weight and reaction frame) can be either top-down for compression type loading or top-up for tension or uplift type loading. The latter two types (i.e., statnamic and O-cell) are both newer technologies; however, comparisons of their test results with the former two types are not straightforward. While the loading mode of O-cell test detailed below is different from the top-down static dead weight or reaction frame setup, the instantaneous loading in case of statnamic type requires adjustments to the measured response for inertia and

damping forces to estimate the corresponding static response, thereby, adding a certain level of complexity in post-processing.

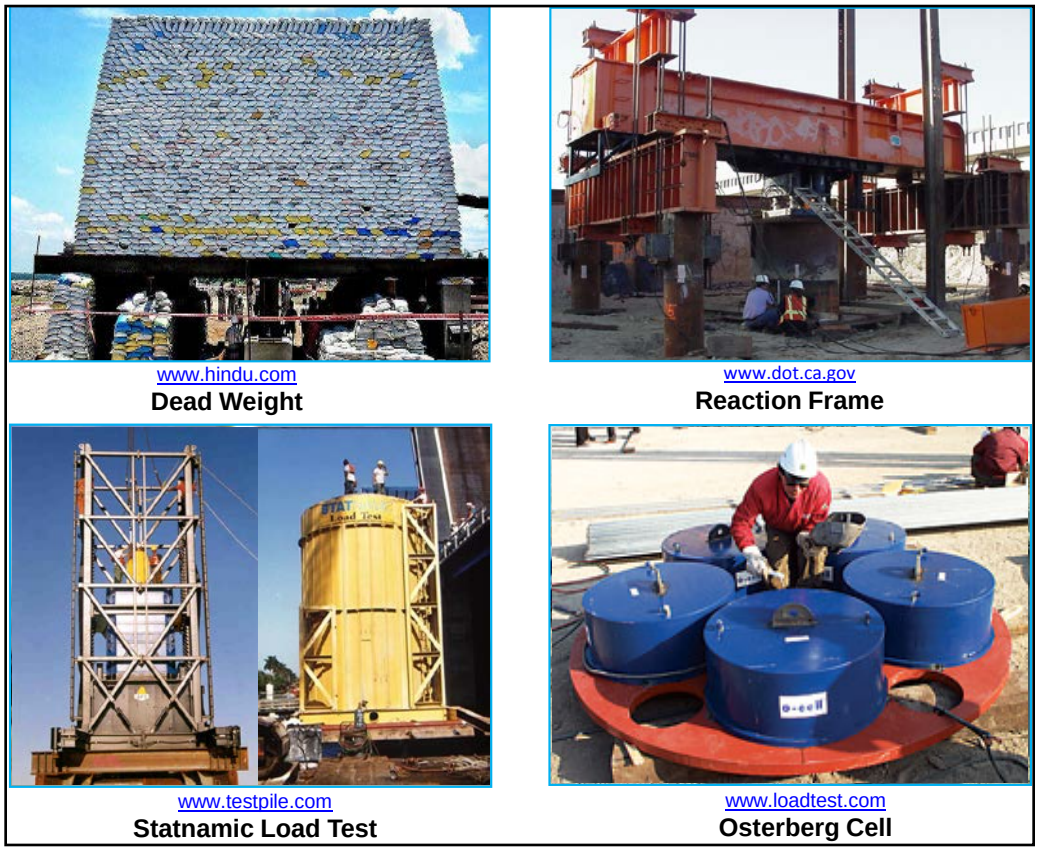

Figure 1.5. Different arrangements of pile load tests.

The O-cell type of load test has been well-established since its inception in 1989 and is frequently being integrated into performance-based design. The hydraulically-driven sacrificial high-capacity multiple O-cell device is installed within the foundation. The amount of load that can possibly be measured (i.e., up to 320 MN) via staged sequences of loading is unprecedented. The O-cell works simultaneously in two directions, upward against the side-shear and downward against the end-bearing, separating the side and base resistance components (LoadTest, 2012; Osterberg, 1989).

The availability of a wide range of materials, methods and equipment in the piling industry warrants a thorough study to be undertaken based on the ever-growing database on a variety of deep foundations investigated to-date via load tests in different types of soils. This exercise from the back-analysis of a large, recent, and reliable documented database can be integrated into a hybrid empirical-analytical approach towards complete pile analysis and design within the framework of an established analytical solution. Such a research program allows updating of the design methodologies for pile foundations by metaphorically connecting the dots in an attempt for cognitive solution of the unresolved issues discussed later.

1.5 Limitations of the Analytical Elastic Solution

The Randolph-type of closed-form analytical solution that is utilized in this research was originally designed to estimate the top and base settlements of a pile foundation under a given axial compressive load ($Q_t - w_t$, and $Q_b - w_b$). It was developed for piles loaded in top-down axial compression mode, embedded in a linear elastic two-layered general Gibson-type soil model with the boundary lying at the pile tip elevation. Since this solution was originally developed for top-down compression loading, there is a need to extend it to other situations, namely tension (or uplift) and O-cell loading arrangements, as well as to multi-layer soil media presenting unconventional stiffness profiles. Effects of differences in the pile material (i.e., steel vs. concrete) and installation (i.e. driving vs. drilling) on the axial load response are not explicitly addressed in the solution. In addition, the original model does not account for the concept of progressive failure with depth where the shaft resistance mobilizes prior to base resistance, as identified in pile load tests.

Evaluation of the soil deformation properties is probably the most delicate phase of the analysis of load–settlement performance of a single pile. The mechanical non-linearity is exhibited in the form of soil stiffness that softens with shear strains exceeding

the linear threshold value (γ_{tl}), resulting in marked reductions in shear moduli for small-, intermediate-, and large-strains. The original Randolph elastic pile solution does not explicitly account for the non–linear soil stiffness softening at increasing loads which is a physical phenomenon observed in all types of geomaterials. This creates a principal difficulty in the selection of elastic stiffness properties of soil for use in this solution to estimate settlements corresponding to varying levels of load. Many algorithms have been developed and documented through wide range of research to describe this non-linear stiffness reduction for different geomaterials towards use in geotechnical engineering applications [e.g., simple hyperbolic stress-strain relationship by Kondner (1963), modified hyperbolic function by Fahey and Carter (1993), modulus reduction curves as functions of plasticity presented by Vucetic and Dobry (1991), and a periodic logarithmic function proposed by Jardine et al. (1986)]. It becomes difficult to strike a compromise between simplicity, without regard for imprecise description of rather complicated stiffness reduction trends, and improved accuracy at the cost of highly complex algorithms. The soil stiffness reduction algorithms adopted from the literature for application in the Randolph elastic pile solution require manipulation of curve fitting parameters to obtain a better match to the measured load-displacement response.

1.6 Interpretation of Pile Load Tests

The interpretation of axial pile load test results incurs some dilemmas. Load-displacement curves obtained from axial load tests on pile foundations exhibit differing shapes and resulting conclusions. There is only a single value of load termed "capacity" that is selected from the entire curve for design purposes. Yet, there are at least 42 different criteria available for defining the "axial capacity" (Hirany and Kulhawy, 1988). An example of the results from the application of selected criteria on a load-displacement curve obtained from a load test conducted on a 0.76 m diameter, 16.9 m long drilled shaft installed at Georgia Institute of Technology is shown in Figure 1.6. As evident, there is

no consensus and the various capacities interpreted via different criteria range from 2231 kN to 5103 kN. This hampers a convenient selection of the most suitable capacity value without considerable experience and engineering judgment. Towards that effect, it is relevant to cite the closing remarks of the 2nd Annual Osterberg Memorial Lecture by Bengt H. Fellenius at Deep Foundations Institute: "Don't get stuck in the capacity singularity, rise above the pack and let settlement issues govern your foundation design."

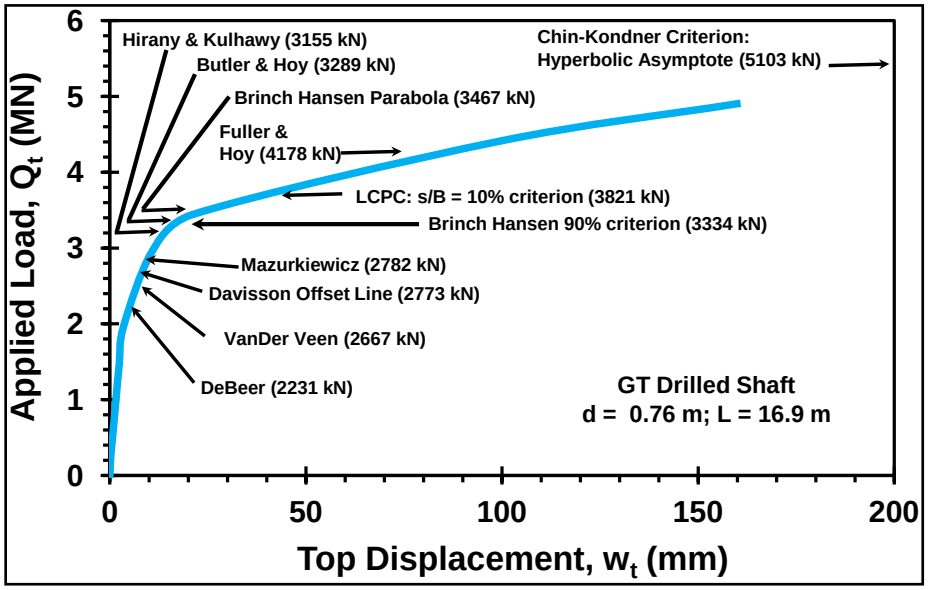

Figure 1.6. Comparison of capacity interpretation criteria from axial pile load tests.

1.7 Limitations of the Existing CPT-based Pile Design Methods

The optimal utilization of SCPTu data has yet to be appreciated for an all-encompassing pile design. Barring aside the individual limitations of different CPT-based pile design methods, the most common observations include:

- Most existing CPT-based methods focus only on an estimate of "axial capacity", without recourse to the behavior in terms of the complete load-displacement-capacity response.

- With the exception of a few approaches (i.e., KTRI by Takesue et al., 1998, and UNICONE by Eslami and Fellenius, 1997), all of the existing methods rely on measured q_c readings (or more proper, q_t) alone to evaluate both f_p as well as q_b.
- In particular, the V_s component of SCPTu that provides the fundamental stiffness (G_{max}) has not been fully exploited and developed towards extension of pile design from capacity to complete load-displacement response.
- Most of the recent CPT research and development have addressed driven pipe piles in sands for the offshore environment. In particular, much less effort has been applied to bored piles in clays, silts and/or sands, as well as newer composite piles and developments in the deep foundations industry.
- The response of pile foundations to axial loading is influenced by multiple factors including fundamental properties of geomaterials, non-linear soil behavior, pile type and geometry, pile installation techniques, and pile loading direction and loading rate. Current CPT-based pile design methods do not account for all such factors, and thus do not yield ideally match results for a variety of pile types.

1.8 Objectives

In view of the background detailed above, the specific objectives identified for this research study are enlisted below:

- Compile a large database of published and unpublished well-documented case records of pile load tests conducted at geotechnical sites from different parts of the world to encompass a wide variety of geomaterials and pile types where CPT soundings had also been advanced, with special focus to acquire SCPTu soundings.
- Derive stiffness softening scheme(s) based on the back-analysis of from pile load test data and site-specific G_{max} profiles obtained from the V_s component of SCPTu for a variety of geomaterials and pile types within the framework of the

Randolph analytical pile solution. Various factors affecting the consistency and reliability of results are studied.

- Refine the Randolph analytical pile solution to account for the concept of progressive failure with depth and extend it for application to tensile (or uplift) and the newer O-cell arrangements of load tests. Such a model will be able to account for layered soil profiles with contrasting stiffness properties.
- Study new alternatives to establish direct correlations between pile capacity components (f_p and q_b) and multiple penetrometer readings of SCPTu (q_t, f_s and u_2). This will consist of first explicitly defining the basis of capacity criteria and then comparing measurements from pile load tests with penetrometer readings. The effects of various contributing factors like properties/characteristics of geomaterials, pile types, geometries, installation techniques, and loading rates on the new CPTu-based capacity estimation method will be analyzed.

1.9 Overview of Thesis Content

Besides the introductory chapter, this thesis has been divided into nine more chapters, as listed below:

- Chapter 2: Review of deep foundation systems. This chapter presents a review of the existing pile foundation systems and various load testing and interpretation schemes.
- Chapter 3: Review of pile capacity evaluations from CPT data (published as a state-of-the-art review in *Geotechnical and Geological Engineering – An International Journal*). This chapter presents a concise, yet comprehensive review of the correlations between static axial capacity of pile foundations and CPT readings developed during the past over six decades.
- Chapter 4: Review of settlement analysis methods for pile foundations. In this chapter, different approaches for pile settlement analysis are briefly reviewed:

empirical, analytical spring, elastic continuum, and numerical methods (finite element method, boundary element methods, and finite layer methods). A more detailed review of the elastic continuum solution by Randolph and Wroth (1978; 1979) is presented. In addition, different shear stiffness reduction schemes from the literature are also reviewed.

- Chapter 5: Pile-SCPT database and case records. In this chapter, an overview of the database of 330 piles from 70 sites, gathered for this research, is presented. It includes information on site locations, pile types, load testing methods, soil deposits at the sites, and types of CPT data. This is presented in the form of summary statistics, charts, graphs, and figures, besides their descriptions.
- Chapter 6: Modified UniCone direct piezocone test method for axial pile capacity (tentatively accepted for the ASCE *Journal of Geotechnical and Geoenvironmental Engineeing*, subject to revisions; and a subset of this chapter has also been accepted for the *Deep Foundations Institute Journal*)
- Chapter 7: Operational soil stiffness from the back-analysis of pile load tests within elastic continuum framework (a subset of this chapter was submitted for the *3rd International Symposium on Cone Penetration Testing*, CPT'14, which has been accepted; a comprehensive paper on this topic is also under submission for review and possible publication in the special issue of the *Geotechnical Engineering Journal of the South East Asian Geotechnical Society*)
- Chapter 8: Elastic continuum solution of stacked pile model for axial load-displacement analysis (currently being submitted for review and possible publication in the special issue of the *Geotechnical Engineering Journal of the South East Asian Geotechnical Society* as a companion to the above paper submission)

- Chapter 9: Axial pile response of O-cell loading from modified elastic solution and shear wave velocity (tentatively accepted for the *Canadian Geotechnical Journal*, subject to revisions)
- Chapter 10: Summary of research findings and recommendations for future research

The dissertation contains following thirteen (13) appendices:

- Appendix A: Characteristics and uses of common pile types
- Appendix B: Schematics of pile load test arrangements and load application procedures
- Appendix C: Interpretive methods for evaluating failure load from axial load test on deep foundations
- Appendix D: Procedure for measuring the distribution of residual loads during a pile load test
- Appendix E: Presentation of database and case records
- Appendix F: Axial pile and CPTu information of Group 1 dataset
- Appendix G: Pile and soil parameters for back-figured operational shear moduli
- Appendix H: Initial shear stiffness (G_{max}) profiles from shear wave velocity (V_s) measurements: Group 2 dataset
- Appendix I: Results of study on the influence of plasticity index on shear modulus reduction
- Appendix J: Application of elastic continuum solution of stacked pile model for axial load-displacement analysis
- Appendix K: Piles and soils characteristics of Group 3 dataset: O-cell load tests
- Appendix L: Initial shear stiffness (G_{max}) profiles from shear wave velocity (V_s) readings

- Appendix M: Sample calculations from modified analytical solution for loads corresponding to selected displacements in multi-stage O-cell load test at Pinners Point Interchange

CHAPTER 2

REVIEW OF DEEP FOUNDATION SYSTEMS

Synopsis

This chapter presents a review of the existing pile foundation systems and various load testing and interpretation schemes. The chapter has been broadly divided into four parts. Part 1 provides information on the different types and characteristics of deep foundations used in practice world-wide, detailed further in the associated Appendix A. Part 2 details different mechanisms through which the static axial performance of a test piles is measured, with its accompanying Appendix B giving supplementary information. Part 3 presents a summary of various schemes for the interpretation of ultimate failure load from the data of pile load test, while Appendix C provides listing of 45 different interpretive schemes with details of selected ten methods. Finally, part 4 offers a brief discussion on the concept of residual loads, with its associated Appendix D summarizing the procedure for measuring the distribution of residual loads in a pile load test.

2.1 Deep Foundations Classification System

The choice of deep foundations over shallow footings for the support of structural loads is dictated by the characteristics and limitations of the project requirements and underlying site-specific local ground conditions (Hannigan et al., 2006). Typical situations requiring use of deep foundations to withstand axial loads include, but are not limited to the following (also see Figure 2.1):

- Compressible or weak shallower subsurface soil layers that are incompetent to support heavy axial loads, thus warranting transfer of loads to deeper firm soils or bedrock.
- Foundations expected to experience axial tensile loading, necessitating deeper layers to provide the required resistance against uplift.

- Anticipated future loss of partial bearing capacity from the expected scour/erosion, requiring foundations to derive their full capacity primarily from deeper strata.
- Subsurface soils located in a zone likely to be subjected to liquefaction in a seismic event, resulting in undesirable settlement and the consequent loss of bearing capacity.
- Structure with heavy axial loads to be constructed on a recent fill that has not reached required degree of consolidation before/during the construction period.
- Protection of bridge piers against damage due to vessel impact via installation of deep foundations for the support of fender systems.
- Sites characterized by multilayered soil profiles with contrasting stiffness and consolidation properties.
- To avoid later retrofitting for support of structures adjacent to the sites where future deep excavation has been planned or it is expected.
- At the site of expansive soils to resist undesirable seasonal uplift. Deep foundations enable transfer of loads to deeper strata unaffected by seasonal moisture variations.

A wide variety of different types of deep foundations is currently in use in geotechnical engineering practice worldwide. The selection of a particular type of deep foundation for a given situation merits consideration to various factors like: soil conditions, building designs, loading requirements, performance standards, construction limitations, time constraints, topography, and economy. Accordingly, the response of these foundations to loading varies greatly. A concise review of the modern available systems that collectively form part of the deep foundations industry is presented herein.

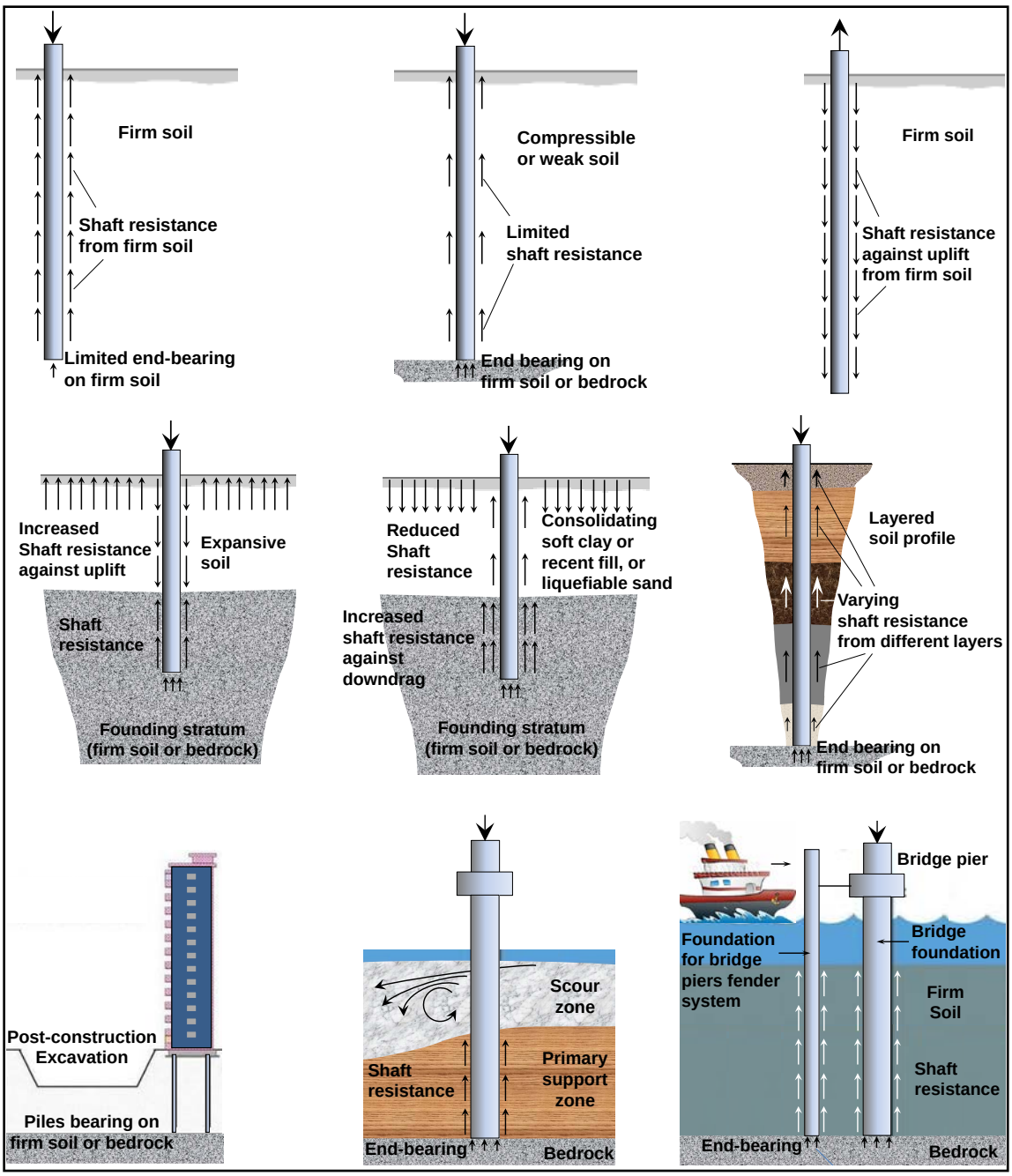

Figure 2.1. Typical situations requiring use of deep foundations for axial loading (modified from Hannigan et al., 2006).

One of the categorizations of deep foundations is based on the mechanism of load transfer from pile to the surrounding soil mass. Thus, deep foundations may be termed as floating type piles (also called friction piles) or end-bearing type piles (also called toe-

bearing piles). The *floating piles* withstand the structural loads by deriving their resistance primarily from the interactions between pile shaft and the adjacent soil layers; whereas *end-bearing piles* draw their resistance mainly from the pile base resting on competent hard soil or bedrock. Another simplistic classification is commonly done on the basis of pile installation effects, termed as *full-displacement piles* [e.g., driven closed-ended (CE) pipe piles, solid precast and prestressed reinforced concrete piles, timber piles] versus *non-displacement piles* [e.g., bored piles or drilled shafts, augered piles, driven open-ended (OE) pipe piles].

An elaborate classification system of deep foundations for the support of structural loads should be derived from the type of pile material, configuration, installation technique, and equipment used for installation. Accordingly, Figure 2.2 shows a comprehensive classification chart for deep foundations. A system for sub-classification of auger piles proposed by Basu et al. (2010) is shown in Figure 2.3, where the salient differences in the terminologies for auger piles in Europe vs. North-America are also presented. Table A.1 in Appendix A summarizes typical characteristics and uses of common pile types. Newer alternatives like helical piles, spun-cast concrete cylinder piles, and heli-crete piles are being added to give new dimensions to the inventory of piling industry for more efficient, versatile and environmental-friendly construction applications, and to cope with a growing spectrum of civil engineering structures.

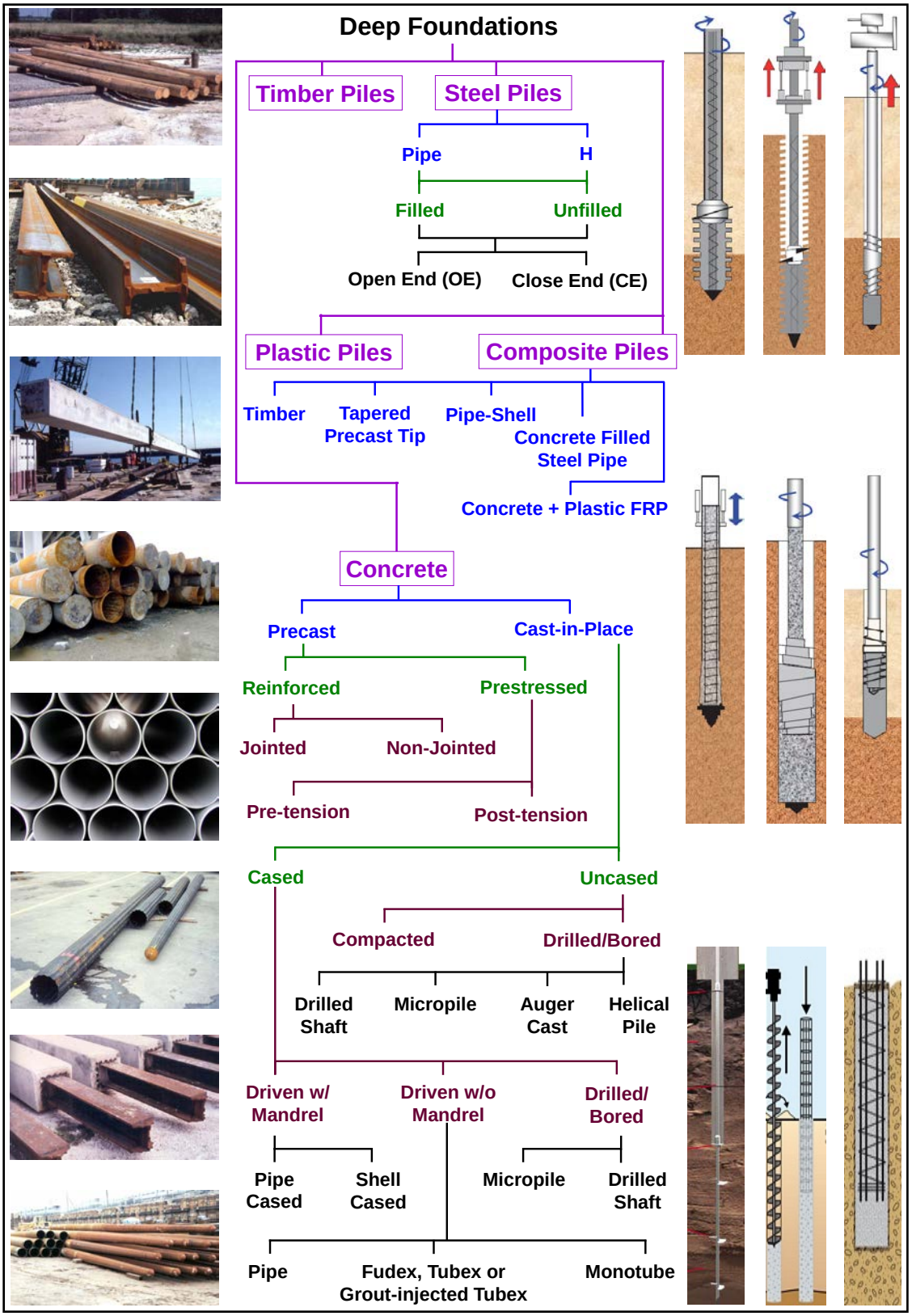

Figure 2.2. Deep foundations classification system
(adapted from Hannigan et al., 2006 and Basu et al., 2010).

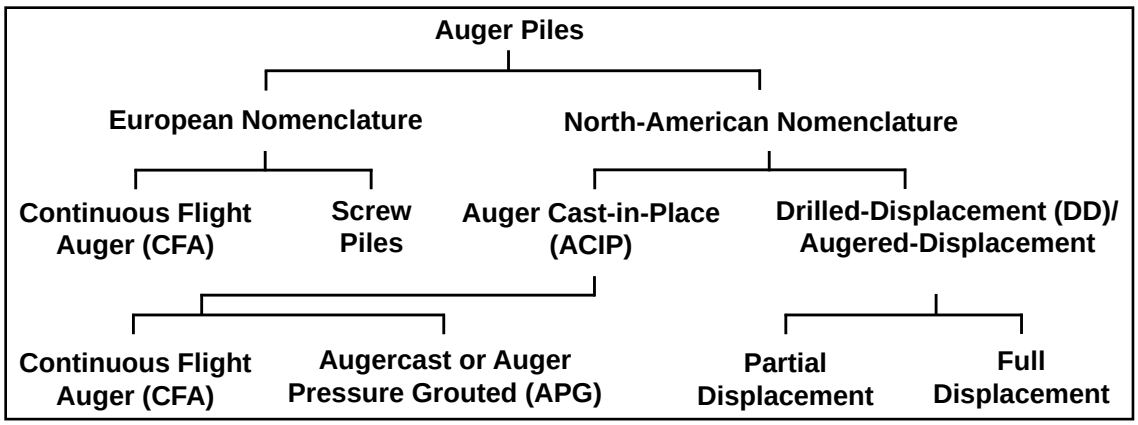

Figure 2.3. Nomenclature used for auger piles in Europe and North-America (after Basu et al., 2010).

2.2 Load Testing of Deep Foundations

In many instances, several different pile types can meet most of the requirements for a particular structure. Accordingly, for large-scale projects, alternative pile foundation options are considered. In such cases, amongst other equally important planning, design and execution steps, physical measurements of the response of different candidate piles are generally conducted, either during the design or the construction phases. These measurements enable selection/adjustment of the pile type, length and section requirements for design loads and constructability. Load testing minimizes risks to the structure by confirming the suitability of the deep foundation to support the design loads. It develops information for use in future design and/or construction of a deep foundations, and allows calibrations and implementation of new analysis and design methods or procedures such as: the LRFD (Samtani and Nowatzki, 2006), dynamic formulas (Peck, 1942; Chellis, 1961; Sowers, 1979; Fragasny et al., 1988; Rausche et al., 1996), Wave Equation Analysis (e.g., Cheney and Chassie, 2000), field solutions (e.g., Case Method by Eiber, 1958; Goble and Rausche, 1970; Goble et al., 1975; Rausche et al., 2004), rigorous numerical modeling techniques (e.g., CAse Pile Wave Analysis Program or CAPWAP by Hannigan et al., 2006; Bradshaw and Baxter, 2006).

Within the domain of performance-based axial pile measurement methods, static load testing of deep foundations is universally considered to be the most authentic and dependable option. Such a level of reliance has been derived through decades of its worldwide frequented use on a variety of deep foundations, and refinements in the testing procedures and instrumentation via research and development.

A pile load test can be conducted on either an uninstrumented or instrumented full-scale pile. With technological advancements, the methodologies and instrumentations for pile load testing have continuously remained under refinement. Figure 2.4 shows different pile load test systems currently being used in practice based on: (1) static dead weight, (2) reaction frame setup, (3) statnamic test, and (4) Osterberg load cell or O-cell arrangement. The direction of axial loading in the former two types (i.e., dead weight and reaction frame) can be either top-down for compression type loading or top-up for tension or uplift type loading. The latter two types (i.e., statnamic and O-cell) are both newer technologies; however, comparisons of their test results with the former two types are not straightforward. While the loading mode of O-cell test detailed below is different from the top-down static dead weight or reaction frame setup, the instantaneous loading in case of statnamic type requires adjustments to the measured response for inertia and damping forces to estimate the corresponding static response, thereby, adding a certain level of complexity in post-processing. The schematics of different static load test arrangements are detailed in Appendix B.

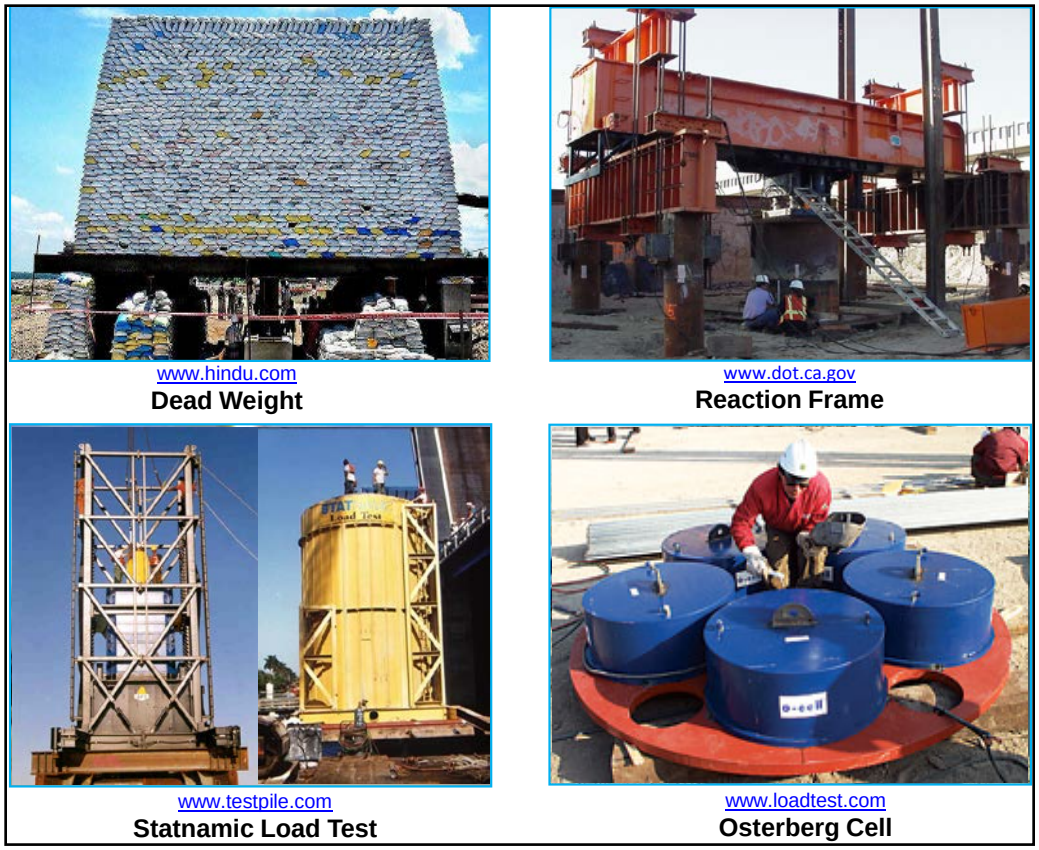

Figure 2.4. Different arrangements of pile load tests.

2.2.1 Tension vs. Compression Loading

Some special considerations are noteworthy with respect to the uplift loading as compared to the conventional top-down compression loading. The pile may be in tension (load applied at top of the pile) or compression (load applied at the pile base or some intermediate depth) depending on the test arrangements shown in Appendix B. A test pile which is loaded in uplift typically has the load applied to the pile shaft by pulling at the top of the shaft, thus placing the foundation into tension. With O-cell loading system, the pile shaft is placed in compression for an uplift loading. The pile shaft as well as base resistance response for these two conditions is expected to be different as illustrated in Figure 2.5. The Poisson's ratio effect due to elastic deformation of the pile material for

tension case will tend to reduce the lateral stress at the pile-geomaterial interface, whereas the opposite occurs for the case where the shaft is loaded in compression.

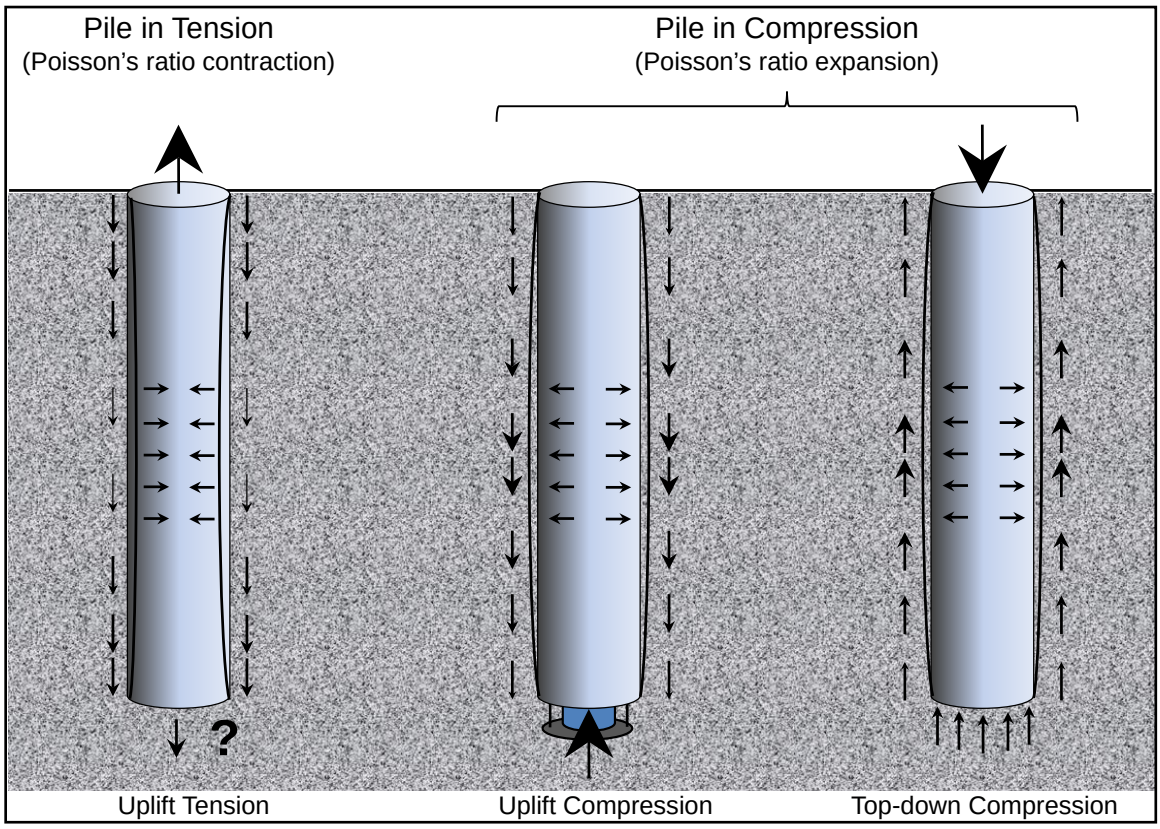

Figure 2.5. Poisson's ratio effect due to elastic deformation of the pile material for tension vs. compression loading (modified from Brown et al., 2010).

Many researchers have attempted to study the effect of loading direction on both shaft and base resistances of pile foundations (e.g., Coyle and Castello, 1981; DeNicola and Randolph, 1993; 1999; Elhakim and Mayne, 2002; Brown et al., 2010). Most of these works have concluded that there is a noticeable reduction in shaft capacity under tensile loading compared to that in compressive loading. The range of the reported tensile to compressive shaft capacity ratio [$Q_{s(t)}/Q_{s(c)}$] spans between 0.50 and 0.90 with an overall average of around 0.70. De Nicola and Randolph (1993) explored a theoretical basis for the differences in tensile and compressive shaft capacity of piles in sand. They

presented numerical work and analysis to quantify this difference from changes in mean effective stress levels related to the direction of loading and Poisson's ratio expansion and contraction of the pile. Accordingly, the following expression was proposed quantifying the ratio $Q_{s(t)}/Q_{s(c)}$, in terms of length to diameter ratio, L/d, and compressibility factor, η:

$$Q_{s(t)}/Q_{s(c)} \approx \{1 - 0.2 \log_{10}[100/(L/d)]\}(1 - 8\eta + 25\eta^2) \quad (2.1)$$

where L = pile length, d = pile diameter, $\eta = \nu_p \cdot \tan\delta \cdot (L/d) \cdot (G_{avg}/E_p)$, δ is the soil-pile interface friction, ν_p is the Poisson's ratio of the pile, G_{avg} = average shear modulus along the pile length (L), and E_p = Young's modulus of an equivalent solid pile. A slight tendency for the ratio to decrease with increasing density has been reported by De Nicola and Randolph (1999). The measurements of base capacity from different tensile loading tests reported in the literature (e.g., Coyle and Castello, 1981; Brittsan and Speer, 2008) span between negligible and some nominal values corresponding to the atmospheric pressure (i.e., 100 kPa) (McManus and Kulhawy, 1994). Accordingly, in coarse grained soils q_b may be neglected, whereas, in fine grained soils, a nominal value equivalent to the excess porewater pressure at the pile base may be considered to account for the suction effect at the pile base.

2.2.2 Load Application Procedures

Besides the loading arrangements, an important aspect in the axial load testing of pile foundations is the procedure of load application to the test pile. The term "procedure" refers only to the different load increment schemes (Hirany and Kulhawy, 1988). Details of different procedures can be found in the literature (e.g. ASTM D1143; ASTM D3689; Crowthers, 1988; Fuller and Hoy, 1970; Hirany and Kulhawy, 1988; Joshi and Sharma, 1987; Prakash and Sharma, 1990). Different agencies adopt their

standardized codes with slight variants in the procedures thereof. Alsamman (2012) summarized the procedures cited in the literature and used in practice under two main categories: stress-controlled and strain-controlled. The sub-categorization of the standardized load increment schemes are shown in a chart form in Figure 2.6. Discussions on the variants of these procedures recommended under different building codes, their comparative advantages/disadvantages and the most suitable applications were presented in Hirany and Kulhawy (1988), while the procedures are summarized in Appendix B.

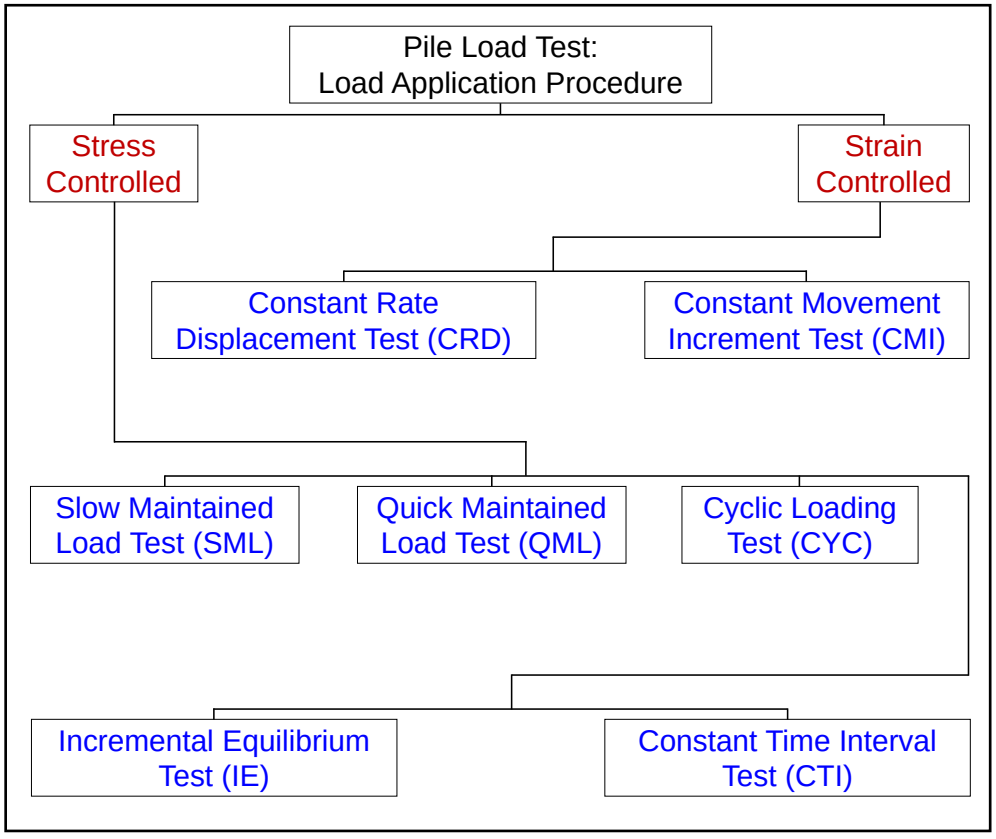

Figure 2.6. Different load increment schemes for pile load tests.

2.3 Interpretation of Axial Load Test Results

The raw data obtained from the static axial load test on pile foundations requires post processing to derive meaningful results that can be used in the design process. The two main components of the results so derived are: (1) the load transfer distribution curves (Q – z) for different levels of applied load obtained from strain gages installed at multiple depths along the pile shaft and load cells placed at the pile top and base, and (2) the load-displacement response curves ($Q_t - w_t$, $Q_s - w_t$, $Q_b - w_t$, and $Q_b - w_b$) obtained from a system of load cells at the pile top and base, dial gages at the pile top, and telltales through the pile shaft. Although, some of these measurements are costly and optional, $Q_t - w_t$ curve is considered to be the bare minimum result that a load test must generate. The Q – z curves present the pile shaft and base resistance components (Q_s and Q_b, respectively) offered via pile soil interaction upon the application of axial load. In turn, the Q_s profile enables calculations for estimating the variation of the unit shaft resistance along the pile shaft: $f_{pi} = Q_{si}/(\pi\, d\, \Delta z_i)$, while q_b provides unit base resistance: $q_b = Q_b/(\pi\, d^2/4)$. Here the subscript 'i' pertains to the i^{th} soil layer along the pile shaft.

It is customary to present the Q – w readings graphically in the first quadrant with the loads on a linear scale on the ordinate and displacements on a linear scale on the abscissa (Fellenius, 1990). The readings may also be flipped between the axes to enable an alternative presentation. This graph (or curve) is then used to estimate the failure load so that a "capacity" may be selected. Hirany and Kulhawy (2002) suggested that the term “ultimate capacity” lacks a universally accepted definition. Instead a term “interpreted failure load (Q_{fi})” was proposed to emphasize that a certain criterion be adopted. In a geotechnical but not structural sense, the "failure load" for a pile can be defined as the force when the pile either plunges or displacements occur rapidly. Plunging, however, may require large movements that may exceed the acceptable range of the soil-pile system (Prakash and Sharma, 1990). Table C.1 in Appendix C (updated from Hirany and Kulhawy, 1988) presents a list of 45 interpretive methods recommended by different

researchers, agencies, or codes for evaluating the failure load (Q_{fi}) from the measured Q_t – w_t results of axial load test on deep foundations, while the application procedures of selected ten methods are also illustrated in Appendix C.

The enlisted methods are based either on the following criteria or a combination of the following criteria used to interpret the failure load:

- Absolute displacement limitation
- Displacement per unit load (limiting secant modulus)
- Relative displacement limitation (function of pile diameter)
- Displacement rate limitation (function of load)
- Displacement ratio limitation
- Graphical construction
- Mathematical modeling

Figure 2.7 shows the frequency (expressed as percent use) of each criterion amongst different interpretive methods.

The procedural steps for implementation of selected methods most frequently used in practice are reviewed in the next sub-section. The applicability of each of these methods may be found in Fellenius (1990; 2001a), Hirany and Kulhawy (1988), and Prakash and Sharma (1990).

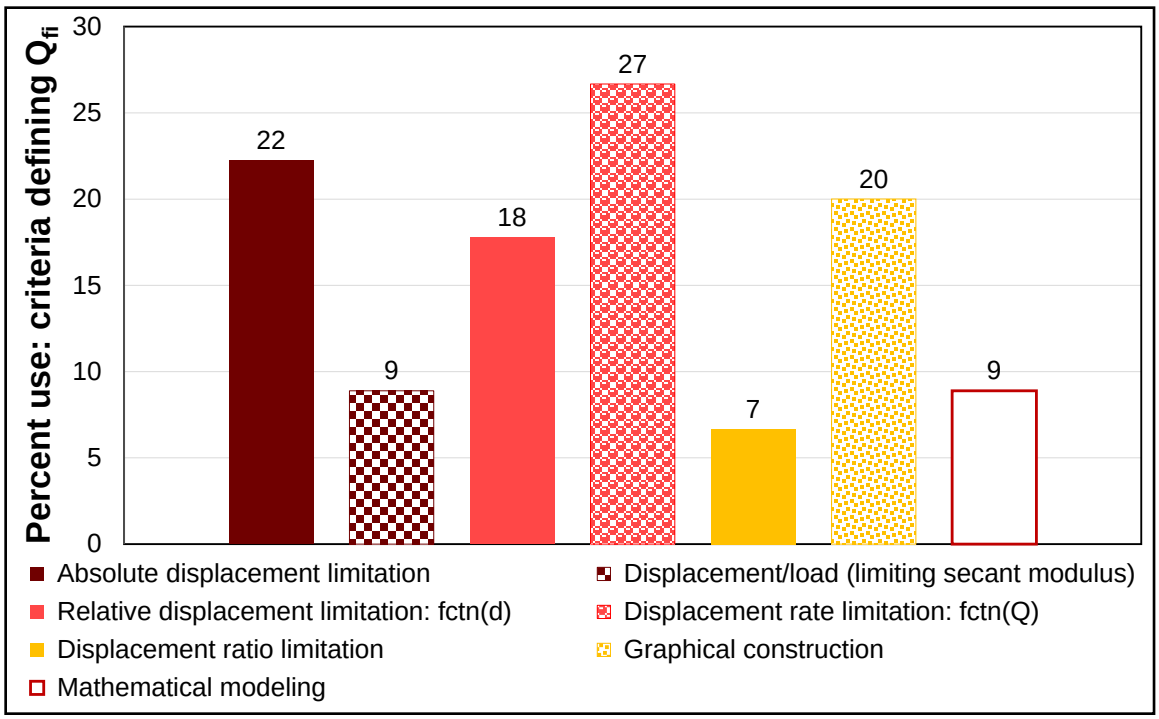

Figure 2.7. Frequency (expressed as percent use) of different criteria defining the failure load (Q_{fi}) used in various interpretive methods.

2.4 Concepts of Residual Loads and Critical Depth

Load tests on pile foundations for important large scale projects usually include instrumentation ranging from telltales, electronic displacement transducers (i.e., LVDTs or DCDTs), strain gages, and/or load cells for measuring the distribution of load along the embedded pile shaft, in addition to the measurement of load vs. movement response. In one viewpoint, however, before the commencement of a load test, installation-induced forces already exist within the pile shaft due to locked-in stresses and strains. Such loads may be attributed to the pile installation effects and are commonly termed as "residual loads." According to the proponents of residual loads in a pile, these may be caused due to: (1) "set-up" or "reconsolidation" related to the soil recovery from the disturbances caused by pile installation; (2) shear stress developed between a displacement pile and the adjacent soil during its driving; and (3) stresses due to thermal or chemical changes, such as curing of concrete.

In analyzing the data from the instrumentation, however, it is also a common practice to consider that the test starts at a condition with no (or negligible) prior history of load, strain, and stress along the pile shaft. Accordingly, most of the field testing program of instrumented piles is based on "zeroing" all gages immediately before commencing the load test. Fellenius (2002a) termed such approach as "solving a problem by declaring it not to exist, as it were." Thus, a conflict exists in the reporting of pile load test data, depending upon whether or not residual loads are included.

Altaee et al. (1992) showed from the results of load tests on a precast concrete pile driven in a sand deposit that neglect of the residual loads can result in incorrect interpretations of constant unit shaft resistance below a certain depth, termed "critical depth (L_c)" in the Canadian Foundation Engineering Manual (Canadian Geotechnical Society, 1985). Fellenius (2002a) termed the concept of critical depth as a fallacy leading to the erroneous conclusion that unit shaft resistance would be essentially constant with depth in a homogeneous soil. A constant unit shaft resistance would mean that the basic physical principle of resistance to sliding movement being a function of normal stress is invalid. Fellenius (2001b) points out that the concept of residual load may be traced back to the works presented by Nordlund (1963), Hunter and Davisson (1969), Hanna and Tan (1973), Holloway et al. (1978), Briaud (1984), and others.

The procedure recommended by Altaee et al. (1992), and Fellenius (1989; 2001b; 2002a) for measuring the distribution of residual loads during a pile load test are presented in Appendix D.

As noted earlier, most of the practitioners still consider the effects of residual loads insignificant or follow the approach of zeroing the gages immediately before the load test. Following logical reasoning could be presented for the practitioners following this approach:

- Premchitt et al. (1988) observed that the pattern of residual stresses developed after pile driving was complex and erratic. Fellenius (2002a) pointed out that it

was not easy to demonstrate that test data are influenced by residual loads, and quantification of the effects of residual loads is even more difficult. It is, therefore, difficult to generalise for design purposes. Accordingly, the cost, effort and time consumed in estimating these residual loads vs. their productive use warrant simplifying assumptions to be preferred.

- It was noted by Premchitt et al. (1988) that the residual shaft resistance and end-bearing resistance locked in after pile driving were not associated with well-defined displacements or an applied loading. Furthermore, consideration of the shaft resistance associated with the applied loading in a load test (i.e. zeroing the instrumentation prior to a load test) represents the condition of actual working piles supporting superstructure loads. A simpler explanation follows.
- Any specific pile, whether a test pile or a production type, having certain dimensions, installed at a particular site, may or may not carry the locked-in residual loads before it is subjected to the planned test or structural load, respectively. Within the bounds of expected variability at a site, the response of a test as well as its compatible production pile is expected to be similar. In a load test on a pile, if gages are zeroed before application of test loads, the response to the applied loads would tell what happens to the pile after its installation and wait period, no matter it carries residual loads or not. The production pile of same type and dimensions installed at the same site should respond comparably on application of structural loads. From that viewpoint, any prior measurements of residual loads do not matter significantly in estimating the post installation response of a pile to the applied loads.

2.5 Summary

A four-part review of the deep foundation systems and their full-scale load testing and interpretations is presented in this chapter. It includes: classification of deep

foundations based on pile materials and installation methods, their characteristics and applications, various load testing arrangements (including compression, tension and O-cell loading), load application procedures (including various stress controlled and strain controlled methods), summary of 45 different criteria for pile capacity interpretation from the results of load test, and a brief discussion on the concept of residual loads.

The database of piles collected for this research (detailed later in Chapter 5) covers most of the piles presented in the classification system shown in Figures 2.2 and 2.3, and Table A.1 of Appendix A. These piles were tested using all the different loading modes and the load increment procedures explained in Appendix B. The application procedures of selected ten methods of capacity interpretations were specifically explained in Appendix C, as some these were applied later in this research. It was also recognized that the cost, effort and time consumed in estimating the residual loads vs. their productive use warrant simplifying assumptions (i.e. zeroing the instrumentation prior to a load test) to be preferred, since consideration of the shaft resistance associated with the applied loading in a load test represents the condition of actual working piles supporting superstructure loads.

CHAPTER 3

REVIEW OF PILE CAPACITY EVALUATIONS FROM CPT DATA

Synopsis

This chapter presents a concise, yet comprehensive review of the correlations between static axial capacity of pile foundations and cone pentrometer readings (q_c or more proper q_t, f_s, and $u_{2)}$, developed during the past over six decades. Broadly, the pile capacity analysis from CPT data can be accomplished via two main approaches: *rational* (*or indirect*) *methods*, and *direct methods*. The rational methods require a two-step approach, wherein CPT data are first used to provide assessments of geoparameters that are further utilized as input values within a selected analytical framework to enable the assessment of pile capacity components of shaft and base resistance (f_p and q_b, respectively). The direct CPT methods use the measured penetrometer readings by scaling relationships or algorithms in a single-step process to obtain f_p and q_b for evaluation of full-size pilings. The compilation effort presented in this chapter results in assembling of maximum published methods of the two approaches, proposed as a result of past investigations in one resource to afford researchers and practitioners with convenient access to the respective design equations and charts. In addition to all-inclusive summary tables and the design charts, a compilation of significant findings, discussions thereof, and potential future research directions are also presented towards the end.

3.1 Introduction

The methods for the assessment of pile capacity in terms of its components of shaft and base resistance (f_p and q_b, respectively) have followed a constant evolution over the past five decades. Starting from some basic formulations where shaft capacity

was related solely to the shear strength of the soil, alternative approaches such as those incorporating the influence of lateral effective stress coefficients and pile-soil interface friction were advanced. Subsequently, other variables which influence the magnitude of shaft capacity were studied, including: stress history, pile length, pile slenderness ratio, soil sensitivity, plasticity of clayey soils, relative density of sandy soils, effective stress strength of soil, progressive failure mechanism, plugging effect in open-ended pipe piles, soil compressibility characteristics, pile material, and installation methods. Similarly, the base resistance component of pile capacity depends primarily on the conditions around the pile base, including: pile tip configuration, installation method, strength and stiffness properties of the geomaterial encountered at the pile base, rate of loading, and drainage characteristics. Different researchers have proposed various bearing capacity theories, and modifications thereof, to evaluate end bearing resistance of pile foundations, e.g., limit plasticity, elasto-plasticity, cavity expansion, strength dilatancy theory, and particle breakage. This continual process of evolution has led to a variety of sophisticated formulae.

Despite significant contributions being made to the literature in terms of different design methods, many of the approaches have a number of inherent drawbacks. Soil behavior is, of course, governed by a series of complex stress-strain changes that occur during installation and subsequent loading. Owing to the difficulties and the uncertainties in assessing the pile capacity on the basis of the soil strength-deformation characteristics, the most frequently followed design practice is to refer to the formulae correlating directly the pile capacity components of q_b and f_p to the results of the prevalent in-situ tests. The pile axial bearing capacity evaluation from cone penetrometer readings is one of the most frequented applications of CPT data. Since the historical use of CPT in geotechnical investigations, research efforts have advanced the very

elementary idea of considering CPT as mini-pile foundation. This has resulted in plethora of correlative relationships being developed between the CPT readings (q_c, or more proper q_t, f_s, and u_2) and the pile capacity components of q_b and f_p. These correlations, although empirical, have been worked out on the basis of load test results from both instrumented and un-instrumented full scale piles and are able to accommodate the following important variables (Jamiolkowski, 2003):

- Soil characteristics, macro-fabric and stress-history
- Construction method
- Soil stratigraphy
- Type of loading, i.e., compression vs. tension, static vs. cyclic, stepped vs. constant rate of loading

As commonly reported (e.g., Ardalan et al., 2009; Cai et al., 2009; 2012; Mayne, 2007), there are two main approaches to accomplish axial pile capacity analysis from CPT data: (a) "rational (or indirect) methods" and/or (b) "direct methods." Figure 3.1 below presents a chart showing different paths to evaluate the two components of q_b and f_p from CPT readings.

3.2 Rational (Indirect) Methods

The rational methods require a two-step approach. As a first step, CPT data are used to provide assessments of stress history [preconsolidation stress, (σ_p') and overconsolidation ratio, (OCR)], in-situ lateral stress coefficient (K_o), undrained shear strength (s_u), relative density (D_r), effective stress strength (ϕ'), soil total unit weight (γ_t), fundamental soil stiffness [intial shear modulus (G_{max}), or initial Young's Modulus (E_{max})], interface friction between soil and pile material (δ), and/or bearing capacity coefficient (N_q). A summary of selected correlations is given in Table 3.1. Utilizing these input values of geoparameters, the second step enables the assessment of f_p and q_b components of pile capacity within a selected analytical framework. Herein, f_p can be

evaluated using either total stress analyses (α-method) for clays, or the effective stress analysis (β-method) for both sands and clays. On the other hand, the evaluation of q_b is based on different bearing capacity theories.

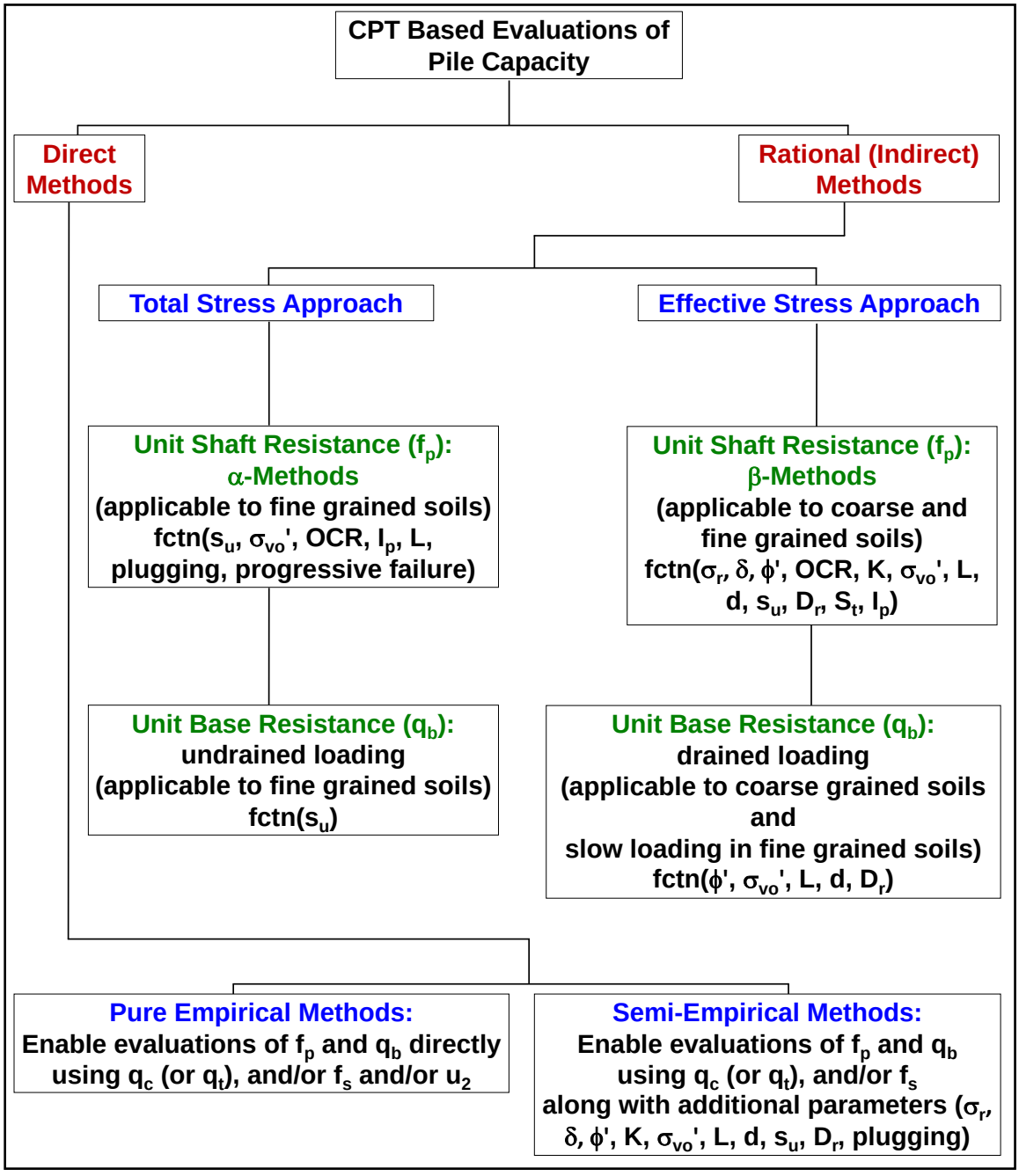

Figure 3.1. Alternative paths for CPT-based evaluations of f_p and q_b components of pile capacity.

Table 3.1. Selected CPT-based correlations for use in rational (indirect) pile design methods.

Engineering Parameter Relationship	Applicable Soil Type	Reference
Soil Classification $I_c = [(3.47 - \log Q_{tn})^2 + (\log F_r + 1.22)^2]^{0.5}$ $n = 0.381\ (I_c) + 0.05\ (\sigma'_{vo}/\sigma_{atm}) - 0.15 \leq 1.0$	All	Robertson (2009)
Total Unit Weight $\gamma_t = 1.95 \cdot \gamma_w \cdot (\sigma_{vo}'/\sigma_{atm})^{0.06} \cdot (f_s/\sigma_{atm})^{0.06}$	All	Mayne et al. (2010)
$\gamma_t\ (kN/m^3) = 11.46 + 0.33 \cdot \log[z\ (m)] + 3.1 \cdot \log[f_s\ (kPa)] + 0.7 \cdot \log[q_t\ (kPa)]$	All	Mayne et al. (2010)
$\gamma_t\ (kN/m^3) = 8.32 \cdot \log[V_s\ (m/s)] + 1.61 \cdot \log[z\ (m)]$	All	Mayne (2007)
Effective Stress Friction Angle $\phi'\ (deg.) = 17.6^o + 11.0 \cdot \log(q_{t1})$; where $q_{t1} = (q_t/\sigma_{atm})/(\sigma_{vo}'/\sigma_{atm})^{0.5}$	Sands	Kulhawy and Mayne (1990)
$\phi'\ (deg.) = 29.5^o \cdot B_q^{0.121}\ [0.256 + 0.336 \cdot B_q + \log Q]$	Clays	Senneset et al. (1989)
Shear Wave Velocity $V_s\ (m/s) = \{10.1 \cdot \log[q_t\ (kPa)] - 11.4\}^{1.67} \cdot [f_s\ (kPa)/q_t\ (kPa)\ 100]^{0.3}$	All	Hegazy and Mayne (1995)
$V_s\ (m/s) = 118.8 \cdot \log[f_s\ (kPa)] + 18.5$	All	Mayne (2006)
$V_s\ (m/s) = 277 \cdot [(q_t)\ (MPa)]^{0.13} \cdot [(\sigma_{vo}')\ (MPa)]^{0.27}$	Uncemented unaged sands	Baldi et al. (1989)

Notes: $Q_{tn} = [(q_t - \sigma_{vo})/\sigma_{atm}](\sigma_{atm}/\sigma_{vo}')^n$, $F_r = f_s \cdot 100/(q_t - \sigma_{vo})$, $n = 0.381(I_c) + 0.05(\sigma_{vo}'/\sigma_{atm}) - 0.15 \leq 1.0$, σ_{vo}' (effective vertical stress) $= \sigma_{vo} - u_o$; σ_{vo} (total overburden stress) $= \Sigma\gamma_{ti} \cdot z_i$, u_o (hydrostatic porewater pressure) $= \gamma_w \cdot h_w$; h_w is the height of water, γ_{ti} and z_i are the total unit weight and depth of i^{th} soil layer, respectively, and γ_w (unit weight of water) = 9.8 kN/m^3; I_c = soil classification index: clays: $2.95 < I_c < 3.60$; silt mix: $2.60 < I_c < 2.95$; sand mix: $2.05 < I_c < 2.60$; sands: $1.31 < I_c < 2.05$; and gravelly sands: $I_c < 1.31$; σ_{atm} is a reference stress = 100 kPa; For soft sensitive soils: $Q_{tn} < 12\exp(-1.4F_r)$.

Table 3.1. (continued).

Engineering Parameter Relationship	Applicable Soil Type	Reference
Fundamental Soil Stiffness (Modulus) $G_{max} = \rho_T \cdot V_s^2$; where, ρ_t is the total mass density = γ_t/g_a; and g_a is the gravitational acceleration constant = 9.8 m/s^2	All	Timoshenko and Goodier (1951)
$E_{max} = 2 \cdot G_{max} \cdot (1 + \nu)$; Drained: $\nu_d \approx 0.2$, Undrained: $\nu_u \approx 0.5$	All	Lehane and Cosgrove (2000)
Stress History $\sigma_p' = 0.33 \cdot (q_t - \sigma_{vo})^{m'} (\sigma_{atm}/100)^{1-m'}$, where $m' = 1 - 0.28/[1 + (I_c/2.65)^{25}]$	All	Mayne et al. (2010)
$\sigma_p' = 0.101 \cdot \sigma_{atm}^{0.102} \cdot G_{max}^{0.478} \cdot \sigma_{vo}'^{0.420}$	All	Mayne (2007)
$OCR = \{[0.192 \cdot (q_t/\sigma_{atm})^{0.22}]/[(1-\sin\phi') \cdot (\sigma_{vo}'/\sigma_{atm})]\}^{\{1/(\sin\phi' - 0.27)\}}$	Sands	Mayne (2005)
Lateral Stress State Coefficient $K_o = (1-\sin\phi') OCR^{\sin\phi'}$	All	Mayne and Kulhawy (1982)
Relative Density $D_r = 100 \cdot \{q_{t1}/(300 \cdot OCR^{0.2})\}^{0.5}$; where $q_{t1} = (q_t/\sigma_{atm})/(\sigma_{vo}'/\sigma_{atm})^{0.5}$	Quartz Sands	Kulhawy and Mayne (1990)
$D_r = 100 \cdot \{0.268 \cdot \ln(q_{t1}) - 0.675\}$; where $q_{t1} = (q_t/\sigma_{atm})/(\sigma_{vo}'/\sigma_{atm})^{0.5}$	Silica Sands	Jamiolkowski et al. (2001)
Normalized Undrained Shear Strength (in direct simple shear) $(s_u/\sigma_{vo}') = \frac{1}{2} \cdot \sin\phi' \cdot OCR^{\Lambda}$	Clays	Ladd and Degroot (2003)

σ_{atm} is a reference stress = 1 bar = 100 kPa; Poisson's ratio ν_d values at working loads increase to larger values at failure state; parameter Λ is the plastic volumetric strain potential that generally varies between 0.8 and 0.9 for many clays.

3.2.1 Total Stress Approach (α-Method)

The basic form of the total stress approach links the f_p to the average undrained shear strength (s_u) of the clay along the pile shaft through an adhesion factor: $\alpha = f_p/s_u$. Many correlations have been advanced since the inception of this approach by Tomlinson (1957). In later approaches, α has been also empirically related to σ_{vo}', OCR, pile slenderness ratio (L/d), plasticity index (I_p), effects of progressive failure, effects of soil plugging in OE pipe piles, and other factors. Doherty and Gavin (2011), Jamiolkowski (2003), and Patrizi and Burland (2001) reported some of these works. Significant contributions in this regard include works by Skempton (1959), McClelland (1974), API (1969, 1976), Vijayvergiya and Focht (1972), Drewry et al. (1977), Vesić (1977), API (1975, 1976), Kraft et al. (1981a), Randolph (1983), Semple and Rigden (1984), Dennis and Olson (1983), Randolph and Murphy (1985), API (1987, 1993), Karlsrud et al. (1993), Chen and Kulhawy (1994), Kolk and Van der Vende (1996), Miller and Luttenegger (1997), Goh et al. (2005), Karlsrud et al. (2005; 2012), Salgado (2006, 2008, 2010), and Chakraborty et al. (2013). Table 3.2 provides a summary list of the various different factors considered by these researchers in their respective studies in order to make improvements in the predictive reliability of their total stress approach. The design equations and related charts derived from these studies are presented in Table 3.3 and accompanying Figures 3.2 to 3.11.

Table 3.2. Factors considered by the total stress approach, α-methods, for estimating pile unit shaft resistance (f_p) in fine grained soils.

Reference	Length effect	Stress history	I_p	s_u	σ_{vo}'	ϕ'	Progressive failure	Plugging effect
Tomlinson (1957)	x	x	x	✓	x	x	x	x
Peck (1958)	x	x	x	✓	x	x	x	x
Skempton (1959)	x	x	x	✓	x	x	x	x
Woodward et al. (1961)	x	x	x	✓	x	x	x	x
Kerisel (1965)	x	x	x	✓	x	x	x	x
API (1969)	x	✓	x	x	✓	x	x	x
McClelland (1974)	x	✓	x	✓	x	x	x	x
Vijayvergiya and Focht (1972)	✓	x	x	✓	✓	x	x	x
Vesić (1977)	x	x	x	✓	x	x	x	x
Drewry et al. (1977)	x	x	x	✓	x	x	x	x
API (1975, 1976)	x	✓	✓	✓	✓	x	x	x
Kraft et al. (1981a)	✓	x	x	✓	✓	x	✓	x
Dennis and Olson (1983)	✓	x	x	✓	x	x	x	x
Randolph (1983)	✓	x	x	✓	x	x	✓	x
Semple and Rigden (1984)	✓	✓	x	✓	✓	x	x	x
Randolph and Murphy (1985)	x	✓	x	✓	✓	x	x	x
API (1987)	x	✓	x	✓	✓	x	x	x
API (1993)	x	✓	x	✓	✓	x	x	x
Karlsrud et al. (1993)	x	x	✓	✓	✓	x	x	x

Notes: I_p = plasticity index; s_u = undrained shear strength; σ_{vo}' = effective overburden stress; ϕ' = friction angle.

Table 3.2. (continued).

Reference	Length effect	Stress history	I_p	s_u	σ_{vo}'	ϕ'	Progressive failure	Plugging effect
Chen and Kulhawy (1994)	x	x	x	✓	x	x	x	x
Kolk and Van der Vende (1996)	✓	✓	x	✓	✓	x	x	x
Miller and Lutenegger (1997)	x	x	x	x	x	x	x	✓
O'Neill and Reese (1999)	x	x	x	✓	x	x	x	x
Jamiolkowski (2003)	x	✓	x	✓	✓	x	x	x
Goh et al. (2005)	x	✓	x	✓	✓	x	x	x
Karlsrud et al. (2005) NGI-05	x	✓	✓	✓	✓	x	x	x
Salgado (2006, 2008, 2010)	x	x	x	✓	x	x	x	x
German Method (Kempfert and Becker, 2010)	x	x	x	✓		x	x	x
Karlsrud (2012)	x	✓	✓	✓	✓	x	x	x
Chakraborty et al. (2013)	x	x	x	✓	✓	✓	x	x

Notes: I_p = plasticity index; s_u = undrained shear strength; σ_{vo}' = effective overburden stress; ϕ' = friction angle.

Table 3.3. Design equations for pile unit shaft resistance (f_p) from total stress approach (common α-methods) for fine grained soils.

Method/Reference	**Pile Type**	**Design Equations**
Tomlinson (1957); Peck (1958); Woodward et al. (1961); Kerisel (1965); Drewry et al. (1977); API (1975)	Driven piles	$f_p = \alpha \cdot s_u$ α = fctn(s_u) (see Figure 3.2)
Skempton (1959)	Drilled shafts Diameter: 0.3m to 0.6m Length: 6m to 15m	$f_p = \alpha \cdot s_u$ $\alpha = 0.45$
API (1969; 1976)	Driven piles	$f_p = \sigma_{vo}'/3$ (for NC high I_p deposit, where α is assumed to be unity)
Vijayvergiya and Focht (1972)	Driven piles	$f_p = \lambda \cdot (2s_u + \sigma_{vo}')$ (see Figure 3.3)
Vesić (1977)	Driven and drilled shafts in stiff clays	$f_p = \alpha \cdot s_u$ α = 0.2 to 1.5 depending on the pile type
Kraft et al. (1981a)	Driven piles	$f_p = \alpha \cdot s_u$ For $s_u/\sigma_{vo}' \leq 0.4$ $\alpha = 1.34+0.126 \ln(L)$ For $s_u/\sigma_{vo}' > 0.4$ $\alpha = 0.89+0.103 \ln(L)$
Semple and Rigden (1984)	Driven piles	$f_p = \alpha \cdot s_u$ α = fctn(L/d, s_u/σ_{vo}') (see Figure 3.4)

Notes: σ_{atm} is a reference stress = 100 kPa; NC = normally consolidated; I_p = plasticity index; L = pile embedded length; d = pile diameter.

Table 3.3. (continued).

Method/Reference	Pile Type	Design Equations
Dennis and Olson (1983)	Steel pipe piles	$f_p = \alpha \cdot s_u \cdot F_c \cdot F_L$ (see Figure 3.2 for s_u from UU tests) F_c = adjustment factor for s_u from other tests (1.1 for CU tests; 1.8 for unconfined samples from dynamically embedded samples; 0.7 for on site vane tests) F_L = correction factor for length (1 for length upto 30 m and 1.8 for length > 53 m)
API (1987)	Driven piles	$f_p = \alpha \cdot s_u$ $\alpha = 0.5(s_u/\sigma_{vo}')^{-0.5}$ for $(s_u/\sigma_{vo}') \leq 1$ $\alpha = 0.5(s_u/\sigma_{vo}')^{-0.25}$ for $(s_u/\sigma_{vo}') > 1$ (also see Figure 3.2)
Randolph and Murphy (1985) (for non-structured fine grained soils)	Drilled shafts and CFA piles	$f_p = \alpha \cdot s_u$ $\alpha = \text{fctn}(s_u/\sigma_{vo}')$ (see Figure 3.5a)
Karlsrud et al. (1993)	Driven piles	$f_p = \alpha \cdot s_u$; $\alpha = \text{fctn}(s_u/\sigma_{vo}', I_p)$ (see Figure 3.6)
API (1993)	Driven piles	f_p is given as the larger of: $f_p = \alpha \cdot s_u = 0.5(s_u \cdot \sigma_{vo}')^{0.5}$ $f_p = \alpha \cdot s_u = 0.5(s_u^{0.75} \cdot \sigma_{vo}')^{0.25}$
Chen and Kulhawy (1994)	Drilled shafts	$f_p = \alpha \cdot s_u$ $\alpha = 0.21+0.26(\sigma_{atm}/s_u) \leq 1$
Kolk and Van der Vlede (1996)	Driven piles	$f_p = \alpha \cdot s_u$ $\alpha = (0.5\ h/d)^{-0.2} \cdot [s_u(z)/\sigma_{vo}'(z)]^{-0.3} \leq 1$

Notes: I_p = plasticity index; z = depth below seafloor; h = distance between pile tip level and z; d = pile diameter.

Table 3.3. (continued).

Method/Reference	Pile Type	Design Equations
Miller and Lutenegger (1997)	Driven and jacked piles	$f_p = \alpha \cdot s_u$ α = fctn(PLR) (see Figure 3.7)
O'Neill and Reese (1999)	Drilled shaft in stiff clay	$f_p = \alpha \cdot s_u$ α=0.55 (for $s_u/\sigma_{atm} \leq 1.5$); $0.55 - 0.1(s_u/\sigma_{atm} - 1.5)$ (for $1.5 < s_u/\sigma_{atm} < 2.5$); 0.45 (for $s_u/\sigma_{atm} \geq 2.5$)
Jamiolkowski (2003) (for non-structured fine grained soils)	Screw piles	$f_p = \alpha \cdot s_u$; α = fctn(s_u/σ_{vo}') (see Figure 3.5b)
Goh et al. (2005)	Drilled shafts	$f_p = \alpha_{CIUC} \cdot s_u$ α_{CIUC} = fctn(USR, σ_{vo}') (see Figure 3.8)
NGI-05 Method (Karlsrud et al., 2005)	Driven piles	For NC clays with $\psi < 0.25$: $f_p = \alpha^{NC} \cdot \psi^{NC} \cdot \sigma_{vo}'$ $f_p = 0.32 \cdot (I_p - 10)^{0.3} \cdot \psi^{NC} \cdot \sigma_{vo}'$ For OC clays with $\psi \geq 1$: $f_p = \alpha \cdot s_u^{UU} \cdot F_{tip}$ $f_p = 0.57 \cdot \psi^{-0.3} \cdot s_u^{DSS} \cdot F_{tip}$ For clays with $0.25 < \psi < 1$: Linearly interpolate α between 0.5 and $0.32 \cdot (I_p - 10)^{0.3}$; (also see Figure 3.9) f_p should be $\geq \beta_{Min} \cdot \sigma_{vo}'$ $\beta_{Min} = 0.06 \cdot (I_p - 12\%)^{0.33}$ $0.05 < \beta_{Min} < 0.2$

Notes: PLR (%) = L_p/L = plug length ratio, where L_p = plug length; USR = undrained strength ratio = s_u/σ_{vo}'; Strength ratio $\psi = s_u^{UU}/\sigma_{vo}'$; $s_u^{UU} = 1.14 \cdot s_u^{DSS}$; $F_{tip\ (open)} = 1.0$ (driven OE); $F_{tip\ (closed)} = 0.8 + 0.2 \cdot \psi^{0.5}$ (driven CE); $1.0 < F_{tip\ (closed)} < 1.25$; NC = normally consolidated; OC = overconsolidated.

Table 3.3. (continued).

Method/Reference	Pile Type	Design Equations
Salgado (2006, 2008, 2010)	Drilled shafts	$f_p = \alpha \cdot s_u$ $\alpha = 0.4[1 - 0.12\ln(s_u/\sigma_{atm})]$ (for clay fraction > 50% and OCR = 3 to 5)
German Method* (Kempfert and Becker, 2010)	See Figure 3.9	Provides lower bound estimated of f_p (kPa) based on s_u (measured in kPa) (see Figure 3.10)
Karlsrud (2012)	Driven piles	Modified from NGI-05 Method by Karlsrud et al. (2005) $f_p = \alpha \cdot \psi \cdot \sigma_{vo}'$ where $\psi = s_u^{DSS}/\sigma_{vo}'$ α = fctn(ψ and I_p) (also see Figure 3.11)
Chakraborty et al. (2013)	Drilled shafts	$f_p = \alpha \cdot s_u$ $\alpha = (s_u/\sigma_{vo}')^{-0.05}\{A_1 + (1-A_1)\exp[-(\sigma_{vo}'/\sigma_{atm})(\phi_c - \phi_{r,min})^{A2}]\}$ $A_1 = 0.4$ for $\phi_c - \phi_{r,min} = 12^o$, $A_1 = 0.75$ for $\phi_c - \phi_{r,min} = 5^o$ $A_2 = 0.4 + 0.3\ln(s_u/\sigma_{vo}')$

Notes: ψ = normalized undrained shear strength; DSS = direct simple shear strength, taken as reference undrained shear strength; I_p = plasticity index; $\phi_c - \phi_{r,min}$ = residual friction angle, where ϕ_c = critical-state friction angle and $\phi_{r,min}$ = minimum residual state friction angle.

*The German method is classically not a total stress approach (α-method). However, it utilizes s_u values which, in turn, can be estimated from the CPT-based correlation. Therefore, this method falls into the category of indirect methods and has been listed here.

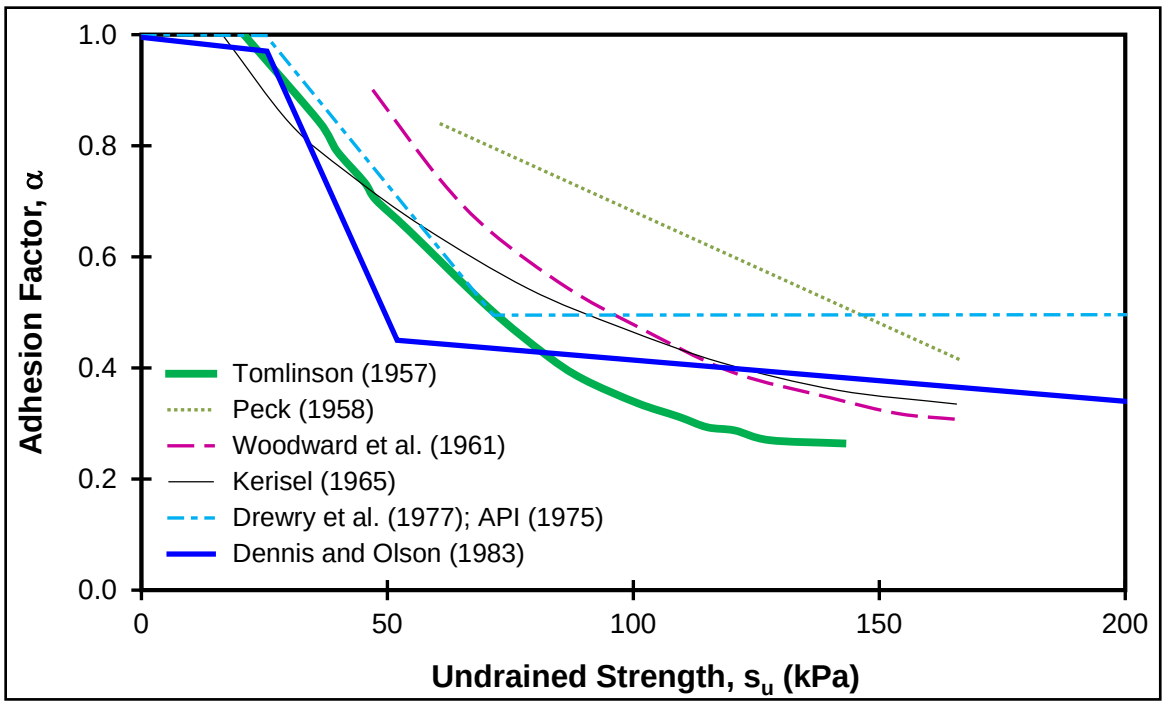

Figure 3.2. Early alpha correlations (adapted from Doherty and Gavin, 2011).

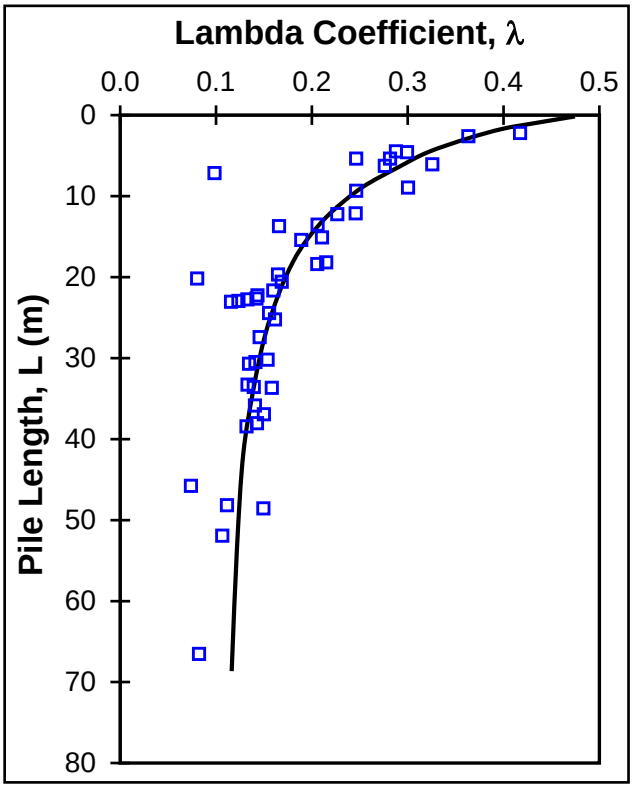

Figure 3.3. Lambda coefficient as a function of pile length (adapted from Vijayvergiya and Focht, 1972).

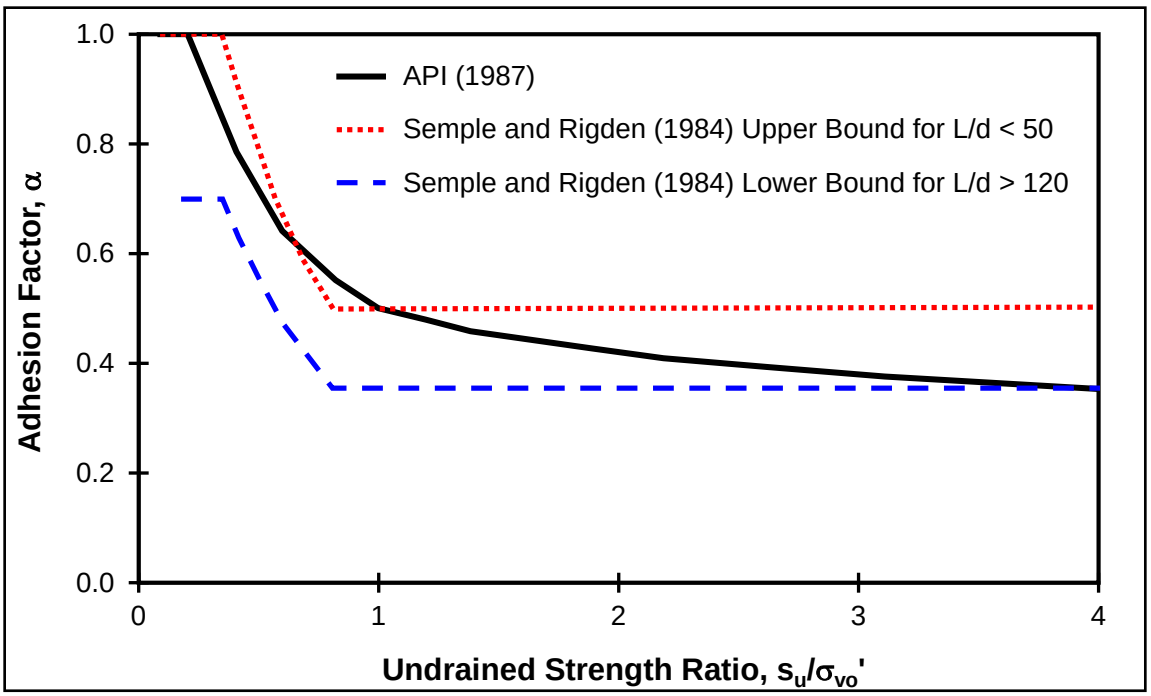

Figure 3.4. Variation of alpha with undrained strength ratio (after Semple and Rigden, 1984).

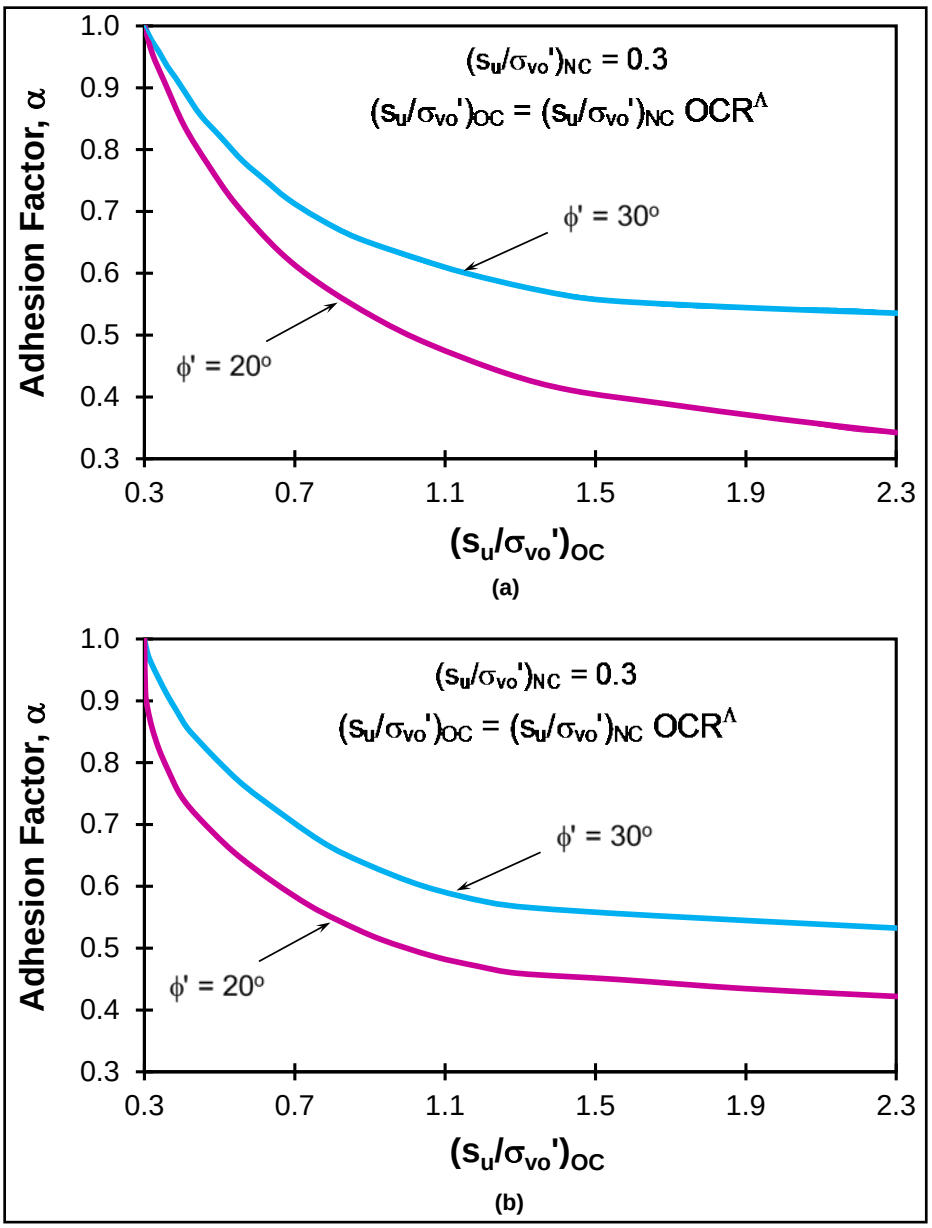

Figure 3.5. α-factor for: (a) bored and CFA piles; (b) screw piles (adapted from Randolph and Murphy, 1985).

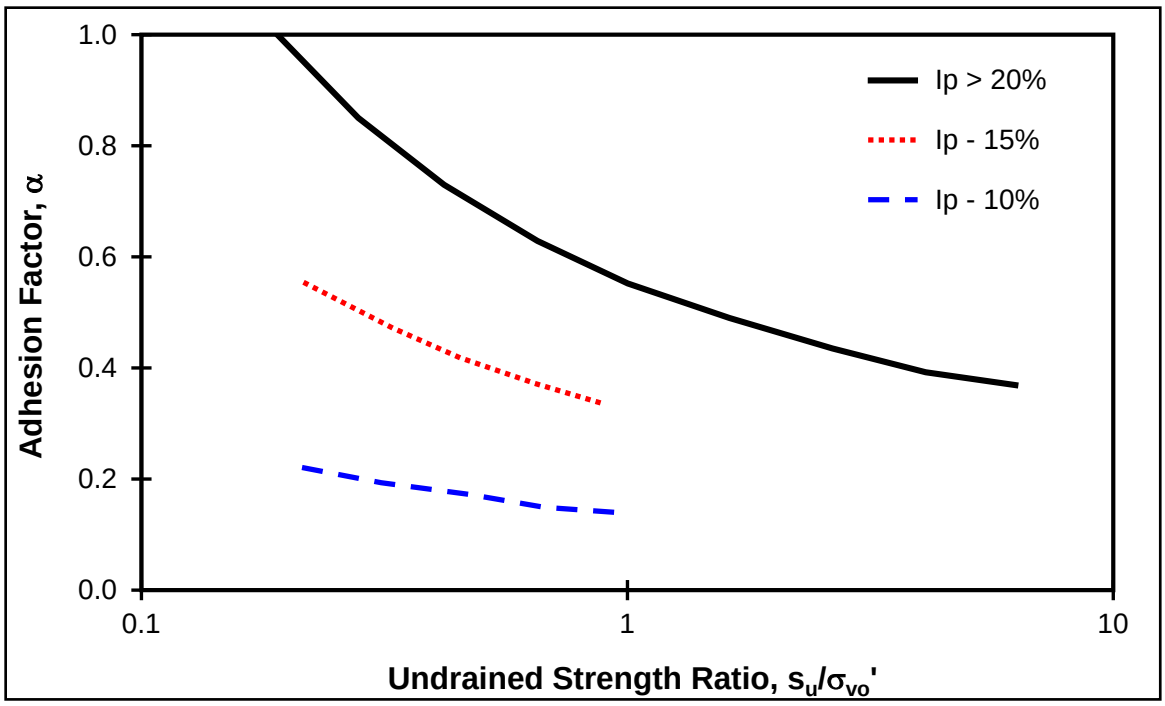

Figure 3.6. Correlation for alpha parameter with undrained strength ratio for low plasticity clays (adapted from Karlsrud et al., 1993).

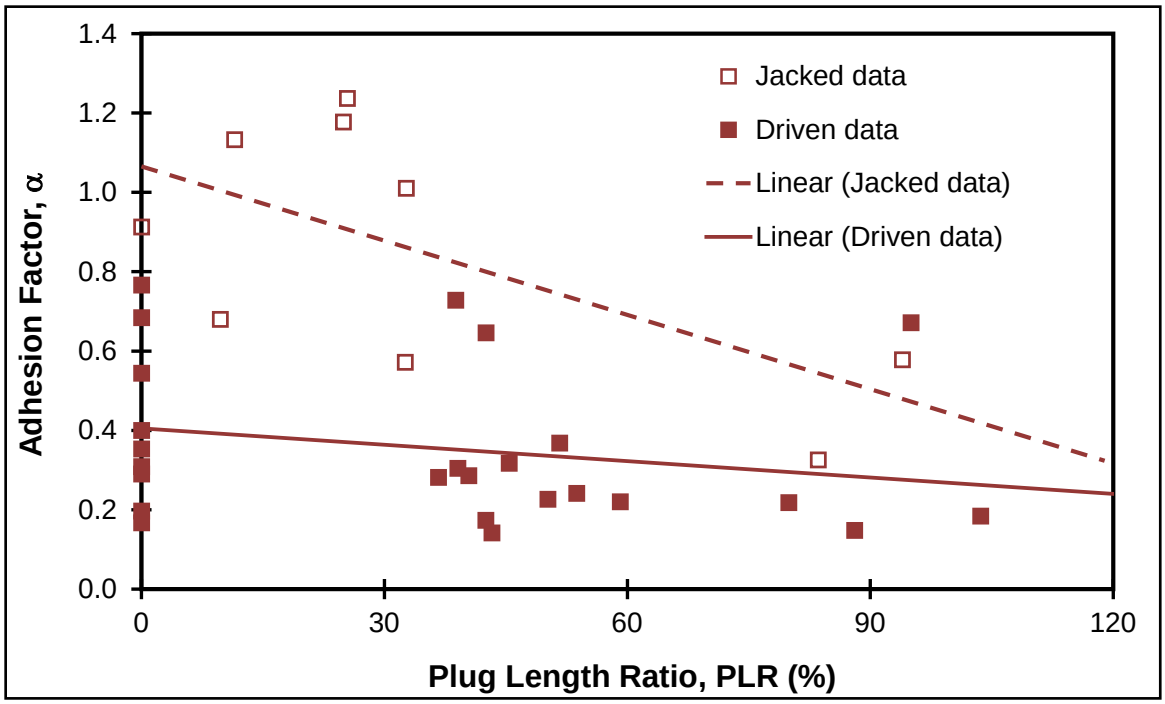

Figure 3.7. Relationship between adhesion factor, a, and the plug length ratio (PLR) (adapted from Miller and Lutenegger, 1997).

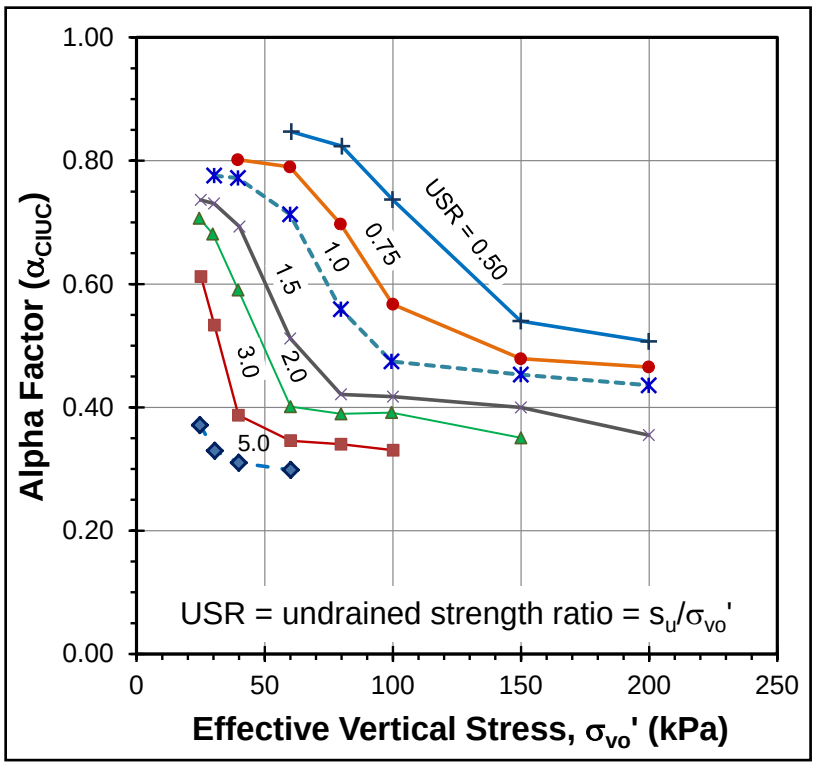

Figure 3.8. Correlation of aCIUC with svo' and USR (Goh et al., 2005).

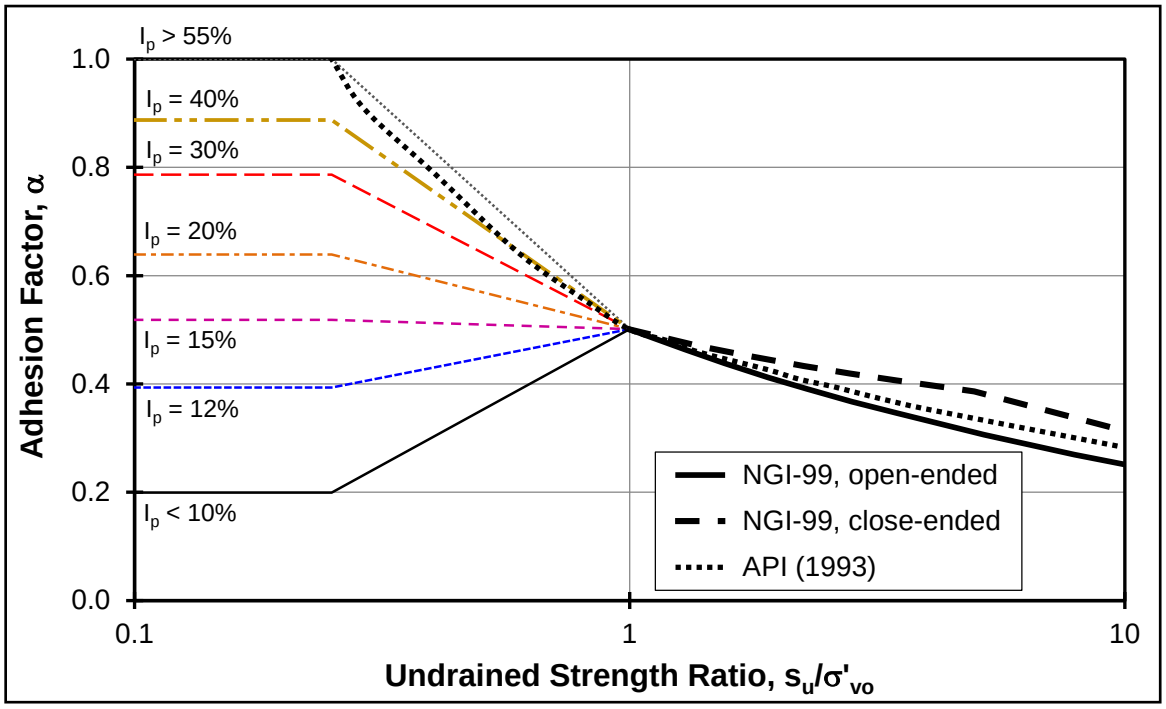

Figure 3.9. Proposed chart for determination of α-value (after Karlsrud et al., 2005).

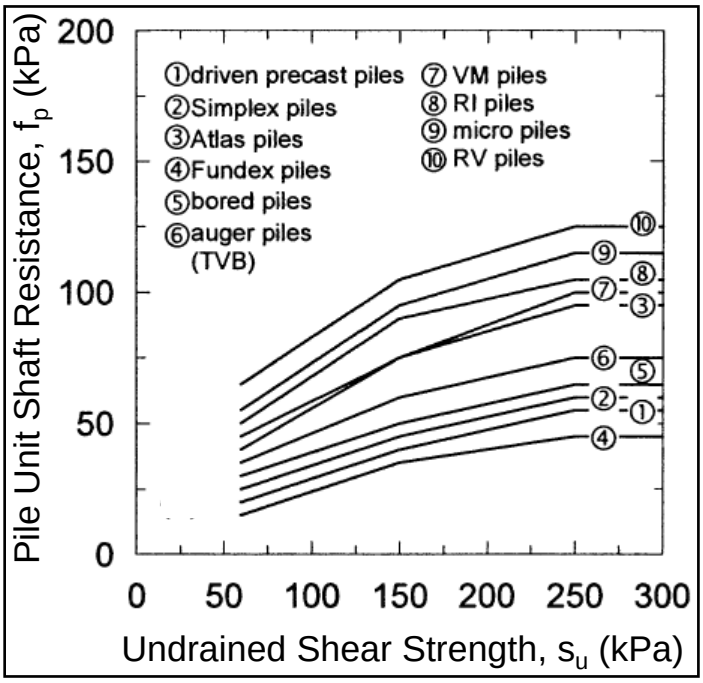

Figure 3.10. Lower empirical values of skin friction for different pile types in clays (after Kempfert and Becker, 2010).

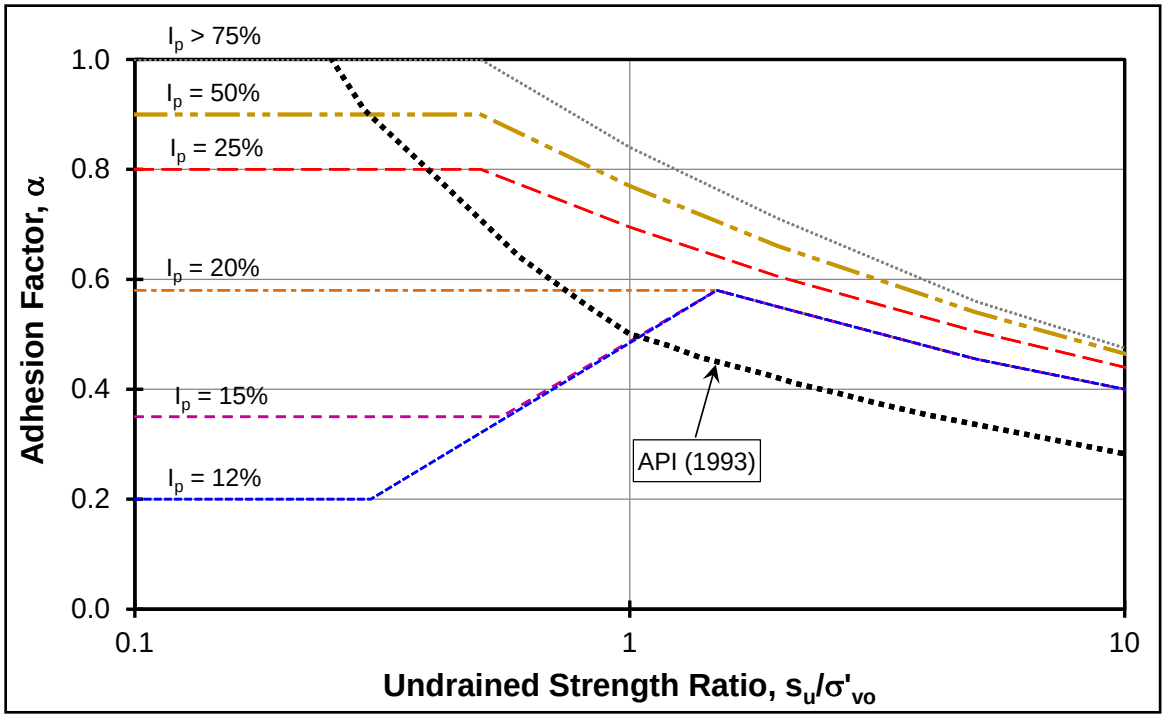

Figure 3.11. Proposed chart for determination of α-value (after Karlsrud, 2012).

The inherent drawbacks in total stress design methods cannot be fully addressed. Some of these shortcomings, identified by Doherty and Gavin (2011), are summarized below:

- The complex stress–strain changes during pile installation and axial loading are influenced by effective soil stresses that cannot be fully described solely by the undrained shear strength of the soil.
- The location of the failure surface on which the shear resistance develops during pile loading depend on the interface roughness, and thus the interface friction angle (δ) plays a role in the shear resistance at the interface.
- The effects of pile length and stress history considered in some of these methods are applicable only to the types of piles and soils considered in the respective databases. Extension to the situations outside of the database results in poor predictions of pile capacity and makes for questionable estimates.

3.2.2 Effective Stress Approach (β-Method)

The effective stress approach is termed the β-method which starts from the fact that the two dominant variables affecting the shaft capacity are the effective horizontal stress (σ_{ho}') and frictional characteristics (ϕ') at the soil-pile interface:

$$f_p \approx \sigma_{ho}' \cdot \tan\phi' \tag{3.1}$$

$$\text{Since } \sigma_{ho}' = K_o \cdot \sigma_{vo}' \tag{3.2}$$

$$f_p \approx K_o \cdot \sigma_{vo}' \cdot \tan\phi' = \beta \cdot \sigma_{vo}' \tag{3.3}$$

This method in its original formulation applies to sands. However, a number of researchers and practitioners have also realized that very little porewater pressures

develop along the sides of the pile during axial loading; therefore, it also applies to all soil types (clays, silts, sands, gravels). It is thought that the pile interface acts as a drain during axial loading, thus $\Delta u \approx 0$. Since the inception of this method by Burland (1973), many researchers have made attempts to study different factor affecting the predictive performance of this method. Michael W. O'Neill in his thirty-fourth Terzaghi lecture, delivered in 1998 provided a concise update of the earlier references of deep foundations by presenting important pre-1998 research on selected aspects of the topic of shaft resistance (Smith, 2001). A summary list of such factors thus studied is presented in Table 3.4, while their respective proposed design equations are given in Table 3.5.

Table 3.4. Factors considered by the effective stress approach (β-method) for estimating pile unit shaft resistance (f_p).

Method/Reference	σ_r'	δ	ϕ'	**OCR**	**K**	σ_{vo}'	**L**	**d**	s_u	D_r	S_t	I_p
Chandler (1968); Burland (1973); Pelletier and Doyle (1982)	✓	✓	✓	x	✓	✓	x	x	x	x	x	x
Meyerhof (1976)	x	✓	✓	✓	x	✓	x	x	x	x	x	x
Flaate and Selnes (1977)	x	x	x	✓	x	✓	✓	x	x	x	x	x
Coyle and Castello (1981)	x	x	✓	✓	x	x	✓	✓	x	x	x	x
Kulhawy et al. (1983)	✓	✓	✓	x	✓	✓	x	x	x	x	x	x
Twine (1987); Patel (1989)	x	x	x	x	x	✓	x	x	x	x	x	x
Reese and O'Neill (1988)	x	x	x	x	x	✓	✓	x	x	x	x	x
Fleming et al. (1992)	✓	✓	x	x	✓	✓	x	x	x	x	x	x
Burland (1993)	x	x	x	✓	x	✓	x	x	✓	x	x	x
de Nicola and Randolph (1999)	x	x	x	x	x	✓	x	x	x	✓	x	x
Patrizi and Burland (2001)	x	x	x	✓	x	✓	x	x	✓	x	x	x
ICP-05 Method (Jardine et al., 2005)	✓	✓	x	✓	✓	x	✓	✓	✓	x	✓	✓
Karlsrud (2012)	x	x	x	✓	x	✓	x	x	x	x	x	✓

Notes: σ_r' = radial effective stress; δ = soil-pile interface friction angle; ϕ' = effective friction angle; OCR ($=\sigma_p'/\sigma_{vo}'$) is the overconsolidation ratio; K ($=\sigma_r'/\sigma_v'$) radial effective stress coefficient; σ_{vo}' = effective vertical stress; L = pile length; d = pile diameter; s_u = undrained shear strength of clay; D_r = relative density of sand; S_t = clay sensitivity; I_p = plasticity index.

Table 3.5. Design equations for pile unit shaft resistance (f_p) from effective stress approach (β-method).

Method/Reference	Pile/Soil Type	Design Equations
Chandler (1968); Burland (1973); Pelletier and Doyle (1982)	Bored and driven pipe piles in NC clays	$f_p=\beta\cdot\sigma_{vo}'=\sigma_{rf}'\cdot\tan\delta_f'=K_f\cdot\tan\delta_f'\cdot\sigma_{vo}'$ Assuming radial effective stress coefficient at failure equal to the at-rest radial effective stress coefficient, the design equation reduces to: $f_p=\beta\cdot\sigma_{vo}'=K_o\cdot\tan\delta_f'\cdot\sigma_{vo}'=(1-\sin\phi_{cv}')\cdot\tan\delta_f'\cdot\sigma_{vo}'$
Meyerhof (1976)	Driven piles in OC clays	$f_p=\beta\cdot\sigma_{vo}'=[(1.5\pm0.5)(1-\sin\phi_{cv}')\cdot\tan\delta_f'\cdot OCR^{0.5}]\cdot\sigma_{vo}'$
Flaate and Selnes (1977)	Driven piles in OC clays	$f_p=\beta\cdot\sigma_{vo}'=\{(0.4\pm0.1)[(L+20)/(2L+20)\cdot OCR^{0.5}]\}\cdot\sigma_{vo}'$ Also see Figure 3.12 for β vs. OCR relationship
Coyle and Castello (1981)	Driven piles in sands	$f_p=\beta\cdot\sigma_{vo}'=K\cdot\tan\delta\cdot\sigma_{vo}'$ See Figure 3.13 for Ktanδ = fctn[relative depth (D/d), ϕ']
Kulhawy et al. (1983)	All	$f_p=\beta\cdot\sigma_{vo}'=C_M\cdot C_K\cdot K_o\cdot\sigma_{vo}'\cdot\tan\phi'$ C_M=1.0 (rough concrete); 0.9 (smooth concrete); 0.8 (timber); 0.7 (rough steel); 0.6 (smooth steel); 0.5 (stainless steel) C_K=0.6 (jetted pile); 0.9 (drilled/bored); 1.0 (driven HP or pipe); 1.1 (driven CE or precast)
Reese and O'Neill (1988)	Bored piles in sandy soils	$f_p=\beta\cdot\sigma_{vo}'$ < 2.0 tsf, for $0.25\leq\beta\leq1.2$ where $\beta=1.5-0.135z^{0.5}$, z in ft

Notes: σ_{rf}' = radial effective stress at failure; δ_f' = soil-pile interface friction angle; K_f ($=\sigma_{rf}'/\sigma_{vo}'$) is the radial effective stress coefficient at failure; K_o ($=\sigma_{ro}'/\sigma_{vo}'$) is the at-rest radial effective stress coefficient; ϕ_{cv}' = constant volume friction angle; L = pile length; OCR = overconsolidation ratio; C_M ($=\tan\delta_f'/\tan\phi'$) and C_K ($=K/K_o$) are modifiers for soil-pile interaction and installation effects, respectively; $K=\sigma_h'/\sigma_v'$ (acting lateral stress coefficient); z = depth below the ground surface.

Table 3.5. (continued).

Method/Reference	Pile/Soil Type	Design Equations
Twine (1987); Patel (1989)	Bored piles in OC clays	$f_p=\beta\cdot\sigma_{vo}'=0.6\cdot\sigma_{vo}'$
Fleming et al. (1992); Jamiolkowski (2003)	Bored and CFA piles in clays	$f_p=\beta\cdot\sigma_{vo}'=\sigma_{rf}'\cdot\tan\delta_f'=[0.5(1+K_o)\cdot\sigma_{vo}']\cdot\tan\delta_f'$ where $\tan\delta_f'=C_M\cdot\tan\phi'$; C_M=1.0 (rough surface), 0.9 (smooth surface)
Burland (1993); Jamiolkowski (2003)	Driven and screw piles in medium to high plasticity clays	$f_p=\beta\cdot\sigma_{vo}'=[0.1+0.4\ (s_u/\sigma_{vo}')_{OC}]\cdot\sigma_{vo}'$ assuming $(s_u/\sigma_{vo}')_{NC}=0.3$ where $(s_u/\sigma_{vo}')_{OC}=(s_u/\sigma_{vo}')_{NC}\cdot OCR^{\Lambda}$ usual range of β=0.2 (NC to lightly OC clay: $s_u/\sigma_{vo}'\leq0.4$), 0.5 (heavily OC clay: $s_u/\sigma_{vo}'\geq1.0$)
UWA-99 (de Nicola and Randolph, 1999)	Driven pipe piles in medium to very dense homogeneous sand	$f_p=\beta\cdot\sigma_{vo}'$ β=fctn[D_r (%)] (see Figure 3.14)
Patrizi and Burland (2001)	Driven piles in medium to high plasticity intact clays	$f_p=\beta\cdot\sigma_{vo}'$ NC clays: $f_p=0.25\cdot\sigma_{vo}'$ OC clays: $f_p=[0.1+0.4\ (s_u/\sigma_{vo}')_{OC}]\cdot\sigma_{vo}'$

Notes: σ_{rf}' = radial effective stress at failure; δ_f' = soil-pile interface friction angle; K_o ($=\sigma_{ho}'/\sigma_{vo}'$) = at-rest lateral effective stress coefficient; C_M = $\tan\delta_f'/\tan\phi'$ is the modifier term used for soil-pile interaction effects; NC = normally consolidated; OC = overconsolidated; OCR = overconsolidation ratio; D_r = relative density; s_u = undrained shear strength of clay.

Table 3.5. (continued).

Method/Reference	Pile/Soil Type	Design Equations
ICP-05 Method (Jardine et al., 2005) (for driven piles in clays) (Jamiolkowski, 2003) (for screw displacement piles in clays)	Driven OE and CE pipe and screw displacement piles in clays	$f_p=\sigma_{rf}'\tan\delta_f'=(K_f/K_c)\sigma_{rc}'\tan\delta_f'$ $K_f/K_c=0.8$; $K_c=[2.2+0.016\ OCR–0.87\Delta I_p]OCR^{0.42}(h/r^*)^{-0.2}$ or: $K_c=[2–0.625\Delta I_{vo}]OCR^{0.42}(h/r^*)^{-0.2}$; $h/r^*\geq 8$ (see Figure 3.15 for terms used in K_c) $\Delta I_p=\log_{10}S_t$; where $S_t=s_{uo}/s_{ur}$ determined from field vane test or laboratory strength test; alternatively s_{ur} (in kPa)$=1.7[10^{2(1–LI)}]$; $LI=(w–PL)/I_p$ δ_f' between δ_{peak}' and $\delta_{ultimate}'$ measured in ring shear tests (alternatively estimate from Figure 3.16 based on PI) $r^* = (r^2–r_i^2)^{0.5}$
Karlsrud (2012)	Driven piles	$f_p=\beta\cdot\sigma_{vo}'$ where β=fctn(OCR and I_p) (see Figure 3.17)

Notes: σ_{rf}' = radial effective stresses at failure; δ_f' = soil-pile interface friction angle; K_f/K_c = loading factor; K_f ($=\sigma_{rf}'/\sigma_{vo}'$) and K_c ($=\sigma_{rc}'/\sigma_{vo}'$) are radial effective stress coefficients at failure and after equalization, respectively; OCR ($=\sigma_p'/\sigma_{vo}'$) is the overconsolidation ratio (also called yield stress ratio, YSR); h = height above pile tip; r* = equivalent pile radius; r_i = pile inner radius; ΔI_p and ΔI_{vo} are oedometer test sensitivity parameters defined in terms of compression curves of undisturbed intact samples and reconstituted samples undergoing virgin compression, respectively (see Figure 3.15); S_t = clay sensitivity; s_{uo} and s_{ur} are the clay's peak intact and its remoulded undrained shear strengths; LI = liquidity index; w = water content; PL = plastic limit; I_p = plasticity index.

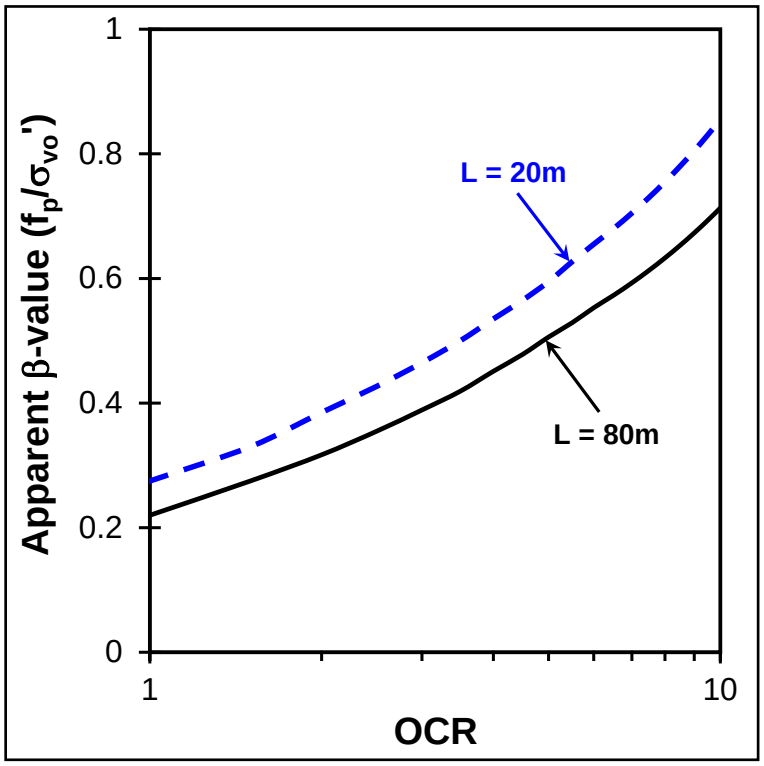

Figure 3.12. Values of β vs. OCR (after Flaate and Selnes, 1977).

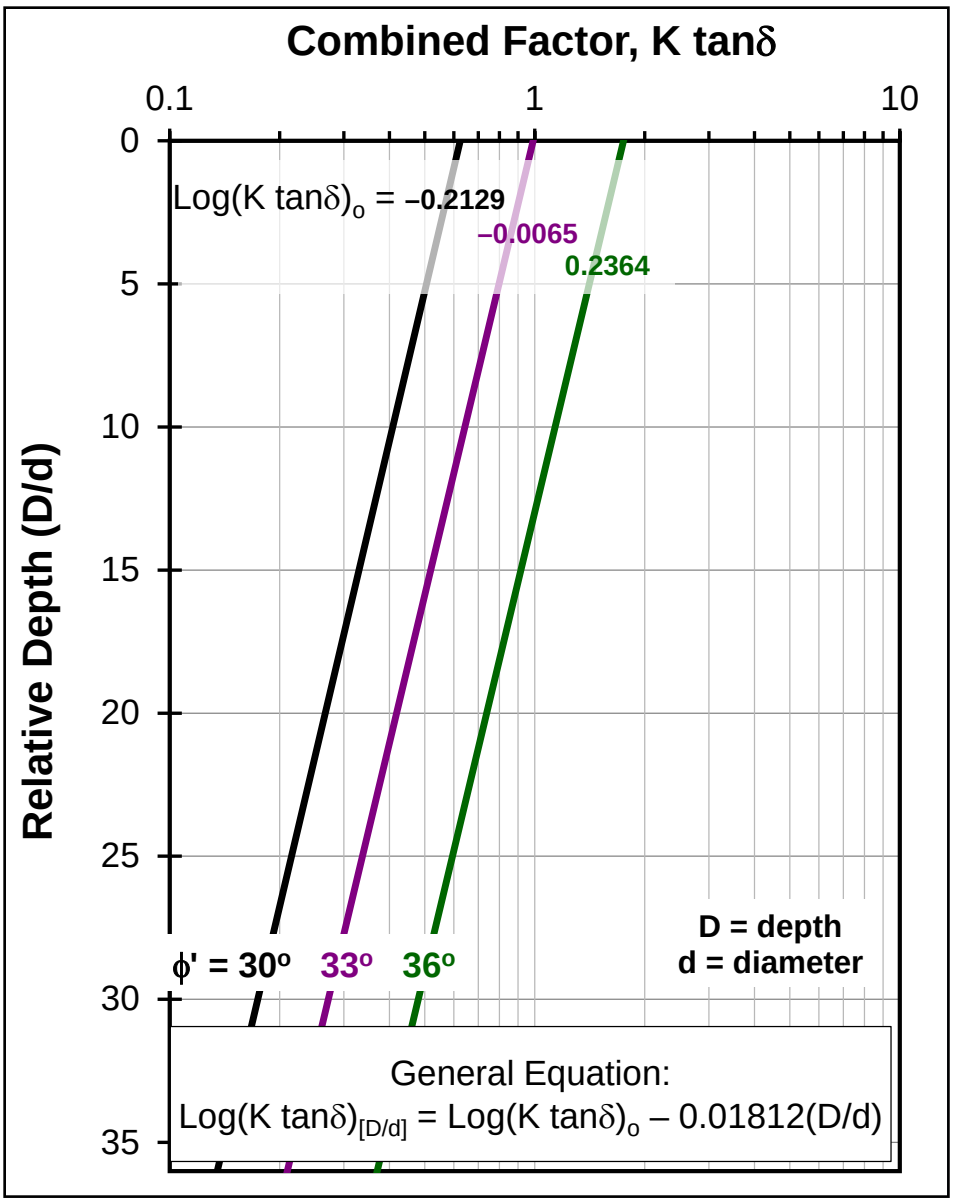

Figure 3.13. Combined factor K tand vs. relative depth (D/d) (after Coyle and Costello, 1981).

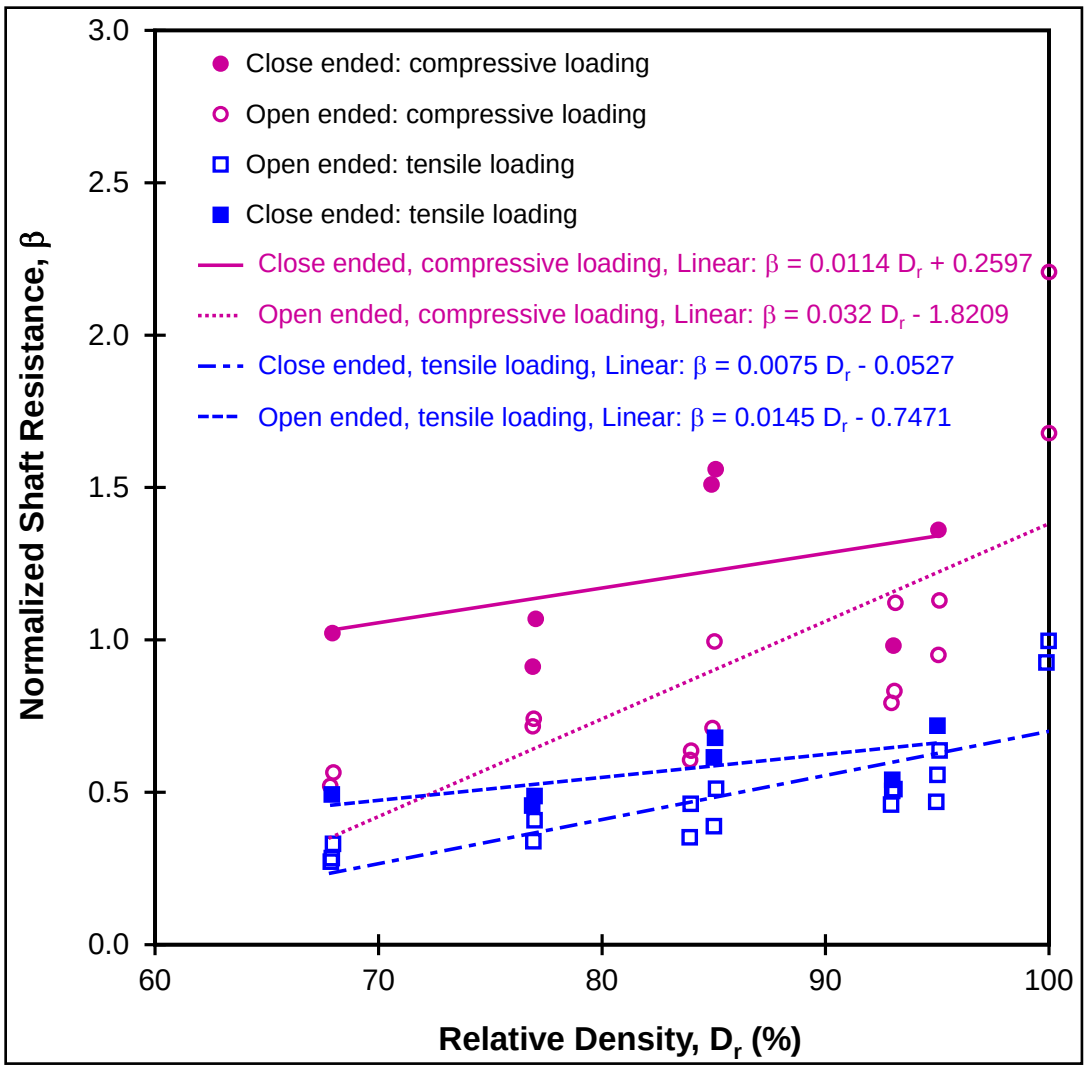

Figure 3.14. Normalized shaft resistance (f_p/σ_{vo}' at 0.05d) for compressive and tensile loading on driven pipe piles in medium to very dense homogeneous sand (adapted from de Nicola and Randolph, 1999).

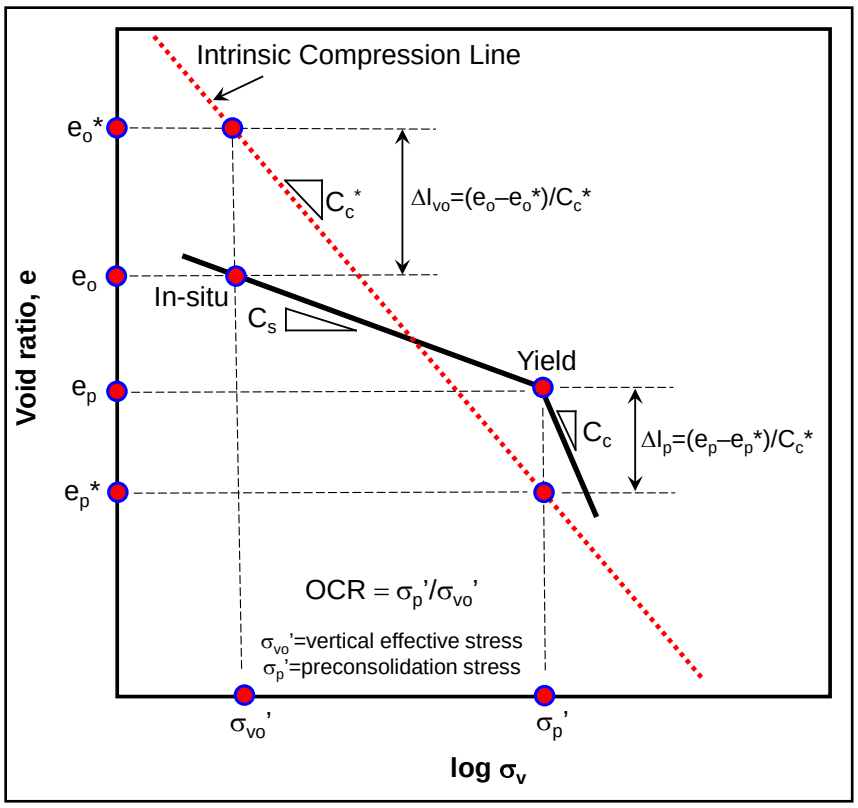

Figure 3.15. Definitions of intrinsic properties of clay relating to oedometer behavior (adapted from Jardine et al., 2005).

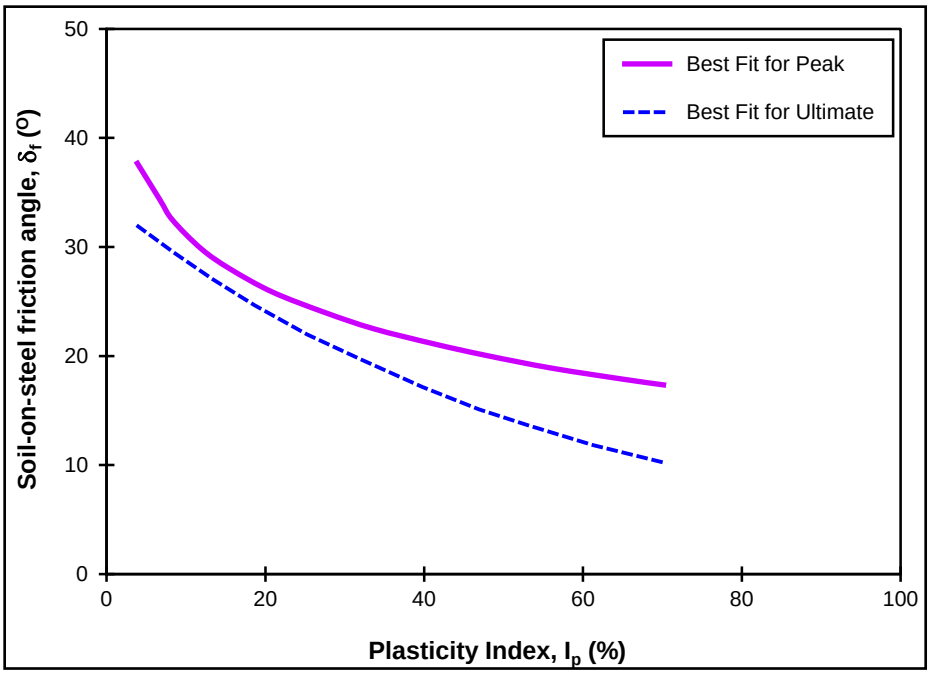

Figure 3.16. Best fit lines for peak and ultimate interface friction angles in clays from the results of ring shear tests as related to I_p (adapted from Jardine et al., 2005).

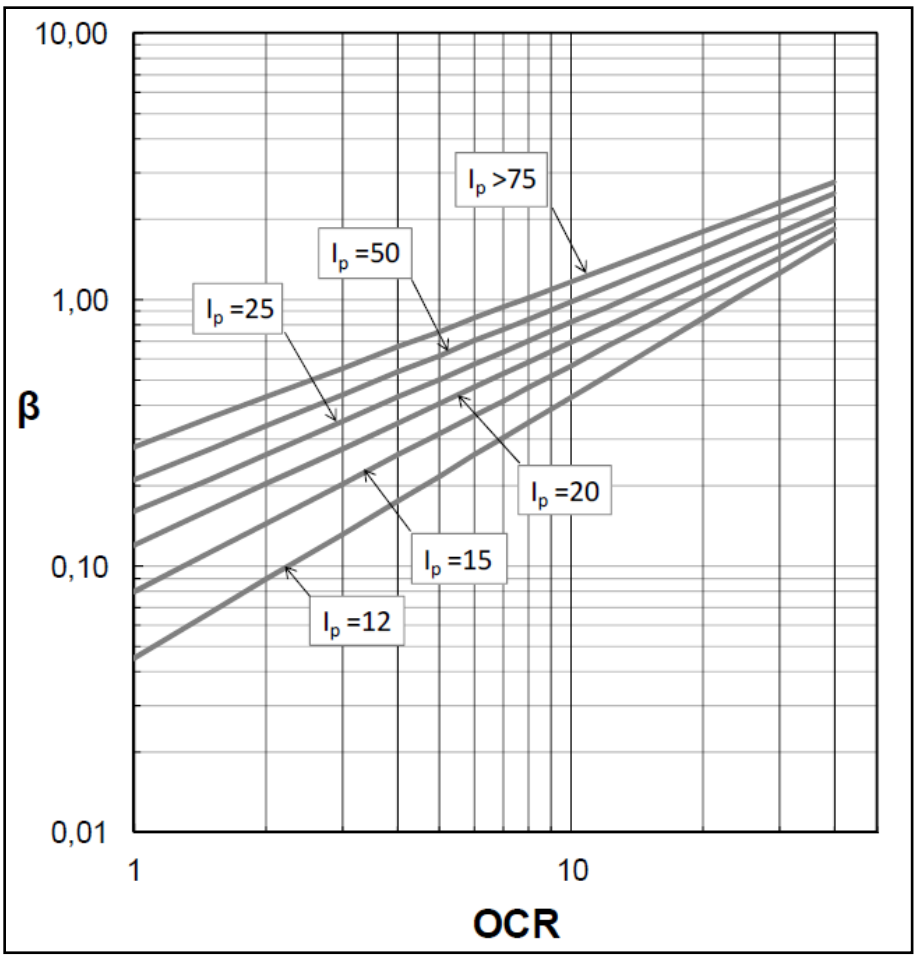

Figure 3.17. Proposed chart for determination of β-values (after Karlsrud, 2012).

3.2.3 CPT Based Rational (Indirect) End Bearing Capacity Methods

For a vertically-loaded pile foundation, the maximum force its base can take without failure is referred to as the end bearing capacity which is associated with mobilization of the shear strength of the underlying soil along a prescribed failure surface. An important factor of relevance to end bearing resistance is the likely strain compatibility differences occurring between the unmatched mobilization of side resistance and end bearing components during pile loading.

For undrained loading (primarily in clays and cohesive silts) beneath the base of a pile foundation, the base resistance can fully mobilize within tolerable limits of vertical displacements, i.e. $w_b/d = 0.05$, where w_b = settlement of the pile base and d = base diameter. In the case of drained loading (primarily sands and granular materials), however, it is impractical to assume that full mobilization of the end bearing resistance occurs for the range of tolerable settlements. Consequently, to achieve a settlement ratio corresponding to $w_b/d = 0.05$, it has been recommended to use an operational value of q_{ult} that is reduced from the theoretical value [$q_{ult(theory)}$] (e.g., Reese and O'Neill, 1988; Chen and Kulhawy, 1994; Van Impe, 1994; Ghionna et al., 1994). Based on the results from calibration chamber tests, Ghionna et al. (1994) recommended a value of $q_{ult} = 0.1q_{ult(theory)}$ for $w_b/d = 0.05$ to account for the strain incompatibility differences. It is, however, noted that most of the European methods recommend use of $w_t/d = 0.10$, instead of $w_b/d = 0.05$. This will be covered in the later sections of this chapter.

As such, the end bearing capacity of foundations is derived from different bearing capacity theories. These include the use of upper and lower bound plasticity theorems, limit equilibrium, cavity expansion, and other theoretical frameworks. Depending upon the specific assumptions made regarding the soil stress-strain characteristics, drainage, rate of loading, boundary conditions, initial stress state, homogeneity, uniformity, or layering, a number of different solutions have been published in the geotechnical

literature. The general shear solution used most commonly in conventional practice is based on limit plasticity theory and assumes the following:

- Plastic equilibrium
- Plain strain conditions
- Active Rankine, radial shear (Prandtl), and passive Rankine zones
- Soil above the foundation is surcharge

The form of the bearing capacity equation has three components, namely cohesion, friction and surcharge (or overburden):

$$q_{ult} = c\, N_c^* + \tfrac{1}{2}\, B\, \gamma\, N_\gamma^* + \sigma_{vo}'\, N_q^* \qquad (3.4)$$

where c is either c' = effective cohesion intercept for drained effective stress behavior, or $c = c_u = s_u$ = undrained shear strength for constant volume case, σ_{vo}' = effective overburden stress, B = foundation width (or d = diameter), γ is soil unit weight (either effective unit weight or total unit weight of the soil depending upon groundwater conditions), and the N terms are bearing factor terms that are functions of the foundation shape and effective stress friction angle (ϕ') of the soil. Specifically, these correspond to the respective bearing capacity factors for cohesion (N_c^*), friction (N_γ^*), and overburden (N_q^*). In sands as well as slow loading (or long-term analysis) in clays and silts ($\Delta u \approx 0$), usually drained conditions are assumed (use bearing capacity term for overburden, N_q^* corresponding to effective stress analysis). In clays, silts, and soils with low permeability (assuming $\phi' = 0$ for fast loading), usually undrained conditions are evaluated (use bearing capacity term for cohesion, N_c^* corresponding to total stress analysis). For practical pile situations, the limit plasticity solutions for drained and undrained conditions reduce to the equations shown in Table 3.6.

Coyle and Castello (1981) presented a comparison of N_q values as a function of ϕ' obtained from field test data and theories, covering a wide range of possible values and curves of well known theories (see Figure 3.18). An alternative solution for piles in sand, based on elasto-plasticity and strength dilatancy theory,was presented by Berezantzev (1970) and Bolton (1986) (see Table 3.6) accounting for pile slenderness ratio (L/d), relative dilatancy (I_D), relative density (D_r), particle strength and frictional characteristics.

These end-bearing capacity methods become relevant to cone penetration testing since various goe-parameters used in their formulations can be estimated from CPT readings via correlations, such as those listed in Table 3.1.

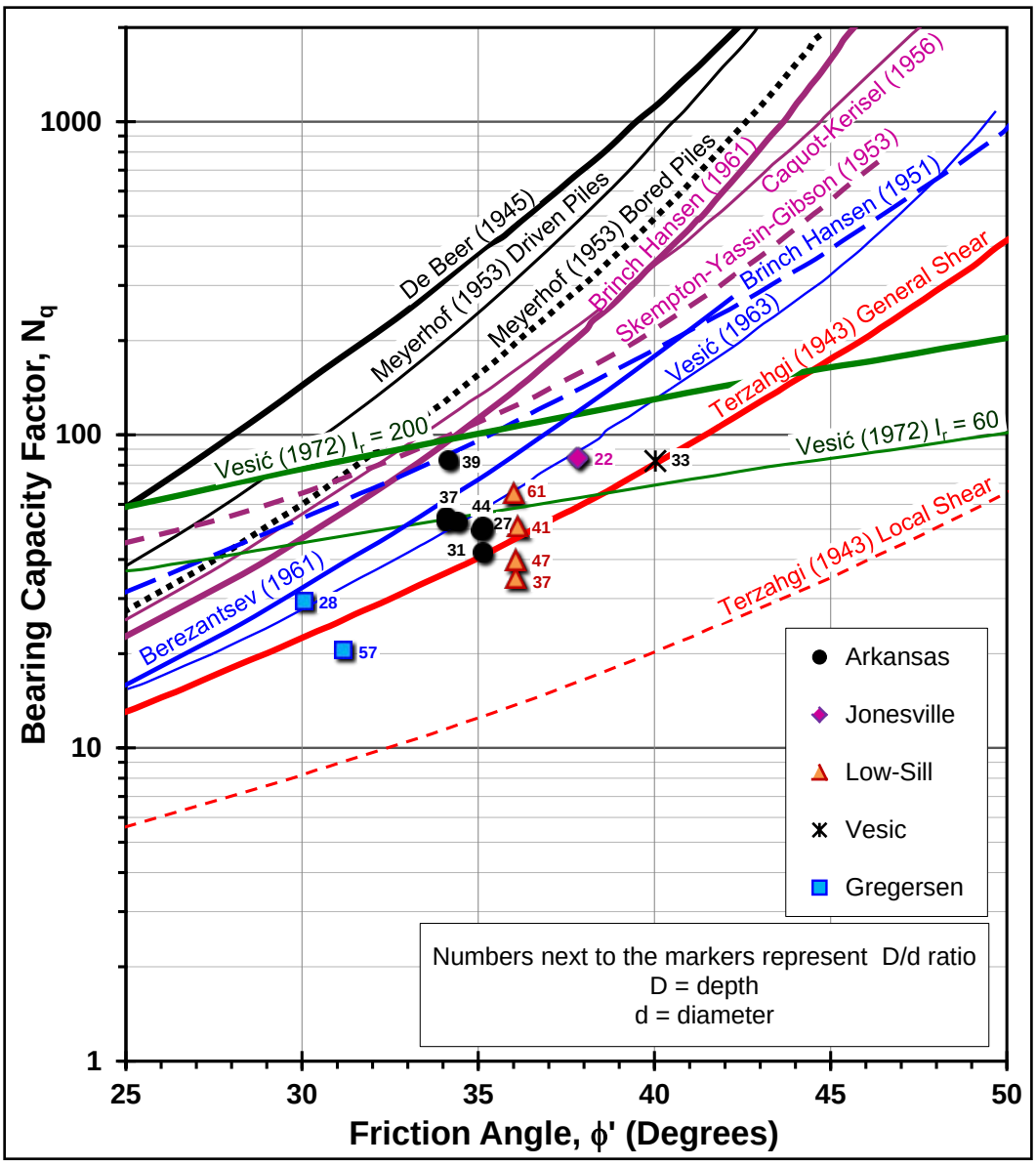

Figure 3.18. Bearing factor N_q vs. ϕ' (Coyle and Costello, 1981).

Table 3.6. Design equations for pile unit end bearing (q_b) from bearing capacity theories.

Method/Theory	**Pile/Soil type**	**Design Equations**
Limit plasticity (Lee et al., 2003; Vesić, 1977)	All pile types in all soil types	Drained: $q_{b,0.1} = 0.1 \cdot N_q^* \cdot \sigma_{vo}'$; Undrained: $q_b = N_c^* \cdot s_u$
Elasto-plasticity and strength dilatancy (Berezantzev, 1970; Bolton, 1986)	Circular and square bored and CFA piles in clean un-cemented siliceous sand deposits	$q_{b(crit)} = N_{\gamma q} \cdot d \cdot \gamma'$ $N_{\gamma q}$ = fctn(ϕ_p' and L/d) (see Figure 3.19); $\phi_p' = \phi_{cv}' + 5 \cdot I_D$ $I_D = D_r \cdot (Q - \ln\sigma_{mf}') - R$ Q = 10 (Quartz and Feldspar); 8 (Limestone); 7 (Anthracite); 5.5 (Chalk) ϕ_{cv}' = 31.6 to 33.5(Quartz); 34.5 (Siliceous); 40.5 (Calcareous) $\sigma_{mf}' = (N_q^*)^{0.5} \cdot \sigma_{vo}'$
NGI-05 (Karlsrud et al., 2005)	for CE or plugged driven piles in clays	Undrained: $q_b = 9 \cdot s_u$ For piles subjected to long-term tensile loads, a crack could form at the base, before the clay strength is fully mobilized in reversed end-bearing

Notes: $N_q^* = [1 + (B/A)\cdot\tan\phi'] \cdot [1 + 2\tan\phi' \cdot (1 - \sin\phi')^2 \cdot \tan^{-1}(L/B)] \cdot e^{\pi\tan\phi'} \cdot \tan^2(45° + \phi'/2)$; $N_c^* \approx 9.33$ for square and circular piles; A and B are side dimensions of rectangular piles; B/A = 1 for circular piles; L = pile length. Operational drained q_b at working load is reduced for tolerable displacements. σ_{vo}' and s_u are the average values from depth z = L to depth z = L + d, where d = pile diameter; $q_{b(crit)}$ = critical unit end bearing at a relative displacement of $w/d \approx 0.2$; $N_{\gamma q}$ = bearing capacity factor; ϕ_p' = peak angle of shearing resistance in the vicinity of pile tip; L = pile embedded length; γ' = average effective bulk density of the soil at the elevation of pile tip; ϕ_{cv}' = constant volume angle of friction at critical state; I_D = relative dilatancy index; D_r = relative density; Q = particle strength parameter corresponding to the natural logarithm of σ_{mf}' (in kPa) at which dilation of the soil is inhibited; σ_{mf}' = mean effective stress at failure.

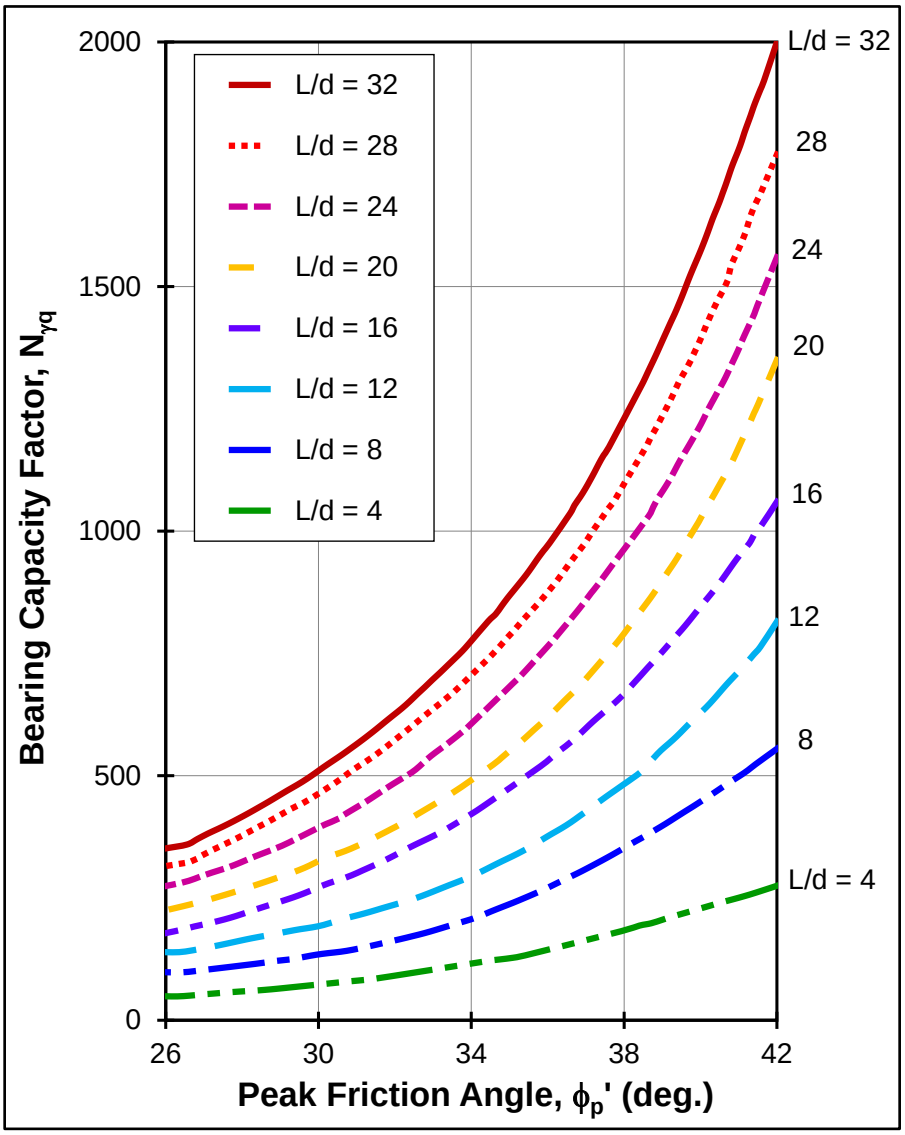

Figure 3.19. Bearing capacity factors for critical base resistance of bored pile and CFA piles (adapted from Berezantzev, 1970).

3.3 Direct CPT-based Methods

In contrast to the rational methods, the direct CPT methods use the measured penetrometer readings by scaling relationships or algorithms in a one-step process to obtain f_p and q_b for evaluation of full-size pilings. In one viewpoint, the cone penetrometer can be considered as a mini-pile foundation, whereby the measured tip stress and sleeve resistance correspond to the pile end bearing and component of side friction (Mayne, 2007). As noted by Ardalan et al. (2009) and Eslami and Fellenius (1997), the mean effective stress, compressibility and rigidity of the surrounding soil medium affect the pile and the cone in a similar manner; thus, eliminating the need to supplement the field data with laboratory testing and to calculate intermediate values for use in the CPT methods for pile capacity evaluations. This concept has led to the development of many direct CPT methods, whereby the measured readings are simply scaled up empirically for the evaluation of full-scale piling. The initial formulations of such methods was based solely on the measured tip resistance (q_c) derived from mechanical cone penetrometers. Subsequently, with the introduction of the electrical cone penetrometer, the additional channels measuring sleeve friction (f_s) and porewater pressure (u_1 and u_2), the correction of porewater pressures to the measured tip resistance to yield corrected tip resistance (q_t), and continuously increasing database of CPT and pile load tests has resulted in a variety of direct CPT based pile evaluations. Some of these methods provide design equations for either f_p or q_b, while others account for both the components.

In addition to the purely empirical CPT-based direct methods, f_p and q_b can also be estimated using the applicable semi-empirical direct methods which require measurements or estimation of additional parameters along with the penetrometer readings of CPT. Within the scope of this study, the semi-empirical direct methods have also been grouped with the direct methods.

The design equations and charts of 36 direct CPT methods are presented in Table 3.7, particularly noting newly available approaches that have recently been developed.

Chen and Zhang (2013) adopted a probabilistic approach for predicting the impact of spatial correlation between q_c values of different soil layers on the bearing capacity of driven piles in clay. They considered the spatial correlations via the correlation coefficients $[\rho_{(b)(i)}]$ and $[\rho_{(i)(j)}]$ between q_{cbV} (the spatial average of q_c over an interval near the pile base) and q_{csVi} (the spatial average of q_c of the i^{th} soil layer), and between q_{csVi} and q_{csVj} (the spatial average of q_c of the j^{th} soil layer), respectively. Adopting the LCPC method and conducting parametric studies they indicated the importance of such spatial correlations in the probabilistic prediction of the bearing capacity. The proposed approach was calibrated against 14 pile load tests. At present, the procedure for implementation of this approach is considered to be fairly intricate for simple frequent application by the practitioners. Therefore, further details have not been included herein.

Table 3.7. Summary of CPT-based direct pile design methods.

Method/Reference	Design Equations	
	Pile unit side resistance (f_p)	Pile unit end bearing (q_b)
Bogdanovic (1961) (for driven and jacked concrete piles in dense sand)	$f_p = f_s \cdot [(\pi \cdot d_{CPT})/(\pi \cdot d)]$	$q_b = q_{ca(tip)}$
Begemann (1963; 1965; 1969) (for driven piles in sandy soils)	f_p = fctn(q_c, f_s and pile type) (Figure 3.20)	$q_b = (q_{c1} + q_{c2})/2$ (also see Figure 3.21) $q_{c1} = [(q_1 + q_2 + q_3 + ... + q_n) + nq_n]/2n$
Meyerhof (1956; 1976; 1983) (for driven and bored piles in sandy soils)	$f_p \approx n_{sf} \cdot f_s$, or f_p(kPa) $\approx 0.5 \cdot n_{sq} \cdot q_c$ (q_c in MPa) n_{sf} = 1 (driven piles), 0.7 (bored piles) n_{sq} = 1 (driven piels); 0.5 (bored piles)	***Driven piles***: *Short piles in sand* ($L < L_c$): $q_b = q_l \cdot L/L_c \leq q_l$ *Long piles driven through weak strata to bearing embedment depth*, z_d (where $L > L_c$): Deep firm sand deposit of great thickness, H ($H/d \geq 20$): $q_b = q_{l1} + (q_{l2} - q_{l1}) \cdot z_d/(10d) \leq q_{l2}$ (also see Figures 3.22 and 3.23) Thin sand bearing layer ($H/d < 20$) overlying a weak deposit: $q_b = q_{l2} + (q_{l1} - q_{l2}) \cdot H'/(10d) \leq q_{l1}$ (also see Figures 3.22 and 3.23) For $d \geq 0.5$m multiply q_b with reduction factor: $R_b = [(d+0.5)/2d]^n \leq 1$ where n = 1 for loose sand, 2 for medium dense sand, and 3 for dense sand ***Bored piles***: Reduce q_b to 30% form above

Notes: n_{sf} and n_{sq} = reduction factors applied to the unit shaft resistance according to the pile type; L and L_c = pile embedment and critical depth, respectively (L_c = 10d – 40d); d = pile diameter; q_l = limiting unit base resistance (= limiting static cone resistance) = average of q_c in a zone ranging from 4d above to 1d below pile base; z_d = embedment depth in dense sand layer (in m); q_{ll} and q_{l2} = limiting unit base resistance in upper/middle and lower soil strata = average of q_c in the respective strata (see Figure 3.22); H' = distance between pile base and the surface of underlying weak deposit (see Figure 3.22).

Table 3.7. (continued).

Method/Reference	Design Equations	
	Pile unit side resistance (f_p)	Pile unit end bearing (q_b)
Aoki and De Alencar (1975) (for piles in all soil types)	$f_p = q_{ca(side)}\ \alpha_s/F_S \leq 120$ kPa α_s depends on soil type: sand = 1.4; silty sand = 2.0; sandy silt = 2.2; silty sand with clay or sandy clay = 2.4; clay-sand-silt mix = 2.8–3.0; clayey silt = 3.4; silty clay = 4.0; clay = 6 F_S depends on pile type: bored=7.0; driven cast-in-situ =5.0; steel and PCC=3.5	$q_b = q_{ca(tip)}/F_b \leq 15$ MPa F_b depends on pile type: bored = 3.5; driven cast-in-situ = 2.5; steel and PCC = 1.75
Nottingham (1975); Schmertmann (1978) (for driven concrete, steel and timber piles in all soil types)	In clay: $f_p = \alpha_c f_s \leq 120$ kPa, α_c = fctn(f_s) = 0.2–1.25 (see Figure 3.24 for different pile types) In sand: $Q_s = \alpha_s[\sum_{y=0}^{8d} \frac{y}{8d} f_s A_s + \sum_{y=8d}^{L} f_s A_s]$ α_s = fctn(z/d) (see Figure 3.25)	$q_b = (q_{c1} + q_{c2})/2 \leq 15$ MPa
Penpile Method (Clisby et al., 1978) (for piles in all soil types)	f_p (in MPa) = $f_s/(1.5 + 14.47 f_s)$ (in MPa)	$q_b = 0.25 q_{ca(tip)}$ for pile tip in clay $q_b = 0.125 q_{ca(tip)}$ for pile tip in sand
Dutch Method (de Ruiter and Beringen, 1979) (for offshore piles in all soil types)	In clay: $f_p = \alpha s_{u(side)} \leq 120$ kPa; α = 1 for NC clay and 0.5 for OC clay; $s_{u(side)} = q_{c(side)}/N_{kt}$ In sand: f_p = min[f_s, $q_{c(side)}/300$ for compression, $q_{c(side)}/400$ for tension, 120 kPa]	In clay: $q_b = N_c s_{u(tip)} \leq 15$ MPa, $s_{u(tip)} = q_{ca(tip)}/N_{kt}$, N_c = 9, N_k = 15–20; $q_{ca(tip)} = (q_{c1}+q_{c2})/2$ In sand: similar to Schmertmann (1978)

Notes: q_{ca} = arithmetic average of q_c in a specified zone that depends on the method; d = pile diameter; A_s = shaft area; z/d = pile embedment depth to diameter ratio; y = depth at which side resistance is calculated; N_{kt} = cone factor range between 15 to 20 depending on local experience; L is the pile length; q_{c1}: minimum of the average q_c values of zones ranging from 0.7d to 4d below the pile tip; q_{c2}: average minimum q_c values 6d to 8d above the pile tip.

Table 3.7. (continued).

Method/Reference	Design Equations	
	Pile unit side resistance (f_p)	Pile unit end bearing (q_b)
Philipponnat (1980) (for all pile types in all soil types)	$f_p = q_{c(side)}\alpha_s / F_S$ α_s = 1.25 (driven PCC piles and drilled shaft with casing); 0.85 [drilled shaft (diameter < 1.5 m]; 0.75 [drilled shaft (diameter > 1.5 m)]; 1.10 [H-piles (circumscribed perimeter)]; 0.6 (driven and jacked steel pipe piles); 0.3 (OE steel pipe pile) F_S = 50 (chalk); 60 (silt, sandy clay and clayey sand); 100 (loose sand); 150 (medium sand); 200 (dense sand and gravel)	$q_b = k_b q_{ca(tip)}$ k_b: depends on soil type = 0.35 for gravel; 0.4 for sand; 0.45 for silt; and 0.5 for clay $q_{ca(tip)} = [q_{ca(A)} + q_{ca(B)}]/2$
LCPC or French Method (Bustamante and Gianeselli, 1982; Bustamante and Frank, 1997; Poulos, 1989) (for all pile types in all soil types)	$f_p = q_{eq(side)}/k_s \leq f_{p(max)}$ k_s = 30–150 depending on soil type, pile type, and installation procedure [also see Figure 3.26 for specific values of k_s and $f_{p(max)}$]	$q_b = k_b q_{eq\ (tip)}$ k_b for non-displacement pile: 0.375 (clay and/or silt), 0.15 (sand and/or gravel), 0.20 (chalk) k_b for displacement pile: 0.60 (clay and/or silt), 0.375 (sand and/or gravel), 0.40 (sand and/or gravel) [see Figure 3.27 for calculating $q_{eq(tip)}$]

Notes: $q_{ca(A)}$ = average cone tip resistance within 3d above the pile tip and $q_{ca(B)}$ = average cone tip resistance within 3d below the pile tip, after removing spikes if $q_{ca(A)} > q_{ca(B)}$; $q_{eq(tip)}$ = equivalent average of q_c values of zone ranging from 1.5d below pile tip to 1.5d above pile tip.

Table 3.7. (continued).

Method/Reference	Design Equations	
	Pile unit side resistance (f_p)	Pile unit end bearing (q_b)
Cone-m Method (Tumay and Fakhroo, 1982) (piles in clays)	$f_p = m\, f_{sa} \leq f_{p(max)}$ ($\leq$ 72 kPa) $m = 0.5 + 9.5e^{(-9fsa)}$	$q_b = (q_{c1} + q_{c2})/4 + q_a/2 \leq 15$ MPa
Price and Wardle (1982) (for jacked, driven and bored piles based on load tests in stiff London clay)	$f_p = k_s\, f_s$ where k_s=0.53 (driven piles), 0.62 (jacked piles), and 0.49 (bored piles)	$q_b = k_b q_{c(tip)}$ k_b = 0.35 (driven piles) and 0.3 (jacked piles)
Gwizdala (1984) (for drilled shafts in cohesionless soils)	$f_p = k_s\, q_{ca(side)}$ Respective values of k_s for q_c values of 2.5, 10 and 20 MPa = gravel: (80, 120, 180); coarse to medium sand: (100, 150, 230); fine sand, silty sand: (130, 190, 300)	$q_b = k_b\, q_{ca(tip)}$ ($d < 5$); $q_b = (5/d)^{0.5}\, k_b\, q_{ca(tip)}$ ($d > 5$) k_b values for q_c of 2.5, 5, 7.5, 10, 15 and 20 MPa = gravel: (0.8, 0.65, 0.54, 0.45, 0.35, 0.3); coarse to medium sand: (0.7, 0.55, 0.45, 0.36, 0.27, 0.23); fine sand, silty sand: (0.6, 0.47, 0.39, 0.31, 0.22, 0.18)
Kulhawy and Phoon (1993); Kulhawy (2004); Lunne et al. (1997) for bored piles in clays	$f_p = 0.5\sigma_{atm}(s_{uCIUC}/\sigma_{atm})^{0.5}$ $f_p = 0.158[q_{t(net)}\cdot\sigma_{atm}]^{0.5}$ using N_{kt} = 10 for CIUC	$q_b = 0.62\cdot q_{t(net)}$; using N_{kt} = 15
UIUC Method (Alsamman, 1995) (for bored piles in sands and clays)	f_p (kPa) = fctn[q_c (MPa)] (see Figure 3.28a for sands and Figure 3.29a for clays)	q_b (MPa) = fctn[q_c (MPa)] (see Figure 3.28b for sands and Figure 3.29b for clays)
NGI-BRE Method (Almeida et al., 1996; Powell et al., 2001; Powell and Quarterman, 1988) (for driven and jacked piles in clays)	$f_p = q_{t(net)}/k_1$ $k_1 = 10.5 + 13.3\log(q_{t(net)}/\sigma_{vo}')$	$q_b = q_{t(net)}/k_2$ $k_2 = N_{kt}/9$; N_{kt} = 15 (soft – firm intact clays), 25 to 35 (fissured to hard clays)

Notes: $f_{sa}=F_t/L$ is the average local friction in tons/ft^2, and F_t is the total cone sleeve friction determined for pile penetration length (L); q_{c1}: average of q_c values of zones 4d below tip; q_{c2}: average of the minimum q_c values 4d below the cone tip; d: pile diameter; q_a: average of the minimum q_c values 8d above the cone tip; $q_{t(net)} = q_t - \sigma_{vo}$; s_{uCIUC} = undrained shear strength from isotropically-consolidated triaxial compression tests.

Table 3.7. (continued).

Method/Reference	Design Equations	
	Pile unit side resistance (f_p)	Pile unit end bearing (q_b)
Politecnico di Torino Method (Fioravante, 1994; Fioravante et al., 1995) (for drilled shafts in clean uncemented NC sands)	f_p (MPa) $\approx [q_t$ (MPa)/274$]^{0.75}$	$q_b \approx q_t/[1.90 + 0.62/(w_b/d)]$ $q_{b,0.1} \approx 0.123q_t$ (for $w_b/d = 0.1$)
Unicone Method (Eslami and Fellenius, 1997; Fellenius, 2002b) (for all pile types in all soil types)	$f_p = C_{se} \cdot q_E$ $q_E = q_t - u_2$ (see Figure 3.30 for C_{se})	$q_b = C_{te} \cdot q_{Eg}$ C_{te} is generally taken as 1; for pile diameter d > 0.4 m, $C_{te} = 1/(3d)$
KTRI Method (Takesue et al., 1998) (for all pile and soil types)	Estimates f_p from measured f_s and Δu_2 (see Figure 3.31)	This method does not indicate a means for evaluating q_b
UWA-99 Method (De Nicola and Randolph, 1999) (for driven pipe piles in medium to very dense homogeneous sand)	This method utilizes effective stress approach (β-method) as a means for evaluating f_p. No direct use of CPT reading is involved. Accordingly, it has been listed in Table 3.5.	CE: $q_{b0.1} = q_c \cdot \lambda \cdot m \cdot (w_b/d)/(w_b/d + c)$ at $w_b/d = 0.1$ where m = 0.7, c = 0.03; $\lambda = 1.75–0.5\sigma_{vo}'/\sigma_{atm}$ (for $\sigma_{vo}' < 200$kPa), $\lambda = 0.75$ (for $\sigma_{vo}' \geq 200$ kPa) (also see Figure 3.32) OE: see Figure 3.32

Notes: C_{se} is the side correlation coefficient based on soil classification chart derived from q_t, f_s and u_2; C_{te} is the toe correlation coefficient; q_{Eg} is the geometric average of q_E values over the influence zone after correction for u_2 and adjustment to σ_{vo}'; influence zone varies from 4d below pile tip to 8d above pile toe if pile is installed from weak soil into dense soil, and from 4d below pile toe to 2d above pile toe when pile is installed from dense soil into weak soil; Δu_2 = excess porewater pressure = $u_2 - u_o$ (measured in kPa); w_b = displacement at the pile base; d = pile diameter.

Table 3.7. (continued).

Method/Reference	Design Equations	
	Pile unit side resistance (f_p)	Pile unit end bearing (q_b)
Lee and Salgado (1999) (for piles in sands)	This method does not indicate a means for evaluating f_p	$q_b \approx q_t/[1.90 + 0.62/(w_b/d)]$ $q_{b,0.1} \approx 0.123q_t$ (for $w_b/d = 0.1$)
TCD-01 Method (Lehane and Gavin, 2001) (for base capacity of OE and CE jacked pipe piles installed in sandy soils where IFR is measured during pile installation)	This method does not indicate a means for evaluating f_p	CE: $q_{ann} \approx q_c$ OE: q_{plug} = fctn(q_c, IFR) and $q_{ann} \approx q_c$ (see Figure 3.33) $Q_b = q_{plug}A_{plug} + q_{ann}A_{ann}$
TCD-03 Method (Gavin and Lehane, 2003; de Nicola and Randolph, 1999) (for OE driven pipe piles installed in sandy soils where the IFR is measured during pile installation)	$f_p = f_L \cdot \sigma_{rc}' \cdot \tan\delta_f'$ $f_L = 0.8$ for piles in tension and 1.0 for piles in compression; $\sigma_{rc}' = 0.029q_b(\sigma_{vo}'/\sigma_{atm})^{0.12} \cdot (h/r^*)^{-0.38}$; where $q_b = (q_{plug}r_i^2 + q_{ann}2rt)/r^2$ For IFR $\leq$ 1: $q_{plug} = q_c(1 - IFR) + IFR \cdot q_{plug,min}$ For IFR > 1: $q_{plug} = q_{plug,min}$ $q_{ann} = q_c$ $q_{plug,min} = 0.1q_c$	$q_{b0.1} = \{\zeta q_c[(1 - 0.9IFR) \cdot r_i^2 + 2rt]\}/r^2$ For $\sigma_{vo}' < 200$ kPa: $\zeta = 1.23 - 0.35\sigma_{vo}'/\sigma_{atm}$ For $\sigma_{vo}' \geq 200$ kPa: $\zeta = 0.53$

Notes: w_b = base displacement; IFR is the incremental filling ratio = $\Delta L_p/\Delta z$; ΔL_p = incremental change of plug length; Δz = change in penetration depth; f_L = reduction factor for loading direction; δ_f' = interface friction angle at failure; σ_{rc}' = radial effective stress following full equalization of pore pressure; q_b = base capacity mobilized during installation; h = height above the pile tip; r* = modified radius term for OE piles = $(r^2 - r_i^2)^{0.5}$; r = external diameter; r_i = internal radius; t = pile wall thickness; q_{plug} = plug unit end bearing resistance; q_{ann} = unit resistance below the base of pile annulus; $q_{plug,min}$ = minimum plug base resistance; A_{plug} and A_{ann} are the pile plug and annulus areas, respectively; $q_{b0.1}$ = static capacity at a base displacement of 10% of the radius; ζ = reduction factor for σ_{vo}'.

Table 3.7. (continued).

Method/Reference	Design Equations	
	Pile unit side resistance (f_p)	Pile unit end bearing (q_b)
Fugro-05 Method (Kolk et al., 2005) (for driven piles in sandy soils mostly for offshore pilings)	Compression loading $h/r^* \geq 4$: $f_p = 0.08q_c(\sigma_{vo}'/\sigma_{atm})^{0.05} \cdot (h/r^*)^{-0.9}$ Compression loading $h/r^* \leq 4$: $f_p = 0.08q_c(\sigma_{vo}'/\sigma_{atm})^{0.05} (4)^{-0.9}(h/4r^*)$ Tension loading: $f_p = 0.045q_c(\sigma_{vo}'/\sigma_{atm})^{0.15} \cdot [\max(h/r^*, 4)^{-0.85}$ $r^* = (r^2 - r_i^2)^{0.5}$ For noncircular piles, equivalent circular area is used to assess r^*	$q_{b0.1} = 8.5q_{c,avg} \cdot (\sigma_{atm}/q_{c,avg})^{0.5}A_r^{0.25}$ $A_r = 1 - (d_i/d)^2$
UCD-05 Method Gavin and Lehane (2005) (for base resistance of OE and CE driven and jacked pipe piles in dense sand)	This method does not indicate a means for evaluating f_p	For CE pile: $q_b = q_{c,avg}$ For OE pile: $q_{ann} = q_{c,avg}$ and $q_{plug} = (0.8 - 0.7\,FFR)q_{c,avg}$ ($FFR \leq 1$) $Q_b = q_{plug}A_{plug} + q_{ann}A_{ann}$

Notes: h = height above pile tip; r* = equivalent pile radius; r_i = internal pile radius = $d_i/2$; d_i = internal pile diameter; $q_{b0.1}$ = unit end bearing at a tip displacement of 10% of the pile diameter; $q_{c,avg}$ = q_c averaged $\pm$ 1.5d over pile tip level; A_r = area ratio; q_{plug} = plug unit end bearing resistance; q_{ann} = unit resistance below the base of pile annulus; FFR is the final filling ratio = IFR at the end of pile installation; IFR = incremental filling ratio = $\Delta L_p/\Delta z$; ΔL_p = incremental change of plug length; Δz = change in penetration depth; Q_b = end bearing at a pile head displacement of up to about one diameter penetration.

Table 3.7. (continued).

Method/Reference	Design Equations	
	Pile unit side resistance (f_p)	Pile unit end bearing (q_b)
ICP-05 Method (Jardine et al., 2005) (for driven piles loaded first time via SML test conducted around 10 days after driving in sandy soils)	$f_p = a(\sigma_{rc}' + \Delta\sigma_{rd}')\tan\delta_f'$ $\sigma_{rc}' = 0.029bq_c(\sigma_{vo}'/\sigma_{atm})^{0.13}\cdot[\max(h/r^*,8)]^{-0.38}$ $\Delta\sigma_{rd}' = 2G\Delta y/r^*$; $\Delta y \approx 2R_a \approx 0.02$ mm a = 0.9 (OE piles in tension), 1.0 (all other cases) b = 0.8 (tension), 1.0 (compression); δ_f' measured or estimated as fctn(d_{50}) (see Figure 3.34) $r^* = (r^2 - r_i^2)^{0.5}$ $G \approx 185q_c q_{c1N}^{-0.7}$, or $G \approx q_c [0.0203 + 0.00125q_{c1N} - 1.216e^{-6}q_{c1N}^2]^{-1}$ $q_{c1N} = (q_c/\sigma_{atm})/(\sigma_{vo}'/\sigma_{atm})^{0.5}$	CE pipe piles: $q_{b0.1} = q_{c,avg}\cdot\max[1 - 0.5\log(d/d_{CPT}), 0.3]$ OE pipe piles: Unplugged: $q_{b0.1} = q_{c,avg}\cdot A_r$ Plugged:$q_{b0.1} = q_{c,avg}\cdot\max[0.5 - 0.25\cdot\log(d/d_{CPT}), 0.15, A_r]$; where $A_r = 1 - (d_i/d)^2$ If $d_i \geq 2.0(D_r - 0.3)$ or $d_i \geq 0.083q_{c,avg}/\sigma_{atm}d_{CPT}$, pile is unplugged, otherwise plugged (d_i in meters) Non-circular piles (use equivalent base area): Square/rectangular section: $q_{b0.1} = 0.7q_{c,avg}$ H section: $q_{b0.1}=q_{c,avg}$

Notes: σ_{rc}' = local radial effective stress after equalization; h = height above pile tip; r* = equivalent pile radius; r_i = pile inner radius = $d_i/2$; d_i = pile inner diameter; $\Delta\sigma_{rd}'$ = change in radial stress during pile loading; δ_f' = interface friction angle at failure; G = operational shear modulus; Δy = radial displacement due to dilation during pile loading; R_a = average roughness of the pile; $q_{b0.1}$ = unit end bearing at a tip displacement of 10% of the pile diameter; $q_{c,avg} = q_c$ averaged $\pm$ 1.5d over pile tip level; d_{CPT} = 0.036 m; A_r = area ratio; d = pile outer diameter; for square, rectangular and H piles r* = $(A_b/\pi)0.5$; A_b = base area = w·b (square/rectangular section), $A_s + 2X_p(D - 2T)$ (H section); w = width, b = breadth; A_s = area of H section, X_p = B/8 if $B/2 < (D - 2T) < B$, $X_p = B^2/[16(D - 2T)]$ if $(D - 2T) \geq B$, B = flange width, D = total depth, T = flange thickness.

Table 3.7. (continued).

Method/Reference	Design Equations	
	Pile unit side resistance (f_p)	Pile unit end bearing (q_b)
ICP-05 Method (Jardine et al., 2005) (for driven piles in clays)	This method utilizes effective stress approach (β-method) as a means for evaluating f_p. No direct use of CPT reading is involved. Accordingly, it has been listed in Table 3.5.	CE pipe piles: $q_b = 0.8q_{c,avg}$ (undrained loading) $q_b = 1.3q_{c,avg}$ (drained loading) OE pipe piles: Unplugged: $q_b = q_{c,avg}$ (undrained loading) $q_b = 1.6q_{c,avg}$ (drained loading) Plugged: $q_b = 0.4q_{c,avg}$ (undrained loading) $q_b = 0.65q_{c,avg}$ (drained loading) If $(d_i/d_{CPT} + 0.45q_{c,avg}/\sigma_{atm}) < 36$, pile is plugged otherwise unplugged during static loading

Notes: $q_{c,avg} = q_c$ averaged $\pm$ 1.5d over pile tip level; $d_{CPT} = 0.036$ m; d_i = pile inner diameter; for non-circular piles equivalent pile diameter is adopted in the manner described above for piles in sand.

Table 3.7. (continued).

Method/Reference	Design Equations	
	Pile unit side resistance (f_p)	Pile unit end bearing (q_b)
UWA-05 Method (Lehane et al., 2005) (for driven piles in sandy soils)	$f_p = \frac{f_t}{f_c}[0.03 q_c A_{rs,eff}^{0.3}[\max(\frac{h}{d},2)^{-0.5}] + \Delta\sigma_{rd}']\tan\delta_f$ f_t/f_c=1 (compression), 0.75 (tension) $A_{rs,eff} = 1 - IFR\,(d_i/d)^2$; where $IFR = \Delta L_p/\Delta z$ If IFR is not measured: Average $IFR = \min\{1,[d_i(m)/1.5]^{0.2}\}$ $\Delta\sigma_{rd}' \approx 2G\Delta y / r^*$ $G \approx 185 q_c q_{c1N}^{-0.7}$, or $G \approx q_c[0.0203 + 0.00125 q_{c1N} - 1.216e^{-6} q_{c1N}^2]^{-1}$ $\Delta y \approx 2R_a \approx 0.02$ mm $q_{c1N} = (q_c/\sigma_{atm})/(\sigma_{vo}'/\sigma_{atm})^{0.5}$ $r^* = (r^2 - r_i^2)^{0.5}$	$q_{b0.1} = q_{c,avg} \cdot (0.15 + 0.45 A_{rb,eff})$ $A_{rb,eff} = 1 - FFR(d_i/d)^2$; FFR = IFR averaged over last 3d of the pile penetration, where $IFR = \Delta L_p/\Delta z$ If IFR not measured: $FFR = \min\{1,[d_i(m)/1.5m]^{0.2}\}$

Notes: f_t/f_c = ratio of tension to compression capacity; $A_{rs,eff}$ = effective shaft area ratio; h = height above pile tip; IFR = incremental filling ratio; ΔL_p = incremental change of plug length; Δz = change in penetration depth; d_i = pile inner diameter; d = pile outer diameter; $\Delta\sigma_{rd}'$ = change in radial stress during pile loading; G = operational shear modulus; Δy = interface dilation (radial displacement during pile loading); R_a = average roughness of the pile; r* = equivalent pile radius; where r_i = internal pile radius = $d_i/2$; $q_{b0.1}$ = unit end bearing at a tip displacement of 10% of the pile diameter; $q_{c,avg}$ = q_c averaged using Dutch averaging technique; $A_{rb,eff}$ = effective base area ratio; FFR = final filling ratio.

Table 3.7. (continued).

Method/Reference	Design Equations	
	Pile unit side resistance (f_p)	Pile unit end bearing (q_b)
NGI-05 Method (Clausen et al., 2005) (for driven piles in sandy soils)	$f_p = (z/L)\cdot\sigma_{atm}F_{Dr}F_{sig}F_{tip}F_{load}F_{mat} \geq 0.1\cdot\sigma_{vo}'$ $F_{Dr} = 2.1(D_r - 0.1)^{1.7}$ $F_{sig} = (\sigma_{vo}'/\sigma_{atm})^{0.25}$ F_{tip} = 1.0 (driven OE), 1.6 (driven CE) F_{load} = 1.0 (tension), 1.3 (compression) F_{mat} = 1.0 for steel and 1.2 for concrete $D_r = 0.4\ln(q_{c1N}/22)$ $q_{c1N} = (q_c/\sigma_{atm})/(\sigma_{vo}'/\sigma_{atm})^{0.5}$	CE: $q_{b0.1} = q_{c,tip}\cdot[0.8/(1+D_r^2)]$ OE: $q_{b0.1} = \min[q_{b0.1(plugged)}, q_{b0.1(unplugged)}]$ Plugged: $q_{b0.1} = q_{c,tip}\cdot[0.7/(1 + 3D_r^2)]$ Unplugged: $q_{b0.1} = q_{c,tip}\cdot A_r + 12\cdot f_{p,avg}\cdot L\cdot(1 - A_r)/(\pi d_i)$ $D_r = 0.4\ln(q_{c1N}/22)$ $q_{c1N} = (q_c/\sigma_{atm})/(\sigma_{vo}'/\sigma_{atm})^{0.5}$ $A_r = 1 - (d_i/d)^2$
Cambridge-05 Method (White and Bolton, 2005) [for CE and PCC piles jacked or driven, and driven cast-in-situ (Franki) piles in two layered strata]	This method does not indicate a means for evaluating f_p	$q_b \approx 0.9q_{c,avg}$ $q_{c,avg}$ = average q_c in zone $\pm$1.5d; for partial embedment in transition zone ($-2<z_b/d<8$): $q_{c,avg} = \{q_{c,weak} + [(q_{c,hard} - q_{c,weak})(z_b/d + 2)]/10\}$ (see Figure 3.35 for further description of partial embedment reduction factor)
Togliani (2008) (for cylindrical and tapered driven and bored piles in all soil types)	$f_p = k_1 q_c^{0.5}$ $k_1 = 1.2(0.8+R_f/8)$ for $R_f < 1$ $k_1 = 1.1(0.4+\mathrm{Ln}(R_f))$ for $R_f \geq 1$ $R_f = (f_s/q_c)100$	$q_b = k_3 q_{c(toe)}$ $k_3 = \lambda + [0.01(L_{pile}/d_{toe})]$ λ = 0.2 (driven piles), 0.1 (bored piles) L_{pile}/d_{toe} = pile slenderness ratio

Notes: $q_{c(toe)}$=average q_c between $+8d_{toe}$ and $-4d_{toe}$; z/L = layer depth to pile length ratio; D_r = relative density in decimal, may be greater than 1.0; $q_{b0.1}$ = unit end bearing at a tip displacement of 10% of the pile diameter; $q_{c,tip}$ = average q_c in the zone at the pile base; A_r = area ratio at pile base; d_i = pile inner diameter; d = pile outer diameter; $f_{p,avg}$ = average external friction over pile embedment depth L; $q_{c,avg}$ = average q_c in zone around the pile base described in Figure 3.35.

Table 3.7. (continued).

Method/Reference	Design Equations	
	Pile unit side resistance (f_p)	Pile unit end bearing (q_b)
German Method (Kempfert and Becker, 2010) (for piles in sandy soils)	Provides upper and lower bound estimates of f_p (kPa) based on q_c (measured in MPa) (see Figures 3.36a and 3.37)	Provides upper and lower bound estimates of q_b (MPa) based on q_c (measured in MPa) (see Figure 3.36b)
UCD-11 Method Igoe et al. (2010; 2011) (for shaft capacity of OE piles in sandy soils)	$f_p = \sigma_{rf}' \cdot \tan\delta_f'$, where $\sigma_{rf}' = \sigma_{rc}' + \Delta\sigma_{rd}'$ $\sigma_{rc}' = q_c[0.025 - 0.0025(h/d)]A_{r,eff} > \sigma_{rc}'_{,min}$ $A_{rs,eff} = 1 - IFR(d_i/d)^2$; where $IFR = \Delta L_p/\Delta z$ $\sigma_{rc}'_{,min} = \lambda q_c$ $\lambda = 0.003$(loose sand), 0.006(dense sand) $\Delta\sigma_{rd}' \approx 2G\Delta y/r^*$ $G \approx 185 q_c q_{c1N}^{-0.7}$, or $G \approx q_c[0.0203 + 0.00125q_{c1N} - 1.216e^{-6}q_{c1N}^2]^{-1}$ $\Delta y \approx 2R_a \approx 0.02$ mm; $r^* = (r^2 - r_i^2)^{0.5}$ $q_{c1N} = (q_c/\sigma_{atm})/(\sigma_{vo}'/\sigma_{atm})^{0.5}$	This method does not indicate a means for evaluating q_b
V-K Method Van Dijk and Kolk (2011) (for offshore piles in clays)	$f_p = k_{s(z)} \cdot q_{t(net),z}$ $k_{s(z)} = 0.16(h/uL)^{-0.3}[Q_{t(z)}]^{-0.4} \leq 0.08$ $uL = 1.0$ m (=3.3 feet) $Q_{t(z)} = q_{t(net),z}/\sigma_{vo}'$ at z; where $q_{t(net)} = q_t - \sigma_{vo}$	$q_b = 0.7q_{t(net),avg}$ $q_{t(net)} = q_t - \sigma_{vo}$

Notes: σ_{rf}' = peak radial effective stress at failure; σ_{rc}' = radial effective stress measured after installation but before loading; $A_{rs,eff}$ = effective shaft area ratio; h = distance from pile toe; IFR = incremental filling ratio; ΔL_p = change in the soil plug length during an increase in pile penetration Δz; d_i = inner pile diameter; d = pile outer diameter; λ = scalar reduction factor that accounts for friction fatigue; $\Delta\sigma_{rd}'$ = change in radial stress during pile loading; G = operational shear modulus; Δy = interface dilation (radial displacement during pile loading); R_a = average roughness of the pile; r* = equivalent pile radius; where r_i = internal pile radius = $d_i/2$; z = depth below seafloor; h = distance between pile tip level and z; uL = unit length to render expression dimensionless; $q_{t(net),avg} = q_{t(net)}$ averaged $\pm$ 1.5d over pile tip level.

Table 3.7. (continued).

Method/Reference	Design Equations	
	Pile unit side resistance (f_p)	Pile unit end bearing (q_b)
SEU Method (Cai et al., 2011; 2012) [for PCC thin-wall and high-strength caissons, cement fly-ash grave pile in soft clays (driven or jacked)]	Estimates f_p from measured f_s and Δu_2 (see Figure 3.38)	Similar to Unicone Method: $q_b=C_{te}q_E$ $q_E = q_t - u_2$
HKU Method (Yu and Yang, 2012) (for base capacity of OE steel pipe piles in sandy soils)	This method does not indicate a means for evaluating f_p	$Q_b=(\pi/4)[d^2q_{plug} + (d^2 - d_i^2)q_{ann}]$ $q_{plug} = 1.063\exp(-1.933PLR)q_{ca}$; where PLR=H/L $q_{ann} = [1.063 - 0.045(L/d)]q_{ca} \geq 0.46q_{ca}$ $q_{ca} = 0.5(M_A + M_B)$ if $M_A \leq M_B$; otherwise = M_B (also see Figure 3.39 for further description)
UWA-13 Method (Lehane et al., 2013) (for shaft capacity of driven and jacked piles in clays)	$f_p = 0.055\, q_t\, [\max(h/r^*, 1)]^{-0.2}$	This method does not indicate a means for evaluating q_b

Notes: Δu_2 = excess porewater pressure = $u_2 - u_o$ (measured in kPa); C_{te} is a factor constant for pile unit tip resistance similar to the bearing capacity factor, N_c, and empirical cone factor N_{kt}; Q_b = total base capacity; d = outer pile diameter; d_i = inner pile diameter; PLR = plug length ratio; H = plug length measured at the end of pile installation; L = pile length; q_{ca} = average q_c in the influence zone at the pile base; M_A and M_B are the averages of q_c trace within the ranges of A or B determined by the geometric means: $(q_{c1}\, q_{c2} \ldots q_{ci} \ldots q_{cn})^{1/n}$; $q_{ci} = i^{th}$ q_c reading recorded over the range of A or B (see Figure 3.39 for further description); h = height above the pile toe; r* = modified radius term for OE piles = $(r^2 - r_i^2)^{0.5}$; r = external radius; r_i = internal radius.

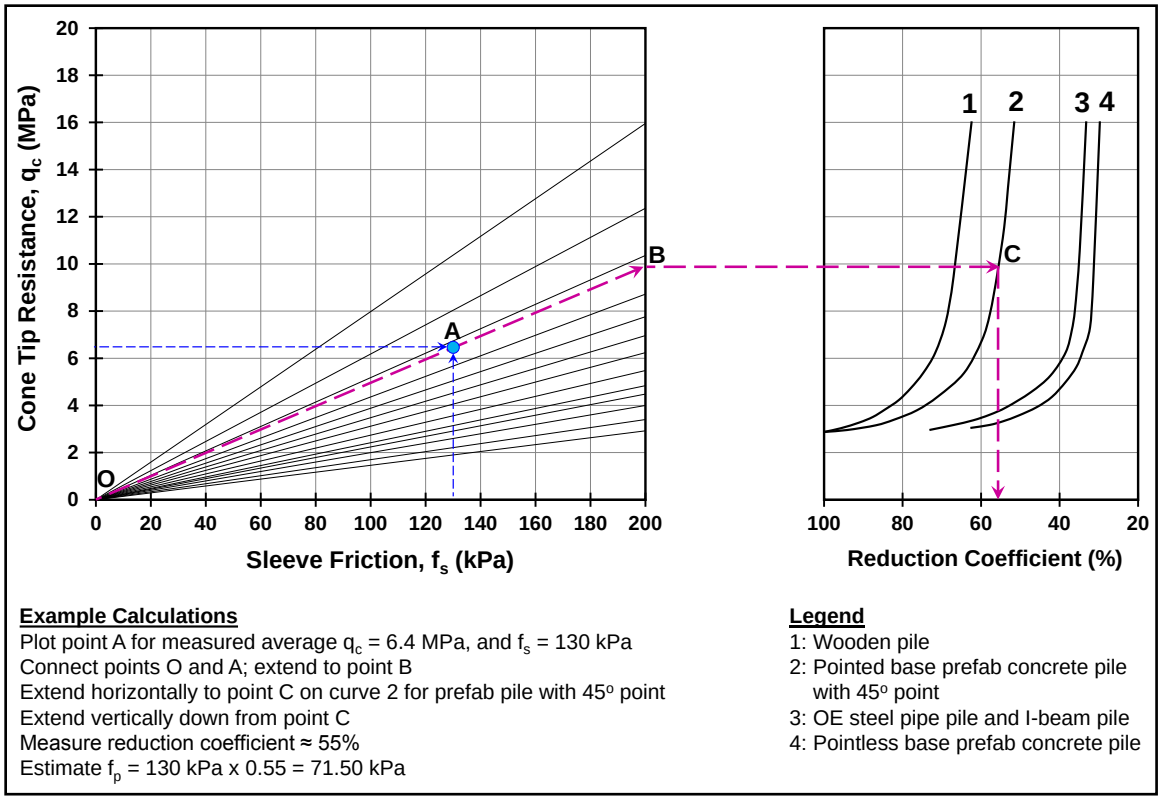

Figure 3.20. Begemann's graph for predicting pile f_p (adapted from Begemann, 1965).

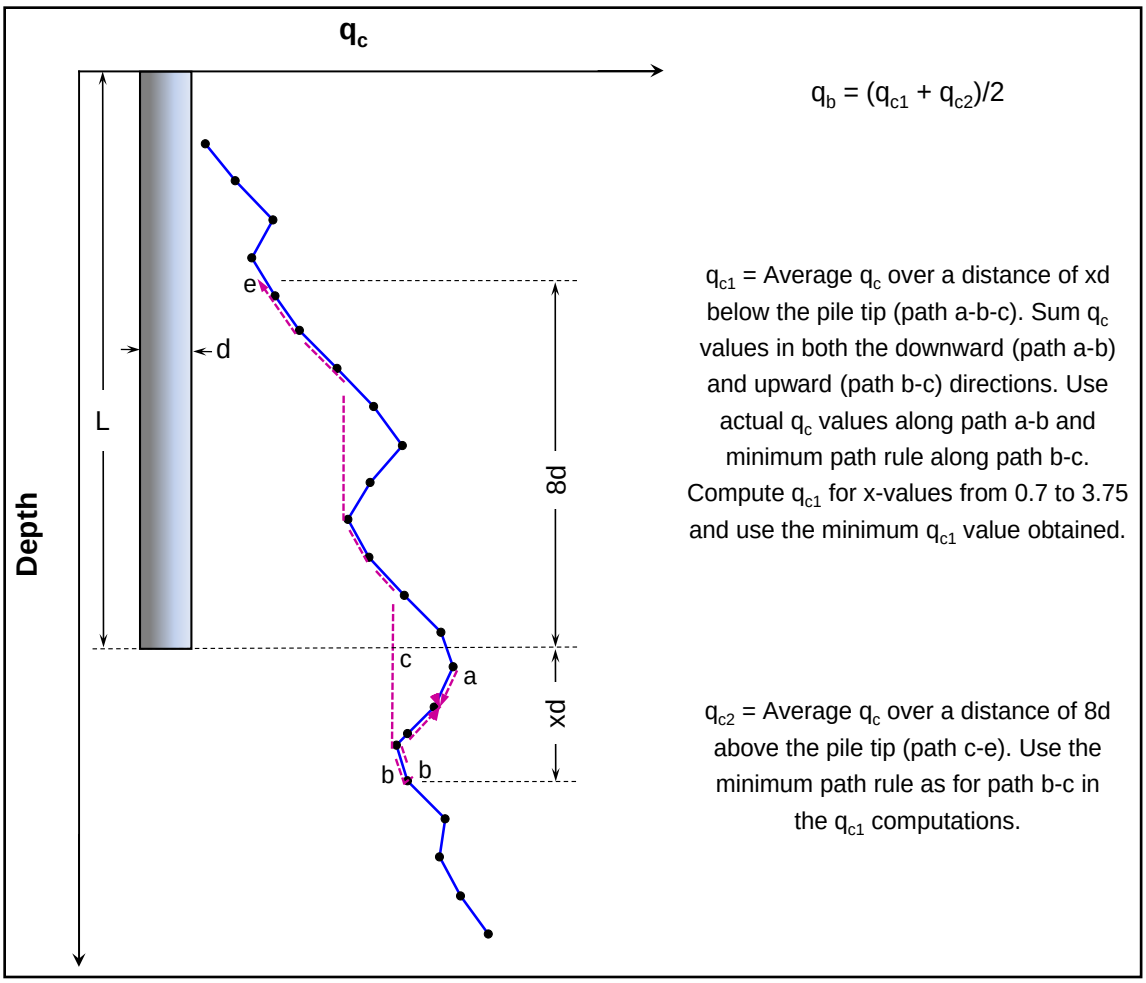

Figure 3.21. Begemann procedure for predicting pile q_b (adapted from Begemann, 1963).

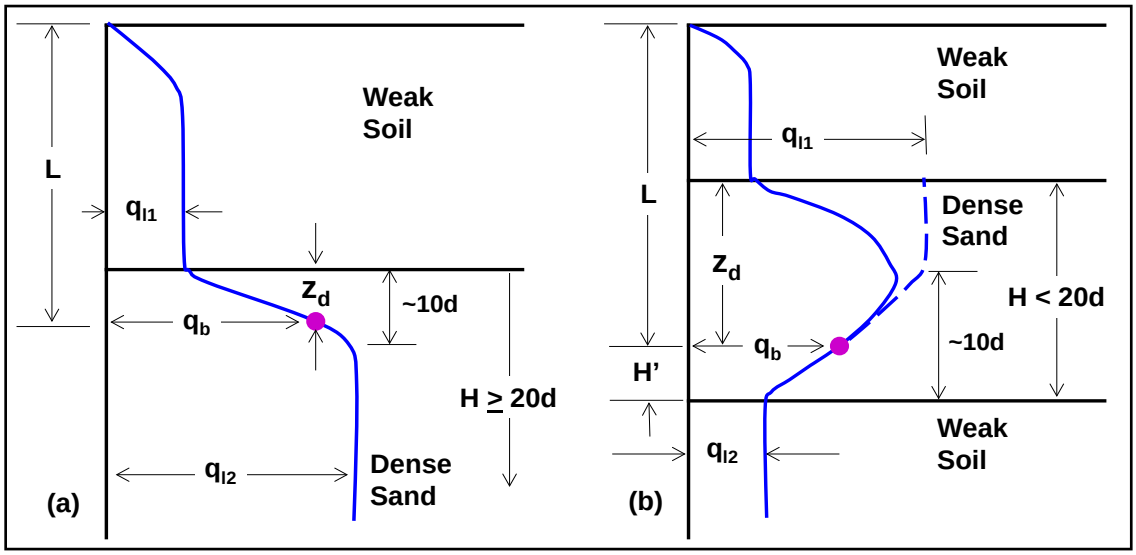

Figure 3.22. Pile unit base resistance and depth in sand stratum beneath weak soil layer: (a) thick sand stratum; (b) thin sand stratum overlying weak soil (after Meyerhof, 1983).

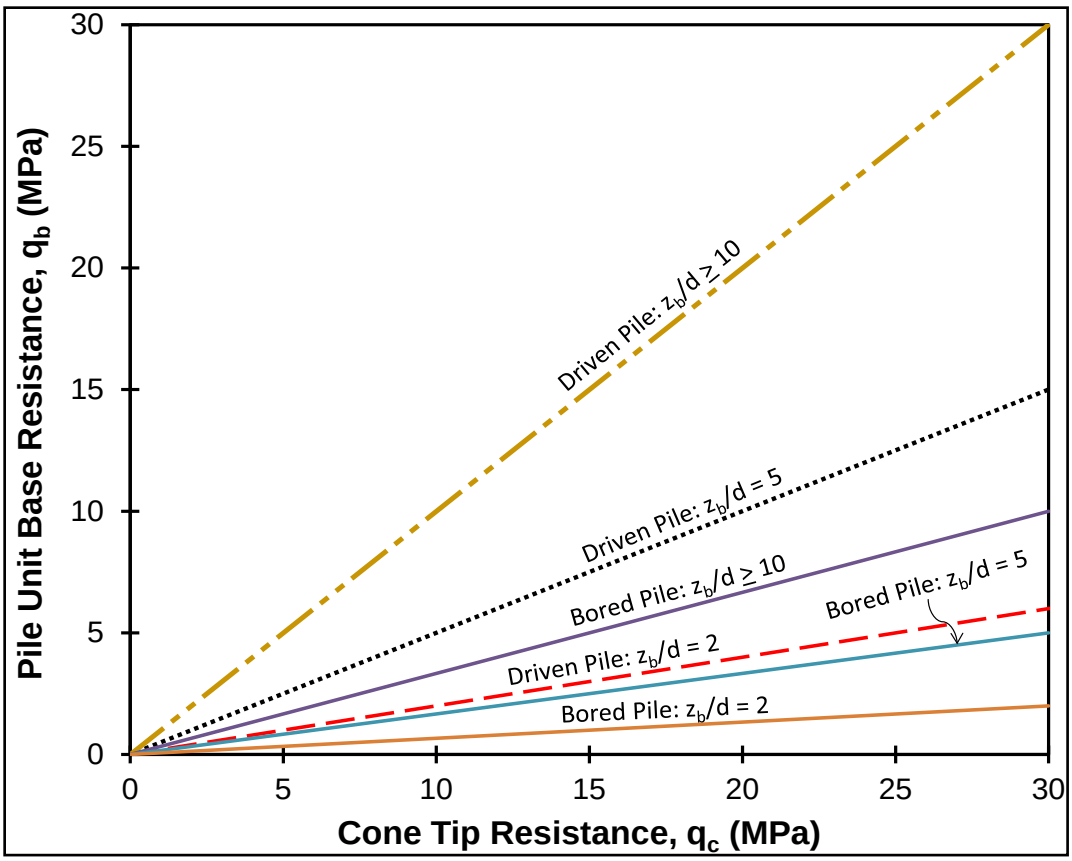

Figure 3.23. Relation between ultimate point resistance of driven and bored piles vs. static cone resistance in sand (after Meyerhof, 1983).

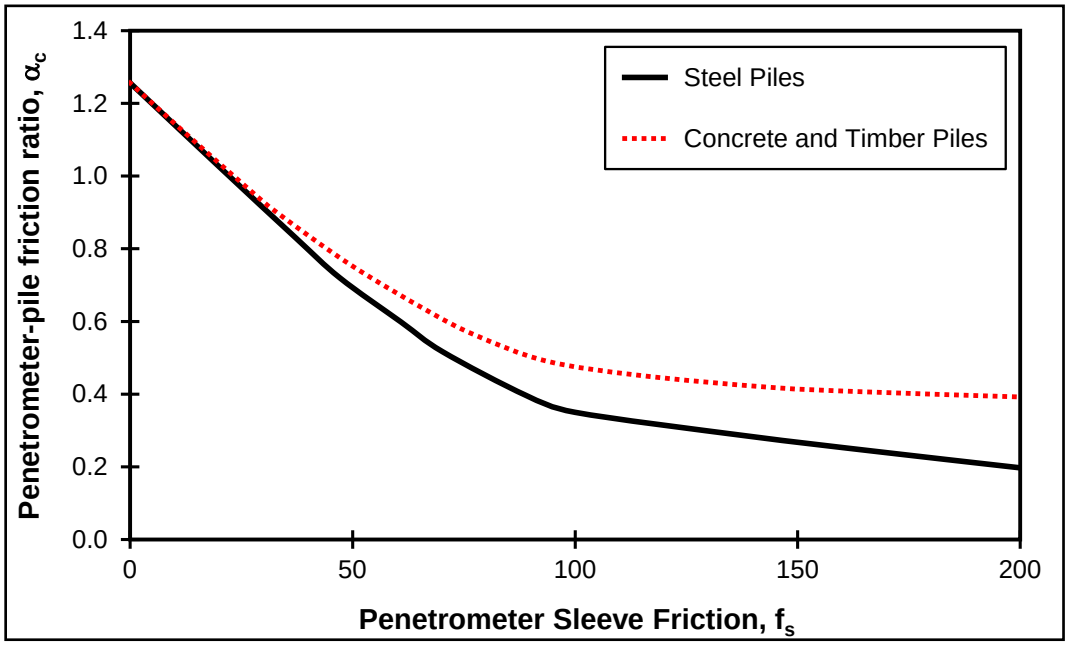

Figure 3.24. Penetration design curves for pile side friction in clays (after Nottingham, 1975; Schmertmann, 1978).

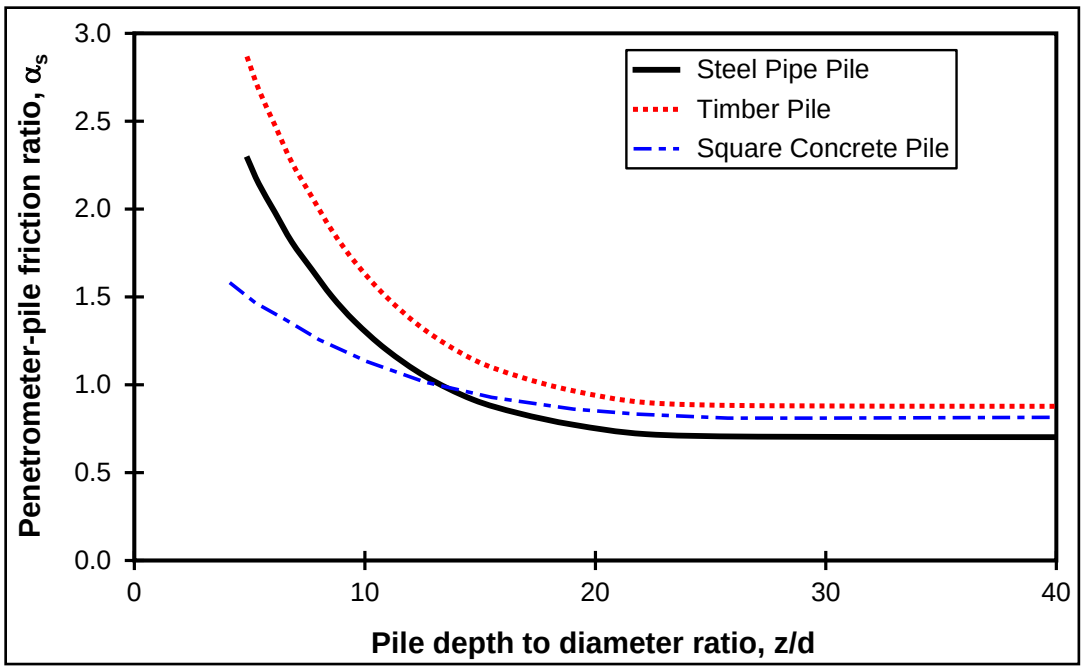

Figure 3.25. Penetrometer design curves for side pile friction in sand (after Nottingham, 1975; Schmertmann, 1978).

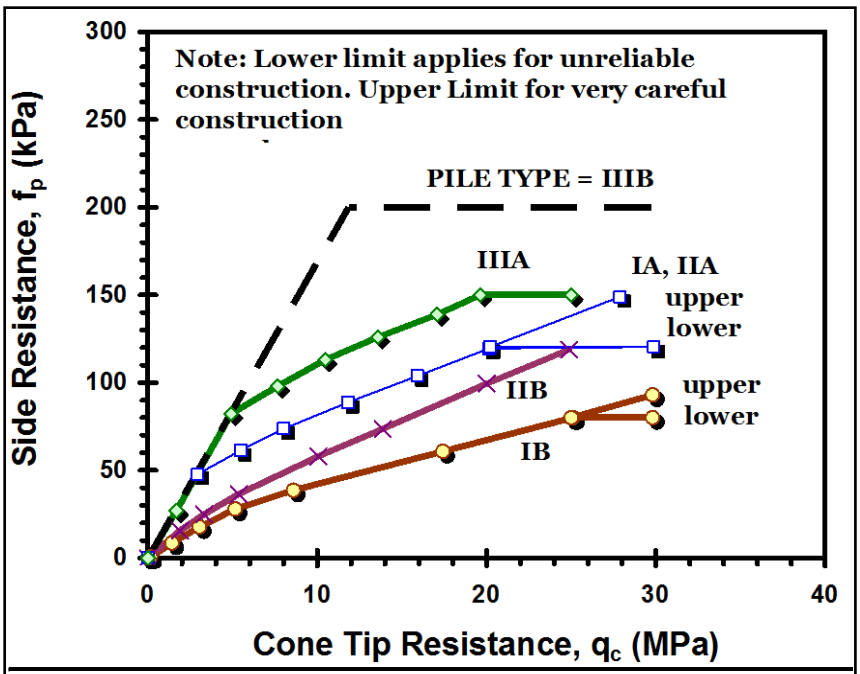

Pile Category	Type of Pile
IA	Plain bored piles, mud bored piles, hollow auger bored piles, case screwed piles, Type I micropioles, piers, barrettes
IB	Cased bored piles, driven cast piles
IIA	Driven precast piles, prestressed tubular piles, jacked concerete piles
IIB	Driven steel piles, jacked steel piles
IIIA	Driven grouted piles, driven rammed piles
IIIB	High pressure grouted piles (d > 0.25 m), Type II micropiles

(a)

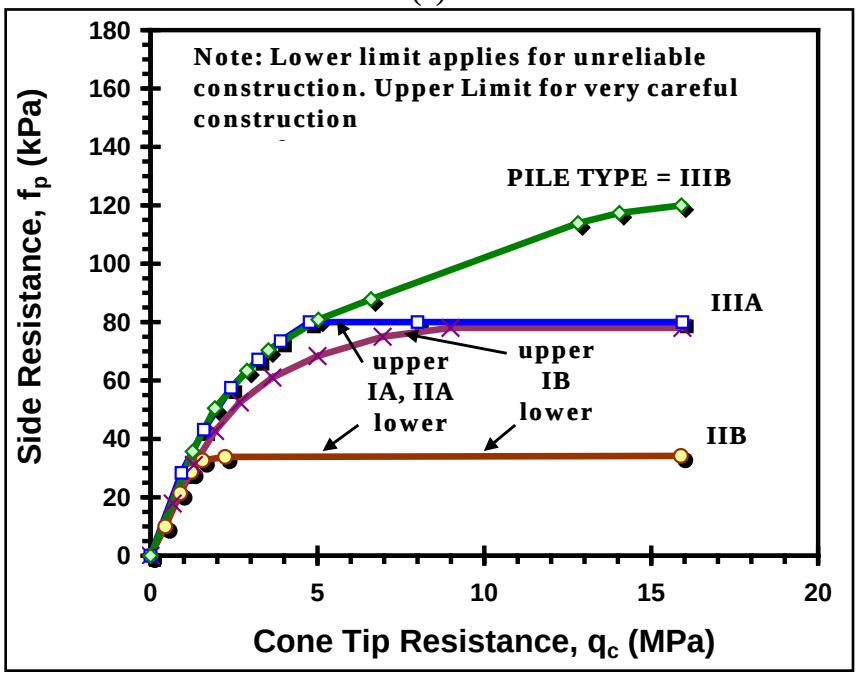

(b)

Figure 3.26. LCPC method for pile side resistance evaluation from CPT in: (a) sands; (b) clays (based on Bustamante and Gianeselli, 1982; adapted from Poulos, 1989).

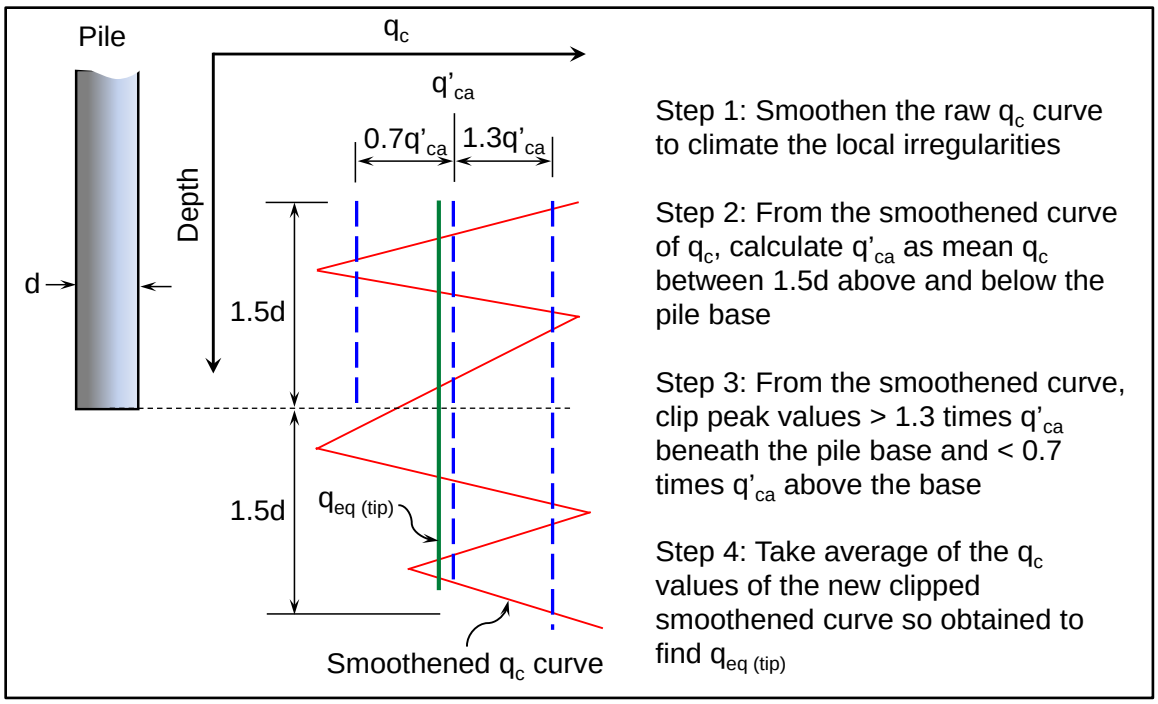

Figure 3.27. Calculation procedure for equivalent q_c for LCPC method (adapted from Bustamante and Gianeselli, 1982).

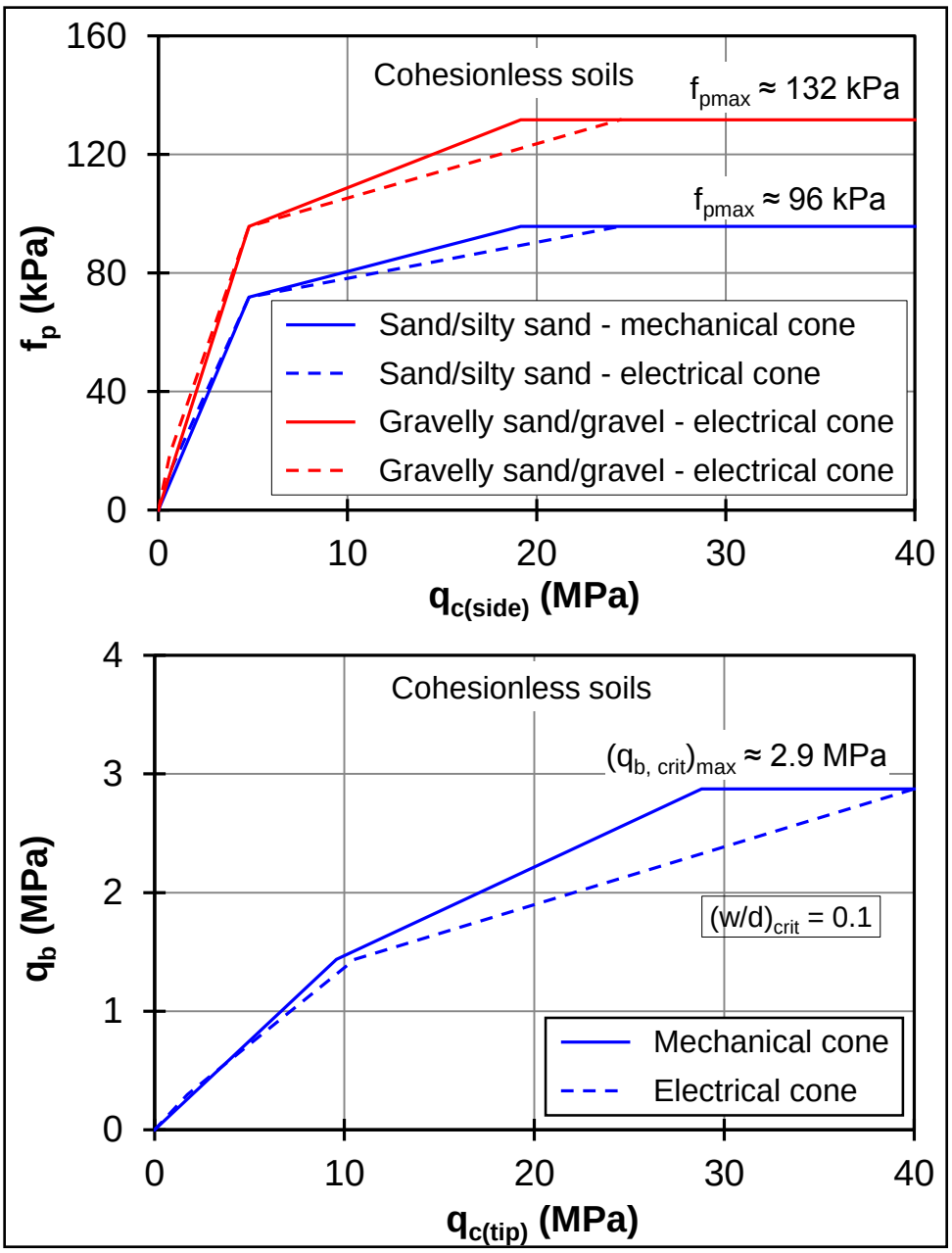

Figure 3.28. Design curves for pile f_p and q_b in cohesionless soils (after Alsamman, 1995).

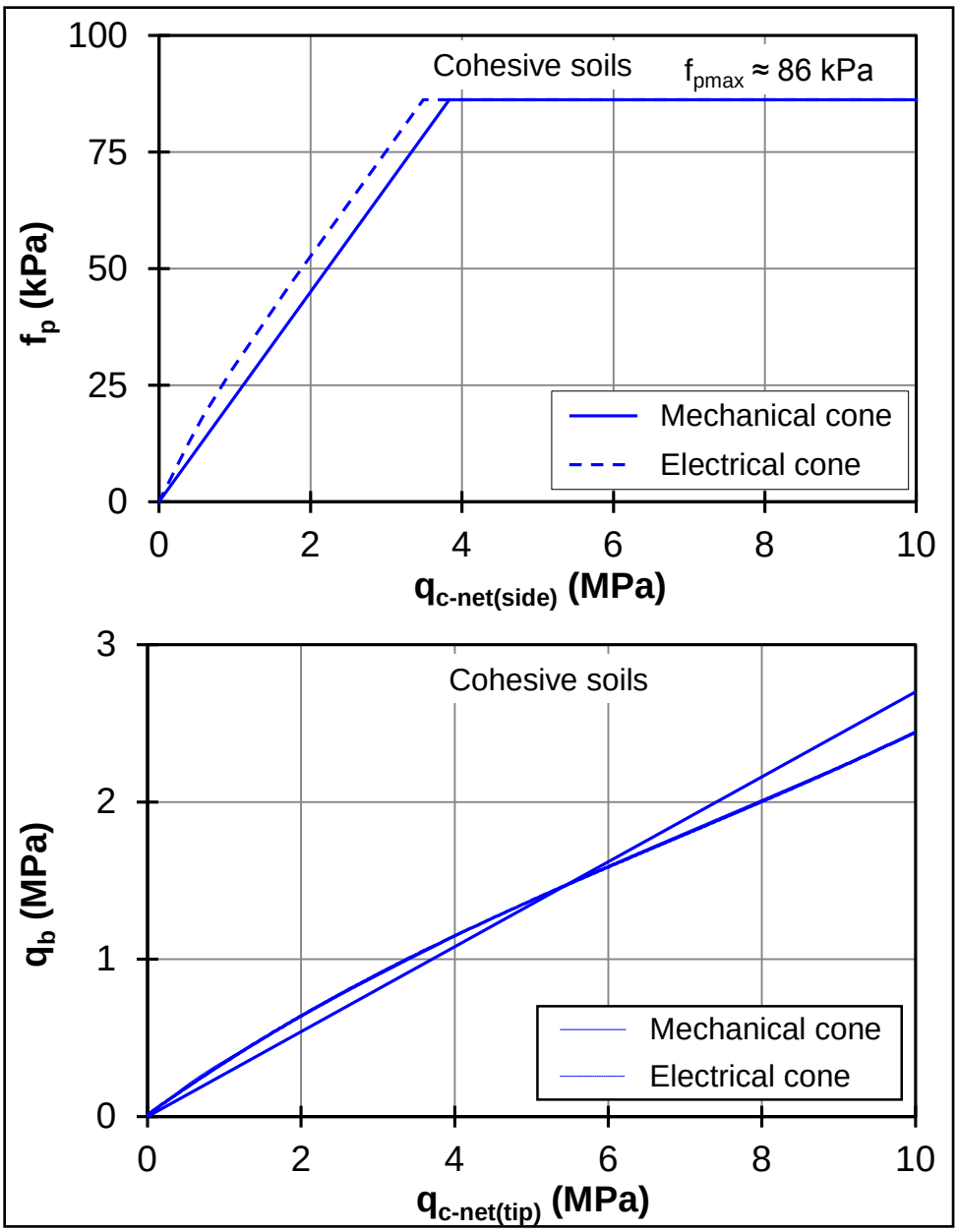

Figure 3.29. Design curves for pile f_p and q_b in cohesive soils (after Alsamman, 1995).

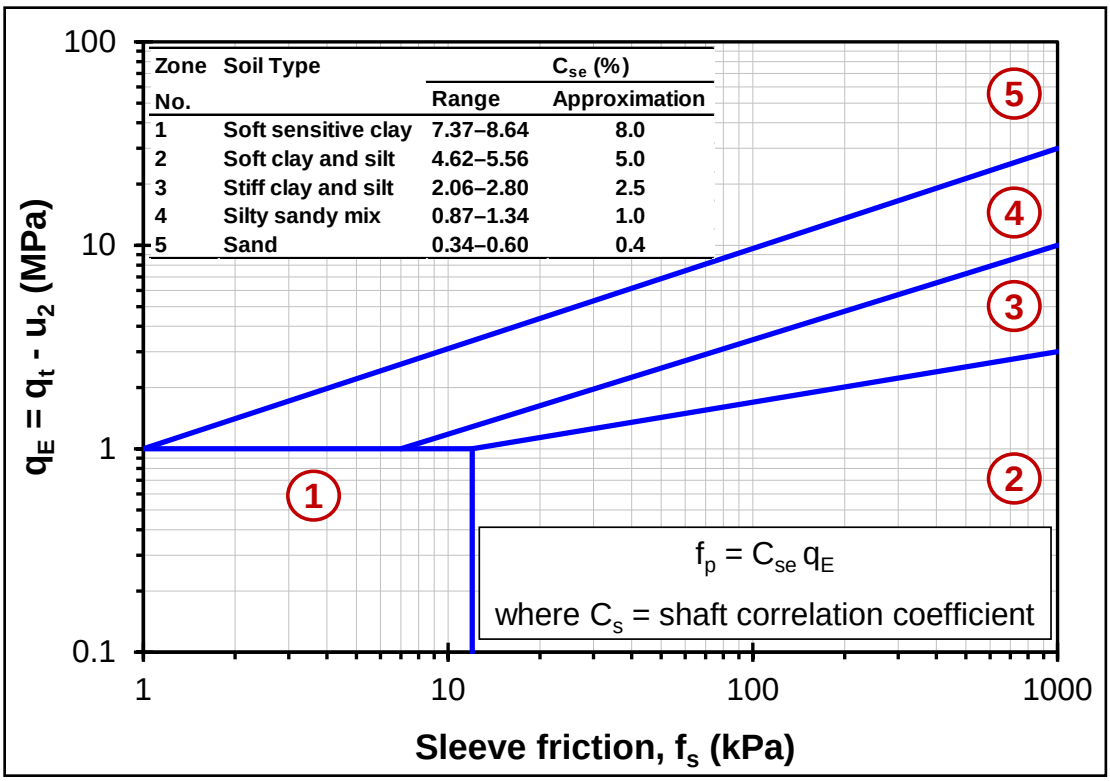

Figure 3.30. UniCone chart for zone numbers and soil types
(after Eslami and Fellenius, 1997).

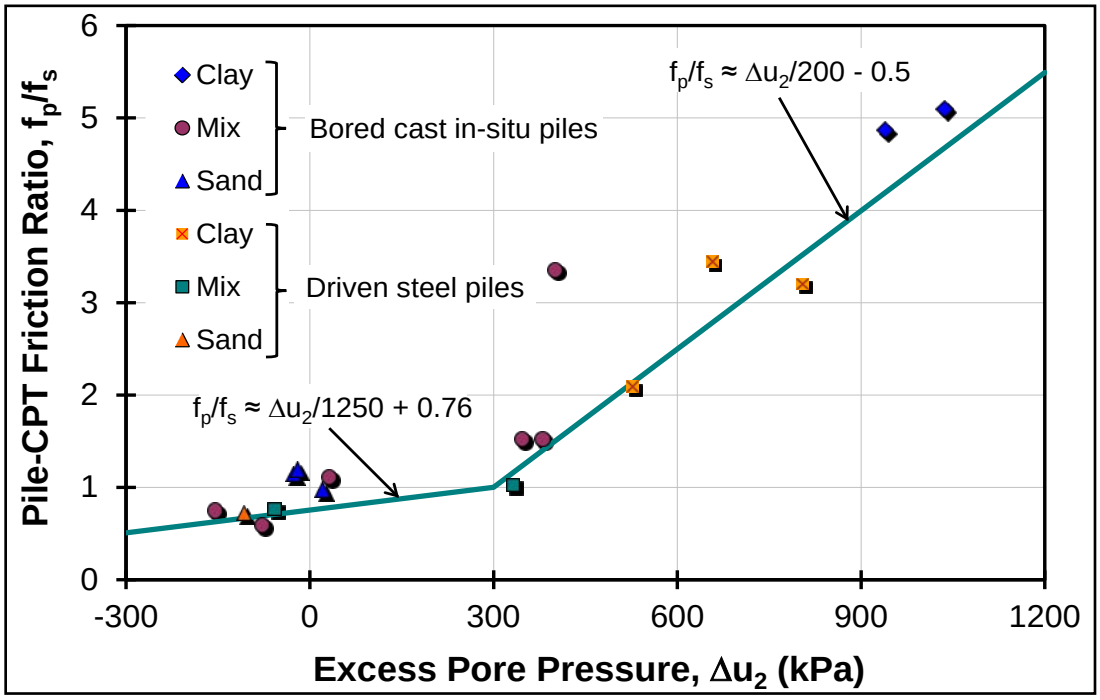

Figure 3.31. KTRI chart for estimating pile f_p from CPTu data
(after Takesue et al., 1998).

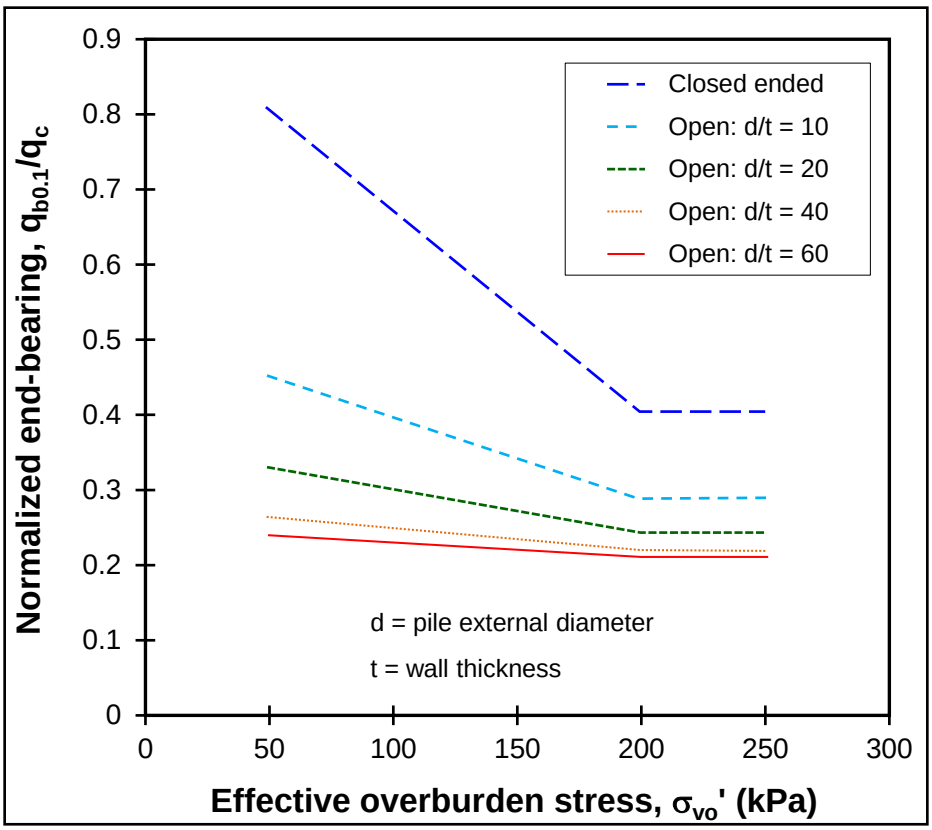

Figure 3.32. Variation of normalized end-bearing resistance with effective overburden stress for $w_b/d = 0.1$ (adapted from de Nicola and Randolph, 1999).

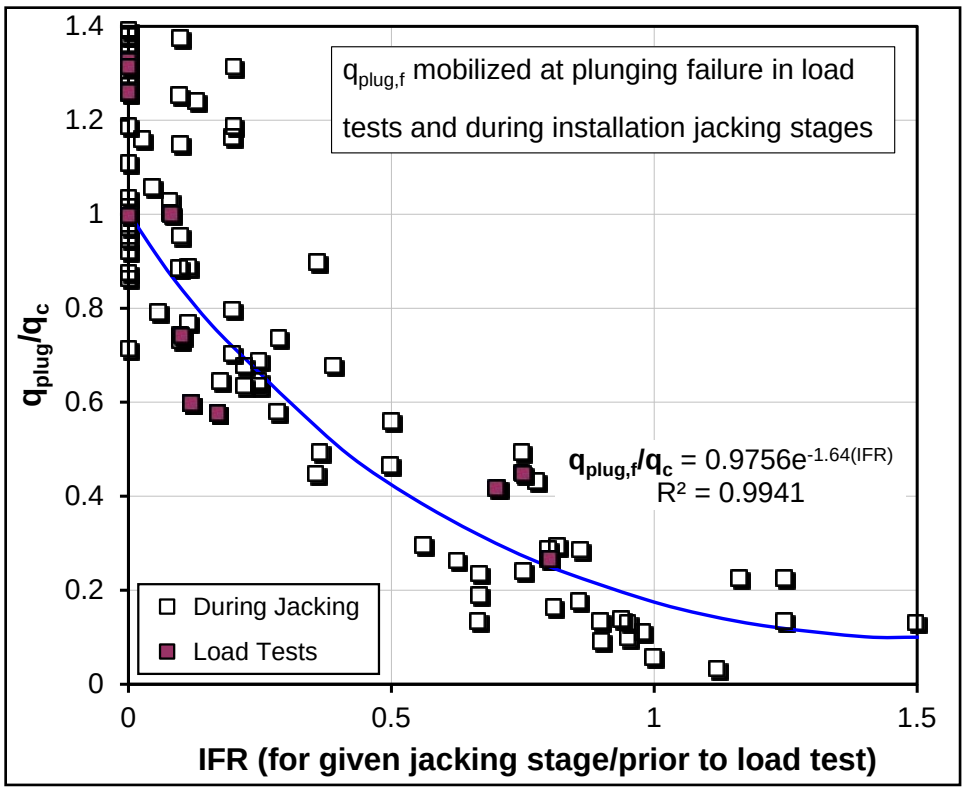

(a)

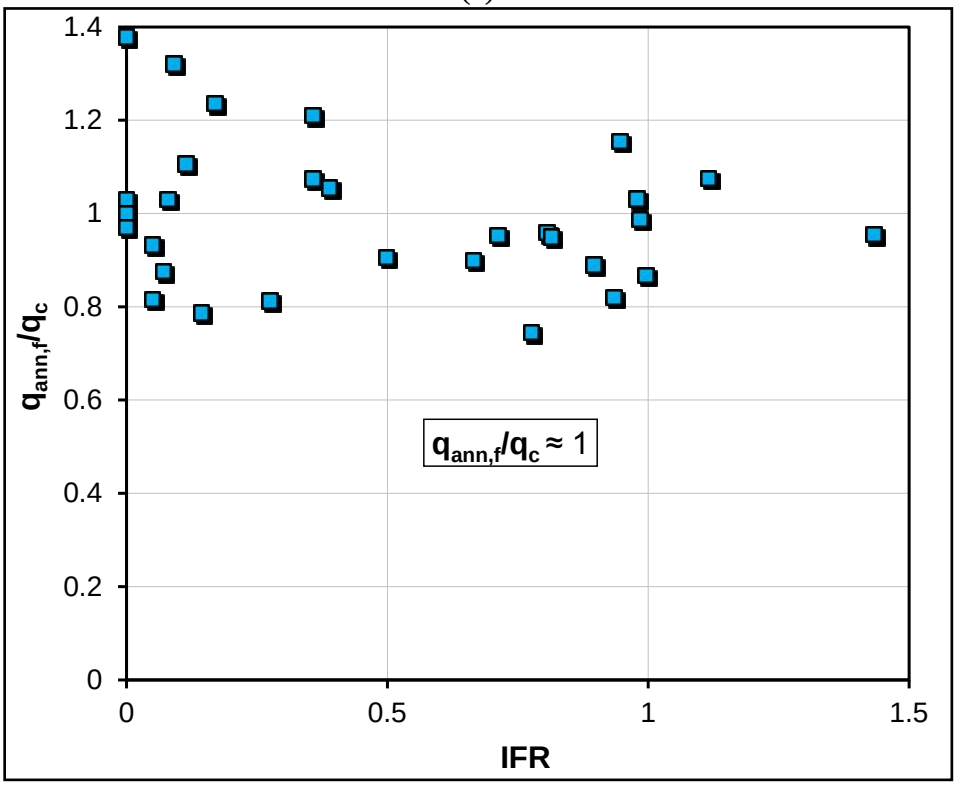

(b)

Figure 3.33. Dependence of: (a) $q_{plug,f}/q_c$ on IFR; (b) $q_{ann,f}/q_c$ on IFR for OE jacked pipe piles in sand (after Lehane and Gavin, 2001).

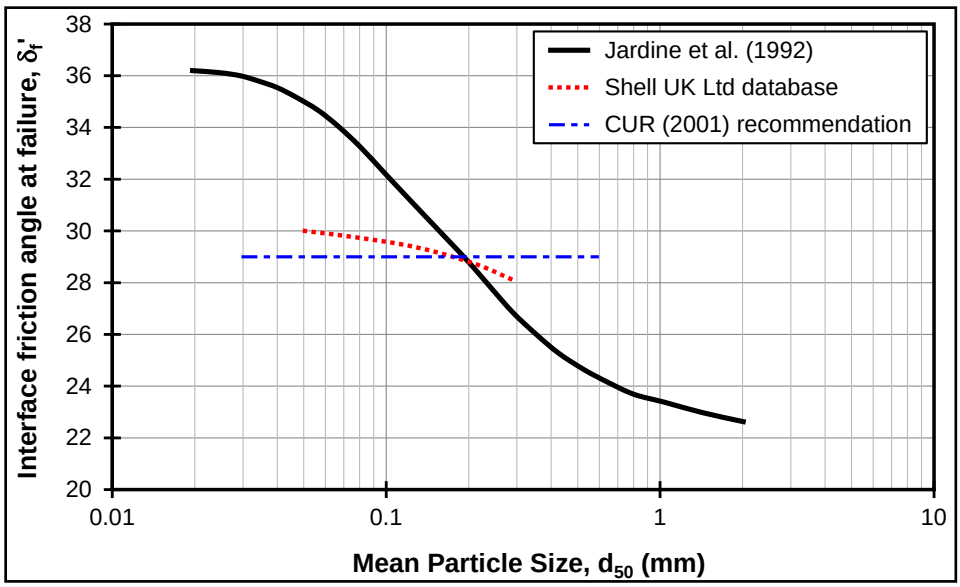

Figure 3.34. lnterface friction angle in sand trends from direct shear interface tests (after Jardine et al., 2005).

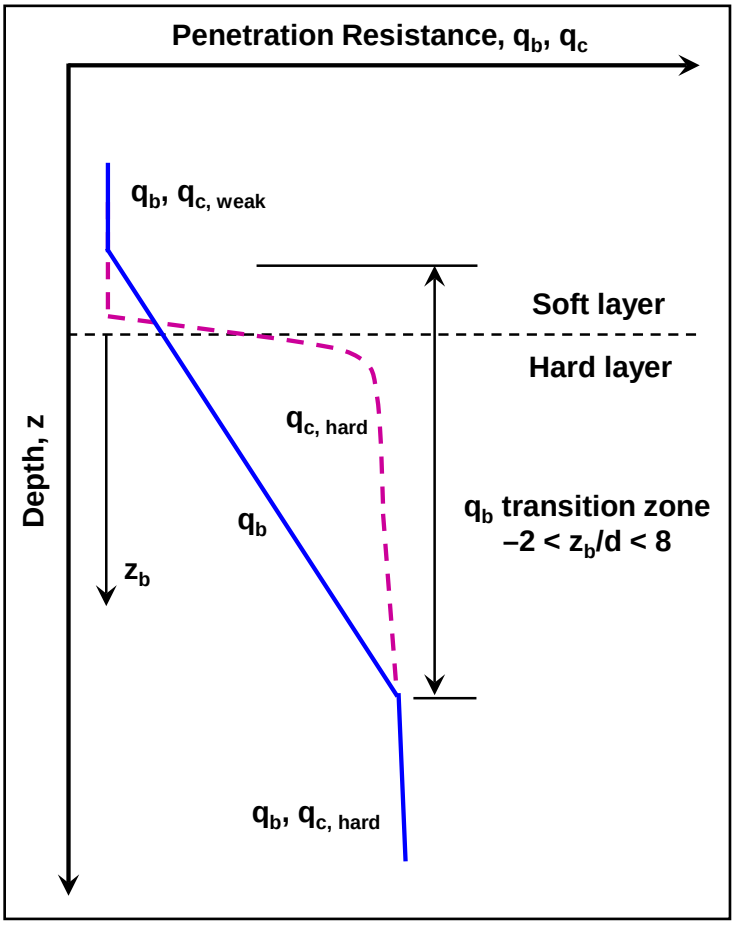

Figure 3.35. Partial embedment reduction factor on base resistance (after White and Bolton, 2005).

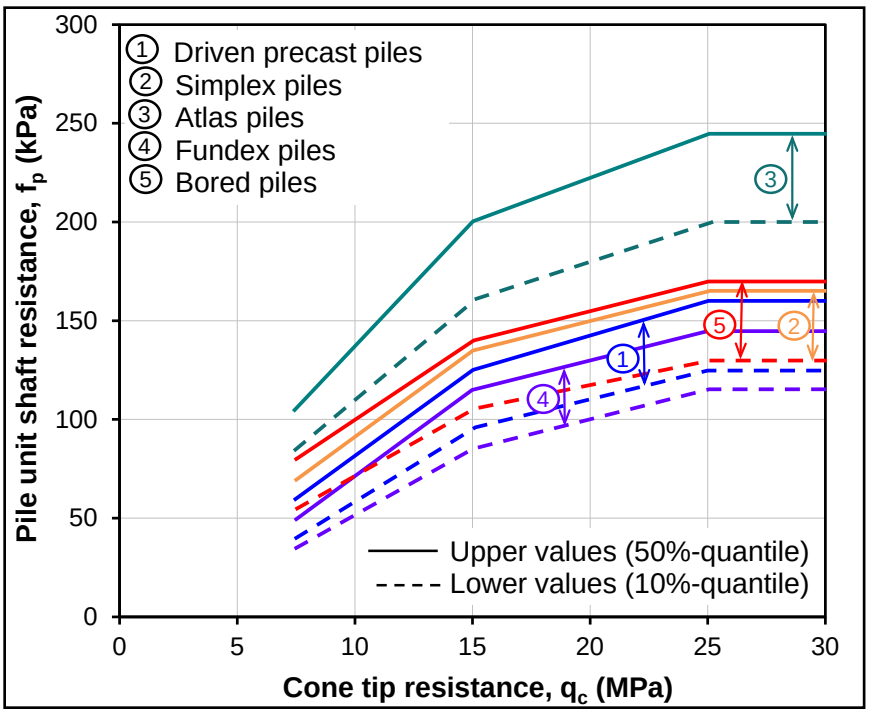

(a)

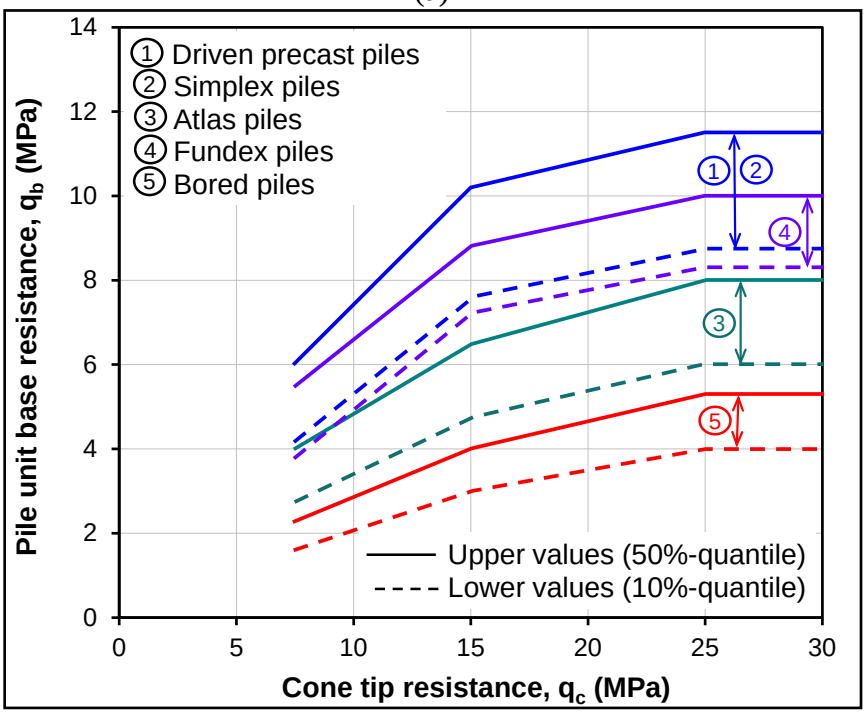

(b)

Figure 3.36. Upper and lower empirical values of different piles in coarse grained soils for: (a) unit shaft resistance; (b) unit base resistance (after Kempfert and Becker, 2010).

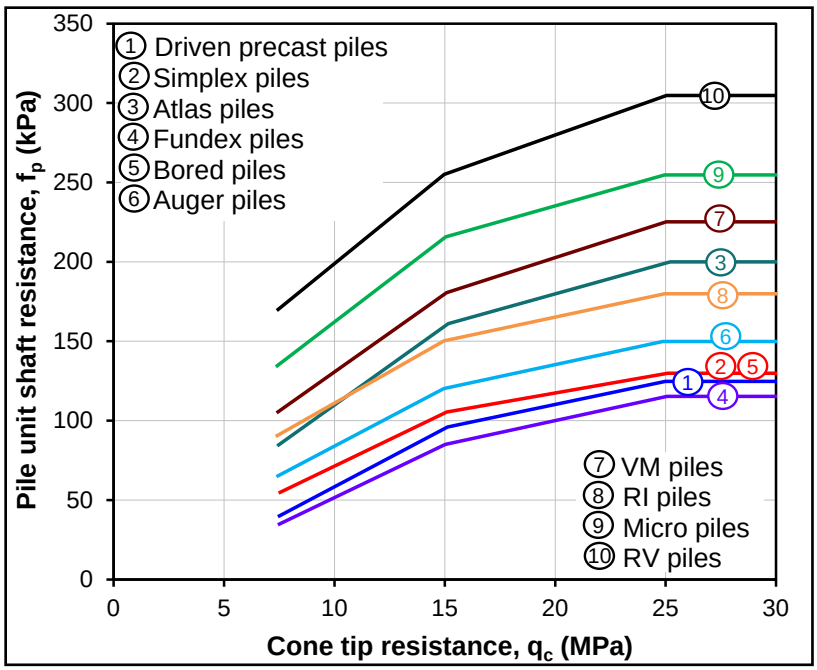

Figure 3.37. Lower empirical values of unit shaft resistance for different piles in coarse grained soils (after Kempfert and Becker, 2010).

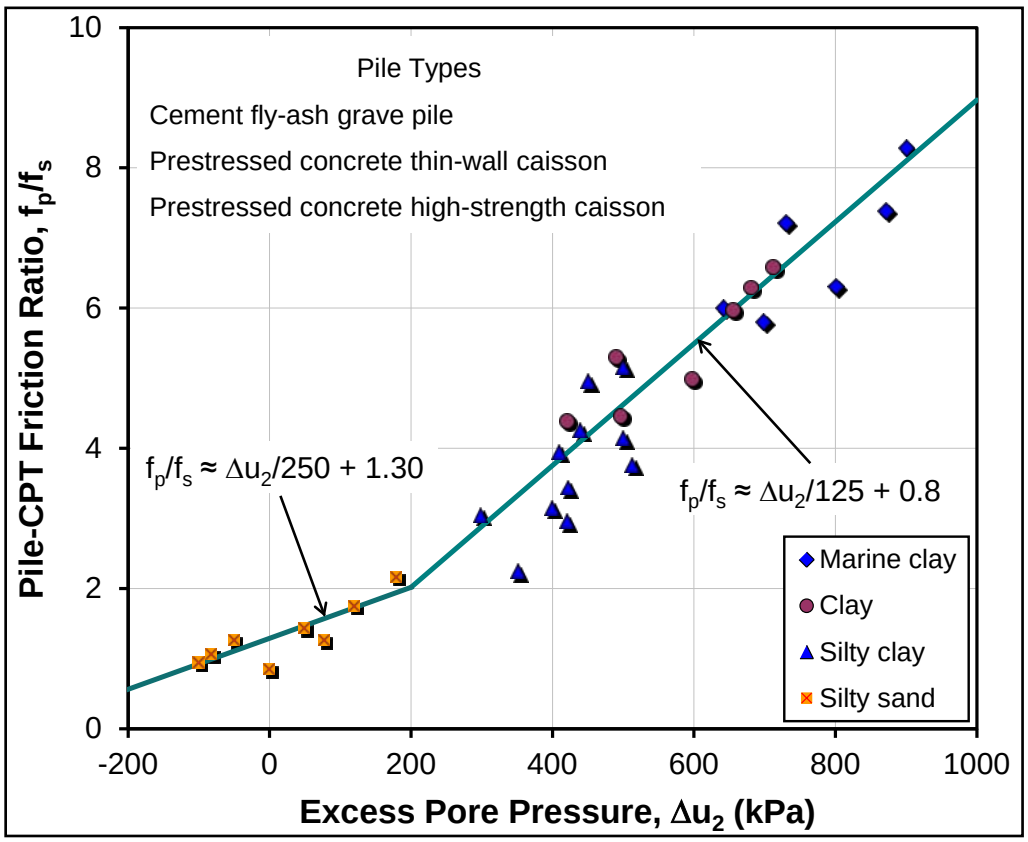

Figure 3.38. Relationship between f_p/f_s and excess pore water pressure based on the CPTu data (after Cai et al., 2012).

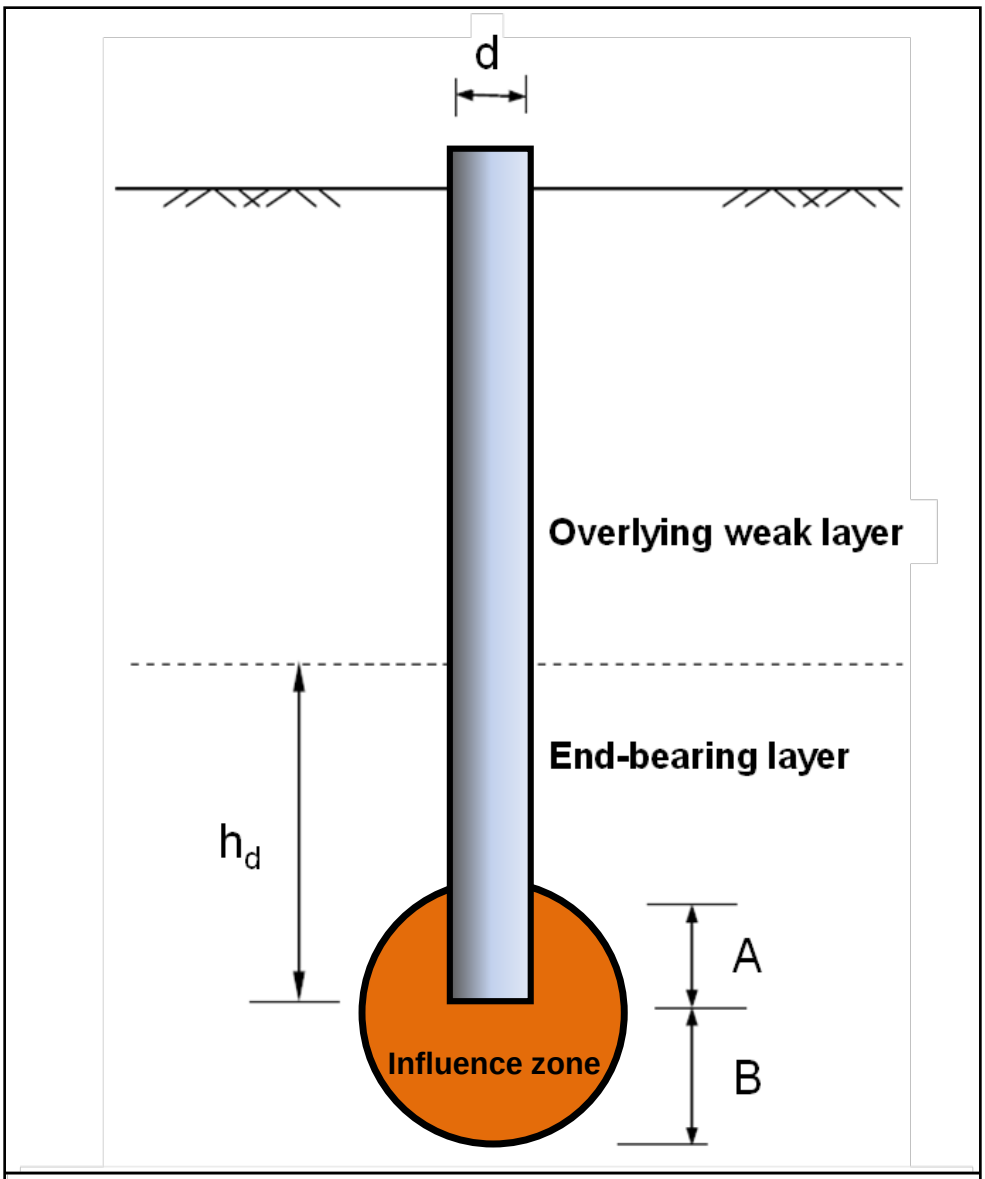

		Range above pile base: A	Range below pile base: B
Case 1 (partial embedment: h_d < 8d)	Extreme variation in qc	8d	1d
	Other situations	1.5d	1.5d
Case 2 (full embedment: $h_d \geq$ 8d)	Embedded in sand of low compressibility	2d	4.5d
	Embedded in sand of high compressibility	1d	2.5d

Figure 3.39. Influence zone for averaging cone tip resistance near pile base (adapted from Yu and Yang, 2012).

3.4 Discussion on CPT-Based Direct Methods

With regard to the selection and implementation of a suitable CPT-based direct method, numerous factors need particular reflection and consideration. Some of these issues are discussed here.

3.4.1 Reliance on CPT Readings and Additional Parameters

It may be noticed from Table 3.7 and Figure 3.1 above that, in essence, there are two tiers of CPT-based direct methods. In one set of methods, referred to herein as *pure-empirical direct methods*, simple direct relationships between CPT readings and f_p and q_b components of pile capacity have been suggested based on the field measurements. Examples include UIUC method, SEU method, German method, KTRI method, UniCone method, Penpile method, and Politecnico di Torino method. For the second type of these CPT methods, listed in Table 3.7 and termed herein as *semi-empirical direct methods*, additional parameters must be evaluated, beyond just reliance on the CPT readings. These additional parameters, measured either via laboratory experimentation and from field investigations, or estimated from CPT-based correlations, include: pile characteristics, pile base conditions (OE vs. CE), plugging vs. coring, installation methods, pile and soil types, pile material, pile-soil interface friction, overburden stress, soil shear strength, soil relative density or plasticity characteristics, soil frictional characteristics.

Some of the methods falling in the category of semi-empirical direct methods take their original concept from the rational methods, i.e., total stress approach or effective stress approach. However, these methods also demonstrate direct use of CPT reading in their design equations/charts. The ICP-05 method, Dutch method, UCD-11 method, TCD-03 method, and UWA-05 method are the examples belonging to this category.

From the list of CPT-based direct methods, 28 methods provide estimates for both f_p and q_b, while the remaining 8 methods account for either f_p or q_b. Figure 3.40

provides an overview of the percent reliance of these methods on the different combinations of readings to estimate f_p and q_b.

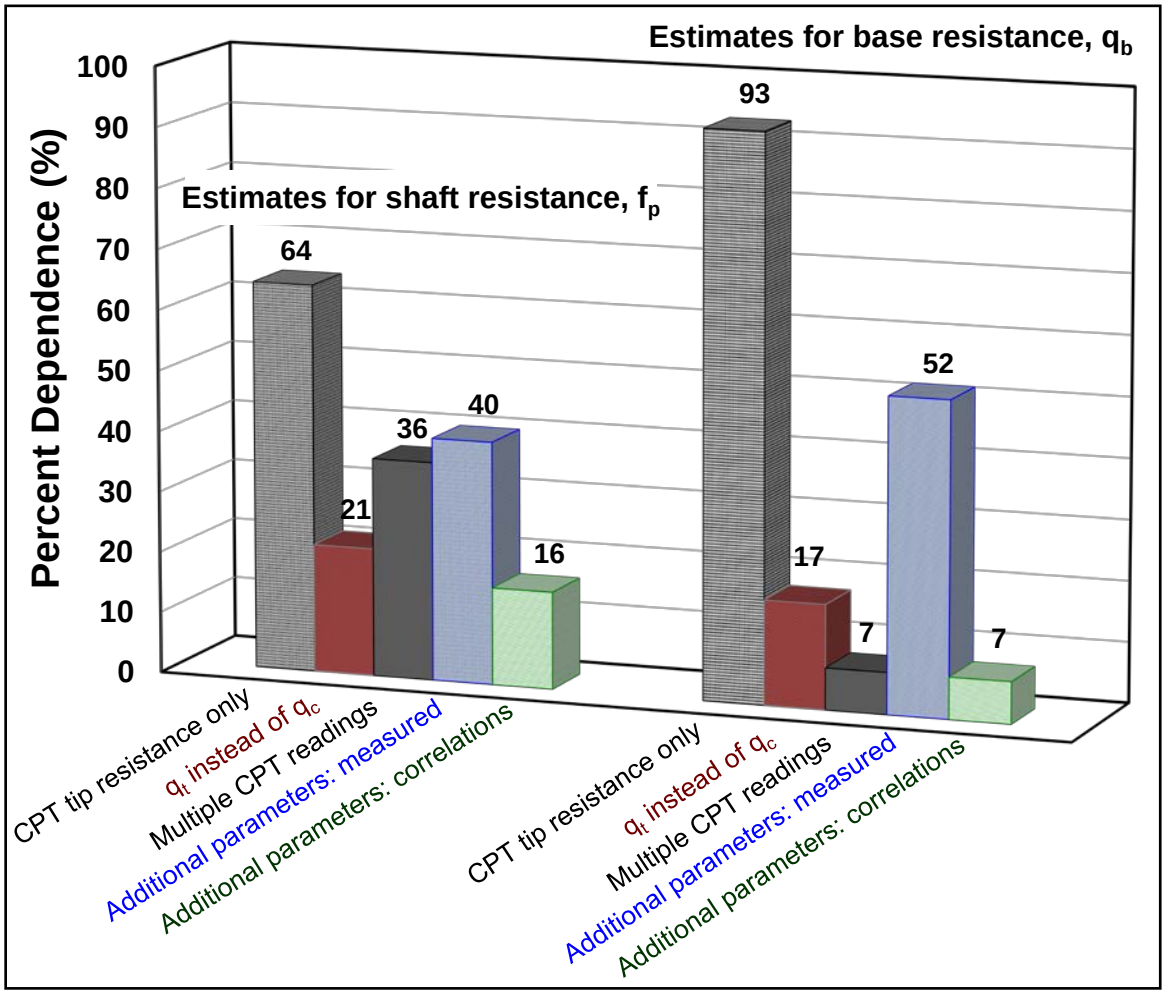

Figure 3.40. Reliance of different CPT-based direct methods on combinations of CPT readings and additional parameters.

3.4.2 Correction of Measured Cone Tip Resistance for the Porewater Pressure

According to the design equations and charts, together with Figure 3.40, most of the CPT-based direct methods rely solely on CPT tip resistance. Only a few draw on multiple readings from the CPTu tests. The methods that utilize tip stress, either solely or in combination with other CPT readings to estimate f_p and/or q_b, generally do not

account for correction of porewater pressures acting on unequal tip area of the cone to obtain corrected tip stress, q_t. The exceptions include Unicone method, KTRI method, SEU method, Togliani (2008) method, and Dutch method. The resistance q_t is given by the following expression:

$$q_t = q_c + (1 - a_n)u_2 \tag{3.5}$$

where a_n = net area ratio of the particular penetrometer determined through calibration in a triaxial chamber, and u_2 is the field excess porewater pressure measured at the shoulder (behind the tip) position. In clean sands and dense granular soils, it may be reasonable to assume $q_t \approx q_c$ because u_2 remains essentially hydrostatic. In soft to stiff intact clayey and silty soils, however, considerable excess porewater pressures are generated during cone penetration, warranting significant corrections to the measured q_c in order to obtain q_t (Mayne, 2007).

3.4.3 Influence Zone for Pile Base Resistance

All the CPT-based direct methods relate unit base resistance to the cone tip resistance (either q_c, or more proper q_t). In doing so, the cone tip resistance data are averaged over a certain depth interval near the pile base. This range of depth is commonly termed as an *influence zone*. Different methods provide different recommendations for the extent of influence zone above and below the pile toe, which have been detailed in Table 3.7. This extent, which is principally taken to account for the rupture path around to the pile toe, has been defined on the basis of different theories, including punching failure, general shear failure, and other regions. Eslami and Fellenius (1997) pointed out that there is no specific evidence to support these theories in relation to the deep foundations. Yet, some recommendations based on limited experimentation and numerical works (e.g., Meyerhof, 1976; DeBeer, 1963; Altaee et al., 1992, Eslami

and Fellenius, 1997) are commonly implemented in practice (see the method specific details in Table 3.7). Various considerations that have led to these recommendations include: (1) the trend of cone tip resistance values around the pile toe, (2) extent of soil variability around the pile toe, (3) pile diameter, (4) pile embedment depth into the bearing soil layer, (5) existence of weak layer beneath the bearing layer, and (6) soil compressibility.

3.4.4 Averaging Technique for Representative Values of Cone Tip Resistance

The averaging technique over the influence zone is another factor to be considered for adopting a representative value of cone tip stress for use in the design equations for unit base resistance. Arithmetic averaging is the most common technique implemented in practice. The CPT readings, typically in coarse grained soils, display squiggly profiles of arbitrary peaks and troughs that may be representative of thin seams of variable soil. However, in relation to their influence on the pile, having a much larger size, retaining such readings while averaging can possibly result in non-representative values of unit base resistance. Therefore, such readings are usually filtered out applying a "minimum path" rule (e.g. Begemann, 1963), or by simply removing the peaks and troughs from the records (e.g., Bustamante and Gianeselli, 1982). Eslami and Fellenius (1997) recommend the use of a geometric averaging technique (i.e., geomean) over arithmetic averaging, since the former automatically results in a filtered representative value.

3.4.5 Shaft and Base Areas for Pile Capacity Calculations

The total axial capacity (Q_t) of deep foundations is calculated from the sum of the shaft capacity (Q_s) and base capacity (Q_b):

$$Q_t = Q_s + Q_b = \Sigma f_{pi} A_{si} + q_b A_b \quad (3.6)$$

where f_{pi} = unit shaft resistance of the i^{th} soil layer through which the pile shaft is embedded, determined from a suitable CPT-based method; A_{si} = shaft area providing frictional resistance with the adjacent soil in the i^{th} layer against axial displacement; q_b is the unit end bearing resistance, also determined from a suitable CPT-based method; A_b is the pile base area.

The shaft area of the i^{th} layer is simply given as the product of the pile perimeter and the layer thickness (Δz_i). For a circular pile, the perimeter is conveniently obtained as $\pi \cdot d_i$, where d_i is the pile diameter in the i^{th} layer. For non-circular solid piles, an equivalent pile diameter can be adopted. Therefore, for square and rectangular piles, equivalent pile diameter, $d_i = (2b_i + 2w_i)/\pi$, where b_i and w_i are the depth and width of the pile cross-section, respectively, in the i^{th} layer. For piles that are not solid (e.g., OE pipe piles, H shaped piles), selection of equivalent pile diameter becomes a bit more complicated, as described subsequently.

For OE driven pipe piles, a soil column enters into the pile through the open base during driving and forms a plug. During the subsequent static loading of the pile, some amount of shaft friction is additionally mobilized along the interface between the soil column and the inner pile wall. However, this fricitonal resistance is accounted for by considering it part of pile base resistance (and so, it is being discussed later). Therefore, the outer diameter of OE pipe pile is used for calculations of its shaft capacity.

For the case for H piles, the contact area contributing to shaft capacity is also complicated. During driving, soil enters the space between the flanges of H piles. Seo et al. (2009) gave the following explanation concerning the shaft area of H piles. "The vibrations during driving cause the soil near the ground surface to detach from the pile. During static loading of the pile, depending on the soil type and state, the soil in the space between the flanges of the pile may behave as a plug and therefore become an integral part of the pile. During loading of the pile, the soil plug may be further compressed or it may slide with respect to the pile. It is difficult to ascertain in practice what occurs at the

time of loading. If the soil in the space between the flanges becomes fully attached to the pile, then the outer perimeter of the H pile is typically used in shaft capacity calculations. Otherwise, the full steel-soil interface contact perimeter, which includes not only the outside and inside of the flanges and their tips but also the web, is used in shaft capacity calculations." Based on load tests on a fully instrumented H pile driven in a multilayer soil, Seo et al. (2009) concluded that assumption of full soil-pile interface contact perimeter results in overprediction of shaft capacity. Accordingly, they recommended two options: (1) consider a reduction factor between 0.41 and 0.88 (average 0.65) when assuming full soil-pile interface contact perimeter; or (2) assume outer perimeter in shaft capacity calculations to get comparable estimates.

The base area (A_b) of a circular solid or CE pipe pile is simply obtained as $\pi \cdot d^2/4$, where d = pile base diameter. For non-circular solid piles of square or rectangular cross-sections, an equivalent base diameter is obtained from: $d = (4\ b \cdot w/\pi)^{0.5}$, where b and w are the depth and width of the pile cross-section at the base, respectively. For OE pipe piles, following the recommendations by Lehane and Gavin (2001), Gavin and Lehane (2005), and Yu and Yang (2012), separate contributions from annulus and plug should be considered (also detailed in Table 3.7):

$$Q_b = (\pi/4) \cdot [d^2 q_{plug} + (d^2 - d_i^2) \cdot q_{ann}] \tag{3.7}$$

where q_{plug} = unit plug resistance of pile; q_{ann} = unit annulus resistance of pile; d = pile outer diameter; d_i = pile inner diameter. Here, q_{plug} accounts for the inner shaft resistance (also pointed out earlier) by incorporating the plug length ratio (PLR = H/L) at the end of pile installation, where H = plug length measured at the end of pile installation, and L = pile length.

For H piles, on the other hand, the base area should be selected depending upon the soil response in the space between the flanges in the influence zone of the pile base.

If the soil in the space between the flanges becomes fully attached to the pile, then the gross cross-sectional area (flange width x depth) should be used, otherwise use the actual cross-sectional area. Since it is difficult to ascertain the actual situation at the time of loading, use of specific formulation for H piles given in ICP-05 method (see Table 3.7) is recommended (also proposed by Seo et al., 2009).

3.4.6 Reference to the Capacity Criteria

The load-displacement (Q – w) curves obtained from axial load tests on pile foundations can exhibit different shapes and results. Only a single value of "axial load capacity" is selected from this entire curve for design load purposes. As for all other geotechnical engineering applications, a common practice in the design of pile foundations is to apply appropriate factors of safety (FS) to this axial load capacity under the allowable stress (ASD) design [also called working stress (WSD) design], the serviceability limit state (SLS) design, or the load and resistance factors (LRFD) design. These FS, in part, account for the inaccuracies and uncertainties of the prediction method.

As noted earlier in Chapters 1 and 2, there are as many as 45 different criteria defining the pile capacity from the load-displacement curves. It has previously been observed that there is no consensus and the capacities interpreted via different criteria span over a wide range (e.g., Niazi 2011). For the most part, the CPT-based direct methods do not explicity refer to any specific capacity criterion on the basis of which the design equations were formulated, thus adding a certain level of uncertainty. Without reference to any specific criterion, the engineer in-charge of a piling project using these methods has to rely considerably on experience and subjective engineering judgment for selecting appropriate FS to strike a balance between economical and safe design.

3.4.7 Pile Setup

The CPT readings in a given soil formation are recorded at a high strain rate of loading corresponding to the penetration rate at 20 mm/s. As such, the measured penetrometer resistances can differ from the pile resistance in long-term behavior, which involves setup and increased capacity over time. Eslami and Fellenius (1997) noted that the CPT methods employ total stress values, whereas effective stress (or the drained characteristics) governs the long-term behavior of piles, especially in clayey soils, following dissipation of excess porewater pressures. In addition, ageing and other rheological effects (i.e., pile "freeze", thixotropy) can occur in clays, silts, and sands following the pile installation.

Pile setup has two major components: (1) short-term setup caused by the dissipation over time of the excess pore water pressures generated during the pile installation, (2) and long-term setup, i.e., additional gain in strength over time at constant effective stress due to other factors, such as secondary compression (creep), bonding, and/or ageing (Konrad and Roy, 1987; Whittle and Sutabutr, 1999; Svinkin and Skov, 2000; Randolph, 2003; Karlsrud and Haugen, 1985; Schmertmann, 1991; Basu et al., 2013). While creep in the surrounding soil may lead to an increase in the horizontal effective stress on the shaft, soil ageing can result in an increase in stiffness and dilatancy effect (Chow et al., 1998). Basu et al. (2013) indicated that the mechanisms of setup and the setup periods are different for fine-grained and coarse-grained soils, because of the drainage characteristics and other intrinsic properties of these geomaterials that affect the soil-structure interactions and their response to the loading.

In any direct pile-CPT correlations, the shaft and toe correlation coefficients (C_{se} and C_{te}, respectively) were derived by comparing a specific set of readings from the database of cone penetrometer tests (q_t, u_2, f_s) with the pile capacity components (f_p and q_b) from a corresponding foundation load dataset at their respective sites. As such, these load tests were conducted (mostly as a one-time measurement) over a variable span of

time subsequent to the pile installation. From that fact, the approximations for these correlations, implicitly account for the pile setup effects.

In order to rationally incorporate the effects of pile setup in the proposed correlations, a set of multiple load tests at each of these sites should have been conducted, starting immediately after the pile installation and at regular intervals thereafter (e.g., one month, one year, 3 years). With availability of such data, more definitive correlations could be developed between the CPT readings and the load test results from the first time pile loading, and then setup effects could be included, based on soil and pile typology, using adjustment factors derived from the subsequent sets of load tests on the same piles. Note that loading and reloading of the same pile at increasing times does not provide reliable information, as each loading changes the geostatic and frictional stress regimes around the pile; i.e. altered K_o and reduced ϕ'_p to $\phi'_{softened}$, plus time effects.

Selected works addressing pile setup with time are summarized in Table 3.8. These studies have focused on the setup phenomenon in both sandy as well as clayey soils. However, clearly the majority of these studies have investigated driven and jacked pile foundations in the full-displacement category, with little or no attention to the bored piles (or drilled shafts) and augered pilings in the category of non-displacement and partial-displacement type foundations. Since the databases used in some of the CPT - based methods consist of a variety of pile types, an important research need is felt that quantification of pile setup should also be explored for different pile types in similar or comparative studies.

Table 3.8. Summary of selected studies on pile setup.

Source/ Reference	Title of study	Database summary	Pile types/material	Soil type	Length (m)	diameter (mm)	Set-up time after EOD (days)
1. Axelsson (2000); 2. Axelsson (2002)	1. Long-term set-up of driven piles in sand 2. A conceptual model of pile set-up for driven piles in non-cohesive soil	196 load tests on 75 piles at 17 sites	Driven concrete hexagonal pile, steel H-pile, concrete square pile	Sand, gravel, silty sand, sandy silt	8.5 – 47.0	270 – 915	16 – 3,310
Basu et al. (2013)	Shaft resistance and setup factors for piles jacked in clay	Finite element model using an advanced plasticity-based constitutive model	Jacked piles	London clay, San Francisco Bay Mud	Variable in the model	Variable in the model	Variable in the model
Bullock et al. (2005a; b)	1. Side shear setup I: Test piles driven in Florida 2. Side shear setup II: Results from Florida test piles	25 O-cell load tests on 5 piles at 5 sites	Driven concrete square piles	Dense fine sand, soft to medium stiff silty clay, and fine sand	9.2 – 25.1	457	0.25 – 1,727
Chow et al. (1998)	Effects of time on capacity of pipe piles in dense marine sand	11 load tests on 4 piles at one site	Driven pipe piles	Medium to very dense Dunkirk sand	11.1 – 22.1	324	159 – 2,055
Doherty and Gavin (2013)	Pile aging in cohesive soils	71 load tests on 16 piles at 9 sites	Driven piles	Clay	5.0 – 70.0	100 – 762	4 – 9,125

Note: EOD = end of driving.

Table 3.8. (continued).

Source/ Reference	Title of study	Database summary	Pile types/material	Soil type	Length (m)	diameter (mm)	Set-up time after EOD (days)
Erbland and McGillivray (2004)	Effects of pile setup on pile design and construction – a case history	14 load tests on 8 piles at one site	Driven piles	Silty to clayey sand	13.0 – 29.0	610	1 – 100
Komurka et al. (2005)	Applying separate safety factors to end-of-drive and set-up components of driven pile capacity	Load tests on 3 piles at one site	Drive pipe piles	Clayey soil	27.5	324 – 406	1 – 200
Long et al. (1999)	Measured time effects for axial capacity of driven piling	80 load tests	Driven steel H-pile, steel pipe pile, concrete square pile, concrete circular pile, timber/wood	Sand, clay, mixed soil	6.7 – 91.5	152 – 610	1 – 1,000
Ng et al. (2013a; b)	1. Pile setup in cohesive soil I: Experimental investigation 2. Pile setup in cohesive soil II: Analytical quantifications and design recommendations	28 load tests on 5 piles at one site	Driven steel H-piles	Clayey soil	14.6 – 17.5	HP 250 x 62	1 – 10
Yang and Liang (2009)	Incorporating setup into load and resistance factor design of driven piles in sand	190 load tests on 73 piles at 13 sites	Driven concrete hexagonal pile, steel H-pile, concrete square pile, steel pipe pile, monotube pile	Loose to dense, fine to coarse sand, gravel, and silty sand	8.5 – 45	305 – 915	1 – 550

Note: EOD = end of driving.

3.5 Concluding Remarks

A concise review of various rational and direct CPT-based methods that focus on axial pile capacity estimation was presented. Accordingly, a comprehensive listing of these methods and their respective design formulations were organized along with information on their applicable pile and soil types. Various design graphs/charts of different methods were also presented. This will serve as a single convenient resource for the practitioners and researchers working in CPT-based pile design and analysis.

The direct methods offer more convenience in their straightforward approach, while the indirect methods are considered more rational as their formulations have been founded on well developed theories.

The design equations and their corresponding charts presented in this chapter are based on empirical methods and theoretical basis, as well as field and laboratory experimentation. Some of these methods are applicable to a wide variety of soils and pile types, while others concern only to specific limited cases. The suitability for use of these methods is dictated by the variety of pile and soil types included in the databases of their respective studies. Of prominance are the larger databases used in the formulation of UniCone method, LCPC method, German method, and UIUC method. Randolph and Wroth (1982) emphasized that empirical approaches may work well in familiar situations, but there will inevitably be uncertainty when novel structures or new types of soil deposits are encountered. Eslami and Fellenius (1997) also noted for UniCone method that the number of cases used was limited, and further correlation experience will result in adjustments of the correlation coefficients used in the design equations. Similarly, Doherty and Gavin (2011) indicated a similar observation on the extension of such methods to the design situations which are outside the scope of the databases used in their respective derivations.

It is clearly evident from the chronological evolution of CPT-based methods that most of the past research and developments (even in the recent years) have addressed driven pipe piles in sands, mostly for the offshore environment. In particular, much less efforts have been directed towards drilled shafts in clays, silts and/or sands.

It is noted that the existing CPT-based methods focus only on an estimate of "axial pile capacity", without recourse to the behavior in terms of the complete load-displacement-capacity response.

In view of the above, it is reasonable to suggest the following:

- Due care must be exercised in applying these empirical approaches to field situations of relevance encountered in design practice. Engineering judgement must be the hallmark for interpretation of the data.
- The reliability of no single method may be regarded as ultimate or universal. The more recent methods that exploit maximum geotechnical parameters from the CPT, and which were developed from larger and latest database of pile load tests may be considered for prediction analysis. However, the results must be checked and validated against the estimates of other recent direct methods as well as the rational methods before finalizing the design.
- Evolution of these methods must continue by supplementing the database with newer piles and latest geotechnical site investigations using the modern multi-channel hybrid geophysical-geotechnical SCPTu. This will enable newer correlation experiences in order to improve the understanding of various mechanisms involved in axial pile behavior and enhance the scope and reliability of such empirical/semi-empirical as well as analytical design methods.
- With the newer multi channel cone penetrometers (i.e., SCPTu), optimal use of all the readings must be made for connecting those to the axial pile response in terms of complete load-displacement-capacity.

- Future work on pile-CPT correlations must attempt to include all soil types in general and clays, silts and mixed soil types, in particular. Any developments in this regard must explicitly indicate the measurement basis for f_p and q_b from their datasets, and the average relationships thereof with some of the more frequently used capacity criteria.

CHAPTER 4

REVIEW OF SETTLEMENT ANALYSIS METHODS FOR PILE FOUNDATIONS

Synopsis

This chapter presents a comprehensive review of the analyses and design methodologies developed during the last six decades in the realm of pile deformations under applied axial working loads in compression. A broad classification of different methodologies is presented, along with a comprehensive table listing different research works accomplished in this direction. These include designs using empirical formulations, analytical solutions, load-transfer (τ-z) methods, numerical methods, variational approaches, and those employing hybrid methods. The application include situations of piles installed in homogeneous soils where the soil stiffness along the pile can be considered constant, Gibson soils for the case of linearly increasing soil stiffness, and others where the soils can be treated as layered media with each layer having its own characteristic stiffness. The analytical solution by Randolph and Wroth (1978; 1979) is covered in more detail since it is simple and convenient in application with extended use in uplift and bidirectional O-cell types of loadings, as well as modeling a stacked pile solution for layered soil profiles.

Various shear stiffness reduction schemes are also reviewed for their applicability in representing the nonlinear load-displacement (Q-w) response of axially loaded piles. These include algorithms derived mostly from laboratory experiments on soil samples in resonant column, triaxial, simple shear, and torsional shear tests. It is identified that the most appropriate scheme applicable to static axial loading of pile foundations is the one that can be derived from the back-analyses of actual load tests within the framework of analytical elastic solution.

4.1 Introduction

The deformation analysis of pile foundations under working loads has been a topic of great interest in the soil-structure interaction problems. Three aspects of the pile response to loading may be identified: (a) the pile-head settlement at working load; (b) the distribution of axial load down the pile; and (c) the degree of the interaction between piles within a group (Guo and Randolph, 1997). Aspects (a) and (b) above will be the focus of this chapter, while analysis of pile groups is beyond the scope of this overall research work, and will not be discussed further.

Many methods of analysis are available for predicting the settlements and the load-transfer of axially loaded piles. In this chapter, an effort will be made to briefly discuss and summarize different varieties of such methods that have evolved in the past six decade.

4.2 Classification of Design Methods for Pile Settlement Analysis

The theoretical methods of settlement of piles and pile groups under axial compression loading can be gathered into the following six broad categories (Poulos, 1989; Southcott and Small, 1996; Zhang et al., 2010) (also see classification chart in Figure 4.1):

- *Empirical Methods*, not founded on soil mechanics principles, where parameters are simply determined from in-situ or laboratory tests, providing direct correlations.
- *Simplified Analytical Methods*, which consider the vertical displacement of the soil induced by the shaft shear stress as a logarithmic relationship of the radial distance away from the pile shaft.
- *Theoretical Load-Transfer Curve Methods*, or the so-called $\tau - z$ curve methods, which use a load-transfer function and model the soil as a series of disjointed springs with spring constants defined in a variety of ways, to describe the

relationship between the unit resistance transferred to the surrounding soil and the pile-soil deformation behavior in each soil layer.

- *Numerical Methods*, which include: (1) *Finite Element Method* (*FEM*), most suitable for pile deformations in dealing with a set of complicated factors such as soil non-homogeneity and anisotropy by means of varied constitutive soil modeling; (2) *Boundary Element Methods* (*BEM*), employing either load-transfer (τ-z) functions to characterize the interaction response, or elastic continuum theory to represent the soil mass response (the pile-soil interface is discretized and the characteristics of the soil response are represented in a lumped form by ascribing the behavioral features of the soil to the interface elements); (3) *Finite Layer Methods* (*FLM*), where the soil continuum is discretized into finite layers on infinite horizontal extent, and the nodes are defined only along the length of each pile segment, in effect reducing the discretization to one dimension; and (4) *Integral Equation Analysis*, based on solution by Mindlin (1936) for a point load acting in an elastic half space, described in detail by Poulos and Davies (1968) and Butterfield and Banerjee (1971).
- *Variational Approach*, applies principle of minimum potential energy to determine the deformation of piles, where both displacements and shear stresses are each represented by a finite series.
- *Hybrid Approach*, which combines the procedures of more than one method in developing solutions and/or calibrations with the other.

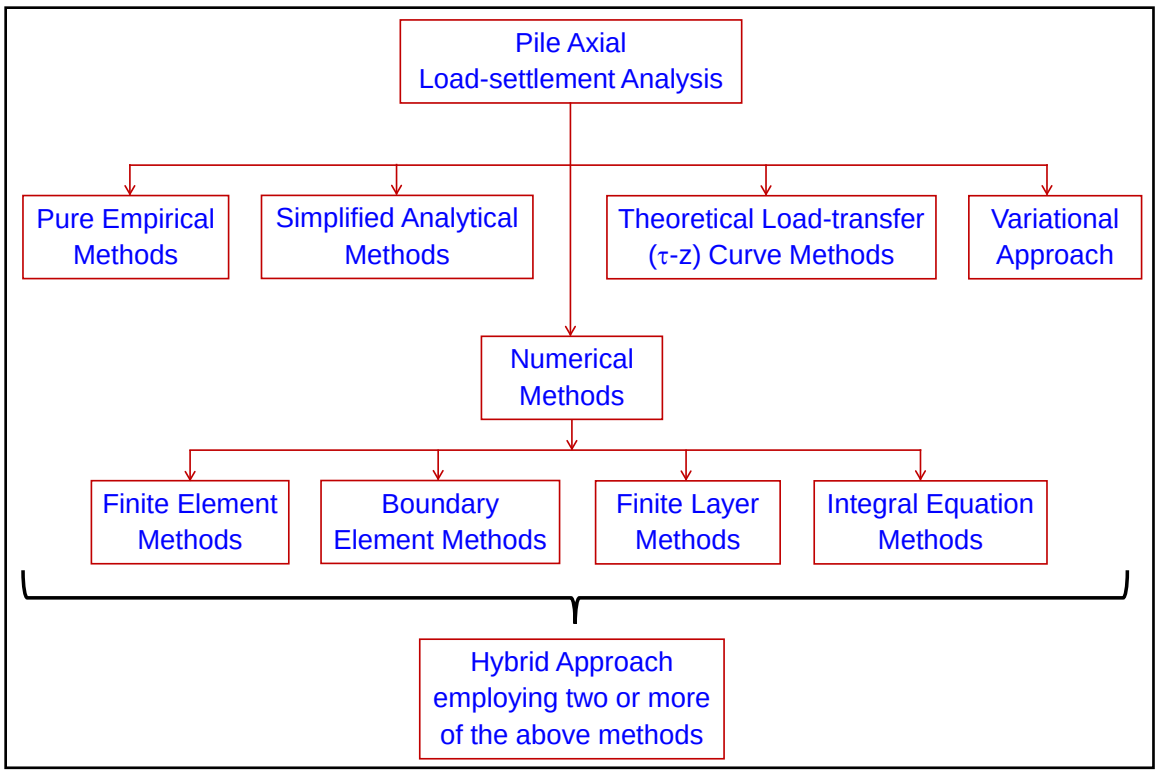

Figure 4.1. Classification chart showing methods of analysis for predicting the settlements of axially loaded piles.

In choosing an appropriate category of analysis and design procedure for a practical problem, the following factors need to be considered (Poulos 1989): (a) the significance and scale of the problem; (b) the available budget for foundation design; (c) the geotechnical data available; and (d) the complexity of both the geotechnical profile and the design loading conditions.

Most of the earlier methods and some of the later ones developed their formulations on Mindlin's point load solution for a homogeneous half-space. Mindlin (1936) presented his solution of the three-dimensional elasticity equations for a homogeneous isotropic solid for the case of a concentrated force acting in the interior of a semi-infinite solid. This represents the fundamental solution having a singular point in a solid bounded by a plane. Mindlin (1936) suggested that from his solution may be derived, by a known method of synthesis, the solutions for the semi-infinite solid. This

suggestion has been exploited by many researchers in the field of pile foundation analysis and design to simulate the pile-soil interaction response, and thus today a large majority of theoretical pile design methods are founded on this solution.

Numerical simulations are considered as the most powerful approaches for the analysis of the behavior of single piles or pile groups. However, their high computational requirements demand complex programs that are not convenient for practical engineering (Zhang and Zhang, 2012). For instance, FEM methods are cumbersome, requiring considerably greater data preparation time and computation time, which makes them too expensive for routine analysis, and therefore, less attractive for practical purposes. Such analyses are valuable in leading to a better understanding of the details of pile behavior, but are unlikely to be readily applicable to practical piling problems because of their complexity and considerable number of required geotechnical parameters (Poulos, 1989). In contrast, empirical methods may be uncertain or unreliable, specifically to situations falling outside of the database from which these were derived, leading to either conservative, and thus uneconomical designs or to solutions which may undesirably render the structure unsafe.

In this regard, the simplified analytical methods, founded on sound theoretical principles and calibrated against alternative methods, offer a better and rational option for practical engineering purposes. Example of such methods includes the one proposed by Randolph and Wroth (1978; 1979) and later adopted by other researchers and updated (e.g., Fleming et al., 1992; Guo and Randolph, 1997; Randolph, 2004; 2007). A summary of this solution will be detailed in a later section of this chapter.

For the purpose of a quick review, Table 4.1 presents a comprehensive list of different design formulations derived in the realm of pile settlement analysis. Although comprehensive, it is still not all-encompassing, as other research studies have also reported similar works by employing one or more of the methodologies listed in this

table. The sole purpose of including this table is to give an overview of the variety and versatility of methods offered for settlement analysis of pile foundations.

Table 4.1. Summary of selected studies in axial pile displacement analysis.

Source/reference	Category of analysis and design procedure	Modeling scheme	Applications
Meyerhof (1959)	Empirical correlations	Approximate correlations with pile diameter	Single driven piles and displacement caissons, and pile groups in sandy soils
Coyle and Reese (1966)	Non-linear load transfer (τ-z) curve	Correlation between the ratio of load transfer to soil shear strength and pile movement in each geological stratum	Steel friction piles in clay
Focht (1967)	Empirical correlations	Column deflection multiplied by a factor	Steel friction piles in clay
Poulos and Davis (1968)	Load transfer (τ-z) method	Analysis using integral equations on Mindlin's point load solution on pile considered as a number of uniformly loaded cylindrical elements together with a uniformly loaded circular base	Single incompressible piles installed in homogeneous compressible soil
Butterfield and Banerjee (1971)	Analytical method	Rigorous analysis based on Mindlin's solution for a point load in the interior of an ideal elastic medium	Rigid and compressible single piles and pile groups embedded in a homogeneous isotropic linear elastic medium
Vesić (1977)	Hybrid empirical, analytical elastic and load-transfer (τ-z) methods	Total settlement treated as sum of elastic pile compression, pile settlement caused by the load at the pile toe, and that caused by the load transmitted along the pile shaft	Single compressible piles in elastic medium
Vijayvergiya (1977)	Empirically derived load transfer (τ-z) functions	Correlations with pile diameter and pile penetration depth	Single bored piles in multi-layered soil medium
Poulos (1979)	Analytical method	Double integration of the Mindlin's equation for vertical displacements of the soil due to the shear stress along the pile shaft	Single piles in Gibson soil, and 3-layered non-homogeneous soil

Table 4.1. (continued).

Source/reference	Category of analysis and design procedure	Modeling scheme	Applications
Randolph and Wroth (1978; 1979)	Analytical method	Vertical displacements of the soil induced by the shaft shear stress considered as a logarithmic relationship of the radial distance away from the pile shaft	Single compressible pile in two layered soil medium
Poulos and Davies (1980)	Boundary element formulation for elastic solution	Analysis based on Mindlin's solution for a point load in the interior of an ideal elastic medium	Single compressible pile in two layered soil medium
Kraft et al. (1981b)	Load-transfer (τ-z) approach	Radial variation of the operative shear stiffness varies linearly	Single pile in homogeneous and Gibson type soils
Frank (1985)	Empirical correlations	Approximate correlations with pile diameter	
Jardine et al. (1986)	Finite element method	Assumption of small strain non-linearity instead of soil linear elastic behavior	Compressible single piles and pile group in low plasticity homogeneous clay
Chow (1987)	Axisymmetric finite element approach	Decomposition of the problem into 2 systems: (1) the group piles acted upon by external applied loads and pile-soil interaction forces, and (2) layered soil continuum acted upon by a system of pile-soil interaction forces at the imaginary positions of the piles	Axially and laterally loaded pile groups embedded in nonhomogeneous soils
Guo et al. (1987)	Non-linear load transfer (τ-z) functions	Soil modeled as a product of polynomial and series expansions of displacement shape functions in vertical and radial directions of infinite layer approach; pile modeled as solid bar elements	Single pile in infinite layered soil medium
Reese and O'Neill (1988)	Non-linear load transfer (τ-z) curves	Relationship between unit resistance transferred to the surrounding soil and displacement of the pile relative to the soil in each geological stratum	Single pile in multi-layered soil medium

Table 4.1. (continued).

Source/reference	Category of analysis and design procedure	Modeling scheme	Applications
McVay et al. (1989)	Non-linear load transfer (τ-z) curves	Relationship between unit resistance transferred to the surrounding soil and displacement of the pile relative to the soil in each geological stratum	Single pile in multi-layered soil medium
Chin et al. (1990)	Elastic continuum boundary element method	Soil flexibility coefficients evaluated using the analytical solutions for a layered elastic half space	Axially loaded piles and pile groups in homogeneous, finite layered soil, and end-bearing on stiffer stratum
Rajapakse (1990)	Variational method	Boundary integral representation based on exact displacement and traction Green's functions (evaluated by using numerical integration) to model the response of the surrounding soil	Single elastic pile embedded in a linearly non-homogeneous incompressible elastic (Gibson) soil
Chin and Poulos (1991)	Hybrid approach: load-tranfer (τ-z) curves and analytical solution	Layered soil approximated as Gibson type	Single piles and pile groups embedded in layered soil medium, approximated as Gibson soil
Lee (1991)	Discrete layer load transfer (τ-z) approach	Linear elastic solutions in a soil profile arbitrarily layered and underlain by either a stiff/rigid stratum (Mindlin's point load solution applied)	Piles and pile groups embedded in finite soil layers
Lee and Small (1991)	Finite layer method	Pile represented as 1D, 2-noded elastic cylindrical solid elements; soil considered as a series of horizontal, isotropic or cross-anisotropic elastic layers of infinite lateral extent, subjected to a system of interaction forces acting at the pile-soil interface	Single piles in isotropic and anisotropic layered soils.
Trochanis et al. (1991a; b)	Finite element method	Pile-soil slippage and separation, and the effect of nonlinear soil behavior on the response of single and pair of piles is modeled using 3D FEM elasto-plastic formulation	Single and pair of piles

Table 4.1. (continued).

Source/reference	Category of analysis and design procedure	Modeling scheme	Applications
Fleming et al. (1992)	Analytical method	A method of linkages, using hyperbolic functions (with definition of origin, asymptote and either initial slope or a single point on the function), elastic soil parameters and ultimate load are used to describe individual shaft and base performance	Single compressible piles
Lee (1993)	Hybrid layer approach	Superposition of the interaction factors between piles within a group in homogeneous and nonhomogeneous soils, computed by the analytical model	Large pile groups with different pile configurations and compressibility, embedded in isotropic elastic half-space
Kodikara and Johnston (1994)	Load transfer (τ-z) approach	Incorporating strain hardening region prior to peak strength for derivation of τ–z curves	Compressible axially loaded cast in-situ large diameter piles in rock
Motta (1994)	Load transfer (τ-z) approach	Use of elastic-perfectly plastic τ-z bilinear curves	Single long friction piles
Southcott and Small (1996)	Finite layer method	Soil idealized as finite layers of infinite horizontal extent, and use of Hankel transform to simplify the equations forming the soil stiffness matrix	Single piles and pile groups in non-uniform soils
Vallabhan and Mustafa (1996)	Variational approach	Use of continuum mechanics principles; distribution of the work done by the applied load as compressive strain energy in the pier, and as shear strain energy in the soil, as well as, the compressive strain energy in the soil surrounding the pier and at the bottom of the pier	Single piles in elastic soil
Guo and Randolph (1997)	Hybrid Load transfer (τ-z) and analytical solution	Calibration of the relationship between load transfer spring stiffness and elastic soil properties to consider the effect of non-homogeneity for the case of elastic-perfectly plastic soil response with stiffness varying as a power law of depth	Single piles in elastic-plastic, nonhomogeneous soil medium

Table 4.1. (continued).

Source/reference	Category of analysis and design procedure	Modeling scheme	Applications
Mandolini and Viggiani (1997)	Boundary element method	Simulation of soil nonlinearity by concentrating it at the pile-soil interface; while in the linear range, the accuracy is checked against known benchmark solutions	Piled rafts
Guo (2000a)	Hybrid Load transfer (τ-z) and analytical solution	Extension of Guo and Randolph (1997) approach in nonhomogeneous, elastic-plastic soil to account for nonzero shear modulus at ground surface	Single piles in non-homogeneous soils with non-zero stiffness at ground surface for overconsolidated soils
Guo (2000b)	Load-transfer (τ-z) approach	Non-linear viscoelastic shaft and base load transfer models, based on integration of a generalized viscoelastic stress-strain model for the soil	Single piles in non-homogeneous soils
Shen et al. (1997; 1999; 2000)	Variational approach	Application of the principle of minimum potential energy to determine the deformations of piles by representing deformations analytically as a function with a set of undetermined constants	Piles and pile groups in homogeneous soils and soils with stiffness varying with depth
Guo and Randolph (1999)	Hybrid Load transfer (τ-z) and analytical method	Extension of Guo and Randolph (1997) model to piles within a group	Elastic settlement of very large pile groups in elastic, nonhomogeneous media
Lee and Xiao (1999)	Variational approach	Extension of Vallabhan and Mustafa (1996) model for layered soil profile, where the displacement shape function of each soil layer is given as the product of an exponential equation along the pile depth and Bessel's solution in the radial direction	Single piles in layered soil
Mendonça and De Paiva (2000)	Boundary element method	Interactions between the plate, the pile and the soil are simultaneously considered, treating soil as a linear homogeneous half space, approximating shear force along each pile in the group by a 2^{nd}-degree polynomial	Piled rafts

Table 4.1. (continued).

Source/reference	Category of analysis and design procedure	Modeling scheme	Applications
Mylonakis (2001)	Analytical method	Depth dependent Winkler springs are used in modeling soil reaction along the pile in homogeneous elastic soil stratum	Single piles in homogeneous soils
Zhu and Chang (2002)	Load-transfer (τ-z) approach	The nonlinear stress-strain behavior of the soil is incorporated into the τ-z curves by considering the nonlinear elastic properties and modulus degradation characteristics of the soil	Single piles in homogeneous and non-homogeneous soils
Xiao et al. (2002)	Load-transfer (τ-z) approach	Load transfer function obtained from the differential equations based on the hyperbolic function, while the analytical solution of the τ-z curve obtained through a series of mathematical derivations	Large diameter piles (diameter > 3 m)
Castelli and Motta (2003)	Load-transfer (τ-z) approach	Use of an incremental procedure taking into account the decrease of the stiffness parameters with increase of the applied load, employing hyperbolic function to simulate non-linear behavior of shaft and base resistance	Single piles and pile groups
Whittle (2003)	Analytical method	Extension of Randolph and Wroth (1978; 1979) approach to layered-soil deposit	Single piles in layered soil deposit
Sheng et al. (2005)	Finite element method	Simulation of pile-soil interaction during installation and loading for large-deformation frictional contact between two or more solid bodies, while soil is treated as a modified Cam clay material and pile as a rigid body	Push-in piles
Cairo and Conte (2006)	Analytical method	Use of dynamic stiffness matrices to simulate the response of layered soils in linear elastic analysis, subsequently including the nonlinearly effects	Single piles and pile groups in layered soils

Table 4.1. (continued).

Source/reference	Category of analysis and design procedure	Modeling scheme	Applications
Randolph (2007)	Analytical method	Extension of Randolph and Wroth (1978; 1979) approach to torsional and lateral loadings, and analysis of pile groups	Single compressible piles and pile groups in two layered soil medium
Basu et al. (2008)	Variational approach	Extension of Vallabhan and Mustafa (1996) approach to rectangular cross-section piles and derivation of differential equations governing the pile and soil displacements using energy principles	Single rectangular cross-section piles in multi-layered soils
Ai and Han (2009)	Boundary element method	The solution for vertical and horizontal axisymmetric ring loads in multi-layered soil applied to the pile with bottom treated as fixed boundary	Single piles in multi-layered soil medium
Said et al. (2009)	Finite element method	2D axisymmetric numerical analysis incorporating the pile-soil installation effects, while the residual loads and shear stresses along the shaft and that around the base are quantified via empirical correlations	Single piles installed in sand
Zhang et al. (2010); Zhang and Zhang (2012)	Analytical approach	Two models: (1) hyperbolic approach to describe the nonlinear relationship between the shaft shear stresses and the displacement surrounding the pile shaft; and (2) bilinear hardening model to simulate the relationship between identical piles including shaft and base interaction in multilayered soil	Single piles and pile groups in multilayered soils

4.3 Analytical Elastic Continuum Solution by Randolph and Wroth (1978; 1979)

Randolph and Wroth (1978; 1979) presented an approximate analytical elastic solution for pile-soil interaction for representing the load-settlement relationship for single pile foundations. It was developed for piles loaded in top-down axial compression mode, embedded in a linear elastic two-layered soil model with the boundary lying at the pile tip elevation (see Figure 4.2, where different terms of the solution are also explained). This analysis assumes elastic stiffness properties for the soil layers. Furthermore, their initial solution employs simplifying assumptions, such that responses of pile shaft and tip are initially treated separately, i.e., the settlements around the pile shaft are due to the shaft load, and those of the tip are due to tip load only, and that the pile material is stiff enough to render pile as rigid [i.e., for any load applied at the pile top (Q_t), the settlements are same all along the pile length, including top-settlements (w_t) and tip-settlements (w_b)]. The rigid pile solutions are presented below:

$$w_t = \frac{Q_t}{G_L\, r_o \left[\frac{4\eta}{(1-\upsilon_s)\xi} + \frac{2\pi\rho_E\, L}{\zeta\, r_o}\right]} \tag{4.1}$$

$$\frac{Q_b}{Q_t} = \frac{1}{\left[1 + \frac{\pi\rho_E(1-\upsilon_s)\xi\, L}{2\,\zeta\,\eta\, r_o}\right]} \tag{4.2}$$

$$w_b = w_t \tag{4.3}$$

where w_t = total settlement at the pile top; Q_b = tip load; G_L = operative soil shear modulus at the reference depth of pile base (z = L); $r_o = d_s/2$ = radius of pile shaft; $\eta = r_b/r_o$ = eta factor for underreamed piles that take greater loads at pile base; $r_b = d_b/2$ =

pile base radius for underreamed piles; ν_s = Poisson's ratio of soil; $\xi = G_L/G_b$ = factor for end bearing piles resting on stiffer stratum (where $G_b > G_L$); G_b = soil shear modulus below pile base (for z > L); $\rho_E = G_M/G_L$ = modulus variation factor; $G_M = [G_o + G_L]/2$ = operative soil shear modulus at mid of pile embedment depth; G_o = operative soil shear modulus at the ground surface (at pile top, where z = 0); L = embedded pile length; $\zeta = \ln(r_m/r_o)$ = measure of average radius of influence in the surrounding soil mass affected by shearing stresses around the pile; $r_m = L\cdot\{0.25 + \xi\cdot[2.5\ \rho_E\cdot(1 - \nu_s) - 0.25]\}$ = average maximum influence radius along the embedded length of the pile [at this radius the shear stresses become negligible (Cooke, 1974; Cooke et al., 1979)].

The solutions for rigid piles were then modified by incorporating appropriate considerations to account for the pile compressibility, thereby presenting solutions for the assessments of separate settlements at the pile top and tip for compressible piles. These modifications were applied by introducing the measure of pile compressibility $\{\mu L = [2/(\zeta\lambda)]^{0.5}\cdot L/r_o\}$, and the factor for pile-to-soil stiffness ratio ($\lambda = E_p/G_L$), where E_p = pile modulus. The solutions are presented below:

$$w_t = \frac{Q_t\left[1+\frac{4\eta\ \tanh(\mu L)L}{\pi\lambda(1-\upsilon_S)\xi\,(\mu L)\,r_o}\right]}{G_L\,r_o\left[\frac{4\eta}{(1-\upsilon_S)\xi}+\frac{2\pi\rho_E\tanh(\mu L)L}{\zeta\,(\mu L)\,r_o}\right]} \tag{4.4}$$

$$\frac{Q_b}{Q_t} = \frac{\left[\frac{4\eta}{(1-\upsilon_S)\xi\cosh(\mu L)}\right]}{\left[\frac{4\eta}{(1-\upsilon_S)\xi}+\frac{2\pi\rho_E\tanh(\mu L)L}{\zeta\,(\mu L)\,r_o}\right]} \tag{4.5}$$

$$\frac{w_b}{w_t} = \frac{1}{\cosh(\mu L)} \tag{4.6}$$

The usefulness of this solution may be explained from the following:

- The solution accounts for piles in homogeneous soils (i.e., constant soil stiffness with depth) as well as Gibson-type soil models (i.e., linearly-increasing soil stiffness with depth).
- It covers floating-type piles and end-bearing type piles. For floating-type piles the stiffness properties beneath the pile base do not contrast significantly from those above the pile base, whereas for end-bearing type piles the base rests on a much stiffer stratum.
- The solution enables evaluation of the fraction of load transferred to the pile base (Q_b) for each stage of total top loading (Q_t).
- Allows derivation of separate load-displacement curves for shaft as well as base (i.e., Q_t vs w_t, Q_s vs w_t, Q_b vs w_t, and Q_b vs w_b).
- Accounts for the compressibility of the pile material via a measure of pile compressibility (μL) and pile-to-soil stiffness ratio (λ).

While the solutions are quite versatile, they still carry following limitations in their original forms presented above:

- Evaluation of the soil deformation properties is probably the most delicate phase of the analysis of load–settlement (Q-w) performance of a single pile. The mechanical non-linearity is exhibited in the form of soil stiffness that softens with shear strains exceeding the linear threshold value (γ_{tl}), resulting in marked reductions in shear moduli for small-, intermediate-, and large-strains. The original solutions do not explicitly account for the non–linear soil stiffness softening at increasing loads which is a physical phenomenon observed in all types of geomaterials. This creates principal difficulty in the selection of elastic

stiffness properties of soil for use in this solution to estimate settlements corresponding to varying levels of load.

- Not all field situations present simple homogeneous or pure Gibson soil profiles for which the solutions were derived, thus warranting appropriate modifications to account for alternative soil models.
- These solutions cannot be applied directly to the case of piles subjected top-applied axial tension (or uplift loading), without appropriate modifications.
- Similarly, the solutions need to be modified for predicting the response of the newer bi-directional O-cell loading arrangements.
- Effects of differences in the pile types and installation methods (i.e., driven vs. jacked vs. bored vs. augered) on the axial load response are not explicitly addressed in the solution.
- In addition, the original model does not account for the concept of progressive failure with depth where the shaft resistance mobilizes prior to base resistance, as identified in pile load tests.

Despite all the constraints listed above, inherent in these solutions are certain provisions such that the exploitation of which provided a recipe for reducing these shortcomings towards the improved performance of this analytical method. The research work presented in the subsequent chapters of this dissertation provides details of these provisions, nitty-gritty of how they were employed for improved design formulations and the ensuing results based on statistical and regression analyses.

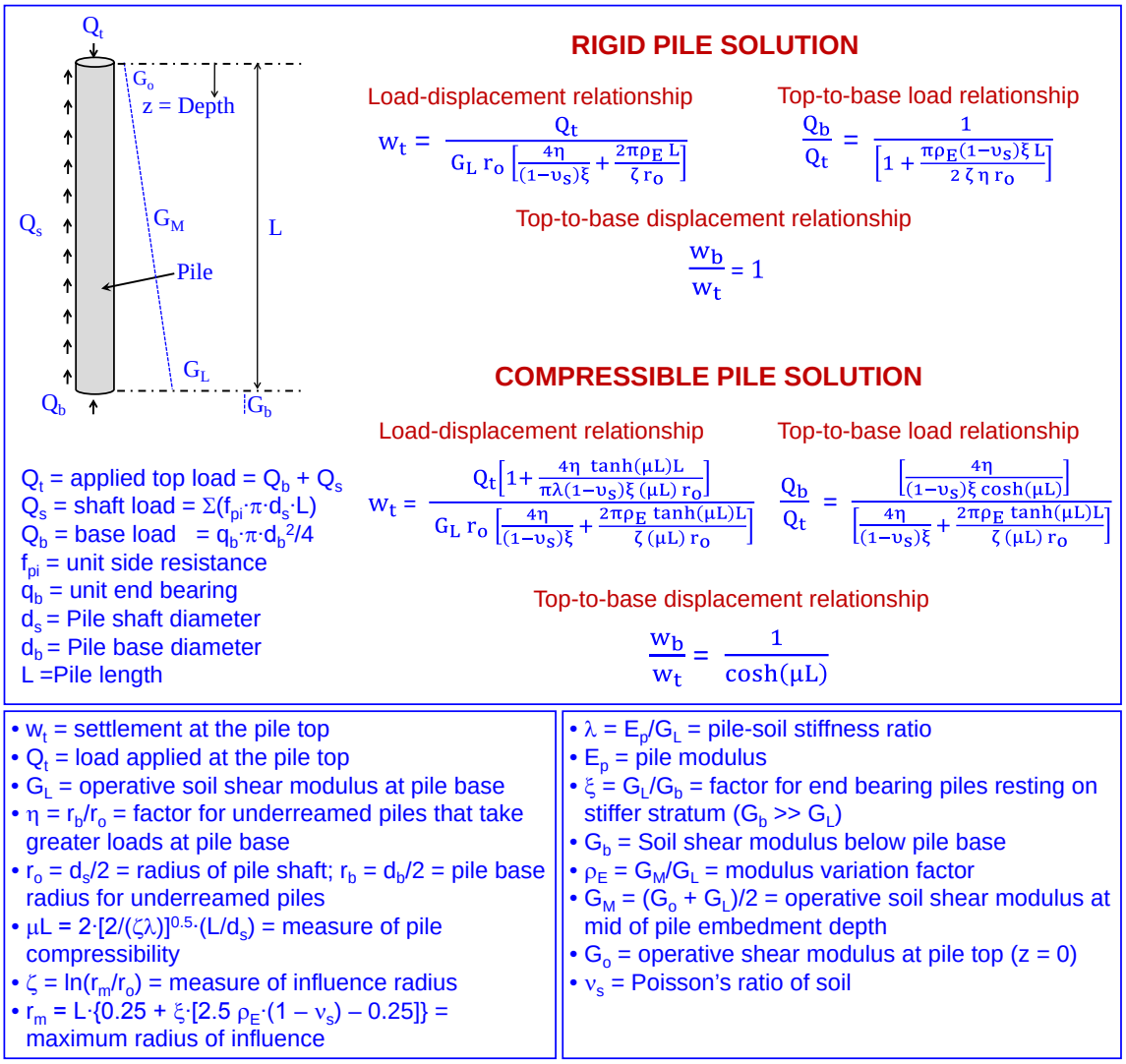

Figure 4.2. Analytical elastic continuum solution for axial pile displacements analysis in a linear elastic two layered soil model (after Randolph and Wroth, 1978; 1979).

4.4 Stiffness Reduction Models

The load-settlement (Q-w) response of single piles is significantly affected by non-homogeneity in stiffness of the ground. Cooke et al. (1979) noted that the operative shear modulus (G) is the most important parameter of the soil affecting the Q-w behavior of a pile under working conditions. Randolph and Wroth (1978) also indicated that use of shear modulus (G) of the soil is preferable over the Young's modulus (E) in pile Q-w analysis because: (1) the soil deforms primarily in shear along the pile shaft, which

contributes to major portion of the pile capacity, and (2) the shear modulus is usually unaffected by whether the loading is drained or undrained. However, as pointed out in the previous section of this chapter, the non-linearity in decay of soil stiffness poses problems in the selection of applicable elastic stiffness properties of soil for use in the estimation of settlements corresponding to increasing levels of load.

Many algorithms have been developed and documented through wide range of research to describe this non-linear stiffness reduction for different geomaterials towards use in geotechnical engineering applications [e.g., simple hyperbolic stress-strain relationship by Kondner (1963), modified hyperbolic function by Fahey and Carter (1993), modulus reduction curves as functions of plasticity presented by Vucetic and Dobry (1991), and a periodic logarithmic function proposed by Jardine et al. (1986)]. It becomes difficult to strike a compromise between simplicity, without regard for imprecise description of rather complicated stiffness reduction trends, and improved accuracy at the cost of highly complex algorithms.

For over 4 decades, the resonant column (RC) device has provided modulus reduction data for dynamically-loaded soils (e.g., Hardin and Drnevich, 1972; Ishibahi-Zhang, 1993; Santos and Correia, 2001). The emphasis of measurement was to define G_{max} and the associated G/G_{max} reduction curves at small- to intermediate strains, as well as damping values (e.g., Vucetic and Dobry, 1991; see Figure 4.3). It is important to note that the rates of loading are quite high for RC tests, thus these G/G_{max} schemes are not directly appropriate to static loadings of pile foundations. Monotonic torsional shear (TS) tests are able to provide a full range of data from small- to high-strain ranges (e.g., Mayne, 2005; see Figure 4.4). These tests replicate more closely to the static loading experienced by the deep foundations.

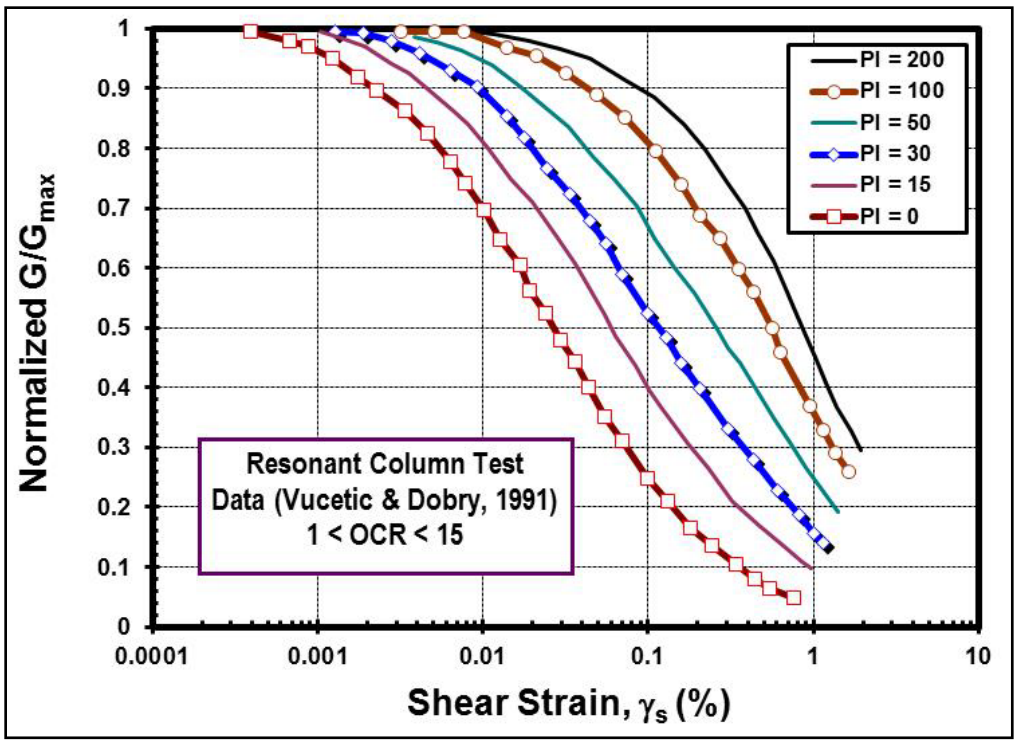

Figure 4.3. Experimental G/G_{max} curves from cyclic resonant column test data (after Vucetic and Dobry, 1991).

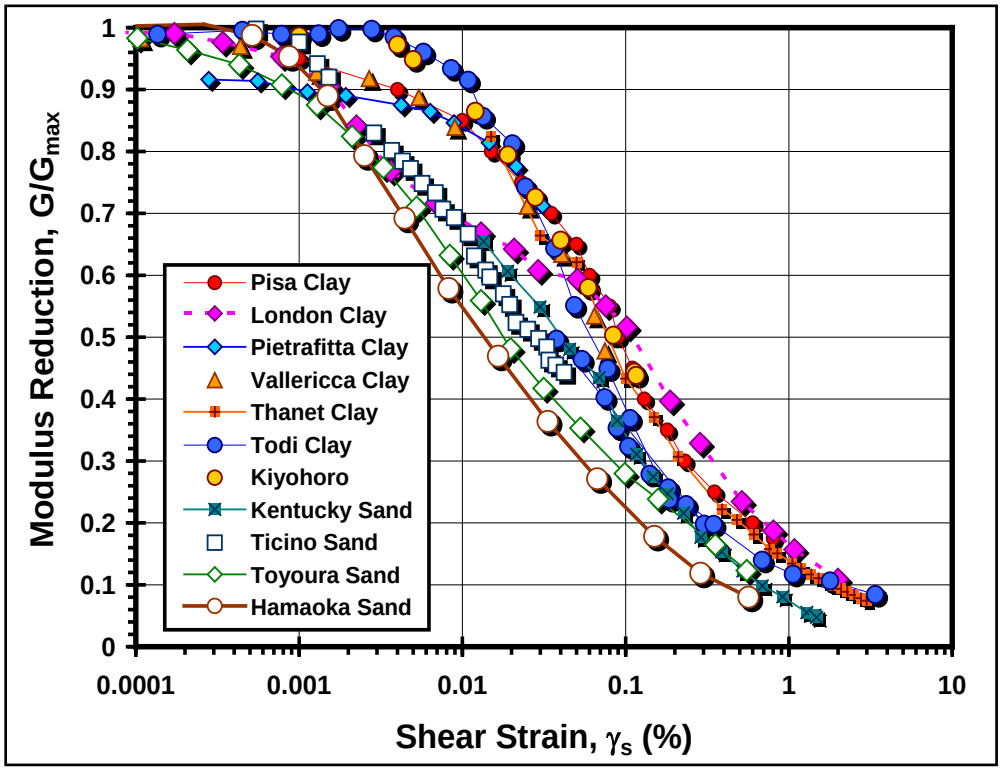

Figure 4.4. Modulus reduction data vs. logarithm of shear strain from monotonic torsional shear (after Mayne, 2005).

The G/G_{max} curves can be presented in terms of logarithm of shear strain (γ_s) (e.g., Vucetic and Dobry, 1991), or alternatively in terms of mobilized shear stress (τ/τ_{max}) (e.g., Fahey and Carter, 1993; see Figure 4.5), or the applied load level (Q/Q_{ult}) (e.g., Mayne, 1999), where τ_{max} = shear strength and Q_{ult} = ultimate load. The mobilized shear stress or applied load level is analogous to the reciprocal of the factor of safety (FS = $\tau_{max}/\tau = Q_{ult}/Q$).

The Vucetic and Dobry (1991) identified plasticity index (PI) as the main factor affecting the G/G_{max} reduction curves for a wide variety of soils. Consequently, they developed design charts showing modulus reduction curves as function of PI. Their use is more appropriate to seismic site amplification studies and cyclic behavioral concerns (Elhakim, 2005). Moreover, these charts were not expressed mathematically for convenient quantification of G/G_{max} vs. logarithm of shear strain (γ_s) relationships.

Recently, using laboratory experimental data from resonant column, triaxial, simple shear, and torsional shear tests on 21 clays and silts, Vardanega and Bolton (2013) advanced this approach and developed G/G_{max} vs. log γ/γ_{ref} curves. Here γ_{ref} refers to the value of shear strain where G_{max} reduces to one-half of its initial maximum value. They characterized their dataset by fitting a modified hyperbola via a transformed system shown in Figure 4.6. To explore the robustness of their relationship to γ_{ref}, regression analyses were performed on individual soil properties, thereby tying γ_{ref} to PI of the soil. They presented new PI based curves similar to the Vucetic and Dobry (1991) type charts for both dynamic and static loading for clays and silts, along with their respective design equations (see Figures 4.6 and 4.7). As seen, the curves of static loading are displaced from the Vucetic and Dobry (1991) curves indicating less stiffer and early yielding response than dynamic loading. This is a clear manifestation of the phenomenon of interpretation of higher stiffness response for increased strain rate due to soil viscosity (e.g., Garner, 2007) and, therefore, provides motivation for introduction of adjustment

factors in the G/G_{max} reduction schemes derived from cyclic and dynamic loading towards static application, or derivation of separate G/G_{max} reduction scheme for use in static loading of pile foundations.

Kraft et al. (1981a) indicated that the shear modulus may be assumed proportional to the shear strength of the soil to deduce modulus next to the pile from the shear strength of the soil after installation and prior to loading. Since the actual distribution of shear strength is not known with a reasonable precision, they proposed idealized linear distribution, with G/G_{max} equal to M_0 at the pile-soil interface and increasing linearly to a value of 1.0 at the elastic-plastic boundary r_1. The resulting normalized shear modulus versus normalized radial distance from the pile/soil interface is as shown in Figure 4.8.

Table 4.2 presents summary of selected expressions, particularly the 'shear modulus' reduction (G/G_{max}) schemes for static, cyclic and dynamic type of loading from laboratory experimental data on a variety of geomaterials.

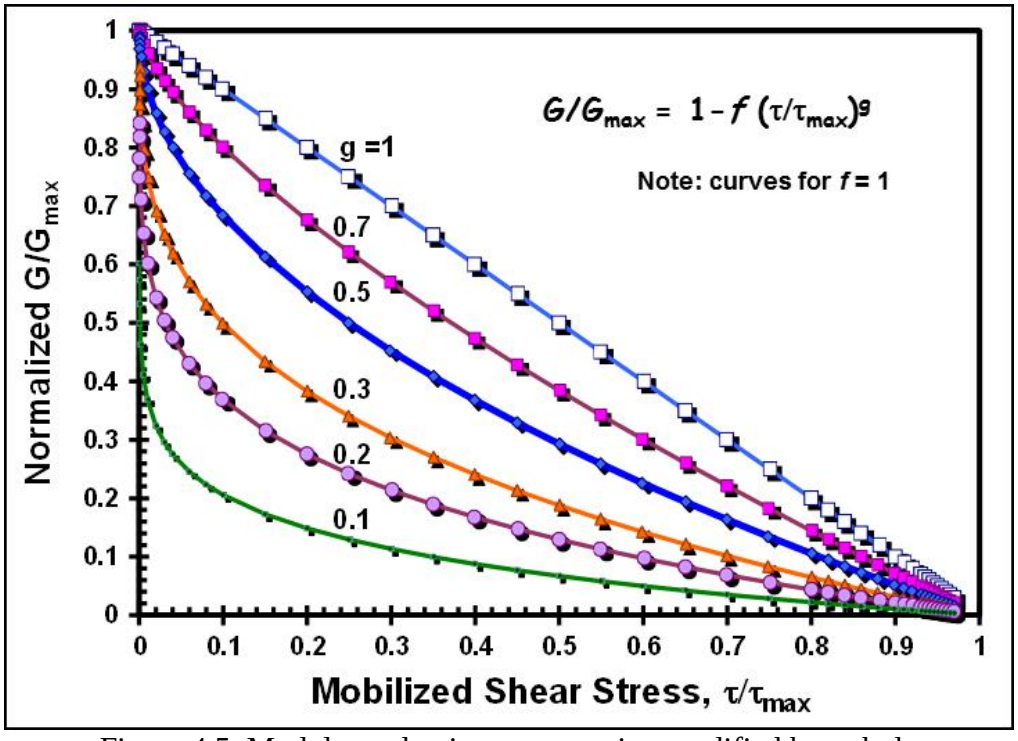

Figure 4.5. Modulus reduction curves using modified hyperbola (Fahey and Carter, 1993).

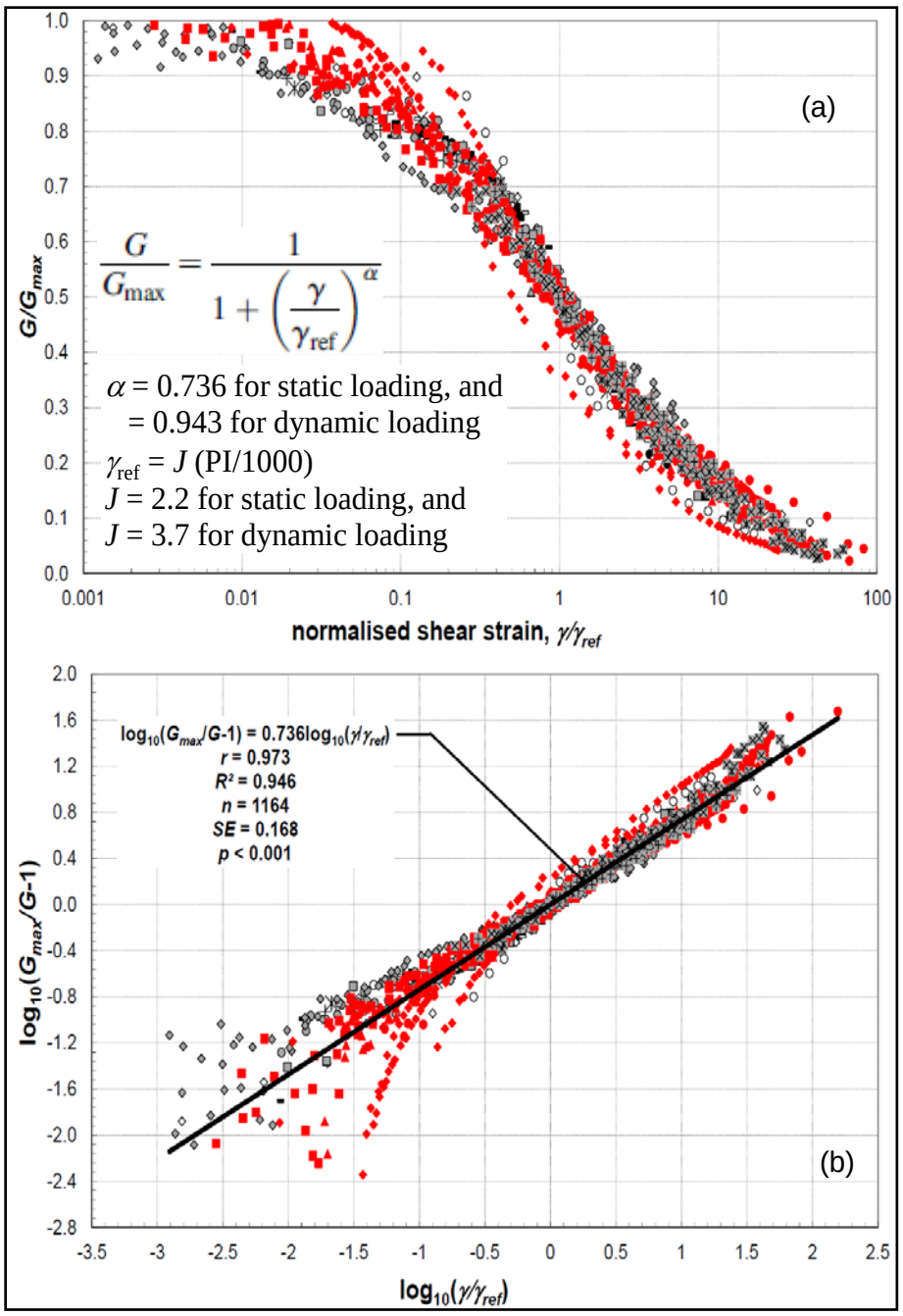

Figure 4.6. Statically adjusted test data and fitted hyperbola: (a) G/G_{max} with static adjustment applied vs. normalized shear strain; (b) modified hyperbola fitted to statically adjusted data (Vardanega and Bolton, 2013).

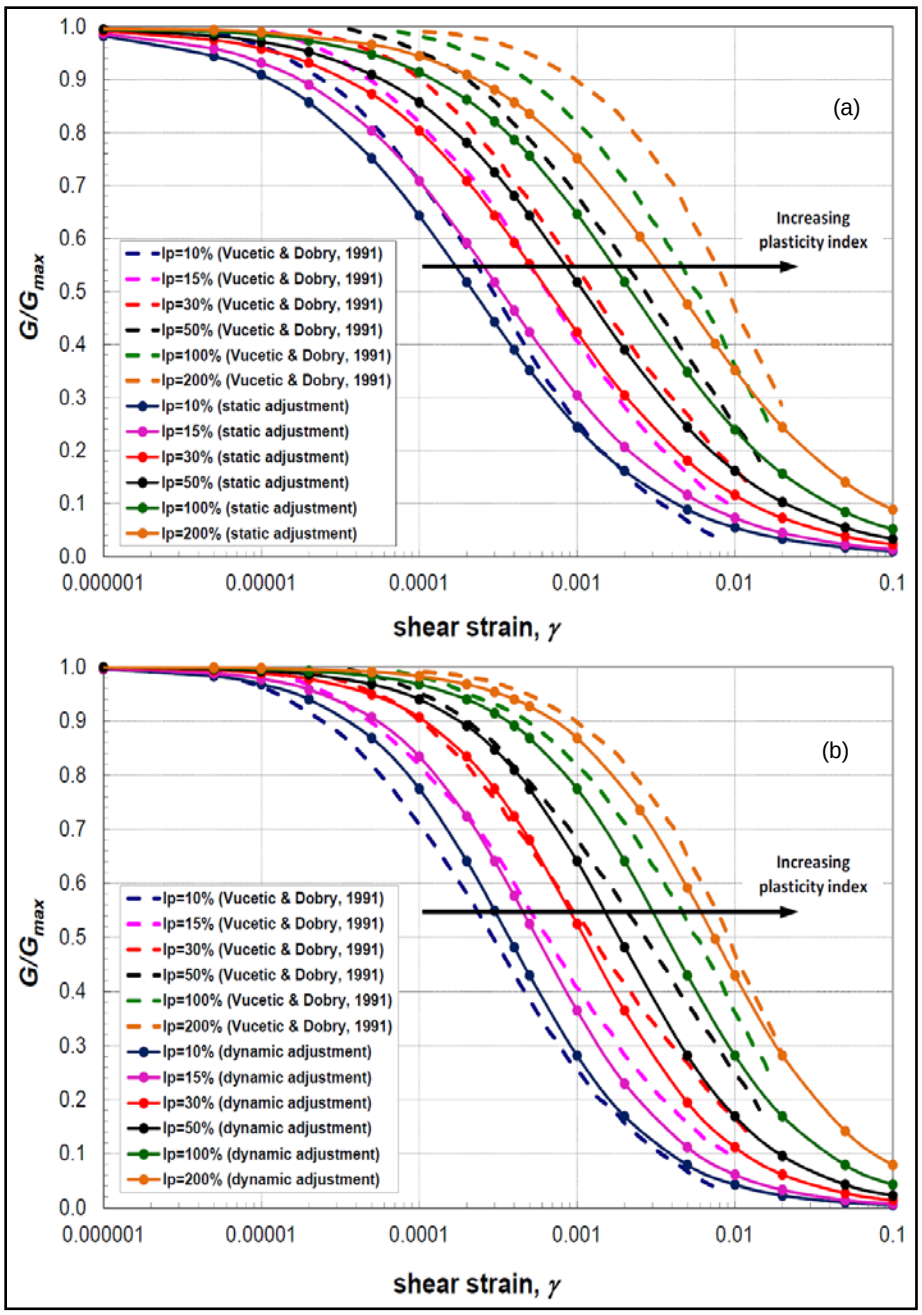

Figure 4.7. Design charts for stiffness degradation of clays and silts: (a) static applications; (b) dynamic applications (Vardanega and Bolton, 2013).

Table 4.2. Summary of selected shear modulus reduction schemes from laboratory experimentations (adapted and updated from Mayne, 2005; and Elhakim, 2005).

Model Type	Expression	Reference	Notes
Power function	$$\frac{\gamma}{\gamma_y} = \frac{\tau}{\tau_y}\left[1 + \alpha\left|\frac{\tau}{\tau_y}\right|^{(r-1)}\right]$$ where γ_y and τ_y are defined at "appropriate levels." Richart (1975) related γ_y and τ_y to the reference strain and shear strength: $$\gamma_y = C_1\,\gamma_r$$ $$\tau_y = C_1\,\tau_{max}$$ where C_1 is a constant less than 1.0. $$\frac{G}{G_{max}} = \frac{1}{\left[1 + \alpha\left|\frac{\tau}{C_1\tau_{max}}\right|^{(r-1)}\right]} = \frac{1}{\left[1 + \alpha\left|\frac{1}{C_1}\frac{G}{G_{max}}\frac{\gamma}{\gamma_r}\right|^{(r-1)}\right]}$$ where α and r are fitting parameters for flexibility in providing actual soil behavior.	Ramberg and Osgood (1943)	See Figure 4.8 for C_1 = 1.0 and for various values of α and r.

Table 4.2. (continued).

Model Type	Expression	Reference	Notes
Rectangular hyperbola	$\tau(\gamma) = \frac{\gamma}{\frac{1}{G_{max}} + \frac{\gamma}{\tau_{max}}}$ $\frac{G}{G_{max}} = \frac{1}{\left(1 + \frac{\gamma}{\gamma_r}\right)}$ $\gamma_r = \frac{\tau_{max}}{G_{max}}$	Kondner (1963)	See Figure 4.9
Modified hyperbolic fitting	$\frac{G}{G_{max}} = \frac{1}{(1 + \gamma_h)}$ $\gamma_r = \frac{\gamma}{\gamma_r}\left[1 + a \cdot e^{-b\left(\frac{\gamma}{\gamma_r}\right)}\right]$ where γ is the current strain, γ_h is the hyperbolic strain, γ_r is the reference strain (= τ_{max}/G_{max}), a and b are soil properties	Hardin and Drnevich (1972)	Based on resonant column tests

Table 4.2. (continued).

Model Type	Expression	Reference	Notes
Idealized linear radial variation of operative modulus	$$G_{ave} = G_{max} \frac{ln\left(\frac{r_m}{r_o}\right)}{\frac{\left(\frac{r_1}{r_o}\right)-1}{\left(\frac{M_o r_1}{r_o}\right)-1} ln\left(\frac{M_o r_1}{r_o}\right) + ln\left(\frac{r_m}{r_1}\right)}$$ where G_{ave} = average equivalent shear modulus along the pile, r_m = limiting radius = $2.5L(1-\nu_s)$, ν_s = Poisson's ratio, r_o = pile radius, see Figure 4.10 for definitions of r_1 and M_0	Kraft et al. (1981a)	Idealized linear distribution of G/G_{max} as function of distance from pile, equal to M_0 at the pile-soil interface and increasing linearly to a value of 1.0 at the elastic-plastic boundary, r_1 From numerical analyses, Zhu (2000) found that the r_1/r_0 value is in the range of 6–8 for stiff clayey soils Field measurements gathered at Houston University in Houston showed that this value could be 2–3 for heavily overconsolidated clay (O'Neill 2001) Also see Figure 4.10

Table 4.2. (continued).

Model Type	Expression	Reference	Notes
Modified hyperbolic fitting	$$\frac{G_{sec}}{G_{max}} = \frac{\tau_1}{\tau_1 + \gamma \cdot G_{max}} - \tau_1 \cdot \frac{\frac{\tau_1}{G_{max}^2}}{\left(\frac{\tau_1}{G_{max}} + \gamma_{max}\right)^2} \cdot \frac{1}{\gamma_{max}^m} \cdot \frac{\gamma^m}{m+1}$$ where τ_1 and m are positive and real numbers of the modified hyperbolic equations; G_{sec} and γ are current secant shear modulus and shear strain, respectively; γ_{max} is the maximum shear strain. Hyperbolic model parameters are obtained from: $$m \geq 4y_{max} - 1 \; and \; \tau_1 = \frac{y_1 \cdot G_{max}}{\gamma_{max}}$$ where $$y_1 = \frac{y_{max} - \frac{1}{2} + \sqrt{\frac{1}{4} - \frac{y_{max}}{m+1}}}{\frac{m}{m+1} - y_{max}}, \qquad y_{max} = \frac{\tau_{max}}{G_{max} \cdot \gamma_{max}}$$	Prevost and Keane (1990)	Both monotonic and cyclic loading at both low- and high-strains

Table 4.2. (continued).

Model Type	Expression	Reference	Notes
Modified hyperbolic fitting	$\frac{G_{sec}}{G_{max}} = 1 - f\left[\frac{\tau}{\tau_{max}}\right]^{g}$ $\frac{G_t}{G_{max}} = \frac{\left[\frac{G}{G_{max}}\right]^2}{\left\{1 - f(1-g)\left[\frac{\tau}{\tau_{max}}\right]^{g}\right\}}$ where G_{sec} = secant shear modulus at current stress level, G_t = tangent shear modulus at current stress level, G_t = maximum shear modulus, τ = current shear stress, τ_{max} = shear strength, f and g = soil parameters describing the nonlinear soil behavior	Fahey and Carter (1991)	Modified hyperbolic formulation. A simple hyperbola obtained for $f = 1$ and $g = 1$
Modified hyperbolic fitting	$\frac{G_{sec}}{G_{max}} = \left[1 - \frac{\tau}{\tau_{max}}\right]^{m}$ where $m = 1$ for simple hyperbola and $m = 2$ to 4 for static loading of soils, τ = current shear stress, τ_{max} = shear strength	Mayne (1994)	

Table 4.2. (continued).

Model Type	Expression	Reference	Notes
Modified hyperbolic fitting	$\frac{G_s}{G_{max}} = \left\{1 - f\left[\frac{(q - q_i)}{(q_{max} - q_i)}\right]^g\right\}\left[\frac{p_o}{p_o'}\right]^{n_g}$ $\frac{G_t}{G_{max}} = \frac{\left(\frac{G_s}{G_o}\right)^2}{\left\{1 - f(1-g)\left[\frac{(q - q_i)}{(q_{max} - q_i)}\right]^g\right\}}\left(\frac{p_o}{p_o'}\right)^{n_g}$ where q is the deviatoric stress invariant, q_i is the initial deviatoric stress invariant at failure, q_i is the deviatoric stress invariant at failure, f , g, n_g are material constants, p_o and p_o' are the octahedral stress invariants at current and initial stress invariant	Lee and Salgado (1999)	Generalized modified hyperbola for 3-D stresses (extension of Fahey and Carter 1993)
Modified hyperbolic fitting	$\frac{G}{G_{max}} = \frac{1}{\left[1 + \frac{\gamma}{\gamma_{ref}}\right]^\alpha}$ $\gamma_{ref} = J\left(\frac{I_p}{1000}\right)$ where γ_{ref} = value of shear strain where G_{max} reduces to one-half of its initial maximum value, α = curvature parameter = 0.736 for static loading and 0.943 for dynamic loading, I_P = plasticity index (expressed numerically, not as a percentage), J = 2.2 for static loading and 3.7 for dynamic loading	Vardanega and Bolton (2013)	Both from dynamic and static loading data from 21 clay and silt sites Also see Figure 4.6

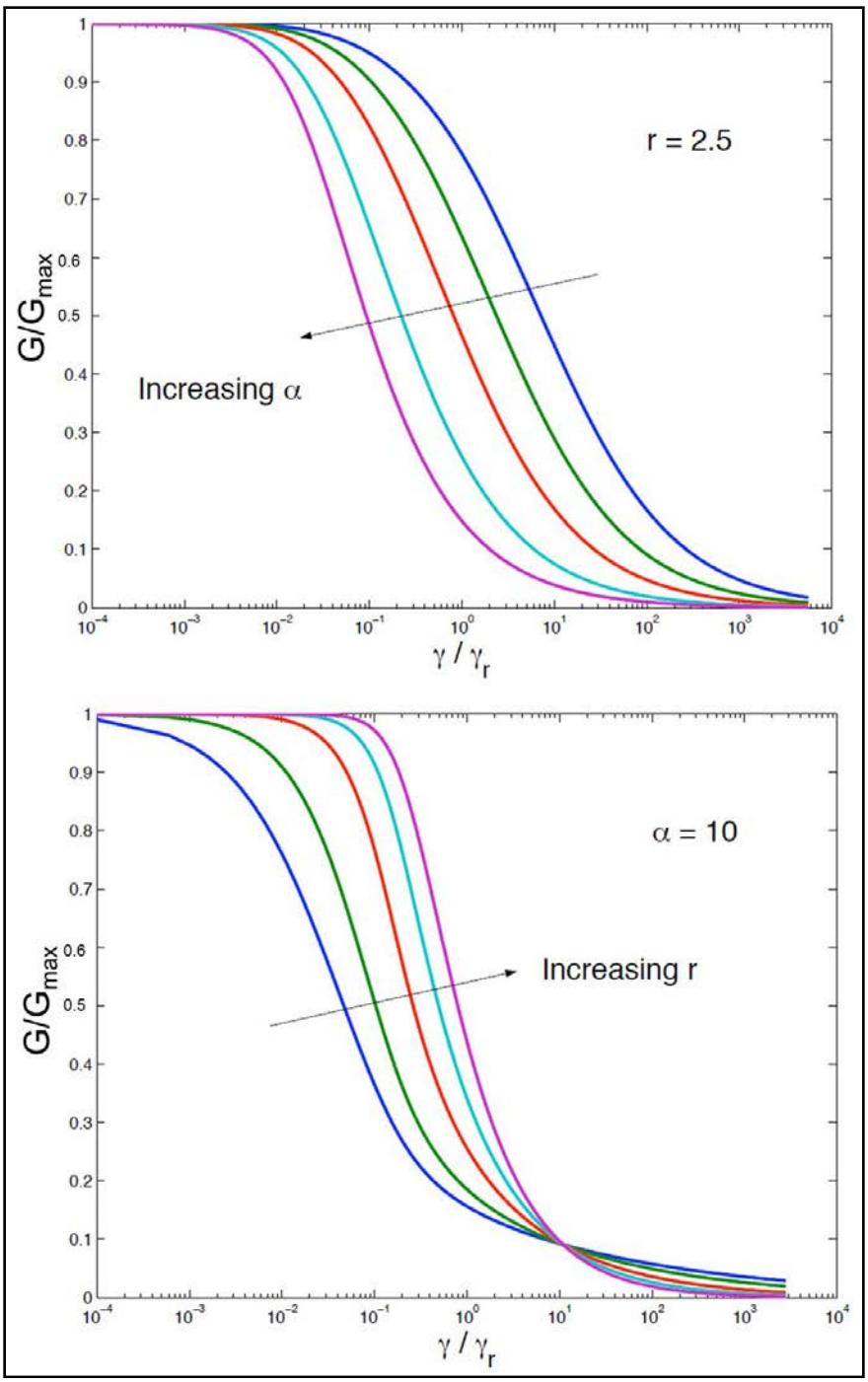

Figure 4.8. Modulus reduction curves for a Ramberg-Osgood stress-strain model.

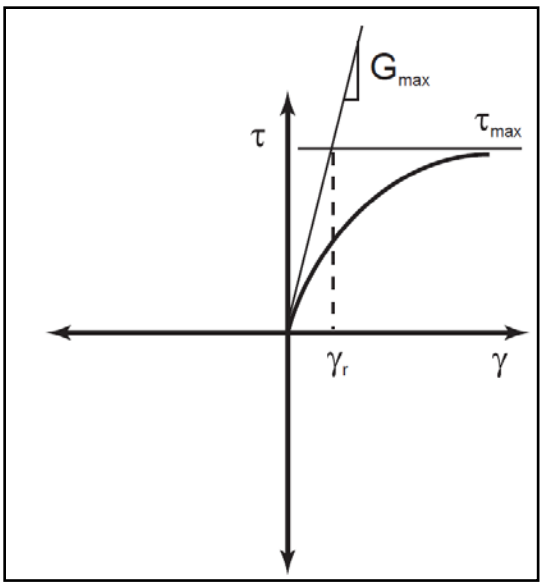

Figure 4.9. Hyperbolic stress-strain curve (Kondner, 1963).

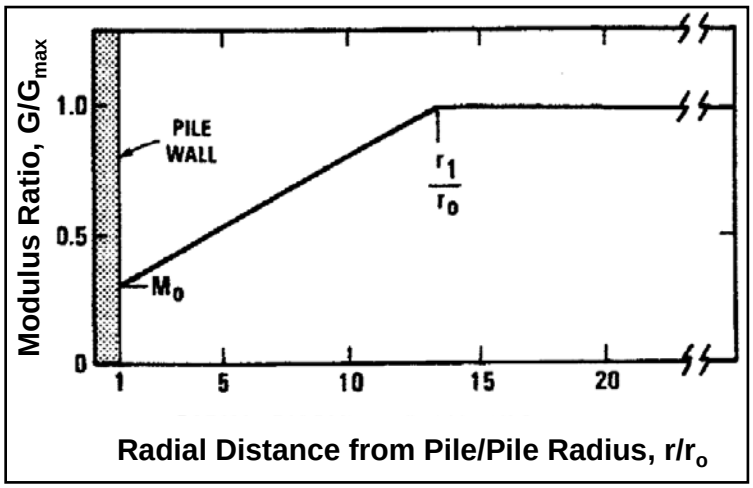

Figure 4.10. Idealized radial distribution of soil modulus ratio (after Kraft et al., 1981a).

The relevance and successful application of the modulus reduction schemes derived from laboratory experimental data to the field situations is highly dependent on the quality of the samples used in their derivations. Another important aspect requiring attention towards selection of applicable shear stiffness values in context of the static pile loading is the effect of pile installation. The analytical pile solution presented in the previous section inexplicitly assumes that the soil parameters are not affected by pile

installation, i.e., the effects of pile installation are not accounted for in the solution. In actuality, the G_{max} profiles obtained from V_s readings at the pile site obtained prior to installation do not truly represent field situation at the time of loading after the pile has been installed. These problems can be significantly addressed by adopting a stiffness reduction schemes [e.g., G/G_{max} vs. percent pseudo-strain, γ_p = w/d (%), where w = pile settlement, and d = pile diameter], such as the one proposed by Berardi and Bovolenta (2005). They proposed a semi-empirical approach of matching actual field measurements via back-analysis of pile load tests using analytical elastic solutions to derive G/G_{max} as a function of γ_p curve (see Figure 4.11). Their curve was based on a limited database of similar situations (pile type, geometry, soil conditions, etc.) for piles tested in axial compression. In Figure 4.12, a simple analogy is presented between the modulus reduction curve generated from the simple shear stress vs. shear strain of a soil element adjacent to the pile, and that generated from the back-analysis of data from the pile load test within the framework of elastic solution. The G values obtained from the later curves can thus be used in the same elastic solution to forecast the nonlinear load-displacement (Q-w) response of piles falling within the range of the database considered.

It is possible to extend this methodology in derivation of shear modulus reduction schemes for different types of piles installed in different types of geomaterials.

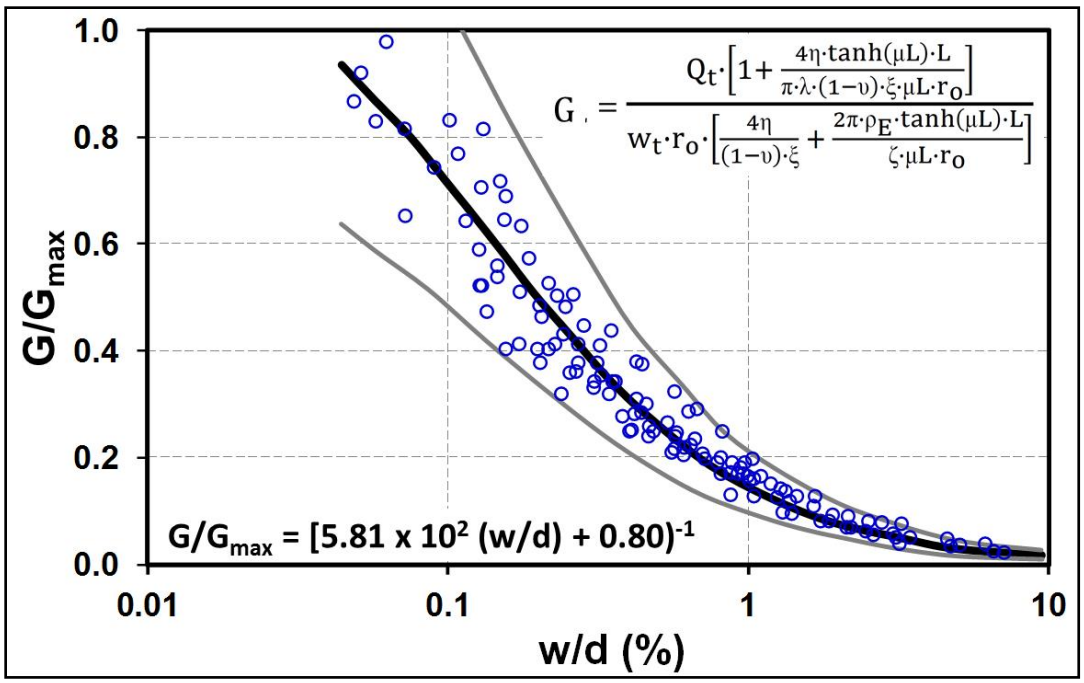

Figure 4.11. Stiffness decay curve (after Berardi and Bovolenta, 2005).

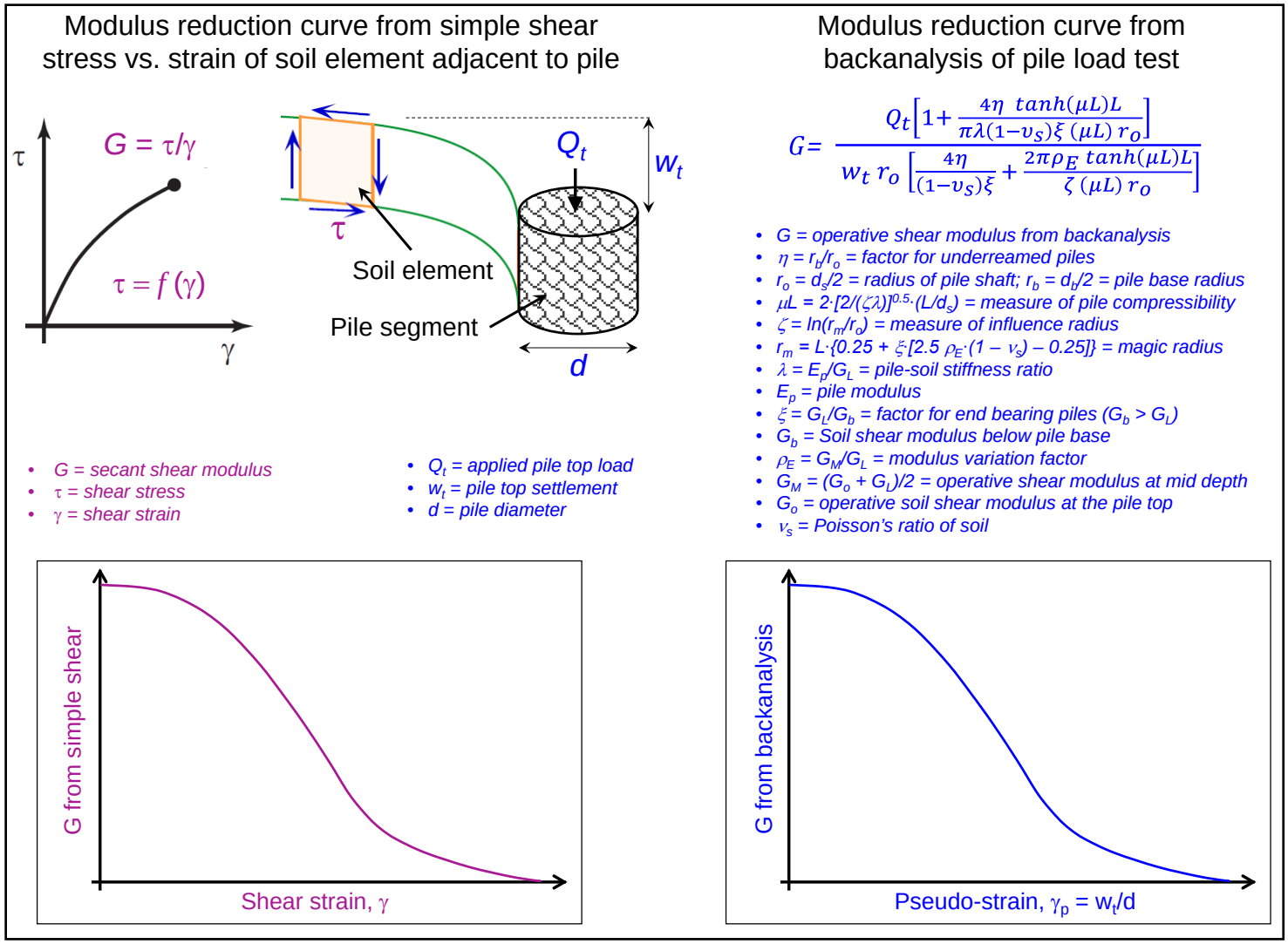

Figure 4.12. Analogy of modulus reduction curves from simple shear stress-strain of soil element adjacent to the pile with modulus reduction curve from back-analysis of data from pile load test.

4.5 Concluding Remarks

In this chapter, different approaches for pile displacement analysis are reviewed: empirical, analytical spring, elastic continuum solutions, and numerical methods (finite elements, boundary elements). In particular, details of the solution proposed by Randolph and Wroth (1978; 1979) for static axial compression loading of single piles embedded in two layered soil model. It is identified that this approximate closed-form analytical elastic solution is simple and convenient to implement, with provisions for its further extension to the cases of uplift (or tension) loading of deep foundations, piles embedded in multi-layered soil media, and bi-directional O-cell loading arrangements. It is also identified that selection of the most appropriate value of operative shear modulus (G) is paramount in the correct assessment of axial displacements corresponding to different loads. Different shear stiffness reduction schemes are reviewed, with the deduction that the most suitable and appropriate modulus reduction scheme for application in the non-linear static load-displacement analysis of pile foundations is the one derived from actual field load tests, in contrast to those derived from laboratory data which are mostly applicable for dynamic and cyclic loadings.

CHAPTER 5

PILE-SCPT DATABASE AND CASE RECORDS

Synopsis

This chapter provides information on the pile load test database compiled with seismic cone penetration test (SCPT) readings that was analyzed as a major part of the current research effort. Herein, the selection criteria, database characteristics, pile types, soil conditions, summary statistics, charts, graphs, and figures are presented to afford an overview of this databank. A summary table listing all the sites is included which is tied to a comprehensive appendix that gives the case-by-case records of cone penetrometer soundings and measured performance results from pile load tests at each site.

5.1 Introduction

An extensive effort was made to collect a large, reliable, and up-to-date database on the topic. During this process, every possible endeavor was made through a wide search of published/unpublished literature, private reports, and personal communications, to include case studies that comprised SCPTu soundings, results of pile load testing, and the allied soil information used in previous research, as well as newly-documented sites. The concept was intended to:

- utilize maximum data (i.e., all 4 SCPTu readings: q_t, f_s, u_2 and V_s) towards axial pile analysis and evaluation;
- refine and improve the formulation of a direct CPTu-based axial pile capacity methodology;
- extend the utilization of penetrometer data from capacity singularity to the assessments of a complete pile load-displacement (Q-w) response via the geophysical measurement of shear wave velocity (V_s) and small-strain stiffness (G_{max}) within a theoretical elastic continuum framework; and

- present this new formulation as a convenient, more consistent, and applicable means for a larger variety of situations, in terms of both pile type, installation, and geomaterial conditions.

5.2 Selection Criteria

The following criteria explain the choices and the selection process applied to the case histories for this research:

- The selected sites were characterized by penetrometer soundings advanced in the proximity of pile locations, providing at least one but often multiple CPT readings, with a primary focus on targeting test sites with SCPTu soundings.
- From the gathered CPT data, the penetrometer readings (q_t, f_s, and u_2) were meant to be utilized in deriving improved correlations for direct axial pile capacity evaluations, while the V_s component was to be exploited in supplying soil stiffness for axial pile Q-w response.
- The maximum depth of CPT soundings at each site extended deeper than the pile length.
- The selected piles were subjected to axial load testing under one or more of the three different primary loading modes: top-down compression (C), top-up tension (T, or uplift), and the newer bi-directional loading utilizing the Osterberg cell (O-cell) device.
- The load test database includes piles that were either partly or fully instrumented. The partly instrumented series provided Q-w data as the minimum result, while those that were fully instrumented also enabled measurements of the complete load transfer (Q-z) distributions along the pile shaft and at the base or toe. In some of the included cases, interpretations of the Q-z distribution were possible from the allied information given in their respective sources, even though the piles were not fully instrumented.

- The master database of load tests includes piles that were either loaded to a certain design value, or to an “ultimate” or “failure” or “capacity” state, or otherwise an intermediate value. For the final analysis, a subset involving a fewer number of piles was tallied where at least two selected criteria defining the pile capacity were reached, namely: (1) Davisson's offset line criterion (Davisson, 1972), and (2) French or European 10% criterion, i.e., w/d = 0.1 (Vesić, 1977), where w = pile top displacement, and d = pile diameter. Nevertheless, data from the remaining load tests were still utilized in this research study in one form or another, including: (1) comparison of pile capacity and Q-w response between compression and tension loadings, (2) effect of pile slenderness ratio (L/d) on the axial loading response, (3) pile response to loading based on the geotechnical properties of soils.

The sites were so selected that many varied soil types form part of the database, including: soft sensitive clay, stiff weathered clay, sandy-gravelly clay till, varved clay, silty clay, silt, residual silty sand, sandy silt, uniform loose sands, very dense medium to coarse sand, gravelly sand, and mudstone. The overall percent distributions of different soil types in the database are shown in Figure 5.1. For all the selected sites, additional data and information were available for adequate geotechnical site characterization.

5.3 Database Characteristics

In contrast to previous studies on pile-CPT correlations, this new database is distinctly characterized with the following features:

- It includes well-documented case records of 330 axial pile load tests conducted at 70 sites from different parts of the world where CPT soundings had also been advanced (see Figure 5.2 for locational orientation of the sites). This is one of the largest databases.

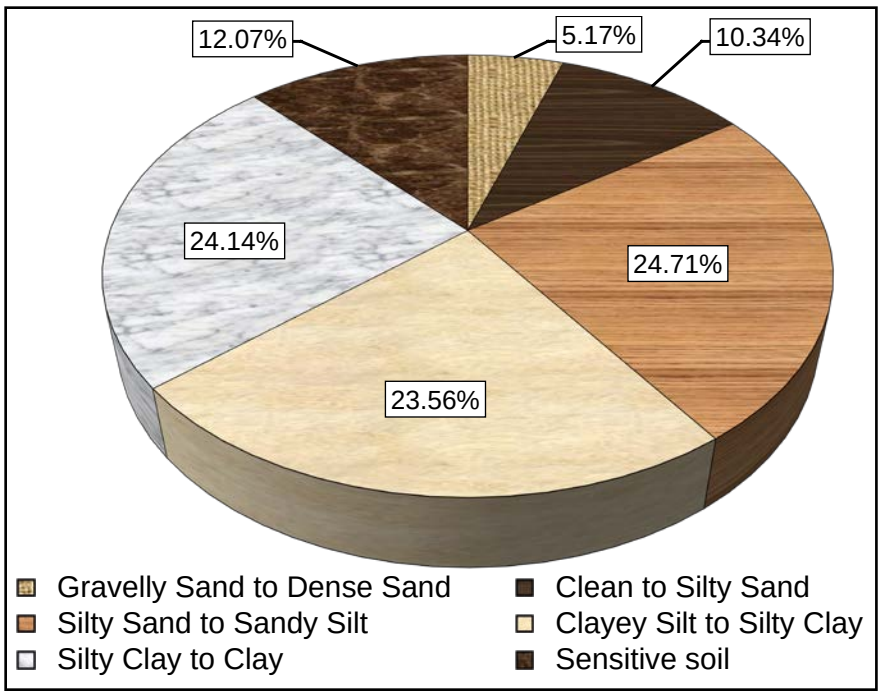

Figure 5.1. Percent distribution of different soil types in the database.

- In past research efforts, the primary focus was on either mechanical CPT, or electric CPT, or electronic CPTu. For the first time, seismic piezocone test (SCPTu) soundings have been comprehensively collected and utilized in a holistic and unified manner in context of the axial pile study.
- The piles in the database include the following types: (1) drilled shafts, (2) open-ended (OE) and close-ended (CE) steel pipe piles, (3) cylinder concrete piles, (4) timber (teak) piles, (5) H-section steel piles, (6) augered piles, and (7) circular as well as square concrete piles. This is a larger range and variety compared to most previous studies on the topic.
- For the first time, cases of O-cell type of bi-directional load testing have been included in the study, whereas previous studies primarily focused on piles that were load-tested in either compression or tension, or both.
- An interesting aspect of the piles in the current database concerns the installation methods. Accordingly, these can categorically sorted and grouped based on the

following installation methods: (1) bored cast in-situ, (2) augered, (3), jacked, and (4) driven.

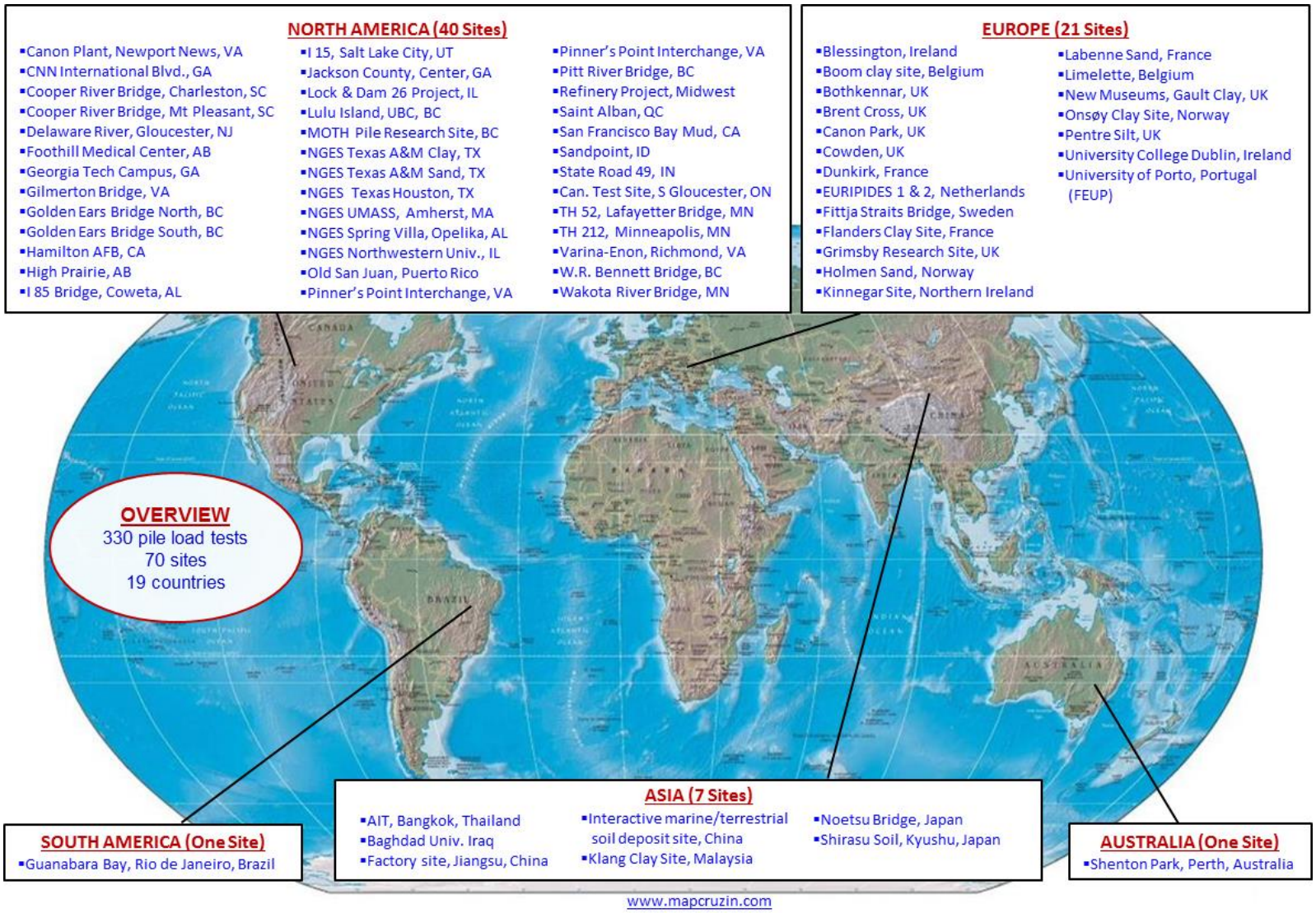

Figure 5.2. Worldwide site locations of axial pile load tests and seismic piezocone tests.

5.4 Case Records

A summary of the information on all 70 worldwide sites in the current database is presented in Table 5.1. Here, the sites have been listed in alphabetical order, assigning a site identification number (ID) to each test location. The information in the summary table presents the name and location of each site, type of soil profile encountered, type(s) of piles, type(s) of in-situ tests, number of test piles, loading mode(s) of the different pile load tests, load test data based on level of instrumentation (Q-w and/or Q-z), and the source(s) of information for each site.

Further details on each site and the field load tests are given in Appendix E. In Table E.1, all pile load tests have been assigned their own IDs, further specifying their respective pile types, dimensions, loading modes, installation methods, and maximum measured loads ($Q_{max\text{-}measured}$), as well as their interpreted capacities based on three definitions: (1) Davisson's offset line criterion, $Q_{Davisson}$ (Davisson, 1972), (2) French criterion, $Q_{w/d=10\%}$, and (3) Chin-Kondner capacity criterion, $Q_{C\text{-}K}$, which is the asymptote of a fitted rectangular hyperbola (Chin, 1970; Kondner, 1963). This table in Appendix E is followed by further detailed information, requiring multiple sheets for presentation of each site. The first sheet concerning each site presents:

- Graphical profiles of CPT readings
- Graphical profiles of CPT SBT classification index
- Tabulated information of the site location/name, soil and pile types, type of cone penetrometer testing, source of V_s data, number of piles and load tests, sources of information, and site-by-site additional significant information.

An additional sheet is given for each pile load test at that site, which provides the following respective set of information, based on available data:

- Plot of Q-w curve

- Plot of the back-analyzed G/G_{max} vs. percent pseudo-strain [w/d (%)] curveTabulated information of the type of pile, pile dimensions, installation method, loading mode, the maximum measured load ($Q_{max\text{-}measured}$), their interpreted capacities based on the three cited criteria (i.e., $Q_{Davisson}$, $Q_{w/d=10\%}$, and $Q_{C\text{-}K}$), and the shaft (Q_s) and base (Q_b) components of $Q_{max\text{-}measured}$ ($= Q_s + Q_b$)

5.5 Test Locations

The compiled database of 70 sites belongs to 19 countries from 5 different continents (see Figure 5.2). Forty sites (i.e., 56.5%) belong to North American continent, twenty one sites (i.e., 30.5%) belong to Europe, seven sites (i.e., 10.2%) are from Asia, while one site each belongs to South America and Australia. The maximum number of sites (i.e., 26) is from USA, followed by 12 from Canada, 7 from UK, and 14 from the other European countries. In most instances, these locations are either internationally recognized and well-established research sites, including national geotechnical experimentation centers, or established as medium- to large-scale project sites for infrastructure and civil engineering works where comprehensive geotechnical investigations have been carried out to obtain sufficient information for large buildings, bridges, highways, or other major facilities.

Table 5.1. Summary of the database of sites and pile load tests.

Site ID	Site Name and Location	Soil Type	Pile Type	In-situ test type	Load test type	Load Test Data		No. of pile load tests	Reference
						Q-w	Q-z		
1	Asian Institute of Technology Test Site, Rangsit, near Bangkok, Thailand	Soft clay over stiff clay	8 Teak piles and 1 DS	SCPTu	C	Yes	Yes	9	Brand et al. (1972); Balasubramaniam et al. (2004); Shibuya and Tamrakar (2003)
2	Baghdad University near River Tigris, Iraq	Clayey silty sand over uniform sand	Sq-C piles	CPT + SPT-N	C and T	Yes	Yes	3	Altaee et al. (1992)
3	Blessington, Ireland	Heavily overconsolidated glacially derived very dense fine sand	CE-S	SCPT	C	Yes	Yes	2	Gavin and O'Kelly (2007)
4	Boom Clay Site, Sint-Kathelijne-Waver, Belgium	Stiff fissured clay	11 Screw piles and 1 Sq-C	SCPT + CPT	C	Yes	Yes	12	Mengé (2001); Huybrechts (2001); Maertens and Huybrechts (2003)
5	Bothkennar clay site, Scotland	Post glacial soft silty clay	CE-S	SCPTu	C and T	Yes	Yes	7	Lehane (1992)
6	Brent Cross, Hendon, UK	Weathered London clay	CE-S	SCPTu	C and T	Yes	Yes	6	Cooke et al. (1979)
7	Canadian Geotechnical Test Site, South Gloucester, ON, Canada	Soft sensitive (Champlain Sea) clay	DS	SCPTu	C and T	Yes	Yes	4	Radhakrishna et al. (1986)
8	Canons Park, North London, UK	Weathered London clay	1 DS and 3 CE-S	SCPTu	C	Yes	Yes	4	Powell and Lunne (2005); Price and Wardle (1982); Bond and Jardine (1991); Jardine et al. (1992)
9	Canon Plant, Newport News, VA, USA	Stiff sandy gravelly clay	Sq-C	SCPTu	C	Yes	No	2	Patton II and Barnhill (1988)
10	CNN International Blvd. Viaduct, Atlanta, GA, USA	Piedmont residual silt and sand grading to partially weathered rock	DS	SCPTu	O-cell	Yes	Yes	1	Ahrens et al. (2003)

Notes: DS: drilled shaft; CFA: continuous flight auger pile; CE-S: closed-ended steel pipe pile; OE-S: open-ended steel pipe pile; OE-SC: open ended concrete filled steel pipe pile; ICP: closed-ended Imperial College Pile; HP: H-section steel pile; PTC: pre-stressed concrete thin-wall caisson; PHC: Pre-stressed concrete high-strength; Sq-C: square precast concrete pile; C-C: circular precast concrete pile; C: top-down compression loading mode; T: top-up tension (or uplift) loading mode; O-cell: bi-directional Osterberg cell loading mode; A: augered piles; D: driven piles; J: jacked piles; B-CIS: bored cast in-situ piles.

Table 5.1. (continued).

Site ID	Site Name and Location	Soil Type	Pile Type	In-situ test type	Load test type	Load Test Data		No. of pile load tests	Reference
						Q-w	Q-z		
11	Cooper River Bridge on HW 17, Charleston site, SC, USA	Loose sand and soft clay overburden underlain by stiff calcareous Cooper Marl	DS	SCPTu	O-cell	Yes	Yes	4	Ahren et al. (2000a, b); Camp (2004); Camp et al. (2002); Simpson et al. (2000 a, b)
12	Cooper River Bridge on HW 17, Mt. Pleasant site, SC, USA	Clayey sand and sandy clay over stiff calcareous Cooper Marl	DS	SCPTu	O-cell	Yes	Yes	4	Ahren et al. (2000c, d); Ahren and Simpson (2000 a, b); Camp et al. (2002); Camp (2004)
13	Cowden, Northeast England, UK	Stiff stony clay till	ICP	SCPTu	C and T	Yes	Yes	6	Powell and Butcher (2003); Lehane (1992); Lehane and Jardine (1994)
14	Dunkirk, Northern Coast of France	Dense to very dense sand	10 OE-S and 12 CE-S	SCPT + CPT	C and T	Yes	Yes	22	Chow (1996)
15	EURIPIDES 1, Eemshaven, Netherlands	Medium dense silty sand over very dense sand	OE-S	SCPTu	C and T	Yes	Yes	8	Baaijens and Kolk (2004)
16	EURIPIDES 2, Eemshaven, Netherlands	Medium dense silty sand over very dense sand	OE-S	SCPTu	C and T	Yes	Yes	5	Baaijens and Kolk (2004)
17	Factory building site, Jiangsu Province, China	Marine silty clay	DS	SCPTu	C	Yes	Yes	1	Miao et al. (2011)
18	Fittja Straits Bridge, Vårby, near Stockholm, Sweden	Layers of sand, silty sand, and gravelly sand	Sq-C	CPTu	C	Yes	Yes	1	Axelsson (2000)
19	Flanders clay site, Merville, France	Silt over stiff homogeneous clay	1 DS, 2 OE-S and 2 HP	CPTu + DHT	C	Yes	Yes	5	Ali (2010); Ferber and Abraham (2002); Rocher-Lacoste et al. (2004); Rocher-Lacoste (2008)
20	Foothill Medical Center (FMC), Calgary, AB, Canada	Sandy clayey silt over hard silty clay till	DS	SCPTu	O-cell	Yes	Yes	1	Kort (2005)
21	Georgia Tech Campus, Sixth Street (west), Atlanta, GA, USA	Piedmont residual silty sand to partially weathered rock	DS	CPT + SASW	C	Yes	Yes	2	Mayne and Harris (1993)

Notes: DS: drilled shaft; CFA: continuous flight auger pile; CE-S: closed-ended steel pipe pile; OE-S: open-ended steel pipe pile; OE-SC: open ended concrete filled steel pipe pile; ICP: closed-ended Imperial College Pile; HP: H-section steel pile; PTC: pre-stressed concrete thin-wall caisson; PHC: Pre-stressed concrete high-strength; Sq-C: square precast concrete pile; C-C: circular precast concrete pile; C: top-down compression loading mode; T: top-up tension (or uplift) loading mode; O-cell: bi-directional Osterberg cell loading mode; A: augered piles; D: driven piles; J: jacked piles; B-CIS: bored cast in-situ piles.

Table 5.1. (continued).

Site ID	Site Name and Location	Soil Type	Pile Type	In-situ test type	Load test type	Load Test Data		No. of pile load tests	Reference
						Q-w	Q-z		
22	Gilmerton Bridge, Pier 12, Chesapeake, VA, USA	Silty sand over Yorktown marl	DS	SCPTu	O-cell	Yes	Yes	1	Pang et al. (2010)
23	Golden Ears Bridge (GEB) site: (N. Bank), Maple Ridge, BC, Canada	Soft thick deltaic silty clay of Fraser River	PTC	SCPTu	C	Yes	No	1	Amini et al. (2008); Naesgaard et al. (2008)
24	Golden Ears Bridge (GEB) site: (S. Bank), Langley, BC, Canada	Silty sand to dense sand over soft silty clay	DS	SCPTu	O-cell	Yes	Yes	1	Amini et al. (2008); Naesgaard et al. (2008)
25	Golden Ears Bridge (GEB) site: (S. Bank), Langley, BC, Canada	Gravelly sand over soft to firm silty clay	DS	SCPTu	C	Yes	Yes	1	Amini et al. (2008); Naesgaard et al. (2008)
26	Grimsby Research Site, Waltham, UK	Very stiff gravelly clay till	DS	SCPTu	C	Yes	Yes	1	Brown (2004); Brown et al. (2006)
27	Guanabara Bay, Rio-de-Janeiro, Brazil	Very soft clay	CE-S	SCPTu	C	Yes	Yes	1	Alves et al. (2009)
28	Hamilton Air Force Base, San Francisco, California, USA	Soft silty clay (San Francisco Bay Mud)	OE-S	CPTu	C	Yes	Yes	1	Heydinger and O'Neill (1986); Robertson (2009)
29	High Prairie Health Complex, Northern Alberta, Canada	Soft to stiff silty clay	CFA	CPTu + SDMT	C	Yes	Yes	2	Padros and Papanicola (2008); Cruz et al. (2008)
30	Holmen sand, Drammen, Norway	Loose medium to coarse river sand	C-C	SCPTu	C and T	Yes	Yes	11	Gregersen et al. (1973); Lunne et al. (2003)
31	Interactive marine and terrestrial deposit soils, China	Marine silty-clayey sand	PHC	SCPTu	C	Yes	No	1	Miao et al. (2011)
32	Interstate Highway I-85 Bridge, Newnan, Coweta County, GA, USA	Silty sand to sandy silt overlying partially weathered gneissic granite bedrock	DS	SCPTu	C	Yes	Yes	1	Mayne and Schneider (2001); O'Neill (1998)

Notes: DS: drilled shaft; CFA: continuous flight auger pile; CE-S: closed-ended steel pipe pile; OE-S: open-ended steel pipe pile; OE-SC: open ended concrete filled steel pipe pile; ICP: closed-ended Imperial College Pile; HP: H-section steel pile; PTC: pre-stressed concrete thin-wall caisson; PHC: Pre-stressed concrete high-strength; Sq-C: square precast concrete pile; C-C: circular precast concrete pile; C: top-down compression loading mode; T: top-up tension (or uplift) loading mode; O-cell: bi-directional Osterberg cell loading mode; A: augered piles; D: driven piles; J: jacked piles; B-CIS: bored cast in-situ piles.

Table 5.1. (continued).

Site ID	Site Name and Location	Soil Type	Pile Type	In-situ test type	Load test type	Load Test Data		No. of pile load tests	Reference
						Q-w	Q-z		
33	Jackson County Electrical Power Facility, Center, GA, USA	Silty sand to sandy silt of Piedmont residuum over partially weathered schist	CE-S	SCPTu	C	Yes	No	2	Mayne and Elhakim (2002)
34	Kinnegar site near Belfast Lough in Northern Ireland	Soft clayey silt (“sleech”)	7 Sq-C, 1 OE-S and 2 CE-S	SCPTu	C and T	Yes	Yes	10	McCabe and Lehane (2006); Doherty and Gavin (2011a, b); Lehane et al. (2000)
35	Klang clay site, western shoreline, Malaysia	Soft marine clay	PTC	CPTu	C	Yes	Yes	4	Liew and Kowng (2005)
36	Kunshan town, eastern Jiangsu province, China	Silty clay	PTC	SCPTu	C	Yes	No	1	Cao et al. (2012)
37	Labenne sand, Bayonne, SW France	Fine-medium uniform sand	ICP	CPT	C and T	Yes	Yes	3	Lehane et al. (1993); Lehane (1992); Chow (1996)
38	Limelette test site, Brussels, Belgium	Silty/sandy clay over clayey sand	10 Screw piles and 2 Sq-C	SCPT + CPT	C	Yes	Yes	12	Alboom and Whenham (2003); Huybrechts and Whenham (2003); Maertens and Huybrechts (2003)
39	LNG storage site, Delaware River, Gloucester county, NJ, USA	Varved clayey silt over dense gravelly sand over dense residual clayey sand	OE-S	SCPTu	C	Yes	Yes	2	Tan and Lin (2013)
40	Lock and Dam 26 Project, Mississippi River, IL, USA	Glacial gravelly sand	6 HP and 14 CE-S	CPTu	C and T	Yes	Yes	20	Tucker and Briaud (1988)
41	Lulu Island, University of British Columbia Pile Research Site (UBC PRS), BC, Canada	Soft silty clay over medium dense sand over clayey silty sand	1 OE-S and 4 CE-S	SCPTu	C	Yes	Yes	5	Davies (1987)

Notes: DS: drilled shaft; CFA: continuous flight auger pile; CE-S: closed-ended steel pipe pile; OE-S: open-ended steel pipe pile; OE-SC: open ended concrete filled steel pipe pile; ICP: closed-ended Imperial College Pile; HP: H-section steel pile; PTC: pre-stressed concrete thin-wall caisson; PHC: Pre-stressed concrete high-strength; Sq-C: square precast concrete pile; C-C: circular precast concrete pile; C: top-down compression loading mode; T: top-up tension (or uplift) loading mode; O-cell: bi-directional Osterberg cell loading mode; A: augered piles; D: driven piles; J: jacked piles; B-CIS: bored cast in-situ piles.

Table 5.1. (continued).

Site ID	Site Name and Location	Soil Type	Pile Type	In-situ test type	Load test type	Load Test Data		No. of pile load tests	Reference
						Q-w	Q-z		
42	Ministry of Transportation & Highways Pile Research Site (MOTH PRS), Alex Fraser Bridge, BC, Canada	Soft silty clay over medium dense sand over clayey silty sand	OE-S	SCPTu	C	Yes	No	3	Davies (1987)
43	New Museums, Gault clay, Central Cambridge, UK	Gravelly fill over stiff fissured clay	DS	SCPTu	C	Yes	Yes	1	Butcher and Lord (1993); Powell et al. (1988)
44	Northwestern University NGES, Evanston, IL, USA	Sand fill over soft-firm clay	2 DS, 1 HP and 1 OE-S	SCPTu	C	Yes	Yes	4	Finno (1989); Finno et al. (1989)
45	Noetsu Bridges No. 3 and 4, Noto Peninsula, Japan	Diatomaceous mudstone	OE-S	SCPTu	C and T	Yes	Yes	3	Matsumoto et al. (1995)
46	Old San Juan site, Puerto Rico	Interbedded sand and clay	DS	SCPTu	C	Yes	Yes	1	Pando et al. (2004)
47	Onsøy clay site, south-eastern Norway	Soft clay with shell fragments	1 OE-S and 6 CE-S	SCPTu	T	Yes	Yes	10	Karlsrud (1988); Lunne et al. (2003)
48	Pentre silt, Shropshire, UK	Soft clayey silt	1 OE-S and 19 CE-S	SCPTu	C and T	Yes	Yes	20	Chow (1996)
49	Pinner's Point Interchange, Portsmouth, VA, USA	Interbedded sand and clay soils of Norfolk Formation overlying medium to dense sand of Yorktown Formation	DS	SCPTu	O-Cell	Yes	Yes	2	Kort et al. (2001a, b)
50	Pitt River Bridge, Vancouver South, BC, Canada	Interbedded silt, clay, and sand over thick layer of silty clay over glacial till	OE-SC	SCPTu	C	Yes	Yes	2	Tara (2012)

Notes: DS: drilled shaft; CFA: continuous flight auger pile; CE-S: closed-ended steel pipe pile; OE-S: open-ended steel pipe pile; OE-SC: open ended concrete filled steel pipe pile; ICP: closed-ended Imperial College Pile; HP: H-section steel pile; PTC: pre-stressed concrete thin-wall caisson; PHC: Pre-stressed concrete high-strength; Sq-C: square precast concrete pile; C-C: circular precast concrete pile; C: top-down compression loading mode; T: top-up tension (or uplift) loading mode; O-cell: bi-directional Osterberg cell loading mode; A: augered piles; D: driven piles; J: jacked piles; B-CIS: bored cast in-situ piles.

Table 5.1. (continued).

Site ID	Site Name and Location	Soil Type	Pile Type	In-situ test type	Load test type	Load Test Data		No. of pile load tests	Reference
						Q-w	Q-z		
51	Refinery Expansion Project, Mid-west, USA	Sand deposit over compressible post-glacial lacustrine clay/silty clay till over limestone bedrock	DS	CPTu	O-Cell	Yes	Yes	2	Fellenius and Ochoa (2009)
52	Saint Alban, QC, Canada	Soft silty marine clay	CE-S	CPTu + SASW	C	Yes	Yes	5	Heydinger (1982); Konrad and Roy (1987); Lefebvre et al. (1995)
53	Sandpoint, along the shores of Lake Pend Oreille, Northern ID, USA	Silty clayey sand over soft thick silty clay	CE-S	SCPTu	C	Yes	Yes	1	Fellenius et al. (2003)
54	San Francisco Bay Mud, I-280 Caltrans Load Tests, CA, USA	Uniform soft silty clay over dense sand	9 OE-SC, 8 Screw piles, 4 OE-S, 8 Sq-C and 3 HP	SCPTu	C and T	Yes	No	32	Brittsan and Speer (1993)
55	Shenton Park, Perth, Western Australia	Siliceous sand	10 OE-S and 2 CE-S	SCPT	T	Yes	Yes	12	Schneider (2007)
56	Shirasu soil, lanima, Southern Kyushu, Japan	Clean sand over silty sand over silty clay	DS	CPTu	C	Yes	Yes	2	Takesue et al. (1996)
57	South Temple test site on I-15, Salt Lake City, Utah, USA	Silty sandy clay over sensitive clay	CE-S	SCPTu	C	Yes	Yes	7	Garner (2007)
58	Spring Villa, Opelika NGES, AL, USA	Clayey-silty sand	10 DS and 1 CFA pile	SCPTu	C	Yes	Yes	11	Brown (2002)
59	State Road 49, Jasper County, Indiana, USA	Silt dominated multilayered soil	1 HP and 1 CE-S	CPTu + SPT N	C	Yes	Yes	2	Seo et al. (2009); Kim et al. (2009)
60	Texas A&M University (TAMU) NGES clay site, College Station, TX, USA	Very stiff Pleistocene clay	DS	SCPTu	C	Yes	Yes	1	Briaud et al. (2000)

Notes: DS: drilled shaft; CFA: continuous flight auger pile; CE-S: closed-ended steel pipe pile; OE-S: open-ended steel pipe pile; OE-SC: open ended concrete filled steel pipe pile; ICP: closed-ended Imperial College Pile; HP: H-section steel pile; PTC: pre-stressed concrete thin-wall caisson; PHC: Pre-stressed concrete high-strength; Sq-C: square precast concrete pile; C-C: circular precast concrete pile; C: top-down compression loading mode; T: top-up tension (or uplift) loading mode; O-cell: bi-directional Osterberg cell loading mode; A: augered piles; D: driven piles; J: jacked piles; B-CIS: bored cast in-situ piles.

Table 5.1. (continued).

Site ID	Site Name and Location	Soil Type	Pile Type	In-situ test type	Load test type	Load Test Data		No. of pile load tests	Reference
						Q-w	Q-z		
61	Texas A&M University (TAMU) NGES sand site, College Station, TX, USA	Medium dense sand over stiff clay	DS	SCPTu	C and O-cell	Yes	Yes	2	Briaud et al. (2000); O'Neill et al. (2002)
62	Trunk Hwy 212 Bridge No. 10038 near Minneapolis, MN, USA	Stiff clay loam glacial till over dense sand	CE-SC	SCPTu	C	Yes	No	2	Reuter (2010)
63	Trunk Hwy 52 Lafayette Bridge over the Mississippi River, St. Paul, MN, USA	Fine to coarse gravelly sand	1 CE-SC and 1 CE-S	SCPTu	C	Yes	Yes	2	Komurka and Grauvogl-Graham (2010)
64	University College Dublin (UCD), Ireland	Uniform loose sand (trenched, backfilled and recompacted)	OE-S	CPT + MASW	C	No	Yes	1	Igoe et al. (2011; 2010)
65	University of Massachusetts-Amherst NGES, Amherst, MA, USA	Silty clay crust over soft varved clay	DS	SCPTu	C	Yes	Yes	2	Iskander et al. (2003)
66	University of Porto, Portugal (FEUP), ISC-2 experimental site	Residual silty sand	1 DS, 1 CFA pile and 1 Sq-C	CPTu + DHT	C	Yes	Yes	3	Viana da Fonseca et al. (2006); Fellenius et al. (2007)
67	University of Texas NGES, Houston, TX, USA	Stiff Beaumont clay over sandy clay	DS	SCPTu	O-cell	Yes	No	1	Ata and O'Neill (1998), O'Neill et al. (2002, 1982), Reese et al. (1976)
68	Varina-Enon Bridge, I-295 over James River, Richmond, VA, USA	Alluvial sands, silts, and clays overlying dense sands and gravels	Sq-C	SCPTu	C	Yes	No	1	Mayne (2002)
69	W. R. Bennett Bridge, Okanagan Lake at Kelowna, BC, Canada	Loose to medium dense lacustrine silts and sandy silt overlying sand	CE-S	CPTu	C	Yes	Yes	1	Naesgaard et al. (2006)
70	Wakota River Bridge site (I-494 Mississippi River Bridge), MN, USA	Sand with intermittent layers of silt and clay	2 OE-S and 2 CE-S	SCPTu	C and T	Yes	No	4	Dasenbrock (2006)

Notes: DS: drilled shaft; CFA: continuous flight auger pile; CE-S: closed-ended steel pipe pile; OE-S: open-ended steel pipe pile; OE-SC: open ended concrete filled steel pipe pile; ICP: closed-ended Imperial College Pile; HP: H-section steel pile; PTC: pre-stressed concrete thin-wall caisson; PHC: Pre-stressed concrete high-strength; Sq-C: square precast concrete pile; C-C: circular precast concrete pile; C: top-down compression loading mode; T: top-up tension (or uplift) loading mode; O-cell: bi-directional Osterberg cell loading mode; A: augered piles; D: driven piles; J: jacked piles; B-CIS: bored cast in-situ piles.

5.6 Pile Characteristics

The 330 pile load tests compiled for the current databank belong to the following 9 main categories:

- Open-ended steel pipe piles (OE-S): 63
- Close-ended steel pipe piles (CE-S), including imperial college piles (ICP): 99
- Open-ended concrete (OE-C), including pre-stressed concrete thin-wall caisson (PTC), pre-stressed concrete high-strength (PHC), and spun cast concrete cylinder piles: 7
- Drilled shafts (DS), also termed bored piles in European nomenclature: 73
- Pre-stressed precast square section concrete piles (Sq-C): 22
- Pre-stressed precast circular section concrete piles (C-C): 11
- Augered piles (A), including continuous flight auger piles (CFA), Atlas piles, Fundex piles, Omega piles, Olivier piles, and De Waal piles: 29
- H-section steel piles (HP): 17
- Timber (teak) or wood piles: 8

The percent distributions of the above types are given in the pie chart shown in Figure 5.3. These piles range in size (diameter or width) from 0.04 to 2.60 m, and range in embedment length from 0.75 to 100.00 m. Also shown below is the alternative classification of piles in the database and their distribution based on the installation methods (see Figure 5.4 for percent distribution):

- Driven piles (D), including OE-S, CE-S, OE-C, Sq-C, C-C, HP, and Teak piles: 169
- Jacked piles (J), including OE-S, CE-S, and OE-C: 58
- Augered piles (A), including CFA, Atlas piles, Fundex piles, Omega piles, Olivier piles, and De Waal piles: 29

- Bored cast in-situ (B-CIS) DS: 73

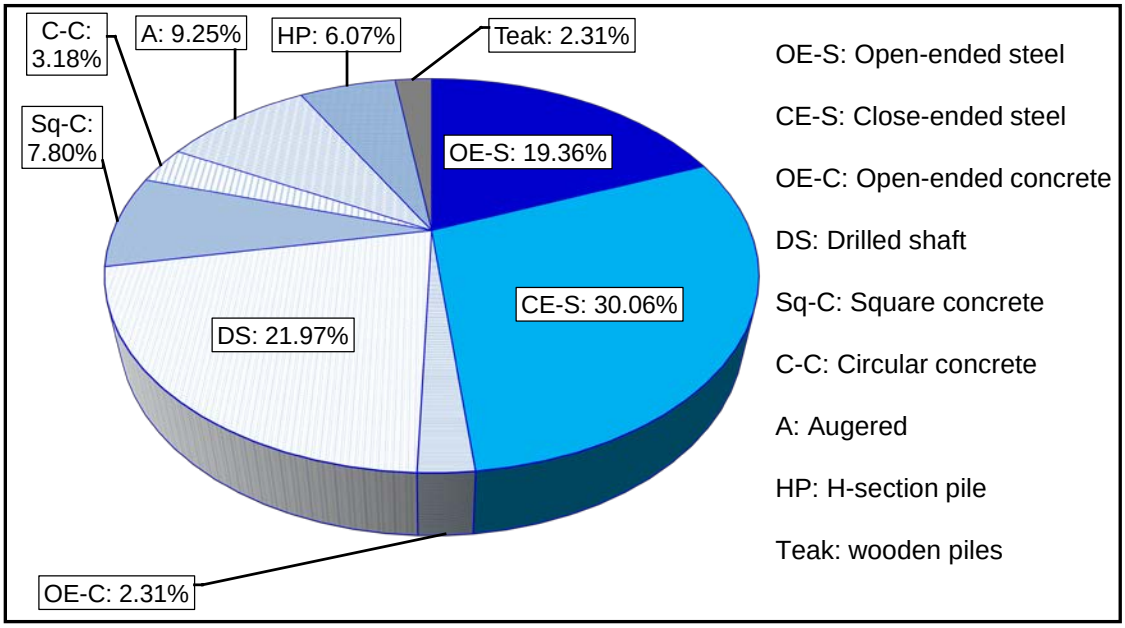

Figure 5.3. Percent distribution of pile types in the database.

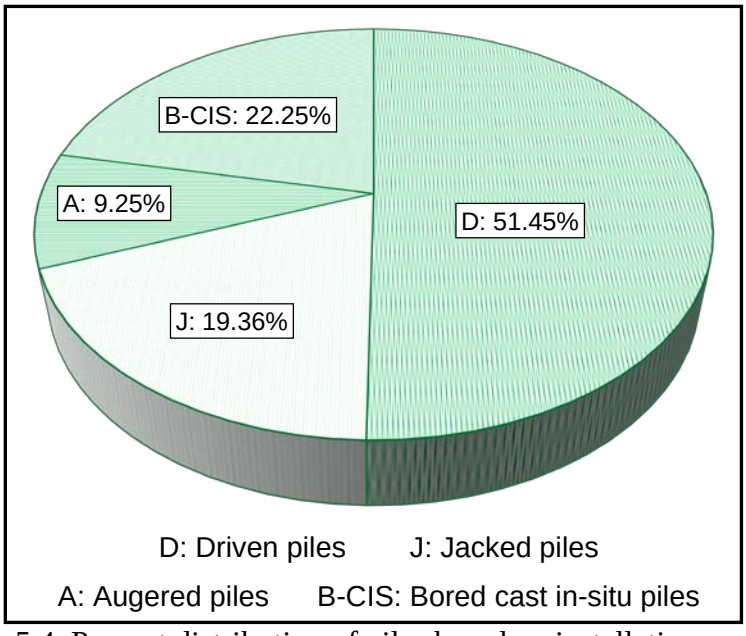

Figure 5.4. Percent distribution of piles based on installation methods.

The piles in the databank vary greatly in both, diameter (or width) and length. Figures 5.5 and 5.6 present frequency distributions of the piles in terms of magnitudes of pile diameter and pile length, respectively. Also presented in these figures are some basic statistics of their respective measurements. Clearly, more than 85% of the piles have diameters within the range of 0.04 m to 0.915 m, with an overall mean of 0.56 m. Similarly, about 88% of piles have lengths ranging between 2.15 m and 35.0 m, with overall mean of 15.5 m. It is also pertinent to mention that for non-circular piles (Sq-C and HP), equivalent shaft diameters were calculated from their outer perimeters, based on the recommendations detailed in Chapter 3. An alternative way of studying the size effects of pile on axial loading response is via pile slenderness ratio (L/d), the frequency distribution of which is shown in Figure 5.7. About 84% of the piles range in slenderness ratio from 8.5 to 100, with an overall mean of 41.6.

5.7 Pile Loading Tests

Indicated earlier is the fact that the load tests included in this databank belong to three different loading modes, and their respective distributions are shown below (also see the pie chart presented in Figure 5.8 for percent distribution of each category):

- Top–down type compression loading (C): 203
- Top –up type uplift (or tension) loading (T): 96
- Osterberg cell type compression loading (O-cell): 31

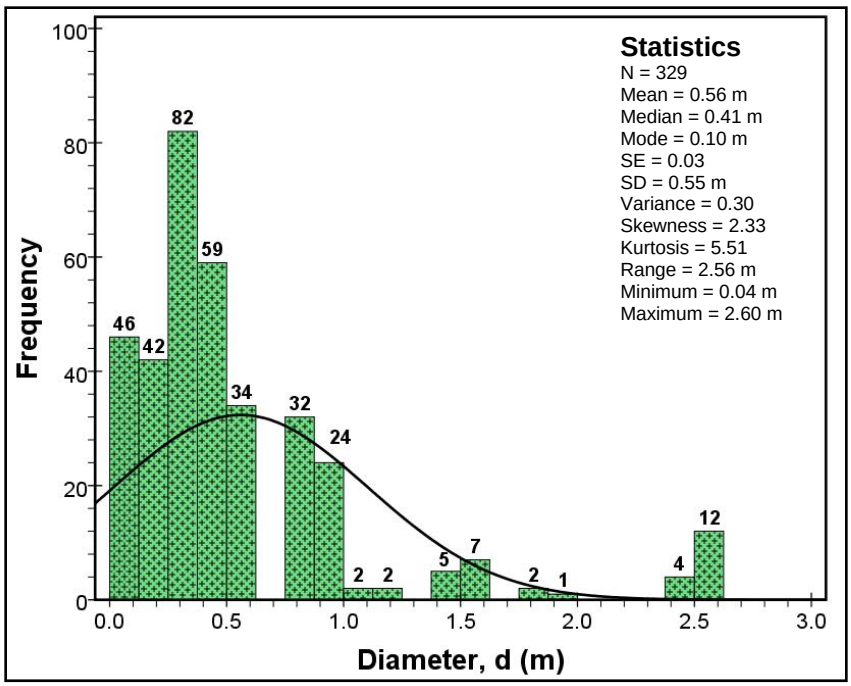

Figure 5.5. Frequency distribution and statistics of pile diameters in the database.

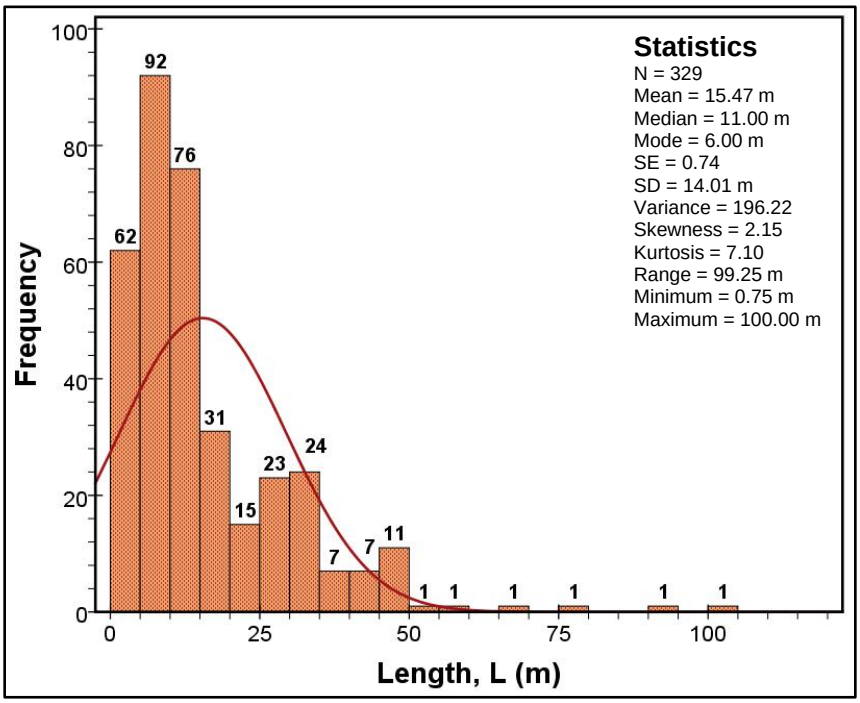

Figure 5.6. Frequency distribution and statistics of pile lengths in the database.

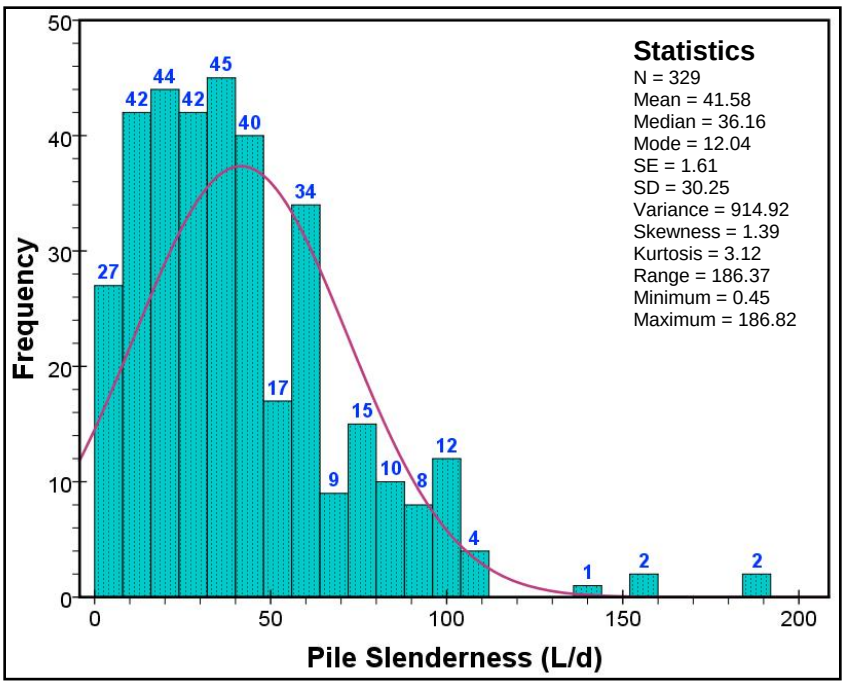

Figure 5.7. Frequency distribution and statistics of pile slenderness ratio in the database.

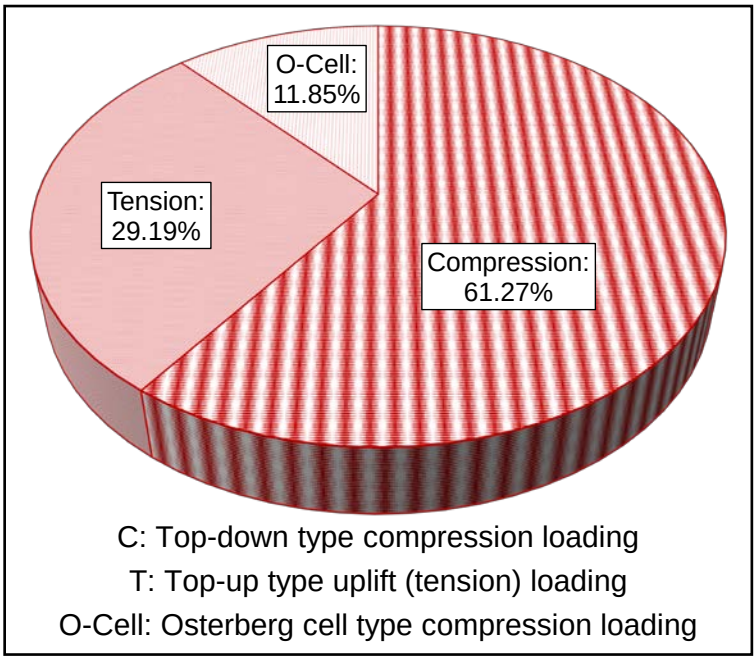

Figure 5.8. Percent distribution based on the loading modes of pile load tests.

The load application procedures used in this database of piles include those of stress-controlled (SMLT or QML) or strain-controlled (CRDT). Here the cases of O-cell

include four loadings arrangements detailed in Chapter 2, namely, case 1: one O-cell at the pile base, single stage, case 2: one O-cell above the pile base, single stage, and cases 5 and 6: two O-cells, lower cell placed above the pile base, multi-stage. Based on the instrumentations and reporting, these load tests provided following sets of output data (also see Figure 5.9 for percent distribution):

- Load-displacement and load transfer distribution (Q-w and Q-z) data: 271 cases
- Load displacement (Q-w) data only: 49 cases
- Load transfer distribution (Q-z) data only: 9 cases

Figure 5.10 shows the frequency distribution of the magnitude of $Q_{max\text{-}measured}$ of piles in database. As presented, the maximum applied loads in these tests range between 5.69 kN for model piles and 44.54 MN for high capacity large diameter pile, with a mean value of 3.36 MN. About 86% of piles experienced $Q_{max\text{-}measured}$ less than 4,000 kN, with more dominant range being 1,000 kN to 1,500 kN.

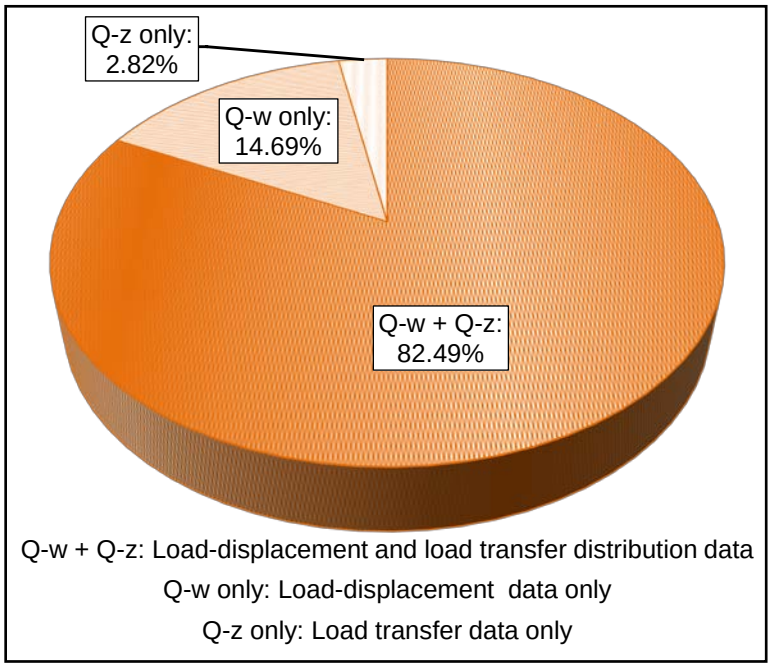

Figure 5.9. Percent distribution based on the data derived from the pile load tests.

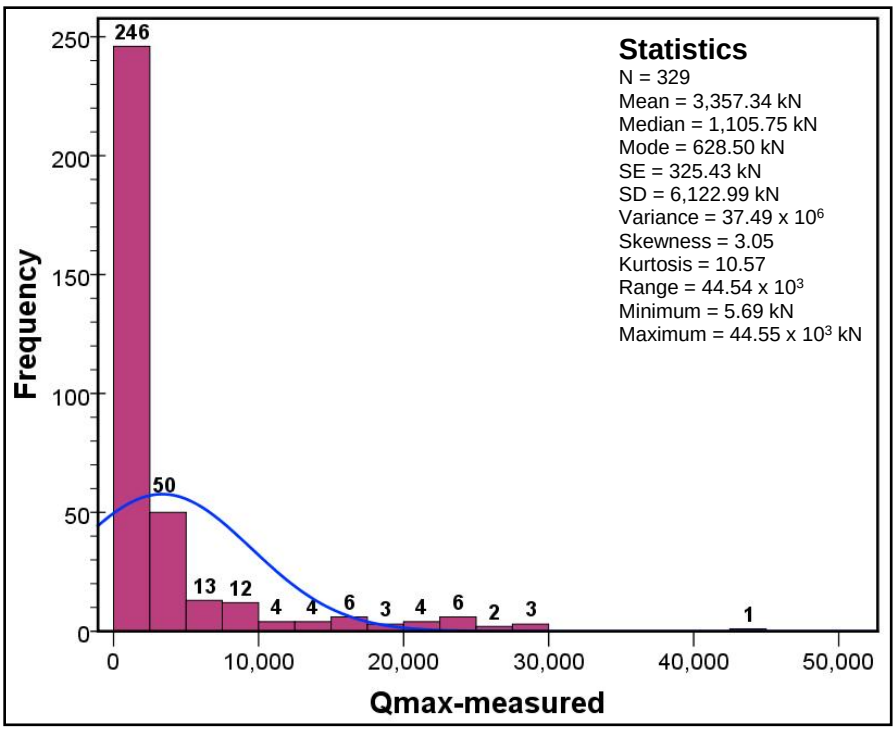

Figure 5.10. Frequency distribution and statistics of $Q_{max\text{-}measured}$ in the database.

5.8 Cone Penetration Tests

Within the purview and scope of this research, a dedicated effort resulted in compilation of the current database of the sites with a predominant majority of SCPT/SCPTu soundings. Accordingly, 80% of the selected sites afforded the shear wave velocity (V_s) directly from the CPT, in addition to the penetrometer readings (q_t, f_s, and u_2). In another 9% of the cases, V_s profiles were available from alternative geophysical measurement, as detailed in subsequent paragraphs. In a few limited cases (11%), V_s was calculated via the well-established correlations listed in Table 3.1 of Chapter 3.

The alternative methods of V_s data acquisition in the current databank include downhole test (DHT): 3 sites; spectral analysis of surface waves (SASW): 2 sites; seismic dilatometer test (SDMT): 1 site; and multichannel analysis of surface waves (MASW): 1 site. The pie charts shown in Figures 5.11 and 5.12 provide information on the percentages of different categories of penetrometer soundings in this databank and the

sources of V_s, respectively. Here, the number of site and sets of readings provided in each category are given below:

- SCPTu (q_t, f_s, u_2 or u_1, and V_s): 51
- SCPT (q_t, f_s, and V_s): 8
- CPTu: q_t, f_s, u_2 or u_1: 11
- CPT: q_t and/or f_s: 6

As shown above, some of the piezocone penetrometers (CPTu or SCPTu) provide porewater pressure readings measured via piezometer element placed at the cone mid-face location (i.e., u_1 readings). In these few cases, well-researched relationships were used for conversion of u_1 readings to u_2, as subsequently detailed in Chapter 6.

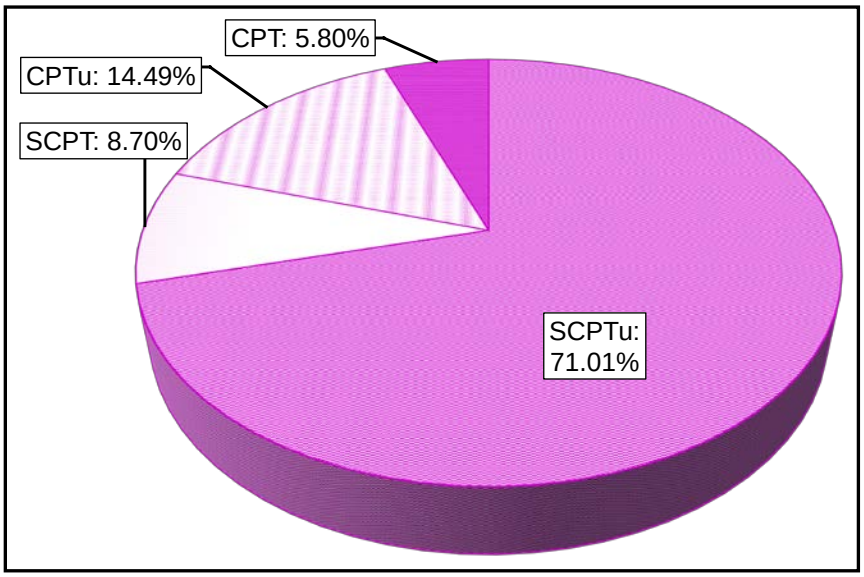

Figure 5.11. Pie chart showing percent proportions of different categories of CPT soundings in the current database.

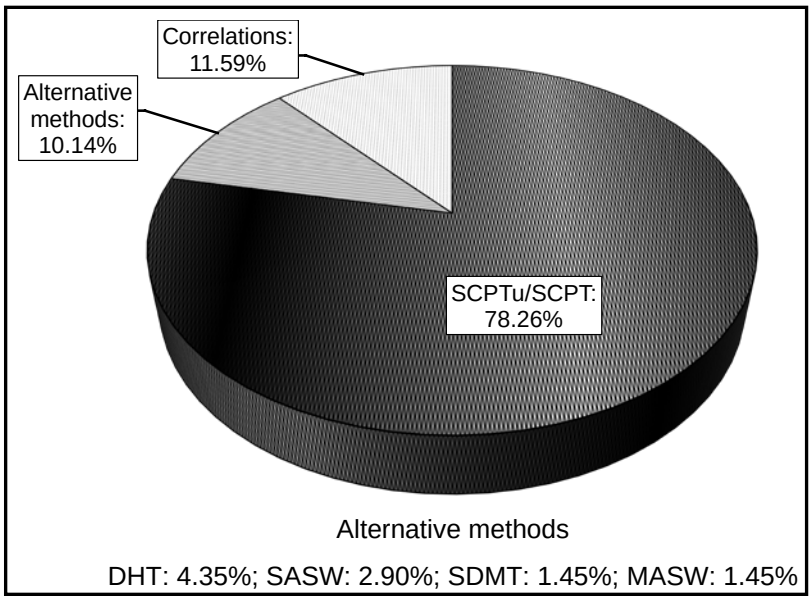

Figure 5.12. Pie chart showing percent proportions of different sources of V_s.

5.9 Categorization of the Database for Analysis

Based on the scope outlined for this research and classification of the compiled database, the sites, piles, and penetrometer data were grouped into following three categories for the purpose of analysis:

- *Group 1*: This group includes 153 pile load tests from 52 sites that provide both Q-z data as well as piezocone readings (q_t, f_s and u_1 or u_2). The load tests include all three types: C, T, and O-cell, while some of the penetrometer soundings that did not provide 'u' readings belong to sand sites, in which case, porewater pressures have been assumed hydrostatic. This subset was used in developing a CPTu-based direct method for pile capacity evaluations. Specific listing of this subset of the database, discussions, details and results are presented in Chapter 6.
- *Group 2*: This group includes 299 pile load tests from 61 sites that provide Q-w data as well as the geophysical component of penetrometer data (i.e., V_s). The load tests include the conventional C and T types only. As explained earlier, for

some of these sites, V_s data were available from alternative investigation methods, while correlations were used for a few sites where pile load test data were very well documented. This subset was used in refining the elastic continuum framework for evaluating the complete Q-w response of piles to axial loading, where new modulus reduction schemes have been developed (see Chapter 7) and stacked pile model is proposed (see Chapter 8). Detailed listing and characteristics of this subset of the database are presented in Chapter 7.

Group 3: A small group of 16 selected and well-documented O-cell load tests from 9 sites was utilized in a separate study. At all these sites, SCPTu soundings had also been advanced; so V_s data were available. This subset was used in extending the elastic continuum model of Q-w evaluations for application to different cases of O-cell loading, besides generating separate modulus reduction trends from back-analysis, specifically meant for O-cell loadings. Case-by-case details of this subset are given in Chapter 9.

5.10 Concluding Remarks

In order to conduct a comprehensive research study on the axial load-displacement-capacity response of piles, a large database was compiled where pile foundations were load tested under top-down compression or top-applied uplift (tension) loading, or both, or by O-cell setups. All test sites had been investigated using CPT soundings; in most cases by the preferred SCPTu that provides all four readings from the same sounding: q_t, f_s, u_2, and V_s. In a few cases, sites were subjected to CPT or CPTu and the profiles of shear wave velocities were obtained by other field geophysical techniques, otherwise by empirical estimations.

In this chapter, a listing of all 330 case records of pile load tests at 70 sites from 5 continents and 19 different countries of the world is presented. Also annexed to this chapter is a more detailed Appendix E that provides further case-by-case information.

Included in this chapter are the locations of the sites, overviews of the distribution of data on the basis of soil types, pile types, pile installation methods, pile loading modes, load test results, and penetrometer data, as well as categorization of the database for subsequent analyses. More specific details of each case and the results of the combined analyses are presented in the ensuing chapters.

CHAPTER 6

MODIFIED UNICONE DIRECT PIEZOCONE TEST METHOD FOR AXIAL PILE CAPACITY

Synopsis

In this chapter, the *UniCone* direct piezocone method (Eslami and Fellenius, 1997) for evaluating the axial capacity of pile foundations is reviewed and improved means of assessing soil resistance factors are recommended. This method uses all three piezocone penetration test (CPTu) readings in a soil behavioral type (SBT) classification chart and provides estimations of axial pile capacity for a wide variety of pile types installed in different assortments of geomaterials. Herein, the *UniCone* soil classification chart is refined using the Group 1 dataset of pile load tests and CPTu soundings (detailed in Appendix F). An alternative soil classification system using the CPT material index I_c (Robertson, 2009) is used to provide improved correlations of higher reliability via continuous functions for estimating the side and tip capacity components of driven pilings, jacked piles, and drilled shafts. An analysis is also included to test the performance of the newly proposed design formulations.

6.1 Introduction

The axial capacity analysis of pile foundations has been a topic of great interest in soil-structure interaction problems because of its importance in safety, economy, and efficiency for infrastructure support. Due to uncertainties in assessing pile capacity via soil strength-deformation characteristics, it is common in design practice to refer the axial components of unit base (or toe or tip) resistance (q_b) and unit shaft (or side) resistance (f_p) directly to the results of the prevalent in-situ tests (Jamiolkowski, 2003). Laboratory tests provide some role in clay strata, but sands are quite difficult and expensive to sample in an undisturbed manner. Therefore, despite improvements in numerical and

analytical solutions, the foremost reliance is still placed on empirical relationships. Evaluations from cone penetration test (CPT) readings fall amongst the most frequented applications of CPT data.

Ever since the initial use of CPT in geotechnical investigations, research efforts have advanced the analogy in considering the cone penetrometer as a mini-pile foundation to correlate its readings with the pile capacity components. The simultaneous evolution of CPT from mechanical to electrical to electronic tool, and single parameter measurement (i.e., cone tip resistance, q_c) to the piezocone penetration test with multiple readings (q_t, f_s, and u_2) has resulted in the contemporaneous development of CPT-based pile design methods. Here pile-CPT correlations have been worked out on the basis of full-scale load test results on both instrumented and un-instrumented piles with site investigations involving cone penetrometers.

As detailed in Chapter 3, there are two main approaches to accomplish axial pile capacity analysis using CPT data: (a) rational (or indirect) methods, and (b) direct methods (Mayne, 2007). Figure 6.1 presents a schematic illustration for implementing these two approaches. In both cases, the unit side friction (f_p) acts over the pile shaft area to obtain the pile shaft capacity (Q_s) and the unit toe resistance (q_b) acts on the pile toe to obtain the pile base capacity (Q_b) that are summed for the total capacity: $Q_t = Q_s + Q_b$.

A comprehensive state-of-the-art review on the historical evolution of direct and indirect CPT-based methods has been included in Chapter 3 (Niazi and Mayne, 2013). Some of these methodologies were developed for selected pile types and geologic soil conditions, while others were derived from several varieties of pile systems installed in a wide range of geomaterials. Most of the older methods were based on q_c readings of the mechanical CPT alone, while later methods incorporated the f_s readings in their design formulations as friction sleeve was attached to the penetrometers.

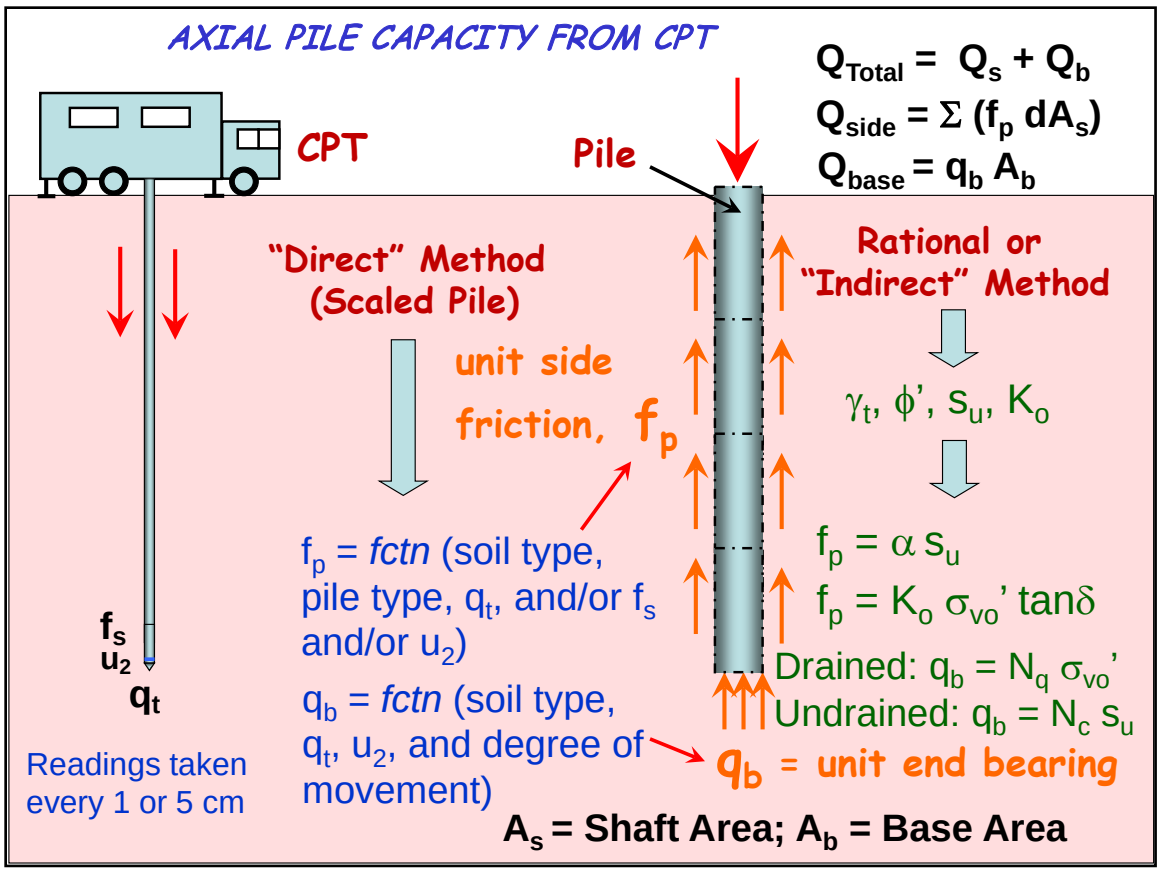

Figure 6.1. Axial pile capacity from direct and rational (or indirect) CPT methods.

6.2 Piezocone Penetrometer Testing

By incorporating piezometer elements into the electric cone penetrometers, piezocone testing (CPTu) was introduced in early 1980's (Torstensson, 1982). The CPTu provides continuous profiles of multiple measurements: corrected tip resistance (q_t), sleeve friction (f_s), and excess porewater pressures measured at the shoulder or behind the tip position (u_2). Here q_t accounts for the correction of pore water pressures (u_2) acting on unequal tip area of the cone, given by (Jamiolkowski et al., 1985):

$$q_t = q_c + (1 - a_n)\, u_2 \qquad (6.1)$$

where a_n = cone dependent net area ratio (cross-sectional steel area at the gap between cone and friction sleeve to the cone toe area). In clean sands and dense granular soils, it may be reasonable to assume $q_t \approx q_c$ because u_2 remains essentially hydrostatic (u_o). However, in soft to stiff intact clayey and silty soils, considerable excess pore water pressures are generated during cone penetration, warranting corrections to the measured q_c in order to obtain q_t (Mayne, 2007).

Some penetrometer designs provide porewater pressure readings measured via a piezometer element placed at the cone tip, either the apex or mid-face (u_1). Analogous to the situations stated above for clean sands and granular soils, u_2 for such cases may also be assumed nearly same as u_1; whereas, for clayey and silty soils that are tested under undrained conditions, either of the following correlations may be used for this conversion:

$$\text{Chen and Kulhawy (1994): } u_2 = 0.742\ (u_1) \tag{6.2}$$

$$\text{Peuchen et al. (2010): } u_2 = K\ (u_1 - u_o) + u_o \tag{6.3a}$$

$$\text{where } K = 0.91 \exp(-0.09\ Q_{tn}^{0.47})\ \{1/[1 + F_r\ (0.17 + 0.061\ (Q_{tn} - 21.6)^{1/3})] - \exp(-2\ F_r)\} \tag{6.3b}$$

The parameters Q_{tn} and F_r represent the stress normalized cone resistance and normalized friction ratio, respectively, that relate to the CPT-based soil behavior type (SBT) classification index, (I_c) which will be discussed later.

6.3 UniCone Method for Pile Capacity Evaluations

Of distinctive interest amongst the CPT-based direct pile capacity evaluations are the formulations of the UniCone method proposed by Eslami and Fellenius (1997), later

updated by Fellenius (2002b). This method utilizes all three penetrometer readings from CPTu by plotting the effective cone resistance ($q_E = q_t - u_2$) at each elevation vs. the sleeve friction (f_s) at same elevation in a soil behavioral classification scheme having 5 zonal regions (Figure 6.2). A pile skin friction coefficient (C_{se}) is assigned to each region: Zone 1: soft sensitive soils: ($C_{se} = 0.08$), Zone 2: soft clays and silts ($C_{se} = 0.05$), Zone 3: stiff clay and silt ($C_{se} = 0.025$), Zone 4: silty sandy mix ($C_{se} = 0.01$), Zone 5: sand ($C_{se} = 0.004$). Table 6.1 shows the calculation procedure to obtain the unit pile side friction ($f_p = C_{se} \cdot q_E$ and unit end-bearing resistance ($q_b = C_{te} \cdot q_{Eg}$).

Table 6.2 shows a summary of the database characteristics that was utilized for development of this method. As evident, it was derived from a large database of soil and pile types, and therefore, it is applicable to a wide variety of situations.

To estimate the unit end bearing resistance (q_b), several of the CPT-based methods rely on an arithmetic averaging of measured resistances to adopt representative values in the "influence zone" around the pile base for use in their respective design equations. The CPT readings in coarse grained soils typically display squiggly profiles of tip resistance with highs and lows that may be characteristic of localized particle breakage, grain crushing, variants in void ratio, and/or thin seams of intermediate silts or lenses. Relative to their influence on the pile having a much larger diameter than the penetrometer, an arithmetic averaging of such q_t readings (or $q_{net} = q_t - \sigma_{vo}$ or $q_E = q_t - u_2$) can result in non-representative values of the pile unit end resistance (q_b). As such, Table 6.1 indicates that the UniCone method prefers use of a geometric averaging technique as a means to acquire filtered and more representative values.

Table 6.1. Design formulations of UniCone method (after Eslami and Fellenius, 1997; Fellenius, 2009).

Pile unit side resistance, f_p	Pile unit end bearing, q_b
$f_p = C_{se}\, q_E$ where $q_E = q_t - u_2$ See note (a) below and Figure 6.2 for C_{se}	$q_b = C_{te}\, q_{Eg}$ where $C_{te} = 1$ for pile diameter $d \leq 0.4$ m and $C_{te} = 1/(3d)$ for $d > 0.4$ m See note (b) below

Note (a): C_{se} = shaft coefficient from soil classification chart (from q_t, f_s and u_2)

Note (b): For C_{te} = toe correlation coefficient, q_{Eg} is the geometric average of q_E values over the influence zone (from 4d below pile toe to 8d above pile toe if pile is installed from weak soil into dense soil, and from 4d below pile toe to 2d above pile toe when pile is installed from dense soil into weak soil) after correction for u_2 and adjustment to σ'_{vo}.

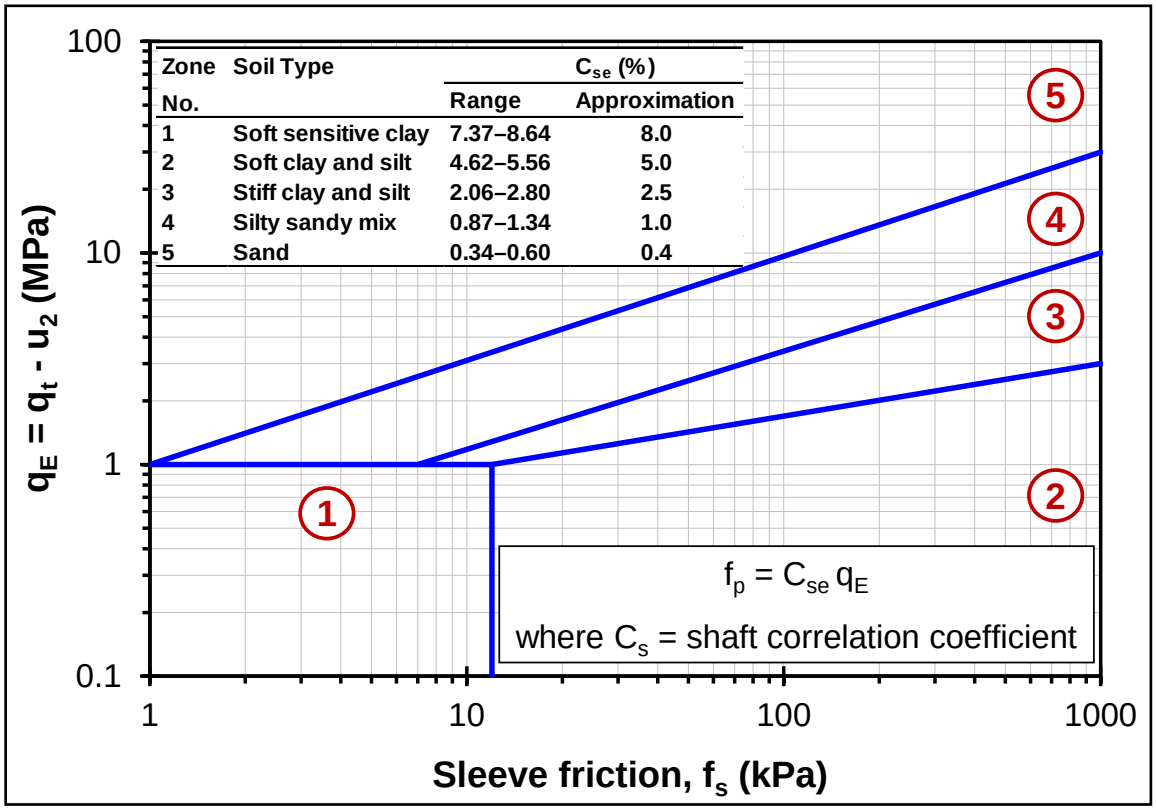

Figure 6.2. UniCone chart for zone numbers, soil types, and shaft coefficients, C_{se} (adapted from Eslami and Fellenius, 1997).

Table 6.2. Summary of Database: *UniCone Method* (after Eslami and Fellenius, 1997).

No. of piles	No. of sites/ countries	Pile diameters (m)	Pile lengths (m)	Pile types	Installation methods	Soil types	Loading mode	Stress history (OCR)
102	40/13	0.203 – 0.915	6.5 – 42.0	OE-S, CE-S, R-C, Sq-C, Tr-C, Oct-C, HP-S, B-C	CIS, D, J	All	C, T	1 – 40

Notes: OE-S: open-ended steel pipe pile; CE-S: closed-ended steel pipe pile; R-C: round concrete, Sq-C: square concrete pile, Tr-C: triangular concrete pile; Oct-C: octagonal concrete pile; HP-S: H section steel pile; B-C: bored concrete pile; CIS: cast-in-situ; D: driving; J: jacking; C: top-down compression loading mode; T: top-up tension (or uplift) loading mode.

One issue with the 1997 UniCone method is the limited and discrete choices of coefficient C_{se} that are selected. The UniCone classification chart presents five major soil zones demarcated by sharp boundaries. The same applies to the abrupt variation in the proposed C_{se} values between any two adjacent soil zones, rather than some gradual transitional values for intermediate soil types. Eslami and Fellenius (1997) noted that the number of cases used to derive this method was limited, and any further experience should result in adjustments of the design shaft and toe correlation coefficients (C_{se} and C_{te}, respectively). As previously noted (Chapter 3), Randolph and Wroth (1982), and Doherty and Gavin (2011) indicated their observations on the extension of empirically derived correlations to the design scenarios which are outside the scope of the databases originally used in their respective derivations. Herein, an improved UniCone methodology was developed by further delineating the SBT classification and adopting a more accommodating pile side friction coefficient (C_{se}).

6.4 Development of a Modified UniCone Method

An effort was made to collect a larger (153 vs. 102), more reliable, and updated database of full-scale pile load tests and cone penetrometer data. Through an extensive search of published and unpublished literature, every possible effort was made to include

high-quality case histories comprising of axial pile load tests, CPTu soundings, and additional allied soil information from laboratory, geophysical, and/or in-situ tests at documented test sites. The concept was to utilize all 3 CPTu readings (q_t, f_s, and u_2) to refine the formulation of the UniCone Method, so as to make it more convenient, consistent, and applicable to a larger variety of pile systems and different types of geomaterials.

6.4.1 Database and Case Records

The record of cases presented in this chapter is the Group 1 subset of the larger database collected in this overall research work. This includes 153 pile load tests from 52 sites in 17 different countries of the world that provide the pile load-displacement response (Q-w), load transfer distributions with depth (Q-z), in part or in full, as well as piezocone readings (q_t, f_s, and either u_1 or u_2). The following criteria explain the choices and the selection process applied to the case histories for the current analysis:

- The selected sites were characterized by penetrometer soundings advanced in the proximity of pile locations, providing multiple CPT readings.
- From the CPT data, only penetrometer readings (q_t, f_s, and u_2) were utilized in derivation of the results offered in this chapter, although most of the soundings were SCPTu based.
- The maximum depth of CPT sounding at each site extended at least as deep, or deeper than the pile base.
- The selected piles were subjected to axial load testing in three different modes: top-down compression (C), top-up tension, or uplift (T), and the newer downhole bidirectional loading utilizing the Osterberg cell (O-cell) device.
- The piles in the load test database were instrumented, enabling measurements of the complete load transfer distributions along the pile shaft and to the pile base. In some of the included cases, interpretations of the load transfer distribution were

possible from the information given in their respective sources, even though the piles were not fully instrumented during load testing.

- The particular load test database includes piles that reached at least two selected criteria defining "capacity" (Q_{cap}), namely: (1) Davisson's offset line criterion (Davisson, 1972), and (2) European or French criterion, load Q when $w_t/d = 10\%$ (Vesić, 1977), where w_t = pile top displacement, and d = pile diameter.
- The sites were so selected that a wide diversity of soil types form the database, including:, soft sensitive to stiff weathered clay, sandy-gravelly clay till, varved clay, silty clay, silt, residual silty sand, sandy silt, uniform loose to very dense medium to coarse sand, gravelly sand, and mudstone.
- The pile types included bored piles (or drilled shafts), continuous flight auger (CFA) piles, driven and jacked open-ended (OE) and closed-ended (CE) steel pipe piles, H-section steel piles, and square as well as circular precast prestressed concrete piles (PSC).

An overview of the Group 1 dataset is presented in Figure 6.3. The piles were installed in geomaterials of varied stress history, with overconsolidation ratios (OCR) ranging from 1 to 40+. The load test application procedures include both constant rate of penetration tests (CRPT) and maintained load tests (MLT) that are often step-loaded. The pile slenderness ratios [i.e., Length (L)/diameter (d)] of the database range from 3.9 to 142.0. Extreme ranges in the load carrying capacities (Q_{cap}) were as low as 10 kN for model piles to as great as 75,500 kN for high capacity production bored piles.

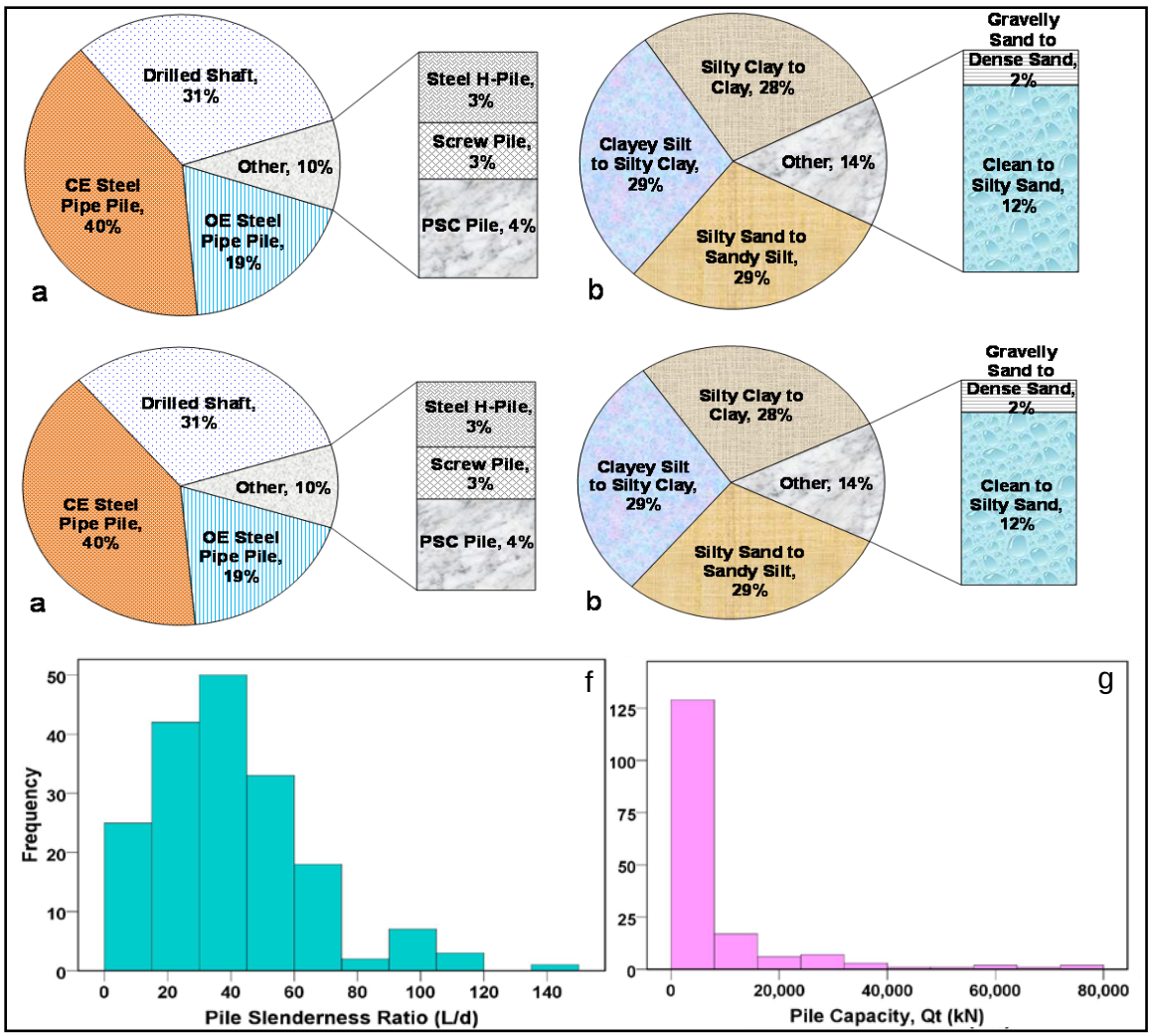

Figure 6.3. Overview summary of database showing: (a) pile types/materials; (b) soil types; (c) pile loading modes; (d) pile installation methods; (e) pile load application procedures; (f) histogram of pile slenderness ratios; (g) histogram of pile capacities.

Within the penetrometer database, CPTu profiles (i.e., q_t, f_s, and u) were available at 46 sites, while for the remaining six sites, both q_c and f_s readings were present. Furthermore, at six of the 46 sites with CPTu soundings, u_1 readings were measured instead of u_2. A concise summary of each case record that presents information on the individual pile, load test, and corresponding CPTu readings is provided in Appendix F. Certain outlines concerning the assumption made and methodologies adopted for the analysis are detailed below:

- The UniCone method was selected for possible refinement because of its versatility for the array of pile types and soil conditions that it accommodates.
- As a first step, the available CPTu data were obtained either in original files or else digitized and recorded in separate spreadsheets for each site.
- The soil profiles at each of the 52 sites were divided into appropriate number of layers based on stratigraphy, followed by calculating the geometric mean values of q_t, f_s, and u_2 for each soil layer. As noted earlier for its inherent advantages, geometric mean was preferred over arithmetic mean.
- The influence zone in context of averaging q_t around the pile base was built on the recommendation of UniCone method, i.e., 2d to 8d above the base to 4d below. In eight out of 152 piles, the maximum depth of soundings did not exceed more than 1.5d below the respective pile bases. Accordingly, the allied information of soil stratigraphy from borings etc. was examined. In all of these eight cases, no significant variations in the soil profile were noticed within a depth zone of 4d below the pile base, and therefore, geometric means were adopted from the existing available sounding depths.
- For the six sites without porewater pressure data, sandy soil profiles were encountered, in which case u_2 readings were assumed hydrostatic (i.e., $u_2 \approx u_o$). Accordingly, the q_t values were also assumed $\approx q_c$ at these sites without loss of accuracy (Robertson, 2009).
- For the few six sites providing u_1 readings, correlations by Chen and Mayne (1994) and Peuchen et al., (2010) [i.e., Equations (6.2) and (6.3), respectively] were used to predict u_2 profiles.
- The digitized pile load test data for each test pile and site were also recorded on their respective spreadsheets.

- The axial pile capacity components of f_p for respective layers and base layer q_b were calculated corresponding to the peak applied load for each test pile. In addition, from the Q-w curve of each case, the axial pile capacity (Q_{cap}) was also calculated based on three different definitions, given in the order from most to least conservative as: (1) Davisson's offset line criterion, (2) European or French criterion, and (3) hyperbolic asymptote criterion by Chin-Kondner (Chin 1970; Kondner, 1963). The aim was to relate these capacity criteria to the measured peak axial load capacities, and therefore the derived relationships are based on measured peak values.
- For circular piles closed at the base (e.g., bored piles, circular precast concrete piles, CFA piles, CE pipe piles), the shaft and base components of pile capacity were calculated using the following expressions:

$$f_{pi} = Q_{si}/A_{si} = Q_{si}/(\pi\, d_{si}\, \Delta z_i) \quad (6.4a)$$

$$q_b = Q_b/A_b = Q_b/(\pi\, d_b^2/4) \quad (6.4b)$$

where, Q_{si} = pile shaft capacity, A_{si} = shaft area, d_{si} = shaft diameter, and Δz_i = thickness of i^{th} soil layer; while Q_b = total base capacity, A_b = pile base area, and d_b = the pile base diameter. For non-circular solid piles, equivalent pile diameters were adopted. Accordingly, for square and rectangular precast concrete piles, equivalent shaft diameter, $d_{si} = (2B_i + 2W_i)/\pi$, where B_i and W_i are the breadth and width (respectively) of the pile cross-section in the i^{th} layer. In contrast, the equivalent d_b of square and rectangular precast concrete piles equals $(4\, B\, W/\pi)^{0.5}$, where B and W are the breadth and width of pile cross-section at the base, respectively. For H piles, based on the recommendations by Seo et al. (2009),

equivalent d_{si} and d_b were calculated in manners identical to the rectangular piles by adopting the outer shaft perimeter for f_p and gross cross-sectional area (flange width x depth) for q_b. For OE pipe piles, Lehane and Gavin (2001), Gavin and Lehane (2005), and Yu and Yang (2012) recommend separate contributions from annulus and plug of the pile base:

$$Q_b = (\pi/4) [d_i^2 q_{plug} + (d_b^2 - d_i^2) q_{ann}]$$

(6.5)

where q_{plug} = unit plug resistance of pile; q_{ann} = unit annulus resistance of pile; d = pile outer diameter; d_i = pile inner diameter. Here, q_{plug} accounts for the inner shaft resistance by incorporating the plug length ratio (PLR = H/L) at the end of pile installation, where H = plug length measured at the end of pile installation, and L = pile length. These calculation methodologies are explained in Figures 6.4 and 6.5. However, from the measured Q_b results of load tests on OE piles in the database, inadequate information on plugging hampered separate calculations of q_{plug} and q_{ann}, and thus simplified combined q_b calculations were adopted identical to CE piles.

- Having obtained unit pile values f_{pi} and q_b and their corresponding averaged piezocone readings for different soil layers at similar elevations onto the respective spreadsheets for each site, statistical trends were established between the two sets of interpreted data, as described subsequently.
- Finally, the statistical significance and correlative experiences from the entire database was summarized onto a master spreadsheet to draw conclusions based upon pile type, construction installation, soil typology, and other factors.

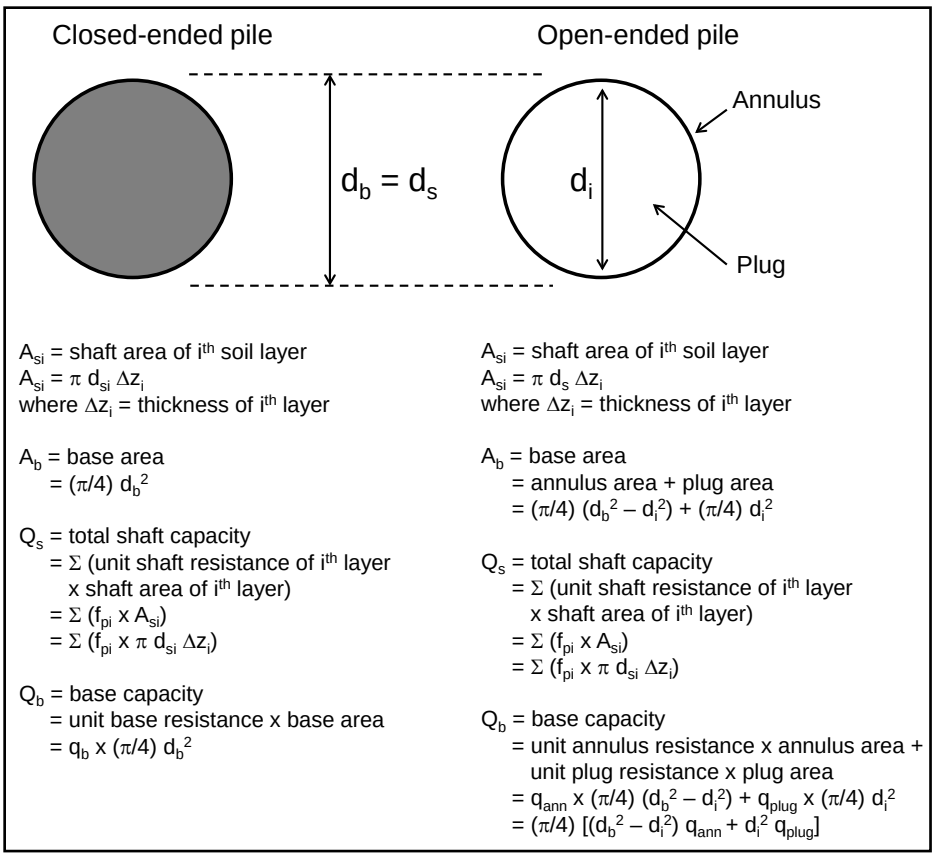

Figure 6.4. Geometry (base cross-section) of closed- and open-ended piles and the recommended calculations methodology for shaft and base capacities.

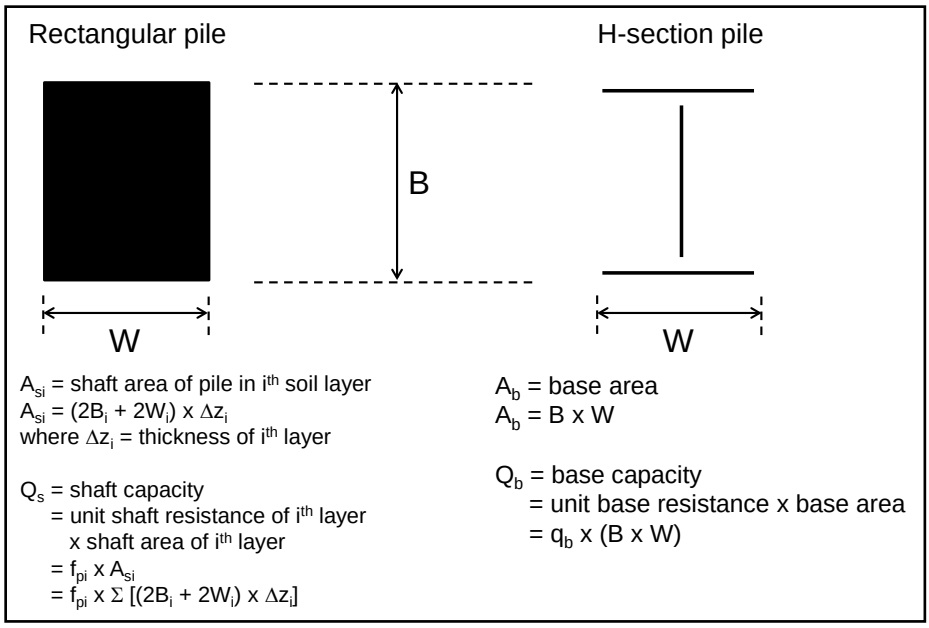

Figure 6.5. Geometry (base cross-section) of rectangular and H-section piles and the recommended calculation methodologies for shaft and base capacities.

6.4.2 Correlation Coefficient for Shaft Capacity

For the UniCone method, it may be noticed in Table 6.1 and Figure 6.2 that 'effective' tip resistance ($q_E = q_t - u_2$) is used instead of q_t in establishing the pile unit side friction coefficient (C_{se}). The same approach was implemented in the current study. Initially, following the original scheme of UniCone method, the corresponding sets of mean values were plotted on the log q_E vs. log f_s diagram of the type used by Eslami and Fellenius (1997). Based on the information of soil classification types and sub-types from the database, new sets of boundaries and sub-boundaries were delineated on the diagram, thus proposing 11 soil zones, in contrast to the 5 originally presented by the UniCone method (see Figure 6.6). It may also be noticed that based on this larger and later database, the new boundaries are slightly displaced from those of the original UniCone method. This process provided an improved CPT soil classification chart. Later, the ratios f_p/q_E were obtained as shaft correlation coefficients (C_{se}). The mean C_{se} values of 11 zones are also presented in Figure 6.6. For an overview of the scatter of C_{se} values within each zone, Table 6.3 presents some basic statistics. Clearly, these values are the synthesis results of calibration from the extended database considered in this study, with potential for further refinement through extension of the test data.

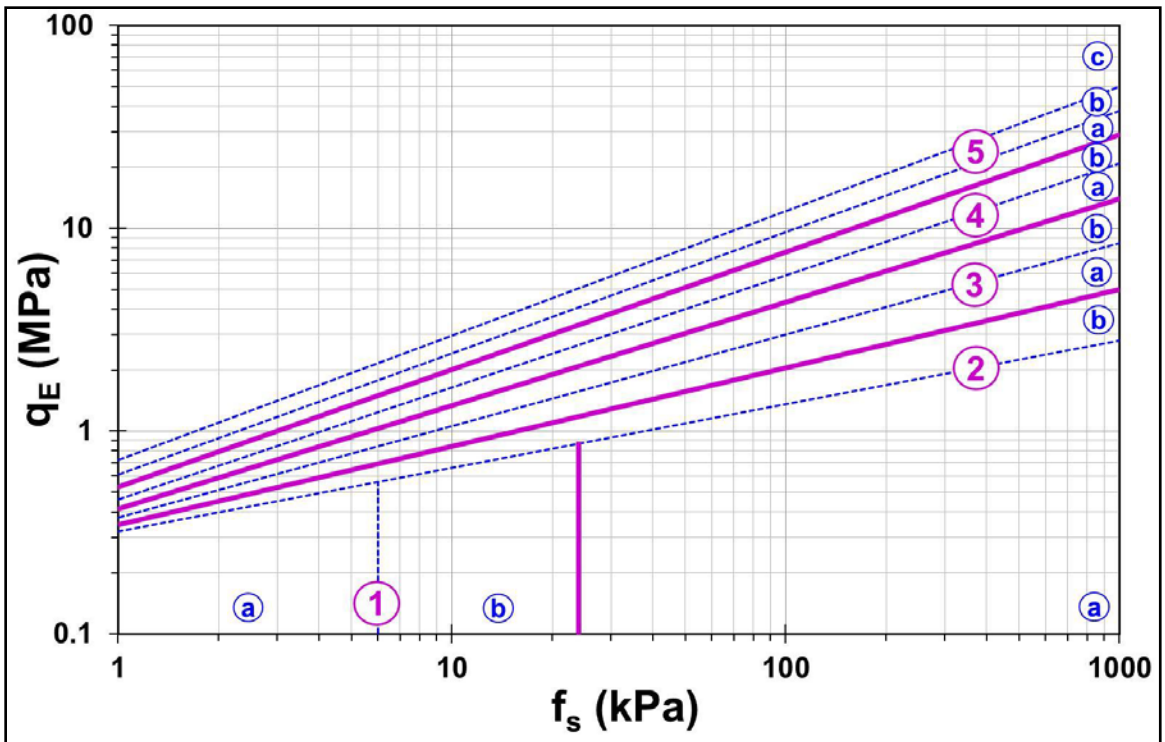

Zone No.	Soil Type	Average C_{se} (%)
1a	Very soft sensitive clay	8.32
1b	Soft clay and silt	6.57
2a	Silty marine and varved clays	4.69
2b	Stiff weathered clay, clay till	3.63
3a	Firm to medium soft silty clay	3.10
3b	Clayey silt, mudstone	2.47
4a	Sandy silt, medium dense silt	1.58
4b	Silty sand, very dense silt	1.09
5a	Uniform loose sand	0.82
5b	Medium dense sand	0.61
5c	Dense sand, gravel-sand mix	0.34

Figure 6.6. Modified UniCone CPTu chart for zone numbers, soil types, pile side friction coefficient (C_{se}).

Table 6.3. Statistics of pile shaft correlation coefficients (C_{se}) for different soil zones of log q_E vs. log f_s chart.

Zone No.	Soil type	N	Mean	Std. error of mean	Median	Mode	Std. deviation	Variance	Skewness	Kurtosis	Range	Minimum	Maximum
Zone 1a	Very soft sensitive clay	21	0.0832	0.00397	0.07857	0.0726	0.01122	0.000126	1.067	-0.162	0.03087	0.0726	0.10347
Zone 1b	Soft clay and silt	57	0.06574	0.00245	0.06166	0.06111	0.01429	0.000204	0.553	-0.946	0.04592	0.04777	0.09369
Zone 2a	Very silty marine and varved clay	48	0.04698	0.00248	0.04967	0.03337	0.01264	0.00016	-0.172	-0.71	0.04476	0.0263	0.07106
Zone 2b	Stiff to firm clay, weathered clay till	46	0.0363	0.00472	0.02886	0.03337	0.02832	0.000802	1.687	2.298	0.08377	0.00629	0.09006
Zone 3a	Firm to soft silty clay	56	0.03107	0.00385	0.02281	0.0144	0.02722	0.000741	1.16	0.007	0.08955	0.00612	0.09567
Zone 3b	Clayey silt, mudstone	23	0.02475	0.00386	0.02577	0.0092	0.0109	0.000119	-0.237	-1.565	0.02929	0.0092	0.03849
Zone 4a	Sandy silt, medium dense silt	35	0.01584	0.00154	0.01527	0.00413	0.00671	0.000045	0.367	-0.242	0.02546	0.00413	0.02959
Zone 4b	Silty sand, very dense silt	44	0.01092	0.00136	0.00922	0.01305	0.00704	0.00005	0.926	0.297	0.02262	0.00455	0.02717
Zone 5a	Uniform fine to coarse loose sand	36	0.00822	0.00058	0.00869	0.00403	0.00209	0.000004	-0.471	0.095	0.0075	0.00403	0.01153
Zone 5b	Medium dense sand	23	0.00612	0.00057	0.00643	0.00438	0.00139	0.000002	-0.143	0.189	0.00403	0.00438	0.00841
Zone 5c	Dense to very dense sand, gravel sand mix	7	0.00338	0.00024	0.00426	0.00065	0.00136	0.000002	0.141	1.684	0.0061	0.00165	0.00776

The delineation of the log q_E vs. log f_s diagram into soil sub-zones, along with their respective C_{se} is the first step in the refinement process, presenting gradual transitional values for intermediate soil types. However, as pointed out earlier, this still presents a two-step process, whereby appropriate relevant values of C_{se} have to be picked up and applied based on first classifying the soil from the log q_E vs. log f_s chart.

To obtain flexibility from the constraints of the two-step approach, an alternative CPT- based soil classification system using the SBT material index, I_c (Robertson, 2009) was considered. Robertson (2009) presented SBT boundaries on a log Q_{tn} – log F_r chart from the contours of I_c, leading to the following (also see Figure 6.7):

$$I_c = [(3.47 - \log Q_{tn})^2 + (\log F_r + 1.22)^2]^{0.5} \quad (6.6a)$$

$$Q_{tn} = [(q_t - \sigma_{vo})/\sigma_{atm}] \, (\sigma_{atm}/\sigma'_{vo})^n \quad (6.6b)$$

$$F_r = [f_s/(q_t - \sigma_{vo})] \, 100\% \quad (6.6c)$$

$$n = 0.381 \, (I_c) + 0.05 \, (\sigma'_{vo}/\sigma_{atm}) - 0.15 \leq 1.0 \quad (6.6d)$$

where σ_{vo} is the total overburden stress, σ'_{vo} = effective overburden stress, σ_{atm} is a reference stress = 100 kPa, and n = stress normalization exponent ($\leq$ 1.0) suggested by Robertson and Wride (1998) and Zhang et al. (2002) and later updated by Robertson (2009). In the above expression, the contour of I_c that demarcates the boundary between zone 3 (clays) and zone 4 (silt mixtures), and that of I_c delineating the boundary between zone 4 (silt mixtures) and zone 5 (sand mixtures) also tend to cross zone 1, that represents

the soft sensitive soils on the log Q_{tn} – log F_r chart. This zone of soft sensitive soil is characterized by the following expression:

$$I_{z1} = Q_{tn} - 12\exp(-1.4F_r) < 0 \qquad (6.6e)$$

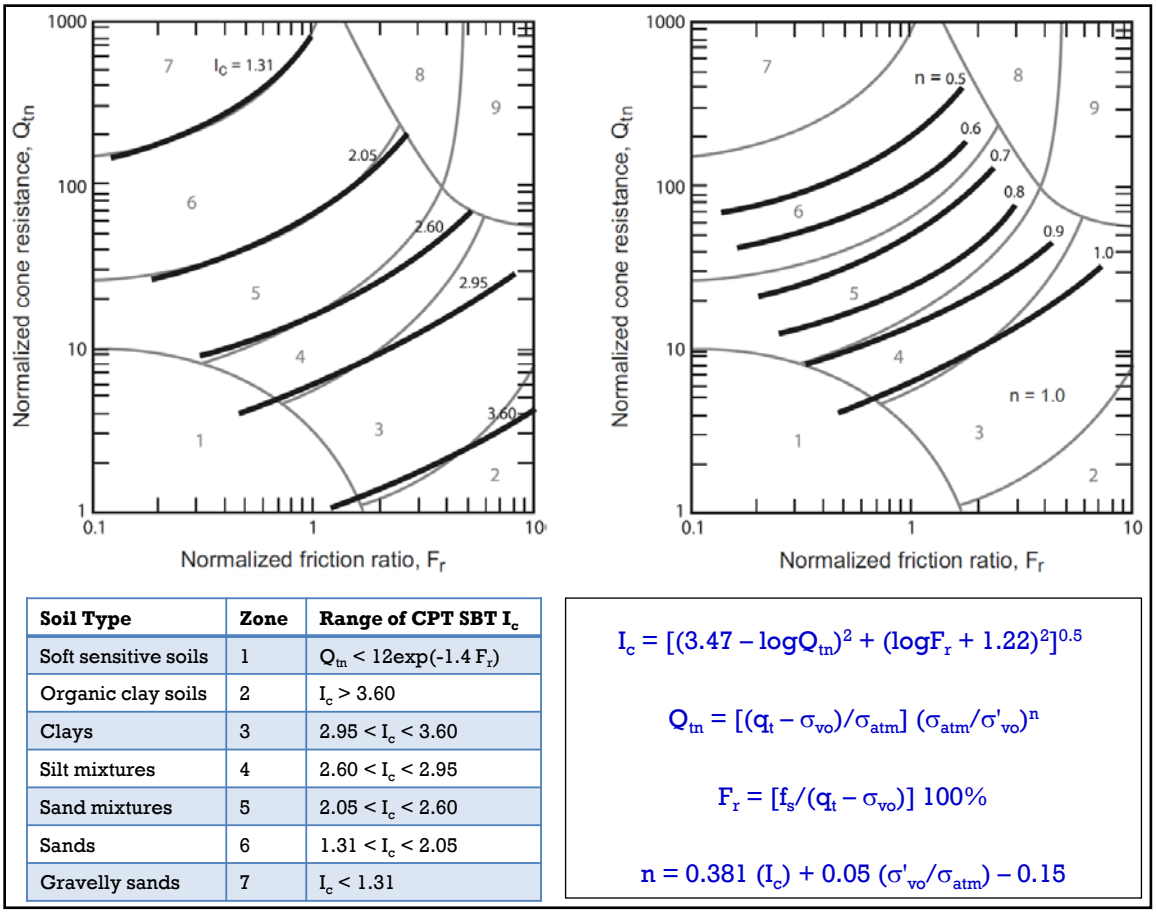

Soil Type	Zone	Range of CPT SBT I_c
Soft sensitive soils	1	$Q_{tn} < 12\exp(-1.4\ F_r)$
Organic clay soils	2	$I_c > 3.60$
Clays	3	$2.95 < I_c < 3.60$
Silt mixtures	4	$2.60 < I_c < 2.95$
Sand mixtures	5	$2.05 < I_c < 2.60$
Sands	6	$1.31 < I_c < 2.05$
Gravelly sands	7	$I_c < 1.31$

$$I_c = [(3.47 - \log Q_{tn})^2 + (\log F_r + 1.22)^2]^{0.5}$$

$$Q_{tn} = [(q_t - \sigma_{vo})/\sigma_{atm}]\ (\sigma_{atm}/\sigma'_{vo})^n$$

$$F_r = [f_s/(q_t - \sigma_{vo})]\ 100\%$$

$$n = 0.381\ (I_c) + 0.05\ (\sigma'_{vo}/\sigma_{atm}) - 0.15$$

Figure 6.7. Contours of SBT index, I_c and stress normalization exponent, n (thick lines), on normalized SBTn Q_{tn} – F_r chart (after Robertson, 1990; 2009).

Accordingly, an investigation was made to establish a direct correlation between I_c and C_{se} from the database of piles and CPTu. Here, log-transformed values of C_{se} were plotted against I_c, giving a continuous and linear relationship, rather than just the five discrete values assigned in the original approach. Figure 6.8 presents the findings of the new log C_{se} vs. I_c trends, where soil zones and SBT boundaries are indicated. Initial

sorting of the trends are made on the basis of installation methods (Figure 6.8a), including: drilled (or bored) piles, jacked piles, and driven pilings. It is pertinent to highlight here that the augered (or screw) piles consist only 3% of the Group 1 dataset, although larger number of these piles (i.e., 29) form part of the overall database of this research. This can be attributed to the difficulty in instrumenting such piles, and then preventing damage during the installation process. Only 4 out of 29 augered piles were fully instrumented providing load transfer data. With such a low number, it was not possible to identify or decipher any definitive trends particular to the augered piles. Accordingly, these were sub-grouped with the bored piles based on their closest match of C_{se} values. However, these values of C_{se} may vary once larger number of augered piles with their load transfer data become available, allowing for their separate trends to be deciphered. The results were also sorted by load application procedure, with maintained load test (MLT) separate from constant rate of penetration (CRPT), as indicated in Figure 6.8b. In Figure 6.8c, the load test data are identified by direction of loading: compression vs. tension (uplift).

From the factors thus investigated, the most clearly discernible trend pertains to the loading direction. Accordingly, on the overall, C_{se} values from tension tests averaged around 76.3% of the corresponding C_{se} values from those of compression tests, i.e., $C_{se(t)}/C_{se(c)} \approx f_{p(t)}/f_{p(c)} \approx 0.763$, where subscripts t and c represent tension and compression, respectively. This is rather consistent with the findings of Brown et al. (2010), De Nicola and Randolph (1999), and Elhakim and Mayne (2002). Plotting the data based on the installation methods (Figure 6.8a) did not yield any well-identified trends. From Figure 6.8b, it can be observed that loading procedure (MLT vs. CRPT) affects the trend between $\log(C_{se})$ and I_c. Even though combined regression analysis of the existing database did not present any significant variations in the trends because of the loading procedure, it appears that strain rate of loading may occur here, particularly in fine-grained soils where $I_c > 2.6$ (zones 4 and 3). As detailed in Chapter 2, MLT are

slow with load applications made on the order of one step increment per hour (or slower), while in CRPT load tests, a continuous load application occurs at a much faster rate.

The following general expression was generated from the overall correlation experience (also see Figure 6.8d):

SBT Zones 3 to 7:

$$\log[C_{se(mean)}] = 0.732\ (I_c) - 3.605 \qquad (6.7a)$$

which can be expressed more conveniently as:

$$C_{se(mean)} = 10^{\,[0.732\ (Ic) - 3.605]} \qquad (6.7b)$$

Equation (6.7) provides reasonable estimates of C_{se}. Based on the averaged trends from compression and tension loadings, C_{se} obtained via Equation (6.7) should be adjusted as follows:

$$C_{se(c)} = 1.11\ [C_{se(mean)}]$$

(6.8)

$$C_{se(t)} = 0.85\ [C_{se(mean)}] \qquad (6.9)$$

Similarly, based on the average trends from the CRPT and MLT load tests in fine grained soils where $I_c > 2.6$ (Zones 4 and 3), C_{se} obtained from Equation (6.7) should also be adjusted as follows. For coarse grained soils, where $I_c < 2.6$ (Zones 5, 6 and 7), such distinction was not possible from the current database. It may still be possible to

further explore this variable by expanding the database from additional newer load test results with specific focus on the loading procedures (e.g., Garner, 2007).

$$C_{se(CRPT)} = 1.09\ [C_{se(mean)}] \tag{6.10}$$

$$C_{se(MLT)} = 0.97\ [C_{se(mean)}] \tag{6.11}$$

It was indicated earlier that sorting of the data on the basis of pile types [bored and augered vs. driven vs. jacked (Figure 6.8a)] did not yield any discernible trends. Yet, this appears to be inconsistent with the expected logical effects of the pile installation and construction methods on the response of these piles to loading, especially based on later analyses on pile displacement response shown herein. Bored piles, which are considered to be nondisplacement type, are constructed by extracting the geomaterial from a cylindrical hole, normally made through an installed tubular casing, which is later retrieved at the time of concrete placement. On the other extreme, during installation of the full-displacement type of the close-ended driven and jacked pipe piles and precast reinforced concrete piles, the displacement of the soil surrounding the pile shaft causes significant changes in the in-situ stress state, resulting in stiffer response to loading. Here, in contrast to the jacked piles which are installed using slower press-in method of static jacking force, the driven piles use dynamic hammering or vibration technique. This results in greater disturbance to the in-situ stress state, and thus subsequent stiffer loading response of driven piles compared to those of the jacked piles, thus resulting in subcategorization within full-displacement type piles. Augered piles fall within the category of partial displacement type piles (Basu et al., 2010). Therefore, their response to loading is intermediate between the jacked type of full-displacement piles and the bored type of non-displacement piles. It was also specified earlier that only 4 out of 29 total augered piles fall in Group-1 dataset used for this analysis, hampering identification

of their distinct trends. Therefore, these were sub-grouped with the bored piles based on their closer response to loading and closest match of C_{se} values.

In view of the above explanations, the data from three categories of piles (bored and augered vs. jacked vs. driven) must display their separate trends. An insight into the results shown in Figure 6.8 suggests that it may be due to the later separations on the basis of the pile loading rate (i.e., Figure 6.8b: MLT vs. CRPT) and the direction of loading (Fig 6.8c: Compression vs. Tension). Accordingly, the following adaptations were made to the results of the data for further analysis: (1) the loading rate effects were removed by converting the C_{se} values from the CRPTs (with I_c values > 2.6 for fine grained soils of zones 3 and 4) to their equivalent C_{se} values for MLT using $C_{se(MLT)}$ = 0.889 [$C_{se(CRPT)}$]; (2) the loading direction effects were removed by converting C_{se} values from all tension load tests to their equivalent C_{se} values for compression loading using $C_{se(C)}$ = 1.31 [$C_{se(T)}$]; (3) to observe the effects of these adaptations, the entire data were then sorted again on the basis of pile type, i.e., bored and augered vs. driven vs. jacked. Figure 6.9 presents the results, where the influence of pile typology and installation method is evident. Accordingly, the following adjustment factors are proposed:

$$C_{se(Bored)} = 0.84\ [C_{se(mean)}] \tag{6.12}$$

$$C_{se(Jacked)} = 1.02\ [C_{se(mean)}] \tag{6.13}$$

$$C_{se(Augered)} = 1.13\ [C_{se(mean)}] \tag{6.14}$$

In use of these correlations, attention must be paid to the applicable range of the database (i.e., $1.28 \leq I_c \leq 3.55$), which belong to zones 3, 4, 5, 6, and 7. From the current database, the minimum calculated value of C_{se} (i.e., 0.165%) belongs to zone 7, which represents gravelly sand to dense sand. On the opposite end, the maximum calculated

value of C_{se} (10.34%) belongs to zone 3, which represents clayey soils and plots very close to the boundary between zone 3 and zone 2 (organic soils). These calculated minimum and maximum values of C_{se} are close to the ones reported by Eslami and Fellenius (1997). Therefore, the expression providing estimates of C_{se} should account for established maximum (upper limit) and minimum (lower limit) values for the soil zones not covered by the existing database. Accordingly, two alternative curve fitting functions were explored that resulted in the following:

SBT Zones 3 to 7:

Hyperbolic Tangent: $C_{se} = 0.044 + 0.0416 \tanh[1.51 (I_c) – 4.53]$ (6.15)

Modified Hyperbola: $C_{se} = 0.1 – 0.097/[1 + (I_c/3.10)^{8.2}]$ (6.16)

The fitting curves of these two expressions (Equations 6.15 and 6.16) are presented on a semi-log plot of C_{se} vs. I_c shown in Figure 6.10 with nearly identical output from both functions.

The evident advantages of using any of the above three formulations include:

- a continuous function allowing estimation of C_{se} for any value of I_c, and
- provision of a simplified single-step (or direct) method eliminating the need for use of the soil classification chart.

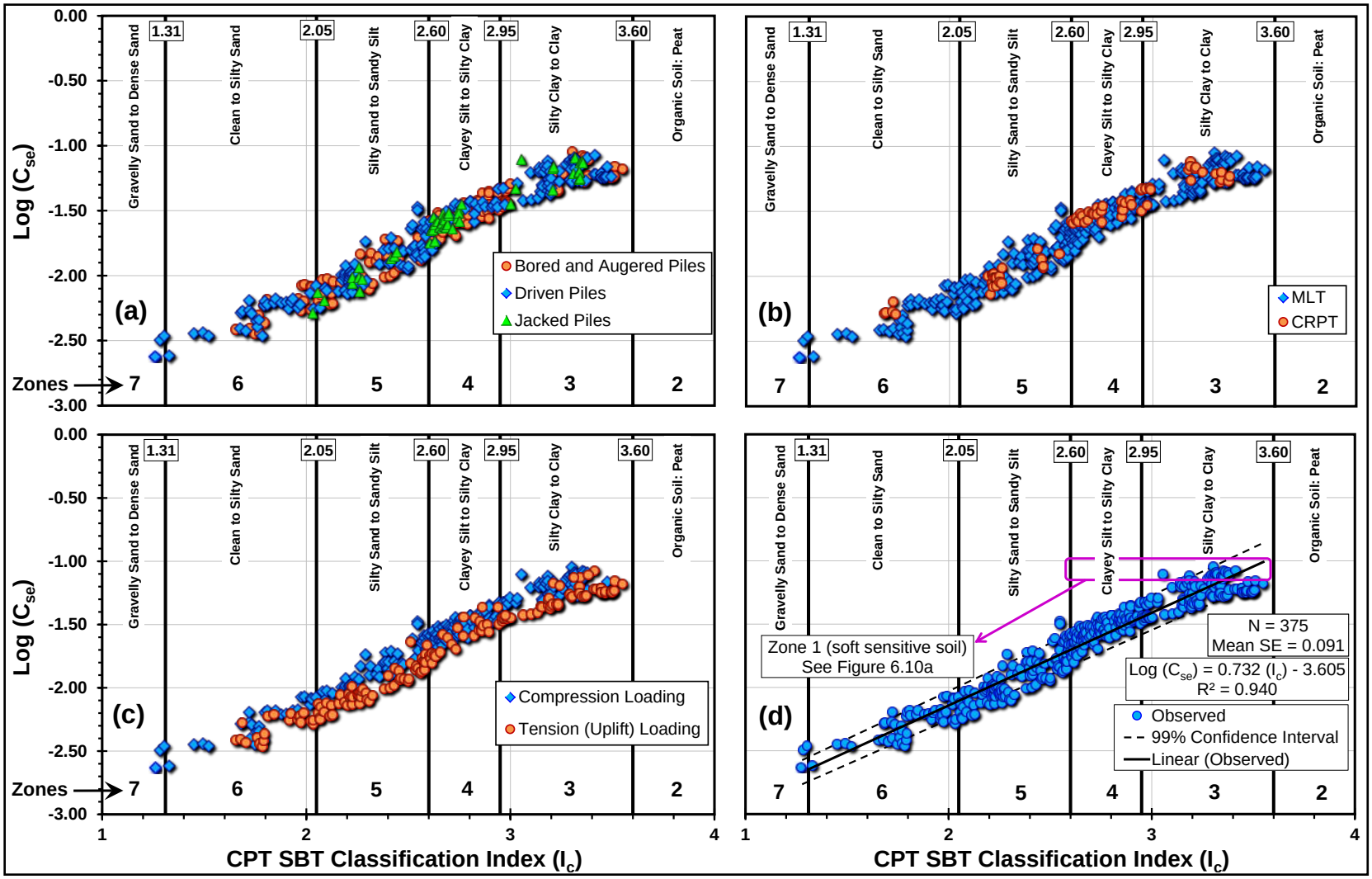

Figure 6.8. Variation of log[C_{se} (= f_p/q_E)] with CPT SBT I_c for zones 2, 3, 4, 5, 6 and 7: (a) influence of pile installation methods; (b) influence of pile loading procedures; (c) influence of pile loading modes; and (d) the overall correlation from linear regression.

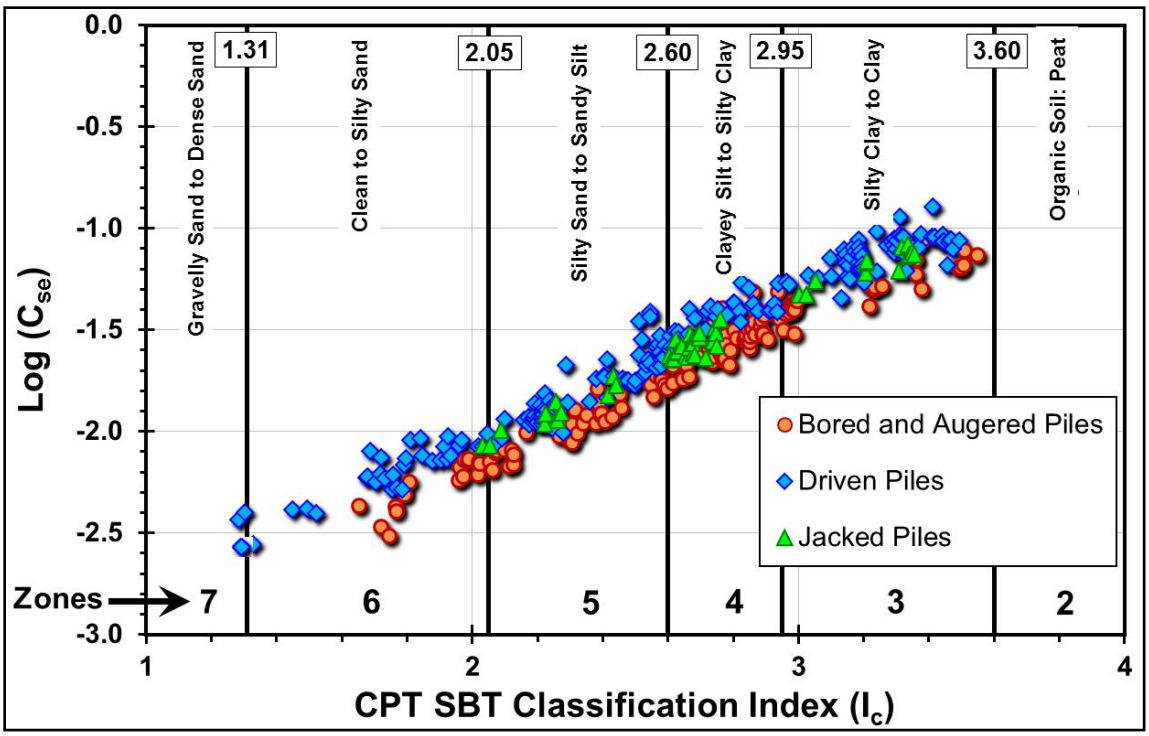

Figure 6.9. Influence of the pile type/installation method on the variation of log[C_{se} (= f_p/q_E)] with CPT SBT I_c for zones 2, 3, 4, 5, 6 and 7.

It may be noted that Equations (6.8) to (6.14) are also applicable to the two functions presented in Equations (6.15) and (6.16). It is also evident from Figures 6.8 to 6.10 that almost the entire database for the shaft correlation coefficient (C_{se}) falls within four soil zones defined via the CPT SBT classification index I_c. For the data pertaining to sensitive soils of zone 1 [i.e., for $Q_{tn} < 12\exp(-1.4F_r)$], the following separate correlations were developed through a similar set of analysis, resulting in coefficient of determination (R^2) value of 0.945 for 21 data points obtained from 4 sites (see Figure 6.11):

Zone 1 (sensitive clays):

Regression Function: $C_{se(mean)} = 0.074 - 0.004\ (I_{z1})$ (6.17)

Hyperbolic Tangent Function: $C_{se} = 0.088 - 0.015 \tanh[0.46 (I_{z1}) + 1.5]$ (6.18)

Modified Hyperbolic Function: $C_{se} = 0.106 - 0.031/[1 + (- I_z/3.5)^{3.3}]$ (6.19)

The scatter and the distribution of C_{se} values within different SBT zones are presented in their histograms shown in Figure 6.12, where some basic statistics are also included. These statistics, besides the synthesis results from Table 6.3, clearly indicate that care and caution, along with a degree of engineering judgment must be exercised in implementing these empirically calibrated correlations.

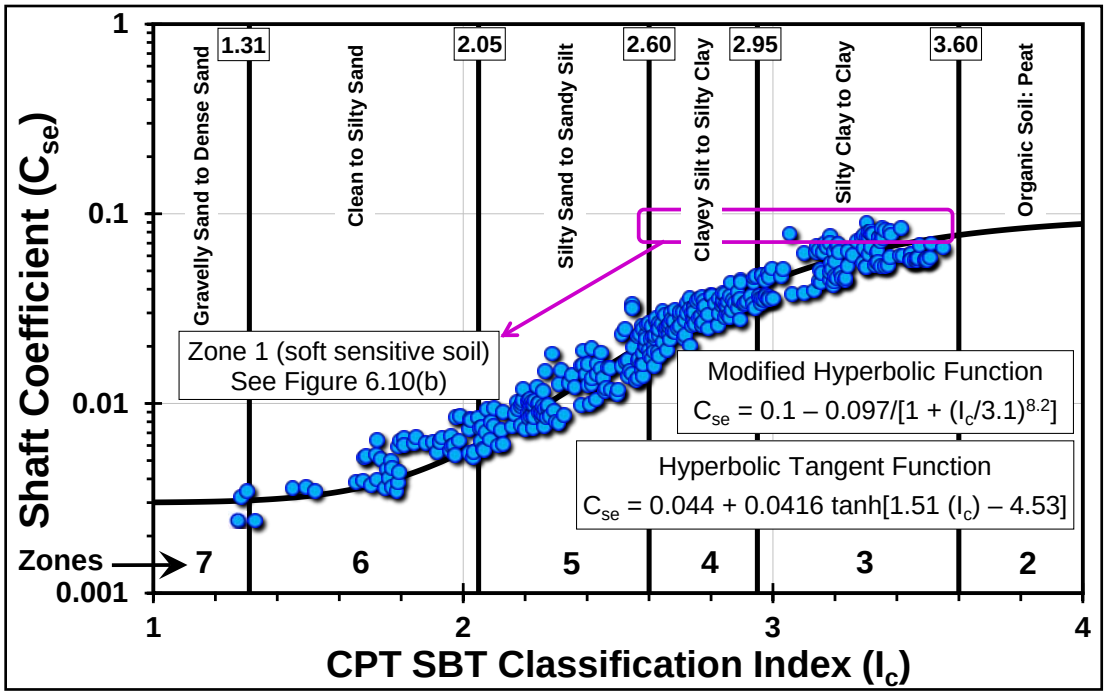

Figure 6.10. Alternative fitting functions for mean pile friction coefficient ($C_{se} = f_p/q_E$) trend with CPT material I_c for soil zones 2, 3, 4, 5, 6 and 7.

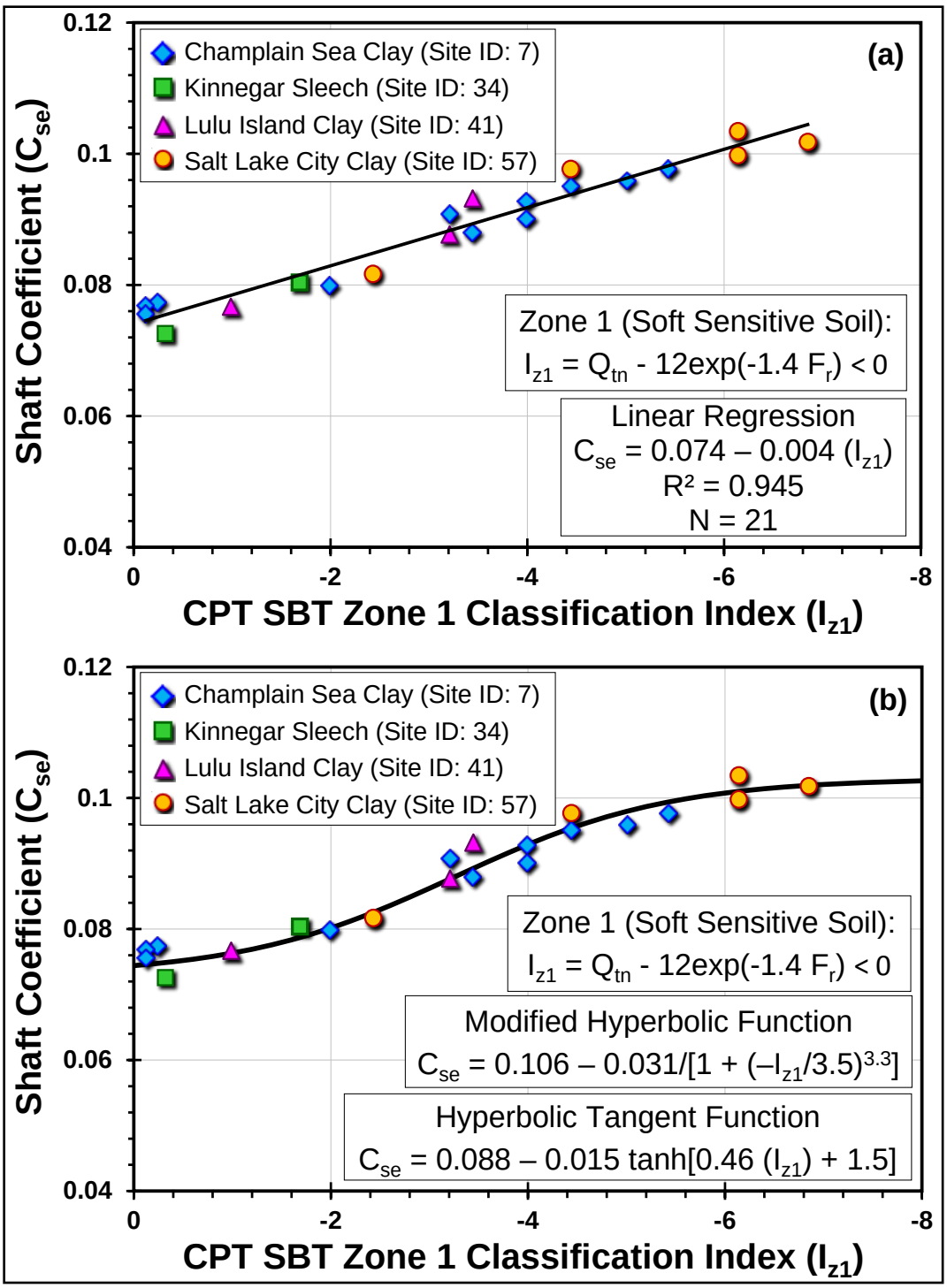

Figure 6.11. Variation of C_{se} (= f_p/q_E) with CPT SBT I_{z1} for zone 1 (soft sensitive soil): (a) linear regression function; and (b) alternative fitting functions.

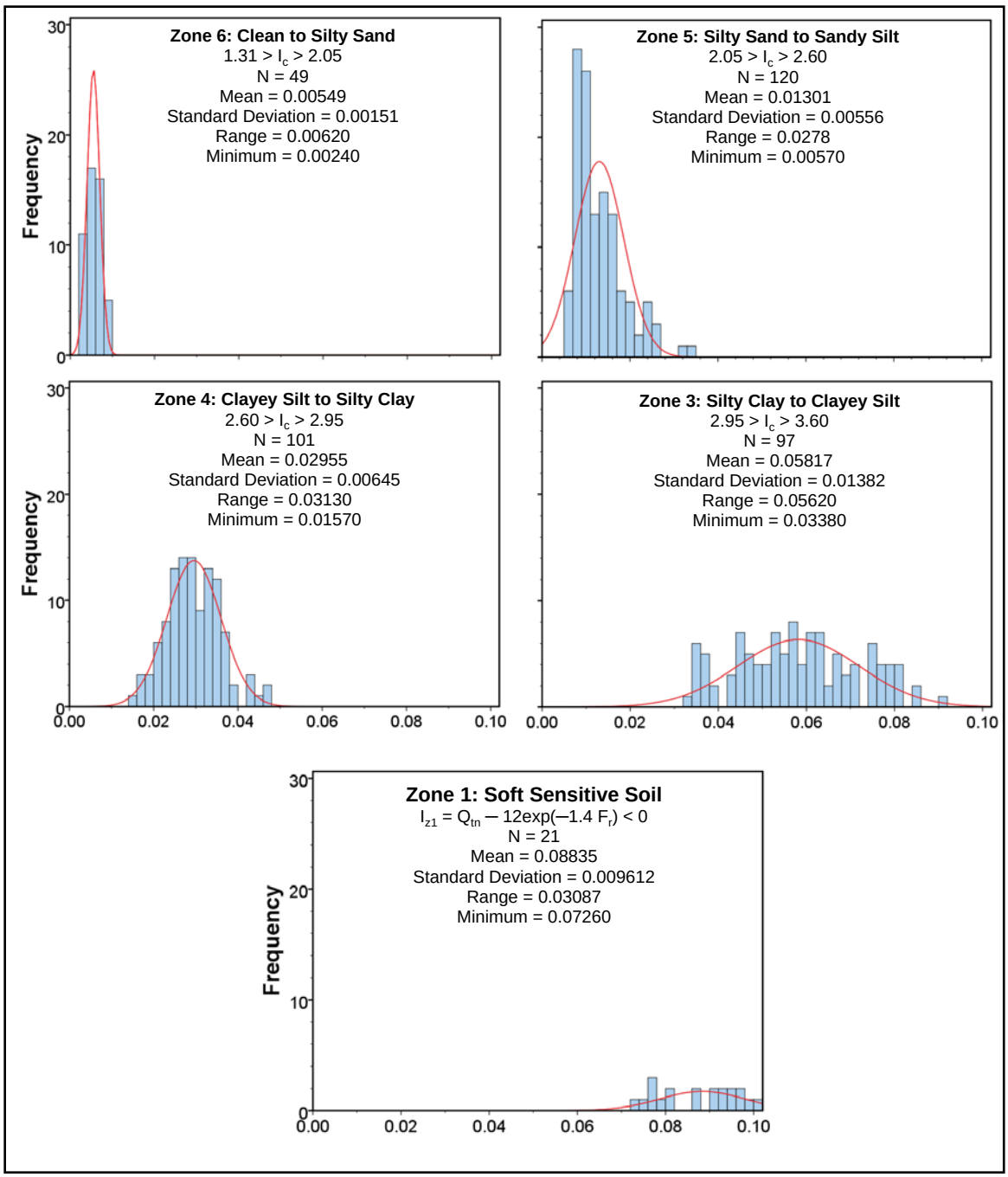

Figure 6.12. Histograms, normal distributions, and basic statistics of measured shaft coefficient [$C_{se(M)}$] for different soil zones based on CPT SBT I_c.

6.4.3 Assessment of New Design Equations

In order to test the performance of the new sets of empirically derived functions, the estimated values of shaft coefficient [$C_{se(E)}$] were plotted against the measured values

[$C_{se(M)}$] for each of the three expressions, applied to the entire database. The results are shown in Figures 6.13 to 6.15. Regression analysis was conducted on each set of the results to obtain the best fit line of estimated/measured ratios of shaft coefficient [$C_{se(E)}/C_{se(M)}$]. The ratio $C_{se(Fit)}/C_{se(M)}$ and the corresponding coefficient of determination (R^2) were then calculated. Inspection of Figures 6.13 to 6.15 shows that the modified hyperbolic function yields a best fit line that matches most closely to the perfect fit line with the highest $R^2 = 0.93$. The next closest match is provided by the hyperbolic tangent functions with a similar $R^2 = 0.93$. This is followed by the linear regression functions which give an R^2 value of 0.90. In these figures, some seemingly greater scatter for the C_{se} values of 0.04 to 0.06 pertain to zone 3 (clayey silt to silty clay), which is consistent with the range of C_{se} values shown in Figure 6.12 as well as those shown for the original UniCone method in Figure 6.2.

Following the reliability approach used by Jardine et al. (2005), Lehane et al. (2013), and Van Dijk and Kolk (2011), the mean values (μ) and the coefficients of variation (COV) of $C_{se(E)}/C_{se(M)}$ for the predictions made by the three proposed equations are shown in Table 6.4. Following observations are noted:

- The $C_{se(E)}/C_{se(M)}$ values derived for each method display approximately normal distribution, with COV for the three equations ranging from 0.178 to 0.207. These low values fall within a reasonable range for reliable predictions, and suggest an improvement over the latest method proposed by Lehane et al. (2013).
- With the assumption of normal distribution for $C_{se(E)}/C_{se(M)}$, the mean values (μ) and COVs for the three sets of new design equations suggest the following probabilities that the estimated shaft coefficient, $C_{se(E)}$ will be less than 1.5 times the measured shaft coefficient, $C_{se(M)}$: 99.64% for hyperbolic tangent function, 99.59% for modified hyperbolic function, and 98.81% for linear regression function.

Potential of bias or skewness in C_{se} calculated using the new formulations was investigated by plotting $C_{se(E)}/C_{se(M)}$ ratios against a number of available independent parameters, e.g., L/d ratios, OCR etc. An illustration of this methodology is shown in Figures 6.16 and 6.17, which plot the ratio $C_{se(E)}/C_{se(M)}$ against L/d ratio and OCR of the entire database. No clear dependence of $C_{se(E)}/C_{se(M)}$ on L/d or OCR is apparent (or any other parameter considered). These results compare well with similar plots of calculated/measured capacity [$Q_{cap(C)}/Q_{cap(M)}$] vs. L/d and OCR presented by Lehane et al. (2013) and Jardine et al. (2005).

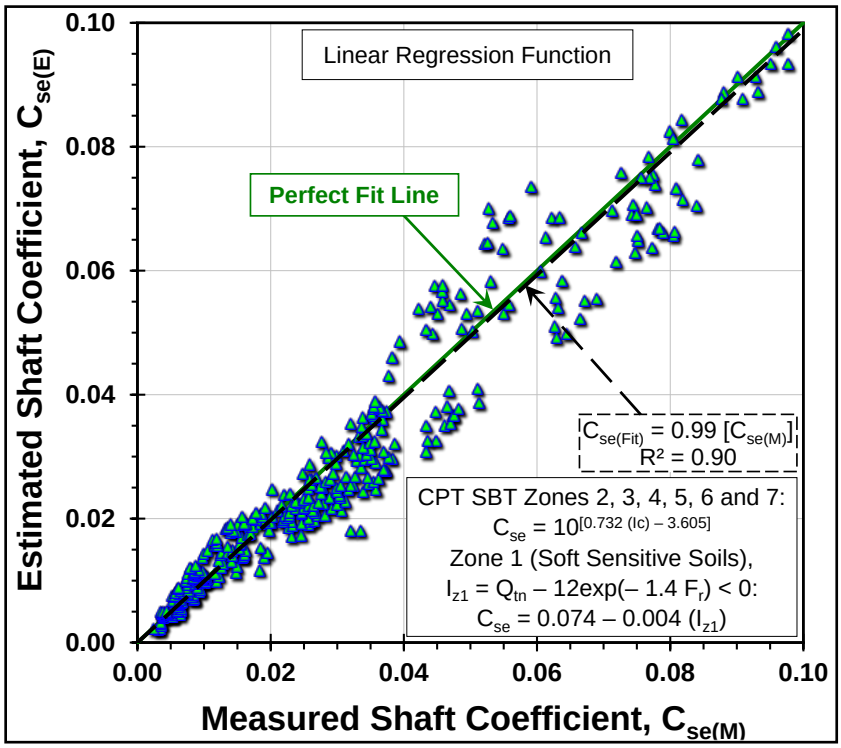

Figure 6.13. Estimated [$C_{se(E)}$] versus measured [$C_{se(M)}$] shaft coefficient from the linear regression function.

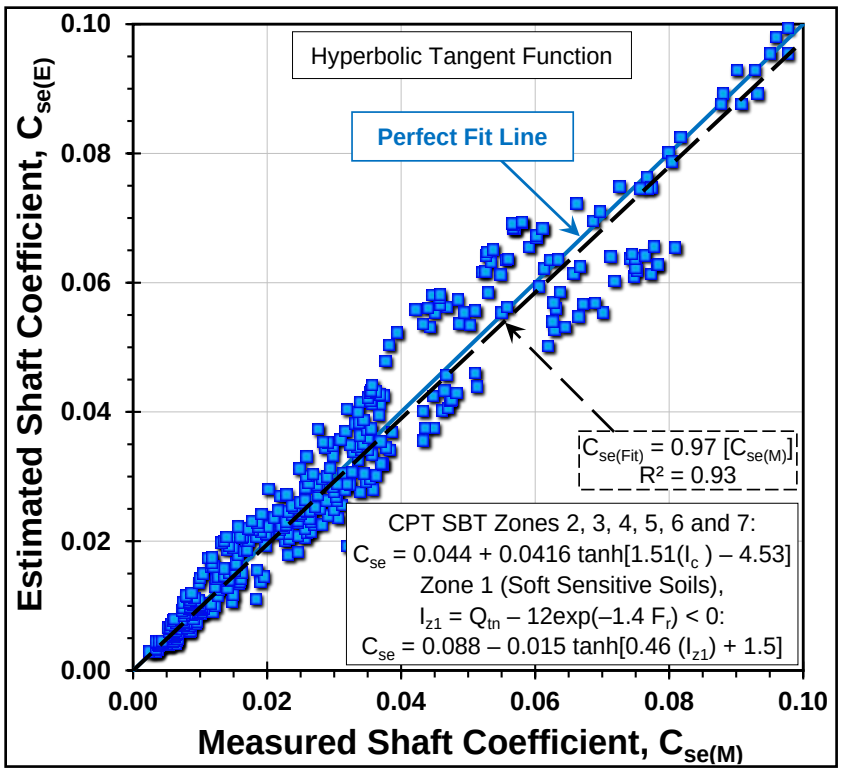

Figure 6.14. Estimated [$C_{se(E)}$] versus measured [$C_{se(M)}$] shaft coefficient from hyperbolic tangent function.

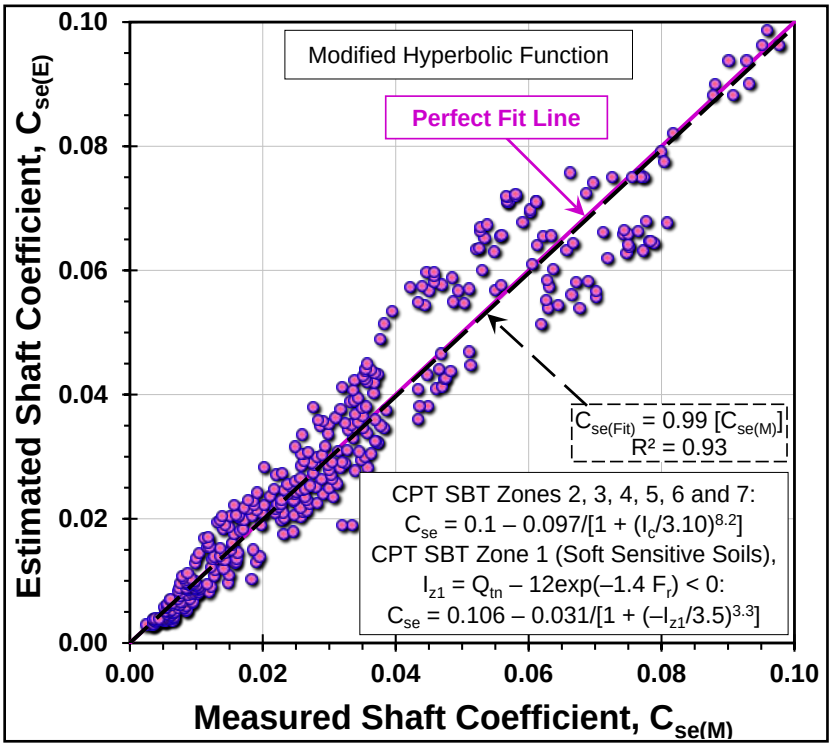

Figure 6.15. Estimated [$C_{se(E)}$] versus measured [$C_{se(M)}$] shaft coefficient from the modified hyperbolic function.

Table 6.4. Statistics of $C_{se(E)}/C_{se(M)}$ for the proposed design formulations.

Proposed Formulation	Mean (μ)	COV	$P[C_{se(E)} < 1.5C_{se(M)}]$
Linear Regression Function	1.021	0.207	98.81%
Hyperbolic Tangent Function	1.025	0.178	99.64%
Modified Hyperbolic Function	1.003	0.191	99.59%

Note: $P[C_{se(E)} < 1.5C_{se(M)}]$ = probability that the estimated shaft coefficient will be less than 1.5 times the measured shaft coefficient.

6.4.4 Correlation Coefficient for Toe Capacity

Following the methodology detailed above, the toe correlation coefficients, C_{te} (= q_b/q_E), were also back-analyzed and then statistically evaluated with their respective I_c values in the influence zones around the pile toes. The resulting trends are plotted in Figure 6.18, with the generalized correlation given in Equation (6.20). The observed data points were limited in number and range of I_c (i.e., $1.69 \leq I_c \leq 3.77$) because: (1) tension tests did not contribute to this part of back-analysis, and (2) number of layers encountered at the base was less than those for the cases of pile shaft. A total of 102 data points include C_{te} calculated from 95 top-down compression tests and 7 O-cell tests.

$$\text{Log}[C_{te(mean)}] = 0.325\,(I_c) - 1.218 \qquad (6.20a)$$

or expressed directly as:

$$C_{te(mean)} = 10^{\,[0.325\,(Ic) - 1.218]} \qquad (6.20b)$$

In Figures 6.18b and 6.18c, it can be seen that the influence of additional factors like pile loading procedures (standard MLT vs. quick MLT vs. CRPT), and pile end conditions (CE vs. OE) were also investigated. Here, the standard MLT refers to the loading procedure specified in ASTM D1143M – 07, while quick MLT is a variant of standard procedure with load maintained for shorter durations (exhibiting not fully

drained conditions in relative terms). The CRPT clearly represents near undrained loading, particularly for fine-grained soils (Zones 2, 3, and 4).

Noticeably, the data points plotted in Figure 6.18 indicate much greater scatter in the log C_{te} vs. I_c correlation than that observed for the shaft coefficient, besides the fact that no clear dependence may be assigned either to the installation method, or to the pile end condition. As noted previously in the discussion of shaft coefficient, Figure 6.18 also indicates that the pile loading procedures may have some influence on the C_{te} vs. I_c correlations, for instance, higher C_{te} values for CRPT, followed by the quick MLT, and least for the standard MLT. Data from CRPT generally display higher C_{te} values than those of the MLT in Zones 2, 3, and 4. This is a possible validation of the earlier findings of gain in the undrained shear strength at higher loading rates (e.g., Garner, 2007). However, with fewer data points it was not possible to define distinct trends, and further correlation analysis did not yield discernible distinction. For OE piles, an added factor restricting further analysis relevant to the end conditions is the adoption of q_b similar to CE piles instead of separate q_{plug} and q_{ann}. Indicated earlier is the fact that this assumption was made due to the non-availability of measured plug information for most of these pile load tests. This study clearly points to the fact that C_{te} cannot be plainly assumed equal to unity, or based solely on pile diameter, as formulated in the original UniCone method.

Equation (6.20) may be reasonable for preliminary analysis and design. However, improved statistical significance of these correlation results may be achieved from additional information from each pile load test, coupled with expansion of the database. More focused studies on the influence of pile end conditions and loading procedures are also warranted. Some of the earlier studies by De Nicola and Randolph (1999), Lehane and Gavin (2001), Gavin and Lehane (2005), and Yu and Yang (2012) have focused on q_b for OE and CE piles in sandy soils. Extension of such research studies in fine grained soils, mixed soil types, and other variety of geomaterials are also warranted.

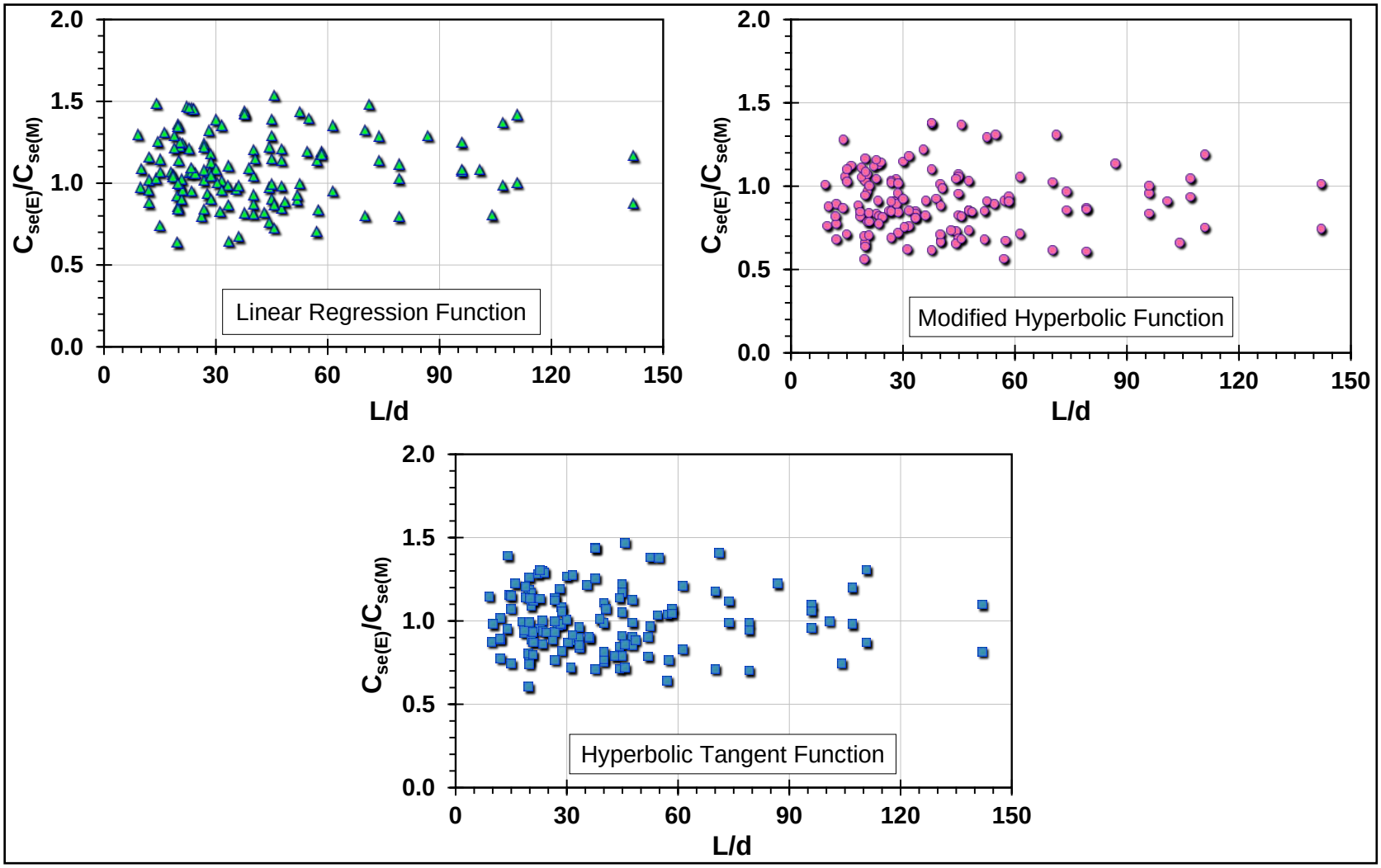

Figure 6.16. Variation of estimated to measured shaft coefficient [$C_{se(E)}/C_{se(M)}$] with pile slenderness ratio (L/d) from the new design formulations.

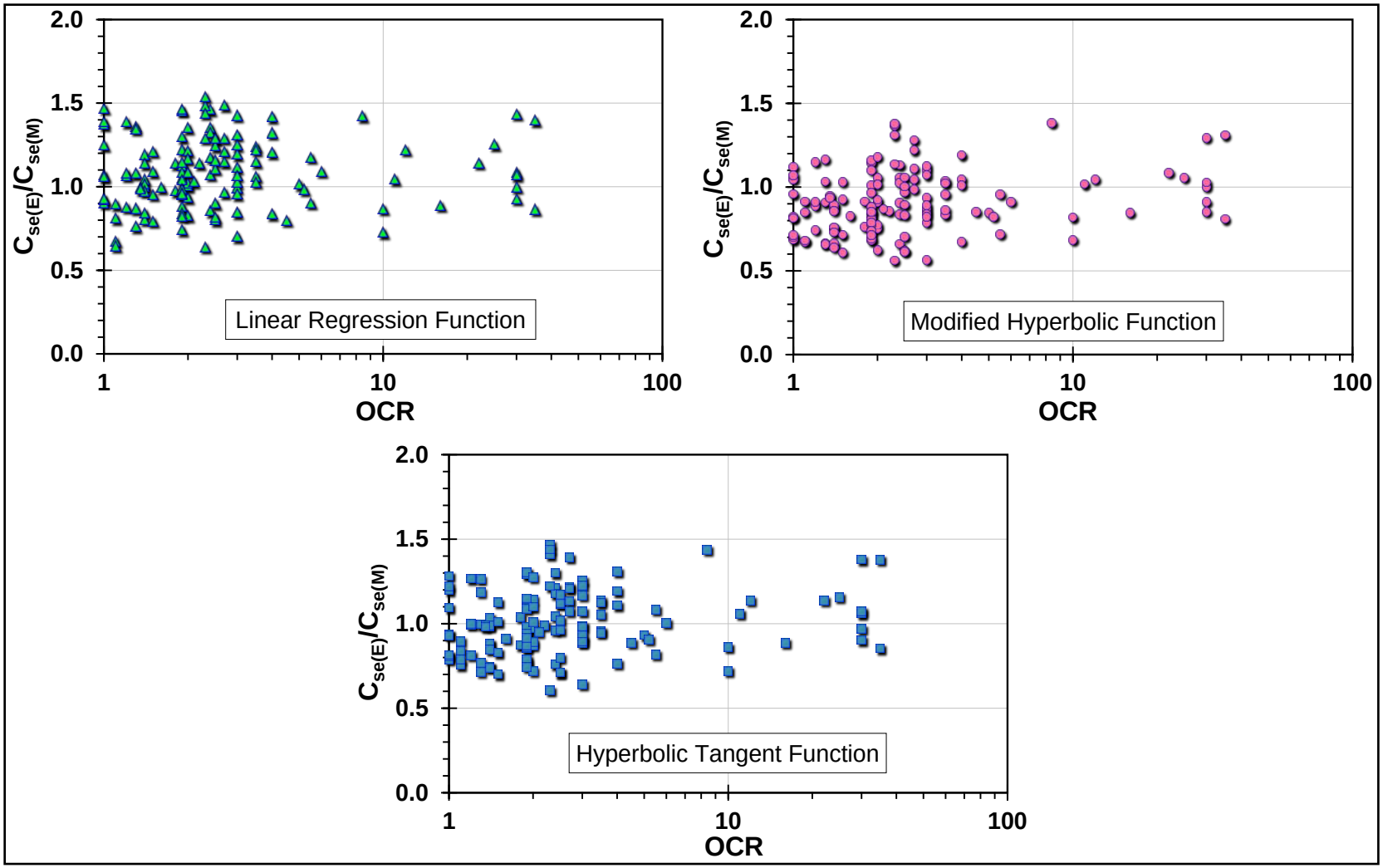

Figure 6.17. Variation of estimated to measured shaft coefficient [$C_{se(E)}/C_{se(M)}$] with overconsolidation ratio (OCR) from the new design formulations.

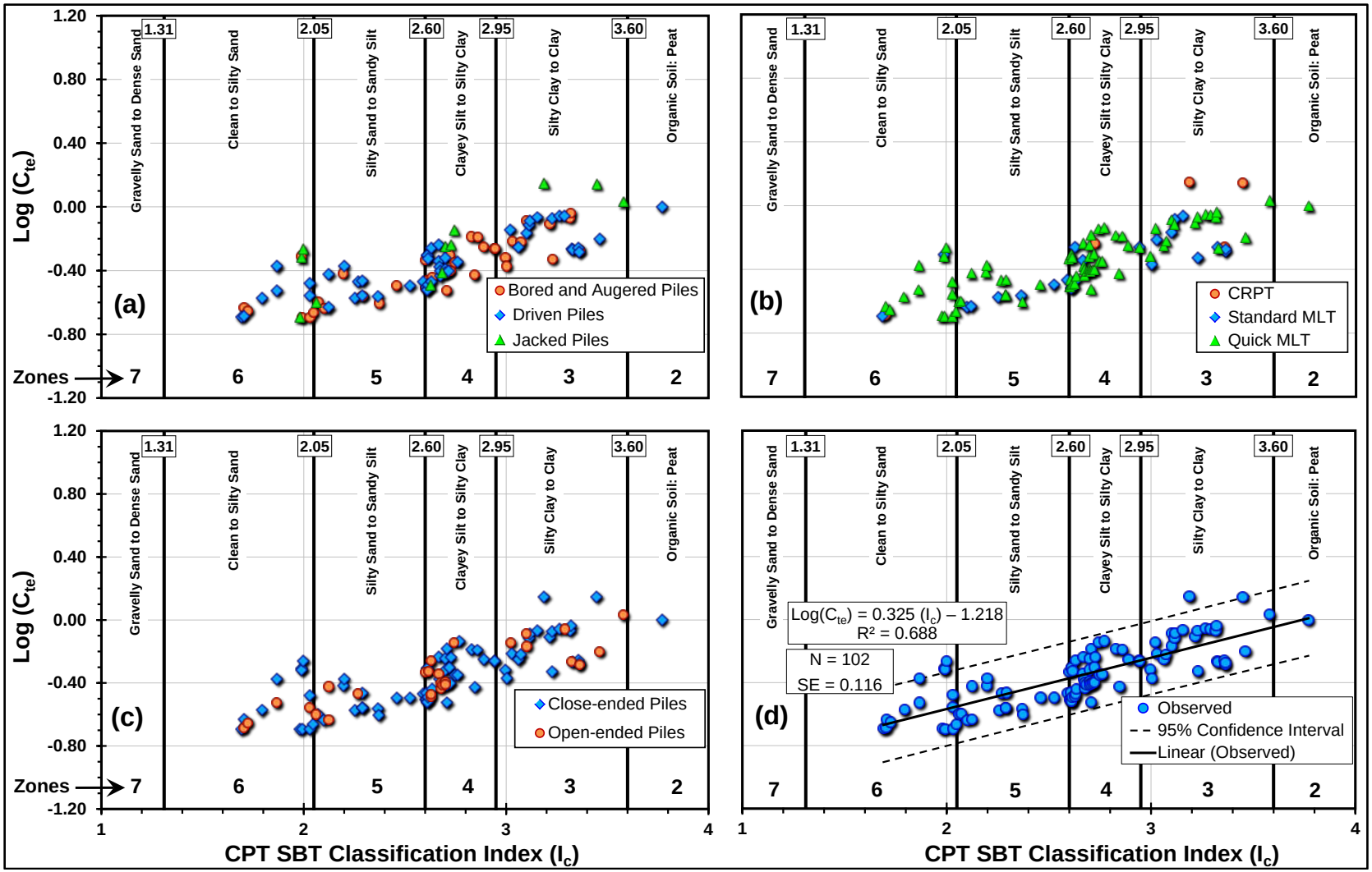

Figure 6.18. Variation of log[C_{te} (= q_b/q_E)] with CPT SBT I_c: (a) influence of pile installation methods; (b) influence of pile loading procedures; (c) influence of pile end conditions; and (d) the overall correlation.

6.5 Reference to the Capacity Criteria

For careful applications of the updated design formulations in future predictions, the measured maximum pile capacity [$Q_{max\ (measured)}$] of each pile load test used in this analysis was related to the pile capacities calculated from three different criteria in the form of simple ratios: (1) $Q_{cap\ (Chin\text{-}Kondner)}/Q_{max\ (measured)}$, (2) $Q_{cap\ (w/d\ =\ 10\%)}/Q_{max\ (measured)}$, and (3) $Q_{cap\ (Davisson)}/Q_{max\ (measured)}$. This was followed by plotting the histograms for each of these ratios for the entire pile dataset of Group 1. These histograms along with their statistics are shown in Figure 6.19. Clearly, Davisson's offset line criterion offers the most conservative definition of axial pile capacity, with mean and standard deviation of the ratios $Q_{cap\ (Davisson)}/Q_{max\ (measured)}$ as 0.852 and 0.104, respectively. The next in the order is the French criterion with its mean and standard deviation of the ratio $Q_{cap\ (w/d\ =\ 10\%)}/Q_{max\ (measured)}$ as 0.986 and 0.084. As expected the Chin-Kondner criterion (i.e., asymptote), which is based on hyperbolic function, slightly over-predicts the capacity with its mean and standard deviation of $Q_{cap\ (Chin\text{-}Kondner)}/Q_{max\ (measured)}$ as 1.101 and 0.112, respectively.

Based on their preference for the capacity definition/criterion, the practitioners applying the above proposed design equations to field situations must clearly relate their prediction outcome to the statistical results presented in Figure 6.19. For interest, the histograms and statistics of two additional sets of ratios from the data, mutually relating capacity definitions are also presented in Figure 6.19: (1) $Q_{cap\ (Davisson)}/Q_{cap\ (Chin\text{-}Kondner)}$, and (2) $Q_{cap\ (w/d\ =\ 10\%)}/Q_{cap\ (Chin\text{-}Kondner)}$.

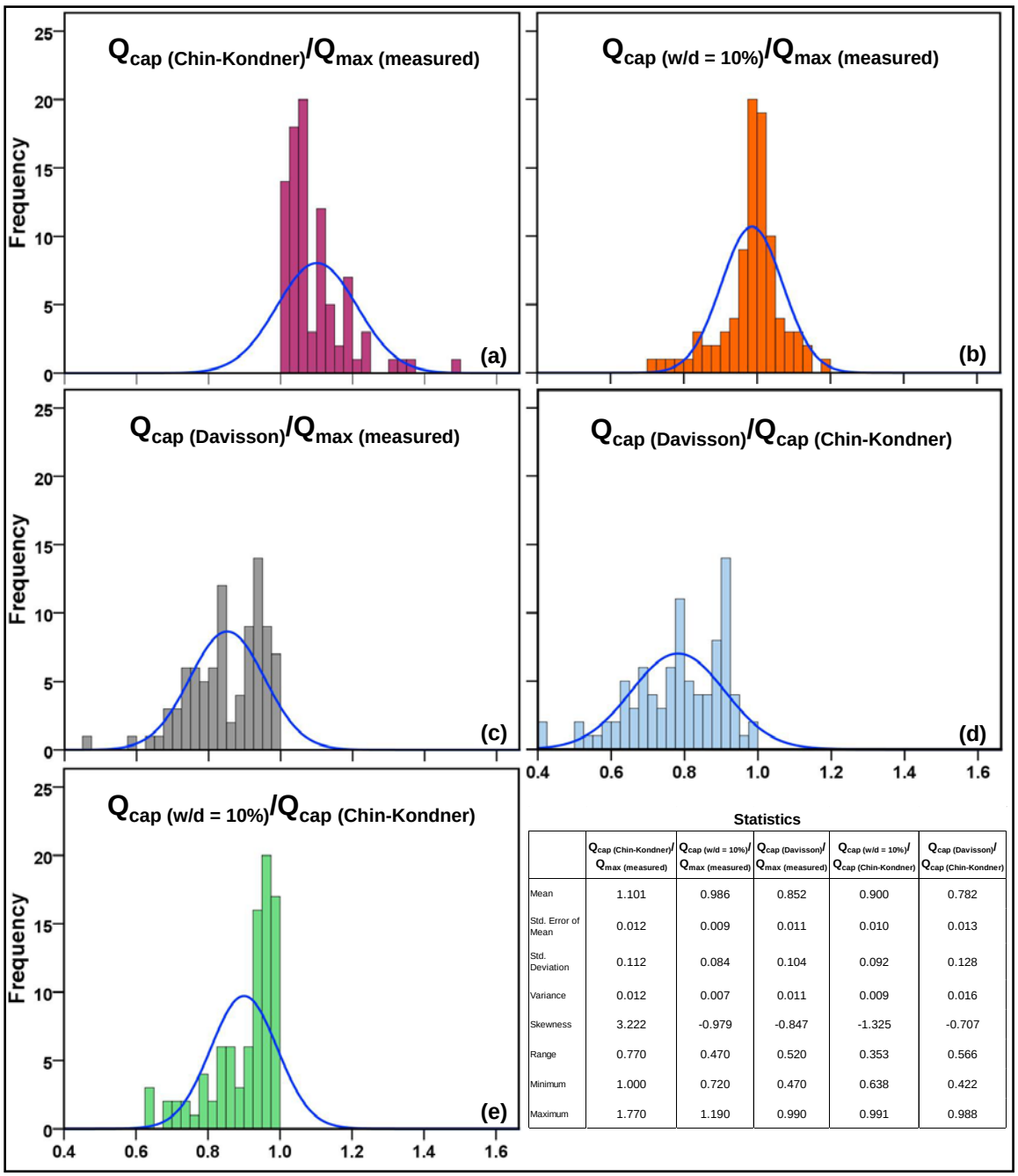

	$Q_{cap\ (Chin\text{-}Kondner)}/Q_{max\ (measured)}$	$Q_{cap\ (w/d\ =\ 10\%)}/Q_{max\ (measured)}$	$Q_{cap\ (Davisson)}/Q_{max\ (measured)}$	$Q_{cap\ (w/d\ =\ 10\%)}/Q_{cap\ (Chin\text{-}Kondner)}$	$Q_{cap\ (Davisson)}/Q_{cap\ (Chin\text{-}Kondner)}$
Mean	1.101	0.986	0.852	0.900	0.782
Std. Error of Mean	0.012	0.009	0.011	0.010	0.013
Std. Deviation	0.112	0.084	0.104	0.092	0.128
Variance	0.012	0.007	0.011	0.009	0.016
Skewness	3.222	-0.979	-0.847	-1.325	-0.707
Range	0.770	0.470	0.520	0.353	0.566
Minimum	1.000	0.720	0.470	0.638	0.422
Maximum	1.770	1.190	0.990	0.991	0.988

Figure 6.19. Histograms, normal distributions, and basic statistics of: (a), (b) and (c) ratios relating different capacity criteria to the maximum applied loads; (d) and (e) ratios mutually relating different capacity criteria.

6.6 Application of New Design Formulations for Pile Capacity Evaluations

The new design formulations can be conveniently applied for reliable prediction of the two components of axial pile capacity, namely total shaft resistance (Q_s) and total base resistance (Q_b). The step-by-step methodology is summarized in the flow chart shown in Figure 6.20. In application of this new formulation via the proposed methodology, care must be exercised in respect of the following:

- The design formulations were derived from the database presenting I_c values between 1.28 and 3.55, and I_{z1} values between – 0.12 and – 6.85 for C_{se}, and 1.69 and 3.77 for C_{te}. Therefore, extension of these formulations to the cases outside of this data range should be carefully applied.
- For the proposed formulations, q_b estimation via C_{te} are statistically not so well defined as that for evaluating f_p via C_{se} correlations. In general, the base capacity component (Q_b) forms a small part of the total axial pile capacity (Q_t). Therefore, discrepancy on the overall Q_t, if any, is expected to be limited. However, it is still recommended that the base capacity estimation should also be tested against alternative and more recent rational methods summarized in Chapter 3.
- In application of the new design formulations, attention must be given to the statistical results of the variability of C_{se} for different soil zones presented in Figure 6.12.
- Similarly, while using the proposed design equations to field situations, the prediction outcome must be compared with the statistical results presented in Figure 6.19, which presents relationships of the predicted pile capacities to three different criteria.
- The final form of expression for shaft coefficient is given below:

$$C_{se} = C_{se(mean)} \cdot \theta_{pile\text{-}type} \cdot \theta_{tc} \cdot \theta_{rate} \qquad (6.21)$$

where $\theta_{pile\text{-}type}$ = adjustment factor for pile type/installation method (0.84 for bored and augered piles vs. 1.02 for jacked piles vs. 1.13 for driven piles), θ_{tc} = adjustment factor for loading direction (0.85 for tension vs. 1.11 for compression), and θ_{rate} = adjustment factor for loading procedure (1.09 for CRPT vs. 0.97 for MLT) for fine grained soils. The adjustment factors for loading rate (θ_{rate}) were derived from pile load tests which present short term loading and offer flexibility in adopting the procedures of load application (CRPT vs. Standard MLT vs. Quick MLT). This convenience is not available for actual production piles, which take the structural loads via long term pile resistance. In that sense, for design purposes, the standard MLT are closer to the field situations compared to the CRPT, and therefore, θ_{rate} = 0.97 becomes more relevant for the actual pile designs.

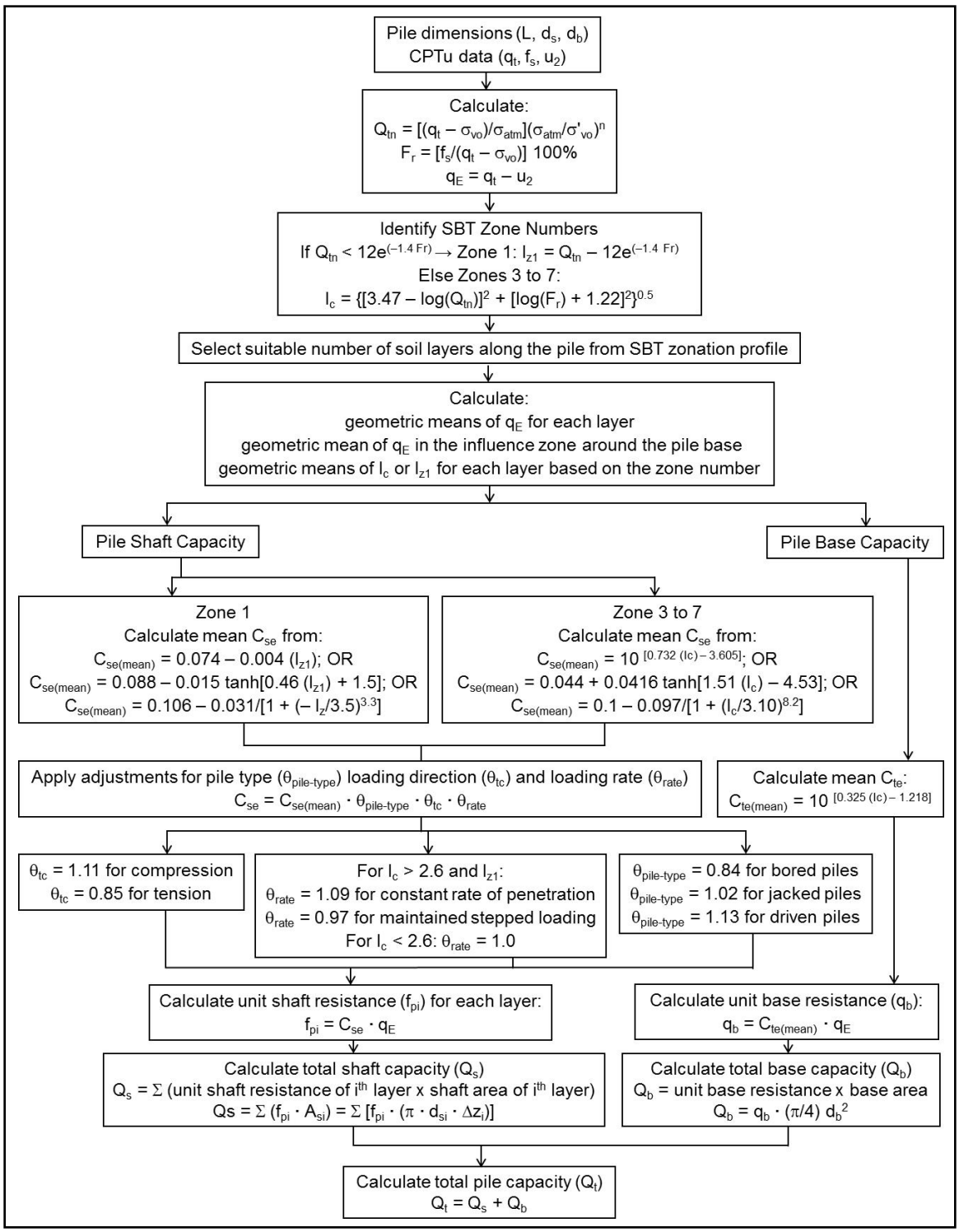

Figure 6.20. Flowchart summarizing steps for evaluating axial pile capacity from the proposed design formulations.

6.7 Concluding Remarks

Direct CPTu methods offer a quick and convenient method for evaluating axial pile capacity using multiple penetrometer readings. They also provide more reliable and accurate results since continuous data are obtained along the length of the pile foundation. In this chapter, a brief review is given on the original UniCone method (Eslami and Fellenius, 1997) that uses a 5-part soil classification system to assign discrete pile side friction coefficients to each elevation of CPTu data. The case is made for making refinements in these relationships and extending their applications based on new test piles and additional soil deposits. A total database of 153 pile load tests from 52 worldwide sites is compiled, representing a 50% increase over the original study. The piles include diversity in terms of pile material, shape, installation method, end conditions, loading procedure, and loading direction, which were installed and tested in a wide assortment of geomaterials. The data selection process aimed at the availability of piezocone type of CPT testing.

Results of the correlation efforts are offered to derive coefficients C_{se} for shaft component, and C_{te} for base component of the axial pile capacity from CPTu data. The UniCone type of log q_E vs. log f_s soil classification chart is refined by delineating 11 soil sub-zones along with their respective shaft coefficients, in contrast to the 5 zones originally proposed by Eslami and Fellenius (1997). For further improvements, the CPT material index, I_c (Robertson, 2009) is used to establish direct correlations linking C_{se} vs. I_c and C_{te} vs. I_c. After identification of sensitive soils (Zone 1), statistical relationships offer a continuous function for estimating the coefficients over a wide value of I_c (Zones 2 to 7), thereby eliminating the need for use of the soil classification chart and improving the reliability in the evaluations of pile side friction (f_p) and unit end-bearing (q_b).

The analysis also reveals that the statistical reliability of estimating f_p is much superior to that for q_b. Many important factors known to affect the f_p and q_b of piles are not incorporated in the proposed design equations. While Ardalan et al. (2009) and

Eslami and Fellenius (1997) argue that the in-situ properties of the surrounding soil medium affect both the pile and cone in a similar manner, it is noted that the CPTu readings are recorded in short term loading and this will differ from the long term pile resistance. Additionally, the apparent effects of the pile loading rates and true end conditions, which were not fully considered in this study due to lack of sufficient data, must also be explored. Any application of the derived trends should be made with due caution and careful engineering judgment, as true for any and all empirical methods.

CHAPTER 7

OPERATIONAL SOIL STIFFNESS FROM BACK-ANALYSIS OF PILE LOAD TESTS WITHIN ELASTIC CONTINUUM FRAMEWORK

Synopsis

In this chapter, new sets of shear stiffness reduction curves are developed from back-analyses of 299 static axial pile load tests from 61 sites towards implementation of a non-linear load-displacement response (Q-w) method for pile foundations. The initial shear modulus (G_{max}) is derived from the measured shear wave velocity (V_s) profiles at the pile sites, normally taken by seismic cone penetration tests (SCPT). A closed-form elastic continuum solution (Randolph, 2007) is used for axial compression loading, and then decoupled and modified for application to the axial tension loading case. The back-analysis of shear moduli performed using this elastic solution results in derivations of new shear modulus reduction curves, specifically normalized shear stiffness (G/G_{max}) vs. logarithm of percent pseudo-strain (γ_p = w/d where w = pile displacement and d = pile diameter). The new sets of curves incorporate the effects of pile type and installation method, as well as the influence of soil plasticity. Three comprehensive appendices are included that provide case-by-case records of key pile and soil input parameters used in this analysis, G_{max} profiles from the test sites, and graphical representations of results indicating the influence of plasticity on G_{max} reduction. A complete step-by-step methodology is presented for use and application of these new stiffness reduction curves within extended system of closed-form elastic solution.

7.1 Introduction

The nonlinear response of geomaterials to loading has been widely researched and documented towards use in geotechnical engineering applications (Burland, 1989). The

mechanical non-linearity is exhibited in the form of soil stiffness that begins at the small-strain shear modulus (G_{max}) and softens when shear strains (γ) exceed the linear threshold value, resulting in marked reductions for small-, intermediate- and large-strains until the shear strength is reached (Tatsuoka and Shibuya, 1992). Many algorithms have been developed to describe this stiffness reduction for different soils. Selected models, along with their respective sources, have been discussed and summarized in Chapter 4. These include hyperbolic stress-strain relationships, power law expressions, and periodic logarithmic functions, as well as constitutive soil models based in elasto-plasticity (Mayne, 2005). It becomes difficult to strike a compromise between simplicity, without regard for imprecise description of rather complicated stiffness reduction trends, and improved accuracy at the cost of highly complex algorithms.

The application of deep foundations provides a common mechanism of load transfer from the heavily built superstructure to the underlying subsurface geomaterials. The determination of the soil stiffness is very important in reckoning the response of deep foundations in terms of allowable displacements (a stringent design criterion) resulting from the applied load, starting from an initial value and leading up to the ultimate pile capacity. The nonlinear axial pile load vs. displacement analysis can be performed via several approaches, including: (a) elastic continuum solutions; (b) spring models (e.g., t-z curves and q-z curves), (c) numerical simulations (e.g., finite elements, finite differences), or (d) empirical approaches. Herein, the nonlinear Q-w behavior is handled using a hybrid method that combines an analytical elastic closed-form solution (e.g. Randolph and Wroth, 1978; 1979; and Randolph, 2007) with an appropriate strain-dependent softening scheme for the profile of operative shear modulus (G) along the pile length. Cooke et al. (1979) noted that G is the most important parameter of the soil affecting the Q-w behavior of a pile under working conditions. The evaluation of the initial shear modulus (G_{max}) in the range of strains less than the linear threshold becomes paramount. Elhakim (2005) showed that the in-situ seismic tests provide much more

definitive and reliable means of assessing G_{max} compared to that from laboratory tests. This fundamental stiffness G_{max} can be conveniently obtained from in-situ measurements of shear wave velocity (V_s) during seismic cone penetration tests (SCPT or SCPTu).

Berardi and Bovolenta (2005) proposed a semi-empirical approach of matching field measurements via back-analysis of pile load tests using analytical elastic solutions. This procedure enables the derivation of the normalized operative field shear stiffness (G/G_{max}) as a function of the pseudo-strain (γ_p), which can be defined as the ratio of pile top displacement to its diameter (w_t/d). Thus, they generated stiffness reduction curve based on actual field measurements from a limited database of similar situations (pile type, geometry, soil conditions, etc.) for piles tested in axial compression. The G values obtained from these curves can thus be used in the same elastic solution to forecast the nonlinear load-displacement (Q-w) response of piles falling within the range of the database considered.

In more recent studies of laboratory stress-strain curves, Vardanega and Bolton (2011; 2013) presented a new scheme for shear modulus estimation of clays and silts, defined via G/G_{max} vs. γ/γ_{ref}. Here γ_{ref} refers to the value of shear strain γ where G_{max} reduces to one-half of its initial maximum value. They characterized their dataset by fitting a modified hyperbola via the following transformed system:

$$\log_{10}[(G_{max}/G) - 1] = \alpha \log_{10}(\gamma/\gamma_{ref}) \tag{7.1}$$

To explore the robustness of their relationship to γ_{ref}, regression analyses were performed on individual soil properties, thereby tying γ_{ref} to the plasticity index (PI) of the soil. These fitting parameters have been presented in Chapter 4.

Herein, a framework has been established that combines these two approaches: (a) back-figured moduli from load tests normalized to field G_{max} measurements (Berardi and

Bovolenta, 2005); and (b) modified hyperbolic fitting of the corresponding G/G_{max} reduction curves versus logarithm of shear strains (Vardanega and Bolton, 2011; 2013). This represents an effort to develop a set of modulus reduction curves from the back-analyses of a large number of pile load tests conducted in a broad assortment of different types of geomaterials. The retro-investigation has been performed within the framework of analytical elastic continuum solutions by Randolph (2007). In addition to tests performed under conventional axial compression loading, this database also encompasses piles load-tested in uplift (or tension). This chapter explains how the elastic solution was de-coupled and modified for adaptation to tension loading cases and subsequently used to back-figure operational stiffnesses for both compression and tension cases. New charts have been developed presenting design curves and their affiliated algorithms for different pile types and soil conditions to be utilized for axial pile Q – w analysis within this elastic continuum framework.

7.2 Modification of Elastic Solution for Tension Loading

The original closed-form analytical elastic solutions by Randolph and Wroth (1978; 1979) were summarized in Chapter 4. The solutions provide a means for evaluating pile displacements under top-down axial compression loadings. To extend this model to top-applied tension (or uplift) loading cases, the following observations (as noted in prior chapters), need consideration:

- A test pile which is loaded in uplift has the load applied to the pile shaft by a system pulling upward at the top, thus placing the foundation into tension.
- The Poisson's ratio effect due to elastic deformation of the pile material for tension case tends to reduce the lateral stress at the pile-geomaterial interface, whereas the opposite occurs for the case where the shaft is loaded in compression.

- As detailed in Chapter 2, previous research studies concluded that the reported range of tensile to compressive shaft capacity ratio [$\theta_{t/c} = Q_{s(t)}/Q_{s(c)}$] spans between 0.50 and 0.90, with an overall average value of 0.70.
- The results of this current research effort indicate that the ratio, $\theta_{t/c}$ averages 0.76.
- In tension loading, shaft resistance (Q_s) is the primary component of axial pile capacity. It implies that the base resistance component (Q_b) may not activate in case of tension loading. This could be true for the drained loading case where the pile foundation is embedded in coarse grained soils. However, for piles installed in silts and clays, undrained conditions exist, whereby suction effects at the pile tip may generate a certain component of Q_b in downward direction. McManus and Kulhawy (1994) reported from field measurements during cyclic axial loading of a drilled shaft in "Cornell clay" that excess pore water pressures up to one atmosphere (σ_{atm} = 100 kPa) may be generated at the pile tip.

To account for the above factors, following modifications are proposed to the Randolph closed form pile solution for the case of tension loading (also see Figure 7.1).

7.2.1 Piles Embedded in Sand

The tension load applied at the pile top (Q_t) is resisted by two components: (1) a reduced shaft resistance in tension [$Q_{s(t)}$] along the pile length; and (2) the pile buoyant weight (W). Accordingly, the mathematical expression for tension load in case of piles embedded in sand reduces to the following form:

$$Q_t = Q_{s(t)} + W = \theta_{t/c} \cdot Q_{s(c)} + W$$
$$= \theta_{t/c} \cdot \Sigma(f_{p(c)} \cdot 2\,\pi\, r_o \cdot L) + W \qquad (7.2)$$

where, $\theta_{t/c}$ is the ratio of tensile to compressive pile shaft capacity averaged at 0.76, $Q_{s(t)}$ = shaft capacity in tension, $Q_{s(c)}$ = shaft capacity in compression, $f_{p(c)}$ = unit shaft

resistance in compression, r_o = shaft radius, W = pile buoyant weight, L = pile length. As noted, the term for pile base resistance (Q_b) has been neglected. Similarly, omitting the applicable terms, i.e., $4\eta/[(1 - \nu_s)\xi]$, in the numerator and denominator terms that relate to the base contribution, the elastic solution reduces to the form shown in Equation 7.3:

$$w_t = \frac{Q_t \, \zeta \, (\mu L)}{2\pi \rho_E \, G_L \tanh(\mu L) L} \tag{7.3}$$

Various terms in the above equation have been defined previously in Chapter 4 and are reproduced here in Figure 7.1 for completeness. The parameter G_L represents the operative soil shear modulus at the reference elevation of pile base (G at depth z = L) corresponding to the applied tensile load at the pile top (Q_t) and the resulting upward pile top displacement (w_t), while ρ_E denotes the shear modulus variation along the pile embedded length: $\rho_E = G_M/G_L$, where G_M = value of G at mid-length depth z = L/2.

7.2.2 Piles Embedded in Clay and/or Silt

In case of piles installed in fine-grained soils, the tension load applied at the pile top (Q_t) is resisted by three components: (1) a reduced shaft resistance [$Q_{s(t)}$] along the pile length; (2) pile buoyant weight (W); and (3) a nominal resistance at the pile base (Q_b) because of possible suction effects from the change in pore water pressure generated beneath the pile tip. This is mathematically expressed in Equation 7.4 below:

$$\begin{aligned} Q_t &= Q_{s(t)} + W + Q_b = \theta_{t/c} \cdot Q_{s(c)} + W + Q_b \\ &= \theta_{t/c} \cdot \Sigma(f_{p(c)} \cdot 2 \, \pi \, r_o \cdot L) + W + q_b \cdot A_b \\ &= \theta_{t/c} \cdot \Sigma(f_{p(c)} \cdot 2 \, \pi \, r_o \cdot L) + W + \Delta u \cdot \pi r_b^2 \end{aligned} \tag{7.4}$$

where, $Q_{s(t)}$ = shaft capacity in tension, $Q_{s(c)}$ = shaft capacity in compression, $f_{p(c)}$ = unit shaft resistance in compression, r_o = shaft radius, W = pile buoyant weight, L = pile length, q_b = unit base resistance, A_b = cross-sectional area of pile tip, Δu = measured change in pore water pressure (ranging between zero and σ_{atm} = 100 kPa, depending on the drainage characteristics of the soil at the pile tip), and r_b = pile base radius. Since some base resistance component forms part of the total resistance in the case of fine-grained soils, the terms of the elastic solution that account for the base resistance components are retained for the load-displacement analysis (Equation 7.5).

$$w_t = \frac{Q_t\left[1+\frac{4\eta\ \tanh(\mu L)L}{\pi\lambda(1-\upsilon_S)\xi\,(\mu L)\,r_o}\right]}{G_L\,r_o\left[\frac{4\eta}{(1-\upsilon_S)\xi}+\frac{2\pi\rho_E\tanh(\mu L)L}{\zeta\,(\mu L)\,r_o}\right]} \tag{7.5}$$

All terms in the above equation have been defined previously in Chapter 4 and are also reproduced here in Figure 7.1.

Uplift or Tension Loading

Solution for clayey soils

$$w_t = \frac{Q_t\left[1 + \frac{4\eta\ tanh(\mu L)\ L}{\pi\lambda(1-\upsilon_s)\xi\ \mu L\ r_o}\right]}{G_L\ r_o\left[\frac{4\eta}{(1-\upsilon_s)\xi} + \frac{2\pi\rho_E\ tanh(\mu L)\ L}{\zeta\ \mu L\ r_o}\right]}$$

$Q_t = Q_{s(t)} + W + Q_b = \theta_{t/c} \cdot Q_{s(c)} + W + Q_b$
$= \theta_{t/c} \cdot \Sigma(f_{p(c)} \cdot 2\ \pi\ r_o \cdot L) + W + q_b \cdot A_b$
$= \theta_{t/c} \cdot \Sigma(f_{p(c)} \cdot 2\ \pi\ r_o \cdot L) + W + \Delta u \cdot \pi r_b^2$

Solution for sandy soils

$$w_t = \frac{Q_t\ \zeta\ (\mu L)}{2\pi\rho_E\ G_L\ tanh(\mu L)L}$$

$Q_t = Q_{s(t)} + W = \theta_{t/c} \cdot Q_{s(c)} + W$
$= \theta_{t/c} \cdot \Sigma(f_{p(c)} \cdot 2\ \pi\ r_o \cdot L) + W$

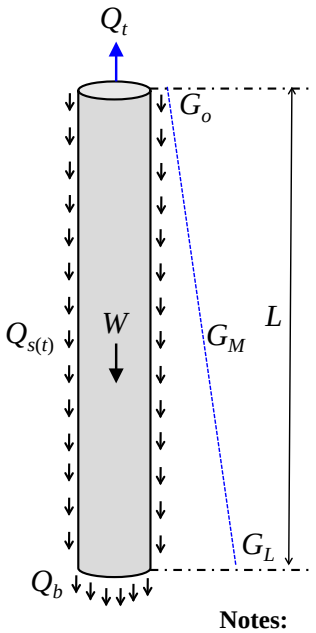

w_t = upward displacement at the pile top; $\theta_{t/c}$ = ratio of tension to compression shaft capacity = 0.763; f_p = mobilized unit side resistance; r_o = shaft radius; W = buoyant weight of the pile; q_b = unit base resistance; r_b = base radius; Δu = excess porewater pressure = 0 to 1 atmosphere (100 kPa)

Pile diameter d
Pile Length L

Notes:

- The solutions compensates for reduction in the uplift capacity due to Poisson's effect
- Base resistance (Q_b) has been assumed negligible in sandy soils, and a nominal value of unit base resistance (q_b) = measured excess pressure (Δu) has been assumed for clayey soils

- G_L = operative soil shear modulus at the pile base
- Q_t = load applied at the pile top
- w_t = total displacement at the pile top
- $\eta = r_b/r_o$ = eta factor for bell-shaped piles
- r_o = d/2 = pile radius; $r_b = d_b/2$ = pile base radius for bell shaped piles
- $\mu L = 2\cdot[2/(\zeta\ \lambda)]^{0.5}\cdot L/d$ = measure of pile compressibility
- $\zeta = \ln(r_m/r_o)$ = measure of influence radius
- $r_m = L\cdot\{0.25 + \xi\cdot[2.5\ \rho_E\cdot(1 - \nu_s) - 0.25]\}$ = influence radius

- $\lambda = E_p/G_L$ = pile-soil stiffness ratio
- E_p = pile modulus
- $\xi = G_L/G_b$ = xi factor for end bearing piles
- G_b = operative soil shear modulus below pile base
- $\rho_E = G_M/G_L$ = modulus variation factor
- $G_M = (G_o + G_L)/2$ = operative soil shear modulus at mid of pile embedment depth
- G_o = operative soil shear modulus at depth
- Q_b = portion of Q_t transferred to the pile base
- ν_s = Poisson's ratio of soil

Figure 7.1. Elastic pile solution for estimating upward displacements for axial tension loading.

7.3 Methodology for Back-Analysis of Shear Moduli from Load Tests

Identifying the versatility and convenience of elastic pile closed-form solutions by Randolph and Wroth (1978; 1979), a scheme of back-analyses of operational shear stiffnesses was formulated similar to the approach adopted by Berardi and Bovolenta (2005). Accordingly, Equations (7.3) and (7.5) were rearranged to the following forms:

$$G_L = \frac{Q_t\, \zeta\,(\mu L)}{2\pi \rho_E\, w_t \tanh(\mu L) L} \tag{7.6}$$

$$G_L = \frac{Q_t\left[1+\frac{4\eta\, \tanh(\mu L) L}{\pi\lambda(1-\upsilon_S)\xi\,(\mu L)\, r_o}\right]}{w_t\, r_o\left[\frac{4\eta}{(1-\upsilon_S)\xi}+\frac{2\pi\rho_E \tanh(\mu L) L}{\zeta\,(\mu L)\, r_o}\right]} \tag{7.7}$$

Further specifics on the methodology of the current retro-investigation are detailed below:

- Equation (7.6) applies to the cases of compression load tests as well as those of tension load tests in clays and silts, while Equation (7.7) was used for the cases of tension load tests in sand.
- The applied loads (Q_t) and their corresponding measured displacements (w_t) from each load test were used in the above equations, duly incorporating expressions (7.2) and (7.4), depending upon their respective cases. The Group 2 dataset, providing measurements of Q-w from the load tests, was utilized. These Q-w data are presented in Appendix E.
- The remaining key input parameters used in the elastic solution are detailed in Appendix G.
- The G_{max} profiles and the related ρ_E factors obtained via V_s measurements mostly indicated either relatively uniform conditions (i.e., homogeneous case where modulus is constant with depth) or general Gibson soil types (modulus increases with depth).
- The pile moduli (E_p), required for calculating the pile-soil stiffness ratios ($\lambda = E_p/G_L$) and the measure of pile compressibility (μL) were adopted from the information given by their respective sources. For other situations, where this

information was not available, appropriate values from similar pile types were assumed.

- For the soil Poisson's ratio (ν_s) values, the following assumptions were made: drained conditions for predominantly sandy soils (ν_s = 0.20), while undrained conditions for predominantly clayey soil layers (ν_s = 0.50). However, where this information was explicitly given in the original data source, the reported values were adopted.
- Inherent in this framework of back-analysis are the following two assumptions that are reasonably acceptable from an engineering point of view: (1) the stiffness is linearly dependent on the depth, although some real situations may portray a different trend, and (2) the back-analyzed field stiffness can be obtained keeping ρ_E constant, i.e., G along the shaft and at the base decrease at the same rate, although the shaft resistance is expected to mobilize prior to the end bearing.
- Hidden in the parameters on the right hand sides of Equations (7.6) and (7.7) is the input of G_L. A trial and error method (or a computer program capable of running the required iterations) can be used to match the values of G_L on both sides of the equation.
- The operative shear stiffness (G) values so obtained and normalized via G/G_{max} as a function of $\gamma_p = w_t/d$ (%) provided the desired stiffness reduction trends.

7.4 Cumulative Results of Back-Analysis

The respective stiffness reduction curves from each load test obtained via the above methodology are shown in Appendix E. The combined back-analyzed stiffness reduction trends from 299 pile load tests of Group 2 dataset are presented in Figure 7.2. As shown here, the pseudo-strain (γ_p) axis has also been normalized with respect to a reference pseudo-strain ($\gamma_{p\text{-}ref}$), taken as w_t/d = 0.01. This low value of $\gamma_{p\text{-}ref}$ has been

adopted to match closely with the previous definitions of reference strain (γ_{ref}) found in the literature, as detailed in Chapter 4.

Clearly evident, the data points in Figure 7.2 present a wide scatter. The database used herein is characterized by a wide variety of differing soil conditions, pile foundation types, and pile installation methods. Logically, such variability is not likely to derive consistent results in a combined plot, such as Figure 7.2, thus hampering its utilization in the development of modulus reduction algorithms which are suitable for future pile Q-w predictions. Accordingly, the results are further segregated and sorted into groups based on pile types and installation methods. These results are shown in Figure 7. 3.

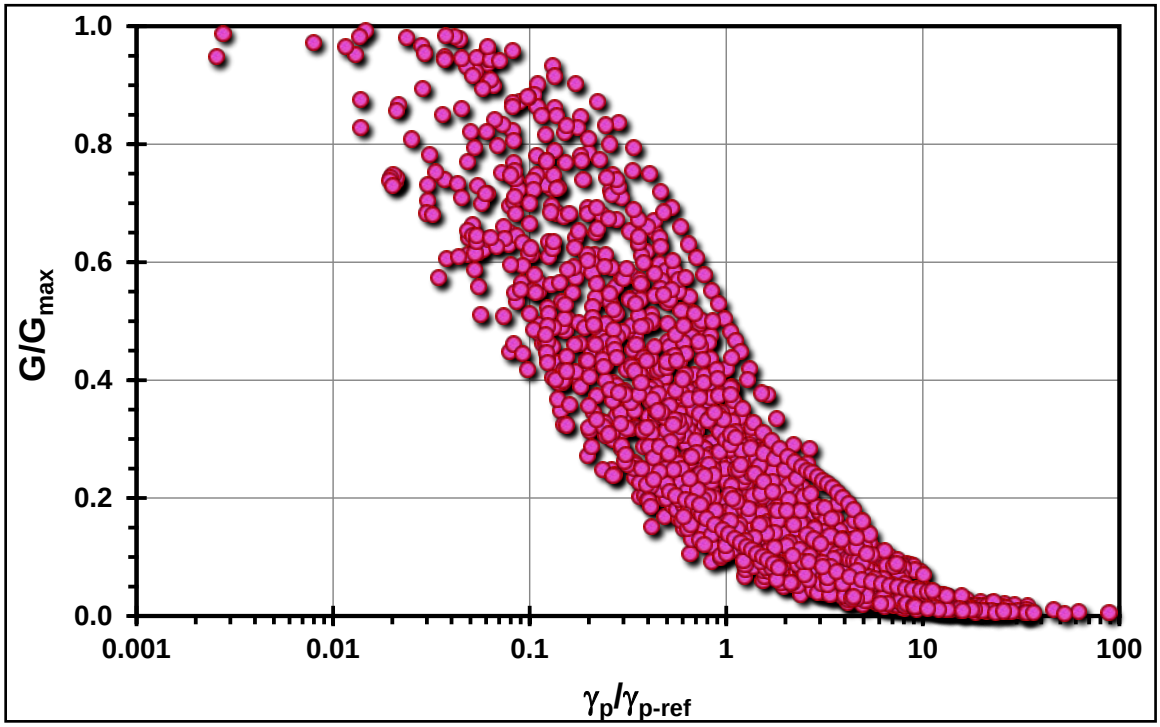

Figure 7.2. Back-analyzed moduli from 299 pile load tests in terms of normalized operative shear stiffnesses (G/G_{max}) vs. normalized pseudo-strain ($\gamma_p/\gamma_{p\text{-}ref}$), where $\gamma_p = w_t/d$ and $\gamma_{p\ -ref} = 0.01$.

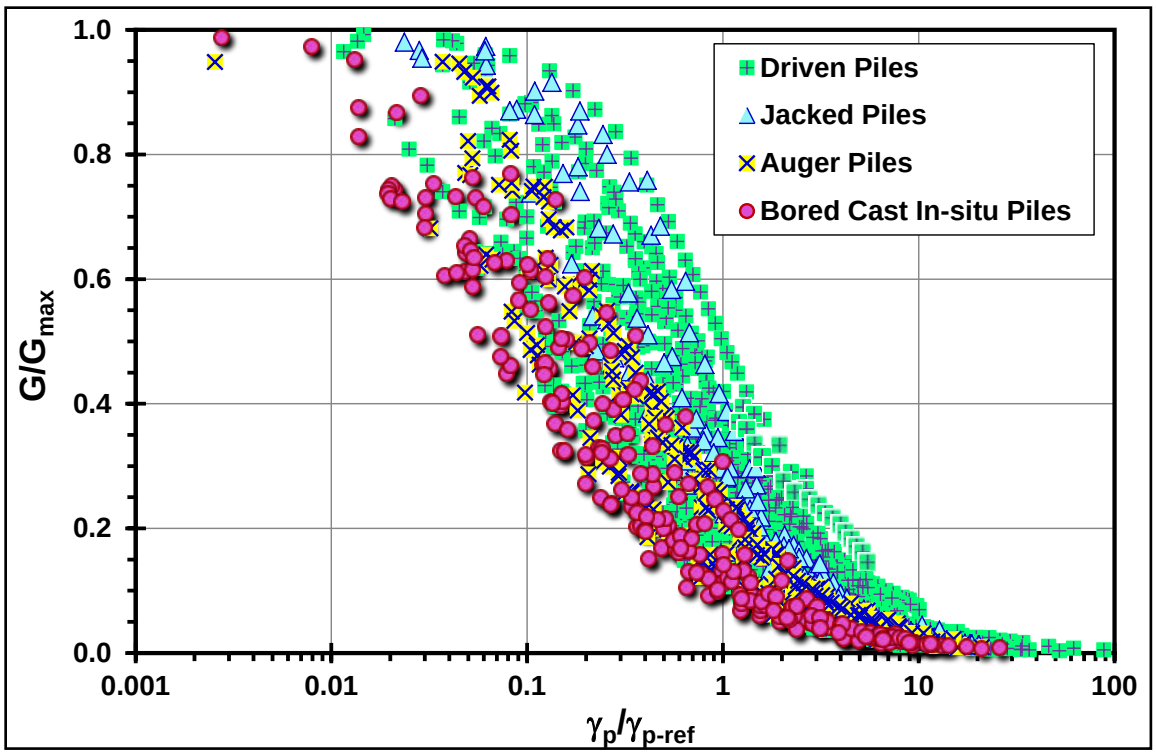

Figure 7.3. Sorted normalized operative shear stiffness vs. normalized pseudo-strain per the pile typology and installation methods.

As observed in Figure 7.3, sorting based on the pile typology and installation method clearly points to a certain hierarchical order in which the stiffness reduction trends may be ranked. In general, the drilled shafts which are installed using bored cast in-situ methods tend to present the most rapid reduction of the soil's operative shear modulus from its initial value of G_{max} in the range of percent γ_p (and even the normalized $\gamma_p/\gamma_{p\text{-}ref}$) < 0.1, beyond which the reduction becomes more gradual. On the other extreme, the steel as well as the precast concrete piles, installed using driven and jacked method largely display the most gradual deterioration of shear stiffness in the initial range of percent γ_p (< 0.1), becoming steeper for higher values. The auger piles fall in the intermediate category. Despite these general observations, significant scatter still exists within each category, which may be attributed to different characteristics of the soil deposits in the database.

Based on experimental laboratory data encompassing clays and sands, Vucetic and Dobry (1991) identified plasticity index (PI) as a main factor affecting G/G_{max} reduction curves for a wide variety of soils. Consequently, they developed design charts showing the modulus reduction curves as functions of PI, applicable to dynamic loading conditions for seismic engineering concerns (see Chapter 4). However, the Vucetic and Dobry (1991) charts were not expressed mathematically for convenient quantification of the G/G_{max} vs log γ_s relationships. Recently, using laboratory experimental data from resonant column, triaxial, simple shear, and torsional shear tests on 21 clays and silts, Vardanega and Bolton (2011, 2013) advanced this approach and developed new PI based curves for both dynamic and static loading, along with their respective design equations. With such trends having already been established, it was considered reasonable to tap into the potential of exploring the effects of PI on this latest framework of G/G_{max} vs. $\gamma_p/\gamma_{p\text{-}ref}$, and then apply this approach to the pile response database in an analogous manner.

Mayne (1999) back-calculated field moduli from bored pile load tests in Piedmont residual soils in Atlanta, using elastic continuum solutions and related the modulus reduction curves (G/G_{max}) to applied load level ($Q_t/Q_{t\text{-}ult}$). Similarly, in a parallel study during the current research, the back-analyzed normalized shear stiffness (G/G_{max}) values were also plotted against normalized $Q_t/Q_{t\text{-}ult}$ (see Appendix I). Here, $Q_{t\text{-}ult}$ represents the interpreted ultimate pile capacity that was determined separately from the Q-w data of each load test using three different definitions of pile capacity, namely: (1) Davisson's offset line criterion, designated $Q_{Davisson}$ (Davisson, 1972), (2) French criterion, i.e., w/d = 10%, designated $Q_{w/d=10\%}$ (Vesić, 1977), and (3) Chin-Kondner capacity criterion, or $Q_{C\text{-}K}$ (Chin, 1970; Kondner, 1963). These interpreted pile capacities have been discussed previously in Chapters 5 and 6, and are individually presented for each pile case study in Appendix E. To observe the effects of soil plasticity on the back-analyzed operative shear modulus curves, G/G_{max} values at reference loading rates of $0.5 \cdot Q_{t\text{-}ult}$ and $0.2 \cdot Q_{t\text{-}ult}$

(corresponding to factors-of-safety of 2 and 5, respectively) from all load tests were plotted against their corresponding PI values. Non-plastic soils (i.e., sands) were assigned a PI of zero, while cases involving fine-grained soils without plasticity information were omitted. Such an exercise was conducted for all three criteria defining the $Q_{t\text{-}ult}$. The resulting plots of different sub-categories (based on the pile and soil typology), and the combined results of the dataset are presented in Figures I.1 to I.8 of Appendix I. The PI effect is clearly validated from these plots, providing a recipe for incorporating this influence into G/G_{max} vs. γ_p formulation.

7.5 Fitting a Model

It is evident from Figures 7.2 and 7.3 that the relationship between the predictor variable ($\gamma_p/\gamma_{p\text{-}ref}$) and the response variable (G/G_{max}) is nonlinear for the entire dataset as well as different categories of pile type and installation. For such a relationship, it is advisable to work with alternative models where the variables are expressed after transformation. In order to linearly characterize the relationship for simple regression purposes, a modified hyperbolic model was fitted to the entire dataset after transforming the response variable to the form ($G_{max}/G - 1$), and taking common logarithms of both predictor variable and the transformed response variable. The resulting plot is shown in Figure 7.4. A simple regression through the data points yields the following expression:

$$\log_{10}\left(\frac{G_{max}}{G} - 1\right) = 0.942 \log_{10}\frac{\gamma_p}{\gamma_{p-ref}} + 0.561 \qquad (7.8)$$

with a coefficient of determination (R^2) = 0.86 for N = 1,968 data points. The reverse-transformation of Equation (7.8) results in the following generalized correlation:

$$\frac{G}{G_{max}} = \frac{1}{\left[1+3.634\left(\frac{\gamma_p}{\gamma_{p-ref}}\right)^{0.942}\right]} \tag{7.9}$$

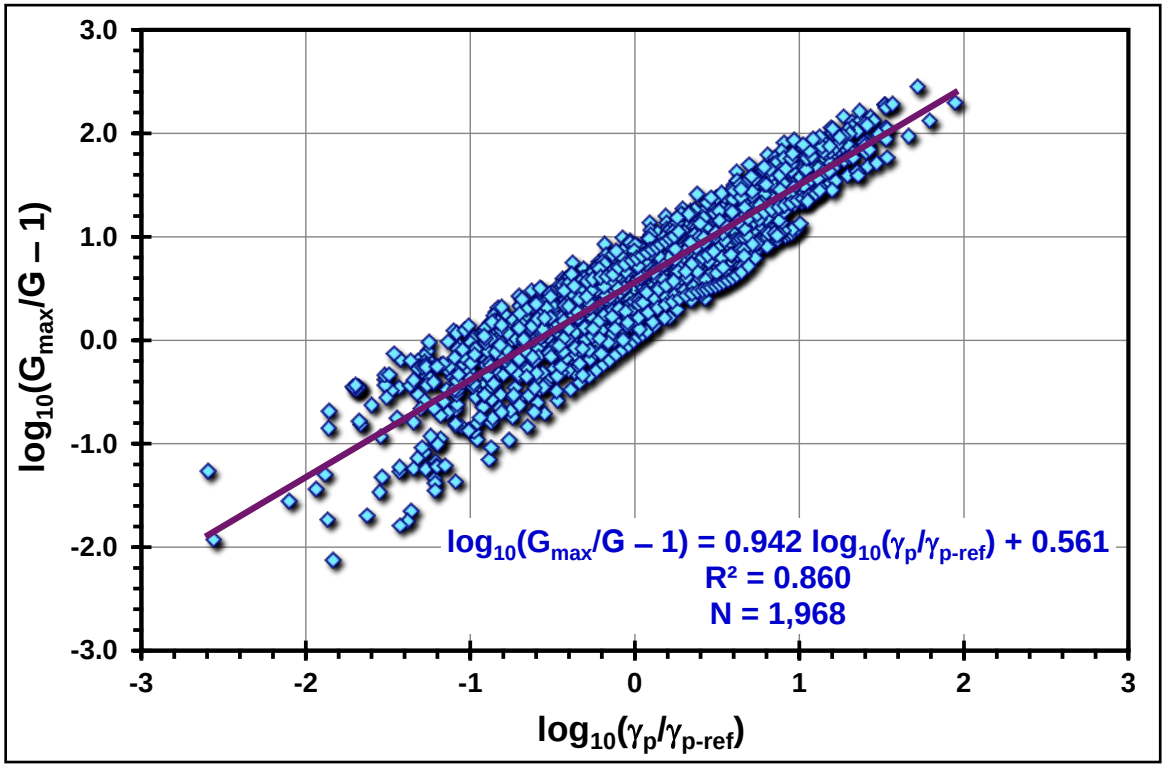

Figure 7.4. Modified hyperbola fitted to the transformed predictor and response variables of G/G_{max} vs. $\gamma_p/\gamma_{p\text{-}ref}$ formulation for all pile load test data.

In order to quantify the influence of pile typology and installation methods, the above methodology was independently applied to the four categories shown in Figure 7.3. These results are presented in Figure 7.5, showing improved R^2 values for each category. The reverse transformations of the linear regression fitting functions for different categories result in the following respective expressions.

Driven Piles: $$\frac{G}{G_{max}} = \frac{1}{\left[1+3.042\left(\frac{\gamma_p}{\gamma_{p-ref}}\right)^{1.006}\right]} \quad (7.10)$$

Jacked Piles: $$\frac{G}{G_{max}} = \frac{1}{\left[1+2.357\left(\frac{\gamma_p}{\gamma_{p-ref}}\right)^{1.175}\right]} \quad (7.11)$$

Auger Piles: $$\frac{G}{G_{max}} = \frac{1}{\left[1+4.275\left(\frac{\gamma_p}{\gamma_{p-ref}}\right)^{0.955}\right]} \quad (7.12)$$

Bored Piles: $$\frac{G}{G_{max}} = \frac{1}{\left[1+6.947\left(\frac{\gamma_p}{\gamma_{p-ref}}\right)^{0.914}\right]} \quad (7.13)$$

To simplify the model, the following unified correlation is proposed to embrace the entire dataset on one end and to account for the pile installation method on the other end:

$$\frac{G}{G_{max}} = \frac{1}{\left[1+3.634\alpha 1\left(\frac{\gamma_p}{\gamma_{p-ref}}\right)^{0.942\beta 1}\right]} \quad (7.14)$$

where the values of coefficient $\alpha 1$ and exponent $\beta 1$ are parameters that, identify with the pile typology and installation methods, as presented in Table 7.1.

Table 7.1. Coefficients and exponents for G/G_{max} vs. $\gamma_p/\gamma_{p\text{-}ref}$ formulation (Equation 7.14).

Pile classification (type/installation method)	**$\alpha 1$**	**$\beta 1$**
Driven	0.837	1.068
Jacked	0.648	1.247
Auger	1.176	1.013
Bored Cast In-situ	1.912	0.971

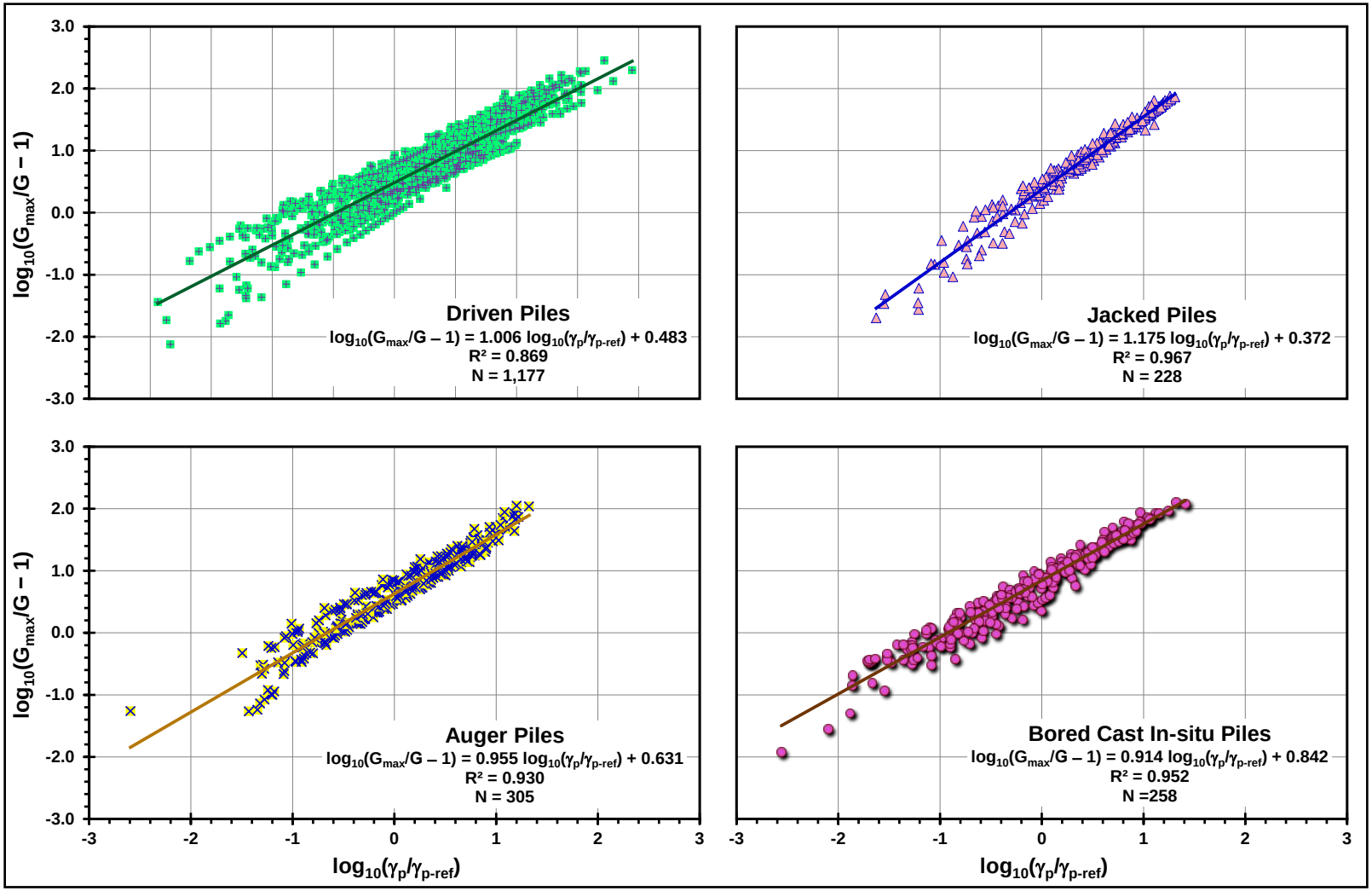

Figure 7.5. Modified hyperbola fitted to the transformed predictor and response variables of G/G_{max} vs. $\gamma_p/\gamma_{p\text{-}ref}$ formulation: (a) driven piles data; (b) jacked piles data; (c) auger piles data; (d) bored cast in-situ piles data.

To mitigate the scatter within each category of piles in an effort of further refinement of the model, it was considered prudent to incorporate the influence of PI in the new design formulation. Therefore, the data were additionally sorted based on the soil plasticity information. Accordingly, the slopes and intercepts from linear regressions of the transformed predictor and response variables were obtained for different PI values within each category of piles. These plots along with their respective PI-based slopes and intercepts are shown in Figure I.9 of Appendix I. The reverse transformation of these linear regression fitting models resulted in additional sets of coefficients and exponents ($\alpha 2$ and $\beta 2$) that present the effect of PI. Equation (7.14) thus takes the following form:

$$\frac{G}{G_{max}} = \frac{1}{\left[1+3.634\ \alpha 1\ \alpha 2 \left(\frac{\gamma_p}{\gamma_{p-ref}}\right)^{0.942\ \beta 1\ \beta 2}\right]} \tag{7.15}$$

Subsequently, separate graphs were plotted for each pile category with percent PI values on the abscissa axis while $\alpha 2$ and $\beta 2$ on the ordinate axis. Different fitting functions were explored to define the trends, followed by superimposing the outcome of these functions on the original datasets. Two functional forms that delivered better results of this superimposition included: (1) exponential function; and (2) hyperbolic tangent function. The plots of the two sets of functions are shown in Figure 7.6. The use of hyperbolic tangent function offers an added advantage of limiting the upper and lower values of the curve fitting coefficient $\alpha 2$ and exponent $\beta 2$, restraining the predicted values from being non-representative near the outer bounds of the dataset, and thereby providing improved fitting.

In summary, the two sets of coefficients ($\alpha 1$ and $\alpha 2$) and exponents ($\beta 1$ and $\beta 2$) of Equation (7.15), identifying the effects of pile typology/installation methods, as well

as the influence of PI on G/G_{max} vs. $\gamma_p/\gamma_{p\text{-}ref}$ formulation for the two proposed fitting functions are presented in Tables 7.2 and 7.3, respectively.

Table 7.2. Coefficient and exponent values for G/G_{max} vs. $\gamma_p/\gamma_{p\text{-}ref}$ formulation by an exponential fitting function (Equation 7.15).

Pile type	**α1**	**β1**	**α2**	**β2**
Driven	0.837	1.068	1.748·exp [– 0.021·PI (%)]	0.854· exp [– 0.005·PI (%)]
Jacked	0.648	1.247	1.453· exp [– 0.017·PI (%)]	0.875· exp [– 0.005·PI (%)]
Auger	1.176	1.013	2.096· exp [– 0.024·PI (%)]	0.867· exp [– 0.005·PI (%)]
Bored cast in-situ	1.912	0.971	1.388· exp [– 0.024·PI (%)]	0.934· exp [– 0.005·PI (%)]

Table 7.3. Coefficient and exponent values for G/G_{max} vs. $\gamma_p/\gamma_{p\text{-}ref}$ formulation by a hyperbolic tangent fitting function (Equation 7.15).

Pile type	**α1**	**β1**	**α2**	**β2**
Driven	0.837	1.068	2.1-1.8·tanh[0.03·PI (%)-0.01]	1.08+0.3·tanh[0.025·PI (%)-0.95]
Jacked	0.648	1.247	1.4-1.3·tanh[0.015·PI (%)-0.2]	1.05+0.21·tanh[0.03·PI (%)-1.2]
Auger	1.176	1.013	1.8-1.5·tanh[0.03·PI (%)-0.23]	1.05+0.17·tanh[0.037·PI (%)-1.5]
Bored cast in-situ	1.912	0.971	1.4-1.3·tanh[0.02·PI (%)-0.07]	1.16+0.3·tanh[0.025·PI (%)-1.0]

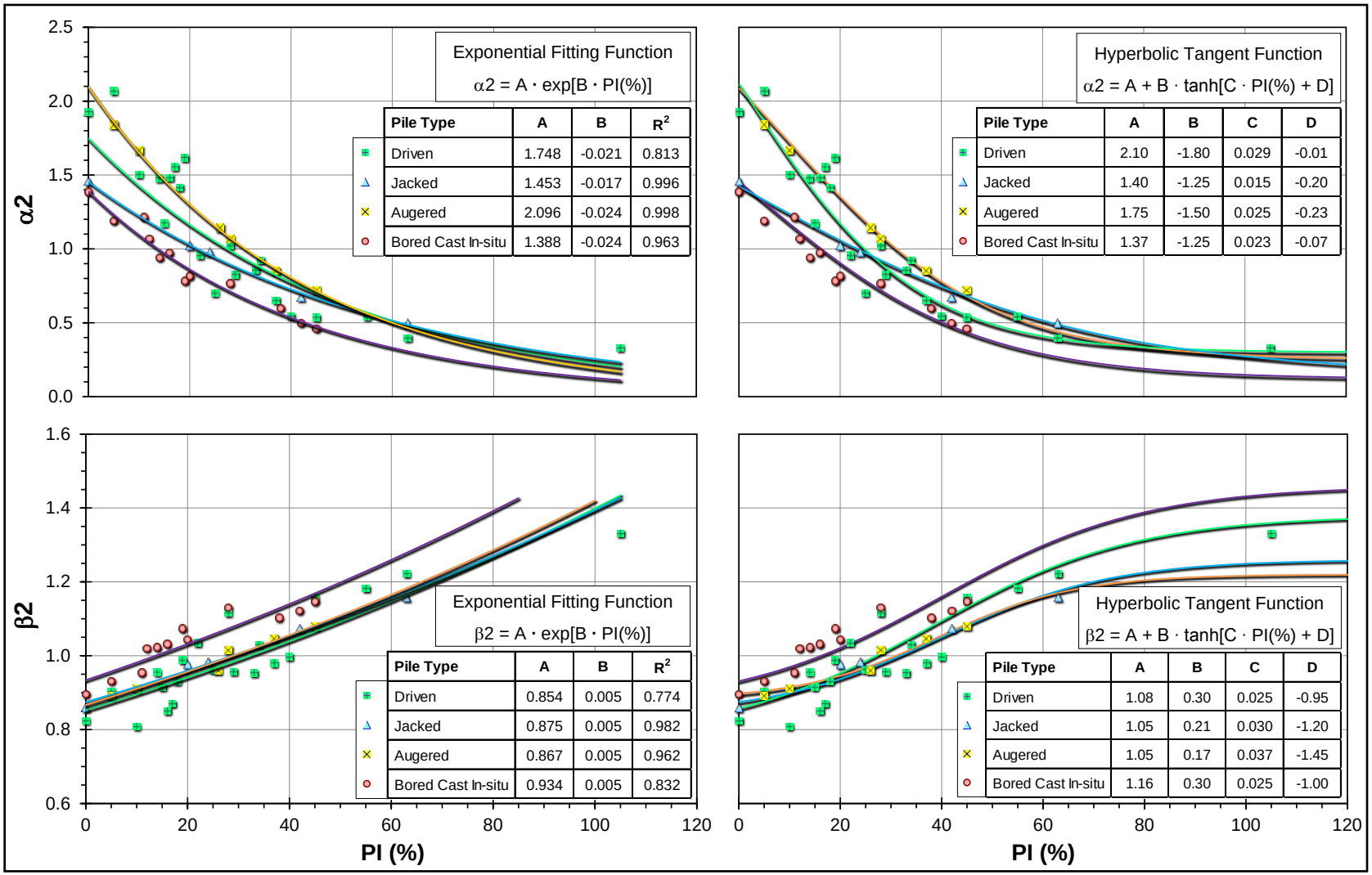

Figure 7.6. Correlations of coefficient α2 and exponent β2 with percent PI: (a) exponential fitting function; (b) hyperbolic tangent fitting function.

7.6 New Design Charts

For convenience and ease in application, it is considered reasonable to present these new design formulations in graphical form. Moreover, the abscissa axis can be simplified to percent pseudo-strain [i.e., γ_p (%)] instead of normalized pseudo-strain ($\gamma_p/\gamma_{p\text{-}ref}$), as the numerical values of both are same because of the selected reference strain [$\gamma_{p\text{-}ref}$ (%) = 1.0]. Accordingly, two sets of design charts have been prepared for the four categories of piles (see Figures 7.7 and 7.8). The first set shown in Figure 7.7 presents design charts derived using exponential fitting function, while that in Figure 7.8 show charts resulting from hyperbolic tangent function. These charts also show their respective design equations pertaining to the pile type and those for estimating their respective coefficients $\alpha 2$ and exponents $\beta 2$ which integrate the influence of PI on shear modulus reduction.

The general trends appear consistent with both the earlier Vucetic and Dobry (1991) charts and recent Vardanega and Bolton (2011; 2013) design charts and equations. A direct simple apple-to-apple comparison is, however, not possible for the fact that the strain values taken in the current analysis have been defined on the basis of relative pile displacements (w_t/d), termed here as pseudo-strains (γ_p), in contrast to the classical strain definitions given for laboratory shear tests. The reference strain at $w_t/d = 0.01$ (used for normalization, i.e., $\gamma_p/\gamma_{p\text{-}ref}$) is also different from the one assumed by Vardanega and Bolton (2011; 2013), as well as other previous research works.

The next section presents assessments of the accuracy of this shear modulus prediction model.

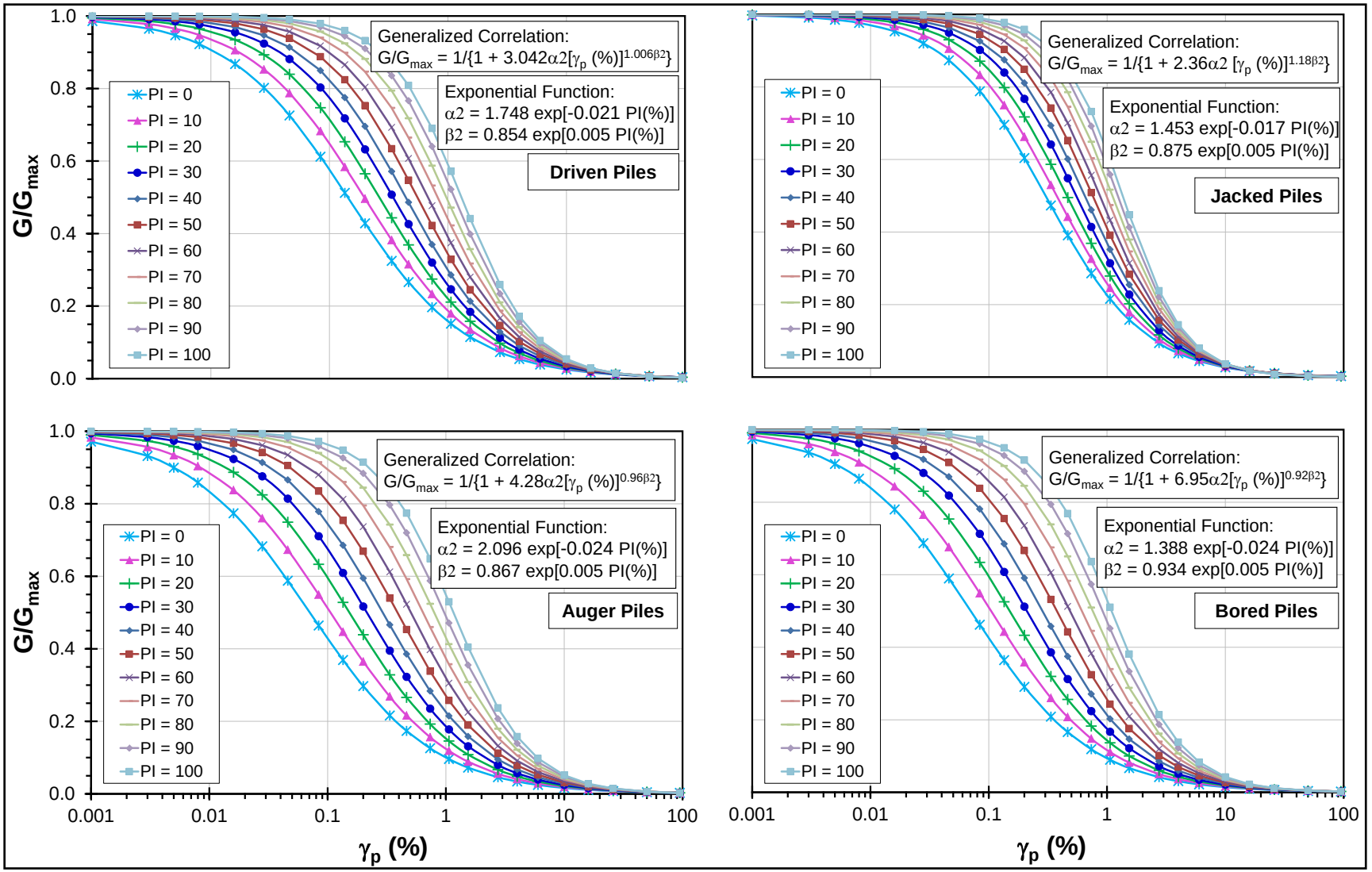

Figure 7.7. Design charts for shear stiffness reduction for application in the pile foundation analysis (exponential fitting function).

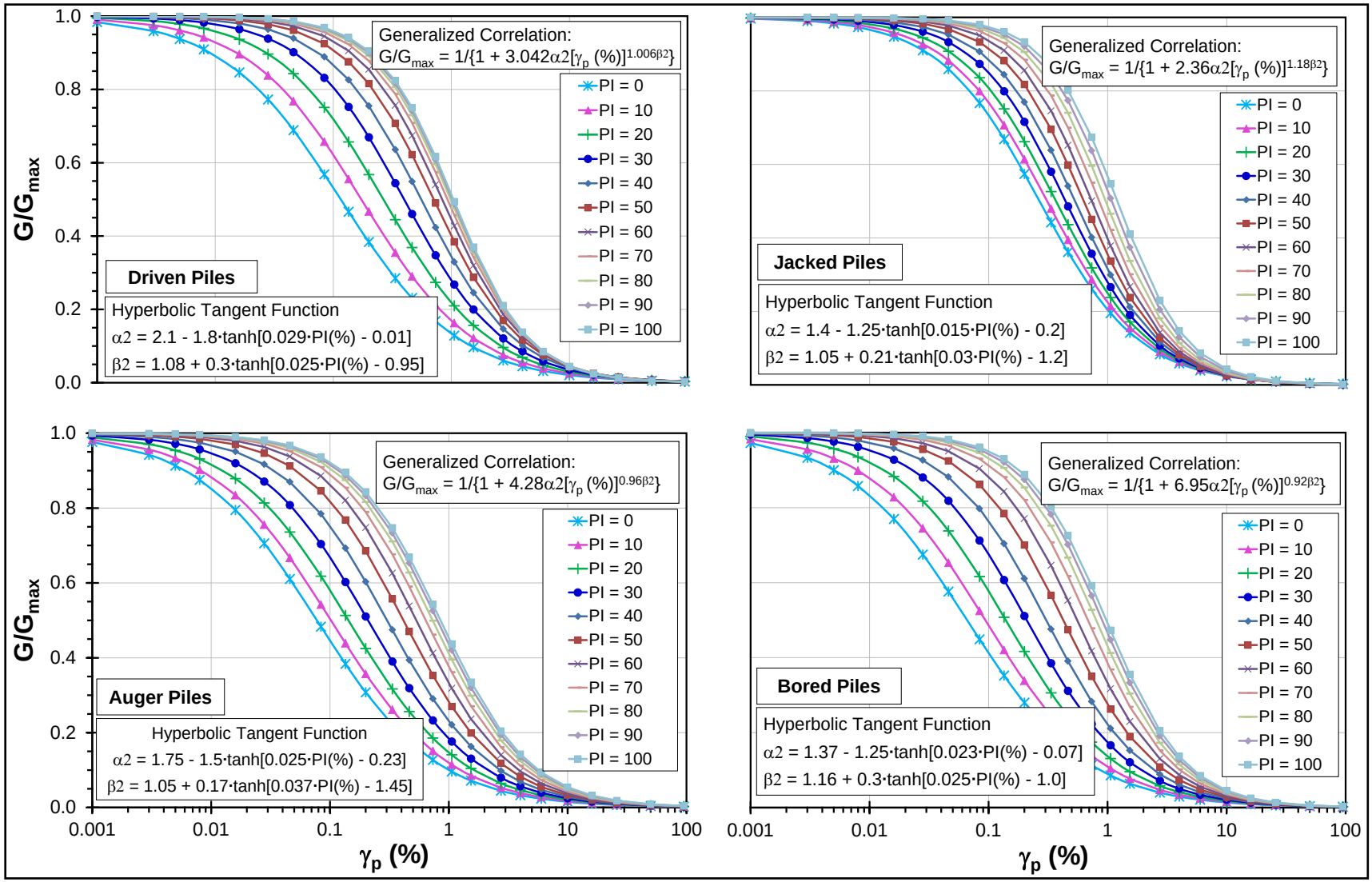

Figure 7.8. Design charts for shear stiffness reduction for application in the pile foundation analysis (hyperbolic tangent function).

7.7 Assessment of New Design Formulation

In order to test the performance of the newly-derived empirically functions, the predicted values of the normalized shear stiffness [$G/G_{max\ (predicted)}$] were plotted against their back-figured values [$G/G_{max\ (back\text{-}figured)}$] for two proposed functions, as applied to the entire dataset. The underlying assumption of the following analysis is the conjecture that the back-figured values of shear modulus are representative of the field values, since there were derived from the actual load tests.

The results are presented in Figure 7.9, while Tables 7.4 and 7.5 show the basic statistics of the two models. Simple linear regression analysis was conducted on each set of the results to obtain the best fit line of the ratios of predicted to back-figured normalized shear stiffness, [$G/G_{max\ (predicted)}$]/[$G/G_{max\ (back\text{-}figured)}$]. The corresponding R^2 of these ratios were then calculated. Inspection of Figure 7.9 shows that both functions yield their trend lines that tie near perfectly to the best fit line with a common R^2 value of 0.975. As evident, more than 90% of the data fall within the $\pm$30% bounds. In Figure 7.9, some seemingly greater scatter for the G/G_{max} values < 0.25 pertain to the range of loading beyond commonly accepted pile capacity definitions. This scatter is consistent with the loss of accuracy at low G/G_{max} reported by Vardanega and Bolton (2013).

Following the comparative approach used by Jardine et al. (2005), Lehane et al. (2013), and Van Dijk and Kolk (2011), the mean values (μ) and the coefficients of variation (COV) of the ratios of [$G/G_{max(predicted)}$]/[$G/G_{max(back\text{-}figured)}$] for the predictions made by the two proposed formulations are shown in Table 7.6. The following observations are noted:

- [$G/G_{max(predicted)}$]/[$G/G_{max(back\text{-}figured)}$] values derived for each method displayed an approximately normal distribution, with COV for the two functions being: 0.246 for exponential function, and 0.239 for hyperbolic tangent function. These values

fall within a reasonable range for reliable predictions, and suggest an improved stiffness reduction models for a wide variety of piles and soils.

- With the assumption of a normal distribution for $[G/G_{max\ (predicted)}]/[G/G_{max\ (back\text{-}figured)}]$, the mean values and COVs for the two sets of new design formulations suggest the following probabilities that the predicted normalized shear stiffness modulus $[G/G_{max\ (predicted)}]$ will be less than 1.5 times the back-figured normalized shear stiffness modulus $[G/G_{max\ (back\text{-}figured)}]$: 98.75% for exponential function, and 99.32% for hyperbolic tangent function.
- To further evaluate the suitability of the two models, they were subjected to additional assessments. Accordingly, the $[G/G_{max\ (predicted)}]/[G/G_{max\ (back\text{-}figured)}]$ ratios were segmented into 5 zones of G/G_{max} values, namely zone 1: 0 to 0.2, zone 2: 0.2 to 0.4, zone 3: 0.4 to 0.6, zone 4: 0.6 to 0.8, and zone 5: 0.8 to 1.0, followed by separate supplementary statistical analyses for each zone. The results are presented in Tables 7.7 to 7.11. The moment statistics of the two models (mean, standard deviation, minimum, maximum, range, variance, skewness, kurtosis) point to the following: (1) the distributions are narrow in zones 2 to 5 (i.e., the data points tend to be close to mean expected values), (2) the distributions are skewed slightly left of the mean values for zones 2 to 5, (3) the data in zone 1 present right skewed wide distributions. Accordingly, the accuracy is maximum in zone 3, 4, and 5, decreasing in zone 2, and least in zone 1. Despite this observed trend, the probabilities in zone 1 that the $G/G_{max\ (predicted)}$ will be less than 1.25 times the $G/G_{max\ (back\text{-}figured)}$ are 80.86% and 88.10% for exponential function, and hyperbolic tangent function, respectively. These probabilities indicate increasing trends for zones 2, 3, and 4, with 100% for zone 5 for both the models.

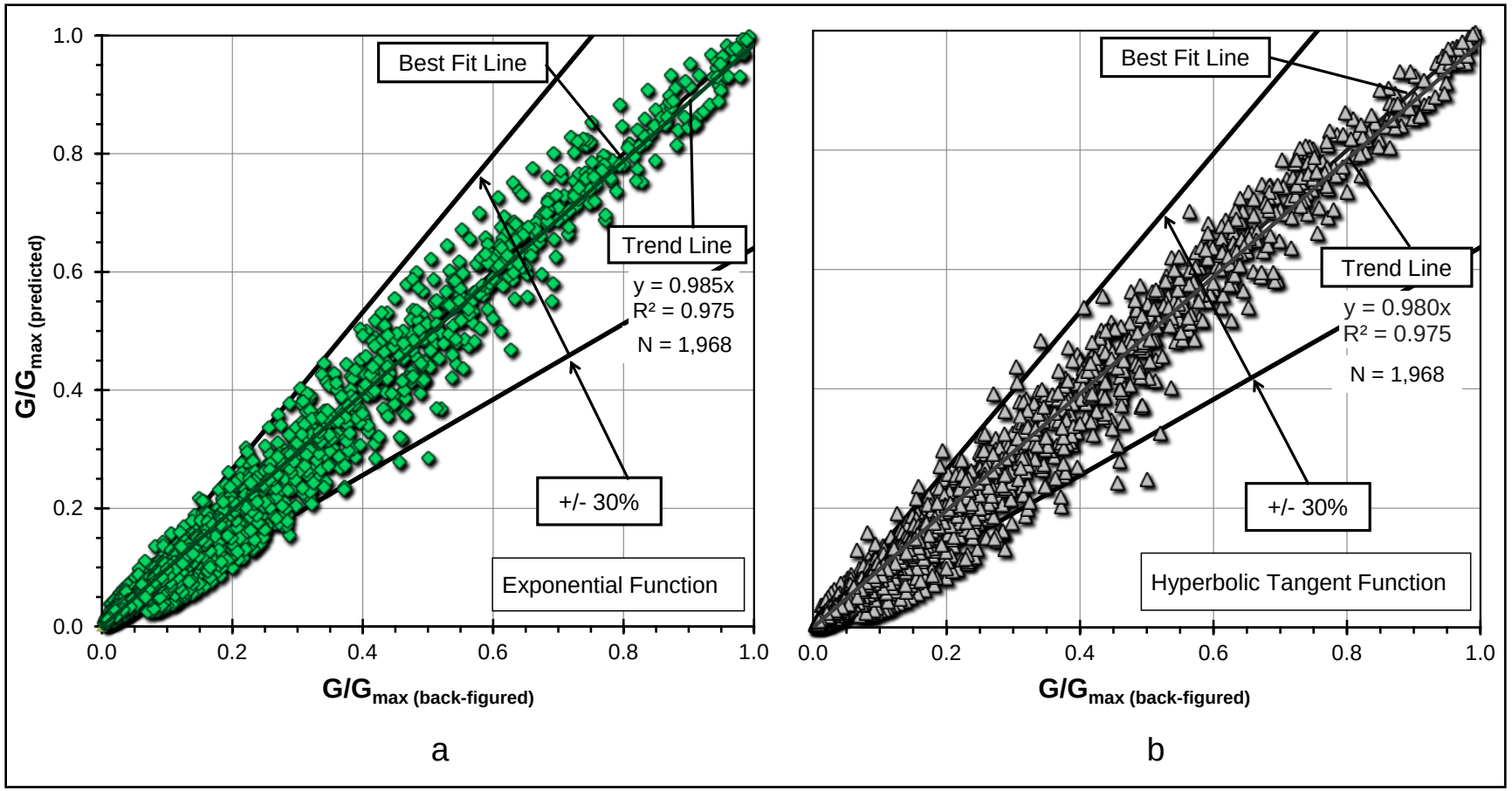

Figure 7.9. Predicted [$G/G_{max\ (predicted)}$] vs. back-figured [$G/G_{max\ (back\text{-}figured)}$] normalized shear stiffness from: (1) exponential fitting function; (2) hyperbolic tangent fitting function.

Table 7.4. Statistics of the exponential function model for G/G_{max} vs. $\gamma_p/\gamma_{p\text{-}ref}$.

Model Summary

R	R Square	Adjusted R Square	Std. Error of the Estimate
0.988	0.975	0.975	0.037

ANOVA

	Sum of Squares	df	Mean Square	F	Sig.
Regression	107.03	1.00	107.032	78854.27	0.00
Residual	2.67	1966.00	0.001		
Total	109.70	1967.00			

Coefficients

	Unstandardized Coefficients		Standardized Coefficients	t	Sig.
	B	Std. Error	Beta		
Measured	1.002	0.004	0.988	280.810	0.000
(Constant)	-0.008	0.001		-6.807	0.000

Table 7.5. Statistics of the hyperbolic tangent function model for G/G_{max} vs. $\gamma_p/\gamma_{p\text{-}ref}$.

Model Summary

R	R Square	Adjusted R Square	Std. Error of the Estimate
0.988	0.975	0.975	0.036

ANOVA

	Sum of Squares	df	Mean Square	F	Sig.
Regression	107.21	1.00	107.207	80847.34	0.000
Residual	2.62	1966.00	0.001		
Total	109.82	1967.00			

Coefficients

	Unstandardized Coefficients		Standardized Coefficients	t	Sig.
	B	Std. Error	Beta		
Measured	1.003	0.004	0.988	284.337	0.000
(Constant)	-0.011	0.001		-9.282	0.000

Table 7.6. Statistics summary of the ratio $[G/G_{max\ (predicted)}]/[G/G_{max\ (back\text{-}figured)}]$ for the proposed design formulations.

Proposed formulation	Mean (μ)	COV	R^2	$P[G/G_{max\ (predicted)} < 1.5\ G/G_{max\ (back\text{-}figured)}]$
Exponential function	0.982	0.246	0.975	98.75%
Hyperbolic tangent function	0.944	0.239	0.975	99.32%

Note: $P[G/G_{max\ (predicted)} < 1.5\ G/G_{max\ (back\text{-}figured)}]$ = probability that the predicted G/G_{max} values will be less than 1.5 times the back-figured G/G_{max}.

Table 7.7. Statistics, G/G_{max} vs. $\gamma_p/\gamma_{p\text{-}ref}$ models for G/G_{max} values in Zone 1: 0 to 0.2.

Statistics	Exponential Function	Hyperbolic Tangent Function
N	515	515
Mean	0.9960	0.9342
Std. Error of Mean	0.0085	0.0078
Median	0.9750	0.9210
Mode	0.9410	0.9120
Std. Deviation	0.2905	0.2676
Variance	0.0844	0.0716
Skewness	1.1628	1.2085
Kurtosis	4.3167	6.8667
Range	2.766	2.818
Minimum	0.329	0.269
Maximum	3.095	3.087
Z-value at 1.25	0.874	1.180
$P[G/G_{max\ (predicted)} < 1.25\ G/G_{max\ (back\text{-}figured)}]$	80.86%	88.10%

Table 7.8. Statistics, G/G_{max} vs. $\gamma_p/\gamma_{p\text{-}ref}$ models for G/G_{max} values in Zone 2: 0.2 to 0.4.

Statistics	Exponential Function	Hyperbolic Tangent Function
N	540	540
Mean	0.9237	0.9193
Std. Error of Mean	0.0086	0.0087
Median	0.9435	0.9295
Mode	0.9880	0.9810
Std. Deviation	0.1696	0.1723
Variance	0.0288	0.0297
Skewness	-0.0483	-0.2575
Kurtosis	-0.2972	0.4496
Range	0.837	1.000
Minimum	0.537	0.451
Maximum	1.374	1.451
Z-value at 1.25	1.923	1.919
$P[G/G_{max\ (predicted)} < 1.25\ G/G_{max\ (back\text{-}figured)}]$	97.28%	97.26%

Table 7.9. Statistics, G/G_{max} vs. $\gamma_p/\gamma_{p\text{-}ref}$ models for G/G_{max} values in Zone 3: 0.4 to 0.6.

Statistics	Exponential Function	Hyperbolic Tangent Function
N	339	339
Mean	0.9914	0.9861
Std. Error of Mean	0.0085	0.0082
Median	1.0030	1.0010
Mode	0.8740	1.0460
Std. Deviation	0.1238	0.1191
Variance	0.0153	0.0142
Skewness	-0.3702	-0.9034
Kurtosis	0.5631	2.2492
Range	0.673	0.824
Minimum	0.570	0.497
Maximum	1.243	1.321
Z-value at 1.25	2.089	2.217
$P[G/G_{max\ (predicted)} < 1.25\ G/G_{max\ (back\text{-}figured)}]$	98.12%	98.67%

Table 7.10. Statistics, G/G_{max} vs. $\gamma_p/\gamma_{p\text{-}ref}$ models for G/G_{max} values in Zone 4: 0.6 to 0.8.

Statistics	Exponential Function	Hyperbolic Tangent Function
N	366	366
Mean	1.0145	1.0071
Std. Error of Mean	0.0064	0.0059
Median	1.0160	1.0160
Mode	1.0070	1.0830
Std. Deviation	0.0741	0.0689
Variance	0.0055	0.0048
Skewness	-0.4229	-0.6711
Kurtosis	1.4562	-0.0883
Range	0.448	0.303
Minimum	0.748	0.822
Maximum	1.196	1.125
Z-value at 1.25	3.177	3.524
$P[G/G_{max\ (predicted)} < 1.25\ G/G_{max\ (back\text{-}figured)}]$	99.92%	99.99%

Table 7.11. Statistics, G/G_{max} vs. $\gamma_p/\gamma_{p\text{-}ref}$ models for G/G_{max} values in Zone 5: 0.8 to 1.0.

Statistics	Exponential Function	Hyperbolic Tangent Function
N	208	208
Mean	0.9918	0.9923
Std. Error of Mean	0.0044	0.0037
Median	1.0010	0.9970
Mode	1.0060	0.9770
Std. Deviation	0.0361	0.0301
Variance	0.0013	0.0009
Skewness	-0.2121	0.0142
Kurtosis	-0.0444	-0.0995
Range	0.176	0.140
Minimum	0.908	0.922
Maximum	1.084	1.062
Z-value at 1.25	7.146	8.548
$P[G/G_{max\ (predicted)} < 1.25\ G/G_{max\ (back\text{-}figured)}]$	100.00%	100.00%

7.8 Application of Design Charts for Pile Load-Displacement Evaluations

The new sets of G/G_{max} vs. γ_p design charts can be used within the elastic continuum framework to predict loads (Q_t) for different values of displacements (w_t), so as to derive their complete non-linear Q-w curves. The methodology is summarized in the flow chart shown in Figure 7.10, and further detailed below:

- Collect information on pile dimensions (length, L and diameter, d) and pile modulus (E_p).
- Acquire downhole shear wave velocity (V_s) profile at the site. Here, downhole V_s has been preferred over alternative methods, since the stiffness reduction curves were developed using G_{max} values calculated from V_s readings obtained predominantly via downhole methods (mostly seismic cone penetration tests). From the V_s profile, determine the initial shear stiffness modulus profile ($G_{max} = \rho_T \cdot V_s^2$) with depth.
- From the G_{max} profile, obtain modulus values at mid-depth, at base of the pile, and below the base [$G_{M(max)}$, $G_{L(max)}$, and $G_{b(max)}$ respectively], and determine the stiffness variation factor [$\rho_E = G_{M(max)}/G_{L(max)}$].
- Select a value of displacement (w_t) and calculate the corresponding pseudo-strain [$\gamma_p = (w_t/d) \cdot 100$] as a percentage.
- Based on the pile type and installation method select the appropriate G/G_{max} vs. γ_p design charts. Using this chart, and from the average representative PI (%) of the soil along the pile length, calculate the coefficient $\alpha 2$ and exponent $\beta 2$.
- Using the same chart, calculate $G_L/G_{L(max)}$ from the applicable algorithm given in that chart, and thus obtain G_L value corresponding to the selected w_t.
- From the accepted assumption of this analysis, keeping ρ_E constant, i.e., G along the shaft and at the base decrease at the same rate, estimate the values of applicable G_M and G_b for the selected w_t.

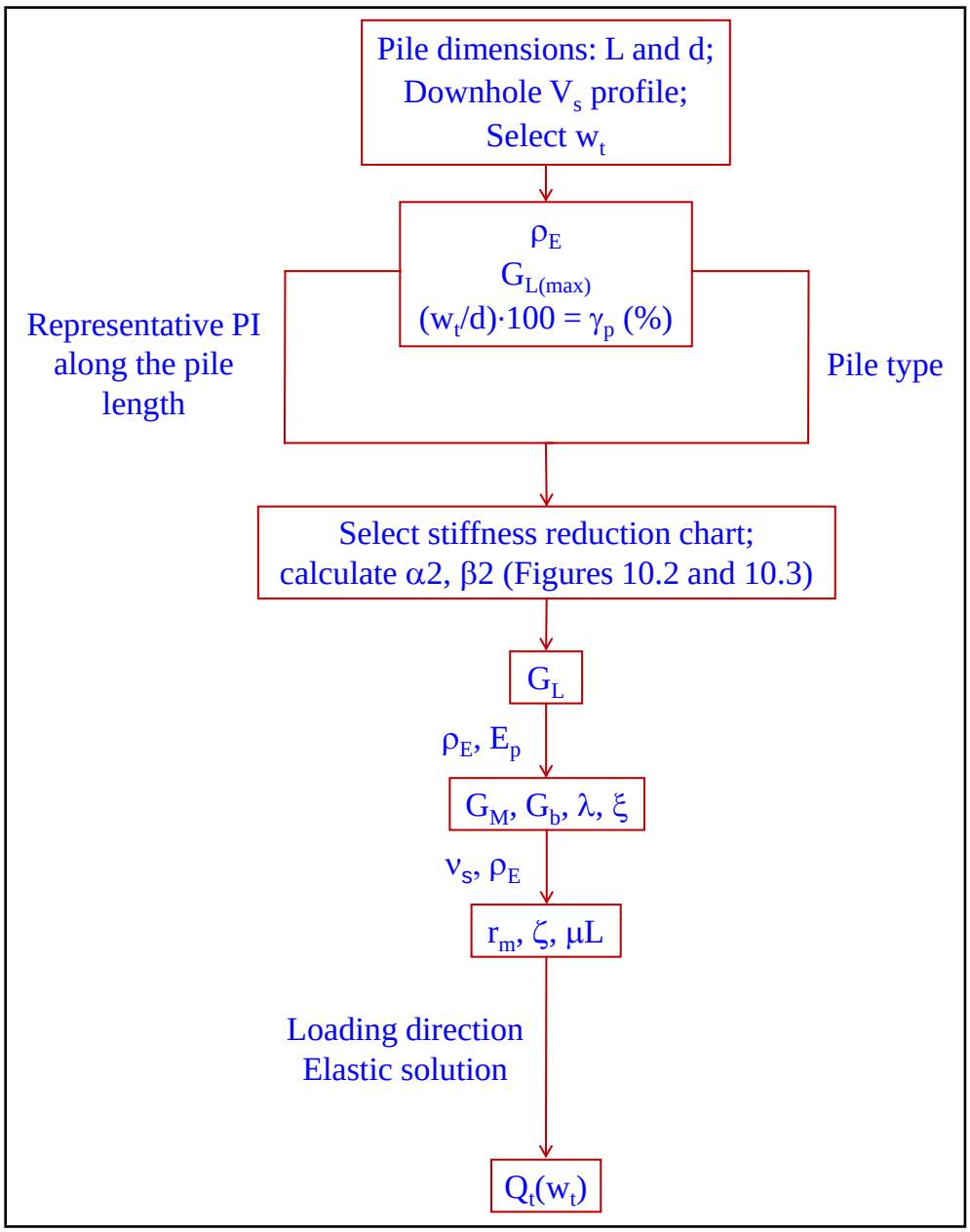

Figure 7.10. Flowchart detailing steps for estimating pairs of load-displacement values from the G/G_{max} vs. percent γ_p type design charts.

- From E_p and G_L, calculate the pile-soil stiffness ratio ($\lambda = E_p/G_L$).
- Calculate ξ factor ($= G_L/G_b$) in case of end-bearing pile.
- From the soil Poisson's ratio (ν_s) and modulus rate parameter (ρ_E), calculate the maximum radius of influence $\{r_m = L\,[0.25 + \xi\,(2.5\,\rho_E\,(1 - \nu_s) - 0.25)]\}$ and the measure of influence radius $[\zeta = \ln(r_m/r_o)]$, where r_o is the shaft radius. In case of

non-availability of ν_s information, use the previously noted assumptions: drained conditions for predominantly sandy soils ($\nu_s = 0.20$), and undrained conditions for predominantly clayey soil layers ($\nu_s = 0.50$).

- Calculate the measure of pile compressibility $\{\mu L = 2[2/(\zeta\lambda)]^{0.5} (L/d)\}$.
- Depending upon the direction of loading and soil type at the site, use the following equations for estimating the load (Q_t) for the selected w_t: Equation (7.3) for the cases of compression loading as well as tension loading in sands, and Equation (7.5) for tension loading in clays and silts.
- Select different values of expected w_t and estimate their corresponding Q_t using the methodology described above.
- Draw complete Q-w curve for the select pile and soil types.

From the details of this methodology, the solution seems to be relatively complicated. However, the solution presents a convenient set of equations that can be implemented into a spreadsheet with a minimal number of geotechnical input parameters (primarily soil stiffness profiles) to estimate the complete Q-w response of piles under axial compression and tension type of loadings.

7.9 Concluding Remarks

Sets of shear stiffness reduction curves are developed from the back-analysis of a dataset of pile load tests. Alternative functions formats are provided in terms of hyperbolic tangent expressions or exponential curves. These charts offer convenience in the axial Q-w analysis of different categories of pile foundation within the framework of elastic continuum solution by Randolph (2007), and Randolph and Wroth (1978; 1979). The charts also account for the plasticity characteristics of the soil deposit at the site. It is likely possible to further refine the methodology by including additional test results from different categories of pile types, by treating the sand sites separately, and further

analyzing these on the basis of relative density information, and/or other geotechnical site characteristics.

CHAPTER 8

ELASTIC CONTINUUM SOLUTION OF STACKED PILE MODEL FOR AXIAL LOAD-DISPLACEMENT ANALYSIS

Synopsis

The stiffness reduction curves presented in Chapter 7 for use in the elastic continuum solution were developed with the following underlying assumptions: (1) soil stiffness is linear with depth (although certain situations may portray a different trend), and (2) the back-analyzed field stiffnesses can be obtained keeping the operative modulus profile constant throughout the loading (even though shaft resistance is expected to be mobilized prior to the end bearing). In an effort to make some improvements with respect to these conditions, certain provisions of the elastic continuum solution are exploited to present a methodology for drawing the stiffness reduction curves as functions of depth. These curves are further utilized in modeling the pile as a stack of smaller segments embedded in multi-layered soils, where each layer is assigned its own distinctive averaged stiffness. The load-displacement analysis of all pile segments, associated with their adjacent soil layers, can thus be performed using the stiffness reduction curves applicable to their respective depths. The overall load-displacement response is obtained through integration of the analysis result of all layers. A flow chart is presented detailing steps for plotting the depth-dependent stiffness reduction curves. Similarly an illustrative figure is included showing the procedures for implementing the stacked pile model. Appendix J presents an example case study in which this model has been applied.

8.1 Introduction

In Chapter 7, a new scheme of shear modulus reduction curves [i.e., normalized shear modulus (G/G_{max}) vs. pseudo-strain ($\gamma_p = w_t/d$)] was presented for use in the non-

linear axial load-displacement (Q-w) analysis of pile foundations within an elastic continuum solution. These schemes were derived via back-analysis from pile load test data. The G and G_{max} values in this framework represent the operative and initial shear moduli, respectively, along the pile shaft at the reference elevation of full pile length (i.e., at depth z = L), while w_t and d are the top displacement and pile diameter, respectively. As such, the following vital and rationally acceptable assumptions were made in the back-analysis approach:

- The back-analyzed field stiffness can be obtained keeping the modulus variation factor (ρ_E) constant, where $\rho_E = G_M/G_L$; G_M = shear modulus at mid-depth of the pile (at z = L/2); and G_L = shear modulus at the full pile length (at z = L). It implies that moduli all along the shaft and that around the base decreases at the same rate. In actual field situations, the shaft resistance is expected to mobilize prior to the end bearing, leading to faster reduction of G in the upper layers than those near the base, thus manifesting the concept of progressive failure with depth.
- The soil stiffness is linear with depth. This assumption was adopted from the shear wave velocity (V_s) profiles of the sites in the database, which provided G_{max} readings. A predominant majority of the sites validated this assumption by presenting either linear or general Gibson types of soil profiles. However, it is expected that some special sites may portray different trends.

In the case of non-uniform or non-linear stiffness profiles of a multi-layered soil medium, it may be prudent to adopt a stacked pile model, where the pile is treated as separate segments of shorter piles stacked one above the other through different layers. In this case, the stiffness profiles of different layers of smaller thicknesses than the

overall pile length may suitably be assumed uniform, and their separate Q-w analyses performed, followed by their integration into the overall Q-w evaluations. On the other hand, the effects of progressive failure can be subsumed in this stacked pile model by making slight modifications to the modulus reduction schemes presented in Chapter 7. Such modifications are possible by adopting certain provisions of the original elastic continuum model by Randolph and Wroth (1978; 1979).

The aim of this chapter is to present a stacked pile model for evaluating the axial pile Q-w as a function of depth within multi-layered soil media.

8.2 Review of Elastic Continuum Solution for Pile Load Displacement Response

The basic formulation of analytical elastic continuum closed-form solution by Randolph and Wroth (1978; 1979) was summarily presented in Chapter 4. This solution, reproduced in Equation (8.1), was developed for piles embedded in a linear elastic two-layered soil model with the boundary lying at the pile base (see Figure 8.1a, where explanation of various terms is also given).

$$w_t = \frac{Q_t\left[1+\frac{4\eta\ \tanh(\mu L)L}{\pi\lambda(1-\upsilon_S)\xi\ (\mu L)\ r_o}\right]}{G_L\ r_o\left[\frac{4\eta}{(1-\upsilon_S)\xi}+\frac{2\pi\rho_E\tanh(\mu L)L}{\zeta\ (\mu L)\ r_o}\right]} \tag{8.1}$$

The top displacement (w_t) may be obtained for an applicable value of the applied top load (Q_t) by utilizing a suitable shear modulus reduction scheme, such as the one presented in Chapter 7. Here, the displacement field of soil around the pile shaft has been modeled via shearing of infinite concentric cylinders of differentially increasing radii with maximum influence radius modeled as shown in Figure 8.1b. This follows from the important observations noted by Cooke (1974), Cook et al. (1979), and Frank (1975) that the load transferred to the adjacent soil through shearing stresses mobilized along the pile shaft extends radially beyond the close proximity of the pile, and that there exists some

magical radius (r_m) around the pile at which these stresses become negligible. Randolph and Wroth (1978; 1979) noted that within this radial distance, the shear stresses and the resulting displacements decrease logarithmically with increasing distance from the pile shaft surface.

As the load transferred to the pile shaft diminishes with depth, so do the shearing stresses, influence radii, axial displacements, and their corresponding reductions in the operative shear stiffness. The shape of the r_m profile, thus hypothesized, is attributable to the horizontal and vertical inhomogeneity of shearing stresses explained by the following: (1) fundamental conjecture that the soil stiffness generally increases with depth describing greater resistance to shearing deformations in deeper layers, and (2) the load applied from the pile top diminishes with depth leaving lesser loads to shear the stiffer soils adjacent to the pile shaft in deeper layers. Also shown in Figure 8.1b is the profile of operative shear stiffness (G) [on qualitative shear stress (τ) vs. shear strain (γ) plots] as function of depth along the pile shaft. Accordingly, the reduction of operative shear stiffness (G) varies inversely with depth (z) below the ground surface.

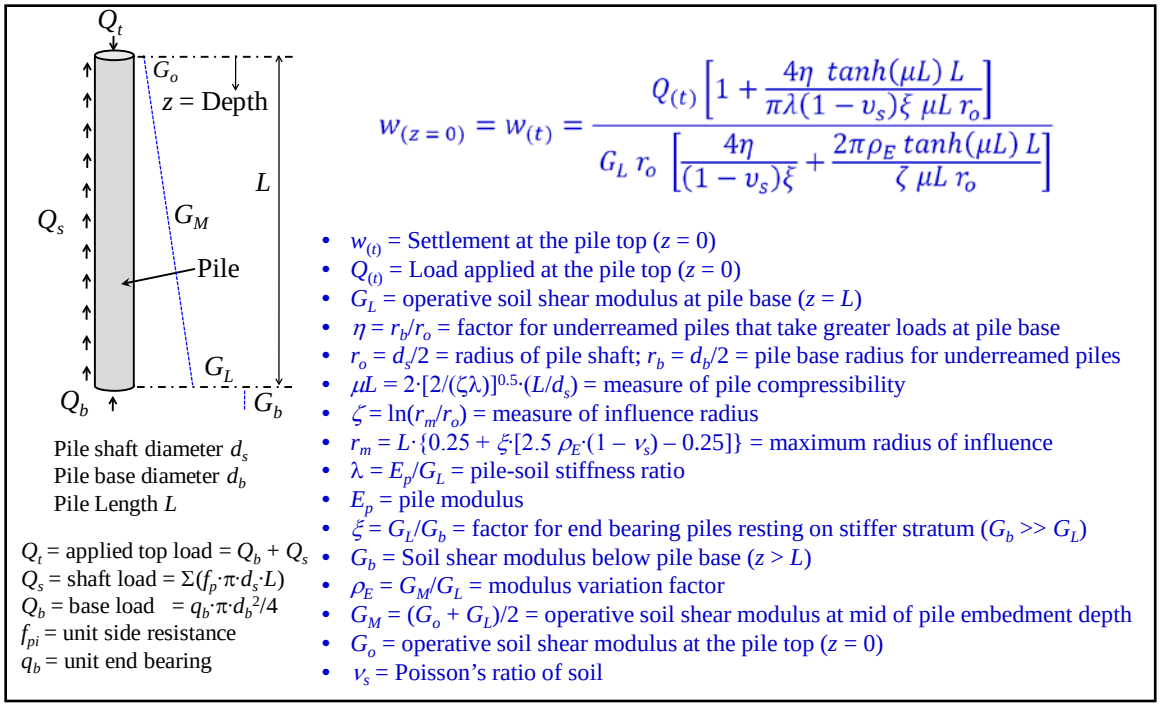

(a)

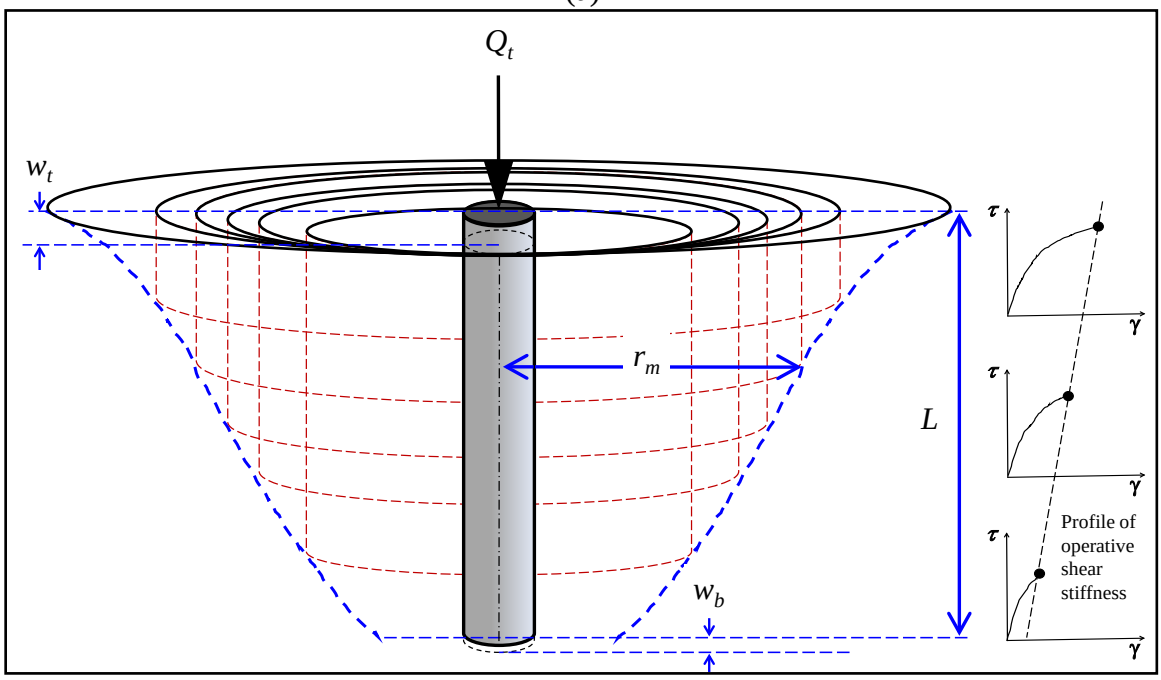

(b)

Figure 8.1. Elastic continuum model for axial pile displacements analysis in a linear elastic two layered soil model (after Randolph and Wroth, 1978; 1979): (a) Randolph pile model of axial pile load-displacement relationship, and (b) displacement field model and profile of maximum influence radius.

8.3 Extension of Elastic Continuum Solution to Stacked Pile in Multi-Layered Soils

8.3.1 Shear Modulus Reduction Curves for Progressive Load Transfer as Function of Depth

Implicit and inherent in the elastic continuum solution are certain provisions whereby it may be employed for predicting the displacements as a function of depth (z) below the ground surface. Accordingly, as shown in Equation (8.2), the term L, which represents the total embedded length of the pile may be replaced with (L – z). Furthermore, Equations (8.3) and (8.4) can be used to calculate the base load (Q_b) corresponding to the top load (Q_t) and base displacement (w_b) corresponding to the top displacement (w_t), respectively. Subsequent to obtaining this set of Q_b vs. w_b, Equations (8.3) and (8.4) can be inverted to the form shown in Equations (8.5) and (8.6) to find the set of load and displacement at any selected depth z [i.e., $Q_{(z)}$ and $w_{(z)}$, respectively] for the same set of top load (Q_t) and top displacement (w_t). Again, all L terms should be replaced with (L – z), as shown in Equations (8.5) and (8.6).

$$w_{(z)} = \frac{Q_{(z)}\left[1+\frac{4\eta\ \tanh[\mu(L-z)](L-z)}{\pi\lambda(1-\upsilon_S)\xi\,[\mu(L-z)]\,r_o}\right]}{G_{L(z)}\,r_o\left[\frac{4\eta}{(1-\upsilon_S)\xi}+\frac{2\pi\rho_E\tanh[\mu(L-z)](L-z)}{\zeta\,[\mu(L-z)]\,r_o}\right]} \tag{8.2}$$

$$\frac{Q_b}{Q_t} = \frac{\left[\frac{4\eta}{(1-\upsilon_S)\xi\cosh(\mu L)}\right]}{\left[\frac{4\eta}{(1-\upsilon_S)\xi}+\frac{2\pi\rho_E\tanh(\mu L)L}{\zeta\,(\mu L)\,r_o}\right]} \tag{8.3}$$

$$\frac{w_b}{w_t} = \frac{1}{\cosh(\mu L)} \tag{8.4}$$

$$Q_{(z)} = \frac{Q_b\left[\frac{4\eta}{(1-\upsilon_S)\xi} + \frac{2\pi\rho_E \tanh[\mu(L-z)](L-z)}{\zeta\,[\mu(L-z)]\,r_O}\right]}{\left[\frac{4\eta}{(1-\upsilon_S)\xi\cosh[\mu(L-z)]}\right]} \tag{8.5}$$

$$w_{(z)} = w_b \cosh[\mu(L-z)] \tag{8.6}$$

where $w_{(z)}$ = pile total displacement at depth z below the top of pile's embedded length; $Q_{(z)}$ = portion of applied top load (Q_t) transferred at depth z corresponding to $w_{(z)}$; η = r_b/r_o = eta factor for underreamed piles; $r_o = d_s/2$ = pile shaft radius; $r_b = d_b/2$ = pile base radius for underreamed piles; $\mu(L - z) = [2/(\zeta\lambda)]^{0.5}\cdot[(L - z)/r_o]$ = measure of pile compressibility for the pile shaft segment between depth z and z = L; $\zeta = \ln(r_m/r_o)$ = measure of average radius of influence in the surrounding soil mass affected by shearing stresses (i.e., the displacement field) around the pile; $r_m = (L - z)\cdot\{0.25 + \xi\cdot[2.5\ \rho_E\cdot(1 - \nu_s) - 0.25]\}$ = average maximum influence radius along the embedded length of the pile [at this radius the shear stresses become negligible]; $\lambda = E_p/G_L$ = pile-to-soil stiffness ratio; E_p = pile modulus; G_L = operative soil shear modulus at pile base (z = L); $\xi = G_L/G_b$ = factor for end bearing piles resting on stiffer stratum (where $G_b > G_L$); G_b = soil shear modulus below pile base (for z > L); $\rho_E = G_{M(z)}/G_L$ = modulus variation factor (between selected depth z and at the pile base, where z = L); $G_{M(z)} = [G_{(z)} + G_L]/2$ = operative soil shear modulus at mid of the pile length under consideration (between selected depth z and z = L); $G_{(z)}$ = operative soil shear modulus at depth z (at pile top, where z = 0, $G_{(z)} = G_o$); ν_s = Poisson's ratio of soil; w_b = pile base displacement at depth z = L.

By using Equations (8.5) and (8.6), sets of loads [$Q_{(z)}$] and displacements [$w_{(z)}$] can be calculated for selected depths (z) below the ground surface for a specific applied top load Q_t. This exercise can be done for different applicable values of top loads. These

sets can be further used to draw their respective shear stiffness reduction curves for selected depths from the back-analysis scheme presented in Chapter 7.

As a case illustration, this methodology was applied to a driven pile of length, L = 30.0 m, and diameter, d = 0.5 m. Sets of top loads (Q_t) vs. top displacements (w_t) were obtained using the modulus reduction algorithm for driven piles from Chapter 7, which is reproduced in Equation (8.7) below:

$$\frac{G}{G_{max}} = \frac{1}{1+3.042\left[\gamma_p(\%)\right]^{1.006}} \tag{8.7}$$

The soil modulus variation factor (ρ_E) was selected over a wide range, with a value $\rho_E = 0.5$ corresponding to a pure Gibson soil stiffness profile (linear with depth), up to a value $\rho_E = 1.0$, representing a constant soil stiffness profile with depth (i.e., homogeneous case). Simplified steps are presented in a flow chart shown in Figure 8.2, which enabled plotting of stiffness reduction curves corresponding to five levels of depth: z = 0 (at the pile top), z = 0.25 L, z = 0.50 L (at pile mid depth), z = 0.75 L, and z = 1.00 L (at the pile tip) for different values of ρ_E. These plots are shown in Figure 8.3. It may be noted that the thick curve with triangular markers representing soil modulus reduction near the ground surface, which is common in all 6 parts of Figure 8.3, was obtained from Equation (8.7). The remaining curves were drawn for different depths by following the steps shown in the flow chart. These curves clearly display the effect of progressive failure with depth and the influence of soil stiffness profile. Such curves can be drawn for any pile type and configuration, and for any soil profile. Subsequently, these curves can be used in a stacked pile model, which will be discussed in the following section.

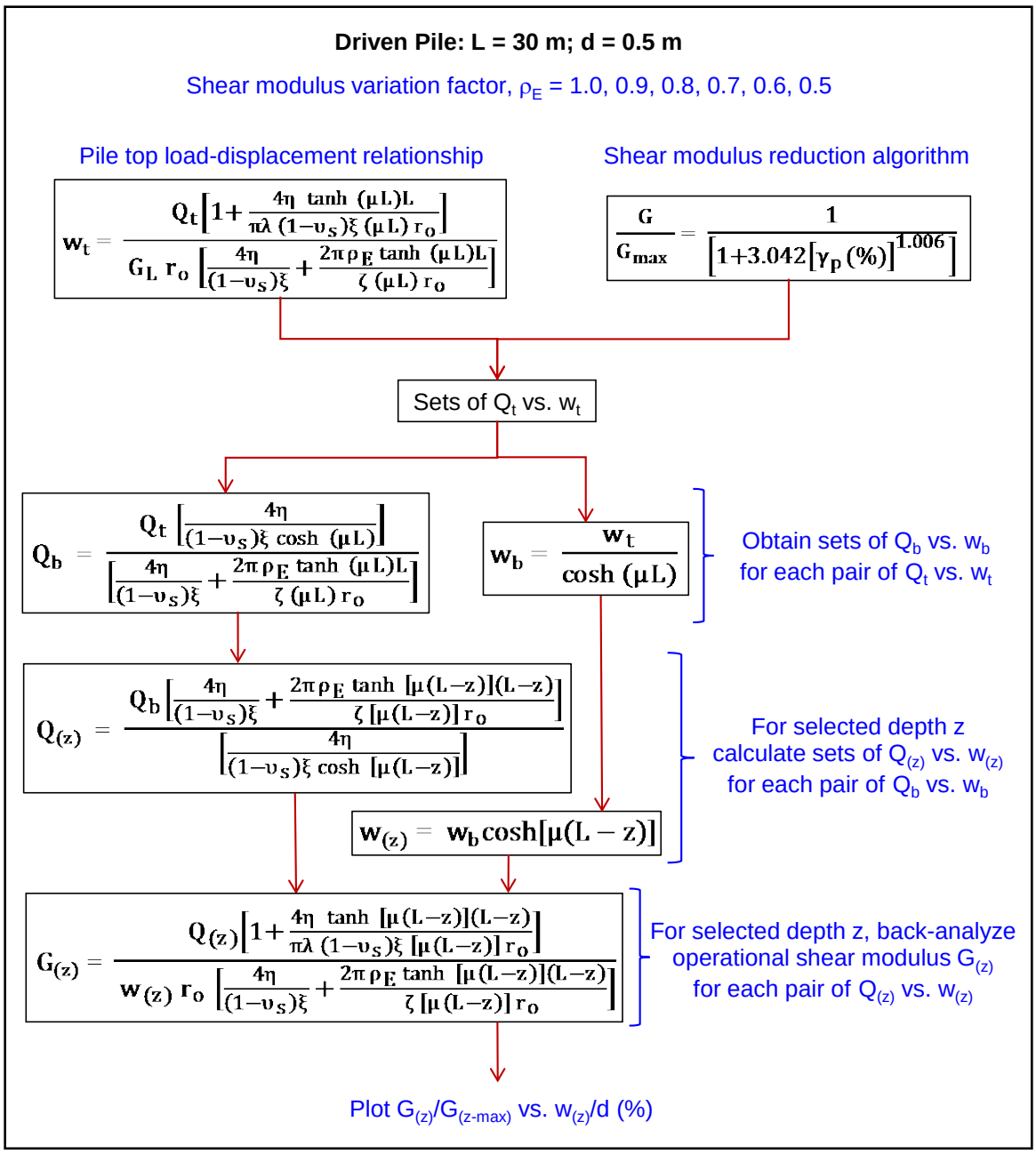

Figure 8.2. Flow chart showing example steps for plotting shear modulus reduction curves for selected depths using solution for compressible stacked pile model.

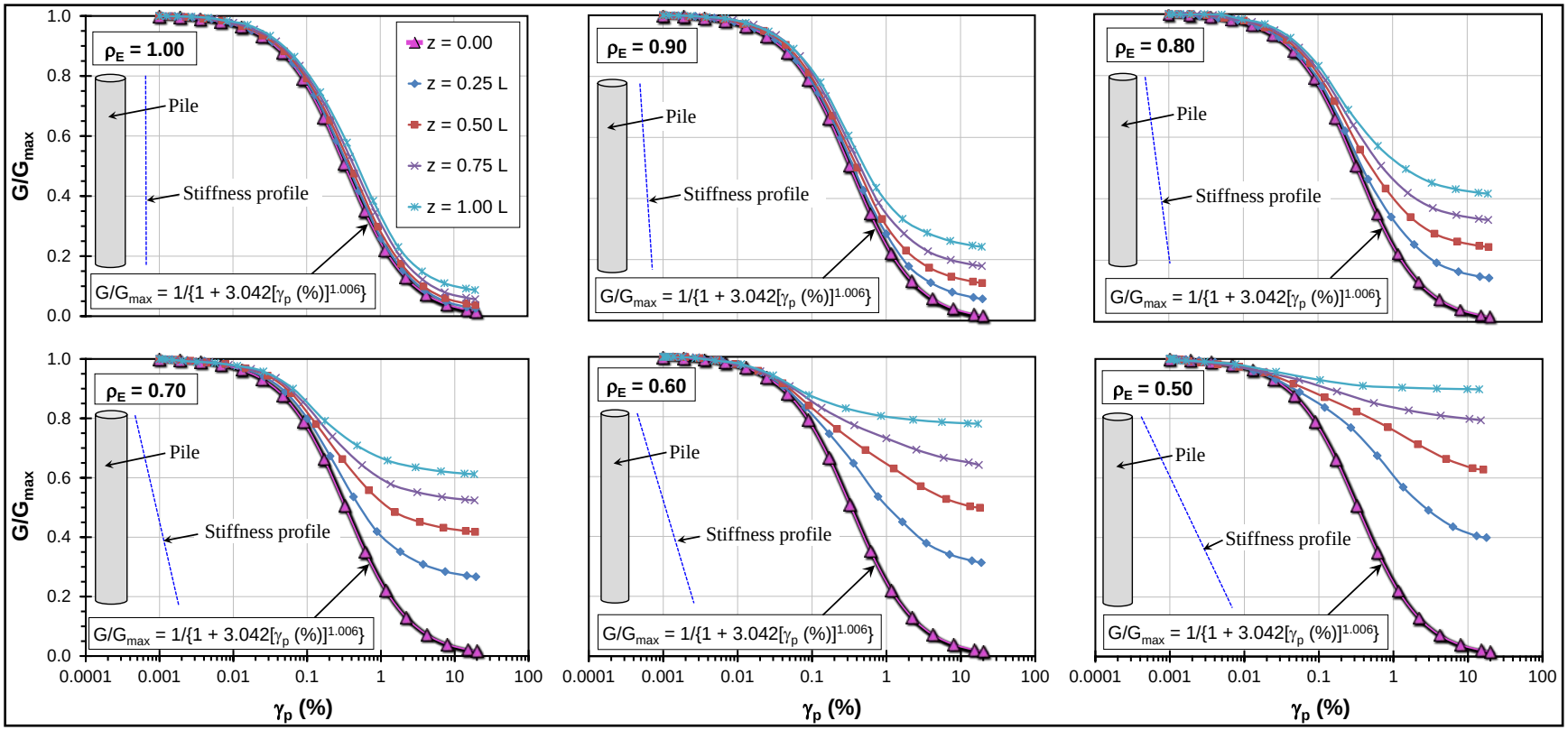

Figure 8.3. Illustration of shear modulus reduction curves as function of depth and soil stiffness variation profile.

8.3.2 Load Displacement Analysis of Stacked Pile Model in a Multi-layered Soil Medium

The basic form of elastic continuum solution, presented in Equation (8.1), works reasonably well for sites where the soil stiffness profile can be idealized as linear or general Gibson type. However, it is expected that certain sites may portray different trends of stiffness variation. For such situations, the pile may be modeled as a stack of shorter pile segments embedded through distinct multilayered soil media, with each layer having its own characteristic averaged stiffness value. As detailed previously, the tendency of stiffness reduction due to progressive failure can be quantified via slight adaptations in the basic solution to obtain stiffness reduction curves as function of depth. These trends can also be integrated into the solution of stacked pile model. In implementing such model, following vital assumptions are applicable:

- The number of layers is chosen on the basis of the measured stiffness profile of the soil, whereby each layer may be assigned its distinct mean modulus value. Thus, a constant stiffness profile is adopted for each layer.
- The component of the applied top load (Q_t) reaching the bottom of the uppermost segments is taken as the base load for this segment (i.e., Q_{b1}). This is calculated using Equation (8.3), and acts as the top load for the next segment below (i.e., Q_{t2}). This applies to all subsequent layers (e.g., $Q_{b1} = Q_{t2}$, $Q_{b2} = Q_{t3}$, and so on).
- A similar approach is applied in calculating the ξ factor as the ratio of soil stiffness at the base of each segment. It implies that the mean stiffness value of the second soil layer is taken as the soil stiffness beneath the base of the top most segment, and the same applies to each of the subsequent segments and layers (i.e., $G_{b1} = G_2$, $G_{b2} = G_3$, and so on).
- The total displacement at the top of each segment is the cumulative displacement of all segments below it (e.g., for a three layered stacked pile model, the total

displacement at the pile top = $w_{t1} + w_{t2} + w_{t3}$, the total displacement at the top of second segment = $w_{t2} + w_{t3}$, and the displacement at the top of third and lower most segment = w_{t3}).

- The pile length used in calculating the averaged maximum radius of influence of each segment is the pile distance between the top of that segment and the pile base (i.e., for a three layered stacked pile model, for the top most segment: use distance $L_1 + L_2 + L_3$, for the middle segment: use distance $L_2 + L_3$, and for the lower most segment: use distance L_3 only).
- The applicable values of operative soil stiffness for each layer and for each applicable load can be calculated from the scheme summarily presented in Figures 8.2 and 8.3.

8.3.3 Application of the Proposed Solution

For purposes of illustration, a four-layer stacked pile model is offered in Figure 8.4, where applicable equations of the solution are also presented, along with explanations of the relevant terms for each layer. This solution is slightly more involved compared to its basic form. However, it can be conveniently implemented in a spreadsheet, besides the fact it is much less laborious than alternative methods [e.g., Winkler springs support model by Mylonakis (2001), rigorous numerical solutions based on advanced constitutive models of soil behavior proposed by Jardine et al. (1986), and the product of polynomial and series expansions of displacement shape functions in vertical and radial directions of infinite layer approach by Guo et al. (1987)].

The stacked pile model was applied to a load test case study of a cast in-situ bored pile in glacial till near the Grimsby research site located at Waltham, UK, where a seismic piezocone test (SCPTu) sounding was also available. The penetrometer readings of tip resistance (q_t), sleeve friction (f_s), and porewater pressure (u_2) were used in the pile capacity evaluation part, while the G_{max} profile from the shear wave velocity (V_s)

readings were utilized in the proposed stacked pile model for the axial load-displacement analysis. This case study was published as a technical paper in the 2nd International Symposium on Cone Penetration Testing (CPT'10) (Niazi et al., 2010) and included in Appendix J.

8.3.4 Solution for Rigid Piles

A simplified version of the analytical elastic solution for a stacked pile model in the case of rigid driven piles in four-layer soil media is summarized in Figures 8.5 and 8.6. This solution can also be applied to other categories of rigid piles (bored, augered, and jacked) by using their applicable stiffness reduction algorithms (such as those presented in Chapter 7). The applicable expressions of the closed-form solution for rigid piles were presented in Chapter 4, and are reproduced below:

$$w_t = \frac{Q_t}{G_L\, r_o \left[\frac{4\eta}{(1-\upsilon_s)\xi} + \frac{2\pi\rho_E\, L}{\zeta\, r_o}\right]} \tag{8.8}$$

$$Q_b = \frac{Q_t}{\left[1 + \frac{\pi\rho_E(1-\upsilon_s)\xi\, L}{2\,\zeta\,\eta\, r_o}\right]} \tag{8.9}$$

$$w_b = w_t \tag{8.10}$$

$$Q_{(z)} = Q_b\left[1 + \frac{\pi\rho_E(1-\upsilon_s)\xi\,(L-z)}{2\,\zeta\,\eta\, r_o}\right] \tag{8.11}$$

$$G_{(z)} = \frac{Q_{(z)}}{w_{(z)}\, r_o \left[\frac{4\eta}{(1-\upsilon_S)\xi} + \frac{2\pi\rho_E\,(L-z)}{\zeta\, r_o}\right]} \tag{8.12}$$

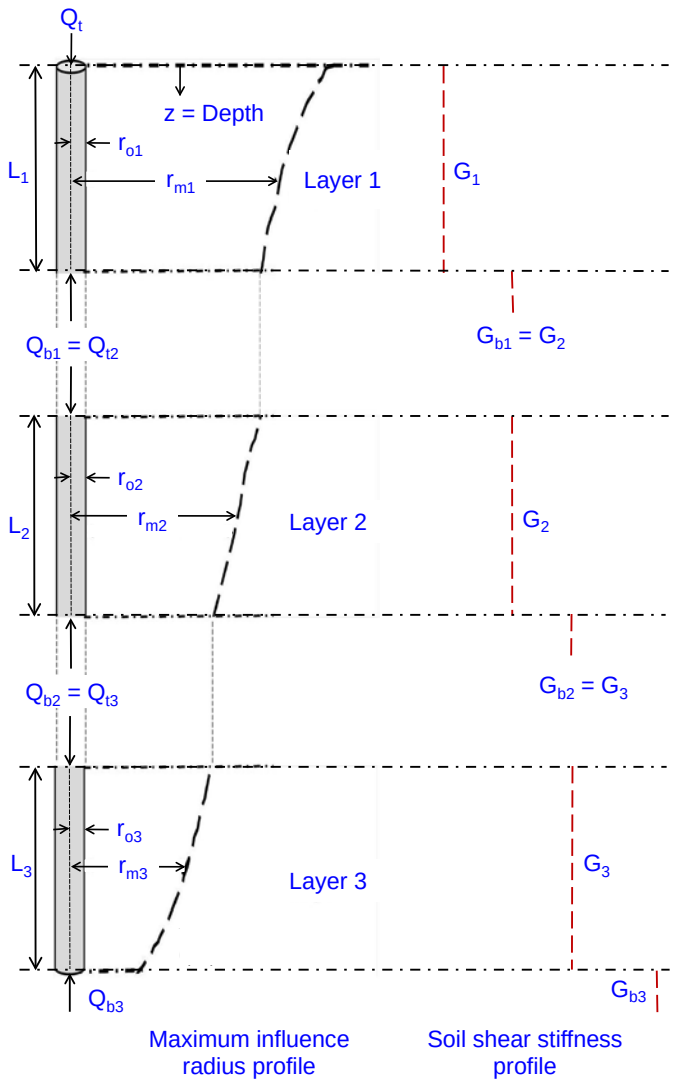

Solution for layer 1

$$w_t = \frac{Q_t\left[1 + \frac{4\eta_1 \tanh(\mu L_1) L_1}{\pi\lambda_1(1-\upsilon_{s1})\xi_1 (\mu L_1) r_{o1}}\right]}{G_1 r_{o1}\left[\frac{4\eta_1}{(1-\upsilon_{s1})\xi_1} + \frac{2\pi\rho_{E1}\tanh(\mu L_1) L_1}{\zeta_1 (\mu L_1) r_{o1}}\right]} + w_{t2}$$

$$\frac{Q_{b1}}{Q_t} = \frac{\left[\frac{4\eta_1}{(1-\upsilon_{s1})\xi_1 \cosh(\mu L_1)}\right]}{\left[\frac{4\eta_1}{(1-\upsilon_{s1})\xi_1} + \frac{2\pi\rho_{E1}\tanh(\mu L_1) L_1}{\zeta_1 (\mu L_1) r_{o1}}\right]}$$

- w_t = cumulative settlement at the pile top
- $\eta_1 = r_{o2}/r_{o1}$
- $\mu L_1 = [2/(\zeta_1\lambda_1)]^{0.5}\cdot(L_1/r_{o1})$
- $\zeta_1 = \ln(r_{m1}/r_{o1})$
- $r_{m1} = (L_1 + L_2 + L_3)\cdot\{0.25 + \xi_1\cdot[2.5\,\rho_{E1}\cdot(1-\nu_{s1}) - 0.25]\}$
- $\lambda_1 = E_p/G_1$
- $\xi_1 = G_{L1}/G_{b1}$
- $G_{b1} = G_2$
- $\rho_{E1} = 1$
- $G_{M1} = G_{o1} = G_{L1} = G_1$
- ν_{s1} = Poisson's ratio of soil in layer 1
- $Q_{b1} = Q_{t2}$

Solution for layer 2

$$w_{t2} = \frac{Q_{t2}\left[1 + \frac{4\eta_2 \tanh(\mu L_2) L_2}{\pi\lambda_2(1-\upsilon_{s2})\xi_2 (\mu L_2) r_{o2}}\right]}{G_2 r_{o2}\left[\frac{4\eta_2}{(1-\upsilon_{s2})\xi_2} + \frac{2\pi\rho_{E2}\tanh(\mu L_2) L_2}{\zeta_2 (\mu L_2) r_{o2}}\right]} + w_{t3}$$

$$\frac{Q_{b2}}{Q_{t2}} = \frac{\left[\frac{4\eta_2}{(1-\upsilon_{s2})\xi_2 \cosh(\mu L_2)}\right]}{\left[\frac{4\eta_2}{(1-\upsilon_{s2})\xi_2} + \frac{2\pi\rho_{E2}\tanh(\mu L_2) L_2}{\zeta_2 (\mu L_2) r_{o2}}\right]}$$

- w_{t2} = cumulative settlement at the top of layer 2
- $\eta_2 = r_{o3}/r_{o2}$
- $\mu L_2 = [2/(\zeta_2\lambda_2)]^{0.5}\cdot(L_2/r_{o2})$
- $\zeta_2 = \ln(r_{m2}/r_{o2})$
- $r_{m2} = (L_2 + L_3)\cdot\{0.25 + \xi_2\cdot[2.5\,\rho_{E2}\cdot(1-\nu_{s2}) - 0.25]\}$
- $\lambda_2 = E_p/G_2$
- $\xi_2 = G_{L2}/G_{b2}$
- $G_{b2} = G_3$
- $\rho_{E2} = 1$
- $G_{M2} = G_{o2} = G_{L2} = G_2$
- ν_{s2} = Poisson's ratio of soil in layer 2
- $Q_{b2} = Q_{t3}$

Solution for layer 3

$$w_{t3} = \frac{Q_{t3}\left[1 + \frac{4\eta_3 \tanh(\mu L_3) L_3}{\pi\lambda_3(1-\upsilon_{s3})\xi_3 (\mu L_3) r_{o3}}\right]}{G_3 r_{o3}\left[\frac{4\eta_3}{(1-\upsilon_{s3})\xi_3} + \frac{2\pi\rho_{E3}\tanh(\mu L_3) L_3}{\zeta_3 (\mu L_3) r_{o3}}\right]}$$

$$\frac{Q_{b3}}{Q_{t3}} = \frac{\left[\frac{4\eta_3}{(1-\upsilon_{s3})\xi_3 \cosh(\mu L_3)}\right]}{\left[\frac{4\eta_3}{(1-\upsilon_{s3})\xi_3} + \frac{2\pi\rho_{E3}\tanh(\mu L_3) L_3}{\zeta_3 (\mu L_3) r_{o3}}\right]}$$

$$w_{b3} = \frac{w_{t3}}{\cosh(\mu L_3)}$$

- w_{t3} = settlement at the top of layer 3
- $\eta_3 = r_b/r_{o3}$
- $\mu L_3 = [2/(\zeta_3\lambda_3)]^{0.5}\cdot(L_3/r_{o3})$
- $\zeta_3 = \ln(r_{m3}/r_{o3})$
- $r_{m3} = L_3\cdot\{0.25 + \xi_3\cdot[2.5\,\rho_{E3}\cdot(1-\nu_{s3}) - 0.25]\}$
- $\lambda_3 = E_p/G_3$
- $\xi_3 = G_{L3}/G_{b3}$
- G_{b3} = shear stiffness beneath pile base
- $\rho_{E3} = 1$
- $G_{M3} = G_{o3} = G_{L3} = G_3$
- ν_{s3} = Poisson's ratio of soil in layer 3
- w_{b3} = displacement at the pile base

Figure 8.4. Analytical elastic continuum solution for compressible stacked pile model in four-layer soil media.

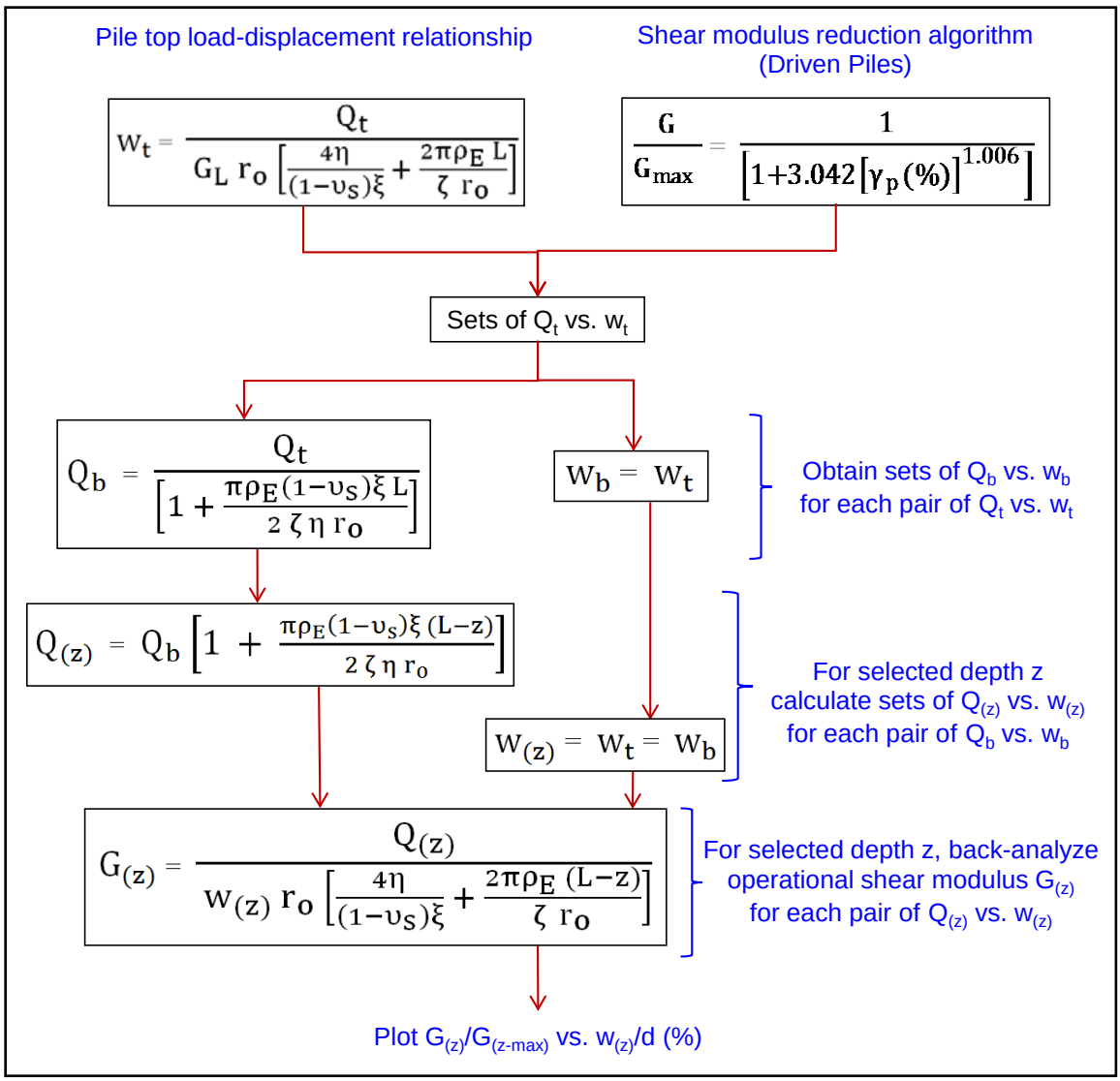

Figure 8.5. Flow chart showing example steps for plotting shear modulus reduction curves for selected depths using solution for rigid stacked pile model.

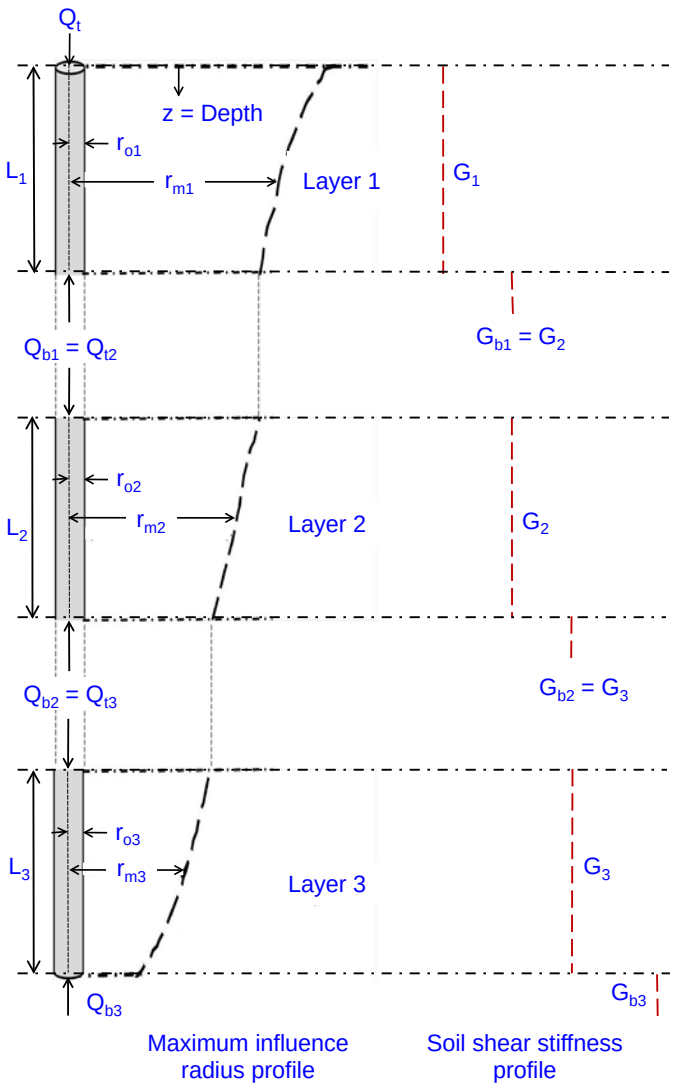

Solution for layer 1

$$w_t = \frac{Q_t}{G_1 r_{o1}\left[\frac{4\eta_1}{(1-\upsilon_{S1})\xi_1} + \frac{2\pi\rho_{E1} L_1}{\zeta_1 r_{o1}}\right]} = w_{t2} \qquad \frac{Q_{b1}}{Q_t} = \frac{1}{\left[1 + \frac{\pi\rho_{E1}(1-\upsilon_{S1})\xi_1 L_1}{2\zeta_1 \eta_1 r_{o1}}\right]}$$

- w_t = cumulative settlement at the pile top
- $\eta_1 = r_{o2}/r_{o1}$
- $\zeta_1 = \ln(r_{m1}/r_{o1})$
- $r_{m1} = (L_1 + L_2 + L_3)\cdot\{0.25 + \xi_1\cdot[2.5\,\rho_{E1}\cdot(1 - \nu_{s1}) - 0.25]\}$
- $\xi_1 = G_{L1}/G_{b1}$
- $G_{b1} = G_2$
- $\rho_{E1} = 1$
- $G_{M1} = G_{o1} = G_{L1} = G_1$
- ν_{s1} = Poisson's ratio of soil in layer 1
- $Q_{b1} = Q_{t2}$

Solution for layer 2

$$w_{t2} = \frac{Q_{t2}}{G_2 r_{o2}\left[\frac{4\eta_2}{(1-\upsilon_{S2})\xi_2} + \frac{2\pi\rho_{E2} L_2}{\zeta_2 r_{o2}}\right]} = w_{t3} \qquad \frac{Q_{b2}}{Q_{t2}} = \frac{1}{\left[1 + \frac{\pi\rho_{E2}(1-\upsilon_{S2})\xi_2 L_2}{2\zeta_2 \eta_2 r_{o2}}\right]}$$

- w_{t2} = cumulative settlement at the top of layer 2
- $\eta_2 = r_{o3}/r_{o2}$
- $\zeta_2 = \ln(r_{m2}/r_{o2})$
- $r_{m2} = (L_2 + L_3)\cdot\{0.25 + \xi_2\cdot[2.5\,\rho_{E2}\cdot(1 - \nu_{s2}) - 0.25]\}$
- $\xi_2 = G_{L2}/G_{b2}$
- $G_{b2} = G_3$
- $\rho_{E2} = 1$
- $G_{M2} = G_{o2} = G_{L2} = G_2$
- ν_{s2} = Poisson's ratio of soil in layer 2
- $Q_{b2} = Q_{t3}$

Solution for layer 3

$$w_{t3} = \frac{Q_{t3}}{G_3 r_{o3}\left[\frac{4\eta_3}{(1-\upsilon_{S3})\xi_3} + \frac{2\pi\rho_{E3} L_3}{\zeta_3 r_{o3}}\right]} \qquad \frac{Q_{b3}}{Q_{t3}} = \frac{1}{\left[1 + \frac{\pi\rho_{E3}(1-\upsilon_{S3})\xi_3 L_3}{2\zeta_3 \eta_3 r_{o3}}\right]}$$

$$w_{b3} = w_{t3} = w_{t2} = w_t$$

- w_{t3} = settlement at the top of layer 3
- $\eta_3 = r_b/r_{o3}$
- $\zeta_3 = \ln(r_{m3}/r_{o3})$
- $r_{m3} = L_3\cdot\{0.25 + \xi_3\cdot[2.5\,\rho_{E3}\cdot(1 - \nu_{s3}) - 0.25]\}$
- $\xi_3 = G_{L3}/G_{b3}$
- G_{b3} = shear stiffness beneath pile base
- $\rho_{E3} = 1$
- $G_{M3} = G_{o3} = G_{L3} = G_3$
- ν_{s3} = Poisson's ratio of soil in layer 3
- w_{b3} = displacement at the pile base

Figure 8.6. Analytical elastic continuum solution for rigid stacked pile model in four-layer soil media.

8.4 Concluding Remarks

A stacked pile model for load-displacement analysis is presented in which certain adaptations are proposed in the elastic continuum solution. These adaptations enable plotting of separate modulus reduction curves (G/G_{max} vs. w/d) as function of depth for each layer, and treating pile as a stack of smaller pile segments embedded in a multi-layered soil medium, where the mean operative stiffness of each layer is adopted. The solution can be used to address the question of progressive failure with depth in a multi-layer soil medium that exhibits nonlinear soil stiffness response.

CHAPTER 9

AXIAL PILE RESPONSE OF O-CELL LOADING FROM MODIFIED ELASTIC SOLUTION AND SHEAR WAVE VELOCITY

Synopsis

The Osterberg cell (O-cell) type of bidirectional pile load testing is a modern full-scale proofing method in the realm of performance-based pile design. It is done at considerable cost, not possible on small to medium size projects, but allows load testing of large drilled shaft foundations to high capacities and requires a minimal footprint for setup. An efficient approach of utilizing the Randolph-type of closed-form analytical elastic solution was previously adopted for evaluating the static pile response from unidirectional top-down axial compression and tension loading. In order to extend this elastic solution to O-cell loadings, the following adaptations are warranted: (1) appropriate modifications to handle the loadings in two directions, and (2) development of non-linear stiffness reduction model, derived from the back-analysis of O-cell pile load tests. Accordingly, a modified analytical solution is presented for the two most common cases of O-cell loading arrangements.

Using these modified sets of solutions and a well-documented database of O-cell load tests on drilled shaft foundations (i.e., Group 3 dataset), stiffness reduction models have been developed. The fundamental shear stiffness modulus (G_{max}) profiles obtained from the shear wave velocity (V_s) readings of the hybrid geophysical-geotechnical seismic piezocone tests (SCPTu), together with the re-arranged modified solution were applied to the axial loads vs. displacements (Q-w) from the database of load tests to back-figure the applicable operational shear stiffness (G) values. Additional sensitivity analyses indicate that pile geometry and soil stiffness profile are the two most significant

factors affecting the outcome of this solution. A comprehensive set of step-by-step example calculations is included to explain the procedure for implementing the new set of solutions.

9.1 Introduction to the Osterberg Cell

The response of pile foundations to top-down axial compression (C) or top-applied axial tension (T) loading is typically described in terms of: (1) the total load applied at the pile top (Q_t), (2) the components of load Q_t transferred to the pile shaft (Q_s) and to the pile base (Q_b), and (3) the magnitudes of pile displacements for different stages of loading, traditionally represented in terms of the load-displacement (Q-w) curves. Depending upon the stiffness properties of pile material, the total axial displacements may also include a component of pile compression or extension. This component can be gaged from the total top displacements corresponding to total, shaft, and base loads (Q_t-w_t, Q_s-w_t, and Q_b-w_t, respectively), and base displacements corresponding to base loads (Q_b-w_b). The geotechnical design of pile foundations is established on the estimates of these responses to anticipated loadings in the soil profile found at any particular site.

It was shown in Chapter 1 that the soil properties obtained from site investigations can be used in one or more of the different interpretive schemes to evaluate the static axial pile response, besides highlighting the importance and reliability of physical load testing. It was also pointed out that other methods can be calibrated against the data obtained from these load tests for improved future predictive performance. Such an approach was adopted in Chapter 7 for the C and T loading cases, where the elastic closed-form solution by Randolph and Wroth (1978; 1979) was used in the back-analysis of soil stiffness reduction trends for different pile and soil types.

The bi-directional Osterberg cell or O-cell type of static axial loading system is a newer, yet now well-established and futuristic pile testing arrangement, which is

frequently being integrated into the performance-based design. As detailed in Chapter 2, the Q-w response from the O-cell system is different than the C and T types of loading. From this perspective, a need was identified for modification of the elastic solution specific to O-cell type of axial loading, both for the back-analysis of stiffness reduction trends, as well as for future predictions of the pile Q-w response.

A point of relevance concerns the use of term 'displacement' instead of 'settlement' throughout this chapter. Displacement has been preferred owing to the fact that the bi-directional axial loadings involved in O-cell tests result in both upward and downward movements of different segment of the pile shaft. The specific details of different cases of such arrangements were discussed in Chapter 2 and presented in Appendix B, while those of certain selected cases will be revisited in the subsequent sections of this chapter.

This chapter presents the details and results of an effort to develop a hybrid empirical-analytical solution for evaluating the pile Q-w response from O-cell loading. By utilizing the shear wave velocity (V_s) measurements from SCPTu tests taken at the O-cell load test sites of Group 3 dataset, and the calibration efforts via back-analysis of the load test data, new modulus reduction schemes are developed. The geophysical V_s component enables determination of the fundamental shear modulus: $G_{max} = \rho_T \cdot V_s^2$, where ρ_T = soil mass density = γ_T/g; γ_T being the soil total unit weight and g the gravitational acceleration = 9.81 m/s^2. Therefore, G_{max} has been formally integrated into the analytical solution to predict the complete O-cell Q-w response. The penetrometer readings (q_t, f_s and u_2) of the SCPTu soundings at these sites were input for assessment of the pile capacity components (side and base), presented in Chapter 6.

9.2 Bi-directional O-cell loading system

In contrast to the conventional C and T types of axial loadings that are applied in dead-weight systems and anchored reaction frame setups, the O-cell is a high-capacity hydraulic jacking device that is positioned either at the foundation base, or at midsection

elevations within the pile shaft. The O-cell jack is sacrificial and becomes part of the final foundation upon completion of load testing.

The O-cell simultaneously works in two directions – upward against the side-shear and downward against the end-bearing, thus separating the upper and lower resistance components. The schematics, basic instrumentations and working of 6 different arrangements of O-cell loading are explained in Appendix B. While mostly used in drilled shafts and bored piles, reported applications also include driven piles, continuous flight auger (CFA), and Fundex piles.

Based on the economic viability, two combinations of O-cell pile load testing presented in Appendix B are considered practicable and thus selected for the current analysis: (1) Case 2 of single O-cell (called here as Case A); and (2) Case 5 of two O-cells (called here as Case B) (see Figures B.1, B.10 and B.12). These cases are schematically explained in Figures 9.1 and 9.2, where their typical responses in terms of load transfer distributions, and load-displacement curves are also shown.

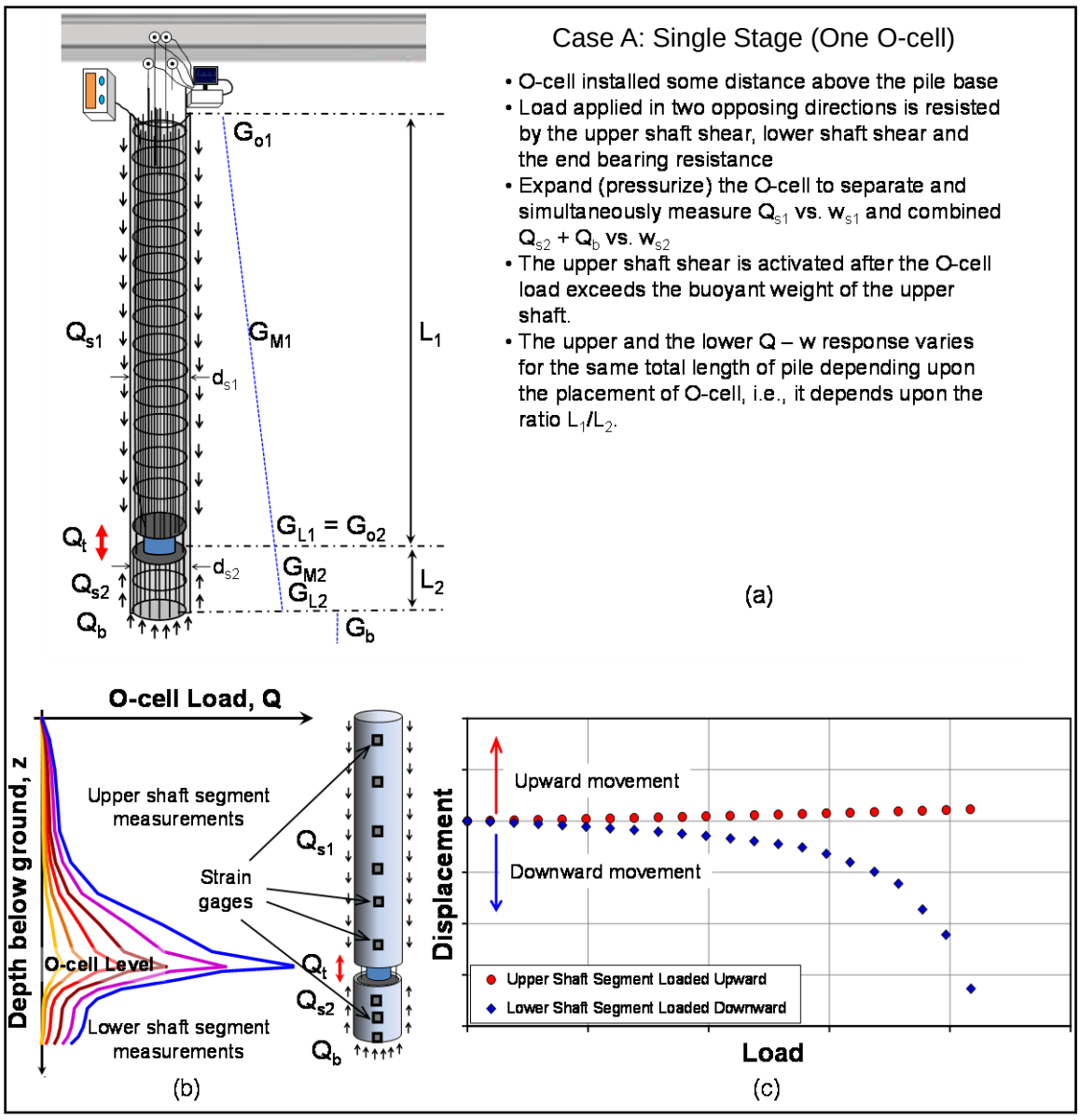

Figure 9.1. Single-stage (one O-cell) load test: (a) typical instrumentation and loading; (b) typical load transfer distributions; (c) typical load-displacement response.

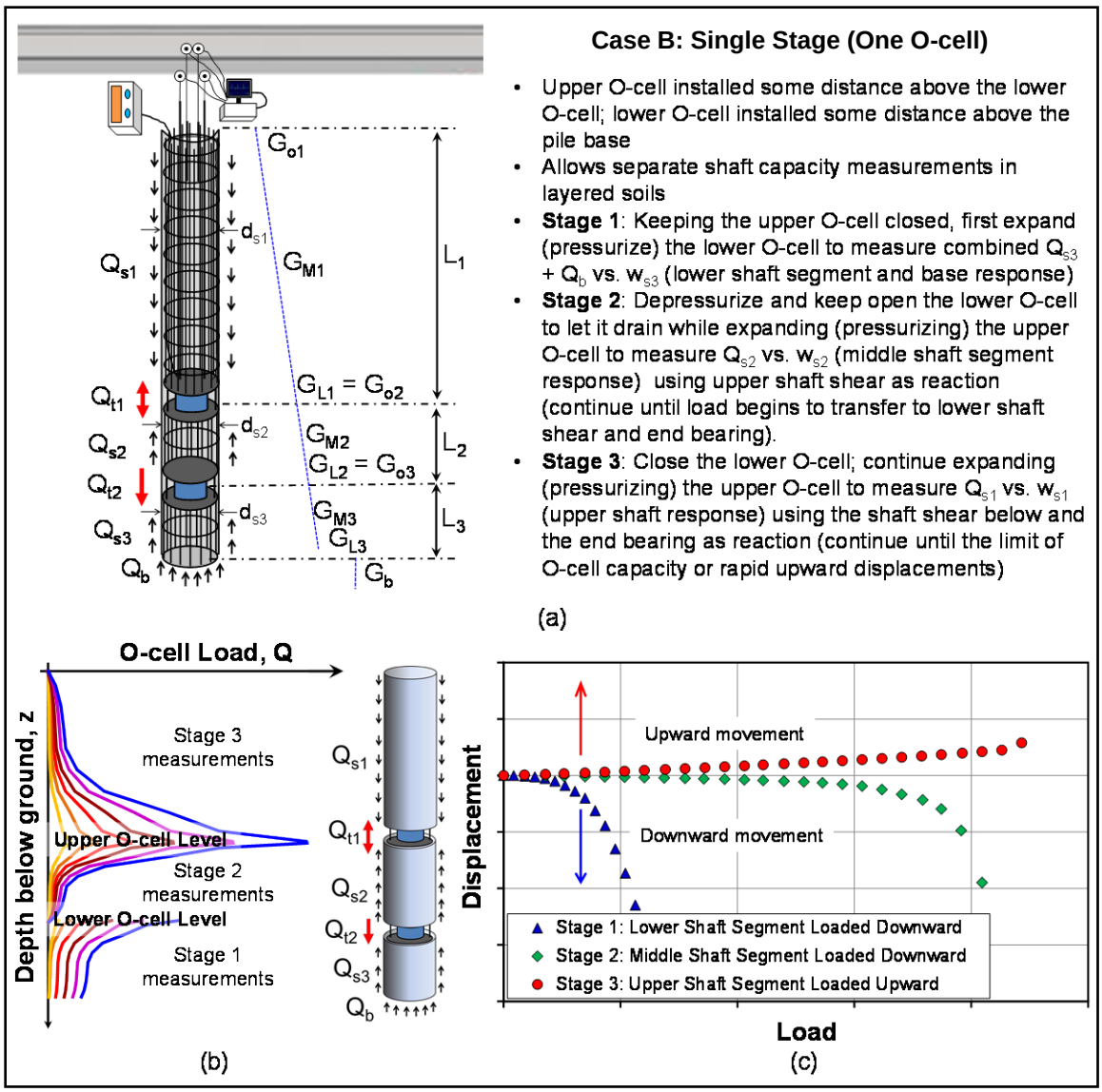

Figure 9.2. Multi-stage (two O-cells) load test: (a) typical instrumentation and loading; (b) typical load transfer distributions; (c) typical load-displacement response.

9.3 Review of Analytical Elastic Solution for Pile Load Displacement Analysis

A summary of the analytical closed-form solution by Randolph and Wroth (1978; 1979) was presented in Chapter 4, while the basic formulation is revisited in the following equations:

$$w_{(z)} = \frac{Q_{(z)}\left[1+\frac{4\eta\ \tanh[\mu(L-z)](L-z)}{\pi\lambda(1-\upsilon)\xi\,[\mu(L-z)]\,r_o}\right]}{G_L\,r_o\left[\frac{4\eta}{(1-\upsilon)\xi}+\frac{2\pi\rho_E\tanh[\mu(L-z)](L-z)}{\zeta\,[\mu(L-z)]\,r_o}\right]} \tag{9.1}$$

where $w_{(z)}$ = pile total displacement at depth z below the top of pile's embedded depth; $Q_{(z)}$ = portion of applied top load (Q_t) transferred at depth z corresponding to $w_{(z)}$; η = r_b/r_o = eta factor for underreamed piles that take greater loads at pile base; r_o = $d_s/2$ = radius of pile shaft; r_b = $d_b/2$ = pile base radius for underreamed piles; $\mu(L - z)$ = $2\cdot[2/(\zeta\lambda)]^{0.5}\cdot[(L - z)/d]$ = measure of pile compressibility for the pile shaft segment between any selected depth z and z = L; ζ = $\ln(r_m/r_o)$ = measure of average radius of influence in the surrounding soil mass affected by shearing stresses around the pile; r_m = $(L - z)\cdot\{0.25 + \xi\cdot[2.5\ \rho_E\cdot(1 - \nu_s) - 0.25]\}$ = average maximum influence radius along the embedded length of the pile – at this radius the shear stresses become negligible (Cooke 1974; Cooke et al. 1979); λ = E_p/G_L = pile-to-soil stiffness ratio; E_p = pile modulus; G_L = operative soil shear modulus at the reference depth of pile base (z = L); ξ = G_L/G_b = factor for end bearing piles resting on stiffer stratum (where $G_b >> G_L$); G_b = soil shear modulus below pile base (for z > L); ρ_E = $G_{M(z)}/G_L$ = modulus variation factor (between any depth z and z = L); $G_{M(z)}$ = $[G_{(z)} + G_L]/2$ = operative soil shear modulus at mid of pile embedment depth (between any depth z and z = L); $G_{(z)}$ = operative soil shear modulus at depth z (at pile top, where z = 0, $G_{(z)} = G_o$); ν_s = Poisson's ratio of soil.

The above solution was derived for top-down static axial compression loading of a single pile foundation. It was developed for piles embedded in a linear elastic two-layered soil model with the soil layer boundary situated at the pile base elevation. The solution was first derived by employing a simplifying assumption that the load-displacement behavior of the pile shaft may be considered separately from that of the pile base and assuming the pile material stiff enough to render pile as rigid (i.e., for any load

applied at the pile top, w_t equals w_b). The separate solutions for pile shaft and base were then tied together by incorporating appropriate modifications to account for the interactions between upper and lower soil layers, and for the pile compressibility, thereby presenting a solution for assessments of separate deformations at pile top and base. These modifications were applied by introducing the soil stiffness variation factor (ρ_E), the xi factor (ξ) for end-bearing piles resting on stiffer stratum, the measure of average influence radius (ζ), and the measure of pile compressibility [$\mu(L - z)$]. A simple insight into all these terms indicates that they are essentially based on the shear stiffness profiles of the two soil layers, which can be conveniently obtained from the V_s measurements.

The operative shear modulus (G) is the most important parameter of the soil affecting the Q-w behavior of a pile under working conditions (e.g., Cooke et al. 1979). However, the non-linearity in decay of soil stiffness poses problem in reliable assessments of the Q-w response. This stiffness decay response can be estimated using a procedure of back-analysis similar to the one presented in Chapter 7. However, as shown in Figures 9.1 and 9.2, the O-cell loading presents it's own typical mechanisms and results, warranting investigations into the factors affecting the outcomes of such back analysis. For this purpose, Group 3 dataset of O-cell load tests on drilled shaft foundations was compiled and exploited in this part of the research.

Following sections present details of the modifications made to the analytical solution to account for the peculiarities of two cases of O-cell loading and the back-analysis of stiffness reduction trends derived from Group 3 dataset.

9.4 Analytical Elastic Solution for Bi-Directional O-cell Loading

The Randolph analytical solution can be de-convoluted into pile shaft and base components to evaluate the bi-directional Q-w response obtained from O-cell type of loading arrangement. Towards that purpose, the basic form of the solution requires to be de-coupled to account for the separate upper and lower pile segments for the two cases of

O-cell pile loading. Moreover, certain other fundamental modifications must also be incorporated into the solution for this newer framework to account for the pile buoyant weight of upper shaft segment, pile installation effect, and radius of influence for different shaft segments above and below the O-cells.

9.4.1 Decoupling of Solution for Separate Upper and Lower Shaft Response

For the two cases of O-cell loading, the responses of the different pile segments are measured separately. Thus, for case A: single stage (one O-cell) load test, the upward displacements are related to pure shaft resistance of the upper pile segment. Similarly, for stage 3 of case B: multi stage (two O-cells) load test, the upward displacements are associated only to shaft resistance of the upper segment. Therefore, the original solution must be modified to disregard the component meant for the pile base response. Putting the set of terms $4\eta/[(1 - \nu_s)\xi]$, which relate only to the pile base, equal to zero in both numerator and denominator, Equation (9.1) reduces to the form applicable only to the compressible shaft Q-w response without a base component:

$$w_{s1} = \frac{Q_{s1}\,\zeta_1\,\mu L_1}{2\pi\,G_{L1}\,\rho_{E1}\tanh(\mu L_1)L_1} \tag{9.2}$$

Here, the subscript 1, as related to Figures 9.1 and 9.2, shows its relevance to the upper shaft segment. Similarly, for stage 2 of case B: multi stage (two O-cells) load test, the only resistance component that activates is the shaft resistance of the middle segment, even though the displacements occur in downward directions. Therefore, the modified solution for the middle segment also reduces to the form similar to Equation (9.2) with subscript 2 relevant to that segment:

$$w_{s2} = \frac{Q_{s2}\,\zeta_2\,\mu L_2}{2\pi\,G_{L2}\,\rho_{E2}\tanh(\mu L_2)L_2} \tag{9.3}$$

For lower segments (L_2 for case 2 and L_3 for stage 1 of case B), the original form of solution from Equation (9.1) still applies since both shaft and base resistance components are activated. Thus, for the downward response in case A: single stage (one O-cell) load test, the applied load from O-cell, which in this case mimics top load for the lower segment, is taken by both shaft resistance of the lower segment (Q_{s2}) and base resistance (Q_b) components. Similarly, for the downward response in stage 1 of case B: multi stage (two O-cells) load test, the applied load from the lower O-cell is taken by shaft resistance of the lower most segment (Q_{s3}) and base resistance (Q_b) components. All the applicable terms in the solutions for the lower segments of the two cases should have their respective subscripts 2 or 3 for each term and the parameters relevant to their respective shaft segments.

Table 9.1 presents two sets of solutions thus derived for the two cases of O-cell loading arrangements shown in Figures 9.1 and 9.2. The expressions are simpler to apply in spreadsheet than they appear at the first sight since some terms and groups of terms occur in both the numerator and the denominator. Referring back to Figures 9.1 and 9.2, the relevant sets of solutions from Table 9.1 along with their respective input parameters should be used for the applicable cases.

9.4.2 Pile Buoyant Weight

An additional aspect relevant to upward loadings for both the cases of O-cell needs attention. In case of upward loading the buoyant weight of the pile must be overcome before any upward displacement in the upper shaft segment may be observed. This means that the measured O-cell loads must be reduced by the amount of buoyant weight of the shaft segment above the O-cell to find the actual shaft resistance offered by that segment. In other words, the applied upward O-cell load is the sum of the buoyant weight of the upper shaft segment ($W_{buoyant}$) and the mobilized shaft resistance along that segment (Q_{s1}). Thus, Equation (9.2) is further modified to the following form:

$$w_{s1} = \frac{(Q_{s1} + W_{buoyant})\,\zeta_1\,\mu L_1}{2\pi\,G_{L1}\,\rho_{E1}\tanh(\mu L_1)L_1} \tag{9.4}$$

9.4.3 Pile Installation Effect

The analytical pile solution inexplicitly assumes that the soil parameters are not affected by pile installation, i.e., the effects of pile installation are not accounted for in the solution. In actuality, the G_{max} profiles obtained from V_s readings at the pile site obtained prior to installation do not truly represent field situation at the time of loading after the pile has been installed. This problem can be significantly addressed by adopting a stiffness reduction schemes [e.g., G/G_{max} vs. percent pseudo-strain, γ_p = w/d (%), where d = pile diameter], such as the one proposed by Berardi and Bovolenta (2005), which can be derived from back-analysis of O-cell pile load tests using the rearranged form of the modified solution. Thus, for case B: multi stage (two O-cells) load test, the rearranged forms of the solution to back-figure their operational stiffness values from the respective measured Q-w response of the upper, middle and lower shaft segments are given in Equations (9.5), (9.6) and (9.7), respectively:

$$G_{L1} = \frac{(Q_{s1} + W_{buoyant})\,\zeta_1\,\mu L_1}{2\pi\,w_{s1}\,\rho_{E1}\tanh(\mu L_1)L_1} \tag{9.5}$$

$$G_{L2} = \frac{Q_{s2}\,\zeta_2\,\mu L_2}{2\pi\,w_{s2}\,\rho_{E2}\tanh(\mu L_2)L_2} \tag{9.6}$$

$$G_{L3} = \frac{(Q_{s3} + Q_b)\left[1 + \frac{4\eta_3\,\tanh(\mu L_3)L_3}{\pi\lambda_3(1-\upsilon_{s3})\xi_3\,\mu L_3\,r_{o3}}\right]}{w_{s3}\;r_{o3}\left[\frac{4\eta_3}{(1-\upsilon_{s3})\xi_3} + \frac{2\pi\rho_{E3}\tanh(\mu L_3)L_3}{\zeta_3\,\mu L_3\,r_{o3}}\right]} \tag{9.7}$$

For case 1: single stage (one O-cell) load test, Equation (9.6) is clearly not applicable; whereas, for Equation (9.7), subscript 2 should be used instead of 3, as related to the lower segment (L_2). This obviously means that the parameters applicable to the lower segment should be used for this case.

Here, the primary input parameters include pile properties and the measured displacements corresponding to measured loads for respective segments of the pile. Since the operational shear stiffness (G_L) values are obtained from back-analysis of actual load test results, these are better representative of the field stiffness values during pile loading (i.e., the installation influence is implicitly taken into account while deriving these stiffness reduction trends from fit-to-field records). In essence, this methodology of back-analysis from a database of load test results entails two advantages: (1) it indirectly accounts for the effects of installation, and (2) it provides a set of modulus reduction trends derived from actual field measurements.

Inherent in this framework of back-analysis are the following assumptions, noted previously in Chapter 7, that are reasonably acceptable from engineering point of view:

- The stiffness is linearly dependent on the depth, although in some real situations may portray a different trend.
- The back-analyzed field stiffness is obtained keeping ρ_E constant, i.e., G all along the shaft segments decreases at the same rate, although greater displacements (and thus greater strains) are expected to be mobilized near the position of O-cell than at the depths closer to the far ends of the shaft segments.

It is also pertinent to mention that hidden in the parameters on the right hand sides of Equations (9.5) to (9.7) is the input of G_L. A trial and error method or a computer program capable of running the required iterations can be used to match the values of G_L on both sides.

9.4.4 Maximum Radius of Influence, r_m

In the Randolph type pile model, the deformations of soil around the pile shaft have been idealized as shearing of infinite concentric cylinders of differentially increasing radii with maximum influence radius modeled as shown in Figure 9.3a. This follows from the vital assumption noted by Cooke (1974), Cooke et al. (1979), and later adopted by Randolph and Wroth (1978; 1979) and Fleming et al. (2009), that the pile load transfers to the adjacent soil through shearing stresses which extend radially away. There is some magical radius (r_m) at some distance from the pile at which these stresses become negligible. Within this radial distance, the shear stresses and resulting displacements decrease inversely with increasing distance from the pile shaft surface. As the load transferred to the pile shaft diminishes with depth, so do the shearing stresses, the resulting influence radius, and their corresponding displacements.

The shape of r_m profile, thus hypothesized for the top-down axial compression and top-applied axial tension loadings, was discussed in Chapter 8. The shape of r_m profile for bottom-up O-cell compression loading for the case of upper shaft segment is expected to be different from that of the top-down compression loading. This may be related to the placement of O-cell(s), and accordingly, the depth at which the maximum load is applied in reference to the overall embedded length of the pile. Here the maximum load is applied to the pile adjacent to the deeper soil layers, where the stiffness is greater compared to that near the ground surface. This should logically result in a reduced r_m compared to the case of top-down compression loading for the same embedded length of the pile (see Figure 9.3b). Accordingly, a reduction factor needs to be introduced in the calculations of r_m for the upward movements of the upper shaft segment. Since the shape of this magical radius profile is noted to be a consequence of the soil stiffness profile at the site, a reduction factor defined in terms of initial shear stiffness profile ($G_{M\ max}/G_{L\ max}$) is introduced in r_m calculations for the upward Q-w response of the upper shaft segment:

$$r_{m1} = \left(\frac{G_{M\,max1}}{G_{L\,max1}}\right) L_1\left[0.25 + \xi_1\left[2.5\rho_{E1}(1 - \upsilon_{s1})\right] - 0.25\right] \quad (9.8)$$

It can be seen that Equation (9.8) applies only to the upper shaft segment of bottom-up O-cell loadings for the two cases presented in Figures 9.1 and 9.2. Here, subscript 1 indicates that all the input parameters pertain to the upper shaft segment (L_1). For all other loadings in downward direction (i.e., the loading of shaft segment L_2 of case A, stage 1 of case B relevant to shaft segment L_3, and stage 2 of case B relevant to shaft segment L_2), the situation mimics the original top-down type of compression loading, and hence the reduction factor needs not be used in these r_m calculations. However, appropriate subscripts representing parameters pertaining to their respective segments should be used. All these expressions are also shown in Table 9.1.

Table 9.1. Modified closed form analytical solutions for two cases of O-cell pile loading.

	Case A (see Figure 9.1)	Case B (see Figure 9.2)
Total pile load	$Q_t = Q_{t1} + Q_{t2} = (Q_{s1} + W_{buoyant}) + (Q_{s2} + Q_b)$ $= [\Sigma(f_{p1}\cdot\pi\cdot d_{s1}\cdot L_1) + \gamma_{buoyant\ (upper\ pile\ shaft)}\cdot\pi\cdot d_{s1}^{\ 2}\cdot L_1/4] +$ $[\Sigma(f_{p2}\cdot\pi\cdot d_{s2}\cdot L_2) + q_b\cdot\pi\cdot d_b^{\ 2}/4]$	$Q_t = Q_{t1} + Q_{t2} = (Q_{s1} + W_{buoyant} + Q_{s2}) + (Q_{s3} + Q_b)$ $= [\Sigma(f_{p1}\cdot\pi\cdot d_{s1}\cdot L_1) + \gamma_{buoyant\ (upper\ pile\ shaft)}\cdot\pi\cdot d_{s1}^{\ 2}\cdot L_1/4 +$ $\Sigma(f_{p2}\cdot\pi\cdot d_{s2}\cdot L_2)] + [\Sigma(f_{p3}\cdot\pi\cdot d_{s3}\cdot L_3) + q_b\cdot\pi\cdot d_b^{\ 2}/4]$
Upper shaft response	$w_{s1} = \frac{(Q_{s1} + W_{buoyant})\,\zeta_1\,\mu L_1}{2\pi\,G_{L1}\,\rho_{E1}\tanh(\mu L_1)L_1}$	$w_{s1} = \frac{(Q_{s1} + W_{buoyant})\,\zeta_1\,\mu L_1}{2\pi\,G_{L1}\,\rho_{E1}\tanh(\mu L_1)L_1}$
Middle shaft response	Not applicable	$w_{s2} = \frac{Q_{s2}\,\zeta_2\,\mu L_2}{2\pi\,G_{L2}\,\rho_{E2}\tanh(\mu L_2)L_2}$
Lower shaft + base response	$w_{s2} = \frac{(Q_{s2} + Q_b)\left[1 + \frac{4\eta_2\tanh(\mu L_2)L_2}{\pi\lambda_2(1-\upsilon_{s2})\xi_2\,\mu L_2\,r_{o2}}\right]}{G_{L2}\,r_{o2}\left[\frac{4\eta_2}{(1-\upsilon_{s2})\xi_2} + \frac{2\pi\rho_{E2}\tanh(\mu L_2)L_2}{\zeta_2\,\mu L_2\,r_{o2}}\right]}$	$w_{s3} = \frac{(Q_{s3} + Q_b)\left[1 + \frac{4\eta_3\tanh(\mu L_3)L_3}{\pi\lambda_3(1-\upsilon_{s3})\xi_3\,\mu L_3\,r_{o3}}\right]}{G_{L3}\,r_{o3}\left[\frac{4\eta_3}{(1-\upsilon_{s3})\xi_3} + \frac{2\pi\rho_{E3}\tanh(\mu L_3)L_3}{\zeta_3\,\mu L_3\,r_{o3}}\right]}$
Additional comments	The respective maximum radius of influence should be calculated from the following expression: $r_{m1} = \left(\frac{G_{M\,max1}}{G_{L\,max1}}\right) L_1\left[0.25 + \xi_1\left[2.5\rho_{E1}(1 - \upsilon_{s1})\right] - 0.25\right]$ $r_{m2} = L_2\left[0.25 + \xi_2\left[2.5\rho_{E2}(1 - \upsilon_{s2})\right] - 0.25\right]$ w_{s1}= upward movement at the top of O-cell w_{s2}= downward movement at the bottom of O-cell ν_{s1} and ν_{s2} are respective soil's Poisson's ratios for upper and lower soil layers	The respective maximum radius of influence should be calculated from the following expression: $r_{m1} = \left(\frac{G_{M\,max1}}{G_{L\,max1}}\right) L_1\left[0.25 + \xi_1\left[2.5\rho_{E1}(1 - \upsilon_{s1})\right] - 0.25\right]$ $r_{m2} = L_2\left[0.25 + \xi_2\left[2.5\rho_{E2}(1 - \upsilon_{s2})\right] - 0.25\right]$ $r_{m3} = L_3\left[0.25 + \xi_3\left[2.5\rho_{E3}(1 - \upsilon_{s3})\right] - 0.25\right]$ w_{s1}= upward movement at the top of upper O-cell w_{s2}=downward movement at the bottom of upper O-cell w_{s3}=downward movement at the bottom of lower O-cell $\nu_{s1,}$ ν_{s2} and ν_{s3} are respective soil's Poisson ratios for upper, middle and lower soil layers

Notes: $W_{buoyant}$ = buoyant weight of pile shaft segment above the O-cell; d_s = shaft diameter; f_p = unit shaft resistance; d_b = pile base diameter; q_b = unit base resistance.

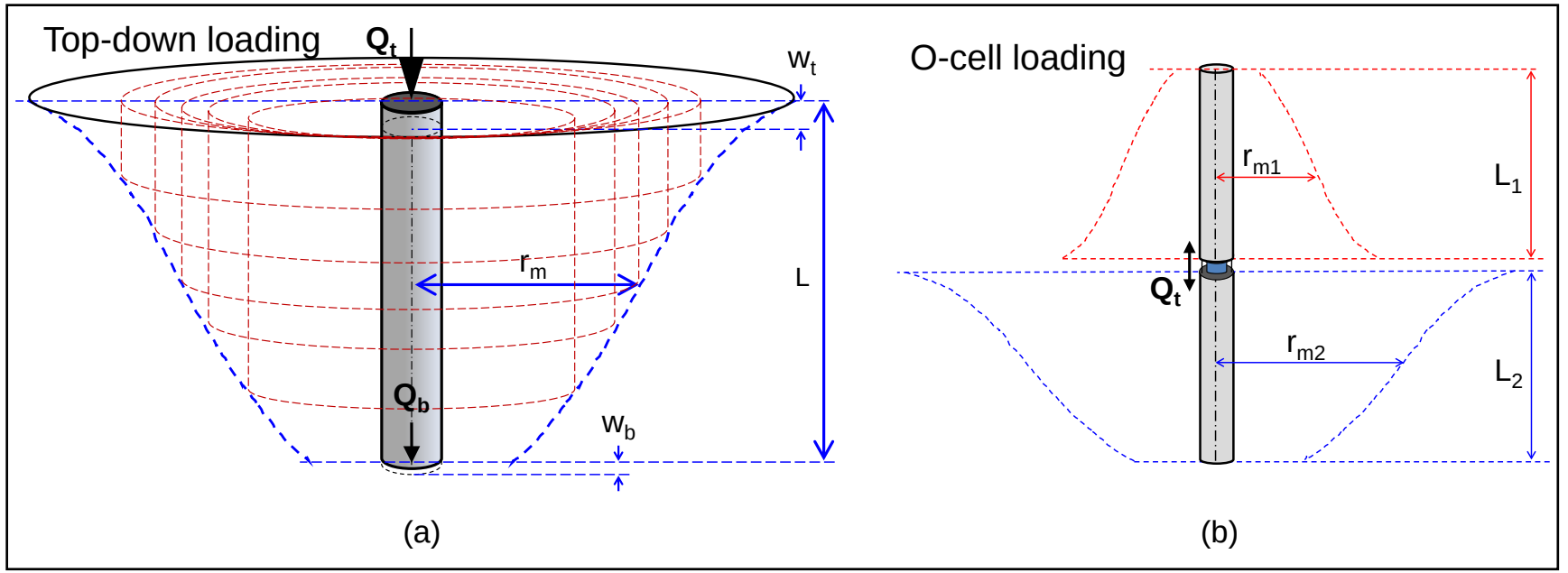

Figure 9.3. Hypothetical model of displacements around the pile shaft and the profile of maximum influence radius: (a) top-down compression loading; (b) bi-directional O-cell loading.

9.5 Field Stiffness Evaluation from Back-analysis of O-cell Load Tests

In order to formulate a field stiffness reduction model for application in the modified closed form solutions for O-cell loading (Table 9.1), the Group 3 dataset was utilized. This dataset consists of well-documented case records of sixteen O-cell pile load tests conducted at nine different sites where SCPTu soundings had also been advanced.

A summary of the pile load test sites indicating their respective locations, soil types and sources of the data is given in Table K.1 of Appendix K. Likewise, Table K.2 provides relevant characteristics of the piles, geomaterials, and O-cell load test specifications. For completeness, the relevant G_{max} profiles obtained from the V_s measurements of SCPTu at these sites are presented in Appendix L. It may be noticed that these sites were made up of a variety of geomaterials ranging from poorly graded sands to stiff clays to partially weathered rock of different geologic origins. The pile foundations in the database were all drilled shafts.

Three additional terms have been introduced in Table K.2 of Appendix K: L/d = pile slenderness ratio, L-ratio = ratio between lengths of pile shaft segment undergoing loading and that of the shaft segment providing resistance, and $\lambda_i = E_p/G_{L\ max}$ = initial pile-to-soil stiffness ratio. Depending on the direction of loadings, the term L-ratio is differently calculated for each shaft segment and each stage to O-cell loading. This will be further explained later in Figures 9.4 and 9.5, and also in the next section showing example application of the modified solution. The G_{max} profiles at these sites indicated nearly uniform or general Gibson soil types. These profiles were further used to evaluate ξ, ρ_E, ζ and λ_i shown in Table K.2 of Appendix K. For the Poisson's ratio values, unless specifically documented as in case of the example presented in this chapter, following assumptions were made: drained conditions for predominantly sandy soil layers (ν_s = 0.20), while undrained conditions taken for predominantly clayey soil layers (ν_s = 0.50).

The equations given in Table 9.1 were all rearranged and used in the forms shown in Equations (9.5) to (9.7) for their respective cases and stages of O-cell loadings. With the measured loads (Q) and their corresponding displacements (w) known from the load test data, and pile and soil characteristics as input, these rearranged equations enabled evaluation of field operational stiffness values (G_L). Such back-analysis was conducted on each stage of loading for all sixteen load tests. The G_L values so obtained were normalized with their respective fundamental shear moduli (i.e., $G_L/G_{L\ max}$) and plotted as function of percent pseudo-strain (γ_p). Thus, separate modulus reduction curves [$G_L/G_{L\ max}$ vs. γ_p (%)] were obtained for each load test and its different stages of loading upper, middle, and lower shaft segments, as applicable. An in-depth study of the results so obtained and other observations from the load test data enabled following conclusion to be drawn:

- The O-cell Q-w responses of the load test dataset clearly indicate a substantial influence of L-ratio (i.e., the placement depth of O-cell in reference to the embedded pile length) on the shear modulus reduction trends. In explanation of that, if the O-cell in case A: single stage (one O-cell) is placed near the pile base, the upward displacements are minimal, and thus result in lesser reduction in the shear modulus values. On the other hand, the downward displacements for this case are considerably large for the same set of O-cell loads, leading to steeper trends in shear modulus reduction (see Figure 9.4a). From another example of the same case, where the O-cell is placed near the mid-depth of the embedded pile, the displacements response to the loadings, and thus the shear modulus reduction trends for both the directions are about similar (see Figure 9.4b). Minor difference can be attributed to the fact that for the upward loading, the load is applied at a depth of greater overburden (and greater stiffness) than that at the other end (i.e., pile top). Therefore, the upward dissipation of load along the shaft is rapid compared to that of the downward loading. All these observations were

further validated from the results of Q-w response, and the back-analyzed shear stiffness values for all the load tests of case B: multi-stage (two O-cells). These are all presented in Appendix E. An actual case from the dataset is also shown in Figure 9.5 as an illustrative example. From these observations, it is established that higher L-ratio points to gradual reduction in shear stiffness under different levels of pseudo-strain.

- On the overall results of the stiffness reduction trends, it is a general observation that the maximum variation exists for the case of upper shaft segment, followed by the lower shaft segment, and tailed by the middle shaft segment responses. Through a closer scrutiny of the database and the load test results, all these trends can be plausibly attributed to the L-ratio as one of the prime factors. Since L-ratio is not a direct part of the closed form solution, it must be incorporated into the stiffness reduction model to be employed for estimation of the applicable stiffness values for use in the modified solution.
- Another element affecting the Q-w measurements and the modulus reduction trends is also related to the pile dimensions. It is noted from the database and its back-analysis that higher L/d ratios also point to gradual reduction in shear stiffness.
- Since the shear stiffness response of each segment varies differently, separate modulus reduction trends/algorithms should be developed for upper, middle, and lower shaft segments.

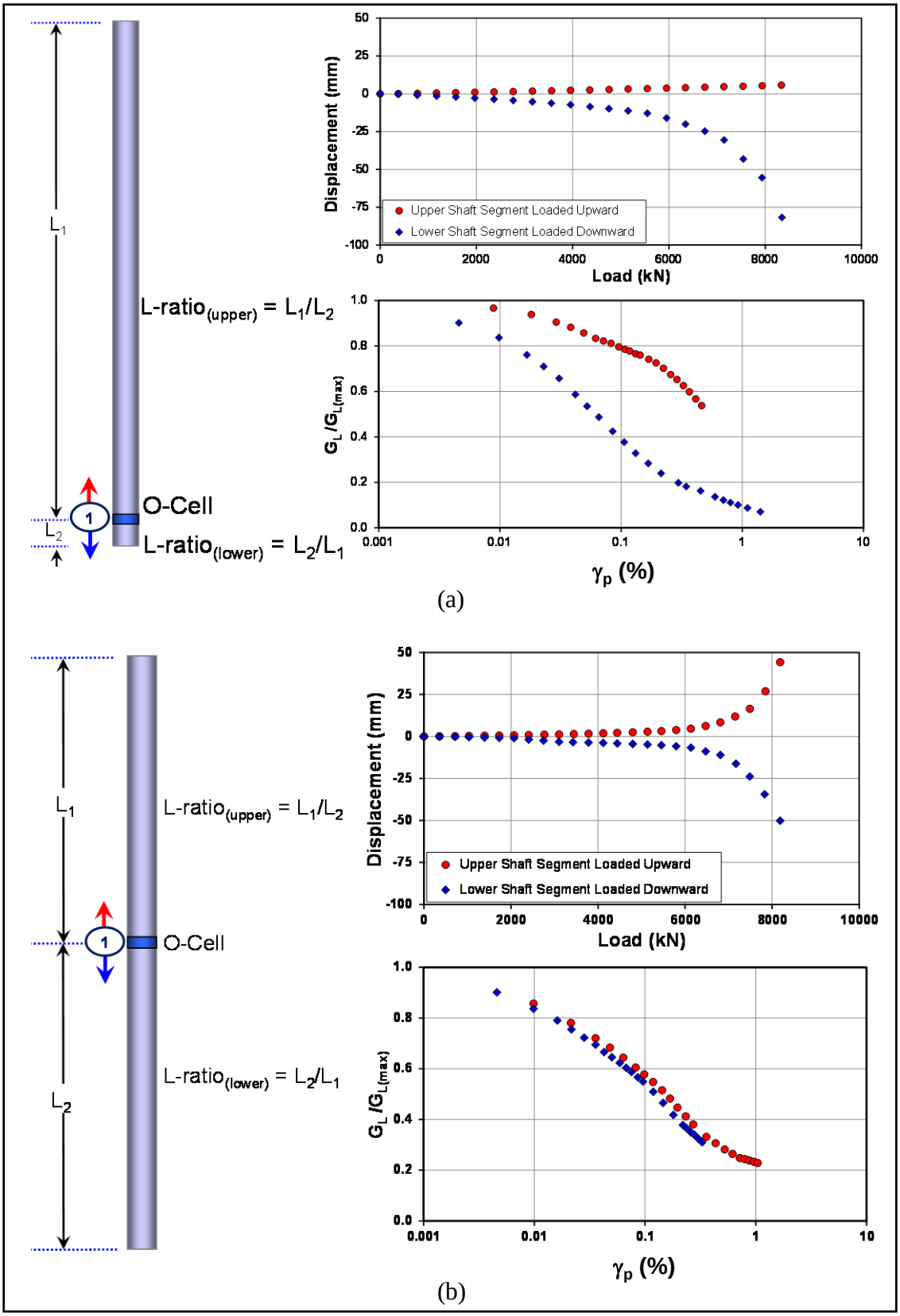

Figure 9.4. Load-displacement and stiffness reduction response, case A: single stage (one O-cell) loading: (a) O-cell placed near the base; (b) O-cell placed at mid-depth.

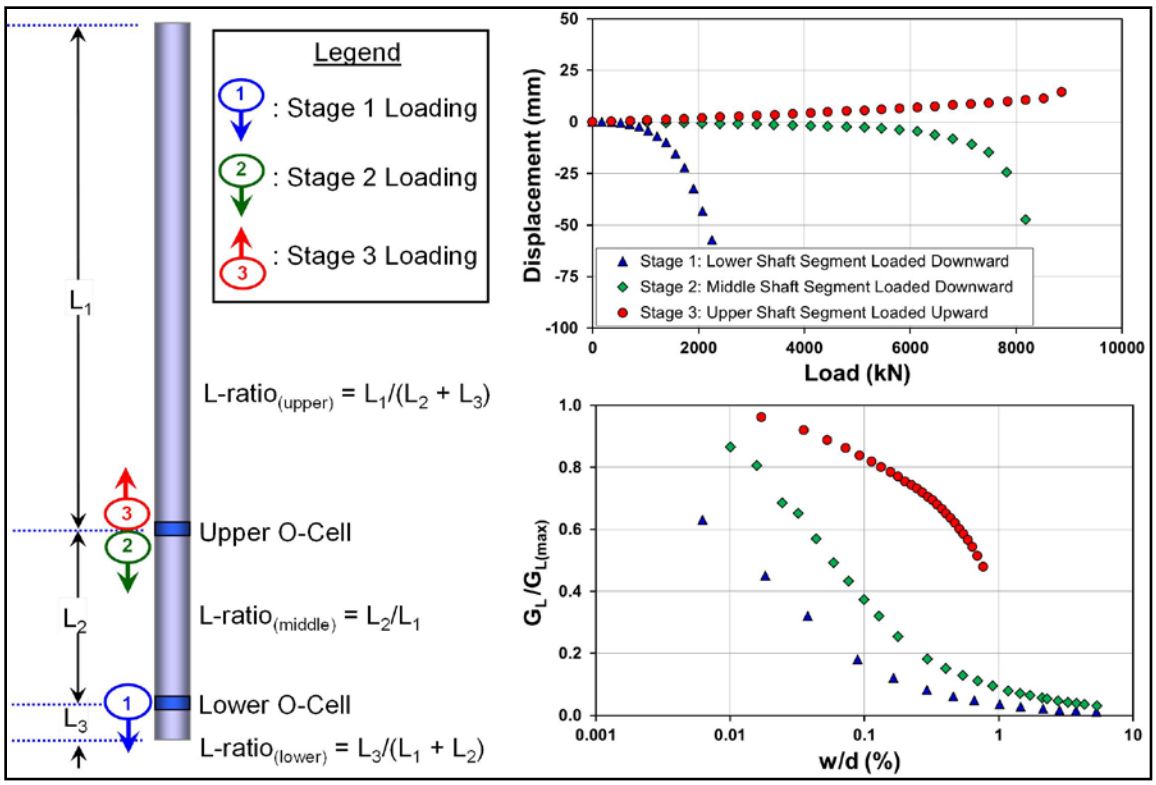

Figure 9.5. Load-displacement and stiffness reduction response, case B: multi stage (two O-cells) load test.

To quantify the influence of input parameters of the solution on the outcome of this retro investigation, simple sensitivity analyses were conducted, wherein the upper and lower limits of the applicable range of values within the dataset were used. The was calculated as the percent contribution of the variation of each parameter within its limits on the overall change in G_L at three levels of percent γ_p separately for upper, middle and lower shaft segments. The results presented in Figure 9.6 demonstrate that the most influential factor on the trends of shear stiffness reduction is the pile slenderness ratio (L/d), followed by ν_s, ξ and ρ_E. For the lower segment, negligible influence is noted for ν_s, ξ, λ_i and ρ_E. At present these results are based on the dataset at hand, as presented in Tables H.1 and H.2. It is possible that the sensitivity analysis results may slightly vary with larger database of different upper and lower limits of the input parameters.

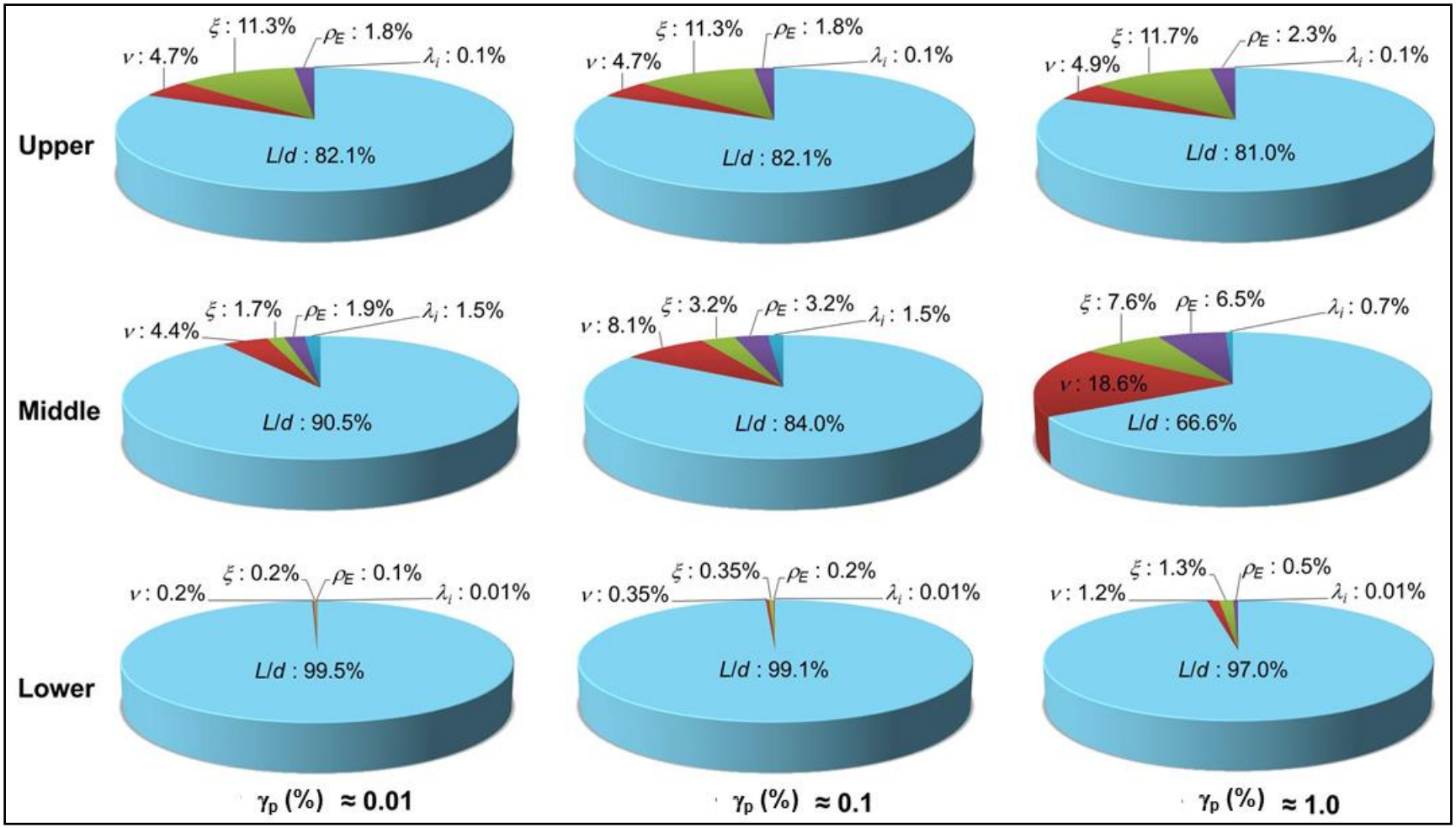

Figure 9.6. Sensitivity analysis of the influence of input parameters on the modified analytical pile solution for axial Q-w response in bi-directional O-cell loading.

It is clear from Figures 9.4 and 9.5 that the relationship between the predictor variable [γ_p (%)] and the response variable ($G_L/G_{L\ max}$) is nonlinear. For such a relationship, it is advisable to work with alternative models where the variables are re-expressed after transformation. Different combinations of variables' transformation were, therefore, attempted to linearize the relationship for simpler regression model. Two statistical software packages (PASW Statistics and R Project), were used in the process. The best curve estimations with highest coefficient of determination (R^2) for upper, middle, and lower shaft segments were obtained via simple linear regression of $\ln(G_L/G_{L\ max})$ against $\ln[\gamma_p$ (%)]. In order to incorporate the influence of L-ratio and L/d in the stiffness softening model (called here as 'Model 1'), following generalized mathematical expression was considered:

$$\frac{G_L}{G_{L\,max}} = j\left[\gamma_p(\%)\right]^k \left(\frac{L}{d}\right)^l (L-\text{ratio})^m (\upsilon_s)^n (\xi)^o \left(\rho_E\right)^p \leq \left(\frac{G_L}{G_{L\,max}}\right)_{lim} \qquad (9.9)$$

where j, k, l, m, n, o and p are dimensionless parameters, and $(G_L/G_{L\ max})_{lim}$ is the upper limit of normalized stiffness value from the back-analyzed results of the dataset. All other input parameters have also been expressed in dimensionless form to avoid investigating the effect of variations of each individual pile or soil factor on the solution. Parameters j, k, l, m, n, o and p were determined from the separate linear regression analyses on the back-analyzed and transformed results of upper, middle and lower shaft segments. The final forms of the modulus reduction algorithms for the three shaft segments, showing the derived parameters are given in Equations (9.10) to (9.12) below. It may be noticed that the insignificant parameters, as applicable to each segment, have been removed from their respective expressions. The $(G_L/G_{L\ max})_{lim}$ values, the applicable ranges of γ_p (%), and the coefficients of determination (R^2) for their respective regression analyses are given in Table 9.2.

Lower segment downward:

$$\frac{G_{L3}}{G_{L\,max3}} = 0.032\left[\gamma_{p3}\,(\%)\right]^{-0.59}\left(\frac{L_3}{d_{s3}}\right)^{0.24}\left[L-\text{ratio}_{(lower)}\right]^{0.13}(\upsilon_{s3})^{-1.06} \quad (9.10)$$

Middle segment downward:

$$\frac{G_{L2}}{G_{L\,max2}} = 0.007\left[\gamma_{p2}\,(\%)\right]^{-0.52}\left(\frac{L_2}{d_{s2}}\right)^{1.22}\left[L-\text{ratio}_{(middle)}\right]^{-0.98}(\upsilon_{s2})^{0.03}(\rho_{E2})^{0.5} \quad (9.11)$$

Upper segment upward:

$$\frac{G_{L1}}{G_{L\,max1}} = 0.026\left[\gamma_{p1}\,(\%)\right]^{-0.55}\left(\frac{L_1}{d_{s1}}\right)^{0.38}\left[L-\text{ratio}_{(upper)}\right]^{-0.2}(\upsilon_{s1})^{-0.18}(\xi_1)^{-0.63} \quad (9.12)$$

Table 9.2. Limiting values and regression R^2 for operational shear stiffness Model 1.

Shaft segment	$(G_L/G_{L\,max})_{lim}$	γ_p (%) range		R^2
		Upper	Lower	
Upper	0.97	0.002	5.4	0.82
Middle	0.91	0.005	3.1	0.88
Lower	0.96	0.004	6.4	0.92

R^2 = coefficient of determination.

A simpler alternative model, termed 'Model 2', was explored by combining groups of similar L/d and L-ratios, since these were established to be the two most sensitive and significant parameters affecting the solution. Here, $G_L/G_{L\,max}$ is expressed solely as function of percent pseudo-strain [γ_p (%)] via the following generalized form of expression, where parameters A, B, C and n (listed in Table 9.3) have been derived from empirical fitting, separately for each group. The grouping has been done on the basis of

certain combinations of L/d and L-ratio; hence, the trends are the result of the combined effects of the two parameters.

$$\frac{G_L}{G_{L\,max}} = \frac{1}{A[\gamma_p\,(\%)]^n + B[\gamma_p\,(\%)] + C} \tag{9.13}$$

Table 9.3. Parameters for operational shear stiffness calculations – Model 2.

Shaft segment	L/d	L–ratio	A	B	C	n
Upper	12.30	1.98	85.0	10.0	1.05	1.95
	12.30	1.55	7.0	2.0	0.95	0.75
	13.00	22.91	200.0	4.0	0.95	1.35
	14.50	2.74	1.0	2.0	1.18	2.0
Middle	3.50	0.27	8.0	1.9	0.95	0.75
	5.60	0.42	7.0	3.0	1.10	1.10
	10.20	0.60	4.0	1.0	1.04	0.85
Lower	1.23	0.07	15.0	1.9	1.00	0.70
	11.80	1.01				
	0.57	0.036	9.0	1.3	0.88	0.60
	0.54	0.038	35.0	1.9	1.00	0.75
	0.47	0.023				
	2.90	0.407	9.0	1.5	1.00	0.70
	10.15	0.762	4.0	1.1	0.90	0.60

9.6 Application of Modified Solution

The proposed modified analytical elastic solution can be conveniently used to predict the Q-w response for the two cases and their different stages of O-cell pile loading.

In order to elaborate the detailed step-by-step procedure, sample calculations for estimation of loads corresponding to selected displacements for three-staged O-cell load

test at Pinners Point Interchange project are presented in Appendix M. The project site is located in Portsmouth, VA, USA. The subsurface explorations indicated approximately 19.5 m of interbedded clay, silt and sand of Sandbridge and Norfolk Formations, overlying medium to dense sand of the Yorktown Formation (Kort et al. 2001a). A SCPTu sounding near the site provides V_s and, therefore, G_{max} profiles (see Figure 9.7). The O-cell load test was conducted on a 26.1 m long, 1.524 m diameter drilled shaft on April 25, 2001 as part of foundation design investigations for the proposed interchange bridge. The two 534 mm O-cells were placed at 19.9 m and 25.2 m depths below the ground elevation, loaded sequentially in three stages (per Figure 9.2). The detailed calculations in Appendix M appear very involved at first glance; however, these are included to explain the complete methodology of implementing the modified solution. The actual Q-w predictions shown in Figure 9.8 were conveniently implemented in a spreadsheet.

It should be noted that the sole purpose of including the example is to explicate the procedure of implementing the modified solution in the new pile loading arrangement. The case shown in the example is one of the tests used in the derivation of stiffness reduction algorithms. As such, the intention was not to demonstrate the reliability of these algorithms. These algorithms, specifically meant for application to O-cell loading, have been derived from limited available dataset. Apparently 'Model 2' gives better prediction results than 'Model 1.' Similar to the case of stiffness reduction algorithms presented in Chapter 7 concerning C and T cases, Model 1 results in loss of accuracy at greater loads (or lower G/G_{max}). The results cannot be authenticated unless these models are applied to any new O-cell load tests, outside of the current dataset. As noted earlier, it is possible to establish and/or improve the validity of these algorithms through further correlation experience on expanded database, as it becomes available.

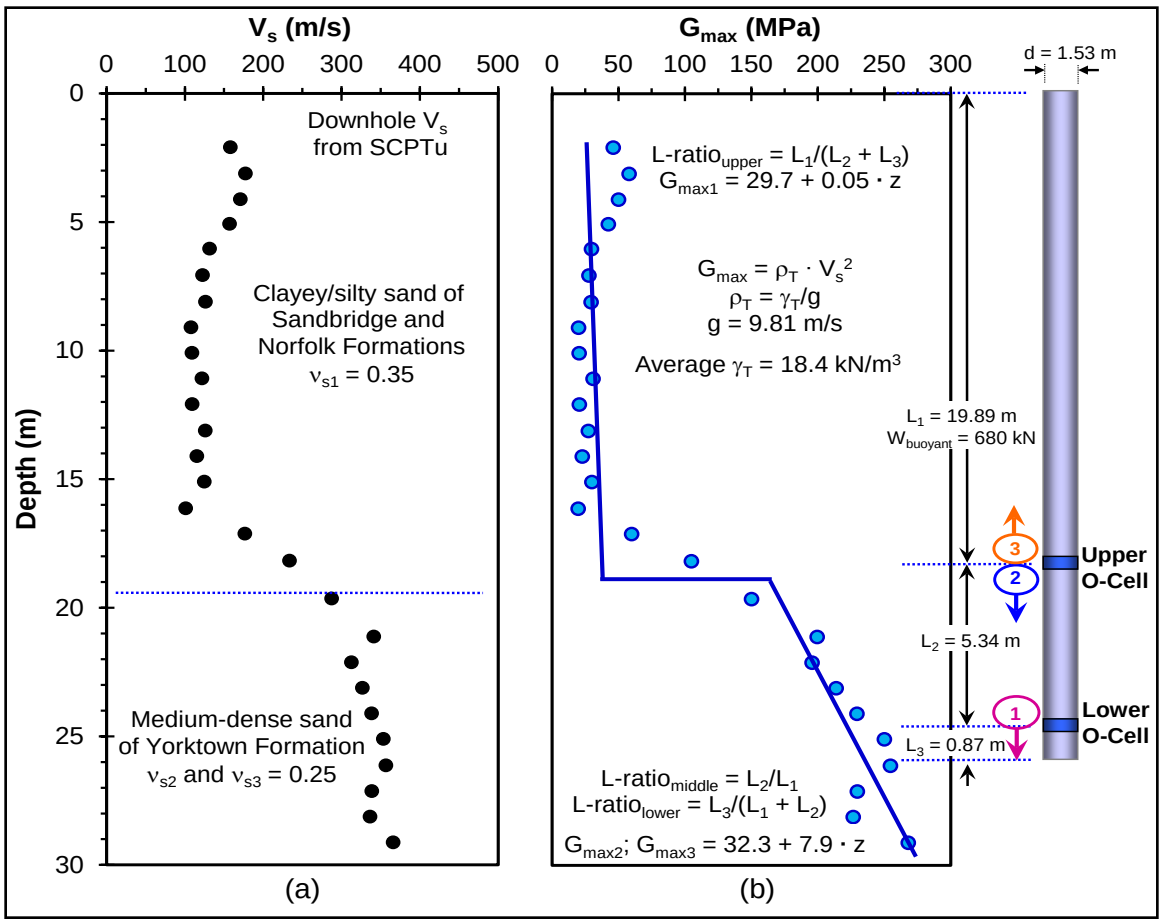

Figure 9.7. O-cell load test on drilled shaft at Pinners Point Interchange, Virginia, USA: (a) V_s profile from SCPTu; and (b) G_{max} profile from V_s readings of SCPTu.

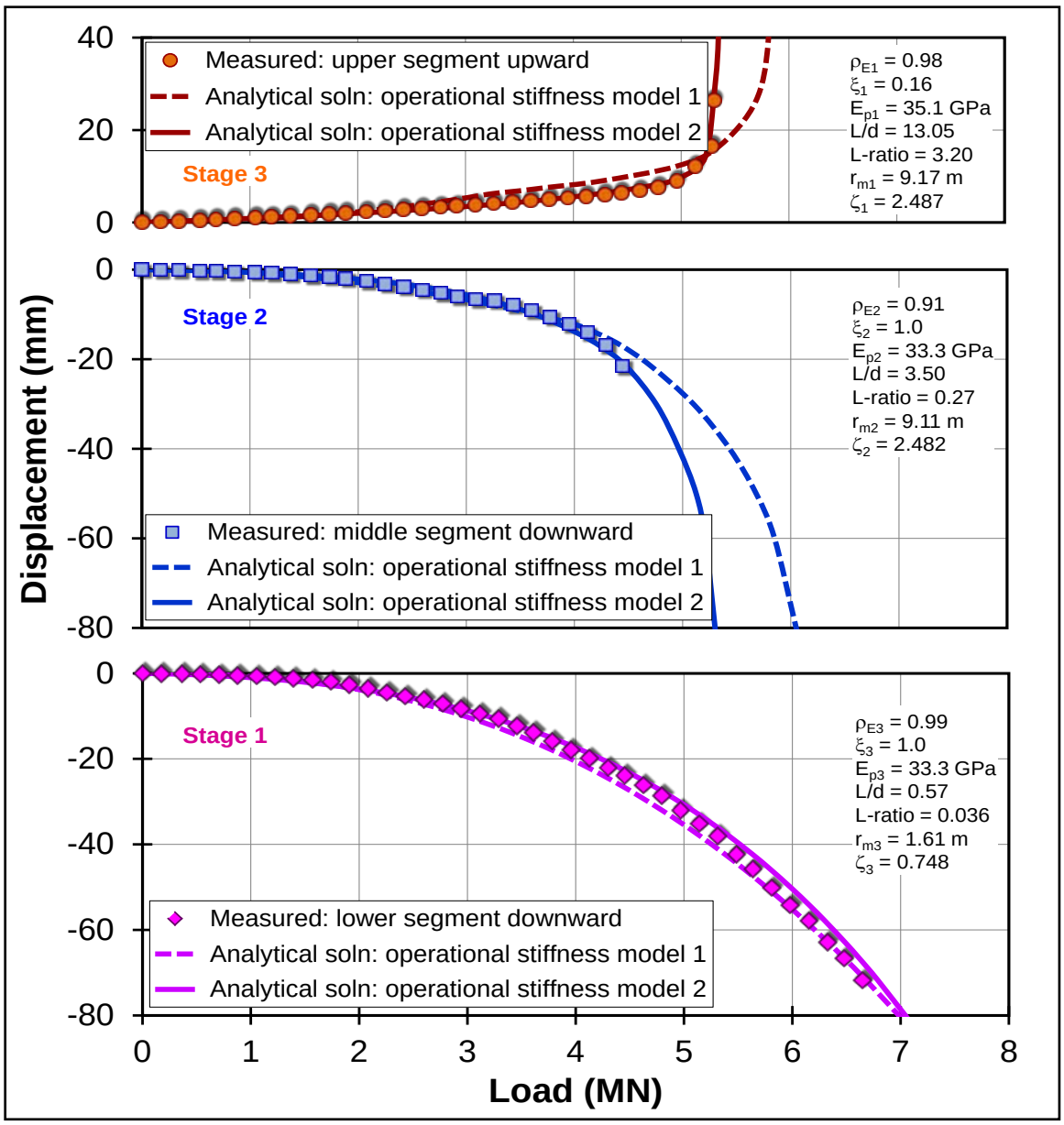

Figure 9.8. Measured vs. predicted Q-w response of multi-stage O-cell load test on drilled shaft at Pinners Point Interchange, Virginia, USA.

9.7 Concluding Remarks

In this chapter, a modified analytical closed form solution is developed for predicting the Q-w response of piles axially loaded using the newer bi-directional O-cell device. The original closed-from solution by Randolph and Wroth (1978; 1979) was

decoupled and modified to account for the different cases and stages of O-cell loading. The decoupling part accounts for separate assessments of the response to axial loading for different segments of pile shaft and different stages of loading, while the modifications include: (1) reduced maximum radius of influence (r_m) for the upper shaft segment, and (2) modeling non-linear ground stiffness (G/G_{max}) from back-analysis of a well-documented dataset of O-cell load tests. The field V_s profiles from hybrid geophysical-geotechnical testing (i.e., SCPTu) enabled use of the soil's fundamental shear stiffness (G_{max}) that provided the starting point in the back-analysis.

The retro-investigation indicated clear variations in the stiffness reduction trends for the upper, middle and lower shaft segments; accordingly, the three sets were separately grouped and analyzed. Further insight into the results of load tests from the database and sensitivity analyses on back-analyzed results indicate that L/d and L-ratio, besides the soil stiffness profiles, are the most influential factors on the results of Q-w predictions from the modified solution. Two stiffness reduction models have been proposed and analyzed. For the predictor variables, the first model uses the significant input parameters of the modified solution [percent pseudo-strain (γ_p), L/d, L-ratio, ν_s, ξ, ρ_E], whereas, the second model is based solely on the percent pseudo-strain (γ_p) for estimating operational shear stiffness.

The stiffness reduction models proposed herein are specifically meant to be applied in the proposed modified solution for O-cell type of pile loading, and should not be considered for universal application in other soil-structure interaction problems. The respective applicable limits of $G_L/G_{L\ max}$ as well as the ranges of γ_p (%) must be considered while applying this solution. It is expected that the proposed model can be further refined by expanding the database and conducting supplementary sensitivity studies.

CHAPTER 10

SUMMARY OF RESEARCH FINDINGS AND RECOMMENDATIONS FOR FUTURE RESEARCH

The conventional use of cone penetrometer testing (CPT) in the analyses of pile foundations has mostly been limited to evaluations of static axial capacity, specifically the two components of unit shaft resistance (f_p) and unit base resistance (q_b). These estimations were made possible in the past by establishing correlations between the field measurements from pile load tests and those from one or more of the three penetrometer readings (q_t, f_s, and u_2) via direct and indirect approaches. While the *indirect CPT approaches* are considered rational in a sense that they provide CPT assessments of the fundamental soil properties within a selected analytical framework (e.g., limit plasticity, cavity expansion, or limit equilibrium) for determining f_p and q_b, they require a two-step process. In contrast, *direct CPT methods* offer a simpler approach with a straightforward relationship between pile and CPT readings from directly-scaled correlations.

The current research effort introduced a new direction to the CPT-based static pile approach by extending it from a sole focus on capacity to a more encompassing axial load-displacement-capacity and load transfer with depth response via use of seismic piezocone penetration testing (SCPT). Towards those goals, all four penetrometer readings (q_t, f_s, u_2, V_s) are used. The penetration readings are utilized in a refinement of the UniCone direct CPT method originally proposed by Eslami and Fellenius (1997), while the shear wave velocity (V_s) readings are exploited to obtain the fundamental soil shear modulus ($G_{max} = \rho_t V_s^2$) for derivation of stiffness reduction curves from the back-analyses of pile load tests within an analytical elastic continuum framework (Randolph and Wroth 1978; 1979; Fleming et al., 2009). In addition, elaborate algorithms are developed for the application of this elastic solution to a stacked pile model in multilayer soil media and to the newer bidirectional O-cell loading arrangements. This was made

possible from a compiled database of 330 pile load tests and 73 SCPT soundings from 70 sites in 19 countries of the world.

10.1 Research Findings

The outcome of this research study can be broadly classified into following four major areas of findings:

10.1.1 Enhanced UniCone CPT Method for Axial Pile Capacity

The original 5-part zonal classification from the UniCone plots of log q_E vs. log f_s system by Eslami and Fellenius (1997) assigns discrete pile side friction coefficients (C_{se}) to each elevation of CPTu data. This UniCone approach was refined by using a 50% increase in the total database of pile load tests and specific earmarking of the diversity in terms of pile material, shape, installation method, end conditions, loading procedure and direction that were installed and tested in a wide assortment of geomaterials. As a result, this soil classification chart was refined by delineating 11 soil sub-zones along with their specific C_{se}, in contrast to the 5 zones originally proposed.

In further improvements, the CPT material index, I_c (Robertson 2009) was used to establish direct correlations, linking C_{se} vs. I_c and toe correlation coefficient, C_{te} vs. I_c. After initial identification of sensitive soils (Zone 1), statistical relationships were developed that offer a continuous function for estimating these pile resistance coefficients over a wide range of I_c values (Zones 2 to 7), thereby eliminating the need for use of the soil classification chart and improving the reliability in the evaluations of pile side friction (f_p) and unit end-bearing (q_b). Adjustment factors were proposed to account for the pile type (bored and augered vs. jacked vs. driven), loading direction (compression vs. tension) and the loading rate applied during pile load tests (constant rate of penetration vs. maintained load tests). Statistical results were presented showing relationships between different capacity criteria and the maximum applied loads used in

this study. A summary flowchart detailing various steps involved in the use of proposed correlations is presented in Figure 10.1. This analysis also reveals that the statistical reliability of estimating f_p is superior to that for q_b.

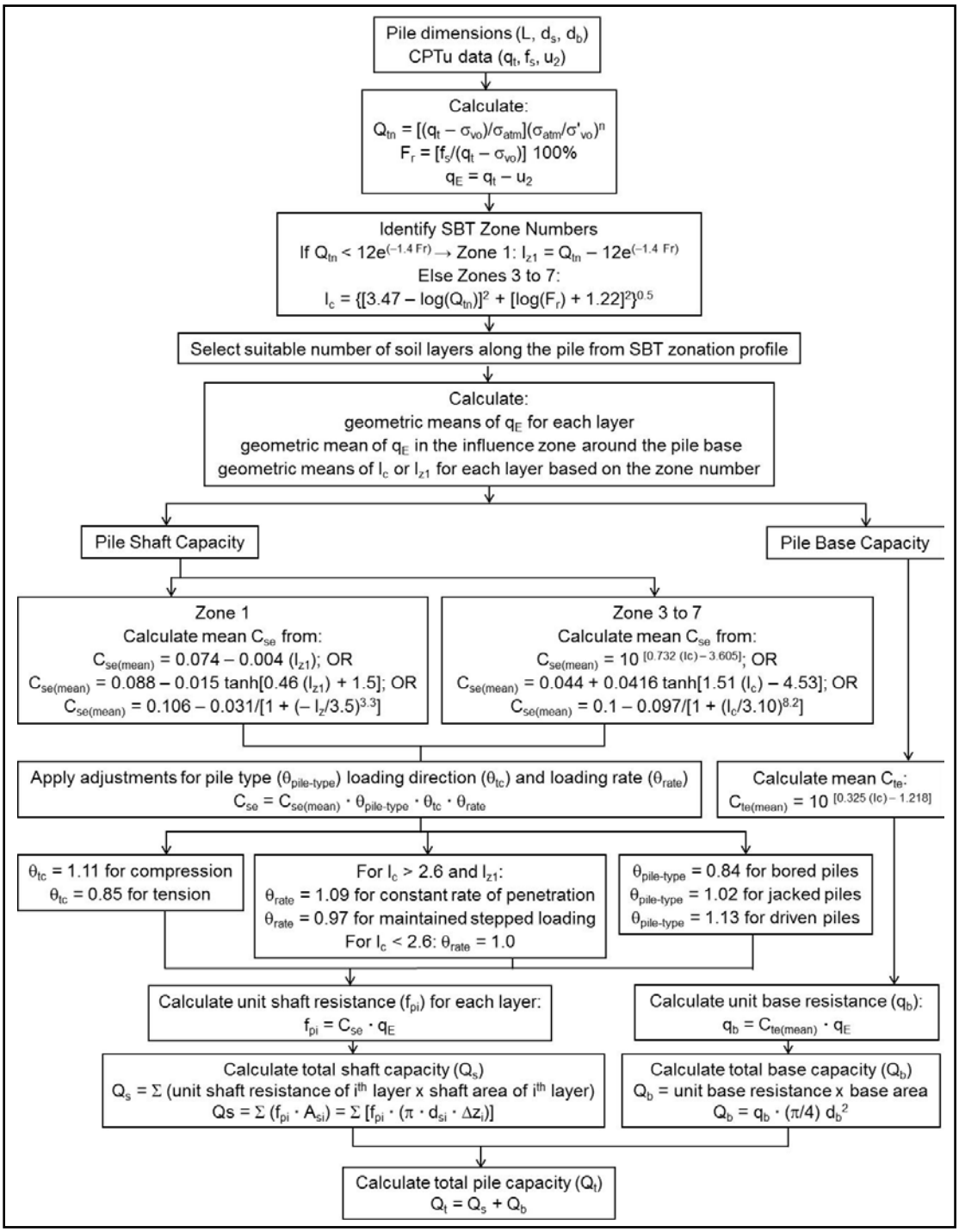

Figure 10.1. Flowchart summarizing steps for evaluating axial pile capacity from the proposed design formulations.

10.1.2 Operational Soil Stiffness for Load-Displacement Response

New sets of shear stiffness reduction curves are developed from back-analyses of 299 static axial pile load tests from 61 sites (Group 2 dataset) towards the implementation of a non-linear Q-w response method for pile foundations. The initial shear modulus (G_{max}), derived from the measured shear wave velocity (V_s) profiles at the pile test sites, were used in these back-analyses. A closed-form elastic continuum solution used for axial compression loading was decoupled and modified to allow application to the axial tension loading case.

The back-analysis of shear moduli performed using this elastic solution resulted in derivations of new shear modulus reduction curves, specifically normalized shear stiffness (G/G_{max}) vs. logarithm of pseudo-strain (γ_p = w/d, where w = pile displacement and d = pile diameter). The new sets of curves incorporate the effects of pile type and installation method (i.e., bored, augered, jacked, or driven), as well as the influence of soil plasticity. Alternative functional formats were provided in terms of exponential curves or hyperbolic tangent expressions to mathematically define these stiffness reduction trends (see Figures 10.2 and 10.3, respectively). A complete step-by-step methodology is presented in Figure 10.4 for use and application of these new stiffness reduction curves within the extended system of closed-form elastic continuum solutions. Statistical evaluations of the design charts show superior overall performance in the comparison of predicted operative stiffness with the back-figured values.

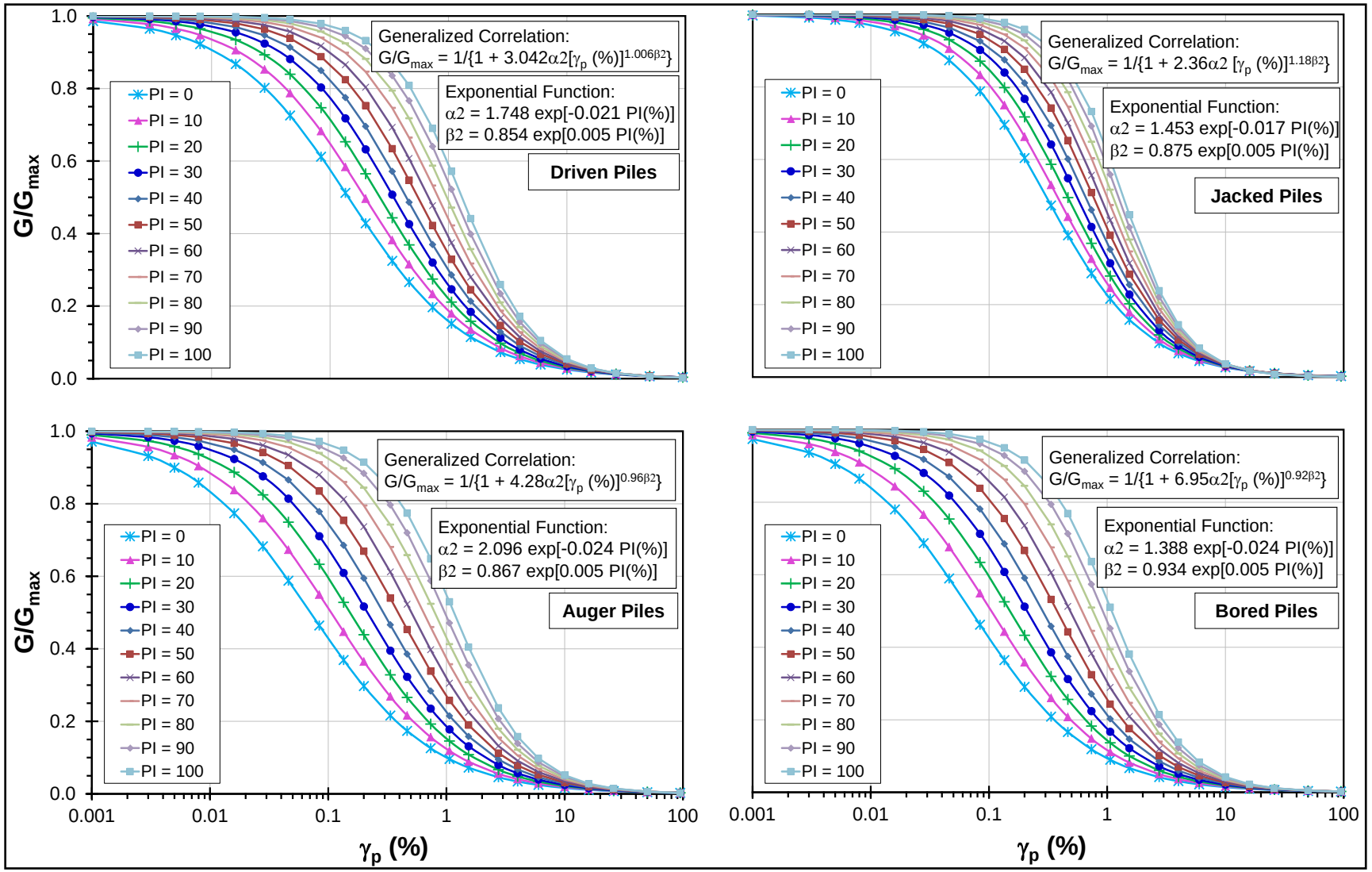

Figure 10.2. Design charts for shear stiffness reduction for application in the pile foundation analysis (exponential fitting function).

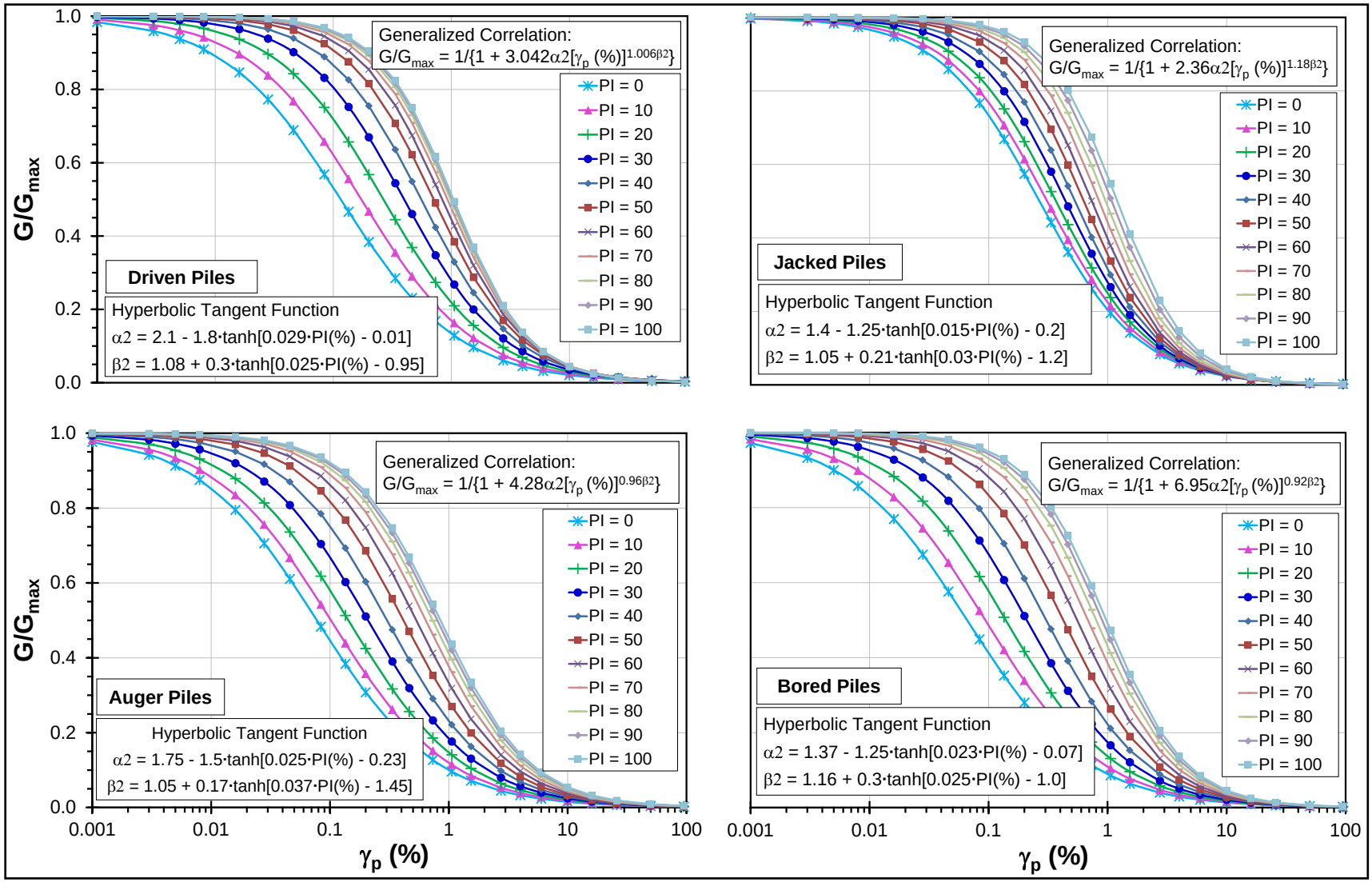

Figure 10.3. Design charts for shear stiffness reduction for application in the pile foundation analysis (hyperbolic tangent function).

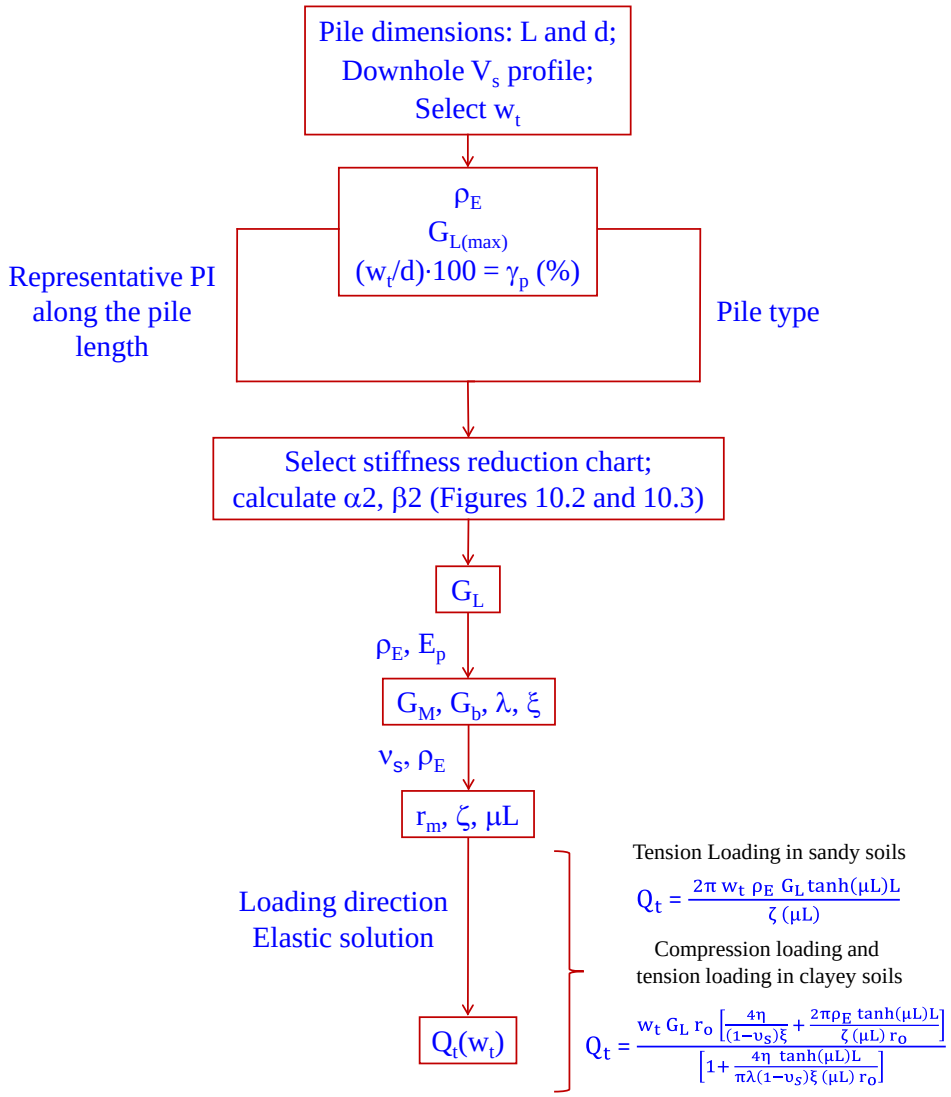

Explanations of Terms

- G_L = operative soil shear modulus at pile base (z = L)
- Q_t = applied top load
- w_t = total settlement at the pile top
- $\eta = r_b/r_o$ = eta factor for bell-shaped piles
- $r_o = d/2$ = pile radius
- $r_b = d_b/2$ = pile base radius for bell shaped piles
- $\mu L = 2\cdot[2/(\zeta\lambda)]^{0.5}\cdot (L/d)$ = measure of pile compressibility
- $\zeta = \ln(r_m/r_o)$ = measure of influence radius
- $r_m = L\cdot\{0.25 + \xi\cdot[2.5\,\rho_E\cdot(1 - \nu_s) - 0.25]\}$ = influence radius
- $\lambda = E_p/G_L$ = pile-soil stiffness ratio
- E_p = pile modulus
- $\xi = G_L/G_b$ = xi factor for end bearing piles
- G_b = operative soil shear modulus below pile base
- $\rho_E = G_M/G_L$ = modulus variation factor
- $G_M = [G_o + G_L]/2$ = operative soil shear modulus at mid of pile embedment depth
- G_o = operative soil shear modulus at the pile top
- ν_s = Poisson's ratio of soil

Figure 10.4. Flowchart detailing steps for estimating load-displacement values from the G/G_{max} vs. percent γ_p type design charts.

10.1.3 Elastic Continuum Solution of Stacked Pile Model

The stiffness reduction curves for use in the elastic continuum solution were developed with the following underlying assumptions: (1) soil stiffness is linear with depth (most common occurrence, although select sites may portray different trends), and (2) back-analyzed field stiffnesses can be obtained keeping the operative modulus profile constant throughout the loading (even though shaft resistance is expected to be mobilized prior to the end bearing). In an effort to make some improvements with respect to these conditions, certain provisions of the elastic continuum solution were exploited to present a methodology for drawing the stiffness reduction curves as functions of depth. These curves can be further utilized in modeling the pile as a stack of smaller segments embedded in multi-layered soils, where each layer is assigned its own distinctive averaged stiffness. The Q-w analysis of all pile segments, associated with their adjacent soil layers, can thus be performed using the stiffness reduction curves applicable to their respective depths. The overall Q-w response is obtained through integration of the analysis result of all layers. The solution can be used to address the question of progressive failure with depth in a multi-layer soil media that exhibits nonlinear soil stiffness response. Flow charts are presented in Figures 10.5 and 10.6, detailing steps for plotting the depth-dependent stiffness reduction curves for compressible and rigid piles, respectively. Similarly, the procedures for implementing the stacked pile model for compressible and rigid piles are summarized in Figures 10.7 and 10.8, respectively.

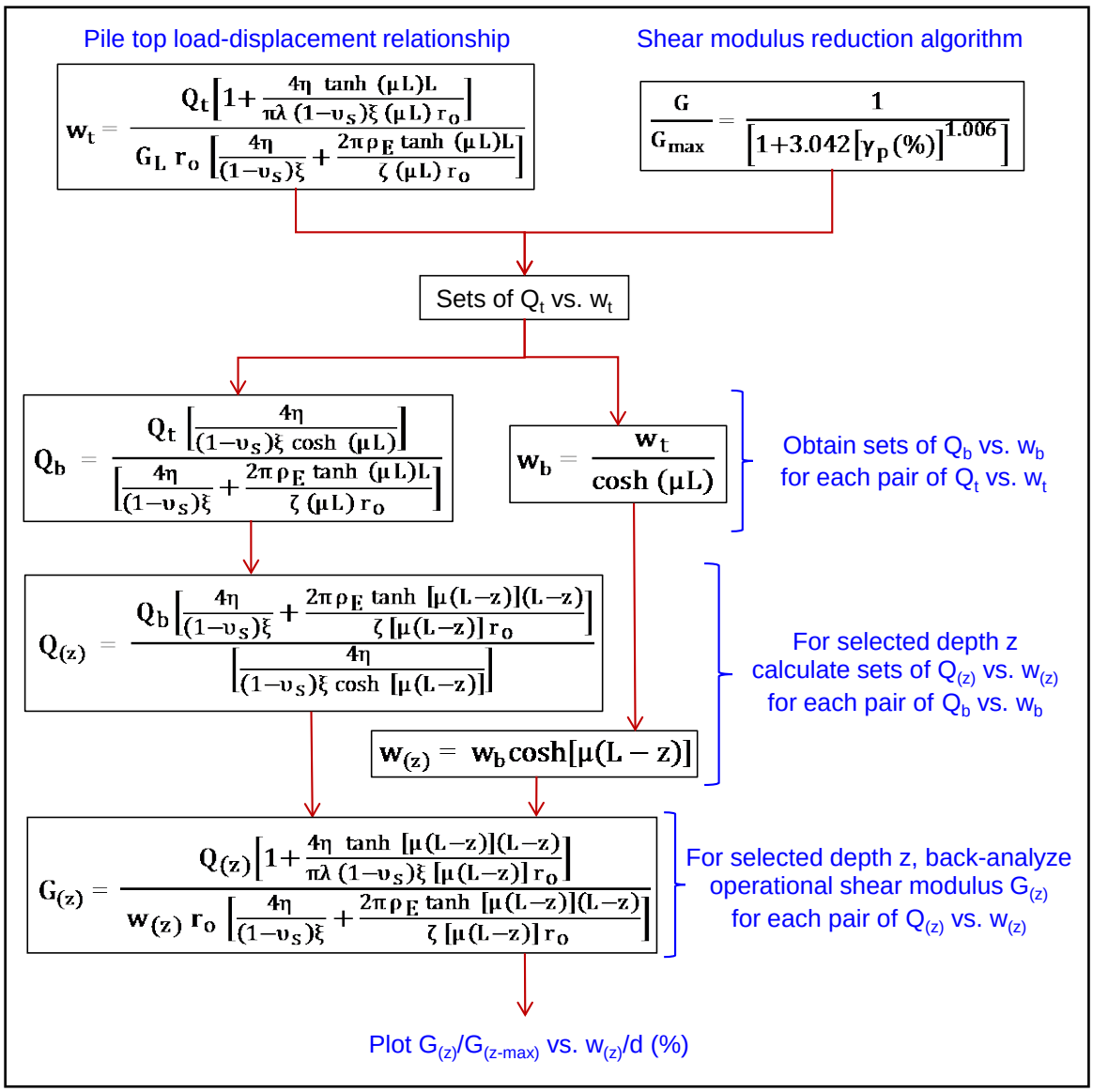

Figure 10.5. Flow chart showing example steps for plotting shear modulus reduction curves at selected depths using solution for compressible stacked pile model.

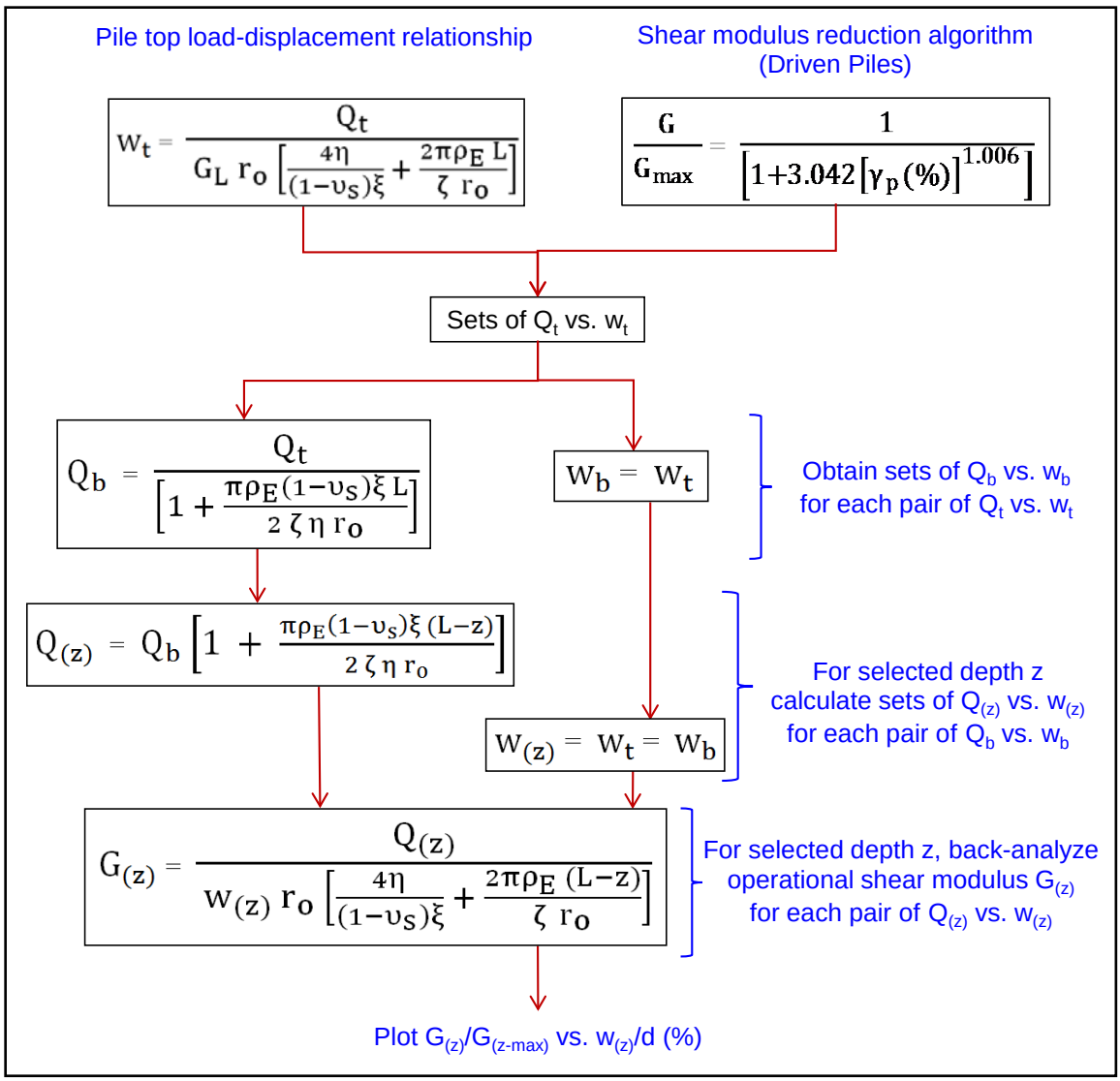

Figure 10.6. Flow chart showing example steps for plotting shear modulus reduction curves at selected depths using solution for rigid stacked pile model.

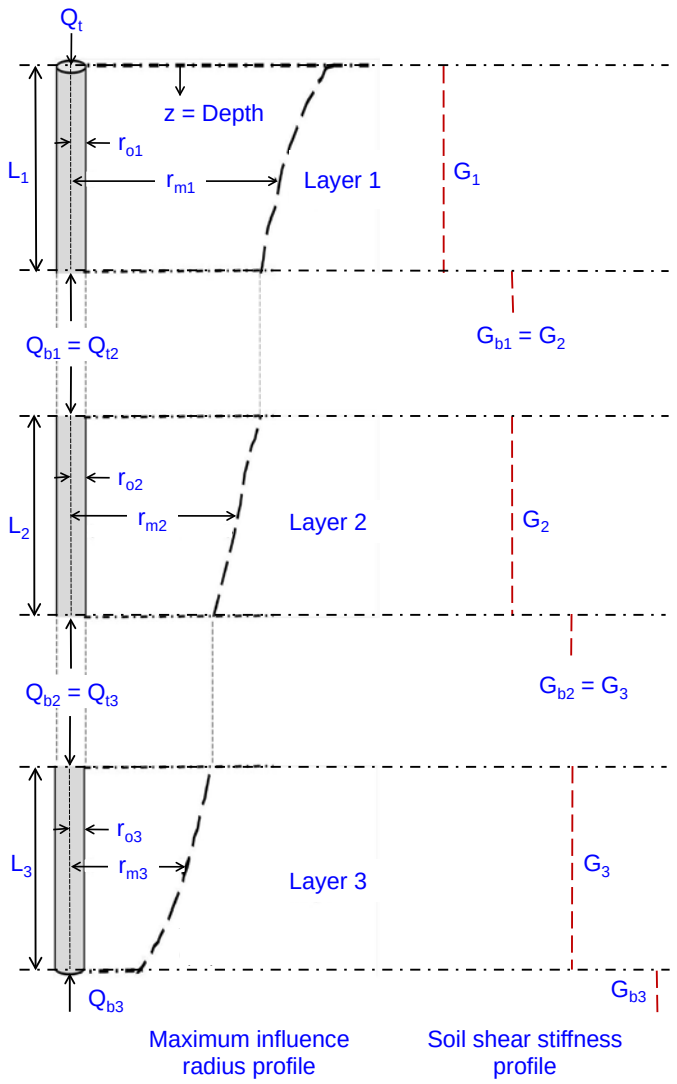

Solution for layer 1

$$w_t = \frac{Q_t\left[1 + \frac{4\eta_1 \tanh(\mu L_1) L_1}{\pi\lambda_1(1-\upsilon_{s1})\xi_1 (\mu L_1) r_{o1}}\right]}{G_1 r_{o1}\left[\frac{4\eta_1}{(1-\upsilon_{s1})\xi_1} + \frac{2\pi\rho_{E1}\tanh(\mu L_1) L_1}{\zeta_1 (\mu L_1) r_{o1}}\right]} + w_{t2}$$

$$\frac{Q_{b1}}{Q_t} = \frac{\left[\frac{4\eta_1}{(1-\upsilon_{s1})\xi_1 \cosh(\mu L_1)}\right]}{\left[\frac{4\eta_1}{(1-\upsilon_{s1})\xi_1} + \frac{2\pi\rho_{E1}\tanh(\mu L_1) L_1}{\zeta_1 (\mu L_1) r_{o1}}\right]}$$

- w_t = cumulative settlement at the pile top
- $\eta_1 = r_{o2}/r_{o1}$
- $\mu L_1 = [2/(\zeta_1\lambda_1)]^{0.5}\cdot(L_1/r_{o1})$
- $\zeta_1 = \ln(r_{m1}/r_{o1})$
- $r_{m1} = (L_1 + L_2 + L_3)\cdot\{0.25 + \xi_1\cdot[2.5\,\rho_{E1}\cdot(1-\nu_{s1}) - 0.25]\}$
- $\lambda_1 = E_p/G_1$
- $\xi_1 = G_{L1}/G_{b1}$
- $G_{b1} = G_2$
- $\rho_{E1} = 1$
- $G_{M1} = G_{o1} = G_{L1} = G_1$
- ν_{s1} = Poisson's ratio of soil in layer 1
- $Q_{b1} = Q_{t2}$

Solution for layer 2

$$w_{t2} = \frac{Q_{t2}\left[1 + \frac{4\eta_2 \tanh(\mu L_2) L_2}{\pi\lambda_2(1-\upsilon_{s2})\xi_2 (\mu L_2) r_{o2}}\right]}{G_2 r_{o2}\left[\frac{4\eta_2}{(1-\upsilon_{s2})\xi_2} + \frac{2\pi\rho_{E2}\tanh(\mu L_2) L_2}{\zeta_2 (\mu L_2) r_{o2}}\right]} + w_{t3}$$

$$\frac{Q_{b2}}{Q_{t2}} = \frac{\left[\frac{4\eta_2}{(1-\upsilon_{s2})\xi_2 \cosh(\mu L_2)}\right]}{\left[\frac{4\eta_2}{(1-\upsilon_{s2})\xi_2} + \frac{2\pi\rho_{E2}\tanh(\mu L_2) L_2}{\zeta_2 (\mu L_2) r_{o2}}\right]}$$

- w_{t2} = cumulative settlement at the top of layer 2
- $\eta_2 = r_{o3}/r_{o2}$
- $\mu L_2 = [2/(\zeta_2\lambda_2)]^{0.5}\cdot(L_2/r_{o2})$
- $\zeta_2 = \ln(r_{m2}/r_{o2})$
- $r_{m2} = (L_2 + L_3)\cdot\{0.25 + \xi_2\cdot[2.5\,\rho_{E2}\cdot(1-\nu_{s2}) - 0.25]\}$
- $\lambda_2 = E_p/G_2$
- $\xi_2 = G_{L2}/G_{b2}$
- $G_{b2} = G_3$
- $\rho_{E2} = 1$
- $G_{M2} = G_{o2} = G_{L2} = G_2$
- ν_{s2} = Poisson's ratio of soil in layer 2
- $Q_{b2} = Q_{t3}$

Solution for layer 3

$$w_{t3} = \frac{Q_{t3}\left[1 + \frac{4\eta_3 \tanh(\mu L_3) L_3}{\pi\lambda_3(1-\upsilon_{s3})\xi_3 (\mu L_3) r_{o3}}\right]}{G_3 r_{o3}\left[\frac{4\eta_3}{(1-\upsilon_{s3})\xi_3} + \frac{2\pi\rho_{E3}\tanh(\mu L_3) L_3}{\zeta_3 (\mu L_3) r_{o3}}\right]}$$

$$\frac{Q_{b3}}{Q_{t3}} = \frac{\left[\frac{4\eta_3}{(1-\upsilon_{s3})\xi_3 \cosh(\mu L_3)}\right]}{\left[\frac{4\eta_3}{(1-\upsilon_{s3})\xi_3} + \frac{2\pi\rho_{E3}\tanh(\mu L_3) L_3}{\zeta_3 (\mu L_3) r_{o3}}\right]}$$

$$w_{b3} = \frac{w_{t3}}{\cosh(\mu L_3)}$$

- w_{t3} = settlement at the top of layer 3
- $\eta_3 = r_b/r_{o3}$
- $\mu L_3 = [2/(\zeta_3\lambda_3)]^{0.5}\cdot(L_3/r_{o3})$
- $\zeta_3 = \ln(r_{m3}/r_{o3})$
- $r_{m3} = L_3\cdot\{0.25 + \xi_3\cdot[2.5\,\rho_{E3}\cdot(1-\nu_{s3}) - 0.25]\}$
- $\lambda_3 = E_p/G_3$
- $\xi_3 = G_{L3}/G_{b3}$
- G_{b3} = shear stiffness beneath pile base
- $\rho_{E3} = 1$
- $G_{M3} = G_{o3} = G_{L3} = G_3$
- ν_{s3} = Poisson's ratio of soil in layer 3
- w_{b3} = displacement at the pile base

Figure 10.7. Analytical elastic continuum solution for compressible stacked pile model in four-layer soil media.

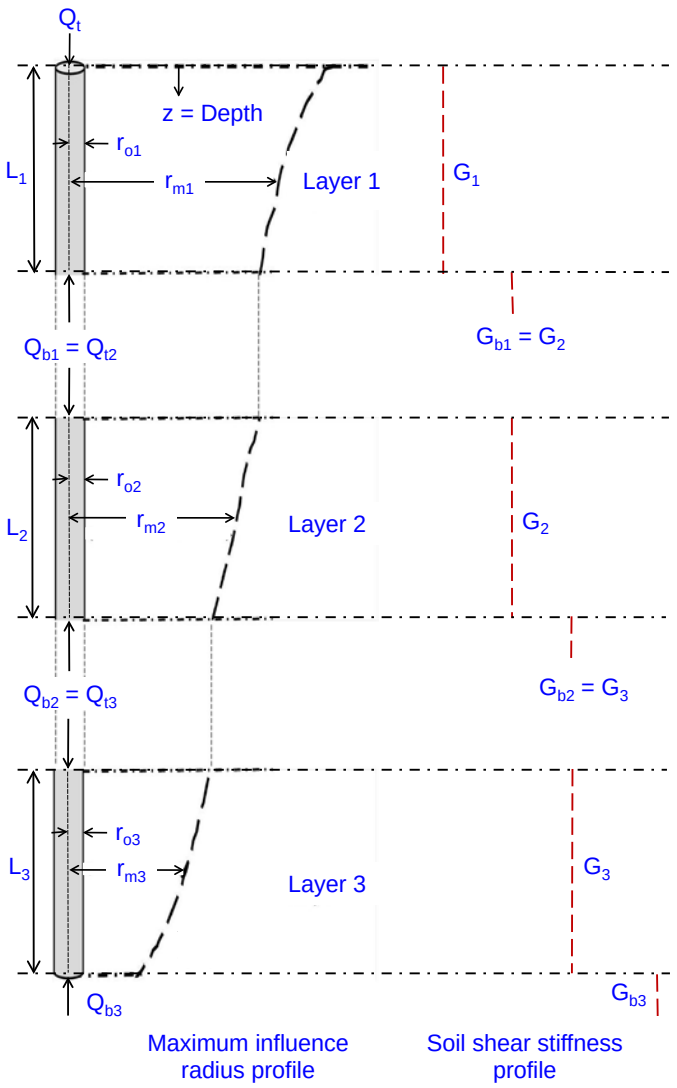

Solution for layer 1

$$w_t = \frac{Q_t}{G_1 r_{o1}\left[\frac{4\eta_1}{(1-\upsilon_{S1})\xi_1} + \frac{2\pi\rho_{E1} L_1}{\zeta_1 r_{o1}}\right]} = w_{t2} \qquad \frac{Q_{b1}}{Q_t} = \frac{1}{\left[1 + \frac{\pi\rho_{E1}(1-\upsilon_{S1})\xi_1 L_1}{2\zeta_1 \eta_1 r_{o1}}\right]}$$

- w_t = cumulative settlement at the pile top
- $\eta_1 = r_{o2}/r_{o1}$
- $\zeta_1 = \ln(r_{m1}/r_{o1})$
- $r_{m1} = (L_1 + L_2 + L_3)\cdot\{0.25 + \xi_1\cdot[2.5\,\rho_{E1}\cdot(1 - \nu_{s1}) - 0.25]\}$
- $\xi_1 = G_{L1}/G_{b1}$
- $G_{b1} = G_2$
- $\rho_{E1} = 1$
- $G_{M1} = G_{o1} = G_{L1} = G_1$
- ν_{s1} = Poisson's ratio of soil in layer 1
- $Q_{b1} = Q_{t2}$

Solution for layer 2

$$w_{t2} = \frac{Q_{t2}}{G_2 r_{o2}\left[\frac{4\eta_2}{(1-\upsilon_{S2})\xi_2} + \frac{2\pi\rho_{E2} L_2}{\zeta_2 r_{o2}}\right]} = w_{t3} \qquad \frac{Q_{b2}}{Q_{t2}} = \frac{1}{\left[1 + \frac{\pi\rho_{E2}(1-\upsilon_{S2})\xi_2 L_2}{2\zeta_2 \eta_2 r_{o2}}\right]}$$

- w_{t2} = cumulative settlement at the top of layer 2
- $\eta_2 = r_{o3}/r_{o2}$
- $\zeta_2 = \ln(r_{m2}/r_{o2})$
- $r_{m2} = (L_2 + L_3)\cdot\{0.25 + \xi_2\cdot[2.5\,\rho_{E2}\cdot(1 - \nu_{s2}) - 0.25]\}$
- $\xi_2 = G_{L2}/G_{b2}$
- $G_{b2} = G_3$
- $\rho_{E2} = 1$
- $G_{M2} = G_{o2} = G_{L2} = G_2$
- ν_{s2} = Poisson's ratio of soil in layer 2
- $Q_{b2} = Q_{t3}$

Solution for layer 3

$$w_{t3} = \frac{Q_{t3}}{G_3 r_{o3}\left[\frac{4\eta_3}{(1-\upsilon_{S3})\xi_3} + \frac{2\pi\rho_{E3} L_3}{\zeta_3 r_{o3}}\right]} \qquad \frac{Q_{b3}}{Q_{t3}} = \frac{1}{\left[1 + \frac{\pi\rho_{E3}(1-\upsilon_{S3})\xi_3 L_3}{2\zeta_3 \eta_3 r_{o3}}\right]}$$

$$w_{b3} = w_{t3} = w_{t2} = w_t$$

- w_{t3} = settlement at the top of layer 3
- $\eta_3 = r_b/r_{o3}$
- $\zeta_3 = \ln(r_{m3}/r_{o3})$
- $r_{m3} = L_3\cdot\{0.25 + \xi_3\cdot[2.5\,\rho_{E3}\cdot(1 - \nu_{s3}) - 0.25]\}$
- $\xi_3 = G_{L3}/G_{b3}$
- G_{b3} = shear stiffness beneath pile base
- $\rho_{E3} = 1$
- $G_{M3} = G_{o3} = G_{L3} = G_3$
- ν_{s3} = Poisson's ratio of soil in layer 3
- w_{b3} = displacement at the pile base

Figure 10.8. Analytical elastic continuum solution for rigid stacked pile model in four-layer soil media.

10.1.4 Elastic Continuum Solution for O-cell Loading

The efficient approach of utilizing the Randolph-type closed-form analytical elastic solution was extended for evaluating the static pile response of bidirectional O-cell loadings. The following adaptations were made: (1) appropriate modifications to handle the loadings in two directions including reduced maximum radius of influence (r_m) for the upper shaft segment, and (2) development of non-linear stiffness reduction model, derived from the back-analysis of O-cell pile load tests. Accordingly, a modified analytical solution was presented for the two most common cases of O-cell loading arrangements: (1) case A: single-stage (one O-cell), and (2) case B: multi-stage (two O-cells) (see Table 10.1). The retro-investigation on 16 O-cell load tests from 9 sites indicated clear variations in the stiffness reduction trends for the upper, middle and lower shaft segments. Accordingly, the three sets were separately grouped and analyzed.

Further insight into the results of load tests from the database and sensitivity analyses on back-analyzed results indicated that pile slenderness ratio (L/d) and the placement depth of the O-cell, via a defined *L-ratio*, besides the soil stiffness profiles, are the most influential factors on the results of Q-w predictions from the modified solution. Here, the L-ratio = ratio between lengths of shaft segment undergoing loading and that of the shaft segment providing resistance. A stiffness reduction models was proposed and analyzed. For the predictor variables, this model uses the significant input parameters of the modified solution identified from sensitivity analysis. Accordingly, the modulus reduction algorithms for the three shaft segments, showing their applicable parameters are given in Equations (10.1) to (10.3) below:

Lower segment downward:

$$\frac{G_{L3}}{G_{L\,max3}} = 0.032\left[\gamma_{p3}\,(\%)\right]^{-0.59}\left(\frac{L_3}{d_{s3}}\right)^{0.24}\left[L-\text{ratio}_{(\text{lower})}\right]^{0.13}(\upsilon_{s3})^{-1.06} \qquad (10.1)$$

Middle segment downward:

$$\frac{G_{L2}}{G_{L\,max2}} = 0.007\left[\gamma_{p2}\,(\%)\right]^{-0.52}\left(\frac{L_2}{d_{s2}}\right)^{1.22}\left[L-\text{ratio}_{(middle)}\right]^{-0.98}(\upsilon_{s2})^{0.03}(\rho_{E2})^{0.5} \quad (10.2)$$

Upper segment upward:

$$\frac{G_{L1}}{G_{L\,max1}} = 0.026\left[\gamma_{p1}\,(\%)\right]^{-0.55}\left(\frac{L_1}{d_{s1}}\right)^{0.38}\left[L-\text{ratio}_{(upper)}\right]^{-0.2}(\upsilon_{s1})^{-0.18}(\xi_1)^{-0.63} \quad (10.3)$$

Table 10.1. Modified closed form analytical solutions for two cases of O-cell pile loading.

	Case A (see Figure 9.1)	Case B (see Figure 9.2)
Total pile load	$Q_t = Q_{t1} + Q_{t2} = (Q_{s1} + W_{buoyant}) + (Q_{s2} + Q_b)$ $= [\Sigma(f_{p1}\cdot\pi\cdot d_{s1}\cdot L_1) + \gamma_{buoyant\ (upper\ pile\ shaft)}\cdot\pi\cdot d_{s1}^2\cdot L_1/4] +$ $[\Sigma(f_{p2}\cdot\pi\cdot d_{s2}\cdot L_2) + q_b\cdot\pi\cdot d_b^2/4]$	$Q_t = Q_{t1} + Q_{t2} = (Q_{s1} + W_{buoyant} + Q_{s2}) + (Q_{s3} + Q_b)$ $= [\Sigma(f_{p1}\cdot\pi\cdot d_{s1}\cdot L_1) + \gamma_{buoyant\ (upper\ pile\ shaft)}\cdot\pi\cdot d_{s1}^2\cdot L_1/4 +$ $\Sigma(f_{p2}\cdot\pi\cdot d_{s2}\cdot L_2)] + [\Sigma(f_{p3}\cdot\pi\cdot d_{s3}\cdot L_3) + q_b\cdot\pi\cdot d_b^2/4]$
Upper shaft response	$w_{s1} = \frac{(Q_{s1} + W_{buoyant})\,\zeta_1\,\mu L_1}{2\pi\,G_{L1}\,\rho_{E1}\tanh(\mu L_1)L_1}$	$w_{s1} = \frac{(Q_{s1} + W_{buoyant})\,\zeta_1\,\mu L_1}{2\pi\,G_{L1}\,\rho_{E1}\tanh(\mu L_1)L_1}$
Middle shaft response	Not applicable	$w_{s2} = \frac{Q_{s2}\,\zeta_2\,\mu L_2}{2\pi\,G_{L2}\,\rho_{E2}\tanh(\mu L_2)L_2}$
Lower shaft + base response	$w_{s2} = \frac{(Q_{s2} + Q_b)\left[1 + \frac{4\eta_2\tanh(\mu L_2)L_2}{\pi\lambda_2(1-\upsilon_{s2})\xi_2\,\mu L_2\,r_{o2}}\right]}{G_{L2}\,r_{o2}\left[\frac{4\eta_2}{(1-\upsilon_{s2})\xi_2} + \frac{2\pi\rho_{E2}\tanh(\mu L_2)L_2}{\zeta_2\,\mu L_2\,r_{o2}}\right]}$	$w_{s3} = \frac{(Q_{s3} + Q_b)\left[1 + \frac{4\eta_3\tanh(\mu L_3)L_3}{\pi\lambda_3(1-\upsilon_{s3})\xi_3\,\mu L_3\,r_{o3}}\right]}{G_{L3}\,r_{o3}\left[\frac{4\eta_3}{(1-\upsilon_{s3})\xi_3} + \frac{2\pi\rho_{E3}\tanh(\mu L_3)L_3}{\zeta_3\,\mu L_3\,r_{o3}}\right]}$
Additional comments	The respective maximum radius of influence should be calculated from the following expression: $r_{m1} = \left(\frac{G_{M\,max1}}{G_{L\,max1}}\right) L_1\left[0.25 + \xi_1\left[2.5\rho_{E1}(1 - \upsilon_{s1})\right] - 0.25\right]$ $r_{m2} = L_2\left[0.25 + \xi_2\left[2.5\rho_{E2}(1 - \upsilon_{s2})\right] - 0.25\right]$ w_{s1}= upward movement at the top of O-cell w_{s2}= downward movement at the bottom of O-cell ν_{s1} and ν_{s2} are respective soil's Poisson's ratios for upper and lower soil layers	The respective maximum radius of influence should be calculated from the following expression: $r_{m1} = \left(\frac{G_{M\,max1}}{G_{L\,max1}}\right) L_1\left[0.25 + \xi_1\left[2.5\rho_{E1}(1 - \upsilon_{s1})\right] - 0.25\right]$ $r_{m2} = L_2\left[0.25 + \xi_2\left[2.5\rho_{E2}(1 - \upsilon_{s2})\right] - 0.25\right]$ $r_{m3} = L_3\left[0.25 + \xi_3\left[2.5\rho_{E3}(1 - \upsilon_{s3})\right] - 0.25\right]$ w_{s1}= upward movement at the top of upper O-cell w_{s2}=downward movement at the bottom of upper O-cell w_{s3}=downward movement at the bottom of lower O-cell $\nu_{s1,}$ ν_{s2} and ν_{s3} are respective soil's Poisson ratios for upper, middle and lower soil layers

Notes: $W_{buoyant}$ = buoyant weight of pile shaft segment above the O-cell; d_s = shaft diameter; f_p = unit shaft resistance; d_b = pile base diameter; q_b = unit base resistance.

10.2 Recommendations

Based on the findings of this research, following recommendations are offered towards future application and research on cone penetrometer based pile evaluations:

10.2.1 Application of the Design Formulations

Due caution must be exercised when applying these semi-empirical approaches to field situations of relevance encountered in design practice. Any application of the derived trends should be made with careful engineering judgment, as true for any and all empirical methods.

10.2.2 Calibration and Validation of Research Results

The research results presented in this dissertation were based on a large variety of pile types. However the number of piles in certain categories (e.g., pre-stressed precast concrete piles) is much less than the others. Similarly, the driven piles form the largest part of the database, compared with jacked, augered, or bored. As a consequence, a certain degree of bias should be expected in the derived results. Accordingly, further calibration with additional data should be conducted to help validate and/or improve the proposed design formulations for reliable use in industrial applications. Towards that, the latest Deep Foundations Load Test Database (DFLTD), comprising of 1307 load tests conducted between the years 1985 and 2003 from all over the world, which has recently been released (in October 2013) by the Federal Highway Administration (FHWA) can be of great use in this calibration effort.

10.2.3 Further Improvement of O-cell Evaluations

The O-cell load test dataset (Group 3) was small and limited in application to bored piles only, although other applications are also known to have been made (e.g., driven piles, continuous flight auger, and Fundex piles). A future collaborative research

effort with Loadtest Incorporated (the most fervent firm in promoting the bidirectional O-cell) should be explored. In such a study, two components of field testing [i.e., the latest and extended O-cell database on wider variety of piles and the seismic piezocone testing (SCPT)] must be combined with focused direction of improving the formulations for O-cell evaluations presented in this dissertation.

10.2.4 Extension of Modified UniCone Method to Stiff Soils of Zones 8 and 9

In developing the Modified UniCone Method, the CPT material index I_c (Robertson 2009) was used to provide continuous functions for shaft and toe correlation coefficients. Based on the existing data, it was possible to first identify sensitive soils of zone 1 at four sites, enabling establishment of their separate correlations. However, not enough sites in the current database presented distinctly viable layers indicating stiff soils of zone 8 ($1.5\% < F_r < 4.5\%$) and zone 9 ($F_r > 4.5\%$). An effort should be made to find pile load test sites particularly of stiff soils clearly falling in zones 8 and 9 and apply a methodology similar to the one used for zone 1 in establishing their separate continuous functions. Following equation should be used in identifying zones 8 and 9:

$$Q_{tn} > 1/[0.005(F_r - 1) - 0.0003(F_r - 1)^2 - 0.002] \quad (10.4)$$

10.2.5 Adjustments for Pile Loading Rates

The adjustment factor for pile loading rate (θ_{rate}) introduced for shaft correlation coefficient in the Modified UniCone Method was based on the assumption that all maintained load tests (MLT) and all constant rate of penetration tests (CRPT) in the database were loaded at identical rates within their respective categories. Of course, this was not the case, however, because of inadequate documentation and unavailability of information on the applied loading rates for each and every load test, yet the above

assumption was accepted. This at least provided a sense of the first-order influence of pile loading rate on the I_c based correlations. As such, pile load test measurements are recorded in short term loading and this will differ from the long term pile resistance under structural loads. A more focused research is warranted to better define the rate parameter by testing different varieties of piles representing identical situations (in terms of pile dimensions and geomaterial types) at a wide range of loading rates (e.g., Garner 2007). Extrapolation of the results of such studies can lead to improved evaluation of the long-term structural response of pile foundations.

10.2.6 Improvement of Base Correlation Coefficient

The analysis conducted during the derivation of the Modified UniCone Method reveals that the statistical reliability of estimating unit base resistance (q_b) is much less reliable than that of the unit shaft resistance (f_p). Many important factors are known to affect the q_b of piles (e.g., apparent influence of the pile true end conditions and the loading rate), yet these were not incorporated into the proposed final design equation for base correlation coefficient due to lack of sufficient data. End conditions (i.e., open-ended vs. close-ended) influence the plug length at the pile base, and thus the base capacity. Seemingly, the pile loading rates are also likely to influence the q_b similar to what was established for f_p. The influence of such factors in the current formulation for base correlation coefficient must also be explored, supported by an effort of specific data acquisition related to the measured plugging and loading rates.

10.2.7 Calibration of Stacked Pile Solution

The stacked pile solution is specifically meant to be applied to the sites which present unconventional stiffness profiles. Its application to common homogeneous and general Gibson type soil models entails considerable work without substantially improved results; and is therefore, not recommended for such use. It is recommended

that this solution be calibrated against alternative methods, e.g., load transfer (τ-z) method, different numerical methods etc.

10.2.8 Recommended Use of SCPTu in Future Site Investigations for Pile Design

It was recognized during this research that geotechnical-geophysical in-situ testing using SCPTu provides continuous and multi-tiered data, thus more detailed information is collected at the sites which is of particular relevance and value to deep foundations. Here the geotechnical readings of q_t, f_s and u_2 can be used in pile capacity evaluation, while the V_s readings are of specific value in axial displacement analysis. It is recommended that SCPTu testing be a mandatory part of all future site investigations for pile design. This will enable further refinement of the SCPTu based axial pile evaluations presented in this research for convenient and reliable industrial applications.

10.2.9 Refinement of Stiffness Reduction Algorithms for Sandy Soils

The plasticity index (PI) based stiffness reduction charts for different pile types presented in this research were derived from that data that include few sand sites also, for which a PI value of zero was simply assumed. It is likely that the design charts can be further refined by collecting more data from additional sand sites, treating them separately, and analyzing these on the basis of either relative density information, state parameter, and/or other geotechnical site characteristics.

10.2.10 Applicability of the Proposed Stiffness Reduction Models

The stiffness reduction models proposed herein are specifically meant to be applied to pile foundations within the framework of the elastic continuum solution originally proposed by Randolph and Wroth (1978; 1979), and modified for extended applications in this research for uplift tensile loadings, O-cell loadings, and in multilayer soil media. As such, these models should not be considered for universal application in

other soil-structure interaction problems. However, their reliability must be tested in alternative applications for possible extended use.

10.2.11 Influence of Pile Setup on CPT Estimations

In view of the possible gain in the axial capacity from the long-term pile setup, the following recommendations are made:

- A more focused research should be conducted through the collection of pile-CPTu database on a wide variety of piles installed in different types of geomaterials. The correlations should be developed between the CPTu readings and the results from the first time pile load test. Then, from the results of subsequent load tests on virgin piles of the same type and size, installed at the same site (i.e., in the same stratigraphic profile), time-dependent adjustment factors should be developed to incorporate the pile setup effects.
- Since previous research on pile setup has focused mainly on full-displacement type (driven and jacked) piles, new research directions should be explored for the partial-displacement type (augered) piles and non-displacement type (bored piles or drilled shafts) for clayey, sandy, and mixed soil types.

10.2.12 Influence of Interface between Pile Material and Surrounding Soil

Because of the fact that the stiffness reduction algorithms developed during this research were derived from the back-analyses of actual pile load tests, the pile installation effects as well as the influence of interface between the pile material and the surrounding soils are considered. Han (1997) specifically studied the interface behavior between Fiber Reinforced Polymer (FRP) composite and sands, and modified the elastic continuum solution by Randolph and Wroth (1978; 1979) to model FRP piles and sand interaction. Similar formulations should be developed for different pile-to-soil interfaces

and this may enable calibrations of the stiffness reduction charts developed in this research into a more unified approach.

APPENDIX A

CHARACTERISTICS AND USES OF COMMON PILE TYPES

Table A.1. Typical characteristics and uses of common pile types (adapted from Hannigan et al., 2006).

Pile Type	Typical Lengths (m)	Cross-sections and Materials	Typical Axial Design Loads (kN)	Applications
Drilled Shafts	5 – 75	Concrete filled circular sections (0.3 – 3.5m diameter) with steel reinforcement, with or without partial/full length steel casing	1,500 – 20,000	• Best for firm incompressible soils • Not suited for soft clays, loose sands • Provide high bearing capacity • Toe bearing of a longer shafts mobilizes after substantial displacement of shaft head
Steel Pipe	5 – 50	Hollow circular steel tube of varying thicknesses (8 – 25mm) and diameters (0.2 – 1m) with or without concrete filled core	800 – 2,500 (w/o concrete cores) 2,500 – 15,000 (w/ concrete cores)	• Offshore or nearshore applications as friction, toe-bearing, or a combination • Driven OE or CE • OE: plugged or unplugged • Concrete-filled or left open
Steel H-Sections	5 – 40	Standard or adopted sizes of flanges and web	600 – 2,500	• Easier to drive, used as toe-bearing and as combination shaft resistance and toe-bearing on firm soil or rock
Prestressed/ Precast Concrete	10 – 15 (reinforced) 15 – 40 (prestressed)	Solid or hollow circular, square or octagonal; typical sizes: square: 0.25–0.92m, circular: 0.25 – 0.61m, hollow circular: 0.92 – 1.68m	400 – 1,000 (reinforced) 400 – 4,500 (prestressed)	• Best for corrosive and hard driving environment owing to durability • Act as friction piles in granular soils • Provide high capacity if used as toe-bearing pile

Table A.1 (continued).

Pile Type	Typical Lengths (m)	Cross-sections and Materials	Typical Axial Design Loads (kN)	Applications
Cast-in-Place Concrete (w/ Mandrel)	3 – 40	With or without thin corrugated or plain steel shell (thickness: 0.5 – 3.3mm), concrete filled with or without reinforcement cage; typical diameters: 0.2 – 0.45m	400 – 1,400	• Best as friction pile in granular materials • Unsuitable for soils containing cobbles and boulders
Cast-in-Place Concrete (w/o Mandrel)	5 – 25	Circular steel fluted or spiral welded shell (thickness: 3 – 64mm), concrete filled with or without reinforcement cage; typical diameters: 0.25 – 0.9m	500 – 1,350	• Best as friction pile of medium length
Composite	15 – 65	Typical combinations: precast concrete over HP section, cased or uncased concrete over timber, steel pipe concrete filled over concrete filled steel shell, steel pipe concrete filled over HP section	300 – 1,800	• Longer piles at lesser cost • More suited where higher uplift resistance is required via longer piles • Weakest material governs the allowable capacity • Suitable in waterfront construction where upper soil layers have high corrosion potential

Table A.1 (continued).

Pile Type	Typical Lengths (m)	Cross-sections and Materials	Typical Axial Design Loads (kN)	Applications
Continuous Flight Auger (CFA)	5 – 25	Pressure injected concrete, circular sections along with reinforcement cage; typical diameters: 0.46 – 0.76m	260 – 875	• Best for urban environment since they cause minimal vibration damage to adjacent structures • Good contact on rock for end-bearing • Best as friction pile in granular material
Timber	5 – 23 (Southern Pine) 5 – 37 (Douglas Fir)	Tree trunks of Southern Pine or Douglas Fir treated with preservatives; typical diameters: 0.12 – 0.55m	100 – 500	• Friction pile for modest loads in all soil types below permanent water table • Not suitable for driving through dense gravel, boulders, or till or as toe-bearing pile on rock. • Suitable as bridge fender systems
Micropile	12 – 25	Sand-cement grout filled circular sections along with steel reinforcement bar, with or without steel casing; typical diameters: 0.13 – 0.23m	300 – 1,100	• Suitable for any soil, rock or fill condition • Low noise and vibration, spoil • Excellent for sites with restricted access • Also suitable for soils containing rubble and boulders

APPENDIX B

SCHEMATICS OF PILE LOAD TEST ARRANGEMENTS AND LOAD APPLICATION PROCEDURES

B.1 Schematics of Pile Load Test Arrangements

A static axial load test is conducted for either of the two loading modes, i.e., compression or tension (i.e., uplift through top loading). Herein, the load transfer distribution (Q – z) and load-displacement ($Q_t - w_t$, $Q_s - w_t$, $Q_b - w_t$ and $Q_b - w_b$) measurements are obtained by attaching vibrating wire strain gages, load cells and telltale rods to a pile at different depths along the pile shaft, and a mechanism that allows application of the desired loading scheme. In order to ensure simultaneous data collection via alternative measurement tools, and to compensate for any undesirable damage during driving or casting, enough redundancy of instrumentation can be ensured for load tests conducted for important projects. Figure B.1 provides detailed categorization of the arrangements of different static axial load tests employed in the piling industry. Schematics of the conventional compression type of load tests are shown in Figures B.2 to B.4. For projects where pile foundations are to be subjected to substantial tensile loading (e.g., because of overturning moments applied to the structure through seismic events or extreme winds, or foundations at the anchorage end of permanent cantilevers), it is appropriate to perform pull-out tests (Brown et al., 2010). Some arrangements for conducting the conventional tension tests of deep foundations are shown in Figures B.5 to B.8. Other types of uplift tests are possible, e.g., O-cell tests that can be used to determine resistance to upward directed load.

The details of these test methods can be seen in the relevant ASTM standards. From the worldwide case histories of pile load testing, it has been observed that modifications from the standardized test methods are often done to adapt to the project

requirements, site and environmental constraints, availability of equipment and cost compulsions etc. (e.g., Davies, 1987; Baaijens and Kolk, 2004; Hirany and Kulhawy, 1988). It is also pertinent to mention that at present time, no ASTM standard test method has been formulated for O-cell type of load test and the testing continues to be performed based on the original formulation and refinements and advancements made during the life of this test method. The method of load testing via O-cell specified by LoadTest International, Inc. is detailed below (after Schmertmann et al., 1998).

The movements during an O-cell load test are measured by electronic gages connected to a computerized data acquisition system. Figure B.9 shows the schematics of basic instrumentation for an O-cell load test. The O-cell placed at the required depth along the pile shaft is expanded by pressurizing it via a hydraulic control system at the ground surface and a supply line leading through the pile shaft down to the cell. The hydraulic pressure injected into the O-cell acts equally on the top and bottom bearing plates of the cell. Knowing the areas of the two plates, this pressure is converted into the O-cell load. The total opening (or expansion) of the O-cell is measured by the displacement transducers, the lower ends of which are attached to the bottom bearing plate of the O-cell. The upward movement of the top of the O-cell is measured directly from steel telltales extending down from above the ground to the top of the upper plate of the O-cell. These telltales also allow the measurement of the compression of the test pile. The difference between the upward movement of top of the O-cell and the total extension of the O-cell (as determined by the displacement transducers) provides the downward movement of the bottom plate. The upward movement of the top of the test pile can also be measured directly with dial gages mounted on any reference frame and set over the top of the test pile. Alternatively, the pile compression can be directly measured with telltales and added to the top-of-pile movement to get the top-plate movement. Optical or electronic leveling is used to check both the stability of the reference beam and the top-of-pile movements.

It can be seen from Figure B.9 relating to the above explanations that the O-cell load test method provides two separate movement curves. One shows the upward movement of the pile above the O-cell vs. the O-cell loading, resisted by downward acting side shear plus the buoyant weight of the pile. The other shows the downward movement of the pile below the O-cell, resisted by end bearing plus any upward acting side shear for that part of the pile between its tip and the O-cell. Load testing with the O-cell continues until ultimate skin friction capacity (Q_s), end bearing capacity (Q_b), and/or the maximum O-cell capacity is reached. The loading capacity of the O-cell can be increased by placing multiple O-cells at the same elevation as shown in Figure 2.4. By utilizing multiple O-cells on different elevations, distinct elements within the pile shaft can be isolated for testing in different stages. Based on the economic viability and various cases reported in the literature, six different combinations of O-cell pile load testing are considered practicable (see Figure B.1, and Figures B.10 to B.12).

Typical Q – w and Q – z results obtained from different types of pile load tests are shown in Figures B.13 and B.14, respectively. Besides the types of load test, the types and dimensions of the pile, installation methods, and the types of geomaterials present at the site also dictate the load transfer distribution. The simultaneous mobilization of shaft resistance and end bearing happens at different rates for different cases. For instance, in case of friction type piles, significant shaft resistance mobilizes before the base of the pile feels the effect of the applied top load, resulting in axial deflections being observed at the pile top. As shown by Davies (1987) and Hirany and Kulhawy (1988), Figure B.15 presents some other alternatives of the load-displacement response obtained from static axial compression loading of different soil and pile types.

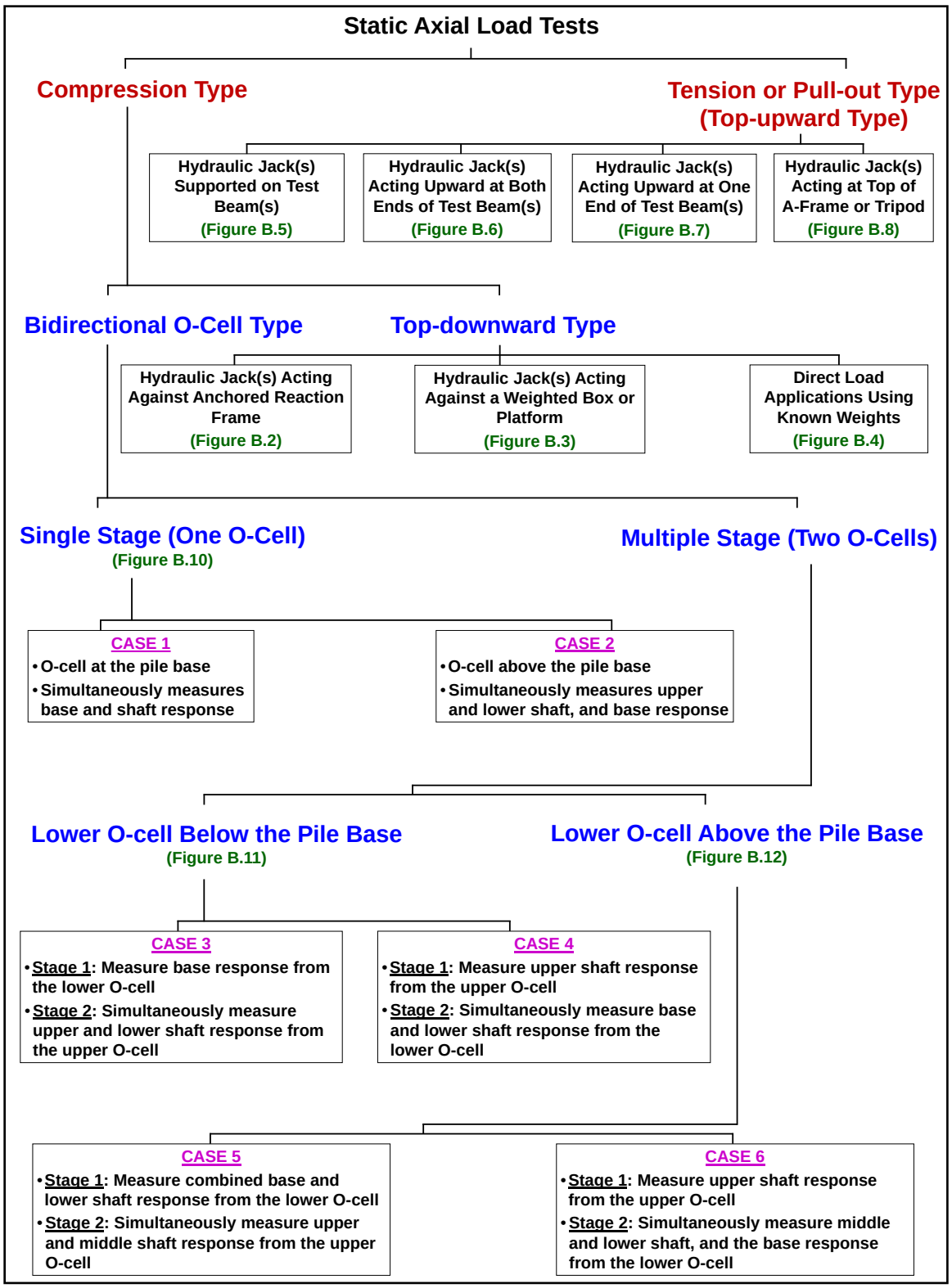

Figure B.1. Different loading modes for static axial pile load tests.

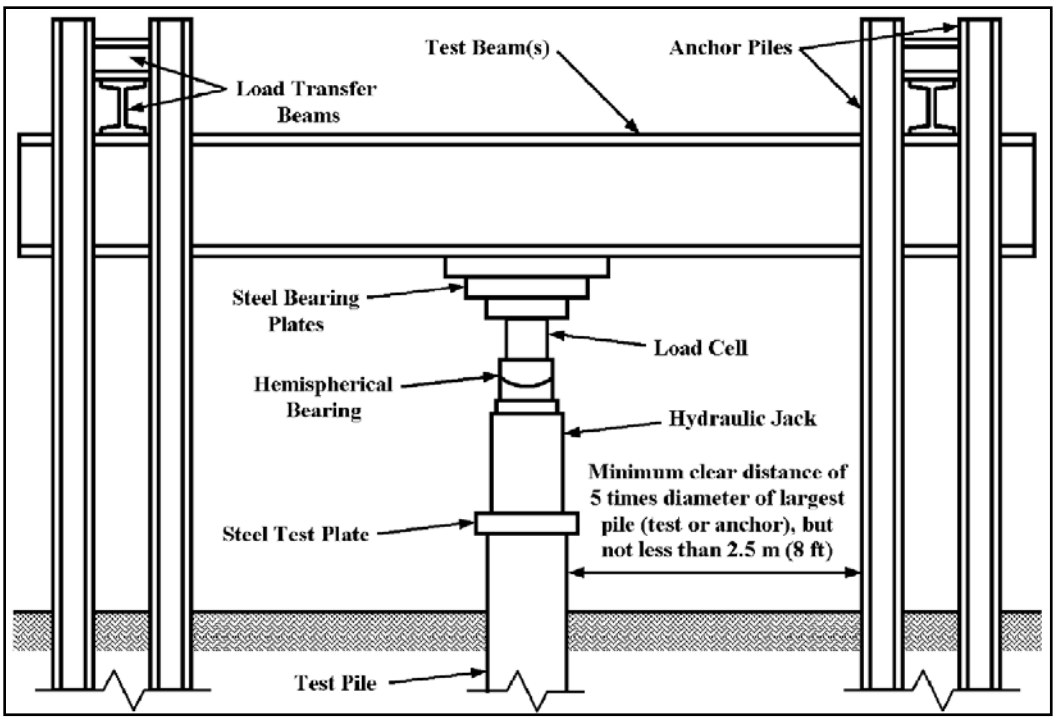

Figure B.2. Schematic of hydraulic jack acting against anchored reaction frame in a typical setup for compression load test (ASTM D1143M – 07).

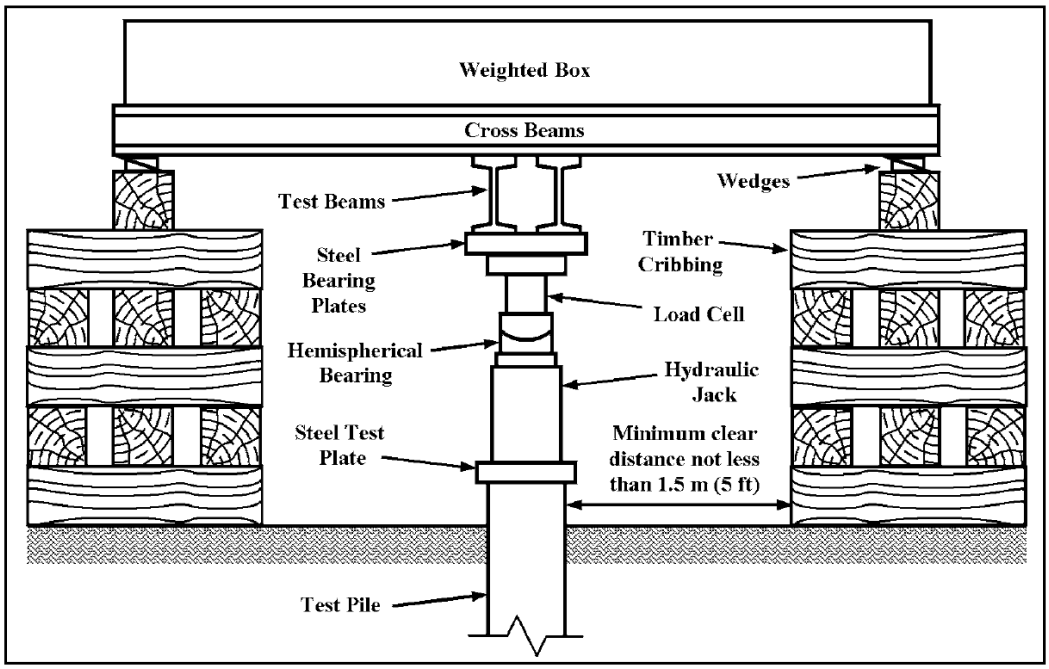

Figure B.3. Schematic hydraulic jack acting against weighted box or platform in a typical setup for compression load test (ASTM D1143M – 07).

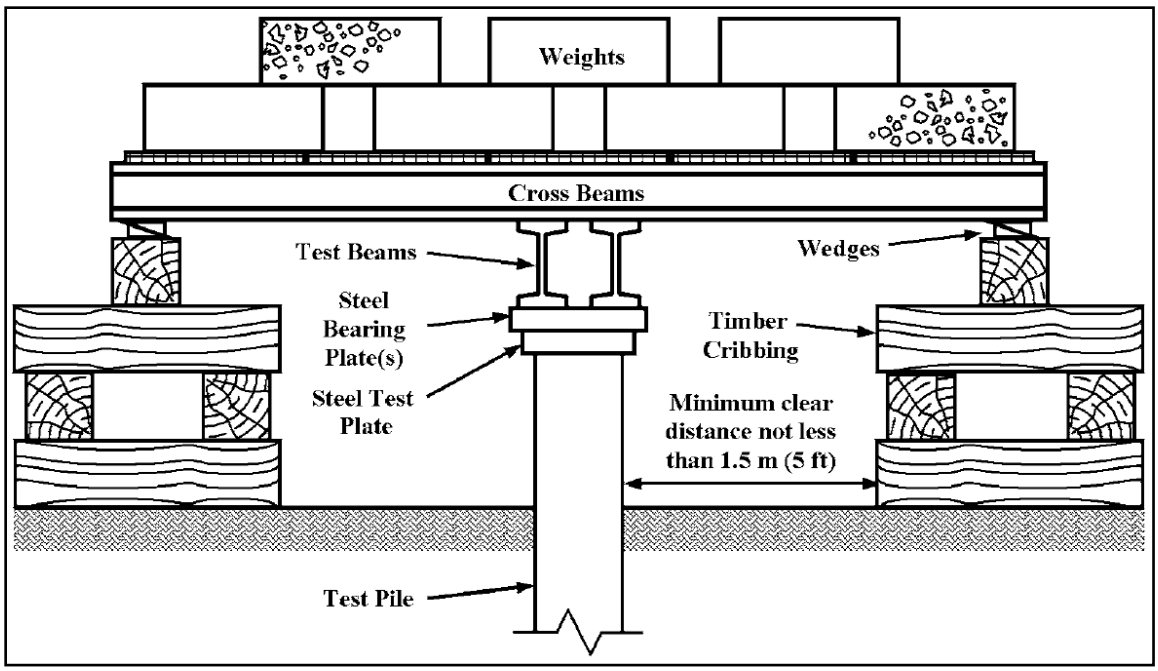

Figure B.4. Schematic of direct loading on a single pile using weighted platform in a typical setup for compression load test (ASTM D1143M – 07).

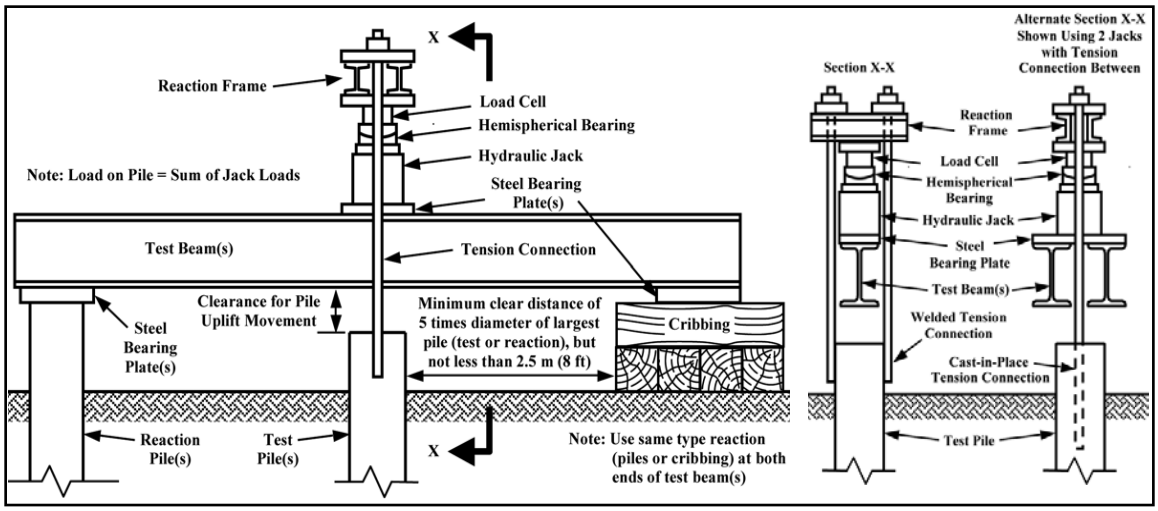

Figure B.5. Typical setup for tensile load test using hydraulic jack(s) supported on test beams (ASTM D3689 – 07).

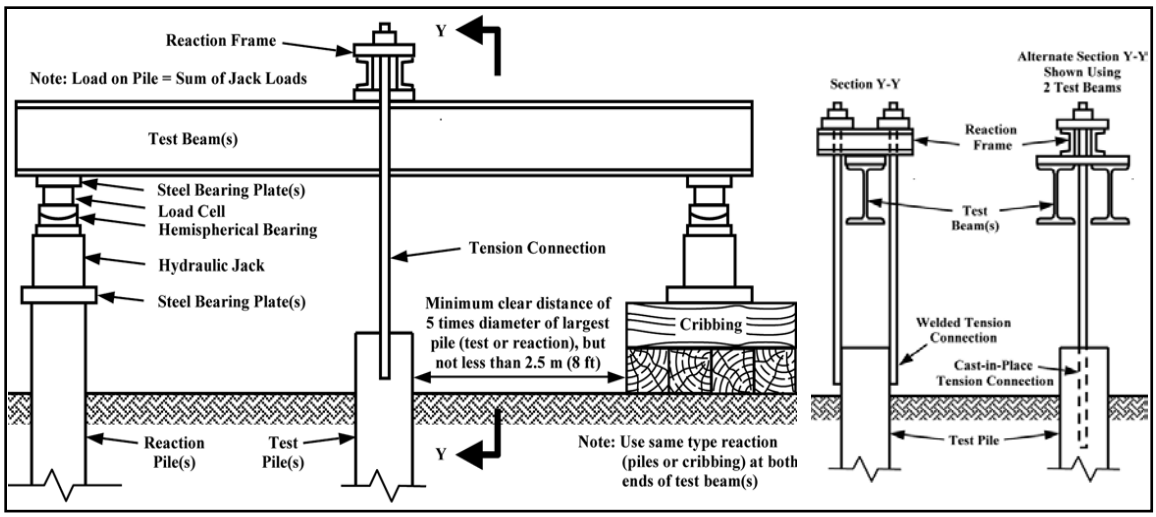

Figure B.6. Typical setup for tensile load test using hydraulic jacks acting upward on both ends of test beam(s) (ASTM D3689 – 07).

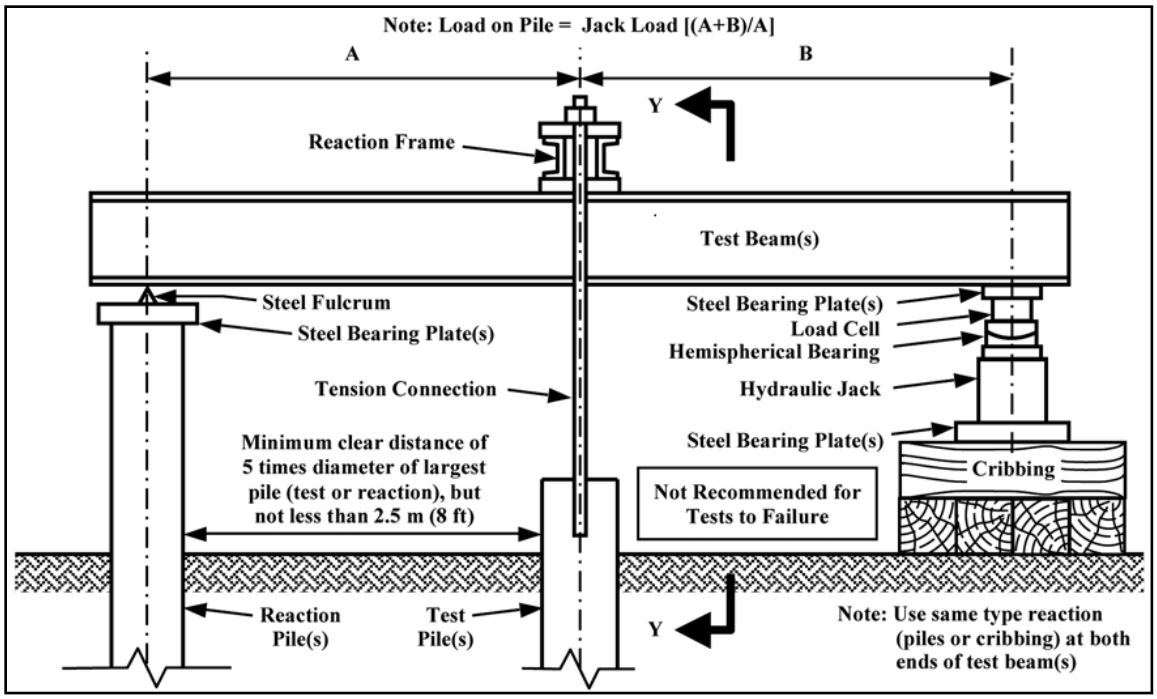

Figure B.7. Typical setup for tensile load test using hydraulic jack(s) acting upward on one end of test beam(s) (ASTM D3689 – 07).

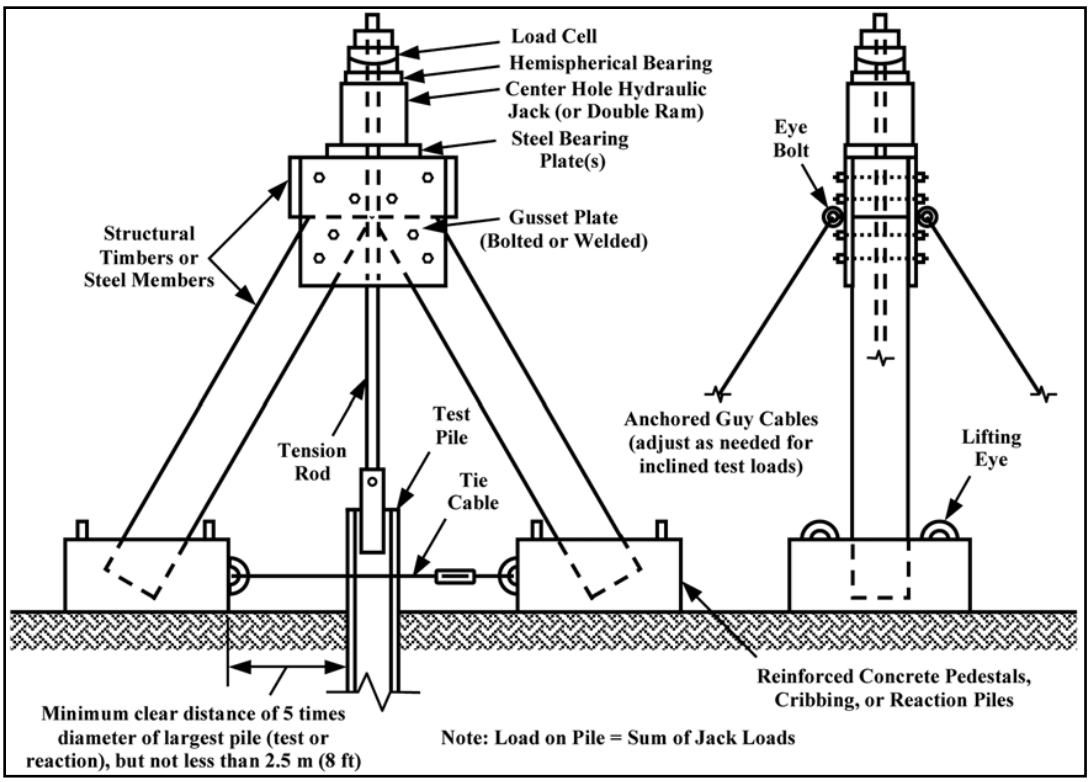

Figure B.8. Typical setup for tensile load test using hydraulic jack(s) acting at top of an A-frame (ASTM D3689 – 07).

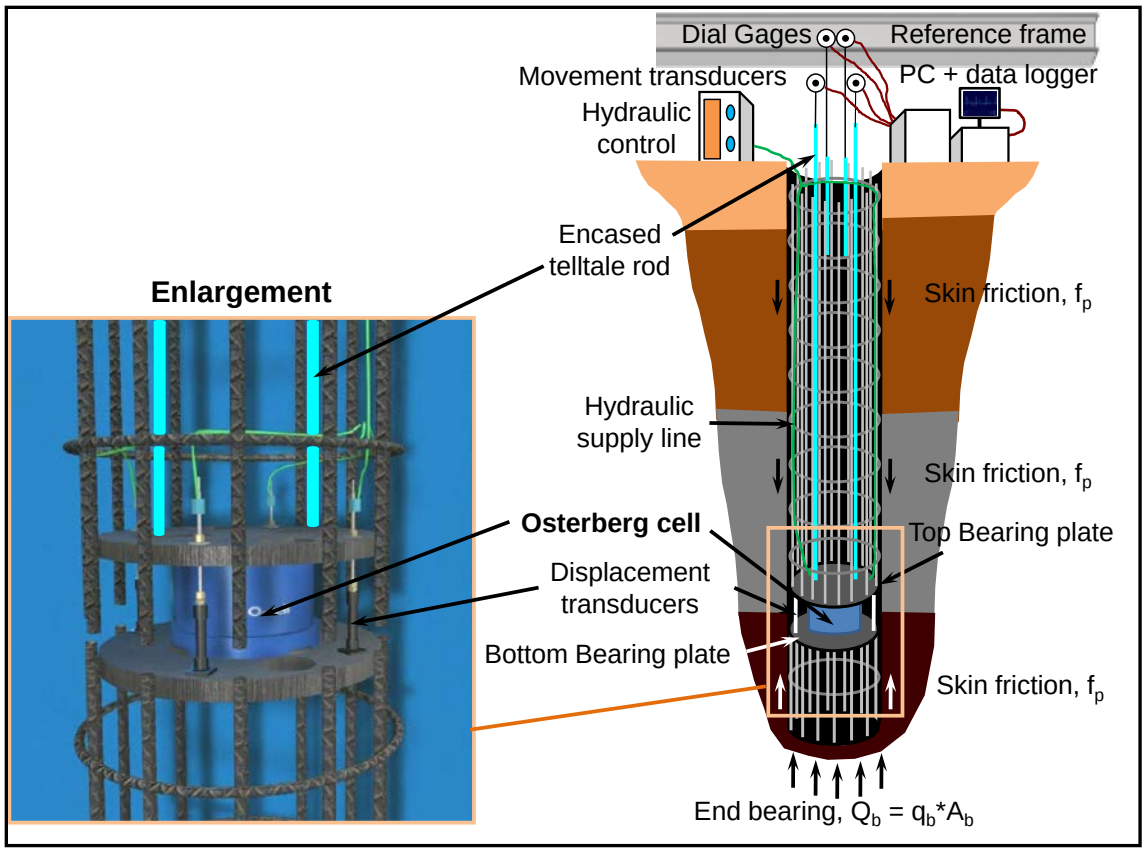

Figure B.9. O-Cell load test arrangement (adapted from LoadTest, 2012).

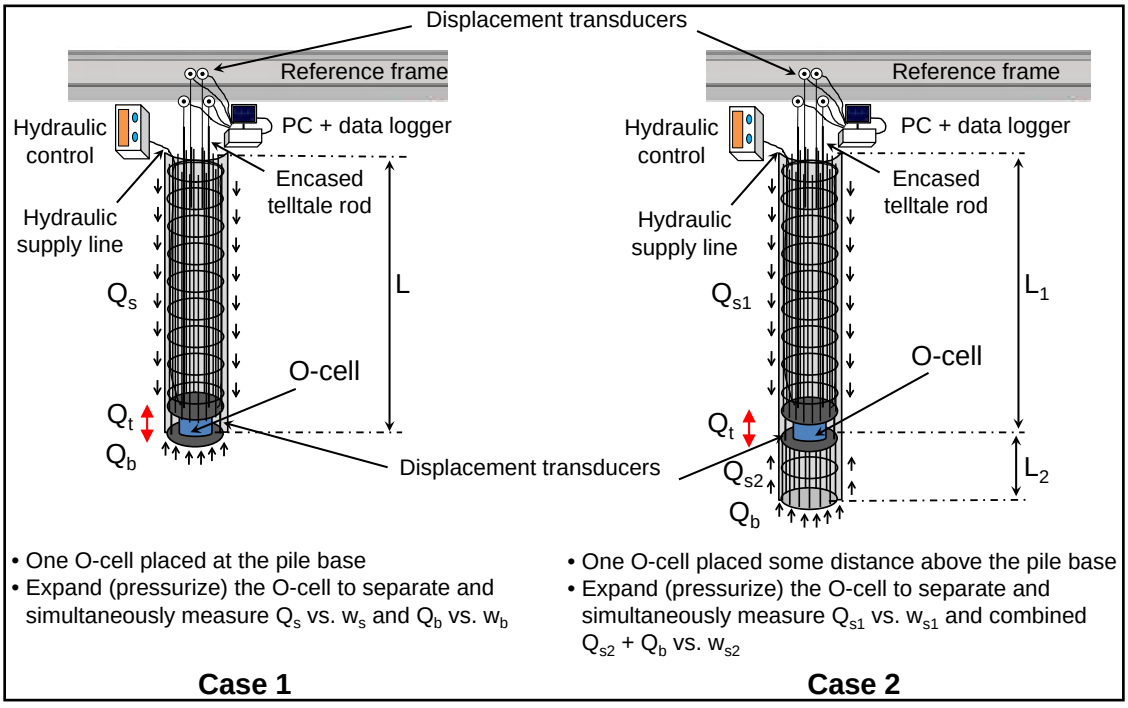

Figure B.10. Typical arrangements of single-stage (one O-cell) load test.

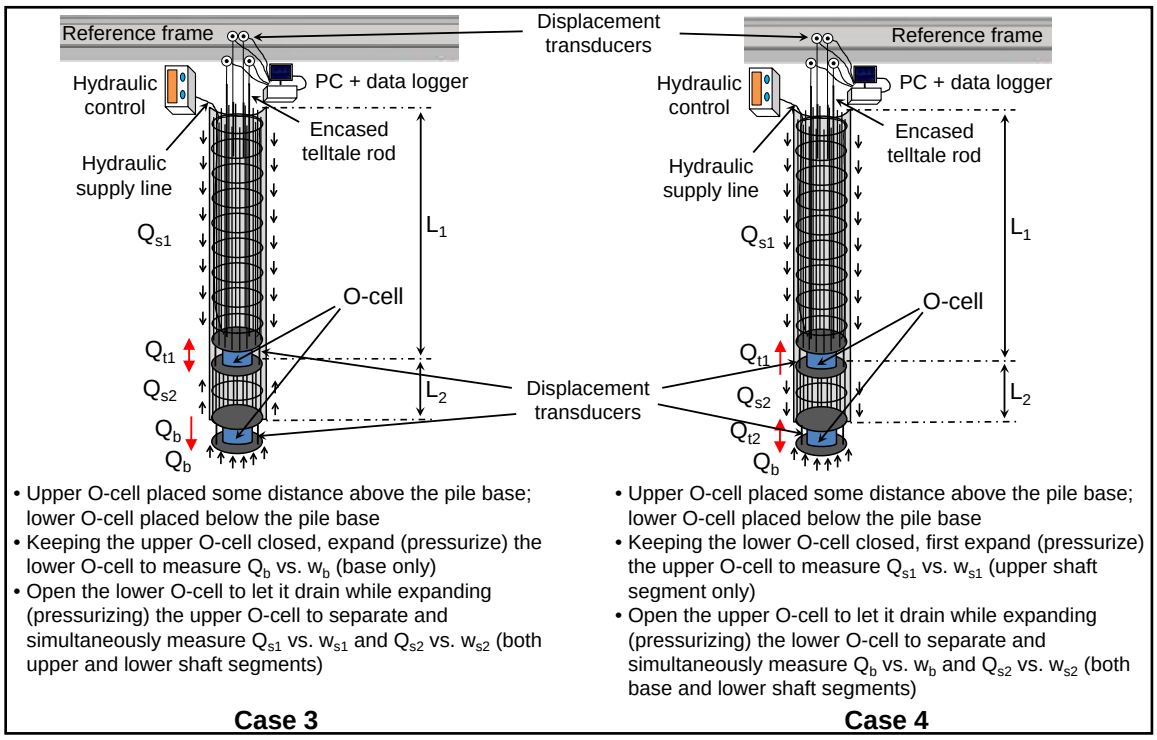

- Upper O-cell placed some distance above the pile base; lower O-cell placed below the pile base
- Keeping the upper O-cell closed, expand (pressurize) the lower O-cell to measure Q_b vs. w_b (base only)
- Open the lower O-cell to let it drain while expanding (pressurizing) the upper O-cell to separate and simultaneously measure Q_{s1} vs. w_{s1} and Q_{s2} vs. w_{s2} (both upper and lower shaft segments)

Case 3

- Upper O-cell placed some distance above the pile base; lower O-cell placed below the pile base
- Keeping the lower O-cell closed, first expand (pressurize) the upper O-cell to measure Q_{s1} vs. w_{s1} (upper shaft segment only)
- Open the upper O-cell to let it drain while expanding (pressurizing) the lower O-cell to separate and simultaneously measure Q_b vs. w_b and Q_{s2} vs. w_{s2} (both base and lower shaft segments)

Case 4

Figure B.11. Typical arrangements of multi-stage (two O-cells) load test (lower O-cell placed below the pile base).

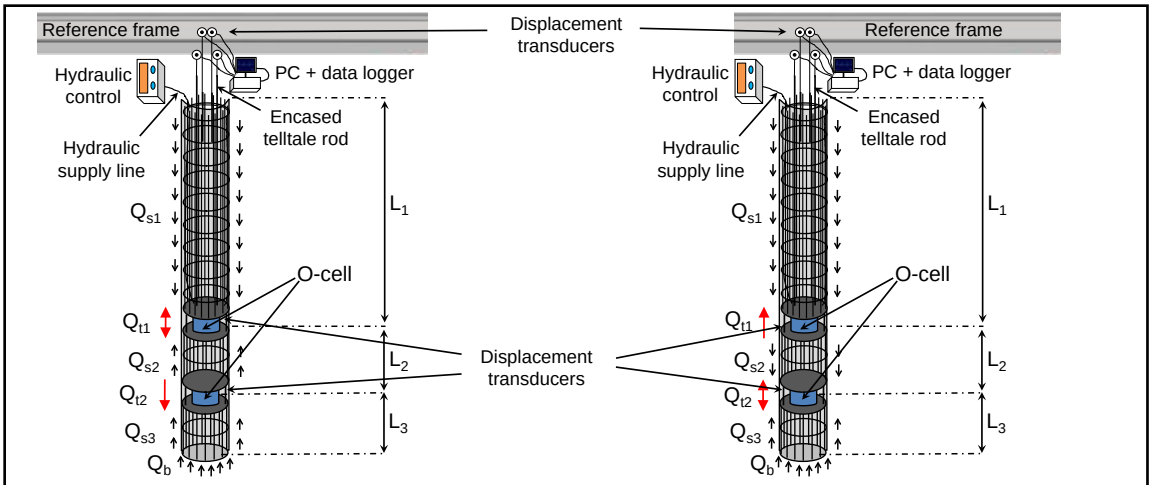

- Upper O-cell placed some distance above the lower O-cell; lower O-cell placed some distance above the pile base
- Allows separate shaft capacity measurements in layered soils
- Keeping the upper O-cell closed, first expand (pressurize) the lower O-cell to measure combined $Q_{s3} + Q_b$ vs. w_{s3} (both base and lower shaft segments)
- Open the lower O-cell to let it drain while expanding (pressurizing) the upper O-cell to separate and simultaneously measure Q_{s1} vs. w_{s1} and Q_{s2} vs. w_{s2} (both upper and middle shaft segments)

Case 5

- Upper O-cell placed some distance above the lower O-cell; lower O-cell placed some distance above the pile base
- Allows separate shaft capacity measurements in layered soils
- Keeping the lower O-cell closed, first expand (pressurize) the upper O-cell to measure Q_{s1} vs. w_{s1} (upper shaft segment only)
- Open the upper O-cell to let it drain while expanding (pressurizing) the lower O-cell to separate and simultaneously measure Q_{s2} vs. w_{s2} and combined $Q_{s3} + Q_b$ vs. w_{s3} (both middle and lower shaft segments, and the base)

Case 6

Figure B.12. Typical arrangements of multi-stage (two O-cells) load test (lower O-cell placed some depth above the pile base).

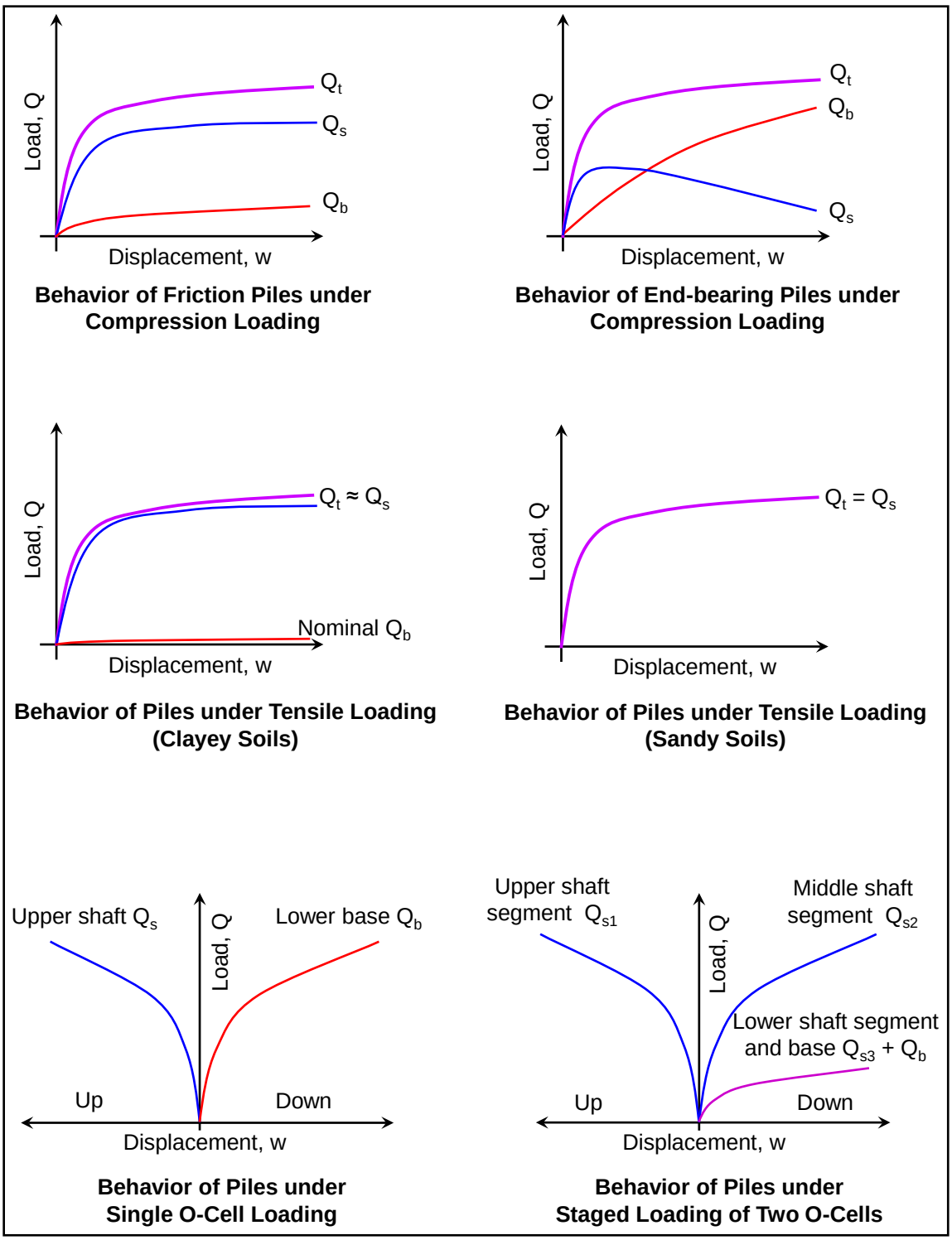

Figure B.13. Typical profiles of load-displacement response for piles tested under different axial loading arrangements.

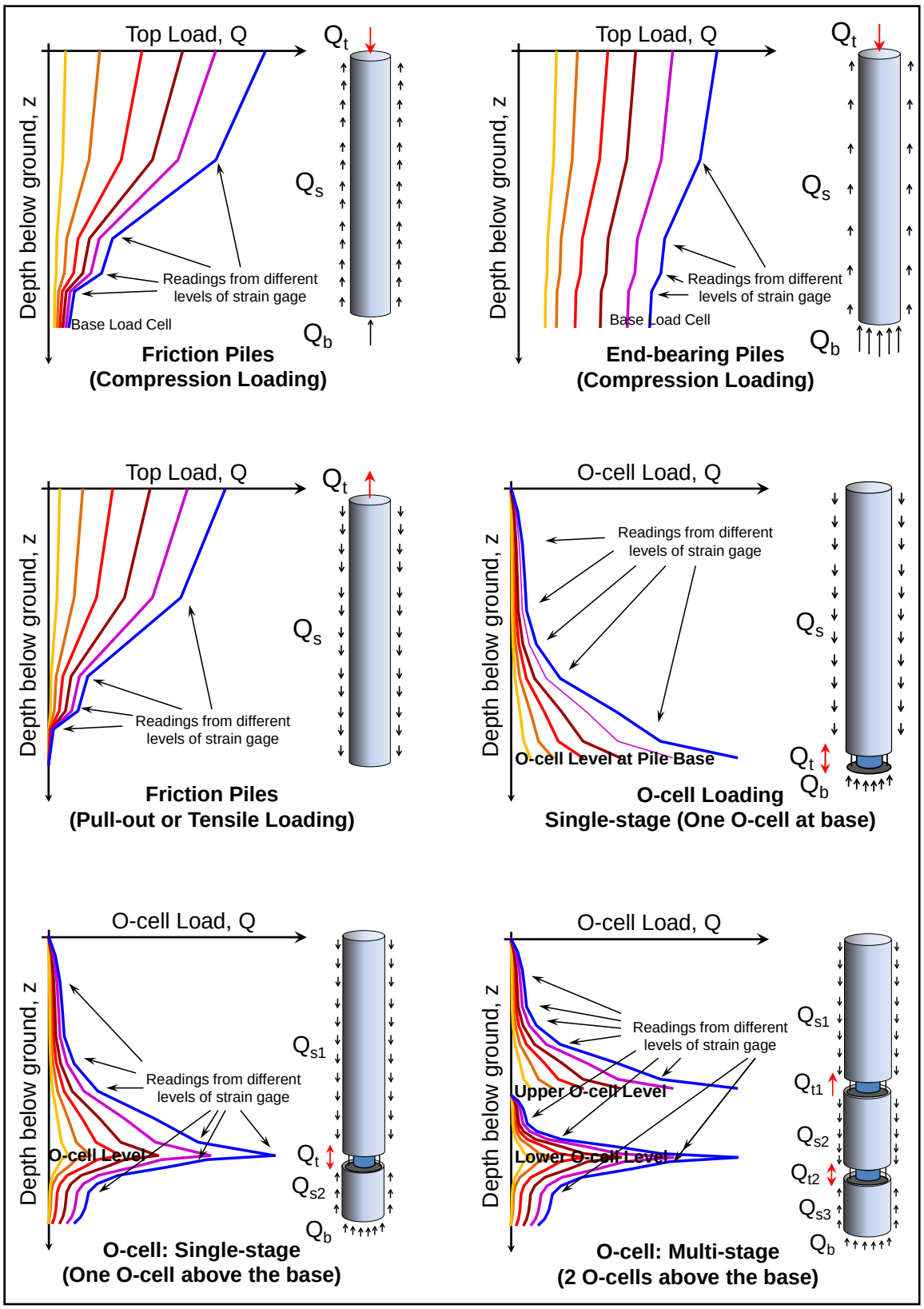

Figure B.14. Typical profiles of load transfer distributions for piles tested under different axial loading arrangements.

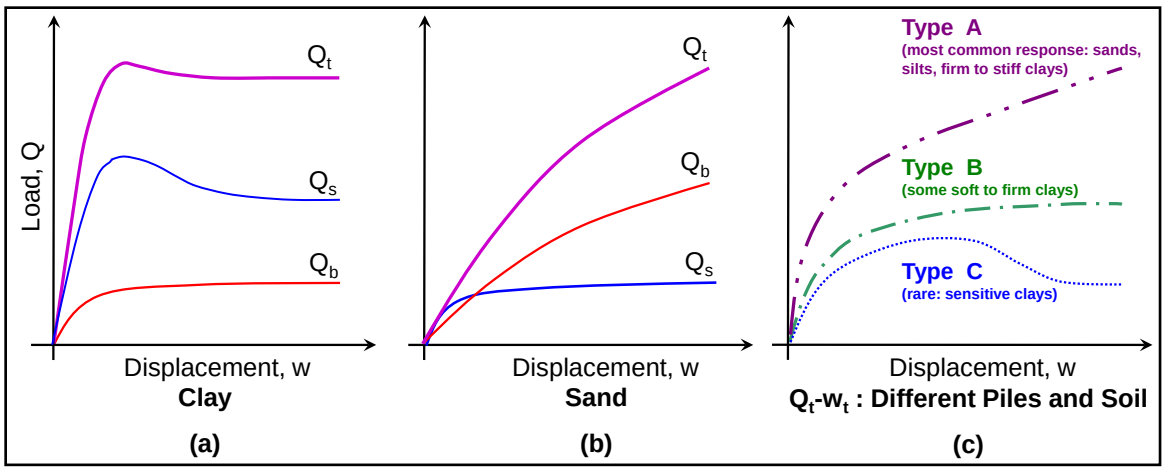

Figure B.15. Schematic concept of pile load-displacement response based on soil type (after Davies, 1987, and Hirany and Kulhawy, 1988).

B.2 Load Application Procedures

Various load application procedures used during static axial load testing of pile foundations were summarily presented in Chapter 2. Here the details of individual load increment schemes are summarized.

B.2.1 Stress-Controlled Procedures

Stress-controlled procedures involve a stepped incremental loading format that relies on maintaining different levels of load until the required displacements or specified period of time. Variations of the stress-controlled procedures are described below.

B.2.1.1 Slow Maintained Load Test (SML)

In this method, the pile is loaded in equal increments of 25% of the design load up to twice the design load. Each increment is maintained until a movement of 0.25 mm/hr is reached. The maximum load is then held typically for 24 hours and then removed in similar decrements. A reloading of the test pile to the maximum maintained load is then performed in increments of 50% of the pile design load, allowing 20 minutes between load increments. Then the load is increased in increments of 10% of design load until

reaching the maximum load or failure, allowing 20 minutes between load increments. This kind of test is the ASTM standard procedure and the most common test, especially in large projects. A typical test lasts between 40 to 70 hours.

B.2.1.2 Quick Maintained Load Test (QML)

In this procedure, 10 to 15% of the design load is added at a time in step load fashion and each held for 2.5 to 15 minutes. The maximum load is usually up to 2 times working loads yet can be up to 3 times the design load. When the total load is reached, unloading is then done with four to ten equal decrements allowing 2.5 to 15 minutes between each two decrements. Typical time of a load test can be between 3 to 5 hours. This method has the advantage of being faster than the SML procedure.

B.2.1.3 Incremental Equilibrium Test (IE)

This test is a modification of the SML test and takes only about one-third of the SML test duration. The IE test is conducted by applying load increments of 15% to 25% of the design load (or 10% of the estimated failure load) and maintaining that load for about 5 to 15 minutes. By closing the jack supplying the pressure, the load is then allowed to drop (with the increase in settlement) until it becomes constant. At this point, equilibrium between the load and displacement is reached and the next increment is applied. Although the total time required for this procedure is about one-third of that required by the SML procedure, the IE test has been reported to provide similar correlations to the SML test (Fellenius, 1975).

B.2.1.4 Constant-Time Interval Test (CTI)

Loading using this method is the same as that for the SML procedure with load increments of 12.5 to 25% of pile design load. Each load is maintained for half to one hour, both during loading as well as unloading. This procedure has a typical duration of about 8 to 10 hours.

B.2.1.5 Cyclic Loading Test (CYC)

The cyclic test is conducted by a series of loading taken to 50, 100 and 150% of the pile design load, subsequent unloading, and then reloading up to the next higher loading (i.e., 100, 150 and 200% of the pile design load). The rate of loading and unloading can be similar to that of the SML or CTI procedures. This test can be used where there is a need to determine the load at which creep displacements exceed certain limits and for separating the capacity of pile foundation into end-bearing and shaft-resistance. This procedure is time-consuming (takes 20 to 44 hours) and is not typically used for routine load testing.

B.2.2 Strain-Controlled Methods

Strain-controlled procedures rely on maintaining a specified rate of movements over various loading levels and these are mainly divided into two categories:

B.2.2.1 Constant-Rate Displacement Test (CRD)

In the CRD load test, the pile is pushed into the ground at a pre-determined constant rate of displacement using a hydraulic jacking system equipped to provide a smooth variable pressure delivery, while the load applied is measured continuously. Rates of pile displacement are maintained at 0.25 to 1.25 mm per minute in cohesive soils and 0.75 to 2.5 mm per minute in granular soils for compression tests, and 0.5 to 1.0 mm per minute for uplift tests. The test continues until one of the following criterion is reached: (a) a total pile displacement equal to 15% of the pile diameter or width, (b) pile top displacement = 60 mm, or (c) until the pile displacement stops. The CRD test can be performed in less than one hour.

B.2.2.2 Constant Movement Increment Test (CMI)

In the CMI procedure, load increments are selected to produce uniform increments of movement of the pile head. Typical movement increments are on the

magnitude of 1% of the pile diameter or width. The load increment is varied in order to maintain the settlement magnitude. The pile is incrementally loaded until obtaining a total pile movement of at least 15% of the average pile diameter or width. Unloading is done in four equal decrements, maintaining each level of unloading until the rate of pile rebound for the preceding load decrement is less than 0.3% of the average pile diameter or width per hour.

B.2.3 Discussion and Comparison

The SML and CYC procedures are the slowest test procedures and the CRP is the fastest (see Figure B.16a). Typical load-displacement curves obtained from four of the above 7 test procedures are compared in Figure B.16b. This figure shows that the shape of load-movement curve by the CRP test procedure is well defined and agrees with the QML load-movement curve before the failure is reached. The interpretation of SML test procedure is based on gross and net settlements, which can be made easily. Therefore, it can furnish a rough estimate of the expected pile settlement under working load (Prakash and Sharma, 1990). According to the ASTM standards, all but CMI test procedure can be applied to static axial tensile loading, whereas, compressive load increments can be applied via any of these schemes. Tests performed using the O-cell arrangement usually follow the ASTM QML test procedure, although other methods are not precluded (Schmertmann and Hayes, 1997).

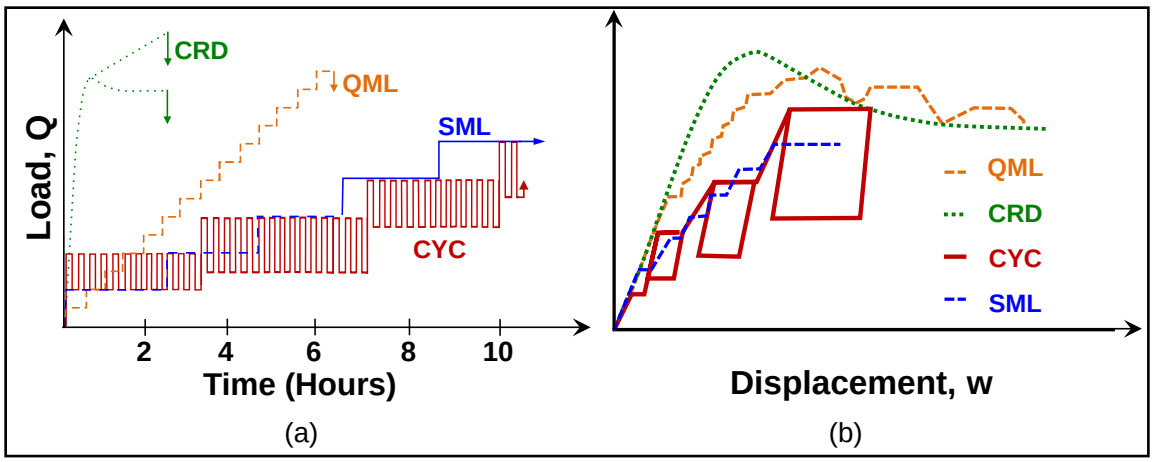

Figure B.16. Conceptual comparison of four load test procedures in axial compression: (a) load versus time; (b) load-displacement curves (adapted from Fellenius, 1975).

APPENDIX C

INTERPRETIVE METHODS FOR EVALUATING FAILURE LOAD FROM AXIAL LOAD TEST ON DEEP FOUNDATIONS

Table C.1. Maximum load criteria for axial compression tests (modified from Hirany and Kulhawy, 1988).

Criterion No.	Interpreted Failure Load (Q_{fi}) Definition	Basis of Definition	Author/Agency/Code/Reference
1	Load at 38 mm total settlement	Absolute displacement limitation	Polish Specs (Klosinski, 1977) Canada (Bertok and Berezowski, 1983)
2	Load at 25 mm total settlement	Absolute displacement limitation	Terzaghi and Peck (1967) Netherlands (Vesić, 1977) Cleveland, OH (Fletcher, 1962) Norforlk, VA (Fletcher, 1962)
3	Load at 20 mm total settlement	Absolute displacement limitation	Muhs (Schultze, 1964)
4	Load at 13 mm total settlement	Absolute displacement limitation	Indian Practice (Mazumder and Bose, 1964)
5	Load at 6 mm plastic settlement	Absolute displacement limitation	AASHTO (1977) NYS DPW (Chellis, 1961) LA Highway Department (Chellis, 1961) Magnel (Vesić, 1977)
6	Load at 8 mm plastic settlement	Absolute displacement limitation	Magnel (Vesić, 1977)
7	Load at 13 mm plastic settlement	Absolute displacement limitation	Boston (Vesić, 1977) Bethlem Steel (Bethlehem, 1979) Milwaukee, WI (Fletcher, 1962)

Table C.1 (continued).

Criterion No.	Interpreted Failure Load (Q_{fi}) Definition	Basis of Definition	Author/Agency/Code/Reference
8	Load at 19 mm plastic settlement	Absolute displacement limitation	NY City Building Code (1981) Standard Building Code (1982) BOCA (1984) Canada (Bertok and Berezowski, 1983)
9	Load at total settlement of 0.029 mm/kN of test load	Displacement per unit load (limiting secant modulus)	California (Vesić, 1977) Pittsburgh, PA (Fletcher, 1962)
10	Load at plastic settlement of 0.029 mm/kN of test load	Displacement per unit load (limiting secant modulus)	NY City Building Code (1981) Standard Building Code (1999) Uniform Building Code (1979) BOCA (1984) Chicago City Building Code (1982) Hartford, CT (Fletcher, 1962) Washington, DC (Fletcher, 1962) Norfolk, VA (Fletcher, 1962) Atlanta, GA (Fletcher, 1962)
11	Load at plastic settlement of 0.014 mm/kN of test load	Displacement per unit load (limiting secant modulus)	New Orleans, LA (Fletcher, 1962)
12	Load at plastic settlement of 0.006 mm/kN of test load	Displacement per unit load (limiting secant modulus)	Milwaukee, WI (Fletcher, 1962)
13	Load at total settlement of 10% of tip diameter	Relative displacement limitation (function of pile diameter)	CIRIA (Weltman, 1980) Bishop et al. (1948)

Table C.1 (continued).

Criterion No.	Interpreted Failure Load (Q_{fi}) Definition	Basis of Definition	Author/Agency/Code/Reference
14	Load at total settlement of 10% of tip diameter for driven piles and 25% of tip diameter for drilled shafts	Relative displacement limitation (function of pile diameter)	Vesić (1977)
15	Load at plastic settlement of 10% of tip diameter	Relative displacement limitation (function of pile diameter)	Danish Standard (Schultze, 1964)
16	Load at plastic settlement of 2% of tip diameter	Relative displacement limitation (function of pile diameter)	Vesić (1977)
17	Load at total settlement of B/30 plus elastic settlement	Relative displacement limitation (function of pile diameter)	Canadian Manual on Foundation Engineering (1985)
18	Load at plastic settlement of 20mm plus B/20 with B in mm	Relative displacement limitation (function of pile diameter)	Swedish Pile Commission (1980)
19	Load at total settlement of elastic pile compression plus 0.15 inch plus B/120, with B in inches	Relative displacement limitation (function of pile diameter) plus graphical construction	Davisson (1972)
20	Load at which total settlement increases without further load increase	Displacement rate limitation (function of load)	Tomlinson (1977)
21	Load beyond which total settlement is disproportionate to load increase	Displacement rate limitation (function of load)	Los Angeles, CA (Chellis, 1961) Uniform Building Code (1979)
22	Load at which plastic settlement is disproportionate to load increase	Displacement rate limitation (function of load)	Tomlinson (1977)

Table C.1 (continued).

Criterion No.	Interpreted Failure Load (Q_{fi}) Definition	Basis of Definition	Author/Agency/Code/Reference
23	Load at which plastic curve breaks sharply	Displacement rate limitation (function of load)	Chellis (1961)
24	Load at which 10% of load increase gives total settlement increase of 20 – 30%	Displacement rate limitation (function of load)	Jorger (Schultze, 1964)
25	Load that gives twice the total settlement as at 90% of that load	Displacement rate limitation (function of load)	Brinch Hansen's 90% criterion (Hansen, 1963)
26	Load that gives four times the total settlement as at 80% of that load	Displacement rate limitation (function of load)	Brinch Hansen's 80% criterion (Hansen, 1963)
27	Load at maximum ratio of total settlement increment to load increment	Displacement rate limitation (function of load)	Vesić (1963)
28	Load at maximum ratio of elastic settlement increment to plastic settlement increment	Displacement ratio limitation	Széchy (1961)
29	Load at ratio of plastic settlement to elastic settlement of 1.5	Displacement ratio limitation	Christiani and Nielsen (Vesić, 1977)
30	Minimum load for a rate of total settlement of 0.057 mm/kN	Displacement rate limitation (function of load)	Dunham (1957)
31	Minimum load for a rate of total settlement of 0.086 mm/kN	Displacement rate limitation (function of load)	Ohio (Vesić, 1977)
32	Minimum load for a rate of total settlement of 0.14 mm/kN	Displacement rate limitation (function of load)	Fuller and Hoy (1970); Nordlund (1966)

Table C.1 (continued).

Criterion No.	Interpreted Failure Load (Q_{fi}) Definition	Basis of Definition	Author/Agency/Code/Reference
33	Minimum load for a rate of plastic settlement of 0.086 mm/kN	Displacement rate limitation (function of load)	Fuller and Hoy (1970)
34	Load at which slope of total settlement curve is four times slope of elastic settlement curve	Displacement ratio limitation	Chellis (1961)
35	Load at intersection of tangents to upper and lower portions of total settlement curve	Graphical construction	Mansur and Kaufman (1956)
36	Load at intersection of tangent sloping at 0.14 mm/kN and tangent to initial straight portion of tital settlement curve	Graphical construction	Butler and Hoy (1977)
37	Load at which change in slope occurs when load is plotted versus total settlement for last 30 minutes from 1 hour load increments	Graphical construction	Housel (1966)
38	Load at which change in slope occurs on log-log total settlement curve	Graphical construction	De Beer (1970)
39	Load equal to inverse slope $1/C_1$, of line $w_t/Q_t = C_1 w_t + C_2$, with Q_t = load and w_t = total settlement	Graphical construction plus mathematical modeling	Chin-Kondner (Chin, 1970; Kondner, 1963)
40	Value of Q_{fi} which gives straight line when $\ln(1 - Q/Q_{fi})$ is plotted versus total settlement	Mathematical modeling	van der Veen (1953)

Table C.1 (continued).

Criterion No.	Interpreted Failure Load (Q_{fi}) Definition	Basis of Definition	Author/Agency/Code/Reference
41	Horizontal lines are drawn from load–displacement curve which correspond to arbitrarily chosen equal displacements. 45^o lines are drawn from points of intersection of these lines with load axis to intersect with adjacent higher horizontal line. These intersections fall on a straight line whose point of intersection with the load axis gives the failure load	Graphical construction plus mathematical modeling	Mazurkiewicz (1972)
42	Load that gives a displacement equal to the initial slope of the $Q_t - w_t$ curve plus 0.15 in. (4 mm) (for uplift type load tests)	Graphical construction plus absolute displacement limitation	O'Rourke and Kulhawy (1985)
43	Load equal to ratio C_2/C_1; C_1 and C_2 are the slope and y-intercept of the line obtained by plotting $Q_t/w_t - Q_t$, with Q_t = load and w_t = total settlement	Graphical construction plus mathematical modeling	Dećourt (1999)
44	Load at total settlement of 4% of tip diameter (for compression type load tests)	Relative settlement limitation (function of pile diameter)	Hirany and Kulhawy (1988)
45	Load at total displacement of 0.5 in. (12.7 mm) (for uplift type load tests)	Absolute displacement limitation	Hirany and Kulhawy (1988)

C.1 Selected Interpretive Methods for Axial Capacity

The following ten methods for defining axial capacity have been chosen here to illustrate their application.

C.1.1 Davisson's Offset Line Method (Davisson, 1972)

- Plot the $Q_t - w_t$ curve as shown in Figure C.1a.
- Obtain and plot elastic movement line OA (Q_t vs. Δ), where Δ, the elastic compression = Q_t L/AE of the pile, where Q_t is the applied load, L is pile length, A is pile cross-sectional area, and E is modulus of elasticity of the pile material.
- Draw line BC parallel to OA at a distance of x where x = 0.15 + d/120 inches (or x = 4 + d/120 mm), where d is the pile diameter.
- The failure load is given by the intersection of BC with load-movement curve.

C.1.2 Chin-Kondner's Method (Chin, 1970; Kondner, 1963)

- The Chin-Kondner method involves the fitting of a rectangular hyperbola to the data.
- Draw the transformed axes with a plot of w_t / Q_t vs. displacement w_t.
- The interpreted failure load (Q_{fi}) is then the inverse of the slope ($1/C_1$) of the best-fit linear relationship through the plotted data points. The relationships given in Figure C.1b assume that the $Q_t - w_t$ curve is a rectangular type hyperbola (refer to Figure C.1b for the explanation of terms).

C.1.3 De Beer's Method (De Beer, 1970)

- Plot $Q_t - w_t$ data on logarithmic scales, so that a bilinear trend is observed.
- The interpreted failure load (Q_{fi}) is then defined as the load at the intersection of these two straight lines (see Figure C.2a).

C.1.4 Brinch Hansen's 90 percent Criterion (Hansen, 1963)

Figure C.2b illustrates this trial and error method, where interpreted failure load (Q_{fi}) is defined as the load that gives twice the movement of the pile head as obtained for 90% of that load obtained from the $Q_t - w_t$ plotted on arithmetic scale.

C.1.5 Brinch Hansen's 80 percent Criterion (Hansen, 1963)

The 80%-criterion failure load defined as the load that gives four times the movement of pile head as obtained from 80% of that load can be estimated by extrapolation from the $Q_t - w_t$ curve directly. It can be obtained more accurately by plotting $\sqrt{w_t}/Q_t$ vs. w_t curve (see Figure C.3a). As shown, interpreted failure load (Q_{fi}) and the corresponding settlement (w_{fi}) are obtained by using the slope (C_1) and the y-intercept (C_2) of the straight line.

C.1.6 Mazurkiewicz's Method (Mazurkiewicz, 1972)

This Mazurkiewicz method is illustrated in Figure C.3b. Subsequent to plotting of the $Q_t - w_t$ curve, a series of equally spaced lines parallel to the load axis are chosen and drawn to intersect with the curve. Horizontal lines are then drawn from each intersection extending beyond the load axis. From the intersection of each horizontal line with the load axis, draw a 45^o line to intersect with the line above. These later intersections fall approximately on a straight line, which when extended back to intersect with the load axis, defines the "failure load."

C.1.7 Nordlund or Fuller and Hoy's Method (Fuller and Hoy, 1970; Nordlund, 1966)

Using a $Q_t - w_t$ curve plotted on linear scales, find the Nordlund-Fuller and Hoy's interpreted failure load (Q_{fi}) estimate on the curve when a tangent line with slope equals 0.05 in/ton (0.14 mm/kN) (see Figure C.4a) meets the measured load-displacement curve.

C.1.8 Butler and Hoy Method (Butler and Hoy, 1977)

With the same plot as above (see Figure C.4a), the tangent drawn at this slope is extended backward to intersect with the tangent to the initial straight portion of the curve, or to a line that is parallel to the rebound portion of the curve (also parallel to elastic line) gives the Butler and Hoy's Q_{fi} estimate.

C.1.9 Vander Veen's Method (Vander Veen, 1953)

The construction of failure load as proposed in the van der Veen's method is shown in Figure C.4b. An estimate of interpreted failure load (Q_{fi}) is chosen and values calculated from $\ln(1 - Q_t/Q_{fi})$ are plotted against w_t on linear scale. When the plot becomes a straight line, the correct Q_{fi} has been chosen.

C.1.10 Dećourt Zero Stiffness Method (Dećourt, 1999)

The construction technique for estimation of failure load as proposed by Dećourt (1999) method involves a plot of stiffness ($K = Q_t/w_t$) vs. applied load (Q_t). When the trendline is extrapolated to a zero stiffness ($K = 0$), then that load is the capacity. Figure C.5 shows a sample plot where the curve apparently tends to be a straight line that is obtained via linear regression over the last few points. Forward forecasting to this line such that it intersects with the abscissa gives the estimate of Q_{fi}.

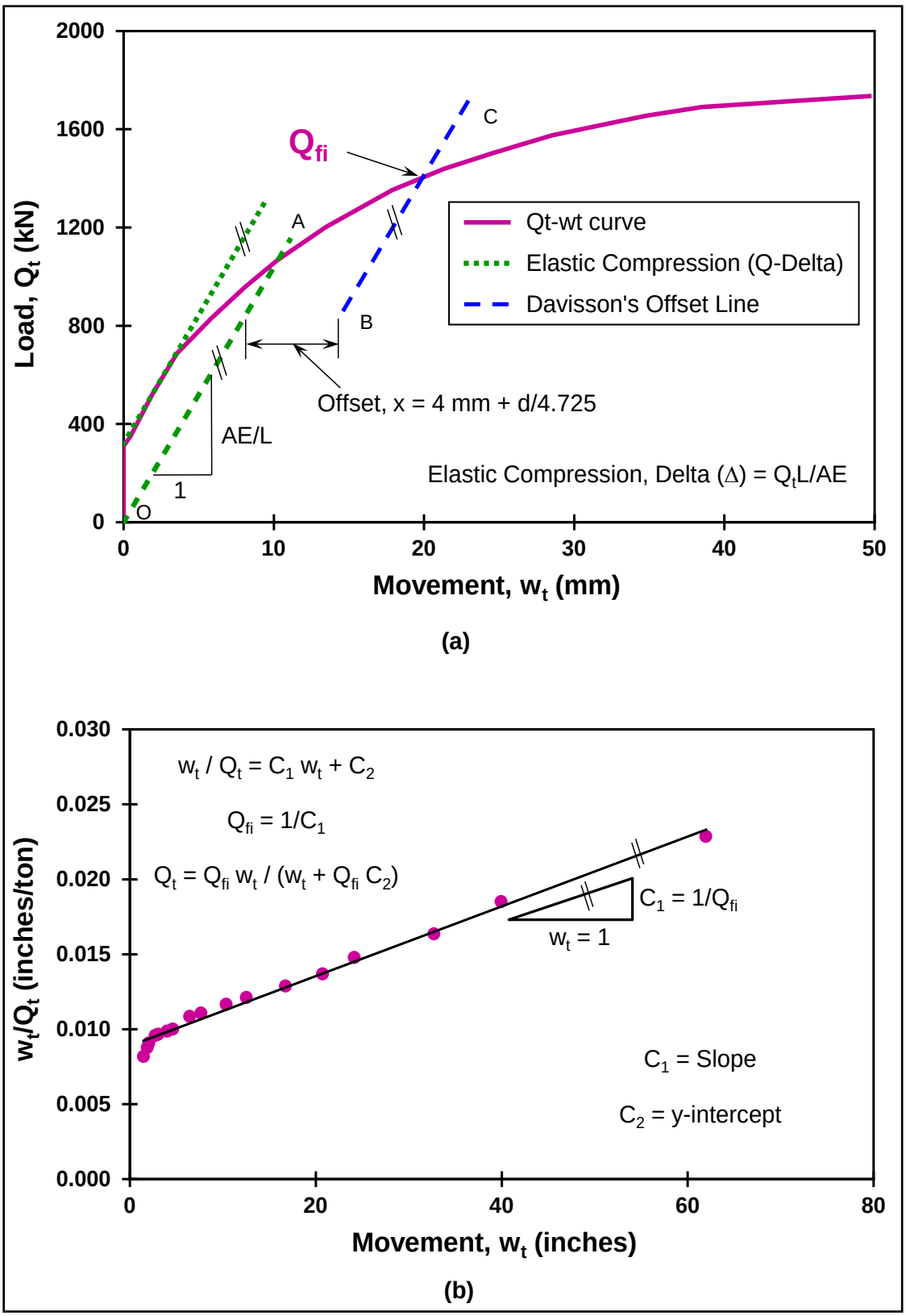

Figure C.1. Failure load interpretation methods: (a) Davisson's method; (b) Chin-Kondner's method (after Fellenius, 1990).

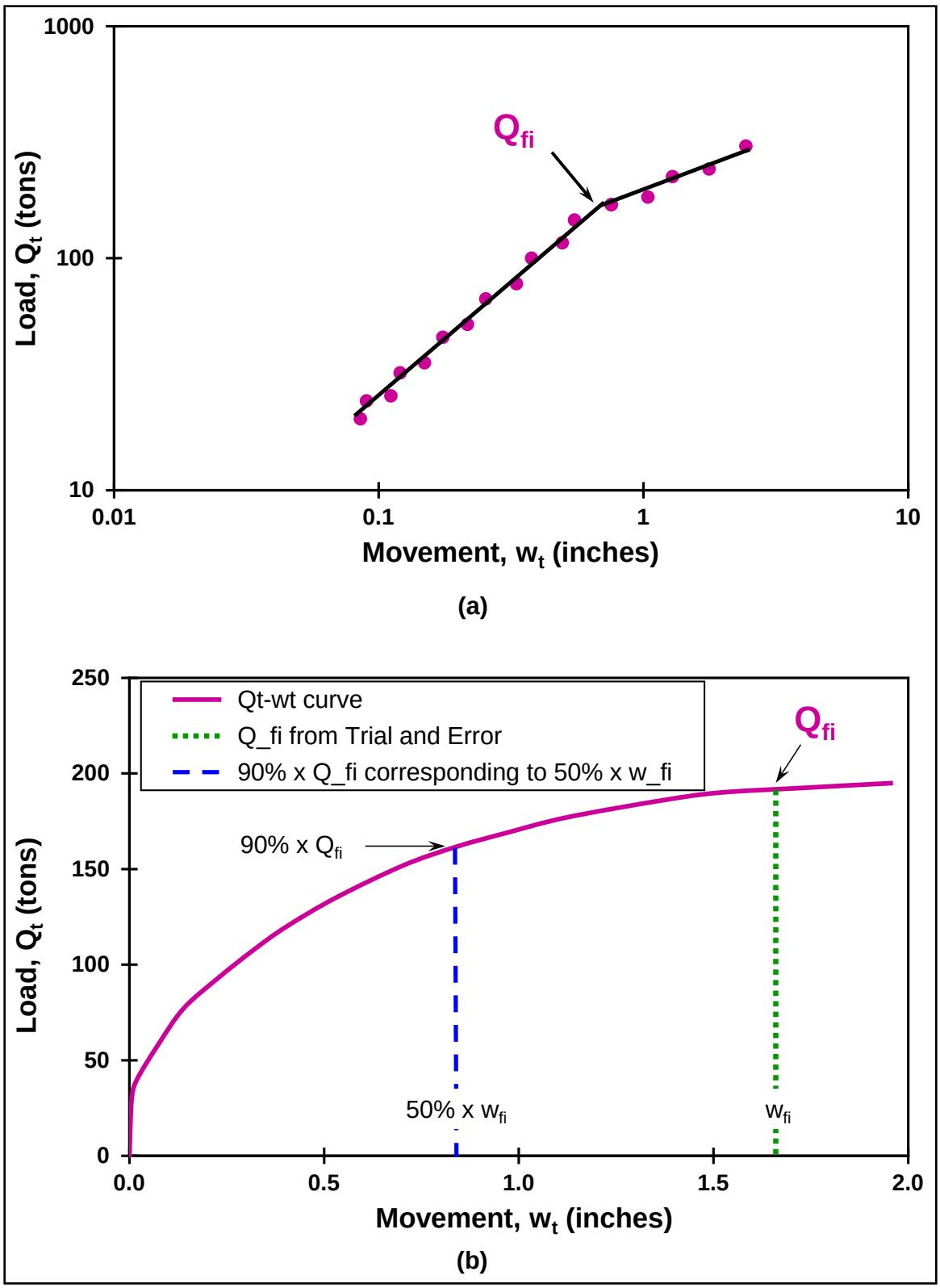

Figure C.2. Failure load interpretation methods: (a) DeBeer's method; (b) Brinch Hansen's 90% criterion method (after Fellenius, 1990).

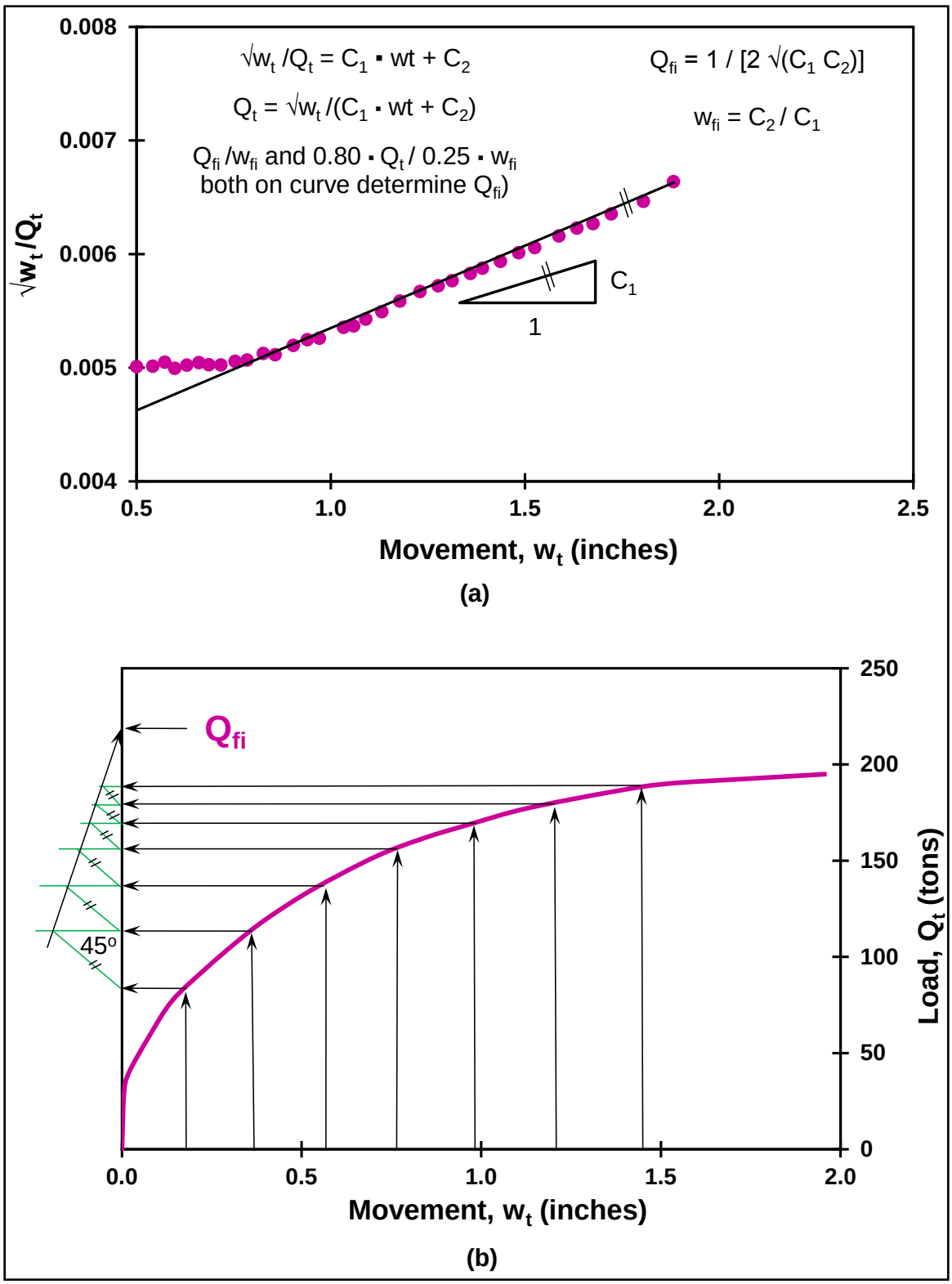

Figure C.3. Failure load interpretation methods: (a) Brinch Hansen's 80% criterion method; (b) Mazurkiewicz's method (after Fellenius, 1990).

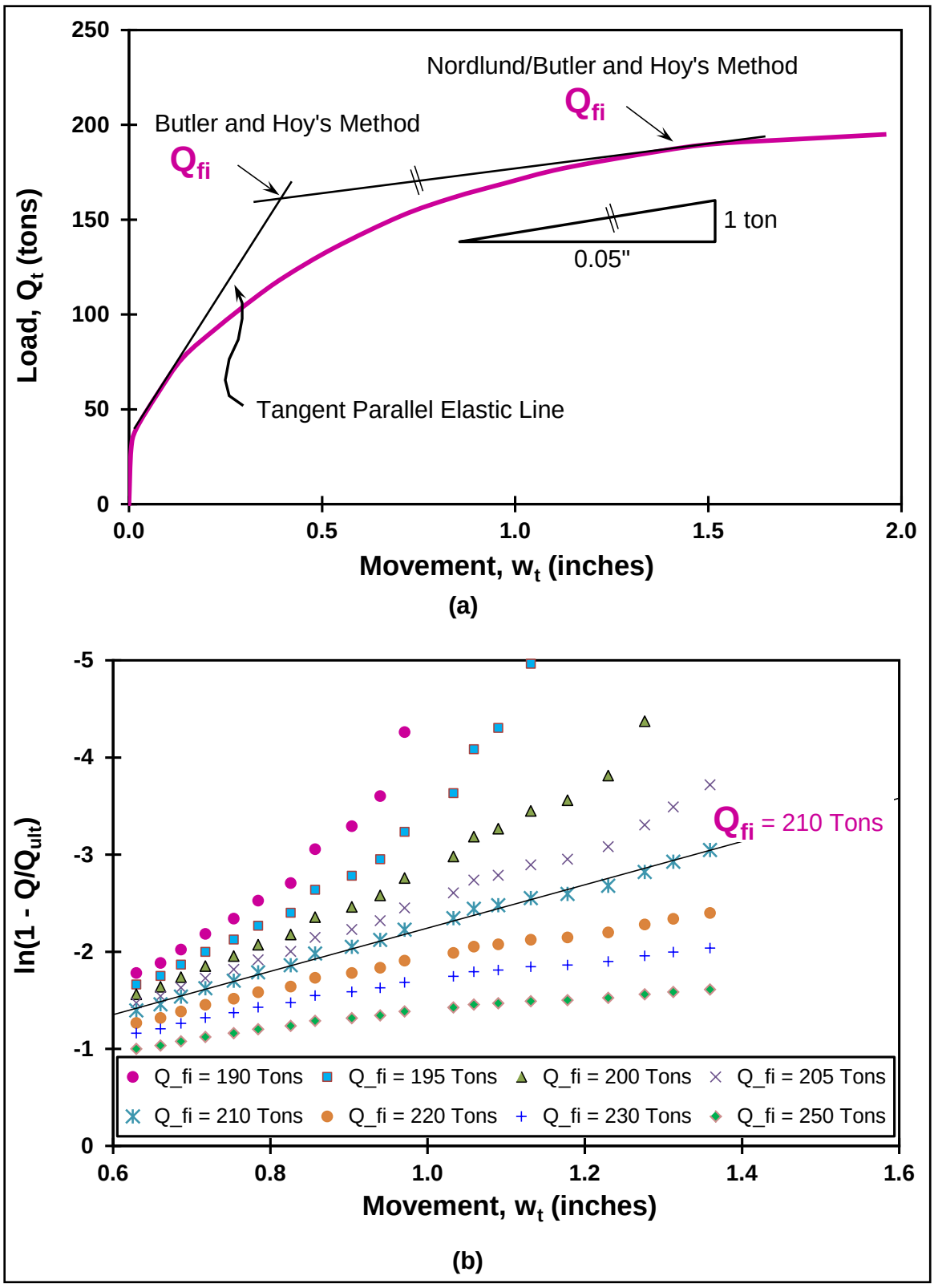

Figure C.4. Failure load interpretation methods: (a) Nordlund/Fuller and Hoy's and Butler and Hoy's methods; (b) van der Veen's method (after Fellenius, 1990).

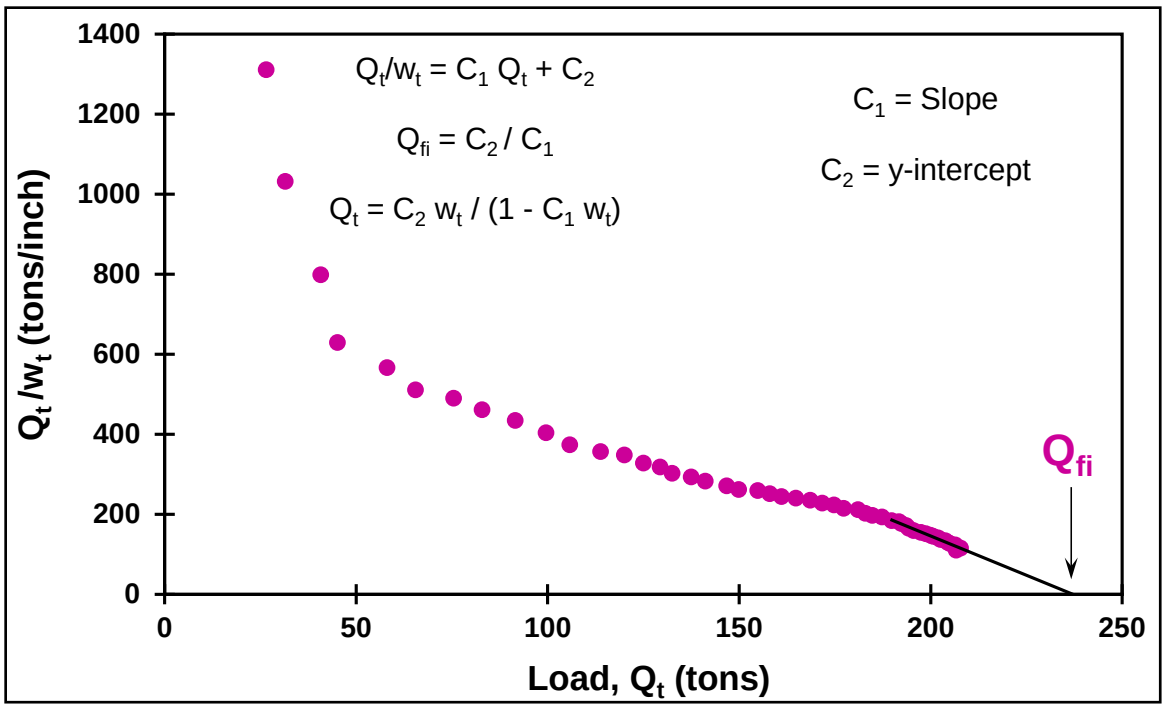

Figure C.5. Zero stiffness failure load interpretation method (after Dećourt, 1999).

APPENDIX D

PROCEDURE FOR MEASURING THE DISTRIBUTION OF RESIDUAL LOADS DURING A PILE LOAD TEST

The distribution of residual loads can be directly measured from the strain gages before commencing the load test. Then proceeding with the load test without zeroing the gages, a true load distribution curve is obtained by measuring the readings from the gages corresponding to the ultimate load applied to the pile head. From the two sets of measured load distributions, subtraction of residual loads from the true loads results in the distribution that would have been found if the gages were zeroed before the start of the test. Figure D.1 presents an example showing the three load distribution curves. If direct measurements of residual loads from the strain gages are not done and the gages are zeroed prior to the load test, following effective stress calculation approach proposed by Fellenius (1989) should be adopted. First, a shear strength distribution along the pile, a residual base load, and a pile base resistance are assumed. These assumptions govern the residual load in the pile, and when adding the residual load to the measured load values, a load distribution is determined which is then compared to the assumed values. The process is iterative, and through trial and error approach selecting different soil parameters and residual load values, a final solution is obtained wherein measured and calculated load distributions agree. More details of the two procedures can be found in Fellenius (1989; 2001b; 2002a), and Altaee et al. (1992).

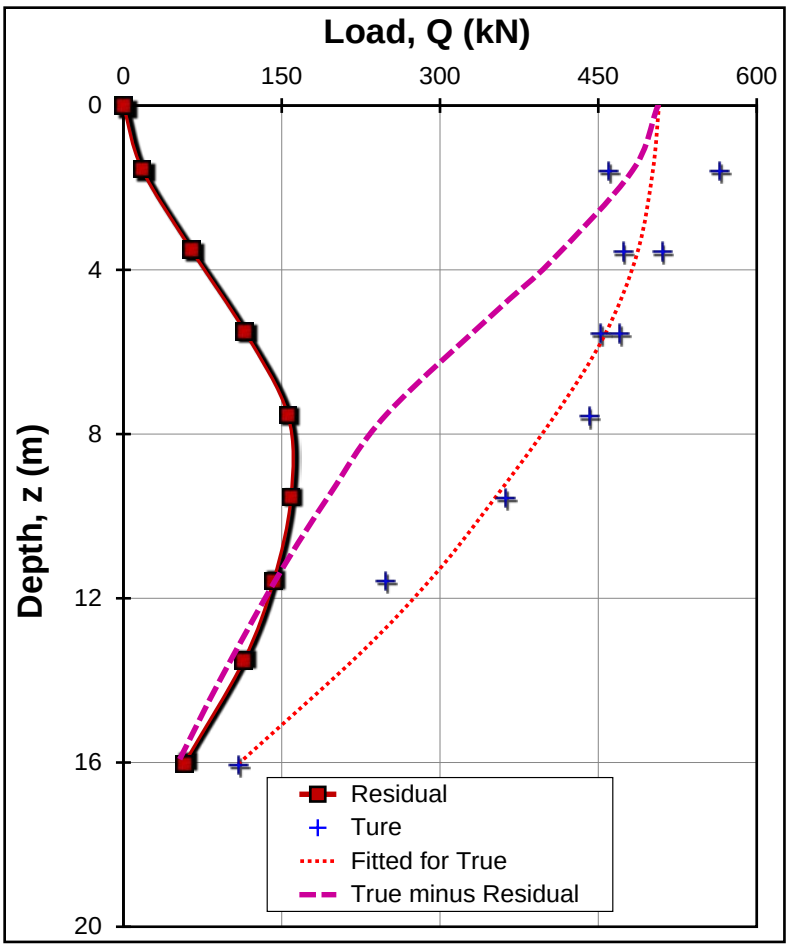

Figure D.1. Residual and true load distributions from pile load tests (modified from Fellenius, 2001b).

APPENDIX E

PRESENTATION OF DATABASE AND CASE RECORDS

This appendix provides a case-by-case summary of the entire database collected as part of this research effort. The first part of this appendix presents Table E.1, detailing information on each pile, the load test results, and their respective "capacity" interpretations, as well as assigns an identification number (ID) for referencing of all 330 load tests. The sites are arranged in alphabetical order.

This table is followed by a second section that contains more comprehensive subsurface information, including a presentation of the complete profiles of cone penetrometer soundings (SCPTu or SCPT or CPTu) from all 70 sites associted to the respective site IDs given in Tables 5.1 and E.1. In addition, the interpreted soil behavioral type (SBT) from the calculated CPT material index (I_c) profiles are also shown. For each site, the individual load-displacement (Q-w) curves, the back-analyzed G/G_{max} vs. percent pseudo-strain [γ_p = w/d (%)] curves, and the allied results and capacity interpretations from the respective pile load tests are presented, again as referenced to their assigned IDs.

Table E.1. Database of pile load tests.

Site ID No.	Pile information, load test results and interpretations									
	Pile ID	**Pile type/ material**	**L (m)**	**d or B (m)**	**Loading mode**	**Installation method**	**$Q_{max\text{-}measured}$ (kN)**	**$Q_{Davisson}$ (kN)**	**$Q_{w/d=10\%}$ (kN)**	**$Q_{C\text{-}K}$ (kN)**
1	AIT 1-1	Teak	6.00	0.150	C	D	38.04	38.70	38.75	38.94
	AIT 1-2	Teak	6.00	0.150	C	D	39.44	39.50	40.16	40.35
	AIT 2-1	Teak	6.00	0.150	C	D	38.62	38.70	40.03	40.40
	AIT 2-2	Teak	6.00	0.150	C	D	33.24	33.30	34.40	34.69
	AIT 3-1	Teak	6.00	0.150	C	D	32.12	32.22	32.51	32.61
	AIT 3-2	Teak	6.00	0.150	C	D	36.13	36.44	36.73	36.88
	AIT 4-1	Teak	6.00	0.150	C	D	41.28	41.51	42.27	42.53
	AIT 4-2	Teak	6.00	0.150	C	D	37.63	37.80	38.11	38.24
	AIT 5	DS	18.00	0.450	C	B-CIS	2,047.28	-	-	-
2	BU 1	Sq-C	11.00	0.285	C	D	1,100.00	985.50	1,066.19	1,117.32
	BU 2	Sq-C	11.00	0.285	T	D	580.00	422.25	554.58	610.87
	BU 3	Sq-C	15.00	0.285	C	D	1,600.00	1,420.15	1,616.83	1,754.39
3	Bl 1	CE-S	2.70	0.073	C	D	150.38	126.62	130.03	152.77
	Bl 2	CE-S	2.49	0.073	C	J	164.02	150.51	156.95	167.14
4	BCS 1	Sq-C	6.35	0.35	C	D	964.20	961.84	1,092.27	1,137.66
	BCS 2	Fundex	6.31	0.38	C	A	807.52	719.14	818.82	861.33
	BCS 3	Fundex	10.48	0.38	C	A	1,291.21	1,193.00	1,329.35	1,390.82
	BCS 4	Sq-C	10.60	0.35	C	D	1,651.00	1,651.00	1,658.97	1,661.13
	BCS 5	De Waal	6.46	0.41	C	A	785.20	647.97	817.56	862.81
	BCS 6	De Waal	10.66	0.41	C	A	1,300.40	1,176.10	1,342.38	1410.44
	BCS 7	Olivier	10.71	0.51	C	A	1,838.14	1,414.16	1,912.64	2,061.86
	BCS 8	Olivier	6.53	0.51	C	A	1,183.74	906.08	1,220.26	1,305.48
	BCS 9	Omega	6.59	0.41	C	A	724.09	619.47	736.58	762.20
	BCS 10	Omega	10.81	0.41	C	A	1,299.36	1,196.38	1,329.36	1,386.96
	BCS 11	Atlas	10.81	0.51	C	A	1,724.11	1,640.10	1,845.60	1,941.75
	BCS 12	Atlas	6.76	0.51	C	A	1,004.98	956.51	1,100.60	1,154.73

Notes: L: pile length; d: pile diameter for piles with circular cross-section; B: pile width for piles with square cross-section; DS: drilled shaft; CFA: continuous flight auger pile; CE-S: closed-ended steel pipe pile; OE-S: open-ended steel pipe pile; OE-SC: open ended concrete filled steel pipe pile; ICP: closed-ended Imperial College Pile; HP: H-section steel pile; PTC: pre-stressed concrete thin-wall caisson; PHC: Pre-stressed concrete high-strength; Sq-C: square precast concrete pile; C-C: circular precast concrete pile; C: top-down compression loading mode; T: top-up tension (or uplift) loading mode; O-cell (U): upward loading mode of bi-directional Osterberg cell; O-cell (D): downward loading mode of bi-directional Osterberg cell; A: augered piles; D: driven piles; J: jacked piles; B-CIS: bored cast in-situ piles; $Q_{max\text{-}measured}$: maximum applied load; $Q_{Davisson}$; estimated capacity from Davisson's offset line criterion; $Q_{w/d=10\%}$: estimated capacity from French criterion (w/d = 10%); $Q_{C\text{-}K}$: estimated capacity from Chin-Kondner criterion.

Table E.1. (continued).

Site ID No.	Pile information, load test results and interpretations									
	Pile ID	**Pile type/ material**	**L (m)**	**d or B (m)**	**Loading mode**	**Installation method**	**$Q_{max\text{-}measured}$ (kN)**	**$Q_{Davisson}$ (kN)**	**$Q_{w/d=10\%}$ (kN)**	**$Q_{C\text{-}K}$ (kN)**
5	BK 1/L1T	ICP	5.00	0.102	T	J	23.74	22.29	24.36	26.73
	BK 2/L1C	ICP	4.80	0.102	C	J	24.75	29.60	33.24	35.52
	BK 2/L2C	ICP	4.80	0.102	C	J	32.31	34.16	38.95	41.81
	BK 3(1)/L1C	ICP	1.95	0.102	C	J	6.81	8.19	9.20	9.45
	BK 3(2)/L1C	ICP	4.70	0.102	C	J	29.04	31.17	33.12	35.32
	BK 4f/L1C	ICP	1.95	0.102	C	J	12.28	13.24	14.65	15.61
	BK 4s/L1C	ICP	4.75	0.102	C	J	25.93	27.23	32.03	34.85
6	BC A1	CE-S	4.50	0.17	C	J	114.40	241.15	415.97	513.08
	BC B1	CE-S	4.50	0.17	C	J	134.54	160.77	187.00	195.05
	BC C1	CE-S	4.50	0.17	C	J	114.56	114.56	115.16	115.23
	BC A2	CE-S	4.50	0.17	T	J	108.59	108.59	108.99	109.19
	BC B2	CE-S	4.50	0.17	T	J	115.27	115.27	116.47	116.75
	BC C2	CE-S	4.50	0.17	T	J	83.31	83.71	88.29	88.85
7	CGTS 1	DS	9.35	0.92	T	B-CIS	974.56	-	-	-
	CGTS 2	DS	5.94	1.48	C	B-CIS	553.95	455.58	564.53	569.80
	CGTS 4	DS	6.51	1.48	T	B-CIS	628.50	605.60	687.56	700.77
	CGTS 9	DS	6.27	1.60	T	B-CIS	974.56	955.47	1,006.24	1,014.20
8	CP 1	CE-S	4.50	0.168	C	J	216.70	216.70	222.24	224.16
	CP 2	CE-S	4.50	0.168	C	D	178.04	-	170.92	-
	CP 3	DS	4.50	0.168	C	B-CIS	143.11	148.38	153.64	157.46
	CP 4	ICP	3.95	0.102	C	J	107.25	-	95.15	-
9	C Pt 1	Sq-C	21.33	0.305	C	D	1,512.46	1,881.00	2,249.55	2,808.99
	C Pt 2	Sq-C	15.24	0.305	C	D	871.89	840.75	888.21	900.90
10	CNN 1-U	DS	14.08	1.60	O-cell (U)	B-CIS	8,058.19	8,058.19	9,055.50	9,225.09
	CNN 1-M	DS	4.45	1.44	O-cell (D)	B-CIS	8,583.18	4,604.68	10,933.90	14,285.71
	CNN 1-L	DS	0.78	1.44	O-cell (D)	B-CIS	5,723.35	2,912.44	6,783.20	10,416.67

Notes: L: pile length; d: pile diameter for piles with circular cross-section; B: pile width for piles with square cross-section; DS: drilled shaft; CFA: continuous flight auger pile; CE-S: closed-ended steel pipe pile; OE-S: open-ended steel pipe pile; OE-SC: open ended concrete filled steel pipe pile; ICP: closed-ended Imperial College Pile; HP: H-section steel pile; PTC: pre-stressed concrete thin-wall caisson; PHC: Pre-stressed concrete high-strength; Sq-C: square precast concrete pile; C-C: circular precast concrete pile; C: top-down compression loading mode; T: top-up tension (or uplift) loading mode; O-cell (U): upward loading mode of bi-directional Osterberg cell; O-cell (D): downward loading mode of bi-directional Osterberg cell; A: augered piles; D: driven piles; J: jacked piles; B-CIS: bored cast in-situ piles; $Q_{max\text{-}measured}$: maximum applied load; $Q_{Davisson}$; estimated capacity from Davisson's offset line criterion; $Q_{w/d=10\%}$: estimated capacity from French criterion (w/d = 10%); $Q_{C\text{-}K}$: estimated capacity from Chin-Kondner criterion.

Table E.1. (continued).

Site ID No.	Pile information, load test results and interpretations									
	Pile ID	**Pile type/ material**	**L (m)**	**d or B (m)**	**Loading mode**	**Installation method**	**$Q_{max\text{-}measured}$ (kN)**	**$Q_{Davisson}$ (kN)**	**$Q_{w/d=10\%}$ (kN)**	**$Q_{C\text{-}K}$ (kN)**
11	CRB-C 1-U	DS	30.57	2.52	O-cell (U)	B-CIS	24,008.30	24,008.30	24,698.10	24,752.48
	CRB-C 1-M	DS	12.19	2.44	O-cell (D)	B-CIS	19,576.58	19,576.58	20,341.80	20,408.16
	CRB-C 1-L	DS	3.65	2.44	O-cell (D)	B-CIS	23,612.32	17,224.45	24,126.70	25,000.00
	CRB-C 2-U	DS	31.39	2.52	O-cell (U)	B-CIS	22,015.67	22,015.67	22,962.30	23,094.69
	CRB-C 2-M	DS	12.19	2.44	O-cell (D)	B-CIS	17,550.95	17,127.57	17,777.70	17,857.14
	CRB-C 2-L	DS	2.62	2.44	O-cell (D)	B-CIS	20,412.40	15,168.48	21,415.60	22,727.27
	CRB-C 3-U	DS	29.74	2.54	O-cell (U)	B-CIS	13,112.60	14,978.89	17,619.70	17,636.68
	CRB-C 3-L	DS	2.41	2.44	O-cell (D)	B-CIS	13,112.60	10,261.29	14,402.50	15,151.52
	CRB-C 4-U	DS	30.81	1.92	O-cell (U)	B-CIS	6,969.25	7,442.35	8,353.40	8,368.20
	CRB-C 4-L	DS	0.92	1.83	O-cell (D)	B-CIS	6,969.25	5,979.52	7,111.40	7,299.27
12	CRB-MP 1-U	DS	30.57	2.52	O-cell (U)	B-CIS	24,393.65	23,939.21	24,536.80	24,570.02
	CRB-MP 1-M	DS	14.02	2.44	O-cell (D)	B-CIS	19,538.06	18,767.31	19,903.70	20,005.40
	CRB-MP 1-L	DS	2.53	2.44	O-cell (D)	B-CIS	20,297.06	15,415.00	21,903.60	23,809.52
	CRB-MP 2-U	DS	30.93	2.54	O-cell (U)	B-CIS	26,898.53	26,898.53	27,633.30	27,700.83
	CRB-MP 2-M	DS	14.02	2.44	O-cell (D)	B-CIS	25,588.31	25,588.31	27,994.00	28,571.43
	CRB-MP 2-L	DS	1.10	2.44	O-cell (D)	B-CIS	17,046.96	13,945.05	18,133.90	18,867.92
	CRB-MP 3-U	DS	30.04	2.56	O-cell (U)	B-CIS	13,834.64	15,224.42	20,380.80	20,474.18
	CRB-MP 3-L	DS	1.31	2.44	O-cell (D)	B-CIS	13,834.64	12,927.05	16,949.10	17,084.51
	CRB-MP 4-U	DS	31.33	2.54	O-cell (U)	B-CIS	9,072.41	13,072.22	18,689.80	18,809.52
	CRB-MP 4-L	DS	1.37	2.44	O-cell (D)	B-CIS	9,072.41	8,381.65	10,709.10	10,204.08
13	CW 1/L1T	ICP	3.00	0.102	T	J	77.54	83.19	82.11	83.54
	CW 2/L1C	ICP	3.66	0.102	C	J	114.42	138.01	139.48	148.08
	CW 2/L3C	ICP	3.66	0.102	C	J	126.50	155.12	154.38	161.50
	CW 3/L1T	ICP	3.88	0.102	T	J	87.57	89.70	94.29	99.37
	CW 4/L1C	ICP	3.51	0.102	C	J	80.13	81.00	79.54	80.73
	CW 4s/L1C	ICP	3.92	0.102	C	J	96.13	114.54	122.52	129.50

Notes: L: pile length; d: pile diameter for piles with circular cross-section; B: pile width for piles with square cross-section; DS: drilled shaft; CFA: continuous flight auger pile; CE-S: closed-ended steel pipe pile; OE-S: open-ended steel pipe pile; OE-SC: open ended concrete filled steel pipe pile; ICP: closed-ended Imperial College Pile; HP: H-section steel pile; PTC: pre-stressed concrete thin-wall caisson; PHC: Pre-stressed concrete high-strength; Sq-C: square precast concrete pile; C-C: circular precast concrete pile; C: top-down compression loading mode; T: top-up tension (or uplift) loading mode; O-cell (U): upward loading mode of bi-directional Osterberg cell; O-cell (D): downward loading mode of bi-directional Osterberg cell; A: augered piles; D: driven piles; J: jacked piles; B-CIS: bored cast in-situ piles; $Q_{max\text{-}measured}$: maximum applied load; $Q_{Davisson}$; estimated capacity from Davisson's offset line criterion; $Q_{w/d=10\%}$: estimated capacity from French criterion (w/d = 10%); $Q_{C\text{-}K}$: estimated capacity from Chin-Kondner criterion.

Table E.1. (continued).

Site ID No.	Pile information, load test results and interpretations									
	Pile ID	**Pile type/ material**	**L (m)**	**d or B (m)**	**Loading mode**	**Installation method**	**$Q_{max\text{-}measured}$ (kN)**	**$Q_{Davisson}$ (kN)**	**$Q_{w/d=10\%}$ (kN)**	**$Q_{C\text{-}K}$ (kN)**
14	DK 1/L1C	ICP	7.40	0.102	C	J	364.92	364.92	363.21	374.11
	DK 1/L2T	ICP	7.40	0.102	T	J	269.37	269.37	267.81	309.31
	DK 1/L3T	ICP	7.40	0.102	T	J	276.27	276.27	277.27	291.80
	DK 2/L1C	ICP	5.96	0.102	C	J	283.38	283.38	282.26	284.82
	DK 2/L2C	ICP	5.96	0.102	C	J	299.79	299.79	307.06	314.96
	DK 2/L3T	ICP	5.96	0.102	T	J	261.30	261.30	263.88	275.86
	DK 2/L4C	ICP	5.96	0.102	C	J	164.89	163.03	164.70	168.89
	DK 3/L1T	ICP	7.40	0.102	T	J	193.37	191.04	194.25	206.70
	DK 3/L2C	ICP	7.40	0.102	C	J	199.86	195.52	197.39	212.90
	DK 3/L4C	ICP	7.54	0.102	C	J	292.41	289.14	291.63	295.86
	DK 3/L5C	ICP	7.54	0.102	C	J	294.55	298.34	298.34	302.11
	DK 3/L6T	ICP	7.54	0.102	T	J	201.77	200.59	202.06	206.83
	DK CS'T89a	OE-S	11.30	0.324	T	D	558.77	556.03	553.74	567.54
	DK CS'T89b	OE-S	11.60	0.324	T	D	612.92	577.38	609.33	624.22
	DK CS'C89a	OE-S	11.30	0.324	C	D	1,198.09	-	-	-
	DK CS'C89b	OE-S	11.60	0.324	C	D	1,224.88	-	-	-
	DK CS'T94	OE-S	11.60	0.324	T	D	1,072.25	1,033.97	1,080.83	1,104.97
	DK CL'T89a	OE-S	11.30	0.324	T	D	669.43	593.74	659.23	691.09
	DK CL'T89b	OE-S	11.60	0.324	T	D	778.61	774.37	770.46	801.28
	DK CL'C89a	OE-S	11.30	0.324	C	D	1,218.15	-	-	-
	DK CL'C89b	OE-S	11.60	0.324	C	D	1,237.21	-	-	-
	DK LS'T94	OE-S	22.10	0.324	T	D	4,433.55	4,433.55	4,489.11	7,812.50
15	E 1/30.5-1	OE-S	30.50	0.762	C	D	11,570.60	6,321.14	7,633.47	14,492.75
	E 1/30.5-2	OE-S	30.50	0.762	T	D	2,938.05	2,368.89	2,942.54	2,985.07
	E 1/38.7-1	OE-S	38.70	0.762	T	D	9,529.93	7,486.70	11,327.33	16,129.03
	E 1/38.7-2	OE-S	38.70	0.762	C	D	16,424.36	10,373.26	12,472.30	18,867.92
	E 1/38.7-3	OE-S	38.70	0.762	T	D	8,704.78	6,386.50	8,786.95	10,101.01
	E 1/47.0-1	OE-S	47.00	0.762	C	D	23,407.80	17,374.30	17,922.79	26,315.79
	E 1/47.0-2	OE-S	47.00	0.762	T	D	13,594.25	12,141.75	13,657.32	16,393.44
	E 1/47.0-3	OE-S	47.00	0.762	C	D	23,407.80	17,095.00	18,292.47	27,777.78

Notes: L: pile length; d: pile diameter for piles with circular cross-section; B: pile width for piles with square cross-section; DS: drilled shaft; CFA: continuous flight auger pile; CE-S: closed-ended steel pipe pile; OE-S: open-ended steel pipe pile; OE-SC: open ended concrete filled steel pipe pile; ICP: closed-ended Imperial College Pile; HP: H-section steel pile; PTC: pre-stressed concrete thin-wall caisson; PHC: Pre-stressed concrete high-strength; Sq-C: square precast concrete pile; C-C: circular precast concrete pile; C: top-down compression loading mode; T: top-up tension (or uplift) loading mode; O-cell (U): upward loading mode of bi-directional Osterberg cell; O-cell (D): downward loading mode of bi-directional Osterberg cell; A: augered piles; D: driven piles; J: jacked piles; B-CIS: bored cast in-situ piles; $Q_{max\text{-}measured}$: maximum applied load; $Q_{Davisson}$; estimated capacity from Davisson's offset line criterion; $Q_{w/d=10\%}$: estimated capacity from French criterion (w/d = 10%); $Q_{C\text{-}K}$: estimated capacity from Chin-Kondner criterion.

Table E.1. (continued).

Site ID No.	Pile information, load test results and interpretations									
	Pile ID	**Pile type/ material**	**L (m)**	**d or B (m)**	**Loading mode**	**Installation method**	**$Q_{max\text{-}measured}$ (kN)**	**$Q_{Davisson}$ (kN)**	**$Q_{w/d=10\%}$ (kN)**	**$Q_{C\text{-}K}$ (kN)**
16	E 2/46.7-1	OE-S	46.70	0.762	C	D	21,631.60	17,409.05	17,657.03	25,000.00
	E 2/46.7-2	OE-S	46.70	0.762	T	D	10,951.70	9,609.60	11,027.86	13,157.89
	E 2/46.7-3	OE-S	46.70	0.762	C	D	23,368.40	18,947.35	19,730.88	26,315.79
	E 2/47.0R-1	OE-S	47.00	0.762	C	D	29,985.00	41,379.30	29,729.82	62,500.00
	E 2/47.0R -2	OE-S	47.00	0.762	T	D	17,062.46	17,062.82	19,481.59	40,000.00
17	FBJ 1	DS	15.00	0.500	C	B-CIS	1,500.26	1,650.29	2,277.68	2,597.40
18	FSB 1	Sq-C	12.80	0.235	C	D	463.00	415.00	458.72	480.54
19	FCS 1	DS	12.00	0.500	C	B-CIS	1,319.75	1,254.35	1,320.15	1,336.90
	FCS 2	OE-S	9.40	0.508	C	D	981.89	936.03	1,074.85	1,107.42
	FCS 3	OE-S	9.40	0.508	C	J	668.98	598.84	664.84	678.43
	FCS 4	HP	10.20	16 x 155	C	D	1,129.66	1,089.17	1,195.25	1,223.99
	FCS 5	HP	10.20	16 x 155	C	J	748.14	637.30	742.81	758.73
20	FMC 1-U	DS	9.95	1.40	O-cell (U)	B-CIS	5,370.52	5,003.13	5,474.30	5,586.59
	FMC 1-L	DS	4.05	1.40	O-cell (D)	B-CIS	5,370.50	5,155.39	6,117.30	6,250.00
21	GT C1	DS	21.40	0.762	C	B-CIS	9,806.65	11,277.65	17,486.22	27,027.03
	GT C2	DS	16.92	0.762	C	B-CIS	4,903.33	3,922.66	4,088.54	5,988.02
22	GB Pier 12-U	DS	24.60	1.57	O-cell (U)	B-CIS	8,338.10	28,776.98	32,092.60	35,971.22
	GB Pier 12-L	DS	0.76	1.57	O-cell (D)	B-CIS	8,338.10	5,950.48	8,757.70	9,259.26
23	GEB N1	PTC	36.00	0.357	C	D	2,497.96	3,247.35	3,357.89	5,494.51
24	GEB S1-U	DS	44.00	2.60	O-cell (U)	B-CIS	28,900.80	27,493.30	31,560.30	32,258.06
	GEB S1-M	DS	26.50	2.60	O-cell (D)	B-CIS	28,713.10	28,843.22	32,766.20	33,333.33
	GEB S1-L	DS	4.00	2.60	O-cell (D)	B-CIS	8,057.85	7,013.55	8,253.70	8,474.58
25	GEB S2	DS	32.00	2.500	C	B-CIS	16,048.10	15,356.90	16,489.66	16,666.67

Notes: L: pile length; d: pile diameter for piles with circular cross-section; B: pile width for piles with square cross-section; DS: drilled shaft; CFA: continuous flight auger pile; CE-S: closed-ended steel pipe pile; OE-S: open-ended steel pipe pile; OE-SC: open ended concrete filled steel pipe pile; ICP: closed-ended Imperial College Pile; HP: H-section steel pile; PTC: pre-stressed concrete thin-wall caisson; PHC: Pre-stressed concrete high-strength; Sq-C: square precast concrete pile; C-C: circular precast concrete pile; C: top-down compression loading mode; T: top-up tension (or uplift) loading mode; O-cell (U): upward loading mode of bi-directional Osterberg cell; O-cell (D): downward loading mode of bi-directional Osterberg cell; A: augered piles; D: driven piles; J: jacked piles; B-CIS: bored cast in-situ piles; $Q_{max\text{-}measured}$: maximum applied load; $Q_{Davisson}$; estimated capacity from Davisson's offset line criterion; $Q_{w/d=10\%}$: estimated capacity from French criterion (w/d = 10%); $Q_{C\text{-}K}$: estimated capacity from Chin-Kondner criterion.

Table E.1. (continued).

Site No.	ID	Pile information, load test results and interpretations								
	Pile ID	Pile type/ material	L (m)	d or B (m)	Loading mode	Installation method	$Q_{max\text{-}measured}$ (kN)	$Q_{Davisson}$ (kN)	$Q_{w/d=10\%}$ (kN)	$Q_{C\text{-}K}$ (kN)
26	GRS 1	DS	11.76	0.600	C	B-CIS	1,794.23	1,571.10	1,950.74	2,032.52
27	GBR 1	CE-S	4.50	0.114	C	D	7.20	7.50	7.80	8.03
28	HAFB 1	OE-S	12.19	0.114	C	J	75.00	71.95	79.50	86.15
29	HPHC TP1	CFA	14.00	0.600	C	A	1,203.81	1,203.81	1,335.59	1,428.57
	HPHC TP2	CFA	18.00	0.600	C	A	1,441.95	1,338.61	1,495.28	1,536.10
30	HSD E1	C-C	3.50	0.28	C	D	215.94	164.31	218.76	234.41
	HSD E2	C-C	7.50	0.28	C	D	204.52	172.22	202.43	214.00
	HSD E3	C-C	11.50	0.28	C	D	333.45	271.16	324.33	371.06
	HSD E4	C-C	15.50	0.28	C	D	473.09	386.68	463.62	506.07
	HSD E5	C-C	19.50	0.28	C	D	652.51	554.65	637.23	706.21
	HSD E6	C-C	23.50	0.28	C	D	933.93	767.56	860.34	1,017.29
	HSD A1	C-C	8.00	0.28	C	D	285.78	233.38	276.88	295.51
	HSD D/A1	C-C	16.00	0.28	C	D	507.25	423.45	494.48	534.47
	HSD E7	C-C	23.50	0.28	T	D	318.16	256.51	311.73	338.41
	HSD A2	C-C	8.00	0.28	T	D	102.08	91.00	102.96	105.37
	HSD D/A2	C-C	16.00	0.28	T	D	275.22	235.17	270.98	287.52
31	IMTDC 1	PHC	29.00	0.50	C	J	2,510.96	1,816.44	2,423.10	2,958.58
32	I-85B 1	DS	19.20	0.914	C	B-CIS	6,908.35	5,314.12	7,605.55	8,474.58
33	JCEPF 1	CE-S	9.45	0.273	C	D	1,087.82	1,087.82	1,154.57	1,213.59
	JCEPF 2	CE-S	17.80	0.273	C	D	1,087.18	1,146.26	1,205.33	1,256.28

Notes: L: pile length; d: pile diameter for piles with circular cross-section; B: pile width for piles with square cross-section; DS: drilled shaft; CFA: continuous flight auger pile; CE-S: closed-ended steel pipe pile; OE-S: open-ended steel pipe pile; OE-SC: open ended concrete filled steel pipe pile; ICP: closed-ended Imperial College Pile; HP: H-section steel pile; PTC: pre-stressed concrete thin-wall caisson; PHC: Pre-stressed concrete high-strength; Sq-C: square precast concrete pile; C-C: circular precast concrete pile; C: top-down compression loading mode; T: top-up tension (or uplift) loading mode; O-cell (U): upward loading mode of bi-directional Osterberg cell; O-cell (D): downward loading mode of bi-directional Osterberg cell; A: augered piles; D: driven piles; J: jacked piles; B-CIS: bored cast in-situ piles; $Q_{max\text{-}measured}$: maximum applied load; $Q_{Davisson}$; estimated capacity from Davisson's offset line criterion; $Q_{w/d=10\%}$: estimated capacity from French criterion (w/d = 10%); $Q_{C\text{-}K}$: estimated capacity from Chin-Kondner criterion.

Table E.1. (continued).

Site ID No.	Pile information, load test results and interpretations									
	Pile ID	**Pile type/ material**	**L (m)**	**d or B (m)**	**Loading mode**	**Installation method**	**$Q_{max\text{-}measured}$ (kN)**	**$Q_{Davisson}$ (kN)**	**$Q_{w/d=10\%}$ (kN)**	**$Q_{C\text{-}K}$ (kN)**
34	KG S2T	Sq-C	6.00	0.32	T	D	60.87	50.19	65.84	71.42
	KG S1C	Sq-C	6.00	0.32	C	D	58.07	54.03	58.36	59.48
	KG G3C	Sq-C	6.00	0.32	C	D	42.50	53.26	64.02	66.35
	KG G1crT(r)	Sq-C	6.00	0.32	T	D	92.16	85.65	93.77	96.24
	KG S4T	Sq-C	6.00	0.32	T	D	64.28	62.03	64.65	65.21
	KG S4T(r)	Sq-C	6.00	0.32	T	D	96.20	86.50	99.84	104.62
	KG S1T	Sq-C	6.00	0.32	T	D	67.65	64.60	69.30	71.12
	KG OE-C1	OE-S	2.01	0.168	C	D	10.75	10.70	10.77	10.92
	KG CE-C1	CE-S	2.80	0.073	C	D	6.24	6.09	6.27	6.60
	KG CE-C4	CE-S	3.25	0.073	C	D	8.42	7.93	8.40	8.96
35	KCS TP-1A	PTC	35.50	0.25	C	J	631.95	580.63	614.10	671.14
	KCS TP-2	PTC	14.50	0.25	C	J	259.23	351.83	406.00	452.28
	KCS TP-3	PTC	23.50	0.25	C	J	414.67	530.50	569.90	663.13
	KCS TP-4	PTC	11.50	0.25	C	J	234.90	217.33	234.00	241.31
36	KTJ 1	PHC	30.00	0.50	C	J	2,527.93	2,429.81	2,513.05	2,597.40
37	LB 1/L1C	ICP	5.95	0.102	C	J	96.41	96.97	102.10	107.65
	LB 2/L1C	ICP	1.83	0.102	C	J	52.63	53.11	56.10	58.12
	LB 2/L1T	ICP	5.95	0.102	T	J	49.07	40.12	46.90	59.10
38	LTS B1	Fundex	8.59	0.45	C	A	3,130.57	2,410.83	3,043.84	3,355.70
	LTS B2	Olivier	8.20	0.55	C	A	3,063.90	2,164.74	3,321.52	3,745.32
	LTS B3	Omega	8.45	0.41	C	A	2,956.52	1,870.33	2,802.36	3,508.77
	LTS B4	De Waal	8.53	0.41	C	A	2,643.24	1,554.55	2,424.60	3,095.98
	LTS B5	Sq-C	8.51	0.35	C	D	2,913.15	2,036.65	2,709.82	3,012.05
	LTS B6	Sq-C	8.57	0.35	C	D	3,568.21	2,483.09	3,554.97	3,875.97
	LTS B7	Atlas	8.43	0.51	C	A	3,619.84	1,987.37	3,453.34	4,166.67
	LTS B8	Atlas	8.43	0.52	C	A	3,427.25	1,986.14	3,357.24	3,636.36
	LTS B9	Fundex	8.65	0.43	C	A	1,654.34	1,203.28	1,755.94	1,937.98
	LTS B10	Olivier	8.13	0.55	C	A	2,691.19	1,796.17	3,026.92	3,623.19
	LTS B11	Omega	8.45	0.41	C	A	2,942.75	1,819.61	2,739.66	3,311.26
	LTS B12	De Waal	9.52	0.43	C	A	2,529.32	1,400.95	2,264.86	2,785.52

Notes: L: pile length; d: pile diameter for piles with circular cross-section; B: pile width for piles with square cross-section; DS: drilled shaft; CFA: continuous flight auger pile; CE-S: closed-ended steel pipe pile; OE-S: open-ended steel pipe pile; OE-SC: open ended concrete filled steel pipe pile; ICP: closed-ended Imperial College Pile; HP: H-section steel pile; PTC: pre-stressed concrete thin-wall caisson; PHC: Pre-stressed concrete high-strength; Sq-C: square precast concrete pile; C-C: circular precast concrete pile; C: top-down compression loading mode; T: top-up tension (or uplift) loading mode; O-cell (U): upward loading mode of bi-directional Osterberg cell; O-cell (D): downward loading mode of bi-directional Osterberg cell; A: augered piles; D: driven piles; J: jacked piles; B-CIS: bored cast in-situ piles; $Q_{max\text{-}measured}$: maximum applied load; $Q_{Davisson}$; estimated capacity from Davisson's offset line criterion; $Q_{w/d=10\%}$: estimated capacity from French criterion (w/d = 10%); $Q_{C\text{-}K}$: estimated capacity from Chin-Kondner criterion.

Table E.1. (continued).

Site ID No.	Pile information, load test results and interpretations									
	Pile ID	**Pile type/ material**	**L (m)**	**d or B (m)**	**Loading mode**	**Installation method**	**$Q_{max\text{-}measured}$ (kN)**	**$Q_{Davisson}$ (kN)**	**$Q_{w/d=10\%}$ (kN)**	**$Q_{C\text{-}K}$ (kN)**
39	DRS P-I	OE-S	40.20	0.48	C	D	4,135.67	3,190.23	4,030.70	4,201.68
	DRS P-D	OE-S	40.20	0.48	C	D	3,278.99	3,111.60	3,280.60	3,322.26
40	L&D 1-1T	HP	18.52	14 x 73	T	D	1,612.30	1,011.73	1,976.10	2,463.05
	L&D 1-2T	HP	16.46	14 x 73	T	D	1,383.82	501.25	1,446.20	2,421.31
	L&D 1-3AC	HP	16.46	14 x 73	C	D	2,875.69	1,987.34	2,904.80	3,802.28
	L&D 1-3BT	HP	16.46	14 x 73	T	D	578.29	324.25	671.10	809.06
	L&D 1-5T	HP	18.44	14 x 73	T	D	1,613.43	1,354.05	2,543.10	3,597.12
	L&D 1-6C	HP	16.15	14 x 73	C	D	3,559.61	2,667.03	4,248.70	6,289.31
	L&D 1-7C	HP	17.98	14 x 73	C	D	3,573.79	5,109.58	5,978.10	9,900.99
	L&D 2-1T	HP	16.76	14 x 73	T	D	1,508.92	957.45	1,621.00	2,057.61
	L&D 2-7C	HP	20.37	14 x 73	C	D	3,566.51	6,347.54	6,307.00	11,363.64
	L&D 2-8T	HP	12.19	14 x 73	T	D	450.46	263.74	505.90	577.03
	L&D 3-1C	CE-S	14.23	0.30	C	D	1,268.93	1,112.85	1,298.50	1,477.10
	L&D 3-2T	CE-S	10.97	0.30	T	D	707.88	680.07	771.20	808.41
	L&D 3-4C	CE-S	14.39	0.36	C	D	1,108.66	881.96	1,223.20	1,385.04
	L&D 3-5T	CE-S	11.12	0.36	T	D	779.96	686.76	862.30	919.12
	L&D 3-7C	CE-S	14.57	0.41	C	D	1,770.12	1,254.71	1,814.70	2,083.33
	L&D 3-8T	CE-S	11.12	0.41	T	D	1,185.85	985.76	1,292.80	1,392.76
	L&D 3-10C	HP	20.02	14 x 73	C	D	3,559.13	4,902.27	5,465.60	7,936.51
	L&D 3-14T	HP	11.89	14 x 73	T	D	1,459.20	1,377.24	1,759.40	1,876.17
	L&D 3-15T	HP	11.28	14 x 73	T	D	957.19	722.69	1,067.10	1,150.75
	L&D 3-16T	HP	11.28	14 x 73	T	D	1,044.99	839.33	1,159.60	1,240.69
41	UBC PRS 1	CE-S	11.83	0.324	C	D	214.34	193.67	220.85	229.52
	UBC PRS 2	CE-S	13.90	0.324	C	D	297.17	248.02	301.78	318.24
	UBC PRS 3	CE-S	16.80	0.324	C	D	653.58	509.95	695.80	870.32
	UBC PRS 4	OE-S	23.20	0.324	C	D	1,102.83	961.22	1,120.92	1,344.09
	UBC PRS 5	CE-S	31.10	0.324	C	D	1,089.20	1,051.95	1,082.76	1,126.13
42	MOTH PRS A	OE-S	67.00	0.915	C	D	7,462.76	7,432.25	7,802.20	8,264.46
	MOTH PRS B	OE-S	78.00	0.915	C	D	7,064.46	7,003.52	7,359.89	7,936.51
	MOTH PRS C	OE-S	94.00	0.915	C	D	7,832.59	7,822.41	7,922.38	8,403.36
43	NMGC 1	DS	21.50	0.760	C	B-CIS	4,980.00	4,980.00	5,981.17	6,329.11

Notes: L: pile length; d: pile diameter for piles with circular cross-section; B: pile width for piles with square cross-section; DS: drilled shaft; CFA: continuous flight auger pile; CE-S: closed-ended steel pipe pile; OE-S: open-ended steel pipe pile; OE-SC: open ended concrete filled steel pipe pile; ICP: closed-ended Imperial College Pile; HP: H-section steel pile; PTC: pre-stressed concrete thin-wall caisson; PHC: Pre-stressed concrete high-strength; Sq-C: square precast concrete pile; C-C: circular precast concrete pile; C: top-down compression loading mode; T: top-up tension (or uplift) loading mode; O-cell (U): upward loading mode of bi-directional Osterberg cell; O-cell (D): downward loading mode of bi-directional Osterberg cell; A: augered piles; D: driven piles; J: jacked piles; B-CIS: bored cast in-situ piles; $Q_{max\text{-}measured}$: maximum applied load; $Q_{Davisson}$; estimated capacity from Davisson's offset line criterion; $Q_{w/d=10\%}$: estimated capacity from French criterion (w/d = 10%); $Q_{C\text{-}K}$: estimated capacity from Chin-Kondner criterion.

Table E.1. (continued).

Site No.	ID	Pile information, load test results and interpretations								
	Pile ID	Pile type/ material	L (m)	d or B (m)	Loading mode	Installation method	$Q_{max\text{-}measured}$ (kN)	$Q_{Davisson}$ (kN)	$Q_{w/d=10\%}$ (kN)	$Q_{C\text{-}K}$ (kN)
44	NWU NGES 1	HP	15.24	14 x 73	C	D	984.05	936.05	986.93	1,000.00
	NWU NGES 2	DS	15.24	0.55	C	B-CIS	1,934.01	1,824.91	2,017.98	2,083.33
	NWU NGES 3	OE-S	15.24	0.46	C	D	1,023.94	956.11	1,029.22	1,044.93
	NWU NGES 4	DS	15.24	0.48	C	B-CIS	1,820.76	1,532.38	1,856.95	1,972.39
45	NP T1	OE-S	8.30	0.80	C	D	4,695.34	3,906.81	4,704.28	4,716.98
	NP T2	OE-S	8.30	0.80	C	D	3,438.85	3,189.78	3,559.40	3,636.36
	NP T3	OE-S	8.80	0.80	T	D	3,587.60	2,712.60	3,819.87	4,201.68
46	OSJS 1	DS	12.80	0.406	C	B-CIS	1,129.06	784.69	1,149.55	1,329.79
47	OC A1	CE-S	5.00	0.219	T	D	95.00	103.27	110.38	114.42
	OC A2	CE-S	5.00	0.219	T	D	160.00	-	-	-
	OC A3	CE-S	5.00	0.219	T	D	231.00	209.14	260.25	295.68
	OC A4	CE-S	5.00	0.219	T	D	262.00	182.11	280.20	335.12
	OC B1	OE-S	5.00	0.219	T	D	453.00	475.73	511.46	521.92
	OC C1-1	CE-S	5.00	0.219	T	D	424.00	295.05	450.19	608.27
	OC C1-2	CE-S	10.00	0.219	T	D	500.00	426.49	515.98	570.45
	OC C1-3	CE-S	5.00	0.219	T	D	66.05	-	-	-
	OC C1-4	CE-S	5.00	0.219	T	D	78.09	-	-	-
	OC C1-5	CE-S	5.00	0.219	T	D	111.80	-	-	-

Notes: L: pile length; d: pile diameter for piles with circular cross-section; B: pile width for piles with square cross-section; DS: drilled shaft; CFA: continuous flight auger pile; CE-S: closed-ended steel pipe pile; OE-S: open-ended steel pipe pile; OE-SC: open ended concrete filled steel pipe pile; ICP: closed-ended Imperial College Pile; HP: H-section steel pile; PTC: pre-stressed concrete thin-wall caisson; PHC: Pre-stressed concrete high-strength; Sq-C: square precast concrete pile; C-C: circular precast concrete pile; C: top-down compression loading mode; T: top-up tension (or uplift) loading mode; O-cell (U): upward loading mode of bi-directional Osterberg cell; O-cell (D): downward loading mode of bi-directional Osterberg cell; A: augered piles; D: driven piles; J: jacked piles; B-CIS: bored cast in-situ piles; $Q_{max\text{-}measured}$: maximum applied load; $Q_{Davisson}$; estimated capacity from Davisson's offset line criterion; $Q_{w/d=10\%}$: estimated capacity from French criterion (w/d = 10%); $Q_{C\text{-}K}$: estimated capacity from Chin-Kondner criterion.

Table E.1. (continued).

Site ID No.	Pile information, load test results and interpretations									
	Pile ID	**Pile type/ material**	**L (m)**	**d or B (m)**	**Loading mode**	**Installation method**	**$Q_{max\text{-}measured}$ (kN)**	**$Q_{Davisson}$ (kN)**	**$Q_{w/d=10\%}$ (kN)**	**$Q_{C\text{-}K}$ (kN)**
48	PT LDP	OE-S	40.00	0.762	C	D	6,070.78	6,372.67	6,674.57	7,352.94
	PT NGI A5-1	CE-S	10.00	0.219	T	D	140.00	118.38	144.57	160.57
	PT NGI A5-2	CE-S	10.00	0.219	T	D	134.05	127.57	134.83	137.04
	PT NGI A6-1	CE-S	10.00	0.219	T	D	356.22	282.70	370.66	422.30
	PT NGI A6-2	CE-S	10.00	0.219	T	D	313.51	300.00	327.85	350.51
	PT 1/L1C	ICP	4.30	0.102	C	J	29.55	28.98	29.46	30.02
	PT 2/L1C	ICP	8.50	0.102	C	J	88.55	90.68	92.81	95.42
	PT 2/L2T	ICP	8.50	0.102	T	J	77.86	84.18	90.50	101.38
	PT 3/L1T	ICP	5.47	0.102	T	J	69.16	68.93	91.66	142.92
	PT 3/L2T	ICP	5.47	0.102	T	J	49.01	49.01	50.89	52.44
	PT 4/L1C	ICP	5.88	0.102	C	J	74.32	80.38	86.44	94.50
	PT 5/L1T	ICP	10.59	0.102	T	J	119.83	114.85	121.04	125.42
	PT 5/L2T	ICP	10.59	0.102	T	J	90.48	90.48	90.86	91.24
	PT 5/L3C	ICP	10.59	0.102	C	J	101.34	124.98	148.62	221.68
	PT 5/L4T	ICP	10.59	0.102	T	J	86.35	85.66	86.92	88.87
	PT 5/L6T	ICP	10.59	0.102	T	J	80.39	81.02	81.65	82.64
	PT 6/L1C	ICP	3.75	0.102	C	J	52.06	52.06	53.87	55.38
	PT 7/L1C	ICP	8.75	0.102	C	J	106.04	93.88	100.36	110.95
	PT 7/L2C	ICP	8.75	0.102	C	J	97.23	95.68	96.89	98.38
	PT 7/L3T	ICP	8.75	0.102	T	J	78.94	78.94	79.79	81.12
49	PPI 1-U	DS	19.86	1.53	O-Cell (U)	B-CIS	5,302.77	5,283.69	5,497.20	5,534.03
	PPI 1-M	DS	5.34	1.53	O-Cell (D)	B-CIS	4,444.41	4,291.81	5,250.30	5,405.41
	PPI 1-L	DS	0.87	1.53	O-Cell (D)	B-CIS	6,821.39	4,299.18	7,306.80	8,130.08
	PPI 2-U	DS	24.40	1.53	O-Cell (U)	B-CIS	9,220.10	8,911.15	9,621.20	9,708.74
	PPI 2-M	DS	9.90	1.53	O-Cell (D)	B-CIS	8,185.17	7,488.98	8,367.60	8,474.58
	PPI 2-L	DS	0.75	1.53	O-Cell (D)	B-CIS	2,426.65	1,738.78	2,646.00	2,958.58
50	PRB '73	OE-SC	55.00	0.610	C	D	3,810.28	4,151.41	4,492.54	4,761.90
	PRB '07	OE-SC	100.00	1.824	C	D	44,548.00	37,899.70	57,255.25	76,923.08

Notes: L: pile length; d: pile diameter for piles with circular cross-section; B: pile width for piles with square cross-section; DS: drilled shaft; CFA: continuous flight auger pile; CE-S: closed-ended steel pipe pile; OE-S: open-ended steel pipe pile; OE-SC: open ended concrete filled steel pipe pile; ICP: closed-ended Imperial College Pile; HP: H-section steel pile; PTC: pre-stressed concrete thin-wall caisson; PHC: Pre-stressed concrete high-strength; Sq-C: square precast concrete pile; C-C: circular precast concrete pile; C: top-down compression loading mode; T: top-up tension (or uplift) loading mode; O-cell (U): upward loading mode of bi-directional Osterberg cell; O-cell (D): downward loading mode of bi-directional Osterberg cell; A: augered piles; D: driven piles; J: jacked piles; B-CIS: bored cast in-situ piles; $Q_{max\text{-}measured}$: maximum applied load; $Q_{Davisson}$; estimated capacity from Davisson's offset line criterion; $Q_{w/d=10\%}$: estimated capacity from French criterion (w/d = 10%); $Q_{C\text{-}K}$: estimated capacity from Chin-Kondner criterion.

Table E.1. (continued).

Site No.	ID	Pile information, load test results and interpretations								
	Pile ID	Pile type/ material	L (m)	d or B (m)	Loading mode	Installation method	$Q_{max\text{-}measured}$ (kN)	$Q_{Davisson}$ (kN)	$Q_{w/d=10\%}$ (kN)	$Q_{C\text{-}K}$ (kN)
51	REP MW B1-U	DS	23.80	0.457	O-Cell (U)	B-CIS	1,974.35	1,801.82	1,902.25	2,100.84
	REP MW B1-L	DS	1.80	0.457	O-Cell (D)	B-CIS	1,974.35	937.40	1,922.31	3,086.42
	REP MW G1-U	DS	24.40	0.457	O-Cell (U)	B-CIS	1,565.93	1,379.25	1,511.29	1,610.31
	REP MW G1-L	DS	1.80	0.457	O-Cell (D)	B-CIS	1,565.93	1,094.98	1,888.52	2,212.39
52	SA 1-1	CE-S	6.40	0.22	C	J	47.73	56.09	64.44	69.88
	SA 1-2	CE-S	6.40	0.22	C	J	67.27	67.27	82.34	88.30
	SA 1-3	CE-S	6.40	0.22	C	J	77.03	77.03	95.78	104.69
	SA 1-4	CE-S	6.40	0.22	C	J	80.94	80.16	96.32	104.01
	SA 1-5	CE-S	6.40	0.22	C	J	85.68	85.68	99.84	106.22
53	SPI 1	CE-S	45.00	0.406	C	D	1,854.23	1,912.73	1,935.24	1,976.28
54	SFBM P10T	OE-SC	38.90	0.25	T	D	1,822.90	1,822.90	1,501.64	2,577.32
	SFBM P11T	OE-SC	26.90	0.26	T	D	1,094.08	1,086.19	1,110.20	1,265.82
	SFBM P12T	OE-SC	38.50	0.25	T	D	2,121.58	2,121.58	1,832.73	2,597.40
	SFBM P13C	OE-SC	26.90	0.27	C	D	982.86	982.86	989.32	1,010.10
	SFBM P13T	OE-SC	26.90	0.27	T	D	823.36	640.15	789.58	938.97
	SFBM P31C	Fundex	25.10	0.57	C	A	865.00	865.00	888.69	896.06
	SFBM P31T	Fundex	25.10	0.57	T	A	825.44	711.24	877.29	930.23
	SFBM P32C	Fundex	33.70	0.57	C	A	3,347.70	2,018.67	3,148.67	3,861.00
	SFBM P32T	Fundex	33.70	0.57	T	A	1,252.13	1,059.22	1,267.27	1,290.32
	SFBM P33C	Fundex	25.10	0.57	C	A	1,775.33	1,758.18	1,799.69	1,811.59
	SFBM P33T	Fundex	25.10	0.57	T	A	1,524.14	860.60	1,586.82	1,841.62
	SFBM P34C	Fundex	33.70	0.57	C	A	4,361.22	2,624.09	5,301.23	10,638.30
	SFBM P34T	Fundex	33.70	0.57	T	A	3,395.91	1,616.39	3,488.48	5,208.33
	SFBM P48C	OE-S	26.10	0.41	C	D	1,316.80	1,316.80	1,330.27	1,340.48
	SFBM P48T	OE-S	26.10	0.41	T	D	1,435.62	1,245.95	1,535.77	1,828.15
	SFBM P49T	OE-S	26.10	0.41	T	D	1,314.48	1,178.89	1,326.73	1,347.71
	SFBM P49C	OE-S	26.10	0.41	C	D	1,135.96	1,127.49	1,138.60	1,146.79
	SFBM P50C	Sq-C	26.50	0.36	C	D	1,149.62	1,132.58	1,177.25	1,196.17

Notes: L: pile length; d: pile diameter for piles with circular cross-section; B: pile width for piles with square cross-section; DS: drilled shaft; CFA: continuous flight auger pile; CE-S: closed-ended steel pipe pile; OE-S: open-ended steel pipe pile; OE-SC: open ended concrete filled steel pipe pile; ICP: closed-ended Imperial College Pile; HP: H-section steel pile; PTC: pre-stressed concrete thin-wall caisson; PHC: Pre-stressed concrete high-strength; Sq-C: square precast concrete pile; C-C: circular precast concrete pile; C: top-down compression loading mode; T: top-up tension (or uplift) loading mode; O-cell (U): upward loading mode of bi-directional Osterberg cell; O-cell (D): downward loading mode of bi-directional Osterberg cell; A: augered piles; D: driven piles; J: jacked piles; B-CIS: bored cast in-situ piles; $Q_{max\text{-}measured}$: maximum applied load; $Q_{Davisson}$; estimated capacity from Davisson's offset line criterion; $Q_{w/d=10\%}$: estimated capacity from French criterion (w/d = 10%); $Q_{C\text{-}K}$: estimated capacity from Chin-Kondner criterion.

Table E.1. (continued).

Site ID No.	Pile information, load test results and interpretations									
	Pile ID	**Pile type/ material**	**L (m)**	**d or B (m)**	**Loading mode**	**Installation method**	**$Q_{max\text{-}measured}$ (kN)**	**$Q_{Davisson}$ (kN)**	**$Q_{w/d=10\%}$ (kN)**	**$Q_{C\text{-}K}$ (kN)**
54	SFBM P50T	Sq-C	26.50	0.36	T	D	598.71	495.75	646.99	710.73
	SFBM P51T	Sq-C	26.50	0.36	T	D	628.50	578.98	673.03	697.35
	SFBM P51C	Sq-C	26.50	0.36	C	D	1,201.34	1,100.47	1,288.31	1,381.22
	SFBM P59T	Sq-C	33.40	0.36	T	D	727.48	725.71	767.45	784.93
	SFBM P59C	Sq-C	33.40	0.36	C	D	2,626.29	2,626.29	4,262.37	9,900.99
	SFBM P61C	Sq-C	33.40	0.36	C	D	2,774.01	3,522.20	4,270.39	7,042.25
	SFBM P61T	Sq-C	33.40	0.36	T	D	676.45	665.32	684.05	690.13
	SFBM P69C	HP	26.50	14 x 89	C	D	1,271.38	1,206.17	1,314.73	1,371.74
	SFBM P69T	HP	26.50	14 x 89	T	D	1,178.08	820.98	1,490.25	2,159.83
	SFBM P70T	HP	26.50	14 x 89	T	D	1,326.95	1,250.38	1,408.82	1,508.30
	SFBM P73T	OE-SC	41.10	0.22	T	D	2,096.16	1,710.63	1,245.91	2,283.11
	SFBM P73C	OE-SC	41.10	0.22	C	D	1,401.55	879.93	713.66	2,247.19
	SFBM P74C	OE-SC	26.70	0.25	C	D	1,633.44	1,633.44	1,575.28	1,908.40
	SFBM P74T	OE-SC	26.70	0.25	T	D	978.64	572.45	735.38	1,295.34
55	SPP P01	OE-S	4.00	0.089	T	D	49.82	33.07	43.35	54.04
	SPP P02	OE-S	4.00	0.043	T	D	26.49	20.63	20.16	28.99
	SPP P03	CE-S	4.00	0.089	T	D	34.70	31.95	33.65	36.56
	SPP P04	OE-S	4.00	0.089	T	D	60.88	48.00	55.89	64.83
	SPP P05	OE-S	4.00	0.114	T	D	68.82	54.13	67.60	70.22
	SPP P06	OE-S	4.00	0.089	T	D	56.54	40.21	49.79	63.85
	SPP P07	OE-S	2.50	0.043	T	D	73.26	-	-	-
	SPP P08	OE-S	2.50	0.043	T	D	12.22	11.90	11.54	12.58
	SPP P09	OE-S	2.50	0.034	T	D	5.69	5.11	4.94	6.02
	SPP P10	OE-S	3.50	0.034	T	D	9.02	8.63	8.30	9.29
	SPP P11	OE-S	2.50	0.089	T	D	22.43	20.77	21.76	23.10
	SPP P12	CE-S	2.50	0.089	T	D	18.68	15.90	17.39	19.77
56	SSK A	DS	52.40	1.100	C	B-CIS	11,750.50	8,759.92	11,891.90	13,698.63
	SSK B	DS	47.00	1.200	C	B-CIS	11,837.28	-	-	-

Notes: L: pile length; d: pile diameter for piles with circular cross-section; B: pile width for piles with square cross-section; DS: drilled shaft; CFA: continuous flight auger pile; CE-S: closed-ended steel pipe pile; OE-S: open-ended steel pipe pile; OE-SC: open ended concrete filled steel pipe pile; ICP: closed-ended Imperial College Pile; HP: H-section steel pile; PTC: pre-stressed concrete thin-wall caisson; PHC: Pre-stressed concrete high-strength; Sq-C: square precast concrete pile; C-C: circular precast concrete pile; C: top-down compression loading mode; T: top-up tension (or uplift) loading mode; O-cell (U): upward loading mode of bi-directional Osterberg cell; O-cell (D): downward loading mode of bi-directional Osterberg cell; A: augered piles; D: driven piles; J: jacked piles; B-CIS: bored cast in-situ piles; $Q_{max\text{-}measured}$: maximum applied load; $Q_{Davisson}$; estimated capacity from Davisson's offset line criterion; $Q_{w/d=10\%}$: estimated capacity from French criterion (w/d = 10%); $Q_{C\text{-}K}$: estimated capacity from Chin-Kondner criterion.

Table E.1. (continued).

Site ID No.	Pile information, load test results and interpretations									
	Pile ID	**Pile type/ material**	**L (m)**	**d or B (m)**	**Loading mode**	**Installation method**	**$Q_{max\text{-}measured}$ (kN)**	**$Q_{Davisson}$ (kN)**	**$Q_{w/d=10\%}$ (kN)**	**$Q_{C\text{-}K}$ (kN)**
57	STTS P24	CE-S	12.20	0.324	C	D	480.91	453.43	542.26	577.70
	STTS P14-1	CE-S	12.20	0.324	C	D	633.45	533.96	700.44	771.60
	STTS P21	CE-S	12.20	0.324	C	D	470.53	470.53	552.92	588.24
	STTS P14-2	CE-S	12.20	0.324	C	D	647.79	587.12	659.91	670.69
	STTS P18	CE-S	12.20	0.324	C	D	768.04	716.31	889.70	971.82
	STTS P15	CE-S	12.20	0.324	C	D	780.24	746.11	934.86	1,023.54
	STTS P14-3	CE-S	12.20	0.324	C	D	615.26	605.23	625.45	634.12
58	S NGES 24LP	DS	11.00	0.914	C	B-CIS	2,802.46	3,912.66	3,987.06	4,484.30
	S NGES 1LP	DS	11.00	0.914	C	B-CIS	3,246.75	2,460.70	3,292.89	3,508.77
	S NGES 24C	DS	11.00	0.914	C	B-CIS	2,597.40	2,050.58	3,279.83	3,389.83
	S NGES 1C	DS	11.00	0.914	C	B-CIS	2,665.75	2,050.58	2,719.86	2,881.84
	S NGES 24CDef	DS	11.00	0.914	C	B-CIS	3,144.22	2,255.64	3,142.61	3,533.57
	S NGES 1CDef	DS	11.00	0.914	C	B-CIS	3,349.28	2,255.64	3,263.70	3,731.34
	S NGES 24B	DS	11.00	0.914	C	B-CIS	1,367.05	922.76	1,389.87	1,512.86
	S NGES 1B	DS	11.00	0.914	C	B-CIS	1,742.99	1,322.88	1,754.12	1,964.64
	S NGES 24DP	DS	11.00	0.914	C	B-CIS	2,870.81	2,460.70	2,925.06	3,012.05
	S NGES 1DP	DS	11.00	0.914	C	B-CIS	2,050.58	1,640.46	2,076.57	2,136.75
	S NGES A1	CFA	11.00	0.450	C	A	1,600.00	-	-	-
59	SR49 P1	HP	17.40	12 x 74	C	D	2,092.00	1,424.00	1,861.70	2,252.25
	SR49 P2	CE-S	17.40	0.356	C	D	1,646.00	1,110.22	1,395.80	1,683.50
60	TAMU-C NGES BP7	DS	9.50	0.915	C	B-CIS	3,024.86	2,499.08	3,056.51	3,154.57
61	TAMU-S NGES BP4	DS	9.40	0.941	C	B-CIS	4,157.03	3,912.66	3,987.06	4,484.30
	TAMU-S NGES O1-U	DS	12.20	0.915	O-cell (U)	B-CIS	3,578.43	3,278.55	3,651.00	3,717.47
	TAMU-S NGES O1-L	DS	9.30	0.915	O-cell (D)	B-CIS	3,578.43	3,583.05	3,608.50	3,610.11

Notes: L: pile length; d: pile diameter for piles with circular cross-section; B: pile width for piles with square cross-section; DS: drilled shaft; CFA: continuous flight auger pile; CE-S: closed-ended steel pipe pile; OE-S: open-ended steel pipe pile; OE-SC: open ended concrete filled steel pipe pile; ICP: closed-ended Imperial College Pile; HP: H-section steel pile; PTC: pre-stressed concrete thin-wall caisson; PHC: Pre-stressed concrete high-strength; Sq-C: square precast concrete pile; C-C: circular precast concrete pile; C: top-down compression loading mode; T: top-up tension (or uplift) loading mode; O-cell (U): upward loading mode of bi-directional Osterberg cell; O-cell (D): downward loading mode of bi-directional Osterberg cell; A: augered piles; D: driven piles; J: jacked piles; B-CIS: bored cast in-situ piles; $Q_{max\text{-}measured}$: maximum applied load; $Q_{Davisson}$; estimated capacity from Davisson's offset line criterion; $Q_{w/d=10\%}$: estimated capacity from French criterion (w/d = 10%); $Q_{C\text{-}K}$: estimated capacity from Chin-Kondner criterion.

Table E.1. (continued).

Site No.	ID	Pile information, load test results and interpretations								
	Pile ID	Pile type/ Material	L (m)	d or B (m)	Loading mode	Installation method	$Q_{max\text{-}measured}$ (kN)	$Q_{Davisson}$ (kN)	$Q_{w/d=10\%}$ (kN)	$Q_{C\text{-}K}$ (kN)
62	TH212 B10038-1	CE-SC	15.90	0.304	C	D	2,087.03	2,015.99	2,118.50	2,288.33
	TH212 B10038-2	CE-SC	15.90	0.406	C	D	3,649.79	3,602.32	3,772.58	3,968.25
63	TH52 PAT2	CE-SC	42.30	0.410	C	D	6,183.43	4,798.26	5,416.31	11,904.76
	TH52 MAT2	CE-S	20.29	0.356	C	D	2,229.69	2,180.26	2,347.76	2,506.27
64	UCD P1	OE-S	4.00	0.168	C	J	51.46	-	-	-
65	UMASS NGES1	DS	13.11	0.878	C	B-CIS	1,290.00	1,025.00	1,286.27	1,345.90
	UMASS NGES2	DS	14.30	0.955	C	B-CIS	1,083.78	968.38	1,108.32	1,135.07
66	FEUP ISC'2 P1	DS	6.00	0.60	C	B-CIS	1,350.00	750.00	1,004.26	1,703.58
	FEUP ISC'2 P2	CFA	6.00	0.60	C	A	1,175.08	899.70	1,117.04	1,264.22
	FEUP ISC'2 P3	Sq-C	6.00	0.35	C	D	1,529.97	1,300.89	1,518.83	1,564.95
67	UH NGES O1-U	DS	10.70	0.920	O-cell (U)	B-CIS	2,541.30	2,441.40	2,635.10	2,666.70
	UH NGES O1-L	DS	10.80	0.92	O-cell (D)	B-CIS	2,541.30	2,660.40	2,879.50	2,915.50
68	VEB I-295 JR 1	Sq-C	16.20	0.610	C	D	6,431.14	7,477.85	11,906.73	14,705.88
69	WRBB 1	CE-S	45.00	0.610	C	D	4,034.78	2,921.74	3,810.10	4,201.68
70	WB I-494 MR1A	OE-S	32.00	0.46	C	D	4,242.01	4,221.19	4,221.19	4,524.89
	WB I-494 MR2	CE-S	32.00	0.46	C	D	4,764.40	4,764.40	4,634.41	5,882.35
	WB I-494 MR1A-2	OE-S	32.00	0.46	C	D	2,867.60	2,465.86	2,707.25	3,194.89
	WB I-494 MR4	CE-S	32.00	0.46	C	D	2,729.32	2,236.97	2,555.26	3,333.33

Notes: L: pile length; d: pile diameter for piles with circular cross-section; B: pile width for piles with square cross-section; DS: drilled shaft; CFA: continuous flight auger pile; CE-S: closed-ended steel pipe pile; OE-S: open-ended steel pipe pile; OE-SC: open ended concrete filled steel pipe pile; ICP: closed-ended Imperial College Pile; HP: H-section steel pile; PTC: pre-stressed concrete thin-wall caisson; PHC: Pre-stressed concrete high-strength; Sq-C: square precast concrete pile; C-C: circular precast concrete pile; C: top-down compression loading mode; T: top-up tension (or uplift) loading mode; O-cell (U): upward loading mode of bi-directional Osterberg cell; O-cell (D): downward loading mode of bi-directional Osterberg cell; A: augered piles; D: driven piles; J: jacked piles; B-CIS: bored cast in-situ piles; $Q_{max\text{-}measured}$: maximum applied load; $Q_{Davisson}$; estimated capacity from Davisson's offset line criterion; $Q_{w/d=10\%}$: estimated capacity from French criterion (w/d = 10%); $Q_{C\text{-}K}$: estimated capacity from Chin-Kondner criterion.

Site ID No. 1

Cone penetrometer data	CPT SBT soil classification index, I_c	Detail	Description
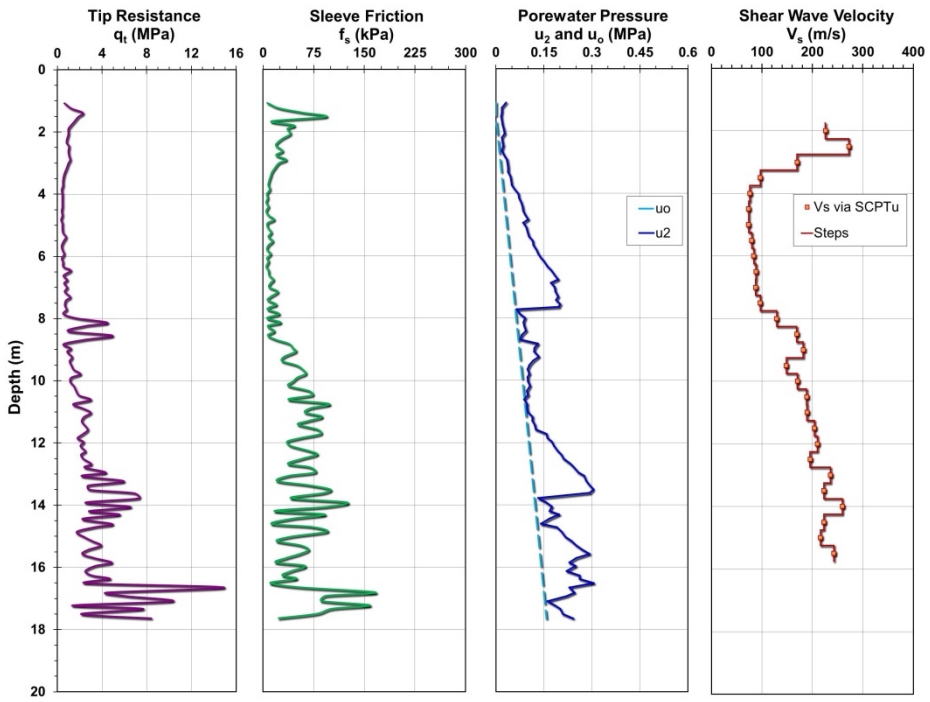	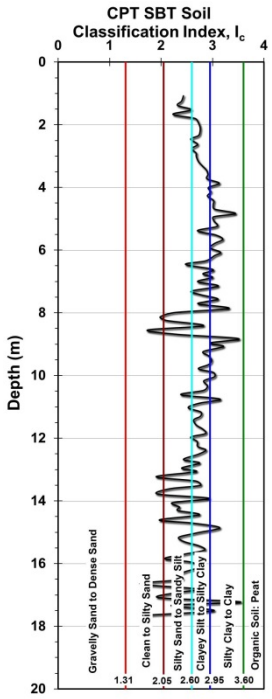	Site name and location	Asian Institute of Technology (AIT) Test Site, Rangsit, near Bangkok, Thailand
		Soil type(s)	Soft to stiff clay
		Pile type(s)	8 Teak piles; 1 drilled shaft
		Type of cone penetrometer testing	SCPTu
		Source of V_s evaluation	SCPTu
		Number of pile load tests	9
		Reference	Brand et al. (1972), Balasubramaniam et al. (2004), Shibuya and Tamrakar (2003)
		Comments	

Pile ID: AIT 1-1

Load-displacement data

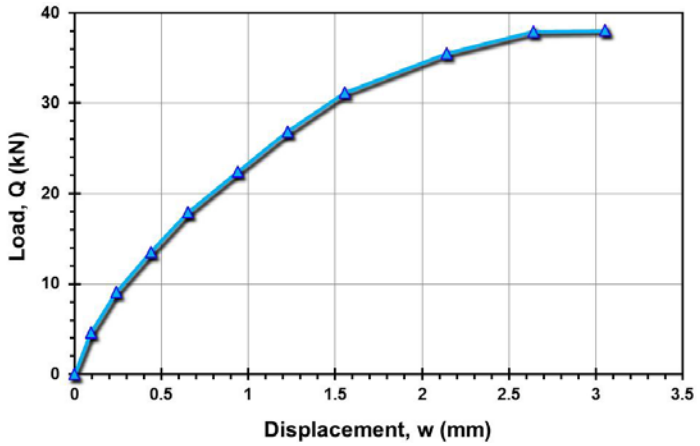

Back-analyzed operational stiffness vs. pseudo-strain

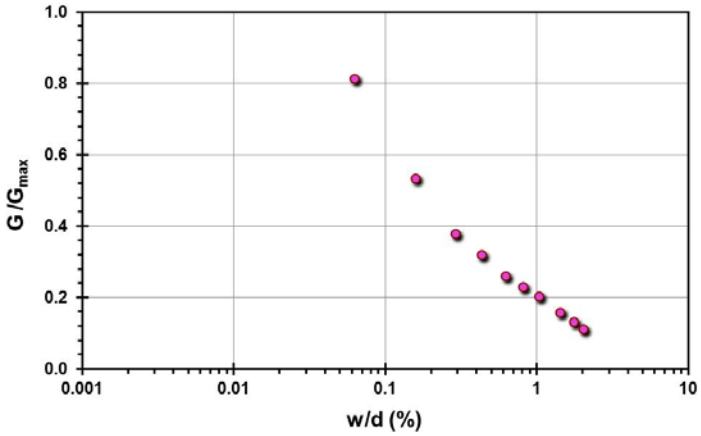

Detail	Description
Pile type/material	Teak
Length, L (m)	6.00
Diameter, d (m)	0.150
Installation method	Driven
Loading mode	Compression
$Q_{max\text{-}measured}$ (kN)	38.04
Q_s (kN)	Not available
Q_b (kN)	Not available
$Q_{Davisson}$ (kN)	38.70
$Q_{w/d=10\%}$ (kN)	38.75
$Q_{C\text{-}K}$ (kN)	38.94

Pile ID: AIT 1-2

Load-displacement data

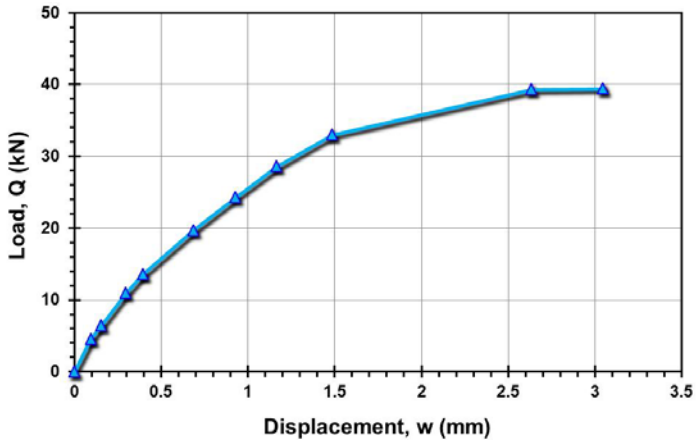

Back-analyzed operational stiffness vs. pseudo-strain

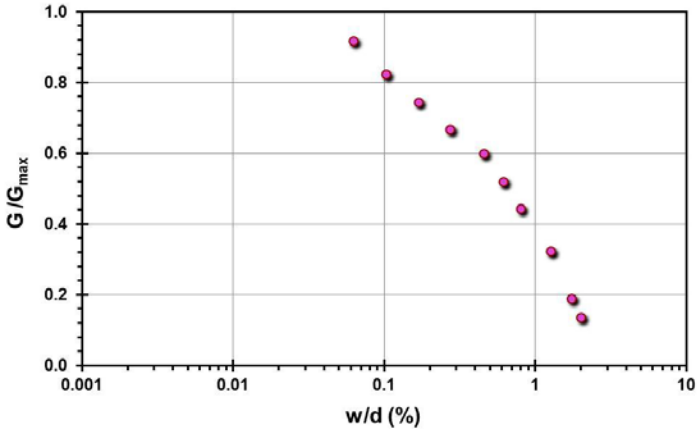

Detail	Description
Pile type/material	Teak
Length, L (m)	6.00
Diameter, d (m)	0.150
Installation method	Driven
Loading mode	Compression
$Q_{max\text{-}measured}$ (kN)	39.44
Q_s (kN)	Not available
Q_b (kN)	Not available
$Q_{Davisson}$ (kN)	39.50
$Q_{w/d=10\%}$ (kN)	40.16
$Q_{C\text{-}K}$ (kN)	40.35

Pile ID: AIT 2-1

Load-displacement data

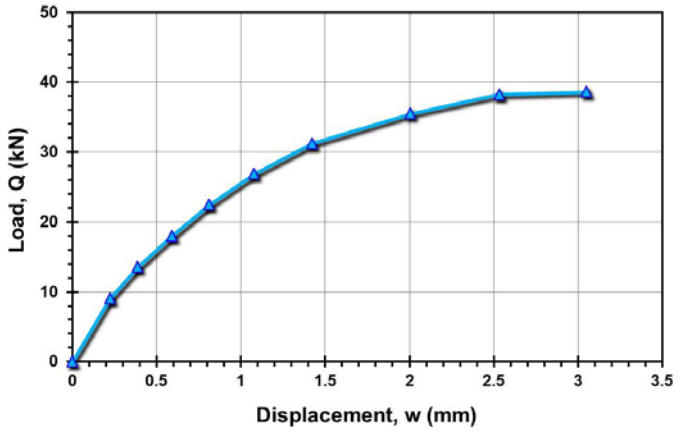

Back-analyzed normalized operational stiffness vs. pseudo-strain

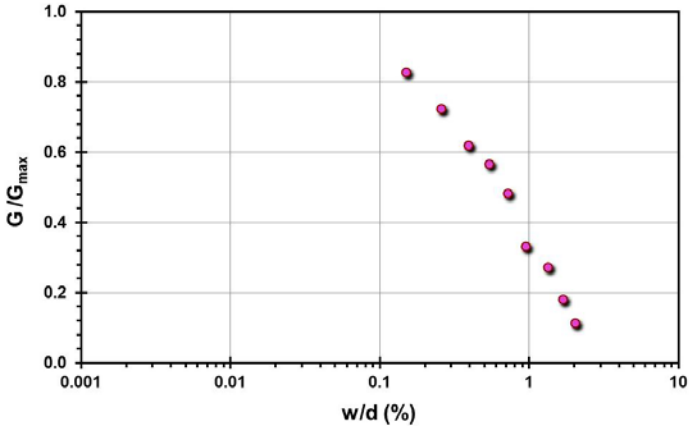

Detail	Description
Pile type/material	Teak
Length, L (m)	6.00
Diameter, d (m)	0.150
Installation method	Driven
Loading mode	Compression
$Q_{max\text{-}measured}$ (kN)	38.62
Q_s (kN)	Not available
Q_b (kN)	Not available
$Q_{Davisson}$ (kN)	38.70
$Q_{w/d=10\%}$ (kN)	40.03
$Q_{C\text{-}K}$ (kN)	40.40

Pile ID: AIT 2-2

Load-displacement data

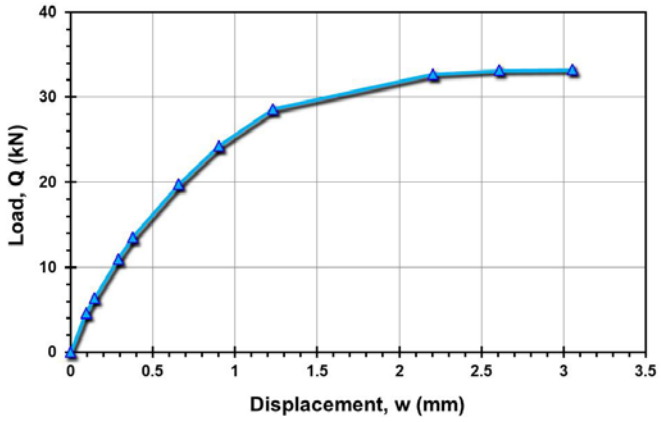

Back-analyzed normalized operational stiffness vs. pseudo-strain

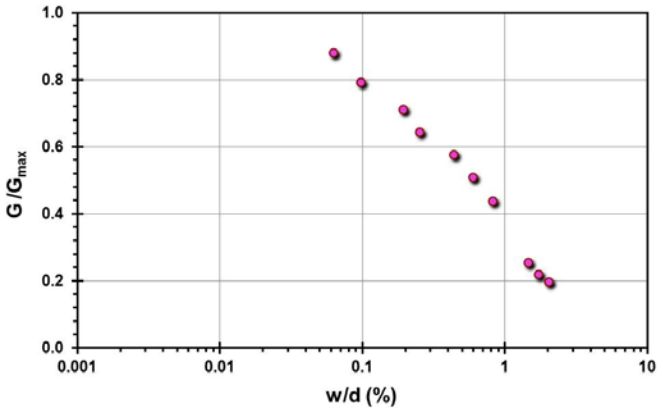

Detail	Description
Pile type/material	Teak
Length, L (m)	6.00
Diameter, d (m)	0.150
Installation method	Driven
Loading mode	Compression
$Q_{max\text{-}measured}$ (kN)	33.24
Q_s (kN)	Not available
Q_b (kN)	Not available
$Q_{Davisson}$ (kN)	33.30
$Q_{w/d=10\%}$ (kN)	34.40
$Q_{C\text{-}K}$ (kN)	34.69

Pile ID: AIT 3-1

Load-displacement data

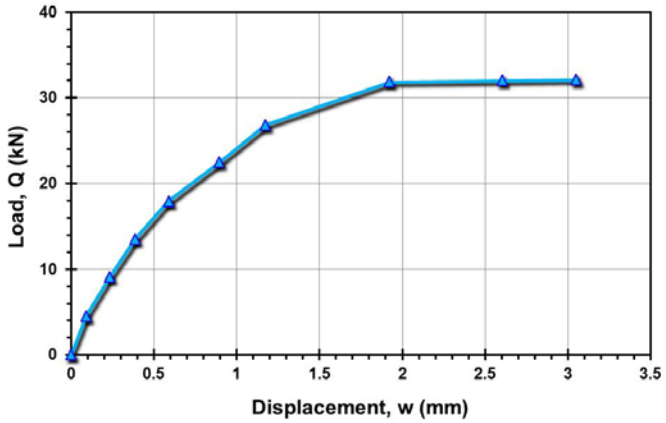

Back-analyzed normalized operational stiffness vs. pseudo-strain

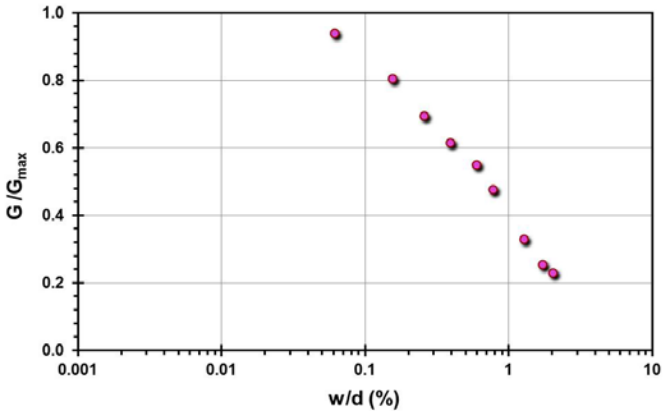

Detail	Description
Pile type/material	Teak
Length, L (m)	6.00
Diameter, d (m)	0.150
Installation method	Driven
Loading mode	Compression
$Q_{max\text{-}measured}$ (kN)	32.12
Q_s (kN)	Not available
Q_b (kN)	Not available
$Q_{Davisson}$ (kN)	32.22
$Q_{w/d=10\%}$ (kN)	32.51
$Q_{C\text{-}K}$ (kN)	32.61

Pile ID: AIT 3-2

Load-displacement data

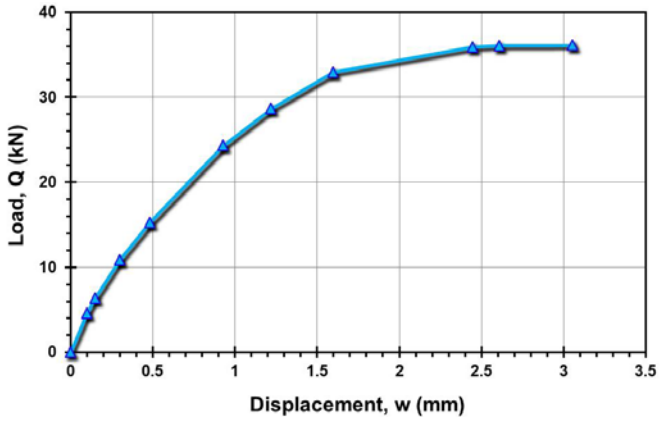

Back-analyzed normalized operational stiffness vs. pseudo-strain

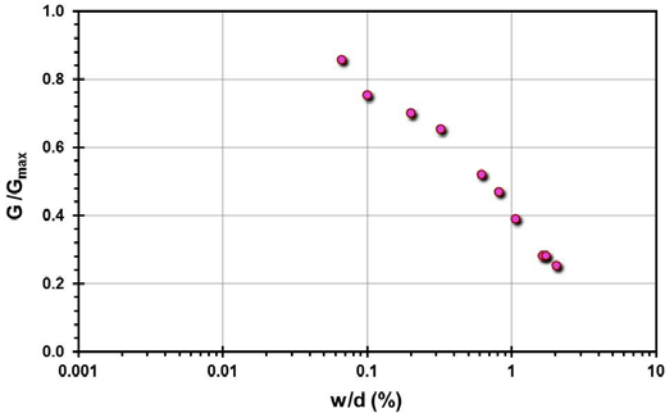

Detail	Description
Pile type/material	Teak
Length, L (m)	6.00
Diameter, d (m)	0.150
Installation method	Driven
Loading mode	Compression
$Q_{max\text{-}measured}$ (kN)	36.13
Q_s (kN)	Not available
Q_b (kN)	Not available
$Q_{Davisson}$ (kN)	36.44
$Q_{w/d=10\%}$ (kN)	36.73
$Q_{C\text{-}K}$ (kN)	36.88

Pile ID: AIT 4-1

Load-displacement data

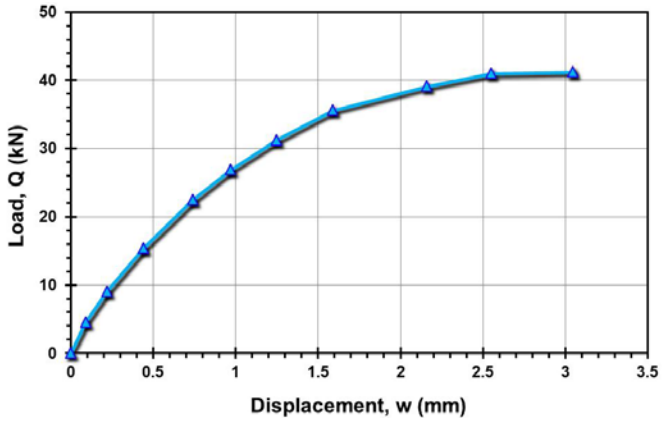

Back-analyzed normalized operational stiffness vs. pseudo-strain

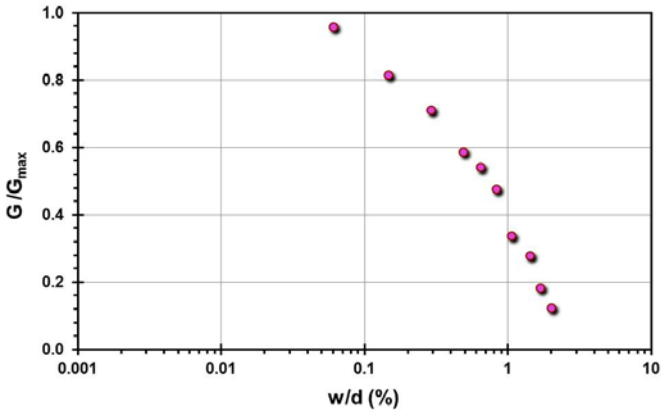

Detail	Description
Pile type/material	Teak
Length, L (m)	6.00
Diameter, d (m)	0.150
Installation method	Driven
Loading mode	Compression
$Q_{max\text{-}measured}$ (kN)	41.28
Q_s (kN)	Not available
Q_b (kN)	Not available
$Q_{Davisson}$ (kN)	41.51
$Q_{w/d=10\%}$ (kN)	42.27
$Q_{C\text{-}K}$ (kN)	42.53

Pile ID: AIT 4-2

Load-displacement data

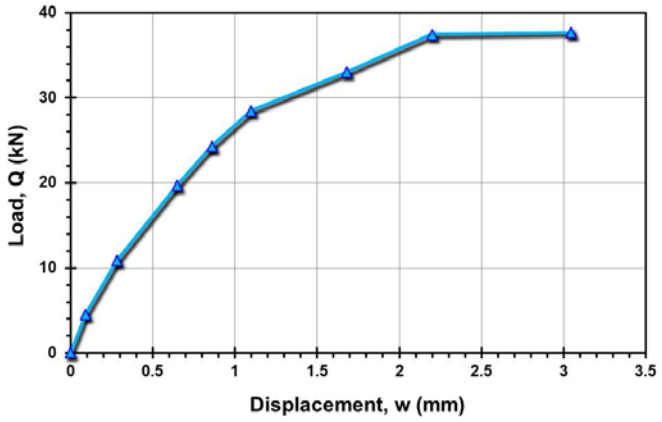

Back-analyzed normalized operational stiffness vs. pseudo-strain

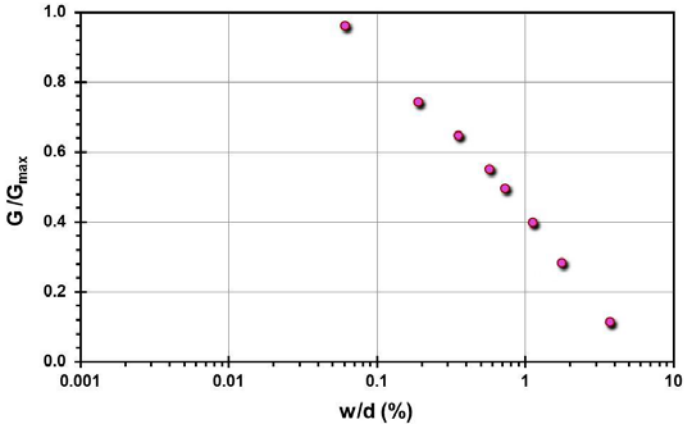

Detail	Description
Pile type/material	Teak
Length, L (m)	6.00
Diameter, d (m)	0.150
Installation method	Driven
Loading mode	Compression
$Q_{max\text{-}measured}$ (kN)	37.63
Q_s (kN)	Not available
Q_b (kN)	Not available
$Q_{Davisson}$ (kN)	37.80
$Q_{w/d=10\%}$ (kN)	38.11
$Q_{C\text{-}K}$ (kN)	38.24

Pile ID: AIT 5

Load-displacement data	Detail	Description
Not available	Pile type/material	Drilled Shaft
	Length, L (m)	18.00
	Diameter, d (m)	0.450
	Installation method	Bored cast in-situ
	Loading mode	Compression
	$Q_{max\text{-}measured}$ (kN)	2,047.28
	Q_s (kN)	1,833.78
	Q_b (kN)	213.50
	$Q_{Davisson}$ (kN)	Not calculated
	$Q_{w/d=10\%}$ (kN)	Not calculated
	$Q_{C\text{-}K}$ (kN)	Not calculated
Back-analyzed normalized operational stiffness vs. pseudo-strain		
Not calculated		

Site ID No. 2

Cone penetrometer data	CPT SBT soil classification index, I_c	Detail	Description
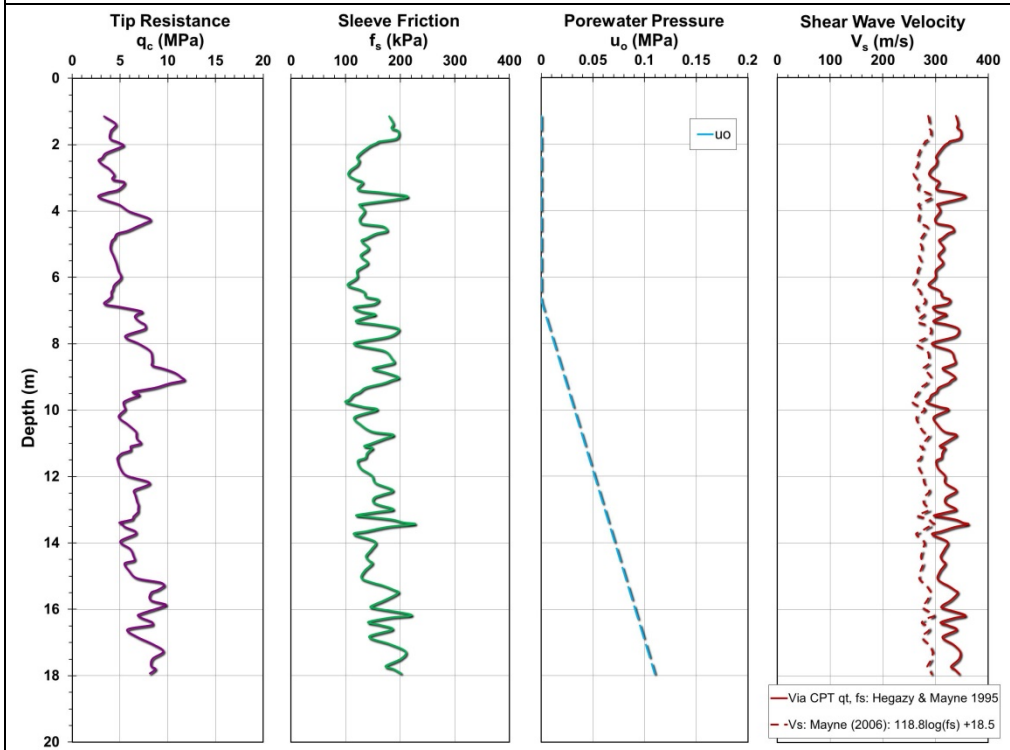	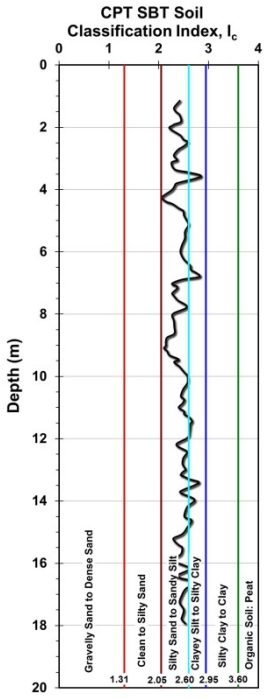	Site name and location	Baghdad University near River Tigris, Iraq
		Soil type(s)	Clayey silty sand over uniform sand
		Pile type(s)	Square concrete piles
		Type of cone penetrometer testing	CPT
		Source of V_s evaluation	Correlations (see Figure opposite and Table 3.1)
		Number of pile load tests	3
		Reference	Altaee et al. (1992)
		Comments	V_s estimated via correlations, u_2 reading assumed ≈ u_o

Pile ID: BU 1

Load-displacement data

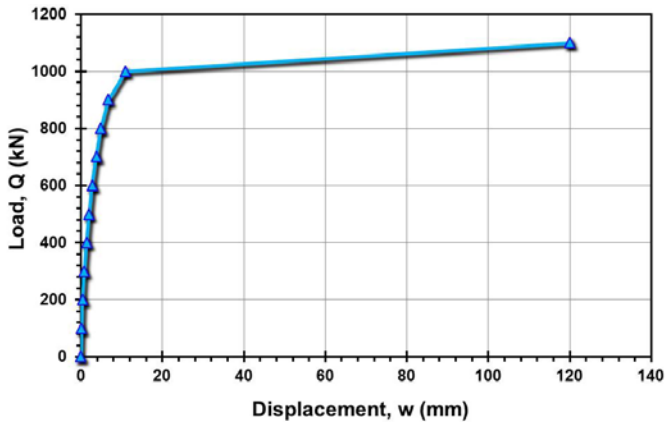

Back-analyzed normalized operational stiffness vs. pseudo-strain

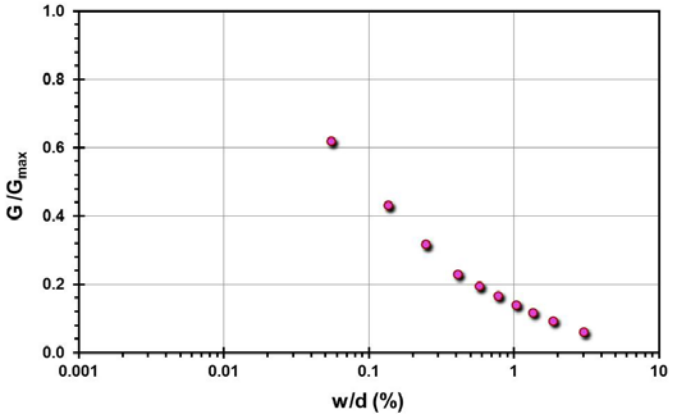

Detail	Description
Pile type/material	Square concrete
Length, L (m)	11.00
Width, B (m)	0.285
Installation method	Driven
Loading mode	Compression
$Q_{max\text{-}measured}$ (kN)	1,100.00
Q_s (kN)	942.93
Q_b (kN)	157.07
$Q_{Davisson}$ (kN)	985.50
$Q_{w/d=10\%}$ (kN)	1,066.19
$Q_{C\text{-}K}$ (kN)	1,117.32

Pile ID: BU 2

Load-displacement data	Detail	Description
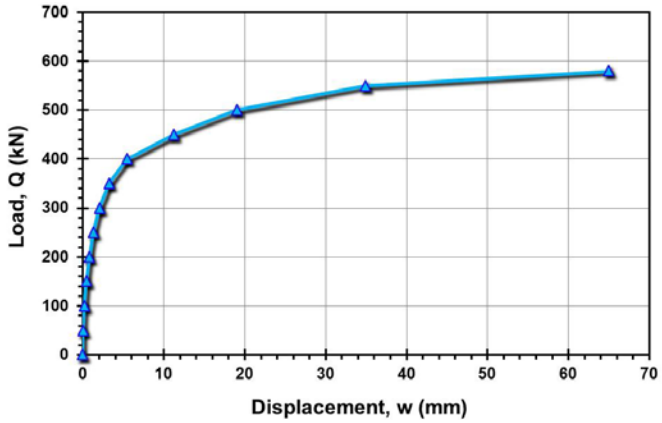	Pile type/material	Square concrete
	Length, L (m)	11.00
	Width, B (m)	0.285
	Installation method	Driven
	Loading mode	Tension
	$Q_{max\text{-}measured}$ (kN)	580.00
	Q_s (kN)	Not reported
	Q_b (kN)	Not reported
	$Q_{Davisson}$ (kN)	422.25
	$Q_{w/d=10\%}$ (kN)	554.58
	$Q_{C\text{-}K}$ (kN)	610.87
Back-analyzed normalized operational stiffness vs. pseudo-strain		
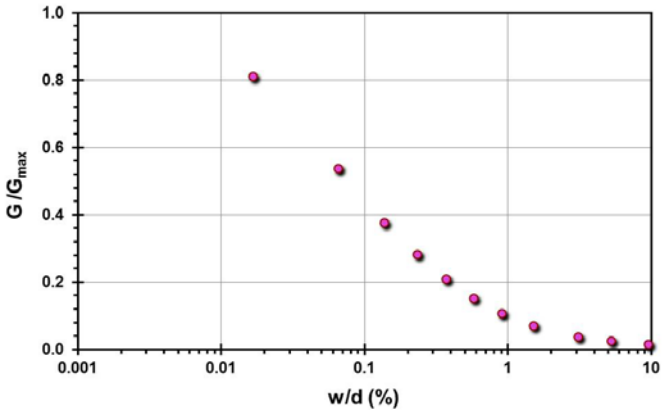		

Pile ID: BU 3

Load-displacement data

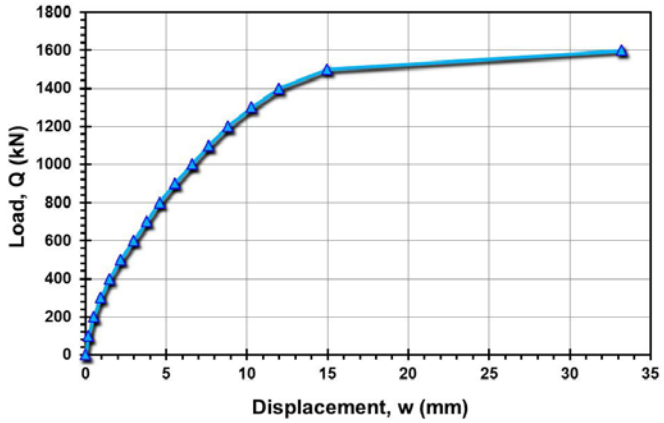

Back-analyzed normalized operational stiffness vs. pseudo-strain

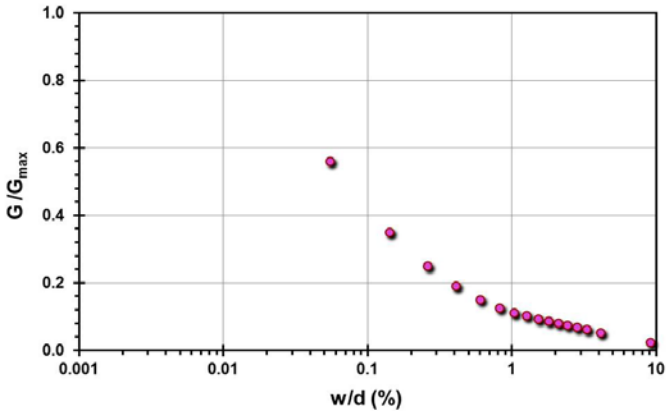

Detail	Description
Pile type/material	Square concrete
Length, L (m)	15.00
Width, B (m)	0.285
Installation method	Driven
Loading mode	Compression
$Q_{max\text{-}measured}$ (kN)	1,600.00
Q_s (kN)	Not reported
Q_b (kN)	Not reported
$Q_{Davisson}$ (kN)	1,420.15
$Q_{w/d=10\%}$ (kN)	1,616.83
$Q_{C\text{-}K}$ (kN)	1,754.39

Site ID No. 3

Cone penetrometer data	CPT SBT soil classification index, I_c	Detail	Description
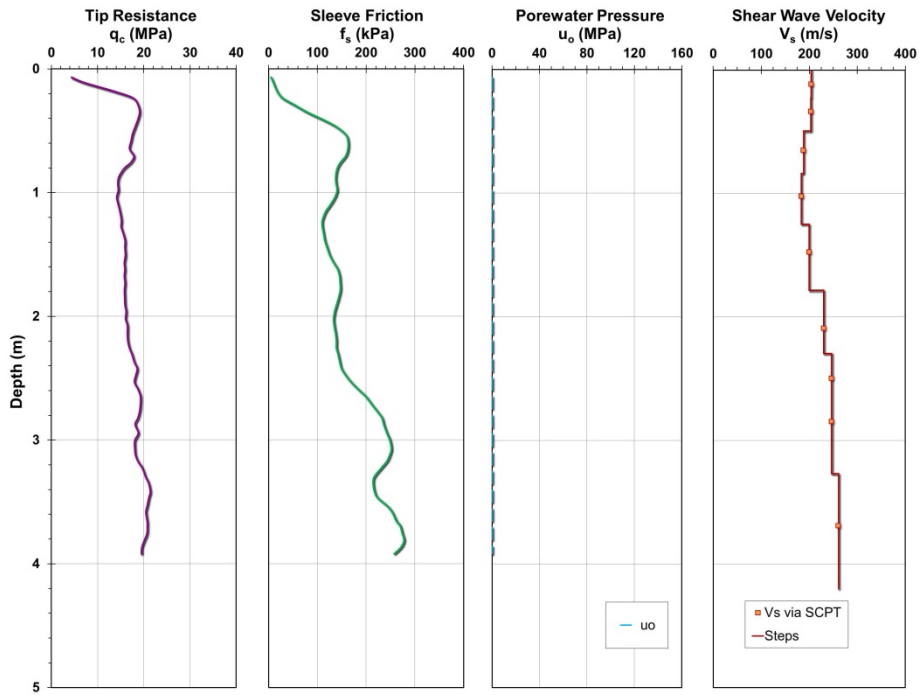	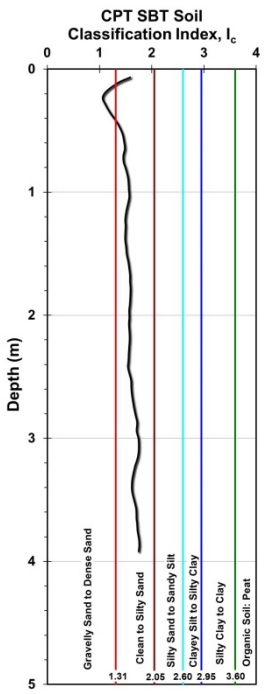	Site name and location	Blessington, Ireland
		Soil type(s)	Heavily overconsolidated glacially derived very dense fine sand
		Pile type(s)	Close-ended steel
		Type of cone penetrometer testing	SCPT
		Source of V_s evaluation	SCPT
		Number of pile load tests	2
		Reference	Gavin & O'Kelly (2007)
		Comments	

Pile ID: Bl 1

Load-displacement data

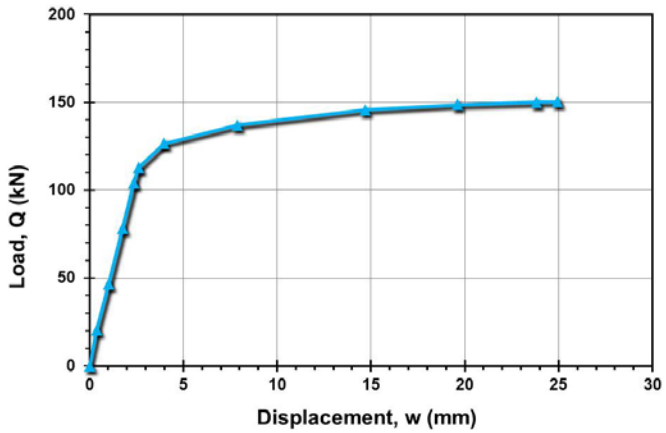

Back-analyzed normalized operational stiffness vs. pseudo-strain

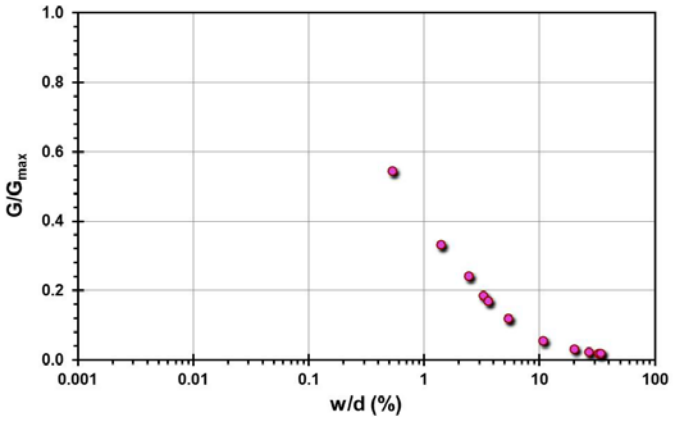

Detail	Description
Pile type/material	Closed-ended steel
Length, L (m)	2.70
Diameter, d (m)	0.073
Installation method	Driven
Loading mode	Compression
$Q_{max\text{-}measured}$ (kN)	150.38
Q_s (kN)	115.67
Q_b (kN)	34.71
$Q_{Davisson}$ (kN)	126.62
$Q_{w/d=10\%}$ (kN)	130.03
$Q_{C\text{-}K}$ (kN)	152.77

Pile ID: Bl 2

Load-displacement data

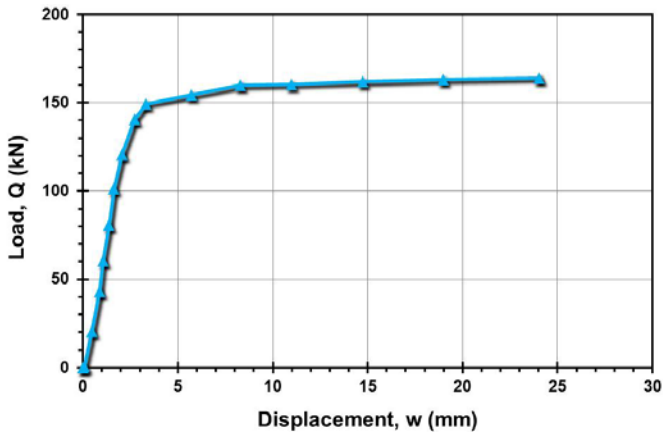

Back-analyzed normalized operational stiffness vs. pseudo-strain

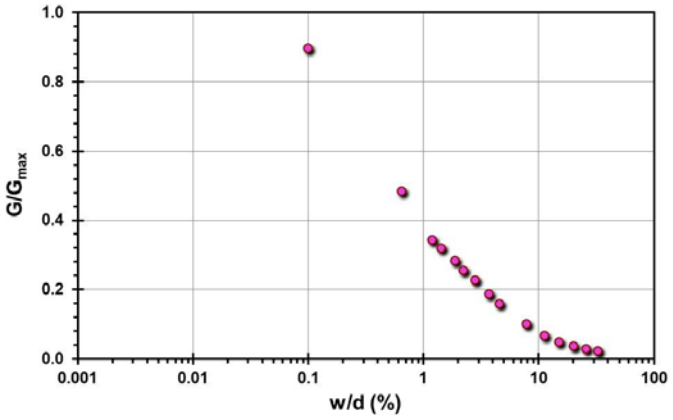

Detail	Description
Pile type/material	Closed-ended steel
Length, L (m)	2.49
Diameter, d (m)	0.073
Installation method	Jacked
Loading mode	Compression
$Q_{max\text{-}measured}$ (kN)	164.02
Q_s (kN)	126.17
Q_b (kN)	37.85
$Q_{Davisson}$ (kN)	150.51
$Q_{w/d=10\%}$ (kN)	156.95
$Q_{C\text{-}K}$ (kN)	167.44

Site ID No. 4

Cone penetrometer data	CPT SBT soil classification index, I_c	Detail	Description
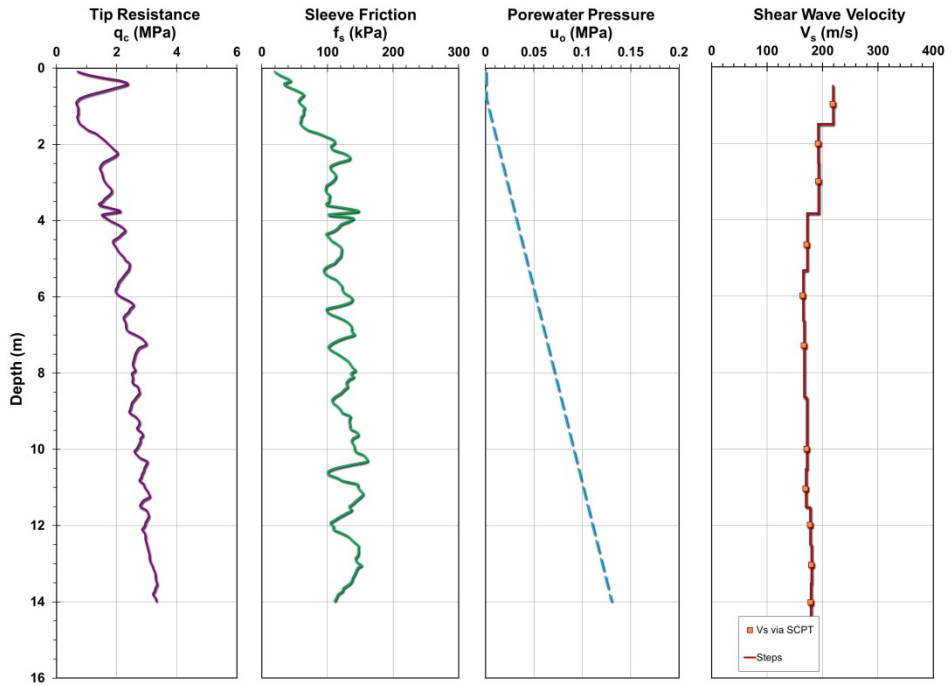	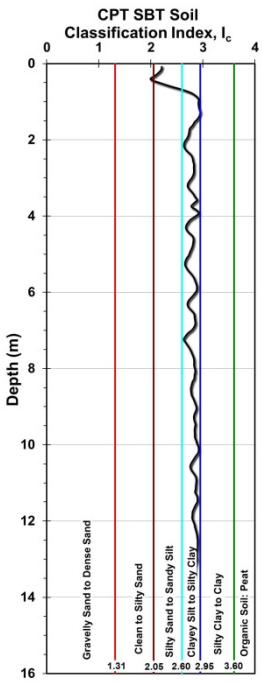	Site name and location	Boom Clay Site, Sint-Kathelijne-Waver, Belgium
		Soil type(s)	Stiff fissured clay
		Pile type(s)	10 Screw piles and 2 square concrete pile
		Type of cone penetrometer testing	SCPT
		Source of V_s evaluation	SCPT
		Number of pile load tests	12
		Reference	Mengé (2001), Huybrechts (2001), and Maertens & Huybrechts (2001)
		Comments	Load transfer distribution (Q-z) for only one pile; u_2 reading not available

Pile ID: BCS 1

Load-displacement data

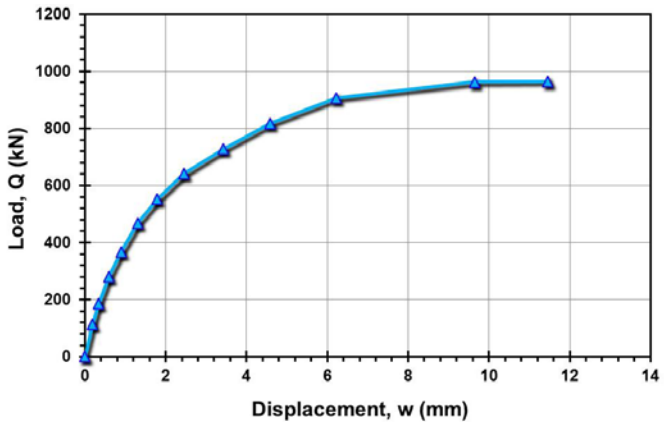

Back-analyzed normalized operational stiffness vs. pseudo-strain

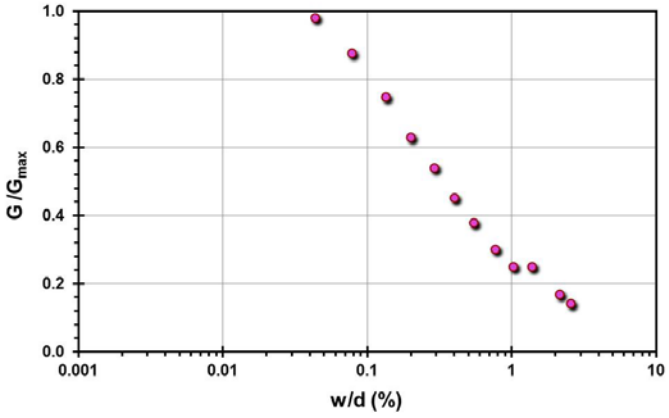

Detail	Description
Pile type/material	Square concrete
Length, L (m)	6.35
Width, B (m)	0.35
Installation method	Driven
Loading mode	Compression
$Q_{max\text{-}measured}$ (kN)	964.20
Q_s (kN)	Not reported
Q_b (kN)	Not reported
$Q_{Davisson}$ (kN)	961.84
$Q_{w/d=10\%}$ (kN)	1,092.27
$Q_{C\text{-}K}$ (kN)	1,137.66

Pile ID: BCS 2

Load-displacement data

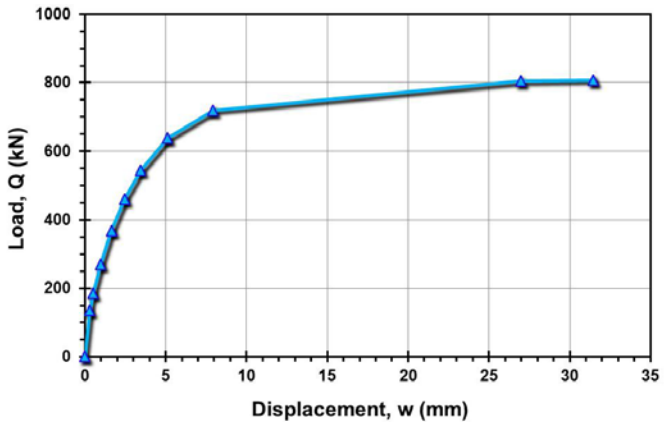

Back-analyzed normalized operational stiffness vs. pseudo-strain

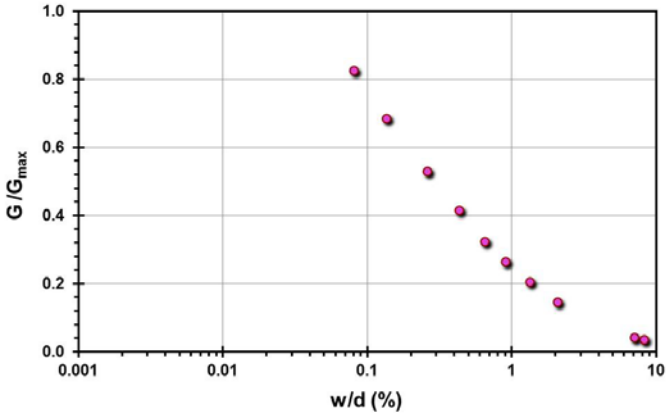

Detail	Description
Pile type/material	Fundex
Length, L (m)	6.31
Diameter, d (m)	0.38
Installation method	Augered
Loading mode	Compression
$Q_{max\text{-}measured}$ (kN)	807.52
Q_s (kN)	Not reported
Q_b (kN)	Not reported
$Q_{Davisson}$ (kN)	719.14
$Q_{w/d=10\%}$ (kN)	818.82
$Q_{C\text{-}K}$ (kN)	861.33

Pile ID: BCS 3

Load-displacement data

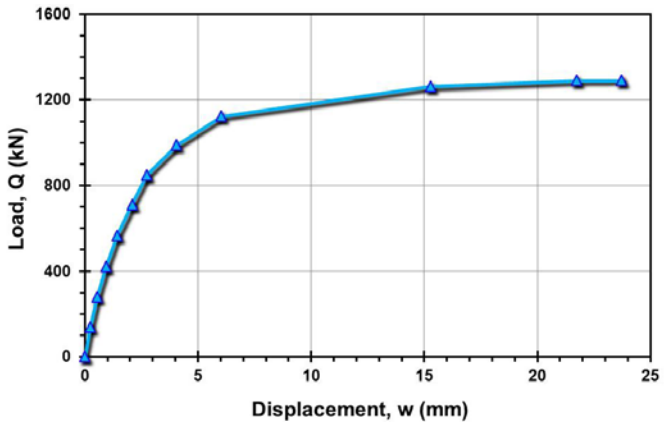

Back-analyzed normalized operational stiffness vs. pseudo-strain

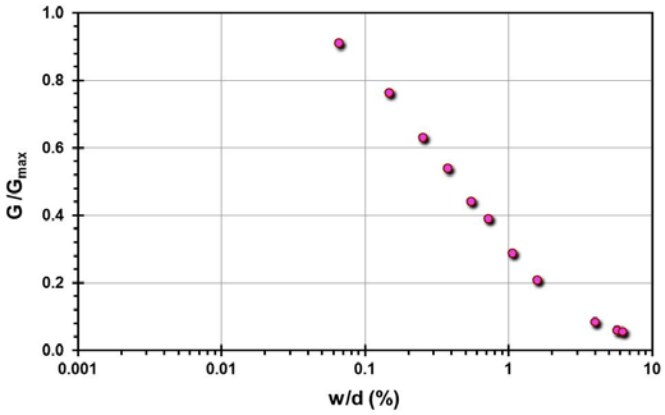

Detail	Description
Pile type/material	Fundex
Length, L (m)	10.48
Diameter, d (m)	0.38
Installation method	Augered
Loading mode	Compression
$Q_{max\text{-}measured}$ (kN)	1,291.21
Q_s (kN)	Not reported
Q_b (kN)	Not reported
$Q_{Davisson}$ (kN)	1,193.00
$Q_{w/d=10\%}$ (kN)	1,329.35
$Q_{C\text{-}K}$ (kN)	1,390.82

Pile ID: BCS 4

Load-displacement data

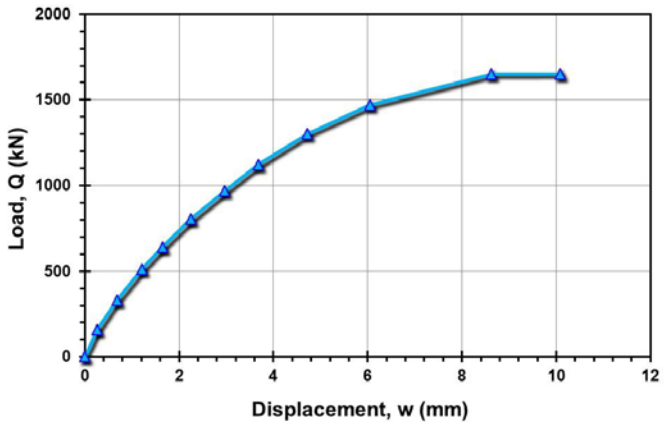

Back-analyzed normalized operational stiffness vs. pseudo-strain

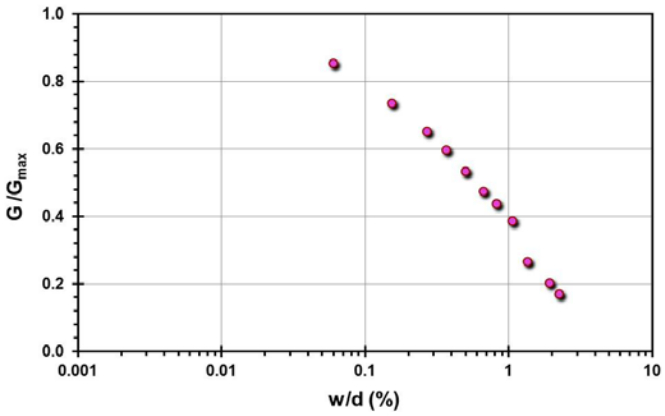

Detail	Description
Pile type/material	Square concrete
Length, L (m)	10.60
Width, B (m)	0.35
Installation method	Driven
Loading mode	Compression
$Q_{max\text{-}measured}$ (kN)	1,651.00
Q_s (kN)	Not reported
Q_b (kN)	Not reported
$Q_{Davisson}$ (kN)	1,651.00
$Q_{w/d=10\%}$ (kN)	1,658.97
$Q_{C\text{-}K}$ (kN)	1,661.13

Pile ID: BCS 5

Load-displacement data

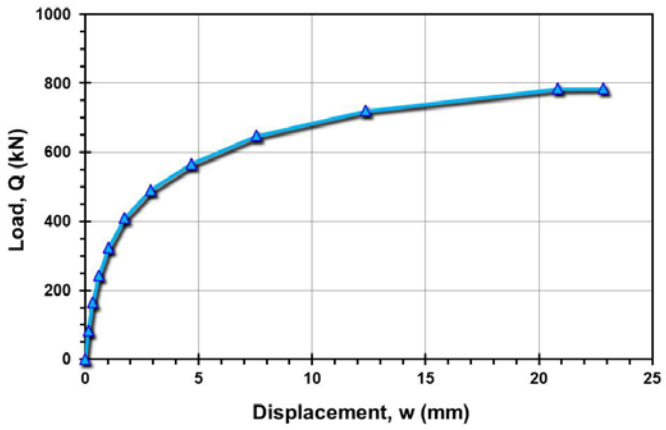

Back-analyzed normalized operational stiffness vs. pseudo-strain

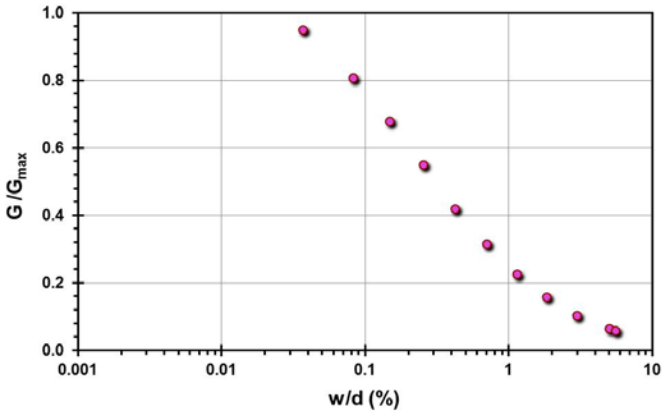

Detail	Description
Pile type/material	De Waal
Length, L (m)	6.46
Diameter, d (m)	0.41
Installation method	Augered
Loading mode	Compression
$Q_{max\text{-}measured}$ (kN)	785.20
Q_s (kN)	Not reported
Q_b (kN)	Not reported
$Q_{Davisson}$ (kN)	647.97
$Q_{w/d=10\%}$ (kN)	817.56
$Q_{C\text{-}K}$ (kN)	862.81

Pile ID: BCS 6

Load-displacement data

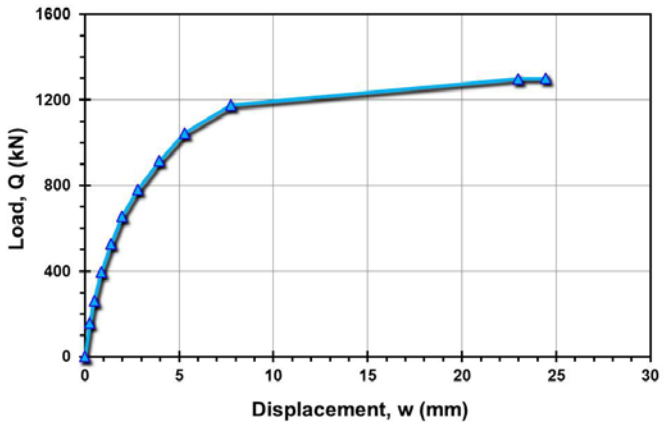

Back-analyzed normalized operational stiffness vs. pseudo-strain

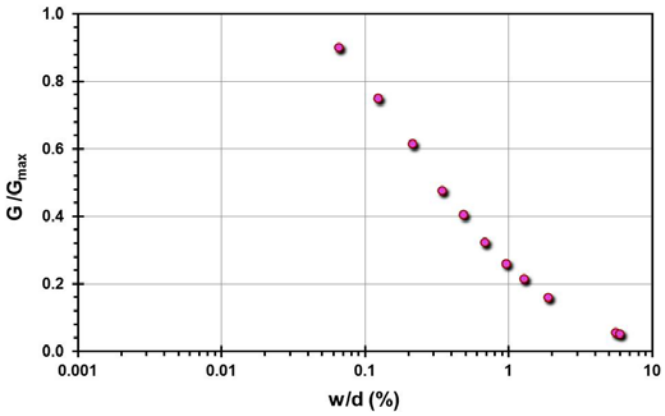

Detail	Description
Pile type/material	De Waal
Length, L (m)	10.66
Diameter, d (m)	0.41
Installation method	Augered
Loading mode	Compression
$Q_{max\text{-}measured}$ (kN)	1,300.40
Q_s (kN)	1,207.41
Q_b (kN)	92.99
$Q_{Davisson}$ (kN)	1,176.10
$Q_{w/d=10\%}$ (kN)	1,342.38
$Q_{C\text{-}K}$ (kN)	1,410.44

Pile ID: BCS 7

Load-displacement data

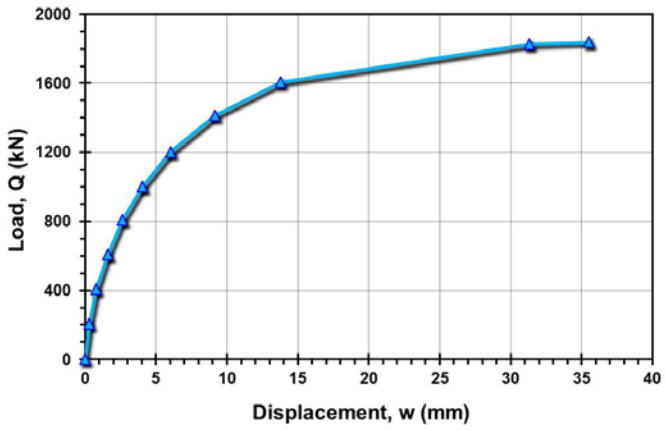

Back-analyzed normalized operational stiffness vs. pseudo-strain

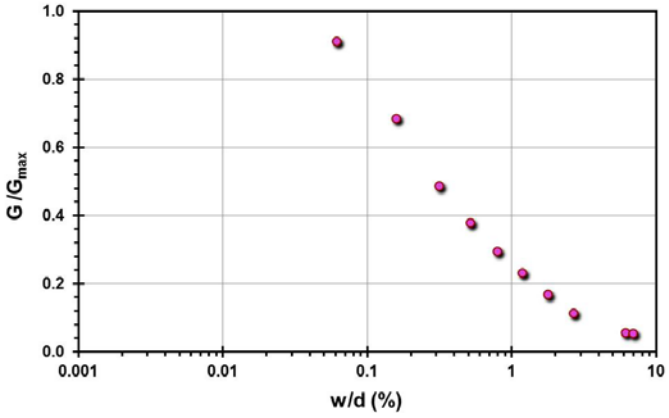

Detail	Description
Pile type/material	Oliver
Length, L (m)	10.71
Diameter, d (m)	0.51
Installation method	Augered
Loading mode	Compression
$Q_{max\text{-}measured}$ (kN)	1,838.14
Q_s (kN)	Not reported
Q_b (kN)	Not reported
$Q_{Davisson}$ (kN)	1,414.16
$Q_{w/d=10\%}$ (kN)	1,912.64
$Q_{C\text{-}K}$ (kN)	2,061.86

Pile ID: BCS 8

Load-displacement data

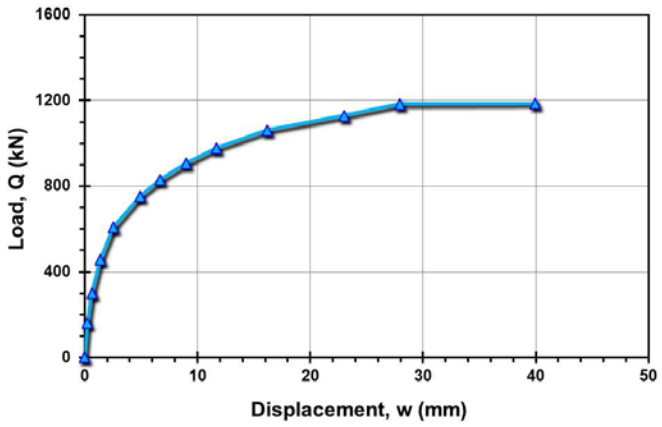

Back-analyzed normalized operational stiffness vs. pseudo-strain

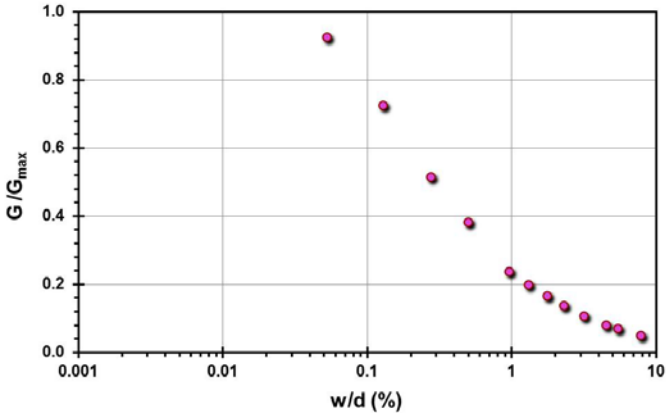

Detail	Description
Pile type/material	Oliver
Length, L (m)	6.53
Diameter, d (m)	0.51
Installation method	Augered
Loading mode	Compression
$Q_{max\text{-}measured}$ (kN)	1,183.74
Q_s (kN)	Not reported
Q_b (kN)	Not reported
$Q_{Davisson}$ (kN)	906.08
$Q_{w/d=10\%}$ (kN)	1,220.26
$Q_{C\text{-}K}$ (kN)	1,305.48

Pile ID: BCS 9

Load-displacement data

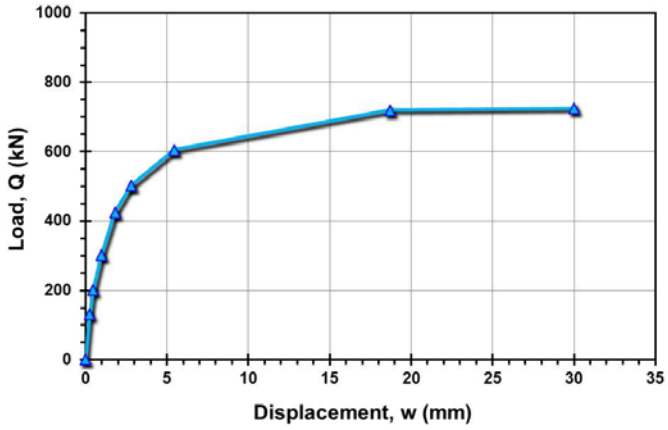

Back-analyzed normalized operational stiffness vs. pseudo-strain

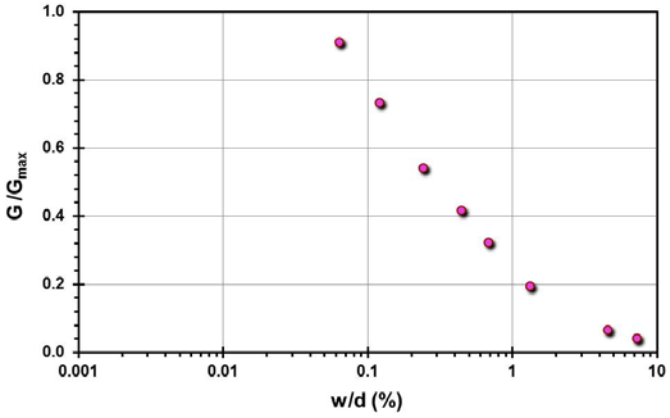

Detail	Description
Pile type/material	Omega
Length, L (m)	6.59
Diameter, d (m)	0.41
Installation method	Augered
Loading mode	Compression
$Q_{max\text{-}measured}$ (kN)	724.09
Q_s (kN)	Not reported
Q_b (kN)	Not reported
$Q_{Davisson}$ (kN)	619.47
$Q_{w/d=10\%}$ (kN)	736.58
$Q_{C\text{-}K}$ (kN)	762.20

Pile ID: BCS 10

Load-displacement data

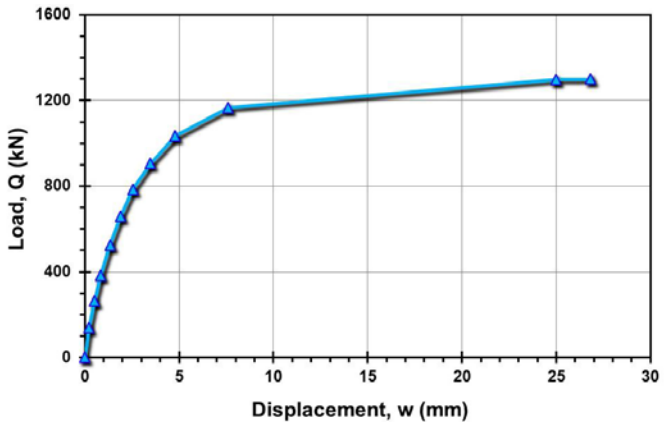

Back-analyzed normalized operational stiffness vs. pseudo-strain

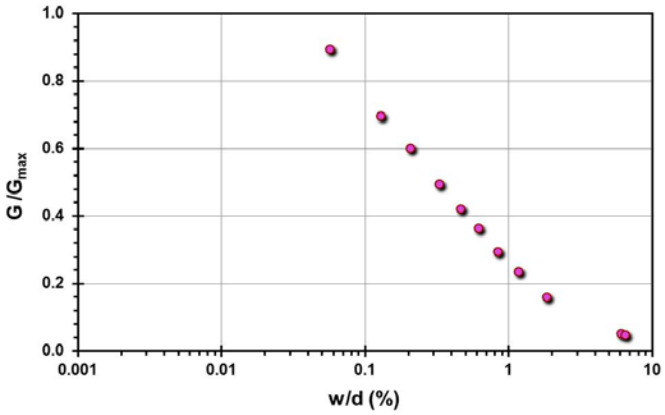

Detail	Description
Pile type/material	Omega
Length, L (m)	10.81
Diameter, d (m)	0.41
Installation method	Augered
Loading mode	Compression
$Q_{max\text{-}measured}$ (kN)	1,299.36
Q_s (kN)	Not reported
Q_b (kN)	Not reported
$Q_{Davisson}$ (kN)	1,196.38
$Q_{w/d=10\%}$ (kN)	1,329.36
$Q_{C\text{-}K}$ (kN)	1,386.96

Pile ID: BCS 11

Load-displacement data

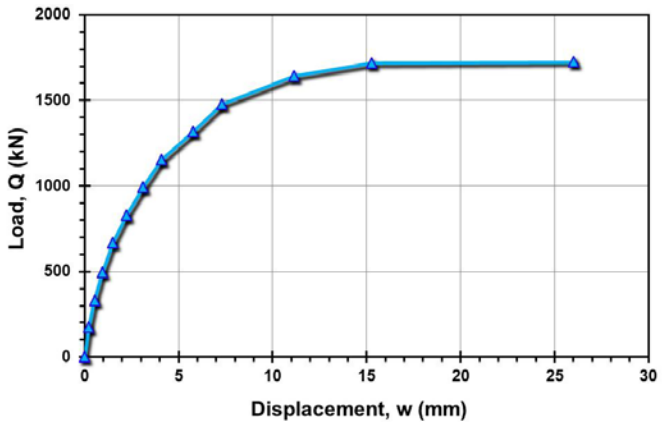

Back-analyzed normalized operational stiffness vs. pseudo-strain

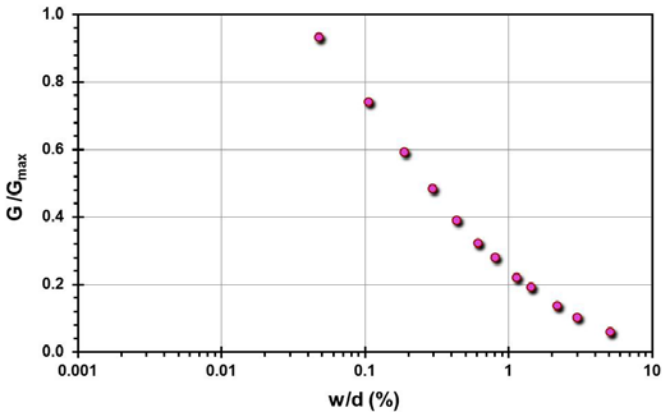

Detail	Description
Pile type/material	Atlas
Length, L (m)	10.81
Diameter, d (m)	0.51
Installation method	Augered
Loading mode	Compression
$Q_{max\text{-}measured}$ (kN)	1,724.11
Q_s (kN)	Not reported
Q_b (kN)	Not reported
$Q_{Davisson}$ (kN)	1,640.10
$Q_{w/d=10\%}$ (kN)	1,845.60
$Q_{C\text{-}K}$ (kN)	1,941.75

Pile ID: BCS 12

Load-displacement data

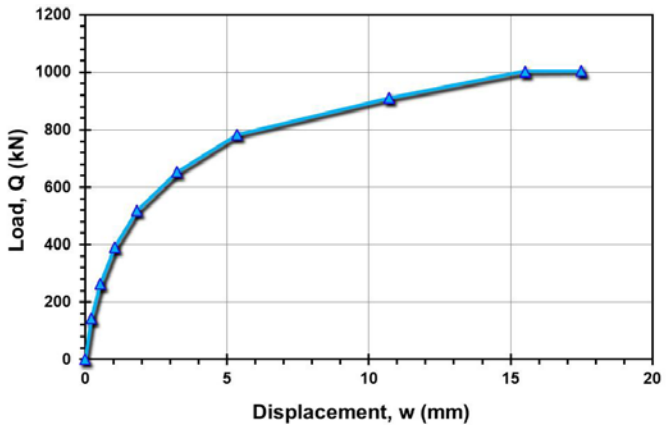

Back-analyzed normalized operational stiffness vs. pseudo-strain

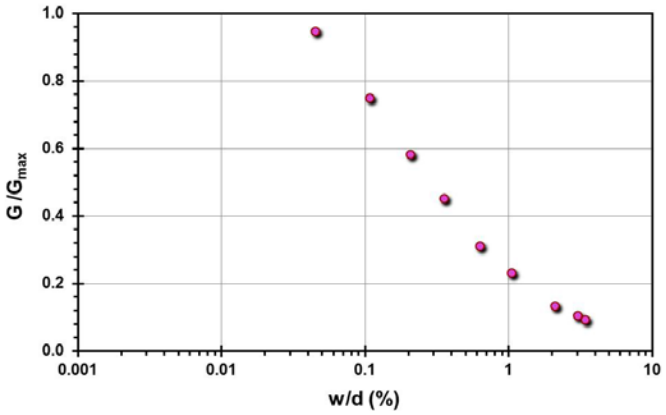

Detail	Description
Pile type/material	Atlas
Length, L (m)	6.76
Diameter, d (m)	0.51
Installation method	Augered
Loading mode	Compression
$Q_{max\text{-}measured}$ (kN)	1,004.98
Q_s (kN)	Not reported
Q_b (kN)	Not reported
$Q_{Davisson}$ (kN)	956.51
$Q_{w/d=10\%}$ (kN)	1,100.60
$Q_{C\text{-}K}$ (kN)	1,154.73

Site ID No. 5

Cone penetrometer data	CPT SBT soil classification index, I_c	Detail	Description
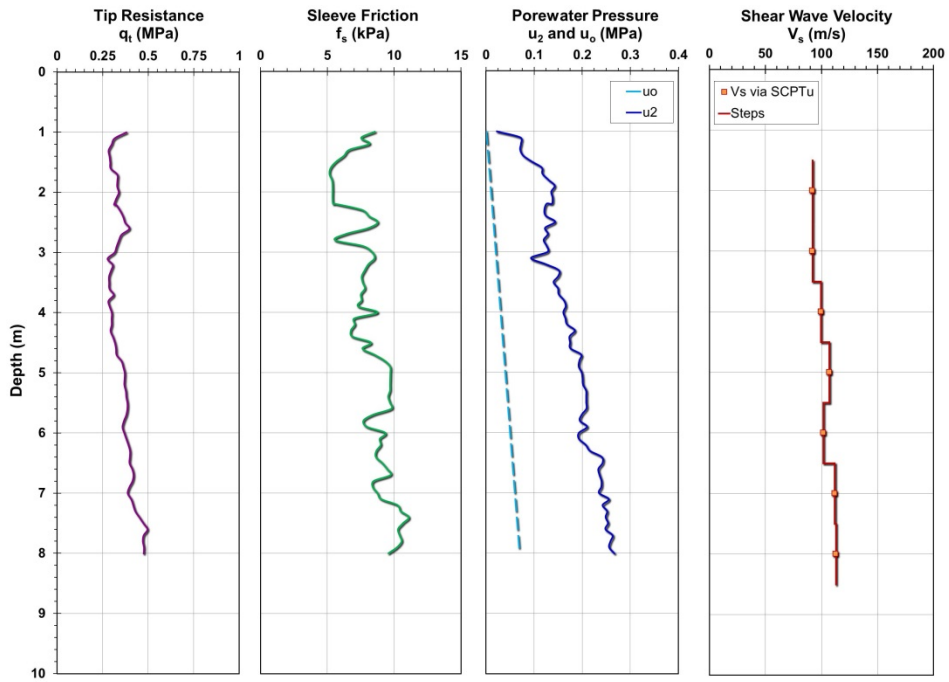	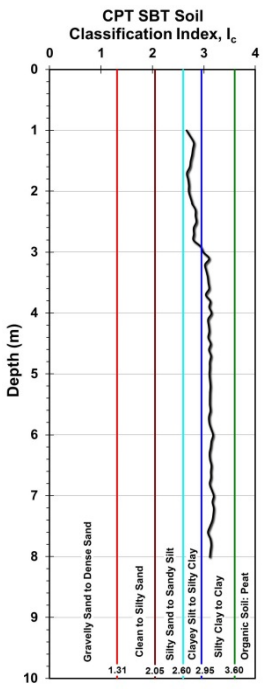	Site name and location	Bothkennar clay site, Scotland
		Soil type(s)	Post glacial soft silty clay
		Pile type(s)	Closed-ended steel pipe piles
		Type of cone penetrometer testing	SCPTu
		Source of V_s evaluation	SCPTu
		Number of pile load tests	7
		Reference	Lehane (1992)
		Comments	Imperial College Instrumented Piles (ICP)

Pile ID: BK 1/L1T

Load-displacement data

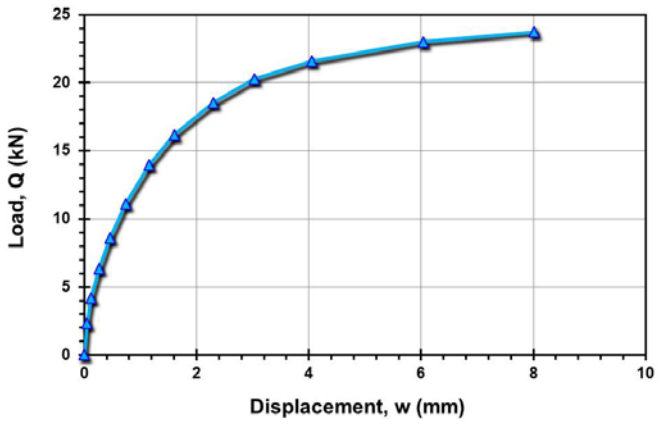

Back-analyzed normalized operational stiffness vs. pseudo-strain

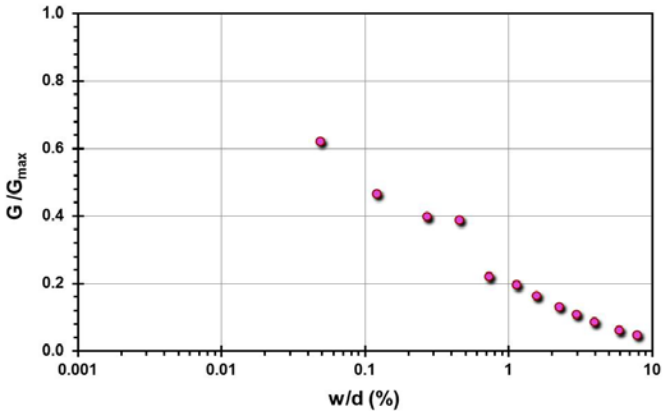

Detail	Description
Pile type/material	Closed-ended steel pipe pile (ICP)
Length, L (m)	5.00
Diameter, d (m)	0.102
Installation method	Jacked
Loading mode	Tension
$Q_{max\text{-}measured}$ (kN)	23.74
Q_s (kN)	23.74
Q_b (kN)	-
$Q_{Davisson}$ (kN)	22.29
$Q_{w/d=10\%}$ (kN)	24.39
$Q_{C\text{-}K}$ (kN)	26.73

Pile ID: BK 2/L1C

Load-displacement data

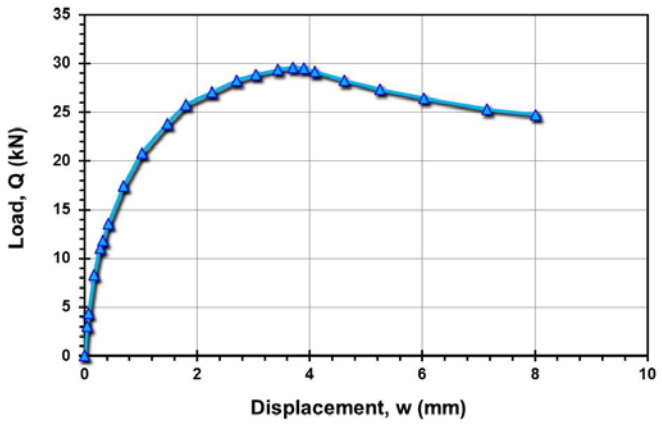

Back-analyzed normalized operational stiffness vs. pseudo-strain

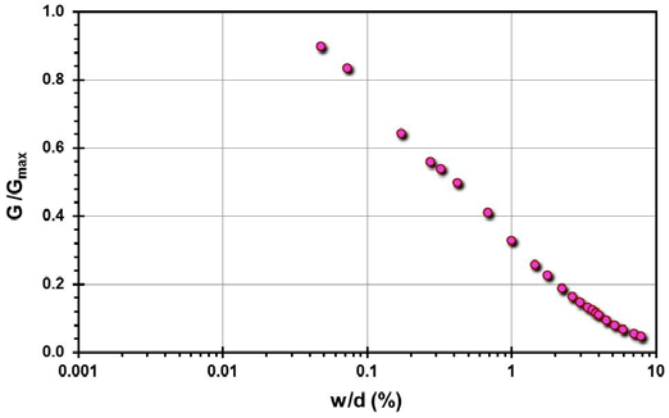

Detail	Description
Pile type/material	Closed-ended steel pipe pile (ICP)
Length, L (m)	4.80
Diameter, d (m)	0.102
Installation method	Jacked
Loading mode	Compression
$Q_{max\text{-}measured}$ (kN)	24.75
Q_s (kN)	20.99
Q_b (kN)	3.76
$Q_{Davisson}$ (kN)	29.60
$Q_{w/d=10\%}$ (kN)	33.24
$Q_{C\text{-}K}$ (kN)	26.73

Pile ID: BK 2/L2C

Load-displacement data

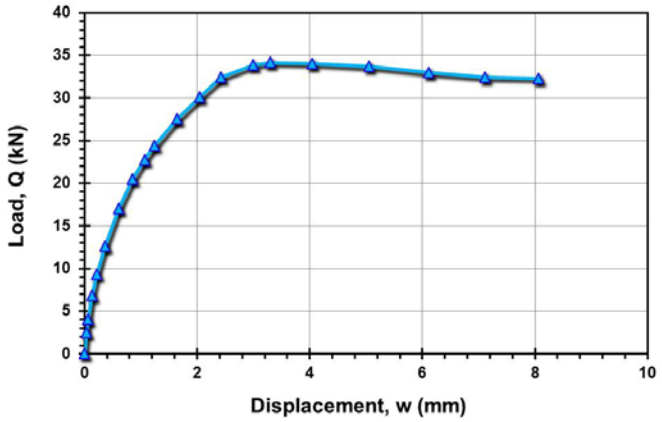

Back-analyzed normalized operational stiffness vs. pseudo-strain

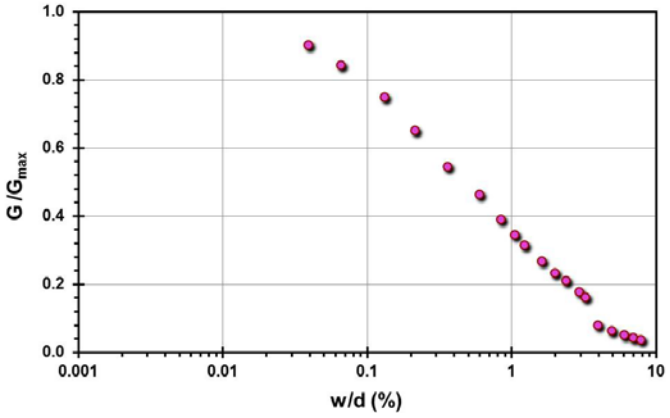

Detail	Description
Pile type/material	Closed-ended steel pipe pile (ICP)
Length, L (m)	4.80
Diameter, d (m)	0.102
Installation method	Jacked
Loading mode	Compression
$Q_{max\text{-}measured}$ (kN)	32.31
Q_s (kN)	24.65
Q_b (kN)	7.66
$Q_{Davisson}$ (kN)	34.16
$Q_{w/d=10\%}$ (kN)	38.95
$Q_{C\text{-}K}$ (kN)	41.81

Pile ID: BK 3(1)/L1C

Load-displacement data

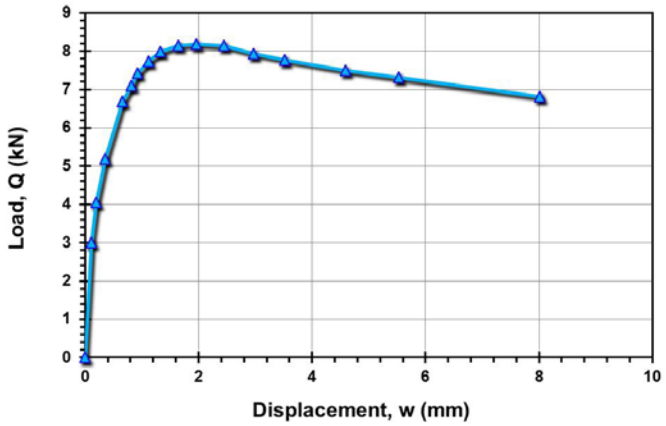

Back-analyzed normalized operational stiffness vs. pseudo-strain

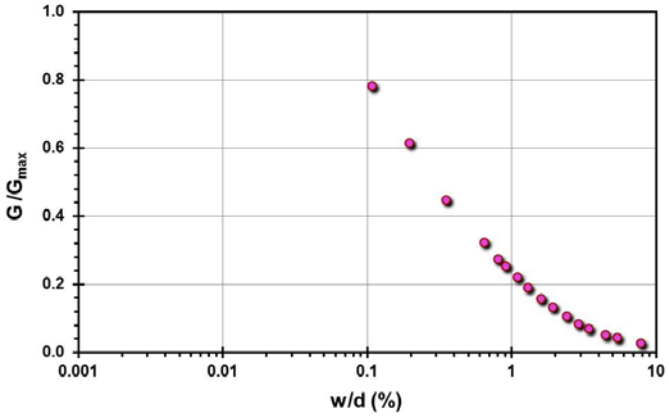

Detail	Description
Pile type/material	Closed-ended steel pipe pile (ICP)
Length, L (m)	1.95
Diameter, d (m)	0.102
Installation method	Jacked
Loading mode	Compression
$Q_{max\text{-}measured}$ (kN)	6.81
Q_s (kN)	Not reported
Q_b (kN)	Not reported
$Q_{Davisson}$ (kN)	8.19
$Q_{w/d=10\%}$ (kN)	9.20
$Q_{C\text{-}K}$ (kN)	9.45

Pile ID: BK 3(2)/L1C

Load-displacement data

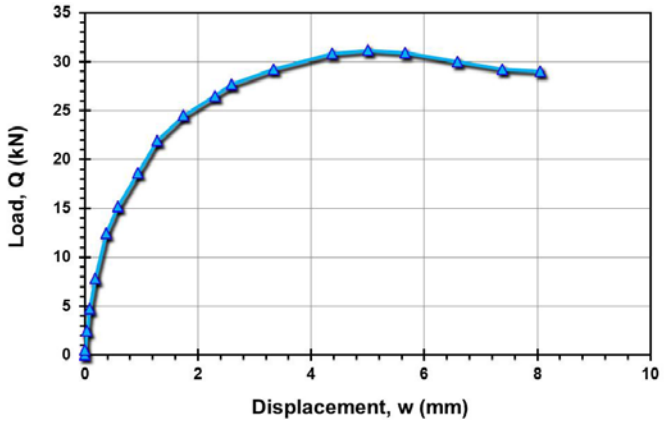

Back-analyzed normalized operational stiffness vs. pseudo-strain

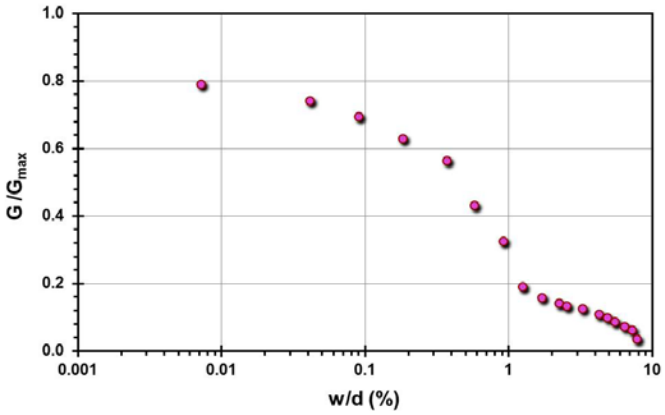

Detail	Description
Pile type/material	Closed-ended steel pipe pile (ICP)
Length, L (m)	4.70
Diameter, d (m)	0.102
Installation method	Jacked
Loading mode	Compression
$Q_{max\text{-}measured}$ (kN)	29.04
Q_s (kN)	22.06
Q_b (kN)	6.98
$Q_{Davisson}$ (kN)	31.17
$Q_{w/d=10\%}$ (kN)	33.12
$Q_{C\text{-}K}$ (kN)	35.32

Pile ID: BK 4f/L1C

Load-displacement data

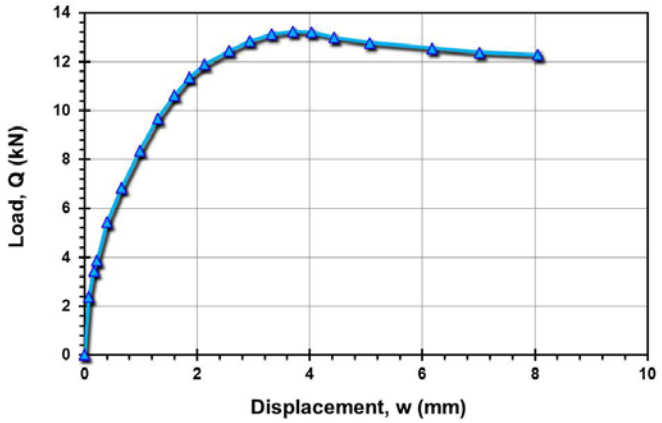

Back-analyzed normalized operational stiffness vs. pseudo-strain

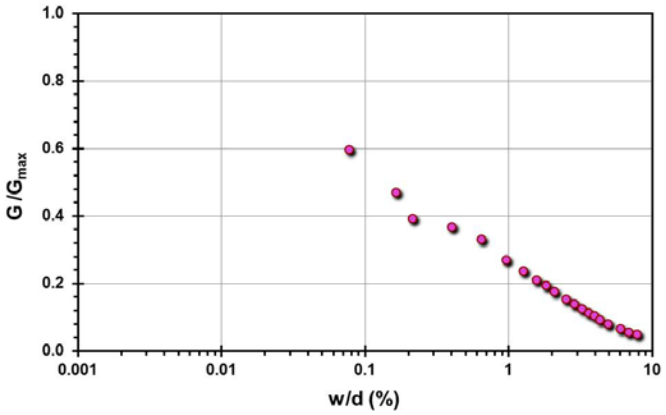

Detail	Description
Pile type/material	Closed-ended steel pipe pile (ICP)
Length, L (m)	1.95
Diameter, d (m)	0.102
Installation method	Jacked
Loading mode	Compression
$Q_{max\text{-}measured}$ (kN)	12.28
Q_s (kN)	10.06
Q_b (kN)	2.22
$Q_{Davisson}$ (kN)	13.24
$Q_{w/d=10\%}$ (kN)	14.65
$Q_{C\text{-}K}$ (kN)	15.61

Pile ID: BK 4s/L1C

Load-displacement data

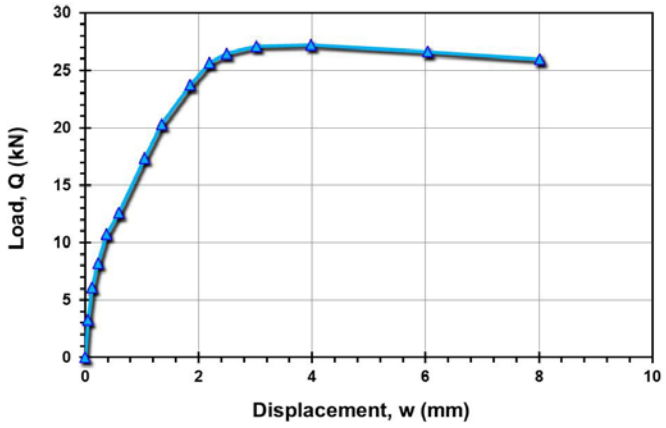

Back-analyzed normalized operational stiffness vs. pseudo-strain

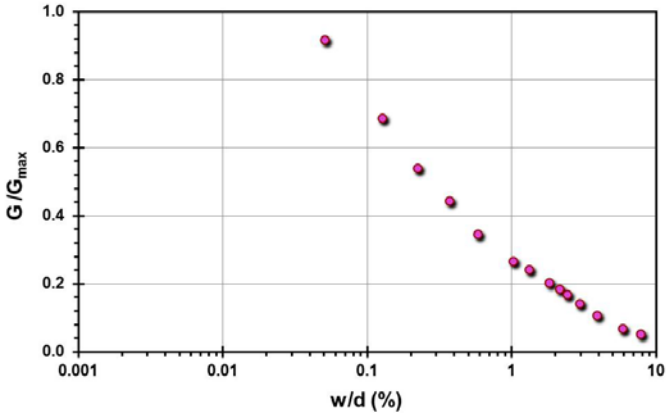

Detail	Description
Pile type/material	Closed-ended steel pipe pile (ICP)
Length, L (m)	4.75
Diameter, d (m)	0.102
Installation method	Jacked
Loading mode	Compression
$Q_{max\text{-}measured}$ (kN)	25.93
Q_s (kN)	20.09
Q_b (kN)	5.84
$Q_{Davisson}$ (kN)	27.23
$Q_{w/d=10\%}$ (kN)	32.03
$Q_{C\text{-}K}$ (kN)	34.85

Site ID No. 6

Cone penetrometer data	CPT SBT soil classification index, I_c	Detail	Description
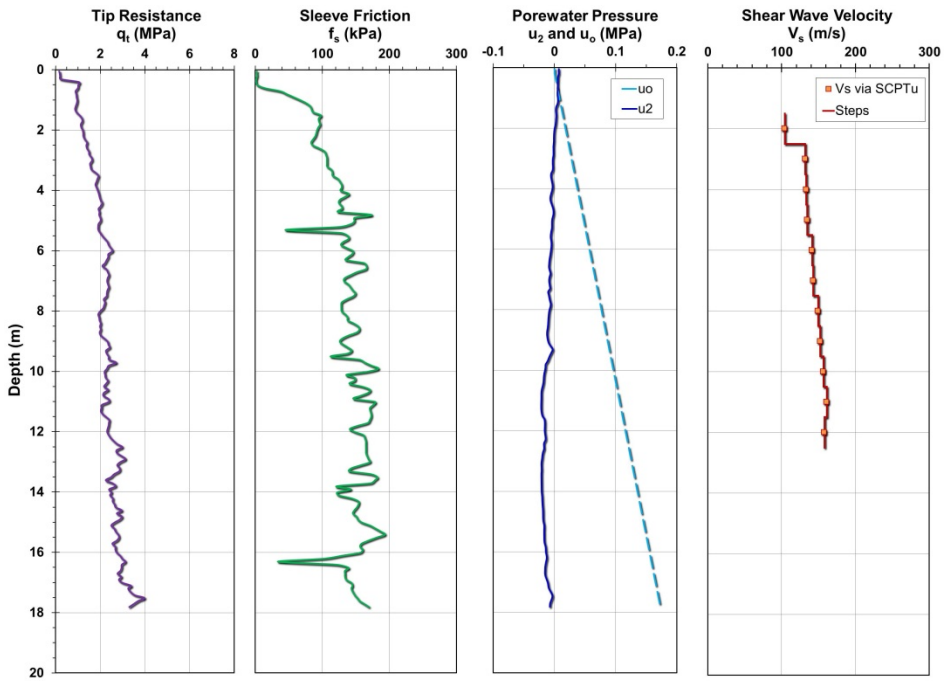	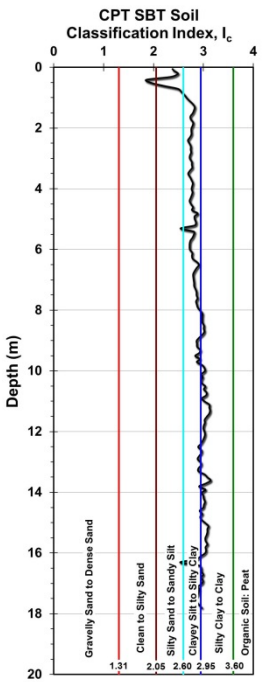	Site name and location	Brent Cross, Hendon, UK
		Soil type(s)	Weathered London clay
		Pile type(s)	Closed-ended steel pipe piles
		Type of cone penetrometer testing	SCPTu
		Source of V_s evaluation	SCPTu
		Number of pile load tests	6
		Reference	Cooke et al. (1979)
		Comments	

Pile ID: BC A1

Load-displacement data

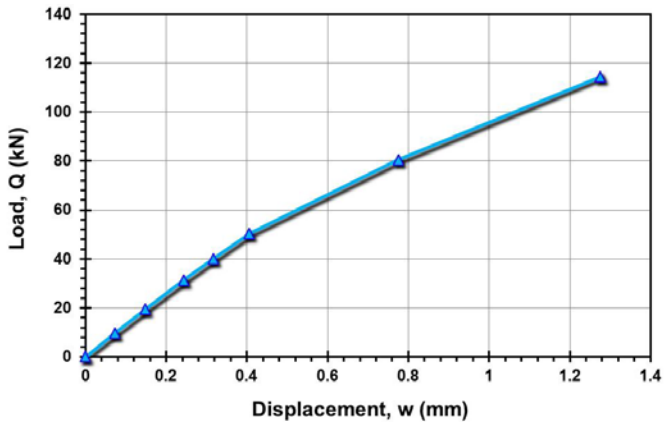

Back-analyzed normalized operational stiffness vs. pseudo-strain

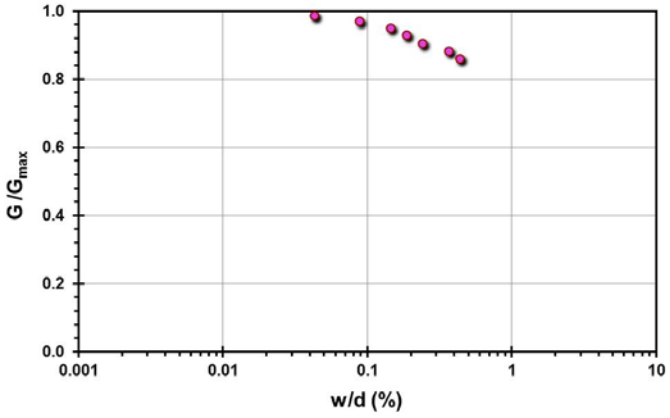

Detail	Description
Pile type/material	Closed-ended steel pipe pile
Length, L (m)	4.50
Diameter, d (m)	0.168
Installation method	Jacked
Loading mode	Compression
$Q_{max\text{-}measured}$ (kN)	114.40
Q_s (kN)	96.96
Q_b (kN)	17.50
$Q_{Davisson}$ (kN)	241.15
$Q_{w/d=10\%}$ (kN)	415.97
$Q_{C\text{-}K}$ (kN)	513.08

Pile ID: BC B1

Load-displacement data

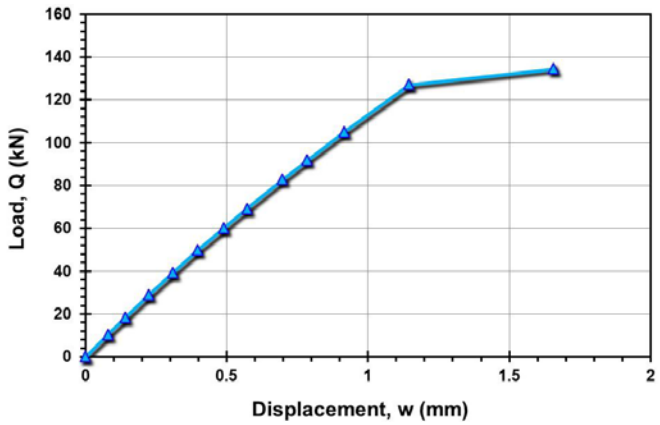

Back-analyzed normalized operational stiffness vs. pseudo-strain

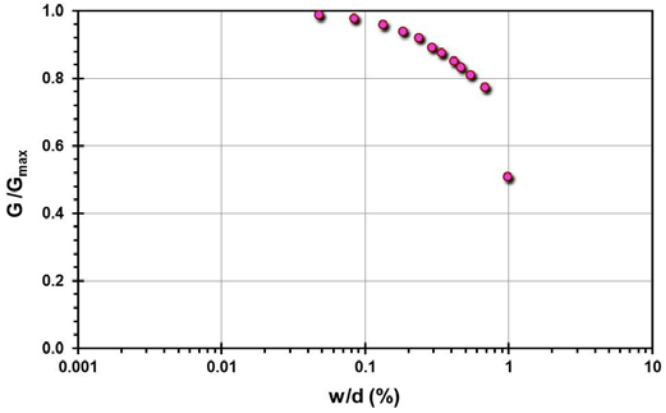

Detail	Description
Pile type/material	Closed-ended steel pipe pile
Length, L (m)	4.50
Diameter, d (m)	0.17
Installation method	Jacked
Loading mode	Compression
$Q_{max\text{-}measured}$ (kN)	134.54
Q_s (kN)	97.77
Q_b (kN)	36.77
$Q_{Davisson}$ (kN)	160.77
$Q_{w/d=10\%}$ (kN)	187.00
$Q_{C\text{-}K}$ (kN)	195.05

Pile ID: BC C1

Load-displacement data

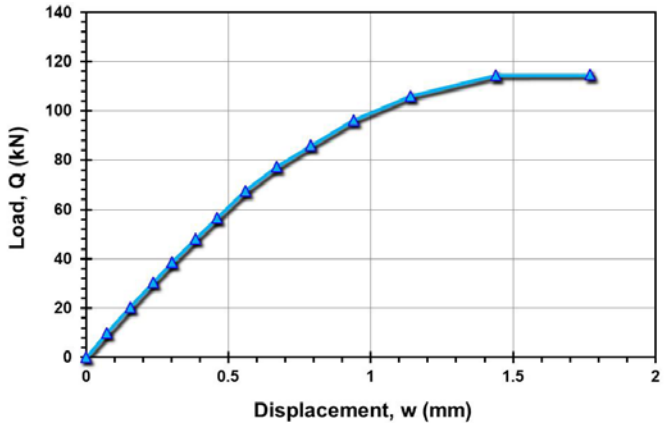

Back-analyzed normalized operational stiffness vs. pseudo-strain

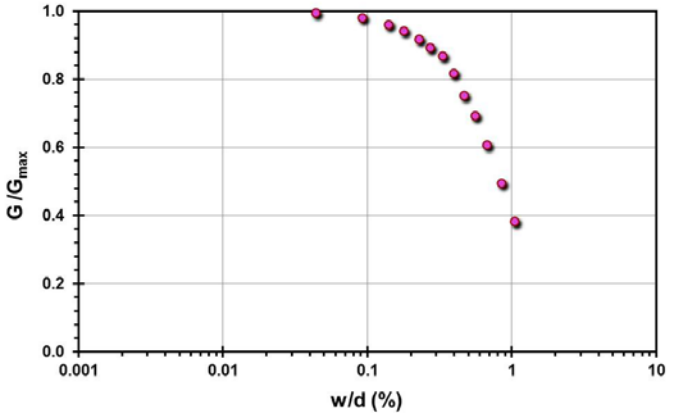

Detail	Description
Pile type/material	Closed-ended steel pipe pile
Length, L (m)	4.50
Diameter, d (m)	0.17
Installation method	Jacked
Loading mode	Compression
$Q_{max\text{-}measured}$ (kN)	114.56
Q_s (kN)	Not reported
Q_b (kN)	Not reported
$Q_{Davisson}$ (kN)	114.56
$Q_{w/d=10\%}$ (kN)	115.16
$Q_{C\text{-}K}$ (kN)	115.23

Pile ID: BC A2

Load-displacement data

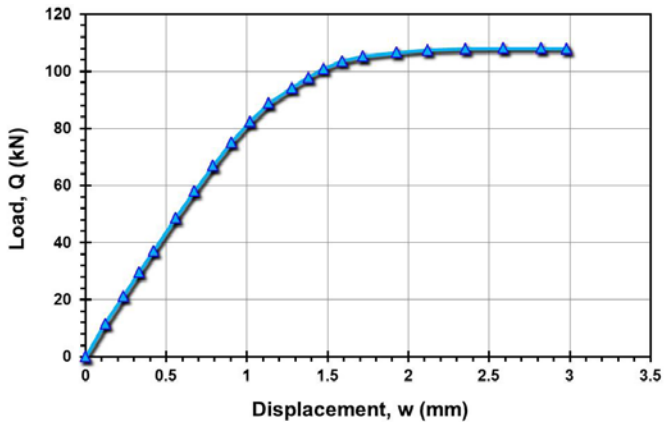

Back-analyzed normalized operational stiffness vs. pseudo-strain

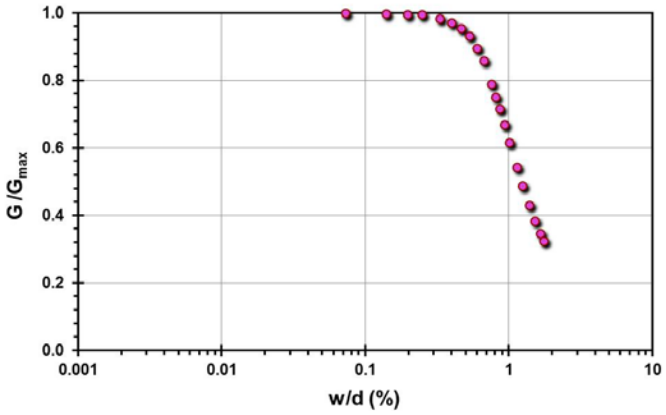

Detail	Description
Pile type/material	Closed-ended steel pipe pile
Length, L (m)	4.50
Diameter, d (m)	0.17
Installation method	Jacked
Loading mode	Tension
$Q_{max\text{-}measured}$ (kN)	108.59
Q_s (kN)	108.59
Q_b (kN)	-
$Q_{Davisson}$ (kN)	108.59
$Q_{w/d=10\%}$ (kN)	108.99
$Q_{C\text{-}K}$ (kN)	109.19

Pile ID: BC B2

Load-displacement data

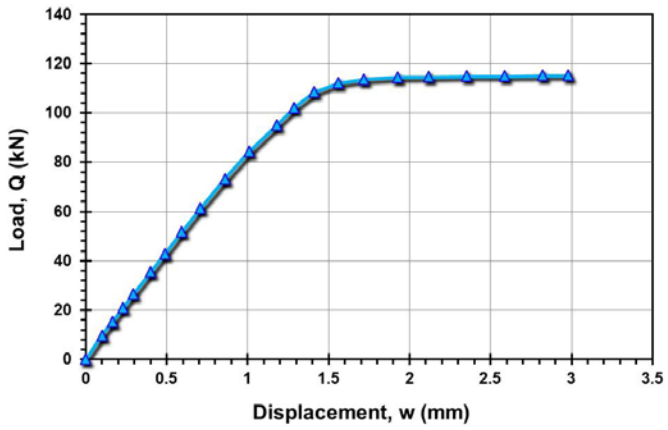

Back-analyzed normalized operational stiffness vs. pseudo-strain

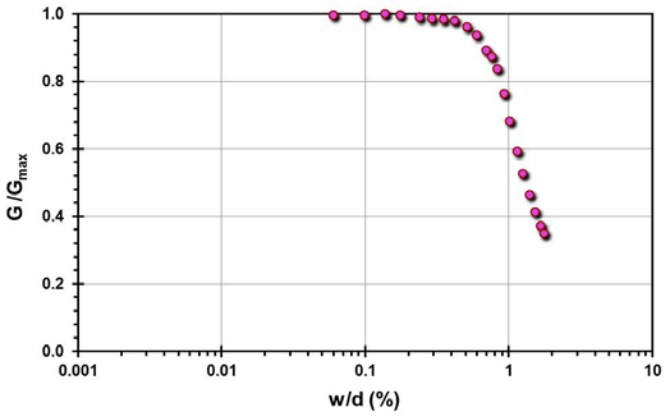

Detail	Description
Pile type/material	Closed-ended steel pipe pile
Length, L (m)	4.50
Diameter, d (m)	0.17
Installation method	Jacked
Loading mode	Tension
$Q_{max\text{-}measured}$ (kN)	115.27
Q_s (kN)	115.27
Q_b (kN)	-
$Q_{Davisson}$ (kN)	115.27
$Q_{w/d=10\%}$ (kN)	116.47
$Q_{C\text{-}K}$ (kN)	116.75

Pile ID: BC C2

Load-displacement data

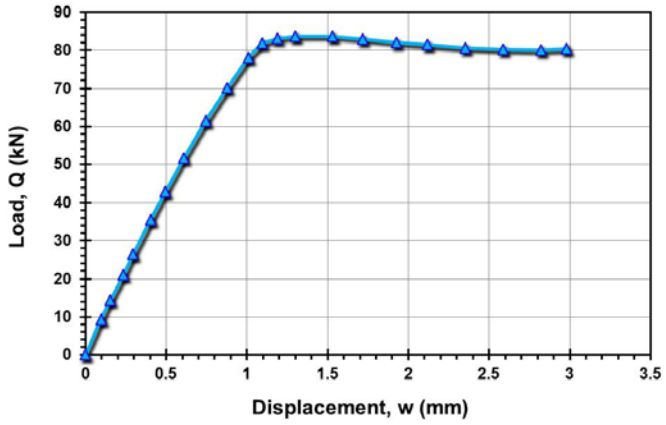

Back-analyzed normalized operational stiffness vs. pseudo-strain

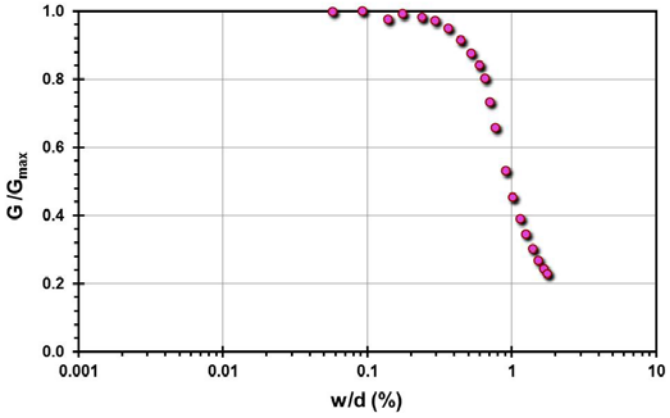

Detail	Description
Pile type/material	Closed-ended steel pipe pile
Length, L (m)	4.50
Diameter, d (m)	0.17
Installation method	Jacked
Loading mode	Tension
$Q_{max\text{-}measured}$ (kN)	83.31
Q_s (kN)	83.31
Q_b (kN)	-
$Q_{Davisson}$ (kN)	83.71
$Q_{w/d=10\%}$ (kN)	88.29
$Q_{C\text{-}K}$ (kN)	88.85

Site ID No. 7

Cone penetrometer data	CPT SBT soil classification index, I_c	Detail	Description
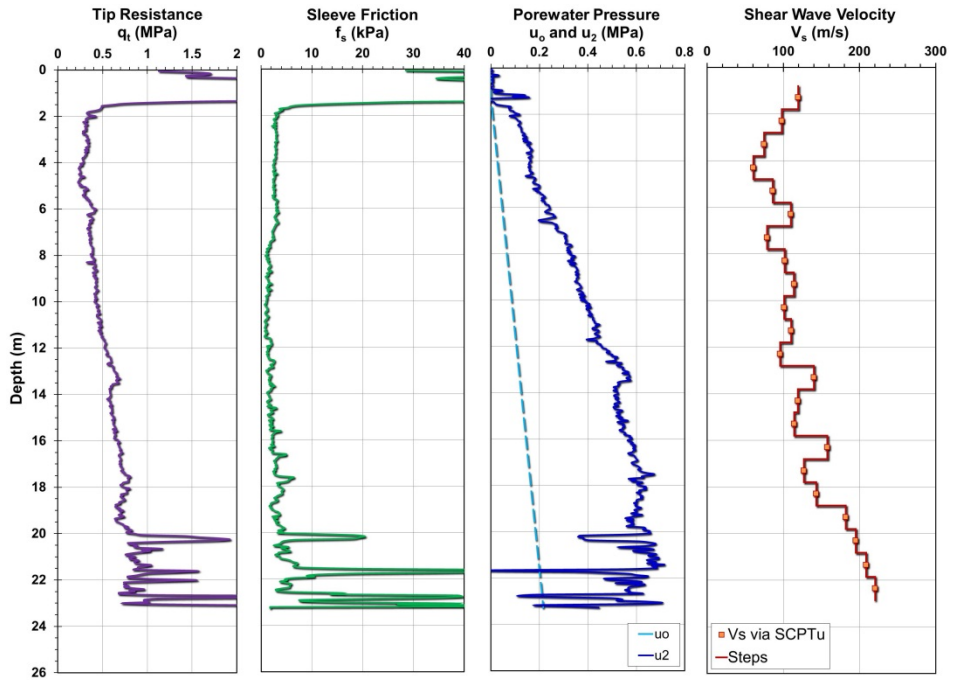	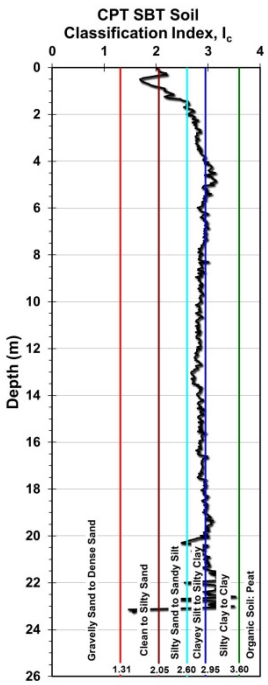	Site name and location	Canadian Geotechnical Test Site, South Gloucester, ON, Canada
		Soil type(s)	Soft sensitive (Champlain Sea) clay
		Pile type(s)	Drilled shaft
		Type of cone penetrometer testing	SCPTu
		Source of V_s evaluation	SCPTu
		Number of pile load tests	4
		Reference	Miller (2012)
		Comments	

Pile ID: CGTS 1

Load-displacement data	Detail	Description
Not reported	Pile type/material	Drilled shaft
	Length, L (m)	9.35
	Diameter, d (m)	0.92
	Installation method	Bored cast in-situ
	Loading mode	Tension
	$Q_{max\text{-}measured}$ (kN)	974.56
	Q_s (kN)	974.56
	Q_b (kN)	-
	$Q_{Davisson}$ (kN)	Not calculated
	$Q_{w/d=10\%}$ (kN)	Not calculated
	$Q_{C\text{-}K}$ (kN)	Not calculated
Back-analyzed normalized operational stiffness vs. pseudo-strain		
Not calculated		

Pile ID: CGTS 2

Load-displacement data

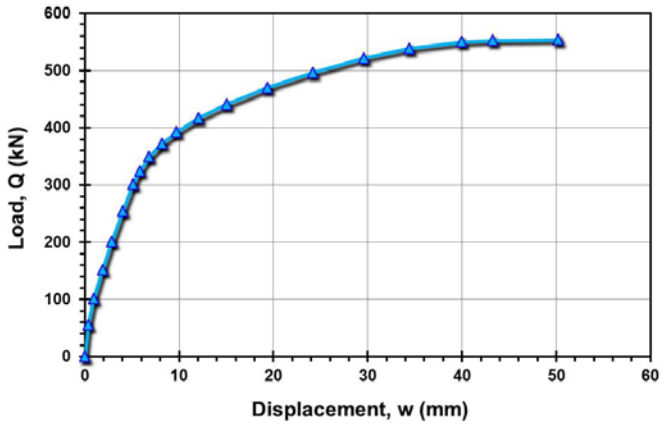

Back-analyzed normalized operational stiffness vs. pseudo-strain

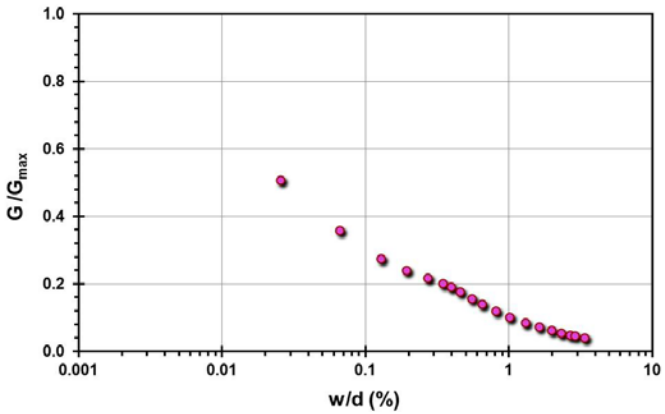

Detail	Description
Pile type/material	Drilled shaft
Length, L (m)	5.94
Diameter, d (m)	1.48
Installation method	Bored cast in-situ
Loading mode	Compression
$Q_{max\text{-}measured}$ (kN)	533.95
Q_s (kN)	Not reported
Q_b (kN)	Not reported
$Q_{Davisson}$ (kN)	455.58
$Q_{w/d=10\%}$ (kN)	564.53
$Q_{C\text{-}K}$ (kN)	569.80

Pile ID: CGTS 4

Load-displacement data

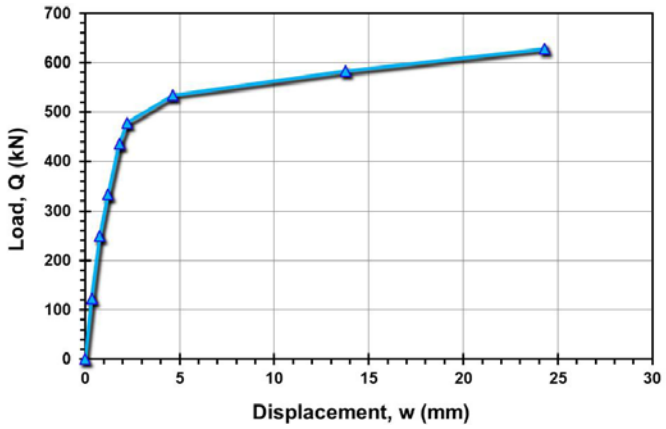

Back-analyzed normalized operational stiffness vs. pseudo-strain

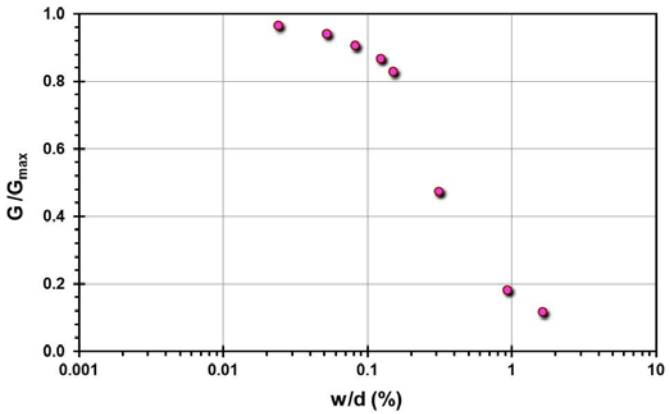

Detail	Description
Pile type/material	Drilled shaft
Length, L (m)	6.51
Diameter, d (m)	1.48
Installation method	Bored cast in-situ
Loading mode	Tension
$Q_{max\text{-}measured}$ (kN)	628.50
Q_s (kN)	628.50
Q_b (kN)	-
$Q_{Davisson}$ (kN)	605.60
$Q_{w/d=10\%}$ (kN)	687.56
$Q_{C\text{-}K}$ (kN)	700.77

Pile ID: CGTS 9

Load-displacement data

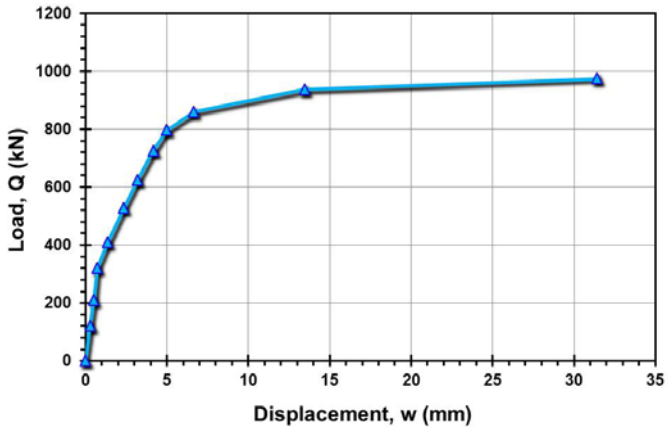

Back-analyzed normalized operational stiffness vs. pseudo-strain

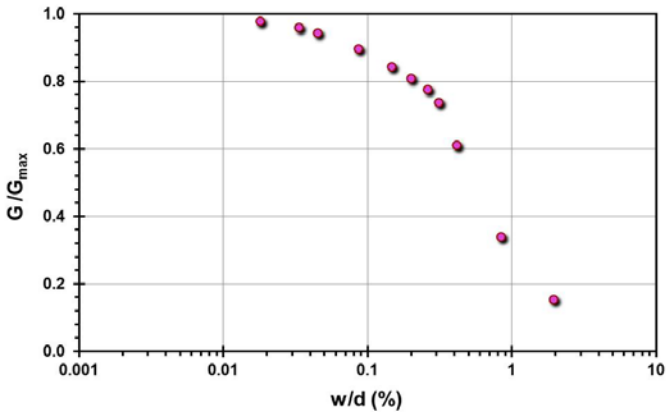

Detail	Description
Pile type/material	Drilled shaft
Length, L (m)	6.27
Diameter, d (m)	1.60
Installation method	Bored cast in-situ
Loading mode	Tension
$Q_{max\text{-}measured}$ (kN)	974.56
Q_s (kN)	974.56
Q_b (kN)	-
$Q_{Davisson}$ (kN)	955.47
$Q_{w/d=10\%}$ (kN)	1,006.24
$Q_{C\text{-}K}$ (kN)	1,014.20

Site ID No. 8

Cone penetrometer data	CPT SBT soil classification index, I_c	Detail	Description
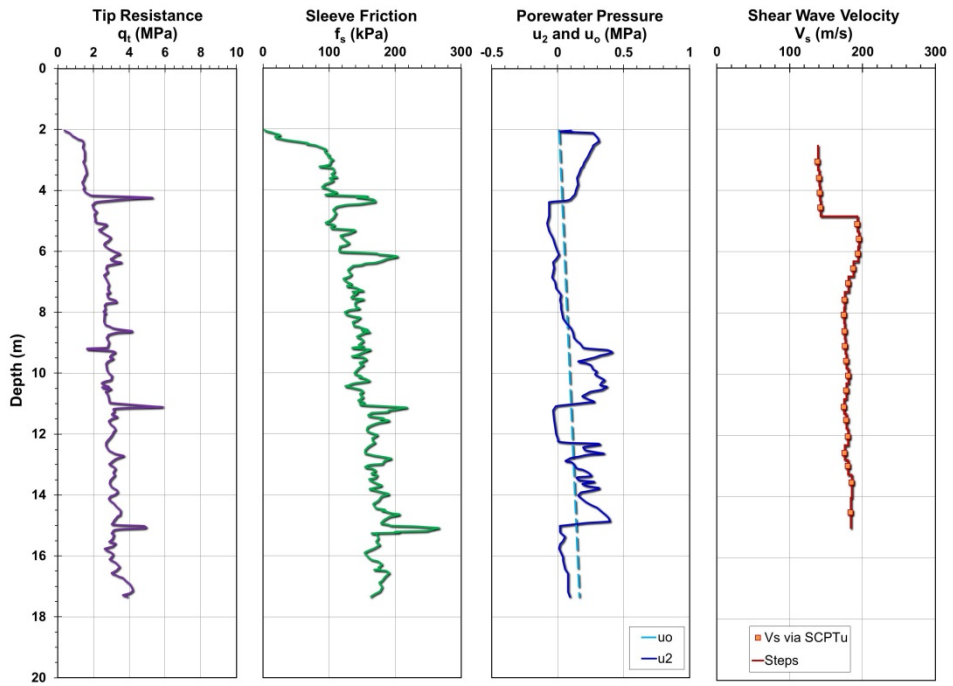	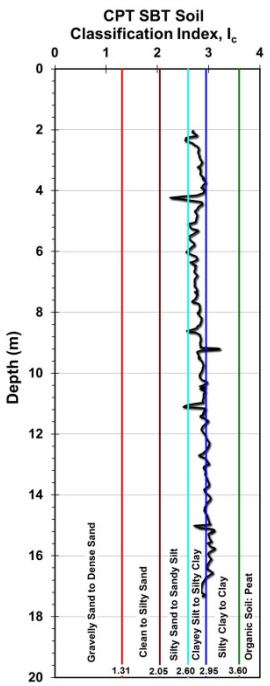	Site name and location	Canons Park, North London, UK
		Soil type(s)	Weathered London clay
		Pile type(s)	1drilled shaft and 3 close-ended steel pipe pile
		Type of cone penetrometer testing	SCPTu
		Source of V_s evaluation	SCPTu
		Number of pile load tests	4
		Reference	Powell and Lunne (2005), Price and Wardle (1982), Bond and Jardine (1991), Jardine et al. (1992)
		Comments	The closed-ended steel pipe piles include one ICP.

Pile ID: CP1

Load-displacement data

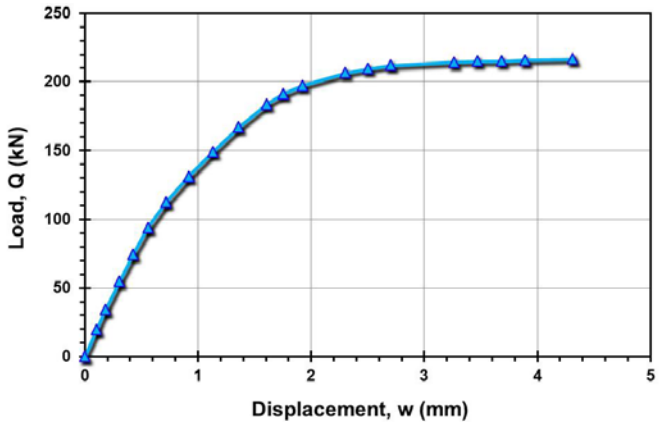

Back-analyzed normalized operational stiffness vs. pseudo-strain

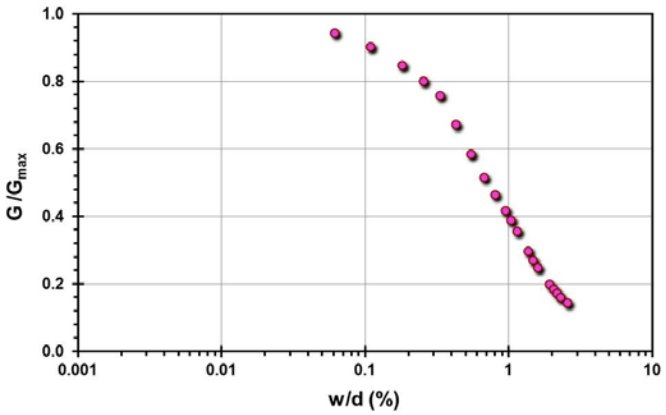

Detail	Description
Pile type/material	Closed-ended steel pipe pile
Length, L (m)	4.50
Diameter, d (m)	0.168
Installation method	Jacked
Loading mode	Compression
$Q_{max\text{-}measured}$ (kN)	216.70
Q_s (kN)	169.71
Q_b (kN)	46.99
$Q_{Davisson}$ (kN)	216.70
$Q_{w/d=10\%}$ (kN)	222.24
$Q_{C\text{-}K}$ (kN)	224.16

Pile ID: CP2

Load-displacement data

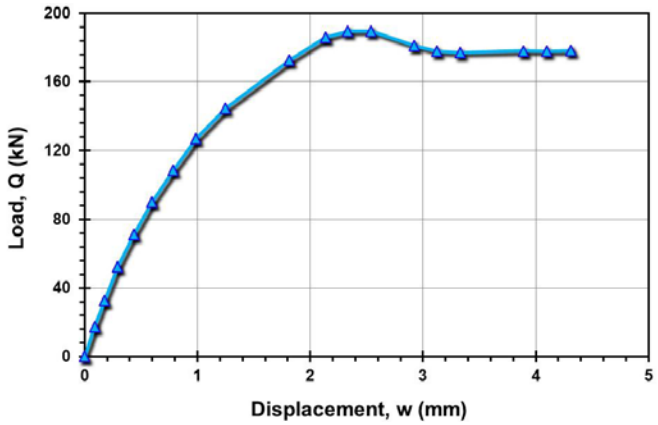

Back-analyzed normalized operational stiffness vs. pseudo-strain

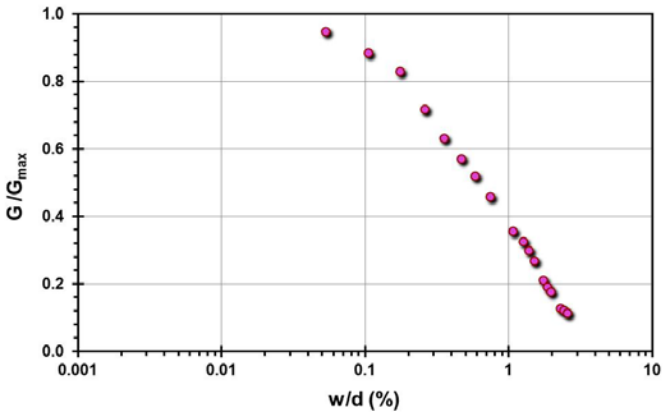

Detail	Description
Pile type/material	Closed-ended steel pipe pile
Length, L (m)	4.50
Diameter, d (m)	0.168
Installation method	Driven
Loading mode	Compression
$Q_{max\text{-}measured}$ (kN)	178.04
Q_s (kN)	147.78
Q_b (kN)	30.26
$Q_{Davisson}$ (kN)	-
$Q_{w/d=10\%}$ (kN)	170.26
$Q_{C\text{-}K}$ (kN)	-

Pile ID: CP3

Load-displacement data

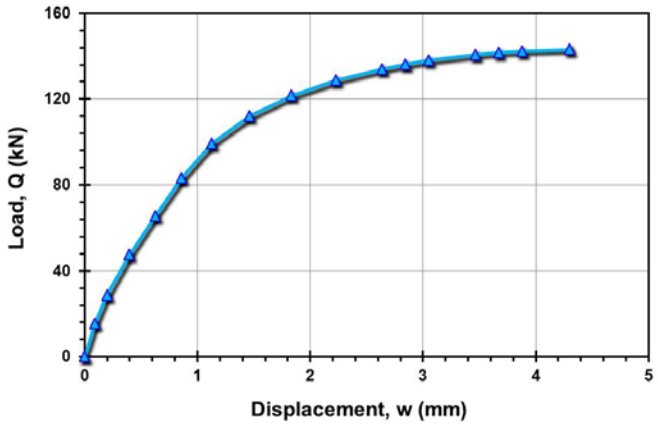

Back-analyzed normalized operational stiffness vs. pseudo-strain

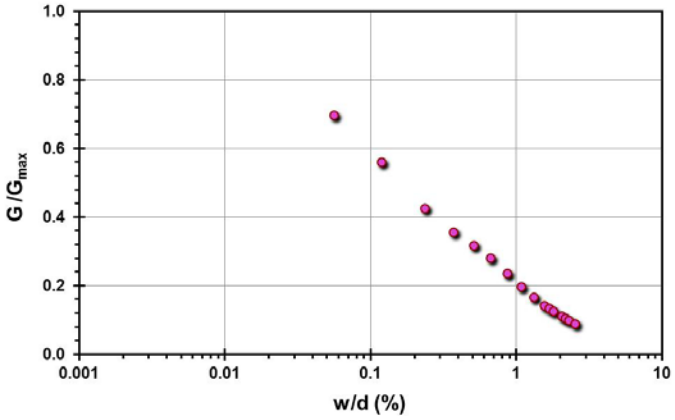

Detail	Description
Pile type/material	Drilled shaft
Length, L (m)	4.50
Diameter, d (m)	0.168
Installation method	Bored cast in-situ
Loading mode	Compression
$Q_{max\text{-}measured}$ (kN)	143.11
Q_s (kN)	Not reported
Q_b (kN)	Not reported
$Q_{Davisson}$ (kN)	148.38
$Q_{w/d=10\%}$ (kN)	153.64
$Q_{C\text{-}K}$ (kN)	157.46

Pile ID: CP4

Load-displacement data

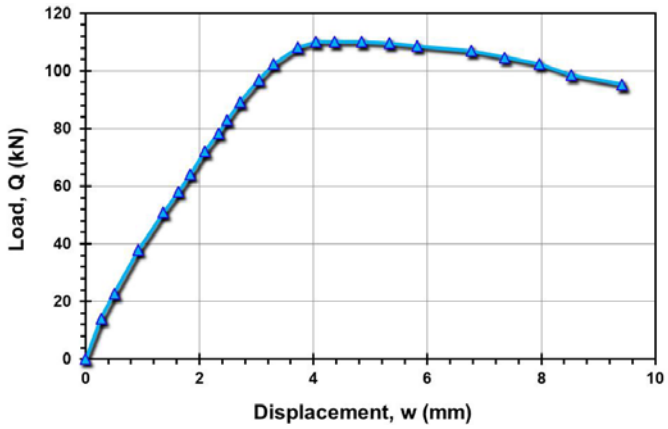

Back-analyzed normalized operational stiffness vs. pseudo-strain

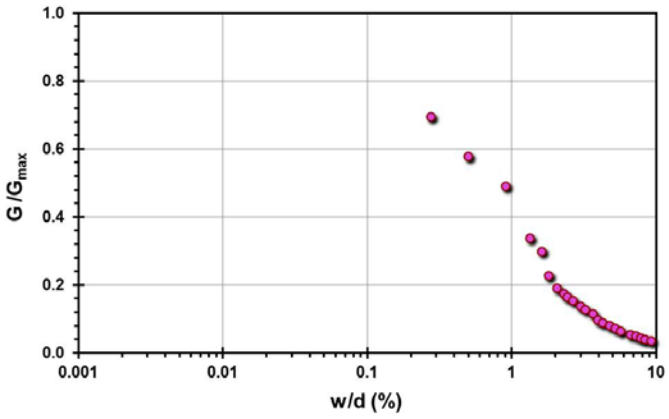

Detail	Description
Pile type/material	Closed-ended steel pipe pile (ICP)
Length, L (m)	3.95
Diameter, d (m)	0.102
Installation method	Jacked
Loading mode	Compression
$Q_{max\text{-}measured}$ (kN)	107.25
Q_s (kN)	73.00
Q_b (kN)	34.25
$Q_{Davisson}$ (kN)	-
$Q_{w/d=10\%}$ (kN)	95.15
$Q_{C\text{-}K}$ (kN)	-

Site ID No. 9

Cone penetrometer data	CPT SBT soil classification index, I_c	Detail	Description
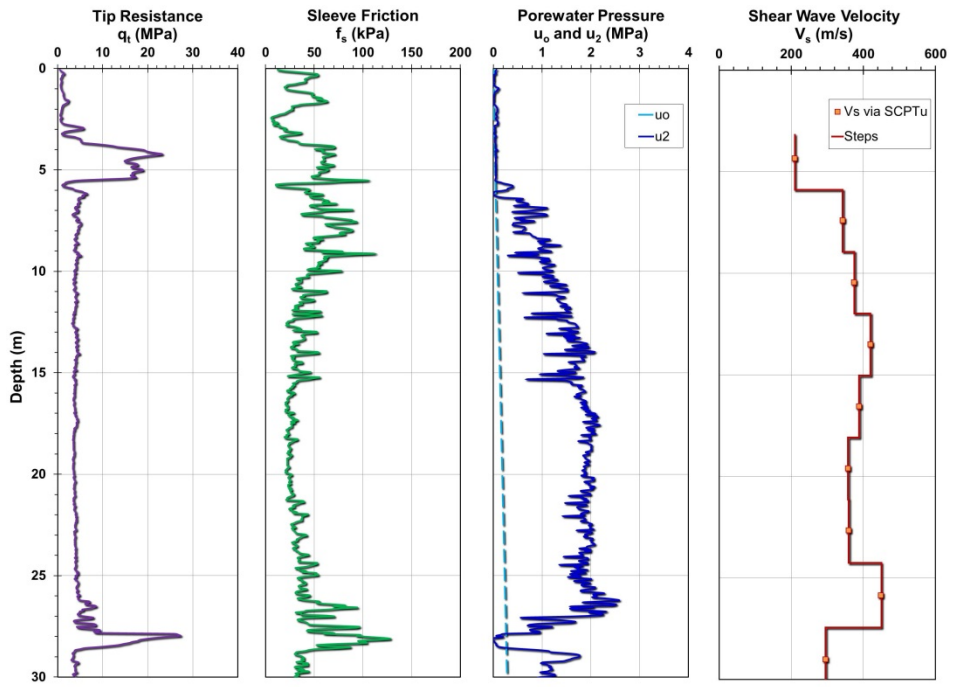	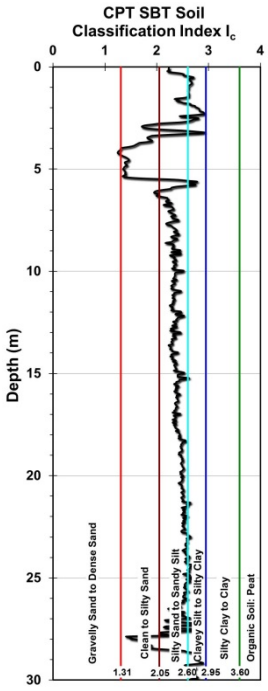	Site name and location	Canon Plant, Newport News, VA, USA
		Soil type(s)	Norfolk Formation (6 m of silts, sands, and clays) over Yorktown Formation (stiff sandy clay)
		Pile type(s)	Square concrete driven pile
		Type of cone penetrometer testing	SCPTu
		Source of V_s evaluation	SCPTu
		Number of pile load tests	2
		Reference	Patton II & Barnhill (1988)
		Comments	

Pile ID: C Pt1

Load-displacement data

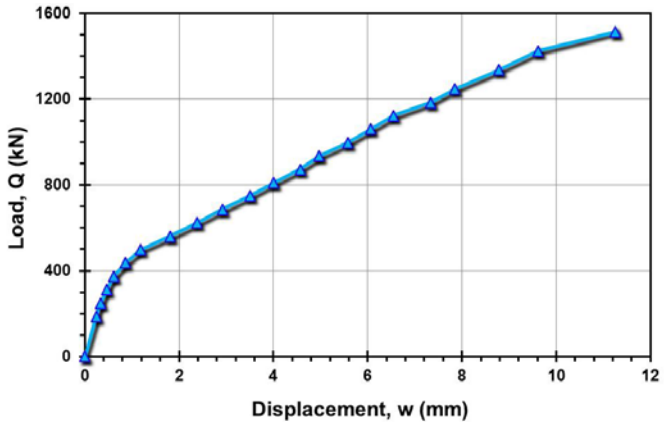

Back-analyzed normalized operational stiffness vs. pseudo-strain

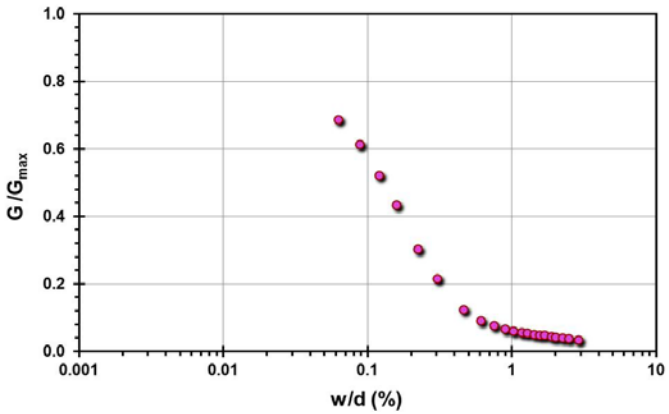

Detail	Description
Pile type/material	Square concrete
Length, L (m)	21.33
Width, B (m)	0.305
Installation method	Driven
Loading mode	Compression
$Q_{max\text{-}measured}$ (kN)	1,512.46
Q_s (kN)	Not reported
Q_b (kN)	Not reported
$Q_{Davisson}$ (kN)	1,881.00
$Q_{w/d=10\%}$ (kN)	2,249.55
$Q_{C\text{-}K}$ (kN)	2,808.99

Pile ID: C Pt2

Load-displacement data

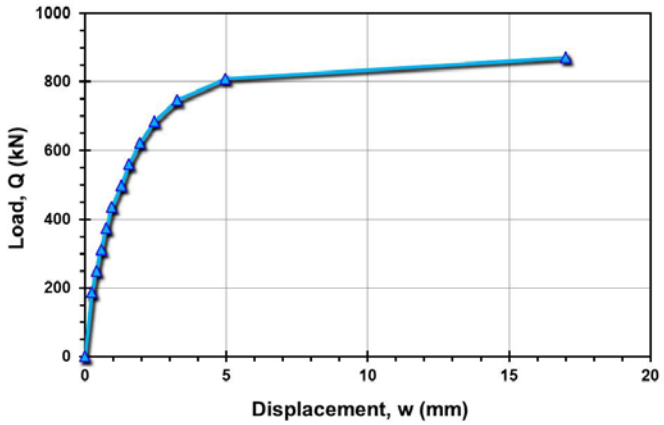

Back-analyzed normalized operational stiffness vs. pseudo-strain

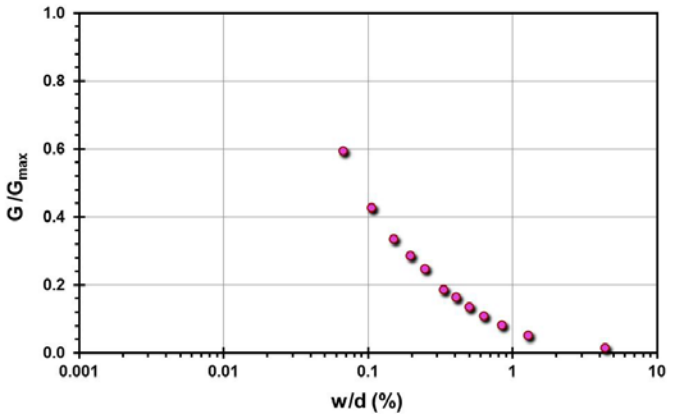

Detail	Description
Pile type/material	Square concrete
Length, L (m)	15.24
Width, B (m)	0.305
Installation method	Driven
Loading mode	Compression
$Q_{max\text{-}measured}$ (kN)	871.89
Q_s (kN)	Not reported
Q_b (kN)	Not reported
$Q_{Davisson}$ (kN)	840.75
$Q_{w/d=10\%}$ (kN)	888.21
$Q_{C\text{-}K}$ (kN)	900.90

Site ID No. 10

Cone penetrometer data	CPT SBT soil classification index, I_c	Detail	Description
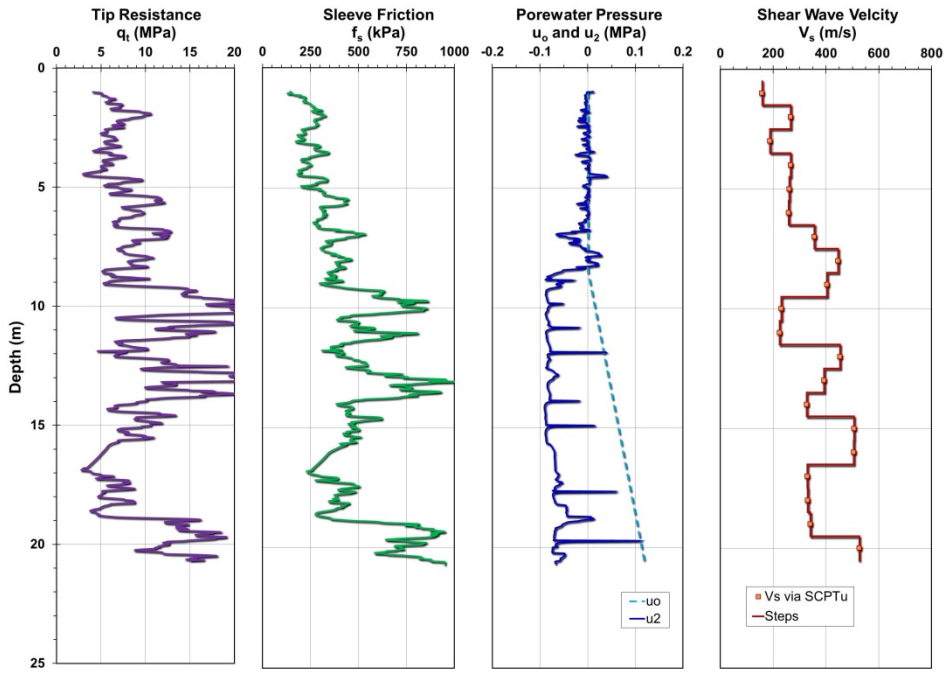	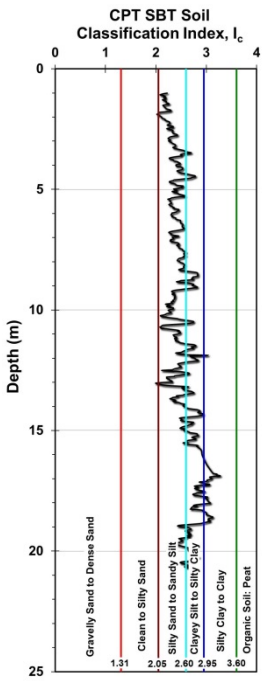	Site name and location	CNN International Blvd. Viaduct, Atlanta, GA, USA
		Soil type(s)	Piedmont residual silt and sand grading to partially weathered rock of Piedmont Geology
		Pile type(s)	Drilled shaft
		Type of cone penetrometer testing	SCPTu
		Source of V_s evaluation	SCPTu
		Number of pile load tests	1
		Reference	Ahrens et al. (2003)
		Comments	SCPTu sounding by GT CPT rig and reported by Mayne, Niazi, & Woeller (2010)

Pile ID: CNN 1

Load-displacement data

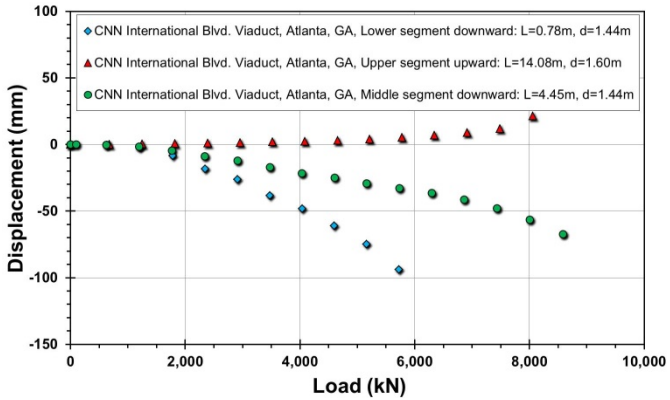

Back-analyzed normalized operational stiffness vs. pseudo-strain

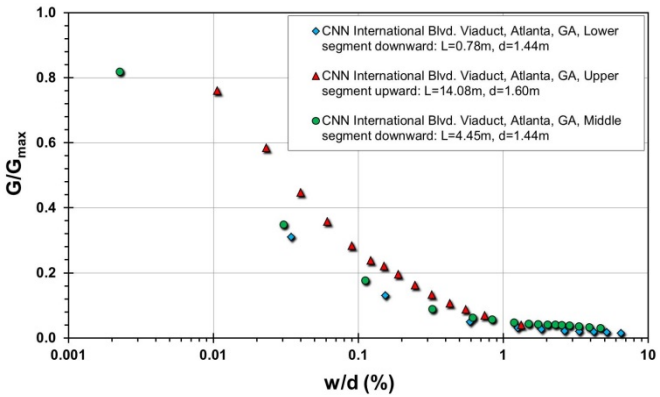

Detail	Description
Pile type/material	Drilled shaft
Length, L (m)	Upper: 14.08; middle: 4.45; lower: 0.78
Diameter, d (m)	Upper: 1.60; middle: 1.44; lower: 0.78
Installation method	Bored cast in-situ
Loading mode	O-cell compression
$Q_{max\text{-}measured}$ (kN)	Upper: 8,058.2; middle: 8,583.2; lower: 5,723.4
Q_s (kN)	Upper: 8,058.2; middle: 8,583.2; lower: 1,313.4
Q_b (kN)	4410.0
$Q_{Davisson}$ (kN)	Upper: 8,058.2; middle: 4,604.7; lower: 2,912.5
$Q_{w/d=10\%}$ (kN)	Upper: 9,055.5; middle: 10,933.9; lower: 6,783.2
$Q_{C\text{-}K}$ (kN)	Upper: 9,225.1; middle: 14,285.7; lower: 10,416.7

Site ID No. 11

Cone penetrometer data	CPT SBT soil classification index, I_c	Detail	Description
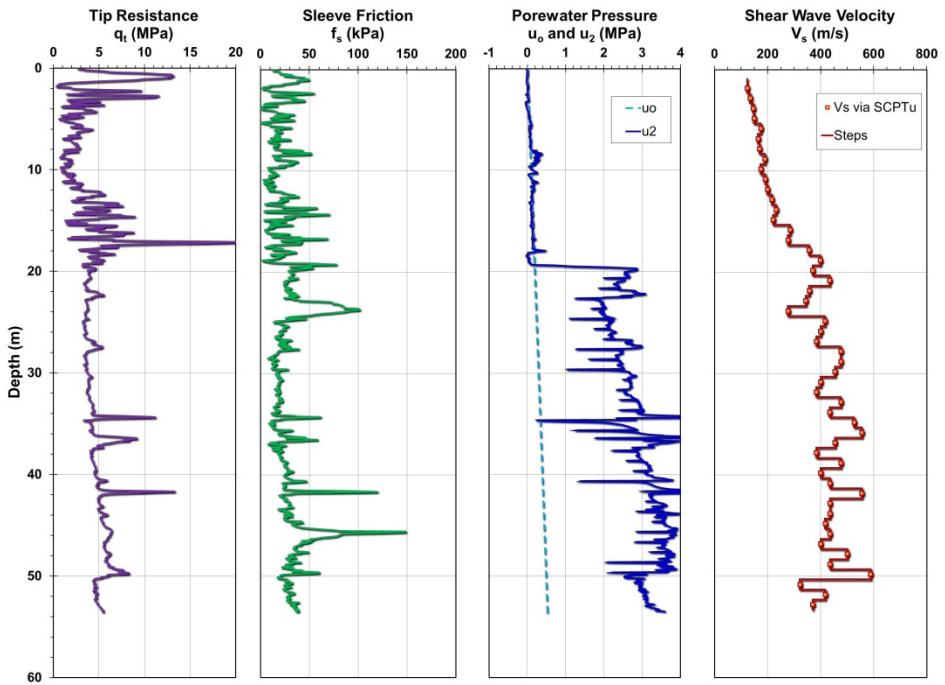	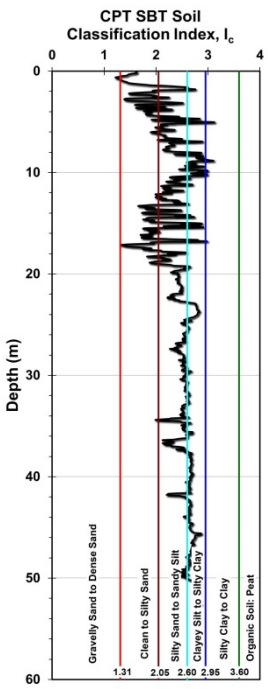	Site name and location	Cooper River Bridge on HW 17, Charleston site, SC, USA
		Soil type(s)	20 m of loose sand and soft clay overburden underlain by stiff calcareous Cooper Marl (sandy clay)
		Pile type(s)	Drilled shaft
		Type of cone penetrometer testing	SCPTu
		Source of V_s evaluation	SCPTu
		Number of pile load tests	4
		Reference	Ahren et al. (2000a, b); Camp (2004); Camp et al. (2002); Simpson et al. (2000 a, b)
		Comments	

Pile ID: CRB-C 1

Load-displacement data

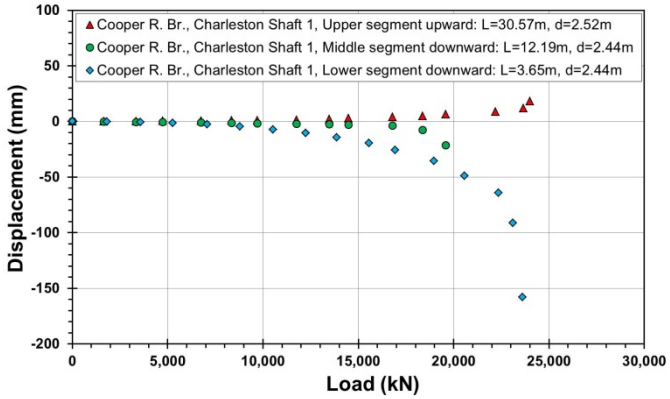

Back-analyzed normalized operational stiffness vs. pseudo-strain

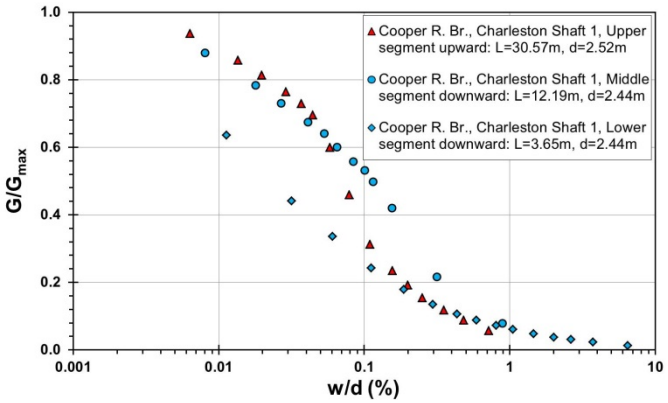

Detail	Description
Pile type/material	Drilled shaft
Length, L (m)	Upper: 30.57; middle: 12.19; lower: 3.65
Diameter, d (m)	Upper: 2.52; middle: 2.44; lower: 2.44
Installation method	Bored cast in-situ
Loading mode	O-cell compression
$Q_{max\text{-}measured}$ (kN)	Upper: 24,008.3; middle: 19,576.6; lower: 23,612.3
Q_s (kN)	Upper: 24,008.3; middle: 19,576.6; lower: 5,812.3
Q_b (kN)	17,800.0
$Q_{Davisson}$ (kN)	Upper: 24,008.3; middle: 19,576.6; lower: 17,224.5
$Q_{w/d=10\%}$ (kN)	Upper: 24,698.1; middle: 20,341.8; lower: 24,126.7
$Q_{C\text{-}K}$ (kN)	Upper: 24,752.5; middle: 20,408.2; lower: 25,000.0

Pile ID: CRB-C 2

Load-displacement data

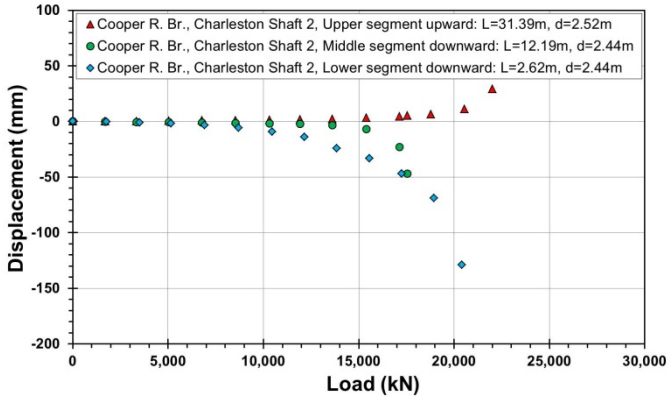

Back-analyzed normalized operational stiffness vs. pseudo-strain

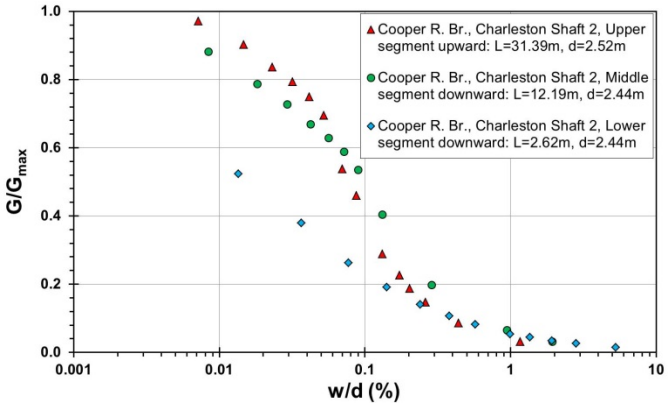

Detail	Description
Pile type/material	Drilled shaft
Length, L (m)	Upper: 31.39; middle: 12.19; lower: 2.62
Diameter, d (m)	Upper: 2.52; middle: 2.44; lower: 2.44
Installation method	Bored cast in-situ
Loading mode	O-cell compression
$Q_{max\text{-}measured}$ (kN)	Upper: 22,015.7; middle: 17,550.9; lower: 20,412.4
Q_s (kN)	Upper: 22,015.7; middle: 17,550.9; lower: 3,712.4
Q_b (kN)	16,700.0
$Q_{Davisson}$ (kN)	Upper: 22,015.7; middle: 17,127.6; lower: 15,168.5
$Q_{w/d=10\%}$ (kN)	Upper: 22,962.3; middle: 17,777.7; lower: 21,415.6
$Q_{C\text{-}K}$ (kN)	Upper: 23,094.7; middle: 17,852.2; lower: 22,727.3

Pile ID: CRB-C 3

Load-displacement data

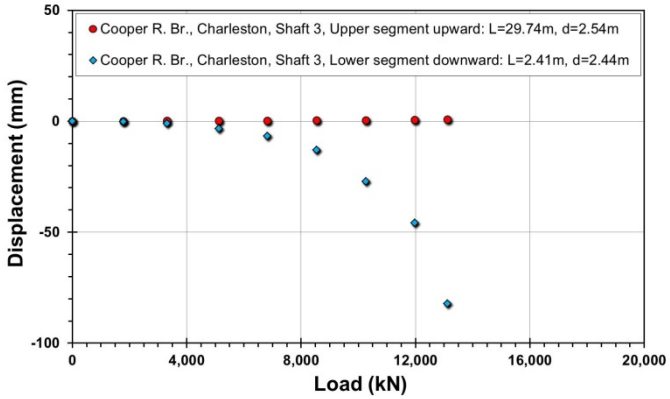

Back-analyzed normalized operational stiffness vs. pseudo-strain

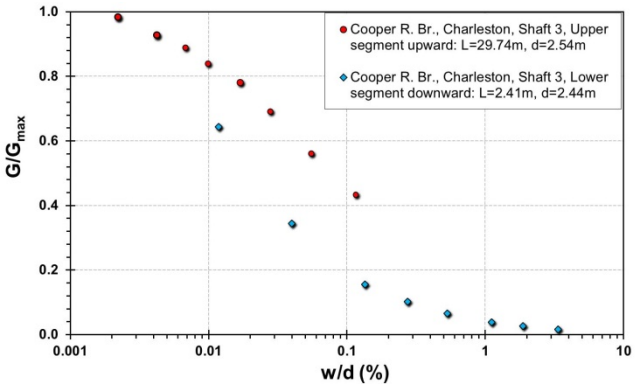

Detail	Description
Pile type/material	Drilled shaft
Length, L (m)	Upper: 29.74; lower: 2.41
Diameter, d (m)	Upper: 2.54; lower: 2.44
Installation method	Bored cast in-situ
Loading mode	O-cell compression
$Q_{max\text{-}measured}$ (kN)	Upper: 13,112.6; lower: 13,112.6
Q_s (kN)	Upper: 13,112.6; lower: 3,392.6
Q_b (kN)	9,720.0
$Q_{Davisson}$ (kN)	Upper: 14,978.9; lower: 10,261.3
$Q_{w/d=10\%}$ (kN)	Upper: 17,619.7; lower: 14,402.5
$Q_{C\text{-}K}$ (kN)	Upper: 17,636.7; lower: 15,151.5

Pile ID: CRB-C 4

Load-displacement data

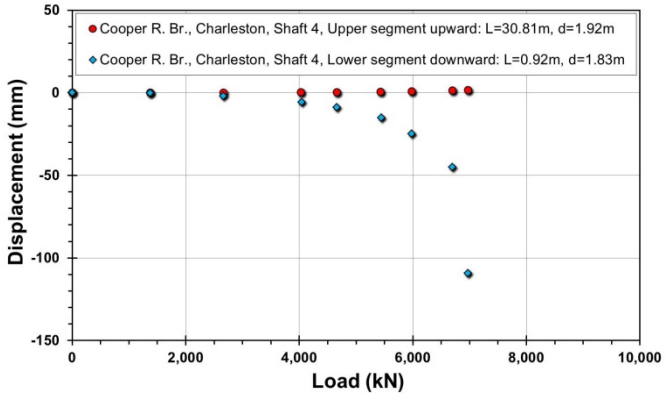

Back-analyzed normalized operational stiffness vs. pseudo-strain

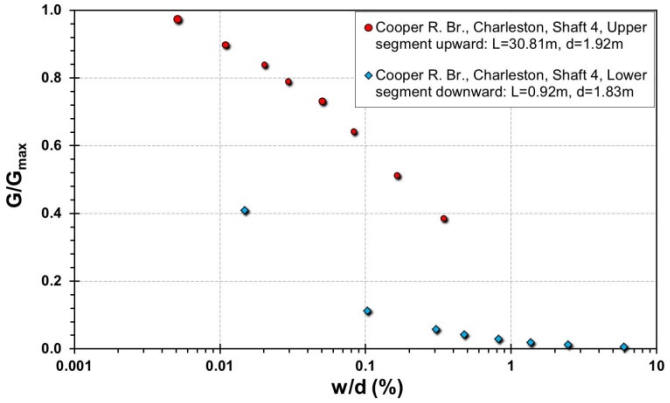

Detail	Description
Pile type/material	Drilled shaft
Length, L (m)	Upper: 30.81; lower: 0.92
Diameter, d (m)	Upper: 1.92; lower: 1.83
Installation method	Bored cast in-situ
Loading mode	O-cell compression
$Q_{max\text{-}measured}$ (kN)	Upper: 6,969.3; lower: 6,969.3
Q_s (kN)	Upper: 6,969.3; lower: 609.3
Q_b (kN)	6,360.0
$Q_{Davisson}$ (kN)	Upper: 7,442.4; lower: 5,979.5
$Q_{w/d=10\%}$ (kN)	Upper: 8,353.4; lower: 7,111.4
$Q_{C\text{-}K}$ (kN)	Upper: 8,368.2; lower: 7,299.3

Site ID No. 12

Cone penetrometer data	CPT SBT soil classification index, I_c	Detail	Description
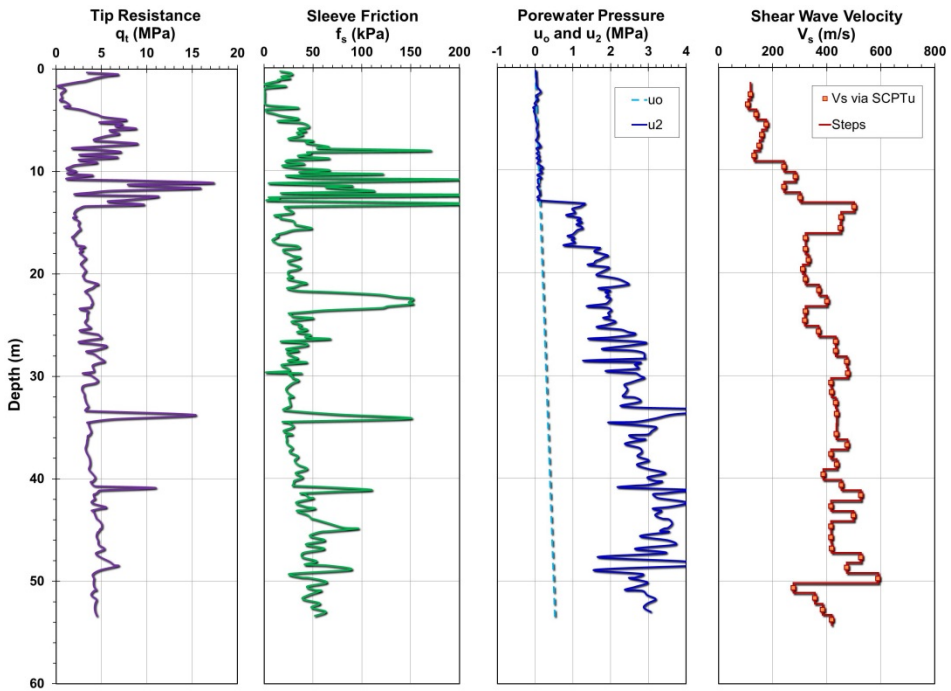	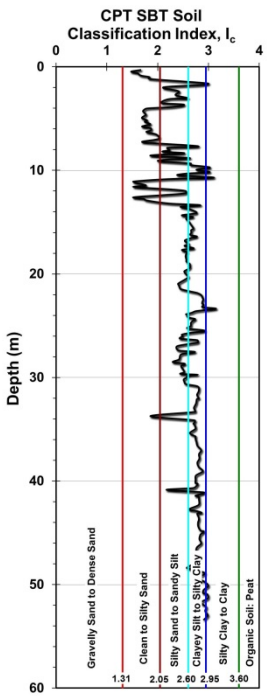	Site name and location	Cooper River Bridge on HW 17, Mount Pleasant site, SC, USA
		Soil type(s)	14 m of clayey sand and sandy clay over stiff calcareous Cooper Marl (sandy clay)
		Pile type(s)	Drilled shaft
		Type of cone penetrometer testing	SCPTu
		Source of V_s evaluation	SCPTu
		Number of pile load tests	4
		Reference	Ahren et al. (2000c, d); Ahren & Simpson (2000 a, b); Camp (2004); Camp et al. (2002)
		Comments	

Pile ID: CRB-MP 1

Load-displacement data

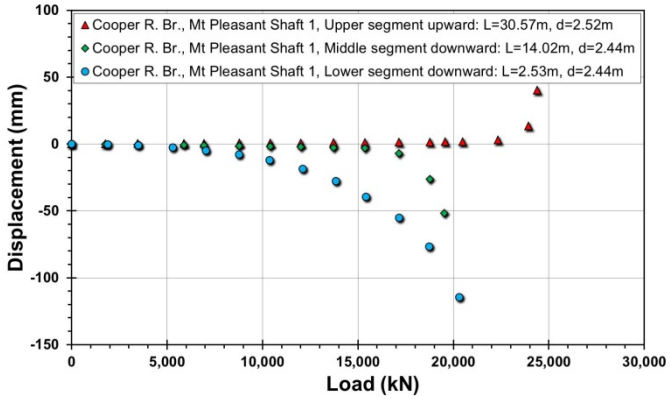

Back-analyzed normalized operational stiffness vs. pseudo-strain

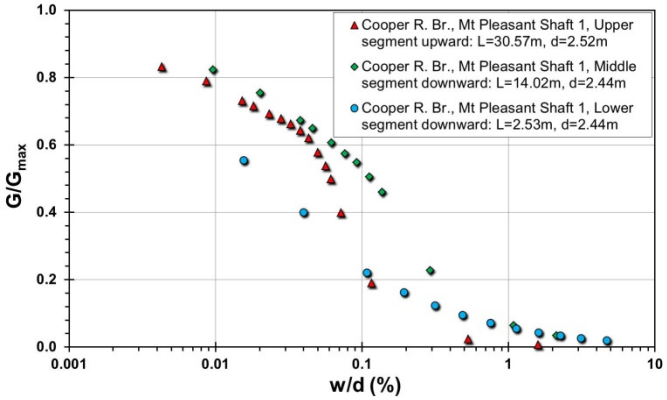

Detail	Description
Pile type/material	Drilled shaft
Length, L (m)	Upper: 30.57; middle: 14.02; lower: 2.53
Diameter, d (m)	Upper: 2.52; middle: 2.44; lower: 2.44
Installation method	Bored cast in-situ
Loading mode	O-cell compression
$Q_{max\text{-}measured}$ (kN)	Upper: 24,393.7; middle: 19,538.1; lower: 20,297.1
Q_s (kN)	Upper: 24,393.7; middle: 19,538.1; lower: 3,547.1
Q_b (kN)	16,750.0
$Q_{Davisson}$ (kN)	Upper: 23,939.2; middle: 18,767.3; lower: 15,415.0
$Q_{w/d=10\%}$ (kN)	Upper: 24,536.8; middle: 19,903.7; lower: 21,903.6
$Q_{C\text{-}K}$ (kN)	Upper: 24,570.0; middle: 20,005.4; lower: 23,809.5

Pile ID: CRB-MP 2

Load-displacement data

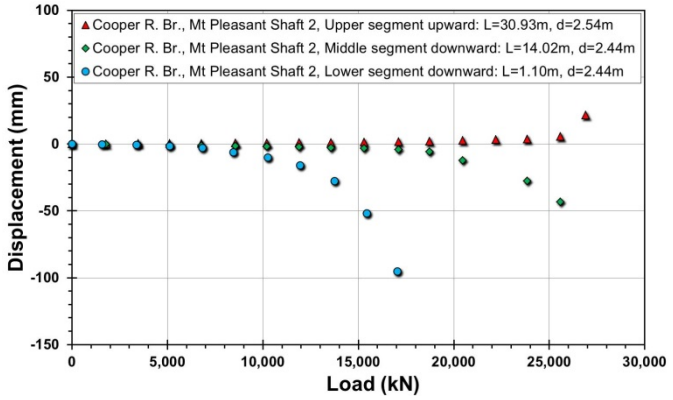

Back-analyzed normalized operational stiffness vs. pseudo-strain

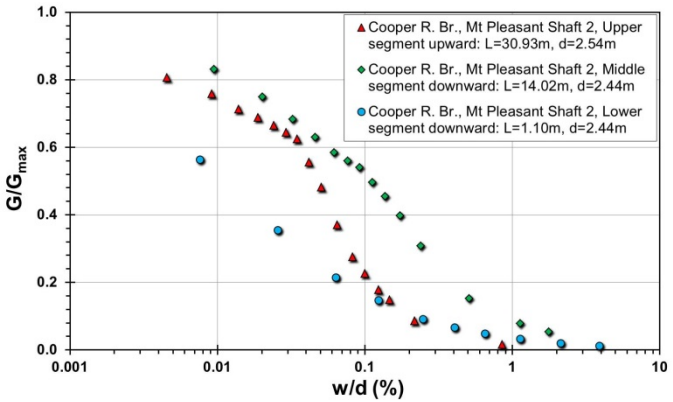

Detail	Description
Pile type/material	Drilled shaft
Length, L (m)	Upper: 30.93; middle: 14.02; lower: 1.10
Diameter, d (m)	Upper: 2.52; middle: 2.44; lower: 2.44
Installation method	Bored cast in-situ
Loading mode	O-cell compression
$Q_{max\text{-}measured}$ (kN)	Upper: 26,898.5; middle: 25,588.3; lower: 17,046.9
Q_s (kN)	Upper: 26,898.5; middle: 25,588.3; lower: 1,776.9
Q_b (kN)	15,270.0
$Q_{Davisson}$ (kN)	Upper: 26,898.5; middle: 25,588.3; lower: 17,046.9
$Q_{w/d=10\%}$ (kN)	Upper: 27,633.3; middle: 27,994.0; lower: 18,133.9
$Q_{C\text{-}K}$ (kN)	Upper: 27,700.8; middle: 28,571.4; lower: 18,867.9

Pile ID: CRB-MP 3

Load-displacement data

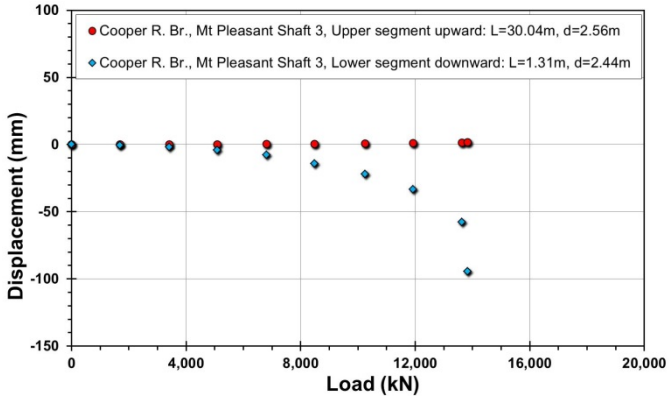

Back-analyzed normalized operational stiffness vs. pseudo-strain

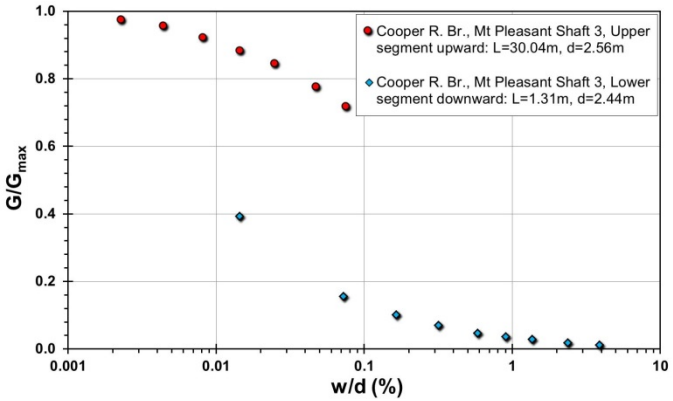

Detail	Description
Pile type/material	Drilled shaft
Length, L (m)	Upper: 30.04; lower: 1.31
Diameter, d (m)	Upper: 2.56; lower: 2.44
Installation method	Bored cast in-situ
Loading mode	O-cell compression
$Q_{max\text{-}measured}$ (kN)	Upper: 13,834.6; lower: 13,834.6
Q_s (kN)	Upper: 13,834.6; lower: 1,674.6
Q_b (kN)	12,160.0
$Q_{Davisson}$ (kN)	Upper: 15,224.4; lower: 12,927.1
$Q_{w/d=10\%}$ (kN)	Upper: 20,380.8; lower: 16,949.1
$Q_{C\text{-}K}$ (kN)	Upper: 20,474.2; lower: 17,084.5

Pile ID: CRB-MP 4

Load-displacement data

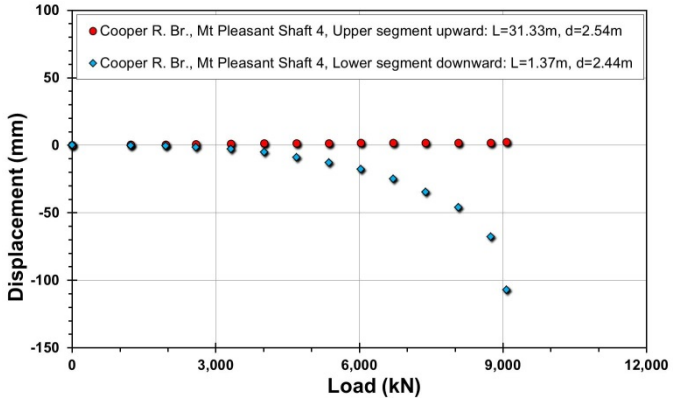

Back-analyzed normalized operational stiffness vs. pseudo-strain

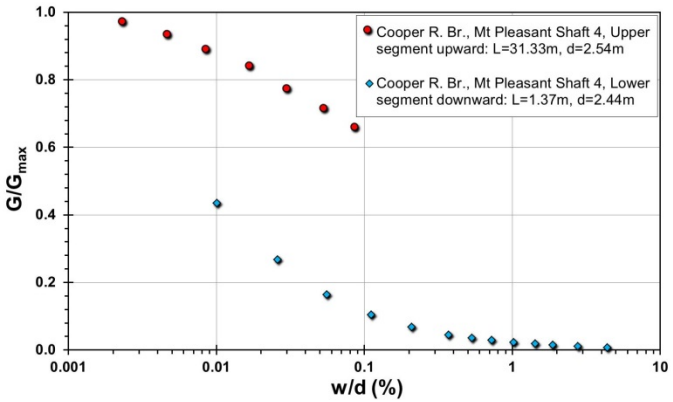

Detail	Description
Pile type/material	Drilled shaft
Length, L (m)	Upper: 31.33; lower: 1.37
Diameter, d (m)	Upper: 2.54; lower: 2.44
Installation method	Bored cast in-situ
Loading mode	O-cell compression
$Q_{max\text{-}measured}$ (kN)	Upper: 9,072.4; lower: 9,072.4
Q_s (kN)	Upper: 9,072.4; lower: 1,092.4
Q_b (kN)	7,980.0
$Q_{Davisson}$ (kN)	Upper: 13,072.2; lower: 8,381.6
$Q_{w/d=10\%}$ (kN)	Upper: 18,689.8; lower: 10,709.1
$Q_{C\text{-}K}$ (kN)	Upper: 18,809.5; lower: 10,204.1

Site ID No. 13

Cone penetrometer data	CPT SBT soil classification index, I_c	Detail	Description
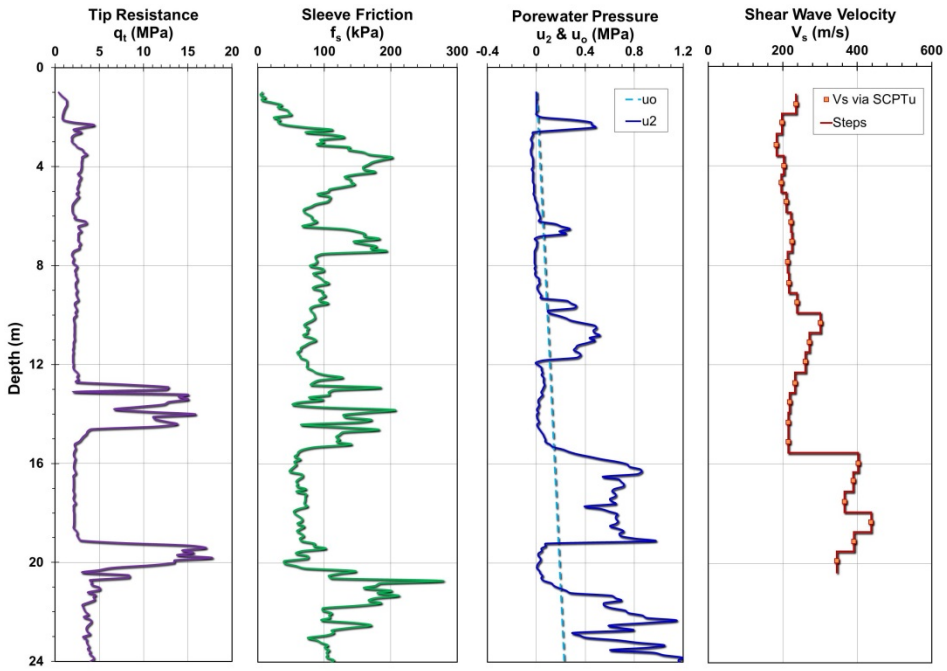	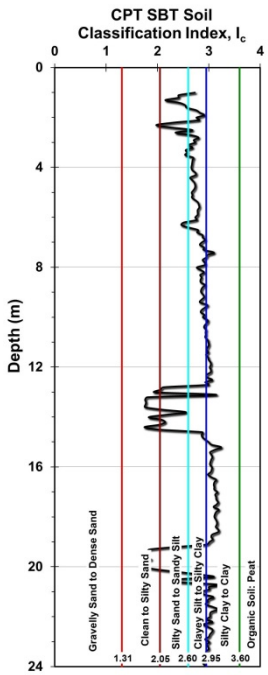	Site name and location	Cowden, Northeast England, UK
		Soil type(s)	Stiff stony clay till
		Pile type(s)	Closed-ended steel pipe piles (ICP)
		Type of cone penetrometer testing	SCPTu
		Source of V_s evaluation	SCPTu
		Number of pile load tests	6
		Reference	Powell and Butcher (2003), Lehane (1992), Lehane and Jardine (1994)
		Comments	

Pile ID: CW 1/L1T

Load-displacement data

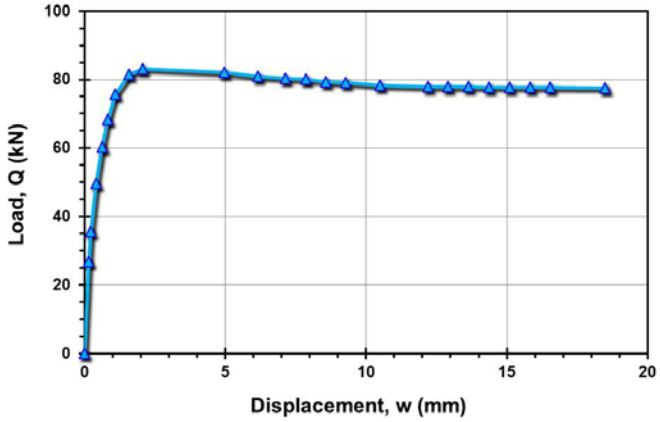

Back-analyzed normalized operational stiffness vs. pseudo-strain

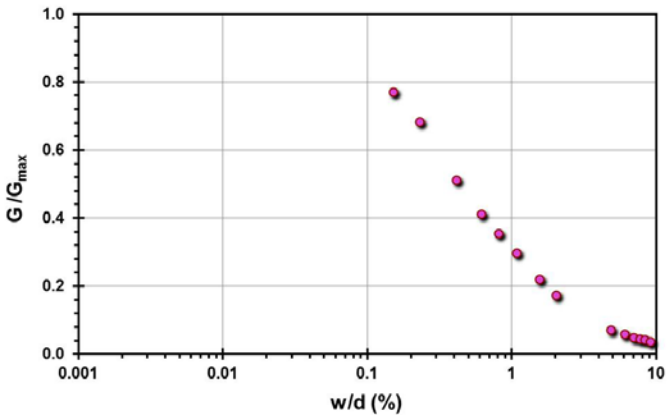

Detail	Description
Pile type/material	Closed-ended steel pipe pile (ICP)
Length, L (m)	3.00
Diameter, d (m)	0.102
Installation method	Jacked
Loading mode	Tension
$Q_{max\text{-}measured}$ (kN)	83.54
Q_s (kN)	83.54
Q_b (kN)	-
$Q_{Davisson}$ (kN)	83.19
$Q_{w/d=10\%}$ (kN)	81.11
$Q_{C\text{-}K}$ (kN)	75.54

Pile ID: CW 2/L1C

Load-displacement data

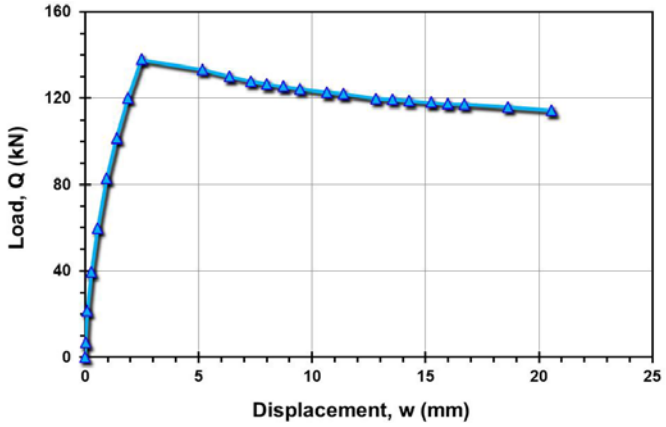

Back-analyzed normalized operational stiffness vs. pseudo-strain

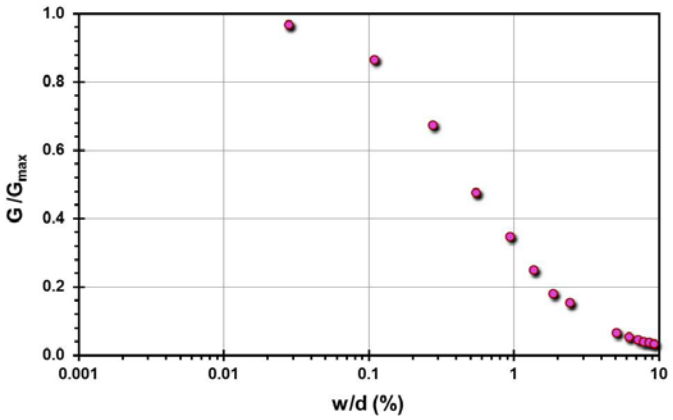

Detail	Description
Pile type/material	Closed-ended steel pipe pile (ICP)
Length, L (m)	3.66
Diameter, d (m)	0.102
Installation method	Jacked
Loading mode	Compression
$Q_{max\text{-}measured}$ (kN)	138.42
Q_s (kN)	123.26
Q_b (kN)	15.16
$Q_{Davisson}$ (kN)	133.01
$Q_{w/d=10\%}$ (kN)	126.48
$Q_{C\text{-}K}$ (kN)	-

Pile ID: CW 2/L3C

Load-displacement data

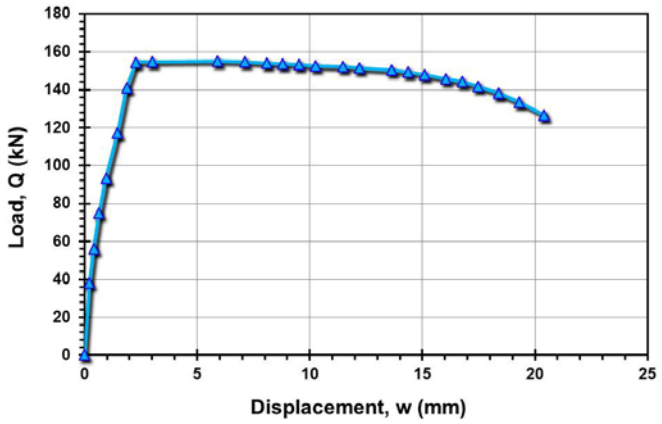

Back-analyzed normalized operational stiffness vs. pseudo-strain

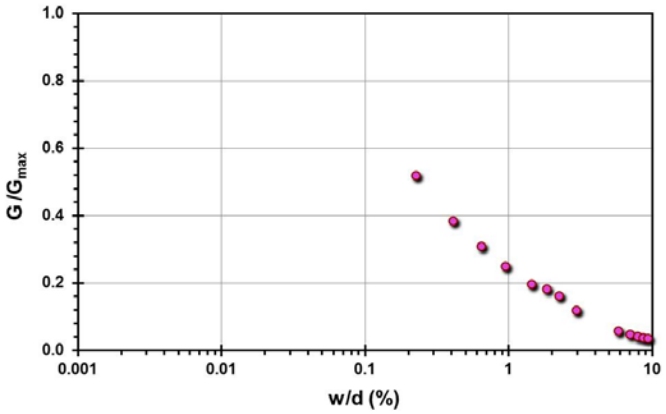

Detail	Description
Pile type/material	Closed-ended steel pipe pile (ICP)
Length, L (m)	3.66
Diameter, d (m)	0.102
Installation method	Jacked
Loading mode	Compression
$Q_{max\text{-}measured}$ (kN)	153.50
Q_s (kN)	134.29
Q_b (kN)	19.21
$Q_{Davisson}$ (kN)	151.12
$Q_{w/d=10\%}$ (kN)	148.38
$Q_{C\text{-}K}$ (kN)	-

Pile ID: CW 3/L1T

Load-displacement data

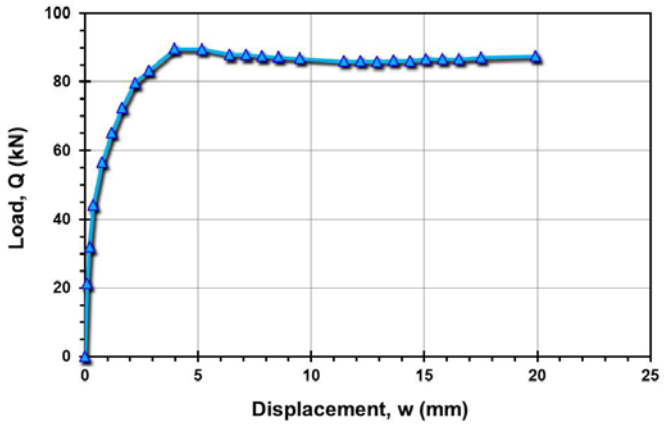

Back-analyzed normalized operational stiffness vs. pseudo-strain

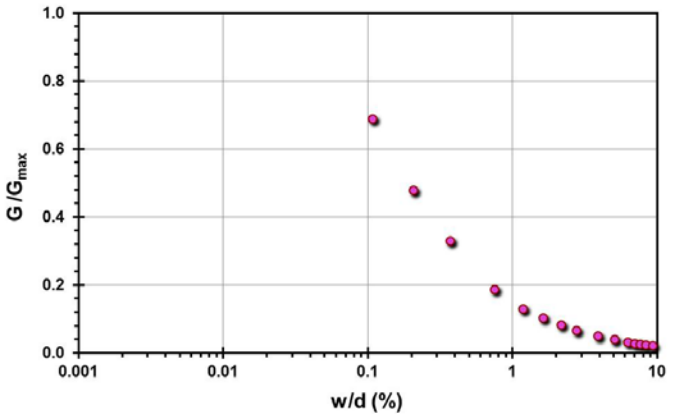

Detail	Description
Pile type/material	Closed-ended steel pipe pile (ICP)
Length, L (m)	3.88
Diameter, d (m)	0.102
Installation method	Jacked
Loading mode	Tension
$Q_{max\text{-}measured}$ (kN)	87.57
Q_s (kN)	87.57
Q_b (kN)	-
$Q_{Davisson}$ (kN)	89.70
$Q_{w/d=10\%}$ (kN)	88.29
$Q_{C\text{-}K}$ (kN)	90.37

Pile ID: CW 4/L1C

Load-displacement data

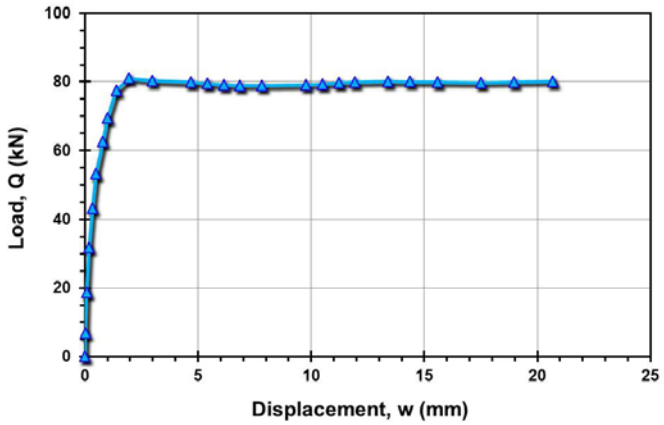

Back-analyzed normalized operational stiffness vs. pseudo-strain

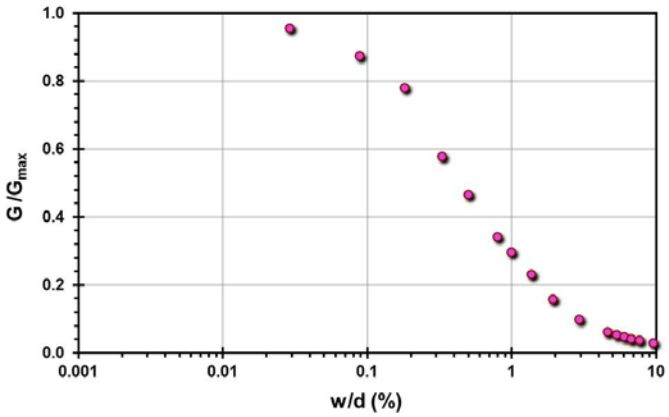

Detail	Description
Pile type/material	Closed-ended steel pipe pile (ICP)
Length, L (m)	3.51
Diameter, d (m)	0.102
Installation method	Jacked
Loading mode	Compression
$Q_{max\text{-}measured}$ (kN)	80.13
Q_s (kN)	67.64
Q_b (kN)	12.49
$Q_{Davisson}$ (kN)	81.00
$Q_{w/d=10\%}$ (kN)	79.54
$Q_{C\text{-}K}$ (kN)	80.73

Pile ID: CW 4s/L1C

Load-displacement data

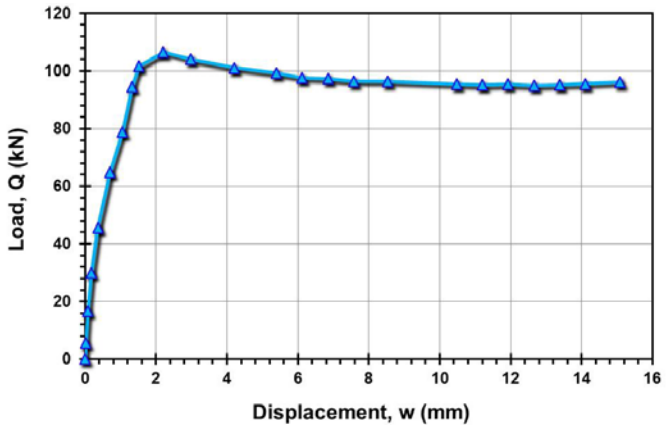

Back-analyzed normalized operational stiffness vs. pseudo-strain

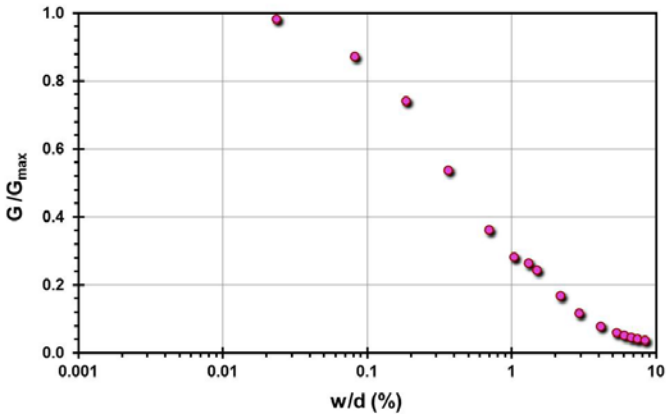

Detail	Description
Pile type/material	Closed-ended steel pipe pile (ICP)
Length, L (m)	3.92
Diameter, d (m)	0.102
Installation method	Jacked
Loading mode	Compression
$Q_{max\text{-}measured}$ (kN)	96.13
Q_s (kN)	81.46
Q_b (kN)	14.67
$Q_{Davisson}$ (kN)	114.54
$Q_{w/d=10\%}$ (kN)	102.52
$Q_{C\text{-}K}$ (kN)	119.50

Site ID No. 14

Cone penetrometer data	CPT SBT soil classification index, I_c	Detail	Description
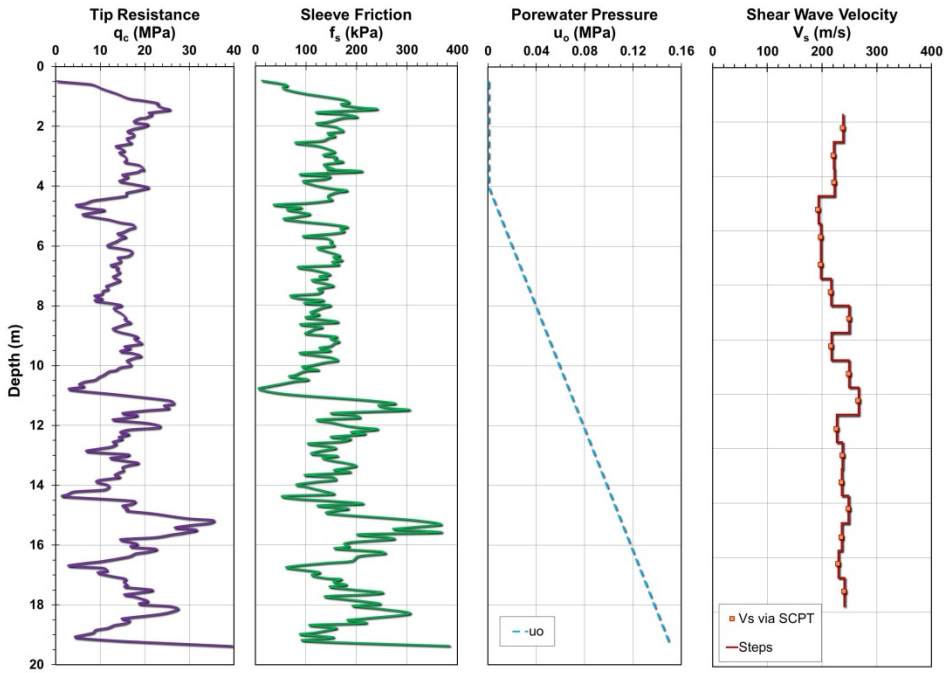	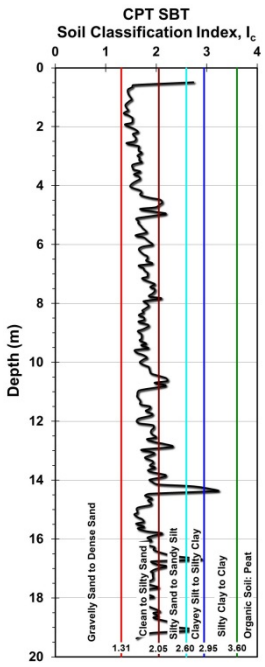	Site name and location	Dunkirk, Northern Coast of France
		Soil type(s)	Dense to very dense sand
		Pile type(s)	10 open-ended steel pipe piles and 12 closed-ended steel pipe piles (ICP)
		Type of cone penetrometer testing	SCPT
		Source of V_s evaluation	SCPT
		Number of pile load tests	22
		Reference	Chow (1996)
		Comments	u_2 reading not available. In sands, assumed to be hydrostatic for this case.

Pile ID: DK 1/L1C

Load-displacement data

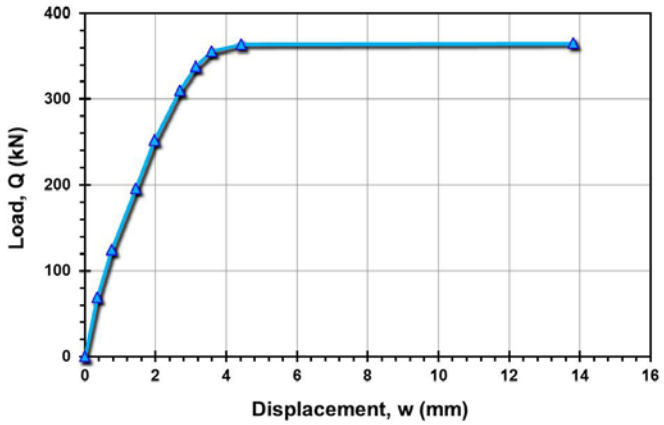

Back-analyzed normalized operational stiffness vs. pseudo-strain

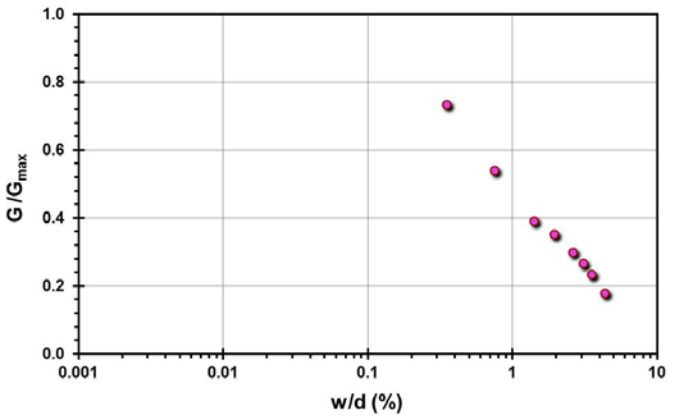

Detail	Description
Pile type/material	Closed-ended steel pipe pile (ICP)
Length, L (m)	7.40
Diameter, d (m)	0.102
Installation method	Jacked
Loading mode	Compression
$Q_{max\text{-}measured}$ (kN)	364.92
Q_s (kN)	273.31
Q_b (kN)	91.61
$Q_{Davisson}$ (kN)	364.92
$Q_{w/d=10\%}$ (kN)	363.21
$Q_{C\text{-}K}$ (kN)	374.11

Pile ID: DK 1/L2T

Load-displacement data

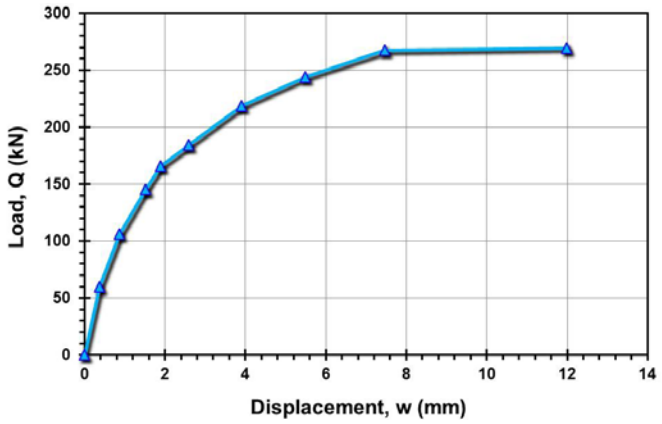

Back-analyzed normalized operational stiffness vs. pseudo-strain

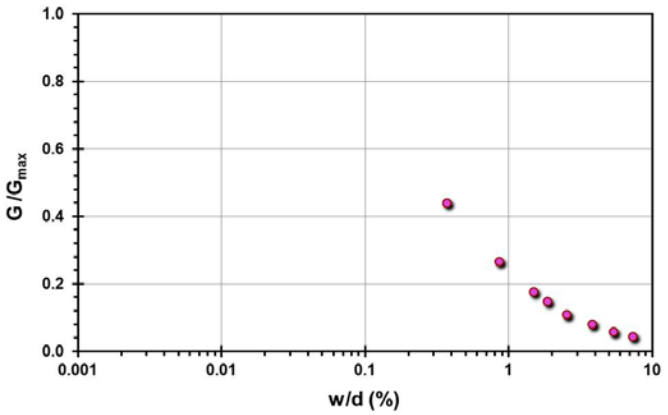

Detail	Description
Pile type/material	Closed-ended steel pipe pile (ICP)
Length, L (m)	7.40
Diameter, d (m)	0.102
Installation method	Jacked
Loading mode	Tension
$Q_{max\text{-}measured}$ (kN)	269.37
Q_s (kN)	269.37
Q_b (kN)	-
$Q_{Davisson}$ (kN)	269.37
$Q_{w/d=10\%}$ (kN)	267.81
$Q_{C\text{-}K}$ (kN)	309.31

Pile ID: DK 1/L3T

Load-displacement data

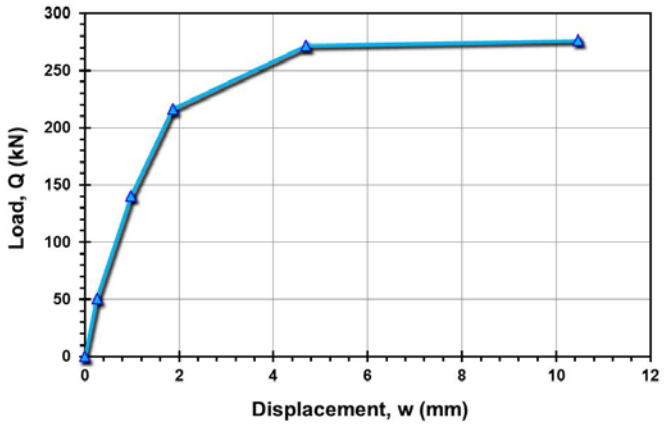

Back-analyzed normalized operational stiffness vs. pseudo-strain

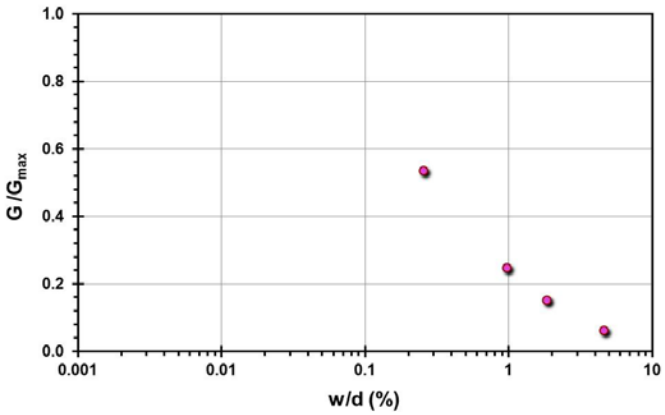

Detail	Description
Pile type/material	Closed-ended steel pipe pile (ICP)
Length, L (m)	7.40
Diameter, d (m)	0.102
Installation method	Jacked
Loading mode	Tension
$Q_{max\text{-}measured}$ (kN)	276.27
Q_s (kN)	276.27
Q_b (kN)	-
$Q_{Davisson}$ (kN)	276.27
$Q_{w/d=10\%}$ (kN)	277.27
$Q_{C\text{-}K}$ (kN)	291.80

Pile ID: DK 2/L1C

Load-displacement data

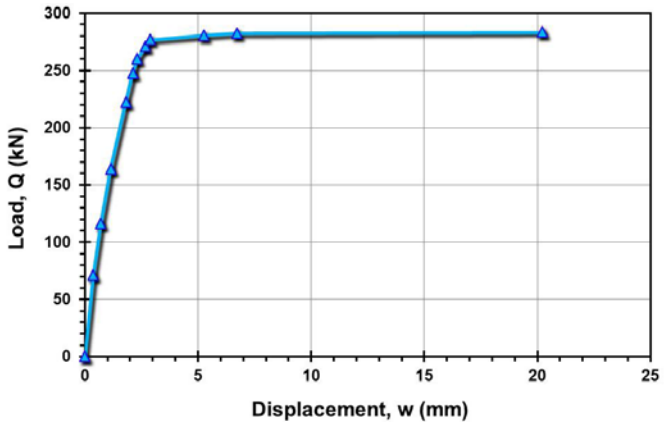

Back-analyzed normalized operational stiffness vs. pseudo-strain

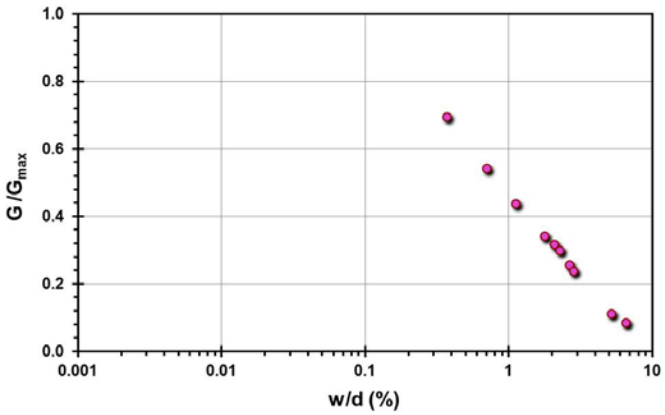

Detail	Description
Pile type/material	Closed-ended steel pipe pile (ICP)
Length, L (m)	5.96
Diameter, d (m)	0.102
Installation method	Jacked
Loading mode	Compression
$Q_{max\text{-}measured}$ (kN)	283.38
Q_s (kN)	199.84
Q_b (kN)	78.64
$Q_{Davisson}$ (kN)	283.38
$Q_{w/d=10\%}$ (kN)	282.26
$Q_{C\text{-}K}$ (kN)	284.82

Pile ID: DK 2/L2C

Load-displacement data

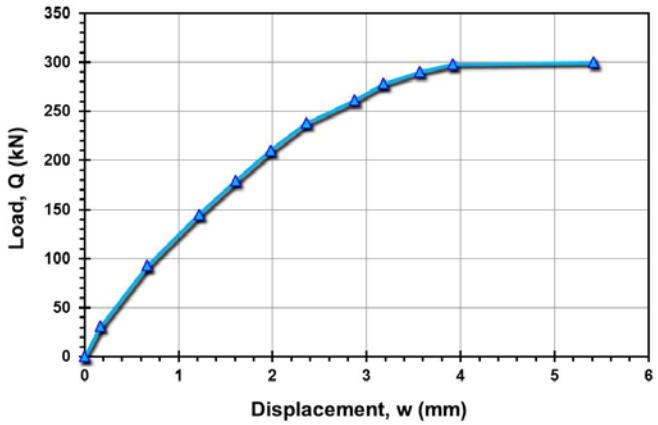

Back-analyzed normalized operational stiffness vs. pseudo-strain

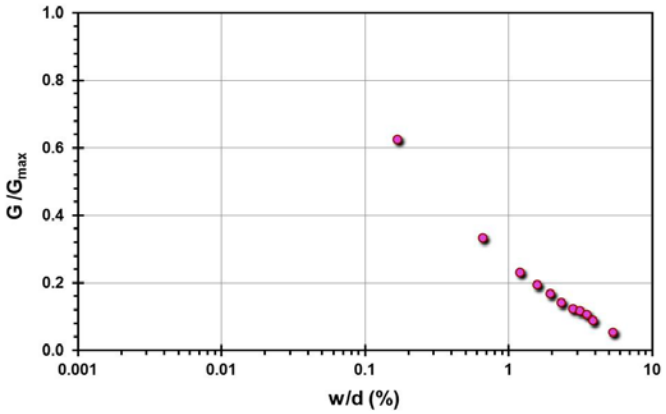

Detail	Description
Pile type/material	Closed-ended steel pipe pile (ICP)
Length, L (m)	5.96
Diameter, d (m)	0.102
Installation method	Jacked
Loading mode	Compression
$Q_{max\text{-}measured}$ (kN)	299.79
Q_s (kN)	254.39
Q_b (kN)	45.40
$Q_{Davisson}$ (kN)	299.79
$Q_{w/d=10\%}$ (kN)	307.06
$Q_{C\text{-}K}$ (kN)	314.96

Pile ID: DK 2/L3T

Load-displacement data

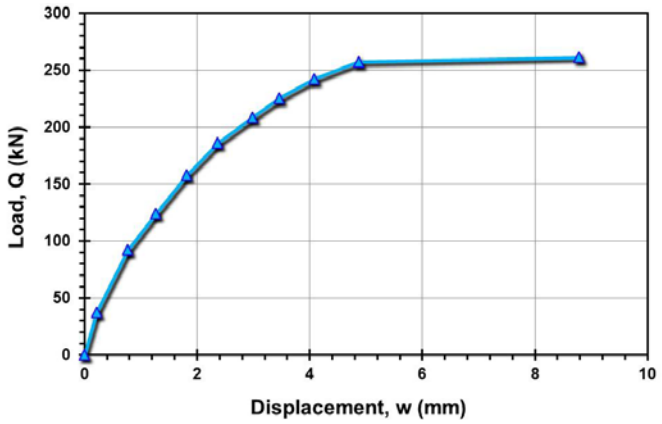

Back-analyzed normalized operational stiffness vs. pseudo-strain

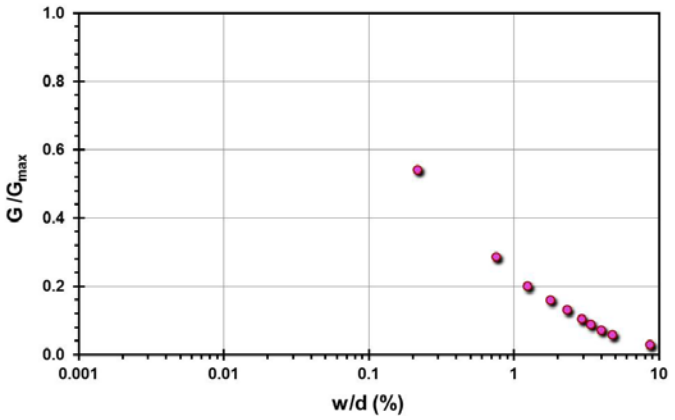

Detail	Description
Pile type/material	Closed-ended steel pipe pile (ICP)
Length, L (m)	5.96
Diameter, d (m)	0.102
Installation method	Jacked
Loading mode	Tension
$Q_{max\text{-}measured}$ (kN)	261.30
Q_s (kN)	261.30
Q_b (kN)	-
$Q_{Davisson}$ (kN)	261.30
$Q_{w/d=10\%}$ (kN)	263.88
$Q_{C\text{-}K}$ (kN)	275.86

Pile ID: DK 2/L4C

Load-displacement data

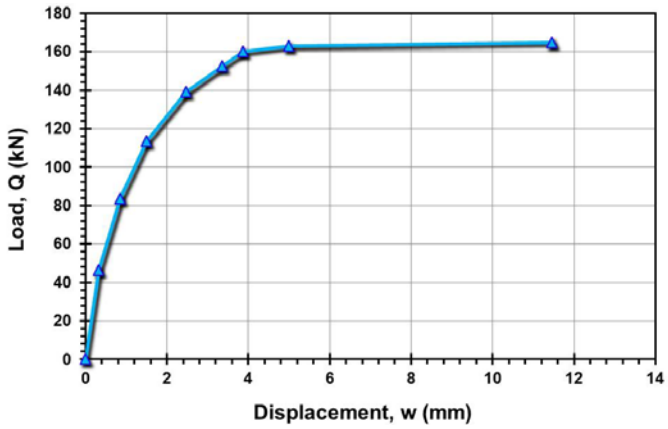

Back-analyzed normalized operational stiffness vs. pseudo-strain

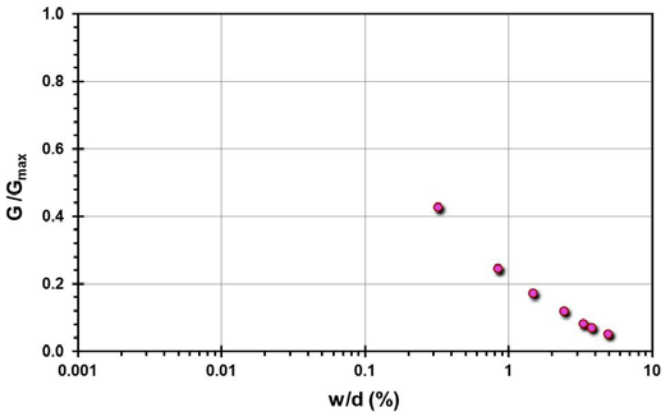

Detail	Description
Pile type/material	Closed-ended steel pipe pile (ICP)
Length, L (m)	5.96
Diameter, d (m)	0.102
Installation method	Jacked
Loading mode	Compression
$Q_{max\text{-}measured}$ (kN)	164.89
Q_s (kN)	144.62
Q_b (kN)	20.27
$Q_{Davisson}$ (kN)	163.03
$Q_{w/d=10\%}$ (kN)	164.70
$Q_{C\text{-}K}$ (kN)	168.89

Pile ID: DK 3/L1T

Load-displacement data

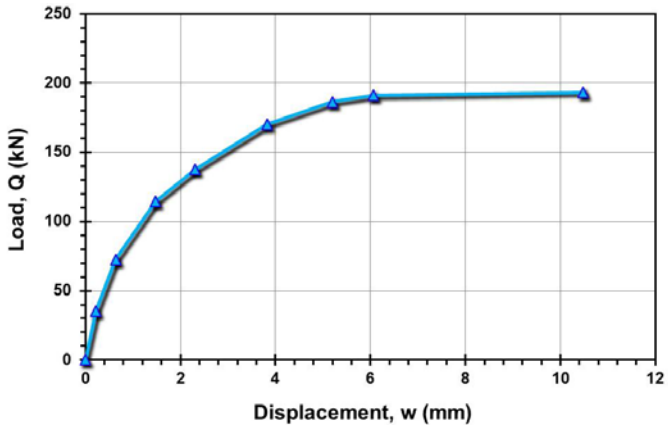

Back-analyzed normalized operational stiffness vs. pseudo-strain

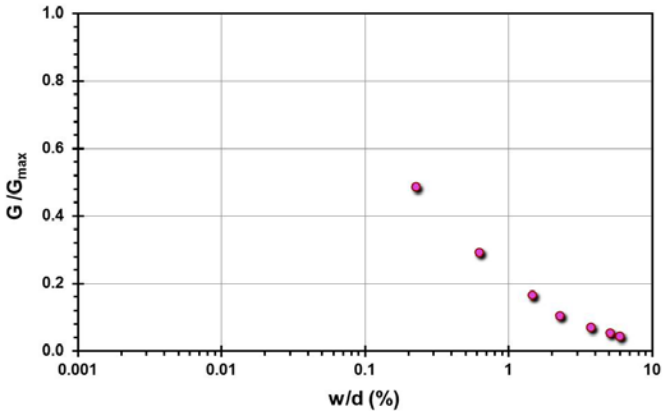

Detail	Description
Pile type/material	Closed-ended steel pipe pile (ICP)
Length, L (m)	7.40
Diameter, d (m)	0.102
Installation method	Jacked
Loading mode	Tension
$Q_{max\text{-}measured}$ (kN)	193.37
Q_s (kN)	193.37
Q_b (kN)	-
$Q_{Davisson}$ (kN)	191.04
$Q_{w/d=10\%}$ (kN)	194.25
$Q_{C\text{-}K}$ (kN)	206.70

Pile ID: DK 3/L2C

Load-displacement data

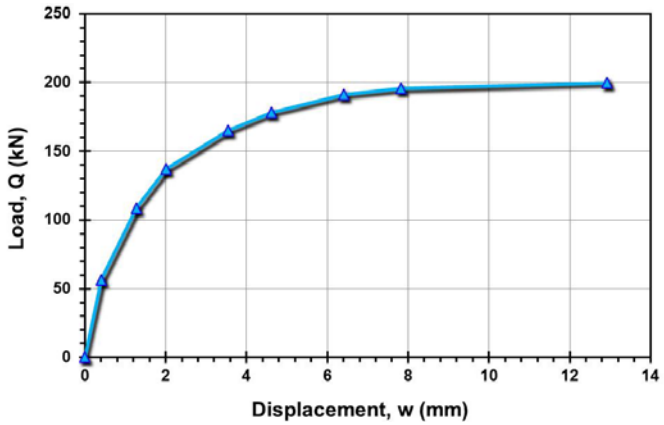

Back-analyzed normalized operational stiffness vs. pseudo-strain

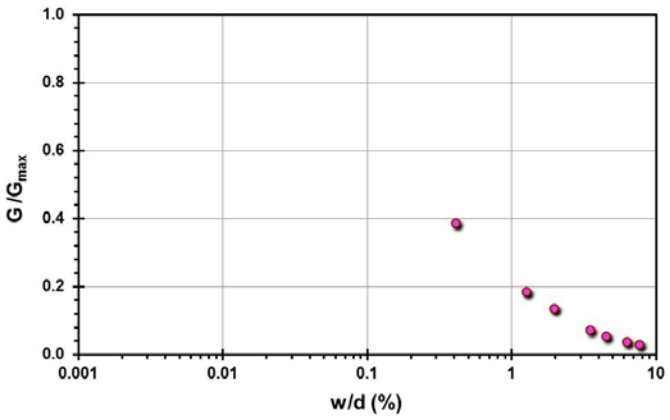

Detail	Description
Pile type/material	Closed-ended steel pipe pile (ICP)
Length, L (m)	7.40
Diameter, d (m)	0.102
Installation method	Jacked
Loading mode	Compression
$Q_{max\text{-}measured}$ (kN)	199.86
Q_s (kN)	149.59
Q_b (kN)	50.27
$Q_{Davisson}$ (kN)	195.52
$Q_{w/d=10\%}$ (kN)	197.39
$Q_{C\text{-}K}$ (kN)	212.90

Pile ID: DK 3/L4C

Load-displacement data

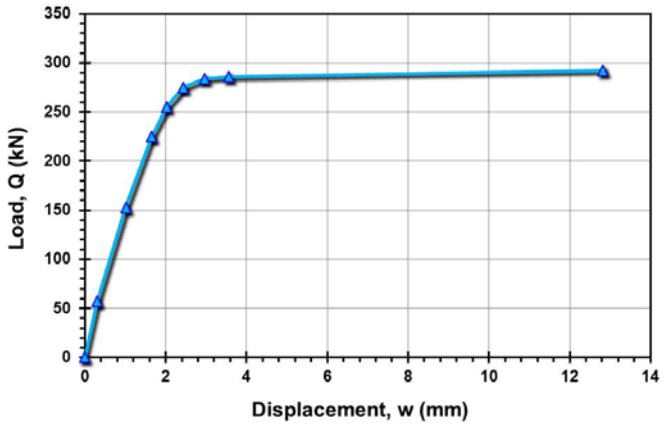

Back-analyzed normalized operational stiffness vs. pseudo-strain

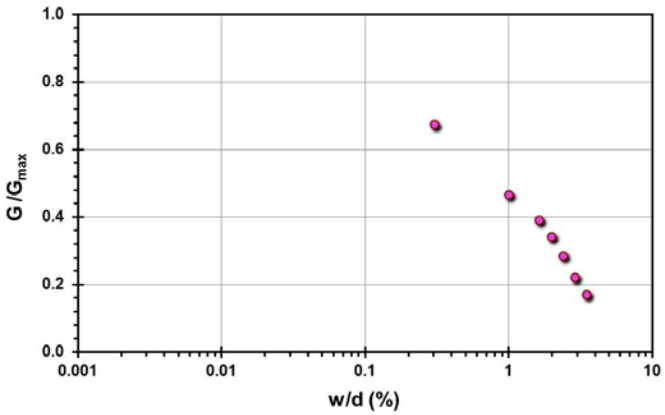

Detail	Description
Pile type/material	Closed-ended steel pipe pile (ICP)
Length, L (m)	7.54
Diameter, d (m)	0.102
Installation method	Jacked
Loading mode	Compression
$Q_{max\text{-}measured}$ (kN)	292.41
Q_s (kN)	222.69
Q_b (kN)	69.72
$Q_{Davisson}$ (kN)	289.14
$Q_{w/d=10\%}$ (kN)	291.63
$Q_{C\text{-}K}$ (kN)	295.86

Pile ID: DK 3/L5C

Load-displacement data

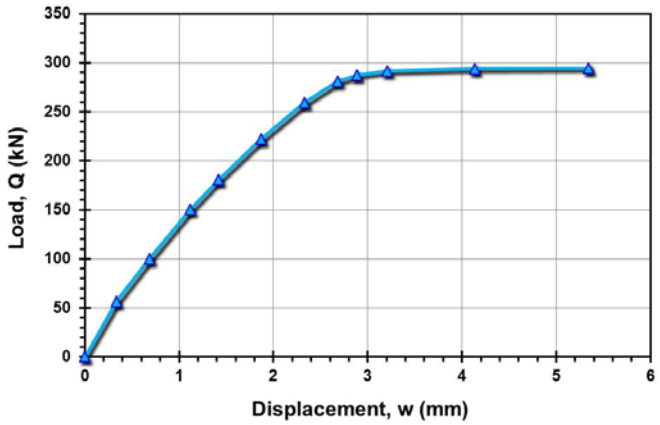

Back-analyzed normalized operational stiffness vs. pseudo-strain

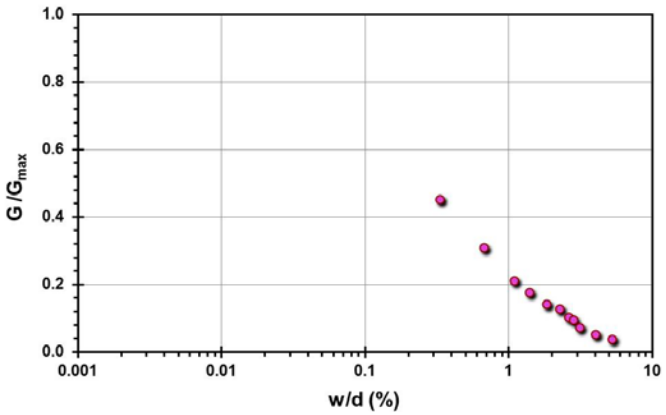

Detail	Description
Pile type/material	Closed-ended steel pipe pile (ICP)
Length, L (m)	7.54
Diameter, d (m)	0.102
Installation method	Jacked
Loading mode	Compression
$Q_{max\text{-}measured}$ (kN)	294.55
Q_s (kN)	224.83
Q_b (kN)	69.72
$Q_{Davisson}$ (kN)	298.34
$Q_{w/d=10\%}$ (kN)	298.34
$Q_{C\text{-}K}$ (kN)	302.11

Pile ID: DK 3/L6T

Load-displacement data

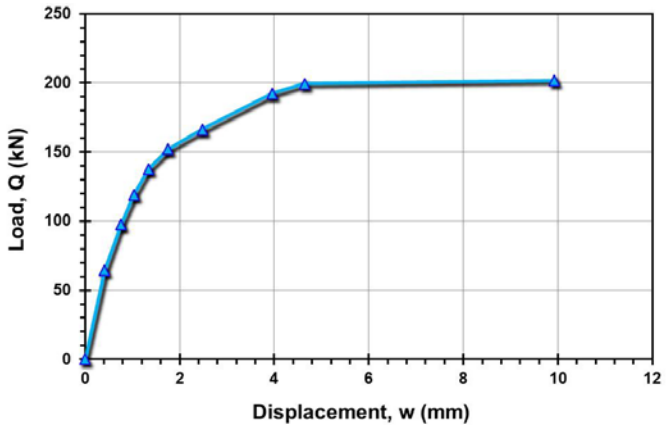

Back-analyzed normalized operational stiffness vs. pseudo-strain

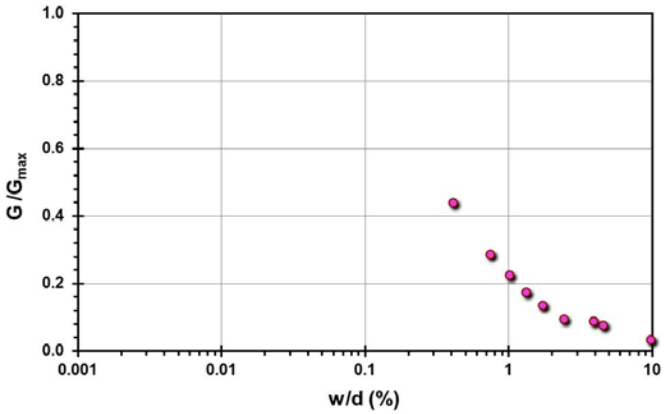

Detail	Description
Pile type/material	Closed-ended steel pipe pile (ICP)
Length, L (m)	7.54
Diameter, d (m)	0.102
Installation method	Jacked
Loading mode	Tension
$Q_{max\text{-}measured}$ (kN)	201.77
Q_s (kN)	201.77
Q_b (kN)	-
$Q_{Davisson}$ (kN)	200.59
$Q_{w/d=10\%}$ (kN)	202.06
$Q_{C\text{-}K}$ (kN)	206.83

Pile ID: DK CS'T89a

Load-displacement data

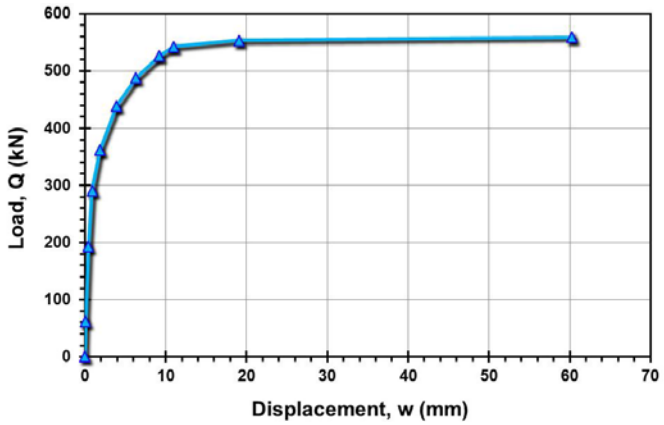

Back-analyzed normalized operational stiffness vs. pseudo-strain

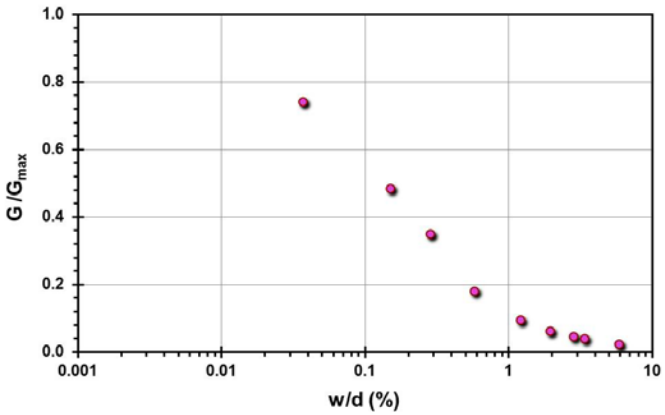

Detail	Description
Pile type/material	Open-ended steel pipe pile
Length, L (m)	11.30
Diameter, d (m)	0.324
Installation method	Driven
Loading mode	Tension
$Q_{max\text{-}measured}$ (kN)	558.77
Q_s (kN)	558.77
Q_b (kN)	-
$Q_{Davisson}$ (kN)	556.03
$Q_{w/d=10\%}$ (kN)	553.74
$Q_{C\text{-}K}$ (kN)	567.54

Pile ID: DK CS'T89b

Load-displacement data

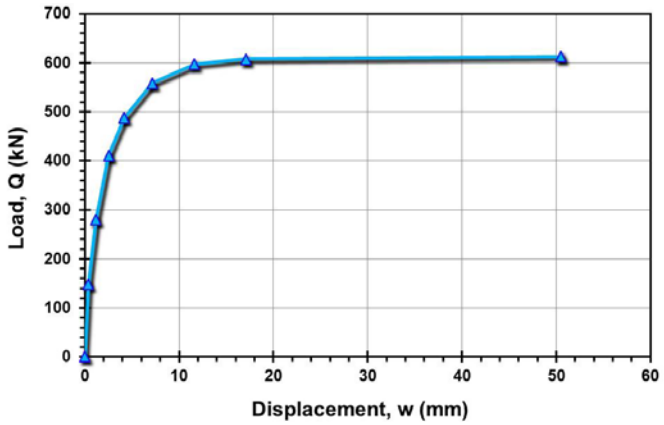

Back-analyzed normalized operational stiffness vs. pseudo-strain

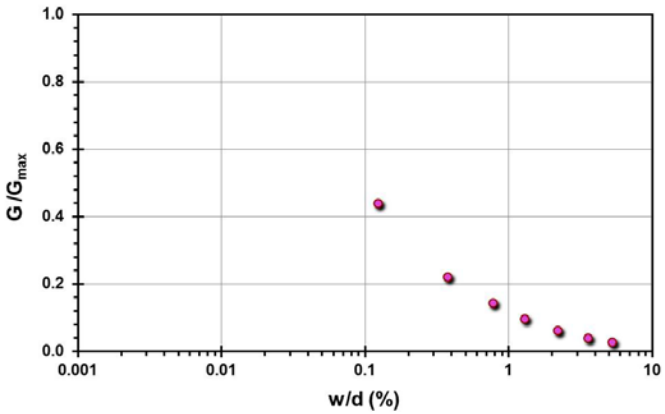

Detail	Description
Pile type/material	Open-ended steel pipe pile
Length, L (m)	11.60
Diameter, d (m)	0.324
Installation method	Driven
Loading mode	Tension
$Q_{max\text{-}measured}$ (kN)	612.92
Q_s (kN)	612.92
Q_b (kN)	-
$Q_{Davisson}$ (kN)	577.38
$Q_{w/d=10\%}$ (kN)	609.33
$Q_{C\text{-}K}$ (kN)	624.22

Pile ID: DK CS'C89a

Load-displacement data

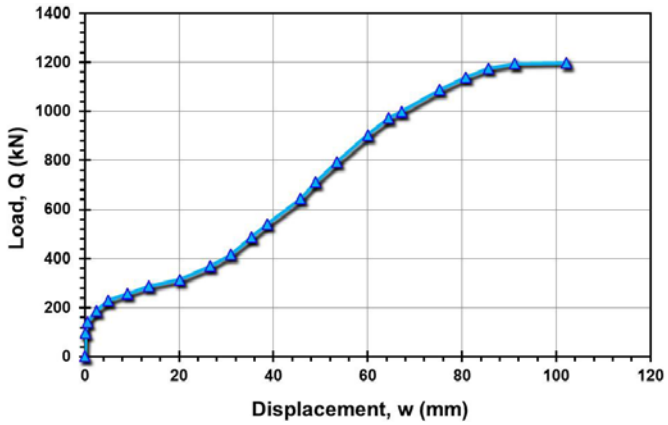

Back-analyzed normalized operational stiffness vs. pseudo-strain

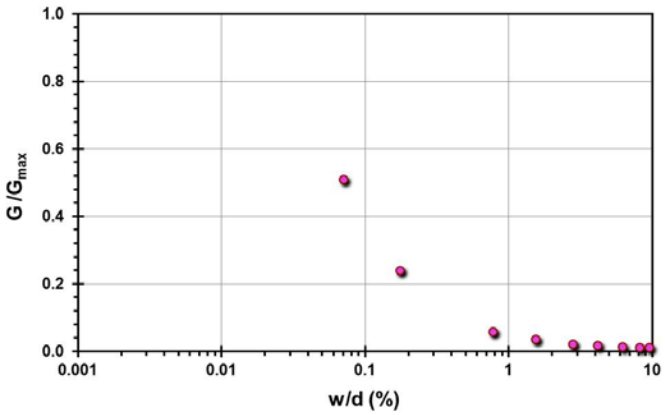

Detail	Description
Pile type/material	Open-ended steel pipe pile
Length, L (m)	11.30
Diameter, d (m)	0.324
Installation method	Driven
Loading mode	Compression
$Q_{max\text{-}measured}$ (kN)	1,198.09
Q_s (kN)	637.44
Q_b (kN)	560.65
$Q_{Davisson}$ (kN)	-
$Q_{w/d=10\%}$ (kN)	-
$Q_{C\text{-}K}$ (kN)	-

Pile ID: DK CS'C89b

Load-displacement data

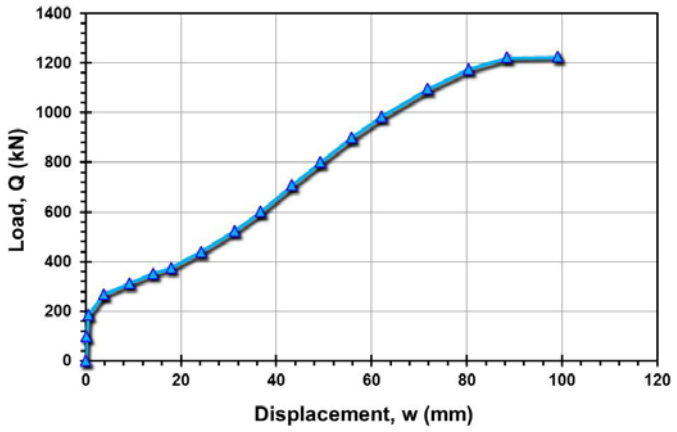

Back-analyzed normalized operational stiffness vs. pseudo-strain

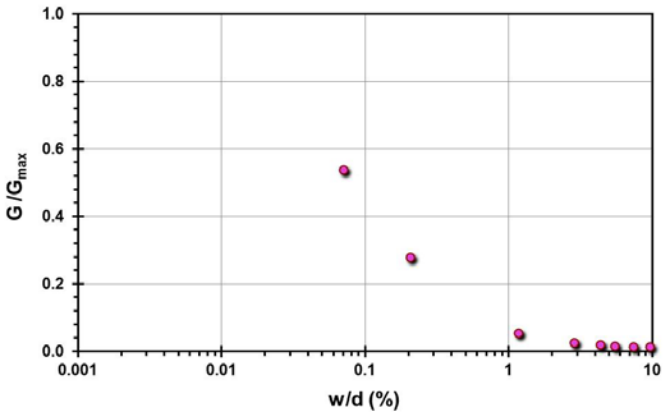

Detail	Description
Pile type/material	Open-ended steel pipe pile
Length, L (m)	11.60
Diameter, d (m)	0.324
Installation method	Driven
Loading mode	Compression
$Q_{max\text{-}measured}$ (kN)	1,224.88
Q_s (kN)	579.31
Q_b (kN)	645.57
$Q_{Davisson}$ (kN)	-
$Q_{w/d=10\%}$ (kN)	-
$Q_{C\text{-}K}$ (kN)	-

Pile ID: DK CS'T94

Load-displacement data

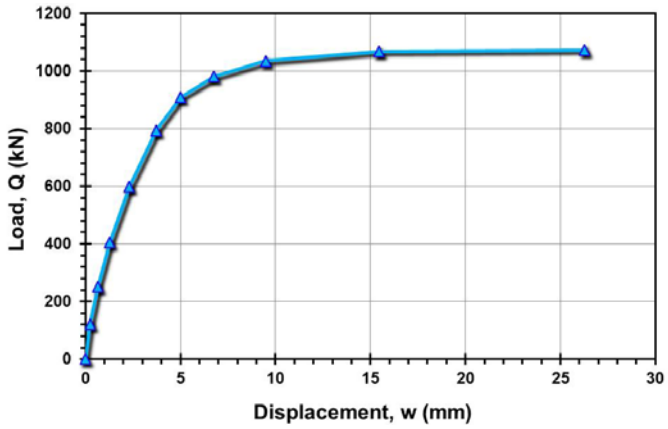

Back-analyzed normalized operational stiffness vs. pseudo-strain

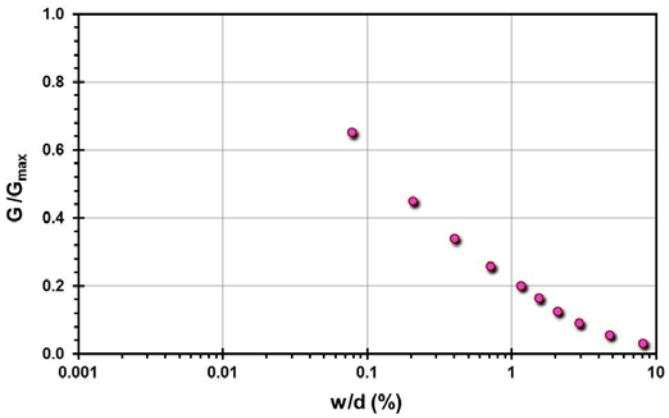

Detail	Description
Pile type/material	Open-ended steel pipe pile
Length, L (m)	11.60
Diameter, d (m)	0.324
Installation method	Driven
Loading mode	Tension
$Q_{max\text{-}measured}$ (kN)	1,072.25
Q_s (kN)	1,072.25
Q_b (kN)	-
$Q_{Davisson}$ (kN)	1,033.97
$Q_{w/d=10\%}$ (kN)	1,080.83
$Q_{C\text{-}K}$ (kN)	1,104.97

Pile ID: DK CL'T89a

Load-displacement data

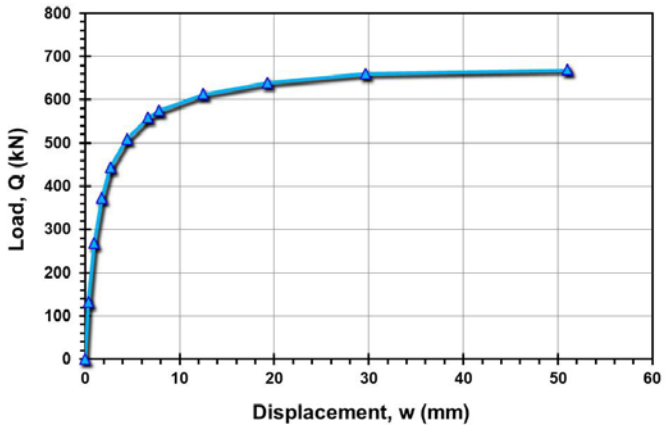

Back-analyzed normalized operational stiffness vs. pseudo-strain

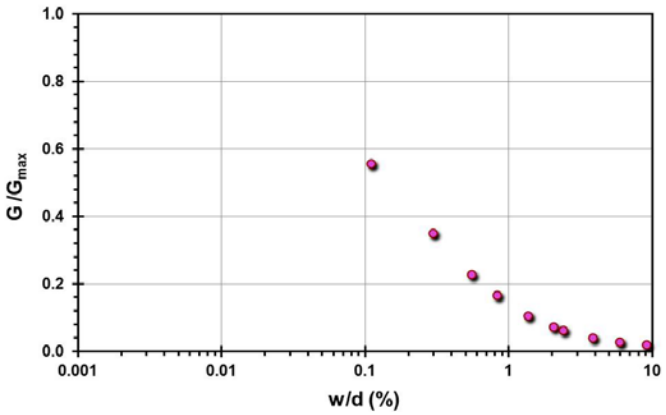

Detail	Description
Pile type/material	Open-ended steel pipe pile
Length, L (m)	11.30
Diameter, d (m)	0.324
Installation method	Driven
Loading mode	Tension
$Q_{max\text{-}measured}$ (kN)	669.43
Q_s (kN)	669.43
Q_b (kN)	-
$Q_{Davisson}$ (kN)	593.74
$Q_{w/d=10\%}$ (kN)	659.23
$Q_{C\text{-}K}$ (kN)	691.09

Pile ID: DK CL'T89b

Load-displacement data

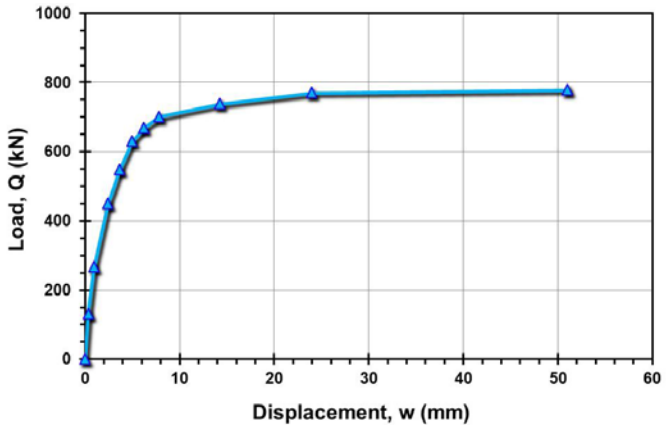

Back-analyzed normalized operational stiffness vs. pseudo-strain

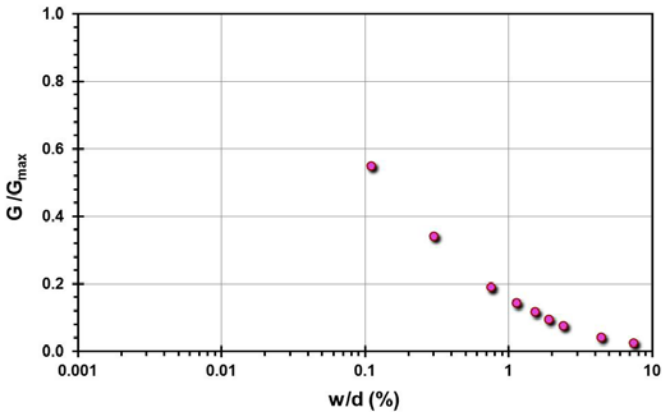

Detail	Description
Pile type/material	Open-ended steel pipe pile
Length, L (m)	11.60
Diameter, d (m)	0.324
Installation method	Driven
Loading mode	Tension
$Q_{max\text{-}measured}$ (kN)	778.61
Q_s (kN)	778.61
Q_b (kN)	-
$Q_{Davisson}$ (kN)	774.37
$Q_{w/d=10\%}$ (kN)	770.46
$Q_{C\text{-}K}$ (kN)	801.28

Pile ID: DK CL'C89a

Load-displacement data

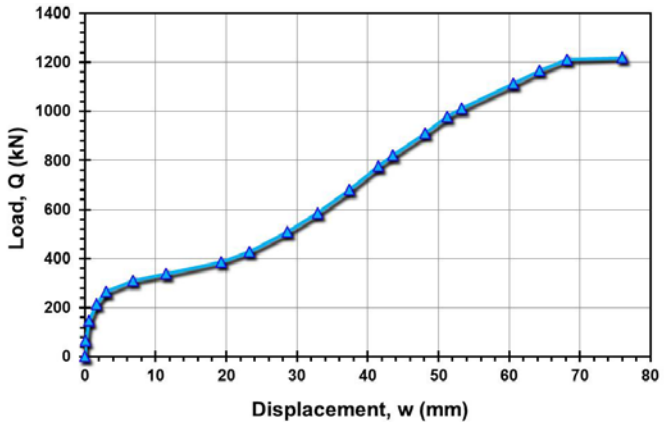

Back-analyzed normalized operational stiffness vs. pseudo-strain

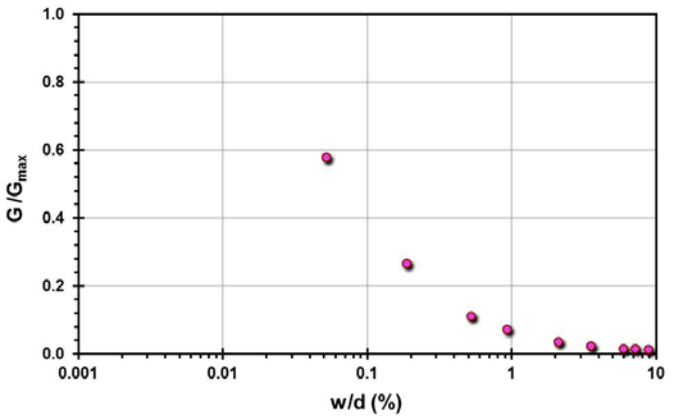

Detail	Description
Pile type/material	Open-ended steel pipe pile
Length, L (m)	11.30
Diameter, d (m)	0.324
Installation method	Driven
Loading mode	Compression
$Q_{max\text{-}measured}$ (kN)	1,198.09
Q_s (kN)	705.05
Q_b (kN)	493.04
$Q_{Davisson}$ (kN)	-
$Q_{w/d=10\%}$ (kN)	-
$Q_{C\text{-}K}$ (kN)	-

Pile ID: DK CL'C89b

Load-displacement data

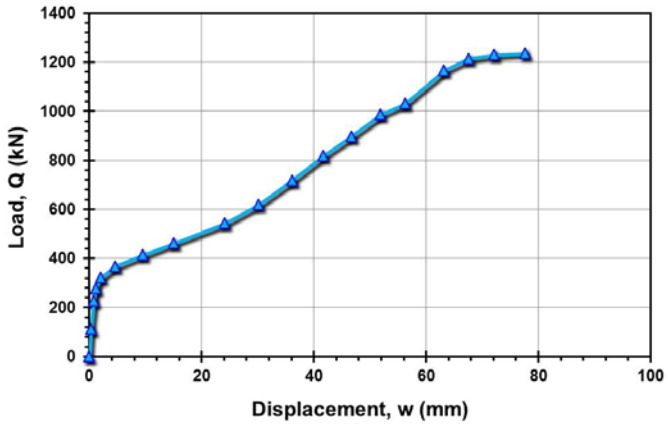

Back-analyzed normalized operational stiffness vs. pseudo-strain

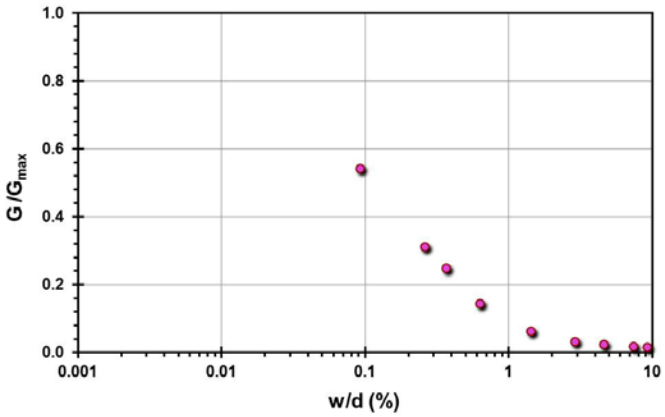

Detail	Description
Pile type/material	Open-ended steel pipe pile
Length, L (m)	11.60
Diameter, d (m)	0.324
Installation method	Driven
Loading mode	Compression
$Q_{max\text{-}measured}$ (kN)	1,237.21
Q_s (kN)	727.68
Q_b (kN)	509.53
$Q_{Davisson}$ (kN)	-
$Q_{w/d=10\%}$ (kN)	-
$Q_{C\text{-}K}$ (kN)	-

Pile ID: **DK LS'T94**

Load-displacement data

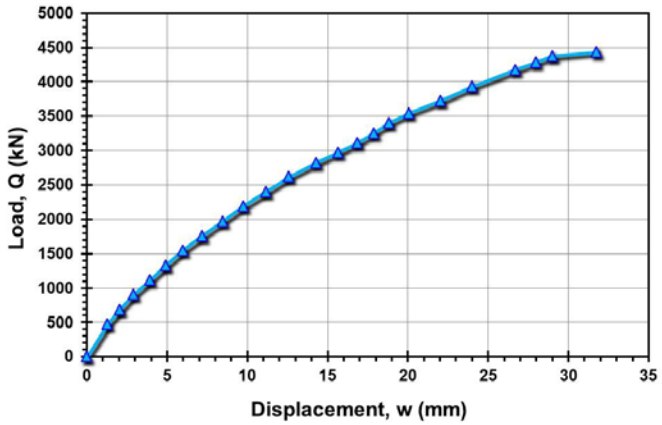

Back-analyzed normalized operational stiffness vs. pseudo-strain

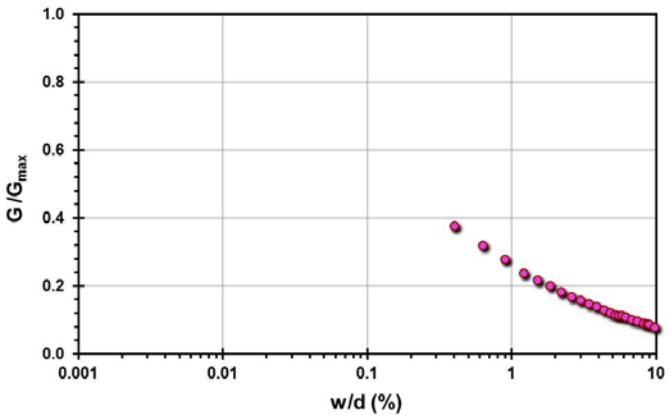

Detail	Description
Pile type/material	Open-ended steel pipe pile
Length, L (m)	22.10
Diameter, d (m)	0.324
Installation method	Driven
Loading mode	Tension
$Q_{max\text{-}measured}$ (kN)	4,433.55
Q_s (kN)	4,433.55
Q_b (kN)	-
$Q_{Davisson}$ (kN)	4,433.55
$Q_{w/d=10\%}$ (kN)	4,489.11
$Q_{C\text{-}K}$ (kN)	7,812.50

Site ID No. 15

Cone penetrometer data	CPT SBT soil classification index, I_c	Detail	Description
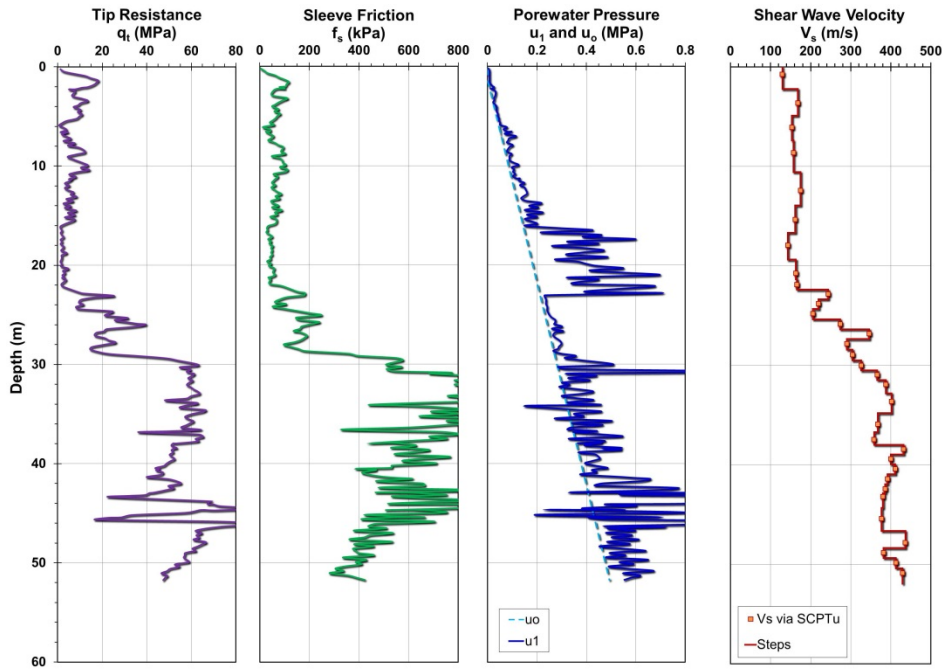	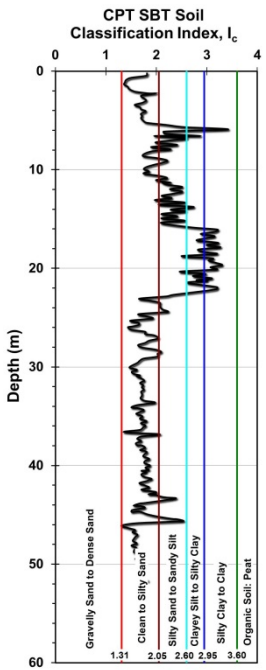	Site name and location	EURIPIDES 1, Eemshaven, Netherlands
		Soil type(s)	30 m of loose to firm silty sands, silts, and clays over very dense sands
		Pile type(s)	Open-ended steel pipe pile
		Type of cone penetrometer testing	SCPTu
		Source of V_s evaluation	SCPTu
		Number of pile load tests	8
		Reference	Baaijens and Kolk (2004)
		Comments	Measured u_1 readings converted to equivalent u_2

Pile ID: E 1/30.5-1

Load-displacement data

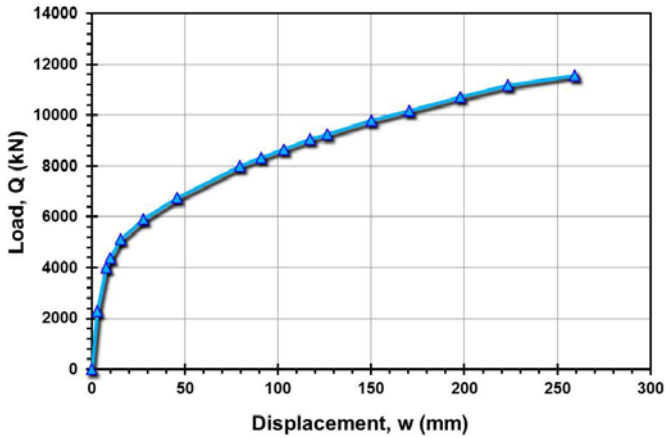

Back-analyzed normalized operational stiffness vs. pseudo-strain

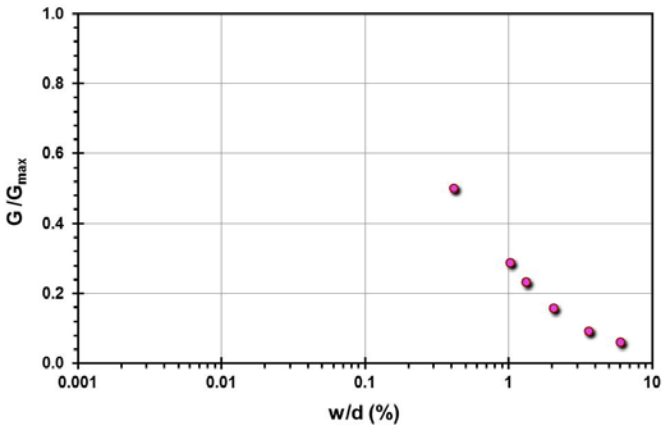

Detail	Description
Pile type/material	Open-ended steel pipe pile
Length, L (m)	30.50
Diameter, d (m)	0.762
Installation method	Driven
Loading mode	Compression
$Q_{max\text{-}measured}$ (kN)	11,570.60
Q_s (kN)	7,472.5
Q_b (kN)	4,098.10
$Q_{Davisson}$ (kN)	6,321.14
$Q_{w/d=10\%}$ (kN)	7,633.47
$Q_{C\text{-}K}$ (kN)	14,492.75

Pile ID: E 1/30.5-2

Load-displacement data

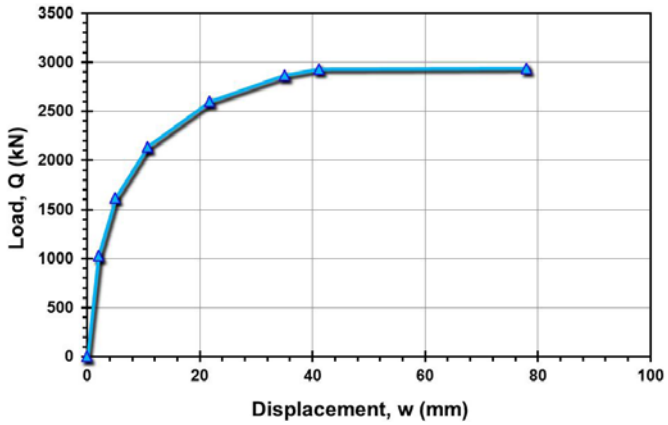

Back-analyzed normalized operational stiffness vs. pseudo-strain

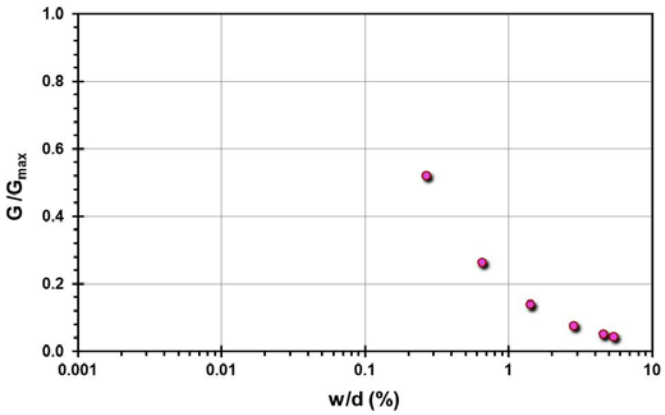

Detail	Description
Pile type/material	Open-ended steel pipe pile
Length, L (m)	30.50
Diameter, d (m)	0.762
Installation method	Driven
Loading mode	Tension
$Q_{max\text{-}measured}$ (kN)	2,938.05
Q_s (kN)	2,938.05
Q_b (kN)	-
$Q_{Davisson}$ (kN)	2,368.89
$Q_{w/d=10\%}$ (kN)	2,942.54
$Q_{C\text{-}K}$ (kN)	2,985.07

Pile ID: E 1/38.7-1

Load-displacement data

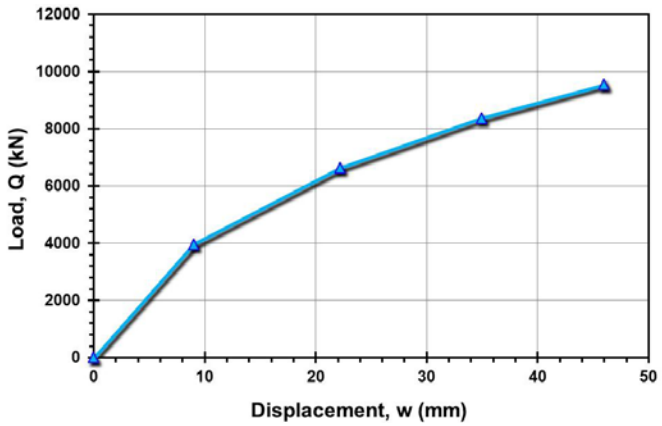

Back-analyzed normalized operational stiffness vs. pseudo-strain

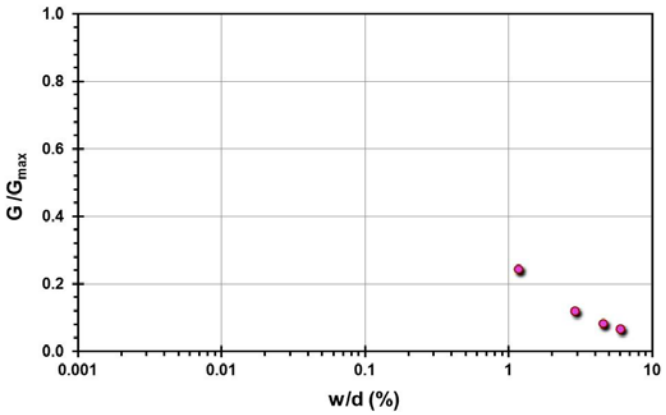

Detail	Description
Pile type/material	Open-ended steel pipe pile
Length, L (m)	38.70
Diameter, d (m)	0.762
Installation method	Driven
Loading mode	Tension
$Q_{max\text{-}measured}$ (kN)	9,529.93
Q_s (kN)	9,529.93
Q_b (kN)	-
$Q_{Davisson}$ (kN)	7,486.70
$Q_{w/d=10\%}$ (kN)	11,327.33
$Q_{C\text{-}K}$ (kN)	16,129.03

Pile ID: E 1/38.7-2

Load-displacement data

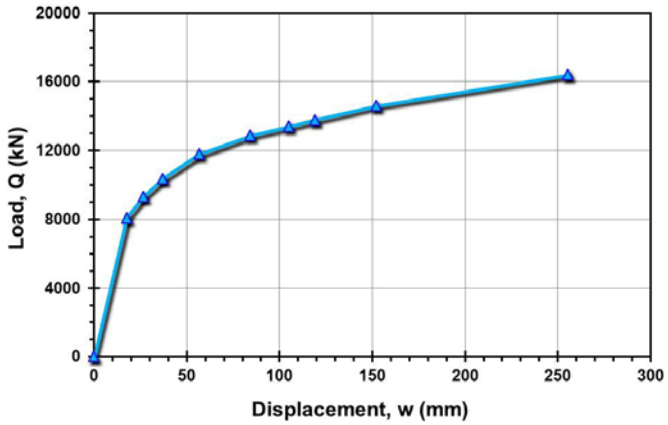

Back-analyzed normalized operational stiffness vs. pseudo-strain

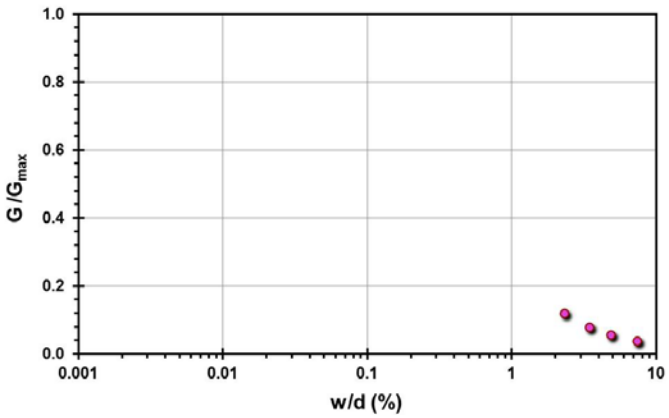

Detail	Description
Pile type/material	Open-ended steel pipe pile
Length, L (m)	38.70
Diameter, d (m)	0.762
Installation method	Driven
Loading mode	Compression
$Q_{max\text{-}measured}$ (kN)	16,424.36
Q_s (kN)	13,064.66
Q_b (kN)	3,359.70
$Q_{Davisson}$ (kN)	10,373.26
$Q_{w/d=10\%}$ (kN)	12,472.30
$Q_{C\text{-}K}$ (kN)	18,867.92

Pile ID: E 1/38.7-3

Load-displacement data

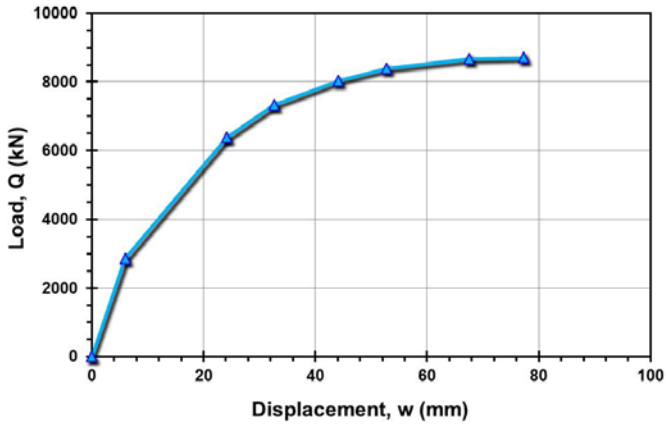

Back-analyzed normalized operational stiffness vs. pseudo-strain

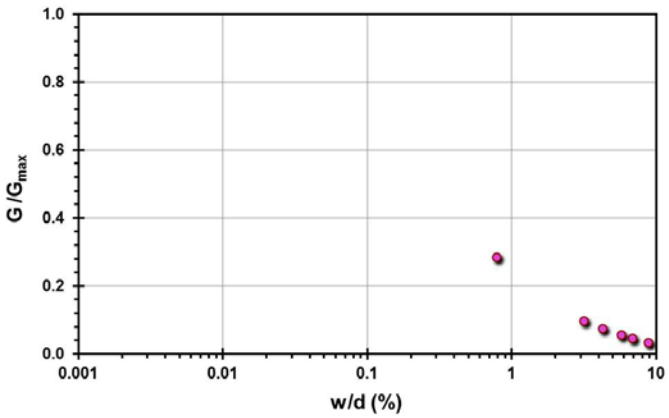

Detail	Description
Pile type/material	Open-ended steel pipe pile
Length, L (m)	38.70
Diameter, d (m)	0.762
Installation method	Driven
Loading mode	Tension
$Q_{max\text{-}measured}$ (kN)	8,704.78
Q_s (kN)	8,704.78
Q_b (kN)	-
$Q_{Davisson}$ (kN)	6,386.50
$Q_{w/d=10\%}$ (kN)	8,786.95
$Q_{C\text{-}K}$ (kN)	10,101.01

Pile ID: E 1/47.0-1

Load-displacement data

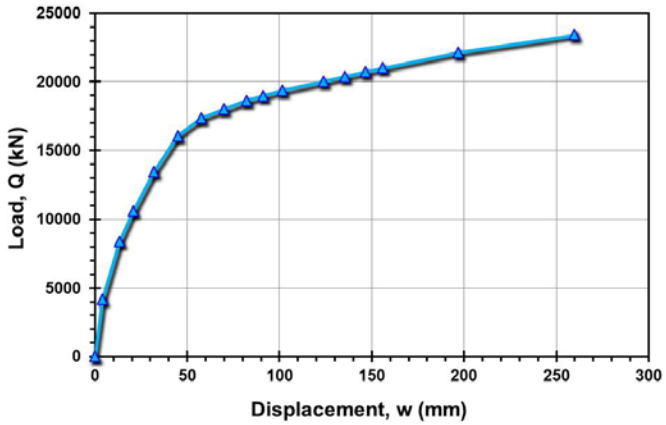

Back-analyzed normalized operational stiffness vs. pseudo-strain

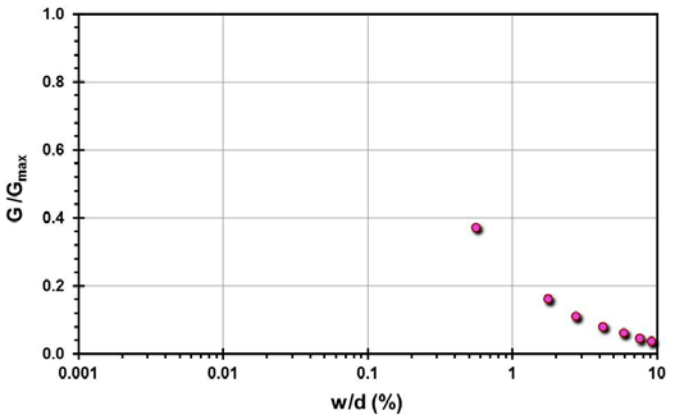

Detail	Description
Pile type/material	Open-ended steel pipe pile
Length, L (m)	47.00
Diameter, d (m)	0.762
Installation method	Driven
Loading mode	Compression
$Q_{max\text{-}measured}$ (kN)	23,407.80
Q_s (kN)	18,718.98
Q_b (kN)	4,688.82
$Q_{Davisson}$ (kN)	17,374.30
$Q_{w/d=10\%}$ (kN)	17,922.79
$Q_{C\text{-}K}$ (kN)	26,315.79

Pile ID: E 1/47.0-2

Load-displacement data

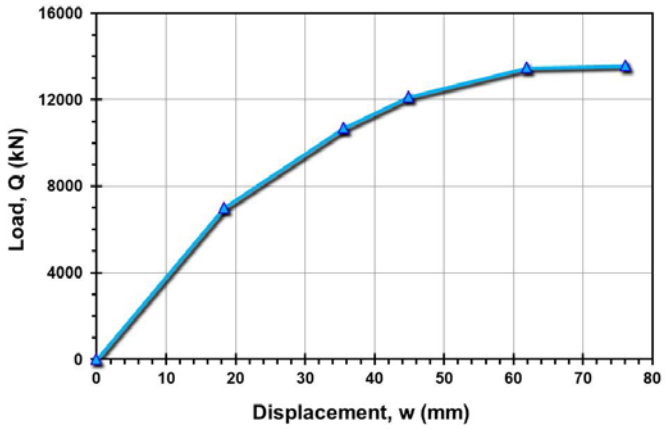

Back-analyzed normalized operational stiffness vs. pseudo-strain

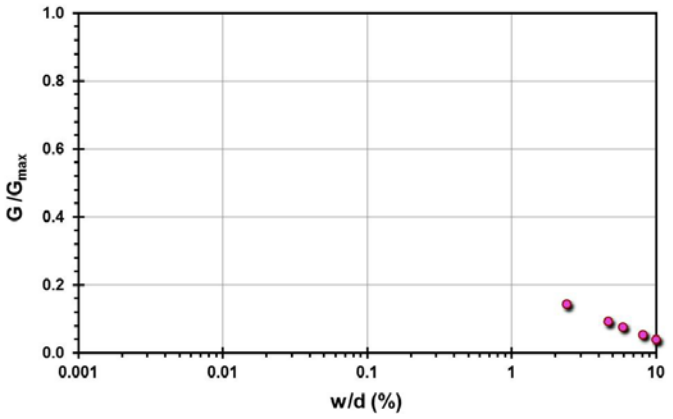

Detail	Description
Pile type/material	Open-ended steel pipe pile
Length, L (m)	47.00
Diameter, d (m)	0.762
Installation method	Driven
Loading mode	Tension
$Q_{max\text{-}measured}$ (kN)	13,594.25
Q_s (kN)	13,594.25
Q_b (kN)	-
$Q_{Davisson}$ (kN)	12,141.75
$Q_{w/d=10\%}$ (kN)	13,657.32
$Q_{C\text{-}K}$ (kN)	16,393.44

Pile ID: E 1/47.0-3

Load-displacement data

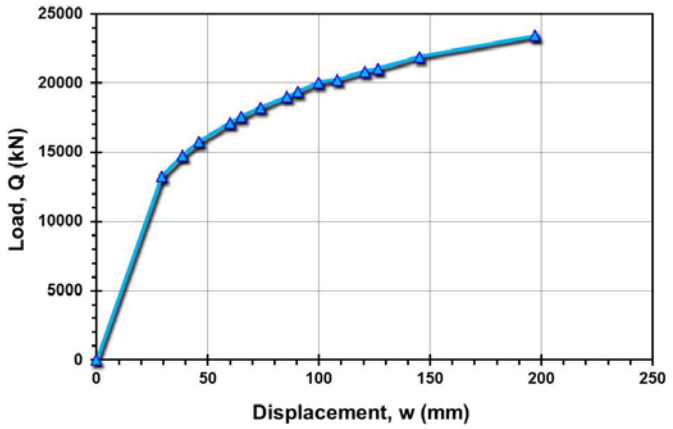

Back-analyzed normalized operational stiffness vs. pseudo-strain

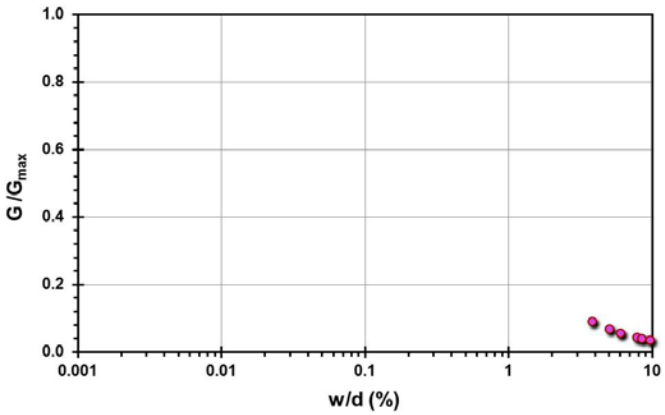

Detail	Description
Pile type/material	Open-ended steel pipe pile
Length, L (m)	47.00
Diameter, d (m)	0.762
Installation method	Driven
Loading mode	Compression
$Q_{max\text{-}measured}$ (kN)	23,407.80
Q_s (kN)	18,792.82
Q_b (kN)	4,614.98
$Q_{Davisson}$ (kN)	17,095.00
$Q_{w/d=10\%}$ (kN)	18,292.47
$Q_{C\text{-}K}$ (kN)	27,777.78

Site ID No. 16

Cone penetrometer data	CPT SBT soil classification index, I_c	Detail	Description
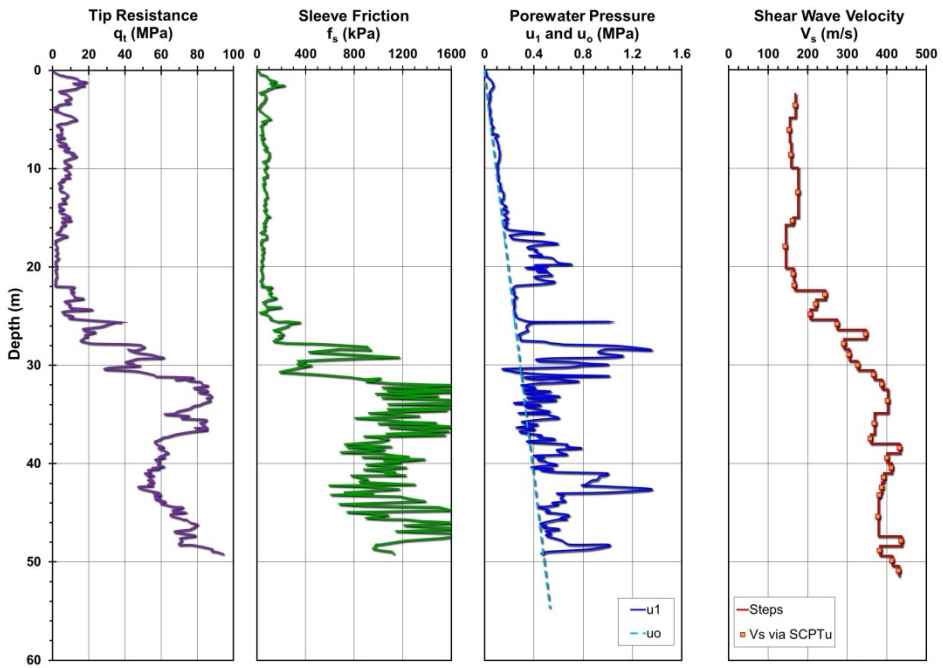	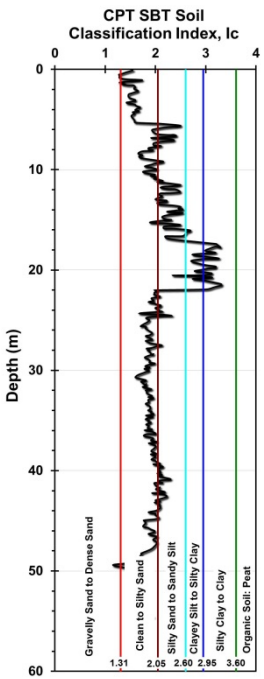	Site name and location	EURIPIDES 2, Eemshaven, Netherlands
		Soil type(s)	Approximately 30 m of loose to medium silty sands, silts, and clays over very dense sands
		Pile type(s)	Open-ended steel pipe pile
		Type of cone penetrometer testing	SCPTu
		Source of V_s evaluation	SCPTu
		Number of pile load tests	5
		Reference	Baaijens and Kolk (2004)
		Comments	u_1 reading converted to u_2

Pile ID: E 2/46.7-1

Load-displacement data

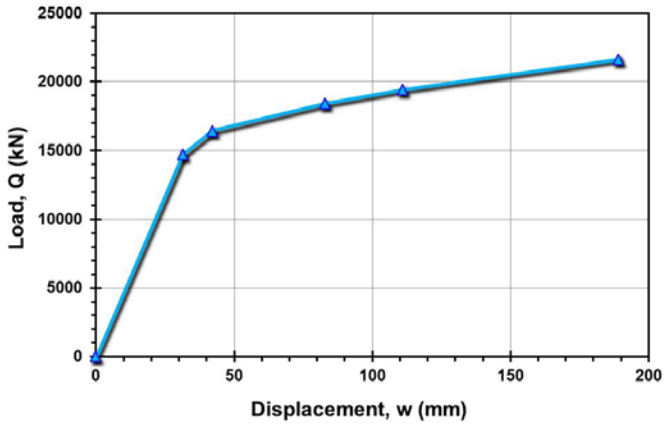

Back-analyzed normalized operational stiffness vs. pseudo-strain

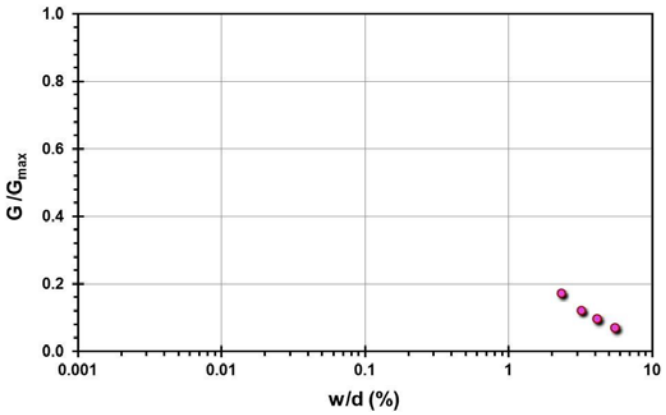

Detail	Description
Pile type/material	Open-ended steel pipe pile
Length, L (m)	46.70
Diameter, d (m)	0.762
Installation method	Driven
Loading mode	Compression
$Q_{max\text{-}measured}$ (kN)	21,631.60
Q_s (kN)	17,016.62
Q_b (kN)	4,614.98
$Q_{Davisson}$ (kN)	17,409.05
$Q_{w/d=10\%}$ (kN)	17,657.03
$Q_{C\text{-}K}$ (kN)	25,000.00

Pile ID: E 2/46.7-2

Load-displacement data

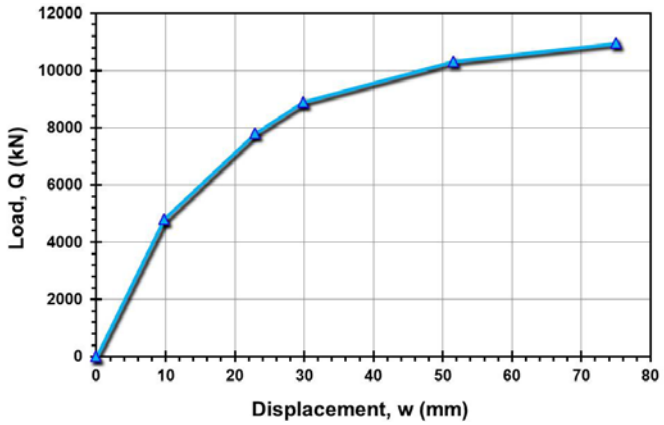

Back-analyzed normalized operational stiffness vs. pseudo-strain

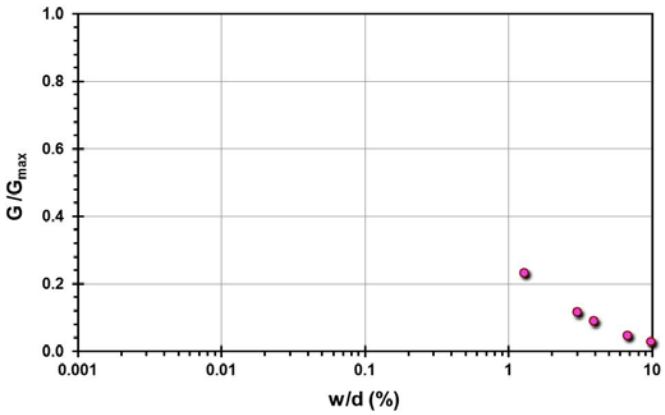

Detail	Description
Pile type/material	Open-ended steel pipe pile
Length, L (m)	46.70
Diameter, d (m)	0.762
Installation method	Driven
Loading mode	Tension
$Q_{max\text{-}measured}$ (kN)	10,951.70
Q_s (kN)	10,951.70
Q_b (kN)	-
$Q_{Davisson}$ (kN)	9,609.60
$Q_{w/d=10\%}$ (kN)	11,027.86
$Q_{C\text{-}K}$ (kN)	13,157.89

Pile ID: E 2/46.7-3

Load-displacement data

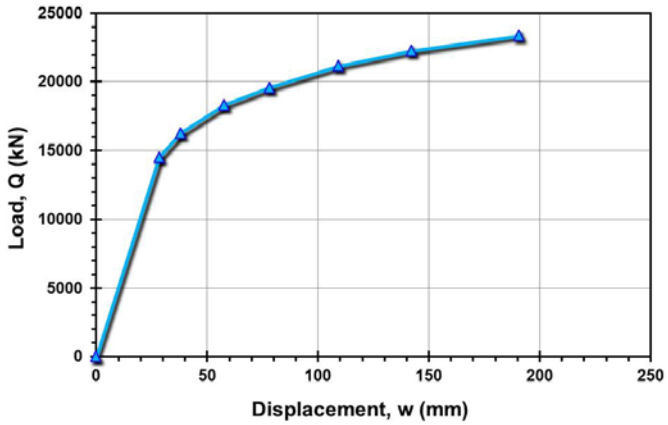

Back-analyzed normalized operational stiffness vs. pseudo-strain

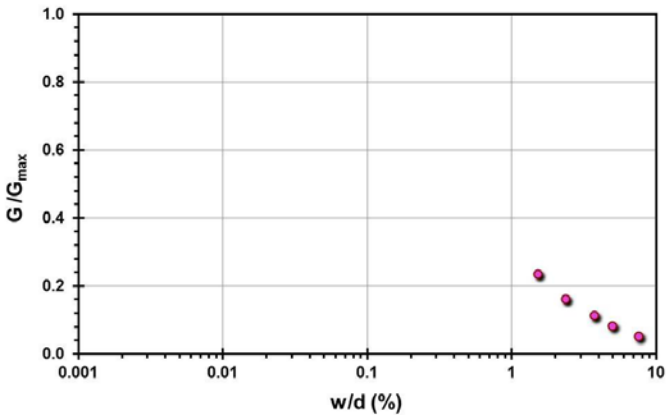

Detail	Description
Pile type/material	Open-ended steel pipe pile
Length, L (m)	46.70
Diameter, d (m)	0.762
Installation method	Driven
Loading mode	Compression
$Q_{max\text{-}measured}$ (kN)	23,368.40
Q_s (kN)	17,678.85
Q_b (kN)	5,689.55
$Q_{Davisson}$ (kN)	18,947.35
$Q_{w/d=10\%}$ (kN)	19,730.88
$Q_{C\text{-}K}$ (kN)	26,315.79

Pile ID: E 2/47.0R-1

Load-displacement data

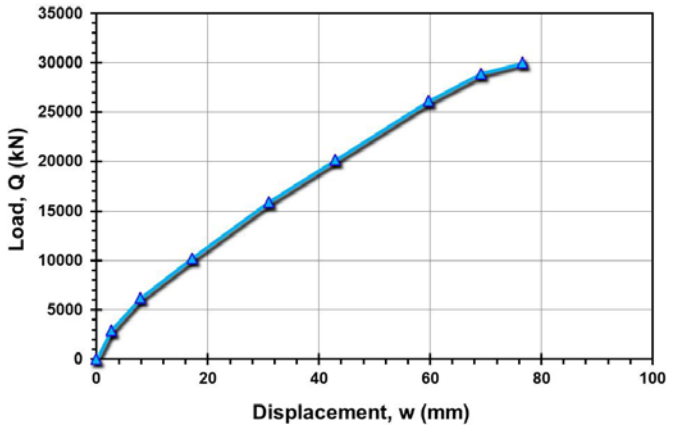

Back-analyzed normalized operational stiffness vs. pseudo-strain

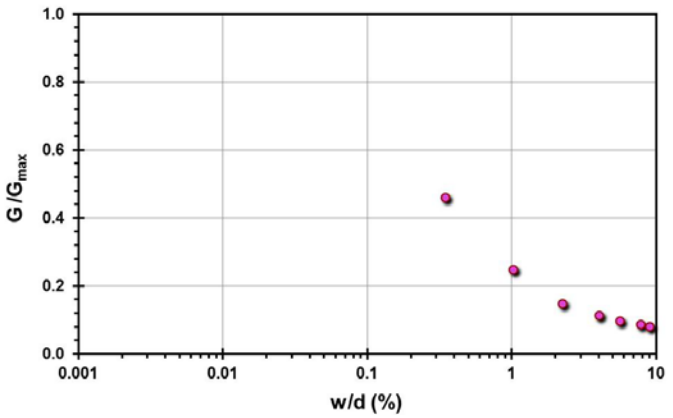

Detail	Description
Pile type/material	Open-ended steel pipe pile
Length, L (m)	47.00
Diameter, d (m)	0.762
Installation method	Driven
Loading mode	Compression
$Q_{max\text{-}measured}$ (kN)	29,985.60
Q_s (kN)	22,761.38
Q_b (kN)	7,224.22
$Q_{Davisson}$ (kN)	41,379.30
$Q_{w/d=10\%}$ (kN)	29,729.82
$Q_{C\text{-}K}$ (kN)	62,500.00

Pile ID: E 2/47.0R-2

Load-displacement data

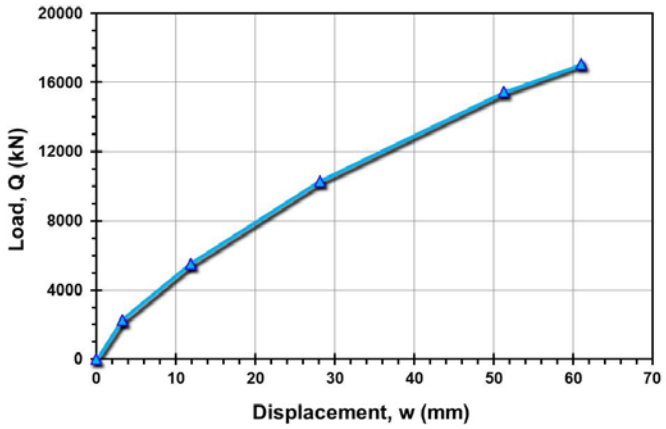

Back-analyzed normalized operational stiffness vs. pseudo-strain

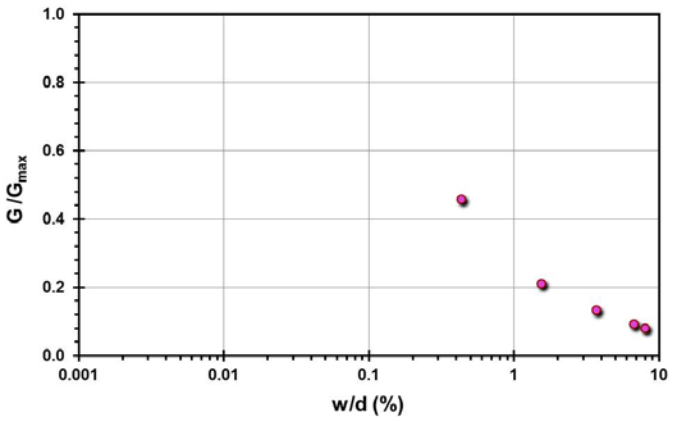

Detail	Description
Pile type/material	Open-ended steel pipe pile
Length, L (m)	47.00
Diameter, d (m)	0.762
Installation method	Driven
Loading mode	Tension
$Q_{max\text{-}measured}$ (kN)	17,062.46
Q_s (kN)	17,062.46
Q_b (kN)	-
$Q_{Davisson}$ (kN)	17,062.82
$Q_{w/d=10\%}$ (kN)	19,481.59
$Q_{C\text{-}K}$ (kN)	40,000.00

Site ID No. 17

Cone penetrometer data	CPT SBT soil classification index, I_c	Detail	Description
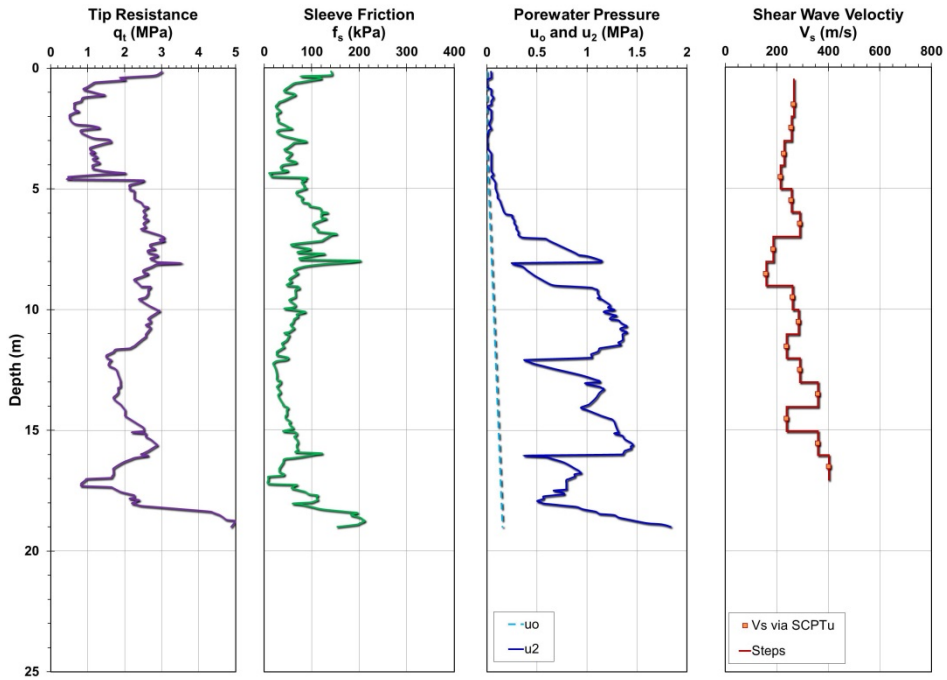	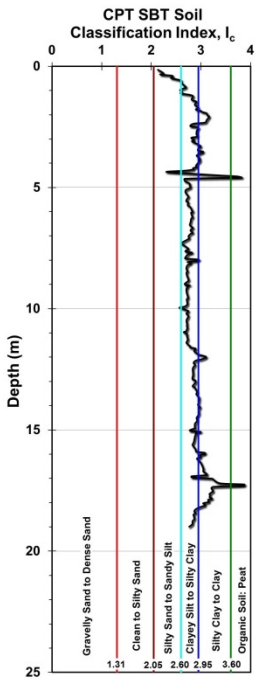	Site name and location	Factory building site, Jiangsu Province, China
		Soil type(s)	Marine silty clay
		Pile type(s)	Drilled shaft
		Type of cone penetrometer testing	SCPTu
		Source of V_s evaluation	SCPTu
		Number of pile load tests	1
		Reference	Miao et al. (2011)
		Comments	

Pile ID: FBJ 1

Load-displacement data

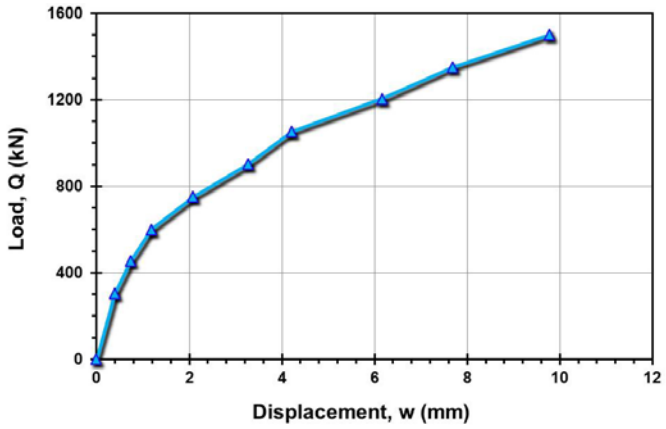

Back-analyzed normalized operational stiffness vs. pseudo-strain

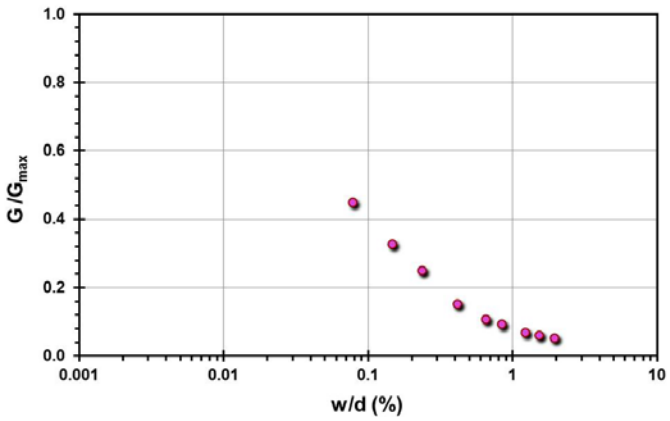

Detail	Description
Pile type/material	Drilled shaft
Length, L (m)	15.00
Diameter, d (m)	0.50
Installation method	Bored cast in-situ
Loading mode	Compression
$Q_{max\text{-}measured}$ (kN)	1,500.00
Q_s (kN)	1345.00
Q_b (kN)	155.00
$Q_{Davisson}$ (kN)	1,650.29
$Q_{w/d=10\%}$ (kN)	2,277.68
$Q_{C\text{-}K}$ (kN)	2,597.40

Site ID No. 18

Cone penetrometer data	CPT SBT soil classification index, I_c	Detail	Description
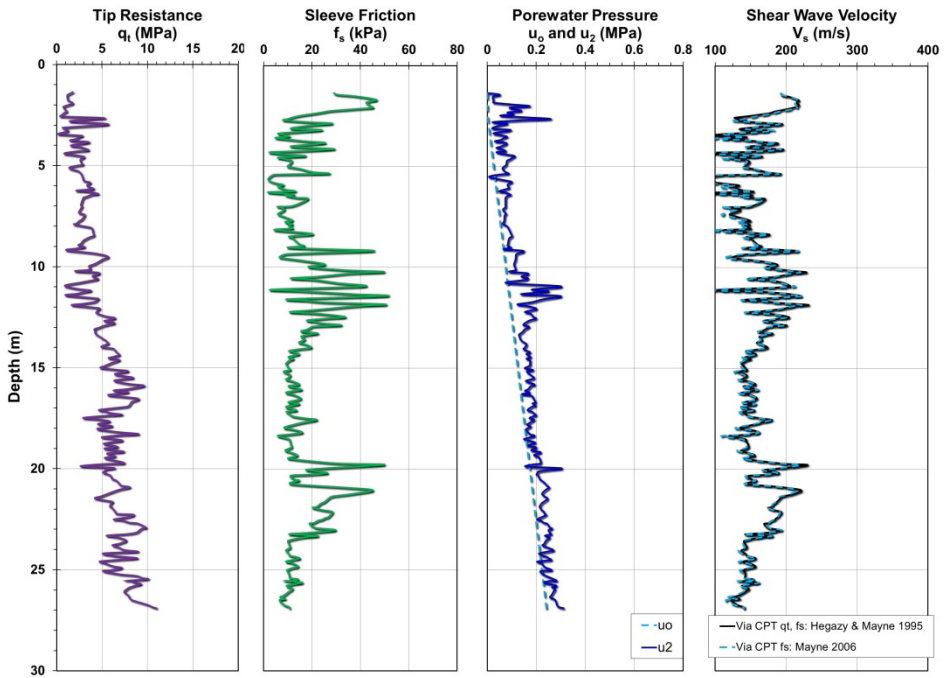	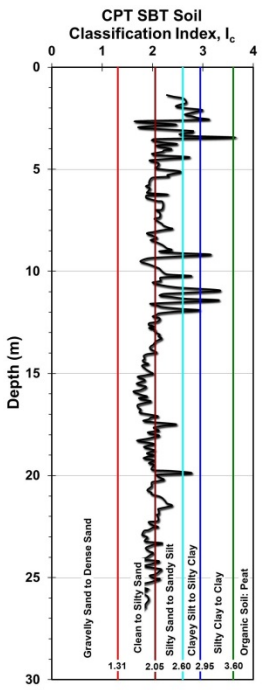	Site name and location	Fittja Straits Bridge, Vårby, near Stockholm, Sweden
		Soil type(s)	Layers of sand, silty sand, and gravelly sand
		Pile type(s)	Square concrete driven pile
		Type of cone penetrometer testing	CPTu
		Source of V_s evaluation	Correlations (see Figure opposite and Table 3.1)
		Number of pile load tests	1
		Reference	Axelsson (2000)
		Comments	V_s estimated via correlations

Pile ID: FSB 1

Load-displacement data

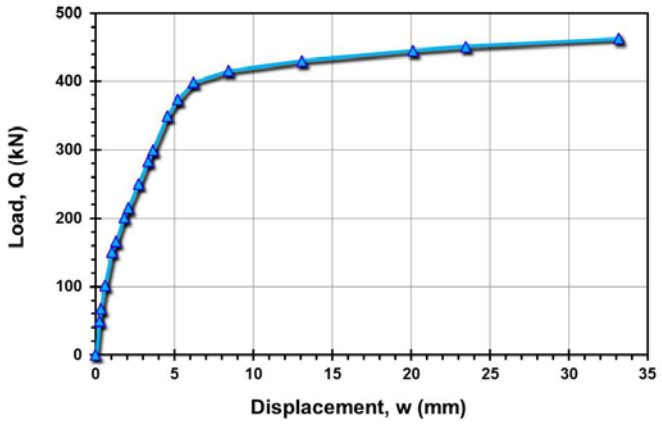

Back-analyzed normalized operational stiffness vs. pseudo-strain

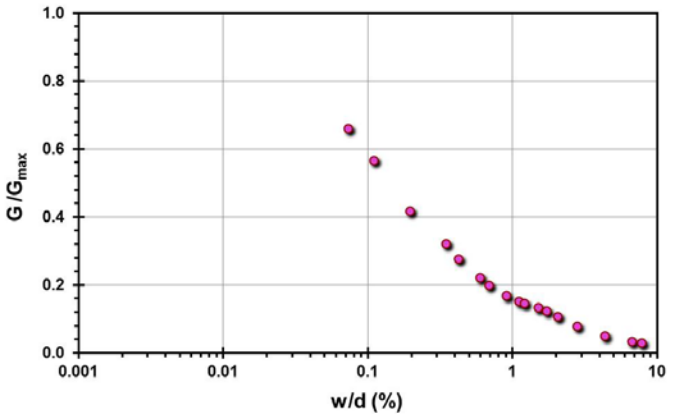

Detail	Description
Pile type/material	Square concrete driven pile
Length, L (m)	12.80
Width, B (m)	0.235
Installation method	Driven
Loading mode	Compression
$Q_{max\text{-}measured}$ (kN)	463.00
Q_s (kN)	340.94
Q_b (kN)	122.06
$Q_{Davisson}$ (kN)	415.00
$Q_{w/d=10\%}$ (kN)	458.72
$Q_{C\text{-}K}$ (kN)	480.54

Site ID No. 19

Cone penetrometer data	CPT SBT soil classification index, I_c	Detail	Description
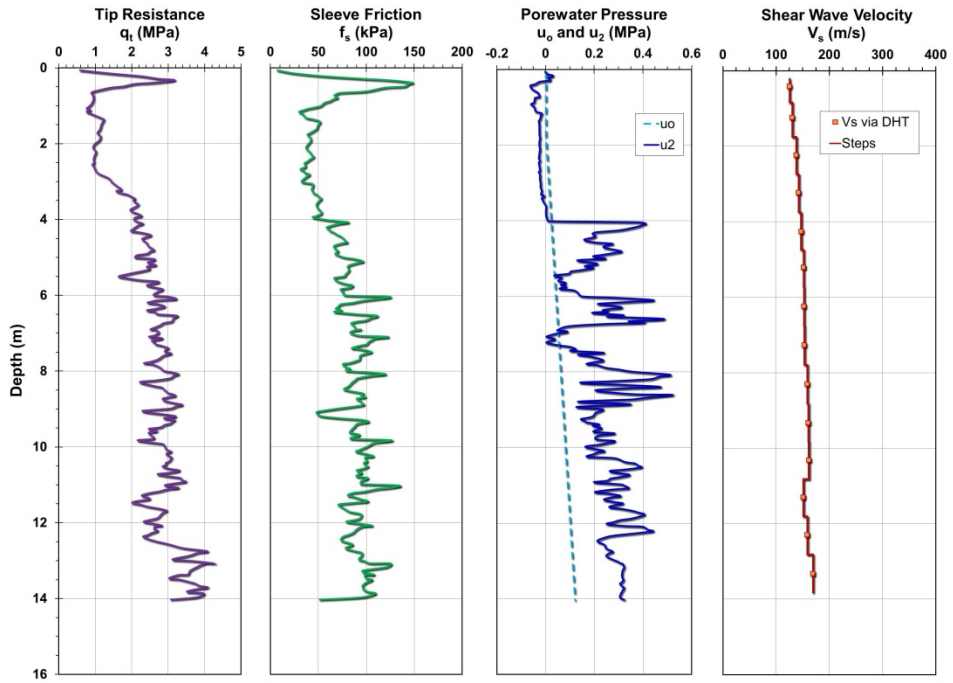	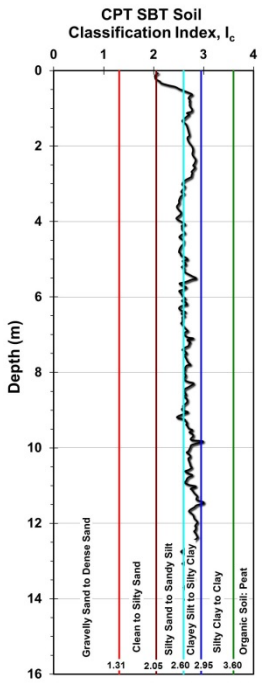	Site name and location	Flanders clay site, Merville, France
		Soil type(s)	Silt over stiff homogeneous clay
		Pile type(s)	1 Drilled shaft, 2 open-ended steel pipe piles and 2 H-section piles
		Type of cone penetrometer testing	CPTu + DHT
		Source of V_s evaluation	DHT
		Number of pile load tests	5
		Reference	Ali (2010), Ferber & Abraham (2002), and Rocher-Lacoste et al. (2004), Rocher-Lacoste (2008)
		Comments	V_s from DHT

Pile ID: FCS 1

Load-displacement data

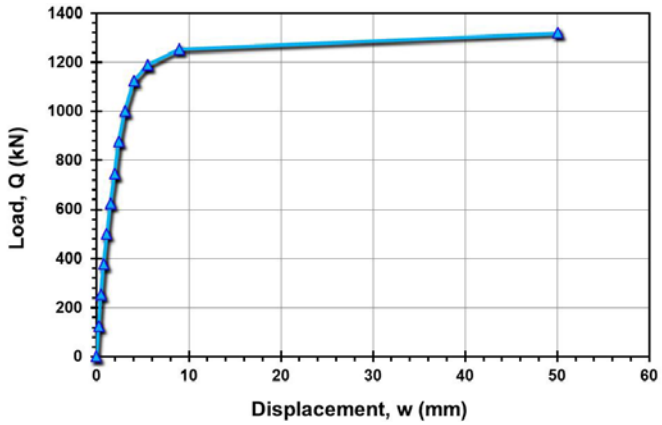

Back-analyzed normalized operational stiffness vs. pseudo-strain

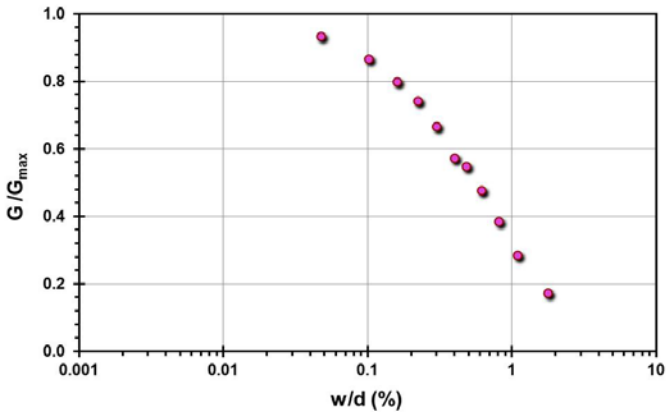

Detail	Description
Pile type/material	Drilled shaft
Length, L (m)	12.00
Diameter, d (m)	0.500
Installation method	Bored cast in-situ
Loading mode	Compression
$Q_{max\text{-}measured}$ (kN)	1,319.75
Q_s (kN)	946.75
Q_b (kN)	373.00
$Q_{Davisson}$ (kN)	1,254.35
$Q_{w/d=10\%}$ (kN)	1,320.15
$Q_{C\text{-}K}$ (kN)	1,336.90

Pile ID: FCS 2

Load-displacement data

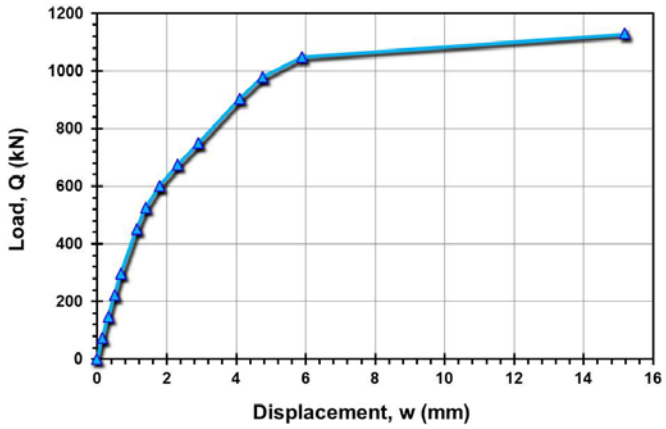

Back-analyzed normalized operational stiffness vs. pseudo-strain

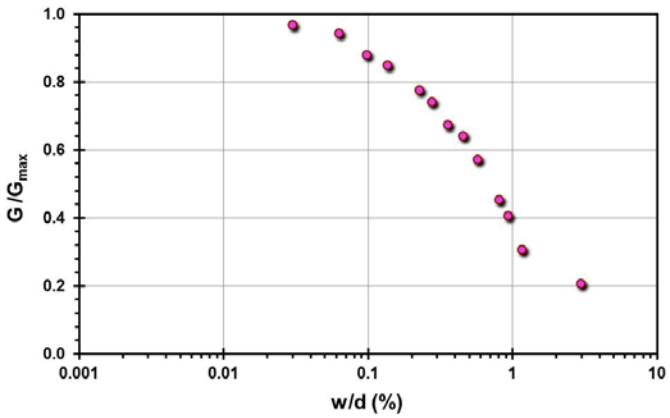

Detail	Description
Pile type/material	Open-ended steel pipe pile
Length, L (m)	9.40
Diameter, d (m)	0.508
Installation method	Driven
Loading mode	Compression
$Q_{max\text{-}measured}$ (kN)	981.89
Q_s (kN)	786.89
Q_b (kN)	195.00
$Q_{Davisson}$ (kN)	936.03
$Q_{w/d=10\%}$ (kN)	1,074.85
$Q_{C\text{-}K}$ (kN)	1,336.90

Pile ID: FCS 3

Load-displacement data

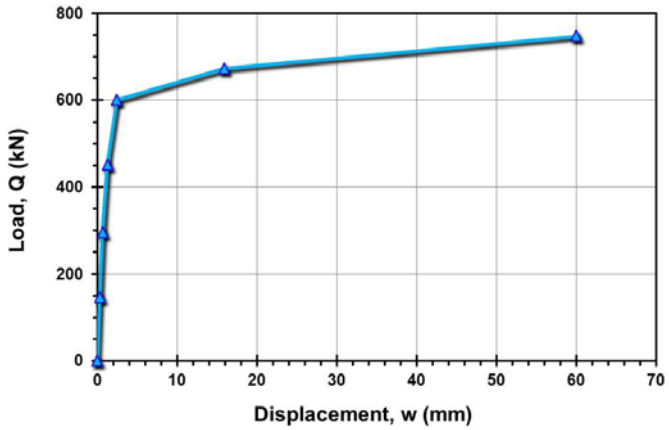

Back-analyzed normalized operational stiffness vs. pseudo-strain

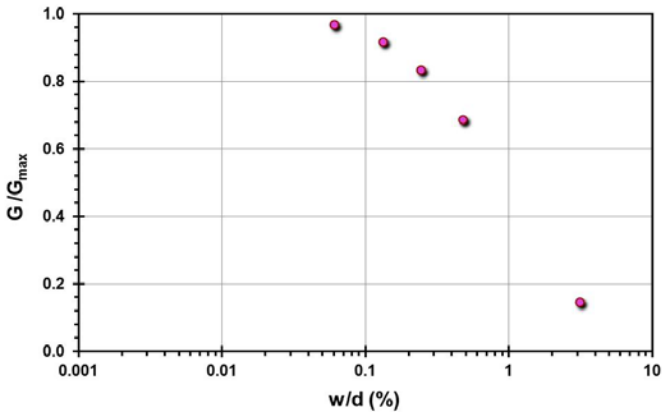

Detail	Description
Pile type/material	Open-ended steel pipe pile
Length, L (m)	9.40
Diameter, d (m)	0.508
Installation method	Jacked
Loading mode	Compression
$Q_{max\text{-}measured}$ (kN)	668.98
Q_s (kN)	533.98
Q_b (kN)	135.00
$Q_{Davisson}$ (kN)	598.84
$Q_{w/d=10\%}$ (kN)	664.84
$Q_{C\text{-}K}$ (kN)	678.43

Pile ID: FCS 4

Load-displacement data

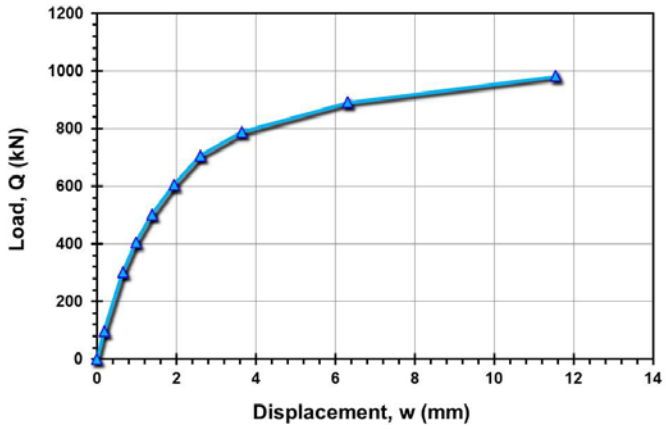

Back-analyzed normalized operational stiffness vs. pseudo-strain

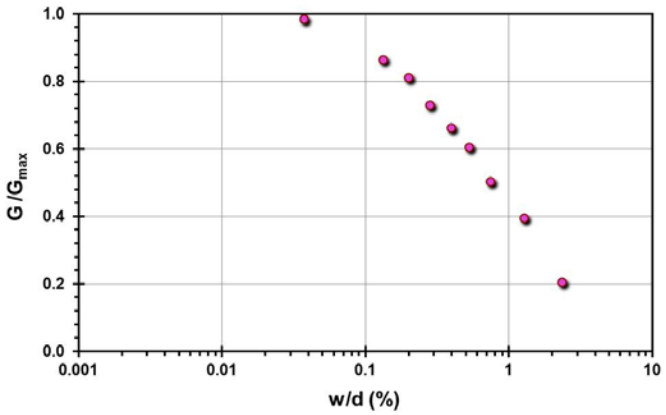

Detail	Description
Pile type/material	H-section steel pipe pile
Length, L (m)	10.20
H-section dimensions	16 x 155
Installation method	Driven
Loading mode	Compression
$Q_{max\text{-}measured}$ (kN)	1,029.66
Q_s (kN)	939.66
Q_b (kN)	190.00
$Q_{Davisson}$ (kN)	1,089.17
$Q_{w/d=10\%}$ (kN)	1,195.25
$Q_{C\text{-}K}$ (kN)	1,223.99

Pile ID: FCS 5

Load-displacement data

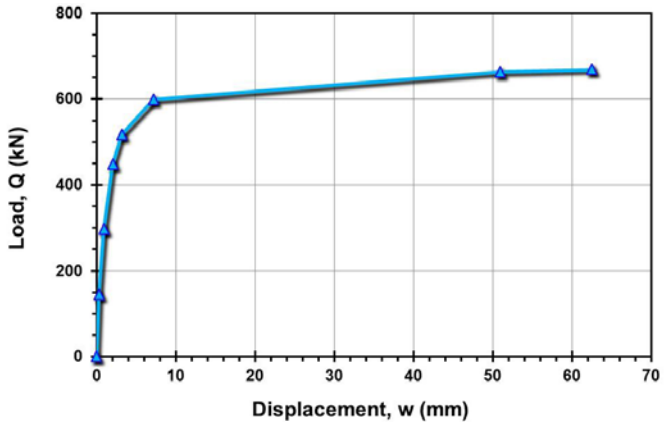

Back-analyzed normalized operational stiffness vs. pseudo-strain

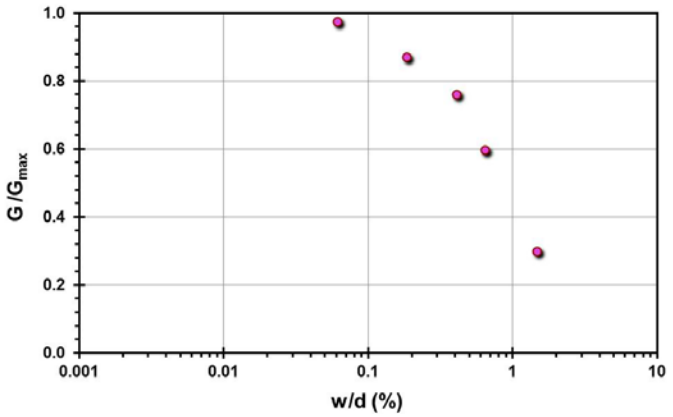

Detail	Description
Pile type/material	H-section steel pipe pile
Length, L (m)	10.20
H-section dimensions	16 x 155
Installation method	Jacked
Loading mode	Compression
$Q_{max\text{-}measured}$ (kN)	748.14
Q_s (kN)	568.14
Q_b (kN)	180.00
$Q_{Davisson}$ (kN)	637.30
$Q_{w/d=10\%}$ (kN)	742.81
$Q_{C\text{-}K}$ (kN)	758.73

Site ID No. 20

Cone penetrometer data	CPT SBT soil classification index, I_c	Detail	Description
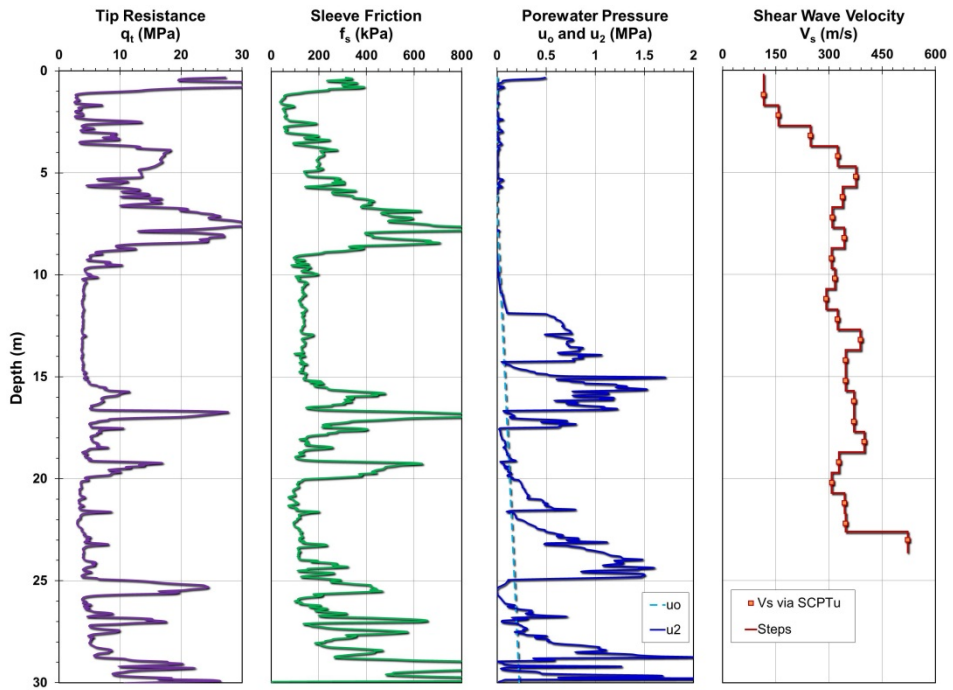	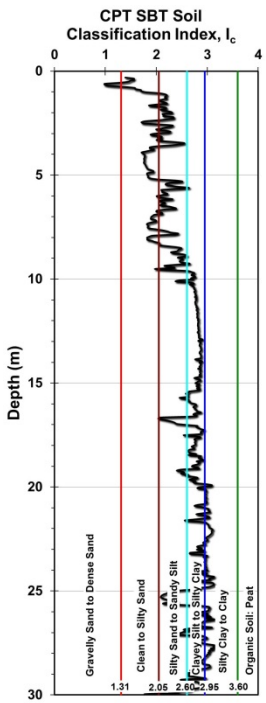	Site name and location	Foothill Medical Center (FMC), Calgary, AB, Canada
		Soil type(s)	Sandy clayey silt over hard silty clay till
		Pile type(s)	Drilled shaft
		Type of cone penetrometer testing	SCPTu
		Source of V_s evaluation	SCPTu
		Number of pile load tests	1
		Reference	Kort (2005)
		Comments	SCPTu data provided by David Woeller of ConeTec, personal communication; permission to use data given by Chris Hendry of Golder Associates. Data reported in Mayne & Woeller (2008).

Pile ID: FMC 1

Load-displacement data

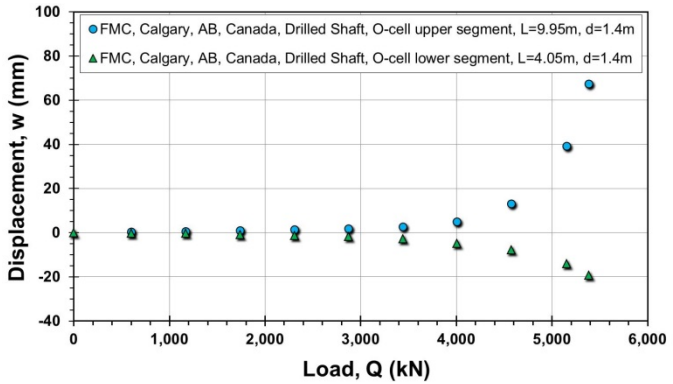

Back-analyzed normalized operational stiffness vs. pseudo-strain

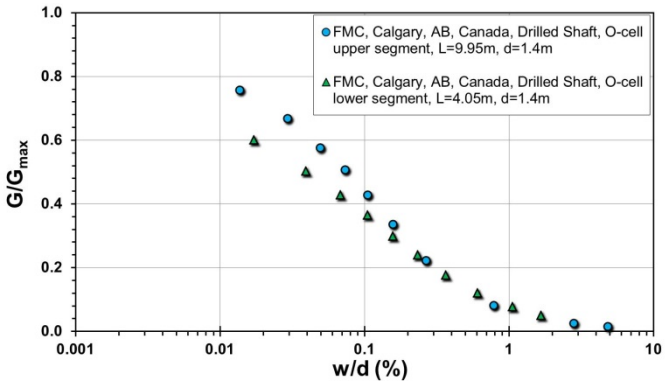

Detail	Description
Pile type/material	Drilled shaft
Length, L (m)	Upper: 9.95; lower: 4.05
Diameter, d (m)	Upper: 1.40; lower: 1.40
Installation method	Bored cast in-situ
Loading mode	O-cell compression
$Q_{max\text{-}measured}$ (kN)	Upper: 5,370.5; lower: 5,370.5
Q_s (kN)	Upper: 5,370.5; lower: 2,163.2
Q_b (kN)	3,207.3
$Q_{Davisson}$ (kN)	Upper: 5,003.2; lower: 5,155.4
$Q_{w/d=10\%}$ (kN)	Upper: 5,474.3; lower: 6,117.3
$Q_{C\text{-}K}$ (kN)	Upper: 5,586.6; lower: 6,250.0

Site ID No. 21

Cone penetrometer data	CPT SBT soil classification index, I_c	Detail	Description
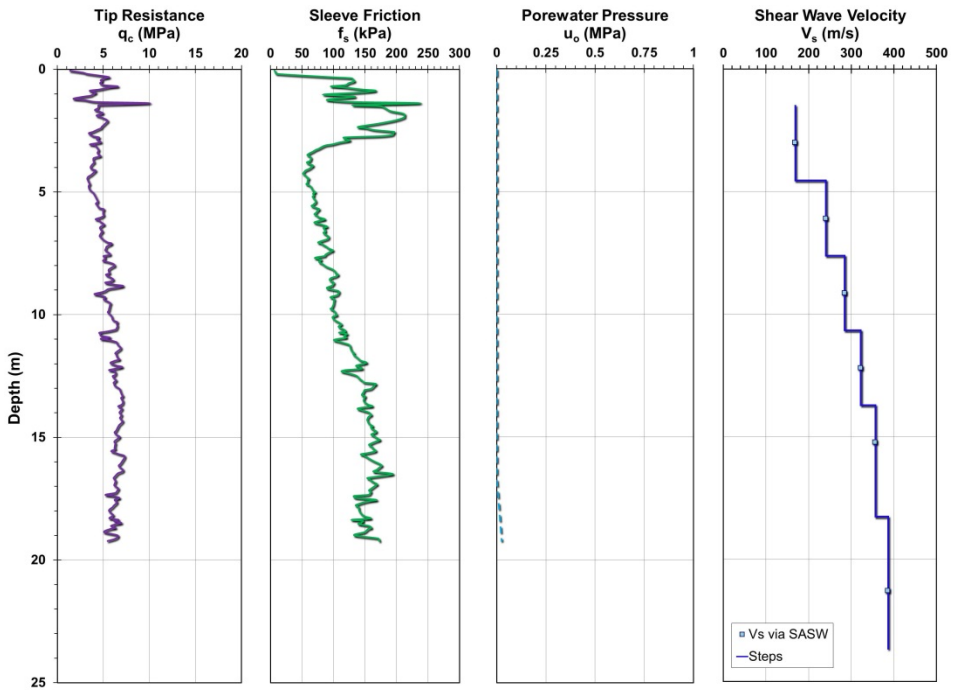	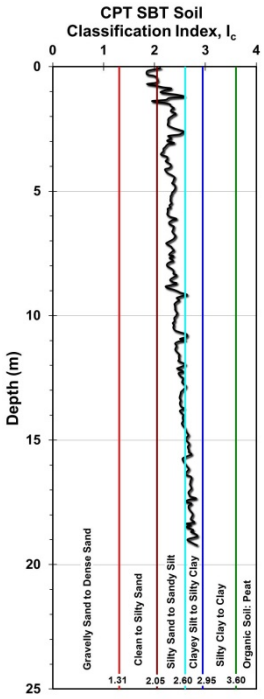	Site name and location	Georgia Tech Campus, Sixth Street (west), Atlanta, GA, USA
		Soil type(s)	Piedmont residual silty sand
		Pile type(s)	Drilled shafts
		Type of cone penetrometer testing	CPT
		Source of V_s evaluation	SASW
		Number of pile load tests	2
		Reference	Mayne and Harris (1993)
		Comments	V_s from SASW survey CPT sounding to 19.2m only Base of longer pile on bedrock u_2 reading assumed ≈ u_o where groundwater table is at 16 m

Pile ID: GT C1

Load-displacement data

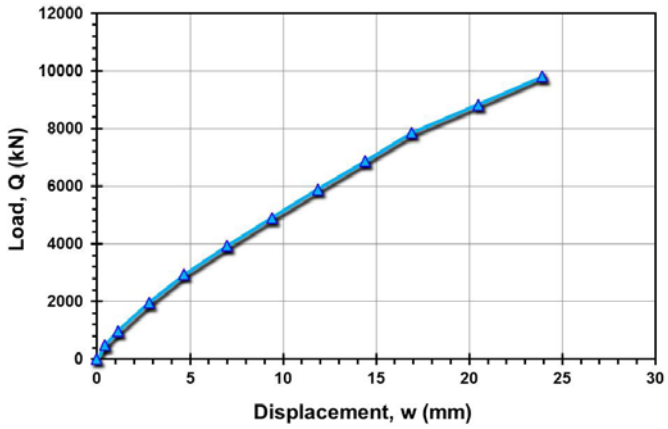

Back-analyzed normalized operational stiffness vs. pseudo-strain

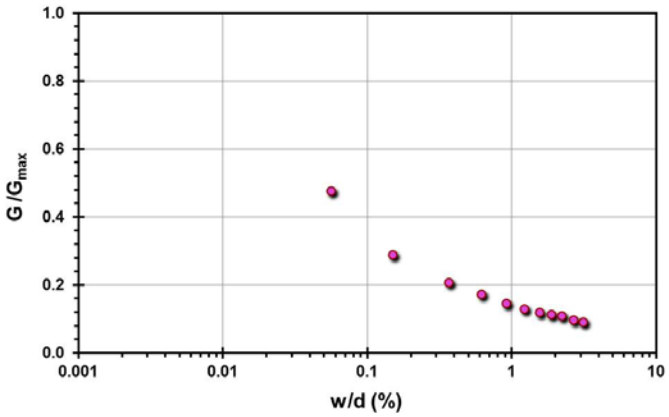

Detail	Description
Pile type/material	Drilled shaft
Length, L (m)	21.40
Diameter, d (m)	0.762
Installation method	Bored cast in-situ
Loading mode	Compression
$Q_{max\text{-}measured}$ (kN)	9,806.65
Q_s (kN)	6,259.58
Q_b (kN)	3,547.07
$Q_{Davisson}$ (kN)	11,277.65
$Q_{w/d=10\%}$ (kN)	17,486.22
$Q_{C\text{-}K}$ (kN)	27,027.03

Pile ID: GT C2

Load-displacement data

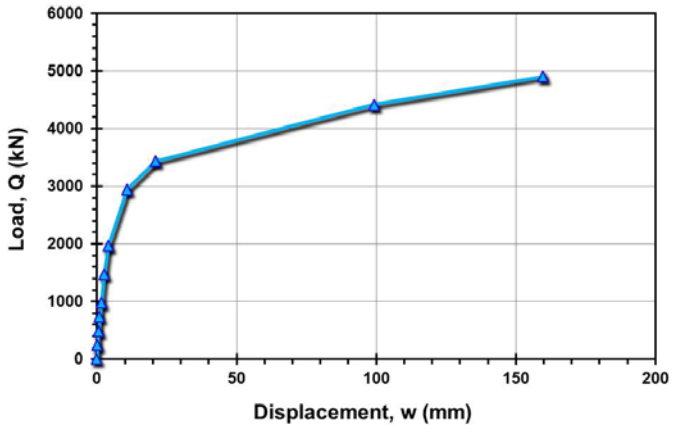

Back-analyzed normalized operational stiffness vs. pseudo-strain

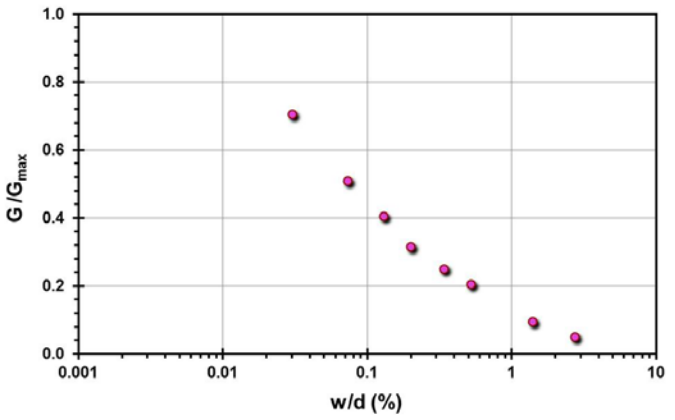

Detail	Description
Pile type/material	Drilled shaft
Length, L (m)	16.92
Diameter, d (m)	0.762
Installation method	Bored cast in-situ
Loading mode	Compression
$Q_{max\text{-}measured}$ (kN)	4,903.33
Q_s (kN)	3,905.99
Q_b (kN)	997.34
$Q_{Davisson}$ (kN)	3,922.66
$Q_{w/d=10\%}$ (kN)	4,088.54
$Q_{C\text{-}K}$ (kN)	5,988.02

Site ID No. 22

Cone penetrometer data	CPT SBT soil classification index, I_c	Detail	Description
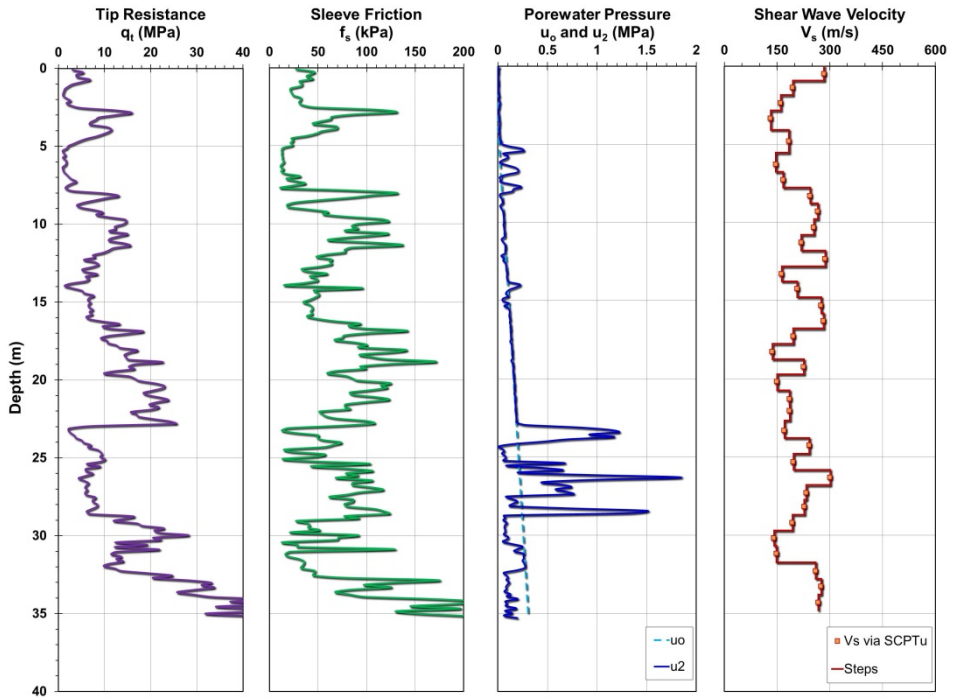	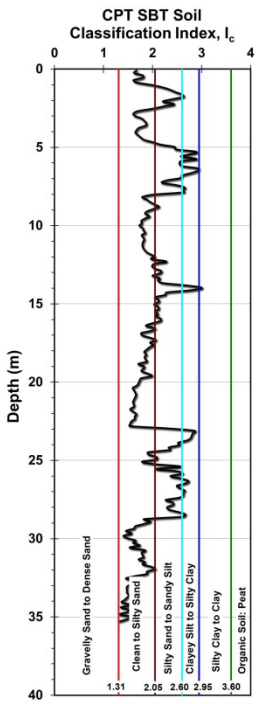	Site name and location	Gilmerton Bridge, Pier 12, Chesapeake, VA, USA
		Soil type(s)	Silty sand and clay over Yorktown marl (calcareous sediments)
		Pile type(s)	Drilled shaft
		Type of cone penetrometer testing	SCPTu
		Source of V_s evaluation	SCPTu
		Number of pile load tests	1
		Reference	Pang et al. (2010)
		Comments	

Pile ID: GB Pier 12

Load-displacement data

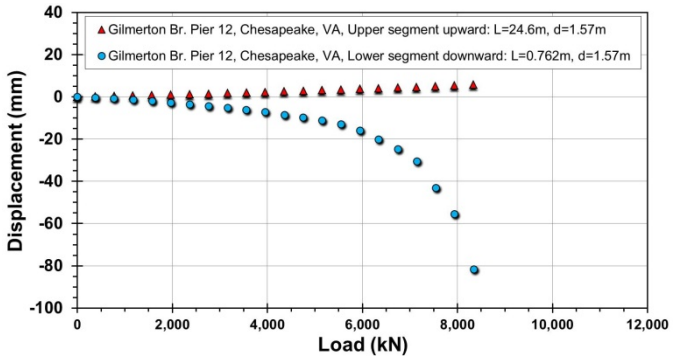

Back-analyzed normalized operational stiffness vs. pseudo-strain

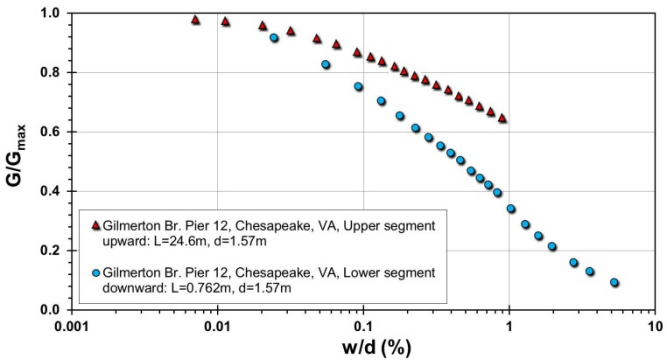

Detail	Description
Pile type/material	Drilled shaft
Length, L (m)	Upper: 24.6; lower: 0.76
Diameter, d (m)	Upper: 1.57; lower: 1.57
Installation method	Bored cast in-situ
Loading mode	O-cell compression
$Q_{max\text{-}measured}$ (kN)	Upper: 8,338.1; lower: 8,338.1
Q_s (kN)	Upper: 8,338.1; lower: 2,841.6
Q_b (kN)	5,496.5
$Q_{Davisson}$ (kN)	Upper: 28,776.9; lower: 5,950.5
$Q_{w/d=10\%}$ (kN)	Upper: 32,092.6; lower: 8,757.7
$Q_{C\text{-}K}$ (kN)	Upper: 35,971.2; lower: 9,259.3

Site ID No. 23

Cone penetrometer data	CPT SBT soil classification index, I_c	Detail	Description
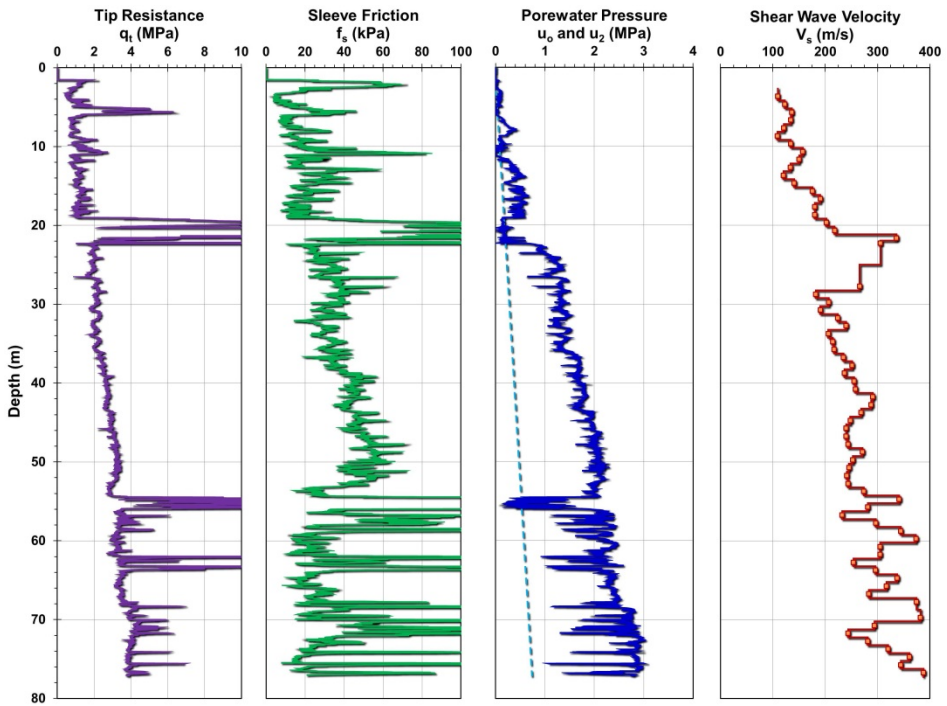	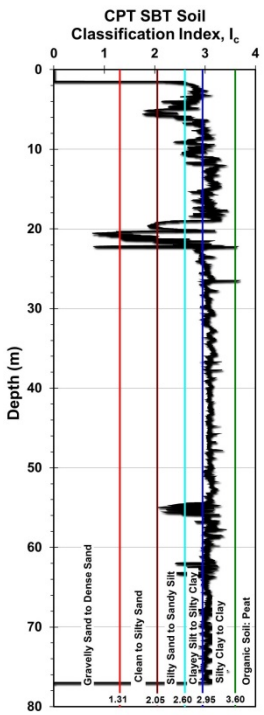	Site name and location	Golden Ears Bridge (GEB) site: (N. Bank), Maple Ridge, BC, Canada
		Soil type(s)	Thick deposits of soft to firm silty clays
		Pile type(s)	Prestressed concrete thin-wall caisson
		Type of cone penetrometer testing	SCPTu
		Source of V_s evaluation	SCPTu
		Number of pile load tests	1
		Reference	Amini et al. (2008), Naesgaard (2008)
		Comments	Shaft capacity obtained through interpretation of available data

Pile ID: GEB N1

Load-displacement data

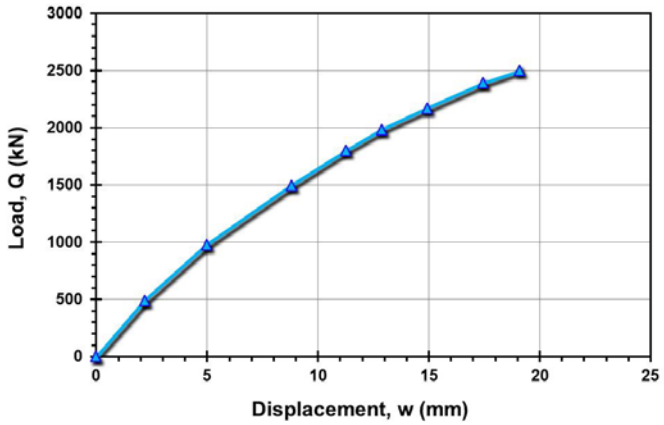

Back-analyzed normalized operational stiffness vs. pseudo-strain

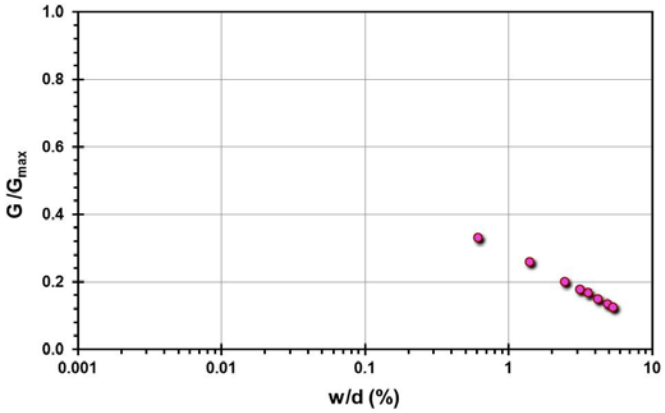

Detail	Description
Pile type/material	Prestressed concrete thin-wall caisson
Length, L (m)	36.00
Diameter, d (m)	0.357
Installation method	Driven
Loading mode	Compression
$Q_{max\text{-}measured}$ (kN)	2,497.96
Q_s (kN)	2,397.96
Q_b (kN)	100.00
$Q_{Davisson}$ (kN)	3,247.35
$Q_{w/d=10\%}$ (kN)	3,357.89
$Q_{C\text{-}K}$ (kN)	5,494.51

Site ID No. 24

Cone penetrometer data	CPT SBT soil classification index, I_c	Detail	Description
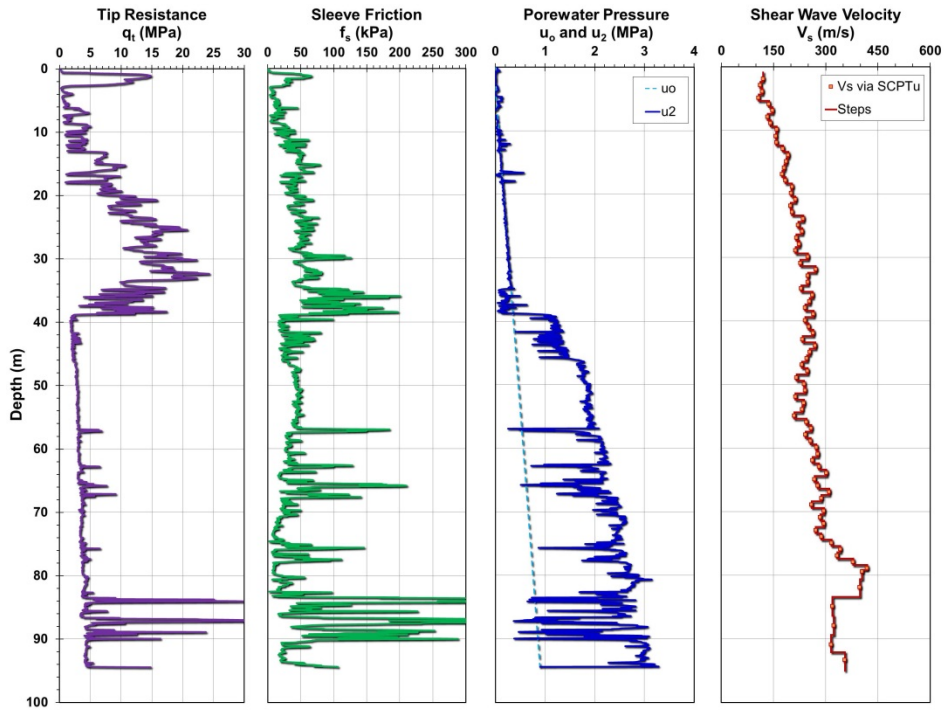	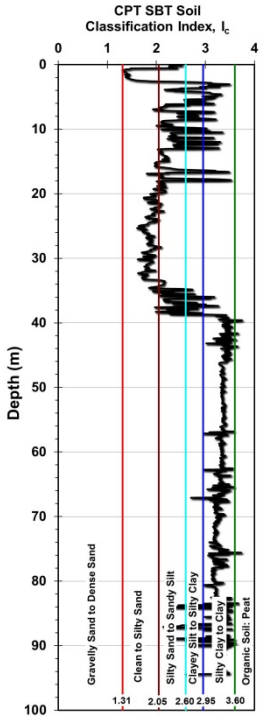	Site name and location	Golden Ears Bridge (GEB) site: (S. Bank), Langley, BC, Canada
		Soil type(s)	Silty sands and silts over dense sand with soft to firm silty clay below 40 m
		Pile type(s)	Drilled shaft
		Type of cone penetrometer testing	SCPTu
		Source of V_s evaluation	SCPTu
		Number of pile load tests	1
		Reference	Amini et al. (2008), Naesgaard (2008)
		Comments	

Pile ID: GEB S1

Load-displacement data

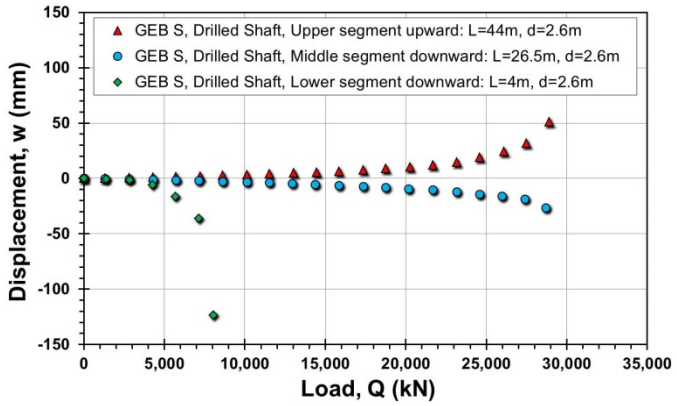

Back-analyzed normalized operational stiffness vs. pseudo-strain

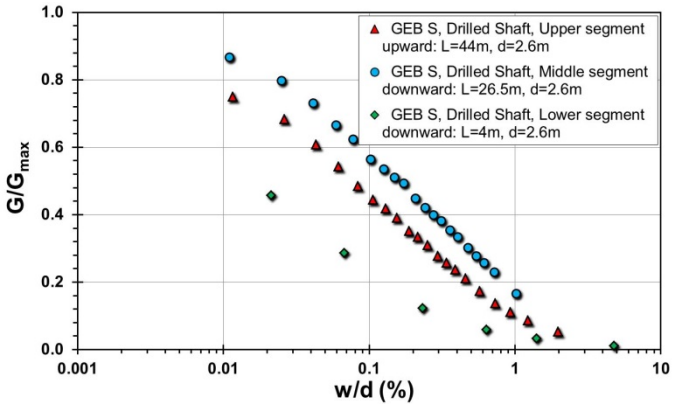

Detail	Description
Pile type/material	Drilled shaft
Length, L (m)	Upper: 44.00; middle: 26.50; lower: 4.00
Diameter, d (m)	Upper: 2.60; middle: 2.60; lower: 2.60
Installation method	Bored cast in-situ
Loading mode	O-cell compression
$Q_{max\text{-}measured}$ (kN)	Upper: 28,900.8; middle: 28,713.1; lower: 8,057.9
Q_s (kN)	Upper: 28,900.8; middle: 28,713.1; lower: 1,068.4
Q_b (kN)	6,989.5
$Q_{Davisson}$ (kN)	Upper: 27,493.3; middle: 28,843.3; lower: 7,013.6
$Q_{w/d=10\%}$ (kN)	Upper: 31,560.3; middle: 32,766.2; lower: 8,253.7
$Q_{C\text{-}K}$ (kN)	Upper: 32,258.0; middle: 33,333.3; lower: 8,474.6

Site ID No. 25

Cone penetrometer data	CPT SBT soil classification index, I_c	Detail	Description
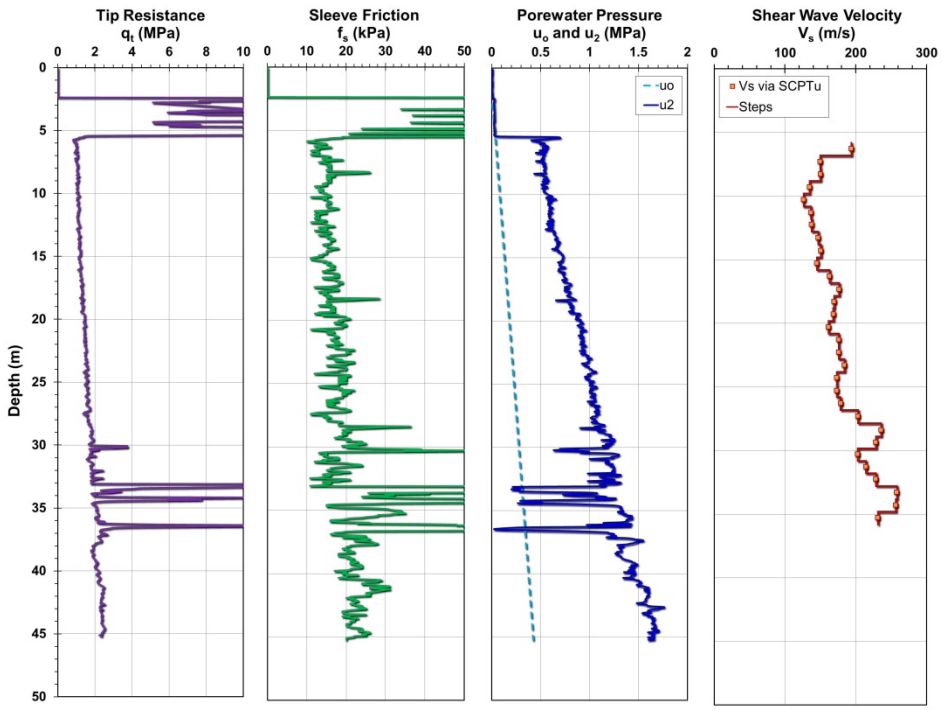	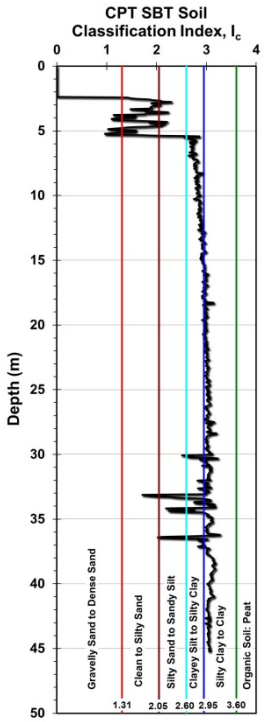	Site name and location	Golden Ears Bridge (GEB) site: (S. Bank), Langley, BC, Canada
		Soil type(s)	Gravelly sand over soft to firm thick silty clays below 6 m
		Pile type(s)	Drilled shaft
		Type of cone penetrometer testing	SCPTu
		Source of V_s evaluation	SCPTu
		Number of pile load tests	1
		Reference	Amini et al. (2008), Naesgaard (2008)
		Comments	Buoyant weight added for base capacity calculations

Pile ID: GEB S1

Load-displacement data

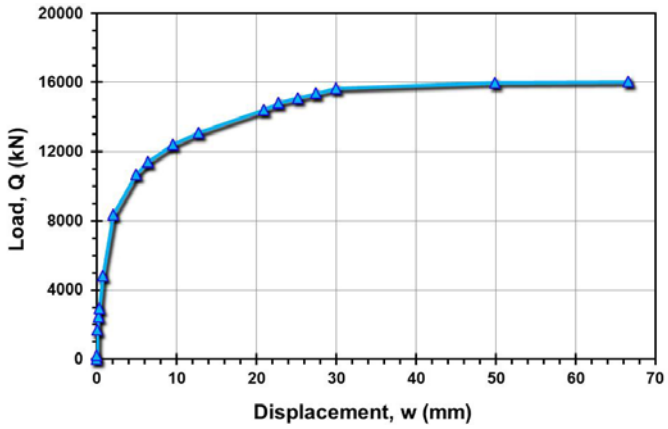

Back-analyzed normalized operational stiffness vs. pseudo-strain

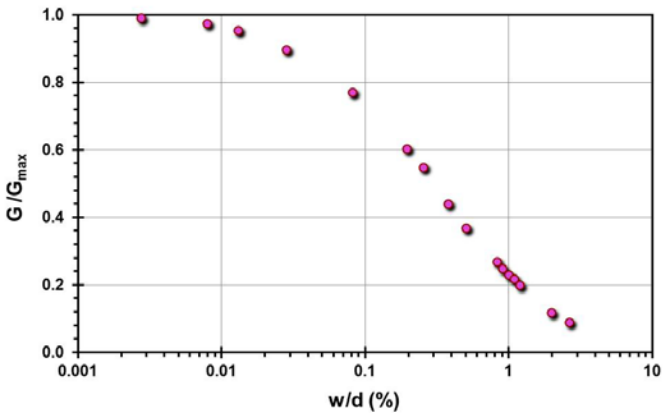

Detail	Description
Pile type/material	Drilled shaft
Length, L (m)	32.00
Diameter, d (m)	2.50
Installation method	Bored cast in-situ
Loading mode	Compression
$Q_{max\text{-}measured}$ (kN)	16,048.10
Q_s (kN)	13,648.1
Q_b (kN)	2,400.00
$Q_{Davisson}$ (kN)	15,356.90
$Q_{w/d=10\%}$ (kN)	16,489.66
$Q_{C\text{-}K}$ (kN)	16,666.67

Site ID No. 26

Cone penetrometer data	CPT SBT soil classification index, I_c	Detail	Description
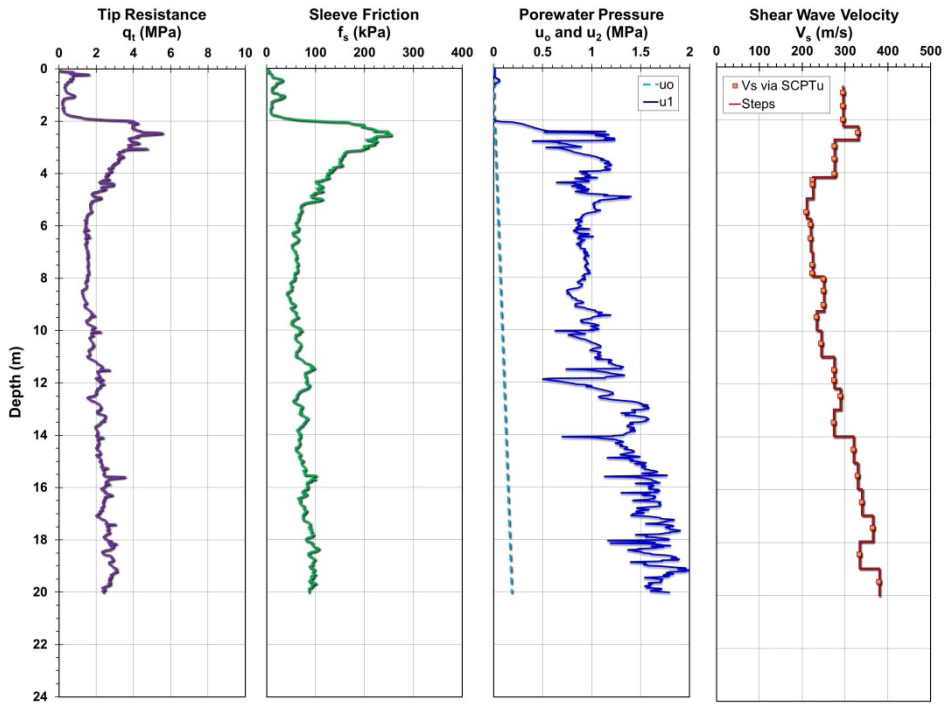	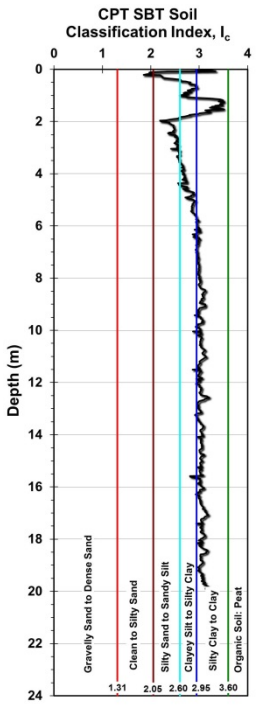	Site name and location	Grimsby Research Site, Waltham, UK
		Soil type(s)	Very stiff gravelly clay till
		Pile type(s)	Drilled shaft
		Type of cone penetrometer testing	SCPTu
		Source of V_s evaluation	SCPTu
		Number of pile load tests	1
		Reference	Brown (2004) and Brown et al. (2006)
		Comments	Measured u_1 reading converted to equivalent u_2

Pile ID: GRS 1

Load-displacement data

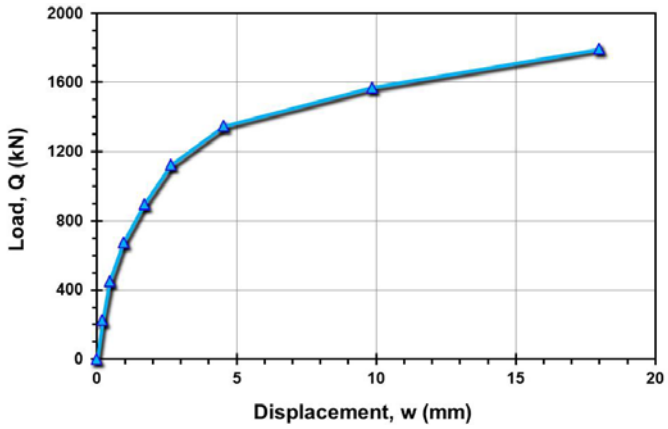

Back-analyzed normalized operational stiffness vs. pseudo-strain

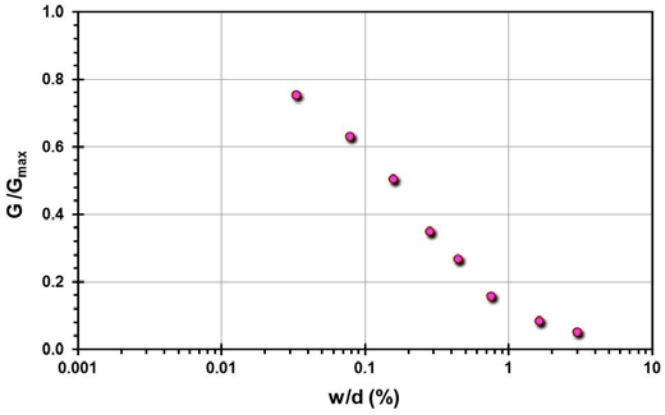

Detail	Description
Pile type/material	Drilled shaft
Length, L (m)	11.76
Diameter, d (m)	0.60
Installation method	Bored cast in-situ
Loading mode	Compression
$Q_{max\text{-}measured}$ (kN)	1,794.23
Q_s (kN)	1,574.72
Q_b (kN)	219.51
$Q_{Davisson}$ (kN)	1,571.10
$Q_{w/d=10\%}$ (kN)	1,950.74
$Q_{C\text{-}K}$ (kN)	2,032.52

Site ID No. 27

Cone penetrometer data	CPT SBT soil classification index, I_c	Detail	Description
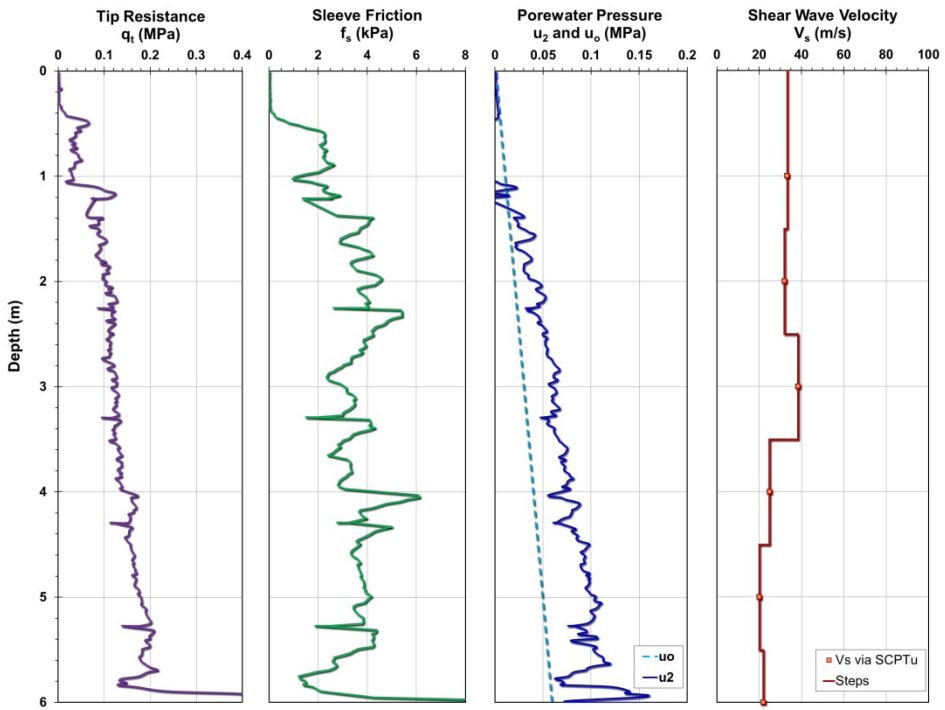	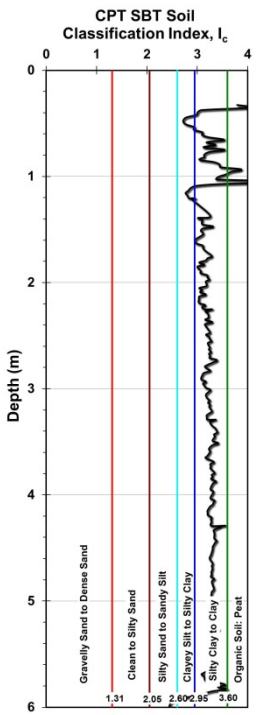	Site name and location	Guanabara Bay, Rio-de-Janeiro, Brazil
		Soil type(s)	Very soft clay
		Pile type(s)	Close-ended steel pipe pile
		Type of cone penetrometer testing	SCPTu
		Source of V_s evaluation	SCPTu
		Number of pile load tests	1
		Reference	Alves et al. (2009)
		Comments	

Pile ID: GBR 1

Load-displacement data

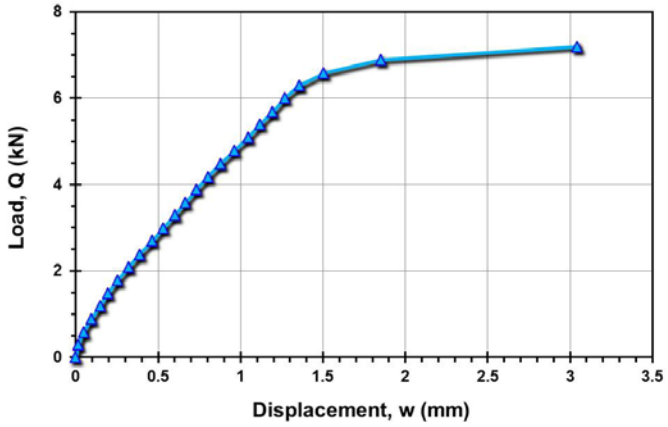

Back-analyzed normalized operational stiffness vs. pseudo-strain

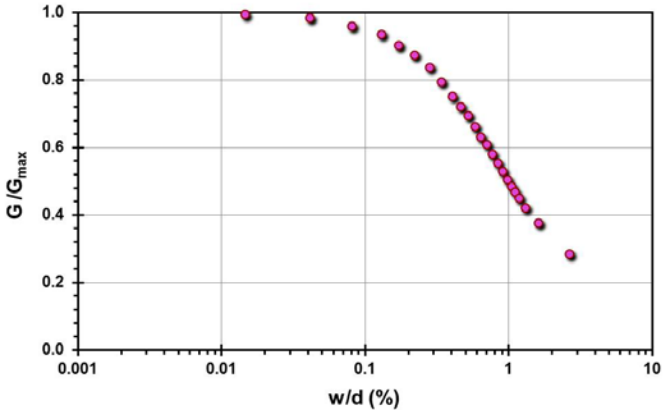

Detail	Description
Pile type/material	Open-ended steel pipe pile
Length, L (m)	4.50
Diameter, d (m)	0.114
Installation method	Driven
Loading mode	Compression
$Q_{max\text{-}measured}$ (kN)	7.20
Q_s (kN)	6.50
Q_b (kN)	0.70
$Q_{Davisson}$ (kN)	7.50
$Q_{w/d=10\%}$ (kN)	7.80
$Q_{C\text{-}K}$ (kN)	8.03

Site ID No. 28

Cone penetrometer data	CPT SBT soil classification index, I_c	Detail	Description
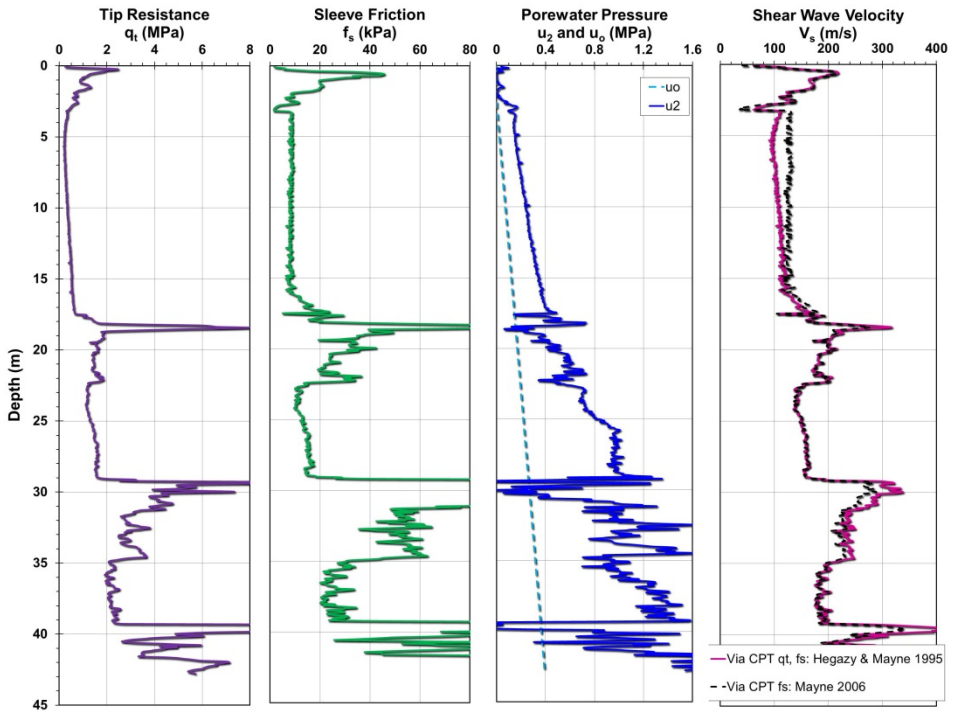	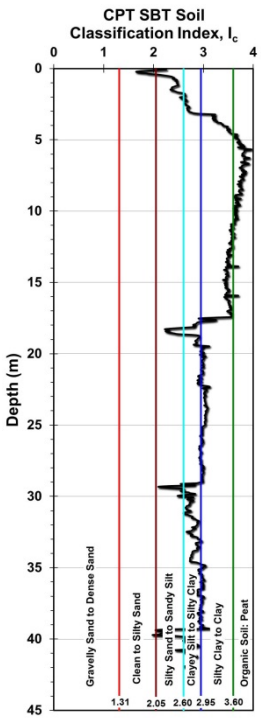	Site name and location	Hamilton Air Force Base, San Francisco, California, USA
		Soil type(s)	Soft silty clay (San Francisco Bay Mud) over stiff clays and silts
		Pile type(s)	Open-ended steel pipe pile
		Type of cone penetrometer testing	CPTu
		Source of V_s evaluation	Correlations (see Figure opposite and Table 3.1)
		Number of pile load tests	1
		Reference	Heydinger & O'Neill (1986), Robertson (2009)
		Comments	Q-z & Q-w data interpreted from f-z curves

Pile ID: HAFB 1

Load-displacement data

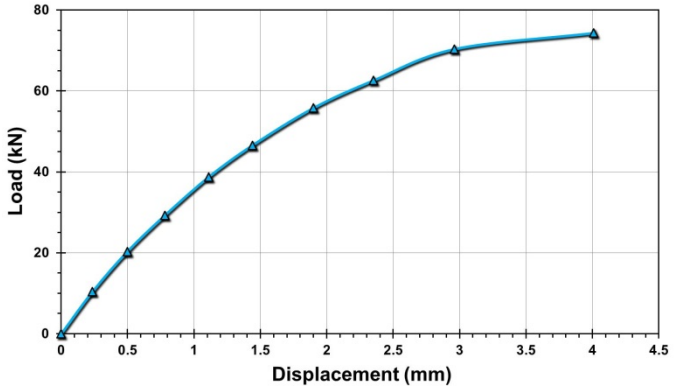

Back-analyzed normalized operational stiffness vs. pseudo-strain

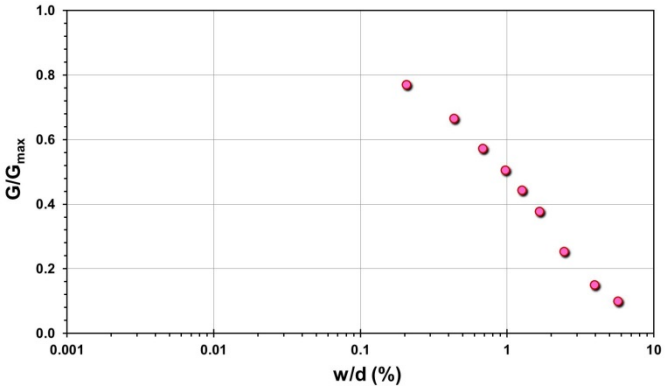

Detail	Description
Pile type/material	Open-ended steel pipe pile
Length, L (m)	12.19
Diameter, d (m)	0.114
Installation method	Jacked
Loading mode	Compression
$Q_{max\text{-}measured}$ (kN)	75.00
Q_s (kN)	69.50
Q_b (kN)	5.50
$Q_{Davisson}$ (kN)	71.95
$Q_{w/d=10\%}$ (kN)	79.50
$Q_{C\text{-}K}$ (kN)	86.15

Site ID No. 29 HPHC1

Cone penetrometer data	CPT SBT soil classification index, I_c	Detail	Description
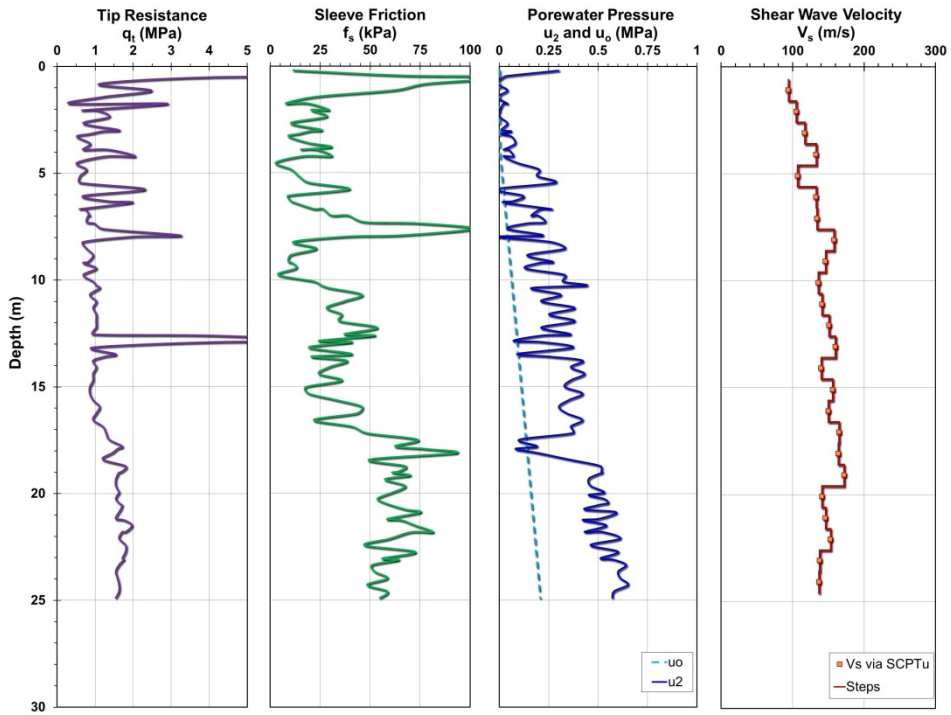	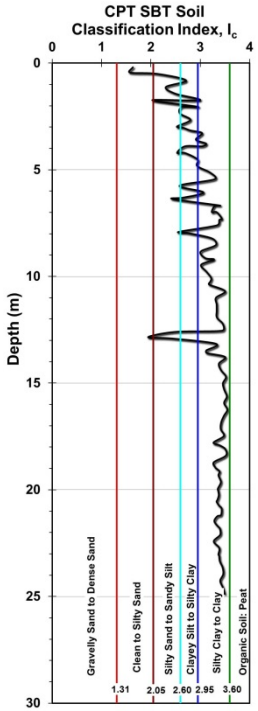	Site name and location	High Prairie Health Complex, Northern Alberta, Canada
		Soil type(s)	Soft to stiff silty clay
		Pile type(s)	Continuous Flight Auger
		Type of cone penetrometer testing	CPTu + SDMT
		Source of V_s evaluation	SDMT
		Number of pile load tests	1
		Reference	Padros and Papanicola (2008), and Cruz et al. (2008)
		Comments	Digital data provided by Ivan Cruz, personal communication

Pile ID: HPHC TP1

Load-displacement data

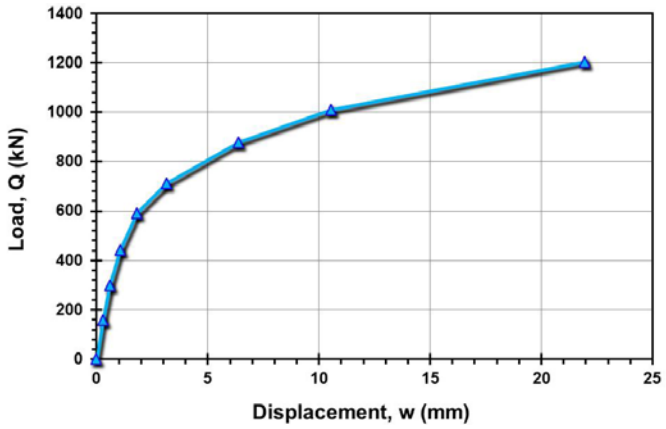

Back-analyzed normalized operational stiffness vs. pseudo-strain

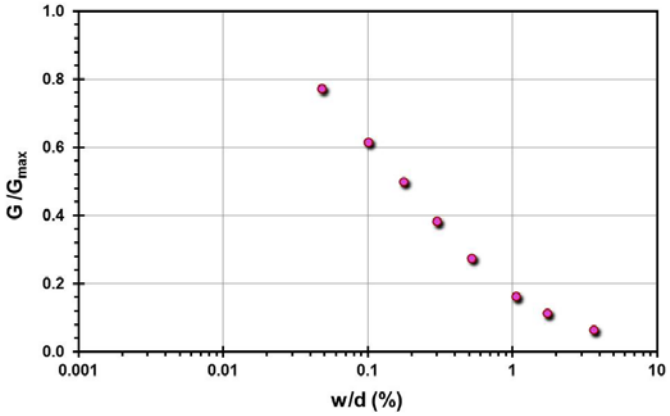

Detail	Description
Pile type/material	Continuous Flight Auger
Length, L (m)	14.00
Diameter, d (m)	0.60
Installation method	Augered
Loading mode	Compression
$Q_{max\text{-}measured}$ (kN)	1,203.81
Q_s (kN)	1,059.32
Q_b (kN)	144.49
$Q_{Davisson}$ (kN)	1,203.81
$Q_{w/d=10\%}$ (kN)	1,335.59
$Q_{C\text{-}K}$ (kN)	1,428.57

Site ID No. 29 HPHC2

Cone penetrometer data	CPT SBT soil classification index, I_c	Detail	Description
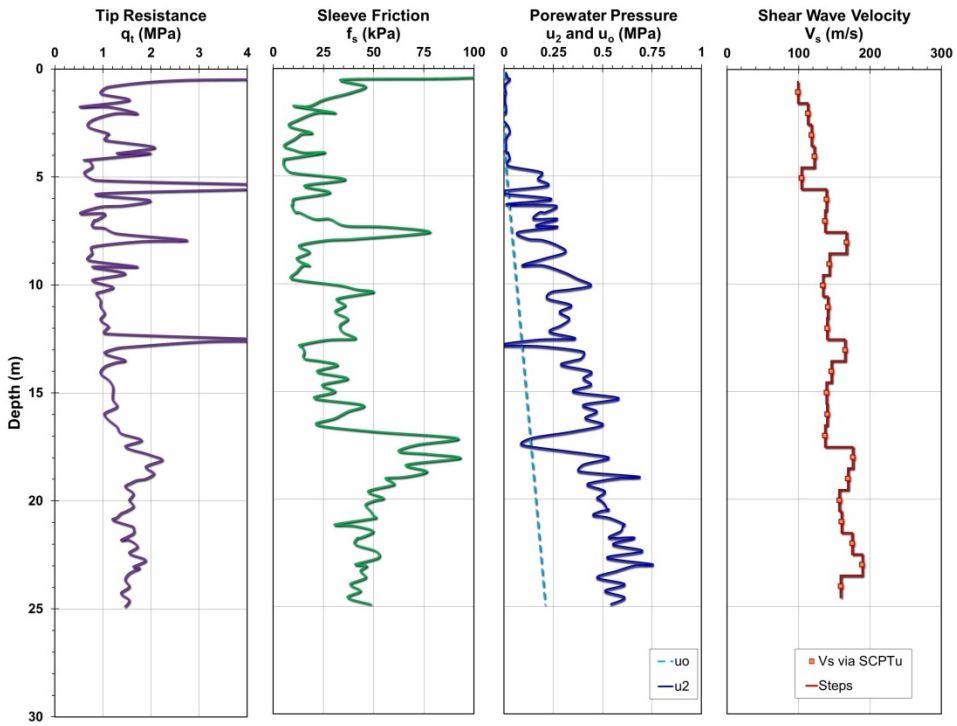	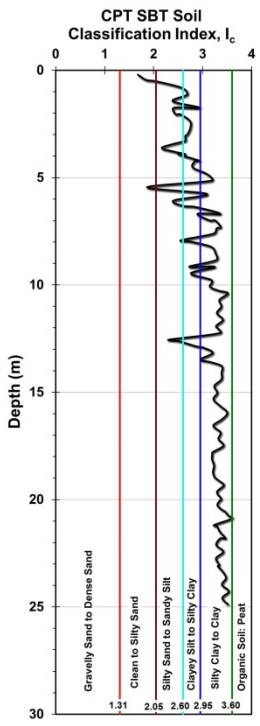	Site name and location	High Prairie Health Complex, Northern Alberta, Canada
		Soil type(s)	Soft to stiff silty clay
		Pile type(s)	Continuous Flight Auger
		Type of cone penetrometer testing	CPTu + SDMT
		Source of V_s evaluation	SDMT
		Number of pile load tests	1
		Reference	Padros and Papanicola (2008), and Cruz et al. (2008)
		Comments	Digital data provided by Ivan Cruz, personal communication

Pile ID: HPHC TP2

Load-displacement data

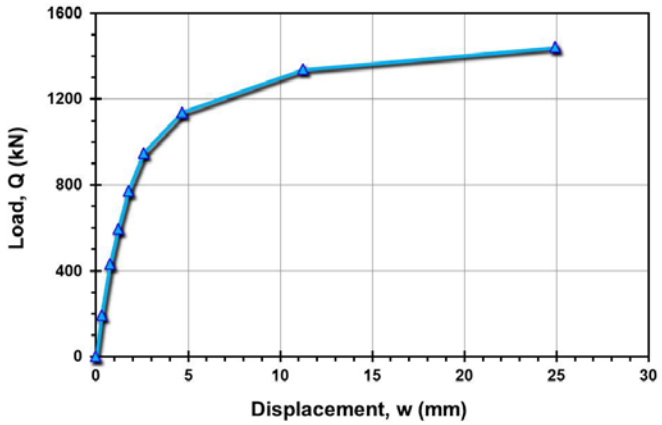

Back-analyzed normalized operational stiffness vs. pseudo-strain

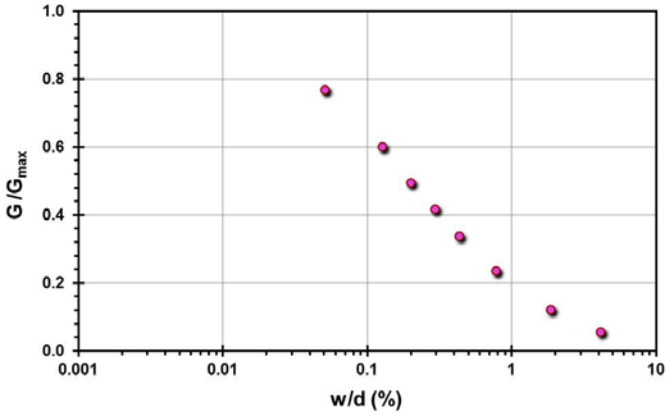

Detail	Description
Pile type/material	Continuous Flight Auger
Length, L (m)	18.00
Diameter, d (m)	0.60
Installation method	Augered
Loading mode	Compression
$Q_{max\text{-}measured}$ (kN)	1,441.95
Q_s (kN)	1,315.5
Q_b (kN)	126.45
$Q_{Davisson}$ (kN)	1,338.61
$Q_{w/d=10\%}$ (kN)	1,495.28
$Q_{C\text{-}K}$ (kN)	1,536.10

Site ID No. 30

Cone penetrometer data	CPT SBT soil classification index, I_c	Detail	Description
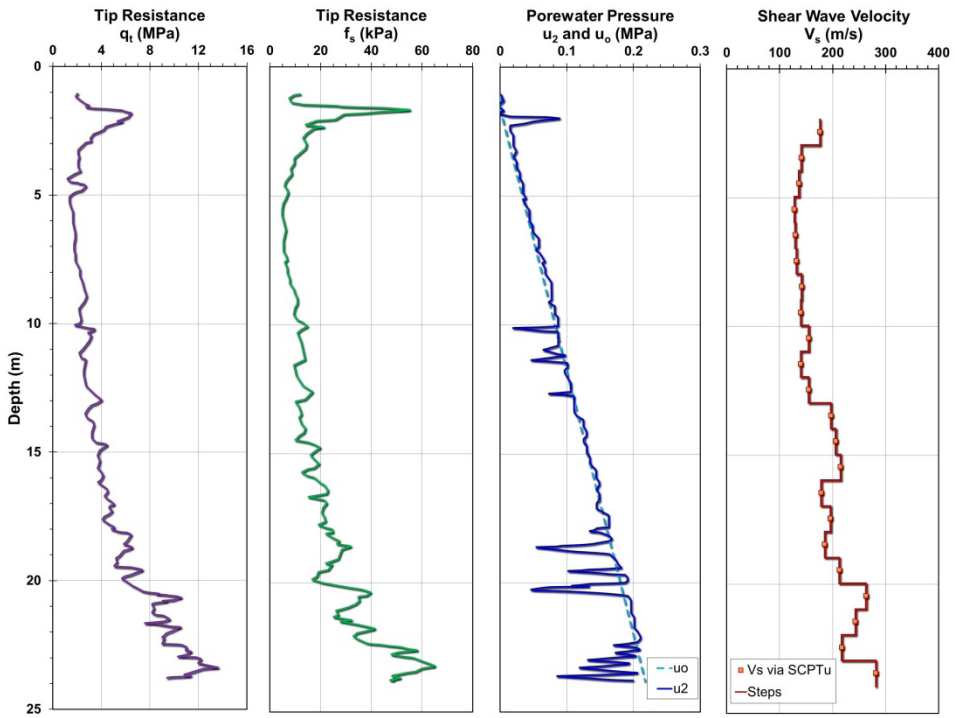	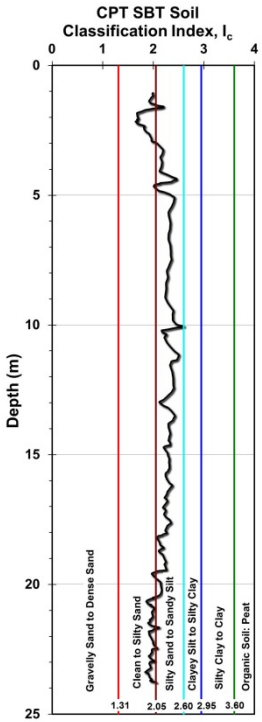	Site name and location	Holmen sand, Drammen, Norway
		Soil type(s)	Loose medium to coarse sand
		Pile type(s)	Circular driven pre-cast concrete pile
		Type of cone penetrometer testing	SCPTu
		Source of V_s evaluation	SCPTu
		Number of pile load tests	11
		Reference	Gregersen et al. (1973), and Lunne et al. (2003)
		Comments	

Pile ID: HSD E1

Load-displacement data

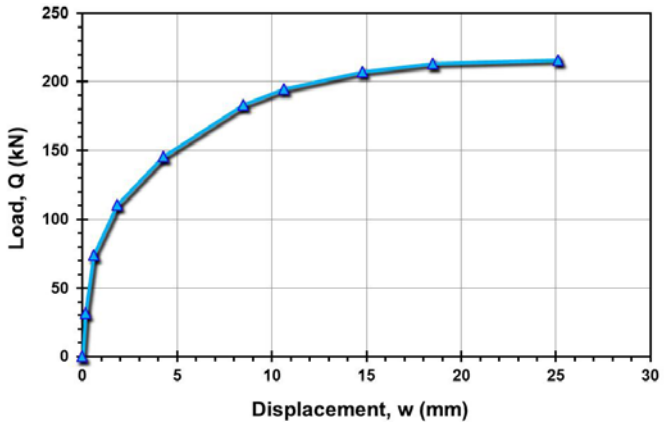

Back-analyzed normalized operational stiffness vs. pseudo-strain

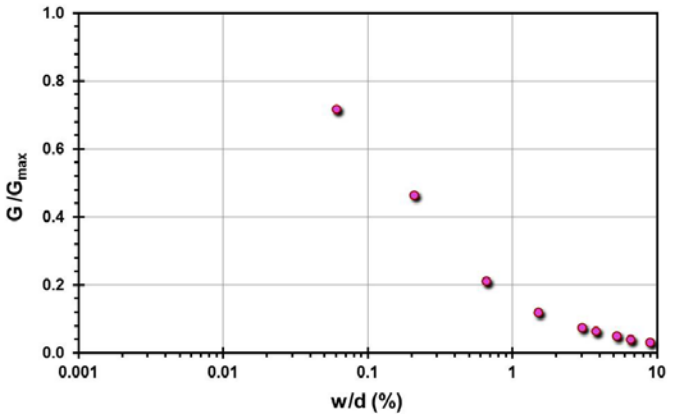

Detail	Description
Pile type/material	Circular driven pre-cast concrete pile
Length, L (m)	3.50
Diameter, d (m)	0.28
Installation method	Driven
Loading mode	Compression
$Q_{max\text{-}measured}$ (kN)	215.94
Q_s (kN)	Not reported
Q_b (kN)	Not reported
$Q_{Davisson}$ (kN)	164.31
$Q_{w/d=10\%}$ (kN)	218.76
$Q_{C\text{-}K}$ (kN)	234.41

Pile ID: HSD E2

Load-displacement data

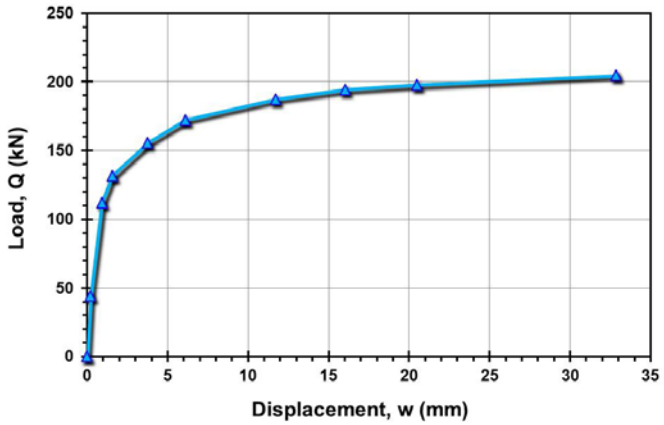

Back-analyzed normalized operational stiffness vs. pseudo-strain

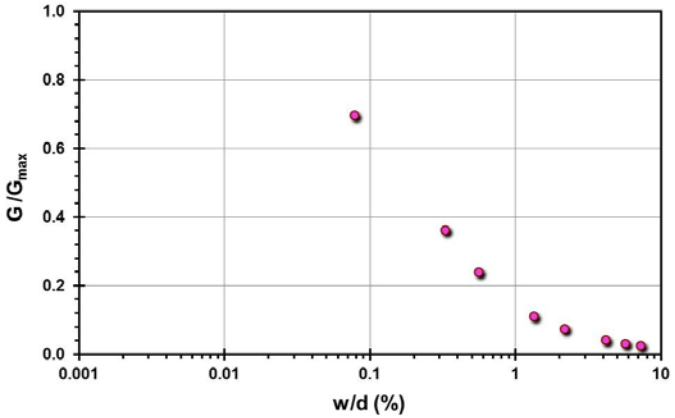

Detail	Description
Pile type/material	Circular driven pre-cast concrete pile
Length, L (m)	7.50
Diameter, d (m)	0.28
Installation method	Driven
Loading mode	Compression
$Q_{max\text{-}measured}$ (kN)	204.52
Q_s (kN)	Not reported
Q_b (kN)	Not reported
$Q_{Davisson}$ (kN)	172.22
$Q_{w/d=10\%}$ (kN)	202.43
$Q_{C\text{-}K}$ (kN)	214.00

Pile ID: HSD E3

Load-displacement data

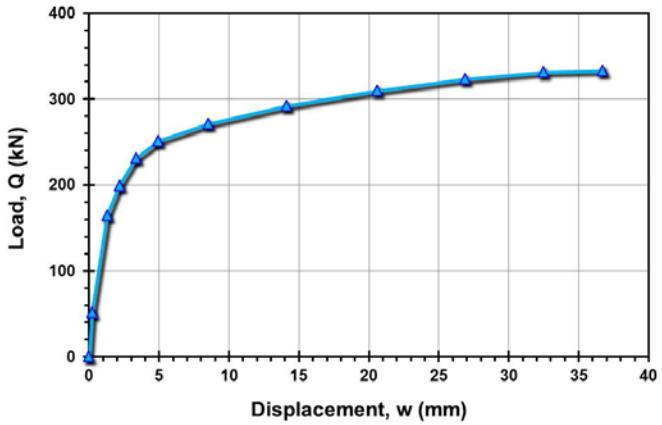

Back-analyzed normalized operational stiffness vs. pseudo-strain

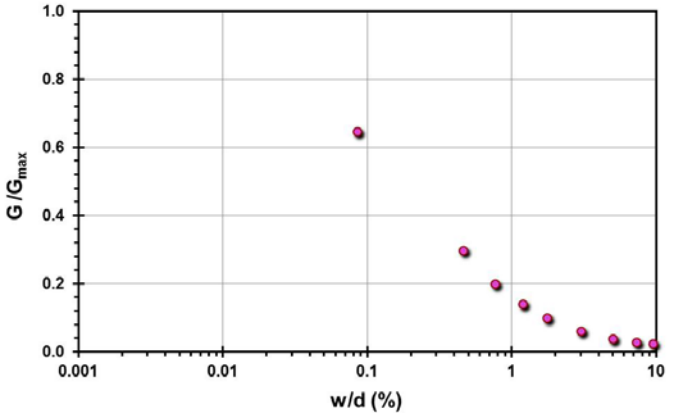

Detail	Description
Pile type/material	Circular driven pre-cast concrete pile
Length, L (m)	11.50
Diameter, d (m)	0.28
Installation method	Driven
Loading mode	Compression
$Q_{max\text{-}measured}$ (kN)	333.45
Q_s (kN)	Not reported
Q_b (kN)	Not reported
$Q_{Davisson}$ (kN)	271.16
$Q_{w/d=10\%}$ (kN)	324.43
$Q_{C\text{-}K}$ (kN)	371.06

Pile ID: HSD E4

Load-displacement data

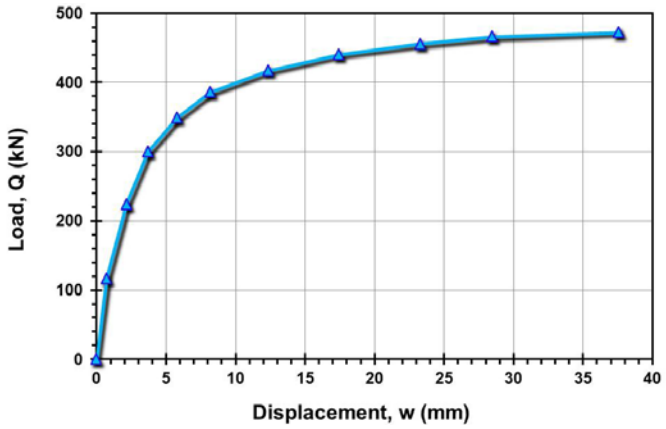

Back-analyzed normalized operational stiffness vs. pseudo-strain

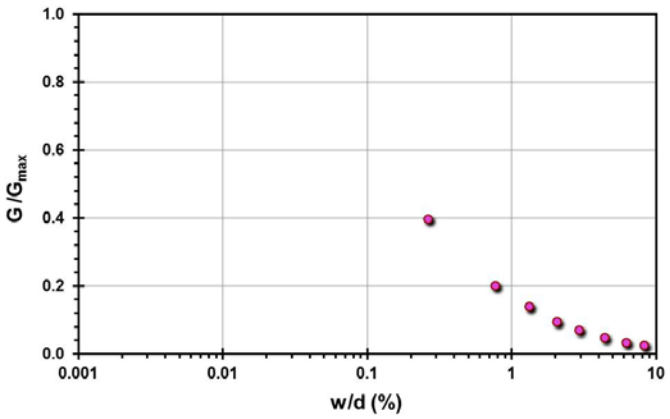

Detail	Description
Pile type/material	Circular driven pre-cast concrete pile
Length, L (m)	15.50
Diameter, d (m)	0.28
Installation method	Driven
Loading mode	Compression
$Q_{max\text{-}measured}$ (kN)	473.09
Q_s (kN)	Not reported
Q_b (kN)	Not reported
$Q_{Davisson}$ (kN)	386.68
$Q_{w/d=10\%}$ (kN)	463.62
$Q_{C\text{-}K}$ (kN)	506.07

Pile ID: HSD E5

Load-displacement data

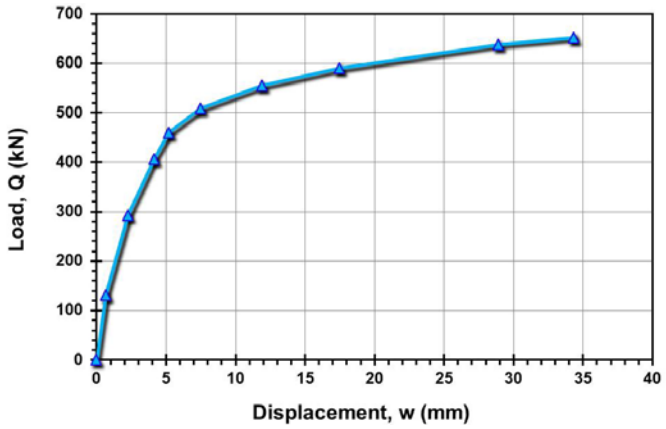

Back-analyzed normalized operational stiffness vs. pseudo-strain

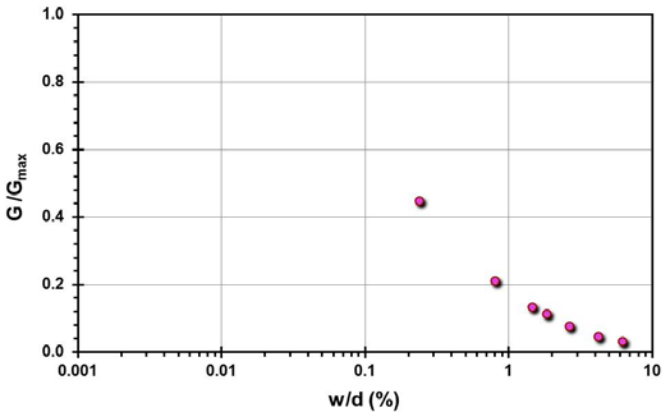

Detail	Description
Pile type/material	Circular driven pre-cast concrete pile
Length, L (m)	19.50
Diameter, d (m)	0.28
Installation method	Driven
Loading mode	Compression
$Q_{max\text{-}measured}$ (kN)	652.51
Q_s (kN)	Not reported
Q_b (kN)	Not reported
$Q_{Davisson}$ (kN)	554.65
$Q_{w/d=10\%}$ (kN)	637.23
$Q_{C\text{-}K}$ (kN)	706.21

Pile ID: HSD E6

Load-displacement data

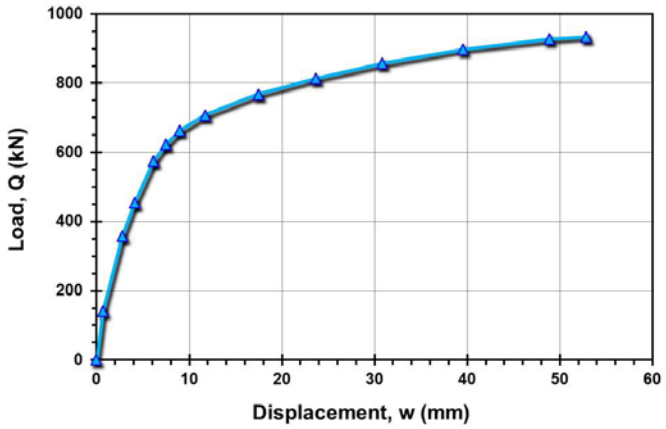

Back-analyzed normalized operational stiffness vs. pseudo-strain

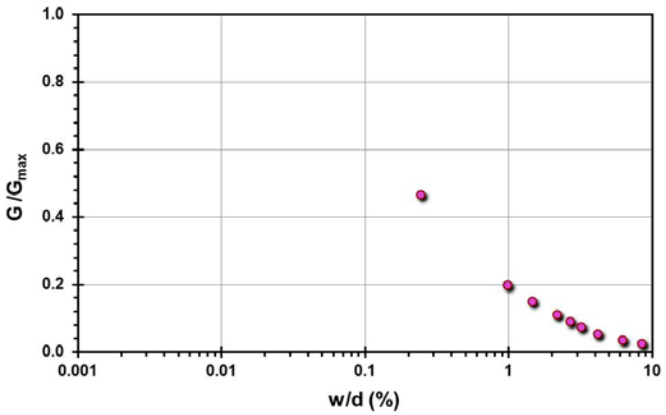

Detail	Description
Pile type/material	Circular driven pre-cast concrete pile
Length, L (m)	23.50
Diameter, d (m)	0.28
Installation method	Driven
Loading mode	Compression
$Q_{max\text{-}measured}$ (kN)	933.93
Q_s (kN)	Not reported
Q_b (kN)	Not reported
$Q_{Davisson}$ (kN)	767.56
$Q_{w/d=10\%}$ (kN)	860.34
$Q_{C\text{-}K}$ (kN)	1,017.29

Pile ID: HSD A1

Load-displacement data

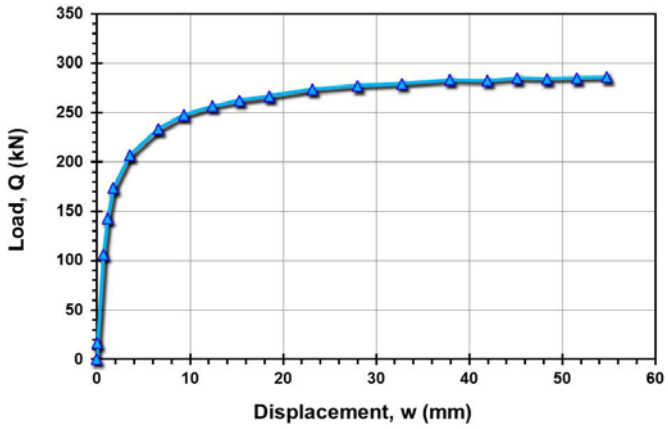

Back-analyzed normalized operational stiffness vs. pseudo-strain

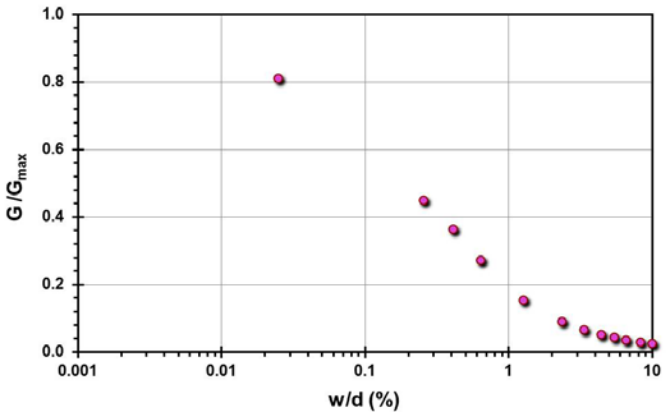

Detail	Description
Pile type/material	Circular driven pre-cast concrete pile
Length, L (m)	8.00
Diameter, d (m)	0.28
Installation method	Driven
Loading mode	Compression
$Q_{max\text{-}measured}$ (kN)	285.78
Q_s (kN)	228.84
Q_b (kN)	56.94
$Q_{Davisson}$ (kN)	233.38
$Q_{w/d=10\%}$ (kN)	276.88
$Q_{C\text{-}K}$ (kN)	295.51

Pile ID: HSD D/A1

Load-displacement data

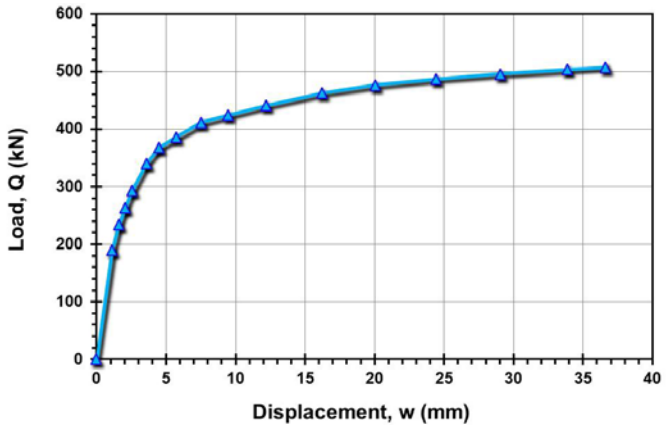

Back-analyzed normalized operational stiffness vs. pseudo-strain

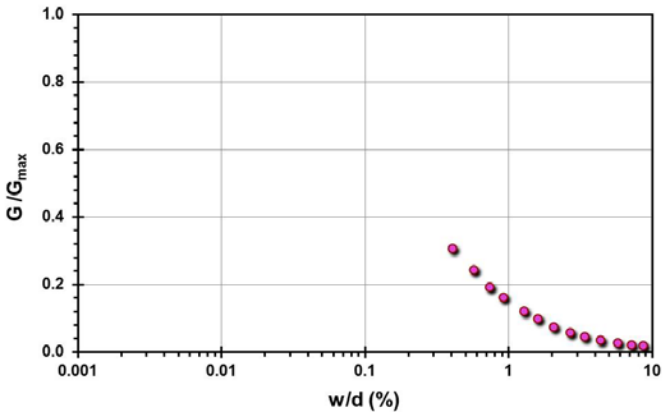

Detail	Description
Pile type/material	Circular driven pre-cast concrete pile
Length, L (m)	16.00
Diameter, d (m)	0.28
Installation method	Driven
Loading mode	Compression
$Q_{max\text{-}measured}$ (kN)	507.25
Q_s (kN)	397.16
Q_b (kN)	110.09
$Q_{Davisson}$ (kN)	423.45
$Q_{w/d=10\%}$ (kN)	494.48
$Q_{C\text{-}K}$ (kN)	534.47

Pile ID: HSD E7

Load-displacement data

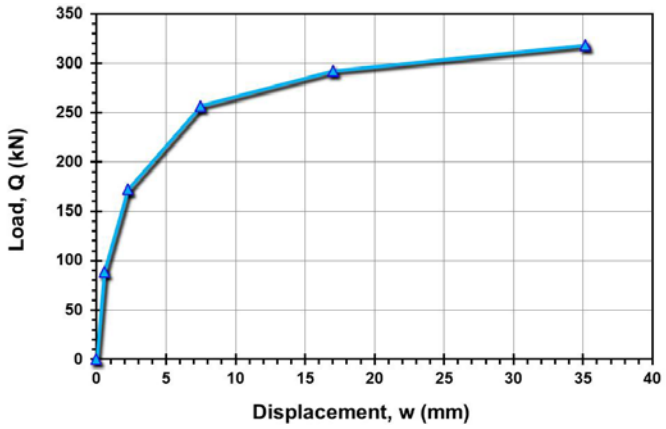

Back-analyzed normalized operational stiffness vs. pseudo-strain

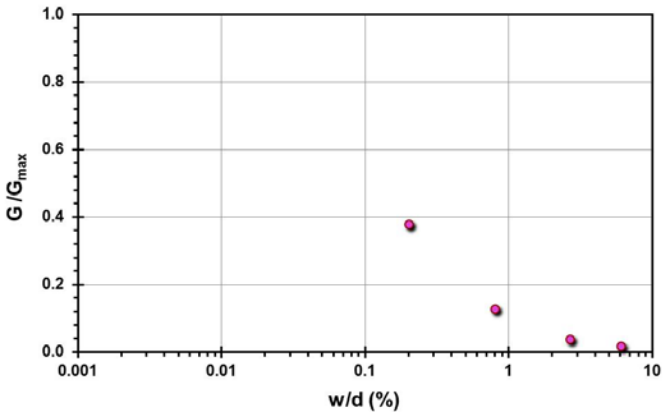

Detail	Description
Pile type/material	Circular driven pre-cast concrete pile
Length, L (m)	23.50
Diameter, d (m)	0.28
Installation method	Driven
Loading mode	Tension
$Q_{max\text{-}measured}$ (kN)	318.16
Q_s (kN)	318.16
Q_b (kN)	-
$Q_{Davisson}$ (kN)	256.51
$Q_{w/d=10\%}$ (kN)	311.73
$Q_{C\text{-}K}$ (kN)	338.41

Pile ID: HSD A2

Load-displacement data

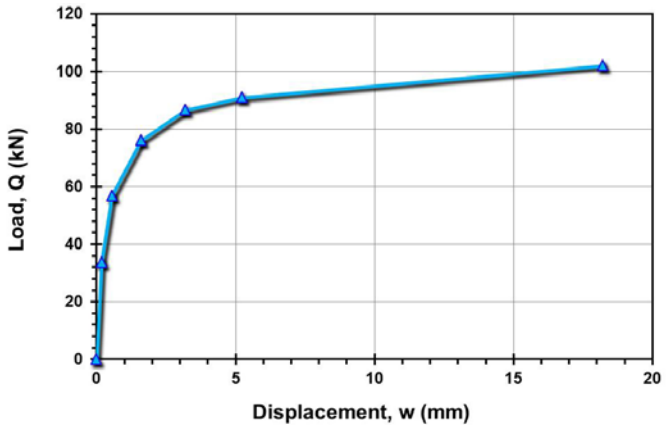

Back-analyzed normalized operational stiffness vs. pseudo-strain

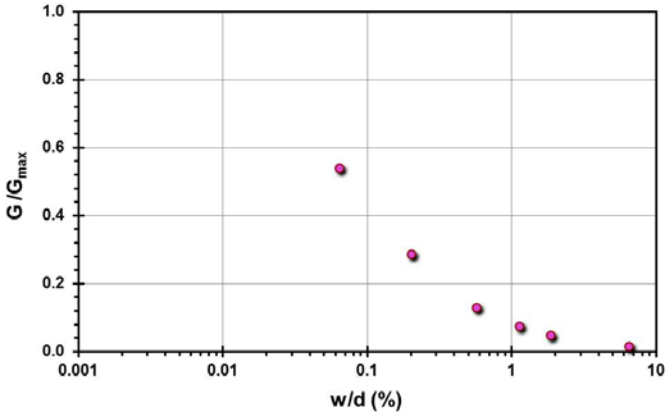

Detail	Description
Pile type/material	Circular driven pre-cast concrete pile
Length, L (m)	8.00
Diameter, d (m)	0.28
Installation method	Driven
Loading mode	Tension
$Q_{max\text{-}measured}$ (kN)	102.08
Q_s (kN)	102.08
Q_b (kN)	-
$Q_{Davisson}$ (kN)	91.00
$Q_{w/d=10\%}$ (kN)	102.96
$Q_{C\text{-}K}$ (kN)	105.37

Pile ID: HSD D/A2

Load-displacement data

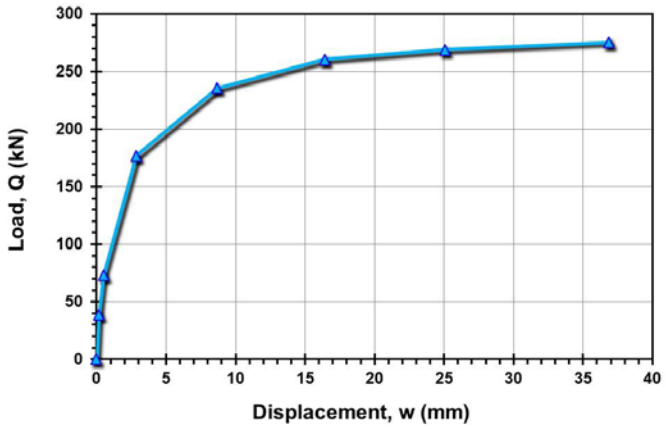

Back-analyzed normalized operational stiffness vs. pseudo-strain

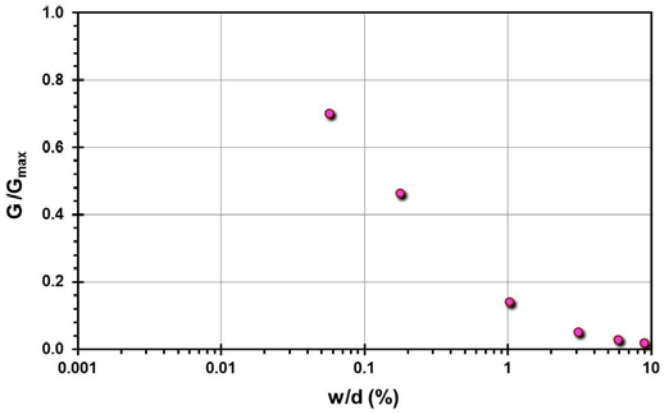

Detail	Description
Pile type/material	Circular driven pre-cast concrete pile
Length, L (m)	16.00
Diameter, d (m)	0.28
Installation method	Driven
Loading mode	Tension
$Q_{max\text{-}measured}$ (kN)	275.22
Q_s (kN)	275.22
Q_b (kN)	-
$Q_{Davisson}$ (kN)	235.17
$Q_{w/d=10\%}$ (kN)	270.98
$Q_{C\text{-}K}$ (kN)	287.52

Site ID No. 31

Cone penetrometer data	CPT SBT soil classification index, I_c	Detail	Description
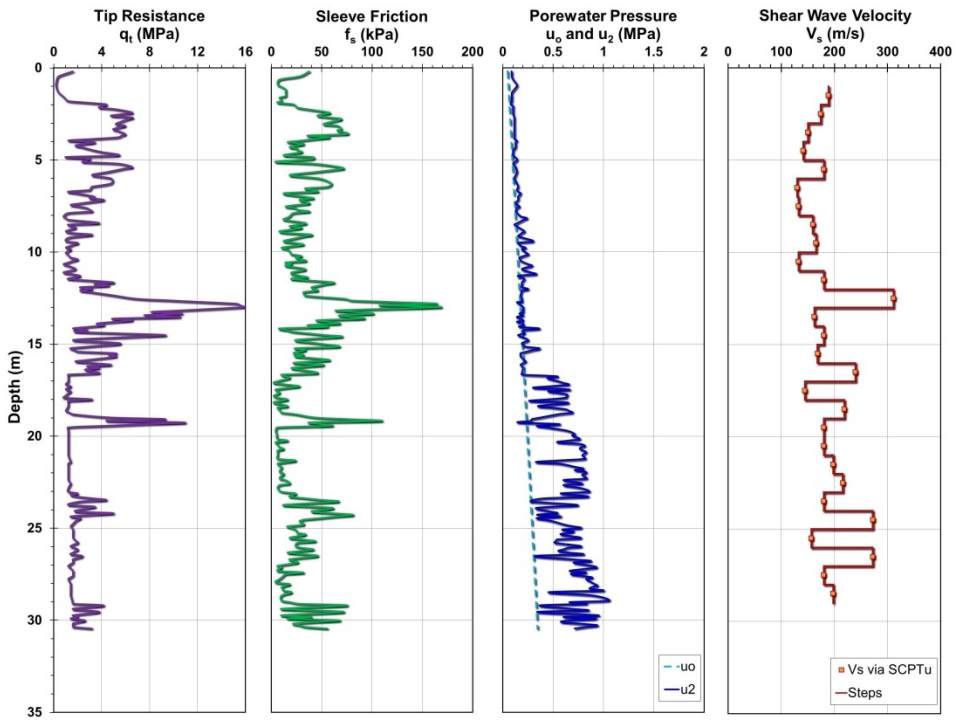	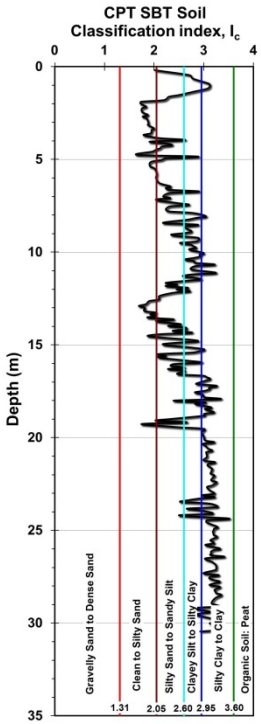	Site name and location	Interactive marine and terrestrial deposits, China
		Soil type(s)	Marine silty-clayey sand
		Pile type(s)	Pre-stressed concrete high-strength (PHC) caisson
		Type of cone penetrometer testing	SCPTu
		Source of V_s evaluation	SCPTu
		Number of pile load tests	1
		Reference	Miao et al. (2011)
		Comments	

Pile ID: IMTDC 1

Load-displacement data

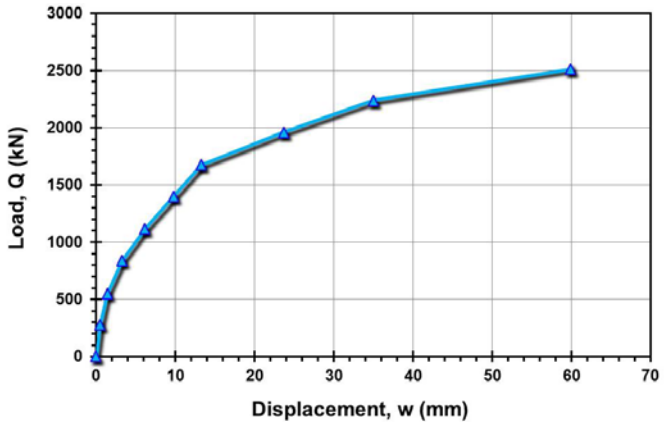

Back-analyzed normalized operational stiffness vs. pseudo-strain

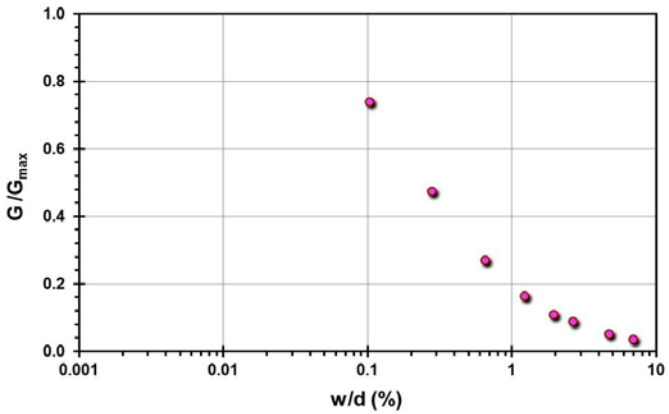

Detail	Description
Pile type/material	Pre-stressed concrete high-strength (PHC) caisson
Length, L (m)	29.00
Diameter, d (m)	0.50
Installation method	Jacked
Loading mode	Compression
$Q_{max\text{-}measured}$ (kN)	2,510.96
Q_s (kN)	Not reported
Q_b (kN)	Not reported
$Q_{Davisson}$ (kN)	1,816.44
$Q_{w/d=10\%}$ (kN)	2,423.10
$Q_{C\text{-}K}$ (kN)	2,958.58

Site ID No. 32

Cone penetrometer data	CPT SBT soil classification index, I_c	Detail	Description
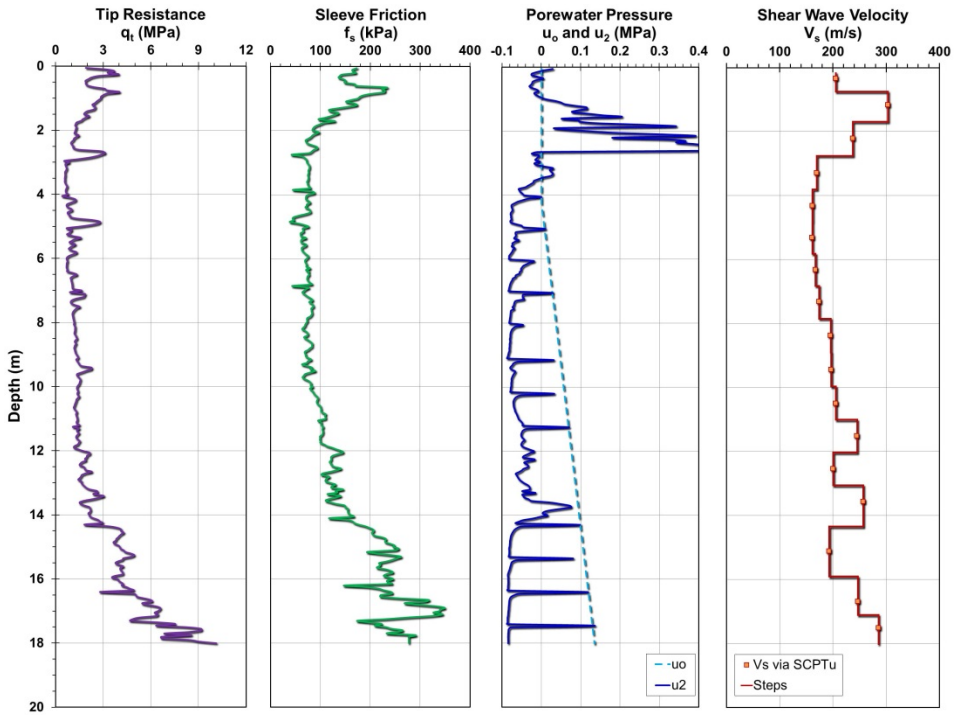	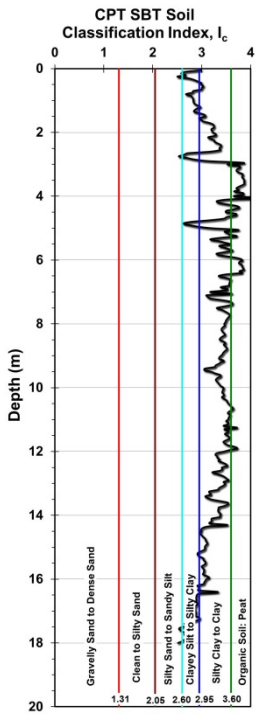	Site name and location	Interstate Highway I-85 Bridge, Newnan, Coweta County, GA, USA
		Soil type(s)	Silty sand to sandy silt overlying partially weathered Gneissic Granite rock
		Pile type(s)	Drilled shaft
		Type of cone penetrometer testing	SCPTu
		Source of V_s evaluation	SCPTu
		Number of pile load tests	1
		Reference	Mayne and Schneider (2001), O'Neill 1998
		Comments	

Pile ID: I-85B 1

Load-displacement data

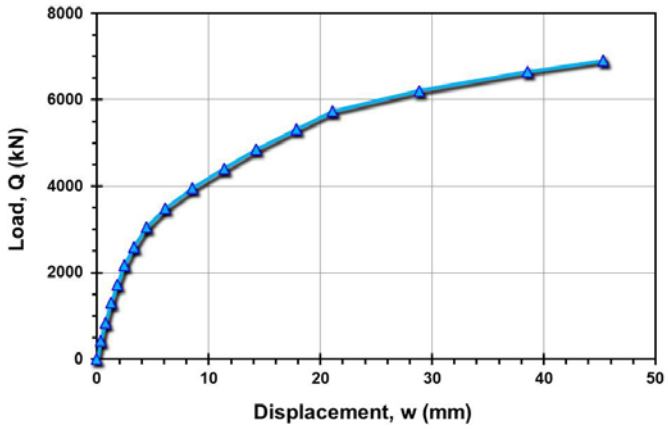

Back-analyzed normalized operational stiffness vs. pseudo-strain

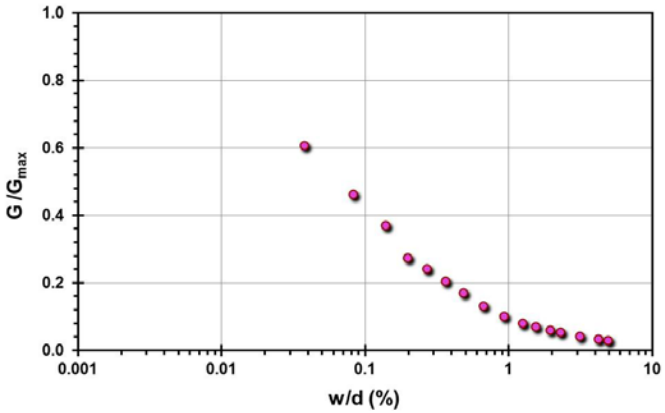

Detail	Description
Pile type/material	Drilled shaft
Length, L (m)	19.20
Diameter, d (m)	0.914
Installation method	Bored cast in-situ
Loading mode	Compression
$Q_{max\text{-}measured}$ (kN)	6,908.35
Q_s (kN)	5,054.13
Q_b (kN)	1,854.22
$Q_{Davisson}$ (kN)	5,314.12
$Q_{w/d=10\%}$ (kN)	7,605.55
$Q_{C\text{-}K}$ (kN)	8,474.58

Site ID No. 33

Cone penetrometer data	CPT SBT soil classification index, I_c	Detail	Description
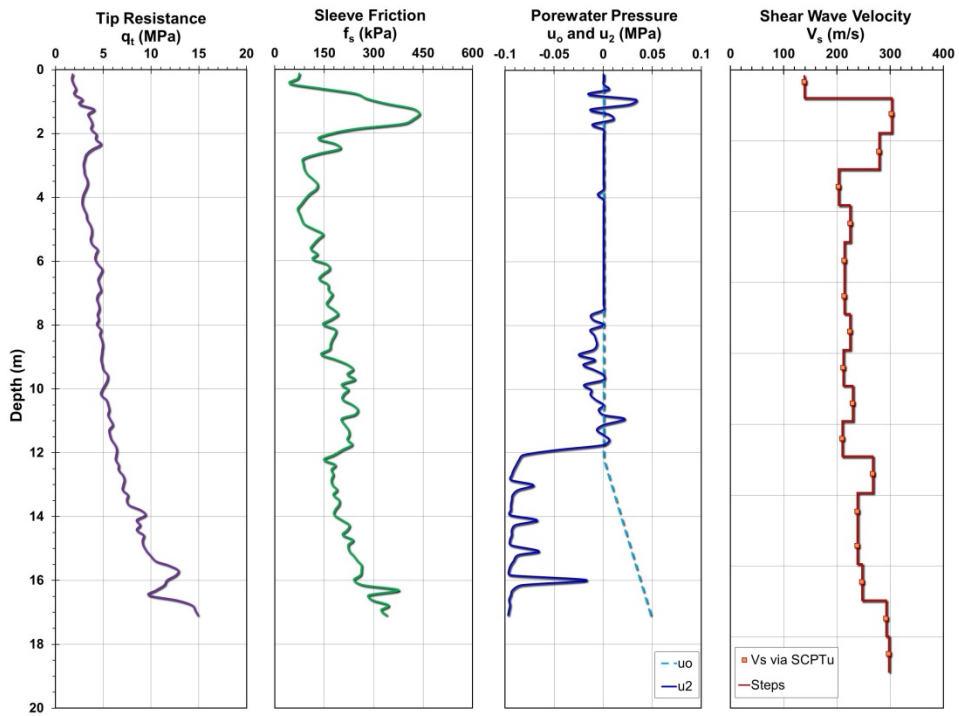	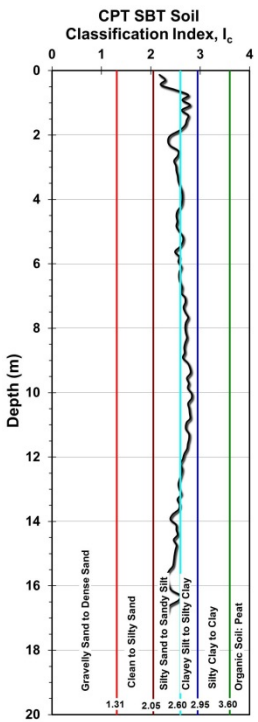	Site name and location	Jackson County Electrical Power Facility, Center, GA, USA
		Soil type(s)	Silty sand to sandy silt of Piedmont residuum over partially weathered schist
		Pile type(s)	Close-ended driven steel pipe piles
		Type of cone penetrometer testing	SCPTu
		Source of V_s evaluation	SCPTu
		Number of pile load tests	1
		Reference	Mayne and Elhakim (2002)
		Comments	

Pile ID: JCEPF 1

Load-displacement data

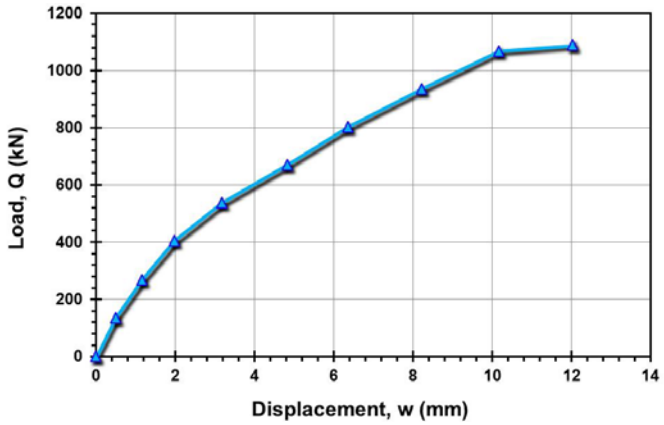

Back-analyzed normalized operational stiffness vs. pseudo-strain

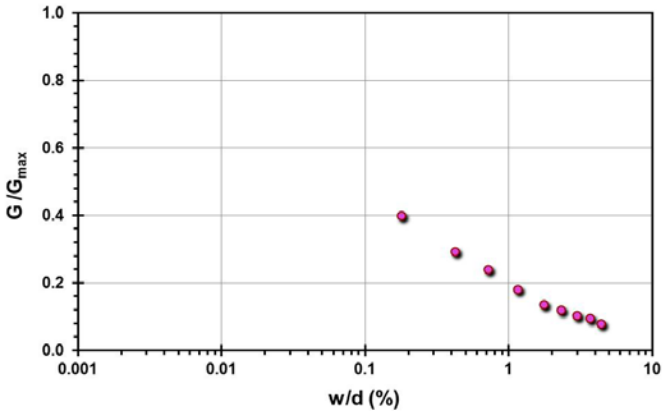

Detail	Description
Pile type/material	Close-ended steel pipe piles
Length, L (m)	9.45
Diameter, d (m)	0.273
Installation method	Driven
Loading mode	Compression
$Q_{max\text{-}measured}$ (kN)	1,087.82
Q_s (kN)	-
Q_b (kN)	-
$Q_{Davisson}$ (kN)	1,087.82
$Q_{w/d=10\%}$ (kN)	1,154.57
$Q_{C\text{-}K}$ (kN)	1,213.59

Pile ID: JCEPF 2

Load-displacement data

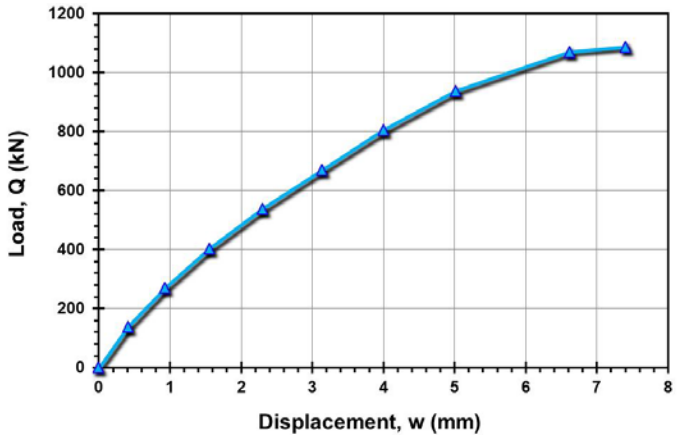

Back-analyzed normalized operational stiffness vs. pseudo-strain

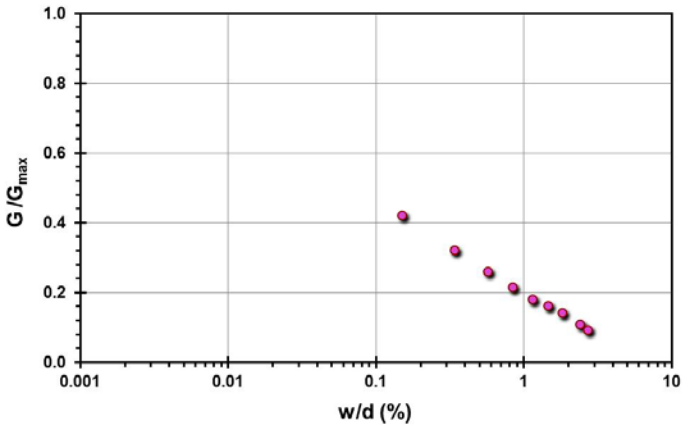

Detail	Description
Pile type/material	Close-ended steel pipe piles
Length, L (m)	17.80
Diameter, d (m)	0.273
Installation method	Driven
Loading mode	Compression
$Q_{max\text{-}measured}$ (kN)	1,087.82
Q_s (kN)	-
Q_b (kN)	-
$Q_{Davisson}$ (kN)	1,146.26
$Q_{w/d=10\%}$ (kN)	1,205.33
$Q_{C\text{-}K}$ (kN)	1,256.28

Site ID No. 34

Cone penetrometer data	CPT SBT soil classification index, I_c	Detail	Description
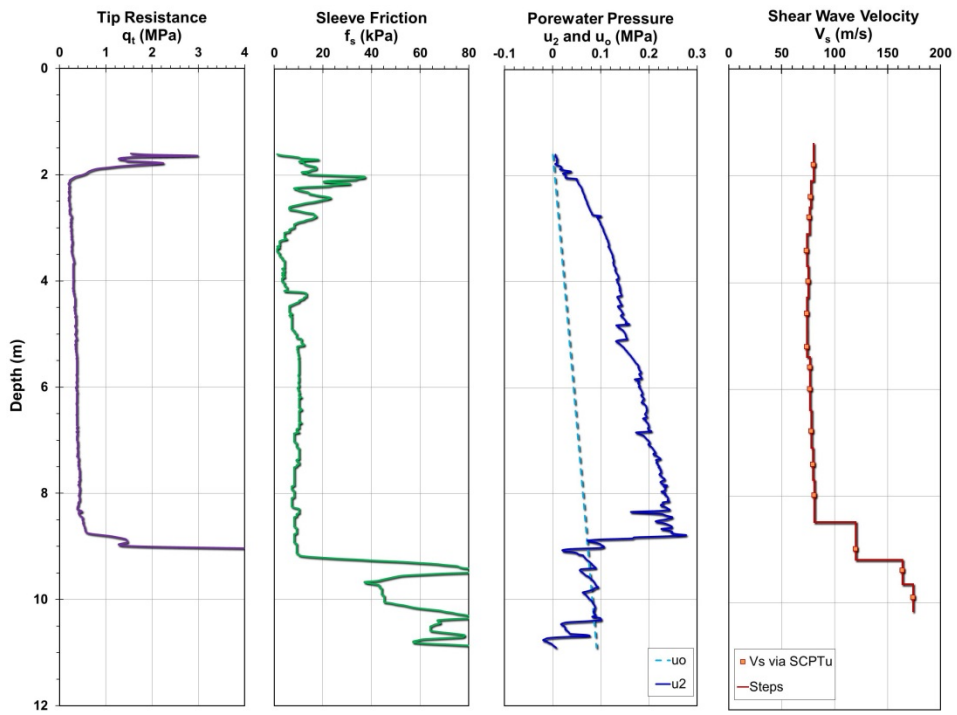	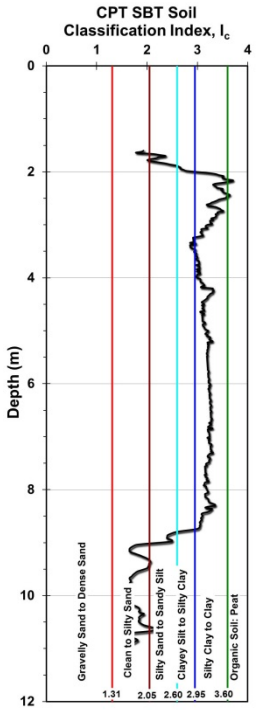	Site name and location	Kinnegar site near Belfast Lough in Northern Ireland
		Soil type(s)	Soft organic clayey silt ("sleech")
		Pile type(s)	7 Square concrete pile, 1 open-ended steel pipe pile, 2 closed-ended steel pipe pile
		Type of cone penetrometer testing	SCPTu
		Source of V_s evaluation	SCPTu
		Number of pile load tests	1
		Reference	McCabe & Lehane (2006), Doherty & Gavin (2011a, b), Lehane et al. (2000)
		Comments	

Pile ID: KG S2T

Load-displacement data

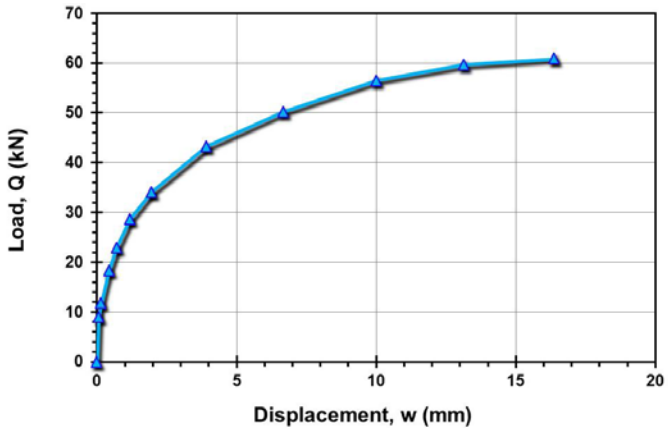

Back-analyzed normalized operational stiffness vs. pseudo-strain

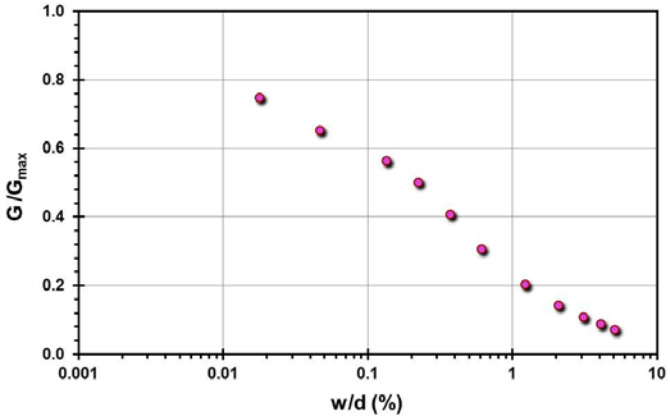

Detail	Description
Pile type/material	Square concrete pile
Length, L (m)	6.00
Width, B (m)	0.32
Installation method	Driven
Loading mode	Tension
$Q_{max\text{-}measured}$ (kN)	60.87
Q_s (kN)	60.87
Q_b (kN)	-
$Q_{Davisson}$ (kN)	50.19
$Q_{w/d=10\%}$ (kN)	65.84
$Q_{C\text{-}K}$ (kN)	71.42

Pile ID: KG S1C

Load-displacement data

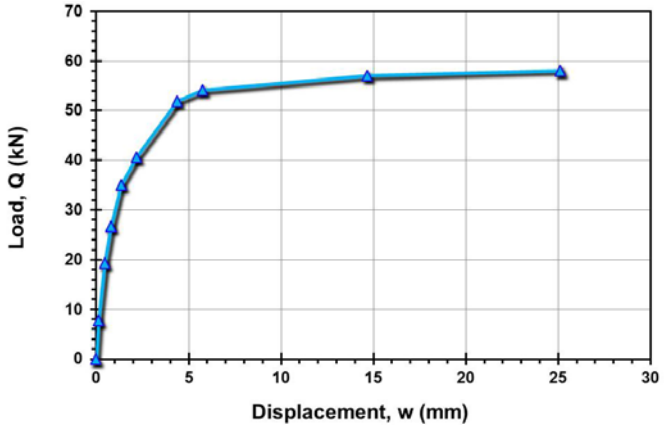

Back-analyzed normalized operational stiffness vs. pseudo-strain

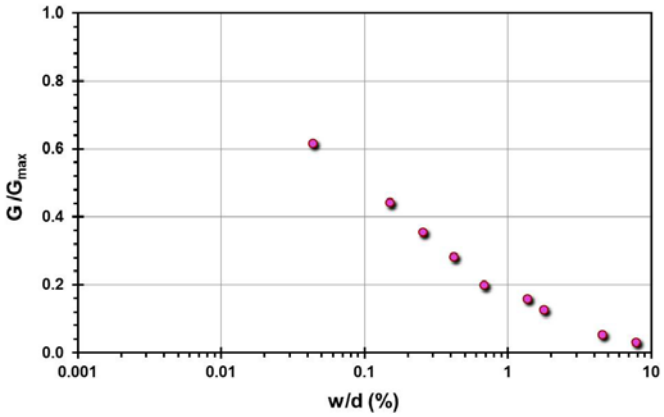

Detail	Description
Pile type/material	Square concrete pile
Length, L (m)	6.00
Width, B (m)	0.32
Installation method	Driven
Loading mode	Compression
$Q_{max\text{-}measured}$ (kN)	58.07
Q_s (kN)	42.44
Q_b (kN)	15.63
$Q_{Davisson}$ (kN)	54.03
$Q_{w/d=10\%}$ (kN)	58.36
$Q_{C\text{-}K}$ (kN)	59.48

Pile ID: KG G3C

Load-displacement data

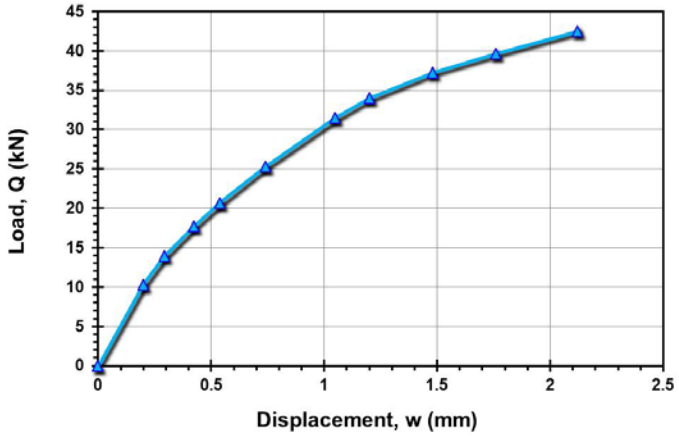

Back-analyzed normalized operational stiffness vs. pseudo-strain

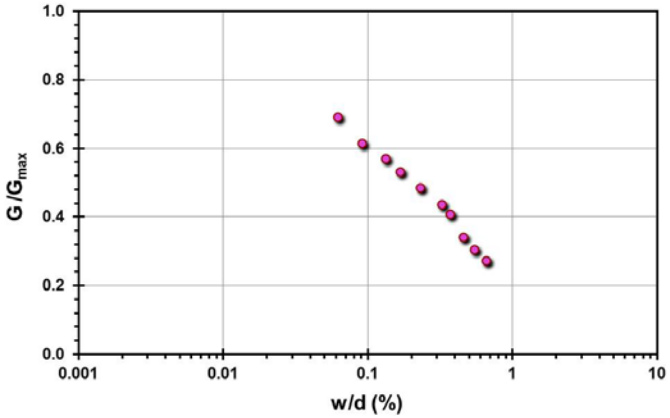

Detail	Description
Pile type/material	Square concrete pile
Length, L (m)	6.00
Width, B (m)	0.32
Installation method	Driven
Loading mode	Compression
$Q_{max\text{-}measured}$ (kN)	42.50
Q_s (kN)	Not reported
Q_b (kN)	Not reported
$Q_{Davisson}$ (kN)	53.26
$Q_{w/d=10\%}$ (kN)	64.02
$Q_{C\text{-}K}$ (kN)	66.35

Pile ID: KG G1crT(r)

Load-displacement data

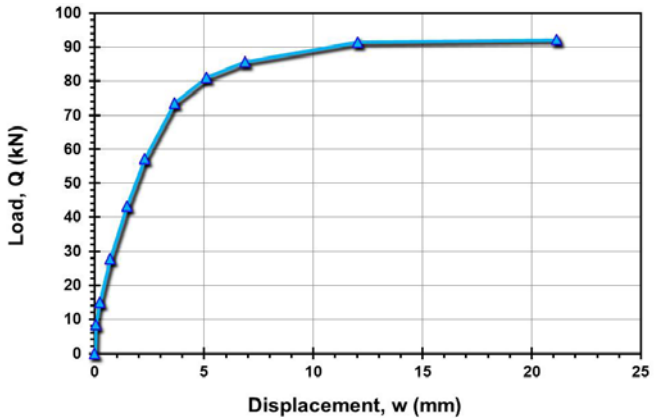

Back-analyzed normalized operational stiffness vs. pseudo-strain

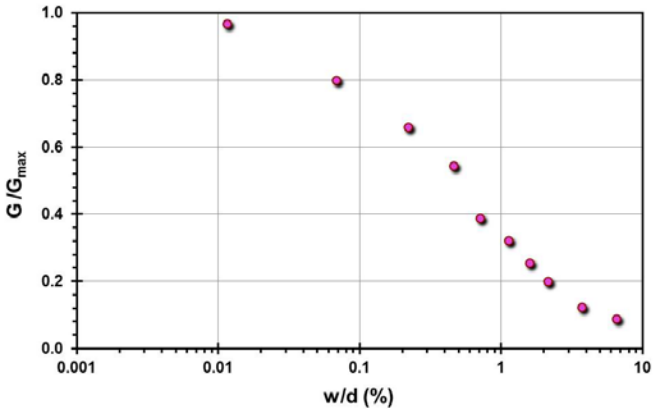

Detail	Description
Pile type/material	Square concrete pile
Length, L (m)	6.00
Width, B (m)	0.32
Installation method	Driven
Loading mode	Tension
$Q_{max\text{-}measured}$ (kN)	92.16
Q_s (kN)	Not reported
Q_b (kN)	Not reported
$Q_{Davisson}$ (kN)	85.65
$Q_{w/d=10\%}$ (kN)	93.77
$Q_{C\text{-}K}$ (kN)	96.24

Pile ID: KG S4T

Load-displacement data

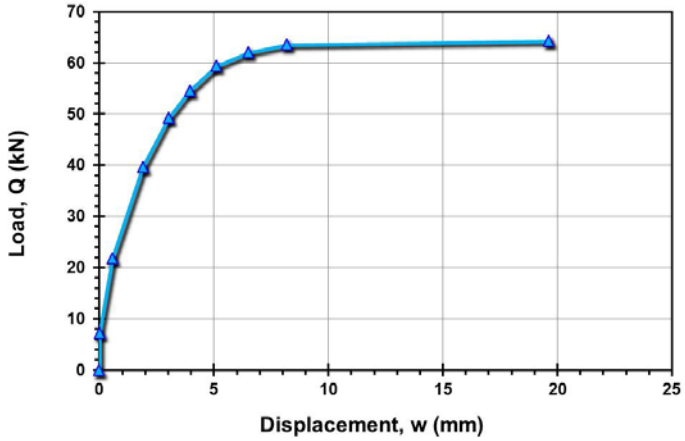

Back-analyzed normalized operational stiffness vs. pseudo-strain

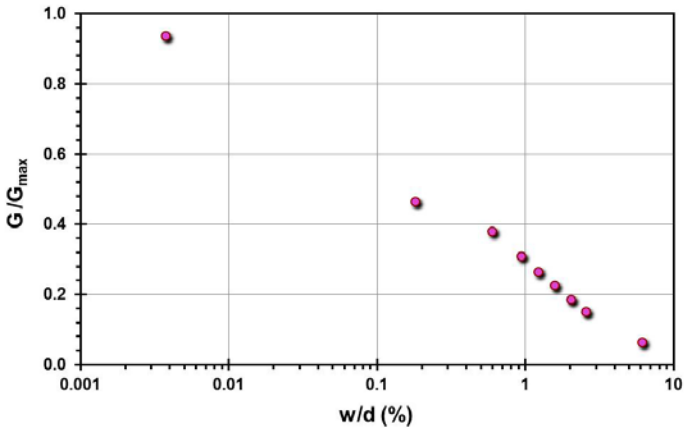

Detail	Description
Pile type/material	Square concrete pile
Length, L (m)	6.00
Width, B (m)	0.32
Installation method	Driven
Loading mode	Tension
$Q_{max\text{-}measured}$ (kN)	64.28
Q_s (kN)	64.28
Q_b (kN)	-
$Q_{Davisson}$ (kN)	62.03
$Q_{w/d=10\%}$ (kN)	64.65
$Q_{C\text{-}K}$ (kN)	65.21

Pile ID: KG S4T(r)

Load-displacement data

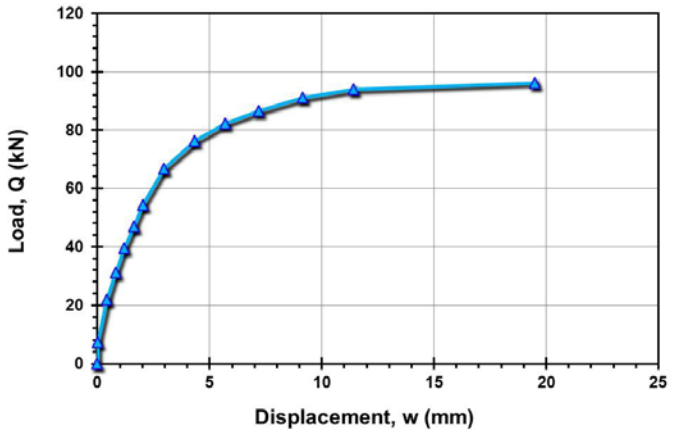

Back-analyzed normalized operational stiffness vs. pseudo-strain

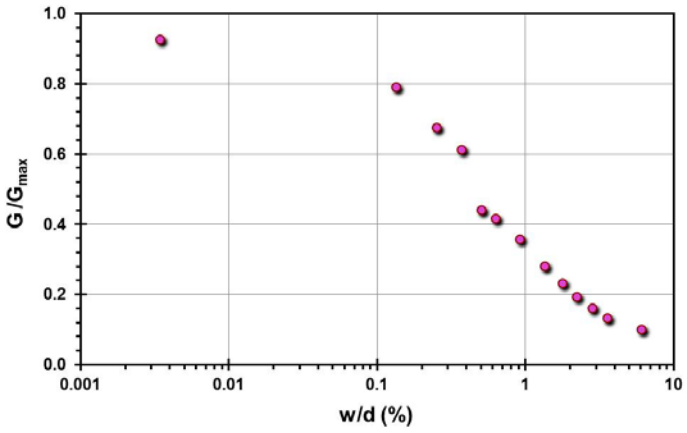

Detail	Description
Pile type/material	Square concrete pile
Length, L (m)	6.00
Width, B (m)	0.32
Installation method	Driven
Loading mode	Tension
$Q_{max\text{-}measured}$ (kN)	96.20
Q_s (kN)	96.20
Q_b (kN)	-
$Q_{Davisson}$ (kN)	86.50
$Q_{w/d=10\%}$ (kN)	99.84
$Q_{C\text{-}K}$ (kN)	104.62

Pile ID: KG S1T

Load-displacement data

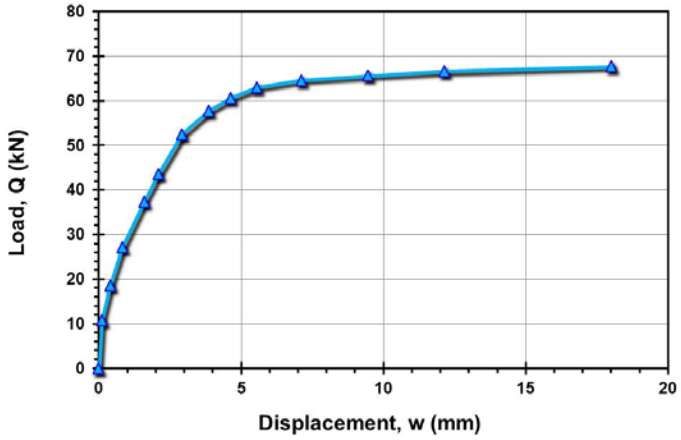

Back-analyzed normalized operational stiffness vs. pseudo-strain

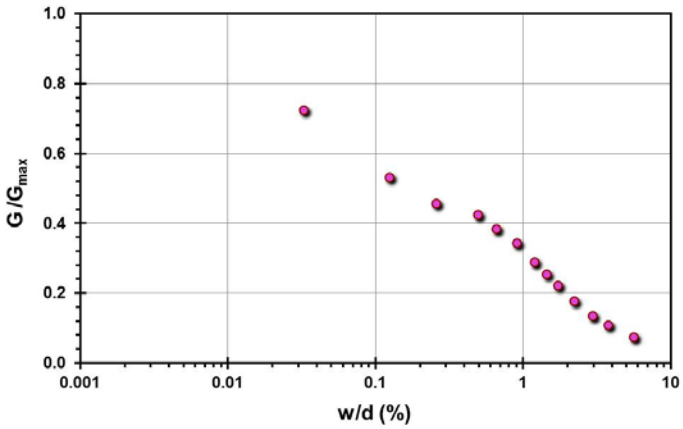

Detail	Description
Pile type/material	Square concrete pile
Length, L (m)	6.00
Width, B (m)	0.32
Installation method	Driven
Loading mode	Tension
$Q_{max\text{-}measured}$ (kN)	67.65
Q_s (kN)	67.65
Q_b (kN)	-
$Q_{Davisson}$ (kN)	64.60
$Q_{w/d=10\%}$ (kN)	69.30
$Q_{C\text{-}K}$ (kN)	71.12

Pile ID: KG OE-C1

Load-displacement data

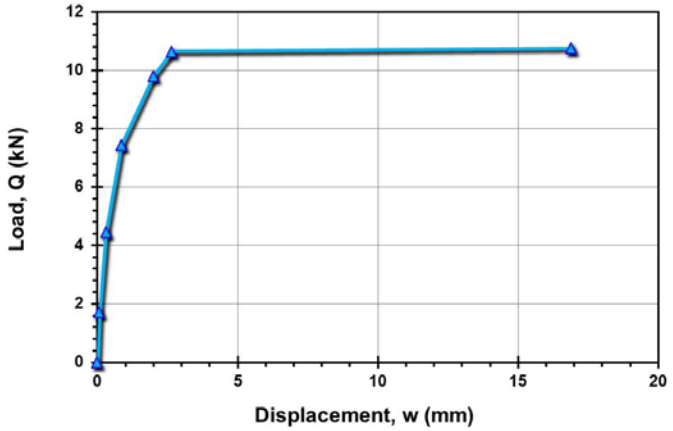

Back-analyzed normalized operational stiffness vs. pseudo-strain

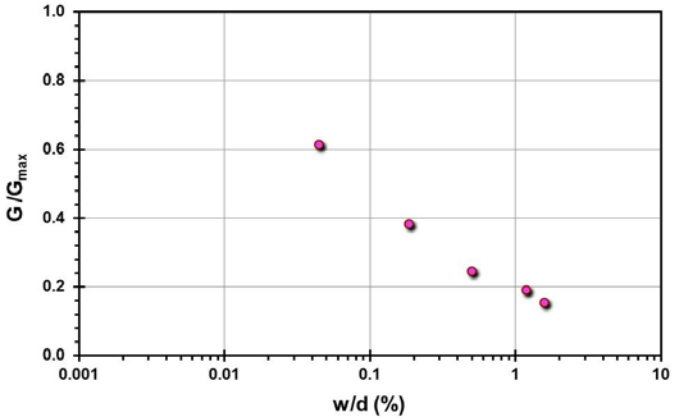

Detail	Description
Pile type/material	Open-ended steel pipe pile
Length, L (m)	2.01
Diameter, d (m)	0.168
Installation method	Driven
Loading mode	Compression
$Q_{max\text{-}measured}$ (kN)	10.75
Q_s (kN)	6.32
Q_b (kN)	4.43
$Q_{Davisson}$ (kN)	10.70
$Q_{w/d=10\%}$ (kN)	10.77
$Q_{C\text{-}K}$ (kN)	10.92

Pile ID: KG CE-C1

Load-displacement data

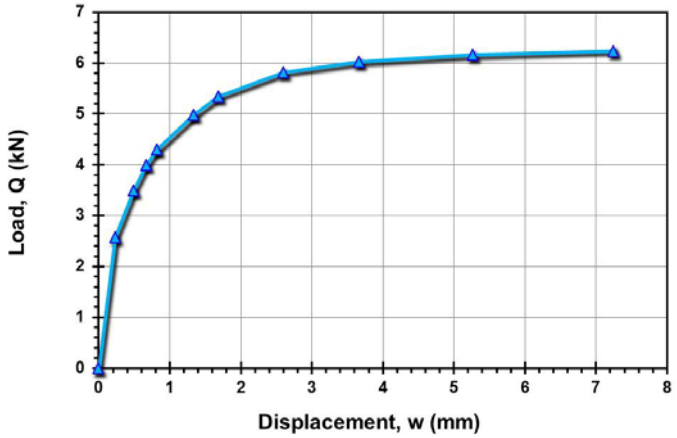

Back-analyzed normalized operational stiffness vs. pseudo-strain

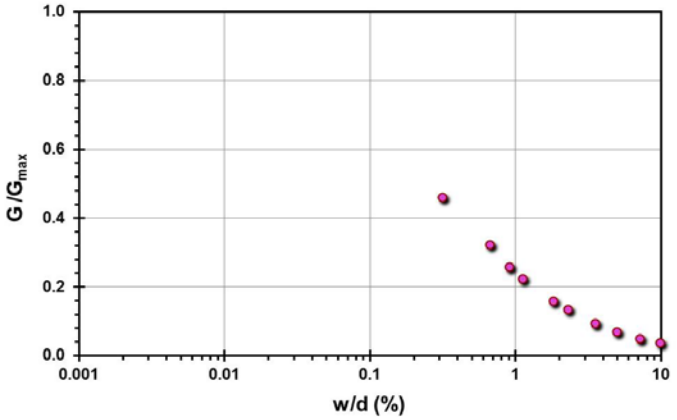

Detail	Description
Pile type/material	Closed-ended steel pipe pile
Length, L (m)	2.80
Diameter, d (m)	0.073
Installation method	Driven
Loading mode	Compression
$Q_{max\text{-}measured}$ (kN)	6.24
Q_s (kN)	5.31
Q_b (kN)	0.96
$Q_{Davisson}$ (kN)	6.09
$Q_{w/d=10\%}$ (kN)	6.27
$Q_{C\text{-}K}$ (kN)	6.60

Pile ID: KG CE-C4

Load-displacement data

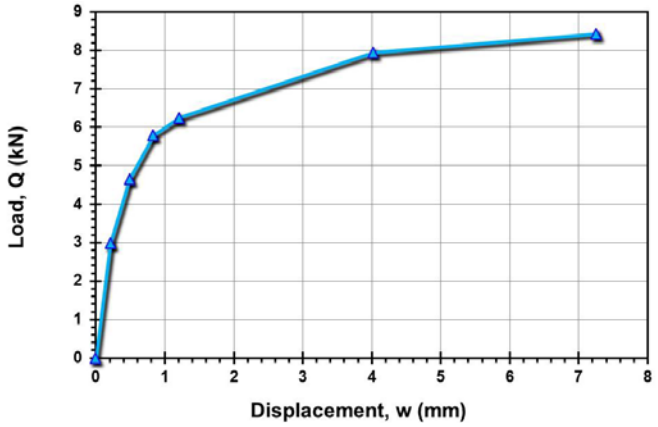

Back-analyzed normalized operational stiffness vs. pseudo-strain

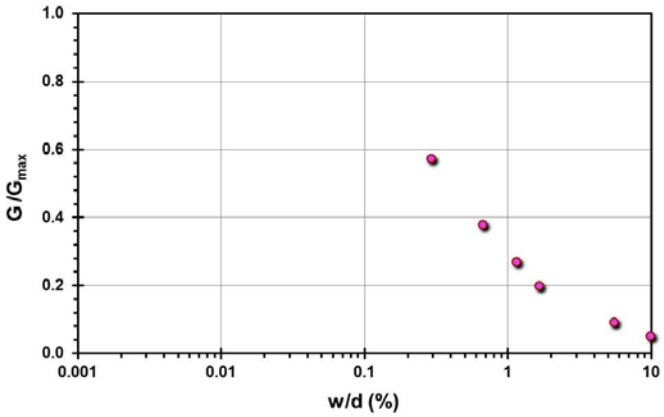

Detail	Description
Pile type/material	Closed-ended steel pipe pile
Length, L (m)	3.25
Diameter, d (m)	0.073
Installation method	Driven
Loading mode	Compression
$Q_{max\text{-}measured}$ (kN)	8.42
Q_s (kN)	7.52
Q_b (kN)	0.90
$Q_{Davisson}$ (kN)	7.93
$Q_{w/d=10\%}$ (kN)	8.40
$Q_{C\text{-}K}$ (kN)	8.96

Site ID No. 35

Cone penetrometer data	CPT SBT soil classification index, I_c	Detail	Description
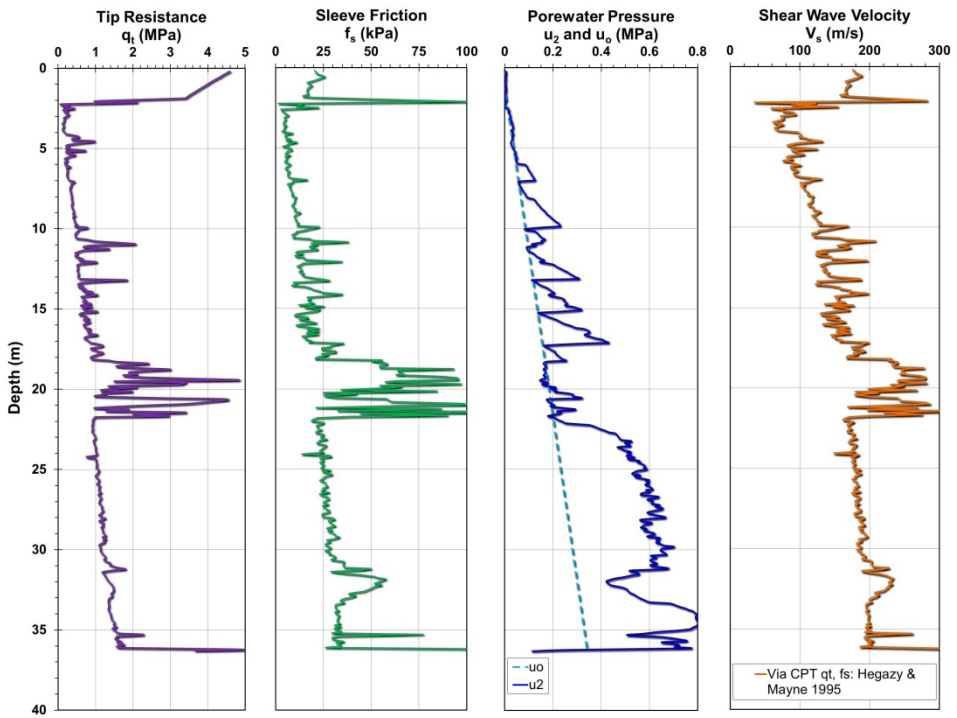	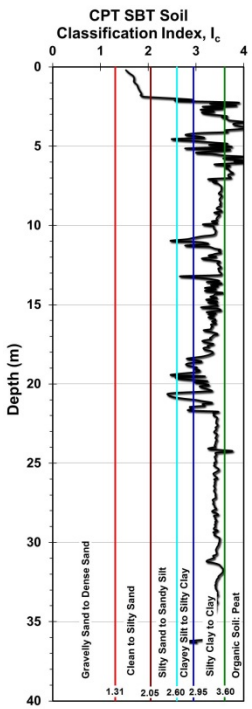	Site name and location	Klang clay site, western shoreline, Malaysia
		Soil type(s)	Soft marine clay
		Pile type(s)	Pre-stressed concrete thin-wall caisson
		Type of cone penetrometer testing	CPTu
		Source of V_s evaluation	Correlations (see Figure opposite and Table 3.1)
		Number of pile load tests	1
		Reference	Liew and Kowng (2005)
		Comments	Vs estimated via correlation by Hegazy and Mayne (1995) In author's opinion, the porewater pressures look ill-developed, perhaps due to loss of saturation of the porous filter element during CPTu

Pile ID: KCS TP-1A

Load-displacement data

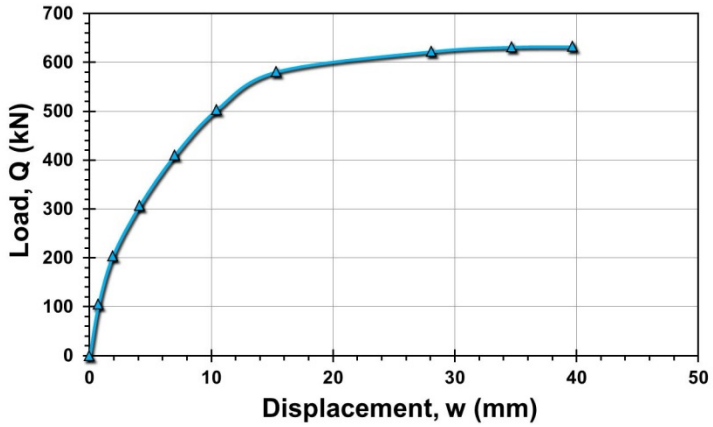

Back-analyzed normalized operational stiffness vs. pseudo-strain

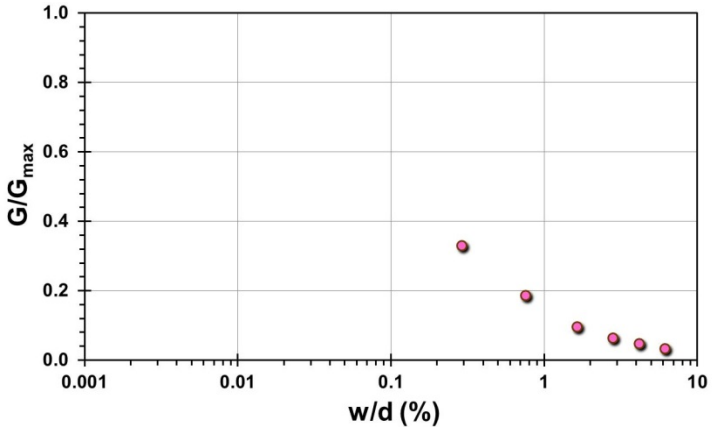

Detail	Description
Pile type/material	Pre-stressed concrete thin-wall caisson
Length, L (m)	35.50
Diameter, d (m)	0.25
Installation method	Jacked
Loading mode	Compression
$Q_{max\text{-}measured}$ (kN)	631.95
Q_s (kN)	586.4
Q_b (kN)	45.55
$Q_{Davisson}$ (kN)	580.63
$Q_{w/d=10\%}$ (kN)	614.10
$Q_{C\text{-}K}$ (kN)	671.14

Pile ID: KCS TP-2

Load-displacement data

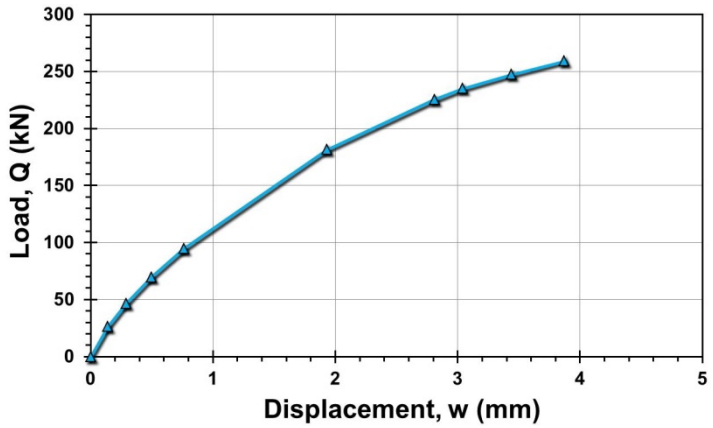

Back-analyzed normalized operational stiffness vs. pseudo-strain

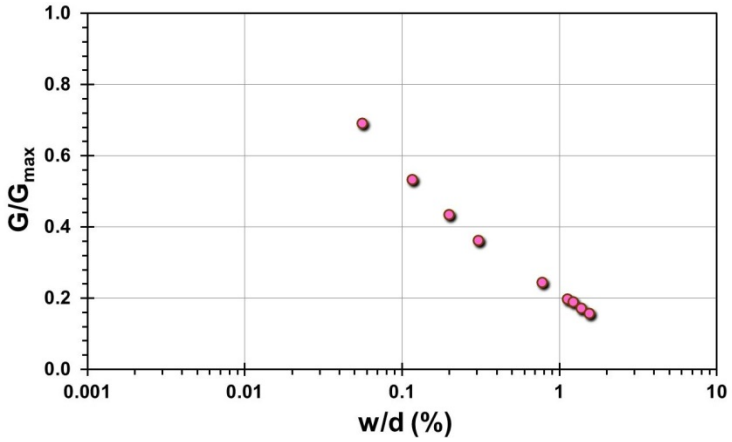

Detail	Description
Pile type/material	Pre-stressed concrete thin-wall caisson
Length, L (m)	14.50
Diameter, d (m)	0.25
Installation method	Jacked
Loading mode	Compression
$Q_{max\text{-}measured}$ (kN)	259.23
Q_s (kN)	Not reported
Q_b (kN)	Not reported
$Q_{Davisson}$ (kN)	351.83
$Q_{w/d=10\%}$ (kN)	406.00
$Q_{C\text{-}K}$ (kN)	452.28

Pile ID: KCS TP-3

Load-displacement data

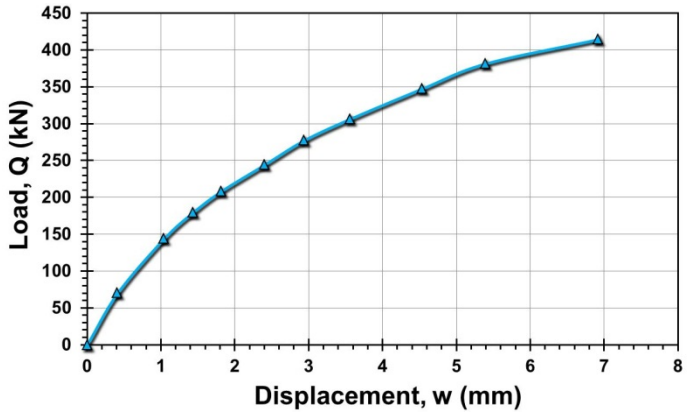

Back-analyzed normalized operational stiffness vs. pseudo-strain

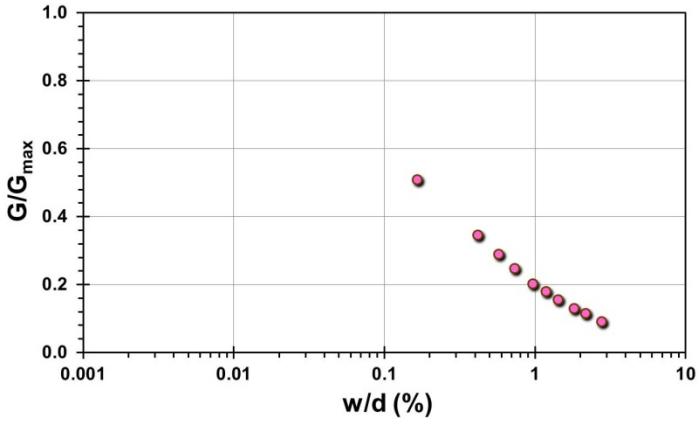

Detail	Description
Pile type/material	Pre-stressed concrete thin-wall caisson
Length, L (m)	23.50
Diameter, d (m)	0.25
Installation method	Jacked
Loading mode	Compression
$Q_{max\text{-}measured}$ (kN)	414.67
Q_s (kN)	Not reported
Q_b (kN)	Not reported
$Q_{Davisson}$ (kN)	530.50
$Q_{w/d=10\%}$ (kN)	569.90
$Q_{C\text{-}K}$ (kN)	663.13

Pile ID: KCS TP-4

Load-displacement data

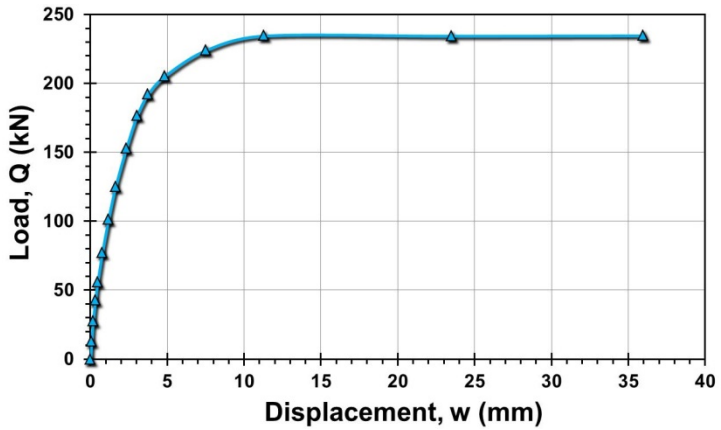

Back-analyzed normalized operational stiffness vs. pseudo-strain

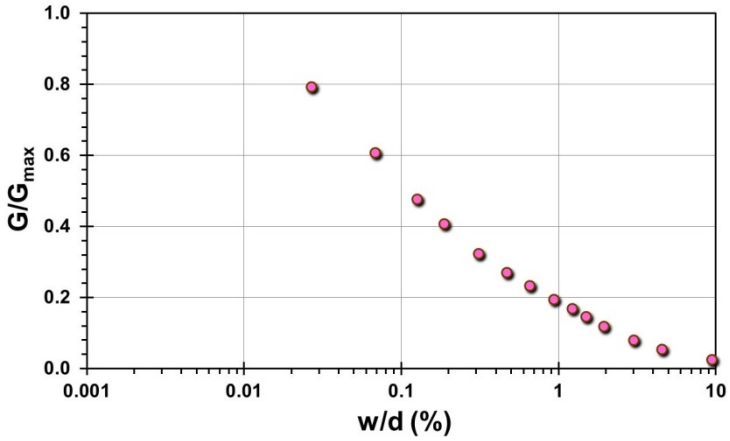

Detail	Description
Pile type/material	Pre-stressed concrete thin-wall caisson
Length, L (m)	11.50
Diameter, d (m)	0.25
Installation method	Jacked
Loading mode	Compression
$Q_{max\text{-}measured}$ (kN)	234.90
Q_s (kN)	Not reported
Q_b (kN)	Not reported
$Q_{Davisson}$ (kN)	217.33
$Q_{w/d=10\%}$ (kN)	234.00
$Q_{C\text{-}K}$ (kN)	241.31

Site ID No. 36

Cone penetrometer data	CPT SBT soil classification index, I_c	Detail	Description
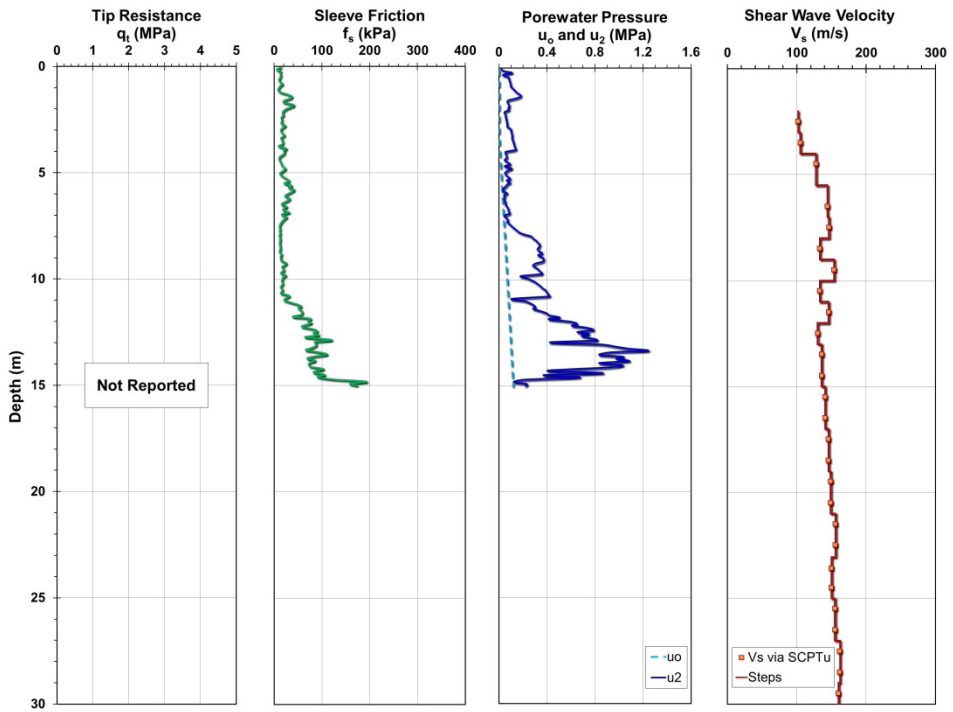	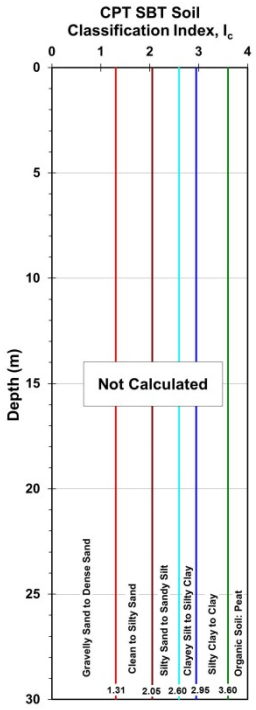	Site name and location	Kunshan town, eastern Jiangsu province, China
		Soil type(s)	Silty clay
		Pile type(s)	Pre-stressed concrete thin-wall caisson
		Type of cone penetrometer testing	SCPTu + DHT
		Source of V_s evaluation	SCPTu + DHT
		Number of pile load tests	1
		Reference	Cao et al. (2012)
		Comments	q_t readings not reported

Pile ID: KTJ 1

Load-displacement data

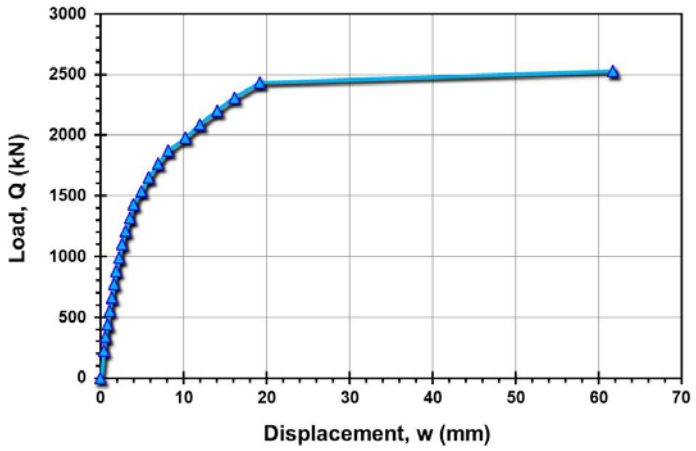

Back-analyzed normalized operational stiffness vs. pseudo-strain

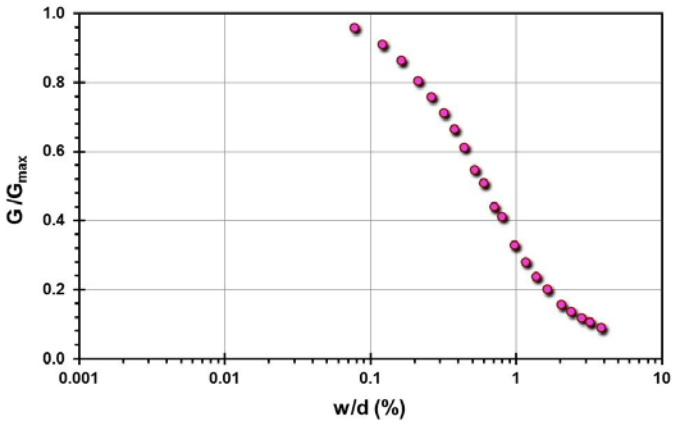

Detail	Description
Pile type/material	Pre-stressed concrete thin-wall caisson
Length, L (m)	30.00
Diameter, d (m)	0.50
Installation method	Jacked
Loading mode	Compression
$Q_{max\text{-}measured}$ (kN)	2,527.93
Q_s (kN)	2,103.71
Q_b (kN)	424.22
$Q_{Davisson}$ (kN)	2,429.81
$Q_{w/d=10\%}$ (kN)	2,513.05
$Q_{C\text{-}K}$ (kN)	2,597.40

Site ID No. 37

Cone penetrometer data	CPT SBT soil classification index, I_c	Detail	Description
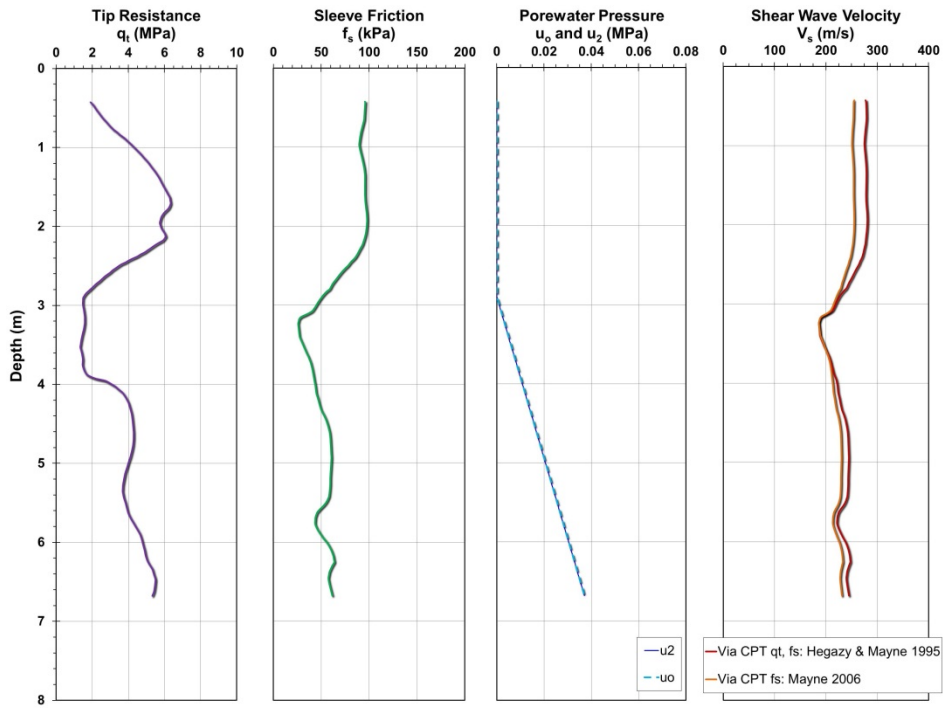	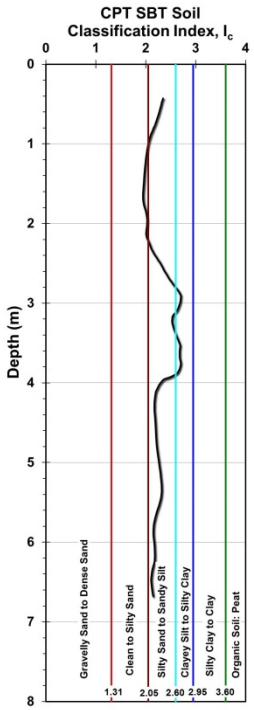	Site name and location	Labenne sand, Bayonne, SW France
		Soil type(s)	Fine-medium uniform sand
		Pile type(s)	Close-ended steel pipe pile (ICP)
		Type of cone penetrometer testing	CPT
		Source of V_s evaluation	Correlations (see Figure opposite and Table 3.1)
		Number of pile load tests	1
		Reference	Lehane et al. (1993), Lehane (1992), Chow (1996)
		Comments	u_2 assumed hydrostatic; V_s via correlations by Hegazy and Mayne (1995) and Mayne (2006)

Pile ID: LB 1/L1C

Load-displacement data

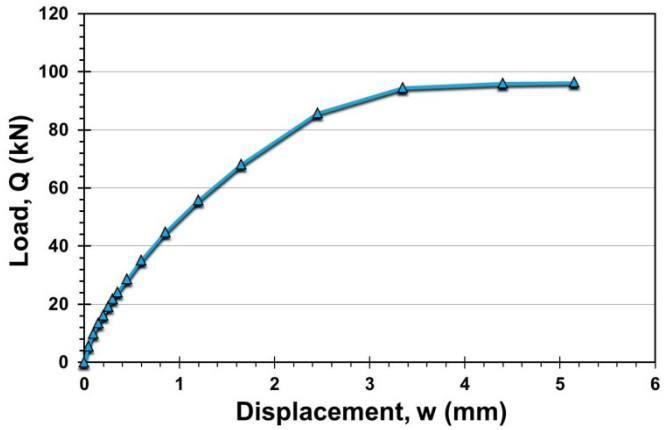

Back-analyzed normalized operational stiffness vs. pseudo-strain

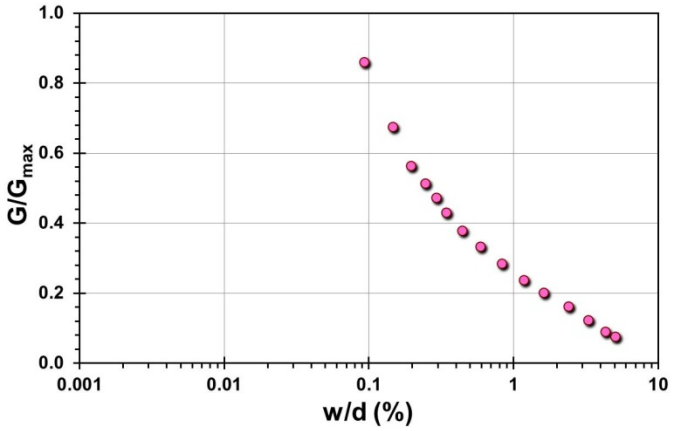

Detail	Description
Pile type/material	Close-ended steel pipe pile (ICP)
Length, L (m)	5.95
Diameter, d (m)	0.102
Installation method	Jacked
Loading mode	Compression
$Q_{max\text{-}measured}$ (kN)	96.41
Q_s (kN)	72.71
Q_b (kN)	23.70
$Q_{Davisson}$ (kN)	96.97
$Q_{w/d=10\%}$ (kN)	102.10
$Q_{C\text{-}K}$ (kN)	107.65

Pile ID: LB 2/L1C

Load-displacement data

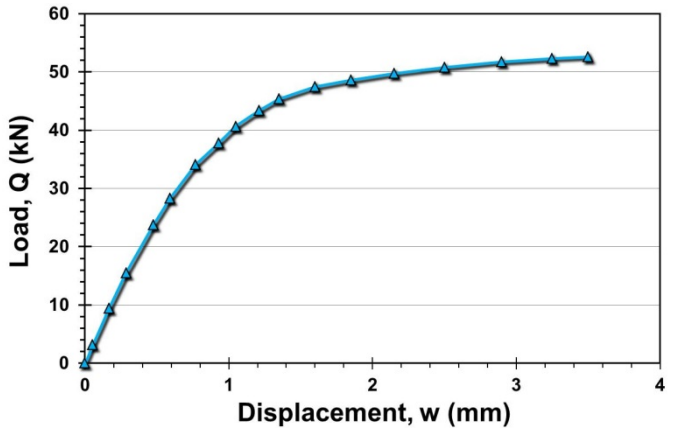

Back-analyzed normalized operational stiffness vs. pseudo-strain

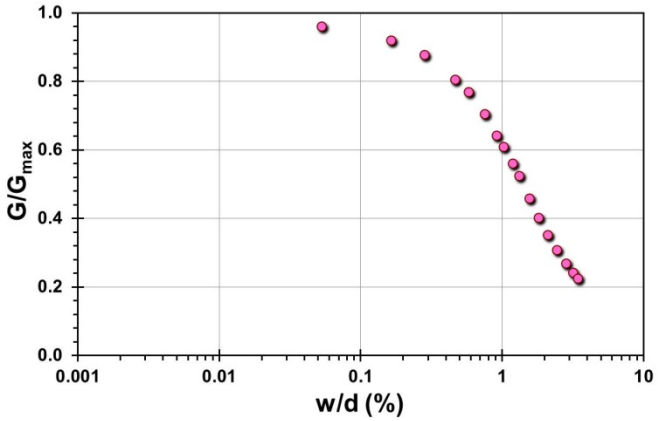

Detail	Description
Pile type/material	Close-ended steel pipe pile (ICP)
Length, L (m)	1.83
Diameter, d (m)	0.102
Installation method	Jacked
Loading mode	Compression
$Q_{max\text{-}measured}$ (kN)	52.63
Q_s (kN)	25.13
Q_b (kN)	27.50
$Q_{Davisson}$ (kN)	53.11
$Q_{w/d=10\%}$ (kN)	56.10
$Q_{C\text{-}K}$ (kN)	58.12

Pile ID: LB 2/L1T

Load-displacement data

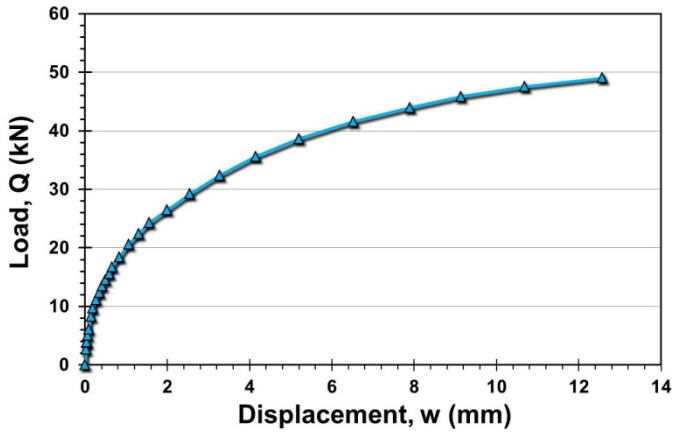

Back-analyzed normalized operational stiffness vs. pseudo-strain

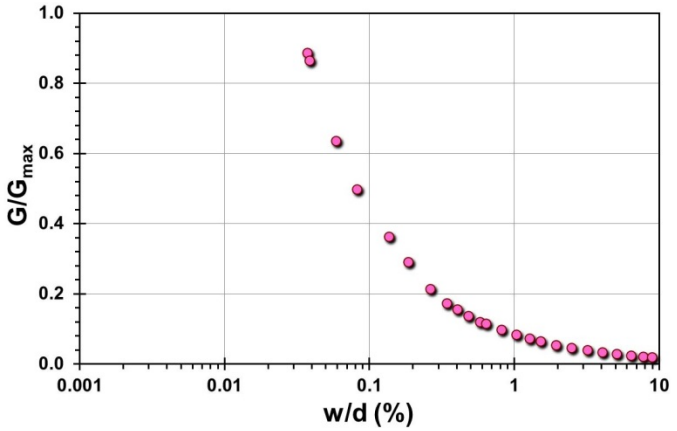

Detail	Description
Pile type/material	Close-ended steel pipe pile (ICP)
Length, L (m)	5.95
Diameter, d (m)	0.102
Installation method	Jacked
Loading mode	Tension
$Q_{max\text{-}measured}$ (kN)	49.07
Q_s (kN)	49.07
Q_b (kN)	-
$Q_{Davisson}$ (kN)	40.12
$Q_{w/d=10\%}$ (kN)	46.90
$Q_{C\text{-}K}$ (kN)	59.10

Site ID No. 38

Cone penetrometer data	CPT SBT soil classification index, I_c	Detail	Description
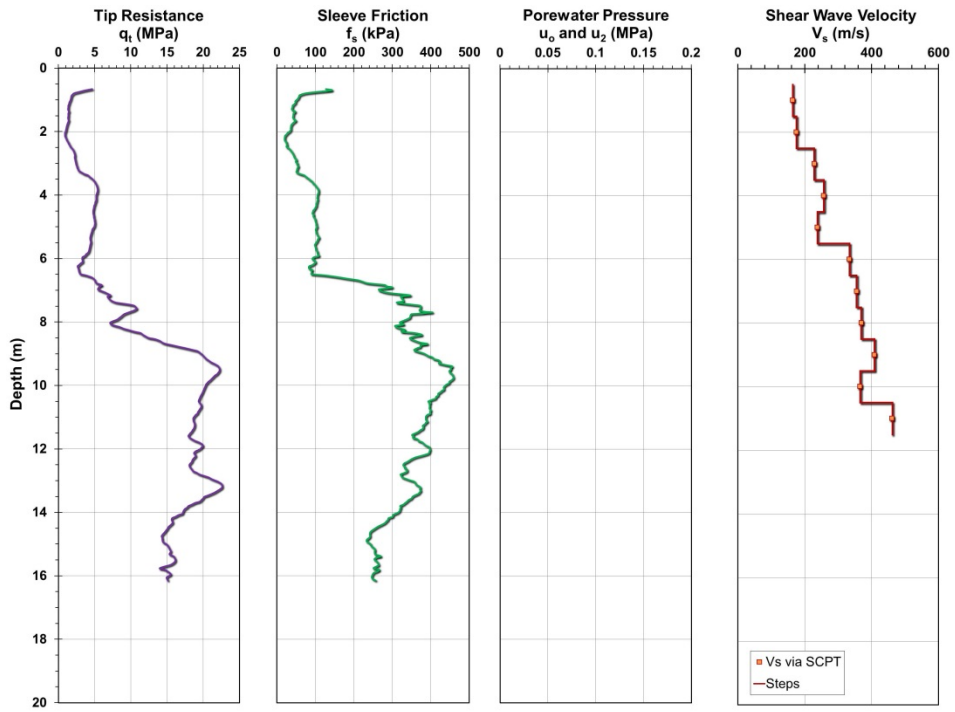	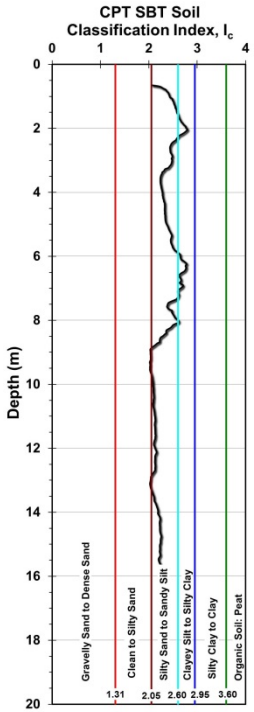	Site name and location	Limelette test site, Brussels, Belgium
		Soil type(s)	Silty/sandy clay over clayey sand
		Pile type(s)	10 Screw piles and 2 Square concrete pile
		Type of cone penetrometer testing	SCPT + CPT
		Source of V_s evaluation	SCPT
		Number of pile load tests	1
		Reference	Alboom & Whenham (2003), Huybrechts and Whenham (2003), and Maertens and Huybrechts (2003)
		Comments	Q-z for only one pile, u_2 reading not available

Pile ID: LTS B1

Load-displacement data

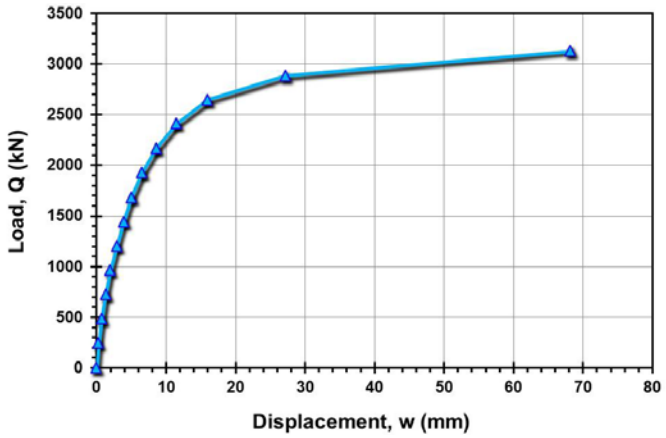

Back-analyzed normalized operational stiffness vs. pseudo-strain

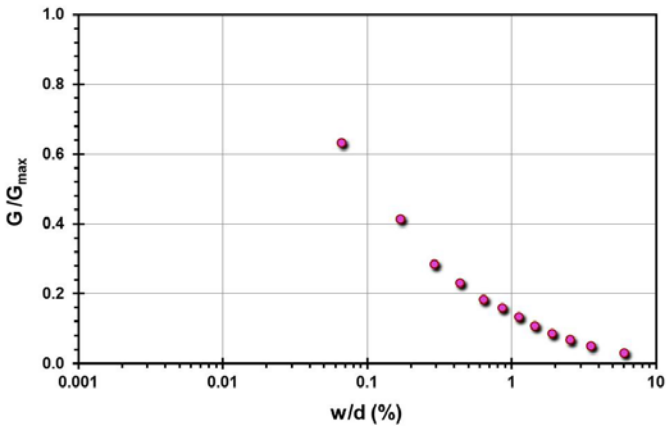

Detail	Description
Pile type/material	Fundex
Length, L (m)	8.59
Diameter, d (m)	0.45
Installation method	Augered
Loading mode	Compression
$Q_{max\text{-}measured}$ (kN)	3,130.57
Q_s (kN)	Not reported
Q_b (kN)	Not reported
$Q_{Davisson}$ (kN)	2,410.83
$Q_{w/d=10\%}$ (kN)	3,043.84
$Q_{C\text{-}K}$ (kN)	3,355.70

Pile ID: LTS B2

Load-displacement data

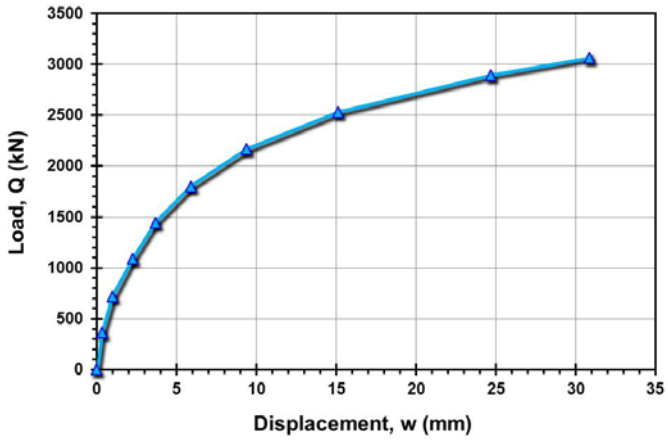

Back-analyzed normalized operational stiffness vs. pseudo-strain

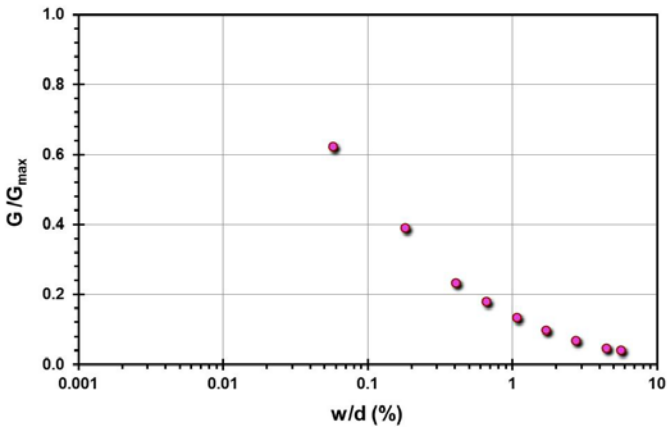

Detail	Description
Pile type/material	Olivier
Length, L (m)	8.20
Diameter, d (m)	0.55
Installation method	Augered
Loading mode	Compression
$Q_{max\text{-}measured}$ (kN)	3,063.90
Q_s (kN)	Not reported
Q_b (kN)	Not reported
$Q_{Davisson}$ (kN)	2,164.74
$Q_{w/d=10\%}$ (kN)	3,321.52
$Q_{C\text{-}K}$ (kN)	3,745.32

Pile ID: LTS B3

Load-displacement data

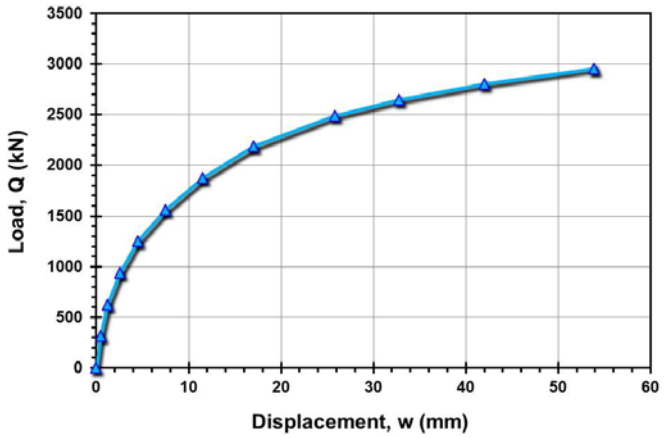

Back-analyzed normalized operational stiffness vs. pseudo-strain

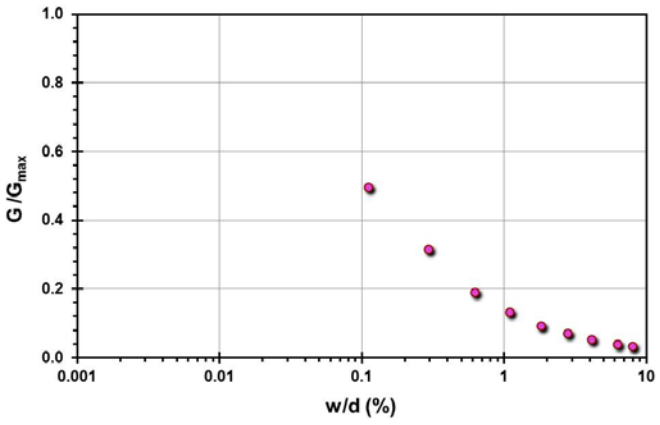

Detail	Description
Pile type/material	Omega
Length, L (m)	8.45
Diameter, d (m)	0.41
Installation method	Augered
Loading mode	Compression
$Q_{max\text{-}measured}$ (kN)	2,956.52
Q_s (kN)	Not reported
Q_b (kN)	Not reported
$Q_{Davisson}$ (kN)	1,870.33
$Q_{w/d=10\%}$ (kN)	2,802.36
$Q_{C\text{-}K}$ (kN)	3,508.77

Pile ID: LTS B4

Load-displacement data

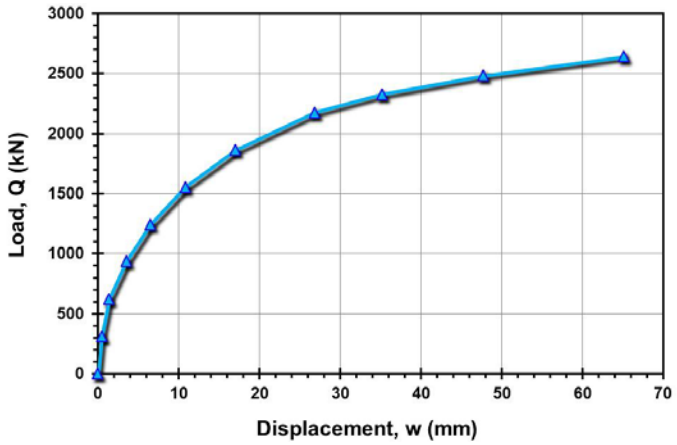

Back-analyzed normalized operational stiffness vs. pseudo-strain

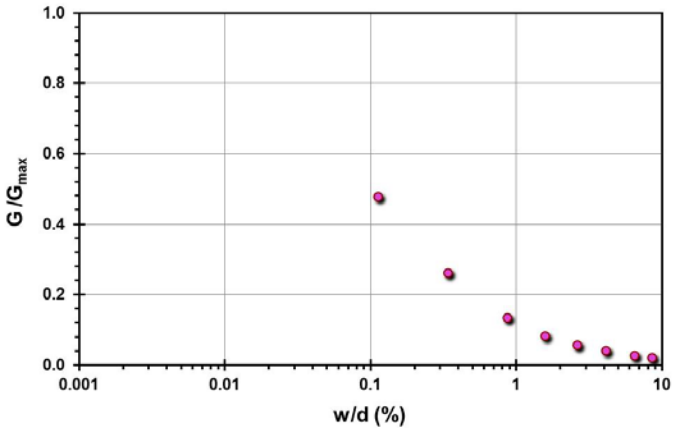

Detail	Description
Pile type/material	De Waal
Length, L (m)	8.53
Diameter, d (m)	0.41
Installation method	Augered
Loading mode	Compression
$Q_{max\text{-}measured}$ (kN)	2,643.24
Q_s (kN)	Not reported
Q_b (kN)	Not reported
$Q_{Davisson}$ (kN)	1,554.55
$Q_{w/d=10\%}$ (kN)	2,424.60
$Q_{C\text{-}K}$ (kN)	3,095.98

Pile ID: LTS B5

Load-displacement data	Detail	Description
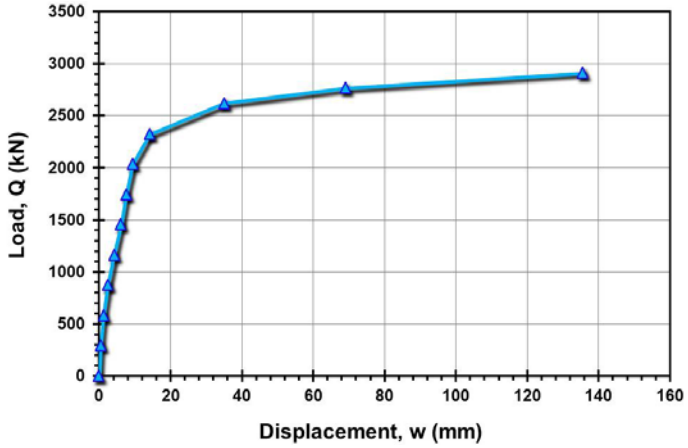	Pile type/material	Square concrete
	Length, L (m)	8.51
	Width, B (m)	0.35
	Installation method	Driven
	Loading mode	Compression
	$Q_{max\text{-}measured}$ (kN)	2,913.15
	Q_s (kN)	Not reported
	Q_b (kN)	Not reported
	$Q_{Davisson}$ (kN)	2,036.65
	$Q_{w/d=10\%}$ (kN)	2,709.82
	$Q_{C\text{-}K}$ (kN)	3,012.05
Back-analyzed normalized operational stiffness vs. pseudo-strain		
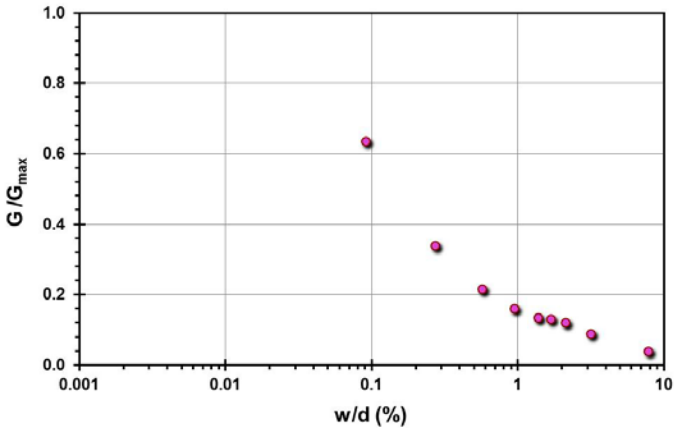		

Pile ID: LTS B6

Load-displacement data

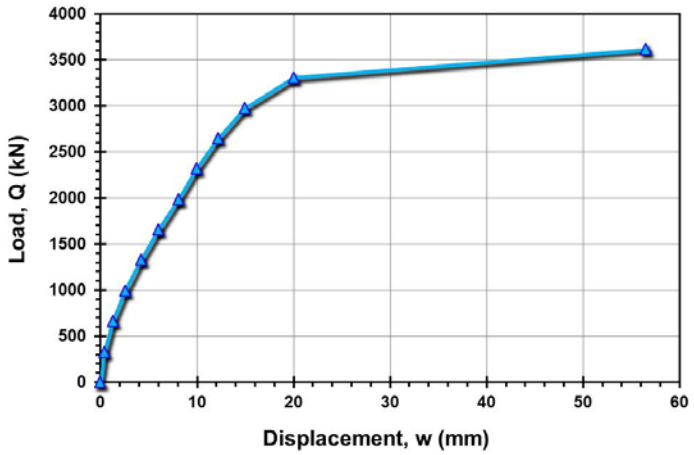

Back-analyzed normalized operational stiffness vs. pseudo-strain

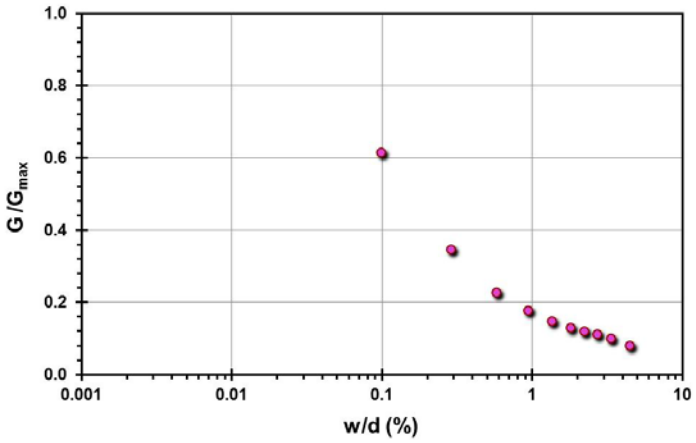

Detail	Description
Pile type/material	Square concrete
Length, L (m)	8.57
Width, B (m)	0.35
Installation method	Driven
Loading mode	Compression
$Q_{max\text{-}measured}$ (kN)	3,568.21
Q_s (kN)	2,654.42
Q_b (kN)	913.79
$Q_{Davisson}$ (kN)	2,483.09
$Q_{w/d=10\%}$ (kN)	3,554.97
$Q_{C\text{-}K}$ (kN)	3,875.97

Pile ID: LTS B7

Load-displacement data

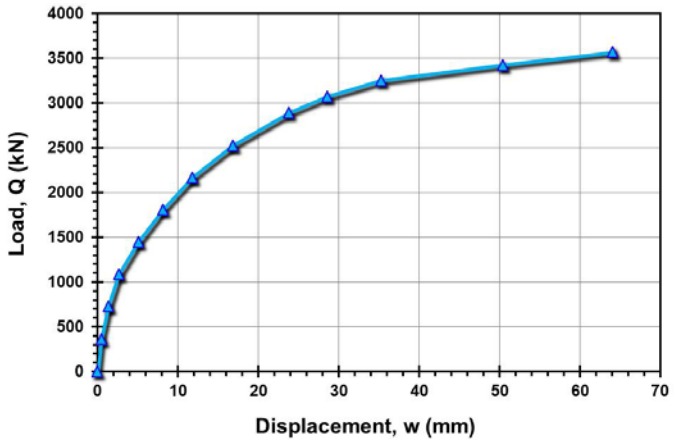

Back-analyzed normalized operational stiffness vs. pseudo-strain

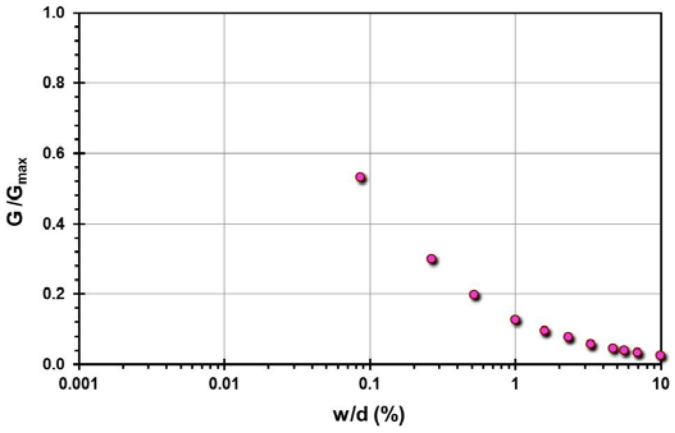

Detail	Description
Pile type/material	Atlas
Length, L (m)	8.43
Diameter, d (m)	0.51
Installation method	Augered
Loading mode	Compression
$Q_{max\text{-}measured}$ (kN)	3,619.84
Q_s (kN)	Not reported
Q_b (kN)	Not reported
$Q_{Davisson}$ (kN)	1,987.37
$Q_{w/d=10\%}$ (kN)	3,453.34
$Q_{C\text{-}K}$ (kN)	4,166.67

Pile ID: LTS B8

Load-displacement data

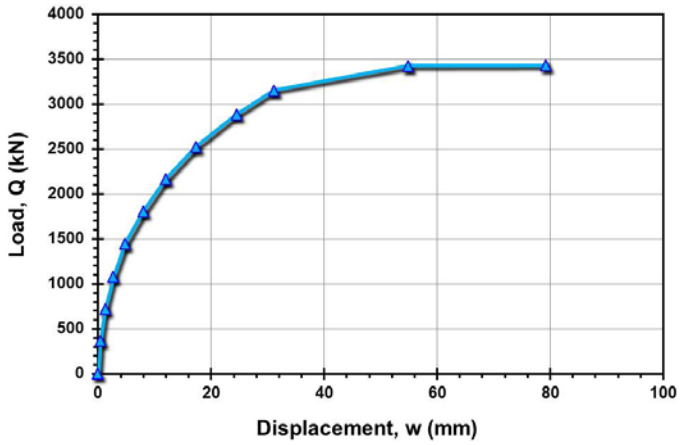

Back-analyzed normalized operational stiffness vs. pseudo-strain

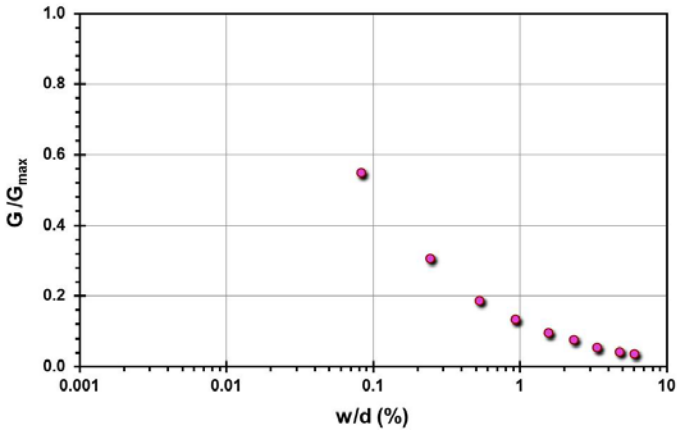

Detail	Description
Pile type/material	Atlas
Length, L (m)	8.43
Diameter, d (m)	0.52
Installation method	Augered
Loading mode	Compression
$Q_{max\text{-}measured}$ (kN)	3,427.25
Q_s (kN)	Not reported
Q_b (kN)	Not reported
$Q_{Davisson}$ (kN)	1,986.14
$Q_{w/d=10\%}$ (kN)	3,357.24
$Q_{C\text{-}K}$ (kN)	3,636.36

Pile ID: LTS B9

Load-displacement data

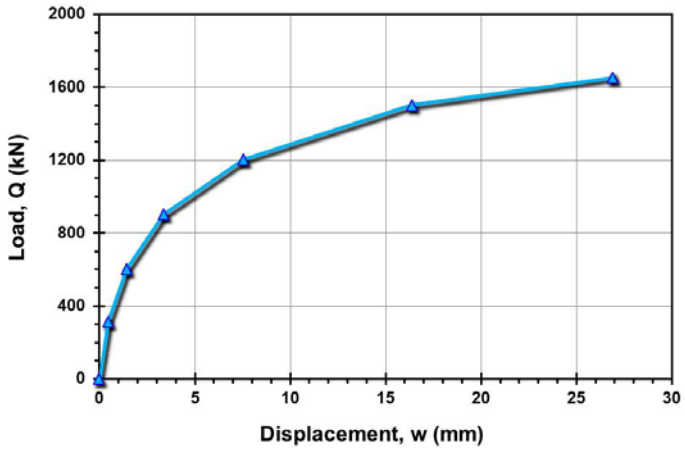

Back-analyzed normalized operational stiffness vs. pseudo-strain

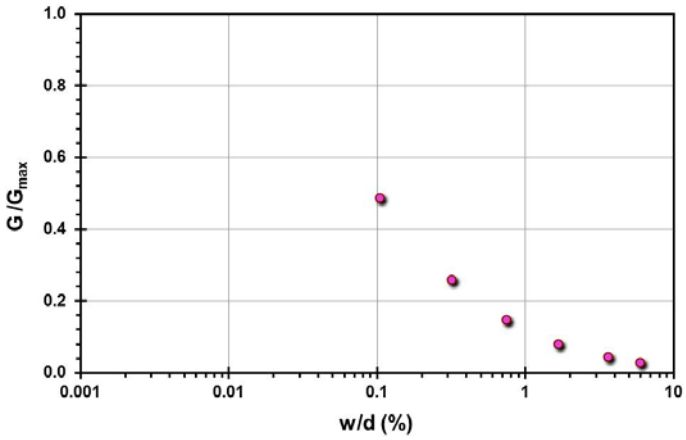

Detail	Description
Pile type/material	Fundex
Length, L (m)	8.65
Diameter, d (m)	0.43
Installation method	Augered
Loading mode	Compression
$Q_{max\text{-}measured}$ (kN)	1,654.34
Q_s (kN)	Not reported
Q_b (kN)	Not reported
$Q_{Davisson}$ (kN)	1,203.28
$Q_{w/d=10\%}$ (kN)	1,755.94
$Q_{C\text{-}K}$ (kN)	1,937.98

Pile ID: LTS B10

Load-displacement data

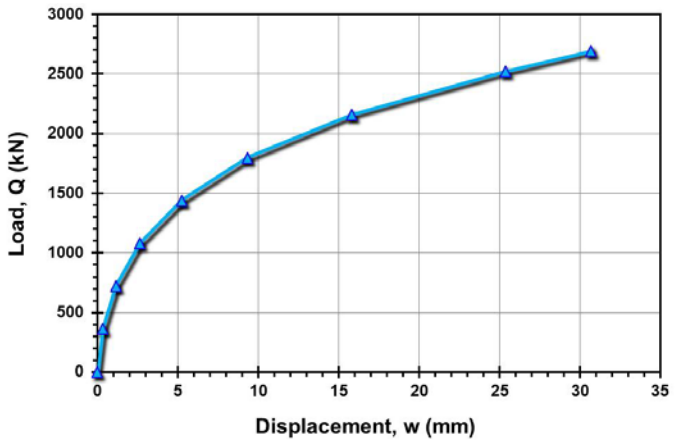

Back-analyzed normalized operational stiffness vs. pseudo-strain

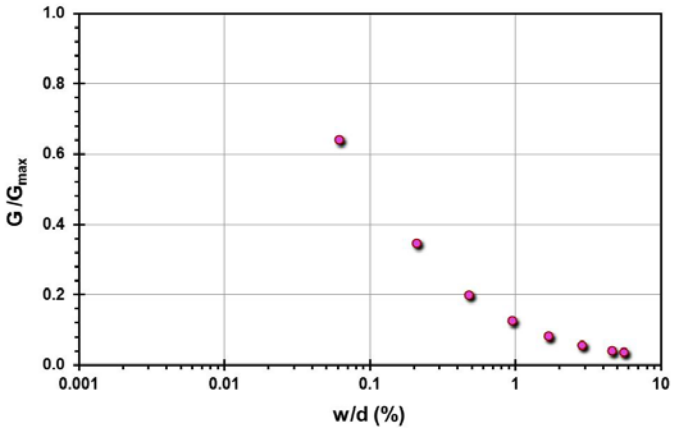

Detail	Description
Pile type/material	Olivier
Length, L (m)	8.13
Diameter, d (m)	0.55
Installation method	Augered
Loading mode	Compression
$Q_{max\text{-}measured}$ (kN)	2,691.19
Q_s (kN)	Not reported
Q_b (kN)	Not reported
$Q_{Davisson}$ (kN)	1,796.17
$Q_{w/d=10\%}$ (kN)	3,026.92
$Q_{C\text{-}K}$ (kN)	3,623.19

Pile ID: LTS B11

Load-displacement data

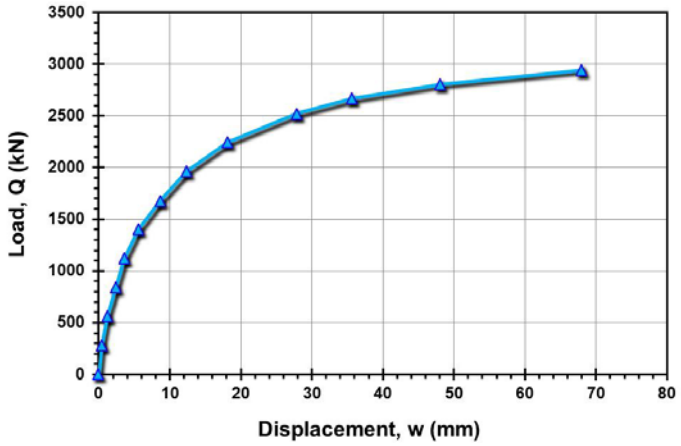

Back-analyzed normalized operational stiffness vs. pseudo-strain

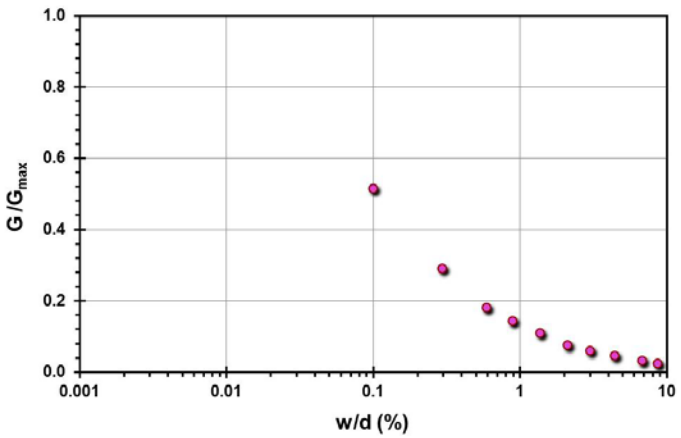

Detail	Description
Pile type/material	Omega
Length, L (m)	8.45
Diameter, d (m)	0.41
Installation method	Augered
Loading mode	Compression
$Q_{max\text{-}measured}$ (kN)	2,942.75
Q_s (kN)	
Q_b (kN)	
$Q_{Davisson}$ (kN)	1,819.61
$Q_{w/d=10\%}$ (kN)	2,739.66
$Q_{C\text{-}K}$ (kN)	3,311.26

Pile ID: LTS B12

Load-displacement data

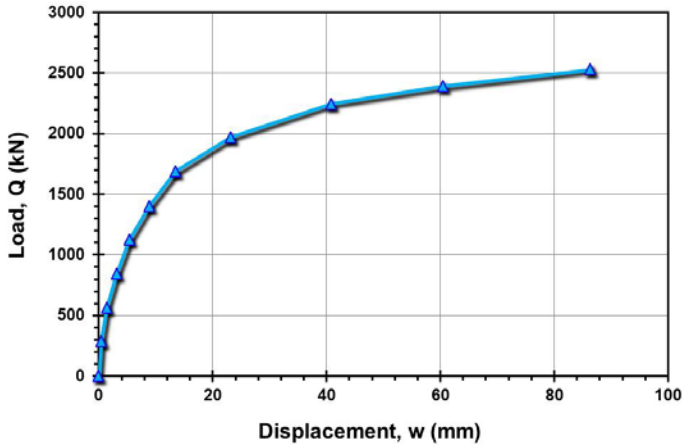

Back-analyzed normalized operational stiffness vs. pseudo-strain

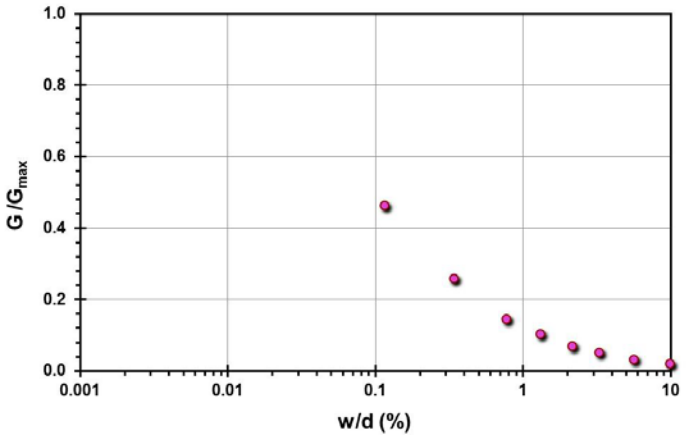

Detail	Description
Pile type/material	De Waal
Length, L (m)	9.52
Diameter, d (m)	0.43
Installation method	Augered
Loading mode	Compression
$Q_{max\text{-}measured}$ (kN)	2,529.32
Q_s (kN)	Not reported
Q_b (kN)	Not reported
$Q_{Davisson}$ (kN)	1,400.95
$Q_{w/d=10\%}$ (kN)	2,264.86
$Q_{C\text{-}K}$ (kN)	2,785.52

Site ID No. 39

Cone penetrometer data	CPT SBT soil classification index, I_c	Detail	Description
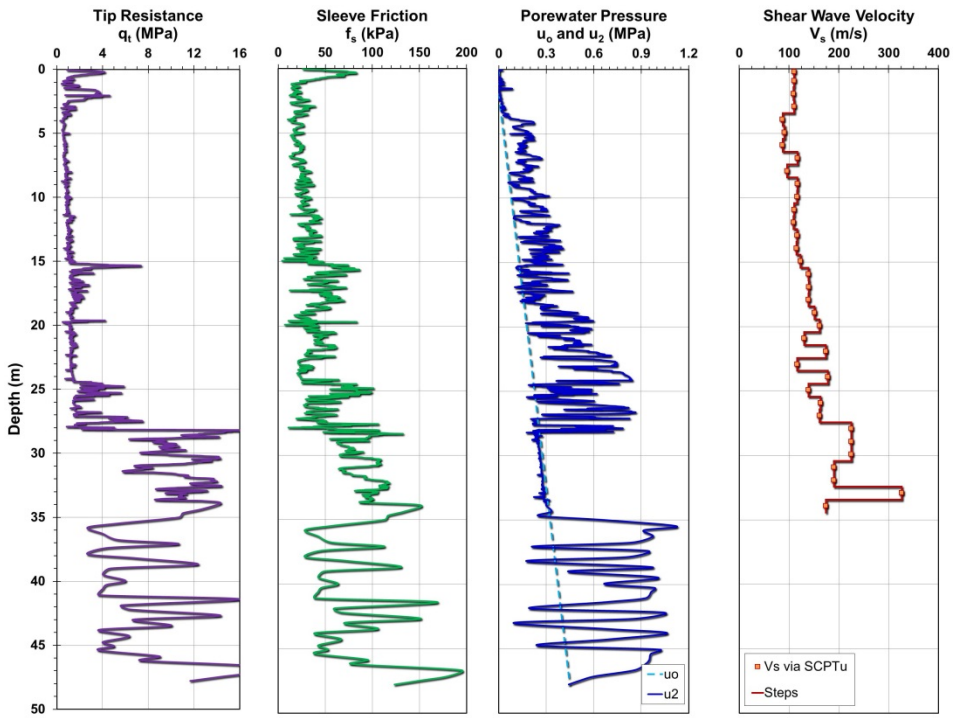	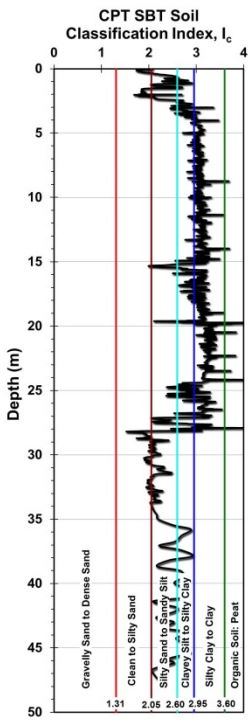	Site name and location	LNG storage site, Delaware River, Gloucester county, NJ, USA
		Soil type(s)	Varved clayey silt over dense gravelly sand over dense residual clayey sand
		Pile type(s)	Open-ended steel pipe piles
		Type of cone penetrometer testing	SCPTu
		Source of V_s evaluation	SCPTu
		Number of pile load tests	2
		Reference	Tan and Lin (2013)
		Comments	Digital data supplied by Guomin Lin, personal communication

Pile ID: DRS P-I

Load-displacement data

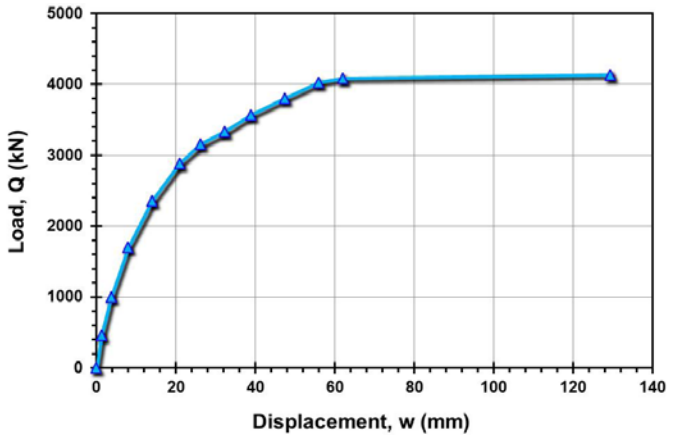

Back-analyzed normalized operational stiffness vs. pseudo-strain

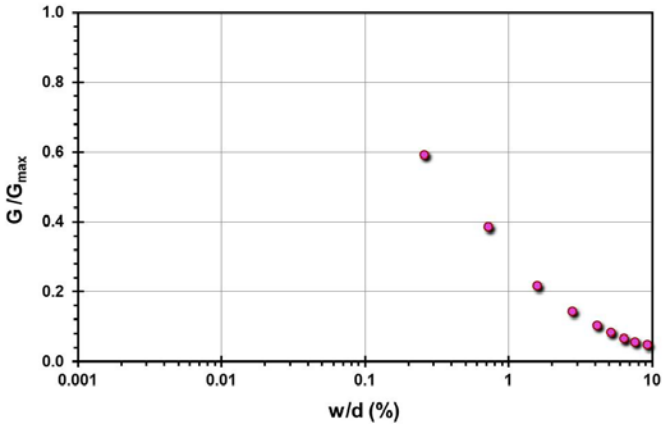

Detail	Description
Pile type/material	Open-ended steel pipe pile
Length, L (m)	40.20
Diameter, d (m)	0.48
Installation method	Driven
Loading mode	Compression
$Q_{max\text{-}measured}$ (kN)	4,135.67
Q_s (kN)	3,391.16
Q_b (kN)	744.51
$Q_{Davisson}$ (kN)	3,190.23
$Q_{w/d=10\%}$ (kN)	4,030.70
$Q_{C\text{-}K}$ (kN)	4,201.68

Pile ID: DRS P-D

Load-displacement data

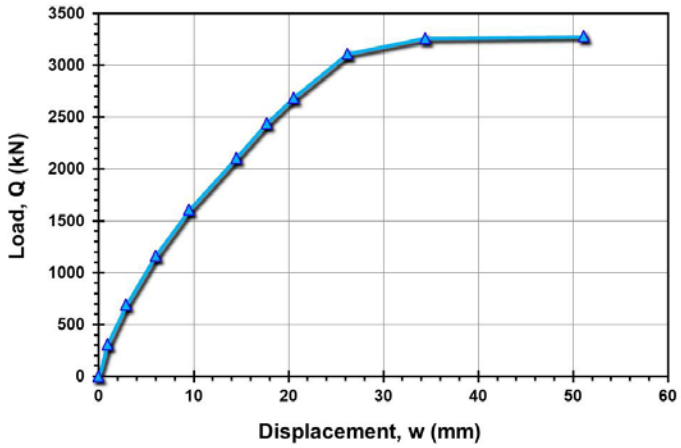

Back-analyzed normalized operational stiffness vs. pseudo-strain

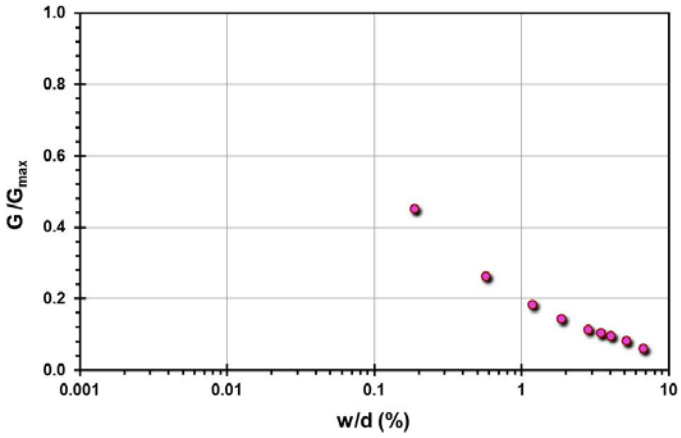

Detail	Description
Pile type/material	Open-ended steel pipe pile
Length, L (m)	40.20
Diameter, d (m)	0.48
Installation method	Driven
Loading mode	Compression
$Q_{max\text{-}measured}$ (kN)	3,278.99
Q_s (kN)	Not reported
Q_b (kN)	Not reported
$Q_{Davisson}$ (kN)	3,111.60
$Q_{w/d=10\%}$ (kN)	3,280.60
$Q_{C\text{-}K}$ (kN)	3,322.26

Site ID No. 40

Cone penetrometer data	CPT SBT soil classification index, I_c	Detail	Description
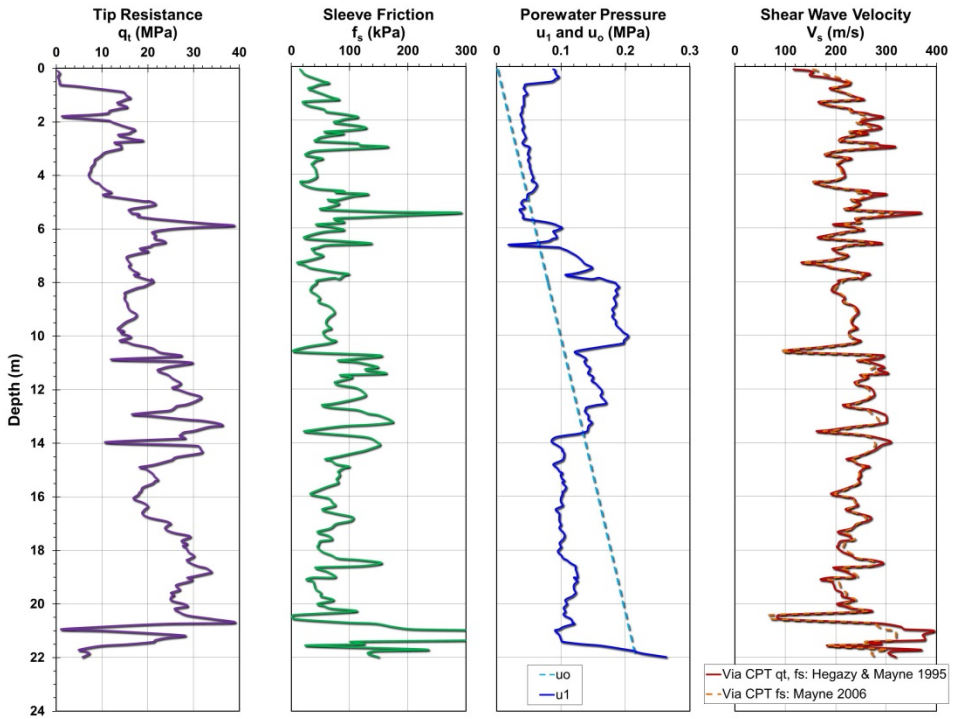	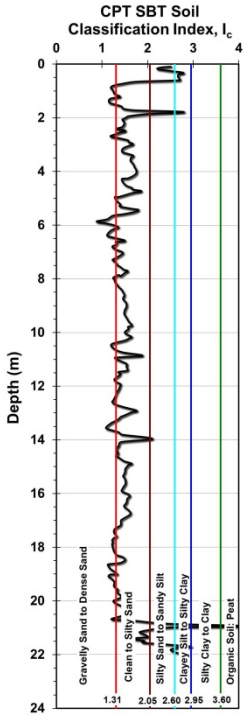	Site name and location	Lock and Dam 26 Project, Mississippi River, IL, USA
		Soil type(s)	Glacial gravelly sand
		Pile type(s)	6 H-piles and 14 Close-ended steel pipe piles
		Type of cone penetrometer testing	CPTu
		Source of V_s evaluation	Correlations (see Figure opposite and Table 3.1)
		Number of pile load tests	20
		Reference	Tucker and Briaud (1988)
		Comments	Measured u_1 reading converted to equivalent u_2

Pile ID: L&D 1-1T

Load-displacement data

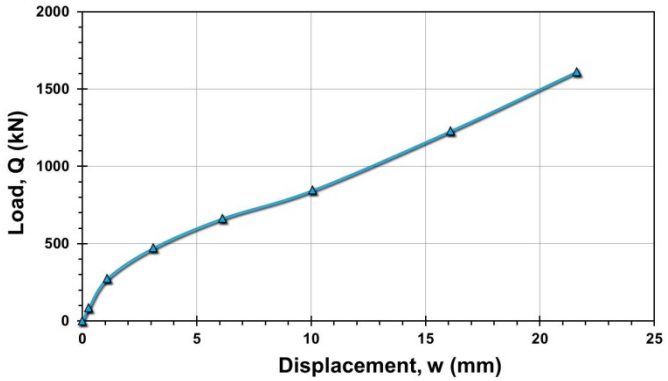

Back-analyzed normalized operational stiffness vs. pseudo-strain

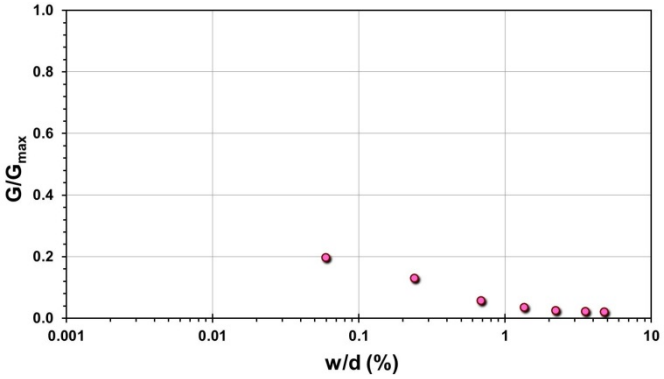

Detail	Description
Pile type/material	H-section pile
Length, L (m)	18.52
H-section sizes	14 x 73
Installation method	Driven
Loading mode	Tension
$Q_{max\text{-}measured}$ (kN)	1,612.30
Q_s (kN)	Not reported
Q_b (kN)	Not reported
$Q_{Davisson}$ (kN)	1,011.73
$Q_{w/d=10\%}$ (kN)	1,976.10
$Q_{C\text{-}K}$ (kN)	2,463.05

Pile ID: L&D 1-2T

Load-displacement data

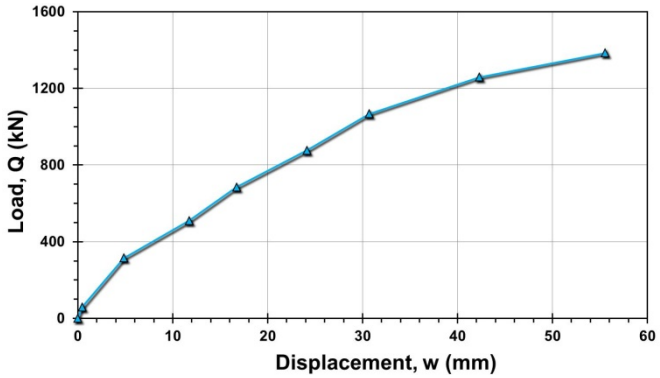

Back-analyzed normalized operational stiffness vs. pseudo-strain

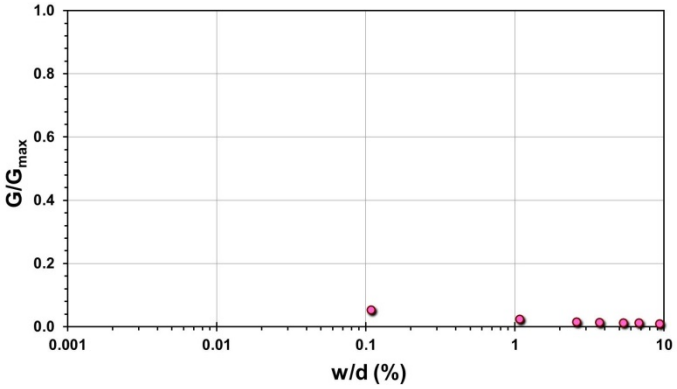

Detail	Description
Pile type/material	H-section pile
Length, L (m)	16.46
H-section sizes	14 x 73
Installation method	Driven
Loading mode	Tension
$Q_{max\text{-}measured}$ (kN)	1,383.82
Q_s (kN)	Not reported
Q_b (kN)	Not reported
$Q_{Davisson}$ (kN)	501.25
$Q_{w/d=10\%}$ (kN)	1,446.20
$Q_{C\text{-}K}$ (kN)	2,421.31

Pile ID: L&D 1-3AC

Load-displacement data

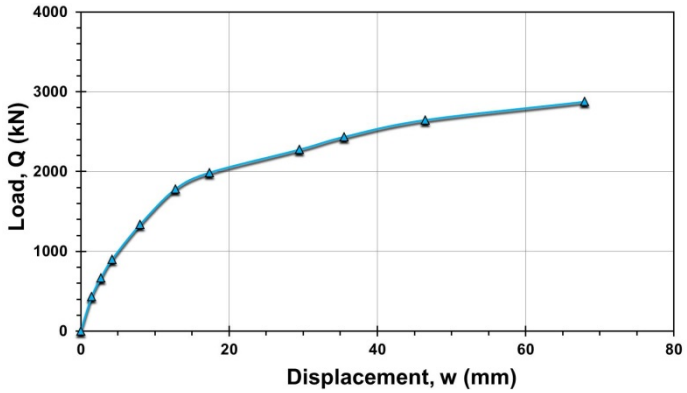

Back-analyzed normalized operational stiffness vs. pseudo-strain

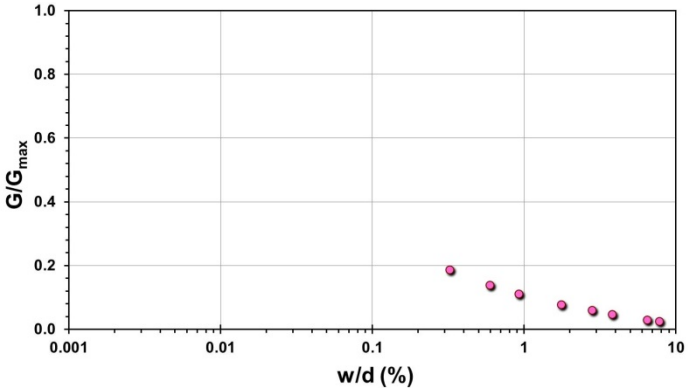

Detail	Description
Pile type/material	H-section pile
Length, L (m)	16.46
H-section sizes	14 x 73
Installation method	Driven
Loading mode	Compression
$Q_{max\text{-}measured}$ (kN)	2,875.69
Q_s (kN)	1,908.08
Q_b (kN)	967.61
$Q_{Davisson}$ (kN)	1,987.34
$Q_{w/d=10\%}$ (kN)	2,904.80
$Q_{C\text{-}K}$ (kN)	3,802.28

Pile ID: L&D 1-3BT

Load-displacement data

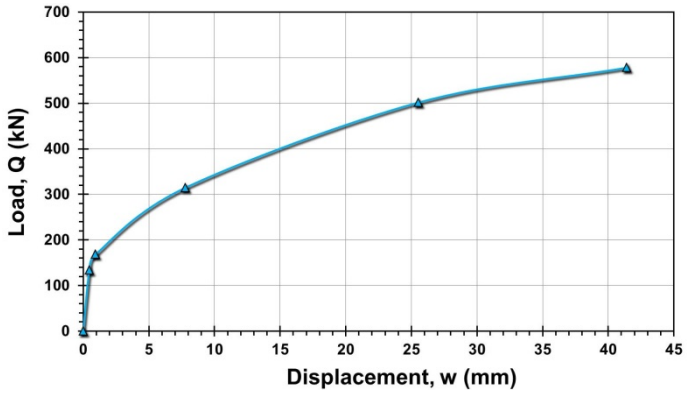

Back-analyzed normalized operational stiffness vs. pseudo-strain

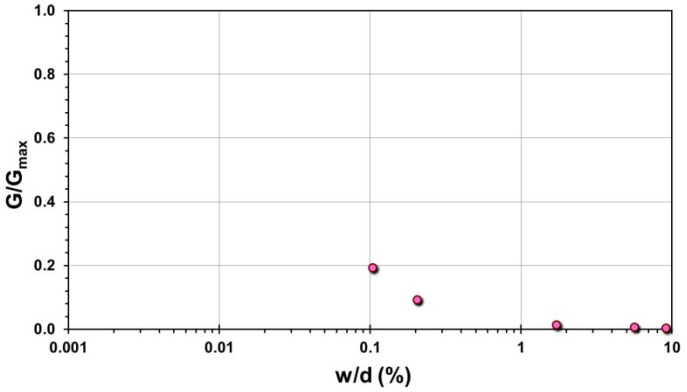

Detail	Description
Pile type/material	H-section pile
Length, L (m)	16.46
H-section sizes	14 x 73
Installation method	Driven
Loading mode	Tension
$Q_{max\text{-}measured}$ (kN)	578.29
Q_s (kN)	Not reported
Q_b (kN)	Not reported
$Q_{Davisson}$ (kN)	324.25
$Q_{w/d=10\%}$ (kN)	671.10
$Q_{C\text{-}K}$ (kN)	809.06

Pile ID: L&D 1-5T

Load-displacement data

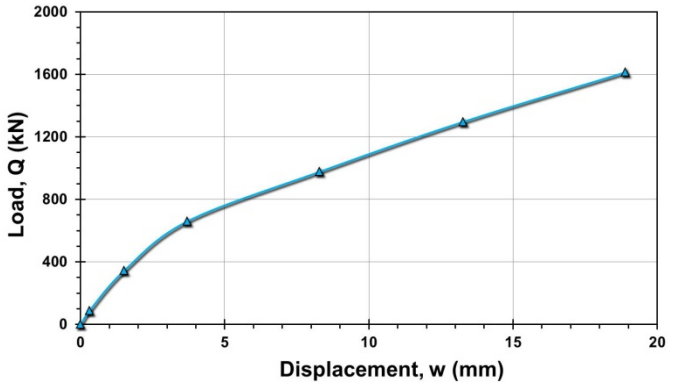

Back-analyzed normalized operational stiffness vs. pseudo-strain

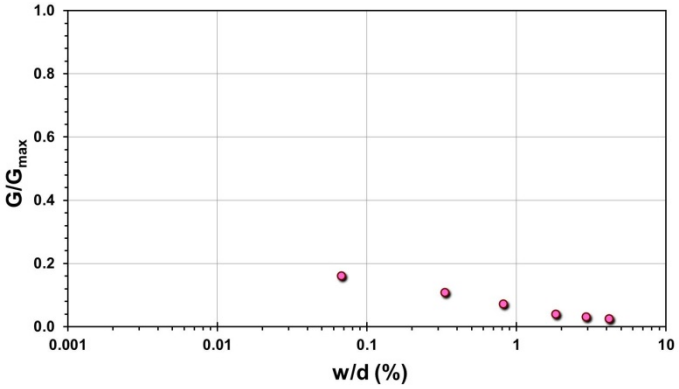

Detail	Description
Pile type/material	H-section pile
Length, L (m)	18.44
H-section sizes	14 x 73
Installation method	Driven
Loading mode	Tension
$Q_{max\text{-}measured}$ (kN)	1,613.43
Q_s (kN)	Not reported
Q_b (kN)	Not reported
$Q_{Davisson}$ (kN)	1,354.05
$Q_{w/d=10\%}$ (kN)	2,543.10
$Q_{C\text{-}K}$ (kN)	3,597.12

Pile ID: L&D 1-6C

Load-displacement data

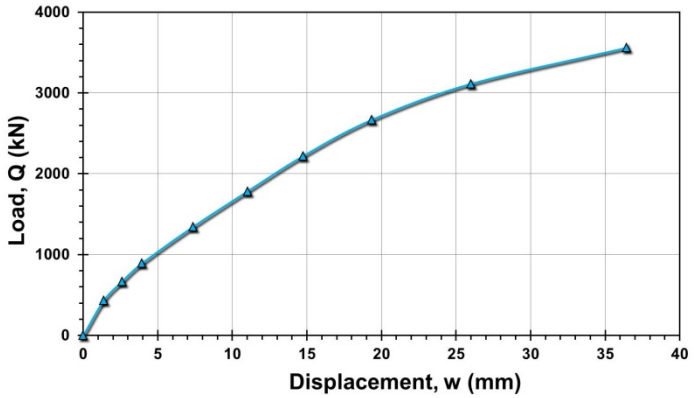

Back-analyzed normalized operational stiffness vs. pseudo-strain

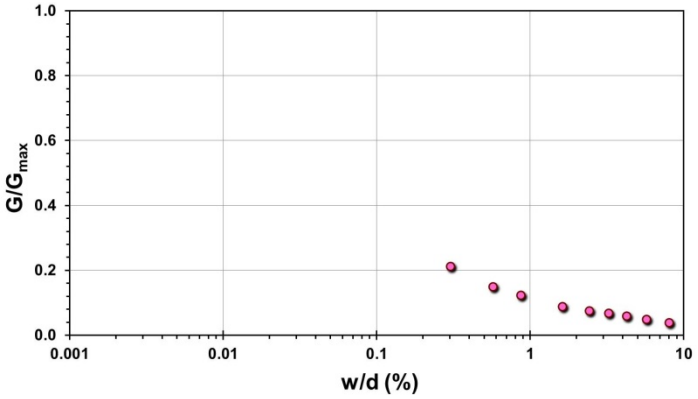

Detail	Description
Pile type/material	H-section pile
Length, L (m)	16.15
H-section sizes	14 x 73
Installation method	Driven
Loading mode	Compression
$Q_{max\text{-}measured}$ (kN)	3,559.61
Q_s (kN)	2,634.11
Q_b (kN)	925.50
$Q_{Davisson}$ (kN)	2,667.03
$Q_{w/d=10\%}$ (kN)	4,248.70
$Q_{C\text{-}K}$ (kN)	6,289.31

Pile ID: L&D 1-7C

Load-displacement data

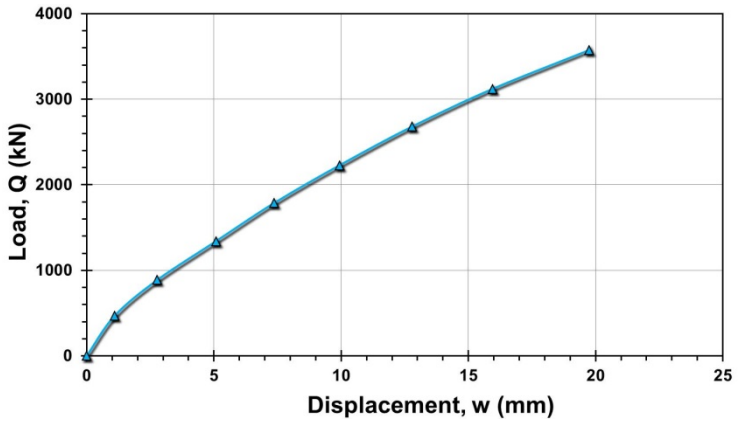

Back-analyzed normalized operational stiffness vs. pseudo-strain

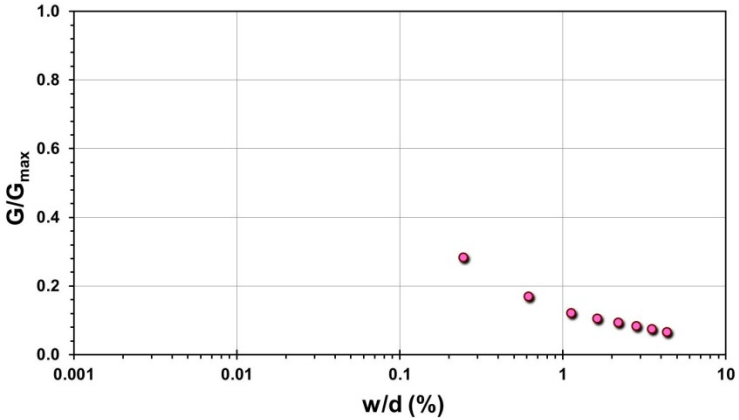

Detail	Description
Pile type/material	H-section pile
Length, L (m)	17.98
H-section sizes	14 x 73
Installation method	Driven
Loading mode	Compression
$Q_{max\text{-}measured}$ (kN)	3,573.79
Q_s (kN)	Not reported
Q_b (kN)	Not reported
$Q_{Davisson}$ (kN)	5,109.58
$Q_{w/d=10\%}$ (kN)	5,978.10
$Q_{C\text{-}K}$ (kN)	9,900.98

Pile ID: L&D 2-1T

Load-displacement data

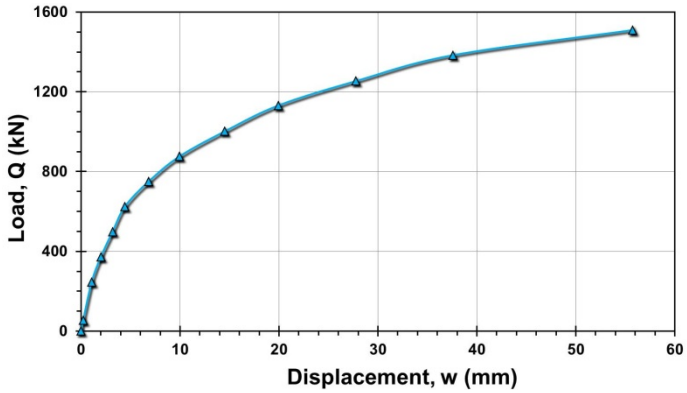

Back-analyzed normalized operational stiffness vs. pseudo-strain

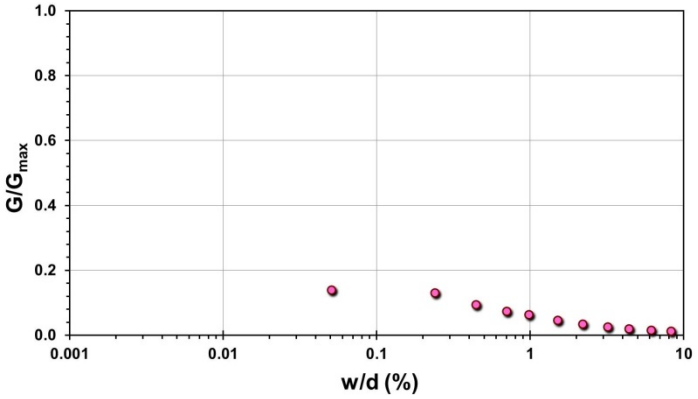

Detail	Description
Pile type/material	H-section pile
Length, L (m)	16.76
H-section sizes	14 x 73
Installation method	Driven
Loading mode	Tension
$Q_{max\text{-}measured}$ (kN)	1,508.92
Q_s (kN)	Not reported
Q_b (kN)	Not reported
$Q_{Davisson}$ (kN)	957.45
$Q_{w/d=10\%}$ (kN)	1,612.00
$Q_{C\text{-}K}$ (kN)	2,057.61

Pile ID: L&D 2-7C

Load-displacement data

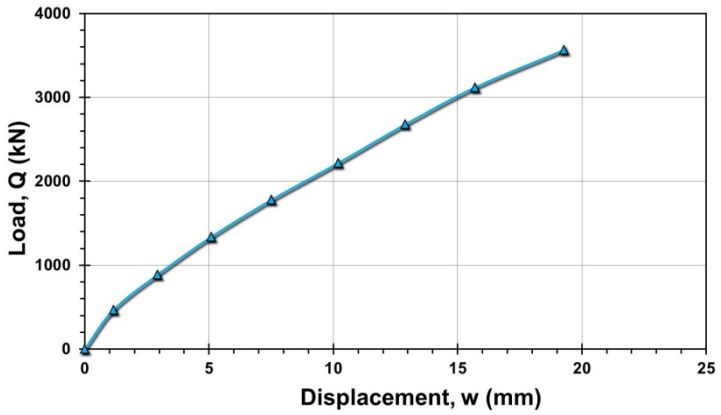

Back-analyzed normalized operational stiffness vs. pseudo-strain

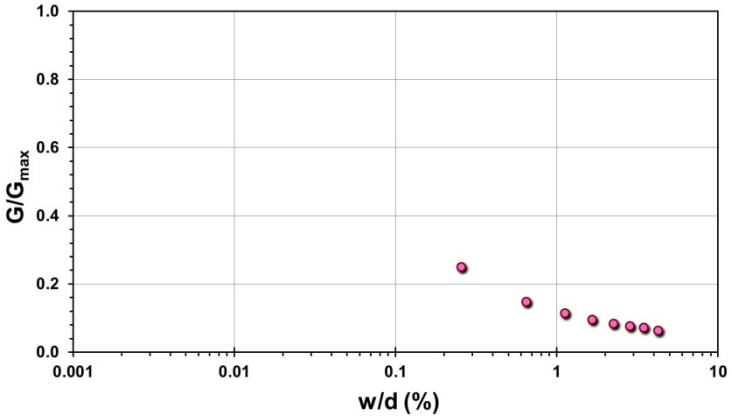

Detail	Description
Pile type/material	H-section pile
Length, L (m)	20.37
H-section sizes	14 x 73
Installation method	Driven
Loading mode	Compression
$Q_{max\text{-}measured}$ (kN)	3,566.51
Q_s (kN)	Not reported
Q_b (kN)	Not reported
$Q_{Davisson}$ (kN)	6,347.54
$Q_{w/d=10\%}$ (kN)	6,307.00
$Q_{C\text{-}K}$ (kN)	11,363.64

Pile ID: L&D 2-8T

Load-displacement data

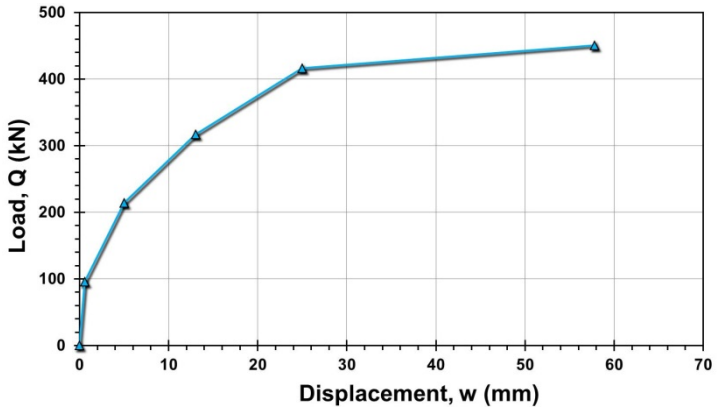

Back-analyzed normalized operational stiffness vs. pseudo-strain

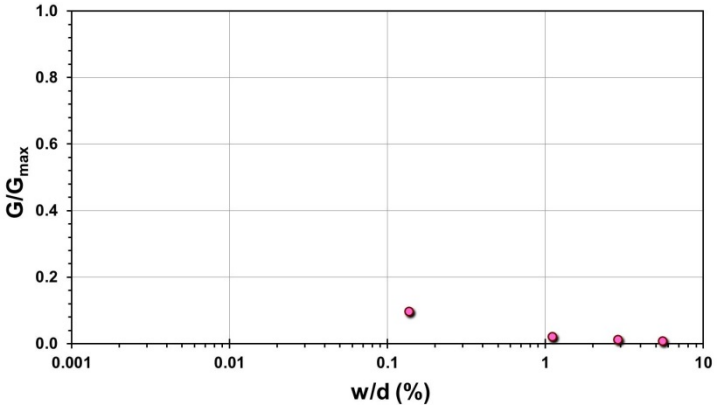

Detail	Description
Pile type/material	H-section pile
Length, L (m)	12.19
H-section sizes	14 x 73
Installation method	Driven
Loading mode	Tension
$Q_{max\text{-}measured}$ (kN)	450.46
Q_s (kN)	Not reported
Q_b (kN)	Not reported
$Q_{Davisson}$ (kN)	263.74
$Q_{w/d=10\%}$ (kN)	505.90
$Q_{C\text{-}K}$ (kN)	577.03

Pile ID: L&D 3-1C

Load-displacement data

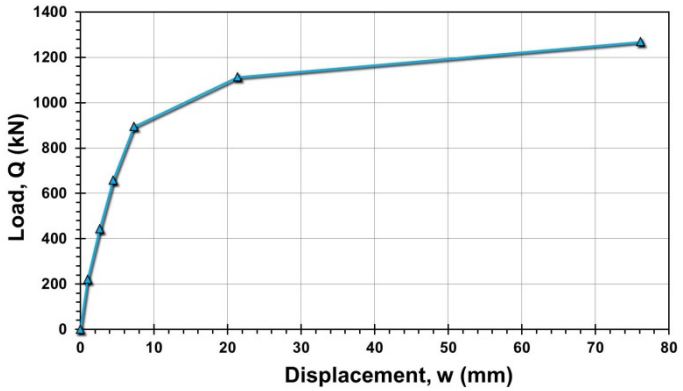

Back-analyzed normalized operational stiffness vs. pseudo-strain

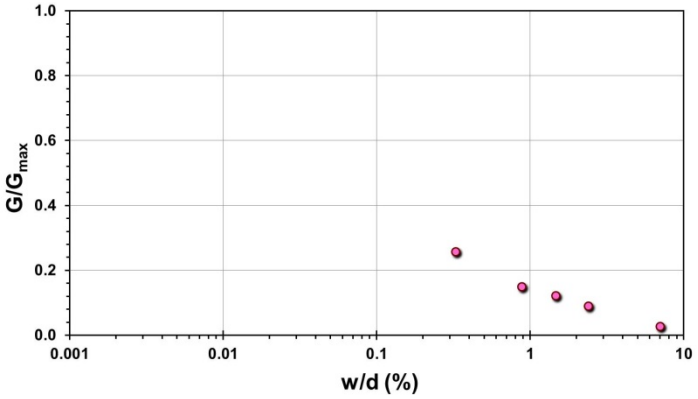

Detail	Description
Pile type/material	Closed-ended steel pipe pile
Length, L (m)	14.23
Diameter, d (m)	0.30
Installation method	Driven
Loading mode	Compression
$Q_{max\text{-}measured}$ (kN)	1,268.93
Q_s (kN)	Not reported
Q_b (kN)	Not reported
$Q_{Davisson}$ (kN)	1,112.85
$Q_{w/d=10\%}$ (kN)	1,298.50
$Q_{C\text{-}K}$ (kN)	1,477.10

Pile ID: L&D 3-2T

Load-displacement data

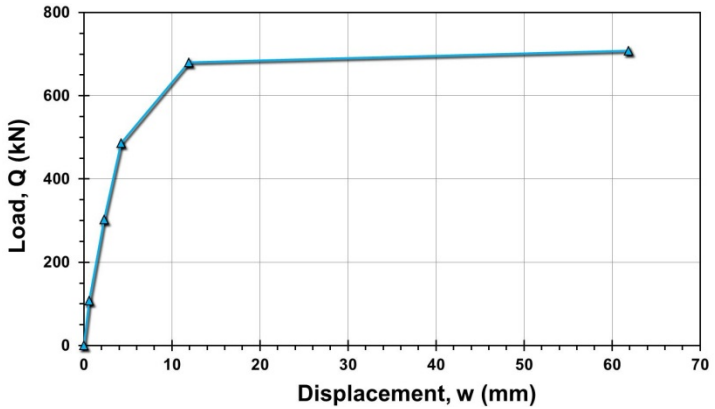

Back-analyzed normalized operational stiffness vs. pseudo-strain

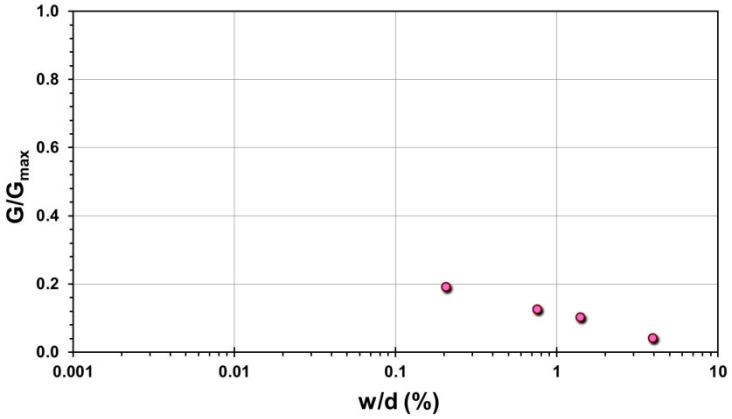

Detail	Description
Pile type/material	Closed-ended steel pipe pile
Length, L (m)	10.97
Diameter, d (m)	0.30
Installation method	Driven
Loading mode	Tension
$Q_{max\text{-}measured}$ (kN)	707.88
Q_s (kN)	Not reported
Q_b (kN)	Not reported
$Q_{Davisson}$ (kN)	680.07
$Q_{w/d=10\%}$ (kN)	771.20
$Q_{C\text{-}K}$ (kN)	808.41

Pile ID: L&D 3-4C

Load-displacement data

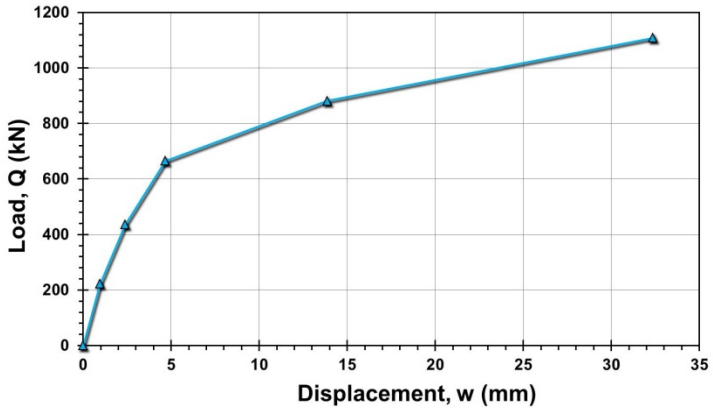

Back-analyzed normalized operational stiffness vs. pseudo-strain

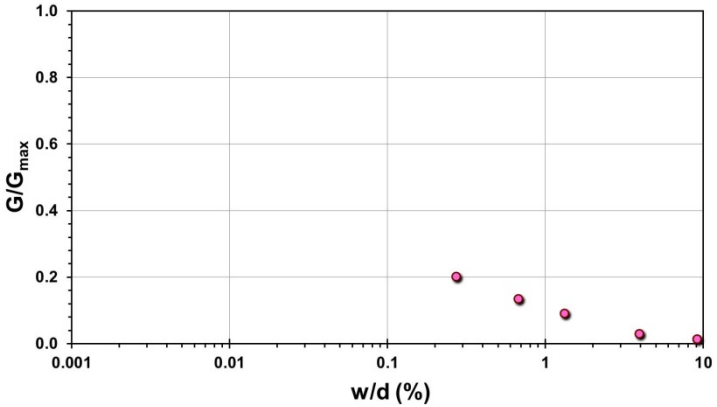

Detail	Description
Pile type/material	Closed-ended steel pipe pile
Length, L (m)	14.39
Diameter, d (m)	0.36
Installation method	Driven
Loading mode	Compression
$Q_{max\text{-}measured}$ (kN)	1,108.66
Q_s (kN)	Not reported
Q_b (kN)	Not reported
$Q_{Davisson}$ (kN)	881.96
$Q_{w/d=10\%}$ (kN)	1,223.20
$Q_{C\text{-}K}$ (kN)	1,385.04

Pile ID: L&D 3-5T

Load-displacement data

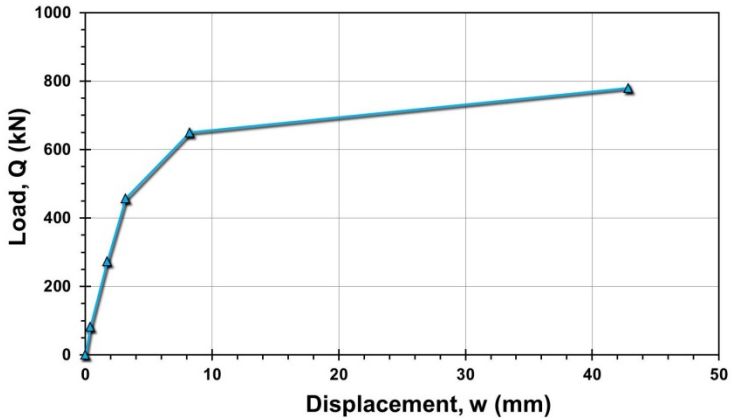

Back-analyzed normalized operational stiffness vs. pseudo-strain

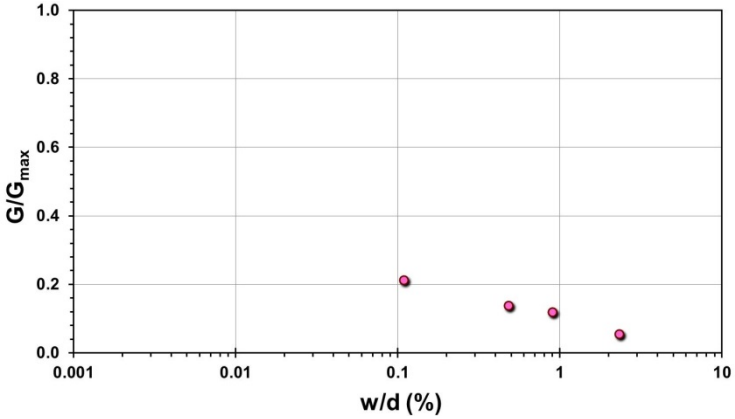

Detail	Description
Pile type/material	Closed-ended steel pipe pile
Length, L (m)	11.12
Diameter, d (m)	0.36
Installation method	Driven
Loading mode	Tension
$Q_{max\text{-}measured}$ (kN)	779.96
Q_s (kN)	Not reported
Q_b (kN)	Not reported
$Q_{Davisson}$ (kN)	686.76
$Q_{w/d=10\%}$ (kN)	862.30
$Q_{C\text{-}K}$ (kN)	919.12

Pile ID: L&D 3-7C

Load-displacement data

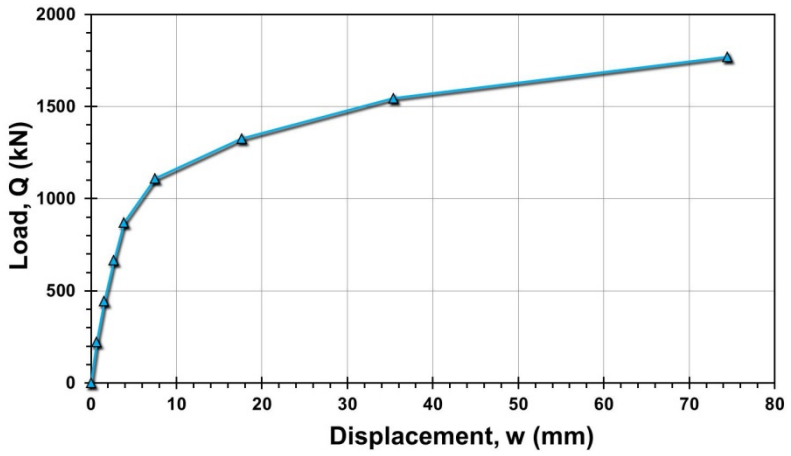

Back-analyzed normalized operational stiffness vs. pseudo-strain

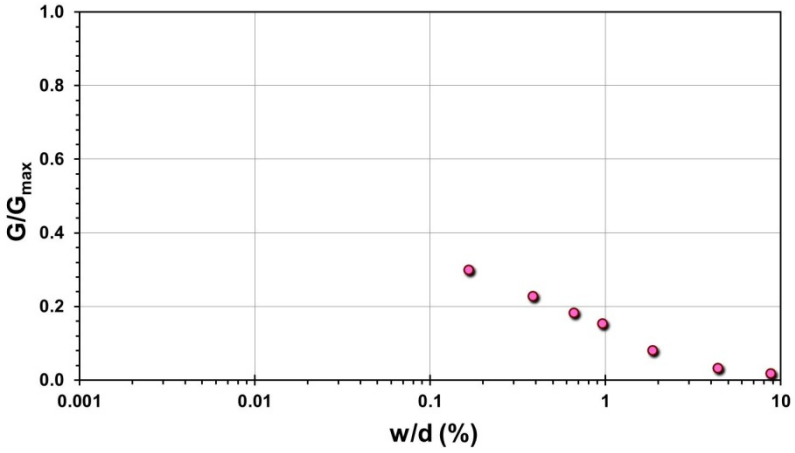

Detail	Description
Pile type/material	Closed-ended steel pipe pile
Length, L (m)	14.57
Diameter, d (m)	0.41
Installation method	Driven
Loading mode	Compression
$Q_{max\text{-}measured}$ (kN)	1,770.12
Q_s (kN)	Not reported
Q_b (kN)	Not reported
$Q_{Davisson}$ (kN)	1,254.71
$Q_{w/d=10\%}$ (kN)	1,814.70
$Q_{C\text{-}K}$ (kN)	2,083.33

Pile ID: L&D 3-8T

Load-displacement data

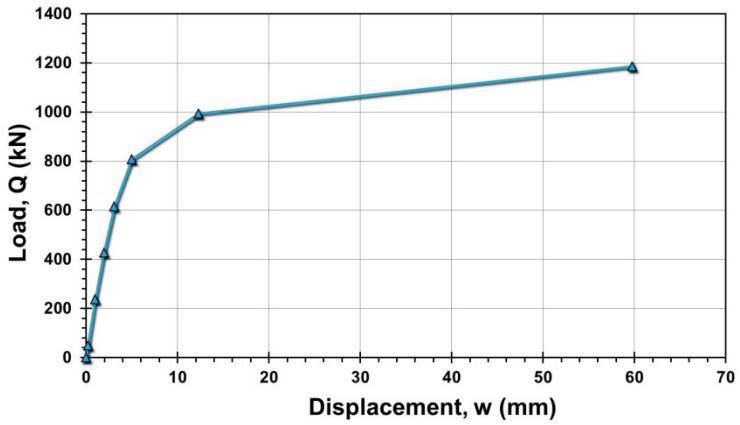

Back-analyzed normalized operational stiffness vs. pseudo-strain

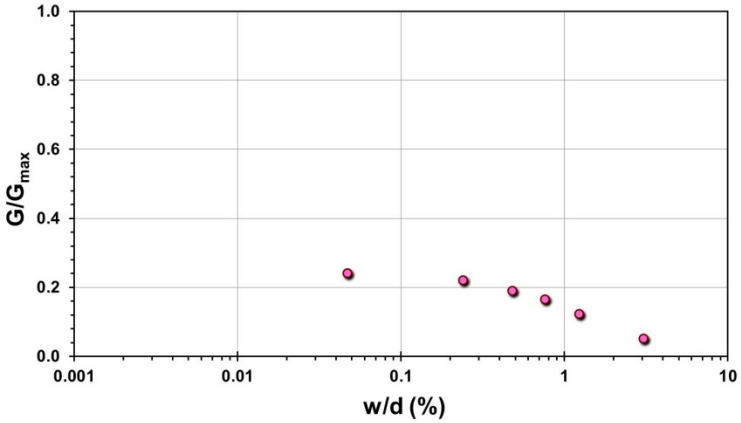

Detail	Description
Pile type/material	Closed-ended steel pipe pile
Length, L (m)	11.12
Diameter, d (m)	0.41
Installation method	Driven
Loading mode	Tension
$Q_{max\text{-}measured}$ (kN)	1,185.85
Q_s (kN)	Not reported
Q_b (kN)	Not reported
$Q_{Davisson}$ (kN)	985.76
$Q_{w/d=10\%}$ (kN)	1,292.80
$Q_{C\text{-}K}$ (kN)	1,392.76

Pile ID: L&D 3-10C

Load-displacement data

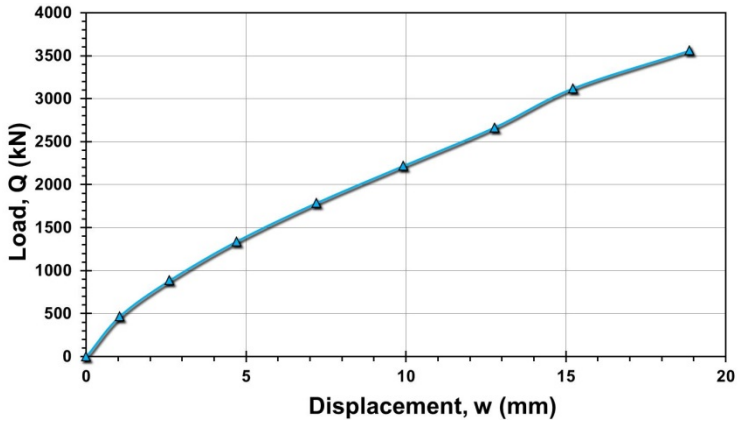

Back-analyzed normalized operational stiffness vs. pseudo-strain

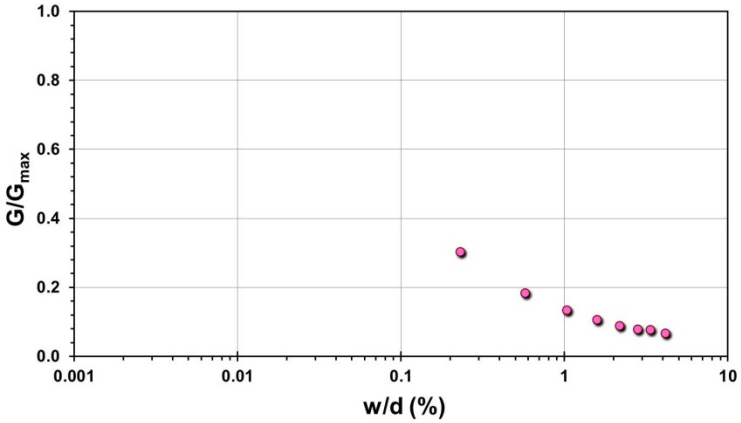

Detail	Description
Pile type/material	H-section pile
Length, L (m)	20.02
H-section sizes	14 x 73
Installation method	Driven
Loading mode	Compression
$Q_{max\text{-}measured}$ (kN)	3,559.13
Q_s (kN)	Not reported
Q_b (kN)	Not reported
$Q_{Davisson}$ (kN)	4,902.27
$Q_{w/d=10\%}$ (kN)	5,465.60
$Q_{C\text{-}K}$ (kN)	7,936.51

Pile ID: L&D 3-14T

Load-displacement data

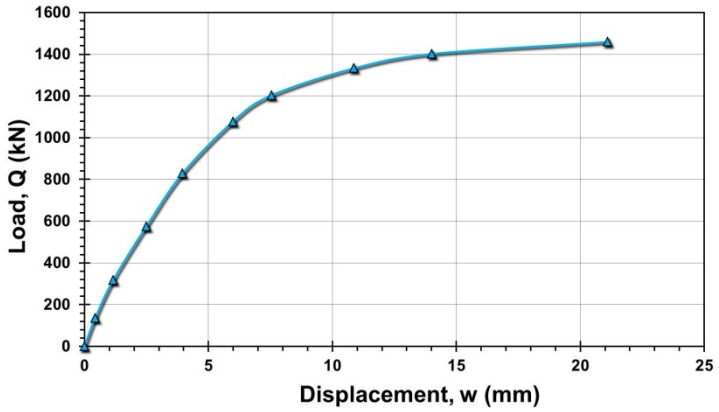

Back-analyzed normalized operational stiffness vs. pseudo-strain

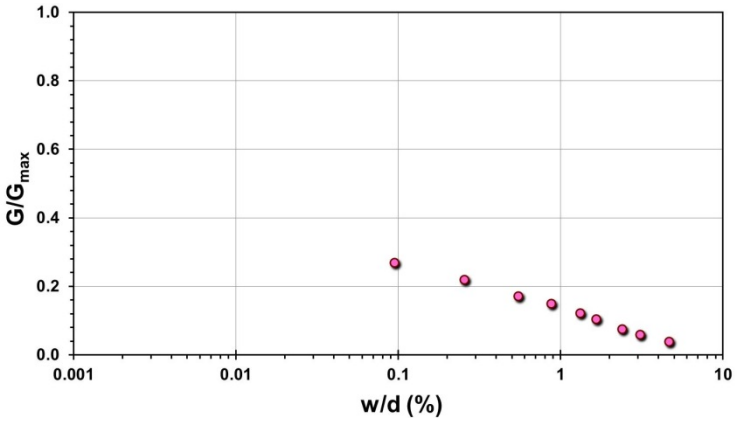

Detail	Description
Pile type/material	H-section pile
Length, L (m)	11.89
H-section sizes	14 x 73
Installation method	Driven
Loading mode	Tension
$Q_{max\text{-}measured}$ (kN)	1,459.20
Q_s (kN)	Not reported
Q_b (kN)	Not reported
$Q_{Davisson}$ (kN)	1,377.24
$Q_{w/d=10\%}$ (kN)	1,759.40
$Q_{C\text{-}K}$ (kN)	1,876.17

Pile ID: L&D 3-15T

Load-displacement data

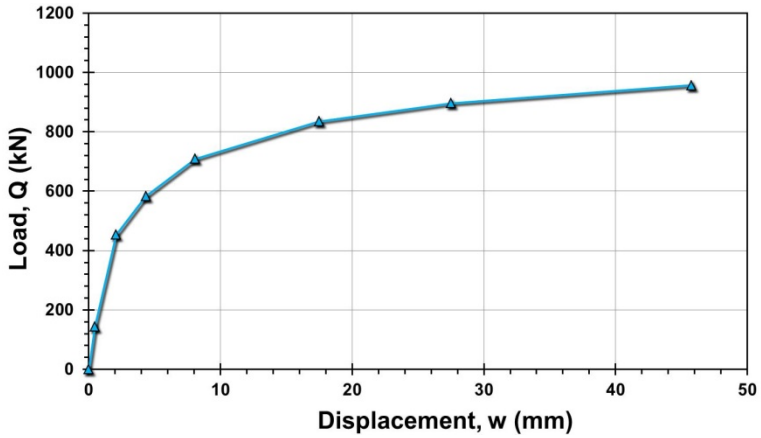

Back-analyzed normalized operational stiffness vs. pseudo-strain

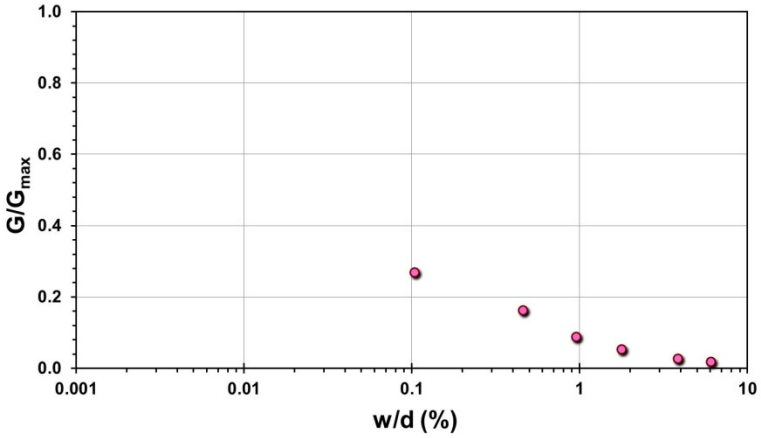

Detail	Description
Pile type/material	H-section pile
Length, L (m)	11.28
H-section sizes	14 x 73
Installation method	Driven
Loading mode	Tension
$Q_{max\text{-}measured}$ (kN)	957.19
Q_s (kN)	Not reported
Q_b (kN)	Not reported
$Q_{Davisson}$ (kN)	722.69
$Q_{w/d=10\%}$ (kN)	1,067.10
$Q_{C\text{-}K}$ (kN)	1,150.75

Pile ID: L&D 3-16T

Load-displacement data

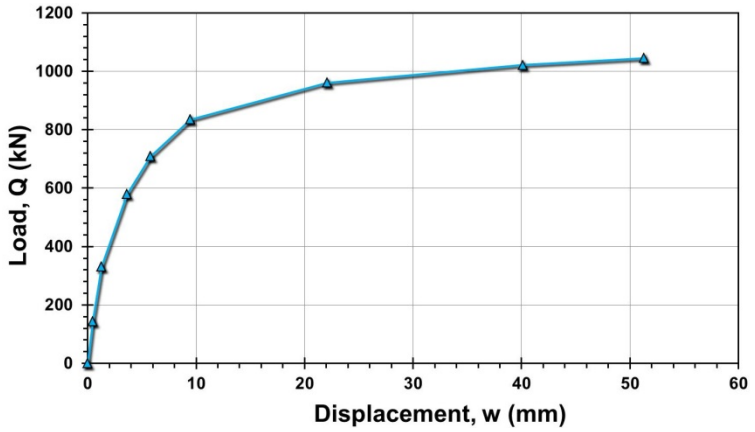

Back-analyzed normalized operational stiffness vs. pseudo-strain

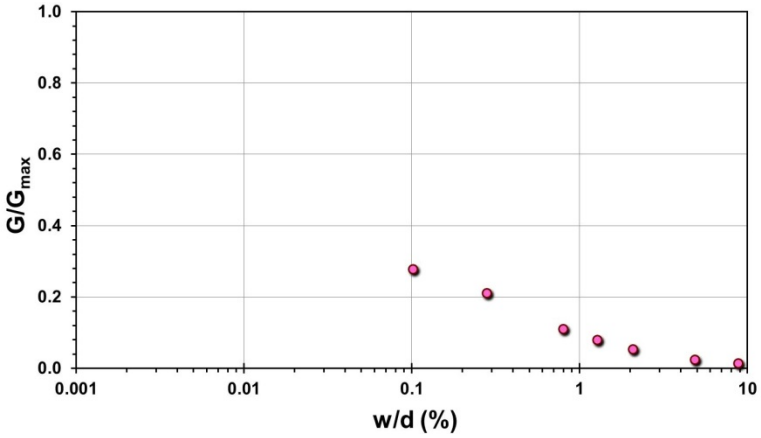

Detail	Description
Pile type/material	H-section pile
Length, L (m)	11.28
H-section sizes	14 x 73
Installation method	Driven
Loading mode	Tension
$Q_{max\text{-}measured}$ (kN)	1,044.99
Q_s (kN)	Not reported
Q_b (kN)	Not reported
$Q_{Davisson}$ (kN)	839.33
$Q_{w/d=10\%}$ (kN)	1,159.60
$Q_{C\text{-}K}$ (kN)	1,240.69

Site ID No. 41

Cone penetrometer data	CPT SBT soil classification index, I_c	Detail	Description
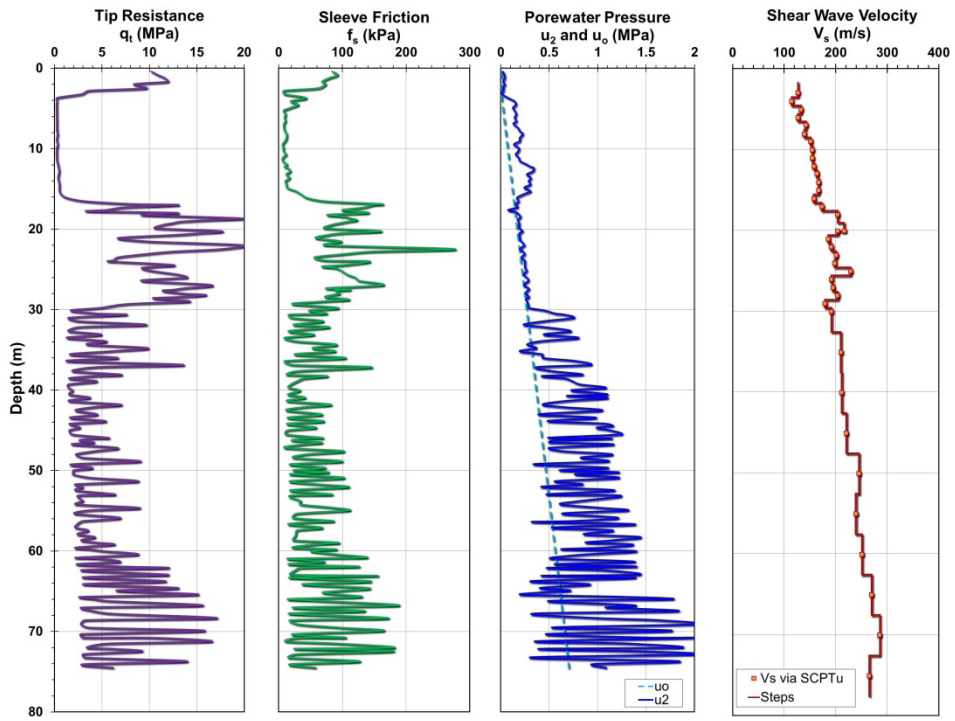	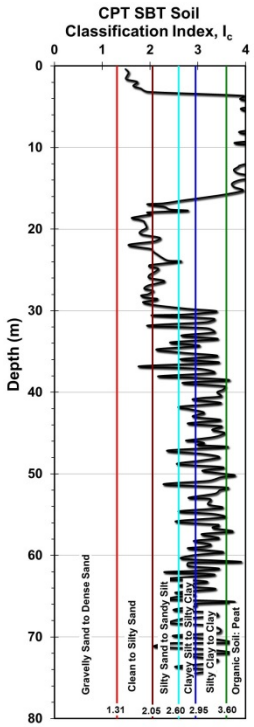	Site name and location	Lulu Island, University of British Columbia Pile Research Site (UBC PRS), BC, Canada
		Soil type(s)	Soft silty clay over medium dense sand over clayey silty sand
		Pile type(s)	1 Open-ended steel pipe pile and 4 closed-ended steel pipe piles
		Type of cone penetrometer testing	SCPTu
		Source of V_s evaluation	SCPTu
		Number of pile load tests	5
		Reference	Davies (1987)
		Comments	

Pile ID: UBC PRS 1

Load-displacement data

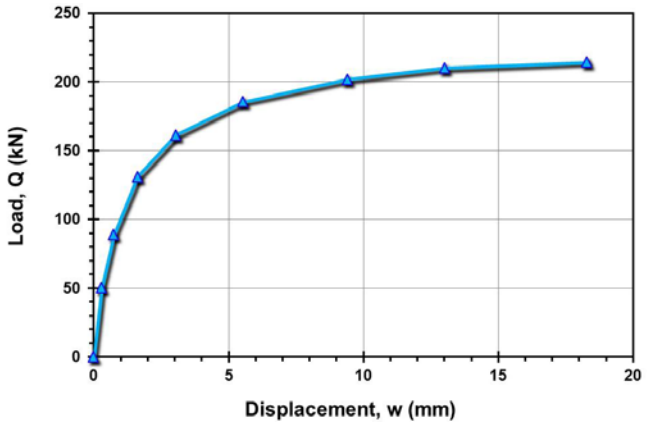

Back-analyzed normalized operational stiffness vs. pseudo-strain

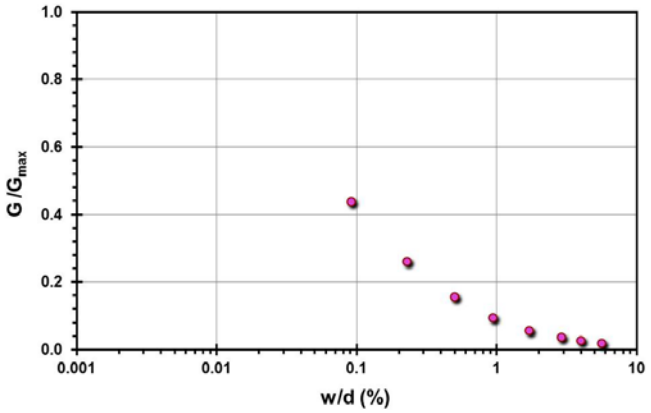

Detail	Description
Pile type/material	Closed-ended steel pipe piles
Length, L (m)	11.83
Diameter, d (m)	0.324
Installation method	Driven
Loading mode	Compression
$Q_{max\text{-}measured}$ (kN)	214.34
Q_s (kN)	146.34
Q_b (kN)	68.00
$Q_{Davisson}$ (kN)	193.67
$Q_{w/d=10\%}$ (kN)	220.85
$Q_{C\text{-}K}$ (kN)	229.52

Pile ID: UBC PRS 2

Load-displacement data

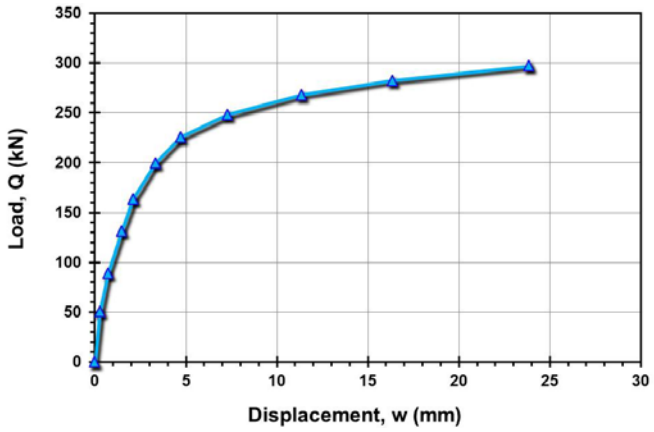

Back-analyzed normalized operational stiffness vs. pseudo-strain

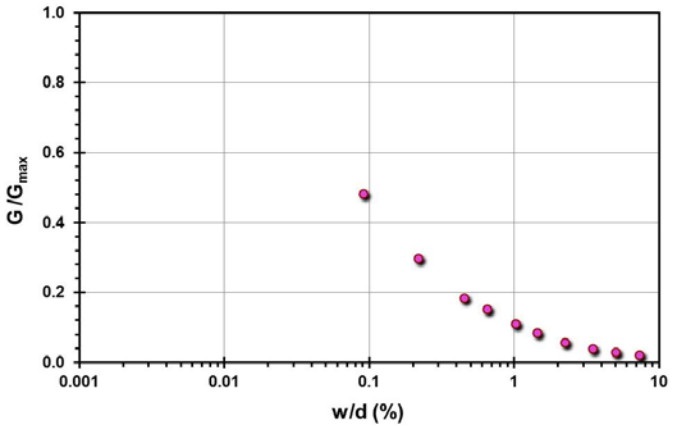

Detail	Description
Pile type/material	Closed-ended steel pipe piles
Length, L (m)	13.90
Diameter, d (m)	0.324
Installation method	Driven
Loading mode	Compression
$Q_{max\text{-}measured}$ (kN)	297.17
Q_s (kN)	253.17
Q_b (kN)	44.00
$Q_{Davisson}$ (kN)	248.02
$Q_{w/d=10\%}$ (kN)	301.78
$Q_{C\text{-}K}$ (kN)	318.24

Pile ID: UBC PRS 3

Load-displacement data

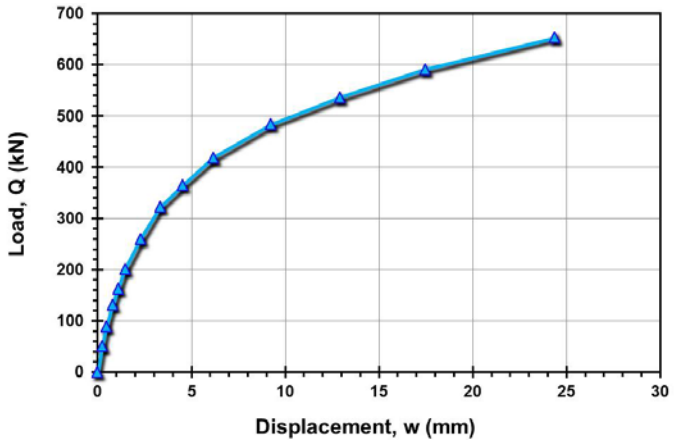

Back-analyzed normalized operational stiffness vs. pseudo-strain

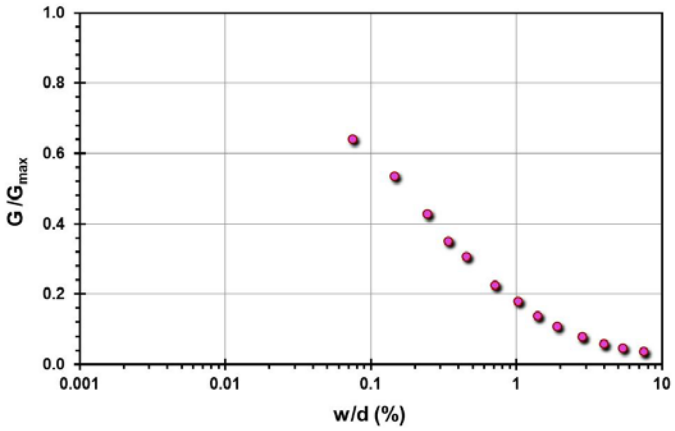

Detail	Description
Pile type/material	Closed-ended steel pipe piles
Length, L (m)	16.80
Diameter, d (m)	0.324
Installation method	Driven
Loading mode	Compression
$Q_{max\text{-}measured}$ (kN)	653.58
Q_s (kN)	348.58
Q_b (kN)	305.00
$Q_{Davisson}$ (kN)	509.95
$Q_{w/d=10\%}$ (kN)	695.80
$Q_{C\text{-}K}$ (kN)	870.32

Pile ID: UBC PRS 4

Load-displacement data

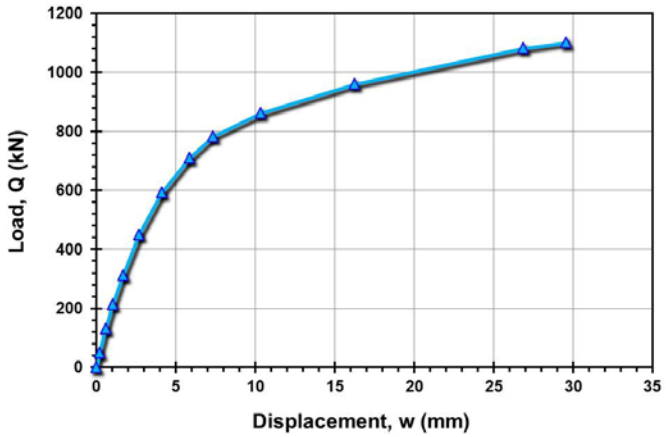

Back-analyzed normalized operational stiffness vs. pseudo-strain

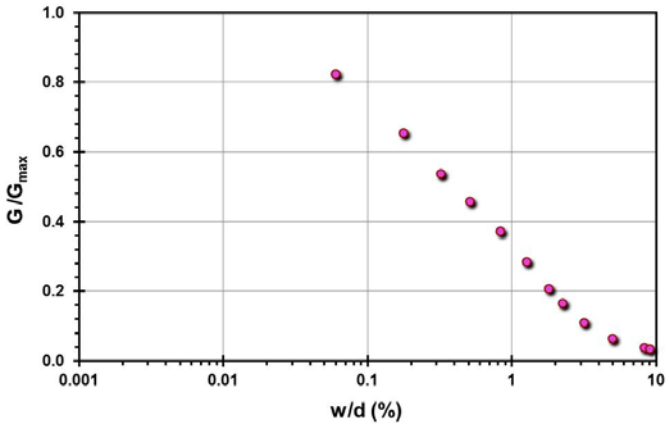

Detail	Description
Pile type/material	Open-ended steel pipe piles
Length, L (m)	23.20
Diameter, d (m)	0.324
Installation method	Driven
Loading mode	Compression
$Q_{max\text{-}measured}$ (kN)	1,102.83
Q_s (kN)	Not reported
Q_b (kN)	Not reported
$Q_{Davisson}$ (kN)	961.22
$Q_{w/d=10\%}$ (kN)	1,120.92
$Q_{C\text{-}K}$ (kN)	1,344.09

Pile ID: UBC PRS 5

Load-displacement data

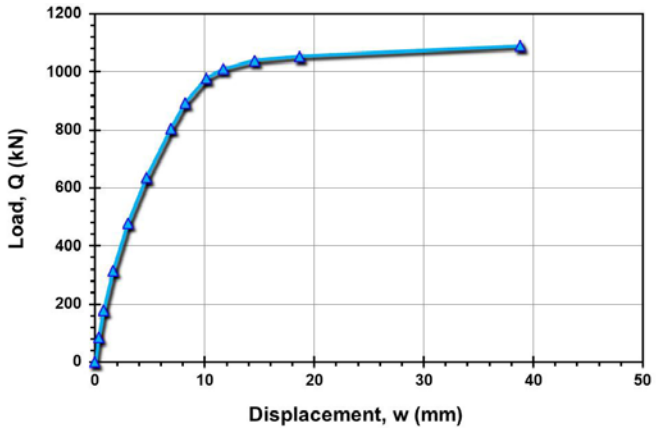

Back-analyzed normalized operational stiffness vs. pseudo-strain

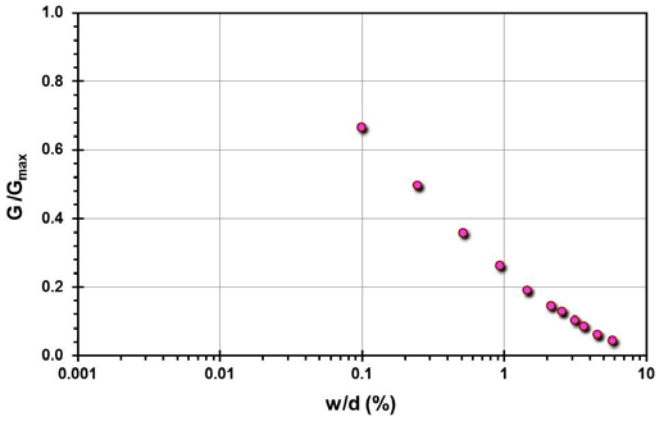

Detail	Description
Pile type/material	Closed-ended steel pipe piles
Length, L (m)	31.10
Diameter, d (m)	0.324
Installation method	Driven
Loading mode	Compression
$Q_{max\text{-}measured}$ (kN)	1,089.20
Q_s (kN)	875.20
Q_b (kN)	214.00
$Q_{Davisson}$ (kN)	1,051.95
$Q_{w/d=10\%}$ (kN)	1,082.76
$Q_{C\text{-}K}$ (kN)	1,126.13

Site ID No. 42

Cone penetrometer data	CPT SBT soil classification index, I_c	Detail	Description
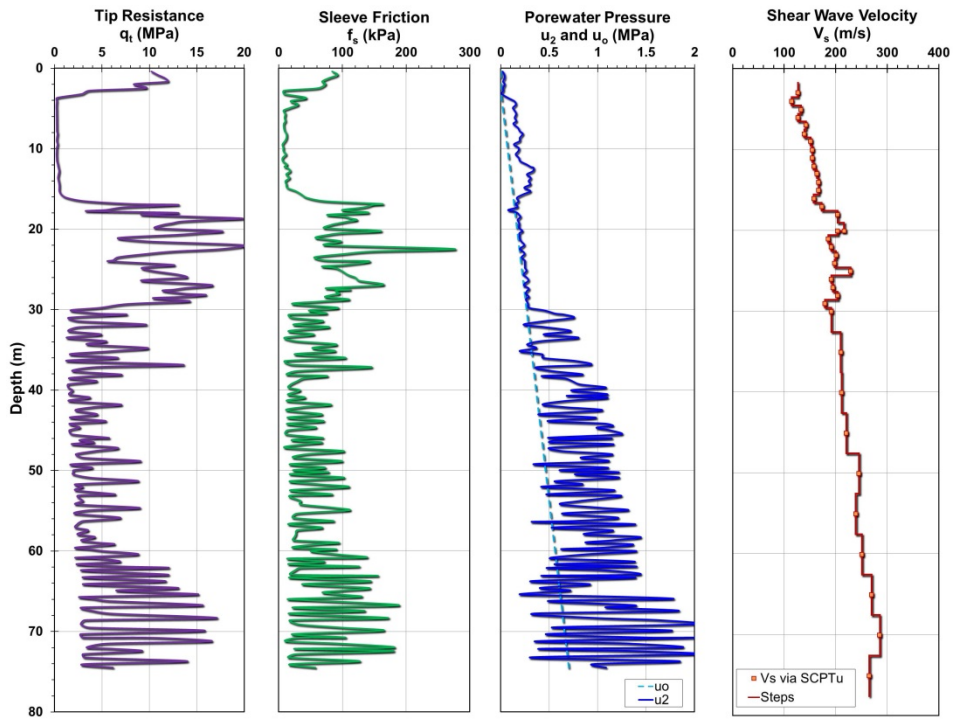	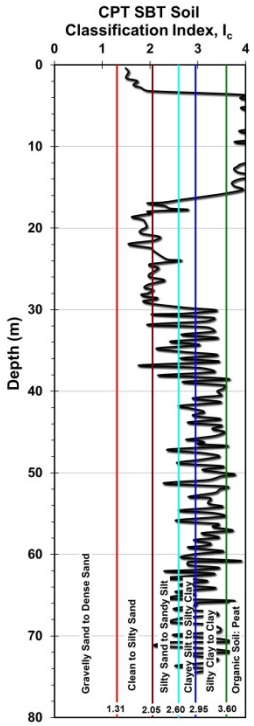	Site name and location	Ministry of Transportation & Highways Pile Research Site (MOTH PRS), Alex Fraser Bridge, BC, Canada
		Soil type(s)	Soft silty clay over medium dense sand over clayey silty sand
		Pile type(s)	Open-ended steel pipe piles
		Type of cone penetrometer testing	SCPTu
		Source of V_s evaluation	SCPTu
		Number of pile load tests	3
		Reference	Davies (1987)
		Comments	

Pile ID: MOTH PRS A

Load-displacement data

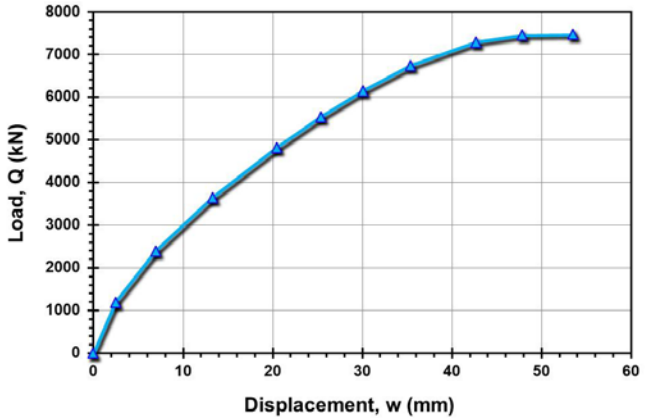

Back-analyzed normalized operational stiffness vs. pseudo-strain

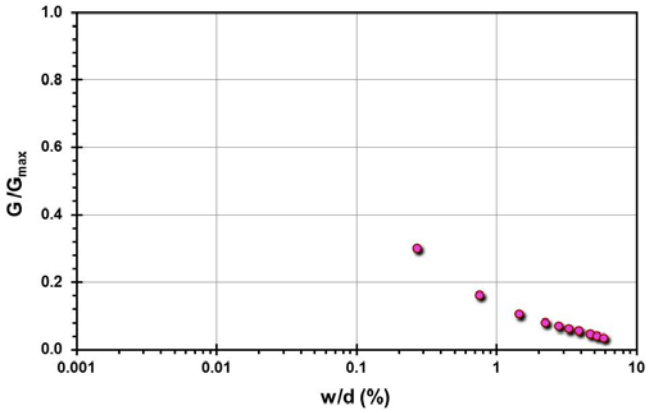

Detail	Description
Pile type/material	Open-ended steel pipe piles
Length, L (m)	67.00
Diameter, d (m)	0.915
Installation method	Driven
Loading mode	Compression
$Q_{max\text{-}measured}$ (kN)	7,462.76
Q_s (kN)	Not reported
Q_b (kN)	Not reported
$Q_{Davisson}$ (kN)	7,432.25
$Q_{w/d=10\%}$ (kN)	7,802.20
$Q_{C\text{-}K}$ (kN)	8,264.46

Pile ID: MOTH PRS B

Load-displacement data

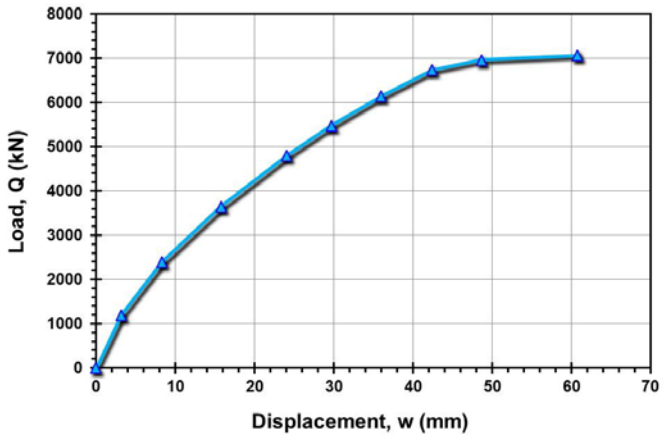

Back-analyzed normalized operational stiffness vs. pseudo-strain

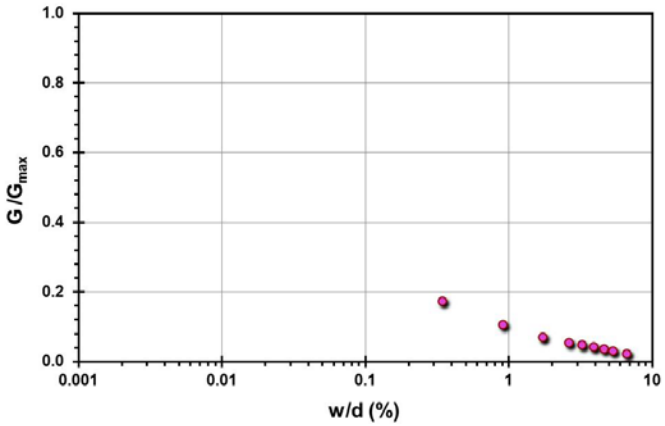

Detail	Description
Pile type/material	Open-ended steel pipe piles
Length, L (m)	78.00
Diameter, d (m)	0.915
Installation method	Driven
Loading mode	Compression
$Q_{max\text{-}measured}$ (kN)	7,064.46
Q_s (kN)	Not reported
Q_b (kN)	Not reported
$Q_{Davisson}$ (kN)	7,003.52
$Q_{w/d=10\%}$ (kN)	7,359.89
$Q_{C\text{-}K}$ (kN)	7,936.51

Pile ID: MOTH PRS C

Load-displacement data

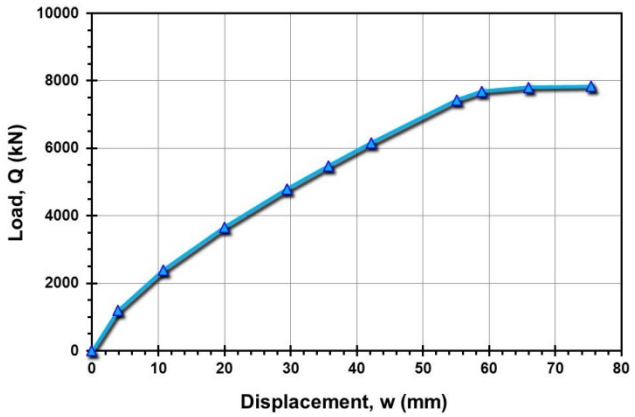

Back-analyzed normalized operational stiffness vs. pseudo-strain

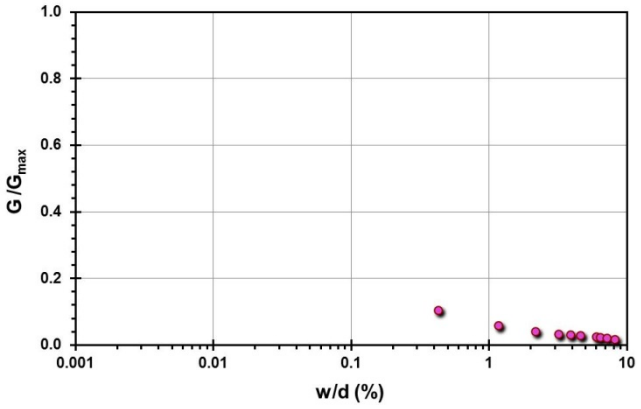

Detail	Description
Pile type/material	Open-ended steel pipe piles
Length, L (m)	94.00
Diameter, d (m)	0.915
Installation method	Driven
Loading mode	Compression
$Q_{max\text{-}measured}$ (kN)	7,832.59
Q_s (kN)	Not reported
Q_b (kN)	Not reported
$Q_{Davisson}$ (kN)	7,822.41
$Q_{w/d=10\%}$ (kN)	7,922.38
$Q_{C\text{-}K}$ (kN)	8,403.36

Site ID No. 43

Cone penetrometer data	CPT SBT soil classification index, I_c	Detail	Description
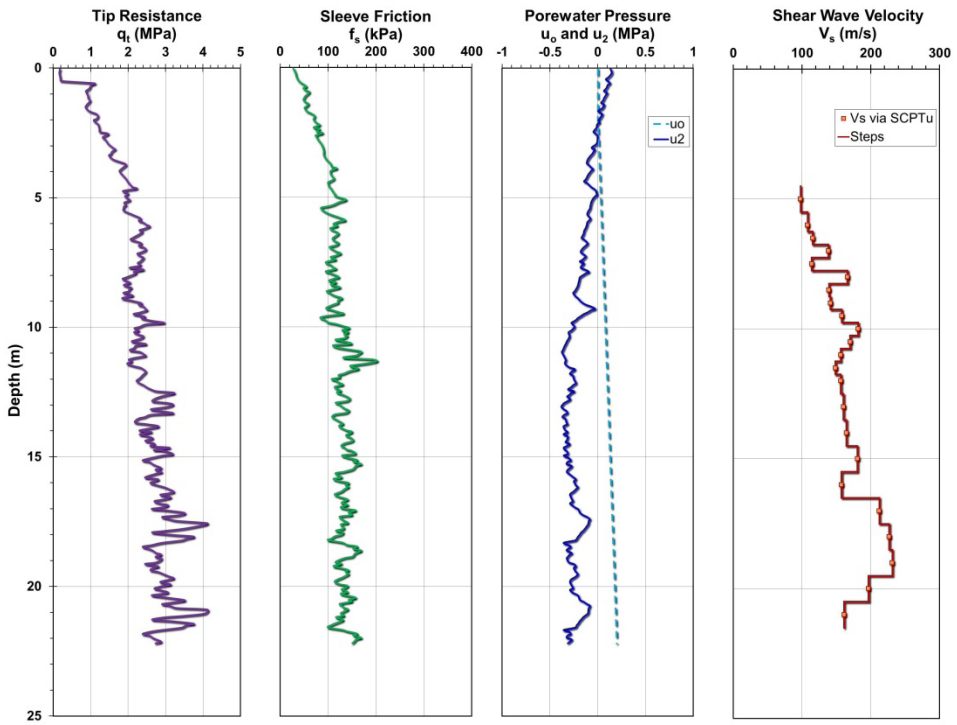	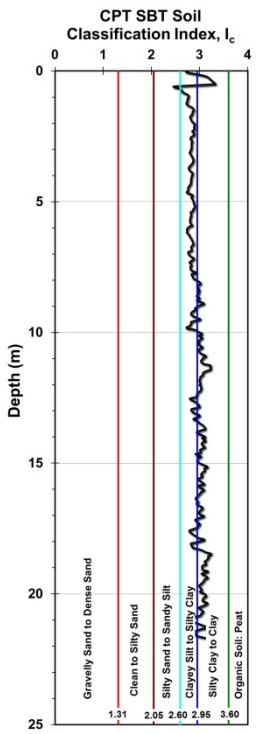	Site name and location	New Museums, Gault clay, Central Cambridge, UK
		Soil type(s)	0.5 m of shallow gravelly fill over stiff fissured clay
		Pile type(s)	Drilled shaft
		Type of cone penetrometer testing	SCPTu
		Source of V_s evaluation	SCPTu
		Number of pile load tests	1
		Reference	Butcher and Lord (1993), Powell et al. (1988)
		Comments	Q-z profile approximate interpretation from the sources

Pile ID: NMGC 1

Load-displacement data

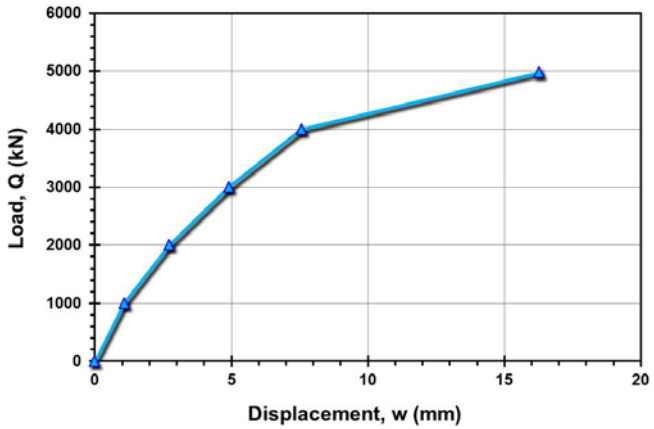

Back-analyzed normalized operational stiffness vs. pseudo-strain

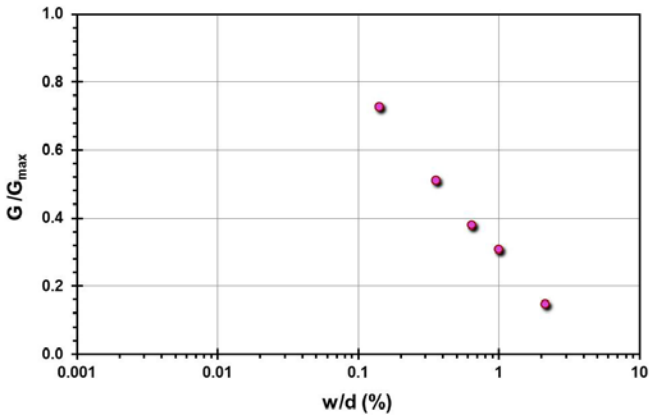

Detail	Description
Pile type/material	Drilled shaft
Length, L (m)	21.50
Diameter, d (m)	0.760
Installation method	Bored cast in-situ
Loading mode	Compression
$Q_{max\text{-}measured}$ (kN)	4,980.00
Q_s (kN)	2,670
Q_b (kN)	2,310.00
$Q_{Davisson}$ (kN)	4,980.00
$Q_{w/d=10\%}$ (kN)	5,981.17
$Q_{C\text{-}K}$ (kN)	6,329.11

Site ID No. 44

Cone penetrometer data	CPT SBT soil classification index, I_c	Detail	Description
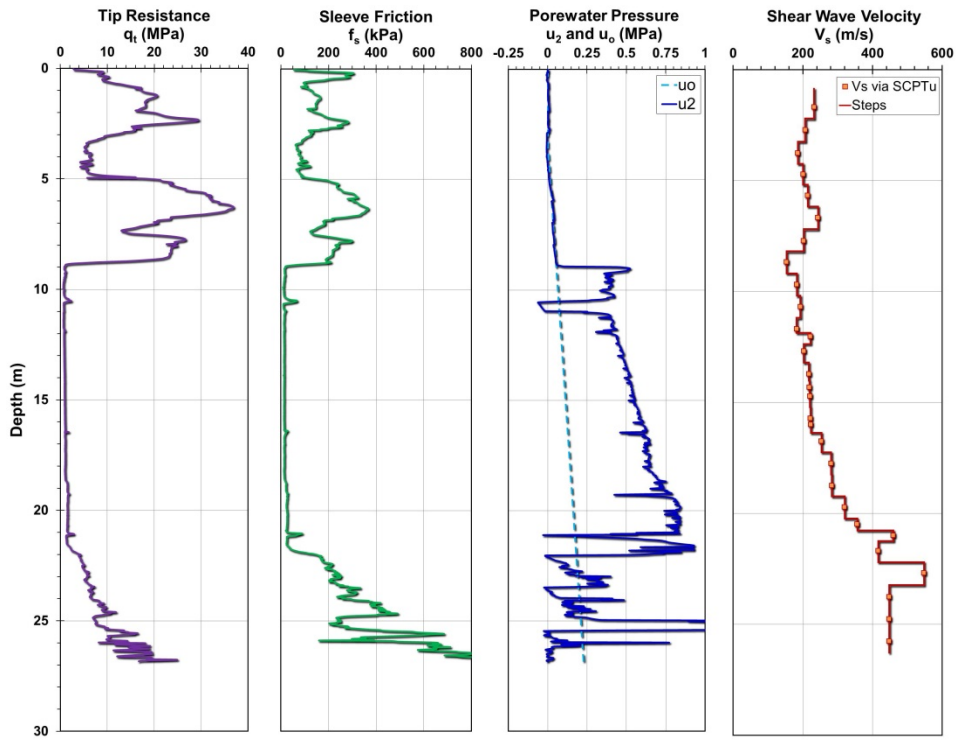	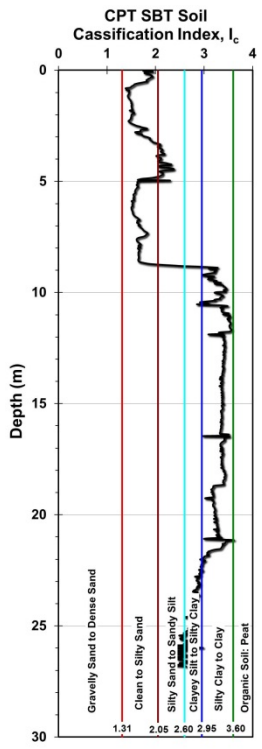	Site name and location	Northwestern University NGES, Evanston, IL, USA
		Soil type(s)	8-m sand fill over soft-medium clay
		Pile type(s)	2 Drilled shafts, 1 H-pile and 1 open-ended steel pipe pile
		Type of cone penetrometer testing	SCPTu
		Source of V_s evaluation	SCPTu
		Number of pile load tests	1
		Reference	Finno (1989), Finno et al. (1989)
		Comments	Some instrumentation went out of function, so not all readings good, some extrapolation of Q-z at base for estimating the base load NOTE: SCPTu obtained by GT CPT rig and reported by Mayne (2007b)

Pile ID: NWU NGES 1

Load-displacement data

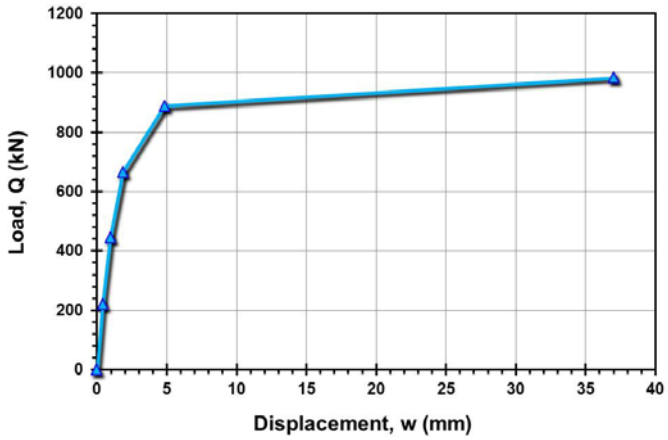

Back-analyzed normalized operational stiffness vs. pseudo-strain

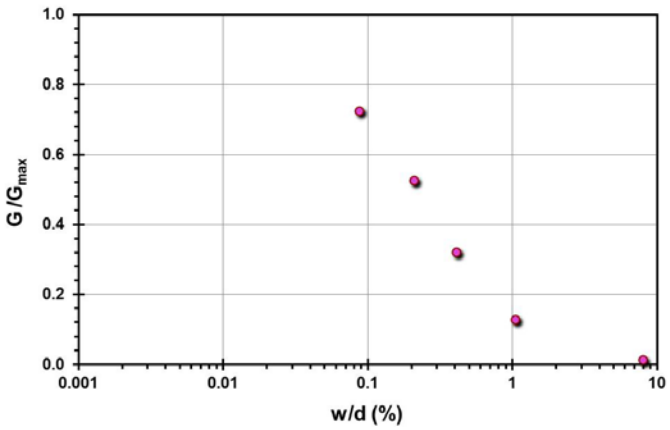

Detail	Description
Pile type/material	H-section pile
Length, L (m)	15.24
H-section sizes	14 x 73
Installation method	Driven
Loading mode	Compression
$Q_{max\text{-}measured}$ (kN)	984.05
Q_s (kN)	944.36
Q_b (kN)	39.69
$Q_{Davisson}$ (kN)	936.06
$Q_{w/d=10\%}$ (kN)	986.93
$Q_{C\text{-}K}$ (kN)	1,004.50

Pile ID: NWU NGES 2

Load-displacement data

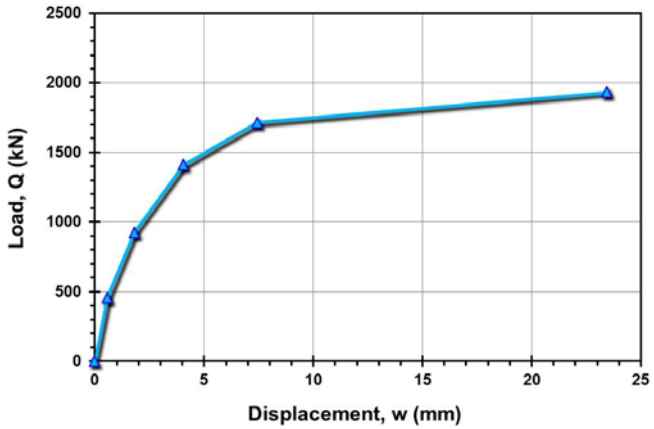

Back-analyzed normalized operational stiffness vs. pseudo-strain

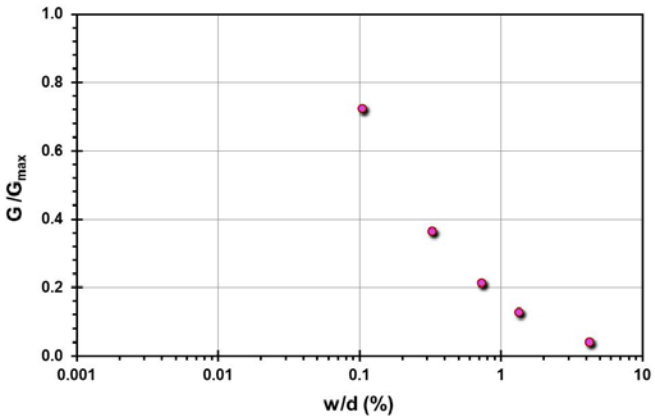

Detail	Description
Pile type/material	Drilled shaft
Length, L (m)	15.24
Diameter, d (m)	0.55
Installation method	Bored cast in-situ
Loading mode	Compression
$Q_{max\text{-}measured}$ (kN)	1,934.01
Q_s (kN)	1,845.79
Q_b (kN)	88.22
$Q_{Davisson}$ (kN)	1,824.91
$Q_{w/d=10\%}$ (kN)	2,017.98
$Q_{C\text{-}K}$ (kN)	2,083.33

Pile ID: NWU NGES 3

Load-displacement data

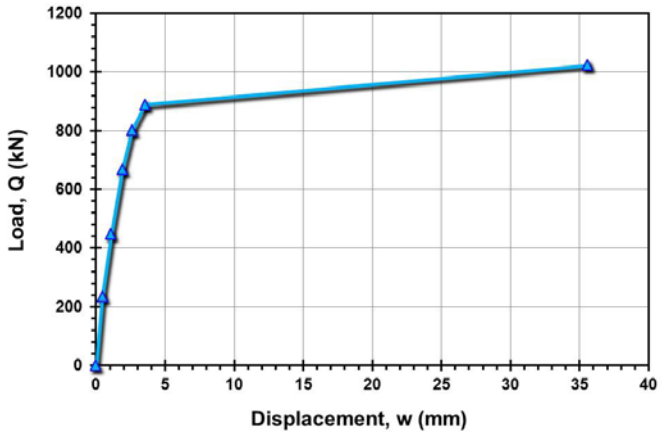

Back-analyzed normalized operational stiffness vs. pseudo-strain

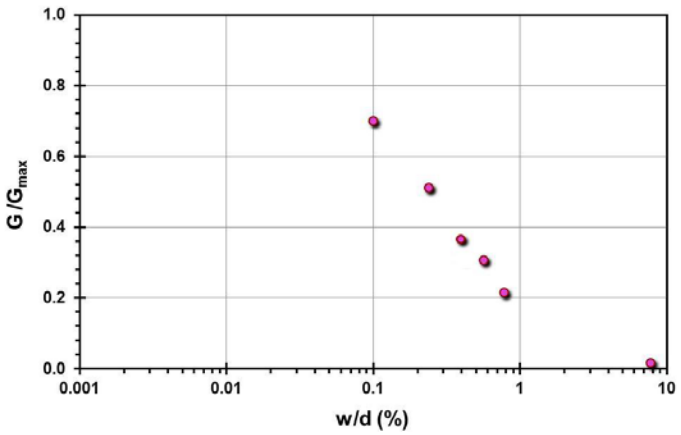

Detail	Description
Pile type/material	Open-ended steel pipe pile
Length, L (m)	15.24
Diameter, d (m)	0.46
Installation method	Driven
Loading mode	Compression
$Q_{max\text{-}measured}$ (kN)	1,023.94
Q_s (kN)	988.98
Q_b (kN)	34.96
$Q_{Davisson}$ (kN)	956.11
$Q_{w/d=10\%}$ (kN)	1,029.22
$Q_{C\text{-}K}$ (kN)	1,044.93

Pile ID: NWU NGES 4

Load-displacement data

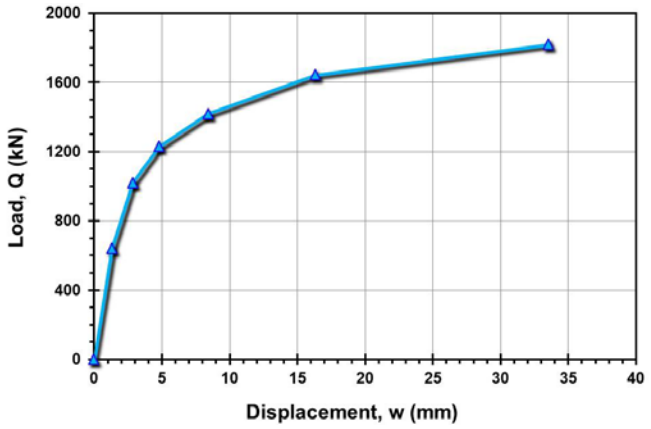

Back-analyzed normalized operational stiffness vs. pseudo-strain

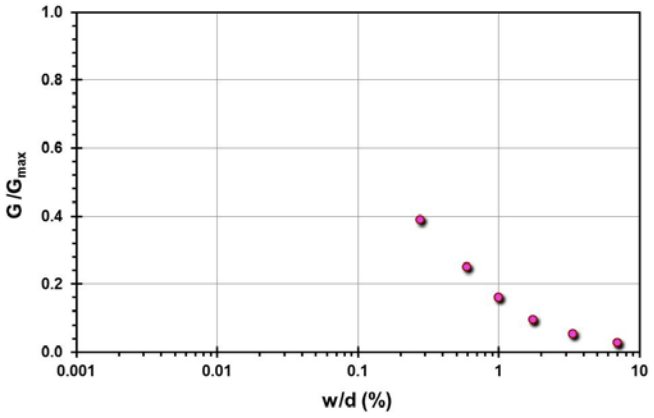

Detail	Description
Pile type/material	Drilled shaft
Length, L (m)	15.24
Diameter, d (m)	0.48
Installation method	Bored cast in-situ
Loading mode	Compression
$Q_{max\text{-}measured}$ (kN)	1,820.76
Q_s (kN)	1,698.51
Q_b (kN)	122.25
$Q_{Davisson}$ (kN)	1,532.38
$Q_{w/d=10\%}$ (kN)	1,856.95
$Q_{C\text{-}K}$ (kN)	1,972.39

Site ID No. 45

Cone penetrometer data	CPT SBT soil classification index, I_c	Detail	Description
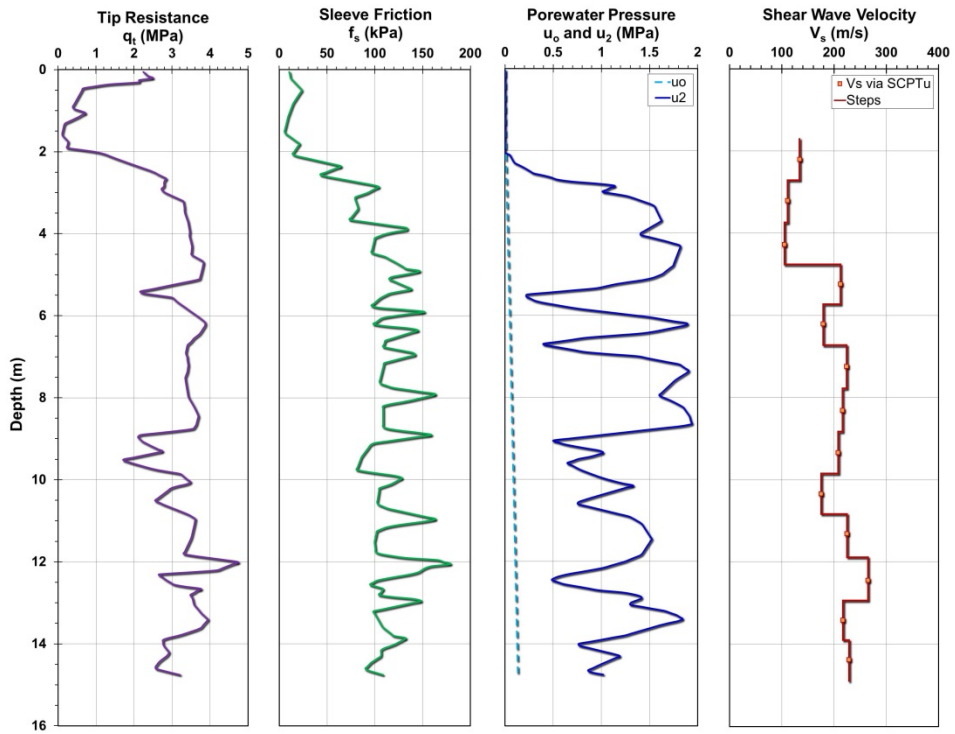	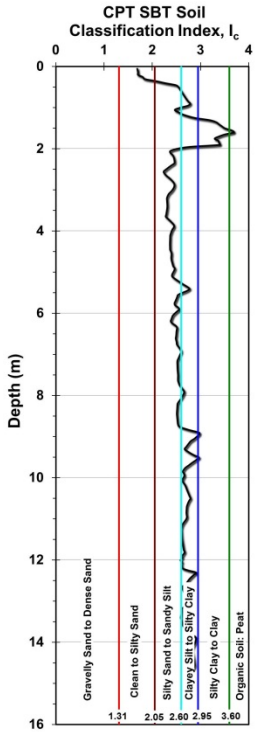	Site name and location	Noetsu Bridges No. 3 and 4, Noto Peninsula, Japan
		Soil type(s)	Diatomaceous mudstone
		Pile type(s)	Open-ended steel pipe piles
		Type of cone penetrometer testing	SCPTu
		Source of V_s evaluation	SCPTu
		Number of pile load tests	3
		Reference	Matsumoto et al. (1995)
		Comments	

Pile ID: NWU NP T1

Load-displacement data

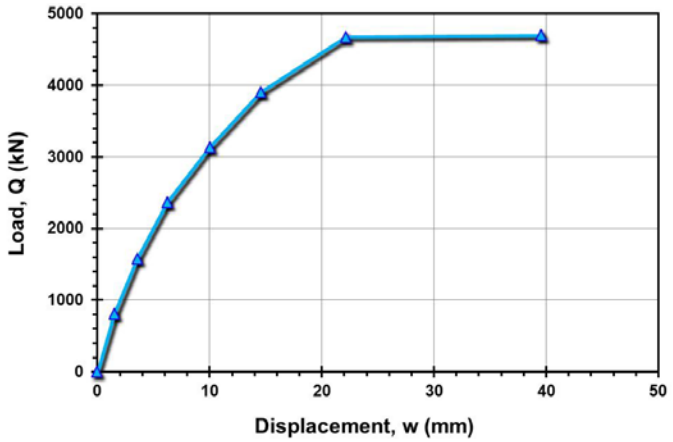

Back-analyzed normalized operational stiffness vs. pseudo-strain

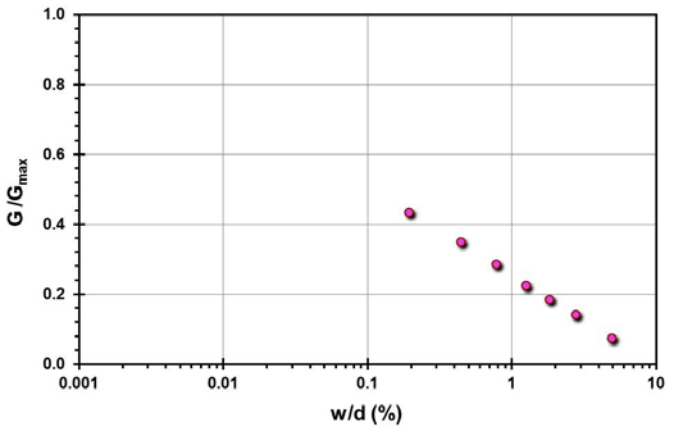

Detail	Description
Pile type/material	Open-ended steel pipe pile
Length, L (m)	8.30
Diameter, d (m)	0.80
Installation method	Driven
Loading mode	Compression
$Q_{max\text{-}measured}$ (kN)	4,695.34
Q_s (kN)	3,725.43
Q_b (kN)	969.91
$Q_{Davisson}$ (kN)	3,906.81
$Q_{w/d=10\%}$ (kN)	4,704.28
$Q_{C\text{-}K}$ (kN)	4,716.98

Pile ID: NWU NP T2

Load-displacement data

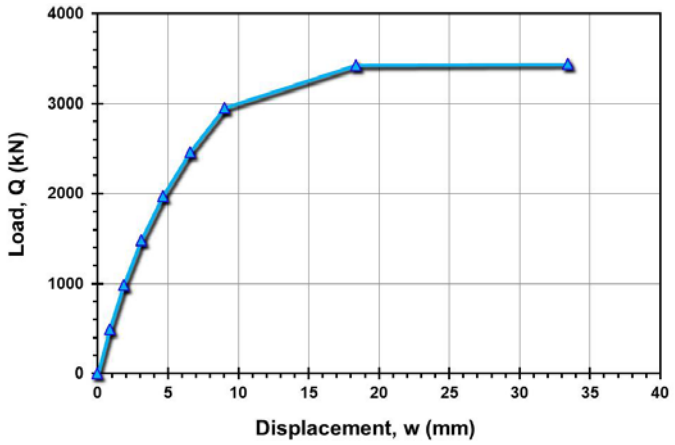

Back-analyzed normalized operational stiffness vs. pseudo-strain

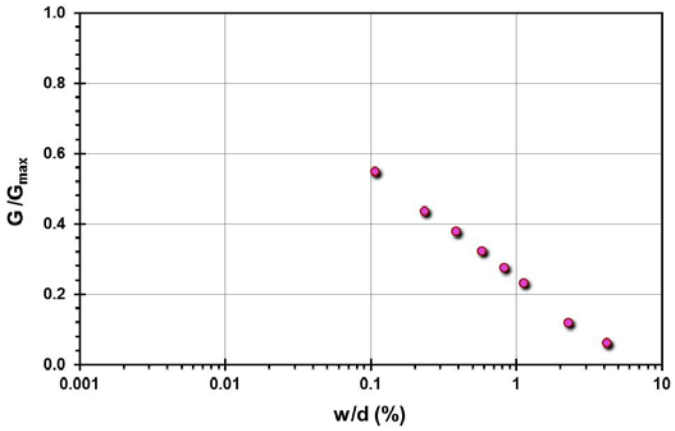

Detail	Description
Pile type/material	Open-ended steel pipe pile
Length, L (m)	8.30
Diameter, d (m)	0.80
Installation method	Driven
Loading mode	Compression
$Q_{max\text{-}measured}$ (kN)	3,438.85
Q_s (kN)	2941.85
Q_b (kN)	497.00
$Q_{Davisson}$ (kN)	3,189.78
$Q_{w/d=10\%}$ (kN)	3,559.40
$Q_{C\text{-}K}$ (kN)	3,636.36

Pile ID: NWU NP T3

Load-displacement data

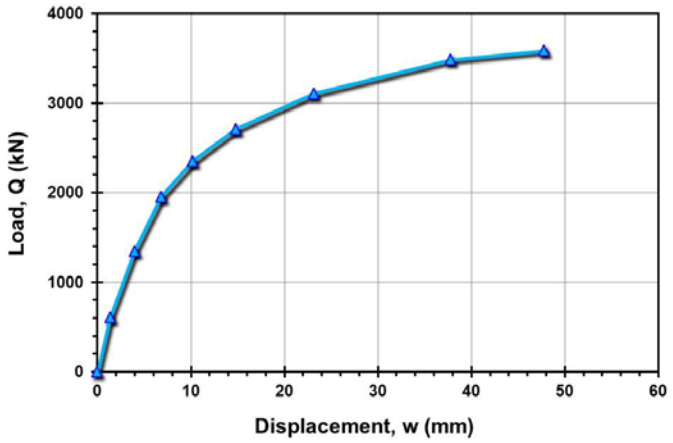

Back-analyzed normalized operational stiffness vs. pseudo-strain

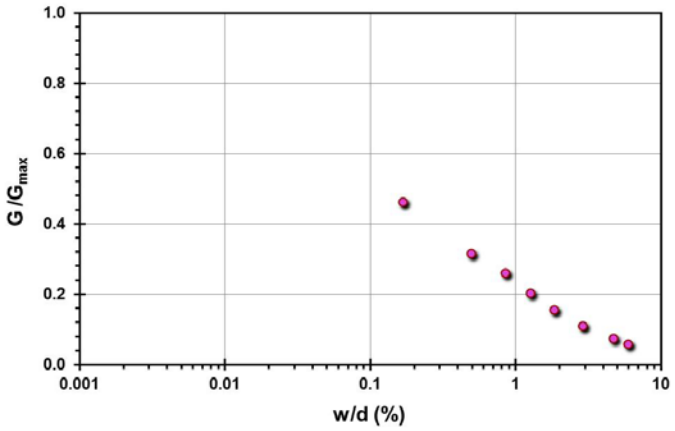

Detail	Description
Pile type/material	Open-ended steel pipe pile
Length, L (m)	8.80
Diameter, d (m)	0.80
Installation method	Driven
Loading mode	Tension
$Q_{max\text{-}measured}$ (kN)	3,587.60
Q_s (kN)	3,587.60
Q_b (kN)	-
$Q_{Davisson}$ (kN)	2,712.60
$Q_{w/d=10\%}$ (kN)	3,819.87
$Q_{C\text{-}K}$ (kN)	4,201.68

Site ID No. 46

Cone penetrometer data	CPT SBT soil classification index, I_c	Detail	Description
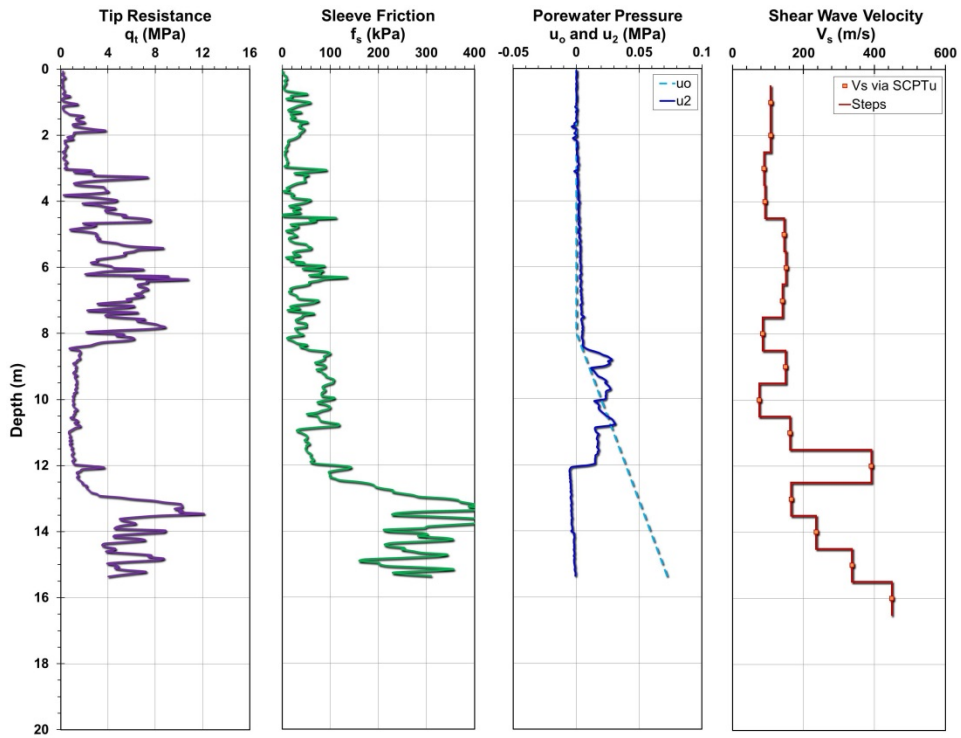	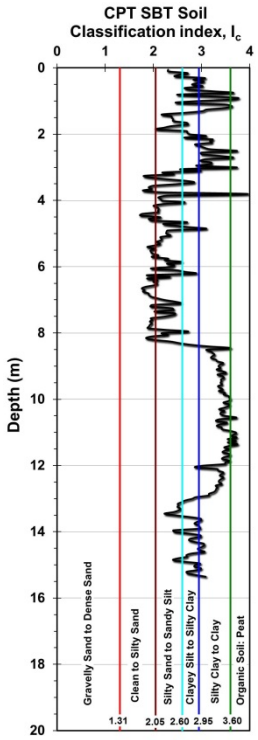	Site name and location	Old San Juan site, Puerto Rico
		Soil type(s)	Interbedded sand and clay
		Pile type(s)	Drilled shaft
		Type of cone penetrometer testing	SCPTu
		Source of V_s evaluation	SCPTu
		Number of pile load tests	1
		Reference	Pando et al. (2004)
		Comments	

Pile ID: OSJS 1

Load-displacement data

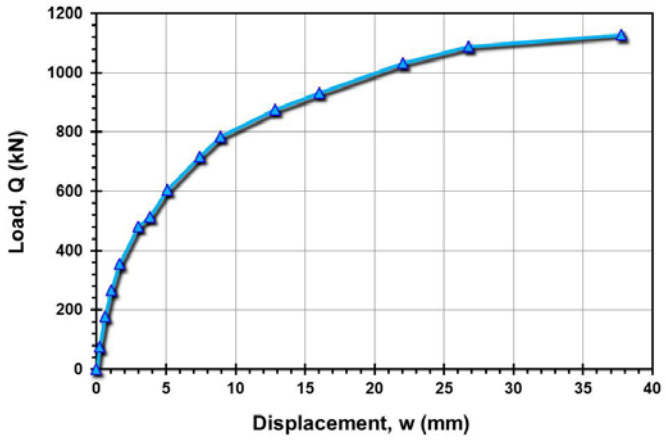

Back-analyzed normalized operational stiffness vs. pseudo-strain

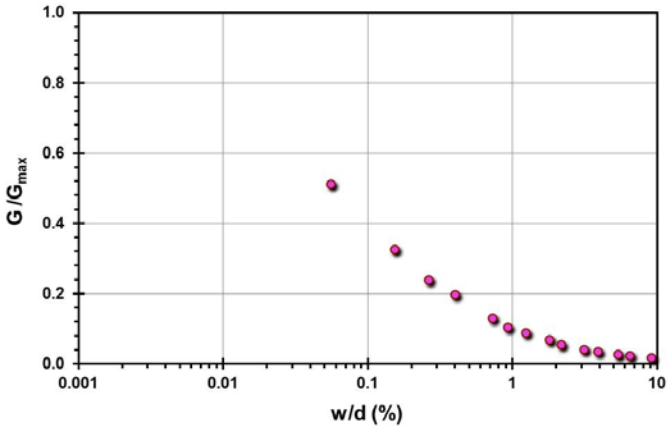

Detail	Description
Pile type/material	Drilled shaft
Length, L (m)	12.80
Diameter, d (m)	0.406
Installation method	Bored cast in-situ
Loading mode	Compression
$Q_{max\text{-}measured}$ (kN)	1,129.06
Q_s (kN)	684.06
Q_b (kN)	445
$Q_{Davisson}$ (kN)	784.69
$Q_{w/d=10\%}$ (kN)	1,149.55
$Q_{C\text{-}K}$ (kN)	1,329.79

Site ID No. 47

Cone penetrometer data	CPT SBT soil classification index, I_c	Detail	Description
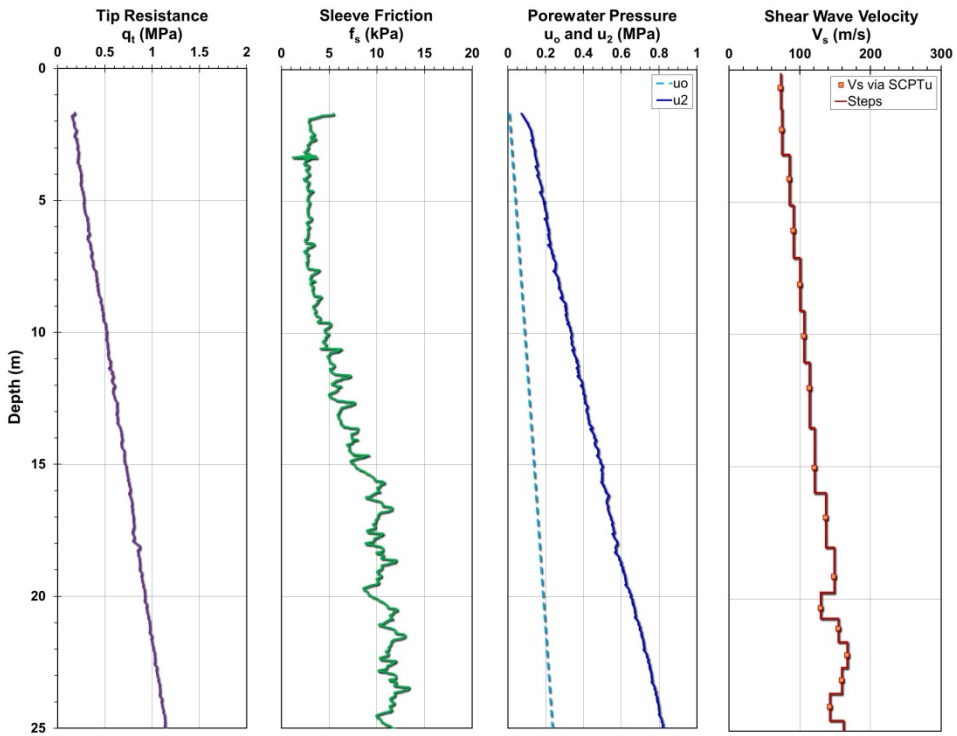	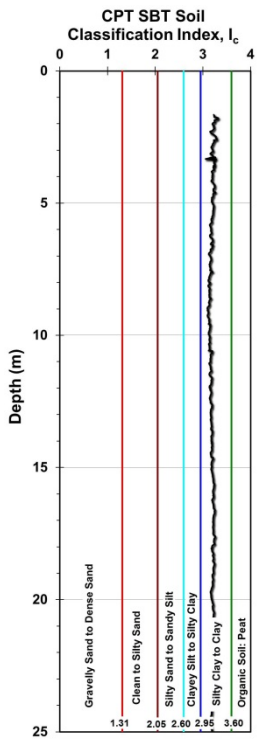	Site name and location	Onsøy clay site, south-eastern Norway
		Soil type(s)	Soft clay with shell fragments
		Pile type(s)	1 Open-ended steel pipe pile and 9 close-ended steel pipe piles
		Type of cone penetrometer testing	SCPTu
		Source of V_s evaluation	SCPTu
		Number of pile load tests	1
		Reference	Karlsrud (1988), Lunne et al. (2003)
		Comments	

Pile ID: OC A1

Load-displacement data

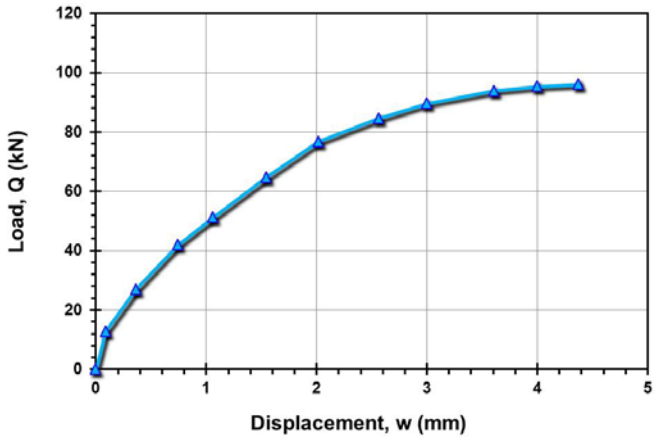

Back-analyzed normalized operational stiffness vs. pseudo-strain

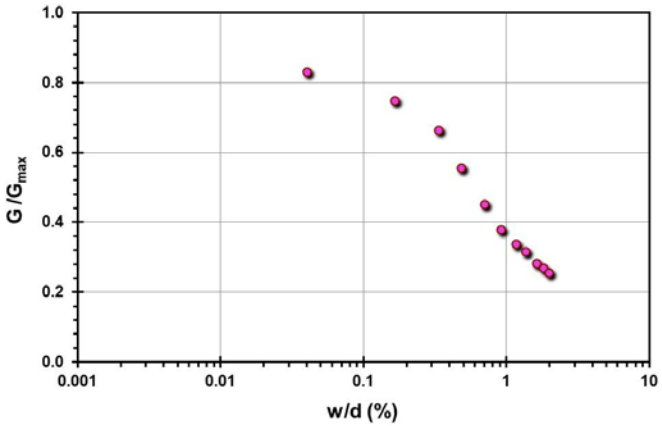

Detail	Description
Pile type/material	Close-ended steel pipe pile
Length, L (m)	5.00
Diameter, d (m)	0.219
Installation method	Driven
Loading mode	Tension
$Q_{max\text{-}measured}$ (kN)	95.00
Q_s (kN)	95.00
Q_b (kN)	-
$Q_{Davisson}$ (kN)	103.27
$Q_{w/d=10\%}$ (kN)	110.38
$Q_{C\text{-}K}$ (kN)	114.42

Pile ID: OC A2

Load-displacement data	Detail	Description
Not reported	Pile type/material	Close-ended steel pipe pile
	Length, L (m)	5.00
	Diameter, d (m)	0.219
	Installation method	Driven
	Loading mode	Tension
	$Q_{max\text{-}measured}$ (kN)	160.00
	Q_s (kN)	160.00
	Q_b (kN)	-
	$Q_{Davisson}$ (kN)	-
	$Q_{w/d=10\%}$ (kN)	-
	$Q_{C\text{-}K}$ (kN)	-
Back-analyzed normalized operational stiffness vs. pseudo-strain		
Not calculated		

Pile ID: OC A3

Load-displacement data

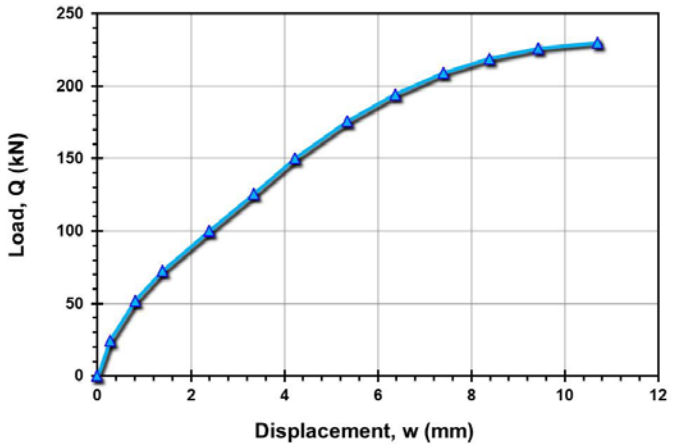

Back-analyzed normalized operational stiffness vs. pseudo-strain

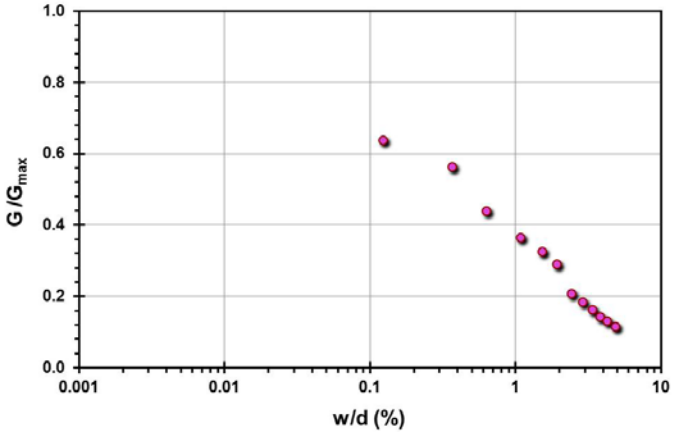

Detail	Description
Pile type/material	Close-ended steel pipe pile
Length, L (m)	5.00
Diameter, d (m)	0.219
Installation method	Driven
Loading mode	Tension
$Q_{max\text{-}measured}$ (kN)	231.00
Q_s (kN)	231.00
Q_b (kN)	-
$Q_{Davisson}$ (kN)	209.14
$Q_{w/d=10\%}$ (kN)	260.25
$Q_{C\text{-}K}$ (kN)	295.68

Pile ID: OC A4

Load-displacement data

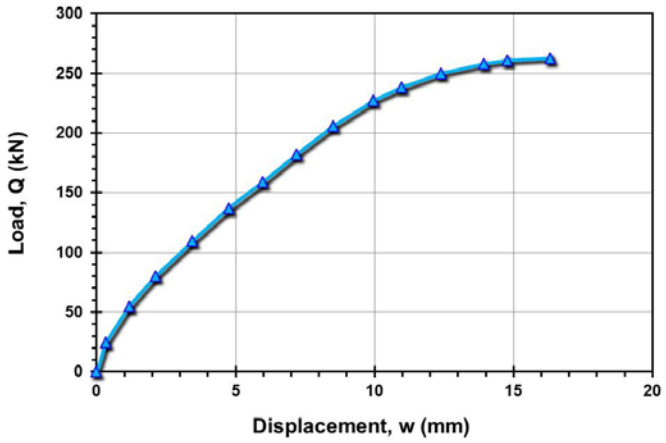

Back-analyzed normalized operational stiffness vs. pseudo-strain

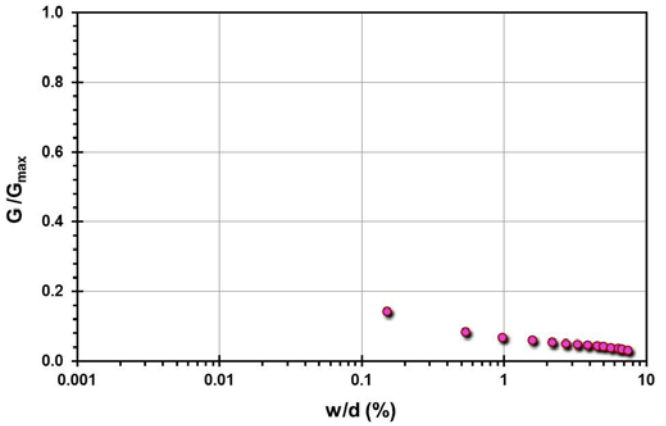

Detail	Description
Pile type/material	Close-ended steel pipe pile
Length, L (m)	5.00
Diameter, d (m)	0.219
Installation method	Driven
Loading mode	Tension
$Q_{max\text{-}measured}$ (kN)	262.00
Q_s (kN)	262.00
Q_b (kN)	-
$Q_{Davisson}$ (kN)	182.11
$Q_{w/d=10\%}$ (kN)	280.20
$Q_{C\text{-}K}$ (kN)	335.12

Pile ID: OC B1

Load-displacement data

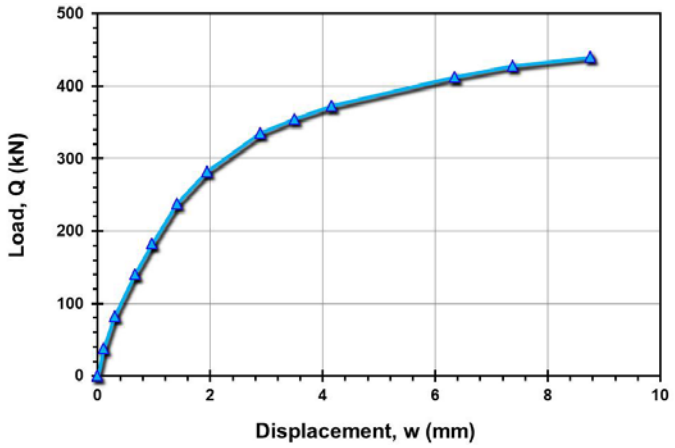

Back-analyzed normalized operational stiffness vs. pseudo-strain

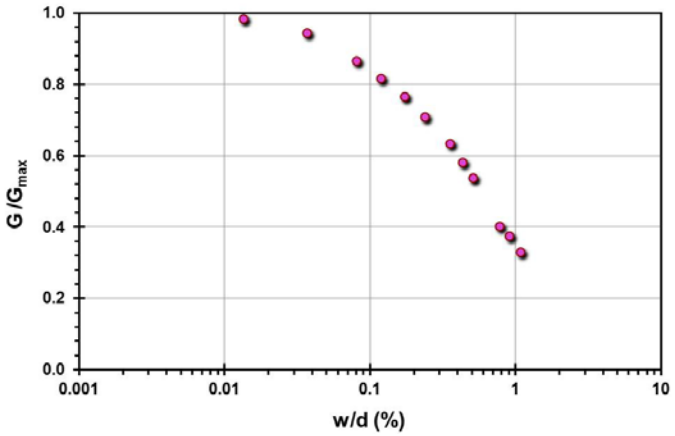

Detail	Description
Pile type/material	Open-ended steel pipe pile
Length, L (m)	5.00
Diameter, d (m)	0.219
Installation method	Driven
Loading mode	Tension
$Q_{max\text{-}measured}$ (kN)	453.00
Q_s (kN)	453.00
Q_b (kN)	-
$Q_{Davisson}$ (kN)	475.73
$Q_{w/d=10\%}$ (kN)	511.46
$Q_{C\text{-}K}$ (kN)	521.92

Pile ID: OC C1-1

Load-displacement data

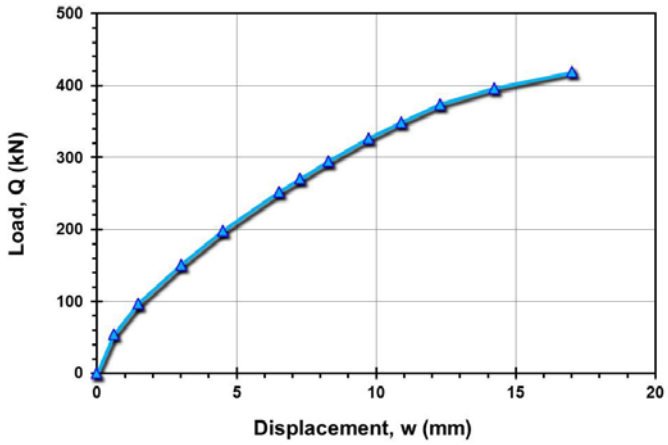

Back-analyzed normalized operational stiffness vs. pseudo-strain

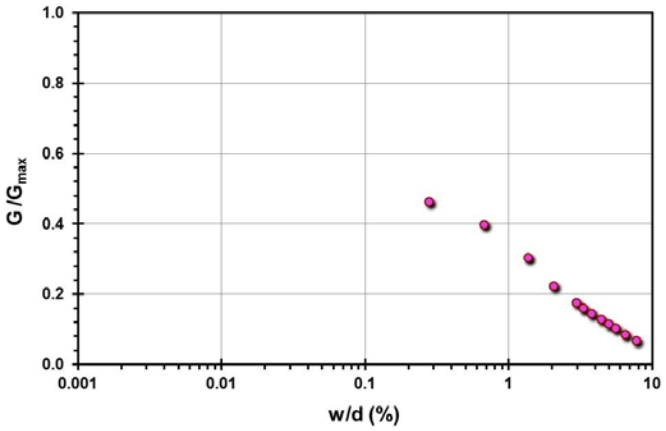

Detail	Description
Pile type/material	Closed-ended steel pipe pile
Length, L (m)	5.00
Diameter, d (m)	0.219
Installation method	Driven
Loading mode	Tension
$Q_{max\text{-}measured}$ (kN)	424.00
Q_s (kN)	424.00
Q_b (kN)	-
$Q_{Davisson}$ (kN)	295.05
$Q_{w/d=10\%}$ (kN)	450.19
$Q_{C\text{-}K}$ (kN)	608.27

Pile ID: OC C1-2

Load-displacement data

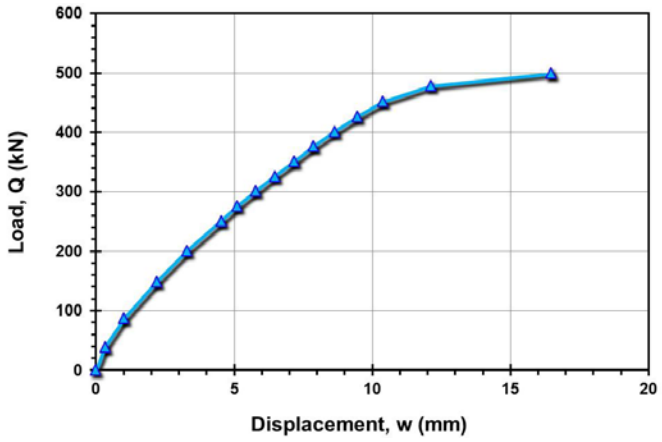

Back-analyzed normalized operational stiffness vs. pseudo-strain

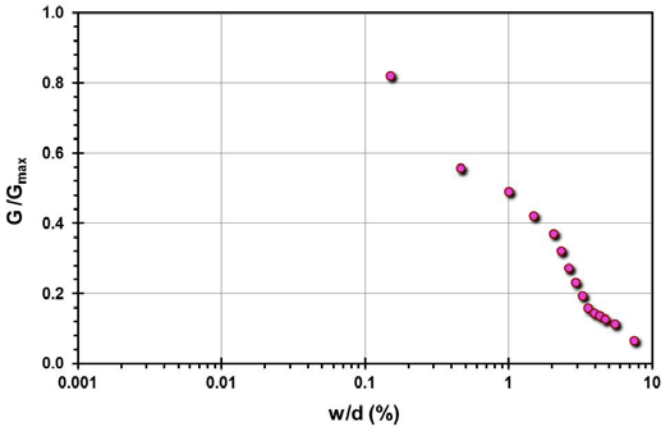

Detail	Description
Pile type/material	Closed-ended steel pipe pile
Length, L (m)	10.00
Diameter, d (m)	0.219
Installation method	Driven
Loading mode	Tension
$Q_{max\text{-}measured}$ (kN)	500.00
Q_s (kN)	500.00
Q_b (kN)	-
$Q_{Davisson}$ (kN)	426.49
$Q_{w/d=10\%}$ (kN)	515.98
$Q_{C\text{-}K}$ (kN)	570.45

Pile ID: OC C1-3

Load-displacement data	Detail	Description
Not reported	Pile type/material	Closed-ended steel pipe pile
	Length, L (m)	5.00
	Diameter, d (m)	0.219
	Installation method	Driven
	Loading mode	Tension
	$Q_{max\text{-}measured}$ (kN)	66.05
	Q_s (kN)	66.05
	Q_b (kN)	-
	$Q_{Davisson}$ (kN)	-
	$Q_{w/d=10\%}$ (kN)	-
	$Q_{C\text{-}K}$ (kN)	-
Back-analyzed normalized operational stiffness vs. pseudo-strain		
Not calculated		

Pile ID: OC C1-4

Load-displacement data	Detail	Description
Not reported	Pile type/material	Closed-ended steel pipe pile
	Length, L (m)	5.00
	Diameter, d (m)	0.219
	Installation method	Driven
	Loading mode	Tension
	$Q_{max\text{-}measured}$ (kN)	78.09
	Q_s (kN)	78.09
	Q_b (kN)	-
	$Q_{Davisson}$ (kN)	-
	$Q_{w/d=10\%}$ (kN)	-
	$Q_{C\text{-}K}$ (kN)	-
Back-analyzed normalized operational stiffness vs. pseudo-strain		
Not calculated		

Pile ID: OC C1-5

Load-displacement data	Detail	Description
Not reported	Pile type/material	Closed-ended steel pipe pile
	Length, L (m)	5.00
	Diameter, d (m)	0.219
	Installation method	Driven
	Loading mode	Tension
	$Q_{max\text{-}measured}$ (kN)	111.80
	Q_s (kN)	111.80
	Q_b (kN)	-
	$Q_{Davisson}$ (kN)	-
	$Q_{w/d=10\%}$ (kN)	-
	$Q_{C\text{-}K}$ (kN)	-
Back-analyzed normalized operational stiffness vs. pseudo-strain		
Not calculated		

Site ID No. 48

Cone penetrometer data	CPT SBT soil classification index, I_c	Detail	Description
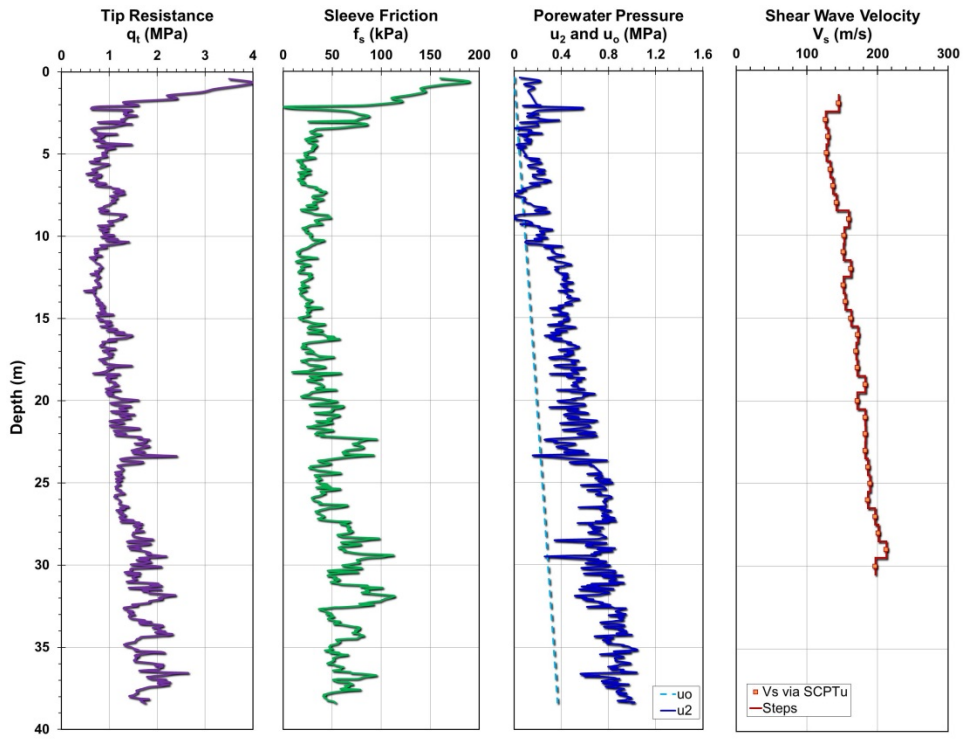	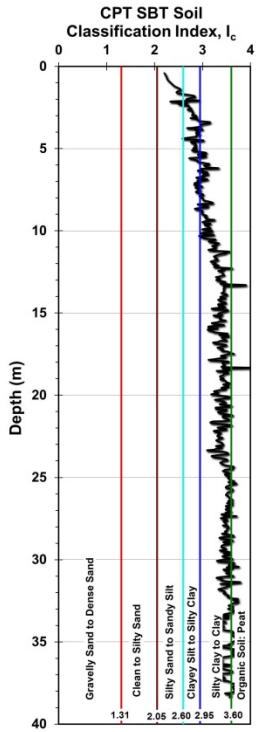	Site name and location	Pentre silt, Shropshire, UK
		Soil type(s)	Very silty clay to silt
		Pile type(s)	1 Open-ended steel pipe pile and 19 close-ended steel pipe piles
		Type of cone penetrometer testing	SCPTu
		Source of V_s evaluation	SCPTu
		Number of pile load tests	20
		Reference	Chow (1996)
		Comments	15 of the 19 close-ended steel pipe piles are Imperial College Piles

Pile ID: PT LDP

Load-displacement data

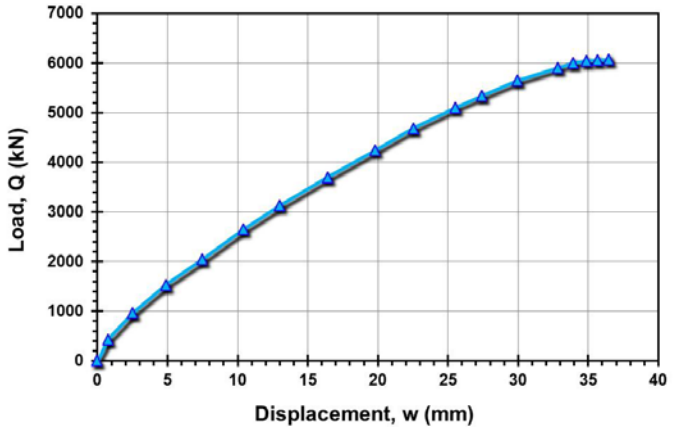

Back-analyzed normalized operational stiffness vs. pseudo-strain

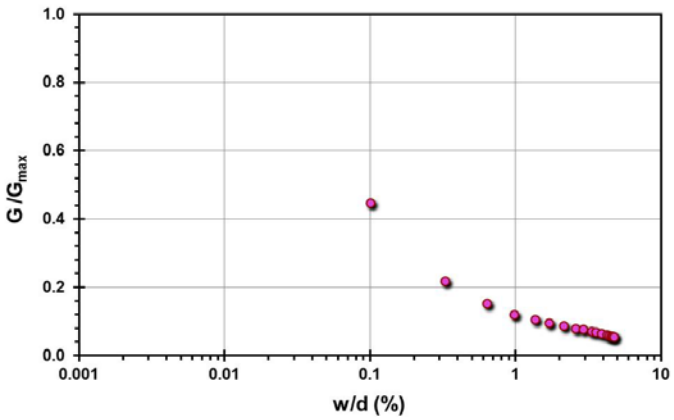

Detail	Description
Pile type/material	Open-ended steel pipe pile
Length, L (m)	40.00
Diameter, d (m)	0.762
Installation method	Driven
Loading mode	Compression
$Q_{max\text{-}measured}$ (kN)	6,070.78
Q_s (kN)	5,210.56
Q_b (kN)	860.22
$Q_{Davisson}$ (kN)	6,372.67
$Q_{w/d=10\%}$ (kN)	6,674.57
$Q_{C\text{-}K}$ (kN)	7,352.94

Pile ID: PT NGI A5-1

Load-displacement data

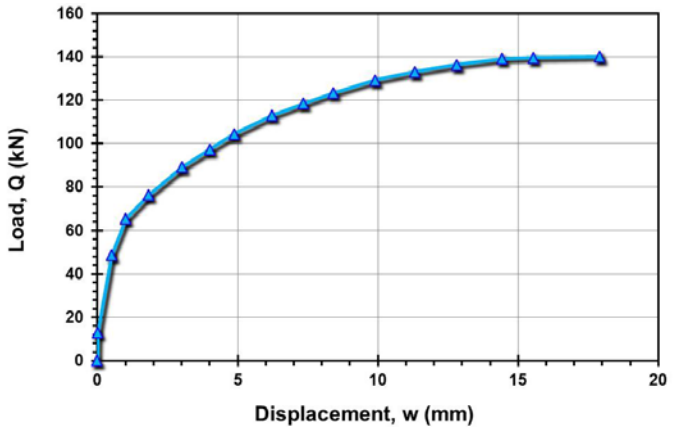

Back-analyzed normalized operational stiffness vs. pseudo-strain

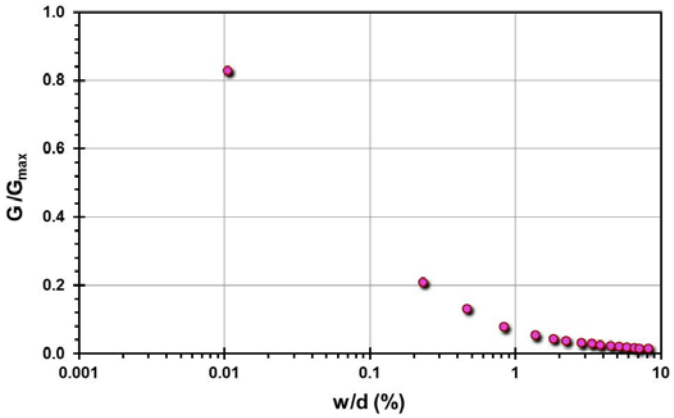

Detail	Description
Pile type/material	Closed-ended steel pipe pile
Length, L (m)	10.00
Diameter, d (m)	0.219
Installation method	Driven
Loading mode	Tension
$Q_{max\text{-}measured}$ (kN)	140.00
Q_s (kN)	140.00
Q_b (kN)	-
$Q_{Davisson}$ (kN)	118.38
$Q_{w/d=10\%}$ (kN)	144.57
$Q_{C\text{-}K}$ (kN)	160.57

Pile ID: PT NGI A5-2

Load-displacement data

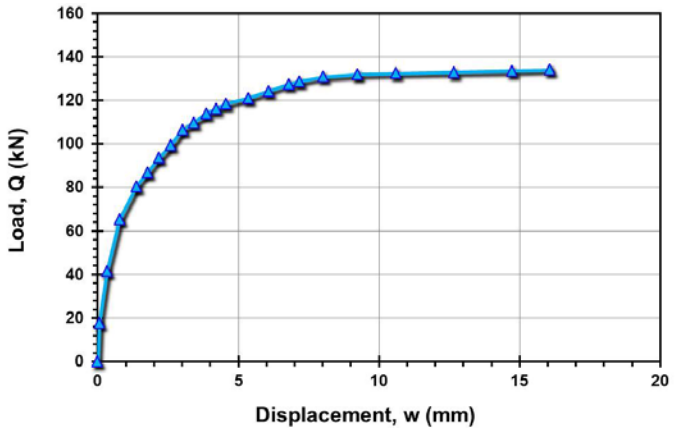

Back-analyzed normalized operational stiffness vs. pseudo-strain

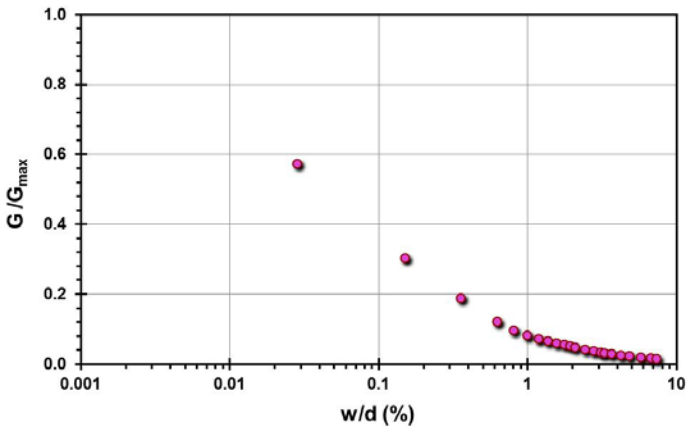

Detail	Description
Pile type/material	Closed-ended steel pipe pile
Length, L (m)	10.00
Diameter, d (m)	0.219
Installation method	Driven
Loading mode	Tension
$Q_{max\text{-}measured}$ (kN)	134.05
Q_s (kN)	134.05
Q_b (kN)	-
$Q_{Davisson}$ (kN)	127.57
$Q_{w/d=10\%}$ (kN)	134.83
$Q_{C\text{-}K}$ (kN)	137.04

Pile ID: PT NGI A6-1

Load-displacement data

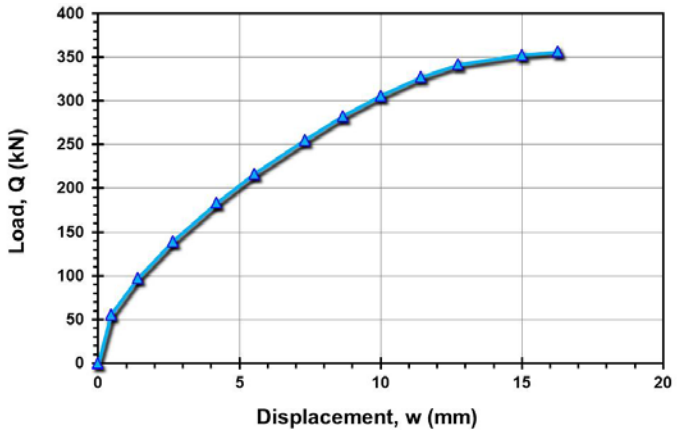

Back-analyzed normalized operational stiffness vs. pseudo-strain

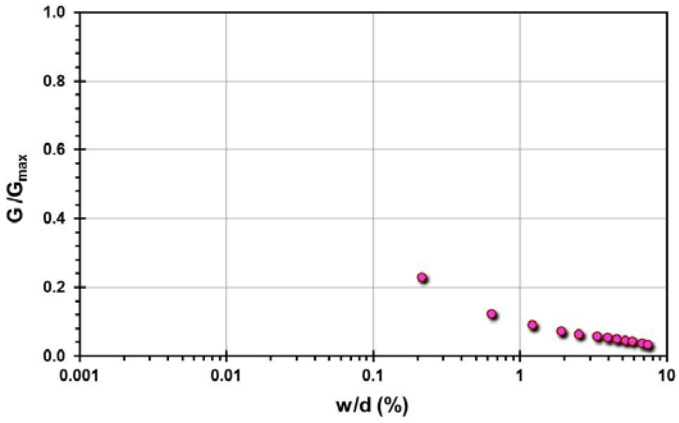

Detail	Description
Pile type/material	Closed-ended steel pipe pile
Length, L (m)	10.00
Diameter, d (m)	0.219
Installation method	Driven
Loading mode	Tension
$Q_{max\text{-}measured}$ (kN)	356.22
Q_s (kN)	356.22
Q_b (kN)	-
$Q_{Davisson}$ (kN)	282.70
$Q_{w/d=10\%}$ (kN)	370.66
$Q_{C\text{-}K}$ (kN)	422.30

Pile ID: PT NGI A6-2

Load-displacement data

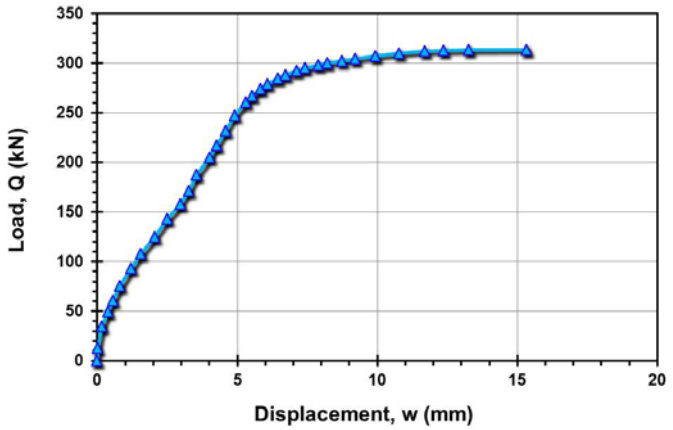

Back-analyzed normalized operational stiffness vs. pseudo-strain

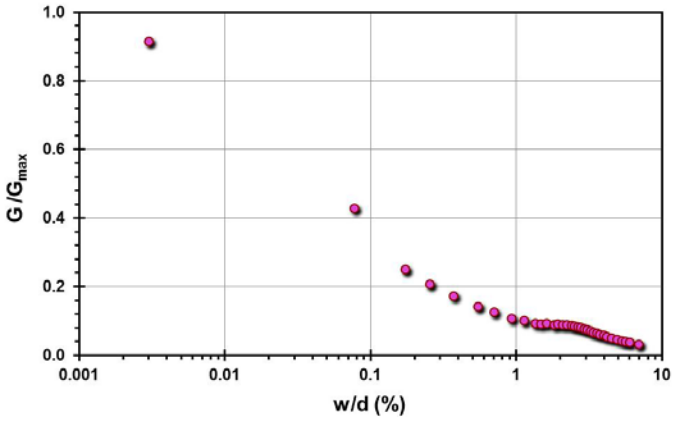

Detail	Description
Pile type/material	Closed-ended steel pipe pile
Length, L (m)	10.00
Diameter, d (m)	0.219
Installation method	Driven
Loading mode	Tension
$Q_{max\text{-}measured}$ (kN)	313.51
Q_s (kN)	313.51
Q_b (kN)	-
$Q_{Davisson}$ (kN)	300.00
$Q_{w/d=10\%}$ (kN)	327.85
$Q_{C\text{-}K}$ (kN)	350.51

Pile ID: PT 1/L1C

Load-displacement data

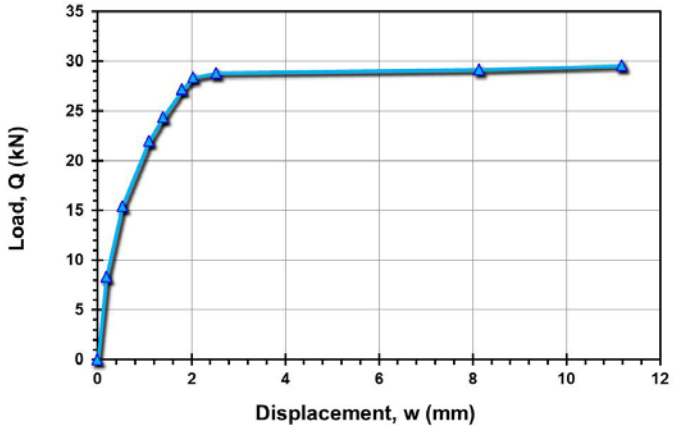

Back-analyzed normalized operational stiffness vs. pseudo-strain

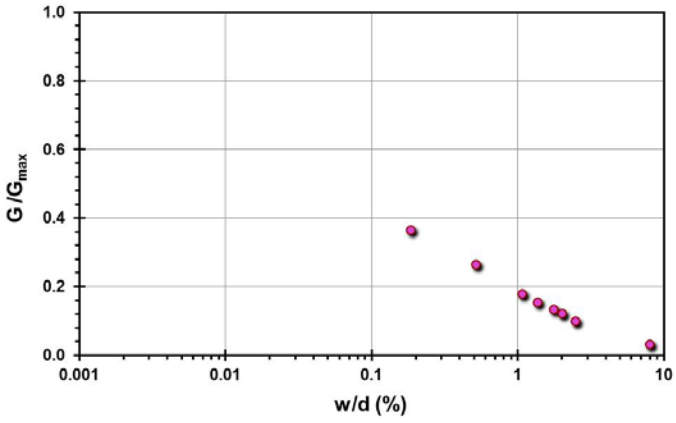

Detail	Description
Pile type/material	Closed-ended steel pipe pile
Length, L (m)	4.30
Diameter, d (m)	0.219
Installation method	Jacked
Loading mode	Compression
$Q_{max\text{-}measured}$ (kN)	29.55
Q_s (kN)	23.53
Q_b (kN)	6.02
$Q_{Davisson}$ (kN)	28.98
$Q_{w/d=10\%}$ (kN)	29.46
$Q_{C\text{-}K}$ (kN)	30.02

Pile ID: PT 2/L1C

Load-displacement data

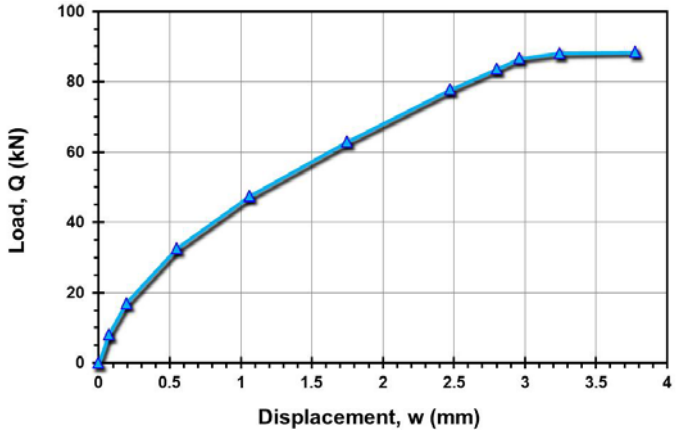

Back-analyzed normalized operational stiffness vs. pseudo-strain

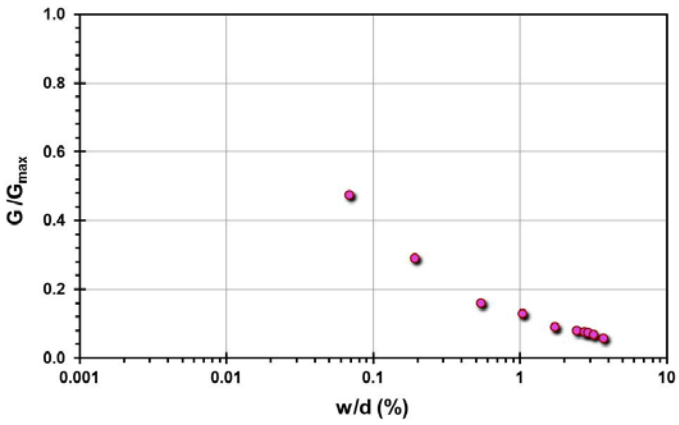

Detail	Description
Pile type/material	Closed-ended steel pipe pile
Length, L (m)	8.50
Diameter, d (m)	0.219
Installation method	Jacked
Loading mode	Compression
$Q_{max\text{-}measured}$ (kN)	88.55
Q_s (kN)	78.98
Q_b (kN)	9.57
$Q_{Davisson}$ (kN)	90.68
$Q_{w/d=10\%}$ (kN)	92.81
$Q_{C\text{-}K}$ (kN)	95.42

Pile ID: PT 2/L2T

Load-displacement data

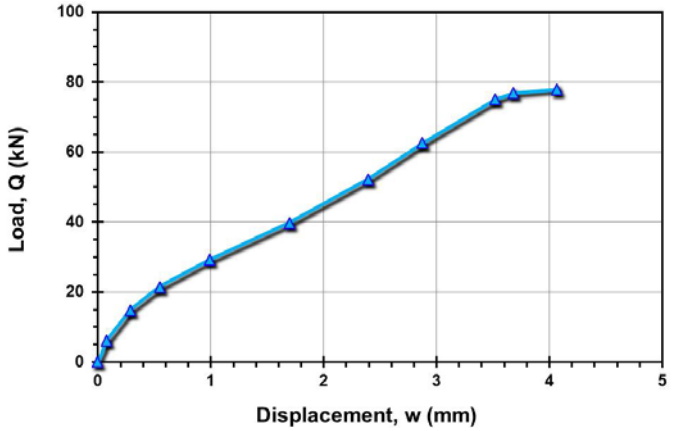

Back-analyzed normalized operational stiffness vs. pseudo-strain

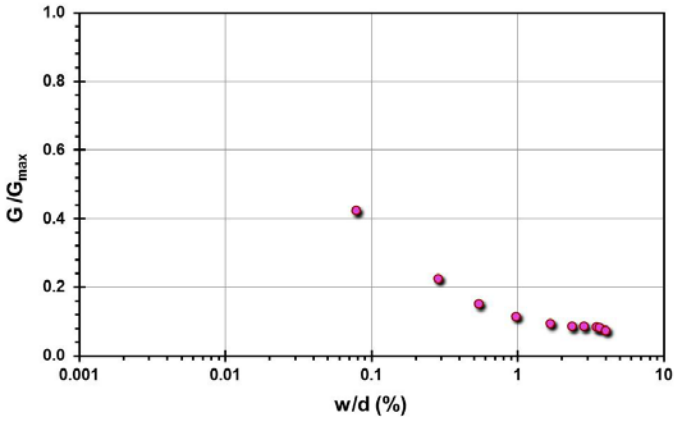

Detail	Description
Pile type/material	Closed-ended steel pipe pile
Length, L (m)	8.50
Diameter, d (m)	0.219
Installation method	Jacked
Loading mode	Tension
$Q_{max\text{-}measured}$ (kN)	77.86
Q_s (kN)	77.86
Q_b (kN)	-
$Q_{Davisson}$ (kN)	84.18
$Q_{w/d=10\%}$ (kN)	90.50
$Q_{C\text{-}K}$ (kN)	101.38

Pile ID: PT 3/L1T

Load-displacement data

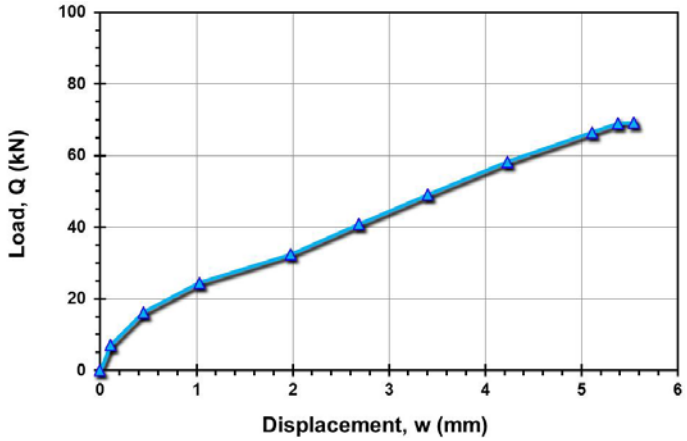

Back-analyzed normalized operational stiffness vs. pseudo-strain

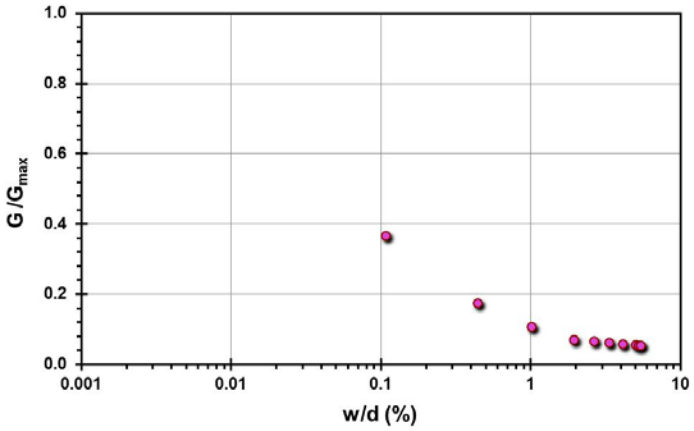

Detail	Description
Pile type/material	Closed-ended steel pipe pile
Length, L (m)	5.47
Diameter, d (m)	0.219
Installation method	Jacked
Loading mode	Tension
$Q_{max\text{-}measured}$ (kN)	69.16
Q_s (kN)	69.16
Q_b (kN)	-
$Q_{Davisson}$ (kN)	68.93
$Q_{w/d=10\%}$ (kN)	91.66
$Q_{C\text{-}K}$ (kN)	142.92

Pile ID: PT 3/L2T

Load-displacement data

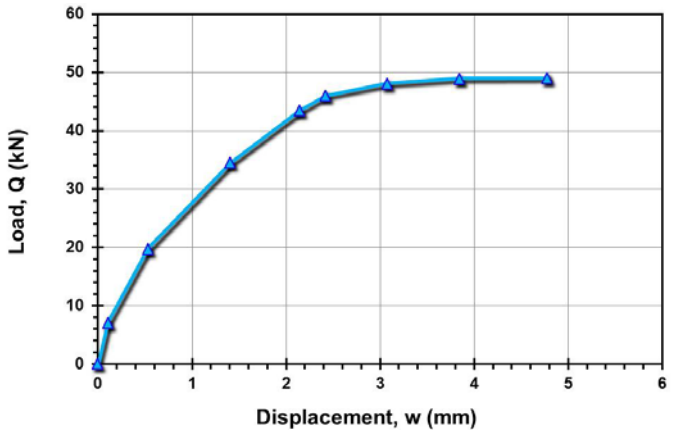

Back-analyzed normalized operational stiffness vs. pseudo-strain

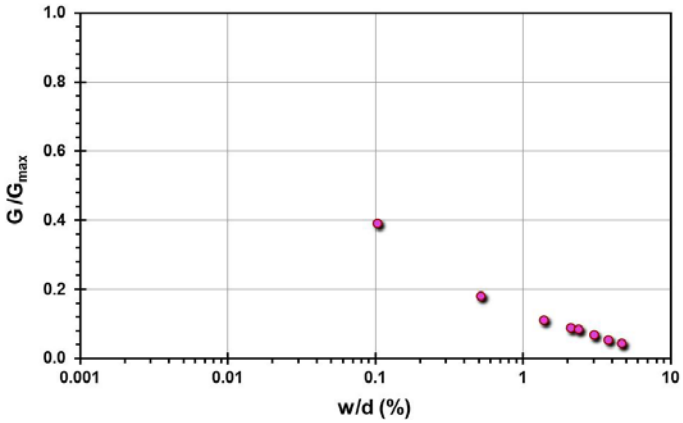

Detail	Description
Pile type/material	Closed-ended steel pipe pile
Length, L (m)	5.47
Diameter, d (m)	0.219
Installation method	Jacked
Loading mode	Tension
$Q_{max\text{-}measured}$ (kN)	49.01
Q_s (kN)	49.01
Q_b (kN)	-
$Q_{Davisson}$ (kN)	49.01
$Q_{w/d=10\%}$ (kN)	50.89
$Q_{C\text{-}K}$ (kN)	52.44

Pile ID: PT 4/L1C

Load-displacement data

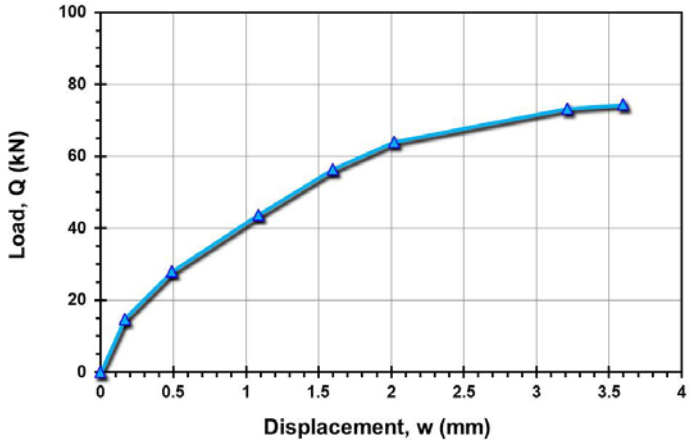

Back-analyzed normalized operational stiffness vs. pseudo-strain

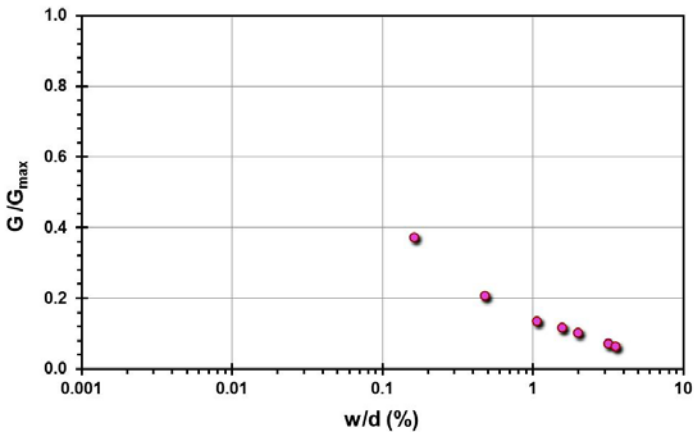

Detail	Description
Pile type/material	Closed-ended steel pipe pile
Length, L (m)	5.88
Diameter, d (m)	0.219
Installation method	Jacked
Loading mode	Compression
$Q_{max\text{-}measured}$ (kN)	74.32
Q_s (kN)	64.35
Q_b (kN)	9.97
$Q_{Davisson}$ (kN)	80.38
$Q_{w/d=10\%}$ (kN)	86.44
$Q_{C\text{-}K}$ (kN)	94.50

Pile ID: PT 5/L1T

Load-displacement data

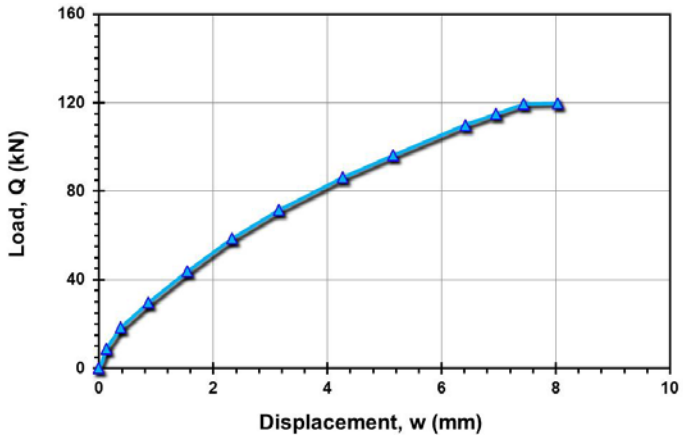

Back-analyzed normalized operational stiffness vs. pseudo-strain

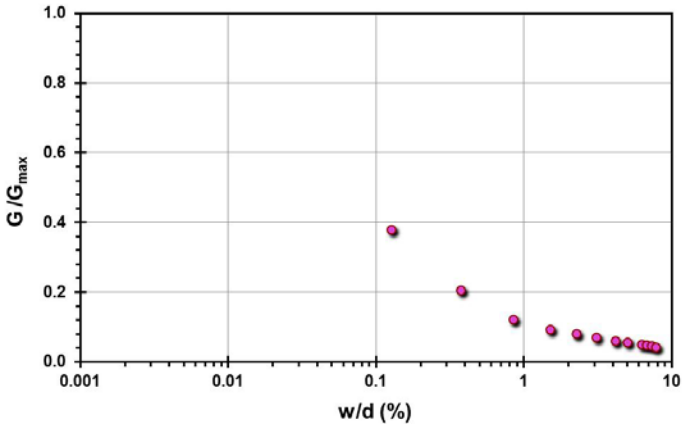

Detail	Description
Pile type/material	Closed-ended steel pipe pile
Length, L (m)	10.59
Diameter, d (m)	0.219
Installation method	Jacked
Loading mode	Tension
$Q_{max\text{-}measured}$ (kN)	119.83
Q_s (kN)	119.83
Q_b (kN)	-
$Q_{Davisson}$ (kN)	114.85
$Q_{w/d=10\%}$ (kN)	121.04
$Q_{C\text{-}K}$ (kN)	125.42

Pile ID: PT 5/L2T

Load-displacement data

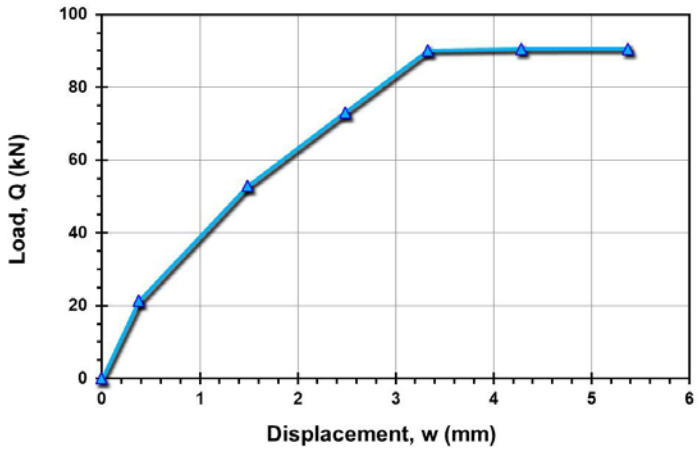

Back-analyzed normalized operational stiffness vs. pseudo-strain

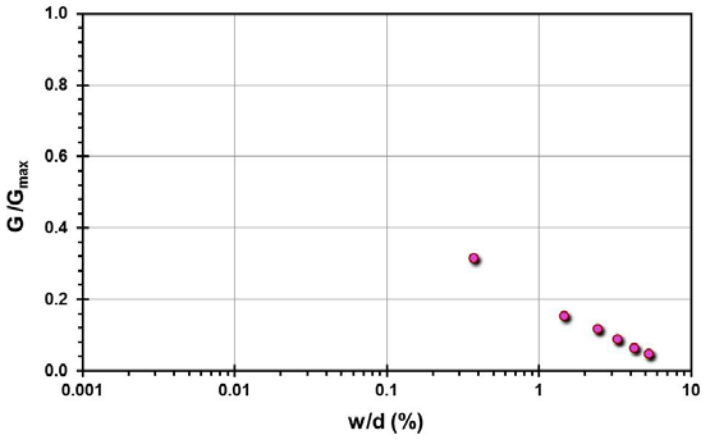

Detail	Description
Pile type/material	Closed-ended steel pipe pile
Length, L (m)	10.59
Diameter, d (m)	0.219
Installation method	Jacked
Loading mode	Tension
$Q_{max\text{-}measured}$ (kN)	90.48
Q_s (kN)	90.48
Q_b (kN)	-
$Q_{Davisson}$ (kN)	90.48
$Q_{w/d=10\%}$ (kN)	90.86
$Q_{C\text{-}K}$ (kN)	91.24

Pile ID: PT 5/L3C

Load-displacement data

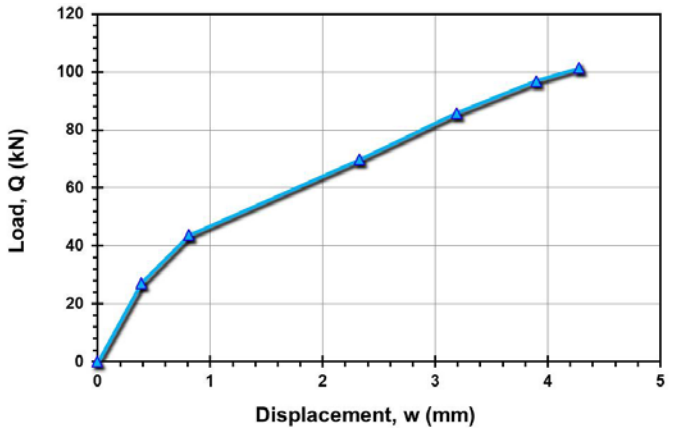

Back-analyzed normalized operational stiffness vs. pseudo-strain

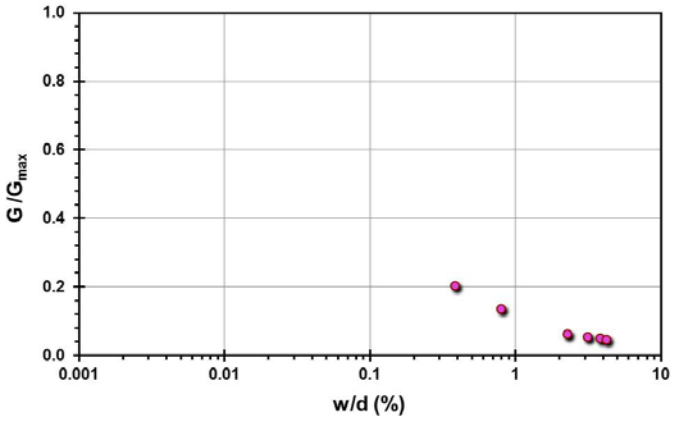

Detail	Description
Pile type/material	Closed-ended steel pipe pile
Length, L (m)	10.59
Diameter, d (m)	0.219
Installation method	Jacked
Loading mode	Compression
$Q_{max\text{-}measured}$ (kN)	101.34
Q_s (kN)	88.79
Q_b (kN)	12.55
$Q_{Davisson}$ (kN)	124.98
$Q_{w/d=10\%}$ (kN)	148.62
$Q_{C\text{-}K}$ (kN)	221.68

Pile ID: PT 5/L4T

Load-displacement data

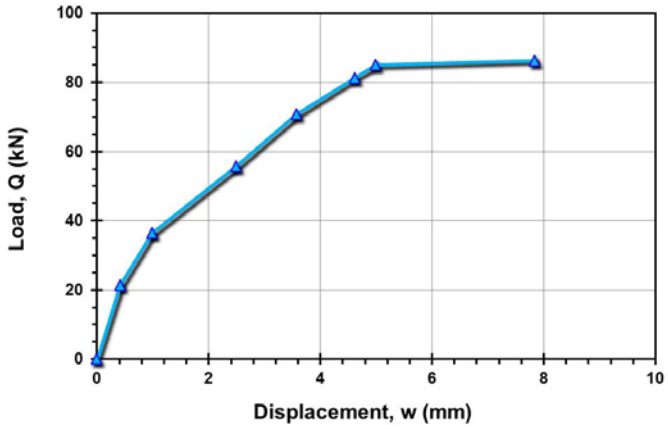

Back-analyzed normalized operational stiffness vs. pseudo-strain

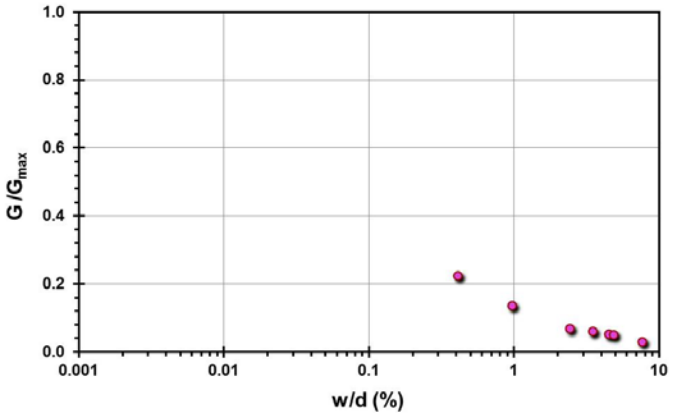

Detail	Description
Pile type/material	Closed-ended steel pipe pile
Length, L (m)	10.59
Diameter, d (m)	0.219
Installation method	Jacked
Loading mode	Tension
$Q_{max\text{-}measured}$ (kN)	86.35
Q_s (kN)	86.35
Q_b (kN)	-
$Q_{Davisson}$ (kN)	85.66
$Q_{w/d=10\%}$ (kN)	86.92
$Q_{C\text{-}K}$ (kN)	88.87

Pile ID: PT 5/L6T

Load-displacement data

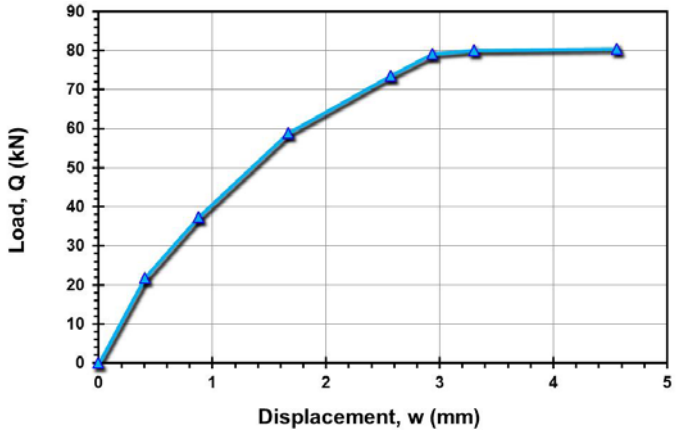

Back-analyzed normalized operational stiffness vs. pseudo-strain

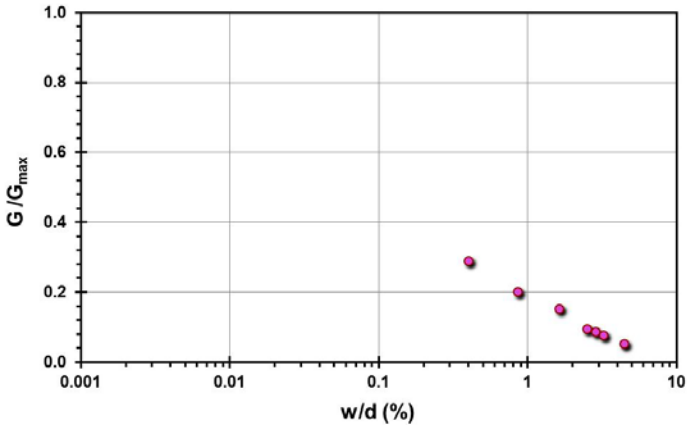

Detail	Description
Pile type/material	Closed-ended steel pipe pile
Length, L (m)	10.59
Diameter, d (m)	0.219
Installation method	Jacked
Loading mode	Tension
$Q_{max\text{-}measured}$ (kN)	80.39
Q_s (kN)	80.39
Q_b (kN)	-
$Q_{Davisson}$ (kN)	81.02
$Q_{w/d=10\%}$ (kN)	81.65
$Q_{C\text{-}K}$ (kN)	82.64

Pile ID: PT 6/L1C

Load-displacement data

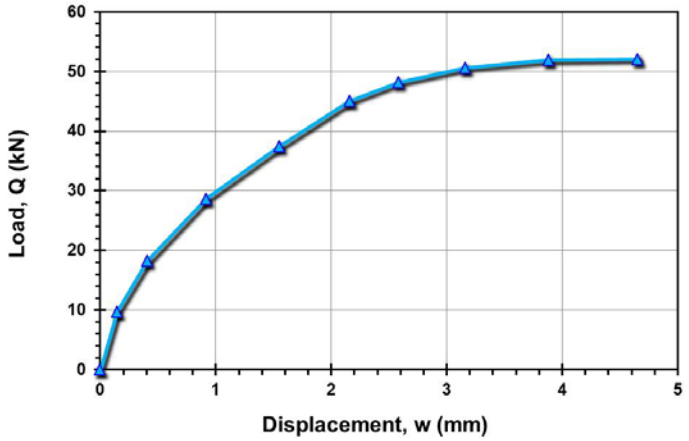

Back-analyzed normalized operational stiffness vs. pseudo-strain

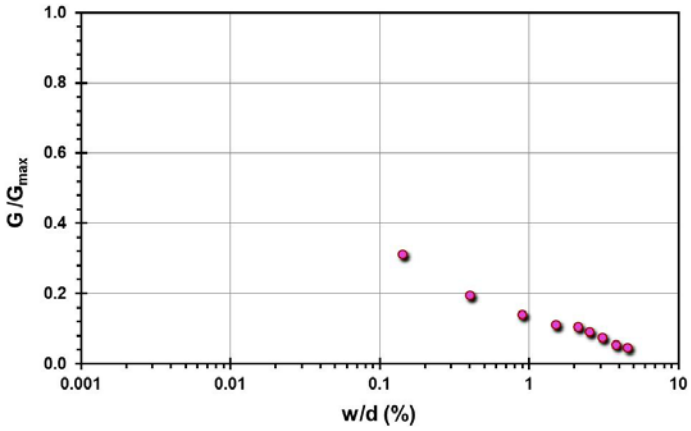

Detail	Description
Pile type/material	Closed-ended steel pipe pile
Length, L (m)	3.75
Diameter, d (m)	0.219
Installation method	Jacked
Loading mode	Compression
$Q_{max\text{-}measured}$ (kN)	52.06
Q_s (kN)	43.55
Q_b (kN)	8.51
$Q_{Davisson}$ (kN)	52.06
$Q_{w/d=10\%}$ (kN)	53.87
$Q_{C\text{-}K}$ (kN)	55.38

Pile ID: PT 7/L1C

Load-displacement data

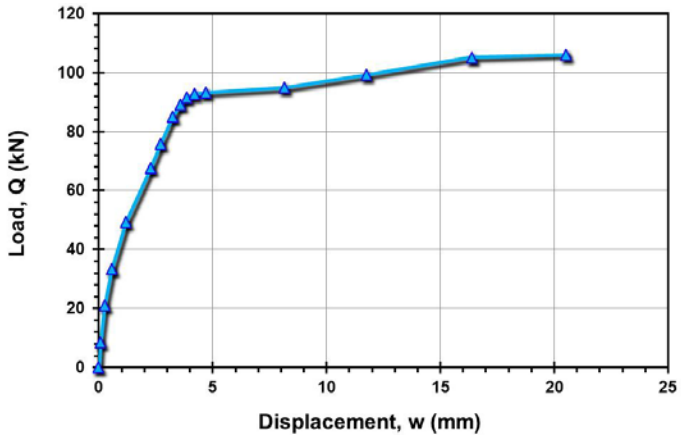

Back-analyzed normalized operational stiffness vs. pseudo-strain

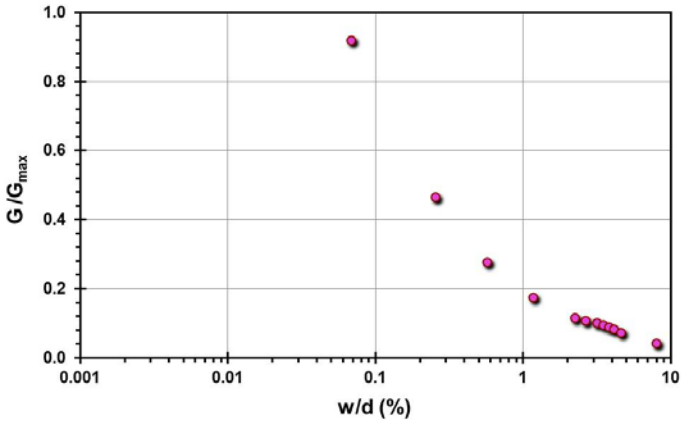

Detail	Description
Pile type/material	Closed-ended steel pipe pile
Length, L (m)	8.75
Diameter, d (m)	0.219
Installation method	Jacked
Loading mode	Compression
$Q_{max\text{-}measured}$ (kN)	106.04
Q_s (kN)	86.88
Q_b (kN)	19.16
$Q_{Davisson}$ (kN)	93.88
$Q_{w/d=10\%}$ (kN)	100.36
$Q_{C\text{-}K}$ (kN)	110.95

Pile ID: PT 7/L2C

Load-displacement data

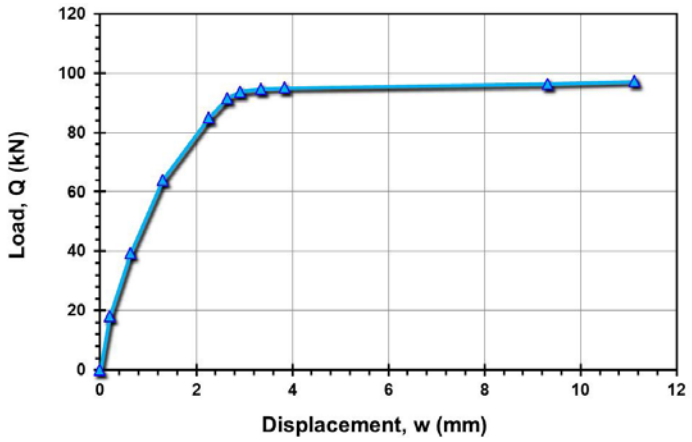

Back-analyzed normalized operational stiffness vs. pseudo-strain

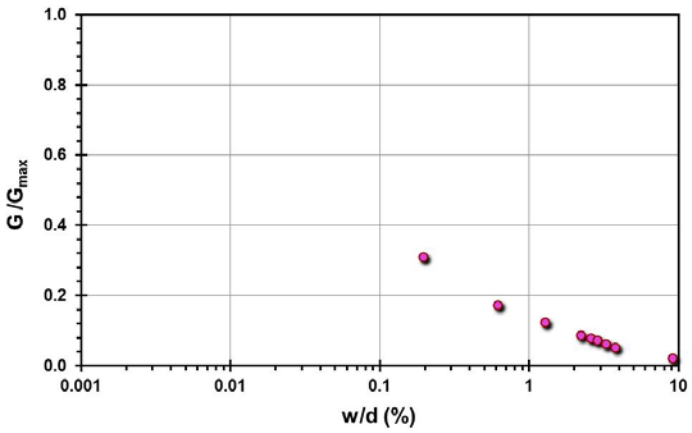

Detail	Description
Pile type/material	Closed-ended steel pipe pile
Length, L (m)	8.75
Diameter, d (m)	0.219
Installation method	Jacked
Loading mode	Compression
$Q_{max\text{-}measured}$ (kN)	97.23
Q_s (kN)	82.47
Q_b (kN)	14.76
$Q_{Davisson}$ (kN)	95.68
$Q_{w/d=10\%}$ (kN)	96.89
$Q_{C\text{-}K}$ (kN)	98.38

Pile ID: PT 7/L3T

Load-displacement data

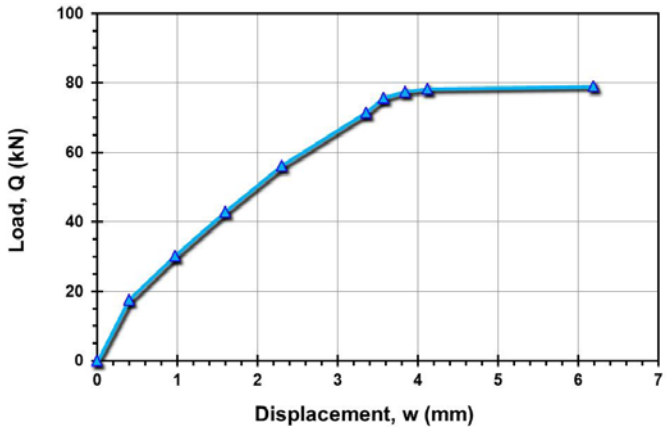

Back-analyzed normalized operational stiffness vs. pseudo-strain

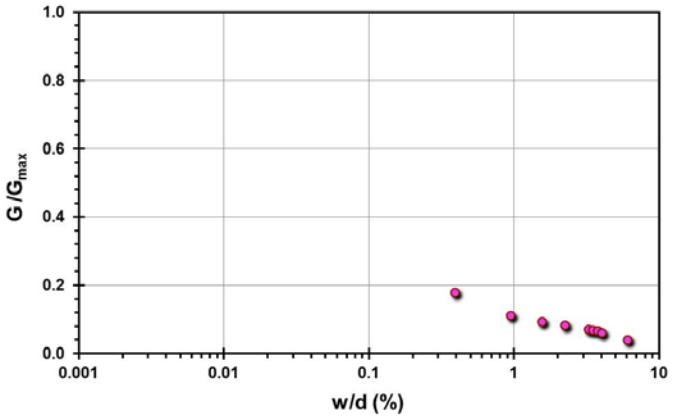

Detail	Description
Pile type/material	Closed-ended steel pipe pile
Length, L (m)	8.75
Diameter, d (m)	0.219
Installation method	Jacked
Loading mode	Tension
$Q_{max\text{-}measured}$ (kN)	78.94
Q_s (kN)	78.94
Q_b (kN)	-
$Q_{Davisson}$ (kN)	78.94
$Q_{w/d=10\%}$ (kN)	79.79
$Q_{C\text{-}K}$ (kN)	81.12

Site ID No. 49

Cone penetrometer data	CPT SBT soil classification index, I_c	Detail	Description
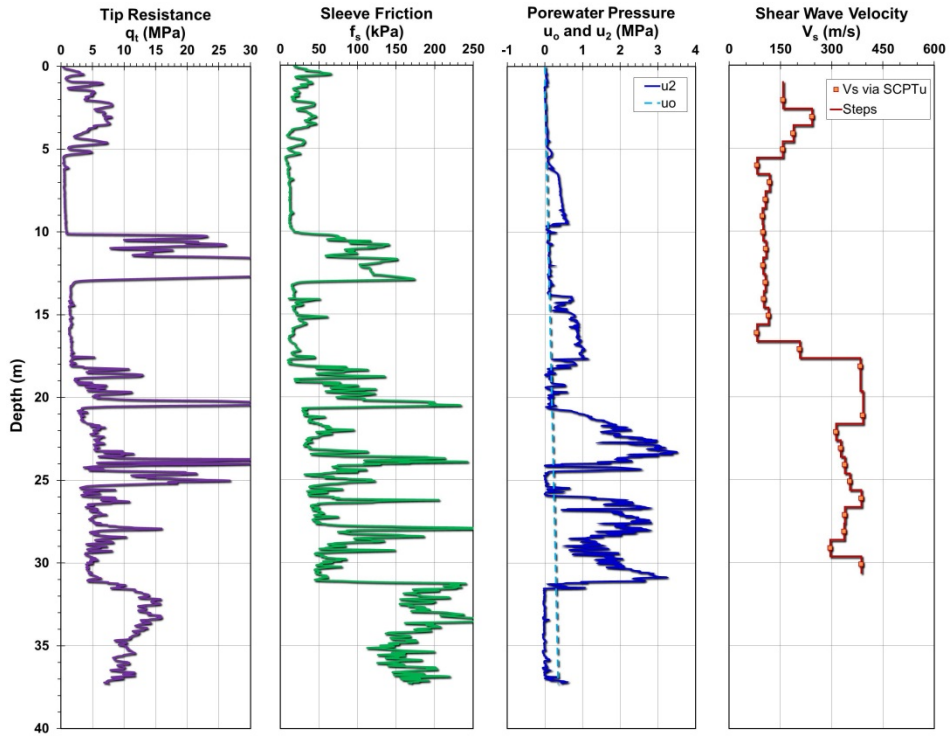	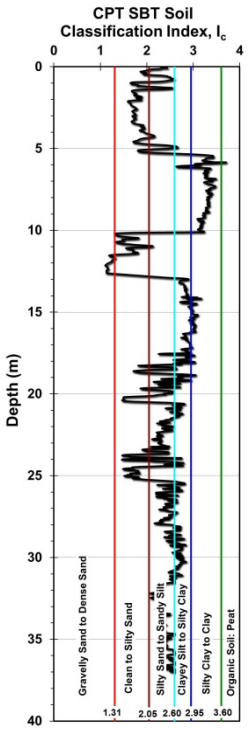	Site name and location	Pinner's Point Interchange, Portsmouth, VA, USA
		Soil type(s)	Interbedded sand and clay soils of Norfolk Formation overlying medium to dense sand of Yorktown Formation
		Pile type(s)	Drilled shaft
		Type of cone penetrometer testing	SCPTu
		Source of V_s evaluation	SCPTu
		Number of pile load tests	2
		Reference	Kort et al. (2001a, b)
		Comments	V_s from SCPTu sounding at a nearby site

Pile ID: PPI 1

Load-displacement data

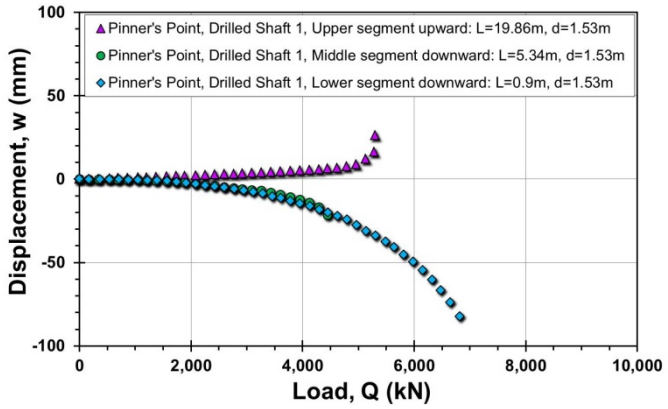

Back-analyzed normalized operational stiffness vs. pseudo-strain

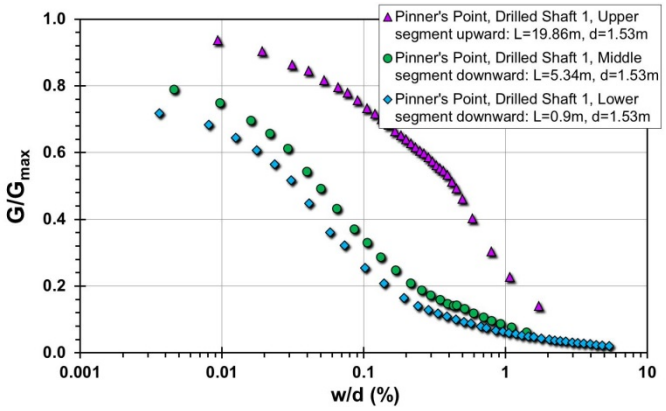

Detail	Description
Pile type/material	Drilled shaft
Length, L (m)	Upper: 19.86; middle: 5.34; lower: 0.87
Diameter, d (m)	Upper: 1.53; middle: 1.53; lower: 1.53
Installation method	Bored cast in-situ
Loading mode	O-cell compression
$Q_{max\text{-}measured}$ (kN)	Upper: 5,302.8; middle: 4,444.4; lower: 6,821.4
Q_s (kN)	Upper: 5,302.8; middle: 4,444.4; lower: 314.4
Q_b (kN)	4,130.0
$Q_{Davisson}$ (kN)	Upper: 5,283.7; middle: 4,291.8; lower: 4,299.2
$Q_{w/d=10\%}$ (kN)	Upper: 5,497.2; middle: 5,250.3; lower: 7,306.8
$Q_{C\text{-}K}$ (kN)	Upper: 5,534.1; middle: 5,405.4; lower: 8,130.1

Pile ID: PPI 2

Load-displacement data

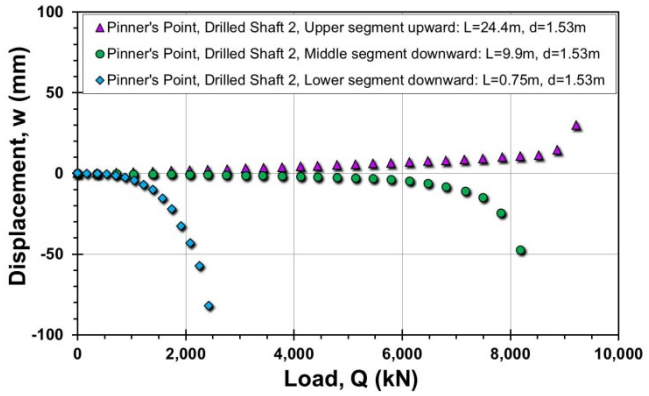

Back-analyzed normalized operational stiffness vs. pseudo-strain

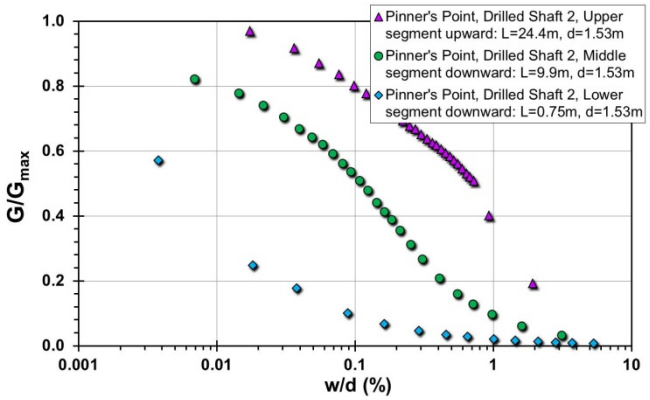

Detail	Description
Pile type/material	Drilled shaft
Length, L (m)	Upper: 24.40; middle: 9.90; lower: 0.75
Diameter, d (m)	Upper: 1.53; middle: 1.53; lower: 1.53
Installation method	Bored cast in-situ
Loading mode	O-cell compression
$Q_{max\text{-}measured}$ (kN)	Upper: 9,220.1; middle: 8,185.2; lower: 2,426.7
Q_s (kN)	Upper: 9,220.1; middle: 8,185.2; lower: 340.3
Q_b (kN)	2,086.4
$Q_{Davisson}$ (kN)	Upper: 8,911.2; middle: 7,489.0; lower: 1,738.8
$Q_{w/d=10\%}$ (kN)	Upper: 9,621.2; middle: 8,367.6; lower: 2,646.0
$Q_{C\text{-}K}$ (kN)	Upper: 9,708.7; middle: 8,474.6; lower: 2,958.6

Site ID No. 50A

Cone penetrometer data	CPT SBT soil classification index, I_c	Detail	Description
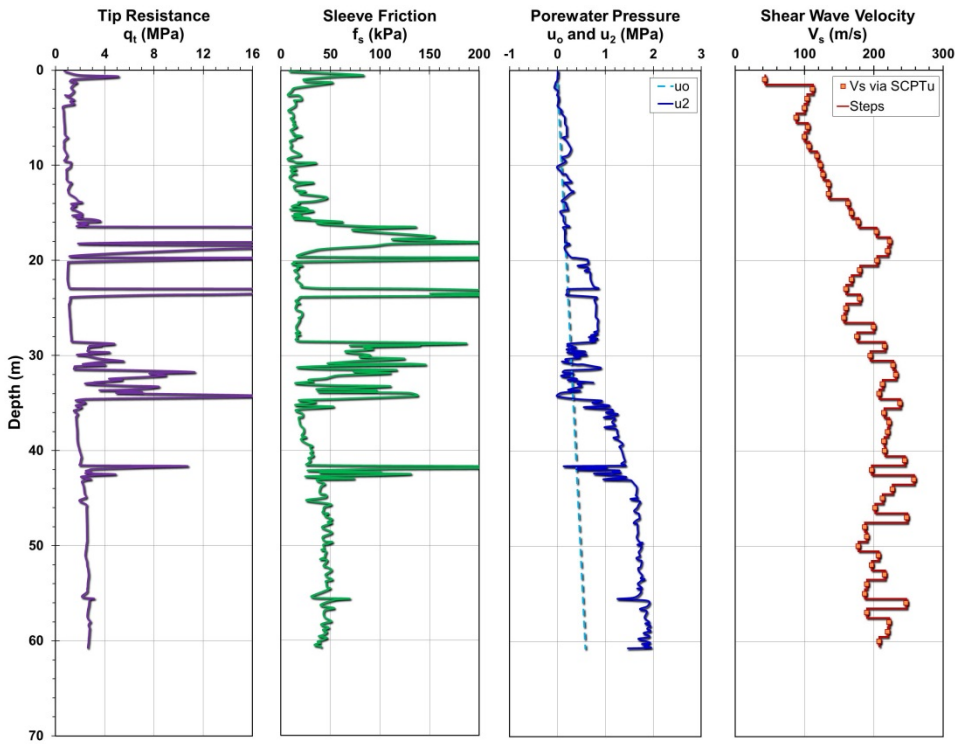	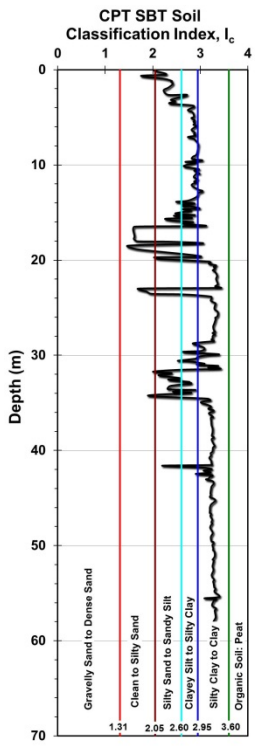	Site name and location	Pitt River Bridge, Vancouver South, BC, Canada
		Soil type(s)	Interbedded silt, clay, and sand over thick layer of silty clay
		Pile type(s)	Open-ended steel-concrete pipe piles
		Type of cone penetrometer testing	SCPTu
		Source of V_s evaluation	SCPTu
		Number of pile load tests	1
		Reference	Tara (2012)
		Comments	

Pile ID: PRB '73

Load-displacement data

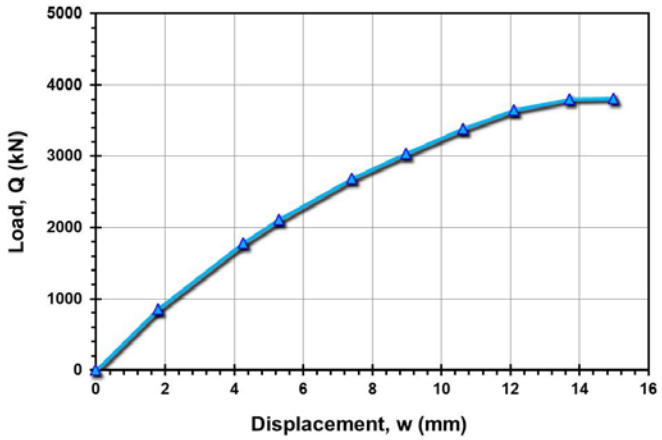

Back-analyzed normalized operational stiffness vs. pseudo-strain

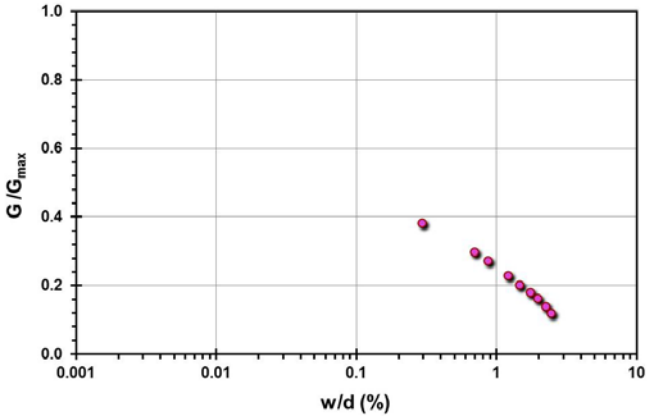

Detail	Description
Pile type/material	Open-ended steel-concrete pile
Length, L (m)	55.00
Diameter, d (m)	0.610
Installation method	Driven
Loading mode	Compression
$Q_{max\text{-}measured}$ (kN)	3,810.28
Q_s (kN)	3,705.16
Q_b (kN)	105.12
$Q_{Davisson}$ (kN)	6,372.67
$Q_{w/d=10\%}$ (kN)	4,492.54
$Q_{C\text{-}K}$ (kN)	4,761.90

Site ID No. 50B

Cone penetrometer data	CPT SBT soil classification index, I_c	Detail	Description
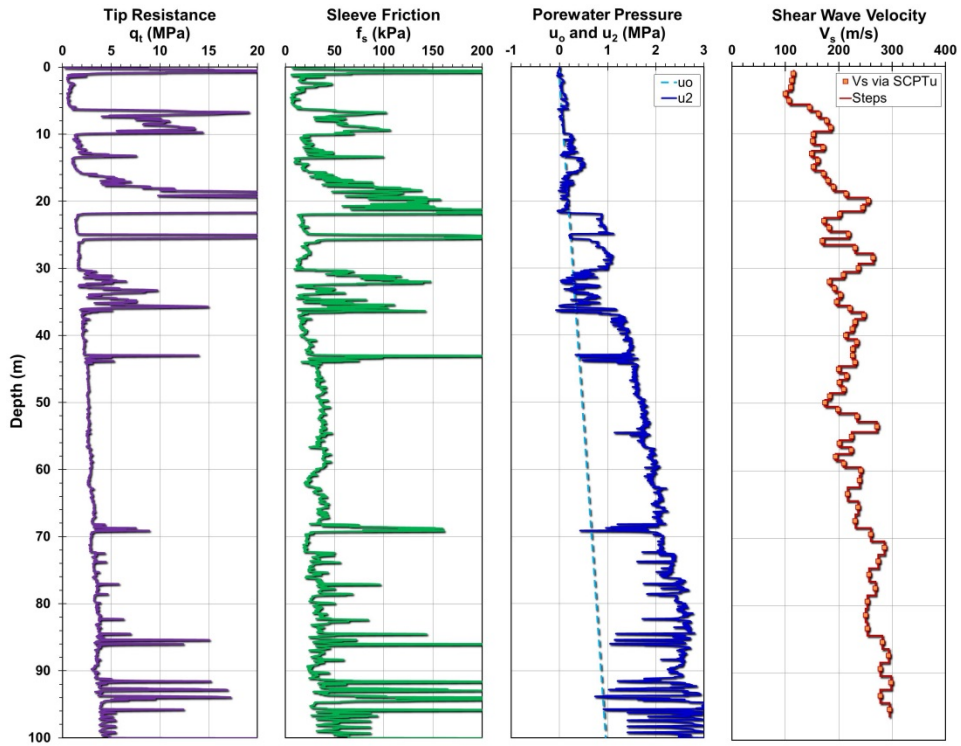	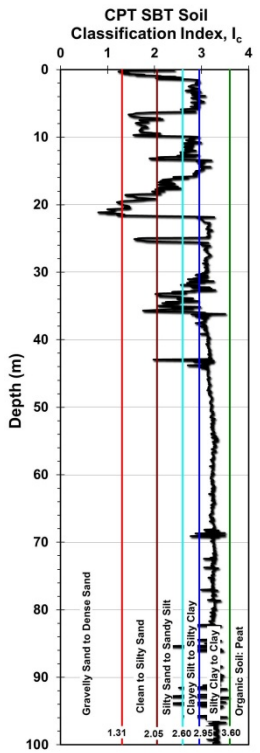	Site name and location	Pitt River Bridge, Vancouver South, BC, Canada
		Soil type(s)	Interbedded silt, clay, and sand over thick layer of soft to firm silty clay
		Pile type(s)	Open-ended steel-concrete pipe piles
		Type of cone penetrometer testing	SCPTu
		Source of V_s evaluation	SCPTu
		Number of pile load tests	1
		Reference	Tara (2012)
		Comments	

Pile ID: PRB '07

Load-displacement data

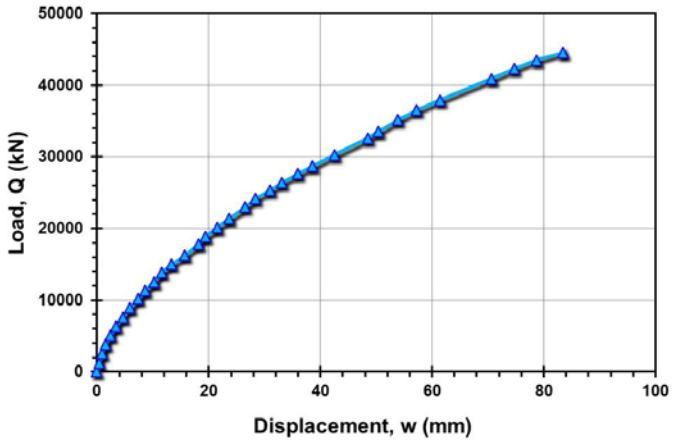

Back-analyzed normalized operational stiffness vs. pseudo-strain

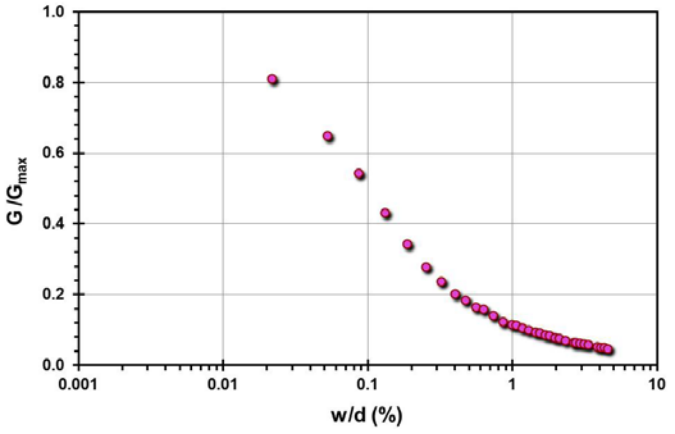

Detail	Description
Pile type/material	Open-ended steel-concrete pile
Length, L (m)	100.00
Diameter, d (m)	1.824
Installation method	Driven
Loading mode	Compression
$Q_{max\text{-}measured}$ (kN)	44,548.00
Q_s (kN)	26,602.86
Q_b (kN)	17,945.14
$Q_{Davisson}$ (kN)	37,899.70
$Q_{w/d=10\%}$ (kN)	57,255.25
$Q_{C\text{-}K}$ (kN)	76,923.08

Site ID No. 51

Cone penetrometer data	CPT SBT soil classification index, I_c	Detail	Description
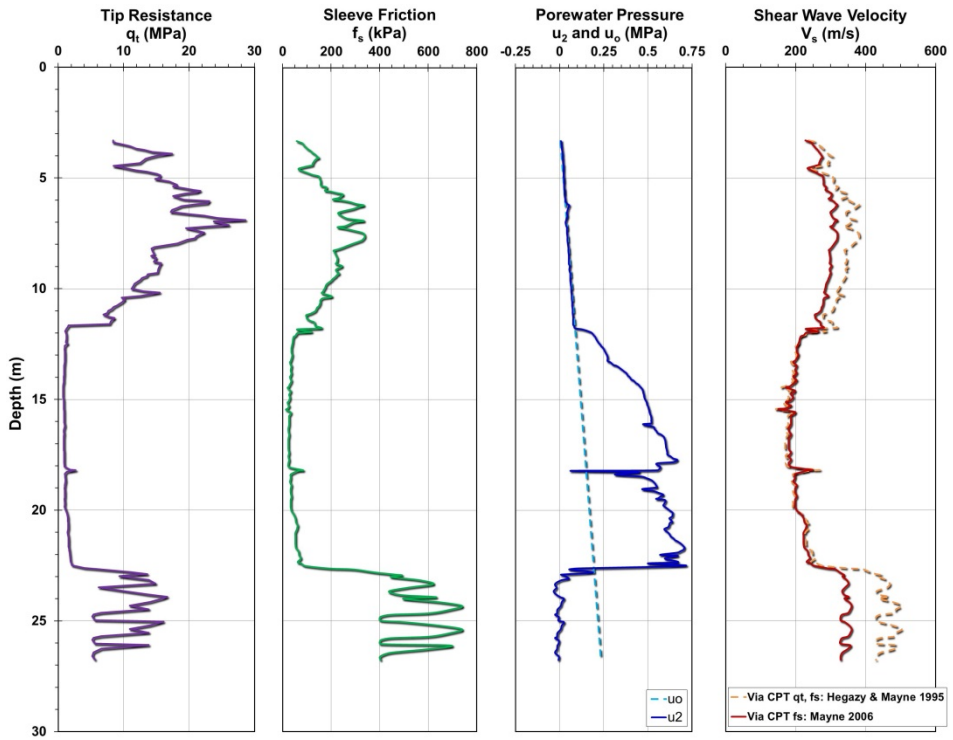	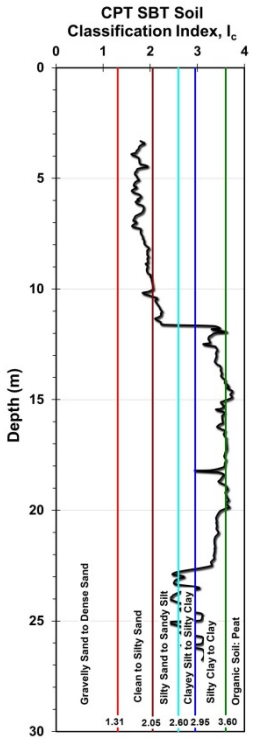	Site name and location	Refinery Expansion Project, Mid-west, USA
		Soil type(s)	Sand deposit over compressible post-glacial lacustrine clay/silty clay till over limestone bedrock
		Pile type(s)	Drilled shaft
		Type of cone penetrometer testing	CPTu
		Source of V_s evaluation	Correlations (see Figure opposite and Table 3.1)
		Number of pile load tests	2
		Reference	Fellenius and Ochoa (2009)
		Comments	

Pile ID: REP MW B1

Load-displacement data

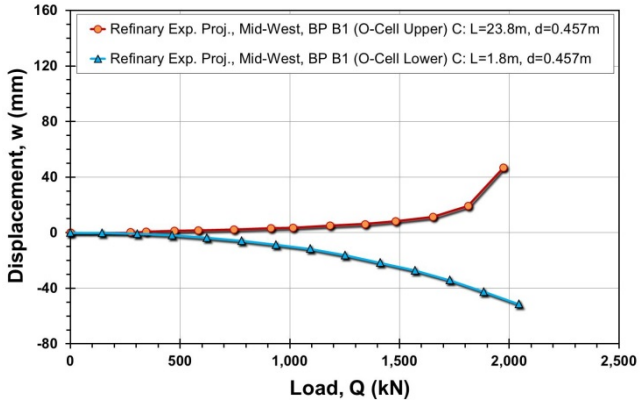

Back-analyzed normalized operational stiffness vs. pseudo-strain

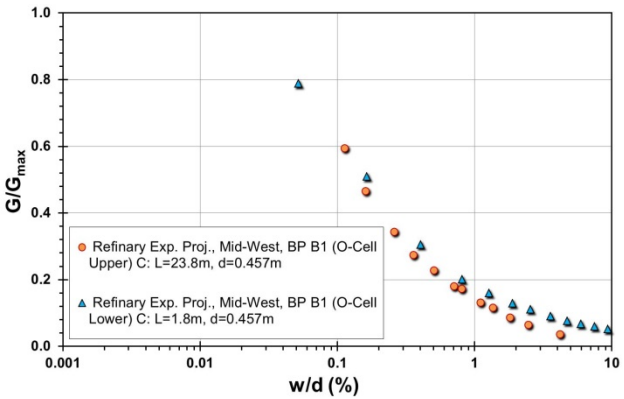

Detail	Description
Pile type/material	Drilled shaft
Length, L (m)	Upper: 23.8; lower: 1.80
Diameter, d (m)	Upper: 0.457; lower: 0.457
Installation method	Bored cast in-situ
Loading mode	O-cell compression
$Q_{max\text{-}measured}$ (kN)	Upper: 1,974.4; lower: 1,974.4
Q_s (kN)	Upper: 1,974.4; lower: 1,345.5
Q_b (kN)	628.9
$Q_{Davisson}$ (kN)	Upper: 1,801.8; lower: 937.4
$Q_{w/d=10\%}$ (kN)	Upper: 1,902.3; lower: 1,922.3
$Q_{C\text{-}K}$ (kN)	Upper: 2,100.8; lower: 3,086.4

Pile ID: REP MW G1

Load-displacement data

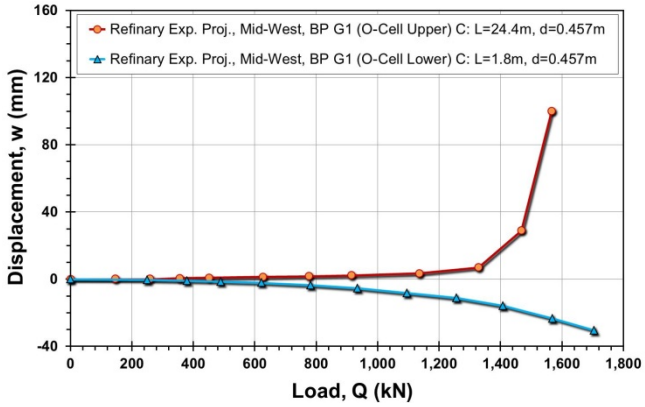

Back-analyzed normalized operational stiffness vs. pseudo-strain

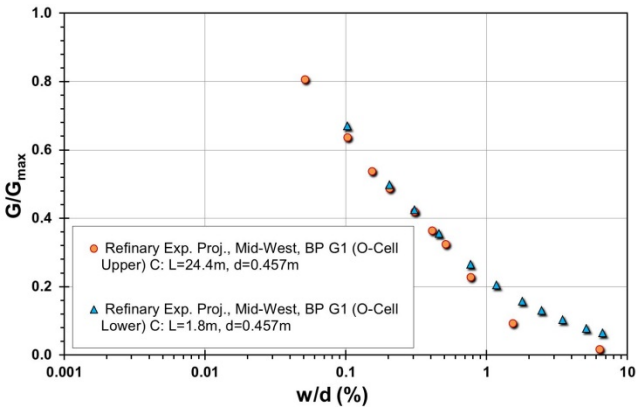

Detail	Description
Pile type/material	Drilled shaft
Length, L (m)	Upper: 24.4; lower: 0.457
Diameter, d (m)	Upper: 1.80; lower: 0.457
Installation method	Bored cast in-situ
Loading mode	O-cell compression
$Q_{max\text{-}measured}$ (kN)	Upper: 1,565.9; lower: 1,565.9
Q_s (kN)	Upper: 1,565.9; lower: 1,112.5
Q_b (kN)	453.4
$Q_{Davisson}$ (kN)	Upper: 1,379.25; lower: 1,094.9
$Q_{w/d=10\%}$ (kN)	Upper: 1,511.3; lower: 1,888.5
$Q_{C\text{-}K}$ (kN)	Upper: 1,610.3; lower: 2,212.4

Site ID No. 52

Cone penetrometer data	CPT SBT soil classification index, I_c	Detail	Description
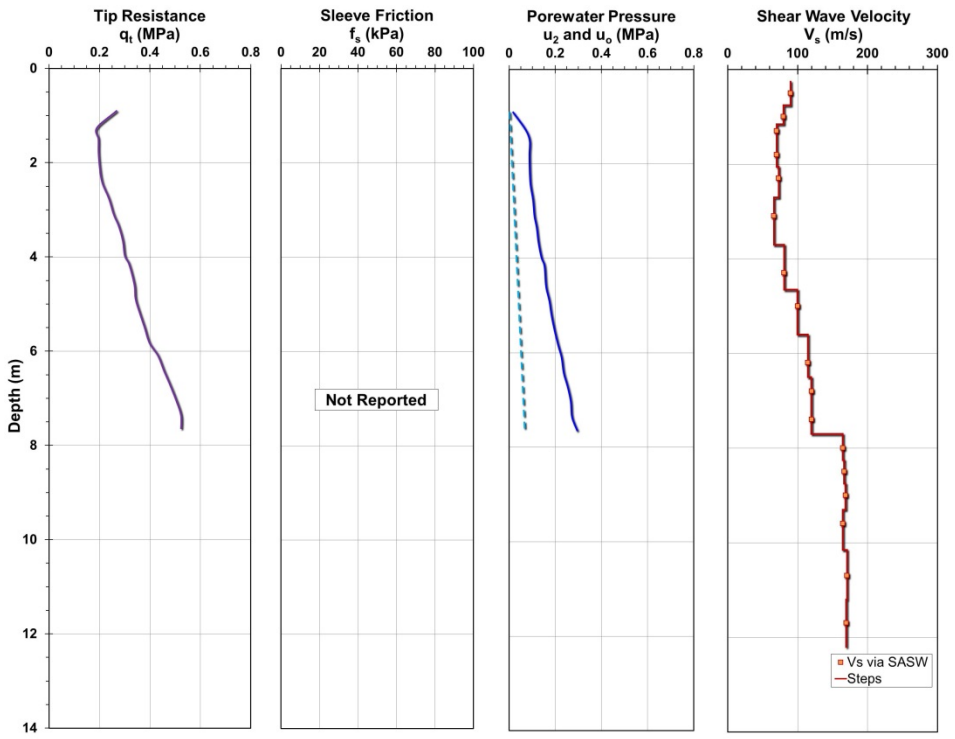	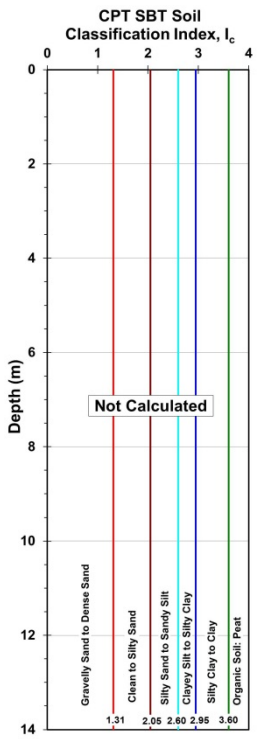	Site name and location	Saint Alban, Quebec, Canada
		Soil type(s)	Soft silty marine clay
		Pile type(s)	Closed-ended steel pipe piles
		Type of cone penetrometer testing	CPTu + SASW
		Source of V_s evaluation	SASW
		Number of pile load tests	5
		Reference	Heydinger (1982), Konrad and Roy (1987), Lefebvre et al. (1995)
		Comments	V_s via SASW, f_s not available

Pile ID: SA 1-1

Load-displacement data

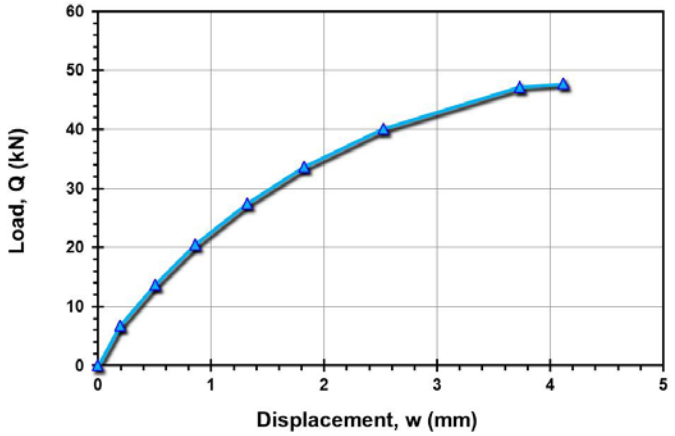

Back-analyzed normalized operational stiffness vs. pseudo-strain

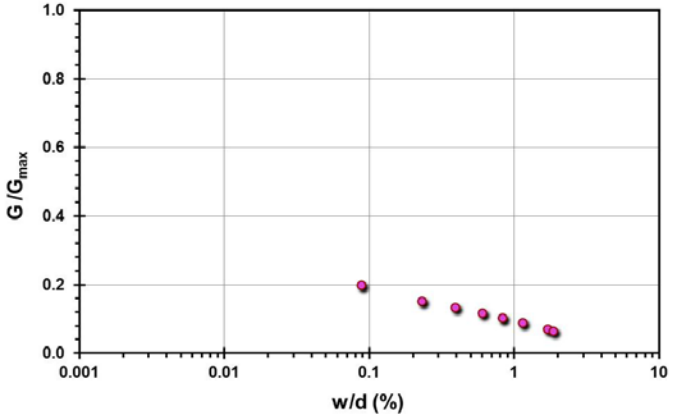

Detail	Description
Pile type/material	Closed-ended steel pipe pile
Length, L (m)	6.40
Diameter, d (m)	0.22
Installation method	Jacked
Loading mode	Compression
$Q_{max\text{-}measured}$ (kN)	47.73
Q_s (kN)	Not reported
Q_b (kN)	Not reported
$Q_{Davisson}$ (kN)	56.09
$Q_{w/d=10\%}$ (kN)	64.44
$Q_{C\text{-}K}$ (kN)	69.88

Pile ID: SA 1-2

Load-displacement data

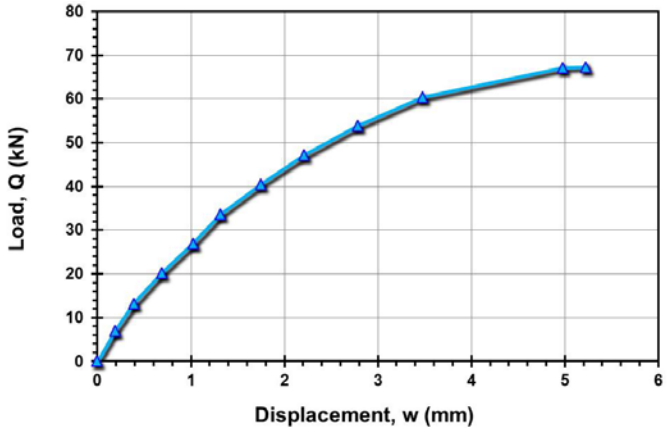

Back-analyzed normalized operational stiffness vs. pseudo-strain

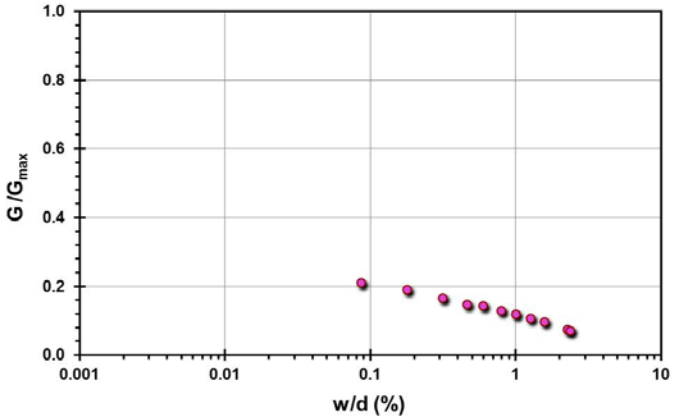

Detail	Description
Pile type/material	Closed-ended steel pipe pile
Length, L (m)	6.40
Diameter, d (m)	0.22
Installation method	Jacked
Loading mode	Compression
$Q_{max\text{-}measured}$ (kN)	67.27
Q_s (kN)	Not reported
Q_b (kN)	Not reported
$Q_{Davisson}$ (kN)	67.27
$Q_{w/d=10\%}$ (kN)	82.34
$Q_{C\text{-}K}$ (kN)	88.30

Pile ID: SA 1-3

Load-displacement data

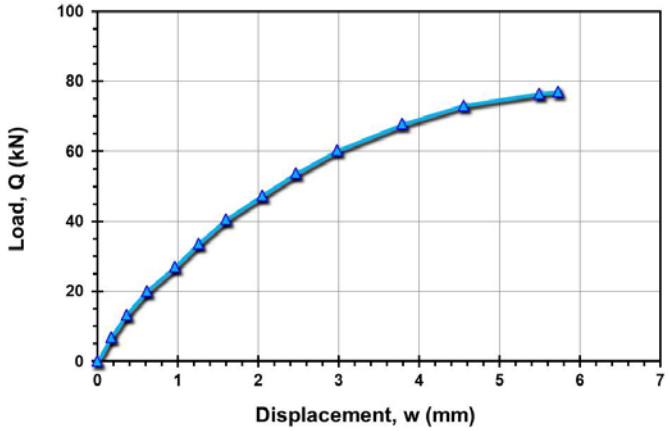

Back-analyzed normalized operational stiffness vs. pseudo-strain

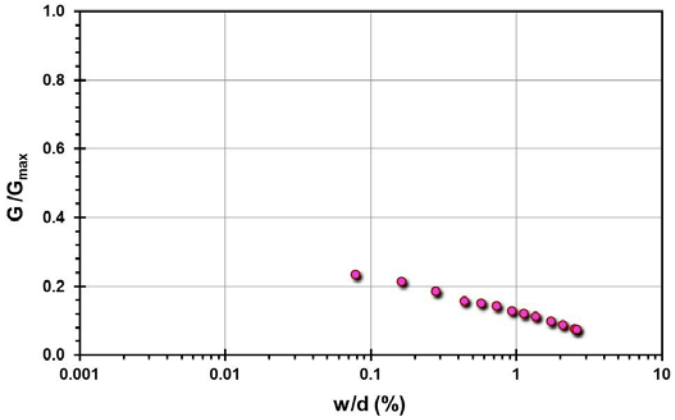

Detail	Description
Pile type/material	Closed-ended steel pipe pile
Length, L (m)	6.40
Diameter, d (m)	0.22
Installation method	Jacked
Loading mode	Compression
$Q_{max\text{-}measured}$ (kN)	77.03
Q_s (kN)	Not reported
Q_b (kN)	Not reported
$Q_{Davisson}$ (kN)	77.03
$Q_{w/d=10\%}$ (kN)	95.78
$Q_{C\text{-}K}$ (kN)	104.69

Pile ID: SA 1-4

Load-displacement data

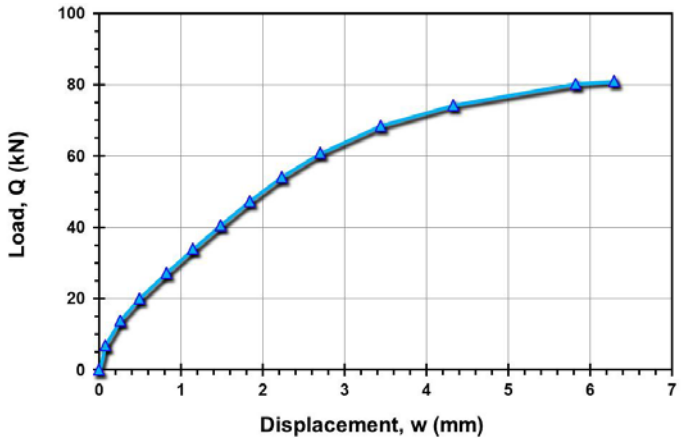

Back-analyzed normalized operational stiffness vs. pseudo-strain

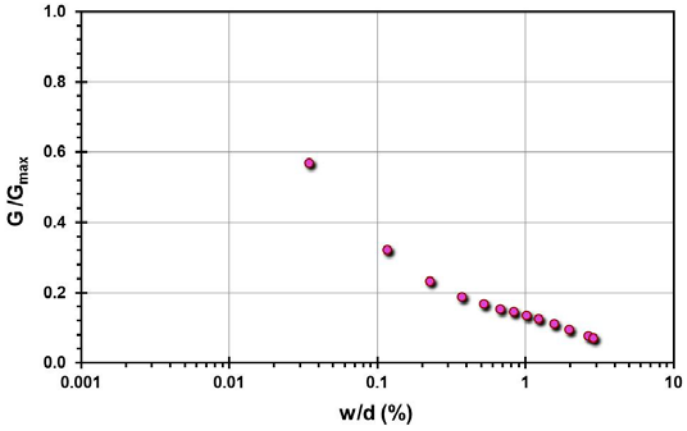

Detail	Description
Pile type/material	Closed-ended steel pipe pile
Length, L (m)	6.40
Diameter, d (m)	0.22
Installation method	Jacked
Loading mode	Compression
$Q_{max\text{-}measured}$ (kN)	80.94
Q_s (kN)	Not reported
Q_b (kN)	Not reported
$Q_{Davisson}$ (kN)	80.16
$Q_{w/d=10\%}$ (kN)	96.32
$Q_{C\text{-}K}$ (kN)	104.01

Pile ID: SA 1-5

Load-displacement data

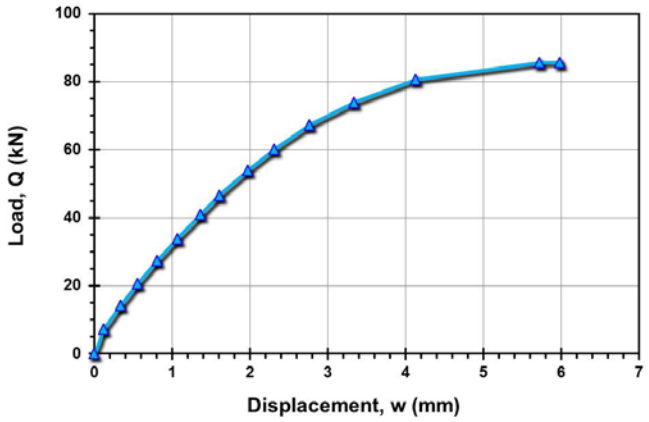

Back-analyzed normalized operational stiffness vs. pseudo-strain

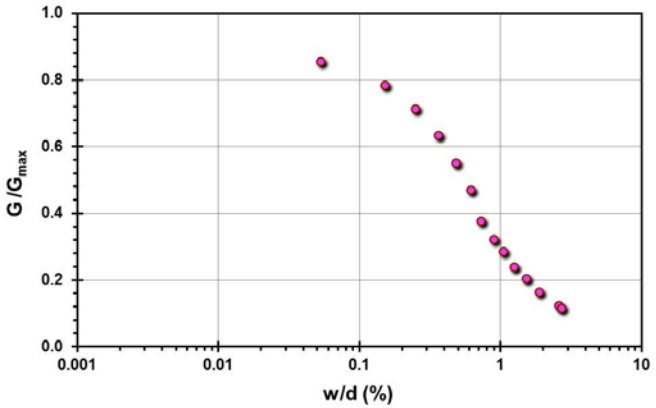

Detail	Description
Pile type/material	Closed-ended steel pipe pile
Length, L (m)	6.40
Diameter, d (m)	0.22
Installation method	Jacked
Loading mode	Compression
$Q_{max\text{-}measured}$ (kN)	85.68
Q_s (kN)	76.8
Q_b (kN)	8.88
$Q_{Davisson}$ (kN)	85.68
$Q_{w/d=10\%}$ (kN)	99.84
$Q_{C\text{-}K}$ (kN)	106.22

Site ID No. 53

Cone penetrometer data	CPT SBT soil classification index, I_c	Detail	Description
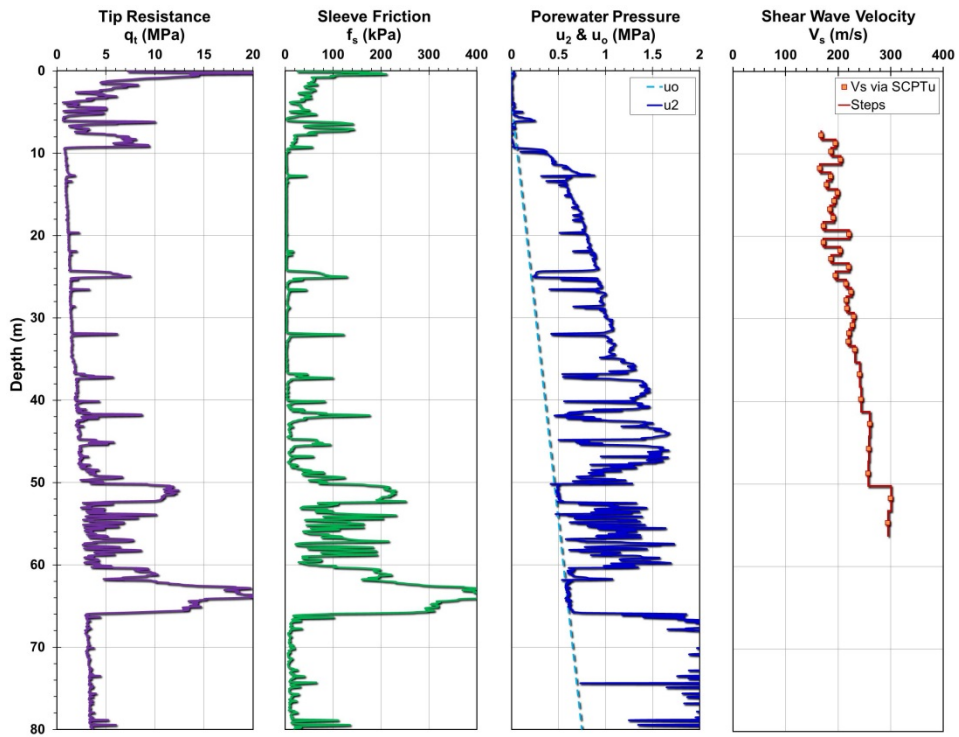	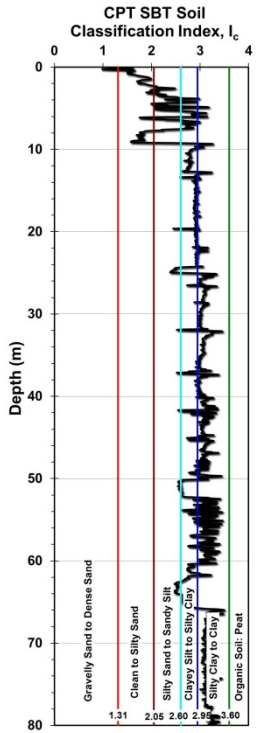	Site name and location	Sandpoint, along the shores of Lake Pend Oreille, Northern Idaho, USA
		Soil type(s)	Silty clayey sand over soft silty clay
		Pile type(s)	Closed-ended steel pipe piles
		Type of cone penetrometer testing	SCPTu
		Source of V_s evaluation	SCPTu
		Number of pile load tests	1
		Reference	Fellenius et al. (2003)
		Comments	

Pile ID: SPI 1

Load-displacement data

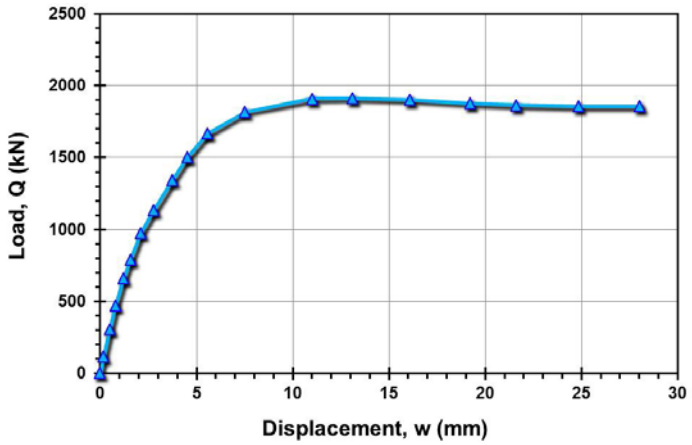

Back-analyzed normalized operational stiffness vs. pseudo-strain

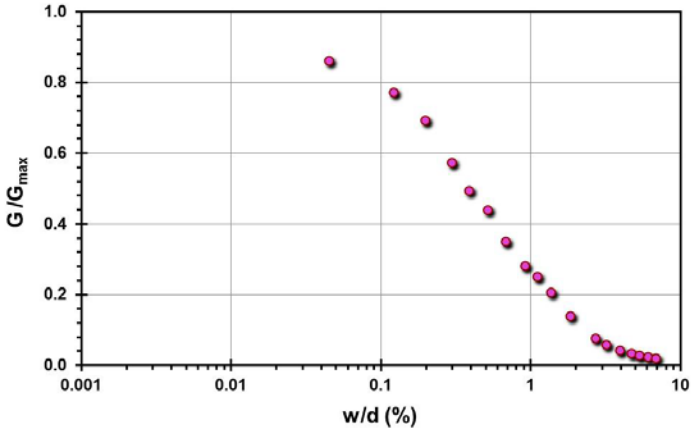

Detail	Description
Pile type/material	Closed-ended steel pipe pile
Length, L (m)	45.00
Diameter, d (m)	0.406
Installation method	Driven
Loading mode	Compression
$Q_{max\text{-}measured}$ (kN)	1,854.23
Q_s (kN)	1,748.72
Q_b (kN)	105.51
$Q_{Davisson}$ (kN)	1,912.73
$Q_{w/d=10\%}$ (kN)	1,935.24
$Q_{C\text{-}K}$ (kN)	1,976.28

Site ID No. 54

Cone penetrometer data	CPT SBT soil classification index, I_c	Detail	Description
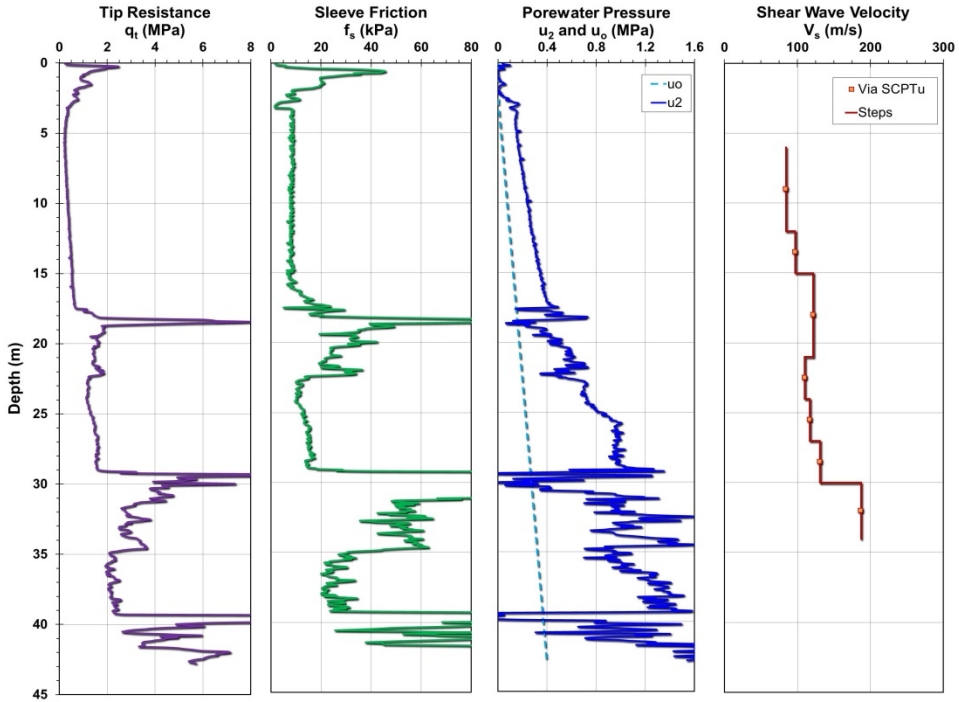	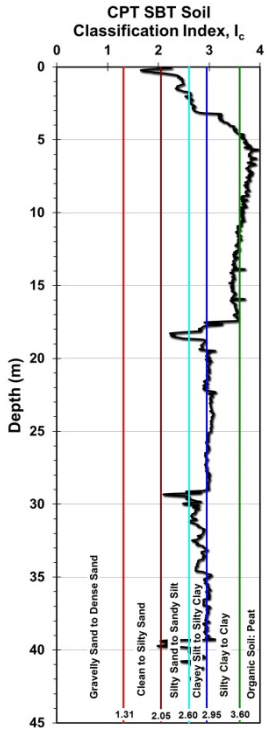	Site name and location	San Francisco Bay Mud, I-280 Caltrans Load Tests, CA, USA
		Soil type(s)	Uniform soft silty clay over clayey to sandy silt
		Pile type(s)	9 Open-ended steel-concrete piles, 8 screw pile, 4 Open-ended steel pipe piles, 8 Square concrete piles, 3 H-section piles
		Type of cone penetrometer testing	SCPTu
		Source of V_s evaluation	SCPTu
		Number of pile load tests	32
		Reference	Brittsan and Speer (2008)
		Comments	

Pile ID: SFBM P10T

Load-displacement data

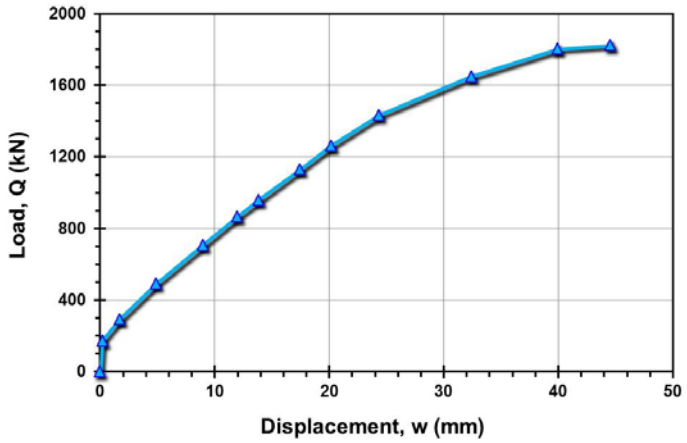

Back-analyzed normalized operational stiffness vs. pseudo-strain

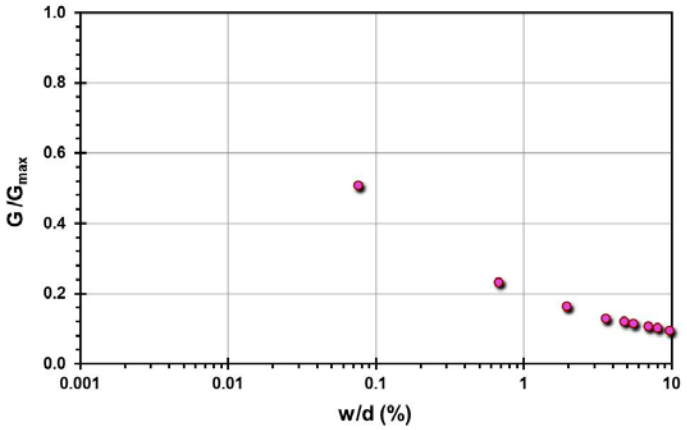

Detail	Description
Pile type/material	Open-ended steel-concrete pile
Length, L (m)	38.90
Diameter, d (m)	0.25
Installation method	Driven
Loading mode	Tension
$Q_{max\text{-}measured}$ (kN)	1,822.90
Q_s (kN)	Not reported
Q_b (kN)	Not reported
$Q_{Davisson}$ (kN)	1,822.90
$Q_{w/d=10\%}$ (kN)	1,501.64
$Q_{C\text{-}K}$ (kN)	2,577.32

Pile ID: SFBM P11T

Load-displacement data

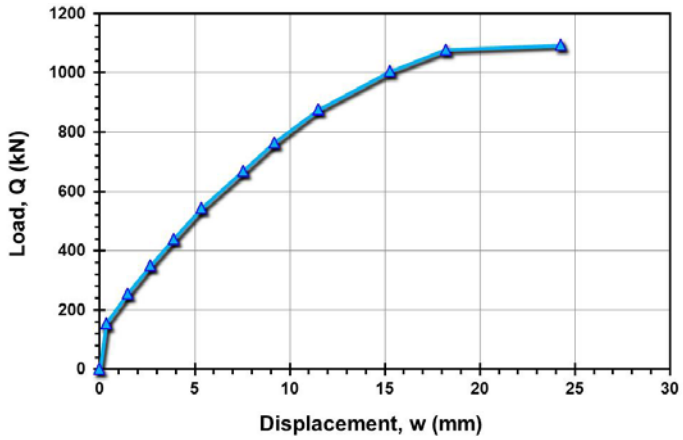

Back-analyzed normalized operational stiffness vs. pseudo-strain

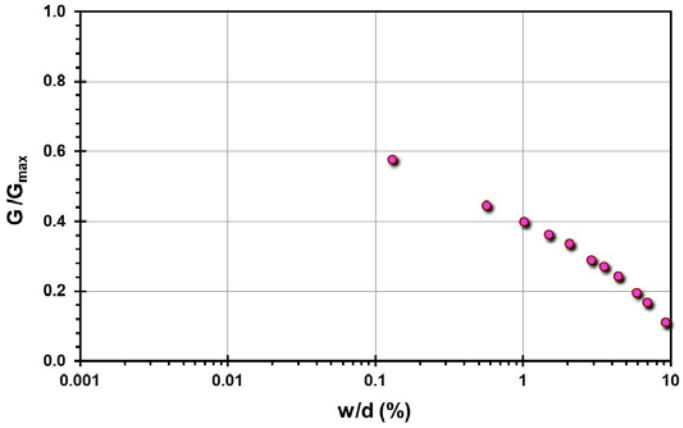

Detail	Description
Pile type/material	Open-ended steel-concrete pile
Length, L (m)	26.90
Diameter, d (m)	0.26
Installation method	Driven
Loading mode	Tension
$Q_{max\text{-}measured}$ (kN)	1,094.08
Q_s (kN)	Not reported
Q_b (kN)	Not reported
$Q_{Davisson}$ (kN)	1,086.19
$Q_{w/d=10\%}$ (kN)	1,110.20
$Q_{C\text{-}K}$ (kN)	1,265.82

Pile ID: SFBM P12T

Load-displacement data

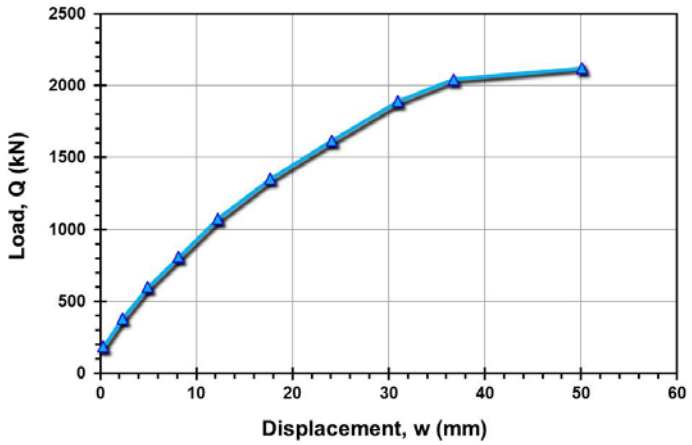

Back-analyzed normalized operational stiffness vs. pseudo-strain

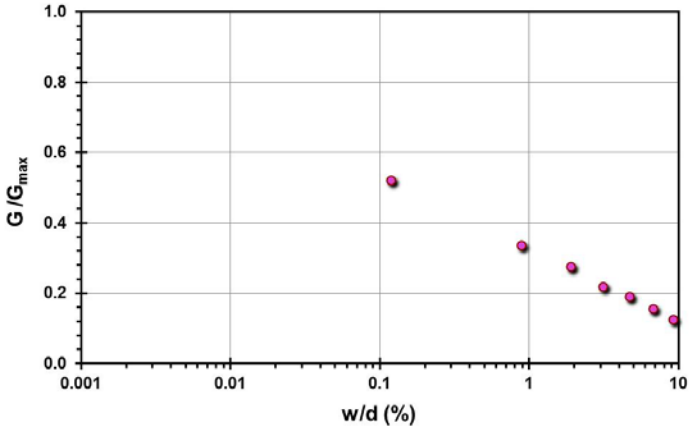

Detail	Description
Pile type/material	Open-ended steel-concrete pile
Length, L (m)	38.50
Diameter, d (m)	0.25
Installation method	Driven
Loading mode	Tension
$Q_{max\text{-}measured}$ (kN)	2,121.58
Q_s (kN)	Not reported
Q_b (kN)	Not reported
$Q_{Davisson}$ (kN)	2,121.58
$Q_{w/d=10\%}$ (kN)	1,832.73
$Q_{C\text{-}K}$ (kN)	2,597.40

Pile ID: SFBM P13C

Load-displacement data

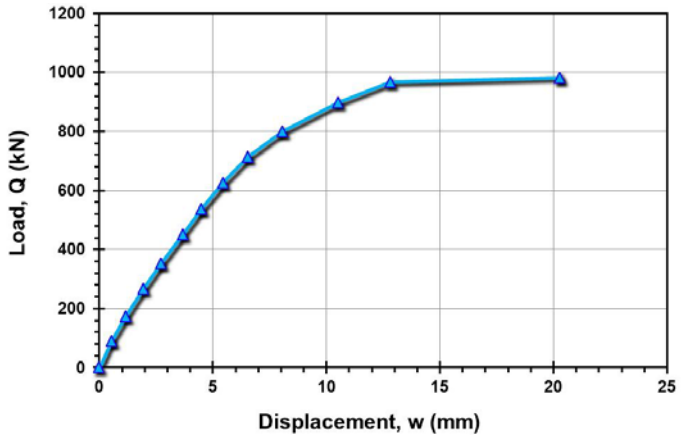

Back-analyzed normalized operational stiffness vs. pseudo-strain

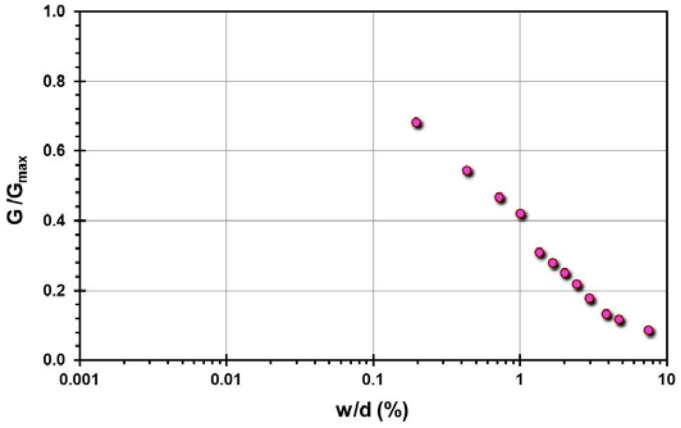

Detail	Description
Pile type/material	Open-ended steel-concrete pile
Length, L (m)	26.90
Diameter, d (m)	0.27
Installation method	Driven
Loading mode	Compression
$Q_{max\text{-}measured}$ (kN)	982.86
Q_s (kN)	Not reported
Q_b (kN)	Not reported
$Q_{Davisson}$ (kN)	982.86
$Q_{w/d=10\%}$ (kN)	989.32
$Q_{C\text{-}K}$ (kN)	1,010.10

Pile ID: SFBM P13T

Load-displacement data

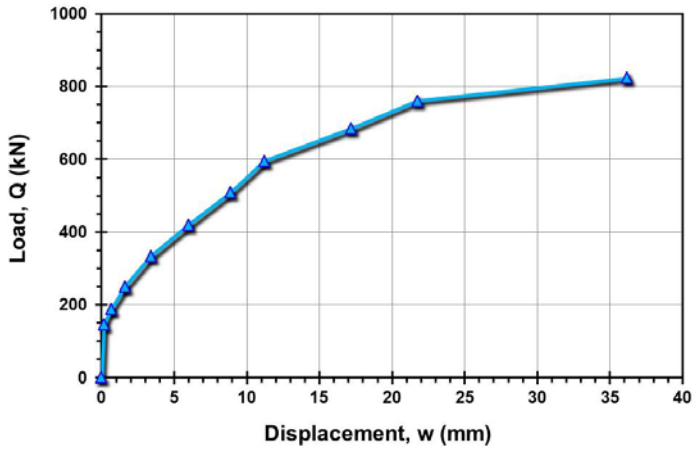

Back-analyzed normalized operational stiffness vs. pseudo-strain

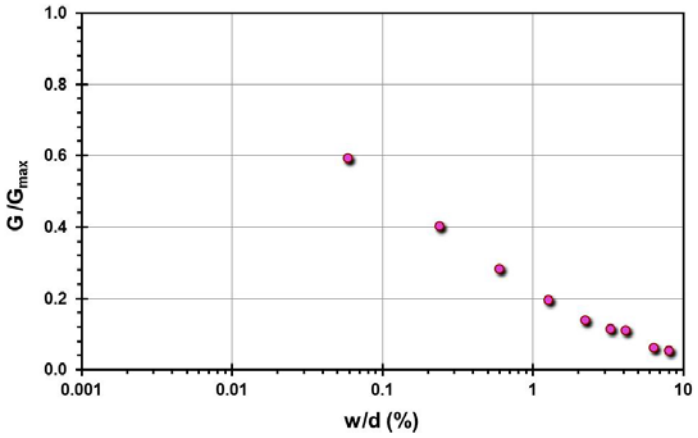

Detail	Description
Pile type/material	Open-ended steel-concrete pile
Length, L (m)	26.90
Diameter, d (m)	0.27
Installation method	Driven
Loading mode	Tension
$Q_{max\text{-}measured}$ (kN)	823.36
Q_s (kN)	Not reported
Q_b (kN)	Not reported
$Q_{Davisson}$ (kN)	640.15
$Q_{w/d=10\%}$ (kN)	789.58
$Q_{C\text{-}K}$ (kN)	938.97

Pile ID: SFBM P31C

Load-displacement data

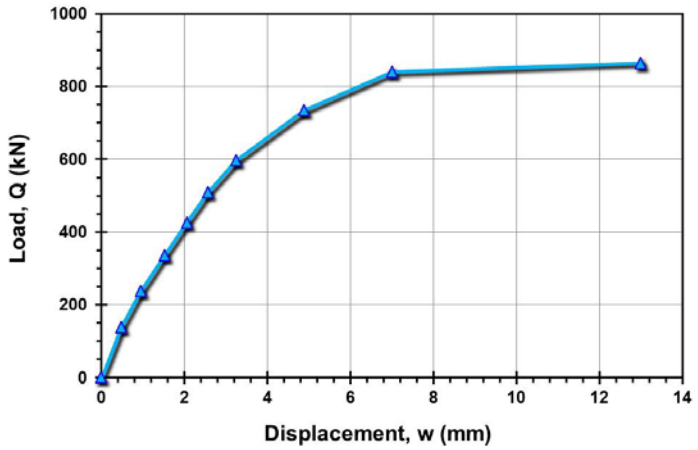

Back-analyzed normalized operational stiffness vs. pseudo-strain

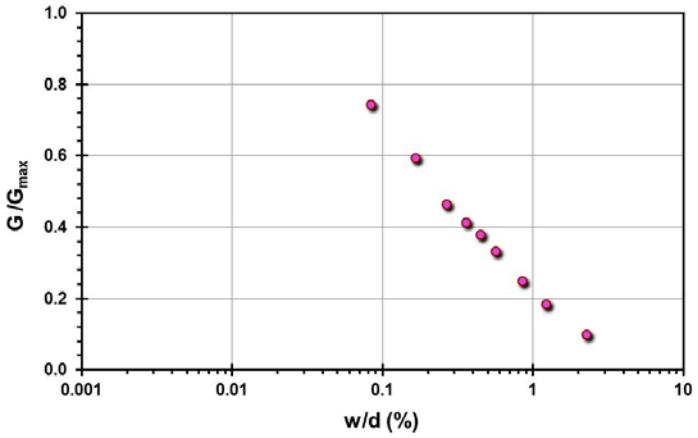

Detail	Description
Pile type/material	Fundex
Length, L (m)	25.10
Diameter, d (m)	0.57
Installation method	Driven
Loading mode	Compression
$Q_{max\text{-}measured}$ (kN)	865.00
Q_s (kN)	Not reported
Q_b (kN)	Not reported
$Q_{Davisson}$ (kN)	865.00
$Q_{w/d=10\%}$ (kN)	888.69
$Q_{C\text{-}K}$ (kN)	896.06

Pile ID: SFBM P31T

Load-displacement data

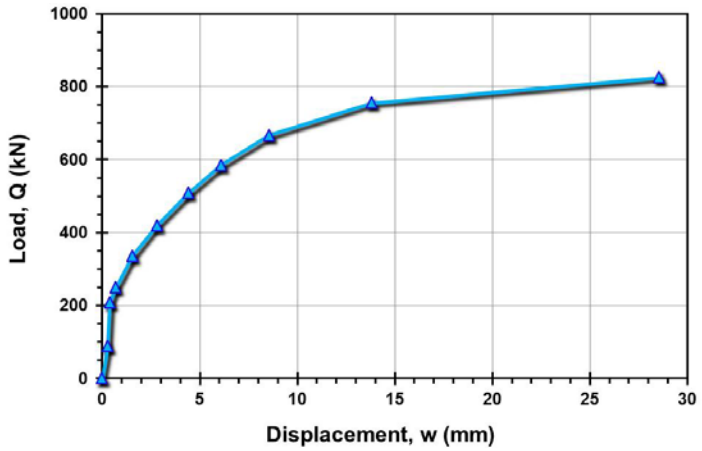

Back-analyzed normalized operational stiffness vs. pseudo-strain

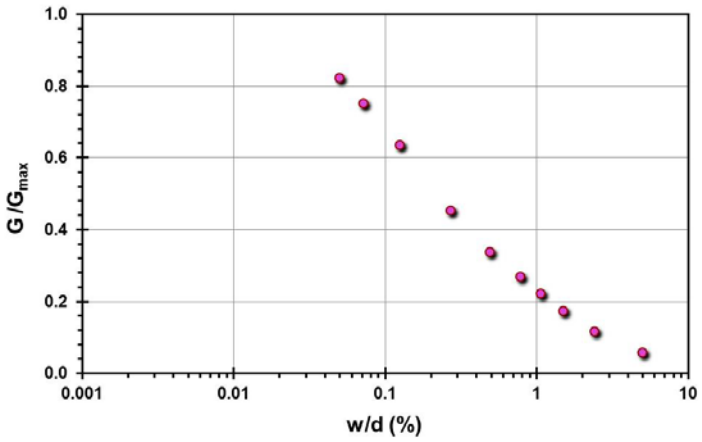

Detail	Description
Pile type/material	Fundex
Length, L (m)	25.10
Diameter, d (m)	0.57
Installation method	Driven
Loading mode	Tension
$Q_{max\text{-}measured}$ (kN)	825.44
Q_s (kN)	Not reported
Q_b (kN)	Not reported
$Q_{Davisson}$ (kN)	711.24
$Q_{w/d=10\%}$ (kN)	877.29
$Q_{C\text{-}K}$ (kN)	896.06

Pile ID: SFBM P32C

Load-displacement data

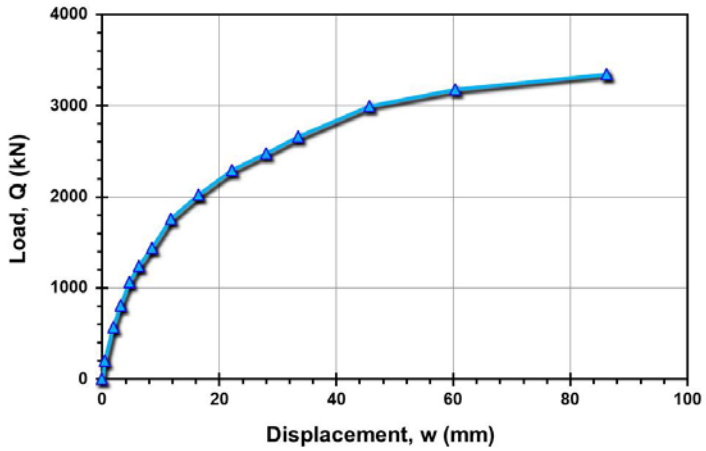

Back-analyzed normalized operational stiffness vs. pseudo-strain

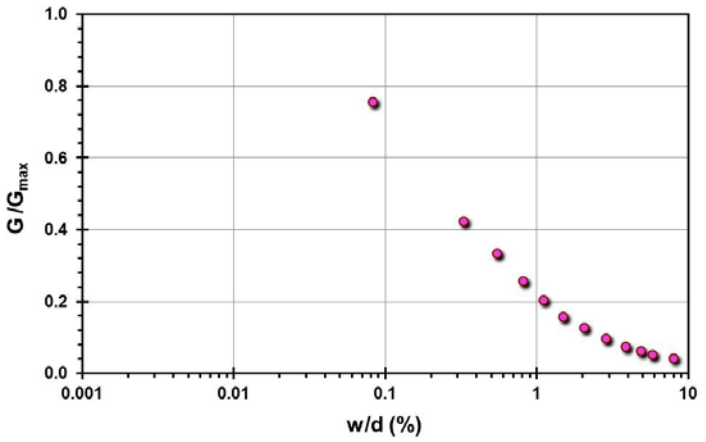

Detail	Description
Pile type/material	Fundex
Length, L (m)	33.70
Diameter, d (m)	0.57
Installation method	Driven
Loading mode	Compression
$Q_{max\text{-}measured}$ (kN)	3,347.70
Q_s (kN)	Not reported
Q_b (kN)	Not reported
$Q_{Davisson}$ (kN)	2,018.67
$Q_{w/d=10\%}$ (kN)	3,148.67
$Q_{C\text{-}K}$ (kN)	3,861.00

Pile ID: SFBM P32T

Load-displacement data

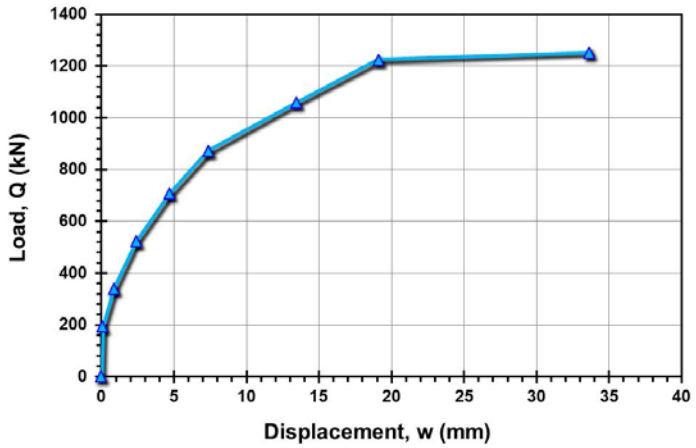

Back-analyzed normalized operational stiffness vs. pseudo-strain

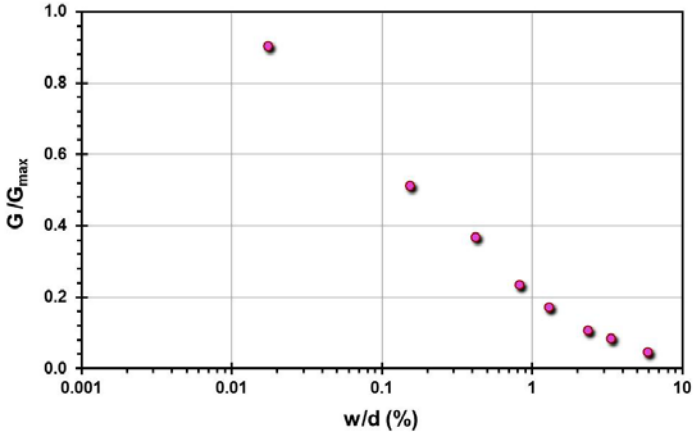

Detail	Description
Pile type/material	Fundex
Length, L (m)	33.70
Diameter, d (m)	0.57
Installation method	Driven
Loading mode	Tension
$Q_{max\text{-}measured}$ (kN)	1,252.13
Q_s (kN)	Not reported
Q_b (kN)	Not reported
$Q_{Davisson}$ (kN)	1,059.22
$Q_{w/d=10\%}$ (kN)	1,267.27
$Q_{C\text{-}K}$ (kN)	1,290.32

Pile ID: SFBM P33C

Load-displacement data

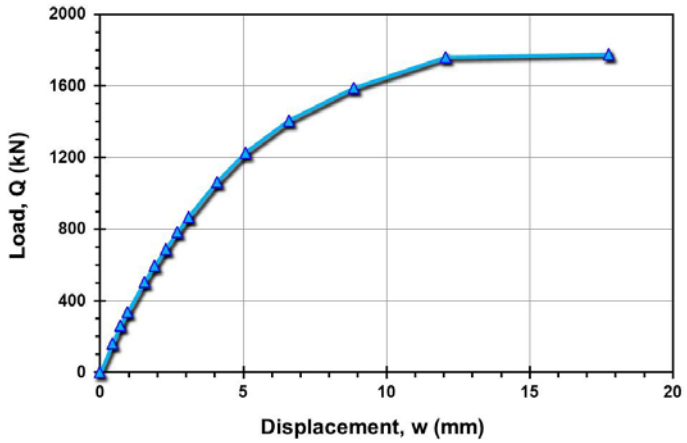

Back-analyzed normalized operational stiffness vs. pseudo-strain

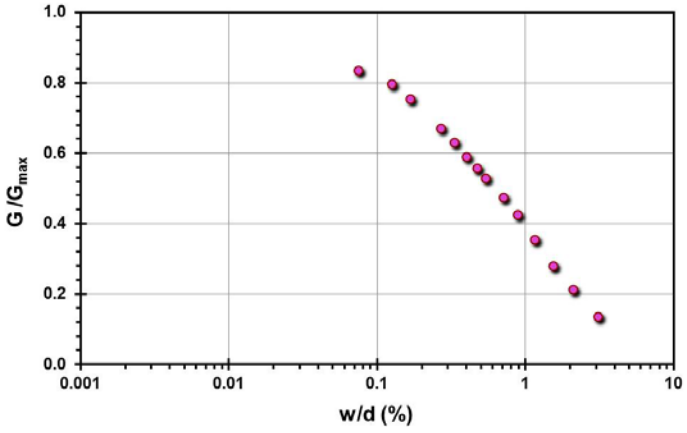

Detail	Description
Pile type/material	Fundex
Length, L (m)	25.10
Diameter, d (m)	0.57
Installation method	Driven
Loading mode	Compression
$Q_{max\text{-}measured}$ (kN)	1,775.33
Q_s (kN)	Not reported
Q_b (kN)	Not reported
$Q_{Davisson}$ (kN)	1,758.18
$Q_{w/d=10\%}$ (kN)	1,799.69
$Q_{C\text{-}K}$ (kN)	1,811.59

Pile ID: SFBM P33T

Load-displacement data

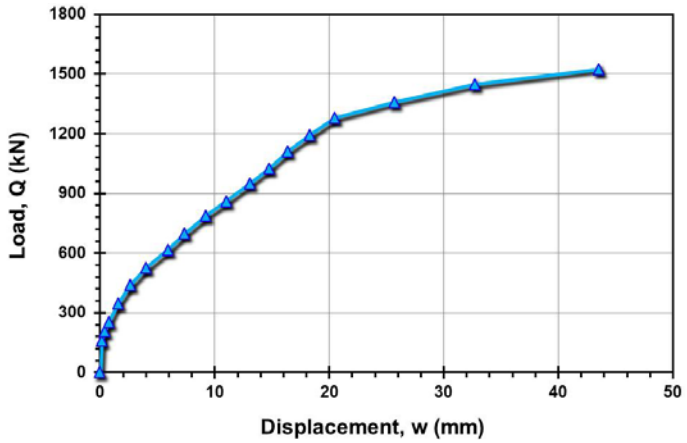

Back-analyzed normalized operational stiffness vs. pseudo-strain

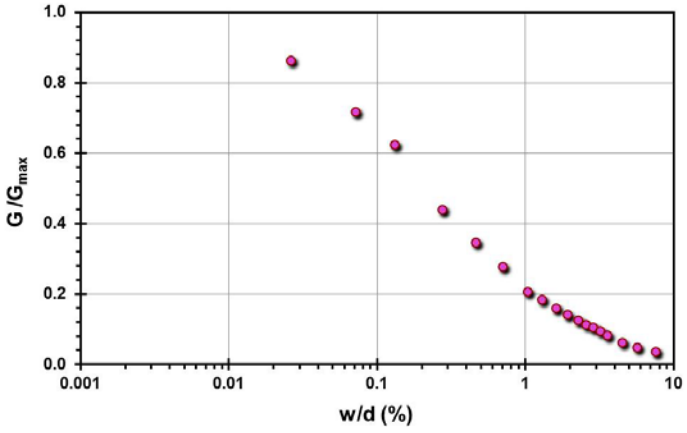

Detail	Description
Pile type/material	Fundex
Length, L (m)	25.10
Diameter, d (m)	0.57
Installation method	Driven
Loading mode	Tension
$Q_{max\text{-}measured}$ (kN)	1,524.14
Q_s (kN)	Not reported
Q_b (kN)	Not reported
$Q_{Davisson}$ (kN)	860.60
$Q_{w/d=10\%}$ (kN)	1,586.82
$Q_{C\text{-}K}$ (kN)	1,841.62

Pile ID: SFBM P34C

Load-displacement data

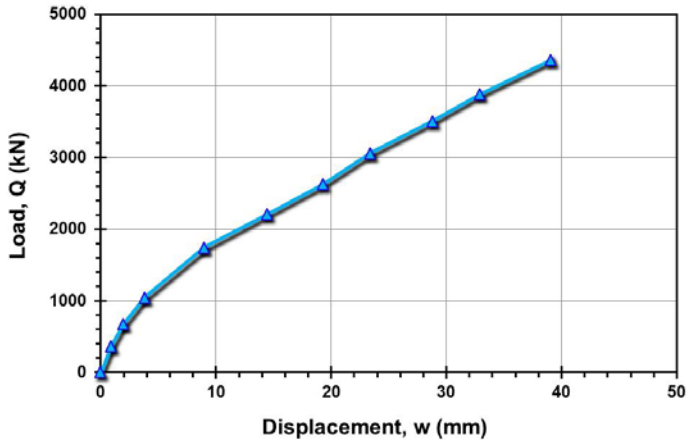

Back-analyzed normalized operational stiffness vs. pseudo-strain

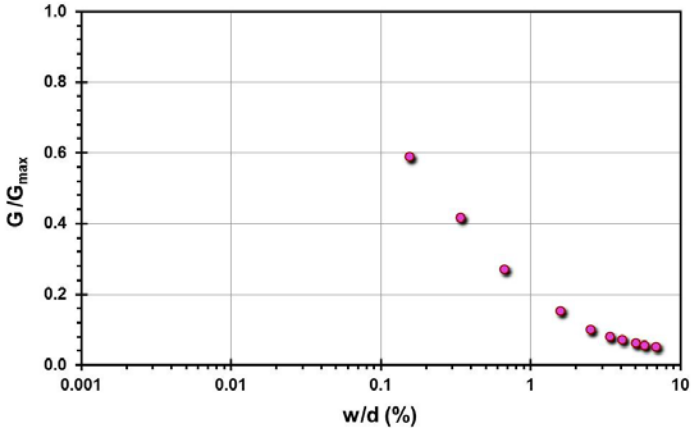

Detail	Description
Pile type/material	Fundex
Length, L (m)	33.70
Diameter, d (m)	0.57
Installation method	Driven
Loading mode	Compression
$Q_{max\text{-}measured}$ (kN)	4,361.22
Q_s (kN)	Not reported
Q_b (kN)	Not reported
$Q_{Davisson}$ (kN)	2,624.09
$Q_{w/d=10\%}$ (kN)	5,301.23
$Q_{C\text{-}K}$ (kN)	10,638.30

Pile ID: SFBM P34T

Load-displacement data

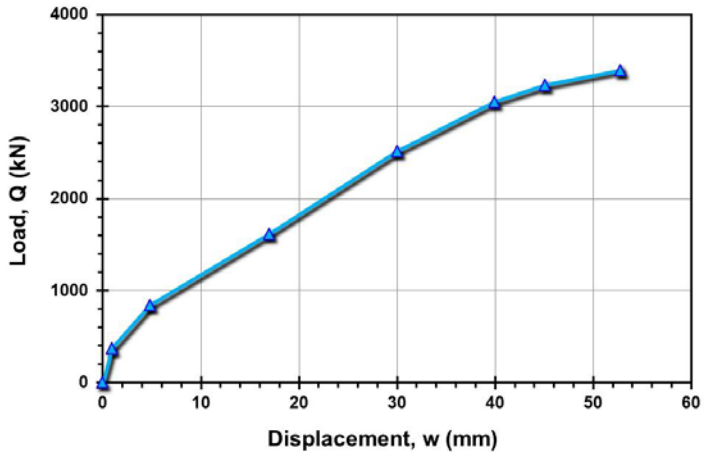

Back-analyzed normalized operational stiffness vs. pseudo-strain

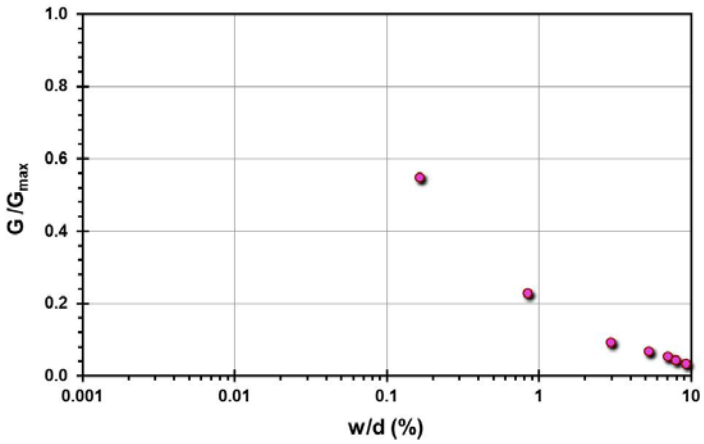

Detail	Description
Pile type/material	Fundex
Length, L (m)	33.70
Diameter, d (m)	0.57
Installation method	Driven
Loading mode	Tension
$Q_{max\text{-}measured}$ (kN)	3,395.91
Q_s (kN)	Not reported
Q_b (kN)	Not reported
$Q_{Davisson}$ (kN)	1,616.39
$Q_{w/d=10\%}$ (kN)	3,488.48
$Q_{C\text{-}K}$ (kN)	5,208.33

Pile ID: SFBM P48C

Load-displacement data

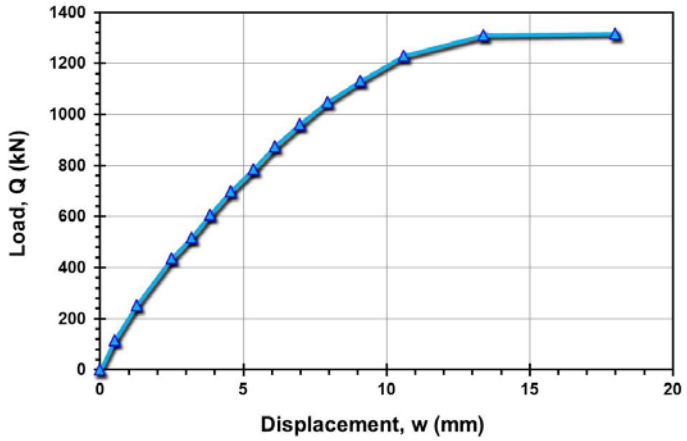

Back-analyzed normalized operational stiffness vs. pseudo-strain

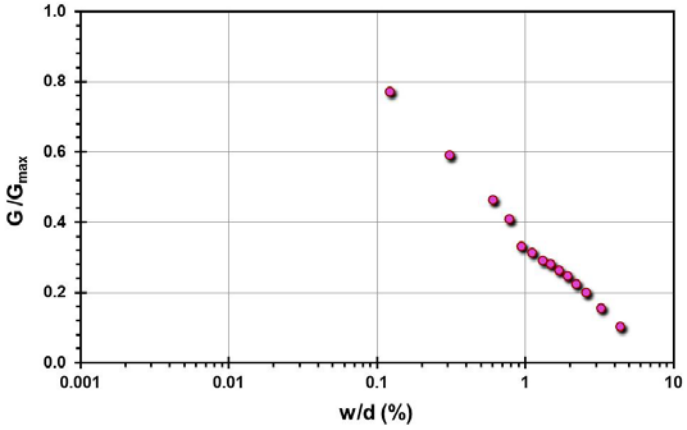

Detail	Description
Pile type/material	Open-ended steel pipe pile
Length, L (m)	26.10
Diameter, d (m)	0.41
Installation method	Driven
Loading mode	Compression
$Q_{max\text{-}measured}$ (kN)	1,316.80
Q_s (kN)	Not reported
Q_b (kN)	Not reported
$Q_{Davisson}$ (kN)	1,316.80
$Q_{w/d=10\%}$ (kN)	1,330.27
$Q_{C\text{-}K}$ (kN)	1,340.48

Pile ID: SFBM P48T

Load-displacement data

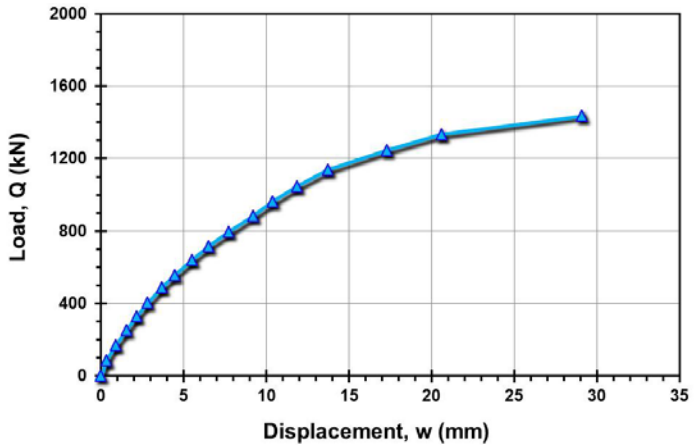

Back-analyzed normalized operational stiffness vs. pseudo-strain

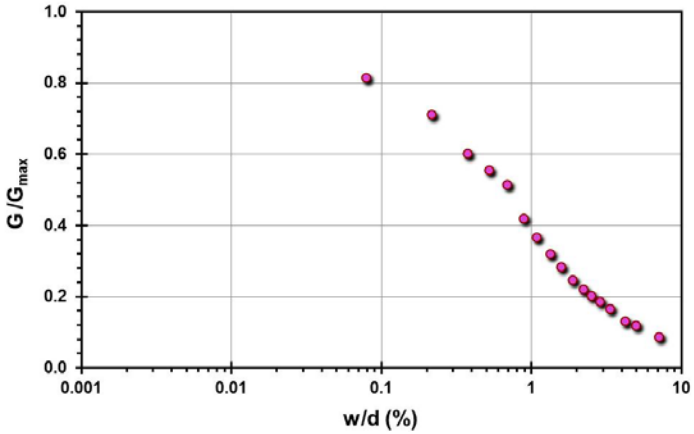

Detail	Description
Pile type/material	Open-ended steel pipe pile
Length, L (m)	26.10
Diameter, d (m)	0.41
Installation method	Driven
Loading mode	Tension
$Q_{max\text{-}measured}$ (kN)	1,435.62
Q_s (kN)	Not reported
Q_b (kN)	Not reported
$Q_{Davisson}$ (kN)	1,245.95
$Q_{w/d=10\%}$ (kN)	1,535.77
$Q_{C\text{-}K}$ (kN)	1,828.15

Pile ID: SFBM P49T

Load-displacement data

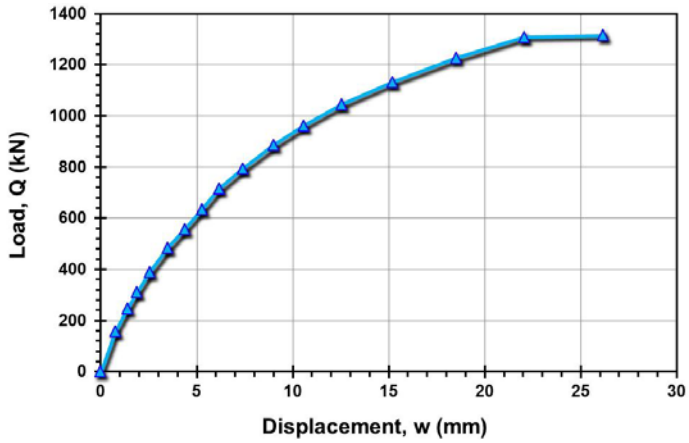

Back-analyzed normalized operational stiffness vs. pseudo-strain

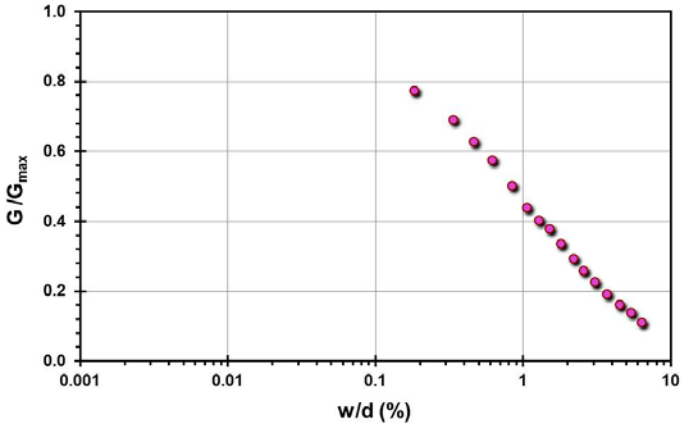

Detail	Description
Pile type/material	Open-ended steel pipe pile
Length, L (m)	26.10
Diameter, d (m)	0.41
Installation method	Driven
Loading mode	Tension
$Q_{max\text{-}measured}$ (kN)	1,314.48
Q_s (kN)	Not reported
Q_b (kN)	Not reported
$Q_{Davisson}$ (kN)	1,178.89
$Q_{w/d=10\%}$ (kN)	1,326.73
$Q_{C\text{-}K}$ (kN)	1,347.71

Pile ID: SFBM P49C

Load-displacement data

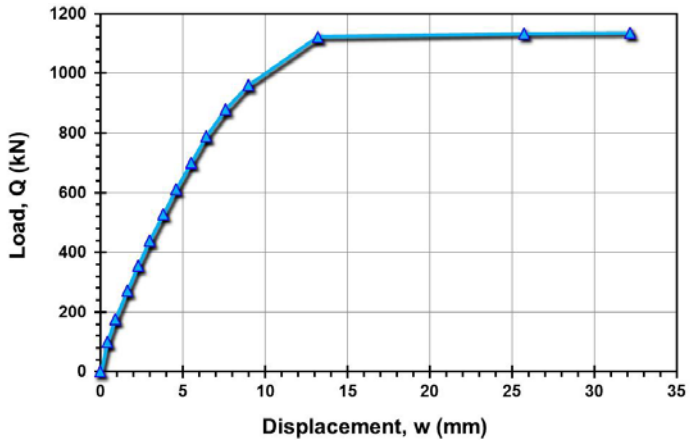

Back-analyzed normalized operational stiffness vs. pseudo-strain

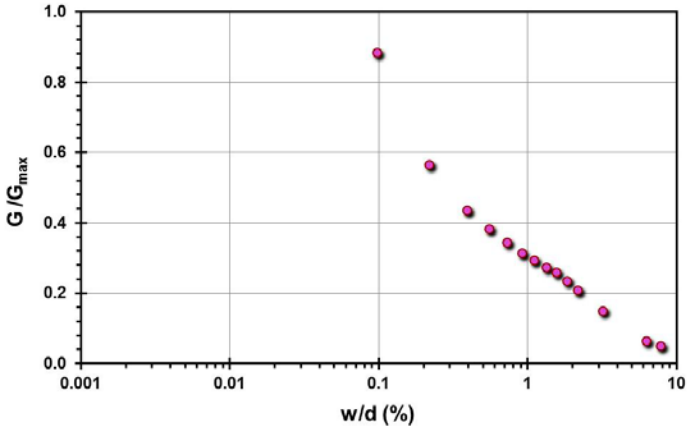

Detail	Description
Pile type/material	Open-ended steel pipe pile
Length, L (m)	26.10
Diameter, d (m)	0.41
Installation method	Driven
Loading mode	Tension
$Q_{max\text{-}measured}$ (kN)	1,135.96
Q_s (kN)	Not reported
Q_b (kN)	Not reported
$Q_{Davisson}$ (kN)	1,127.49
$Q_{w/d=10\%}$ (kN)	1,138.60
$Q_{C\text{-}K}$ (kN)	1,146.79

Pile ID: SFBM P50C

Load-displacement data

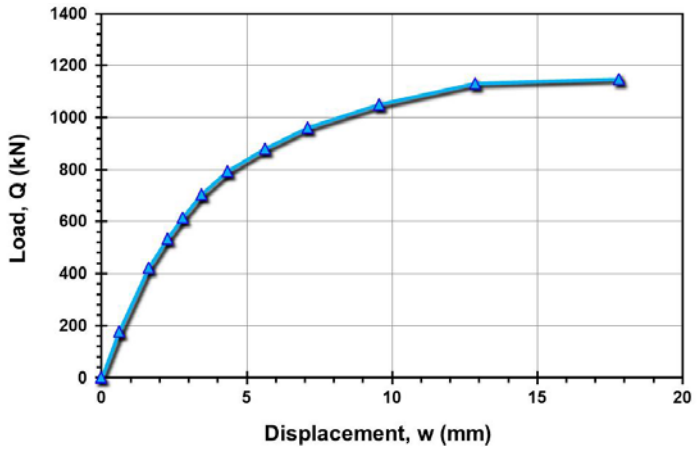

Back-analyzed normalized operational stiffness vs. pseudo-strain

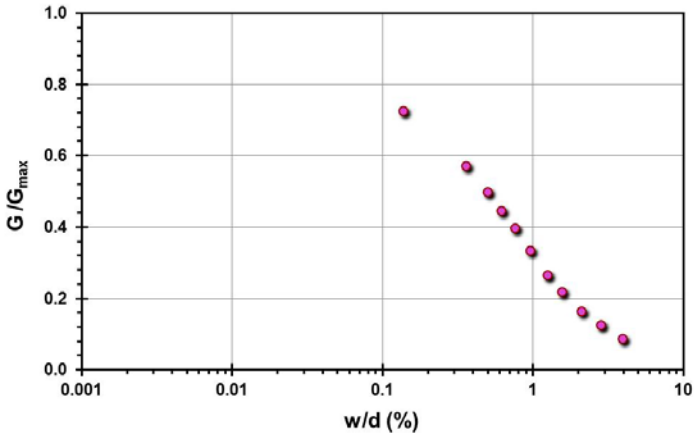

Detail	Description
Pile type/material	Square concrete pile
Length, L (m)	26.50
Width, B (m)	0.36
Installation method	Driven
Loading mode	Compression
$Q_{max\text{-}measured}$ (kN)	1,149.62
Q_s (kN)	Not reported
Q_b (kN)	Not reported
$Q_{Davisson}$ (kN)	1,132.58
$Q_{w/d=10\%}$ (kN)	1,177.25
$Q_{C\text{-}K}$ (kN)	1,196.17

Pile ID: SFBM P50T

Load-displacement data

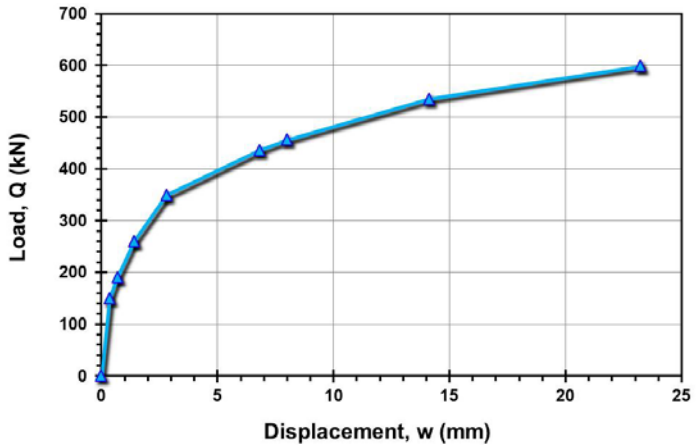

Back-analyzed normalized operational stiffness vs. pseudo-strain

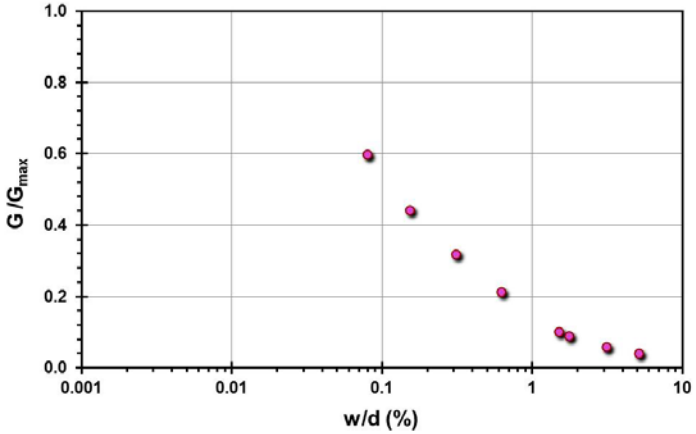

Detail	Description
Pile type/material	Square concrete pile
Length, L (m)	26.50
Width, B (m)	0.36
Installation method	Driven
Loading mode	Tension
$Q_{max\text{-}measured}$ (kN)	598.71
Q_s (kN)	Not reported
Q_b (kN)	Not reported
$Q_{Davisson}$ (kN)	495.75
$Q_{w/d=10\%}$ (kN)	646.99
$Q_{C\text{-}K}$ (kN)	710.73

Pile ID: SFBM P51T

Load-displacement data

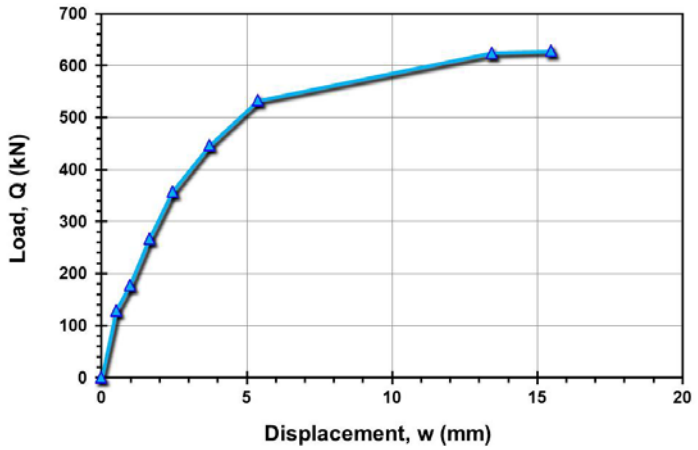

Back-analyzed normalized operational stiffness vs. pseudo-strain

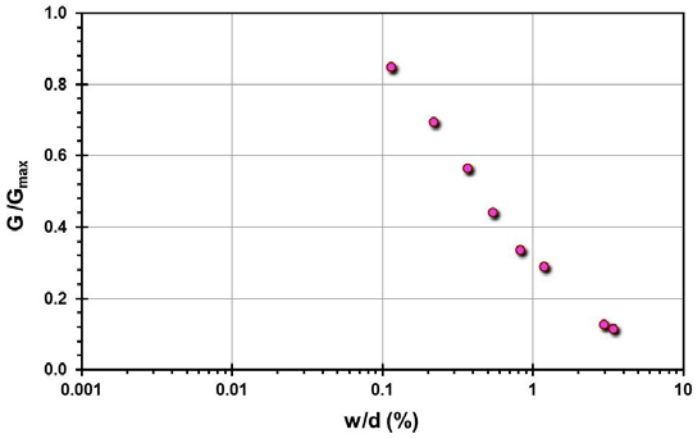

Detail	Description
Pile type/material	Square concrete pile
Length, L (m)	26.50
Width, B (m)	0.36
Installation method	Driven
Loading mode	Tension
$Q_{max\text{-}measured}$ (kN)	628.50
Q_s (kN)	Not reported
Q_b (kN)	Not reported
$Q_{Davisson}$ (kN)	578.98
$Q_{w/d=10\%}$ (kN)	673.03
$Q_{C\text{-}K}$ (kN)	697.35

Pile ID: SFBM P51C

Load-displacement data

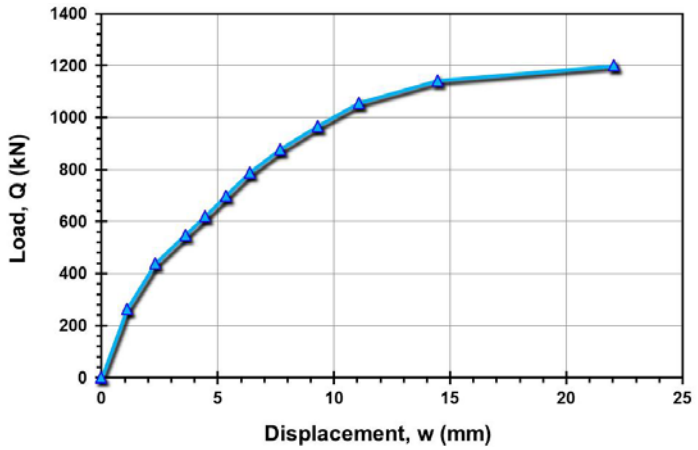

Back-analyzed normalized operational stiffness vs. pseudo-strain

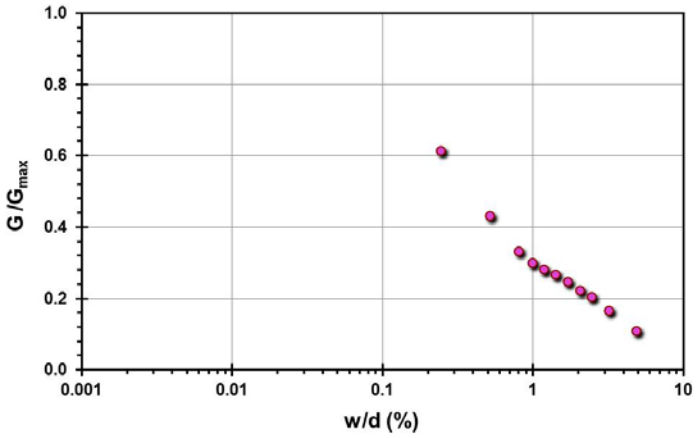

Detail	Description
Pile type/material	Square concrete pile
Length, L (m)	26.50
Width, B (m)	0.36
Installation method	Driven
Loading mode	Compression
$Q_{max\text{-}measured}$ (kN)	1,201.34
Q_s (kN)	Not reported
Q_b (kN)	Not reported
$Q_{Davisson}$ (kN)	1,100.47
$Q_{w/d=10\%}$ (kN)	1,288.31
$Q_{C\text{-}K}$ (kN)	1,381.22

Pile ID: SFBM P59T

Load-displacement data

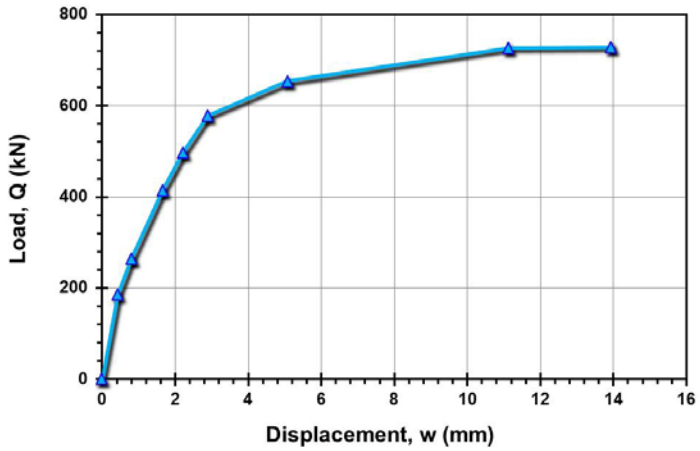

Back-analyzed normalized operational stiffness vs. pseudo-strain

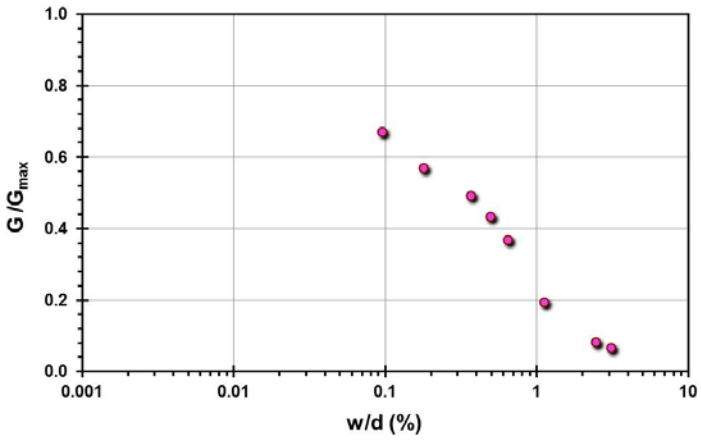

Detail	Description
Pile type/material	Square concrete pile
Length, L (m)	33.40
Width, B (m)	0.36
Installation method	Driven
Loading mode	Tension
$Q_{max\text{-}measured}$ (kN)	727.48
Q_s (kN)	Not reported
Q_b (kN)	Not reported
$Q_{Davisson}$ (kN)	725.71
$Q_{w/d=10\%}$ (kN)	767.45
$Q_{C\text{-}K}$ (kN)	784.93

Pile ID: SFBM P59C

Load-displacement data

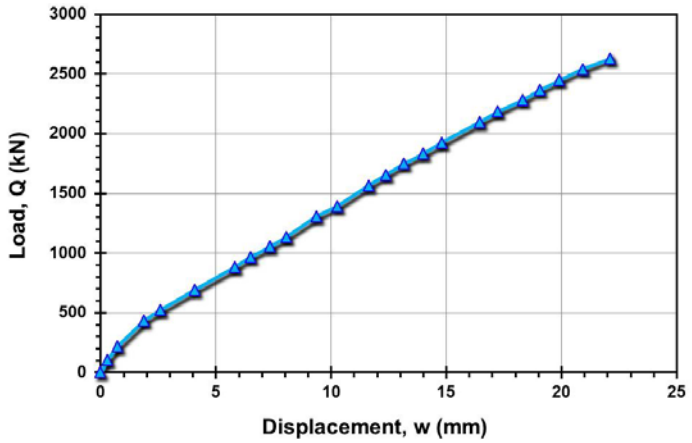

Back-analyzed normalized operational stiffness vs. pseudo-strain

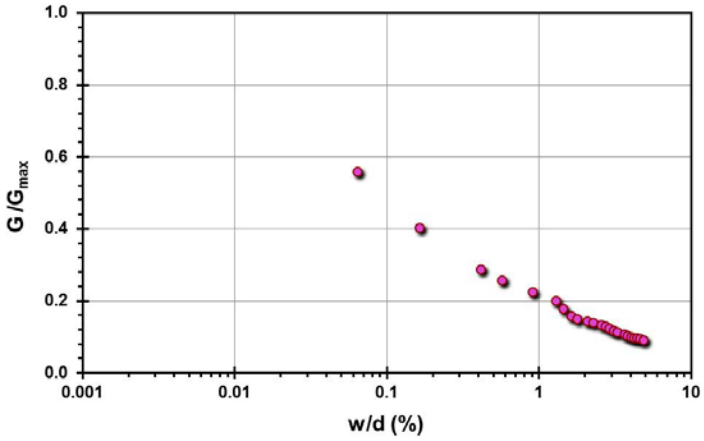

Detail	Description
Pile type/material	Square concrete pile
Length, L (m)	33.40
Width, B (m)	0.36
Installation method	Driven
Loading mode	Compression
$Q_{max\text{-}measured}$ (kN)	2,626.29
Q_s (kN)	Not reported
Q_b (kN)	Not reported
$Q_{Davisson}$ (kN)	2,626.29
$Q_{w/d=10\%}$ (kN)	4,262.37
$Q_{C\text{-}K}$ (kN)	9,900.99

Pile ID: SFBM P61C

Load-displacement data

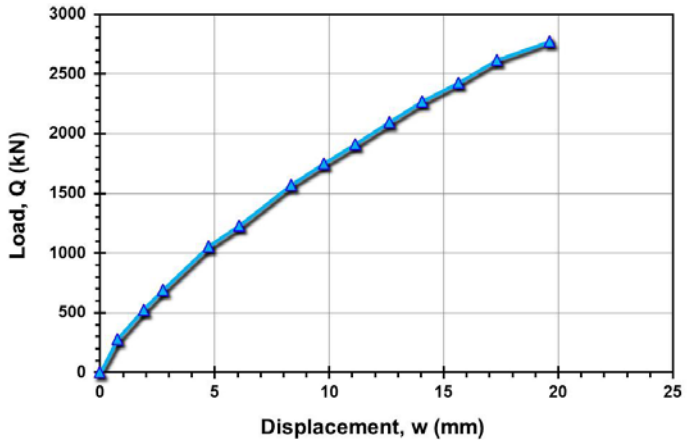

Back-analyzed normalized operational stiffness vs. pseudo-strain

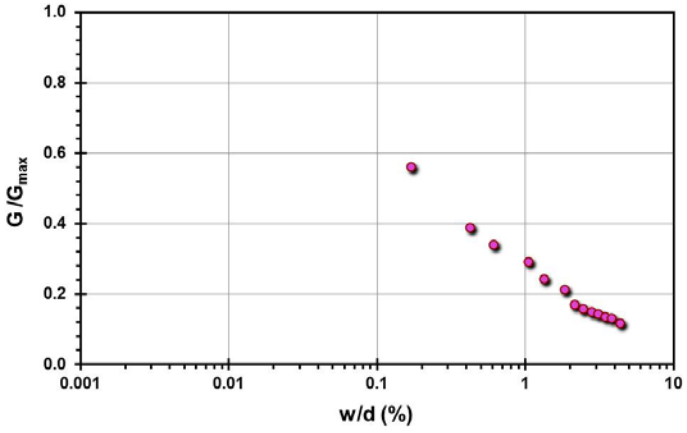

Detail	Description
Pile type/material	Square concrete pile
Length, L (m)	33.40
Width, B (m)	0.36
Installation method	Driven
Loading mode	Compression
$Q_{max\text{-}measured}$ (kN)	2,774.01
Q_s (kN)	Not reported
Q_b (kN)	Not reported
$Q_{Davisson}$ (kN)	3,522.20
$Q_{w/d=10\%}$ (kN)	4,270.39
$Q_{C\text{-}K}$ (kN)	7,042.25

Pile ID: SFBM P61T

Load-displacement data

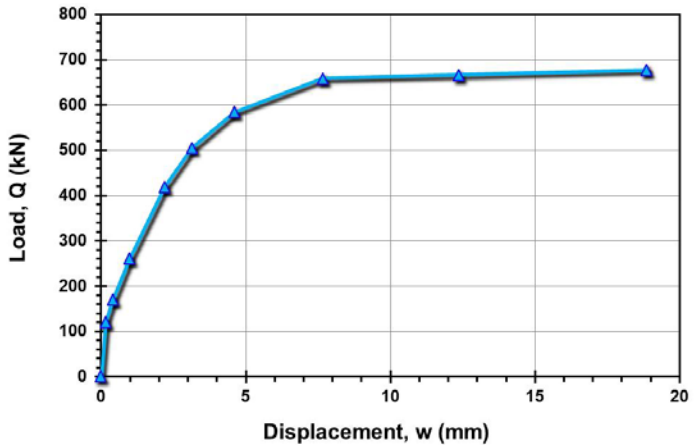

Back-analyzed normalized operational stiffness vs. pseudo-strain

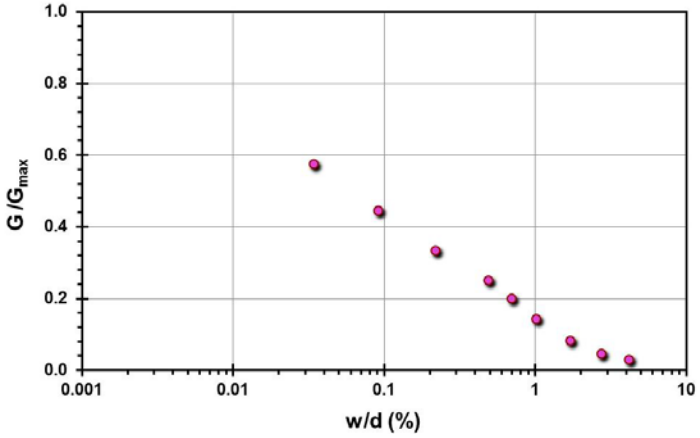

Detail	Description
Pile type/material	Square concrete pile
Length, L (m)	33.40
Width, B (m)	0.36
Installation method	Driven
Loading mode	Tension
$Q_{max\text{-}measured}$ (kN)	676.45
Q_s (kN)	Not reported
Q_b (kN)	Not reported
$Q_{Davisson}$ (kN)	665.32
$Q_{w/d=10\%}$ (kN)	684.05
$Q_{C\text{-}K}$ (kN)	690.13

Pile ID: SFBM P69C

Load-displacement data

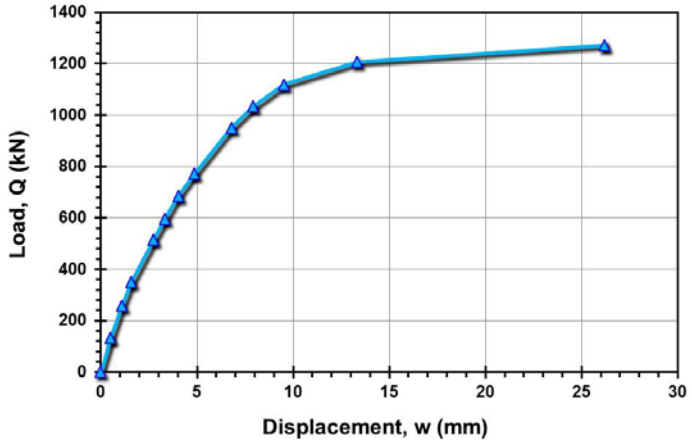

Back-analyzed normalized operational stiffness vs. pseudo-strain

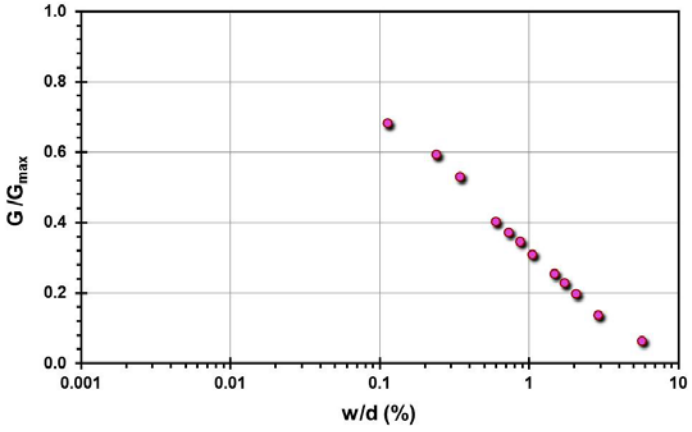

Detail	Description
Pile type/material	H-section pile
Length, L (m)	26.50
H-section size	14 x 89
Installation method	Driven
Loading mode	Compression
$Q_{max\text{-}measured}$ (kN)	1,271.38
Q_s (kN)	Not reported
Q_b (kN)	Not reported
$Q_{Davisson}$ (kN)	1,206.17
$Q_{w/d=10\%}$ (kN)	1,314.73
$Q_{C\text{-}K}$ (kN)	1,371.74

Pile ID: SFBM P69T

Load-displacement data

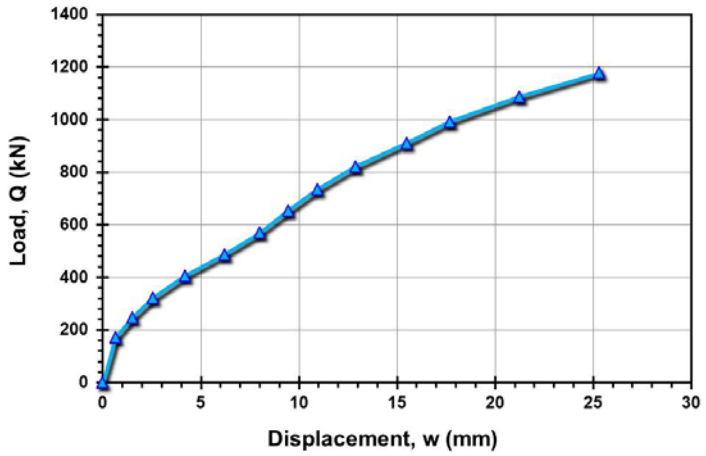

Back-analyzed normalized operational stiffness vs. pseudo-strain

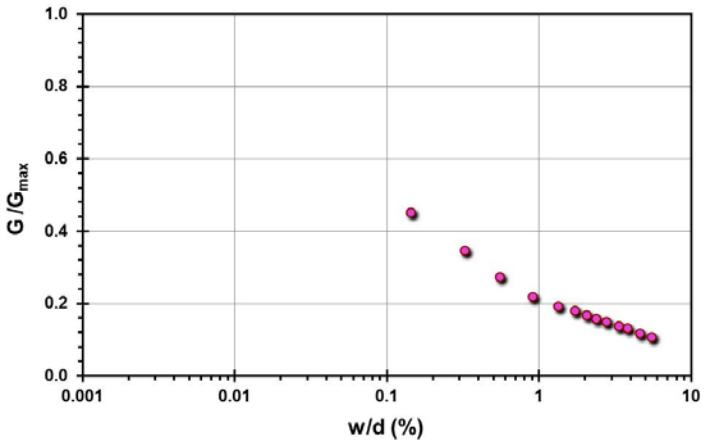

Detail	Description
Pile type/material	H-section pile
Length, L (m)	26.50
H-section size	14 x 89
Installation method	Driven
Loading mode	Tension
$Q_{max\text{-}measured}$ (kN)	1,178.08
Q_s (kN)	Not reported
Q_b (kN)	Not reported
$Q_{Davisson}$ (kN)	820.98
$Q_{w/d=10\%}$ (kN)	1,490.25
$Q_{C\text{-}K}$ (kN)	2,159.83

Pile ID: SFBM P70T

Load-displacement data

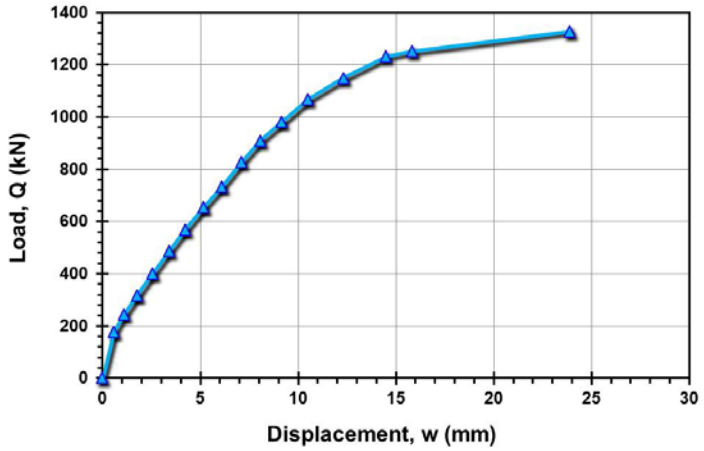

Back-analyzed normalized operational stiffness vs. pseudo-strain

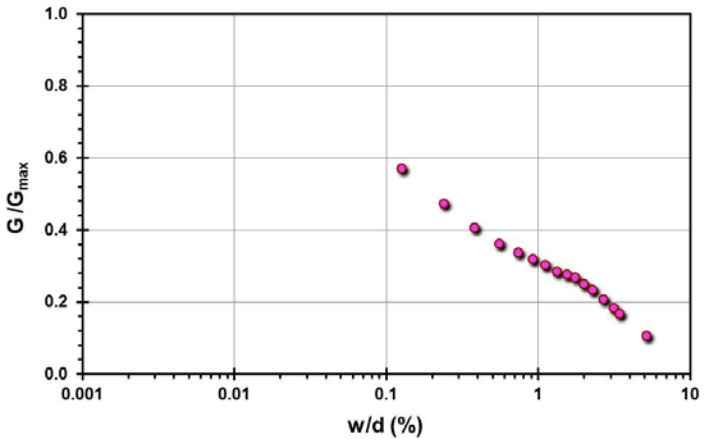

Detail	Description
Pile type/material	H-section pile
Length, L (m)	26.50
H-section size	14 x 89
Installation method	Driven
Loading mode	Tension
$Q_{max\text{-}measured}$ (kN)	1,326.95
Q_s (kN)	Not reported
Q_b (kN)	Not reported
$Q_{Davisson}$ (kN)	1,250.38
$Q_{w/d=10\%}$ (kN)	1,408.82
$Q_{C\text{-}K}$ (kN)	1,508.30

Pile ID: SFBM P73T

Load-displacement data

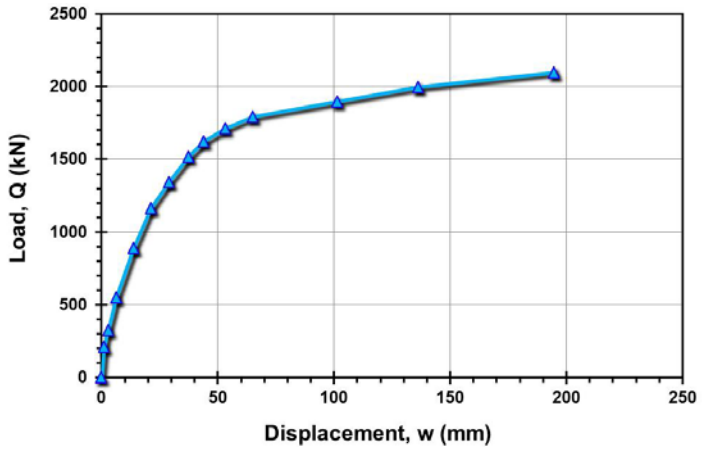

Back-analyzed normalized operational stiffness vs. pseudo-strain

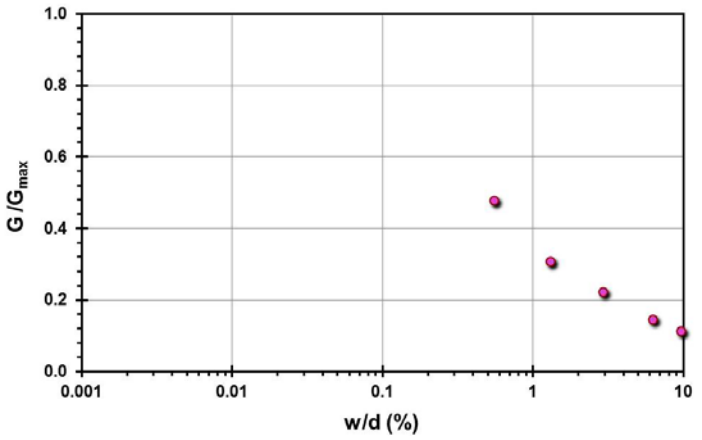

Detail	Description
Pile type/material	Open-ended steel concrete pile
Length, L (m)	41.10
Diameter, d (m)	0.22
Installation method	Driven
Loading mode	Tension
$Q_{max\text{-}measured}$ (kN)	2,096.16
Q_s (kN)	Not reported
Q_b (kN)	Not reported
$Q_{Davisson}$ (kN)	1,710.63
$Q_{w/d=10\%}$ (kN)	1,245.91
$Q_{C\text{-}K}$ (kN)	2,283.11

Pile ID: SFBM P73C

Load-displacement data

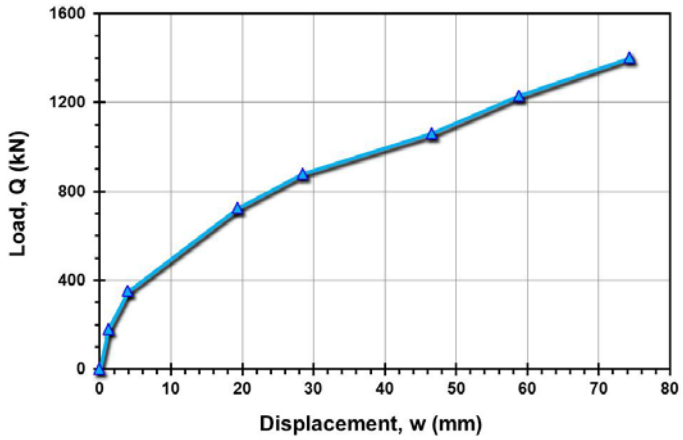

Back-analyzed normalized operational stiffness vs. pseudo-strain

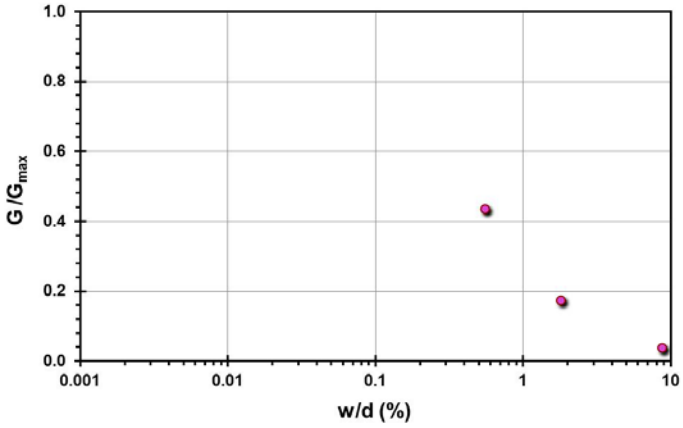

Detail	Description
Pile type/material	Open-ended steel concrete pile
Length, L (m)	41.10
Diameter, d (m)	0.22
Installation method	Driven
Loading mode	Compression
$Q_{max\text{-}measured}$ (kN)	1,401.55
Q_s (kN)	Not reported
Q_b (kN)	Not reported
$Q_{Davisson}$ (kN)	879.93
$Q_{w/d=10\%}$ (kN)	713.66
$Q_{C\text{-}K}$ (kN)	2,247.19

Pile ID: SFBM P74C

Load-displacement data

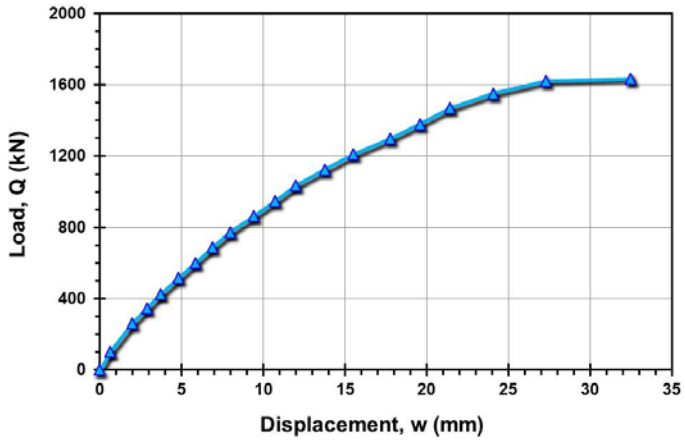

Back-analyzed normalized operational stiffness vs. pseudo-strain

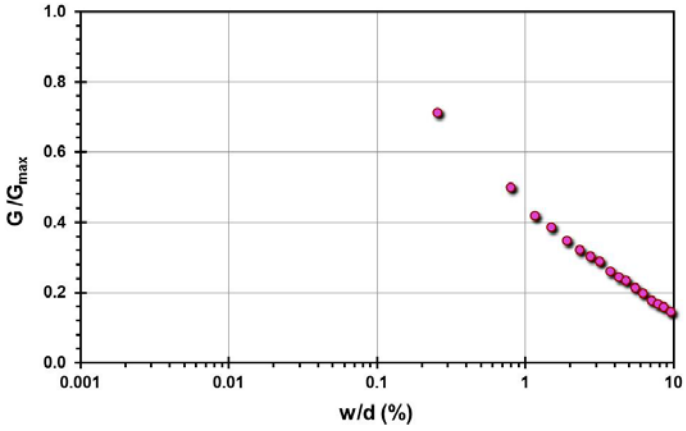

Detail	Description
Pile type/material	Open-ended steel concrete pile
Length, L (m)	26.70
Diameter, d (m)	0.25
Installation method	Driven
Loading mode	Compression
$Q_{max\text{-}measured}$ (kN)	1,633.44
Q_s (kN)	Not reported
Q_b (kN)	Not reported
$Q_{Davisson}$ (kN)	1,633.44
$Q_{w/d=10\%}$ (kN)	1,575.28
$Q_{C\text{-}K}$ (kN)	1,908.40

Pile ID: SFBM P74T

Load-displacement data

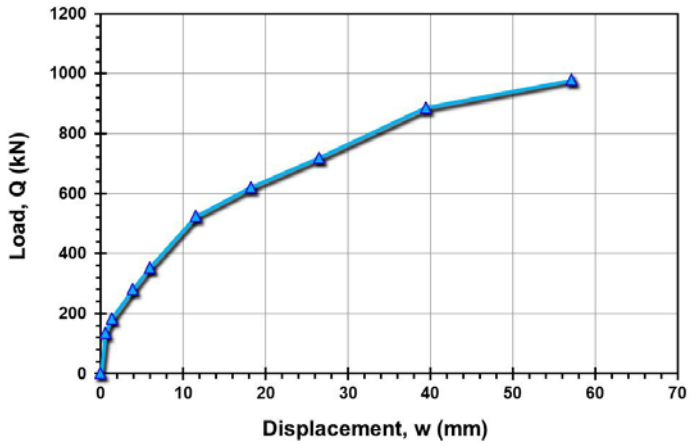

Back-analyzed normalized operational stiffness vs. pseudo-strain

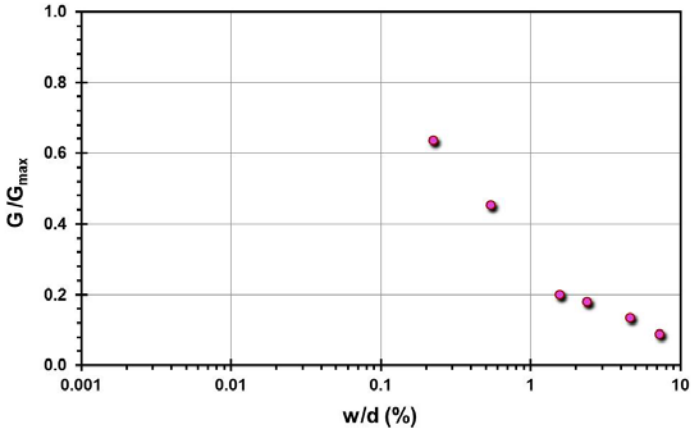

Detail	Description
Pile type/material	Open-ended steel concrete pile
Length, L (m)	26.70
Diameter, d (m)	0.25
Installation method	Driven
Loading mode	Tension
$Q_{max\text{-}measured}$ (kN)	978.64
Q_s (kN)	Not reported
Q_b (kN)	Not reported
$Q_{Davisson}$ (kN)	572.45
$Q_{w/d=10\%}$ (kN)	735.38
$Q_{C\text{-}K}$ (kN)	1,295.34

Site ID No. 55

Cone penetrometer data	CPT SBT soil classification index, I_c	Detail	Description
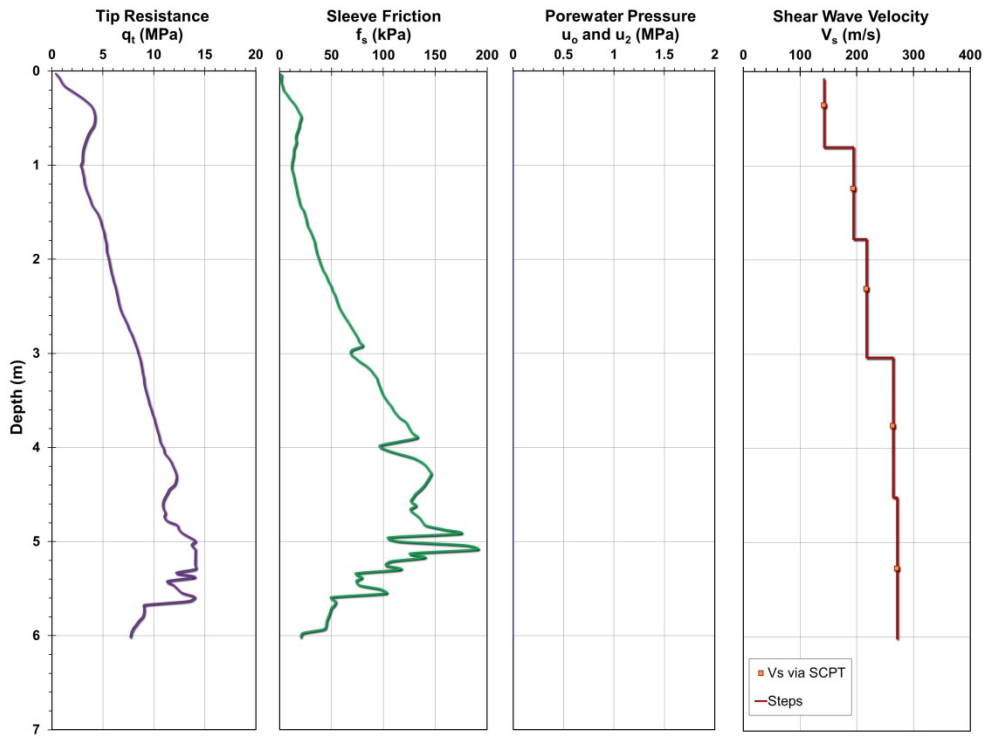	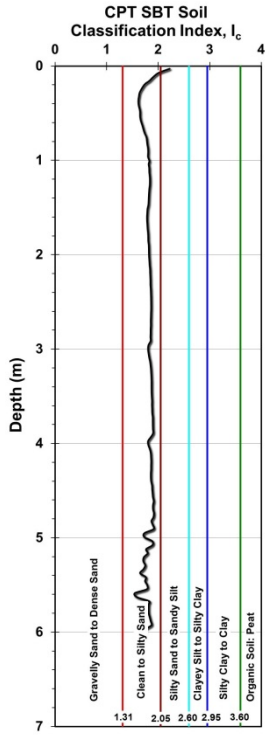	Site name and location	Shenton Park, Perth, Western Australia
		Soil type(s)	Siliceous sand
		Pile type(s)	10 open-ended steel pipe piles and 2 closed-ended steel pipe piles
		Type of cone penetrometer testing	SCPT
		Source of V_s evaluation	SCPT
		Number of pile load tests	11
		Reference	Schneider (2007)
		Comments	u_2 assumed zero; GWT well below the pile base

Pile ID: SPP P01

Load-displacement data

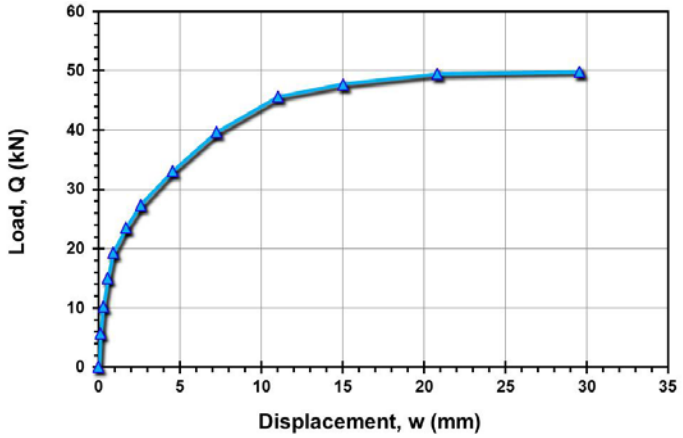

Back-analyzed normalized operational stiffness vs. pseudo-strain

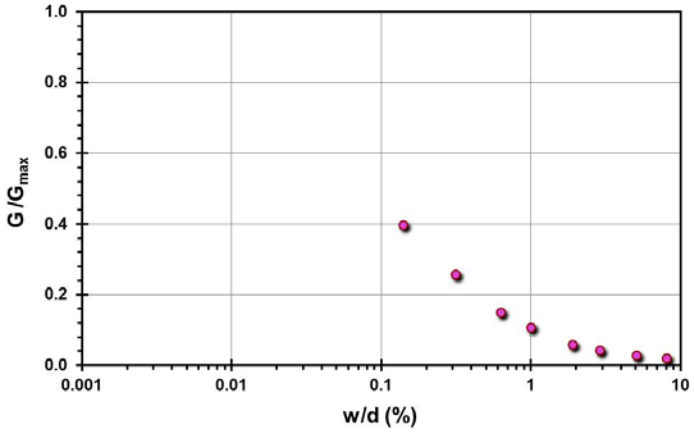

Detail	Description
Pile type/material	Open-ended steel pipe pile
Length, L (m)	4.00
Diameter, d (m)	0.089
Installation method	Driven
Loading mode	Tension
$Q_{max\text{-}measured}$ (kN)	49.82
Q_s (kN)	49.82
Q_b (kN)	-
$Q_{Davisson}$ (kN)	33.07
$Q_{w/d=10\%}$ (kN)	43.35
$Q_{C\text{-}K}$ (kN)	54.04

Pile ID: SPP P02

Load-displacement data

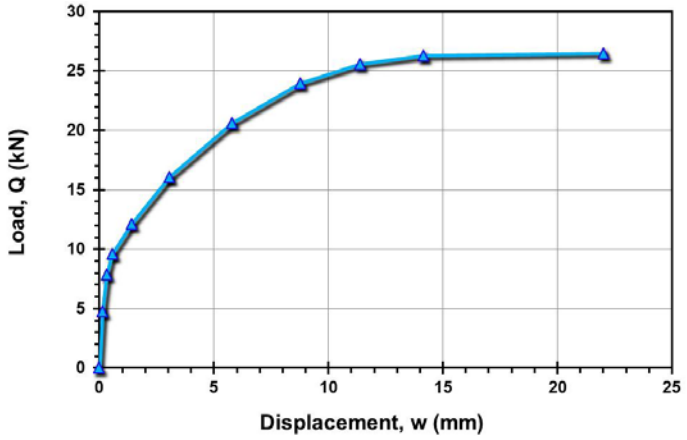

Back-analyzed normalized operational stiffness vs. pseudo-strain

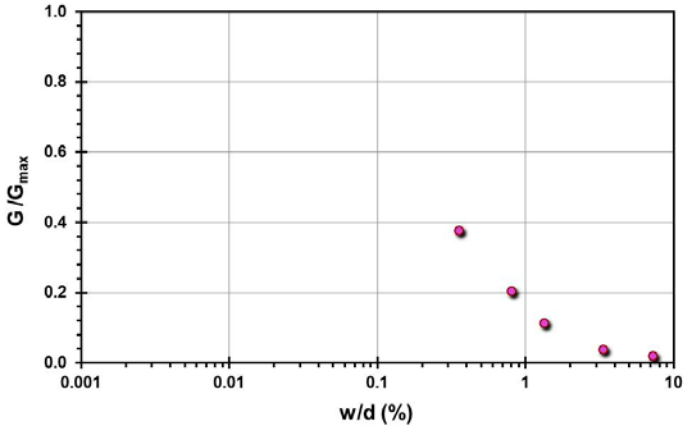

Detail	Description
Pile type/material	Open-ended steel pipe pile
Length, L (m)	4.00
Diameter, d (m)	0.043
Installation method	Driven
Loading mode	Tension
$Q_{max\text{-}measured}$ (kN)	26.49
Q_s (kN)	26.49
Q_b (kN)	-
$Q_{Davisson}$ (kN)	20.63
$Q_{w/d=10\%}$ (kN)	20.16
$Q_{C\text{-}K}$ (kN)	28.99

Pile ID: SPP P03

Load-displacement data

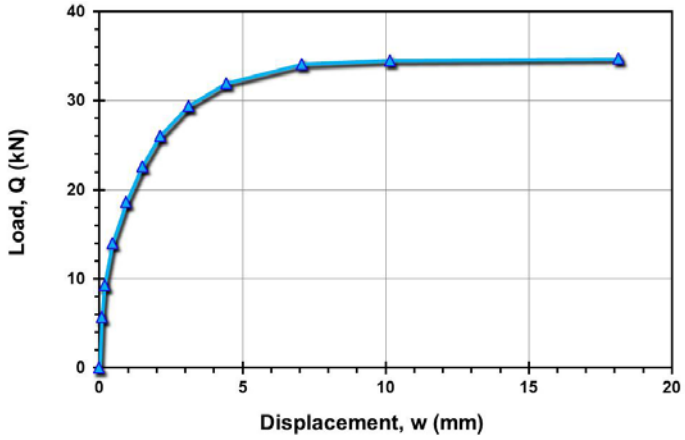

Back-analyzed normalized operational stiffness vs. pseudo-strain

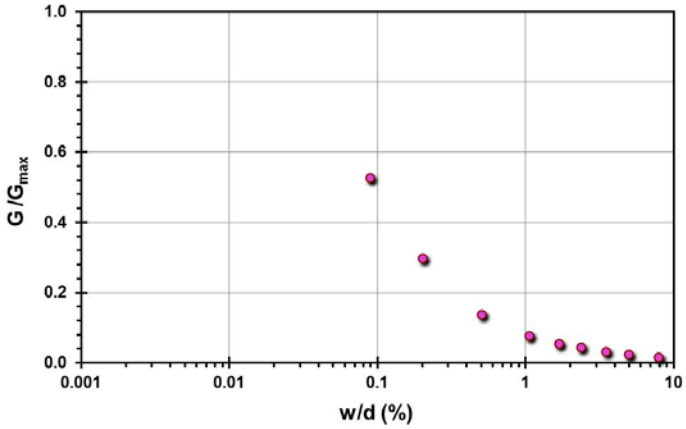

Detail	Description
Pile type/material	Close-ended steel pipe pile
Length, L (m)	4.00
Diameter, d (m)	0.089
Installation method	Driven
Loading mode	Tension
$Q_{max\text{-}measured}$ (kN)	34.70
Q_s (kN)	34.70
Q_b (kN)	-
$Q_{Davisson}$ (kN)	31.95
$Q_{w/d=10\%}$ (kN)	33.65
$Q_{C\text{-}K}$ (kN)	36.56

Pile ID: SPP P04

Load-displacement data

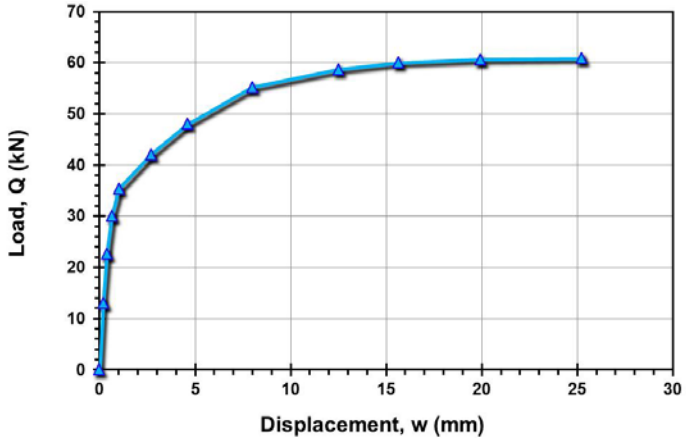

Back-analyzed normalized operational stiffness vs. pseudo-strain

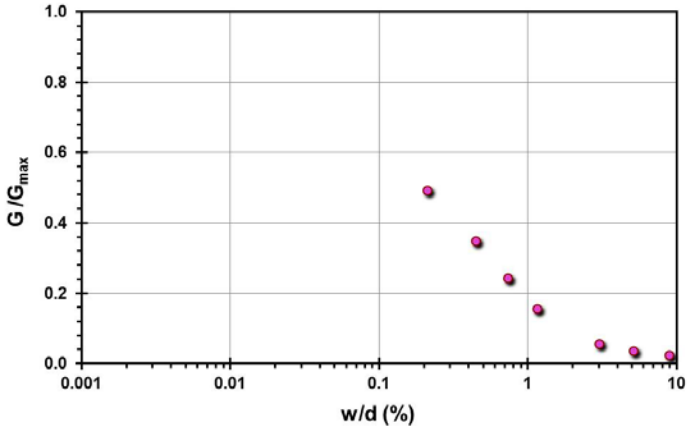

Detail	Description
Pile type/material	Open-ended steel pipe pile
Length, L (m)	4.00
Diameter, d (m)	0.089
Installation method	Driven
Loading mode	Tension
$Q_{max\text{-}measured}$ (kN)	60.88
Q_s (kN)	60.88
Q_b (kN)	-
$Q_{Davisson}$ (kN)	48.00
$Q_{w/d=10\%}$ (kN)	55.89
$Q_{C\text{-}K}$ (kN)	64.83

Pile ID: SPP P05

Load-displacement data

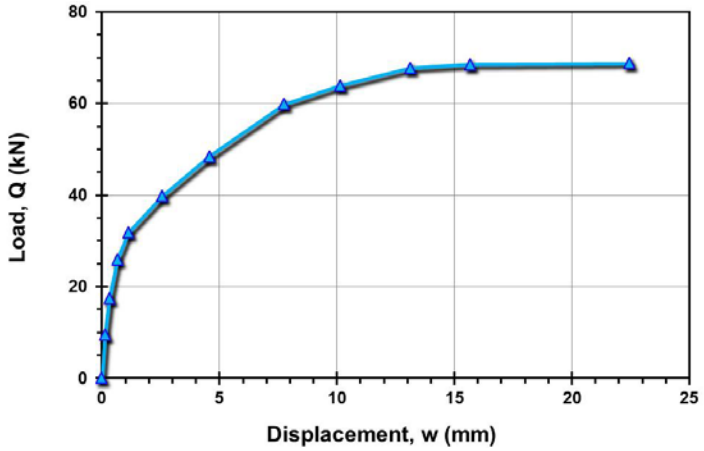

Back-analyzed normalized operational stiffness vs. pseudo-strain

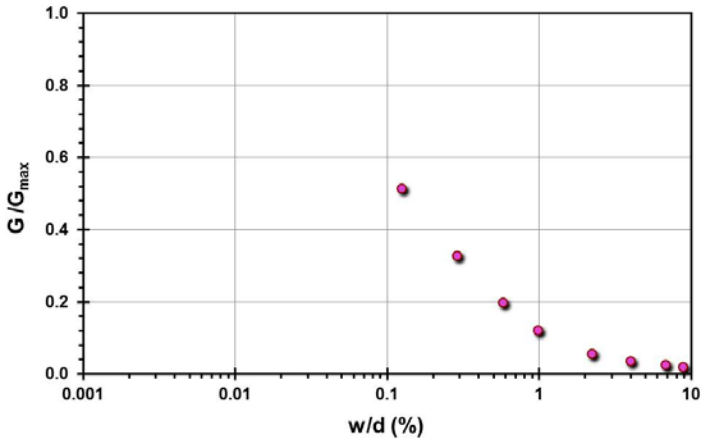

Detail	Description
Pile type/material	Open-ended steel pipe pile
Length, L (m)	4.00
Diameter, d (m)	0.114
Installation method	Driven
Loading mode	Tension
$Q_{max\text{-}measured}$ (kN)	68.82
Q_s (kN)	68.82
Q_b (kN)	-
$Q_{Davisson}$ (kN)	54.13
$Q_{w/d=10\%}$ (kN)	67.60
$Q_{C\text{-}K}$ (kN)	70.22

Pile ID: SPP P06

Load-displacement data

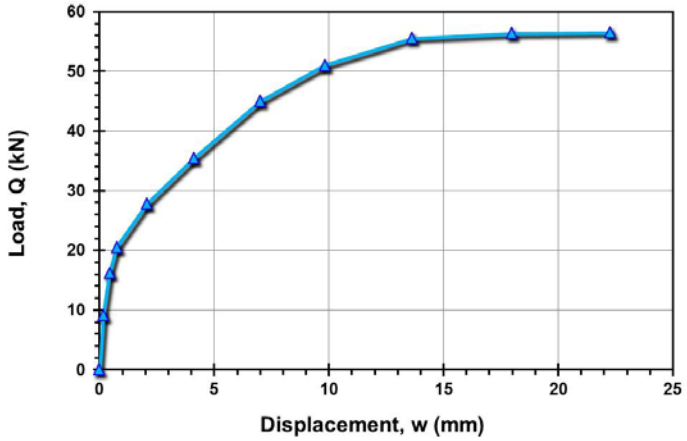

Back-analyzed normalized operational stiffness vs. pseudo-strain

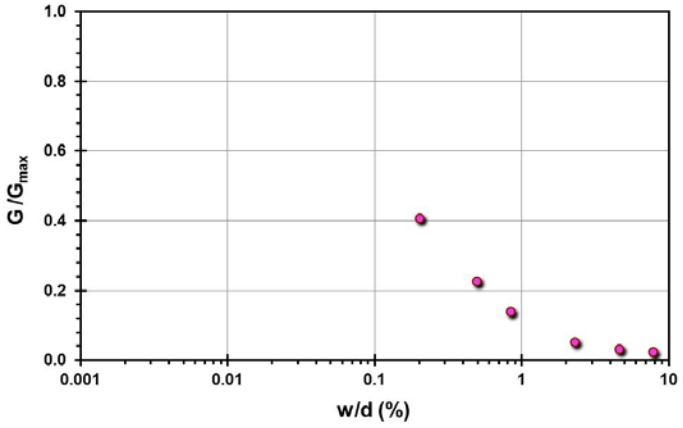

Detail	Description
Pile type/material	Open-ended steel pipe pile
Length, L (m)	4.00
Diameter, d (m)	0.089
Installation method	Driven
Loading mode	Tension
$Q_{max\text{-}measured}$ (kN)	56.54
Q_s (kN)	56.54
Q_b (kN)	-
$Q_{Davisson}$ (kN)	40.12
$Q_{w/d=10\%}$ (kN)	49.79
$Q_{C\text{-}K}$ (kN)	63.85

Pile ID: SPP P07

Load-displacement data	Detail	Description
Not reported	Pile type/material	Open-ended steel pipe pile
	Length, L (m)	2.50
	Diameter, d (m)	0.043
	Installation method	Driven
	Loading mode	Tension
	$Q_{max\text{-}measured}$ (kN)	73.26
	Q_s (kN)	73.26
	Q_b (kN)	-
	$Q_{Davisson}$ (kN)	Not reported
	$Q_{w/d=10\%}$ (kN)	Not reported
	$Q_{C\text{-}K}$ (kN)	Not reported
Back-analyzed normalized operational stiffness vs. pseudo-strain		
Not calculated		

Pile ID: SPP P08

Load-displacement data

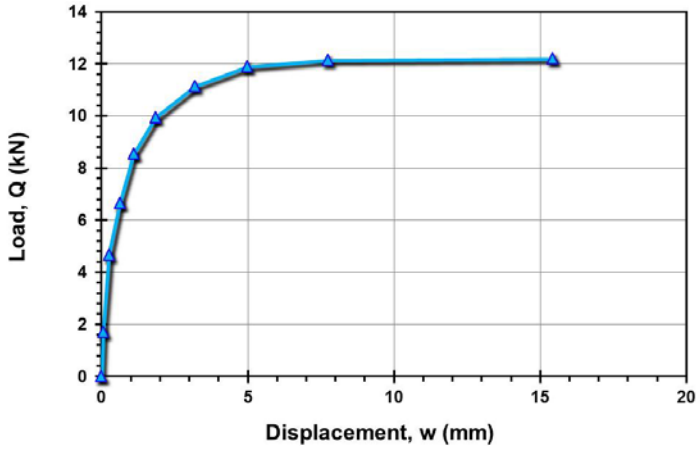

Back-analyzed normalized operational stiffness vs. pseudo-strain

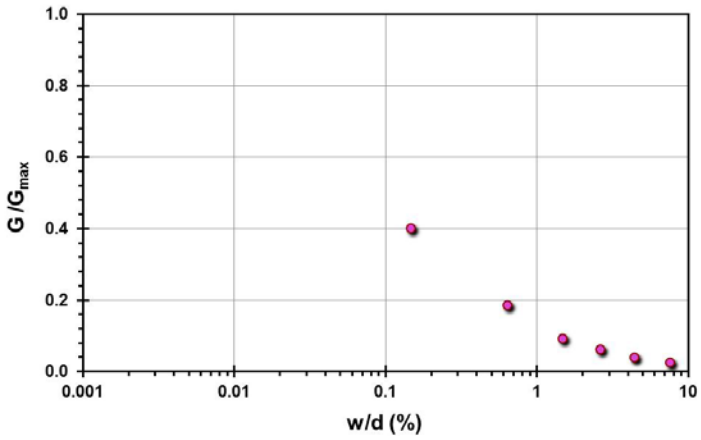

Detail	Description
Pile type/material	Open-ended steel pipe pile
Length, L (m)	2.50
Diameter, d (m)	0.043
Installation method	Driven
Loading mode	Tension
$Q_{max\text{-}measured}$ (kN)	12.22
Q_s (kN)	12.22
Q_b (kN)	-
$Q_{Davisson}$ (kN)	11.90
$Q_{w/d=10\%}$ (kN)	11.54
$Q_{C\text{-}K}$ (kN)	12.58

Pile ID: SPP P09

Load-displacement data

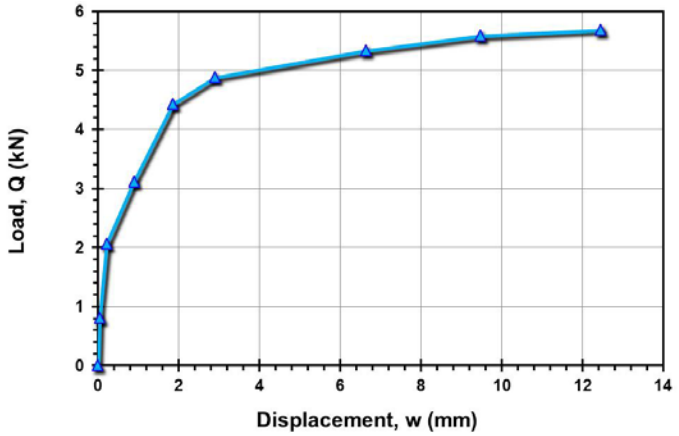

Back-analyzed normalized operational stiffness vs. pseudo-strain

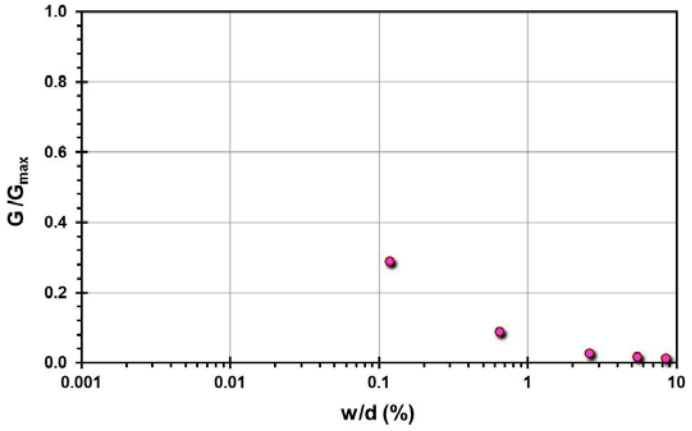

Detail	Description
Pile type/material	Open-ended steel pipe pile
Length, L (m)	2.50
Diameter, d (m)	0.034
Installation method	Driven
Loading mode	Tension
$Q_{max\text{-}measured}$ (kN)	5.69
Q_s (kN)	5.69
Q_b (kN)	-
$Q_{Davisson}$ (kN)	5.11
$Q_{w/d=10\%}$ (kN)	4.94
$Q_{C\text{-}K}$ (kN)	6.02

Pile ID: SPP P10

Load-displacement data

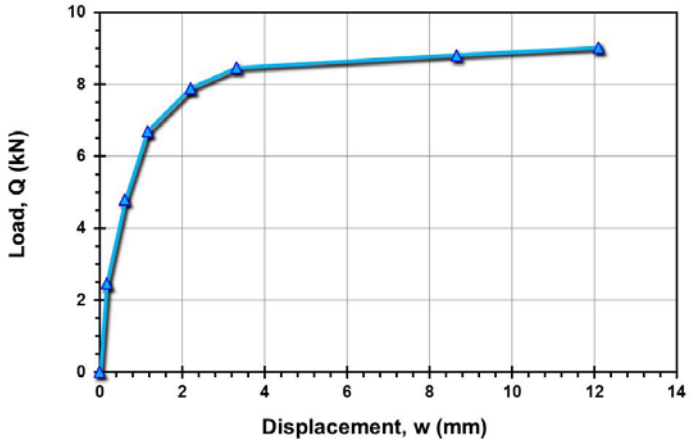

Back-analyzed normalized operational stiffness vs. pseudo-strain

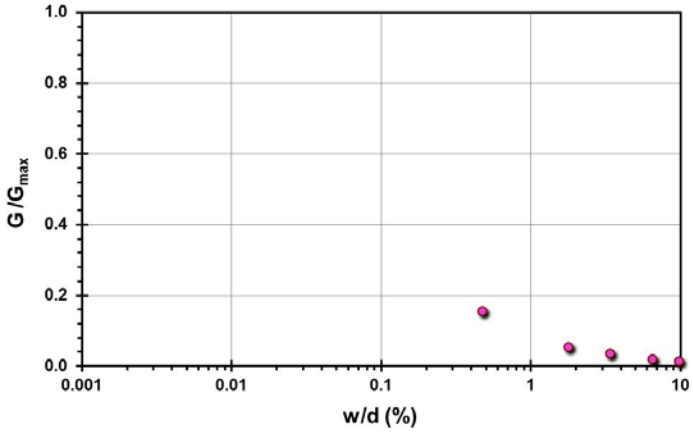

Detail	Description
Pile type/material	Open-ended steel pipe pile
Length, L (m)	3.50
Diameter, d (m)	0.034
Installation method	Driven
Loading mode	Tension
$Q_{max\text{-}measured}$ (kN)	9.02
Q_s (kN)	9.02
Q_b (kN)	-
$Q_{Davisson}$ (kN)	8.63
$Q_{w/d=10\%}$ (kN)	8.30
$Q_{C\text{-}K}$ (kN)	9.29

Pile ID: SPP P11

Load-displacement data

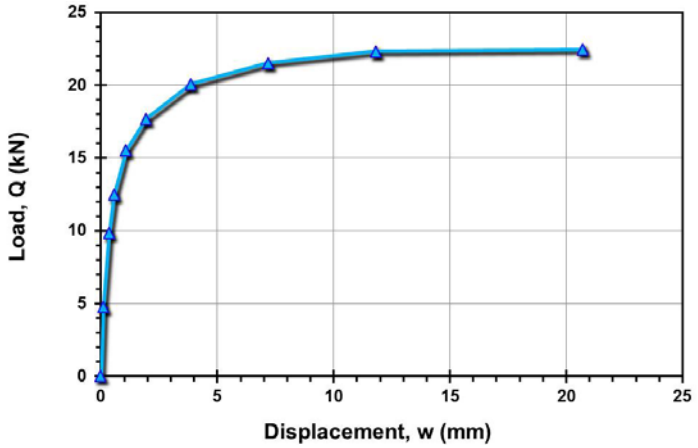

Back-analyzed normalized operational stiffness vs. pseudo-strain

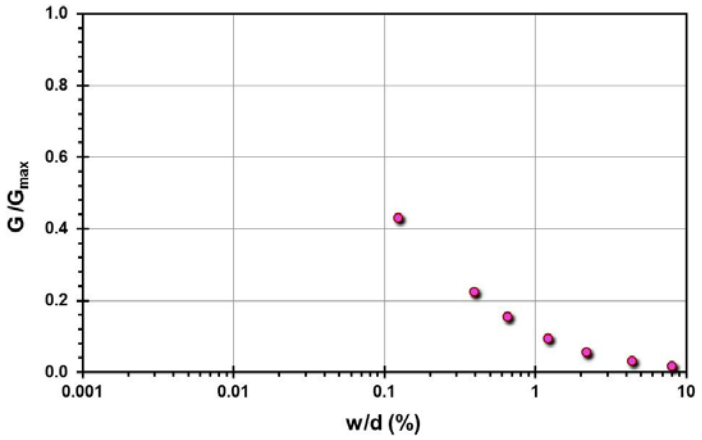

Detail	Description
Pile type/material	Open-ended steel pipe pile
Length, L (m)	2.50
Diameter, d (m)	0.089
Installation method	Driven
Loading mode	Tension
$Q_{max\text{-}measured}$ (kN)	22.43
Q_s (kN)	22.43
Q_b (kN)	-
$Q_{Davisson}$ (kN)	20.77
$Q_{w/d=10\%}$ (kN)	21.76
$Q_{C\text{-}K}$ (kN)	23.10

Pile ID: SPP P12

Load-displacement data

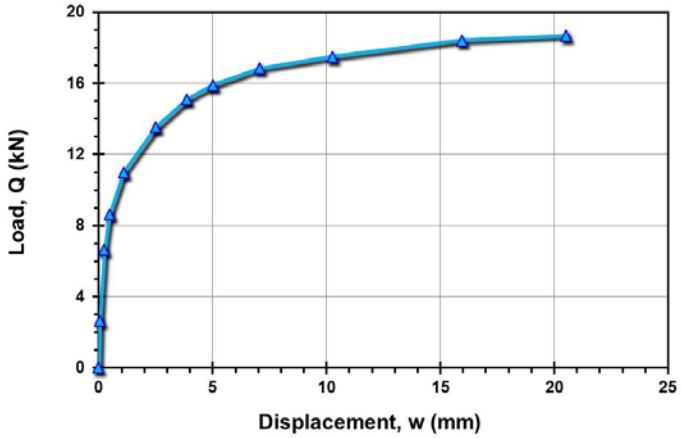

Back-analyzed normalized operational stiffness vs. pseudo-strain

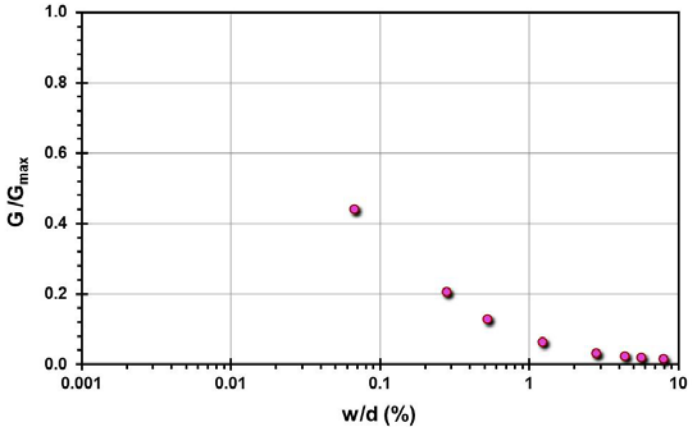

Detail	Description
Pile type/material	Closed-ended steel pipe pile
Length, L (m)	2.50
Diameter, d (m)	0.089
Installation method	Driven
Loading mode	Tension
$Q_{max\text{-}measured}$ (kN)	18.68
Q_s (kN)	18.68
Q_b (kN)	-
$Q_{Davisson}$ (kN)	15.90
$Q_{w/d=10\%}$ (kN)	17.39
$Q_{C\text{-}K}$ (kN)	19.77

Site ID No. 56

Cone penetrometer data	CPT SBT soil classification index, I_c	Detail	Description
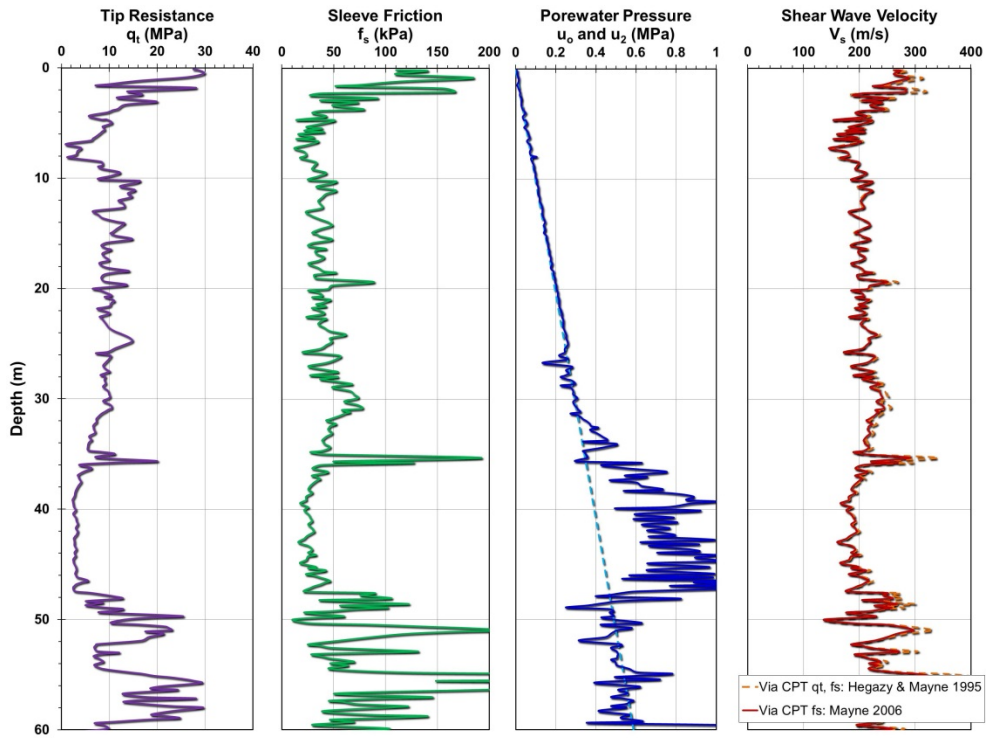	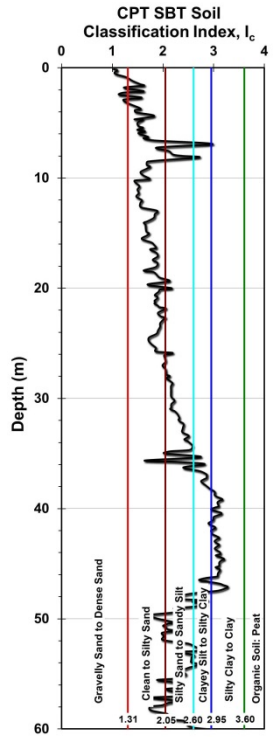	Site name and location	Shirasu soil, lanima, Southern Kyushu, Japan
		Soil type(s)	Clean sand over silty sand over silty clay
		Pile type(s)	Drilled shafts
		Type of cone penetrometer testing	CPTu
		Source of V_s evaluation	Correlations (see Figure opposite and Table 3.1)
		Number of pile load tests	2
		Reference	Takesue et al. (1996)
		Comments	V_s estimated via correlation

Pile ID: SSK A

Load-displacement data

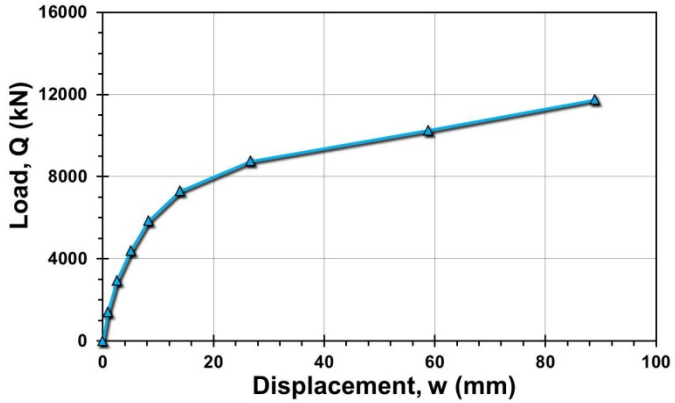

Back-analyzed normalized operational stiffness vs. pseudo-strain

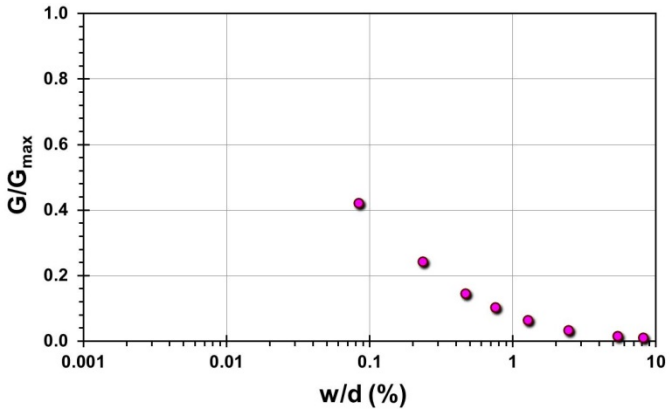

Detail	Description
Pile type/material	Drilled shaft
Length, L (m)	52.40
Diameter, d (m)	1.10
Installation method	Bored cast in-situ
Loading mode	Compression
$Q_{max\text{-}measured}$ (kN)	11,750.50
Q_s (kN)	Not reported
Q_b (kN)	Not reported
$Q_{Davisson}$ (kN)	8,759.92
$Q_{w/d=10\%}$ (kN)	11,891.90
$Q_{C\text{-}K}$ (kN)	13,698.63

Pile ID: SSK B

Load-displacement data	Detail	Description
Not reported	Pile type/material	Drilled shaft
	Length, L (m)	47.00
	Diameter, d (m)	1.20
	Installation method	Bored cast in-situ
	Loading mode	Compression
	$Q_{max\text{-}measured}$ (kN)	11,837.28
	Q_s (kN)	10,411.57
	Q_b (kN)	1,425.71
	$Q_{Davisson}$ (kN)	-
	$Q_{w/d=10\%}$ (kN)	-
	$Q_{C\text{-}K}$ (kN)	-
Back-analyzed normalized operational stiffness vs. pseudo-strain		
Not calculated		

Site ID No. 57

Cone penetrometer data	CPT SBT soil classification index, I_c	Detail	Description
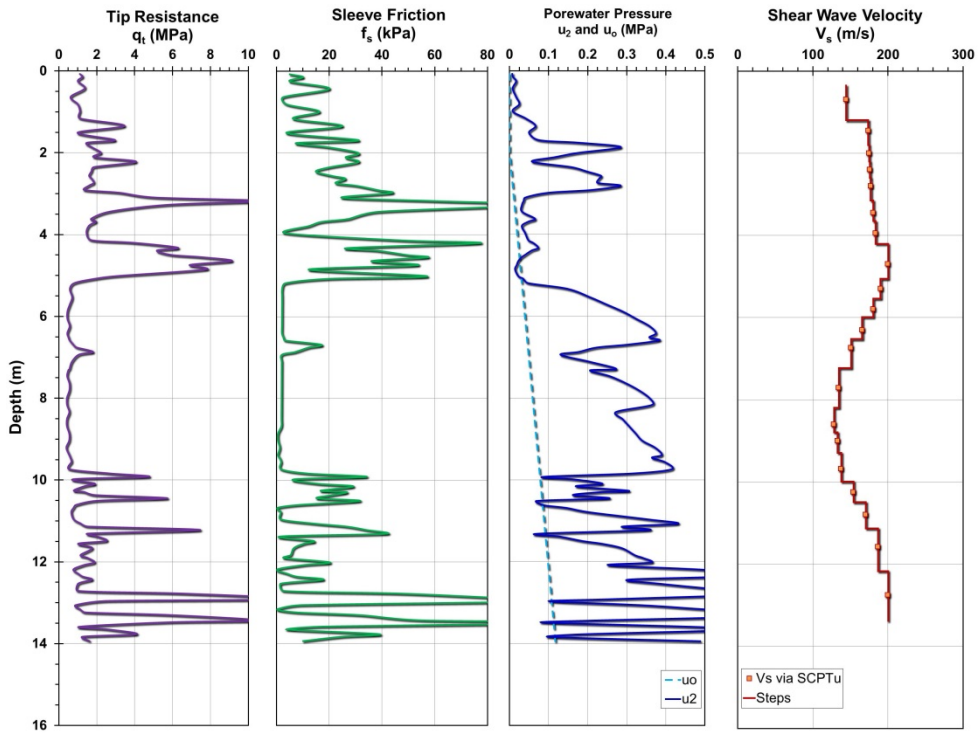	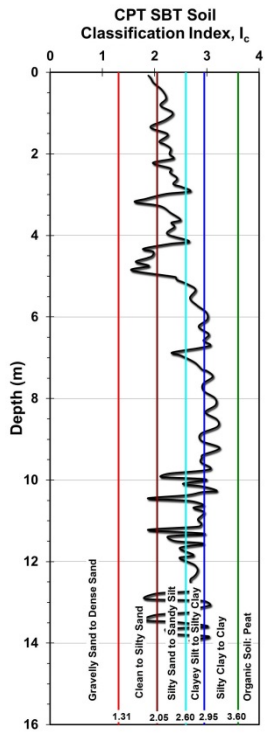	Site name and location	South Temple test site on I-15, Salt Lake City, Utah, USA
		Soil type(s)	Silty sands and sandy clays over sensitive clay below 5 m
		Pile type(s)	Closed-ended steel pipe piles
		Type of cone penetrometer testing	SCPTu
		Source of V_s evaluation	SCPTu
		Number of pile load tests	7
		Reference	Garner (2007)
		Comments	A number of pile load tests were conducted at different rates of loading at this site

Pile ID: STTS P24

Load-displacement data

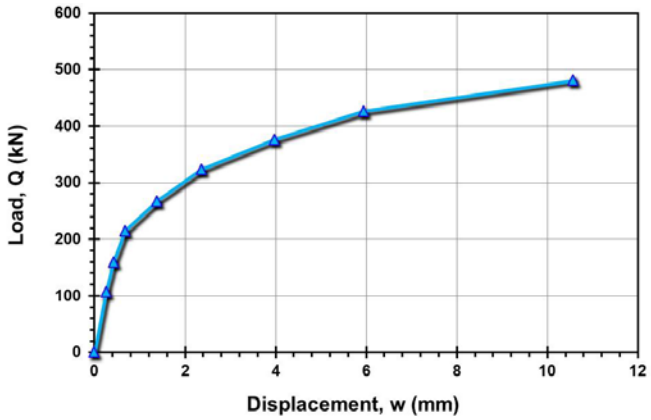

Back-analyzed normalized operational stiffness vs. pseudo-strain

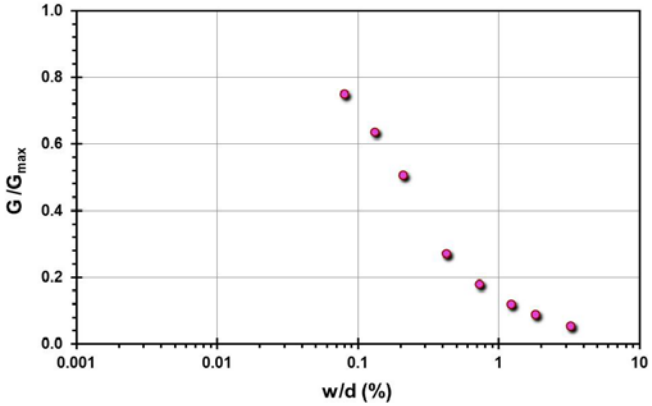

Detail	Description
Pile type/material	Closed-ended steel pipe pile
Length, L (m)	12.20
Diameter, d (m)	0.324
Installation method	Driven
Loading mode	Compression
$Q_{max\text{-}measured}$ (kN)	480.91
Q_s (kN)	442.77
Q_b (kN)	38.14
$Q_{Davisson}$ (kN)	453.43
$Q_{w/d=10\%}$ (kN)	542.26
$Q_{C\text{-}K}$ (kN)	577.70

Pile ID: STTS P14-1

Load-displacement data

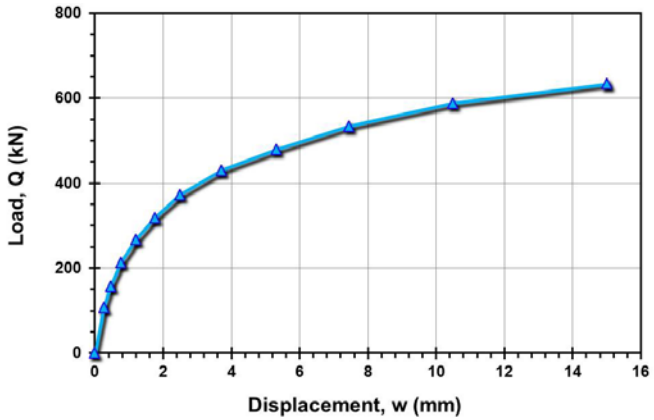

Back-analyzed normalized operational stiffness vs. pseudo-strain

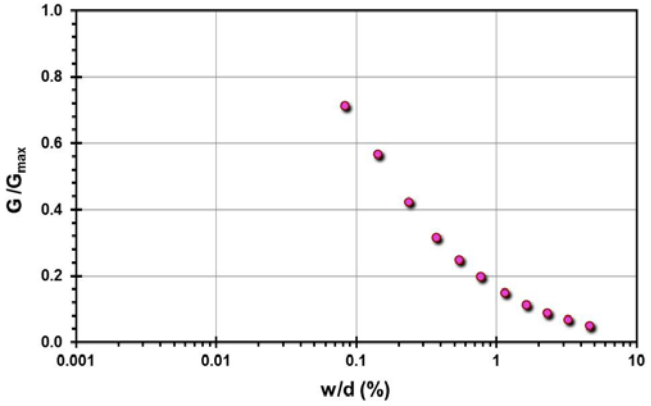

Detail	Description
Pile type/material	Closed-ended steel pipe pile
Length, L (m)	12.20
Diameter, d (m)	0.324
Installation method	Driven
Loading mode	Compression
$Q_{max\text{-}measured}$ (kN)	633.45
Q_s (kN)	597.01
Q_b (kN)	36.44
$Q_{Davisson}$ (kN)	553.96
$Q_{w/d=10\%}$ (kN)	700.44
$Q_{C\text{-}K}$ (kN)	771.60

Pile ID: STTS P21

Load-displacement data

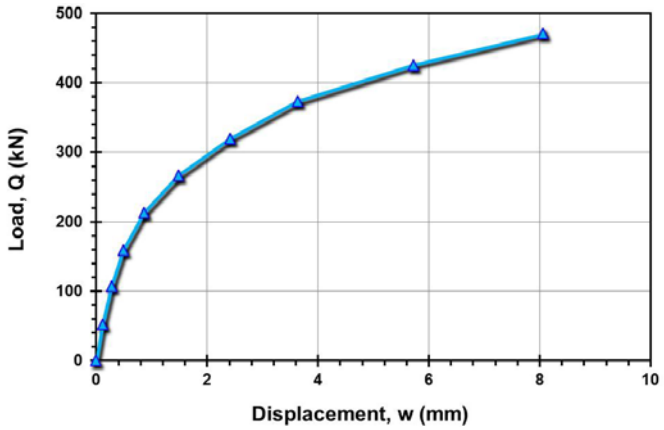

Back-analyzed normalized operational stiffness vs. pseudo-strain

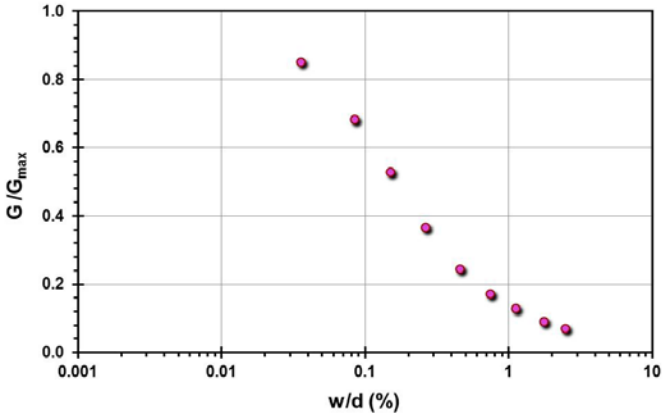

Detail	Description
Pile type/material	Closed-ended steel pipe pile
Length, L (m)	12.20
Diameter, d (m)	0.324
Installation method	Driven
Loading mode	Compression
$Q_{max\text{-}measured}$ (kN)	470.53
Q_s (kN)	Not reported
Q_b (kN)	Not reported
$Q_{Davisson}$ (kN)	470.53
$Q_{w/d=10\%}$ (kN)	552.92
$Q_{C\text{-}K}$ (kN)	588.24

Pile ID: STTS P14-2

Load-displacement data

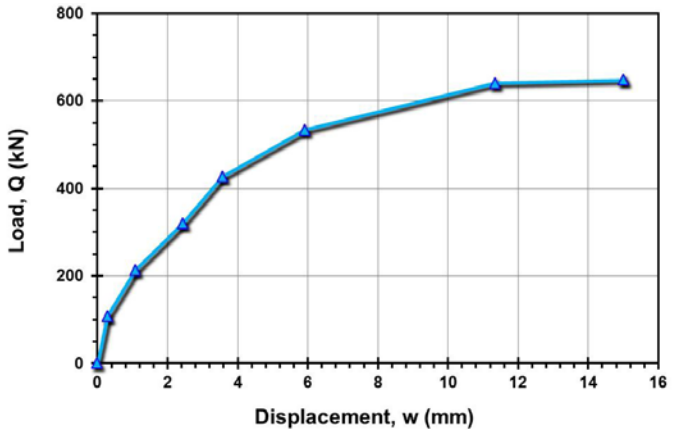

Back-analyzed normalized operational stiffness vs. pseudo-strain

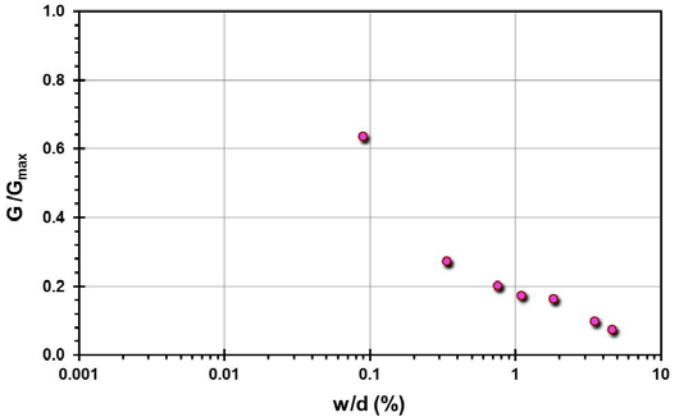

Detail	Description
Pile type/material	Closed-ended steel pipe pile
Length, L (m)	12.20
Diameter, d (m)	0.324
Installation method	Driven
Loading mode	Compression
$Q_{max\text{-}measured}$ (kN)	647.79
Q_s (kN)	Not reported
Q_b (kN)	Not reported
$Q_{Davisson}$ (kN)	587.12
$Q_{w/d=10\%}$ (kN)	659.91
$Q_{C\text{-}K}$ (kN)	670.69

Pile ID: STTS P18

Load-displacement data

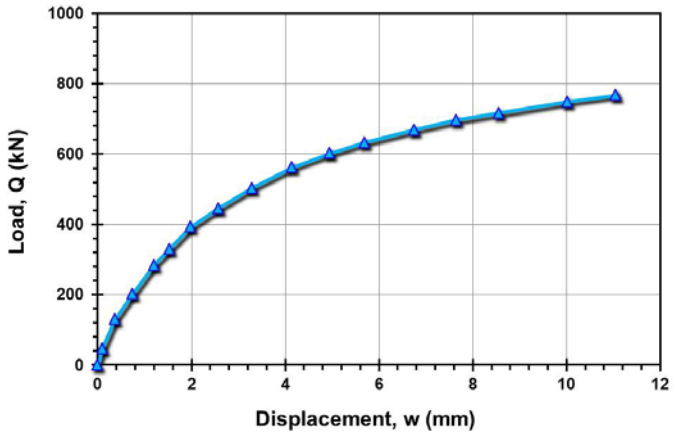

Back-analyzed normalized operational stiffness vs. pseudo-strain

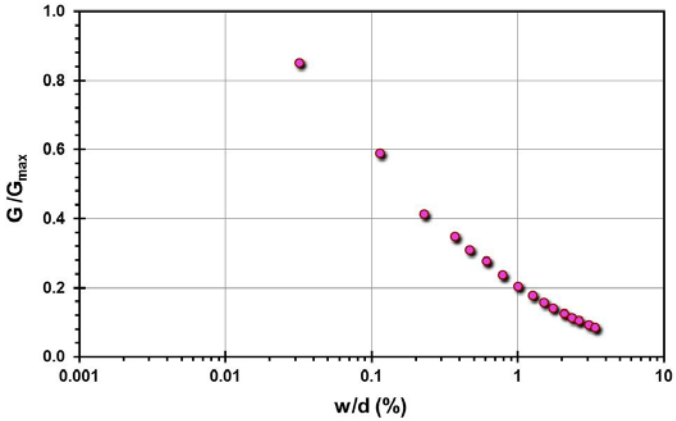

Detail	Description
Pile type/material	Closed-ended steel pipe pile
Length, L (m)	12.20
Diameter, d (m)	0.324
Installation method	Driven
Loading mode	Compression
$Q_{max\text{-}measured}$ (kN)	768.04
Q_s (kN)	Not reported
Q_b (kN)	Not reported
$Q_{Davisson}$ (kN)	716.31
$Q_{w/d=10\%}$ (kN)	889.70
$Q_{C\text{-}K}$ (kN)	971.82

Pile ID: STTS P15

Load-displacement data

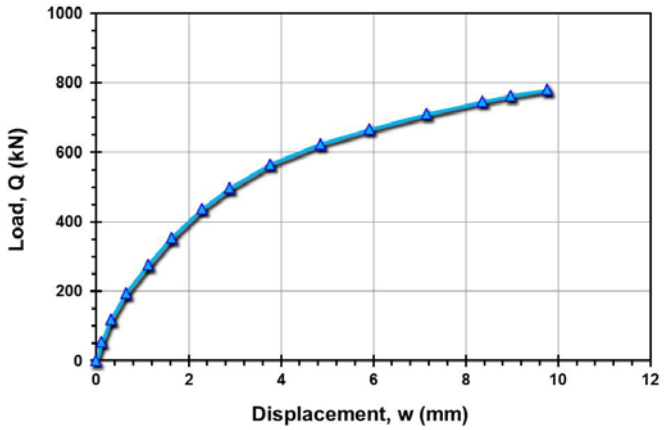

Back-analyzed normalized operational stiffness vs. pseudo-strain

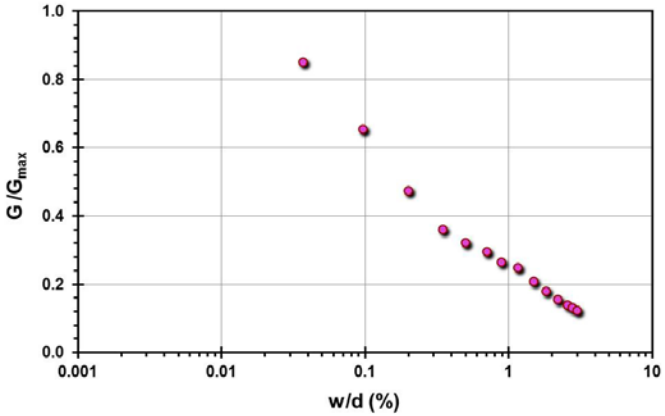

Detail	Description
Pile type/material	Closed-ended steel pipe pile
Length, L (m)	12.20
Diameter, d (m)	0.324
Installation method	Driven
Loading mode	Compression
$Q_{max\text{-}measured}$ (kN)	780.24
Q_s (kN)	Not reported
Q_b (kN)	Not reported
$Q_{Davisson}$ (kN)	746.11
$Q_{w/d=10\%}$ (kN)	934.86
$Q_{C\text{-}K}$ (kN)	1,023.54

Pile ID: STTS P14-3

Load-displacement data

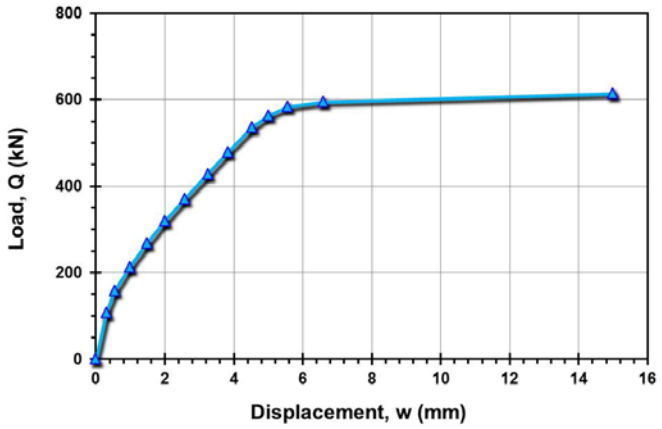

Back-analyzed normalized operational stiffness vs. pseudo-strain

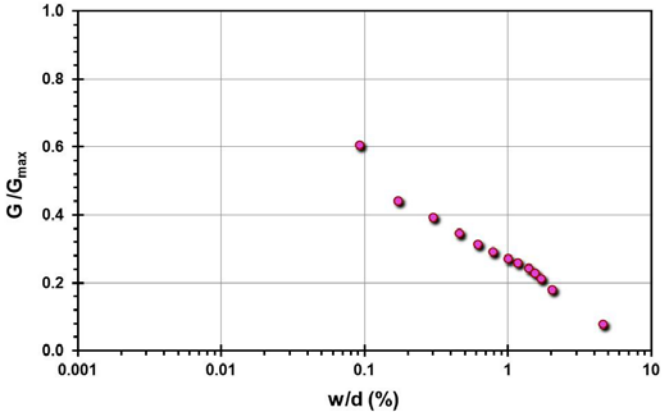

Detail	Description
Pile type/material	Closed-ended steel pipe pile
Length, L (m)	12.20
Diameter, d (m)	0.324
Installation method	Driven
Loading mode	Compression
$Q_{max\text{-}measured}$ (kN)	615.26
Q_s (kN)	Not reported
Q_b (kN)	Not reported
$Q_{Davisson}$ (kN)	605.23
$Q_{w/d=10\%}$ (kN)	625.45
$Q_{C\text{-}K}$ (kN)	634.12

Site ID No. 58

Cone penetrometer data	CPT SBT soil classification index, I_c	Detail	Description
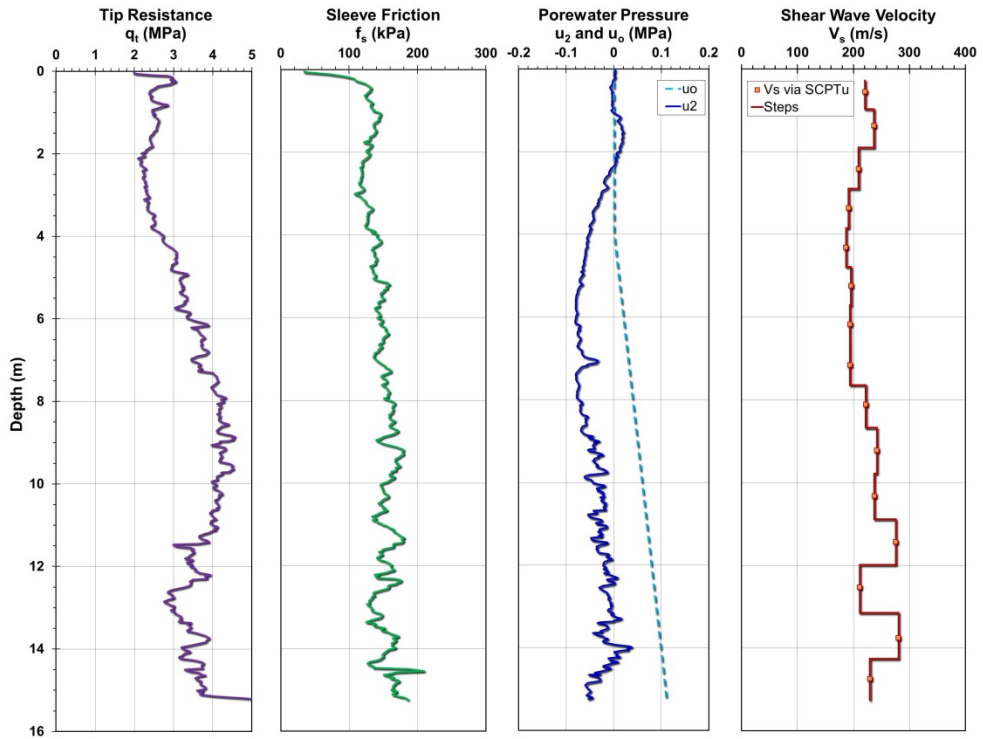	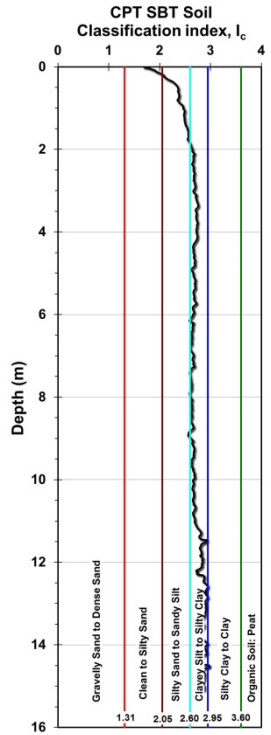	Site name and location	Spring Villa, Opelika NGES, AL, USA
		Soil type(s)	Residual fine sandy silt to silty fine sands of the Piedmont geology
		Pile type(s)	10 Drilled shaft, 1 CFA pile (DeWaal)
		Type of cone penetrometer testing	SCPTu
		Source of V_s evaluation	SCPTu
		Number of pile load tests	11
		Reference	Brown (2002)
		Comments	Note 1: SCPTu data collected by GT CPT rig and reported by Mayne and Brown (2003) Note 2: Multiple drilled shafts were constructed using different installation methods (cased dry, liquid polymer, dry polymer, bentonite slurry) and concreted after 1 hour and after 1 day to investigate these effects on axial pile performance.

Pile ID: S NGES 24LP

Load-displacement data

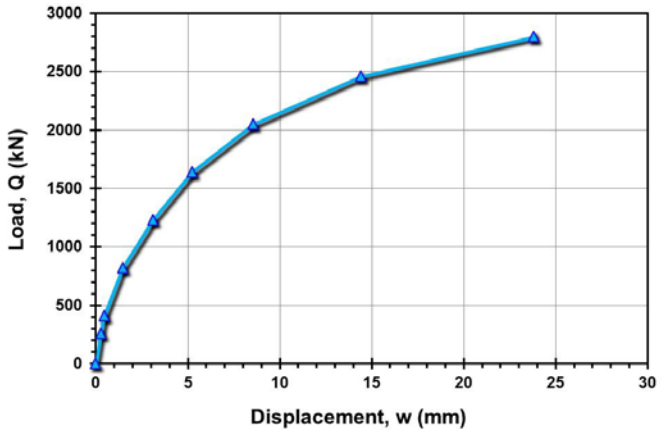

Back-analyzed normalized operational stiffness vs. pseudo-strain

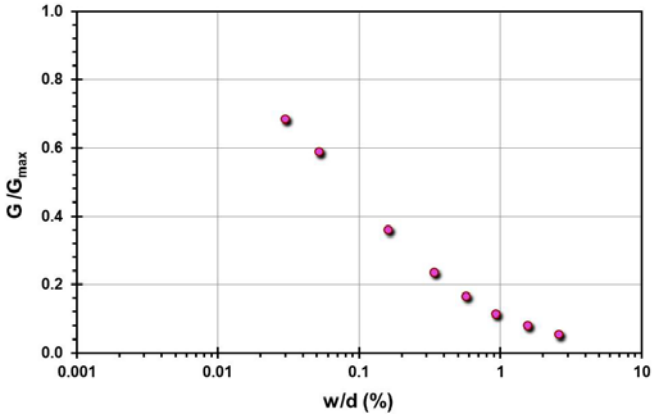

Detail	Description
Pile type/material	Drilled shaft
Length, L (m)	11.00
Diameter, d (m)	0.914
Installation method	Bored cast in-situ
Loading mode	Compression
$Q_{max\text{-}measured}$ (kN)	2,802.46
Q_s (kN)	1,721.23
Q_b (kN)	1,081.23
$Q_{Davisson}$ (kN)	3,912.66
$Q_{w/d=10\%}$ (kN)	3,987.06
$Q_{C\text{-}K}$ (kN)	4,484.30

Pile ID: S NGES 1LP

Load-displacement data

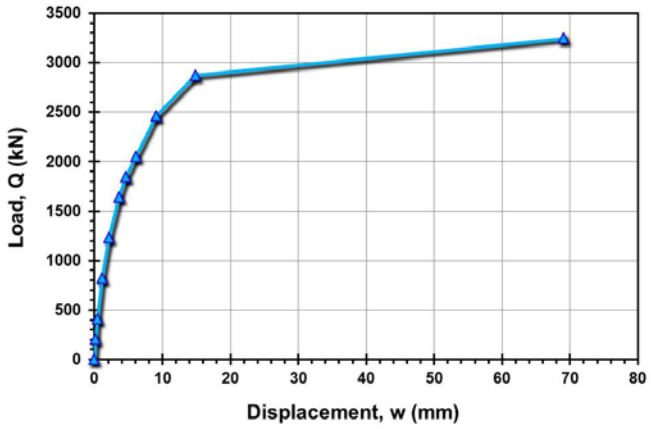

Back-analyzed normalized operational stiffness vs. pseudo-strain

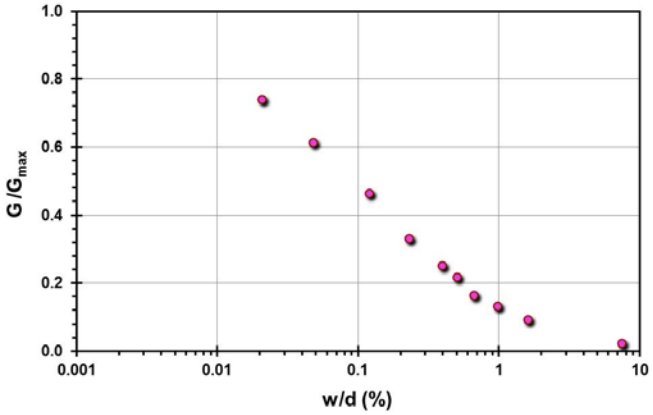

Detail	Description
Pile type/material	Drilled shaft
Length, L (m)	11.00
Diameter, d (m)	0.914
Installation method	Bored cast in-situ
Loading mode	Compression
$Q_{max\text{-}measured}$ (kN)	3,246.75
Q_s (kN)	Not reported
Q_b (kN)	Not reported
$Q_{Davisson}$ (kN)	2,460.70
$Q_{w/d=10\%}$ (kN)	3,292.89
$Q_{C\text{-}K}$ (kN)	3,508.77

Pile ID: S NGES 24C

Load-displacement data

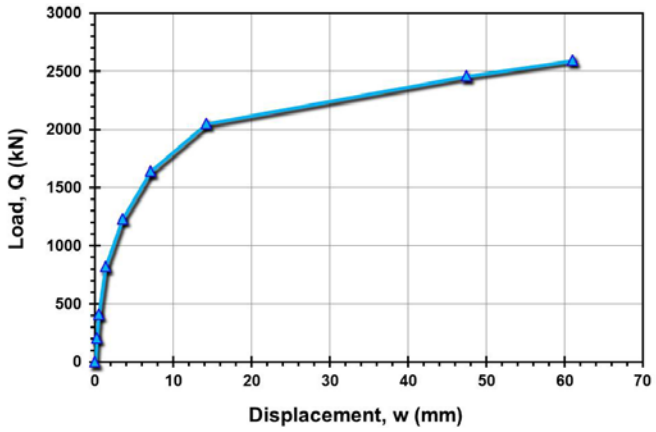

Back-analyzed normalized operational stiffness vs. pseudo-strain

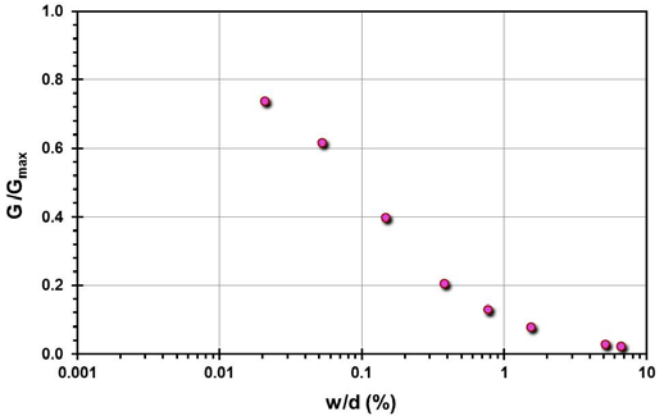

Detail	Description
Pile type/material	Drilled shaft
Length, L (m)	11.00
Diameter, d (m)	0.914
Installation method	Bored cast in-situ
Loading mode	Compression
$Q_{max\text{-}measured}$ (kN)	2,597.40
Q_s (kN)	1,451.82
Q_b (kN)	1,145.58
$Q_{Davisson}$ (kN)	2,050.58
$Q_{w/d=10\%}$ (kN)	3,279.83
$Q_{C\text{-}K}$ (kN)	3,389.83

Pile ID: S NGES 1C

Load-displacement data

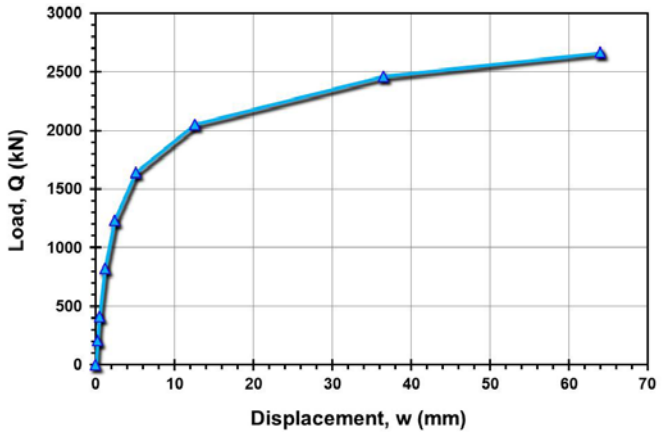

Back-analyzed normalized operational stiffness vs. pseudo-strain

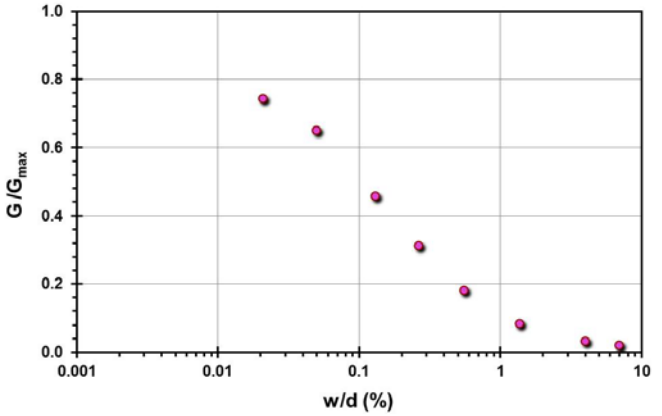

Detail	Description
Pile type/material	Drilled shaft
Length, L (m)	11.00
Diameter, d (m)	0.914
Installation method	Bored cast in-situ
Loading mode	Compression
$Q_{max\text{-}measured}$ (kN)	2,665.75
Q_s (kN)	Not reported
Q_b (kN)	Not reported
$Q_{Davisson}$ (kN)	2,050.58
$Q_{w/d=10\%}$ (kN)	2,719.86
$Q_{C\text{-}K}$ (kN)	2,881.84

Pile ID: S NGES 24CDef

Load-displacement data

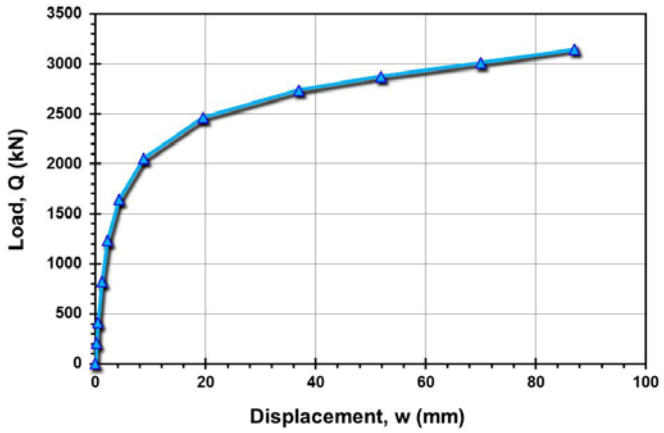

Back-analyzed normalized operational stiffness vs. pseudo-strain

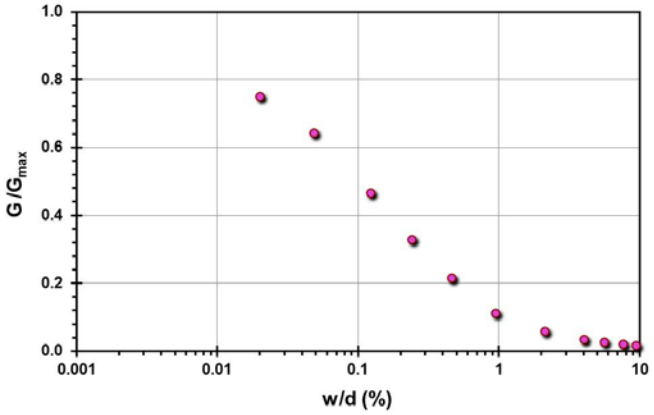

Detail	Description
Pile type/material	Drilled shaft
Length, L (m)	11.00
Diameter, d (m)	0.914
Installation method	Bored cast in-situ
Loading mode	Compression
$Q_{max\text{-}measured}$ (kN)	3,144.22
Q_s (kN)	Not reported
Q_b (kN)	Not reported
$Q_{Davisson}$ (kN)	2,255.64
$Q_{w/d=10\%}$ (kN)	3,142.61
$Q_{C\text{-}K}$ (kN)	3,533.57

Pile ID: S NGES 1CDef

Load-displacement data

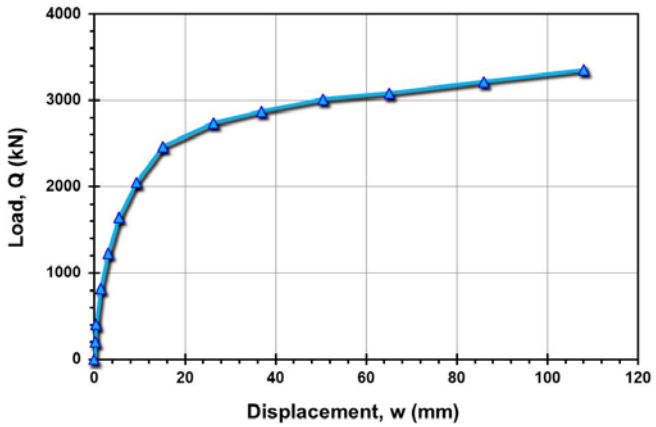

Back-analyzed normalized operational stiffness vs. pseudo-strain

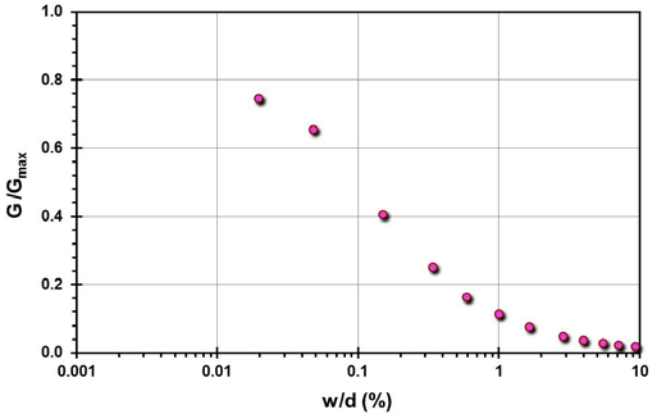

Detail	Description
Pile type/material	Drilled shaft
Length, L (m)	11.00
Diameter, d (m)	0.914
Installation method	Bored cast in-situ
Loading mode	Compression
$Q_{max\text{-}measured}$ (kN)	3,349.28
Q_s (kN)	Not reported
Q_b (kN)	Not reported
$Q_{Davisson}$ (kN)	2,255.64
$Q_{w/d=10\%}$ (kN)	3,263.70
$Q_{C\text{-}K}$ (kN)	3,731.34

Pile ID: S NGES 24B

Load-displacement data

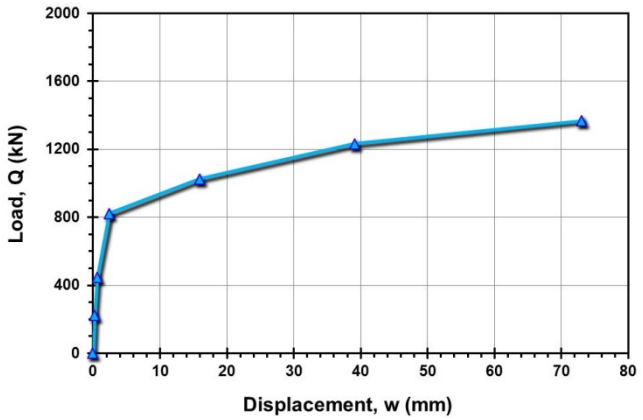

Back-analyzed normalized operational stiffness vs. pseudo-strain

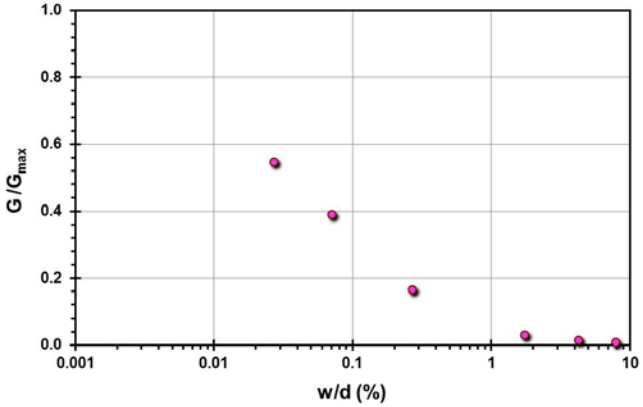

Detail	Description
Pile type/material	Drilled shaft
Length, L (m)	11.00
Diameter, d (m)	0.914
Installation method	Bored cast in-situ
Loading mode	Compression
$Q_{max\text{-}measured}$ (kN)	1,367.05
Q_s (kN)	627.10
Q_b (kN)	739.95
$Q_{Davisson}$ (kN)	922.76
$Q_{w/d=10\%}$ (kN)	1,389.87
$Q_{C\text{-}K}$ (kN)	1,512.86

Pile ID: S NGES 1B

Load-displacement data

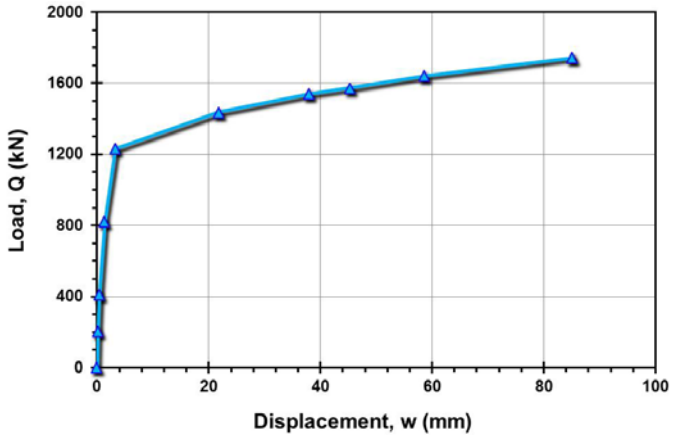

Back-analyzed normalized operational stiffness vs. pseudo-strain

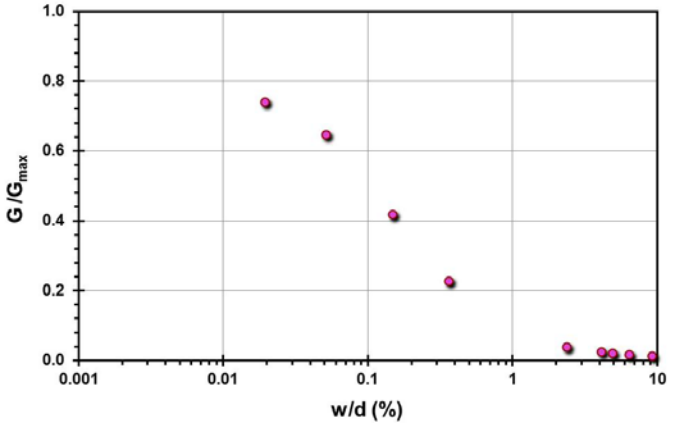

Detail	Description
Pile type/material	Drilled shaft
Length, L (m)	11.00
Diameter, d (m)	0.914
Installation method	Bored cast in-situ
Loading mode	Compression
$Q_{max\text{-}measured}$ (kN)	1,742.99
Q_s (kN)	Not reported
Q_b (kN)	Not reported
$Q_{Davisson}$ (kN)	1,322.88
$Q_{w/d=10\%}$ (kN)	1,754.12
$Q_{C\text{-}K}$ (kN)	1,964.64

Pile ID: S NGES 24DP

Load-displacement data

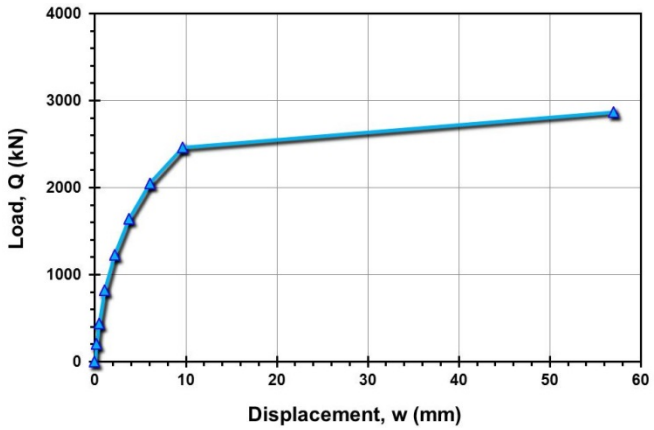

Back-analyzed normalized operational stiffness vs. pseudo-strain

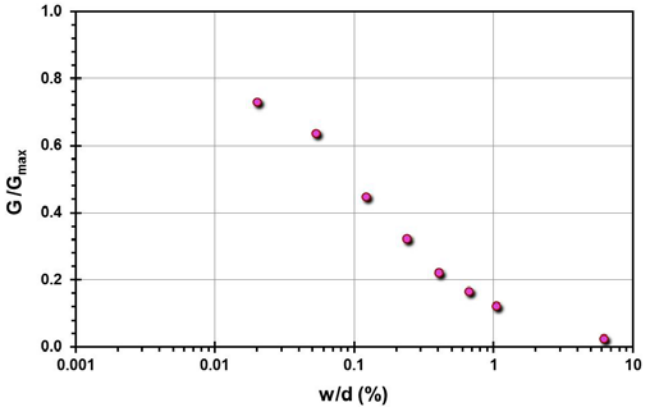

Detail	Description
Pile type/material	Drilled shaft
Length, L (m)	11.00
Diameter, d (m)	0.914
Installation method	Bored cast in-situ
Loading mode	Compression
$Q_{max\text{-}measured}$ (kN)	2,870.81
Q_s (kN)	Not reported
Q_b (kN)	Not reported
$Q_{Davisson}$ (kN)	2,460.70
$Q_{w/d=10\%}$ (kN)	2,925.06
$Q_{C\text{-}K}$ (kN)	3,012.05

Pile ID: S NGES 1DP

Load-displacement data

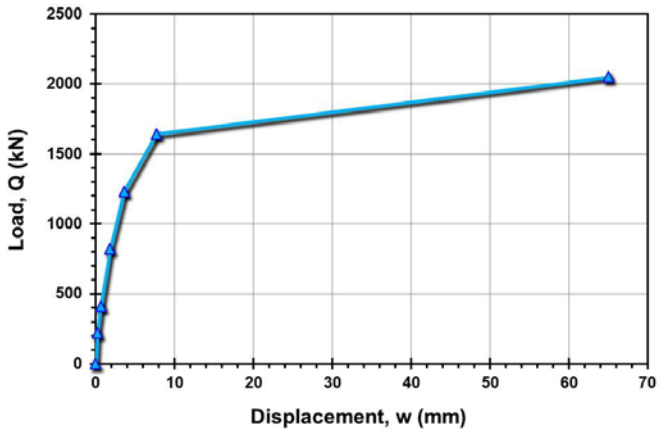

Back-analyzed normalized operational stiffness vs. pseudo-strain

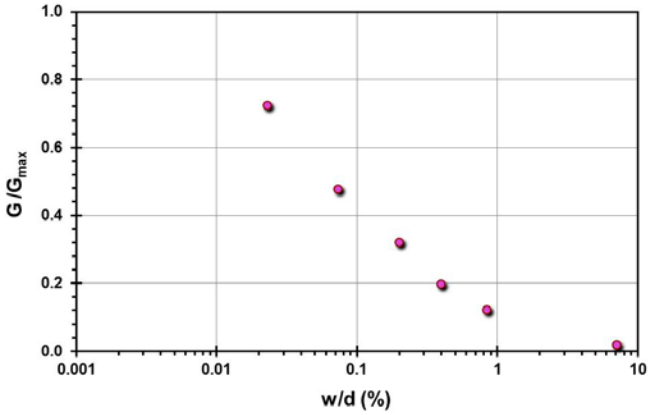

Detail	Description
Pile type/material	Drilled shaft
Length, L (m)	11.00
Diameter, d (m)	0.914
Installation method	Bored cast in-situ
Loading mode	Compression
$Q_{max\text{-}measured}$ (kN)	2,050.58
Q_s (kN)	686.32
Q_b (kN)	1,364.26
$Q_{Davisson}$ (kN)	1,640.46
$Q_{w/d=10\%}$ (kN)	2,076.57
$Q_{C\text{-}K}$ (kN)	2,136.75

Pile ID: S NGES A1

Load-displacement data	Detail	Description
Not reported	Pile type/material	Continuous Flight Auger
	Length, L (m)	11.00
	Diameter, d (m)	0.45
	Installation method	Bored cast in-situ
	Loading mode	Compression
	$Q_{max\text{-}measured}$ (kN)	1,600.00
	Q_s (kN)	1,442.26
	Q_b (kN)	157.74
	$Q_{Davisson}$ (kN)	-
	$Q_{w/d=10\%}$ (kN)	-
	$Q_{C\text{-}K}$ (kN)	-
Back-analyzed normalized operational stiffness vs. pseudo-strain		
Not calculated		

Site ID No. 59A

Cone penetrometer data	CPT SBT soil classification index, I_c	Detail	Description
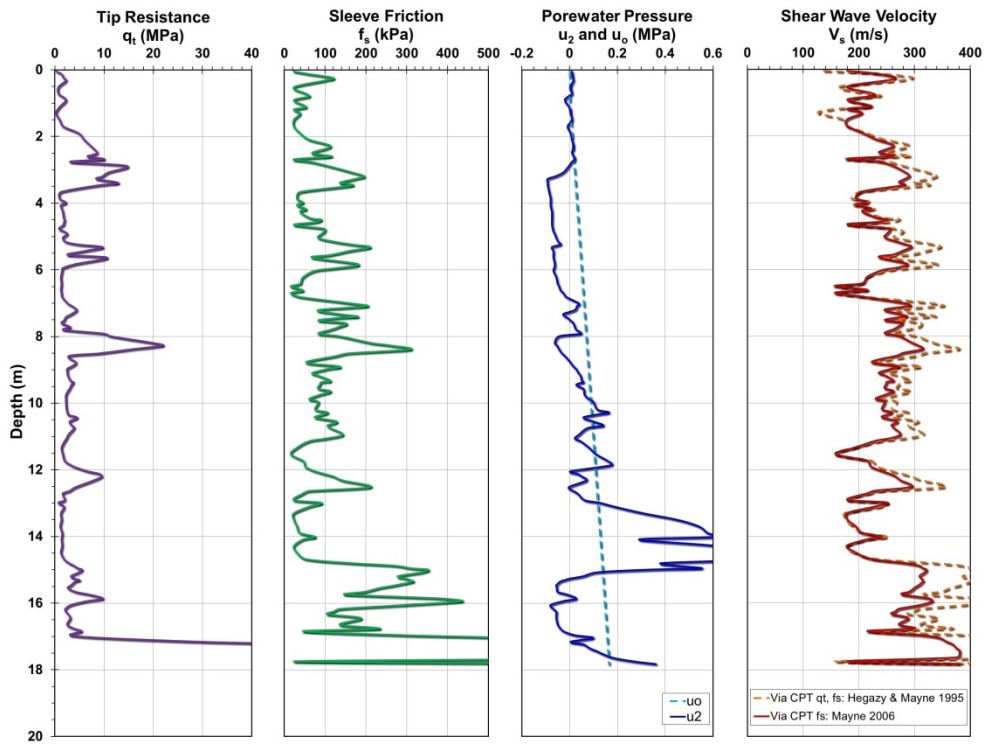	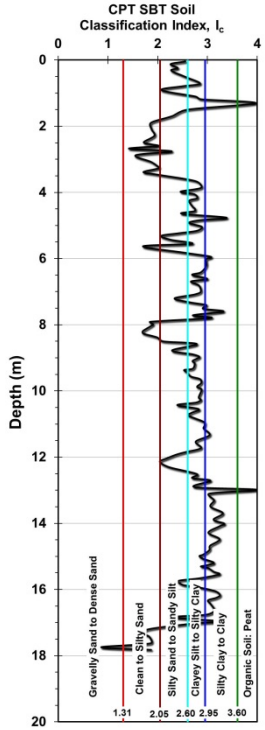	Site name and location	State Road 49, Jasper County, Indiana, USA
		Soil type(s)	Silt dominated multilayered soil
		Pile type(s)	H-section pile
		Type of cone penetrometer testing	CPTu + SPT N
		Source of V_s evaluation	Correlations (see Figure opposite and Table 3.1)
		Number of pile load tests	1
		Reference	Seo et al. (2009), Kim et al. (2009)
		Comments	V_s estimated via correlations

Pile ID: SR49 P1

Load-displacement data

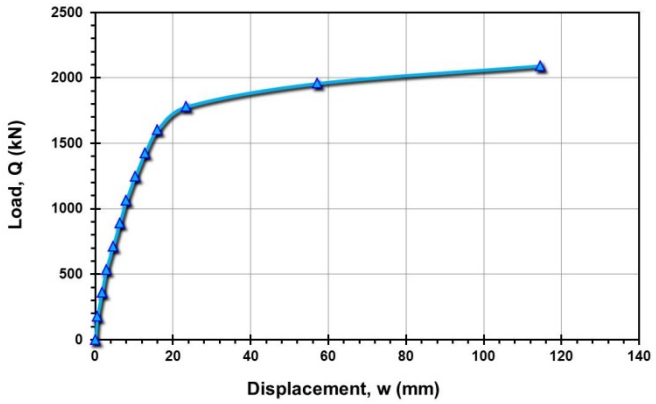

Back-analyzed normalized operational stiffness vs. pseudo-strain

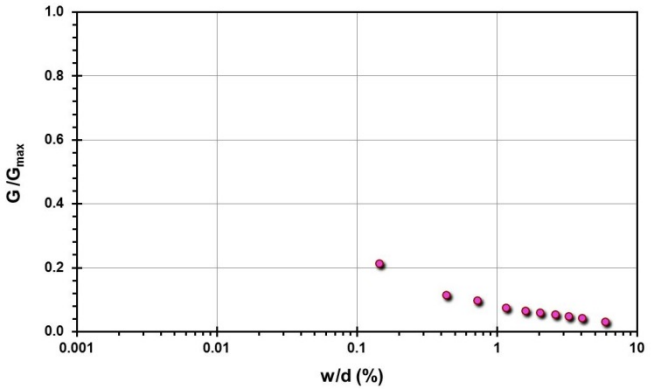

Detail	Description
Pile type/material	H-section pile
Length, L (m)	17.40
H-section size	12 x 74
Installation method	Driven
Loading mode	Compression
$Q_{max\text{-}measured}$ (kN)	2,092.00
Q_s (kN)	1,058.48
Q_b (kN)	1,033.52
$Q_{Davisson}$ (kN)	1,424.00
$Q_{w/d=10\%}$ (kN)	1,861.70
$Q_{C\text{-}K}$ (kN)	2,252.25

Site ID No. 59B

Cone penetrometer data	CPT SBT soil classification index, I_c	Detail	Description
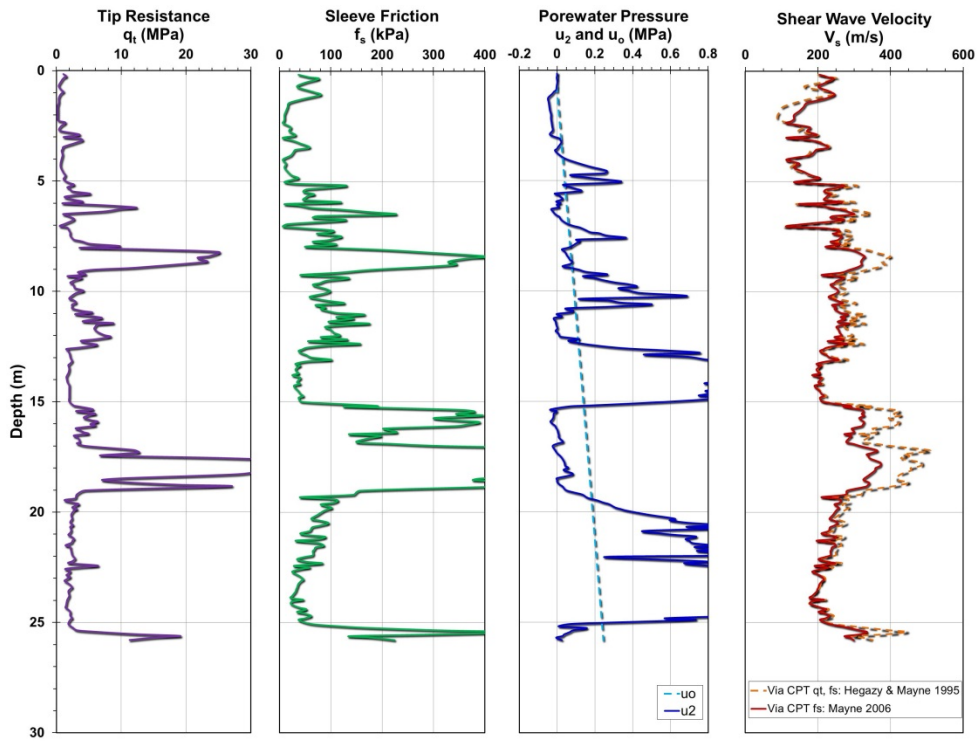	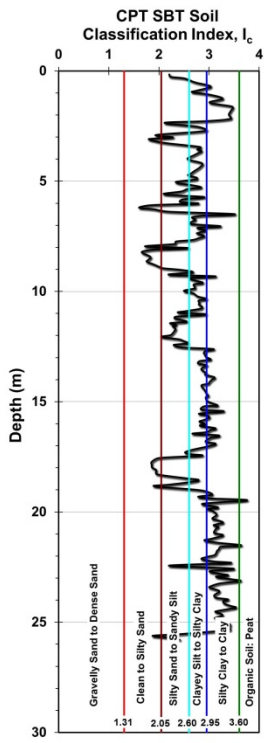	Site name and location	State Road 49, Jasper County, Indiana, USA
		Soil type(s)	Silt dominated multilayered soil
		Pile type(s)	Close-ended steel pipe pile
		Type of cone penetrometer testing	CPTu + SPT N
		Source of V_s evaluation	Correlations (see Figure opposite and Table 3.1)
		Number of pile load tests	1
		Reference	Seo et al. (2009), Kim et al. (2009)
		Comments	V_s estimated via correlations

Pile ID: SR49 P2

Load-displacement data

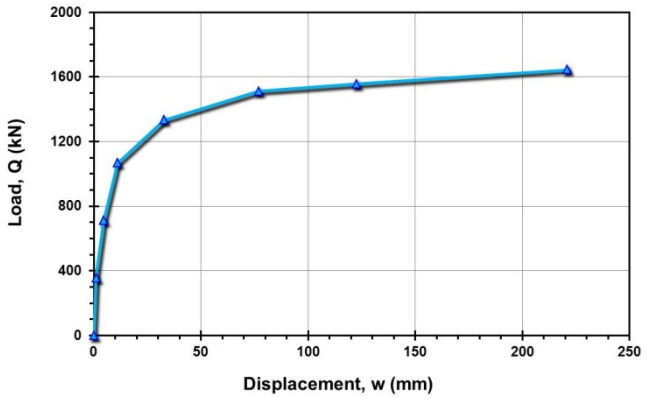

Back-analyzed normalized operational stiffness vs. pseudo-strain

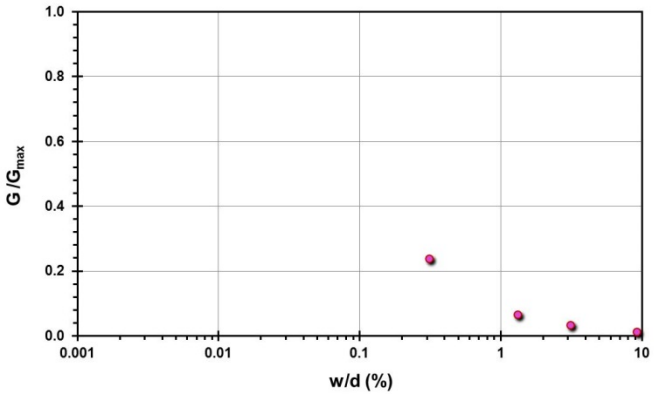

Detail	Description
Pile type/material	Close-ended steel pipe pile
Length, L (m)	17.40
Diameter, d (m)	0.356
Installation method	Driven
Loading mode	Compression
$Q_{max\text{-}measured}$ (kN)	1,646.00
Q_s (kN)	1,198.64
Q_b (kN)	447.36
$Q_{Davisson}$ (kN)	1,110.22
$Q_{w/d=10\%}$ (kN)	1,395.51
$Q_{C\text{-}K}$ (kN)	1,683.50

Site ID No. 60

Cone penetrometer data	CPT SBT soil classification index, I_c	Detail	Description
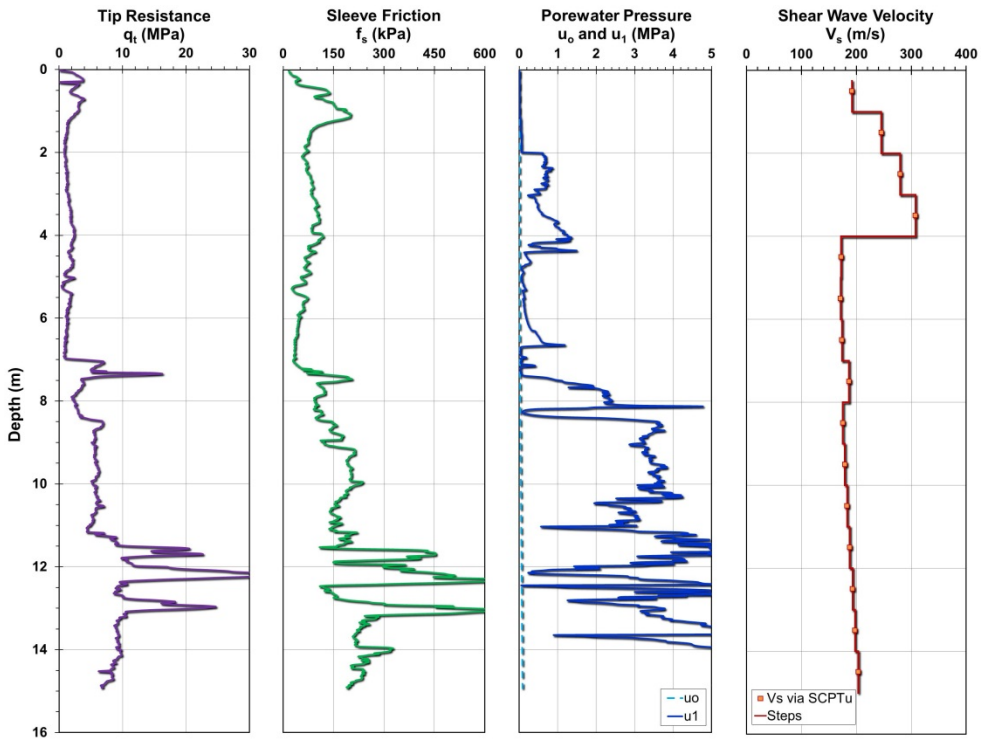	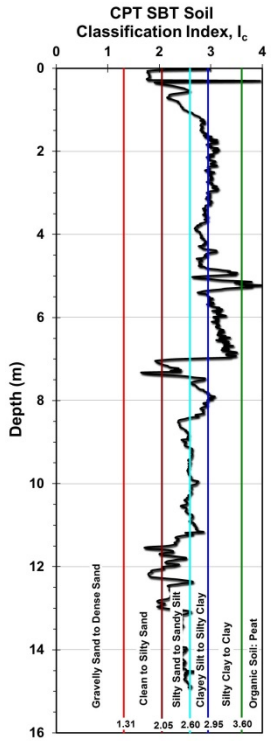	Site name and location	Texas A&M University NGES clay site, College Station, TX, USA
		Soil type(s)	Very stiff clay and stiff to hard sandy clays
		Pile type(s)	Drilled shaft
		Type of cone penetrometer testing	SCPTu
		Source of V_s evaluation	SCPTu
		Number of pile load tests	1
		Reference	Briaud et al. (2000)
		Comments	Meaured u_1 reading converted to equivalent u_2

Pile ID: TAMU-C NGES BP7

Load-displacement data

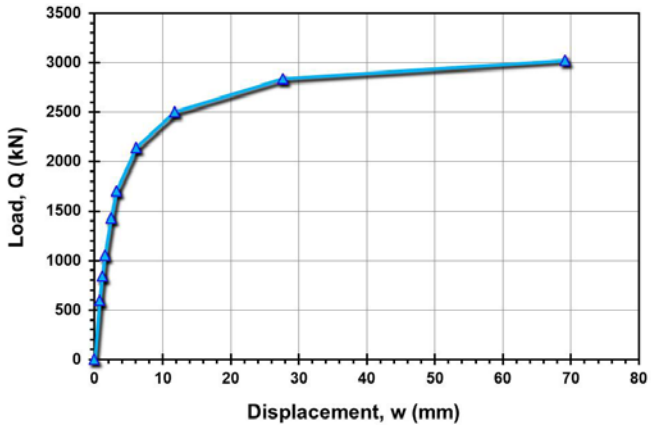

Back-analyzed normalized operational stiffness vs. pseudo-strain

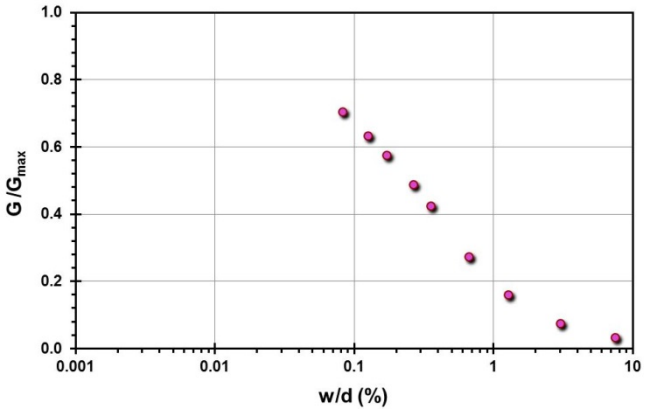

Detail	Description
Pile type/material	Drilled shaft
Length, L (m)	9.50
Diameter, d (m)	0.915
Installation method	Bored cast in-situ
Loading mode	Compression
$Q_{max\text{-}measured}$ (kN)	3,024.86
Q_s (kN)	2,194.87
Q_b (kN)	829.99
$Q_{Davisson}$ (kN)	2,499.08
$Q_{w/d=10\%}$ (kN)	3,056.51
$Q_{C\text{-}K}$ (kN)	3,154.57

Site ID No. 61

Cone penetrometer data	CPT SBT soil classification index, I_c	Detail	Description
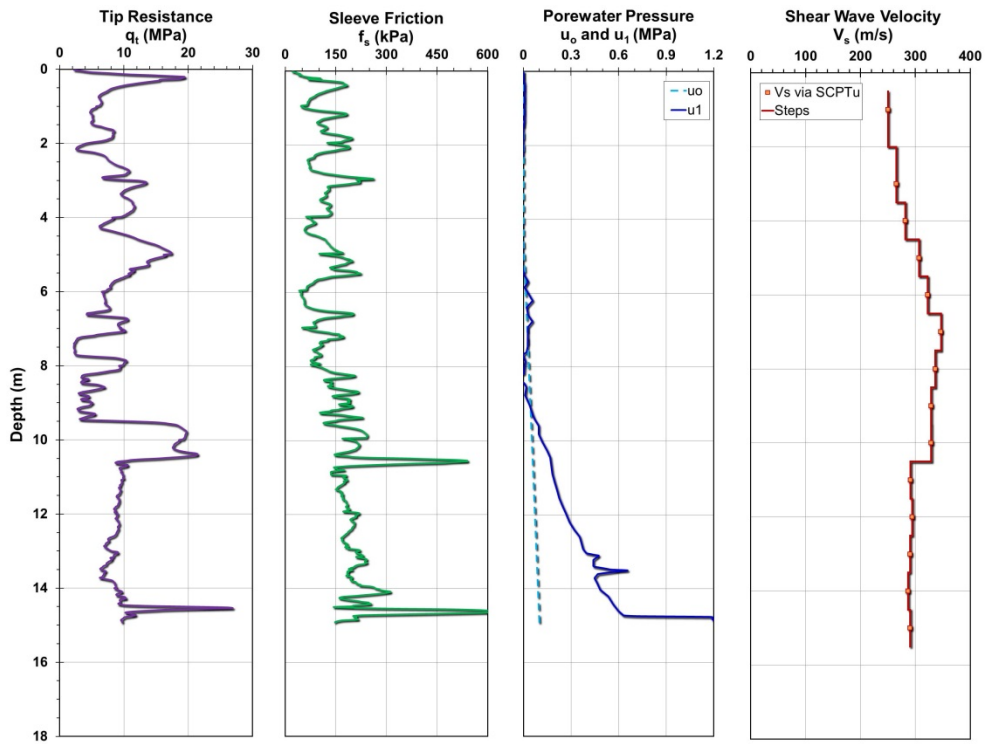	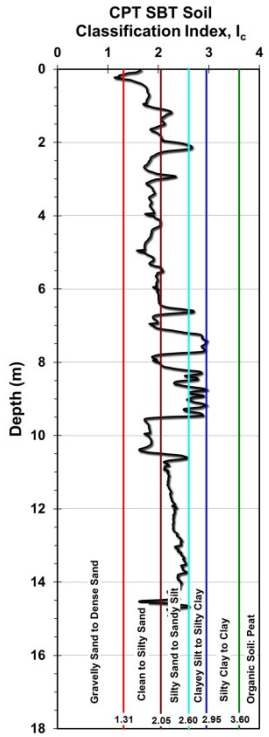	Site name and location	Texas A&M University NGES sand site, College Station, TX, USA
		Soil type(s)	Medium dense sand to silty and clayey sand over stiff clay
		Pile type(s)	Drilled shaft
		Type of cone penetrometer testing	SCPTu
		Source of V_s evaluation	SCPTu
		Number of pile load tests	1
		Reference	Briaud et al. (2000), O'Neill et al. (2002)
		Comments	Measured u_1 reading converted to equivalent u_2

Pile ID: TAMU-S NGES BP4

Load-displacement data

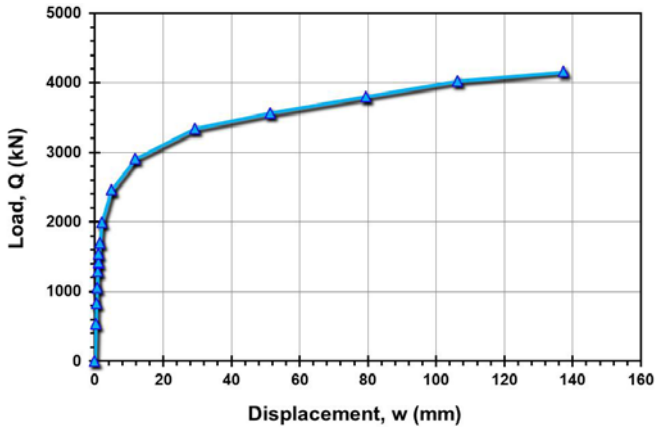

Back-analyzed normalized operational stiffness vs. pseudo-strain

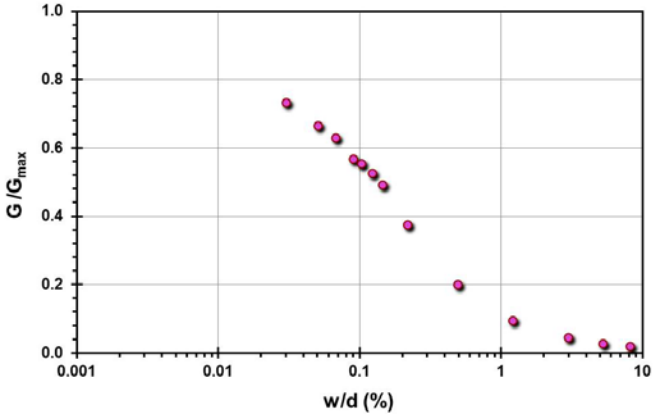

Detail	Description
Pile type/material	Drilled shaft
Length, L (m)	9.40
Diameter, d (m)	0.941
Installation method	Bored cast in-situ
Loading mode	Compression
$Q_{max\text{-}measured}$ (kN)	4,157.03
Q_s (kN)	3,423.05
Q_b (kN)	733.98
$Q_{Davisson}$ (kN)	3,912.66
$Q_{w/d=10\%}$ (kN)	3,987.06
$Q_{C\text{-}K}$ (kN)	4,484.30

Pile ID: TAMU-S NGES O1

Load-displacement data

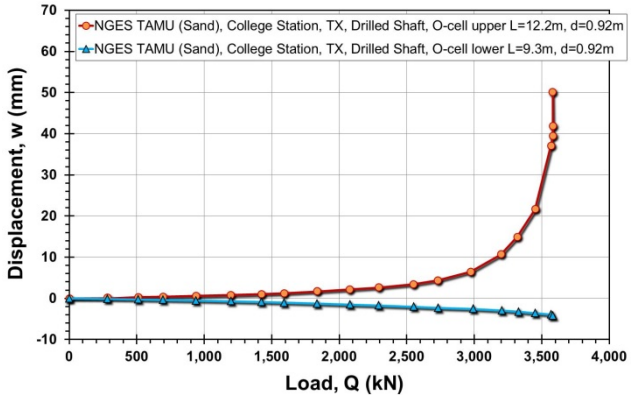

Back-analyzed normalized operational stiffness vs. pseudo-strain

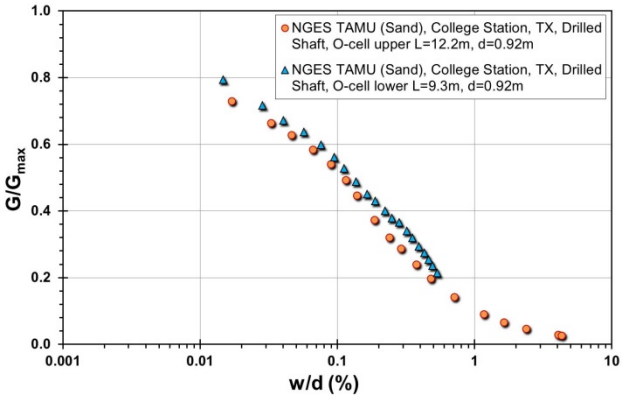

Detail	Description
Pile type/material	Drilled shaft
Length, L (m)	Upper: 12.2; lower: 9.30
Diameter, d (m)	Upper: 0.915; lower: 0.915
Installation method	Bored cast in-situ
Loading mode	O-cell compression
$Q_{max\text{-}measured}$ (kN)	Upper: 3,578.4; lower: 3,578.4
Q_s (kN)	Upper: 3,578.4; lower: 2,930.31
Q_b (kN)	648.09
$Q_{Davisson}$ (kN)	Upper: 3,278.6; lower: 3,583.1
$Q_{w/d=10\%}$ (kN)	Upper: 3,651.0; lower: 3,608.5
$Q_{C\text{-}K}$ (kN)	Upper: 3,717.5; lower: 3,610.1

Site ID No. 62

Cone penetrometer data	CPT SBT soil classification index, I_c	Detail	Description
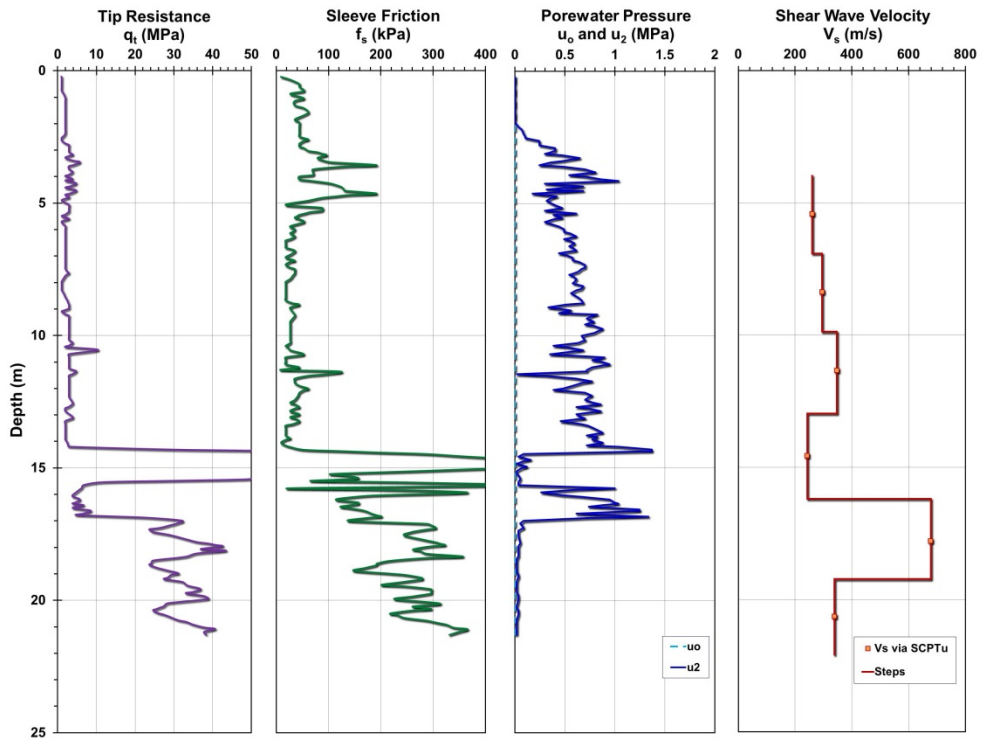	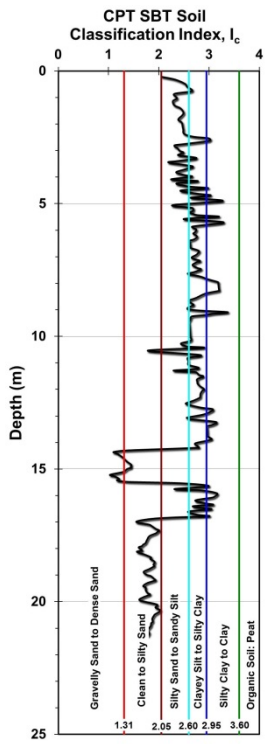	Site name and location	Trunk Hwy 212 Bridge No. 10038 near Minneapolis, MN, USA
		Soil type(s)	Stiff clay loam glacial till over dense sand
		Pile type(s)	Closed-ended steel-concrete pile
		Type of cone penetrometer testing	SCPTu
		Source of V_s evaluation	SCPTu
		Number of pile load tests	2
		Reference	Reuter (2010)
		Comments	

Pile ID: TH212 B10038-1

Load-displacement data

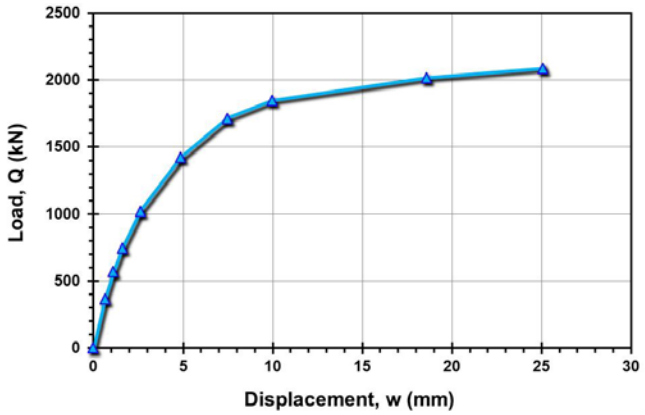

Back-analyzed normalized operational stiffness vs. pseudo-strain

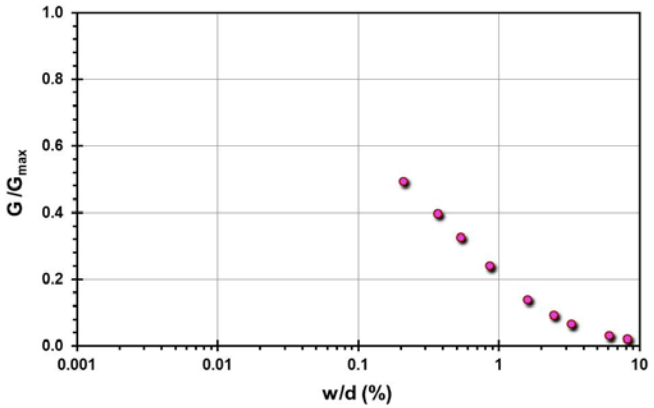

Detail	Description
Pile type/material	Closed-ended steel-concrete pile
Length, L (m)	15.90
Diameter, d (m)	0.304
Installation method	Driven
Loading mode	Compression
$Q_{max\text{-}measured}$ (kN)	2,087.03
Q_s (kN)	Not reported
Q_b (kN)	Not reported
$Q_{Davisson}$ (kN)	2,015.99
$Q_{w/d=10\%}$ (kN)	2,118.50
$Q_{C\text{-}K}$ (kN)	2,288.33

Pile ID: TH212 B10038-2

Load-displacement data

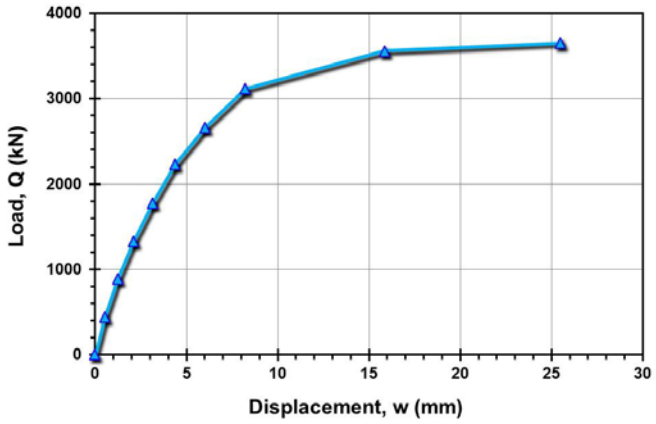

Back-analyzed normalized operational stiffness vs. pseudo-strain

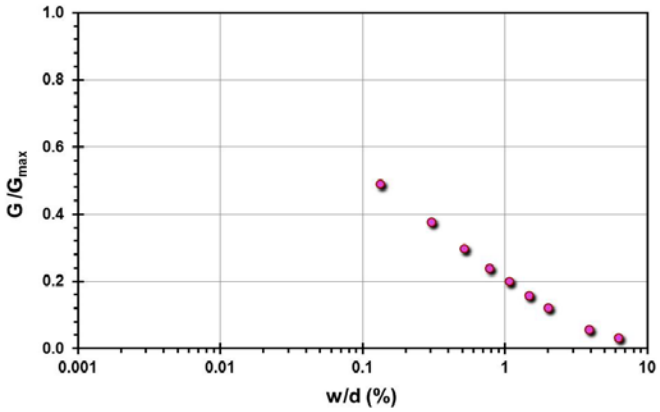

Detail	Description
Pile type/material	Closed-ended steel-concrete pile
Length, L (m)	15.90
Diameter, d (m)	0.406
Installation method	Driven
Loading mode	Compression
$Q_{max\text{-}measured}$ (kN)	3,649.79
Q_s (kN)	Not reported
Q_b (kN)	Not reported
$Q_{Davisson}$ (kN)	3,602.32
$Q_{w/d=10\%}$ (kN)	3,772.58
$Q_{C\text{-}K}$ (kN)	3,968.25

Site ID No. 63

Cone penetrometer data	CPT SBT soil classification index, I_c	Detail	Description
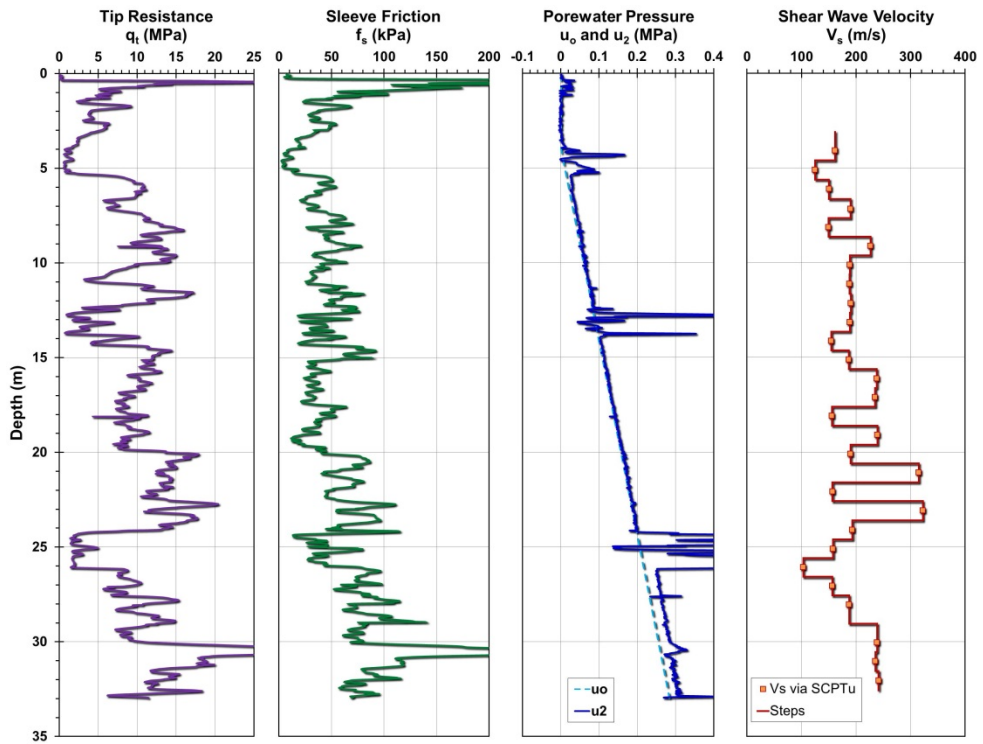	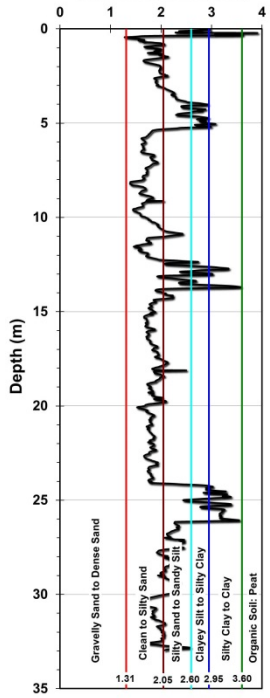	Site name and location	Trunk Hwy 52 Lafayette Bridge over the Mississippi River, St. Paul, MN, USA
		Soil type(s)	Fine to coarse gravelly sands with clay layers
		Pile type(s)	1 Closed-ended steel-concrete pile and 1 mono-pile
		Type of cone penetrometer testing	SCPTu
		Source of V_s evaluation	SCPTu
		Number of pile load tests	2
		Reference	Komurka and Grauvogl-Graham (2010)
		Comments	Digital SCPTu data provided by Derek Dassenbrock and Gary Person of MnDOT

Pile ID: TH52 PAT2

Load-displacement data

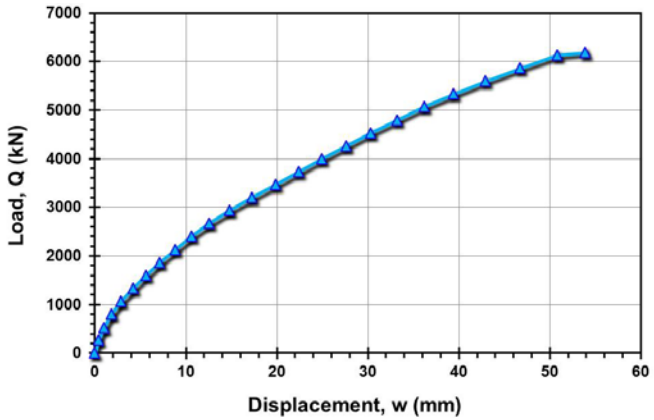

Back-analyzed normalized operational stiffness vs. pseudo-strain

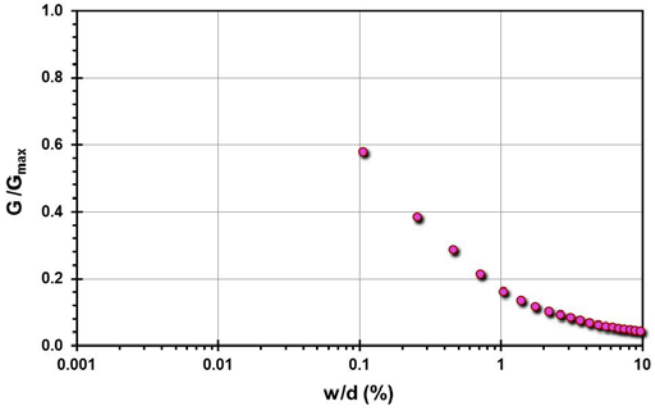

Detail	Description
Pile type/material	Closed-ended steel-concrete pile
Length, L (m)	42.30
Diameter, d (m)	0.410
Installation method	Driven
Loading mode	Compression
$Q_{max\text{-}measured}$ (kN)	6,183.43
Q_s (kN)	2,209.68
Q_b (kN)	3,973.75
$Q_{Davisson}$ (kN)	4,798.26
$Q_{w/d=10\%}$ (kN)	5,416.31
$Q_{C\text{-}K}$ (kN)	11,904.76

Pile ID: TH52 MAT2

Load-displacement data

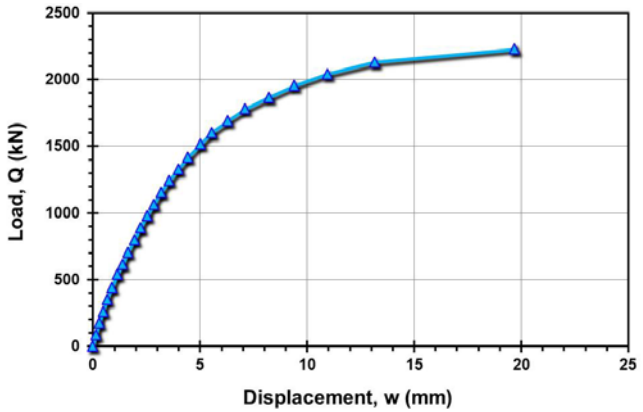

Back-analyzed normalized operational stiffness vs. pseudo-strain

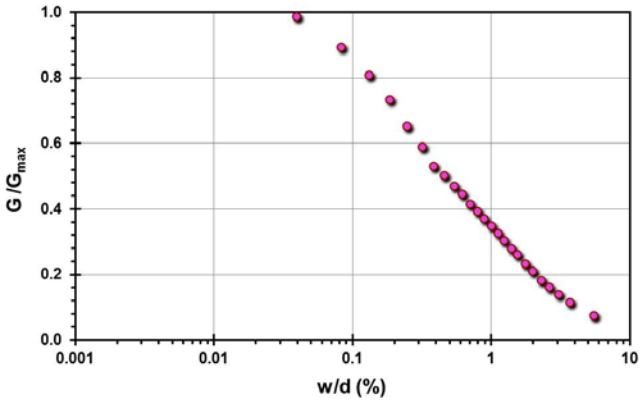

Detail	Description
Pile type/material	Closed-ended steel pile
Length, L (m)	20.29
Diameter, d (m)	0.356
Installation method	Driven
Loading mode	Compression
$Q_{max\text{-}measured}$ (kN)	2,229.69
Q_s (kN)	2,037.02
Q_b (kN)	192.67
$Q_{Davisson}$ (kN)	2,180.26
$Q_{w/d=10\%}$ (kN)	2,347.76
$Q_{C\text{-}K}$ (kN)	2,506.27

Site ID No. 64

Cone penetrometer data	CPT SBT soil classification index, I_c	Detail	Description
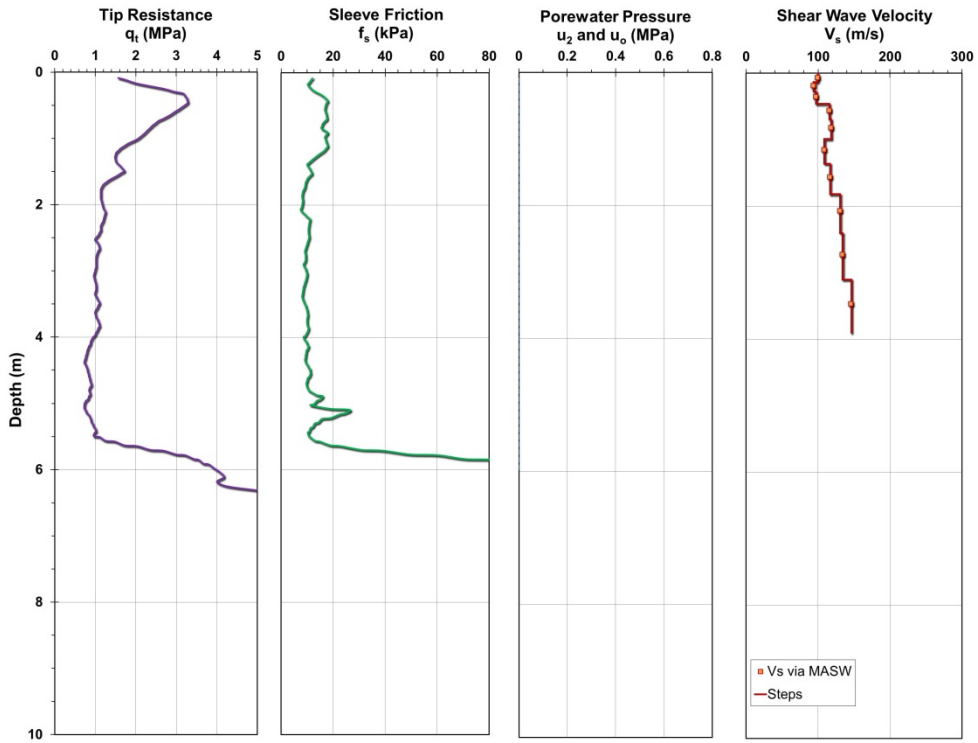	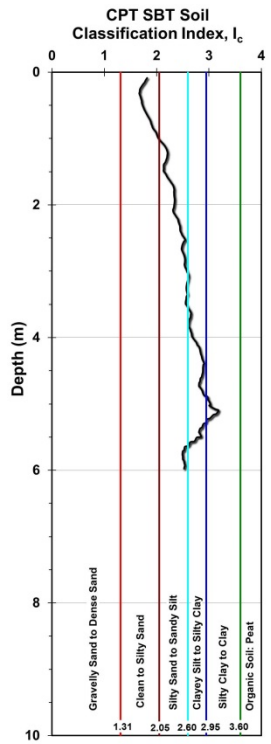	Site name and location	University College Dublin (UCD), Ireland
		Soil type(s)	Uniform loose sand (trenched, backfilled and recompacted)
		Pile type(s)	Open-ended steel pipe pile
		Type of cone penetrometer testing	CPT + MASW
		Source of V_s evaluation	MASW
		Number of pile load tests	1
		Reference	Igoe et al. (2011; 2010)
		Comments	The reading u_2 assumed negligible because GWT below the pile base

Pile ID: UCD P1

Load-displacement data	Detail	Description
Not reported	Pile type/material	Close-ended steel-concrete pile
	Length, L (m)	4.00
	Diameter, d (m)	0.168
	Installation method	Jacked
	Loading mode	Compression
	$Q_{max\text{-}measured}$ (kN)	51.46
	Q_s (kN)	15.16
	Q_b (kN)	36.30
	$Q_{Davisson}$ (kN)	-
	$Q_{w/d=10\%}$ (kN)	-
	$Q_{C\text{-}K}$ (kN)	-
Back-analyzed normalized operational stiffness vs. pseudo-strain		
Not reported		

Site ID No. 65

Cone penetrometer data	CPT SBT soil classification index, I_c	Detail	Description
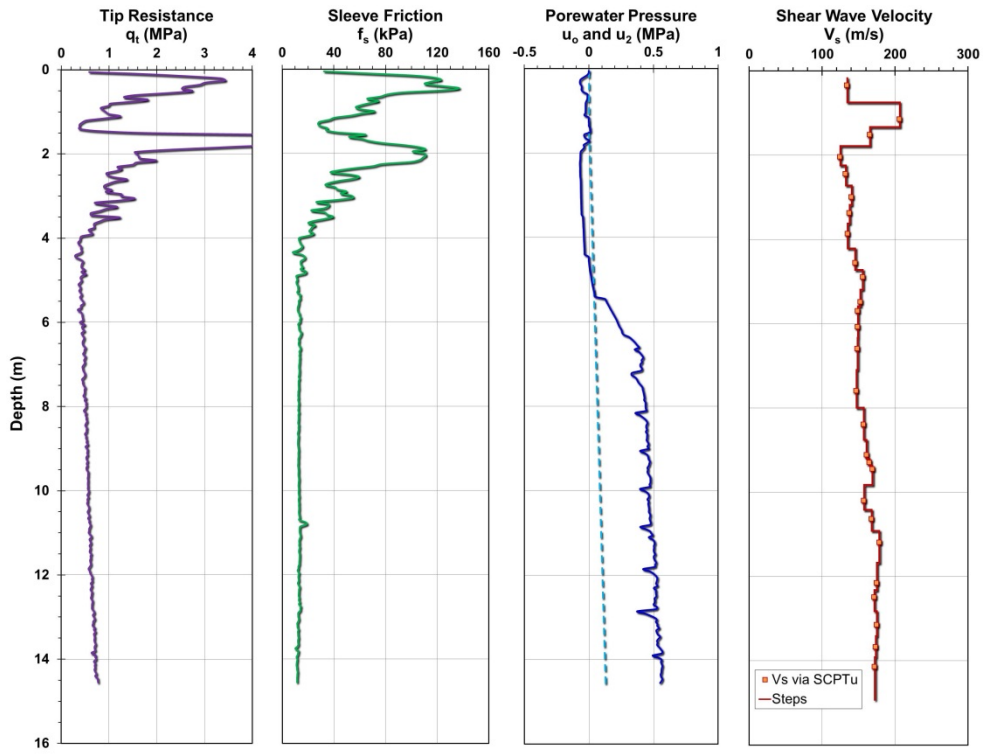	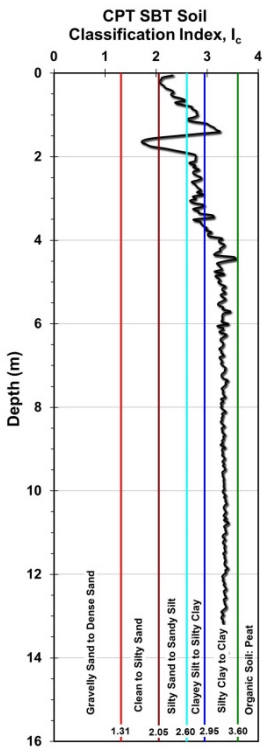	Site name and location	University of Massachusetts-Amherst NGES, Amherst, MA, USA
		Soil type(s)	Desiccated crust over soft varved silty clay
		Pile type(s)	Drilled shaft
		Type of cone penetrometer testing	SCPTu
		Source of V_s evaluation	SCPTu
		Number of pile load tests	2
		Reference	Iskander et al. (2003)
		Comments	SCPTu soundings obtained by GT forces with Hogentogler cone. Data reported in Mayne (2001).

Pile ID: UMASS NGES1

Load-displacement data

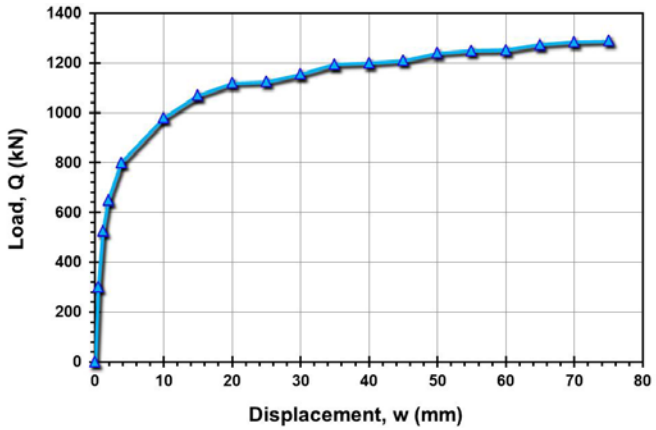

Back-analyzed normalized operational stiffness vs. pseudo-strain

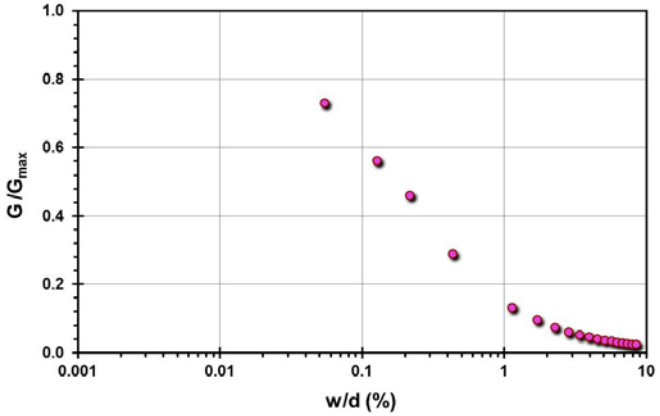

Detail	Description
Pile type/material	Drilled shaft
Length, L (m)	13.11
Diameter, d (m)	0.878
Installation method	Bored cast in-situ
Loading mode	Compression
$Q_{max\text{-}measured}$ (kN)	1,290.00
Q_s (kN)	1,090.00
Q_b (kN)	200.00
$Q_{Davisson}$ (kN)	1,025.00
$Q_{w/d=10\%}$ (kN)	1,286.27
$Q_{C\text{-}K}$ (kN)	1,345.90

Pile ID: UMASS NGES2

Load-displacement data

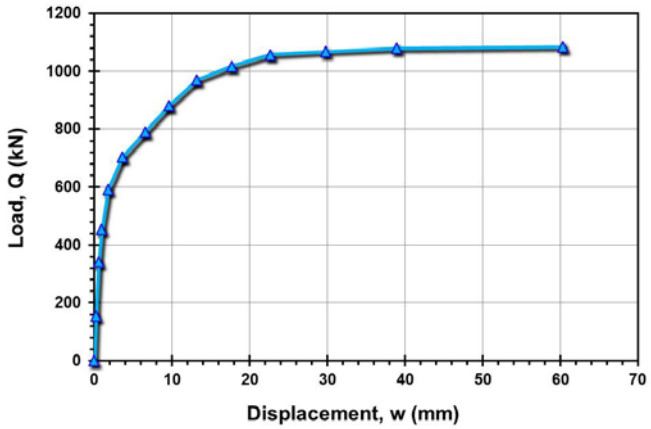

Back-analyzed normalized operational stiffness vs. pseudo-strain

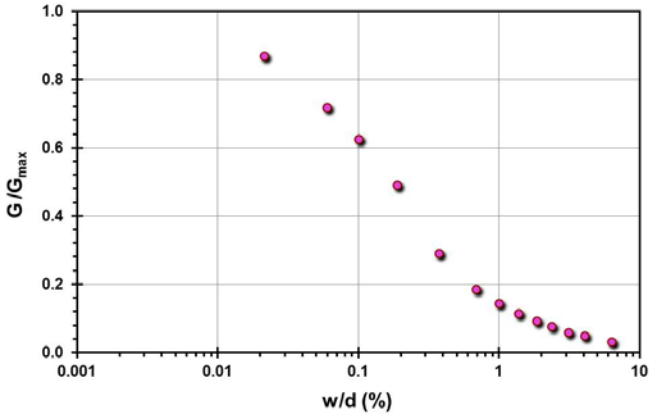

Detail	Description
Pile type/material	Drilled shaft
Length, L (m)	14.30
Diameter, d (m)	0.955
Installation method	Bored cast in-situ
Loading mode	Compression
$Q_{max\text{-}measured}$ (kN)	1,083.78
Q_s (kN)	833.78
Q_b (kN)	250.00
$Q_{Davisson}$ (kN)	968.38
$Q_{w/d=10\%}$ (kN)	1,108.32
$Q_{C\text{-}K}$ (kN)	1,135.07

Site ID No. 66

Cone penetrometer data	CPT SBT soil classification index, I_c	Detail	Description
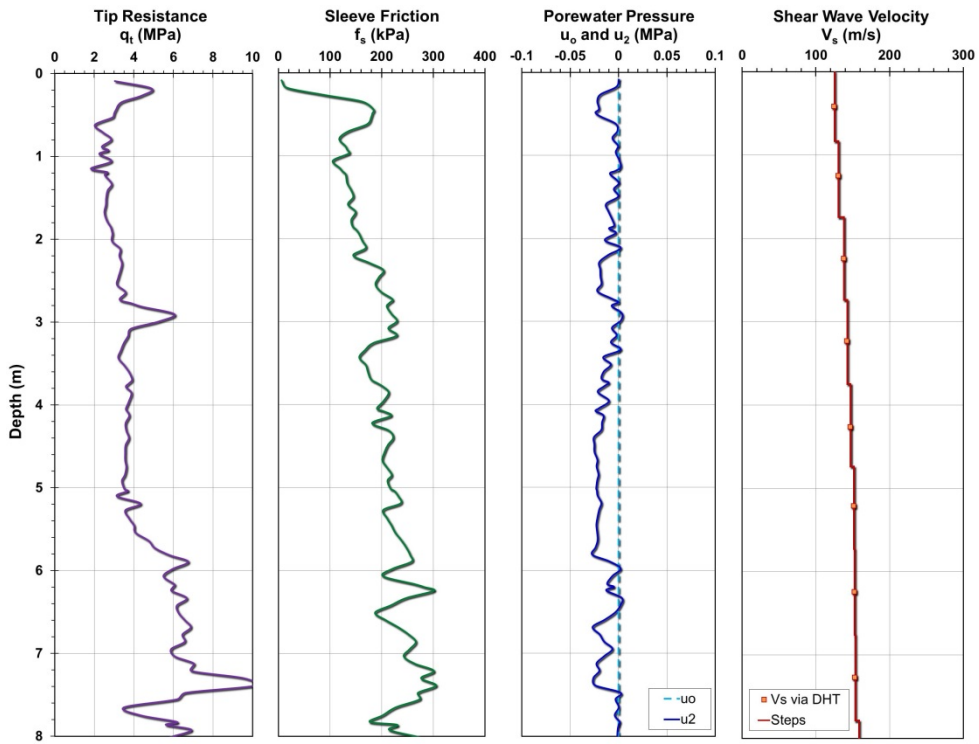	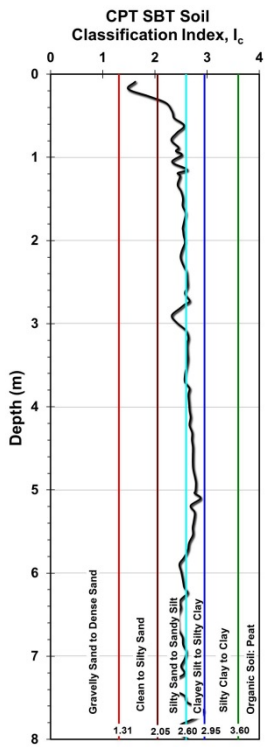	Site name and location	University of Porto, Portugal (FEUP), ISC-2 experimental site
		Soil type(s)	Residual silty sand
		Pile type(s)	1 Drilled shaft, 1 CFA pile and 1 square concrete pile
		Type of cone penetrometer testing	CPTu + DHT
		Source of V_s evaluation	DHT
		Number of pile load tests	3
		Reference	Viana da Fonseca et al. (2006), Fellenius et al. (2007)
		Comments	

Pile ID: FEUP ISC'2 P1

Load-displacement data

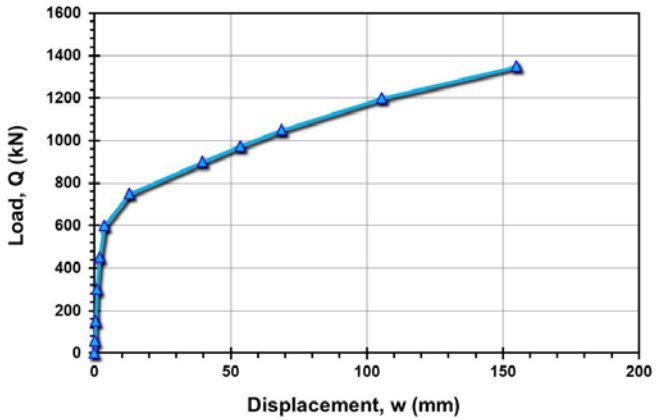

Back-analyzed normalized operational stiffness vs. pseudo-strain

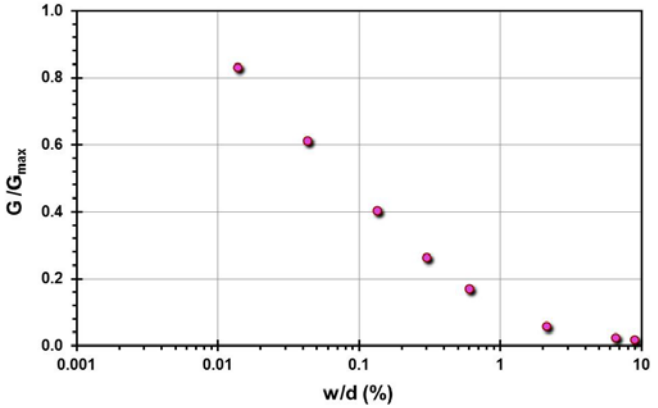

Detail	Description
Pile type/material	Drilled shaft
Length, L (m)	6.00
Diameter, d (m)	0.60
Installation method	Bored cast in-situ
Loading mode	Compression
$Q_{max\text{-}measured}$ (kN)	1,350.00
Q_s (kN)	855.00
Q_b (kN)	495.00
$Q_{Davisson}$ (kN)	750.00
$Q_{w/d=10\%}$ (kN)	1,004.26
$Q_{C\text{-}K}$ (kN)	1,703.58

Pile ID: FEUP ISC'2 P2

Load-displacement data

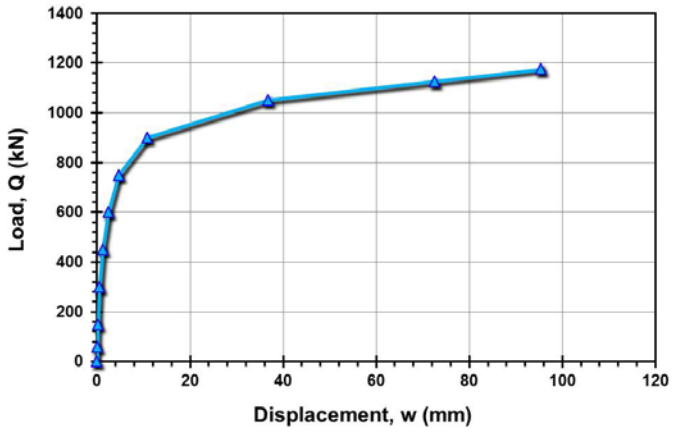

Back-analyzed normalized operational stiffness vs. pseudo-strain

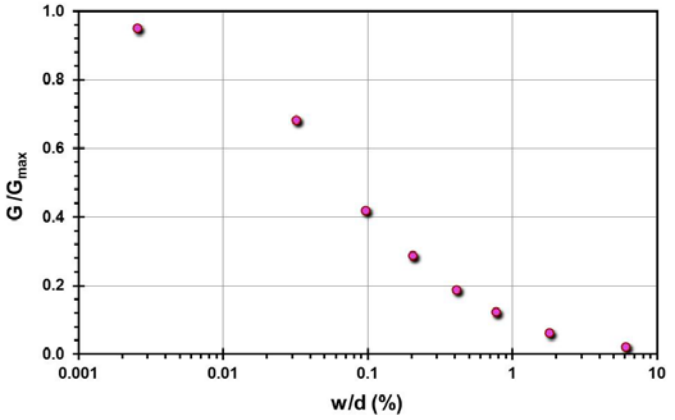

Detail	Description
Pile type/material	Continuous Flight Auger
Length, L (m)	6.00
Diameter, d (m)	0.60
Installation method	Augered
Loading mode	Compression
$Q_{max\text{-}measured}$ (kN)	1,175.08
Q_s (kN)	765.08
Q_b (kN)	410.00
$Q_{Davisson}$ (kN)	899.70
$Q_{w/d=10\%}$ (kN)	1,117.04
$Q_{C\text{-}K}$ (kN)	1,264.22

Pile ID: FEUP ISC'2 P3

Load-displacement data

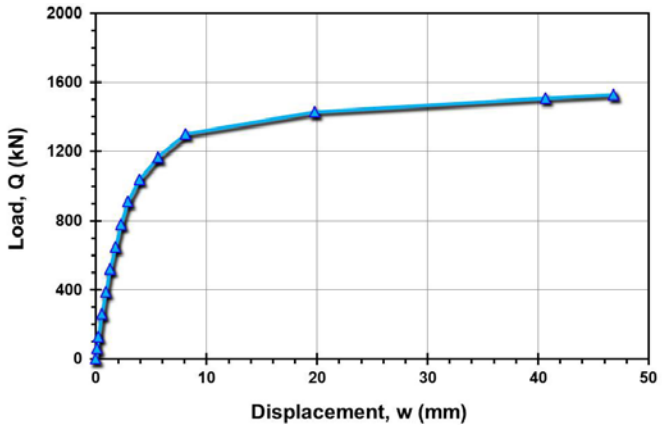

Back-analyzed normalized operational stiffness vs. pseudo-strain

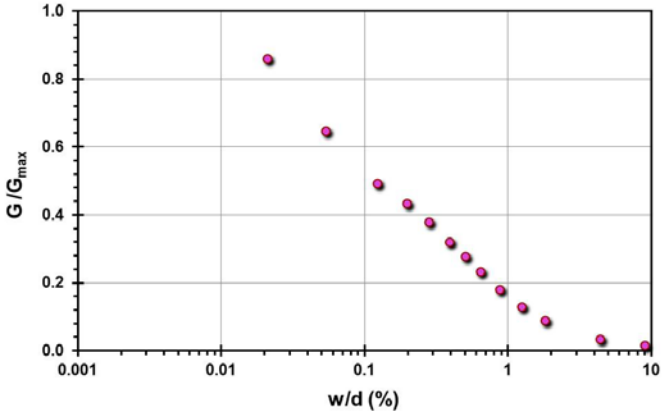

Detail	Description
Pile type/material	Square concrete pile
Length, L (m)	6.00
Width, B (m)	0.35
Installation method	Driven
Loading mode	Compression
$Q_{max\text{-}measured}$ (kN)	1,529.97
Q_s (kN)	Not available
Q_b (kN)	Not available
$Q_{Davisson}$ (kN)	1,300.89
$Q_{w/d=10\%}$ (kN)	1,518.83
$Q_{C\text{-}K}$ (kN)	1,564.95

Site ID No. 67

Cone penetrometer data	CPT SBT soil classification index, I_c	Detail	Description
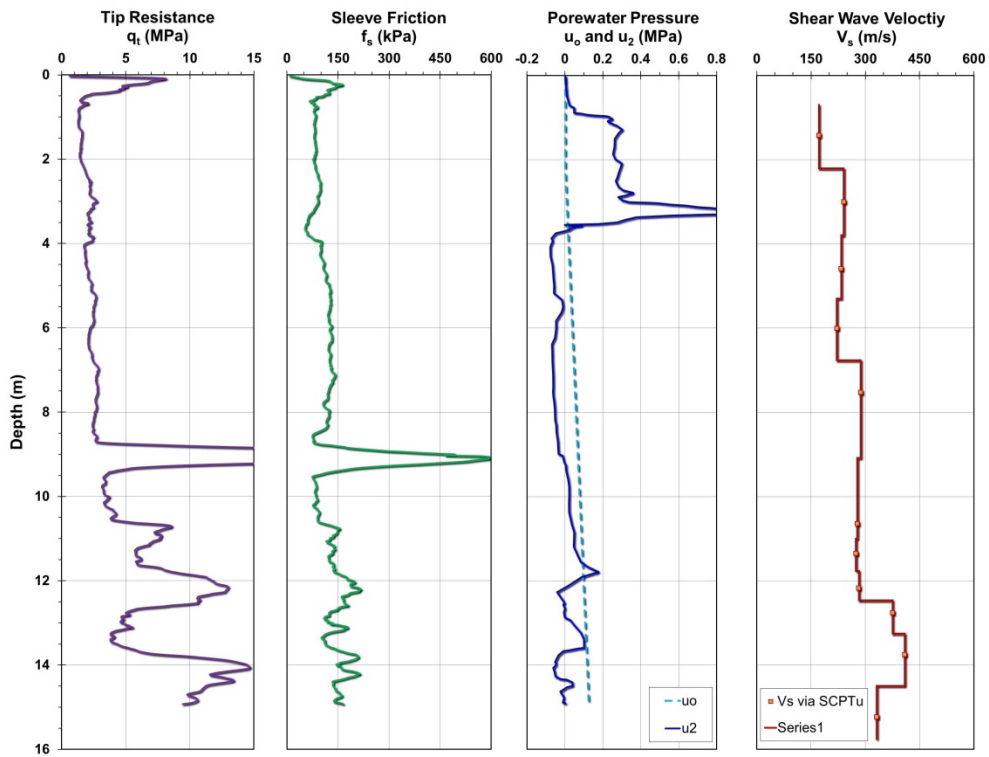	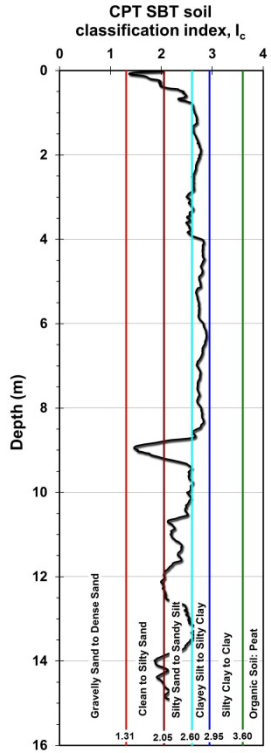	Site name and location	University of Texas NGES, Houston, TX, USA (NGES-UH)
		Soil type(s)	Stiff Beaumont clay over sandy clay
		Pile type(s)	Drilled shaft
		Type of cone penetrometer testing	SCPTu
		Source of V_s evaluation	SCPTu
		Number of pile load tests	1
		Reference	Ata and O'Neill (1998), O'Neill et al. (2002, 1982), Reese et al. (1976)
		Comments	

Pile ID: UH-NGES O1

Load-displacement data

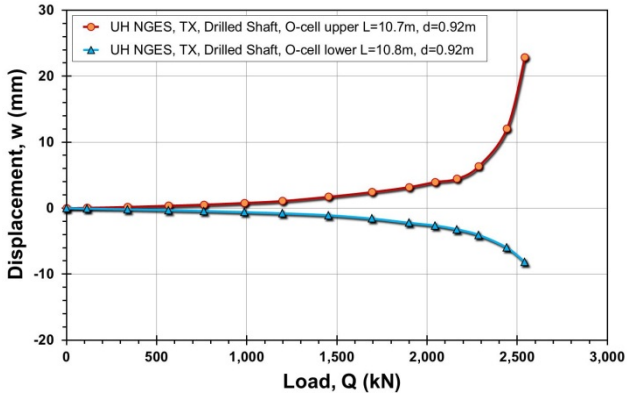

Back-analyzed normalized operational stiffness vs. pseudo-strain

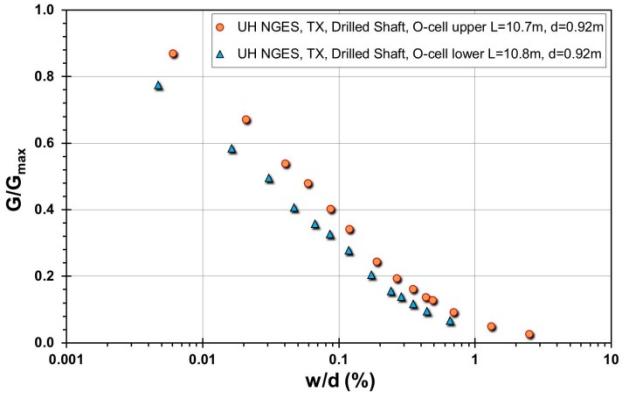

Detail	Description
Pile type/material	Drilled shaft
Length, L (m)	Upper: 10.7; lower: 10.80
Diameter, d (m)	Upper: 0.915; lower: 0.915
Installation method	Bored cast in-situ
Loading mode	O-cell compression
$Q_{max\text{-}measured}$ (kN)	Upper: 2,541.3; lower: 2,541.3
Q_s (kN)	Upper: 2,541.3; lower: 1,596.1
Q_b (kN)	945.2
$Q_{Davisson}$ (kN)	Upper: 2,441.4; lower: 2,660.4
$Q_{w/d=10\%}$ (kN)	Upper: 2,635.1; lower: 2,879.5
$Q_{C\text{-}K}$ (kN)	Upper: 2,666.7; lower: 2,915.5

Site ID No. 68

Cone penetrometer data	CPT SBT soil classification index, I_c	Detail	Description
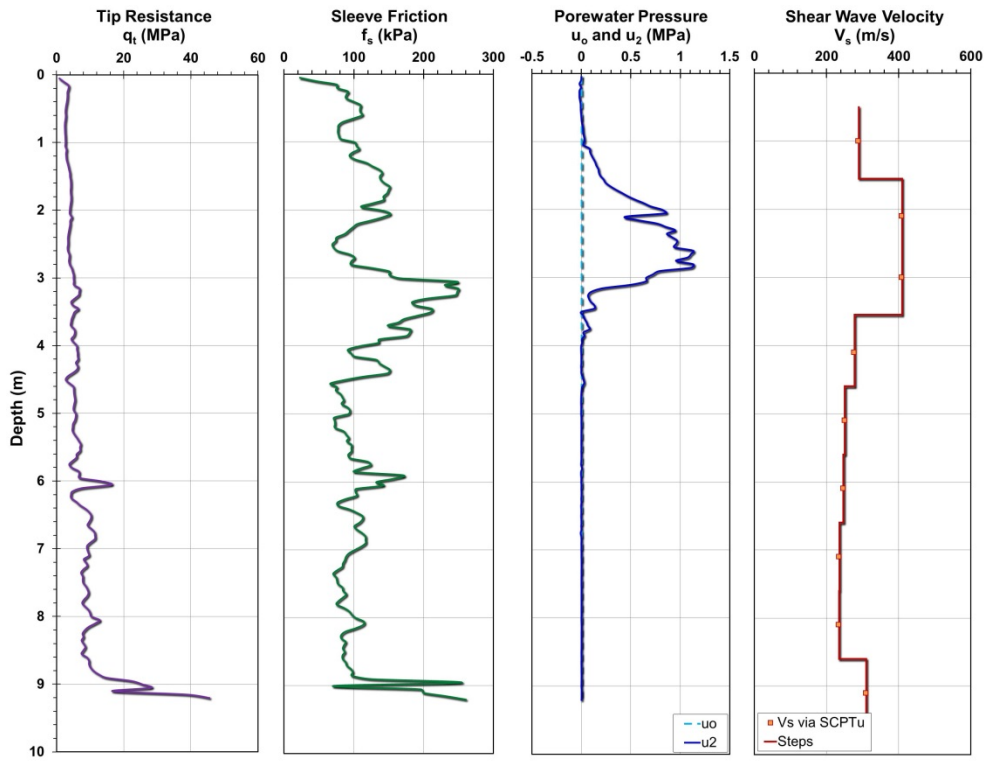	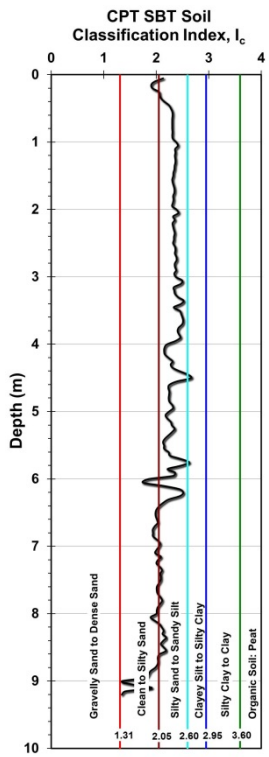	Site name and location	Varina-Enon Bridge, I-295 over James River, Richmond, VA, USA
		Soil type(s)	Alluvial sands, silts, and clays overlying dense sands and gravels
		Pile type(s)	Square concrete pile
		Type of cone penetrometer testing	SCPTu
		Source of V_s evaluation	SCPTu
		Number of pile load tests	1
		Reference	Mayne (2002)
		Comments	

Pile ID: VEB I-295 JR 1

Load-displacement data

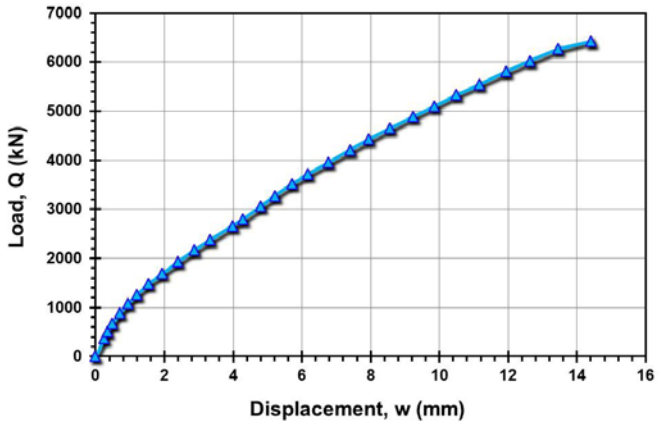

Back-analyzed normalized operational stiffness vs. pseudo-strain

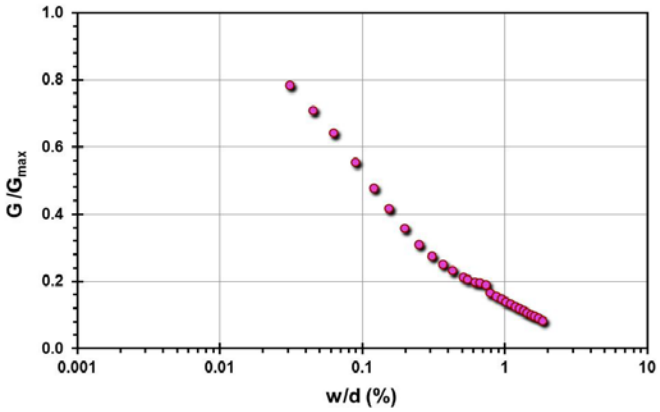

Detail	Description
Pile type/material	Sq-C
Length, L (m)	16.20
Diameter, d (m)	0.61
Installation method	Driven
Loading mode	Compression
$Q_{max\text{-}measured}$ (kN)	6,431.14
Q_s (kN)	Not reported
Q_b (kN)	Not reported
$Q_{Davisson}$ (kN)	7,477.85
$Q_{w/d=10\%}$ (kN)	11,906.73
$Q_{C\text{-}K}$ (kN)	14,705.88

Site ID No. 69

Cone penetrometer data	CPT SBT soil classification index, I_c	Detail	Description
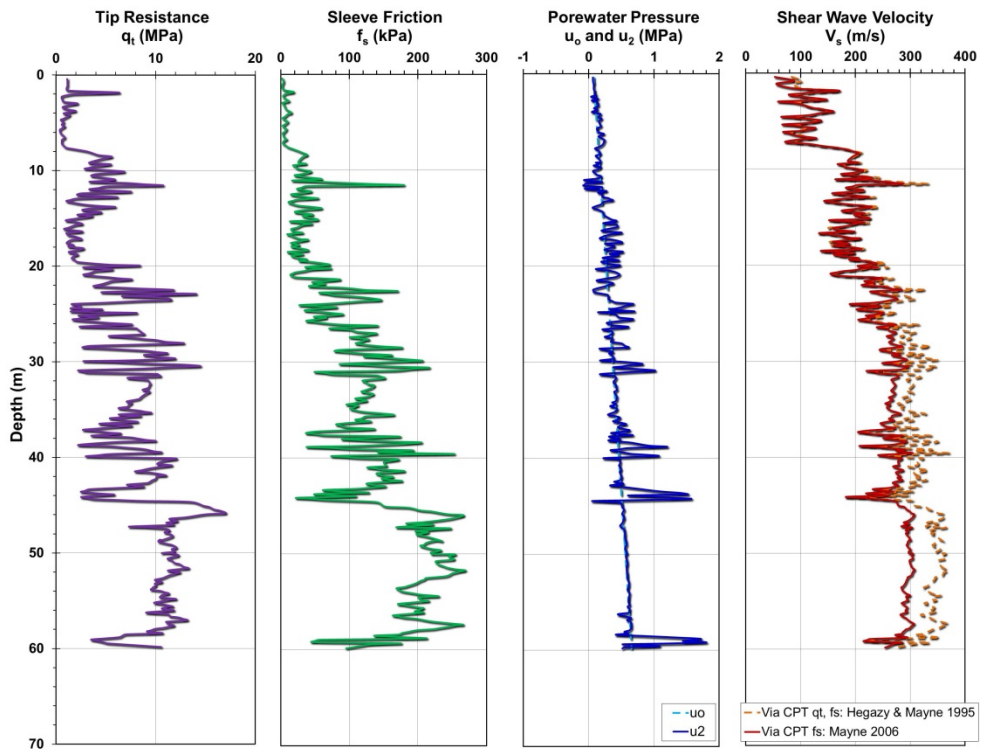	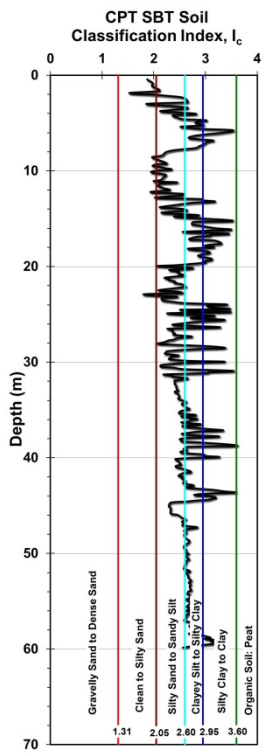	Site name and location	W. R. Bennett Bridge, Okanagan Lake at Kelowna, BC, Canada
		Soil type(s)	Loose to medium dense lacustrine silts and sandy silt overlying sand
		Pile type(s)	Closed-ended steel pile
		Type of cone penetrometer testing	CPTu
		Source of V_s evaluation	Correlations (see Figure opposite and Table 3.1)
		Number of pile load tests	1
		Reference	Naesgaard et al. (2006)
		Comments	

Pile ID: WRBB 1

Load-displacement data

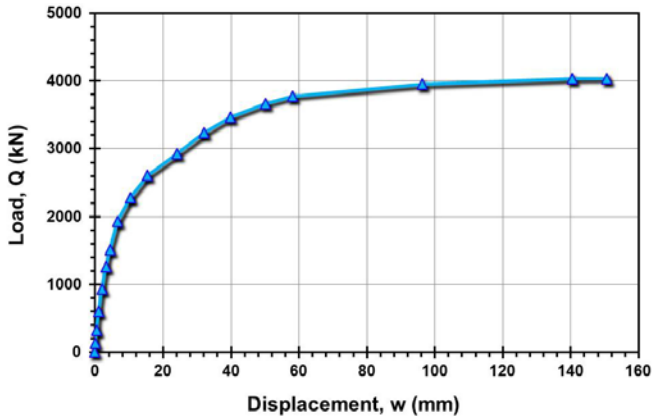

Back-analyzed normalized operational stiffness vs. pseudo-strain

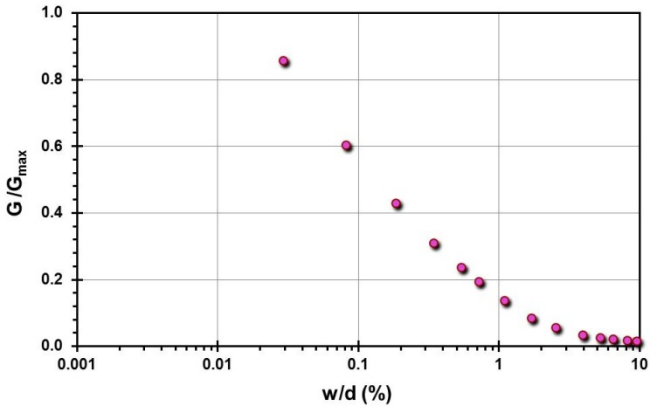

Detail	Description
Pile type/material	Closedended steel pile
Length, L (m)	45.00
Diameter, d (m)	0.61
Installation method	Driven
Loading mode	Compression
$Q_{max\text{-}measured}$ (kN)	4,034.78
Q_s (kN)	1,502.75
Q_b (kN)	2,532.03
$Q_{Davisson}$ (kN)	2,921.74
$Q_{w/d=10\%}$ (kN)	3,810.10
$Q_{C\text{-}K}$ (kN)	4,201.68

Site ID No. 70

Cone penetrometer data	CPT SBT soil classification index, I_c	Detail	Description
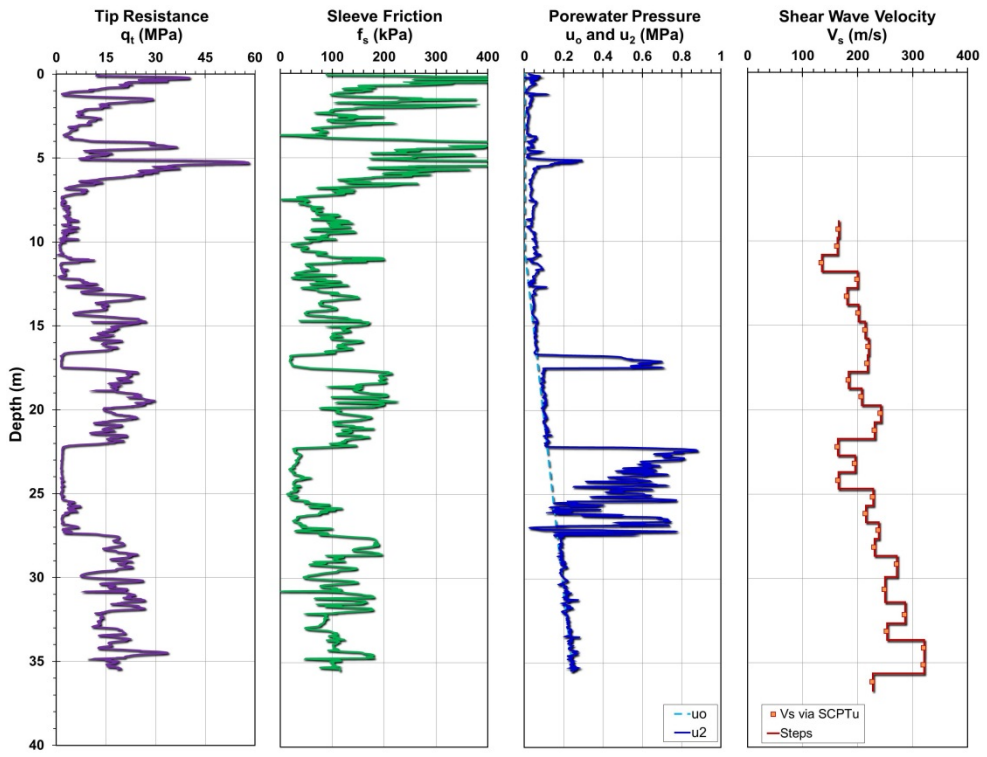	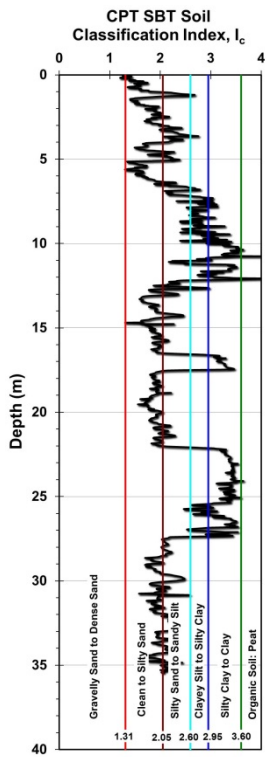	Site name and location	Wakota River Bridge site (I-494 Mississippi River Bridge), MN, USA
		Soil type(s)	Sand with intermittent layers of silt and clay
		Pile type(s)	2 open-ended steel pile and 2 closed-ended steel pile
		Type of cone penetrometer testing	SCPTu
		Source of V_s evaluation	SCPTu
		Number of pile load tests	4
		Reference	Dasenbrock (2006)
		Comments	

Pile ID: WB I-494 MR1A

Load-displacement data

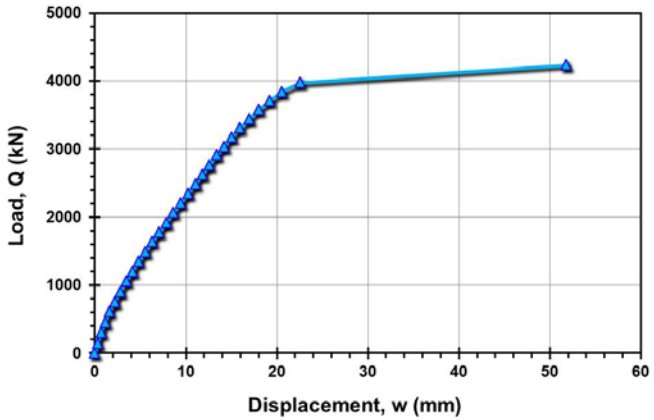

Back-analyzed normalized operational stiffness vs. pseudo-strain

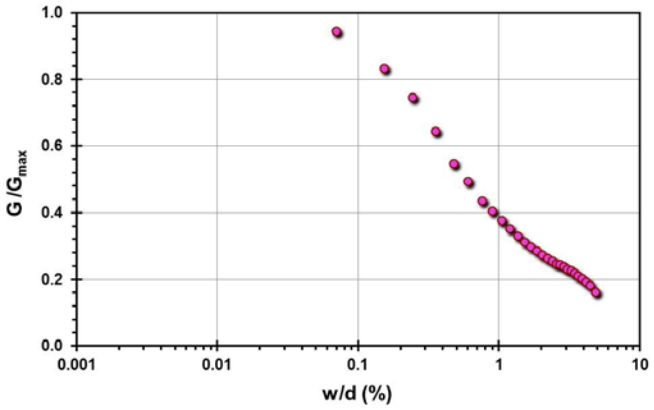

Detail	Description
Pile type/material	Open-ended steel pile
Length, L (m)	32.00
Diameter, d (m)	0.46
Installation method	Driven
Loading mode	Compression
$Q_{max\text{-}measured}$ (kN)	4,242.01
Q_s (kN)	Not reported
Q_b (kN)	Not reported
$Q_{Davisson}$ (kN)	4,221.19
$Q_{w/d=10\%}$ (kN)	4,221.19
$Q_{C\text{-}K}$ (kN)	4,524.89

Pile ID: WB I-494 MR2

Load-displacement data

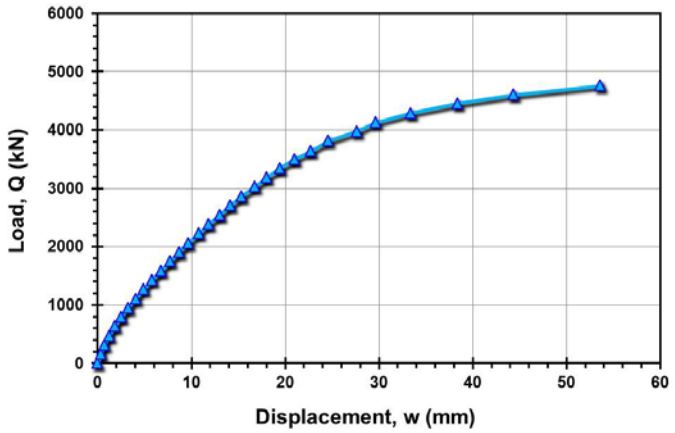

Back-analyzed normalized operational stiffness vs. pseudo-strain

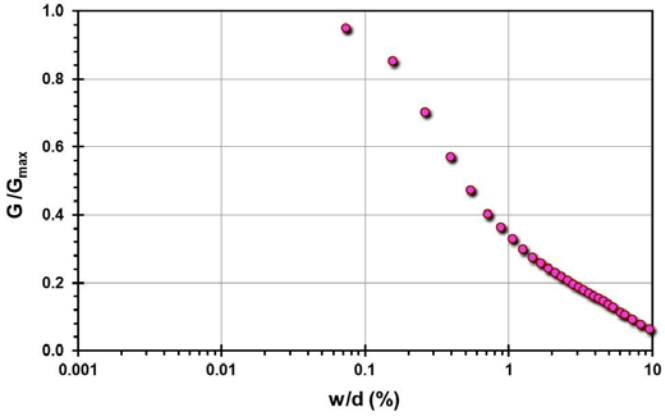

Detail	Description
Pile type/material	Closed-ended steel pile
Length, L (m)	32.00
Diameter, d (m)	0.46
Installation method	Driven
Loading mode	Compression
$Q_{max\text{-}measured}$ (kN)	4,764.40
Q_s (kN)	Not reported
Q_b (kN)	Not reported
$Q_{Davisson}$ (kN)	4,764.40
$Q_{w/d=10\%}$ (kN)	4,634.41
$Q_{C\text{-}K}$ (kN)	5,882.35

Pile ID: WB I-494 MR1A-2

Load-displacement data

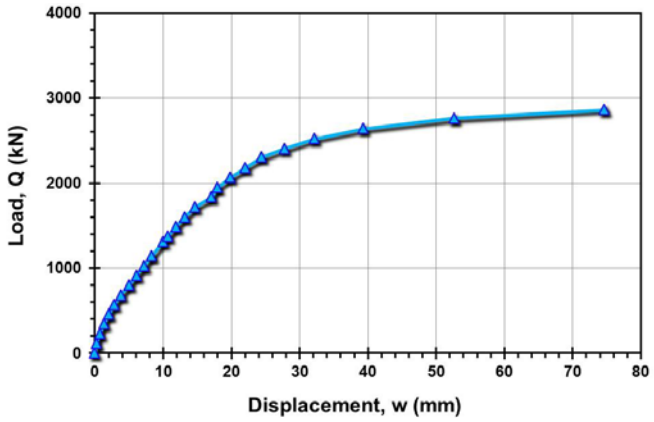

Back-analyzed normalized operational stiffness vs. pseudo-strain

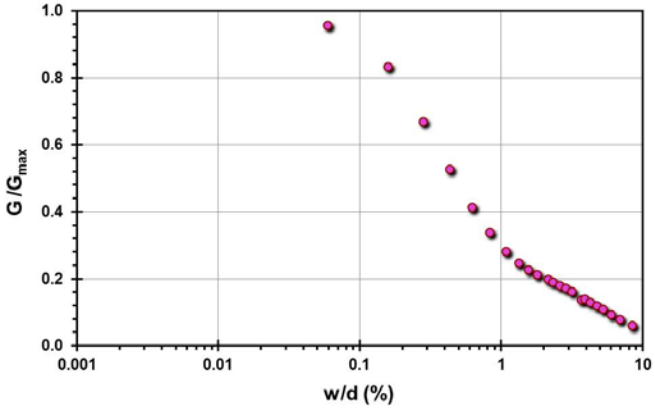

Detail	Description
Pile type/material	Open-ended steel pile
Length, L (m)	32.00
Diameter, d (m)	0.46
Installation method	Driven
Loading mode	Compression
$Q_{max\text{-}measured}$ (kN)	2,867.60
Q_s (kN)	Not reported
Q_b (kN)	Not reported
$Q_{Davisson}$ (kN)	2,465.86
$Q_{w/d=10\%}$ (kN)	2,707.25
$Q_{C\text{-}K}$ (kN)	3,194.89

Pile ID: WB I-494 MR4

Load-displacement data

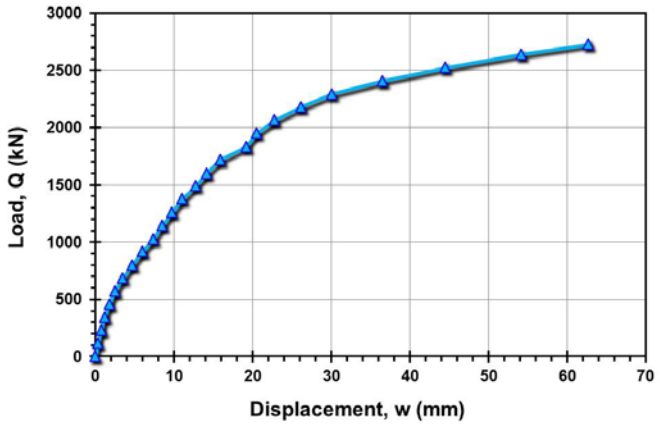

Back-analyzed normalized operational stiffness vs. pseudo-strain

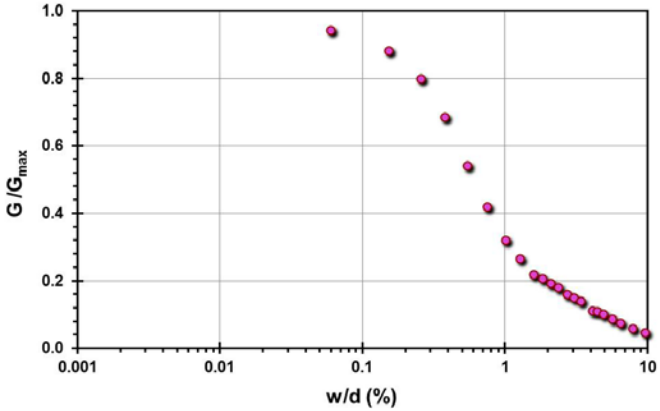

Detail	Description
Pile type/material	Closed-ended steel pile
Length, L (m)	32.00
Diameter, d (m)	0.46
Installation method	Driven
Loading mode	Compression
$Q_{max\text{-}measured}$ (kN)	2,729.32
Q_s (kN)	Not reported
Q_b (kN)	Not reported
$Q_{Davisson}$ (kN)	2,236.97
$Q_{w/d=10\%}$ (kN)	2,555.26
$Q_{C\text{-}K}$ (kN)	3,333.33

APPENDIX F

AXIAL PILE AND CPTu INFORMATION OF GROUP 1 DATASET

This appendix provides a case-by-case tabulated summary of the Group 1 dataset on pile foundation load tests with corresponding CPTu soundings. This dataset consists of 153 pile load tests from 52 sites in 17 different countries. The sites and the axial pile load tests presented here are tied to the comprehensive Table E.1 of Appendix E via the site ID numbers and the pile IDs. The pile information presented here includes pile type/material, pile installation method, pile dimensions, and loading mode. The CPT information includes type of readings collected and depth of investigations at each site, while the detailed profiles are giving in Appendix E.

These data are used in Chapter 6 of this dissertation to improve on the direct pile capacity method (UniCone; Eslami and Fellenius, 1997) by including 50% more pile load test results than the original study. The improvements include a refinement in the grouping of soil type category in the soil behavioral classification charts using effective cone resistance ($q_E = q_t - u_2$) vs. sleeve friction (f_s). This increases the soil classifications from 5 zonal types to a total of 11 types, now expressed as subset soil categories in order to retain the original 5 part zones.

The data are also used to derive continuous and more accurate functions for the unit pile side friction (C_{se}) and unit end bearing resistance (C_{te}). In the original UniCone, only five discrete values of C_{se} are available. Now, a full range of C_{se} is viable ($0.003 < C_{se} < 0.100$) which is shown directly related to the CPT material index, I_c. Also, the type of pile material and method of pile installation are explicitly included in the analysis, improving upon the overall side and base capacity evaluations.

Table F.1. Case record summary for Group 2 dataset: pile data and CPTu soundings.

Site ID no.	Pile data						CPT sounding	
	Pile ID	Type/ material	L (m)	d (m)/ B (m)	Loading mode	Installation method	Available readings	Maximum depth (m)
1	AIT 9	DS	18.00	0.45	C	B-CIS	q_t, f_s, u_2	18.95
2	BU 1	Sq-C	11.0	0.285	C	D	q_c, f_s	17.95
	BU 2	Sq-C	11.0	0.285	T	D		
	BU 3	Sq-C	15.0	0.285	C	D		
5	BK 1/L1T	ICP	5.00	0.102	T	J	q_t, f_s, u_2	8.00
	BK 2/L2C	ICP	4.80	0.102	C	J		
	BK 4s/L1C	ICP	4.75	0.102	C	J		
	BK 3(2)/L1C	ICP	4.70	0.102	C	J		
	BK 2/L1C	ICP	4.80	0.102	C	J		
	BK 4f/L1C	ICP	1.95	0.102	C	J		
6	BC A1	CE-S	4.50	0.168	C	J	q_t, f_s, u_2	17.80
	BC B1	CE-S	4.50	0.168	C	J		
	BC A2	CE-S	4.50	0.168	T	J		
	BC B2	CE-S	4.50	0.168	T	J		
	BC C2	CE-S	4.50	0.168	T	J		
7	CGTS 1	DS	9.35	0.920	T	B-CIS	q_t, f_s, u_2	23.25
	CGTS 2	DS	5.94	1.480	C	B-CIS		
	CGTS 4	DS	6.51	1.480	T	B-CIS		
	CGTS 9	DS	6.27	1.600	T	B-CIS		
8	CP 1	CE-S	4.50	0.168	C	J	q_t, f_s, u_2	17.35
	CP 2	CE-S	4.50	0.168	C	D		
	CP 3	DS	4.50	0.168	C	B-CIS		
	CP 4	ICP	3.95	0.102	C	J		
10	CNN 1	DS	19.30	1.60	O-cell	B-CIS	q_t, f_s, u_2	21.70
13	CW 1/L1T	ICP	3.00	0.102	T	J	q_t, f_s, u_2	24.60
	CW 2/L1C	ICP	3.66	0.102	C	J		
	CW 2/L3C	ICP	3.66	0.102	C	J		
	CW 3/L1T	ICP	3.88	0.102	T	J		
	CW 4/L1C	ICP	3.51	0.102	C	J		
	CW 4s/L1C	ICP	3.92	0.102	C	J		
15	E 1/30.5-1	OE-S	30.50	0.762	C	D	q_t, f_s, u_1	51.75
	E 1/30.5-2	OE-S	30.50	0.762	T	D		
	E 1/38.7-1	OE-S	38.70	0.762	T	D		
	E 1/38.7-2	OE-S	38.70	0.762	C	D		
	E 1/38.7-3	OE-S	38.70	0.762	T	D		
	E 1/47-1	OE-S	47.00	0.762	C	D		
	E 1/47-2	OE-S	47.00	0.762	T	D		
	E 1/47-3	OE-S	47.00	0.762	C	D		
16	E 2/46.7-1	OE-S	46.70	0.762	C	D	q_t, f_s, u_1	54.25
	E 2/46.7-2	OE-S	46.70	0.762	T	D		
	E 2/46.7-3	OE-S	46.70	0.762	C	D		
	E 2/47R-1	OE-S	47.00	0.762	C	D		
	E 2/47R-2	OE-S	47.00	0.762	T	D		
17	FBJ 1	DS	15.00	0.500	C	B-CIS	q_t, f_s, u_2	19.00
18	FSB 1	Sq-C	12.80	0.235	C	D	q_t, f_s, u_2	26.90

Notes: L: pile length; d: pile diameter for piles with circular cross-section; B: pile width for piles with square cross-section; DS: drilled shaft; CFA: continuous flight auger pile; CE-S: closed-ended steel pipe pile; OE-S: open-ended steel pipe pile; OE-SC: open ended concrete filled steel pipe pile; ICP: closed-ended Imperial College pile; HP: H-section steel pile; PTC: pre-stressed concrete thin-wall caisson; PHC: Pre-stressed concrete high-strength; Sq-C: square precast concrete pile; C-C: circular precast concrete pile; C: top-down compression loading mode; T: top-up tension (or uplift) loading mode; O-cell: bi-directional Osterberg cell; A: augered piles; D: driven piles; J: jacked piles; B-CIS: bored cast in-situ piles; q_c = measured cone tip resistance, q_t = corrected cone tip resistance; f_s = sleeve friction; u_2 = excess porewater pressures measured behind the cone tip position; u_1 = excess porewater pressures measured via piezometer element placed at mid-face of the cone tip.

Table F.1. (continued).

Site ID No.	Pile data						CPT sounding	
	Pile ID	Type/ material	L (m)	d (m)/ B (m)	Loading mode	Installation method	Available readings	Maximum depth (m)
19	FCS 1	DS	12.00	0.500	C	B-CIS	q_t, f_s, u_2	14.00
	FCS 2	OE-S	9.40	0.508	C	D		
	FCS 3	OE-S	9.40	0.508	C	J		
	FCS 4	HP	10.20	16 x 155	C	D		
	FCS 5	HP	10.20	16 x 155	C	J		
20	FMC 1	DS	14.00	1.400	O-cell	B-CIS	q_t, f_s, u_2	30.00
21	GT C2	DS	16.92	0.762	C	B-CIS	q_c, f_s	19.20
22	GM Pier 12	DS	25.36	1.570	O-cell	B-CIS	q_t, f_s, u_2	35.30
23	GEB-N1	PTC	36.00	0.357	C	D	q_t, f_s, u_2	77.10
24	GEB-S1	DS	74.5	2.600	O-cell	B-CIS	q_t, f_s, u_2	94.40
25	GEB-S2	DS	32.00	2.500	C	B-CIS	q_t, f_s, u_2	45.20
26	GRS 1	DS	11.76	0.600	C	B-CIS	q_t, f_s, u_1	20.00
27	GBR 1	CE-S	4.50	0.114	C	D	q_t, f_s, u_2	7.80
28	HAFB 1	OE-S	12.19	0.114	C	J	q_t, f_s, u_2	42.75
29	HPHC TP1	CFA	14.00	0.600	C	A	q_t, f_s, u_2	24.90
	HPHC TP2	CFA	18.00	0.600	C	A		
30	HSD A1	C-C	8.00	0.280	C	D	q_t, f_s, u_2	23.80
	HSD D/A1	C-C	16.00	0.280	C	D		
32	I-85B 1	DS	19.20	0.914	C	B-CIS	q_t, f_s, u_2	21.50
34	KG S2T	Sq-C	6.00	0.320	C	D	q_t, f_s, u_2	10.90
	KG S1C	Sq-C	6.00	0.320	T	D		
	KG OE-C1	OE-S	2.01	0.168	C	D		
	KG CE-C1	CE-S	2.80	0.073	C	D		
	KG CE-C4	CE-S	3.25	0.073	C	D		
35	KCS TP-1A	PTC	35.5	0.250	C	J	q_t, f_s, u_2	36.30
37	LB 1/L1C	ICP	5.95	0.102	C	J	q_c, f_s	6.70
	LB 2/L1C	ICP	1.83	0.102	C	J		
	LB 2/L1T	ICP	5.95	0.102	T	J		
38	LTS B6	Sq-C	8.57	0.350	C	D	q_c, f_s	16.15
39	DRS P-I	OE-S	40.20	0.483	C	D	q_t, f_s, u_2	47.75

Notes: L: pile length; d: pile diameter for piles with circular cross-section; B: pile width for piles with square cross-section; DS: drilled shaft; CFA: continuous flight auger pile; CE-S: closed-ended steel pipe pile; OE-S: open-ended steel pipe pile; OE-SC: open ended concrete filled steel pipe pile; ICP: closed-ended Imperial College pile; HP: H-section steel pile; PTC: pre-stressed concrete thin-wall caisson; PHC: Pre-stressed concrete high-strength; Sq-C: square precast concrete pile; C-C: circular precast concrete pile; C: top-down compression loading mode; T: top-up tension (or uplift) loading mode; O-cell: bi-directional Osterberg cell; A: augered piles; D: driven piles; J: jacked piles; B-CIS: bored cast in-situ piles; q_c = measured cone tip resistance, q_t = corrected cone tip resistance; f_s = sleeve friction; u_2 = excess porewater pressures measured behind the cone tip position; u_1 = excess porewater pressures measured via piezometer element placed at mid-face of the cone tip.

Table F.1. (continued).

Site ID No.	Pile data						CPT sounding	
	Pile ID	Type/ material	L (m)	d (m)/ B (m)	Loading mode	Installation method	Available readings	Maximum depth (m)
40	L&D 1-3AC	HP	16.46	14 x 73	C	D	q_t, f_s, u_1	21.95
	L&D 1-6C	HP	16.15	14 x 73	C	D		
41	UBC PRS 1	CE-S	11.83	0.324	C	D	q_t, f_s, u_2	74.45
	UBC PRS 2	CE-S	13.90	0.324	C	D		
	UBC PRS 3	CE-S	16.80	0.324	C	D		
	UBC PRS 5	CE-S	31.10	0.324	C	D		
43	NMGC 1	DS	21.50	0.760	C	B-CIS	q_t, f_s, u_2	22.40
44	NWU NGES 1	HP	15.24	14 x 73	C	D	q_t, f_s, u_2	26.85
	NWU NGES 2	DS	15.24	0.552	C	B-CIS		
	NWU NGES 3	OE-S	15.24	0.457	C	D		
	NWU NGES 4	DS	15.24	0.483	C	B-CIS		
45	NP T1	OE-S	8.30	0.800	C	D	q_t, f_s, u_2	14.75
	NP T2	OE-S	8.30	0.800	C	D		
46	OSJS 1	DS	12.80	0.406	C	B-CIS	q_t, f_s, u_2	15.35
47	OC A1	CE-S	5.00	0.219	T	D	q_t, f_s, u_2	24.70
	OC A2	CE-S	5.00	0.219	T	D		
	OC A3	CE-S	5.00	0.219	T	D		
	OC A4	CE-S	5.00	0.219	T	D		
	OC B1	OE-S	5.00	0.219	T	D		
	OC C1-1	CE-S	5.00	0.219	T	D		
	OC C1-2	CE-S	10.00	0.219	T	D		
	OC C1-3	CE-S	5.00	0.219	T	D		
	OC C1-4	CE-S	5.00	0.219	T	D		
	OC C1-5	CE-S	5.00	0.219	T	D		
48	PT LDP	OE-S	40.00	0.762	C	D	q_t, f_s, u_2	41.25
	PT NGI A5-1	CE-S	10.00	0.219	T	D		
	PT NGI A6-1	CE-S	10.00	0.219	T	D		
	PT 1/L1C	ICP	4.30	0.102	C	J		
	PT 2/L1C	ICP	8.50	0.102	C	J		
	PT 2/L2T	ICP	8.50	0.102	T	J		
	PT 3/L1T	ICP	5.47	0.102	T	J		
	PT 3/L2T	ICP	5.47	0.102	T	J		
	PT 4/L1C	ICP	5.88	0.102	C	J		
	PT 5/L1T	ICP	10.59	0.102	T	J		
	PT 5/L2T	ICP	10.59	0.102	T	J		
	PT 5/L3C	ICP	10.59	0.102	C	J		
	PT 5/L4T	ICP	10.59	0.102	T	J		
	PT 5/L6T	ICP	10.59	0.102	T	J		
	PT 6/L1C	ICP	3.75	0.102	C	J		
	PT 7/L1C	ICP	8.75	0.102	C	J		
	PT 7/L2C	ICP	8.75	0.102	C	J		
	PT 7/L3T	ICP	8.75	0.102	T	J		
49	PPI 1	DS	26.07	1.524	O-Cell	B-CIS	q_t, f_s, u_2	37.25
	PPI 2	DS	35.05	1.524	O-Cell	B-CIS		
50	PRB '73	OE-SC	55.00	0.610	C	D	q_t, f_s, u_2	60.70; 96.85
	PRB '07	OE-SC	100.00	1.824	C	D		

Notes: L: pile length; d: pile diameter for piles with circular cross-section; B: pile width for piles with square cross-section; DS: drilled shaft; CFA: continuous flight auger pile; CE-S: closed-ended steel pipe pile; OE-S: open-ended steel pipe pile; OE-SC: open ended concrete filled steel pipe pile; ICP: closed-ended Imperial College pile; HP: H-section steel pile; PTC: pre-stressed concrete thin-wall caisson; PHC: Pre-stressed concrete high-strength; Sq-C: square precast concrete pile; C-C: circular precast concrete pile; C: top-down compression loading mode; T: top-up tension (or uplift) loading mode; O-cell: bi-directional Osterberg cell; A: augered piles; D: driven piles; J: jacked piles; B-CIS: bored cast in-situ piles; q_c = measured cone tip resistance, q_t = corrected cone tip resistance; f_s = sleeve friction; u_2 = excess porewater pressures measured behind the cone tip position; u_1 = excess porewater pressures measured via piezometer element placed at mid-face of the cone tip.

Table F.1. (continued).

Site ID No.	Pile data						CPT sounding	
	Pile ID	Type/ material	L (m)	d (m)/ B (m)	Loading mode	Installation method	Available readings	Maximum depth (m)
53	SPI 1	CE-S	45.00	0.406	C	D	q_t, f_s, u_2	79.90
55	SPP P01	OE-S	4.00	0.089	T	D	q_c, f_s	6.00
	SPP P02	OE-S	4.00	0.043	T	D		
	SPP P03	CE-S	4.00	0.089	T	D		
	SPP P04	OE-S	4.00	0.089	T	D		
	SPP P05	OE-S	4.00	0.114	T	D		
	SPP P06	OE-S	4.00	0.089	T	D		
	SPP P07	OE-S	2.50	0.043	T	D		
	SPP P08	OE-S	2.50	0.043	T	D		
	SPP P09	OE-S	2.50	0.034	T	D		
	SPP P10	OE-S	3.50	0.034	T	D		
	SPP P11	OE-S	2.50	0.089	T	D		
	SPP P12	CE-S	2.50	0.089	T	D		
56	SSK A	DS	52.40	1.100	C	B-CIS	q_t, f_s, u_2	64.98
57	STTS P24	CE-S	12.20	0.324	C	D	q_t, f_s, u_2	13.95
	STTS P14-1	CE-S	12.20	0.324	C	D		
58	S NGES 24C	DS	11.00	0.914	C	B-CIS	q_t, f_s, u_2	15.24
	S NGES 1LP	DS	11.00	0.914	C	B-CIS		
	S NGES 24B	DS	11.00	0.914	C	B-CIS		
	S NGES 24CDef	DS	11.00	0.914	C	B-CIS		
	S NGES A1	CFA	11.00	0.450	C	A		
59	SR49 P1	HP	17.40	12 x 74	C	D	q_t, f_s, u_2	17.92;
	SR49 P2	CE-S	17.40	0.356	C	D		25.79
60	TAMU-C NGES BP7	DS	9.50	0.915	C	B-CIS	q_t, f_s, u_1	14.92
61	TAMU-S NGES BP4	DS	9.40	0.941	C	B-CIS	q_t, f_s, u_1	14.92
	TAMU-S NGES O1	DS	21.50	0.915	O-cell	B-CIS		
63	TH52 PAT2	CE-SC	42.30	0.410	C	D	q_t, f_s, u_2	42.95
	TH52 MAT2	CE-S	20.29	0.356	C	D		
64	UCD P1	OE-S	4.00	0.168	C	J	q_c, f_s	5.95
65	UMASS NGES1	DS	13.11	0.878	C	B-CIS	q_t, f_s, u_2	15.55
	UMASS NGES2	DS	14.30	0.955	C	B-CIS		
68	WRBB 1	CE-S	45.00	0.610	C	D	q_t, f_s, u_2	59.80

Notes: L: pile length; d: pile diameter for piles with circular cross-section; B: pile width for piles with square cross-section; DS: drilled shaft; CFA: continuous flight auger pile; CE-S: closed-ended steel pipe pile; OE-S: open-ended steel pipe pile; OE-SC: open ended concrete filled steel pipe pile; ICP: closed-ended Imperial College pile; HP: H-section steel pile; PTC: pre-stressed concrete thin-wall caisson; PHC: Pre-stressed concrete high-strength; Sq-C: square precast concrete pile; C-C: circular precast concrete pile; C: top-down compression loading mode; T: top-up tension (or uplift) loading mode; O-cell: bi-directional Osterberg cell; A: augered piles; D: driven piles; J: jacked piles; B-CIS: bored cast in-situ piles; q_c = measured cone tip resistance, q_t = corrected cone tip resistance; f_s = sleeve friction; u_2 = excess porewater pressures measured behind the cone tip position; u_1 = excess porewater pressures measured via piezometer element placed at mid-face of the cone tip.

APPENDIX G

PILE AND SOIL PARAMETERS FOR BACKFIGURED OPERATIONAL SHEAR MODULI

This appendix provides a case-by-case summary of certain specific information of the Group 2 category of the database [i.e., 299 pile load tests of the types C (compression) and T (tension) from 61 sites, affording the Q-w data]. This subset of the database was used to backfigure the operative shear stiffness (G) values using the load test data and Randolph elastic solutions. The profiles of small-strain modulus (G_{max}) were obtained from V_s readings taken along the pile embedment length. Herein, Table G.1 presents the values of different input properties and parameters of test piles and soil conditions at each site. Each load test was evaluated within the framework of the elastic continuum solutions. To tie this set of the data to Table E.1, the following sets of information are reproduced in the first six columns of Table G.1: (1) site ID; (2) pile ID; (3) loading mode; (4) installation method; (5) pile length; and (6) pile diameter. The remaining columns present key pile information and soil properties that were used in the backanalysis of normalized G values (i.e., G/G_{max}) shown as functions of percent pseudo-strains [γ_p (%), where $\gamma_p = w_t/d$], and later in developing the trend-based algorithms and charts for different pile types and soil conditions. In the later part of this appendix, the individual profiles of initial shear stiffness (G_{max}) for each case in the entire Group 2 dataset are presented, followed by the results on investigations for the influence of plasticity characteristics (e.g., PI) on the derived shear modulus reduction curves.

Table G.1. Pile and soil parameters for elastic continuum solution.

Site ID	Pile ID	Loading mode	Installation method	L (m)	d or B (m)	E_p (kN)	$G_{L(max)}$ (kN)	$G_{b\text{-}max}$ (kN)	ρ_E	ν_s	η	ξ	Representative PI (%)
1	AIT 1-1	C	D	6.00	0.150	9,500,000	12,192	51,724	0.85	0.5	1.0	0.24	55
	AIT 1-2	C	D	6.00	0.150	9,500,000	12,192	51,724	0.85	0.5	1.0	0.24	55
	AIT 2-1	C	D	6.00	0.150	9,500,000	12,192	51,724	0.85	0.5	1.0	0.24	55
	AIT 2-2	C	D	6.00	0.150	9,500,000	12,192	51,724	0.85	0.5	1.0	0.24	55
	AIT 3-1	C	D	6.00	0.150	9,500,000	12,192	51,724	0.85	0.5	1.0	0.24	55
	AIT 3-2	C	D	6.00	0.150	9,500,000	12,192	51,724	0.85	0.5	1.0	0.24	55
	AIT 4-1	C	D	6.00	0.150	9,500,000	12,192	51,724	0.85	0.5	1.0	0.24	55
	AIT 4-2	C	D	6.00	0.150	9,500,000	12,192	51,724	0.85	0.5	1.0	0.24	55
2	BU 1	C	D	11.00	0.285	35,000,000	143,880	143,880	0.73	0.2	1.0	1.00	NP
	BU 2	T	D	11.00	0.285	35,000,000	143,880	143,880	0.73	0.2	1.0	1.00	NP
	BU 3	C	D	15.00	0.285	35,000,000	145,695	166,440	0.78	0.2	1.0	0.87	NP
3	Bl 1	C	D	2.70	0.073	39,500,000	123,282	123,282	0.74	0.2	1.0	1.00	NP
	Bl 2	C	J	2.49	0.073	39,500,000	118,387	118,387	0.75	0.2	1.0	1.00	NP
4	BCS 1	C	D	6.35	0.35	35,500,000	61,155	61,155	1.00	0.5	0.9	1.00	45
	BCS 2	C	A	6.31	0.38	33,800,000	61,155	61,155	1.00	0.5	1.2	1.00	45
	BCS 3	C	A	10.48	0.38	33,800,000	61,185	61,185	1.00	0.5	1.2	1.00	45
	BCS 4	C	D	10.60	0.35	35,500,000	61,185	61,185	1.00	0.5	0.9	1.00	45
	BCS 5	C	A	6.46	0.41	37,900,000	61,155	61,155	1.00	0.5	1.0	1.00	45
	BCS 6	C	A	10.66	0.41	38,000,000	61,185	61,185	1.00	0.5	1.0	1.00	45
	BCS 7	C	A	10.71	0.51	35,400,000	61,185	61,185	1.00	0.5	1.0	1.00	45
	BCS 8	C	A	6.53	0.51	35,600,000	61,155	61,155	1.00	0.5	1.0	1.00	45
	BCS 9	C	A	6.59	0.41	39,200,000	61,155	61,155	1.00	0.5	1.0	1.00	45
	BCS 10	C	A	10.81	0.41	39,200,000	61,190	61,190	1.00	0.5	1.0	1.00	45
	BCS 11	C	A	10.81	0.51	37,600,000	61,190	61,190	1.00	0.5	1.0	1.00	45
	BCS 12	C	A	6.76	0.51	38,400,000	61,155	61,155	1.00	0.5	1.0	1.00	45
5	BK 1/L1T	T	J	5.00	0.102	67,800,000	18,060	18,060	0.87	0.5	1.0	1.00	29
	BK 2/L1C	C	J	4.80	0.102	67,800,000	18,060	18,060	0.87	0.5	1.0	1.00	29
	BK 2/L2C	C	J	4.80	0.102	67,800,000	18,060	18,060	0.87	0.5	1.0	1.00	29
	BK 3(1)/L1C	C	J	1.95	0.102	67,800,000	15,340	15,340	0.94	0.5	1.0	1.00	29
	BK 3(2)/L1C	C	J	4.70	0.102	67,800,000	17,965	17,965	0.88	0.5	1.0	1.00	29
	BK 4f/L1C	C	J	1.95	0.102	67,800,000	15,340	15,340	0.94	0.5	1.0	1.00	29
	BK 4s/L1C	C	J	4.75	0.102	67,800,000	18,015	18,015	0.87	0.5	1.0	1.00	29

Notes: C: top-down compression loading mode; T: top-up tension (or uplift) loading mode; A: augered piles; D: driven piles; J: jacked piles; B-CIS: bored cast in-situ piles; L: pile length; d: pile diameter for piles with circular cross-section; B: pile width for piles with square cross-section; E_p = pile modulus; G_{max} = initial soil shear modulus at pile base; $G_{b\text{-}max}$ = initial soil shear modulus below the pile base for end-bearing type piles; ρ_E = modulus variation factor; ν_s = soil's Poisson's ratio; η = factor for underreamed piles = r_b/r_o, where r_b = pile base radius and r_o = pile shaft radius; ξ = $G_{max}/G_{b\text{-}max}$; PI = plasticity index, NP = non-plastic; NR = not reported.

Table G.1. (continued).

Site ID	Pile ID	Loading mode	Installation method	L (m)	d or B (m)	E_p (kN)	$G_{L(max)}$ (kN)	$G_{b\text{-}max}$ (kN)	ρ_E	ν_s	η	ξ	Representative PI (%)
6	BC A1	C	J	4.50	0.17	29,500,000	34,965	34,965	0.74	0.5	1.0	1.00	53
	BC B1	C	J	4.50	0.17	29,500,000	34,965	34,965	0.74	0.5	1.0	1.00	53
	BC C1	C	J	4.50	0.17	29,500,000	34,965	34,965	0.74	0.5	1.0	1.00	53
	BC A2	T	J	4.50	0.17	29,500,000	34,965	34,965	0.74	0.5	1.0	1.00	53
	BC B2	T	J	4.50	0.17	29,500,000	34,965	34,965	0.74	0.5	1.0	1.00	53
	BC C2	T	J	4.50	0.17	29,500,000	34,965	34,965	0.74	0.5	1.0	1.00	53
7	CGTS 2	C	B-CIS	5.94	1.48	30,000,000	13,485	13,485	0.96	0.5	1.0	1.00	24
	CGTS 4	T	B-CIS	6.51	1.48	30,000,000	13,586	13,586	0.96	0.5	1.0	1.00	24
	CGTS 9	T	B-CIS	6.27	1.60	30,000,000	13,543	13,543	0.96	0.5	1.0	1.00	24
8	CP 1	C	J	4.50	0.168	27,500,000	73,575	73,575	0.70	0.5	1.0	1.00	45
	CP 2	C	D	4.50	0.168	27,500,000	73,575	73,575	0.70	0.5	1.0	1.00	45
	CP 3	C	B-CIS	4.50	0.168	30,000,000	73,575	73,575	0.70	0.5	1.0	1.00	45
	CP 4	C	J	3.95	0.102	67,800,000	68,165	68,165	0.72	0.5	1.0	1.00	45
9	C Pt 1	C	D	21.33	0.305	30,000,000	260,540	260,540	0.85	0.2	1.0	1.00	NR
	C Pt 2	C	D	15.24	0.305	30,000,000	238,220	238,220	0.88	0.2	1.0	1.00	NR
13	CW 1/L1T	T	J	3.00	0.102	67,800,000	89,175	89,175	0.98	0.5	1.0	1.00	24
	CW 2/L1C	C	J	3.66	0.102	67,800,000	94,360	94,360	0.95	0.5	1.0	1.00	24
	CW 2/L3C	C	J	3.66	0.102	67,800,000	94,360	94,360	0.95	0.5	1.0	1.00	24
	CW 3/L1T	T	J	3.88	0.102	67,800,000	94,310	94,310	0.95	0.5	1.0	1.00	24
	CW 4/L1C	C	J	3.51	0.102	67,800,000	93,390	93,390	0.95	0.5	1.0	1.00	24
	CW 4s/L1C	C	J	3.92	0.102	67,800,000	94,410	94,410	0.95	0.5	1.0	1.00	24
14	DK 1/L1C	C	J	7.40	0.102	67,800,000	83,775	83,775	1.00	0.2	1.0	1.00	NP
	DK 1/L2T	T	J	7.40	0.102	67,800,000	83,775	83,775	1.00	0.2	1.0	1.00	NP
	DK 1/L3T	T	J	7.40	0.102	67,800,000	83,775	83,775	1.00	0.2	1.0	1.00	NP
	DK 2/L1C	C	J	5.96	0.102	67,800,000	83,775	83,775	1.00	0.2	1.0	1.00	NP
	DK 2/L2C	C	J	5.96	0.102	67,800,000	83,775	83,775	1.00	0.2	1.0	1.00	NP
	DK 2/L3T	T	J	5.96	0.102	67,800,000	83,775	83,775	1.00	0.2	1.0	1.00	NP
	DK 2/L4C	C	J	5.96	0.102	67,800,000	83,775	83,775	1.00	0.2	1.0	1.00	NP
	DK 3/L1T	T	J	7.40	0.102	67,800,000	83,775	83,775	1.00	0.2	1.0	1.00	NP
	DK 3/L2C	C	J	7.40	0.102	67,800,000	83,775	83,775	1.00	0.2	1.0	1.00	NP
	DK 3/L4C	C	J	7.54	0.102	67,800,000	83,775	83,775	1.00	0.2	1.0	1.00	NP
	DK 3/L5C	C	J	7.54	0.102	67,800,000	83,775	83,775	1.00	0.2	1.0	1.00	NP
	DK 3/L6T	T	J	7.54	0.102	67,800,000	83,775	83,775	1.00	0.2	1.0	1.00	NP

Notes: C: top-down compression loading mode; T: top-up tension (or uplift) loading mode; A: augered piles; D: driven piles; J: jacked piles; B-CIS: bored cast in-situ piles; L: pile length; d: pile diameter for piles with circular cross-section; B: pile width for piles with square cross-section; E_p = pile modulus; G_{max} = initial soil shear modulus at pile base; $G_{b\text{-}max}$ = initial soil shear modulus below the pile base for end-bearing type piles; ρ_E = modulus variation factor; ν_s = soil's Poisson's ratio; η = factor for underreamed piles = r_b/r_o, where r_b = pile base radius and r_o = pile shaft radius; ξ = $G_{max}/G_{b\text{-}max}$; PI = plasticity index, NP = non-plastic; NR = not reported.

Table G.1. (continued).

Site ID	Pile ID	Loading mode	Installation method	L (m)	d or B (m)	E_p (kN)	$G_{L(max)}$ (kN)	$G_{b\text{-}max}$ (kN)	ρ_E	ν_s	η	ξ	Representative PI (%)
14	DK CS'T89a	T	D	11.30	0.324	44,500,000	106,860	106,860	0.87	0.2	1.0	1.00	NP
	DK CS'T89b	T	D	11.60	0.324	44,500,000	107,625	107,625	0.86	0.2	1.0	1.00	NP
	DK CS'C89a	C	D	11.30	0.324	44,500,000	106,860	106,860	0.87	0.2	1.0	1.00	NP
	DK CS'C89b	C	D	11.60	0.324	44,500,000	107,625	107,625	0.86	0.2	1.0	1.00	NP
	DK CS'T94	T	D	11.60	0.324	44,500,000	107,625	107,625	0.86	0.2	1.0	1.00	NP
	DK CL'T89a	T	D	11.30	0.324	30,120,000	106,860	106,860	0.87	0.2	1.0	1.00	NP
	DK CL'T89b	T	D	11.60	0.324	30,120,000	107,625	107,625	0.86	0.2	1.0	1.00	NP
	DK CL'C89a	C	D	11.30	0.324	30,120,000	106,860	106,860	0.87	0.2	1.0	1.00	NP
	DK CL'C89b	C	D	11.60	0.324	30,120,000	107,625	107,625	0.86	0.2	1.0	1.00	NP
	DK LS'T94	T	D	22.10	0.324	44,500,000	129,500	129,500	0.81	0.2	1.0	1.00	NP
15	E 1/30.5-1	C	D	30.50	0.762	36,000,000	82,160	82,160	0.80	0.2	1.0	1.00	NP
	E 1/30.5-2	T	D	30.50	0.762	36,000,000	82,160	82,160	0.80	0.2	1.0	1.00	NP
	E 1/38.7-1	T	D	38.70	0.762	36,000,000	281,630	281,630	0.51	0.2	1.0	1.00	NP
	E 1/38.7-2	C	D	38.70	0.762	36,000,000	281,630	281,630	0.51	0.2	1.0	1.00	NP
	E 1/38.7-3	T	D	38.70	0.762	36,000,000	281,630	281,630	0.51	0.2	1.0	1.00	NP
	E 1/47.0-1	C	D	47.00	0.762	36,000,000	339,430	339,430	0.54	0.2	1.0	1.00	NP
	E 1/47.0-2	T	D	47.00	0.762	36,000,000	339,430	339,430	0.54	0.2	1.0	1.00	NP
	E 1/47.0-3	C	D	47.00	0.762	36,000,000	339,430	339,430	0.54	0.2	1.0	1.00	NP
16	E 2/46.7-1	C	D	46.70	0.762	36,000,000	337,450	337,450	0.54	0.2	1.0	1.00	NP
	E 2/46.7-2	T	D	46.70	0.762	36,000,000	337,450	337,450	0.54	0.2	1.0	1.00	NP
	E 2/46.7-3	C	D	46.70	0.762	36,000,000	337,450	337,450	0.54	0.2	1.0	1.00	NP
	E 2/47.0R-1	C	D	47.00	0.762	36,000,000	339,430	339,430	0.54	0.2	1.0	1.00	NP
	E 2/47.0R -2	T	D	47.00	0.762	36,000,000	339,430	339,430	0.54	0.2	1.0	1.00	NP
17	FBJ 1	C	B-CIS	15.00	0.500	35,000,000	201,090	201,090	0.66	0.5	1.0	1.00	NR
18	FSB 1	C	D	12.80	0.235	30,000,000	64,170	64,170	0.64	0.2	1.0	1.00	NP
19	FCS 1	C	B-CIS	12.00	0.500	30,000,000	52,495	52,495	0.81	0.5	1.0	1.00	63
	FCS 2	C	D	9.40	0.508	25,700,000	48,150	48,150	0.84	0.5	1.0	1.00	63
	FCS 3	C	J	9.40	0.508	25,700,000	48,150	48,150	0.84	0.5	1.0	1.00	63
	FCS 4	C	D	10.20	16 x 155	38,800,000	49,480	49,480	0.83	0.5	1.0	1.00	63
	FCS 5	C	J	10.20	16 x 155	38,800,000	49,480	49,480	0.83	0.5	1.0	1.00	63
21	GT C1	C	B-CIS	21.40	0.762	27,600,000	273,735	411,000	0.54	0.5	1.0	1.00	11
	GT C2	C	B-CIS	16.92	0.762	27,600,000	221,070	221,070	0.55	0.5	1.0	1.00	11

Notes: C: top-down compression loading mode; T: top-up tension (or uplift) loading mode; A: augered piles; D: driven piles; J: jacked piles; B-CIS: bored cast in-situ piles; L: pile length; d: pile diameter for piles with circular cross-section; B: pile width for piles with square cross-section; E_p = pile modulus; G_{max} = initial soil shear modulus at pile base; $G_{b\text{-}max}$ = initial soil shear modulus below the pile base for end-bearing type piles; ρ_E = modulus variation factor; ν_s = soil's Poisson's ratio; η = factor for underreamed piles = r_b/r_o, where r_b = pile base radius and r_o = pile shaft radius; ξ = $G_{max}/G_{b\text{-}max}$; PI = plasticity index, NP = non-plastic; NR = not reported.

Table G.1. (continued).

Site ID	Pile ID	Loading mode	Installation method	L (m)	d or B (m)	E_p (kN)	$G_{L(max)}$ (kN)	$G_{b\text{-}max}$ (kN)	ρ_E	ν_s	η	ξ	Representative PI (%)
23	GEB N1	C	D	36.00	0.357	35,000,000	85,915	85,915	0.59	0.5	1.0	1.00	25
25	GEB S2	C	B-CIS	32.00	2.500	40,000,000	89,890	89,890	0.59	0.5	1.0	1.00	42
26	GRS 1	C	B-CIS	11.76	0.600	30,000,000	185,630	198,160	0.81	0.5	1.0	0.94	14
27	GBR 1	C	D	4.50	0.114	75,300,000	4,350	4,350	0.77	0.5	1.0	1.00	105
28	HAFB 1	C	J	12.19	0.114	33,000,000	15,500	15,500	0.60	0.5	1.0	1.00	37
29	HPHC TP1	C	A	14.00	0.600	44,800,000	43,460	43,460	0.71	0.5	1.0	1.00	26
	HPHC TP2	C	A	18.00	0.600	44,800,000	48,560	48,560	0.70	0.5	1.0	1.00	26
30	HSD E1	C	D	3.50	0.28	30,000,000	50,500	39,590	1.00	0.2	1.0	1.20	NP
	HSD E2	C	D	7.50	0.28	30,000,000	36,515	38,850	1.00	0.2	1.0	0.94	NP
	HSD E3	C	D	11.50	0.28	30,000,000	41,215	47,300	0.91	0.2	1.0	0.87	NP
	HSD E4	C	D	15.50	0.28	30,000,000	71,060	62,800	0.60	0.2	1.0	1.12	NP
	HSD E5	C	D	19.50	0.28	30,000,000	85,760	145,700	0.58	0.2	1.0	0.59	NP
	HSD E6	C	D	23.50	0.28	30,000,000	122,275	157,925	0.50	0.2	1.0	0.77	NP
	HSD A1	C	D	8.00	0.28	30,000,000	36,510	38,850	1.00	0.2	1.0	0.94	NP
	HSD D/A1	C	D	16.00	0.28	30,000,000	72,900	62,810	0.60	0.2	1.0	1.16	NP
	HSD E7	T	D	23.50	0.28	30,000,000	122,275	157,925	0.50	0.2	1.0	0.77	NP
	HSD A2	T	D	8.00	0.28	30,000,000	36,510	38,850	1.00	0.2	1.0	0.94	NP
	HSD D/A2	T	D	16.00	0.28	30,000,000	72,900	62,810	0.60	0.2	1.0	1.16	NP
31	IMTDC 1	C	J	29.00	0.50	30,000,000	88,750	106,500	0.71	0.5	1.0	0.83	NR
32	I-85B 1	C	B-CIS	19.20	0.914	30,000,000	132,230	200,000	0.58	0.2	1.0	0.66	NP
33	JCEPF 1	C	D	9.45	0.273	30,000,000	104,360	104,360	0.73	0.2	1.0	1.00	NP
	JCEPF 2	C	D	17.80	0.273	30,000,000	153,380	153,380	0.66	0.2	1.0	1.00	NP

Notes: C: top-down compression loading mode; T: top-up tension (or uplift) loading mode; A: augered piles; D: driven piles; J: jacked piles; B-CIS: bored cast in-situ piles; L: pile length; d: pile diameter for piles with circular cross-section; B: pile width for piles with square cross-section; E_p = pile modulus; G_{max} = initial soil shear modulus at pile base; $G_{b\text{-}max}$ = initial soil shear modulus below the pile base for end-bearing type piles; ρ_E = modulus variation factor; ν_s = soil's Poisson's ratio; η = factor for underreamed piles = r_b/r_o, where r_b = pile base radius and r_o = pile shaft radius; ξ = $G_{max}/G_{b\text{-}max}$; PI = plasticity index, NP = non-plastic; NR = not reported.

Table G.1. (continued).

Site ID	Pile ID	Loading mode	Installation method	L (m)	d or B (m)	E_p (kN)	$G_{L(max)}$ (kN)	$G_{b\text{-}max}$ (kN)	ρ_E	ν_s	η	ξ	Representative PI (%)
34	KG S2T	T	D	6.00	0.32	33,450,000	8,520	8,520	1.00	0.5	1.0	1.00	33
	KG S1C	C	D	6.00	0.32	33,450,000	8,520	8,520	1.00	0.5	1.0	1.00	33
	KG G3C	C	D	6.00	0.32	33,450,000	8,520	8,520	1.00	0.5	1.0	1.00	33
	KG G1crT(r)	T	D	6.00	0.32	33,450,000	8,520	8,520	1.00	0.5	1.0	1.00	33
	KG S4T	T	D	6.00	0.32	33,450,000	8,520	8,520	1.00	0.5	1.0	1.00	33
	KG S4T(r)	T	D	6.00	0.32	33,450,000	8,520	8,520	1.00	0.5	1.0	1.00	33
	KG S1T	T	D	6.00	0.32	33,450,000	8,520	8,520	1.00	0.5	1.0	1.00	33
	KG OE-C1	C	D	2.01	0.168	40,550,000	8,580	8,580	1.00	0.5	1.0	1.00	35
	KG CE-C1	C	D	2.80	0.073	38,090,000	8,460	8,460	1.00	0.5	1.0	1.00	35
	KG CE-C4	C	D	3.25	0.073	38,090,000	8,460	8,460	1.00	0.5	1.0	1.00	35
35	KCS TP-1A	C	J	35.50	0.25	42,300,000	59,350	59,350	0.64	0.5	1.0	1.00	40
	KCS TP-2	C	J	14.50	0.25	42,300,000	34,180	34,180	0.74	0.5	1.0	1.00	31
	KCS TP-3	C	J	23.50	0.25	42,300,000	44,760	44,760	0.68	0.5	1.0	1.00	36
	KCS TP-4	C	J	11.50	0.25	42,300,000	26,300	26,300	0.89	0.5	1.0	1.00	30
36	KTJ 1	C	J	30.00	0.50	35,000,000	42,090	105,220	0.86	0.5	1.0	0.40	NR
37	LB 1/L1C	C	J	5.95	0.102	35,000,000	58,460	58,460	0.63	0.2	1.0	1.00	NP
	LB 2/L1C	C	J	1.83	0.102	35,000,000	28,200	28,200	0.76	0.2	1.0	1.00	NP
	LB 2/L1T	T	J	5.95	0.102	35,000,000	58,460	58,460	0.63	0.2	1.0	1.00	NP
38	LTS B1	C	A	8.59	0.45	37,600,000	279,140	279,140	0.59	0.2	0.9	1.00	10
	LTS B2	C	A	8.20	0.55	39,600,000	269,000	269,000	0.60	0.2	1.0	1.00	10
	LTS B3	C	A	8.45	0.41	37,000,000	275,450	275,450	0.59	0.2	1.0	1.00	10
	LTS B4	C	A	8.53	0.41	34,500,000	277,550	277,550	0.59	0.2	1.0	1.00	10
	LTS B5	C	D	8.51	0.35	35,500,000	277,050	277,050	0.59	0.2	1.0	1.00	10
	LTS B6	C	D	8.57	0.35	35,500,000	278,610	278,610	0.59	0.2	1.0	1.00	10
	LTS B7	C	A	8.43	0.51	36,450,000	274,910	274,910	0.59	0.2	1.0	1.00	10
	LTS B8	C	A	8.43	0.52	36,450,000	274,910	274,910	0.59	0.2	1.0	1.00	10
	LTS B9	C	A	8.65	0.43	36,750,000	280,725	280,725	0.59	0.2	0.9	1.00	10
	LTS B10	C	A	8.13	0.55	36,400,000	266,980	266,980	0.60	0.2	1.0	1.00	10
	LTS B11	C	A	8.45	0.41	35,900,000	275,450	275,450	0.59	0.2	1.0	1.00	10
	LTS B12	C	A	9.52	0.43	34,250,000	277,290	277,290	0.59	0.2	1.0	1.00	10
39	DRS P-I	C	D	40.20	0.48	29,250,000	74,960	74,960	0.57	0.5	1.0	1.00	25
	DRS P-D	C	D	40.20	0.48	29,250,000	74,960	74,960	0.57	0.5	1.0	1.00	25

Notes: C: top-down compression loading mode; T: top-up tension (or uplift) loading mode; A: augered piles; D: driven piles; J: jacked piles; B-CIS: bored cast in-situ piles; L: pile length; d: pile diameter for piles with circular cross-section; B: pile width for piles with square cross-section; E_p = pile modulus; G_{max} = initial soil shear modulus at pile base; $G_{b\text{-}max}$ = initial soil shear modulus below the pile base for end-bearing type piles; ρ_E = modulus variation factor; ν_s = soil's Poisson's ratio; η = factor for underreamed piles = r_b/r_o, where r_b = pile base radius and r_o = pile shaft radius; ξ = $G_{max}/G_{b\text{-}max}$; PI = plasticity index, NP = non-plastic; NR = not reported.

Table G.1. (continued).

Site ID	Pile ID	Loading mode	Installation method	L (m)	d or B (m)	E_p (kN)	$G_{L(max)}$ (kN)	$G_{b\text{-}max}$ (kN)	ρ_E	ν_s	η	ξ	Representative PI (%)
40	L&D 1-1T	T	D	18.52	14 x 73	22,200,000	221,040	442,080	0.66	0.2	1.0	0.50	NP
	L&D 1-2T	T	D	16.46	14 x 73	22,200,000	196,300	196,300	0.68	0.2	1.0	1.00	NP
	L&D 1-3AC	C	D	16.46	14 x 73	22,200,000	196,300	196,300	0.68	0.2	1.0	1.00	NP
	L&D 1-3BT	T	D	16.46	14 x 73	22,200,000	196,300	196,300	0.68	0.2	1.0	1.00	NP
	L&D 1-5T	T	D	18.44	14 x 73	22,200,000	220,400	440,780	0.66	0.2	1.0	0.50	NP
	L&D 1-6C	C	D	16.15	14 x 73	22,200,000	193,950	193,950	0.68	0.2	1.0	1.00	NP
	L&D 1-7C	C	D	17.98	14 x 73	22,200,000	216,630	433,270	0.66	0.2	1.0	0.50	NP
	L&D 2-1T	T	D	16.76	14 x 73	22,200,000	198,590	198,590	0.68	0.2	1.0	1.00	NP
	L&D 2-7C	C	D	20.37	14 x 73	22,200,000	236,135	472,270	0.65	0.2	1.0	0.50	NP
	L&D 2-8T	T	D	12.19	14 x 73	22,200,000	157,680	157,680	0.73	0.2	1.0	1.00	NP
	L&D 3-1C	C	D	14.23	0.30	22,100,000	175,800	175,800	0.70	0.2	1.0	1.00	NP
	L&D 3-2T	T	D	10.97	0.30	22,000,000	149,130	149,130	0.74	0.2	1.0	1.00	NP
	L&D 3-4C	C	D	14.39	0.36	22,100,000	176,950	176,950	0.70	0.2	1.0	1.00	NP
	L&D 3-5T	T	D	11.12	0.36	22,000,000	150,180	150,180	0.74	0.2	1.0	1.00	NP
	L&D 3-7C	C	D	14.57	0.41	22,100,000	178,270	178,270	0.70	0.2	1.0	1.00	NP
	L&D 3-8T	T	D	11.12	0.41	22,000,000	150,180	150,180	0.74	0.2	1.0	1.00	NP
	L&D 3-10C	C	D	20.02	14 x 73	22,200,000	151,600	151,600	0.65	0.2	1.0	1.00	NP
	L&D 3-14T	T	D	11.89	14 x 73	22,050,000	155,580	155,580	0.73	0.2	1.0	1.00	NP
	L&D 3-15T	T	D	11.28	14 x 73	22,050,000	151,300	151,300	0.74	0.2	1.0	1.00	NP
	L&D 3-16T	T	D	11.28	14 x 73	22,050,000	151,300	151,300	0.74	0.2	1.0	1.00	NP
41	UBC PRS 1	C	D	11.83	0.324	23,400,000	46,650	46,650	0.73	0.5	1.0	1.00	20
	UBC PRS 2	C	D	13.90	0.324	23,400,000	45,700	45,700	0.67	0.5	1.0	1.00	20
	UBC PRS 3	C	D	16.80	0.324	23,400,000	51,900	51,900	0.65	0.5	1.0	1.00	20
	UBC PRS 4	C	D	23.20	0.324	23,400,000	75,200	75,200	0.57	0.5	1.0	1.00	20
	UBC PRS 5	C	D	31.10	0.324	28,150,000	89,150	89,150	0.58	0.4	1.0	1.00	20
42	MOTH PRS A	C	D	67.00	0.915	16,750,000	145,700	145,700	0.58	0.2	1.0	1.00	5
	MOTH PRS B	C	D	78.00	0.915	16,750,000	164,000	164,000	0.56	0.2	1.0	1.02	5
	MOTH PRS C	C	D	94.00	0.915	16,750,000	197,800	197,800	0.56	0.2	1.0	1.00	5
43	NMGC 1	C	B-CIS	21.50	0.760	35,000,000	88,900	88,900	0.54	0.5	2.45	1.00	45
44	NWU NGES 1	C	D	15.24	14 x 73	18,500,000	85,600	99,200	1.00	0.5	1.0	0.86	19
	NWU NGES 2	C	B-CIS	15.24	0.55	30,000,000	85,600	99,200	1.00	0.5	1.0	0.86	19
	NWU NGES 3	C	D	15.24	0.46	16,400,000	85,600	99,200	1.00	0.5	1.0	0.86	19
	NWU NGES 4	C	B-CIS	15.24	0.48	30,000,000	85,600	99,200	1.00	0.5	1.0	0.86	19

Notes: C: top-down compression loading mode; T: top-up tension (or uplift) loading mode; A: augered piles; D: driven piles; J: jacked piles; B-CIS: bored cast in-situ piles; L: pile length; d: pile diameter for piles with circular cross-section; B: pile width for piles with square cross-section; E_p = pile modulus; G_{max} = initial soil shear modulus at pile base; $G_{b\text{-}max}$ = initial soil shear modulus below the pile base for end-bearing type piles; ρ_E = modulus variation factor; ν_s = soil's Poisson's ratio; η = factor for underreamed piles = r_b/r_o, where r_b = pile base radius and r_o = pile shaft radius; ξ = $G_{max}/G_{b\text{-}max}$; PI = plasticity index, NP = non-plastic; NR = not reported.

Table G.1. (continued).

Site ID	Pile ID	Loading mode	Installation method	L (m)	d or B (m)	E_p (kN)	$G_{L(max)}$ (kN)	$G_{b\text{-}max}$ (kN)	ρ_E	ν_s	η	ξ	Representative PI (%)
45	NP T1	C	D	8.30	0.80	12,500,000	66,230	66,230	0.71	0.2	1.0	1.00	NP
	NP T2	C	D	8.30	0.80	12,000,000	66,230	66,230	0.71	0.2	1.0	1.00	NP
	NP T3	T	D	8.80	0.80	12,500,000	68,600	68,600	0.70	0.2	1.0	1.00	NP
46	OSJS 1	C	B-CIS	12.80	0.406	25,000,000	42,425	106,100	0.70	0.5	1.0	0.4	NR
47	OC A1	T	D	5.00	0.219	28,800,000	31,000	31,000	0.74	0.5	1.0	1.00	40
	OC A3	T	D	5.00	0.219	28,800,000	53,400	53,400	0.86	0.5	1.0	1.00	45
	OC A4	T	D	5.00	0.219	28,800,000	64,970	64,970	0.88	0.5	1.0	1.00	40
	OC B1	T	D	5.00	0.219	10,500,000	30,200	30,200	0.74	0.5	1.0	1.00	40
	OC C1-1	T	D	5.00	0.219	28,800,000	61,100	61,100	0.62	0.5	1.0	1.00	40
	OC C1-2	T	D	10.00	0.219	28,800,000	61,100	61,100	0.62	0.5	1.0	1.00	40
48	PT LDP	C	D	40.00	0.762	15,500,000	123,290	123,290	0.71	0.5	1.0	1.00	17
	PT NGI A5-1	T	D	10.00	0.219	28,500,000	70,090	70,090	0.87	0.5	1.0	1.00	14
	PT NGI A5-2	T	D	10.00	0.219	28,500,000	70,090	70,090	0.87	0.5	1.0	1.00	14
	PT NGI A6-1	T	D	10.00	0.219	28,500,000	87,600	87,600	0.85	0.5	1.0	1.00	14
	PT NGI A6-2	T	D	10.00	0.219	28,500,000	87,600	87,600	0.85	0.5	1.0	1.00	14
	PT 1/L1C	C	J	4.30	0.102	67,800,000	47,400	47,400	0.97	0.5	1.0	1.00	18
	PT 2/L1C	C	J	8.50	0.102	67,800,000	61,000	61,000	0.85	0.5	1.0	1.00	18
	PT 2/L2T	T	J	8.50	0.102	67,800,000	61,000	61,000	0.85	0.5	1.0	1.00	18
	PT 3/L1T	T	J	5.47	0.102	67,800,000	57,600	57,600	0.88	0.5	1.0	1.00	17
	PT 3/L2T	T	J	5.47	0.102	67,800,000	57,600	57,600	0.88	0.5	1.0	1.00	17
	PT 4/L1C	C	J	5.88	0.102	67,800,000	46,200	46,200	0.96	0.5	1.0	1.00	17
	PT 5/L1T	T	J	10.59	0.102	67,800,000	59,500	59,500	0.83	0.5	1.0	1.00	16
	PT 5/L2T	T	J	10.59	0.102	67,800,000	59,500	59,500	0.83	0.5	1.0	1.00	16
	PT 5/L3C	C	J	10.59	0.102	67,800,000	59,500	59,500	0.83	0.5	1.0	1.00	16
	PT 5/L4T	T	J	10.59	0.102	67,800,000	59,500	59,500	0.83	0.5	1.0	1.00	16
	PT 5/L6T	T	J	10.59	0.102	67,800,000	59,500	59,500	0.83	0.5	1.0	1.00	16
	PT 6/L1C	C	J	3.75	0.102	67,800,000	46,800	46,800	0.97	0.5	1.0	1.00	19
	PT 7/L1C	C	J	8.75	0.102	67,800,000	61,000	61,000	0.84	0.5	1.0	1.00	17
	PT 7/L2C	C	J	8.75	0.102	67,800,000	61,000	61,000	0.84	0.5	1.0	1.00	17
	PT 7/L3T	T	J	8.75	0.102	67,800,000	61,000	61,000	0.84	0.5	1.0	1.00	17
50	PRB '73	C	D	55.00	0.610	35,000,000	94,200	94,200	0.58	0.5	1.0	1.00	25
	PRB '07	C	D	100.0	1.824	35,000,000	147,700	450,000	0.62	0.5	1.0	1.00	35

Notes: C: top-down compression loading mode; T: top-up tension (or uplift) loading mode; A: augered piles; D: driven piles; J: jacked piles; B-CIS: bored cast in-situ piles; L: pile length; d: pile diameter for piles with circular cross-section; B: pile width for piles with square cross-section; E_p = pile modulus; G_{max} = initial soil shear modulus at pile base; $G_{b\text{-}max}$ = initial soil shear modulus below the pile base for end-bearing type piles; ρ_E = modulus variation factor; ν_s = soil's Poisson's ratio; η = factor for underreamed piles = r_b/r_o, where r_b = pile base radius and r_o = pile shaft radius; ξ = $G_{max}/G_{b\text{-}max}$; PI = plasticity index, NP = non-plastic; NR = not reported.

Table G.1. (continued).

Site ID	Pile ID	Loading mode	Installation method	L (m)	d or B (m)	E_p (kN)	$G_{L(max)}$ (kN)	$G_{b\text{-}max}$ (kN)	ρ_E	ν_s	η	ξ	Representative PI (%)
52	SA 1-1	C	J	6.40	0.22	54,500,000	25,950	25,950	0.59	0.5	1.0	1.00	20
	SA 1-2	C	J	6.40	0.22	54,500,000	25,950	25,950	0.59	0.5	1.0	1.00	20
	SA 1-3	C	J	6.40	0.22	54,500,000	25,950	25,950	0.59	0.5	1.0	1.00	20
	SA 1-4	C	J	6.40	0.22	54,500,000	25,950	25,950	0.59	0.5	1.0	1.00	20
	SA 1-5	C	J	6.40	0.22	54,500,000	25,950	25,950	0.59	0.5	1.0	1.00	20
53	SPI 1	C	D	45.00	0.406	45,850,000	114,750	114,750	0.66	0.5	1.0	1.00	22
54	SFBM P10T	T	D	38.90	0.25	36,400,000	66,560	268,620	0.58	0.5	1.0	0.25	37
	SFBM P11T	T	D	26.90	0.26	36,400,000	36,450	36,450	0.63	0.5	1.0	1.00	37
	SFBM P12T	T	D	38.50	0.25	36,400,000	65,990	268,620	0.59	0.5	1.0	0.25	37
	SFBM P13C	C	D	26.90	0.27	36,400,000	36,450	36,450	0.63	0.5	1.0	1.00	37
	SFBM P13T	T	D	26.90	0.27	36,400,000	36,450	36,450	0.63	0.5	1.0	1.00	37
	SFBM P31C	C	A	25.10	0.57	30,000,000	34,640	34,640	0.63	0.5	1.0	1.00	37
	SFBM P31T	T	A	25.10	0.57	30,000,000	34,640	34,640	0.63	0.5	1.0	1.00	37
	SFBM P32C	C	A	33.70	0.57	30,000,000	59,165	139,350	0.60	0.5	1.0	0.42	37
	SFBM P32T	T	A	33.70	0.57	30,000,000	59,165	139,350	0.60	0.5	1.0	0.42	37
	SFBM P33C	C	A	25.10	0.57	30,000,000	34,640	34,640	0.63	0.5	1.0	1.00	37
	SFBM P33T	T	A	25.10	0.57	30,000,000	34,640	34,640	0.63	0.5	1.0	1.00	37
	SFBM P34C	C	A	33.70	0.57	30,000,000	59,165	139,350	0.60	0.5	1.0	0.42	37
	SFBM P34T	T	A	33.70	0.57	30,000,000	59,165	139,350	0.60	0.5	1.0	0.42	37
	SFBM P48C	C	D	26.10	0.41	24,012,000	35,650	35,650	0.63	0.5	1.0	1.00	37
	SFBM P48T	T	D	26.10	0.41	24,012,000	35,650	35,650	0.63	0.5	1.0	1.00	37
	SFBM P49T	T	D	26.10	0.41	24,012,000	35,650	35,650	0.63	0.5	1.0	1.00	37
	SFBM P49C	C	D	26.10	0.41	24,012,000	35,650	35,650	0.63	0.5	1.0	1.00	37
	SFBM P50C	C	D	26.50	0.36	35,000,000	36,050	36,050	0.63	0.5	1.0	1.00	37
	SFBM P50T	T	D	26.50	0.36	35,000,000	36,050	36,050	0.63	0.5	1.0	1.00	37
	SFBM P51T	T	D	26.50	0.36	35,000,000	36,050	36,050	0.63	0.5	1.0	1.00	37
	SFBM P51C	C	D	26.50	0.36	35,000,000	36,050	36,050	0.63	0.5	1.0	1.00	37
	SFBM P59T	T	D	33.40	0.36	35,000,000	58,740	139,350	0.60	0.5	1.0	0.42	37
	SFBM P59C	C	D	33.40	0.36	35,000,000	58,740	139,350	0.60	0.5	1.0	0.42	37
	SFBM P61C	C	D	33.40	0.36	35,000,000	58,740	139,350	0.60	0.5	1.0	0.42	37
	SFBM P61T	T	D	33.40	0.36	35,000,000	58,740	139,350	0.60	0.5	1.0	0.42	37
	SFBM P69C	C	D	26.50	14 x 89	25,700,000	36,050	36,050	0.63	0.5	1.0	1.00	37
	SFBM P69T	T	D	26.50	14 x 89	25,700,000	36,050	36,050	0.63	0.5	1.0	1.00	37
	SFBM P70T	T	D	26.50	14 x 89	25,700,000	36,050	36,050	0.63	0.5	1.0	1.00	37
	SFBM P73T	T	D	41.10	0.22	36,400,000	69,690	268,620	0.58	0.5	1.0	0.26	37
	SFBM P73C	C	D	41.10	0.22	36,400,000	69,690	268,620	0.58	0.5	1.0	0.26	37
	SFBM P74C	C	D	26.70	0.25	36,400,000	36,250	36,250	0.63	0.5	1.0	1.00	37
	SFBM P74T	T	D	26.70	0.25	36,400,000	36,250	36,250	0.63	0.5	1.0	1.00	37

Notes: C: top-down compression loading mode; T: top-up tension (or uplift) loading mode; A: augered piles; D: driven piles; J: jacked piles; B-CIS: bored cast in-situ piles; L: pile length; d: pile diameter for piles with circular cross-section; B: pile width for piles with square cross-section; E_p = pile modulus; G_{max} = initial soil shear modulus at pile base; $G_{b\text{-}max}$ = initial soil shear modulus below the pile base for end-bearing type piles; ρ_E = modulus variation factor; ν_s = soil's Poisson's ratio; η = factor for underreamed piles = r_b/r_o, where r_b = pile base radius and r_o = pile shaft radius; ξ = $G_{max}/G_{b\text{-}max}$; PI = plasticity index, NP = non-plastic; NR = not reported.

Table G.1. (continued).

Site ID	Pile ID	Loading mode	Installation method	L (m)	d or B (m)	E_p (kN)	$G_{L(max)}$ (kN)	$G_{b\text{-}max}$ (kN)	ρ_E	ν_s	η	ξ	Representative PI (%)
55	SPP P01	T	D	4.00	0.089	22,800,000	138,300	138,300	0.65	0.2	1.0	1.00	NP
	SPP P02	T	D	4.00	0.043	46,000,000	138,300	138,300	0.65	0.2	1.0	1.00	NP
	SPP P03	T	D	4.00	0.089	42,500,000	138,300	138,300	0.65	0.2	1.0	1.00	NP
	SPP P04	T	D	4.00	0.089	42,500,000	138,300	138,300	0.65	0.2	1.0	1.00	NP
	SPP P05	T	D	4.00	0.114	21,800,000	138,300	138,300	0.65	0.2	1.0	1.00	NP
	SPP P06	T	D	4.00	0.089	27,800,000	138,300	138,300	0.65	0.2	1.0	1.00	NP
	SPP P08	T	D	2.50	0.043	46,010,000	102,300	102,300	0.71	0.2	1.0	1.00	NP
	SPP P09	T	D	2.50	0.043	56,900,000	102,300	102,300	0.71	0.2	1.0	1.00	NP
	SPP P10	T	D	2.50	0.034	56,900,000	126,300	126,300	0.71	0.2	1.0	1.00	NP
	SPP P11	T	D	3.50	0.034	22,800,000	102,300	102,300	0.71	0.2	1.0	1.00	NP
	SPP P12	T	D	2.50	0.089	22,800,000	102,300	102,300	0.71	0.2	1.0	1.00	NP
56	SSK A	C	B-CIS	2.50	0.089	30,000,000	279,100	279,100	0.69	0.2	1.0	1.00	NP
57	STTS P24	C	D	12.20	0.324	51,850,000	49,400	49,400	0.99	0.5	1.0	1.00	22
	STTS P14-1	C	D	12.20	0.324	51,850,000	49,400	49,400	0.99	0.5	1.0	1.00	22
	STTS P21	C	D	12.20	0.324	51,850,000	49,400	49,400	0.99	0.5	1.0	1.00	22
	STTS P14-2	C	D	12.20	0.324	51,850,000	49,400	49,400	0.99	0.5	1.0	1.00	22
	STTS P18	C	D	12.20	0.324	51,850,000	49,400	49,400	0.99	0.5	1.0	1.00	22
	STTS P15	C	D	12.20	0.324	51,850,000	49,400	49,400	0.99	0.5	1.0	1.00	22
	STTS P14-3	C	D	12.20	0.324	51,850,000	49,400	49,400	0.99	0.5	1.0	1.00	22
58	S NGES 24LP	C	B-CIS	11.00	0.914	27,100,000	84,155	115,200	0.98	0.5	1.0	0.73	11
	S NGES 1LP	C	B-CIS	11.00	0.914	28,150,000	84,155	115,200	0.98	0.5	1.0	0.73	11
	S NGES 24C	C	B-CIS	11.00	0.914	28,400,000	84,155	115,200	0.98	0.5	1.0	0.73	11
	S NGES 1C	C	B-CIS	11.00	0.914	26,400,000	84,155	115,200	0.98	0.5	1.0	0.73	11
	S NGES 24CDef	C	B-CIS	11.00	0.914	26,100,000	84,155	115,200	0.98	0.5	1.0	0.73	11
	S NGES 1CDef	C	B-CIS	11.00	0.914	27,400,000	84,155	115,200	0.98	0.5	1.0	0.73	11
	S NGES 24B	C	B-CIS	11.00	0.914	21,000,000	84,155	115,200	0.98	0.5	1.0	0.73	11
	S NGES 1B	C	B-CIS	11.00	0.914	30,300,000	84,155	115,200	0.98	0.5	1.0	0.73	11
	S NGES 24DP	C	B-CIS	11.00	0.914	27,400,000	84,155	115,200	0.98	0.5	1.0	0.73	11
	S NGES 1DP	C	B-CIS	11.00	0.914	29,700,000	84,155	115,200	0.98	0.5	1.0	0.73	11
59	SR49 P1	C	D	17.40	12 x 74	31,000,000	159,500	242,200	0.73	0.5	1.0	0.66	20
	SR49 P2	C	D	17.40	0.356	28,900,000	285,800	310,400	0.58	0.5	1.0	0.92	20
60	TAMU-C NGES BP7	C	B-CIS	17.40	12 x 74	35,000,000	74,200	74,200	0.83	0.5	1.0	1.00	38

Notes: C: top-down compression loading mode; T: top-up tension (or uplift) loading mode; A: augered piles; D: driven piles; J: jacked piles; B-CIS: bored cast in-situ piles; L: pile length; d: pile diameter for piles with circular cross-section; B: pile width for piles with square cross-section; E_p = pile modulus; G_{max} = initial soil shear modulus at pile base; $G_{b\text{-}max}$ = initial soil shear modulus below the pile base for end-bearing type piles; ρ_E = modulus variation factor; ν_s = soil's Poisson's ratio; η = factor for underreamed piles = r_b/r_o, where r_b = pile base radius and r_o = pile shaft radius; ξ = $G_{max}/G_{b\text{-}max}$; PI = plasticity index, NP = non-plastic; NR = not reported.

Table G.1. (continued).

Site ID	Pile ID	Loading mode	Installation method	L (m)	d or B (m)	E_p (kN)	$G_{L(max)}$ (kN)	$G_{b\text{-}max}$ (kN)	ρ_E	ν_s	η	ξ	Representative PI (%)
61	TAMU-S NGES BP4	C	B-CIS	9.40	0.941	35,000,000	178,400	178,400	0.95	0.2	1.0	1.00	NP
62	TH212 B10038-1	C	D	15.90	0.304	35,000,000	192,000	383,900	0.85	0.5	1.0	0.50	NR
	TH212 B10038-2	C	D	15.90	0.406	35,000,000	192,000	383,900	0.85	0.5	1.0	0.50	NR
63	TH52 PAT2	C	D	42.30	0.410	60,500,000	105,000	262,300	0.76	0.2	1.0	0.40	NP
	TH52 MAT2	C	D	20.29	0.356	52,400,000	79,400	119,000	0.85	0.2	1.0	0.67	NP
65	UMASS NGES1	C	B-CIS	13.11	0.878	31,800,000	49,260	49,260	0.83	0.5	1.0	1.00	20
	UMASS NGES2	C	B-CIS	14.30	0.955	31,800,000	50,770	50,770	0.82	0.5	1.0	1.00	20
66	FEUP ISC'2 P1	C	B-CIS	6.00	0.60	20,000,000	132,600	132,600	0.82	0.2	1.0	1.00	5
	FEUP ISC'2 P2	C	A	6.00	0.60	40,000,000	132,600	132,600	0.82	0.2	1.0	1.00	5
	FEUP ISC'2 P3	C	D	6.00	0.35	35,500,000	132,600	132,600	0.82	0.2	1.0	1.00	5
67	VEB I-295 JR 1	C	D	16.20	0.610	27,500,000	147,400	294,800	1.00	0.2	1.0	0.50	NP
68	WRBB 1	C	D	45.00	0.610	30,000,000	177,400	177,400	0.53	0.2	1.0	1.00	10
69	WB I-494 MR1A	C	D	32.00	0.46	21,000,000	143,500	143,500	0.52	0.2	1.0	1.00	NR
	WB I-494 MR2	C	D	32.00	0.46	21,000,000	143,500	143,500	0.52	0.2	1.0	1.00	NR
	WB I-494 MR1A-2	C	D	32.00	0.46	21,000,000	143,500	143,500	0.52	0.2	1.0	1.00	NR
	WB I-494 MR4	C	D	32.00	0.46	21,000,000	143,500	143,500	0.52	0.2	1.0	1.00	NR

Notes: C: top-down compression loading mode; T: top-up tension (or uplift) loading mode; A: augered piles; D: driven piles; J: jacked piles; B-CIS: bored cast in-situ piles; L: pile length; d: pile diameter for piles with circular cross-section; B: pile width for piles with square cross-section; E_p = pile modulus; G_{max} = initial soil shear modulus at pile base; $G_{b\text{-}max}$ = initial soil shear modulus below the pile base for end-bearing type piles; ρ_E = modulus variation factor; ν_s = soil's Poisson's ratio; η = factor for underreamed piles = r_b/r_o, where r_b = pile base radius and r_o = pile shaft radius; ξ = $G_{max}/G_{b\text{-}max}$; PI = plasticity index, NP = non-plastic; NR = not reported.

APPENDIX H

INITIAL SHEAR STIFFNESS (G_{max}) PROFILES FROM SHEAR WAVE VELOCITY (V_S) MEASUREMENTS: GROUP 2 DATASET

Initial shear stiffness (G_{max}) profiles from shear wave velocity (V_s) readings.

Site ID No. 1: Asian Institute of Technology (AIT) Test Site, Rangsit, near Bangkok, Thailand	Site ID No. 2: Baghdad University near River Tigris, Iraq	Site ID No. 3: Blessington, Ireland
Soft clay over stiff clay	Clayey silty sand over uniform sand	Heavily overconsolidated glacially derived very dense fine sand
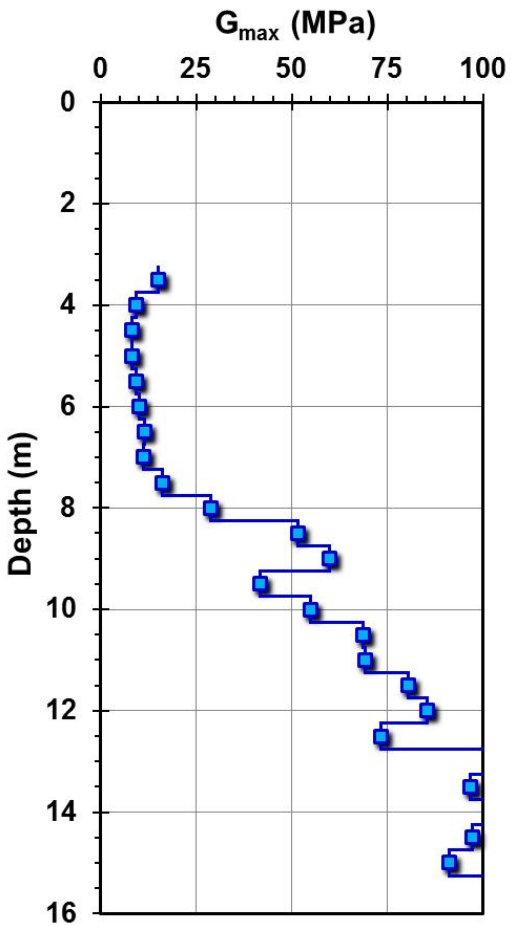	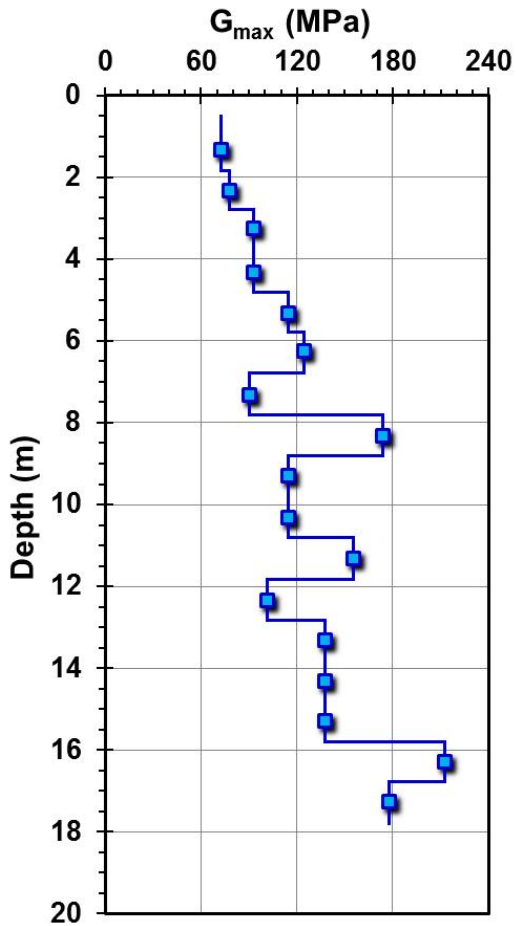	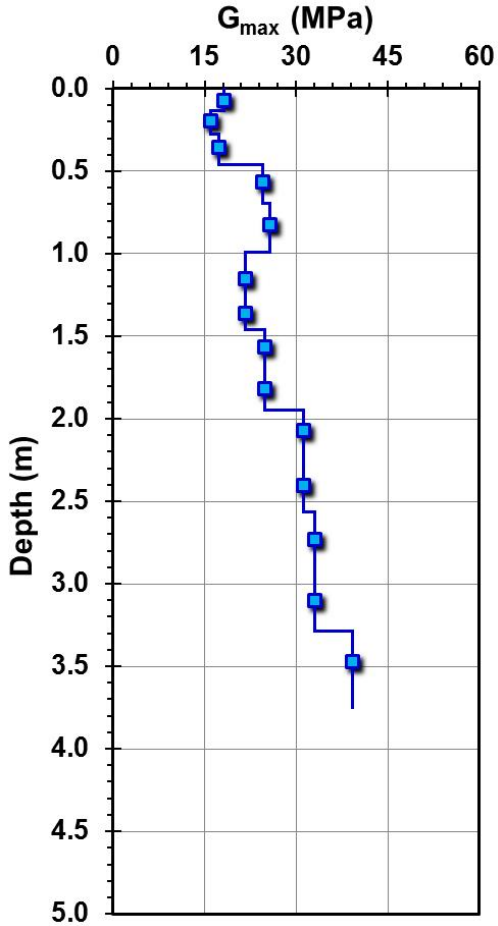

Initial shear stiffness (G_{max}) profiles from shear wave velocity (V_s) readings.

Site ID No. 4: Boom Clay Site, Sint-Kathelijne-Waver, Belgium	Site ID No. 5: Bothkennar clay site, Scotland	Site ID No. 6: Brent Cross, Hendon, UK
Stiff fissured clay	Post glacial soft silty clay	Weathered London clay
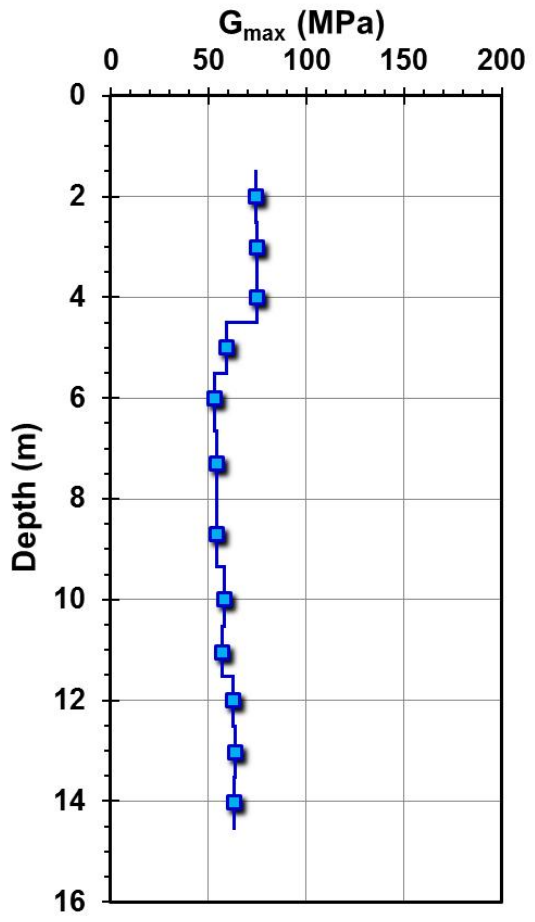	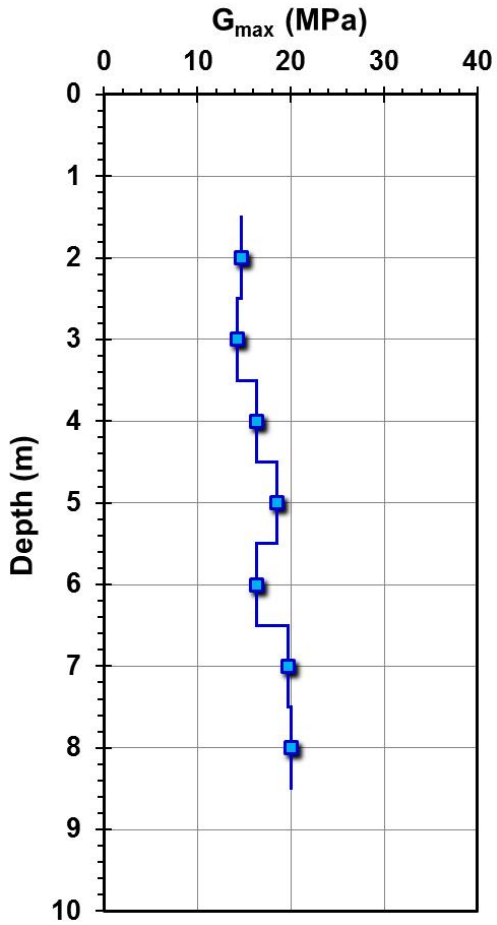	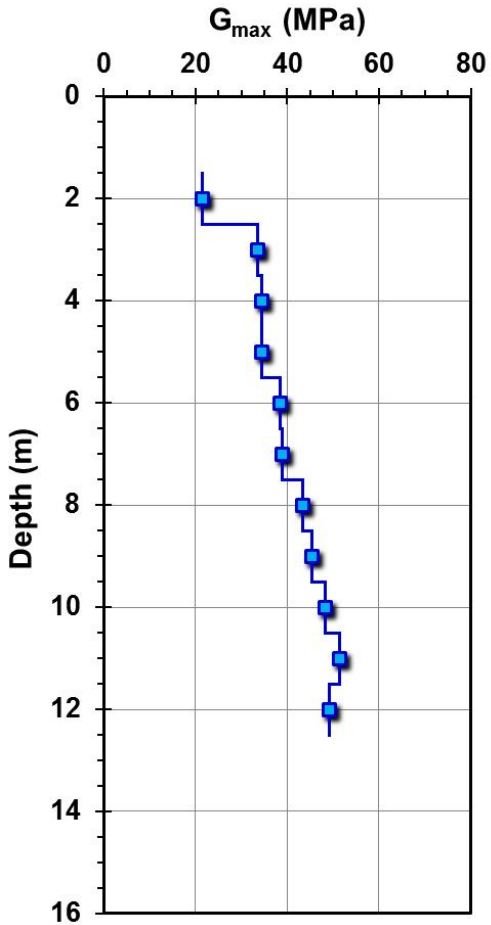

Initial shear stiffness (G_{max}) profiles from shear wave velocity (V_s) readings.

Site ID No. 7: Canadian Geotechnical Test Site, South Gloucester, ON, Canada	Site ID No. 8: Canon Park, North London, UK	Site ID No. 9: Canon Plant, Newport News, VA, USA
Soft sensitive (Champlain Sea) clay	Weathered London clay	Stiff sandy gravelly clay
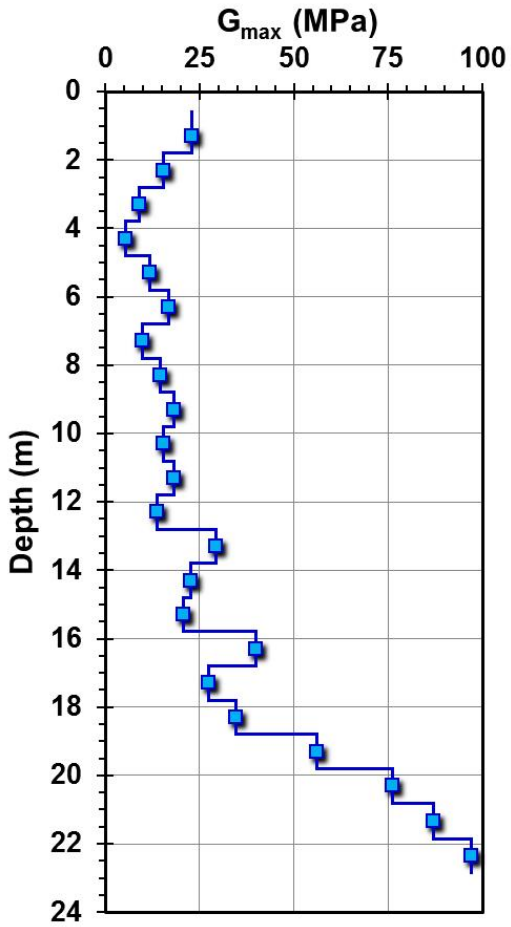	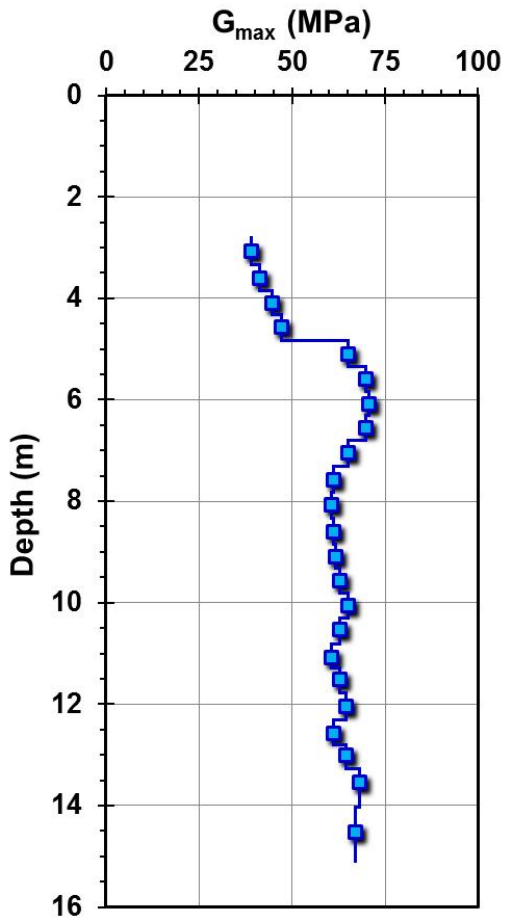	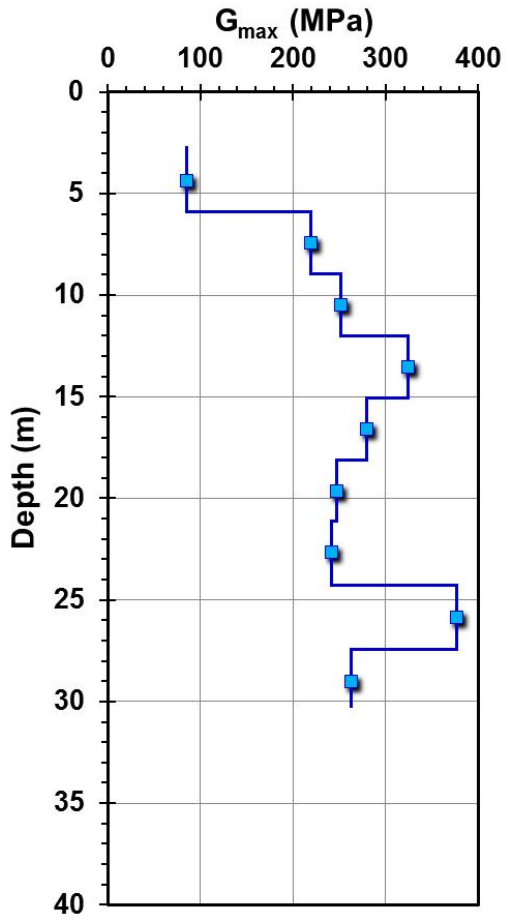

Initial shear stiffness (G_{max}) profiles from shear wave velocity (V_s) readings.

Site ID No. 13: Cowden, Northeast England, UK	Site ID No. 14: Dunkirk, Northern Coast of France	Site ID No. 15: EURIPIDES 1, Eemshaven, Netherlands
Stiff stony clay till	Dense to very dense sand	Medium dense silty sand over very dense sand
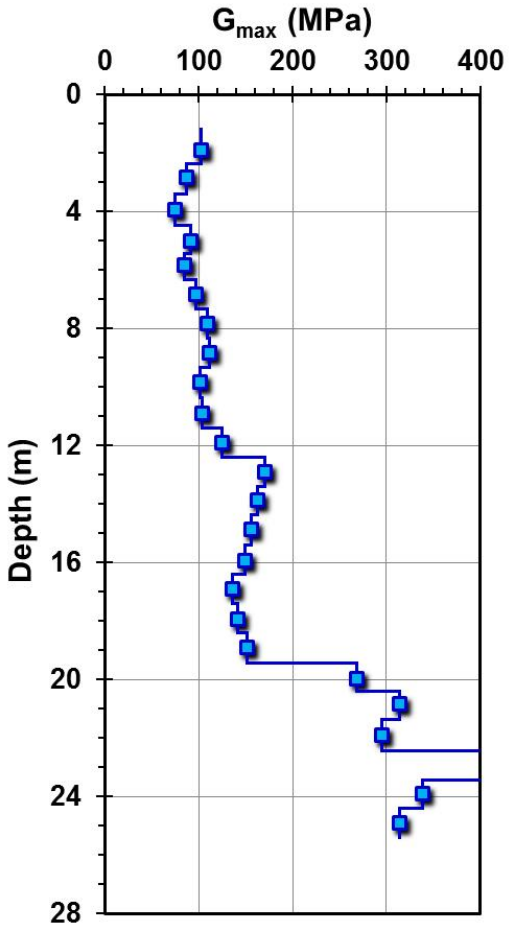	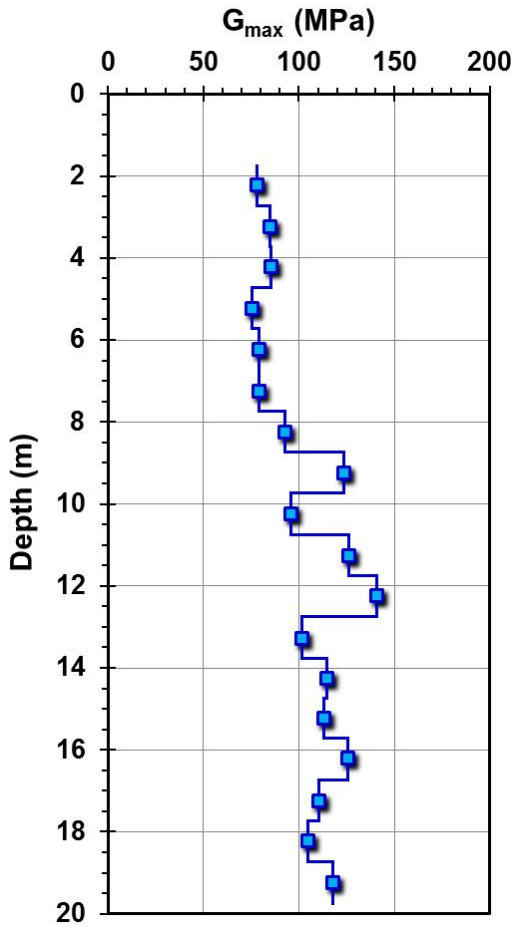	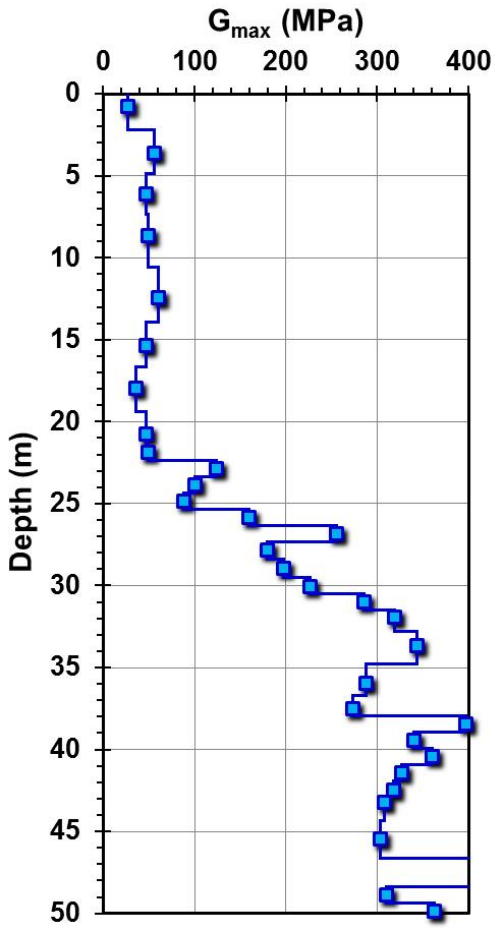

Initial shear stiffness (G_{max}) profiles from shear wave velocity (V_s) readings.

Site ID No. 16: EURIPIDES 2, Eemshaven, Netherlands	Site ID No. 17: Factory building site, Jiangsu Province, China	Site ID No. 18: Fittja Straits Bridge, Vårby, near Stockholm, Sweden
Medium dense silty sand over very dense sand	Marine silty clay	Layers of sand, silty sand, and gravelly sand
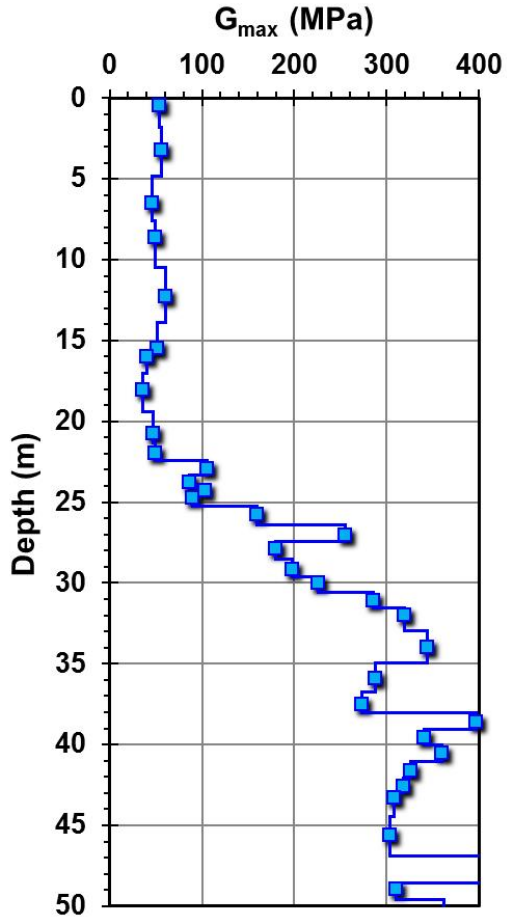	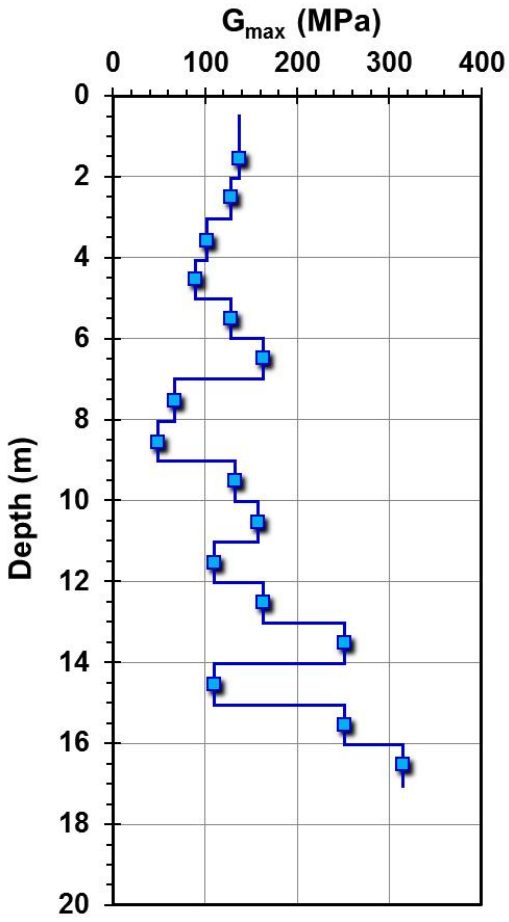	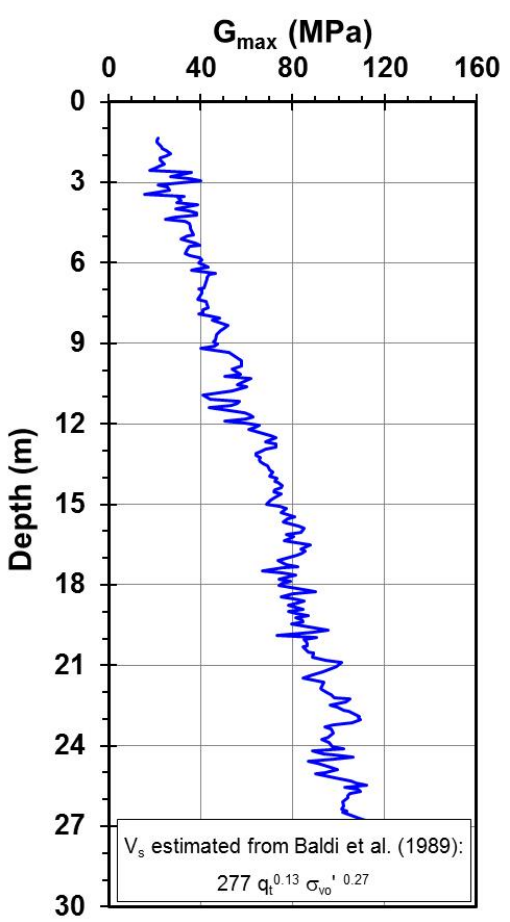

Initial shear stiffness (G_{max}) profiles from shear wave velocity (V_s) readings.

Site ID No. 19: Flanders clay site, Merville, France	Site ID No. 21: Georgia Tech Campus, Sixth Street (west), Atlanta, GA, USA	Site ID No. 23: Golden Ears Bridge (GEB) site: (N. Bank), Maple Ridge, BC, Canada
Silt over stiff homogeneous clay	Piedmont residual silty sand to partially weathered rock	Soft thick deltaic silty clay of Fraser River
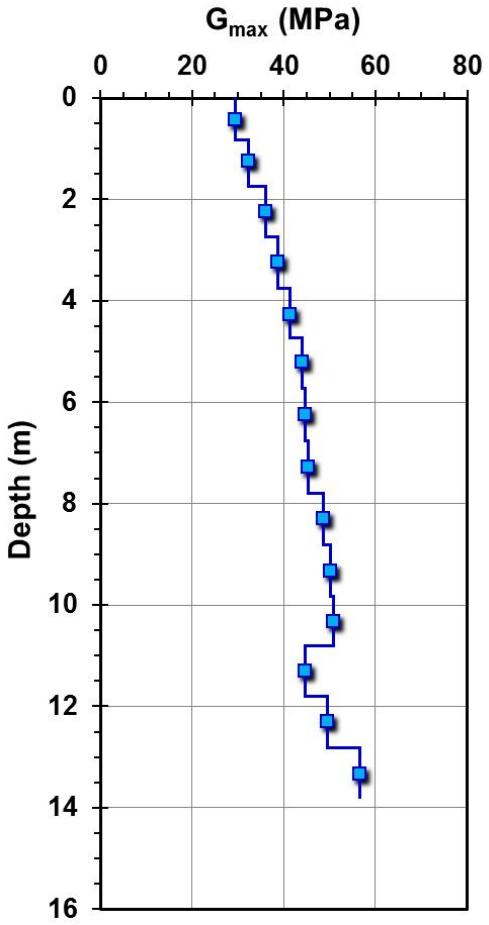	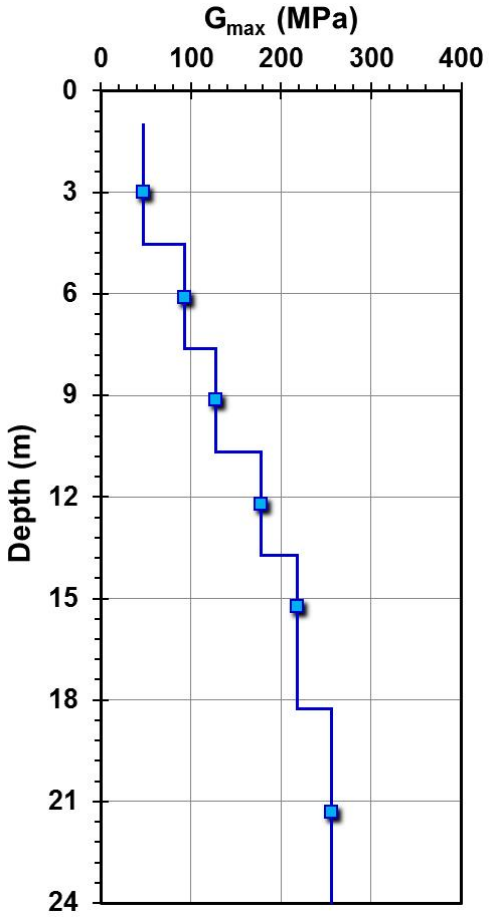	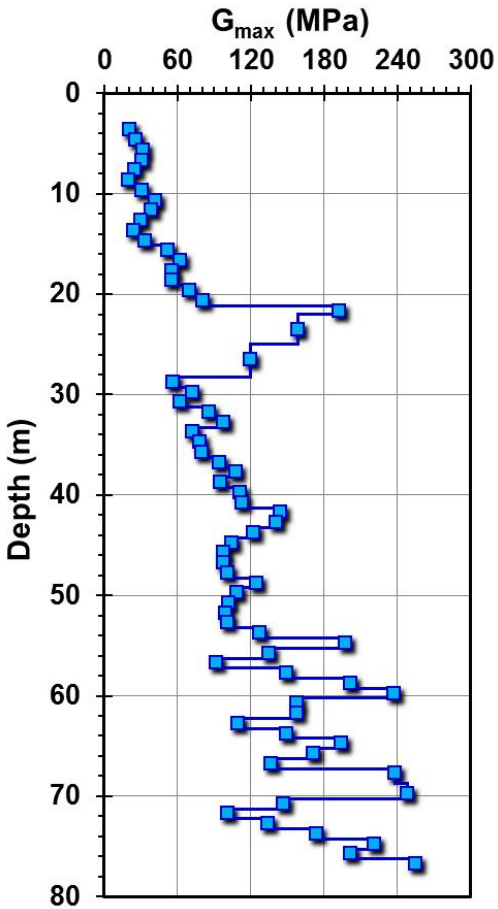

Initial shear stiffness (G_{max}) profiles from shear wave velocity (V_s) readings.

Site ID No. 25: Golden Ears Bridge (GEB) site: (S. Bank), Langley, BC, Canada	Site ID No. 26: Grimsby Research Site, Waltham, UK	Site ID No. 27: Guanabara Bay, Rio-de-Janeiro, Brazil
Gravelly sand over soft to firm silty clay	Very stiff gravelly clay till	Very soft clay
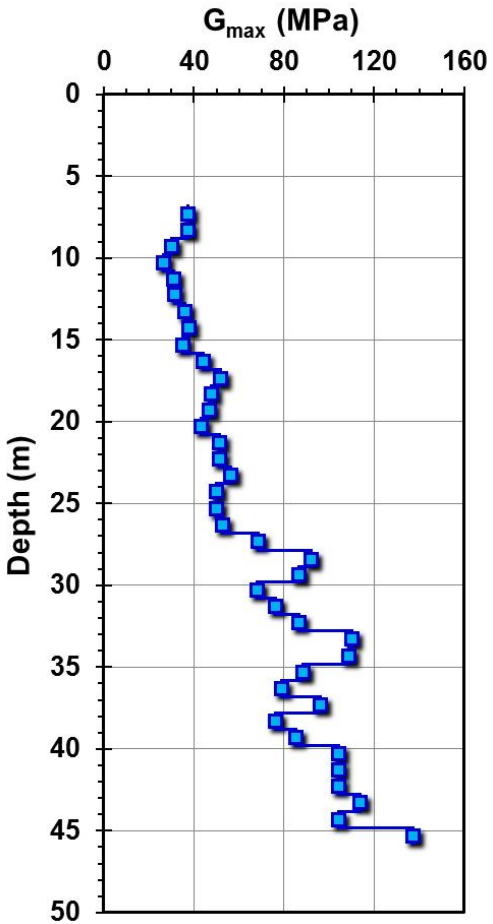	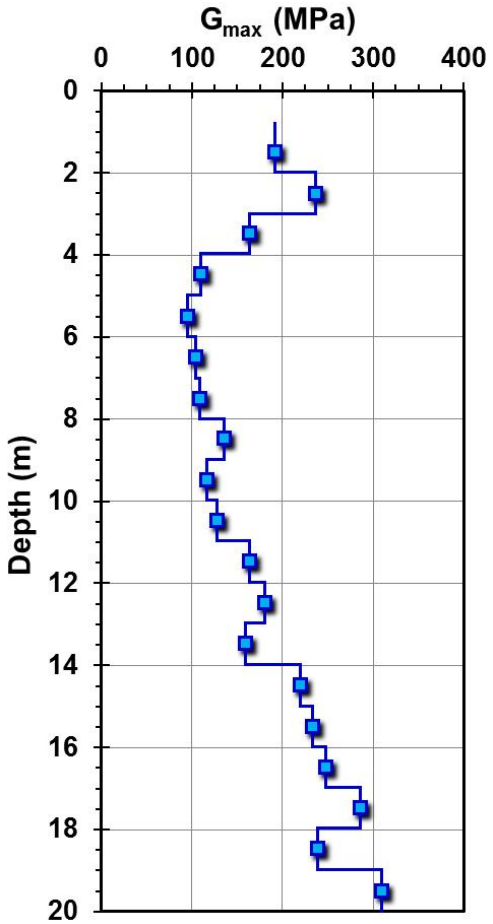	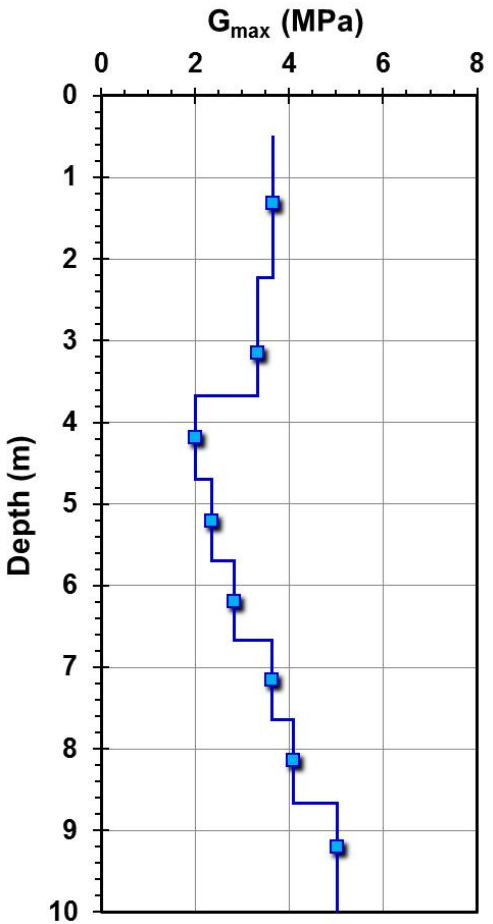

Initial shear stiffness (G_{max}) profiles from shear wave velocity (V_s) readings.

Site ID No. 28: Hamilton Air Force Base, San Francisco, California, USA	Site ID No. 29: High Prairie Health Complex, Northern Alberta, Canada	Site ID No. 30: Holmen sand, Drammen, Norway
Soft silty clay (San Francisco Bay Mud)	Soft to stiff silty clay	Loose medium to coarse river sand
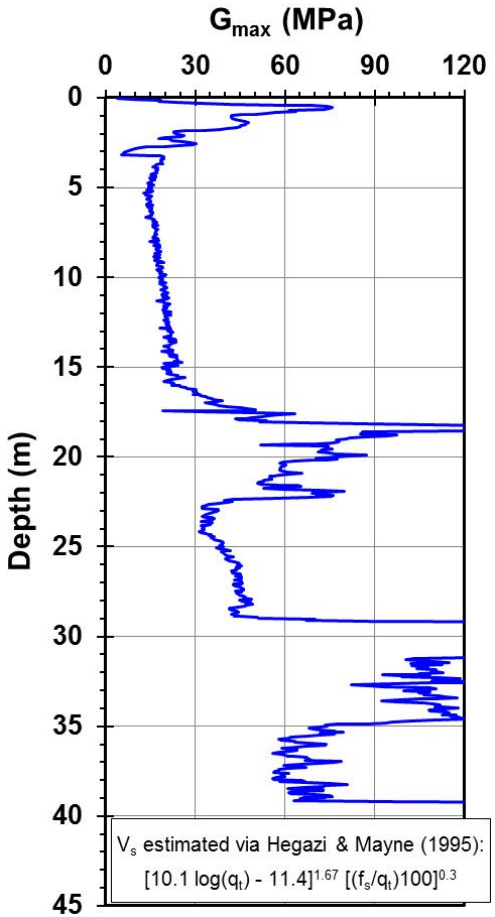	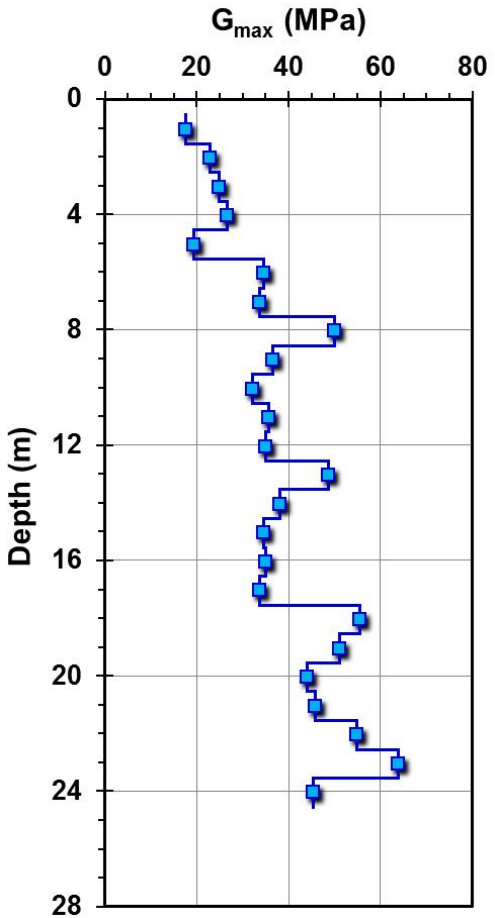	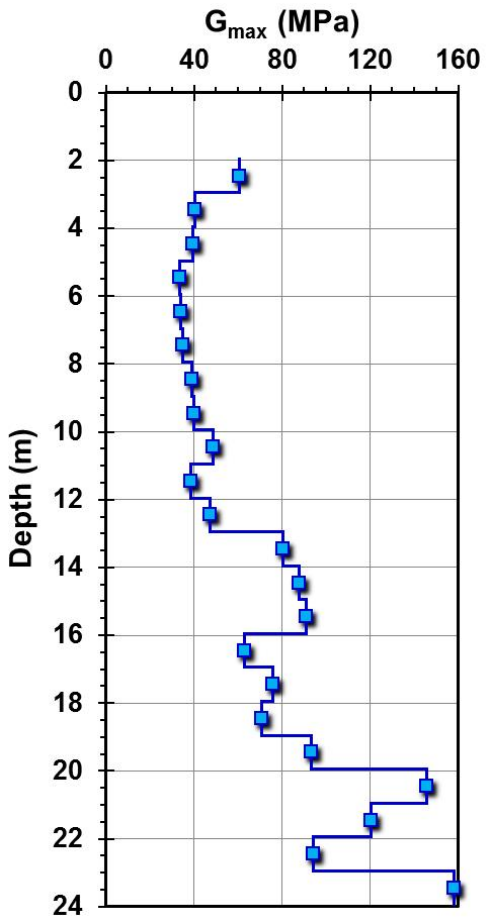

Initial shear stiffness (G_{max}) profiles from shear wave velocity (V_s) readings.

Site ID No. 31: Interactive marine and terrestrial deposit soils, China	Site ID No. 32: Interstate Highway I-85 Bridge, Newnan, Coweta County, GA, USA	Site ID No. 33: Jackson County Electrical Power Facility, Center, GA, USA
Marine silty-clayey sand	Silty sand to sandy silt overlying partially weathered gneissic granite bedrock	Silty sand to sandy silt of Piedmont residuum over partially weathered schist
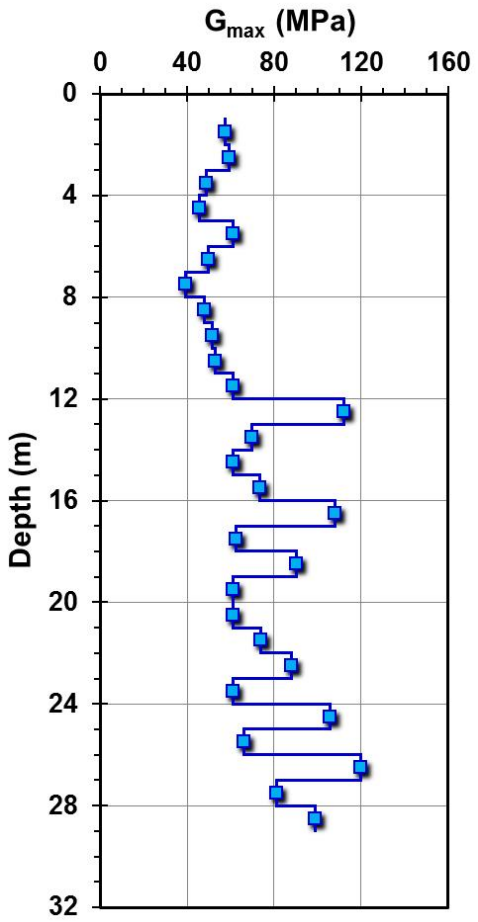	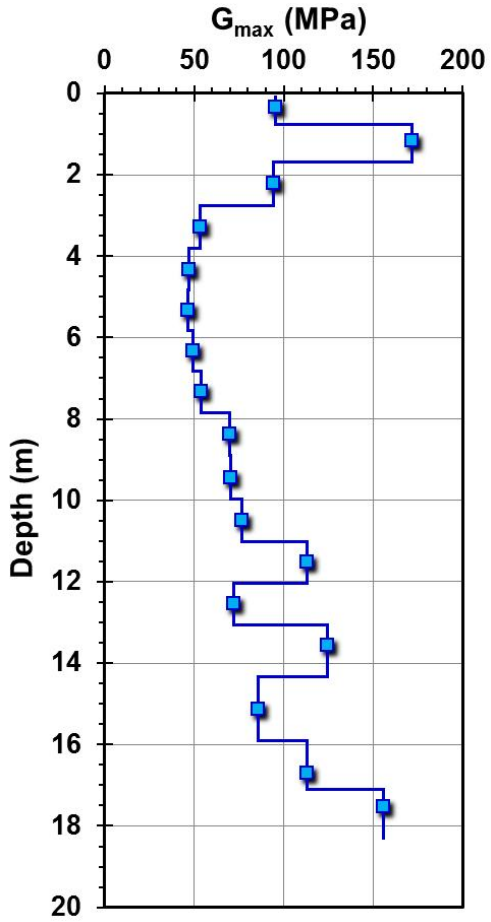	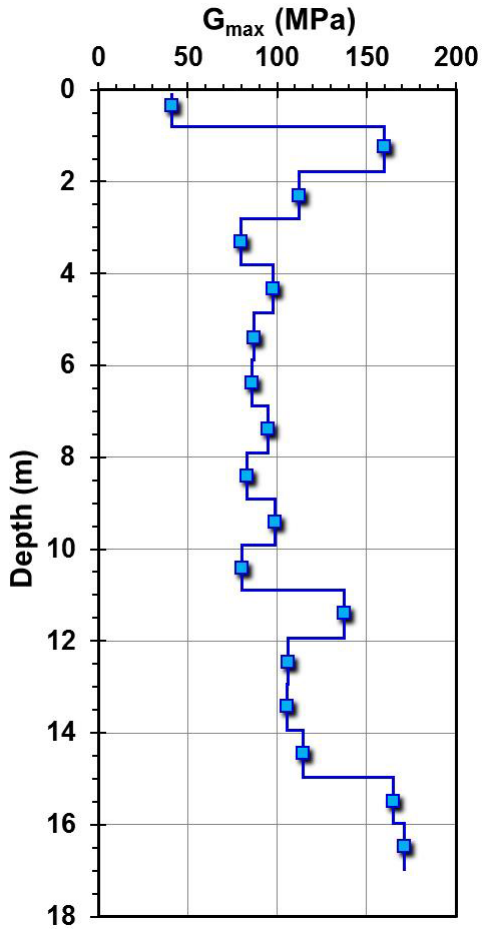

Initial shear stiffness (G_{max}) profiles from shear wave velocity (V_s) readings.

Site ID No. 34: Kinnegar site near Belfast Lough in Northern Ireland	Site ID No. 35: Klang clay site, western shoreline, Malaysia	Site ID No. 36: Kunshan town, eastern Jiangsu province, China
Soft clayey silt (“sleech”)	Soft marine clay	Silty clay
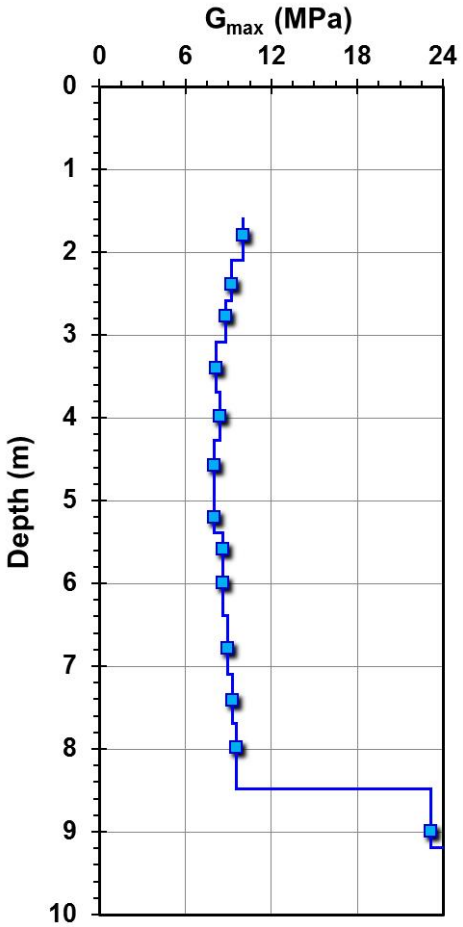	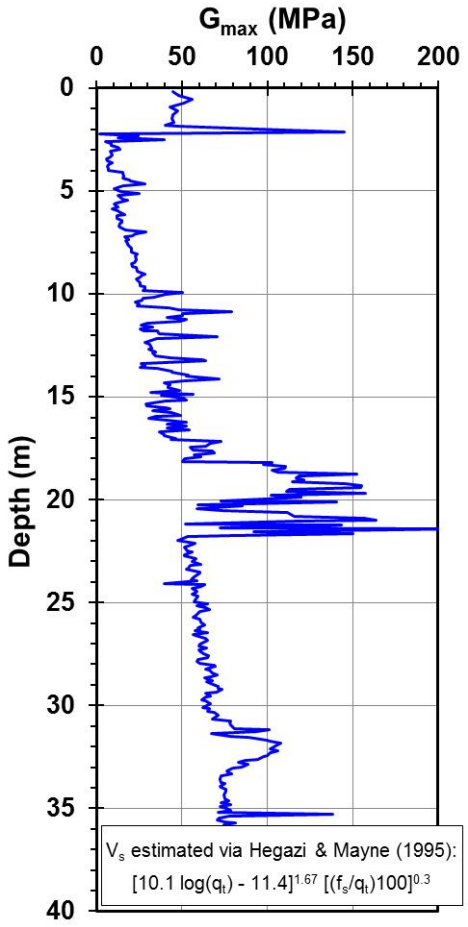	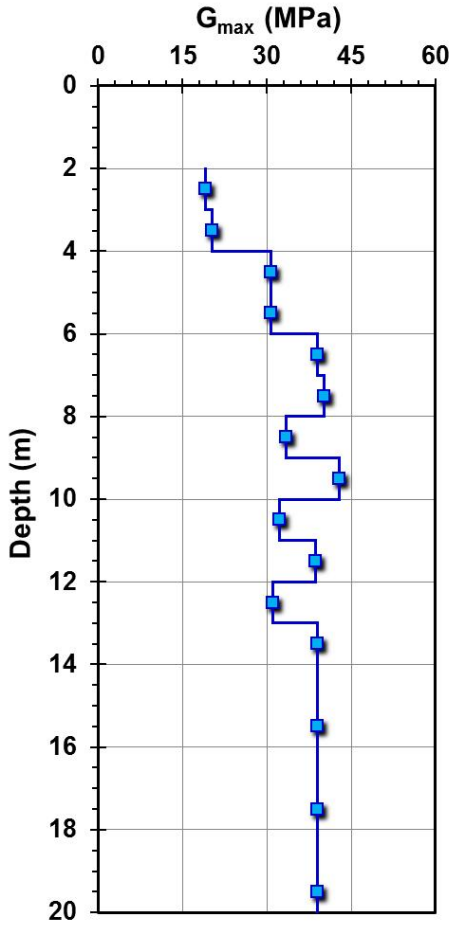

Initial shear stiffness (G_{max}) profiles from shear wave velocity (V_s) readings.

Site ID No. 37: Labenne sand, Bayonne, SW France	Site ID No. 38: Limelette test site, Brussels, Belgium	Site ID No. 39: LNG storage site, Delaware River, Gloucester county, NJ, USA
Fine-medium uniform sand	Silty/sandy clay over clayey sand	Varved clayey silt over dense gravelly sand over dense residual clayey sand
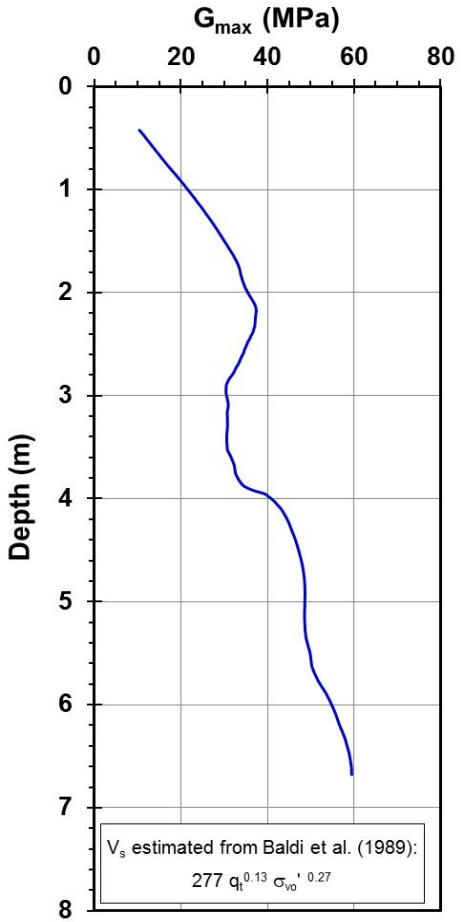	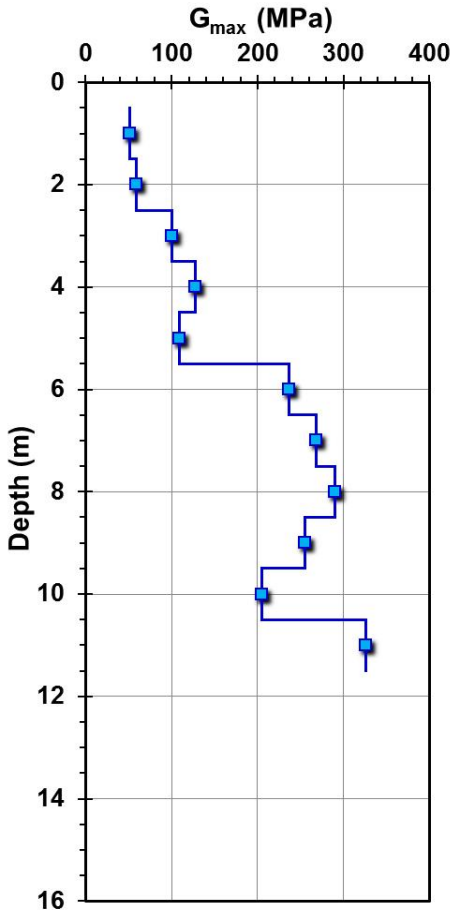	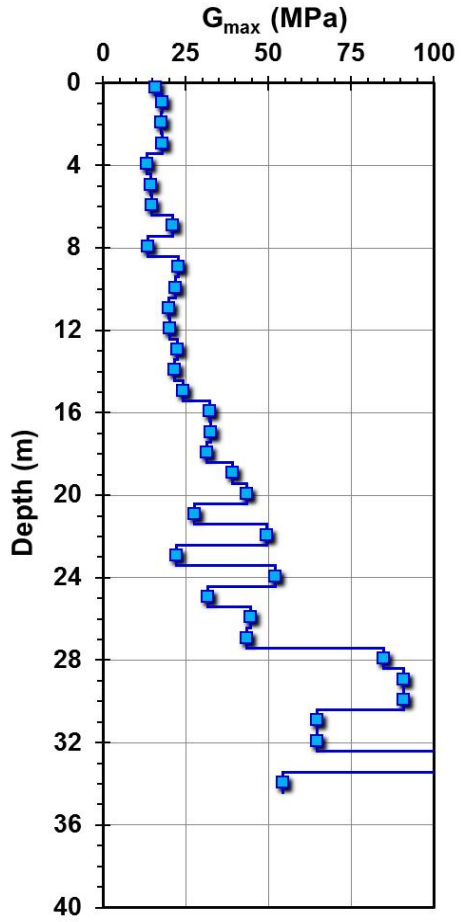

Initial shear stiffness (G_{max}) profiles from shear wave velocity (V_s) readings.

Site ID No. 40: Lock and Dam 26 Project, Mississippi River, IL, USA	Site ID No. 41: Lulu Island, University of British Columbia Pile Research Site (UBC PRS), BC, Canada	Site ID No. 43: New Museums, Gault clay, Central Cambridge, UK
Glacial gravelly sand	Soft silty clay over medium dense sand over clayey silty sand	Gravelly fill over stiff fissured clay
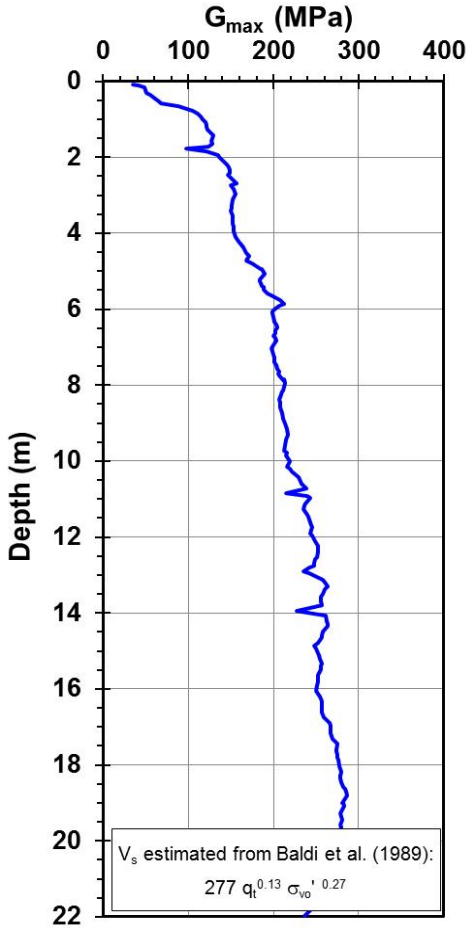	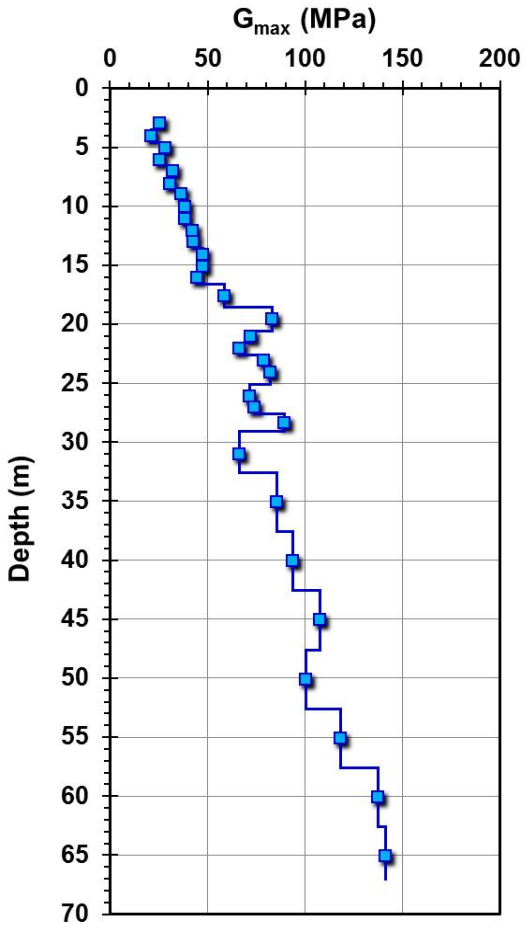	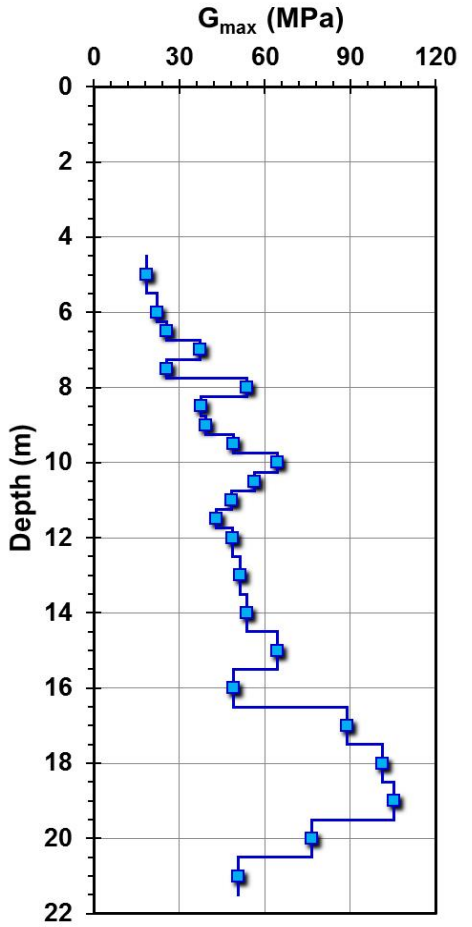

Initial shear stiffness (G_{max}) profiles from shear wave velocity (V_s) readings.

Site ID No. 44: Northwestern University NGES, Evanston, IL, USA	Site ID No. 45: Noetsu Bridges No. 3 and 4, Noto Peninsula, Japan	Site ID No. 46: Old San Juan site, Puerto Rico
Sand fill over soft-firm clay	Diatomaceous mudstone	Interbedded sand and clay
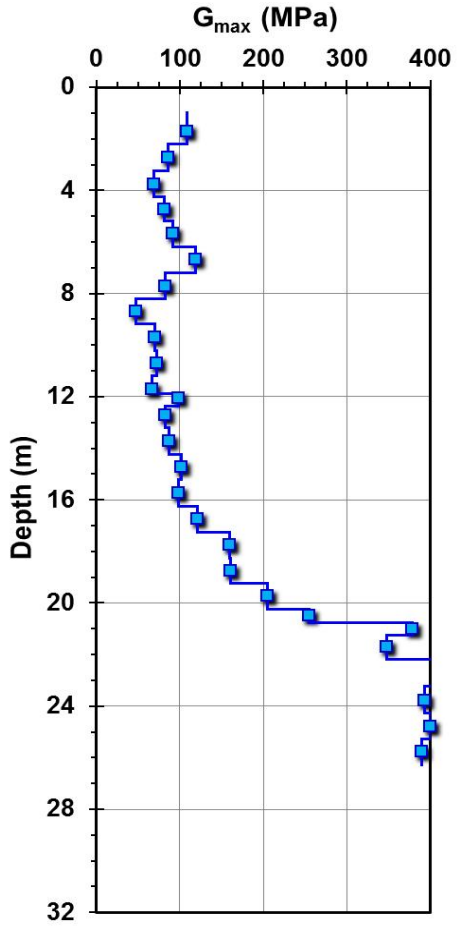	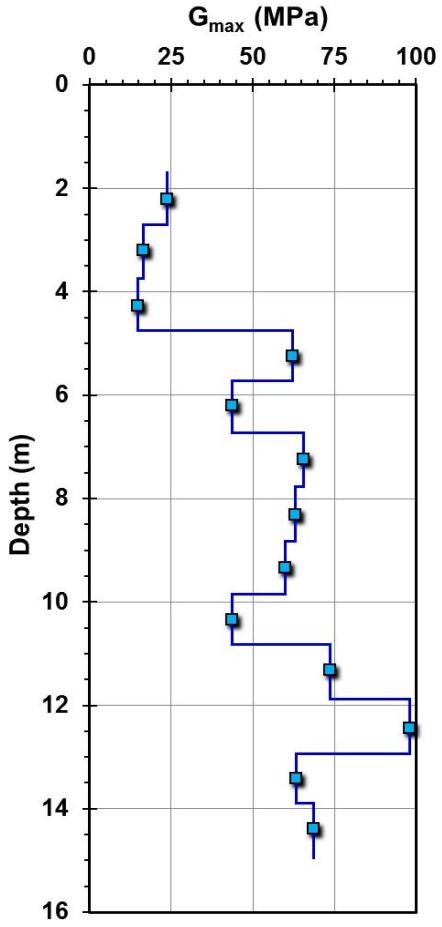	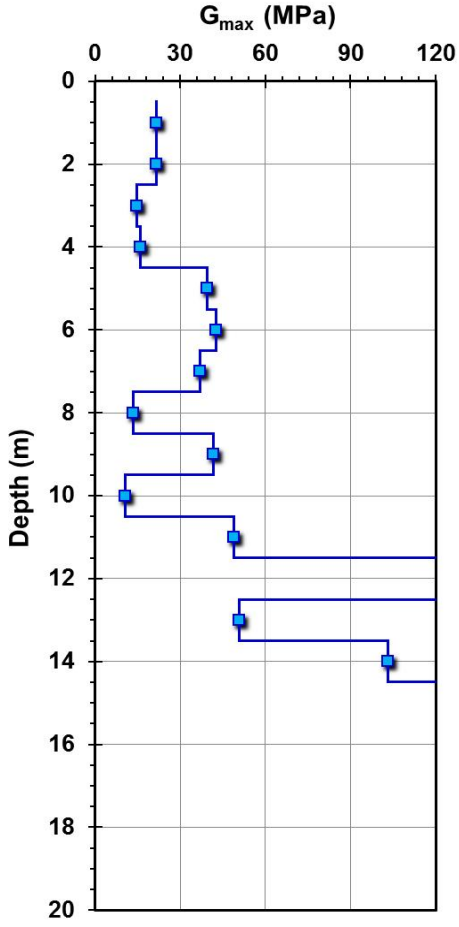

Initial shear stiffness (G_{max}) profiles from shear wave velocity (V_s) readings.

Site ID No. 47: Onsøy clay site, south-eastern Norway	Site ID No. 48: Pentre silt, Shropshire, UK	Site ID No. 50: Pitt River Bridge, Vancouver South, BC, Canada
Soft clay with shell fragments	Soft clayey silt	Interbedded silt, clay, and sand over thick layer of silty clay over glacial till
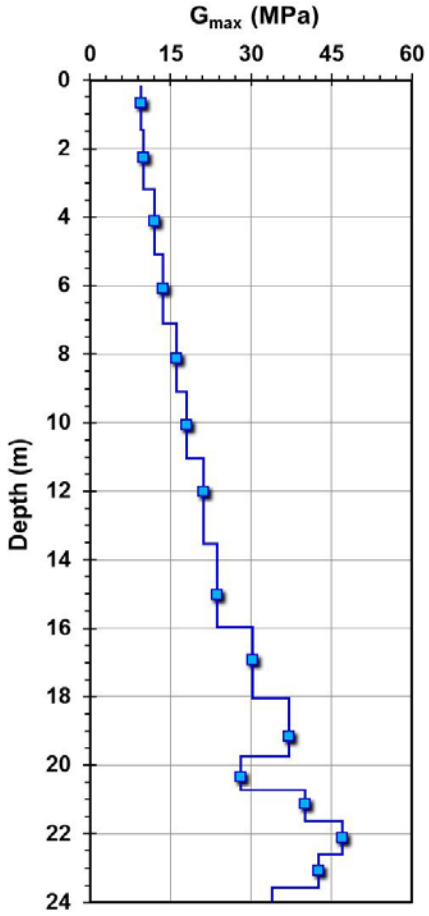	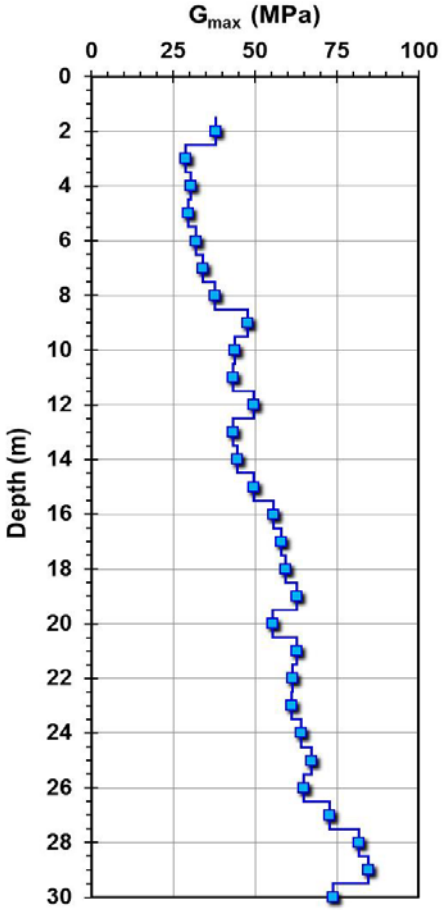	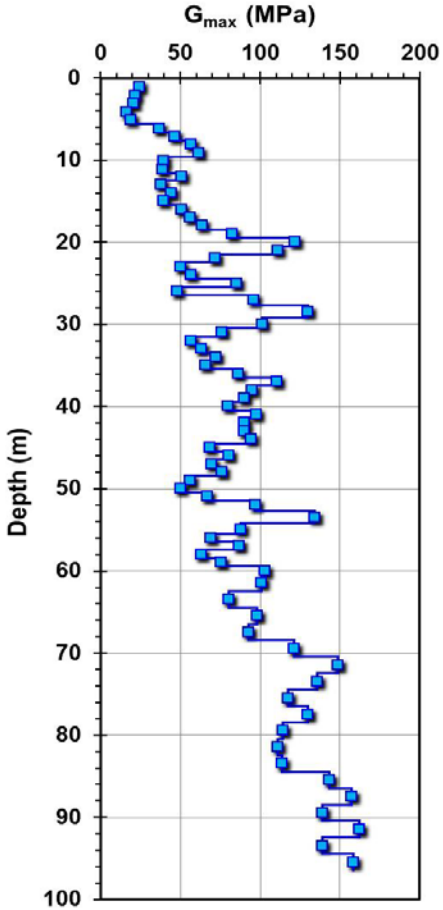

Initial shear stiffness (G_{max}) profiles from shear wave velocity (V_s) readings.

Site ID No. 52: Saint Alban, QC, Canada	Site ID No. 53: Sandpoint, along the shores of Lake Pend Oreille, Northern ID, USA	Site ID No. 55: Shenton Park, Perth, Western Australia
Soft silty marine clay	Silty clayey sand over soft thick silty clay	Siliceous sand
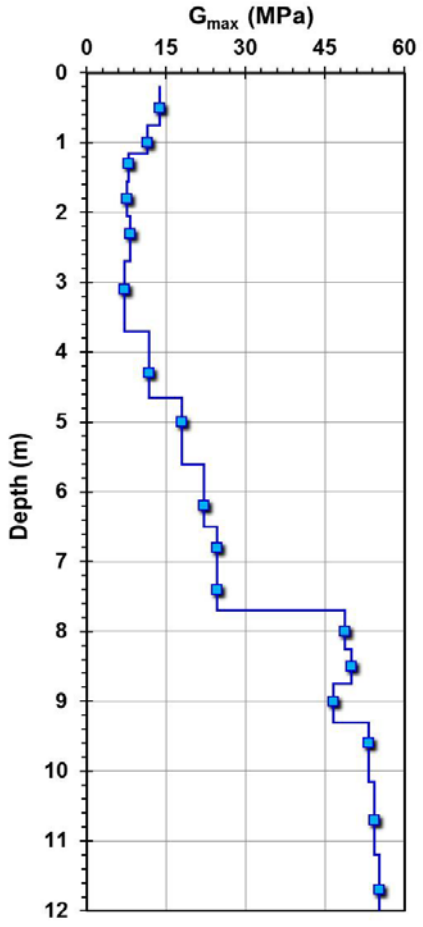	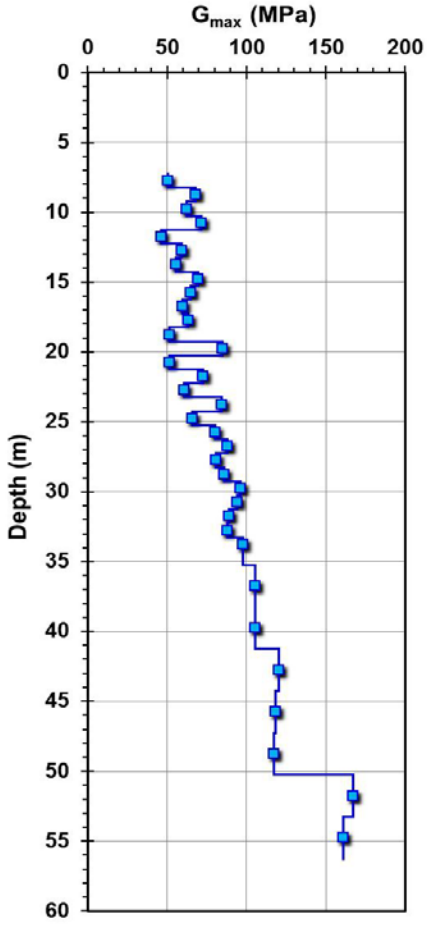	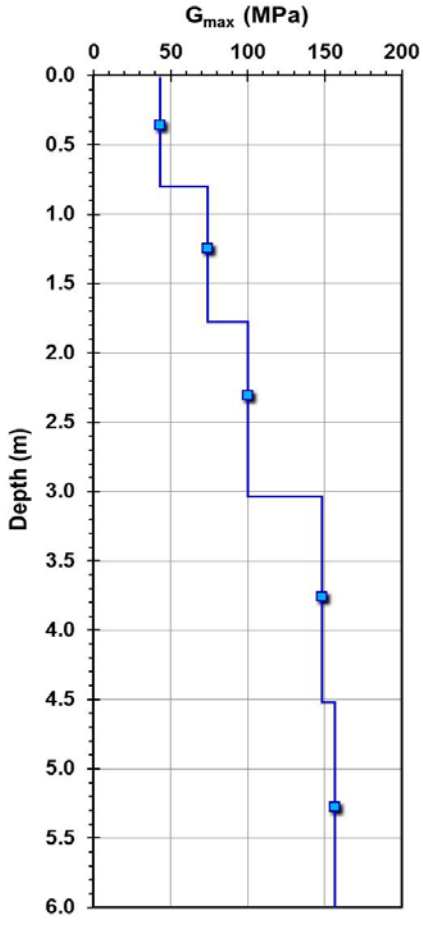

Initial shear stiffness (G_{max}) profiles from shear wave velocity (V_s) readings.

Site ID No. 56: Shirasu soil, lanima, Southern Kyushu, Japan	Site ID No. 57: South Temple test site on I-15, Salt Lake City, Utah, USA	Site ID No. 58: Spring Villa, Opelika NGES, AL, USA
Clean sand over silty sand over silty clay	Silty sandy clay over sensitive clay	Clayey-silty sand
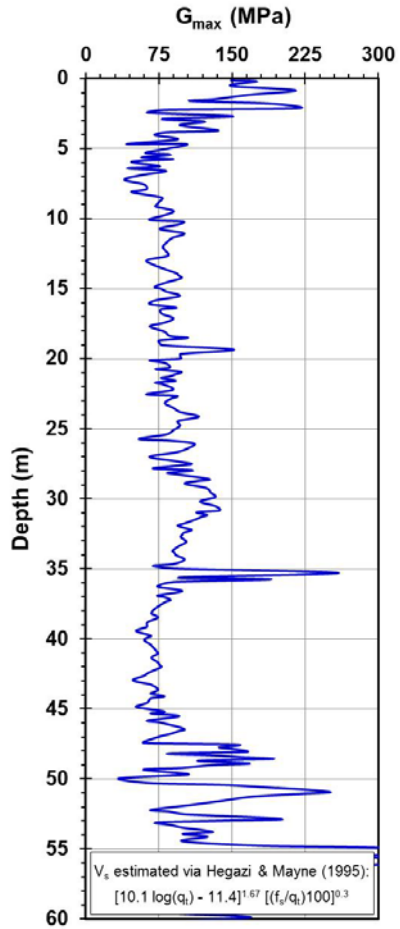	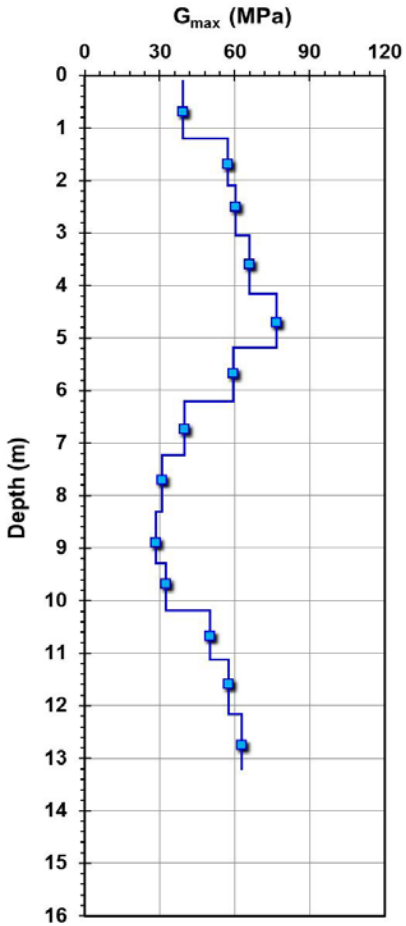	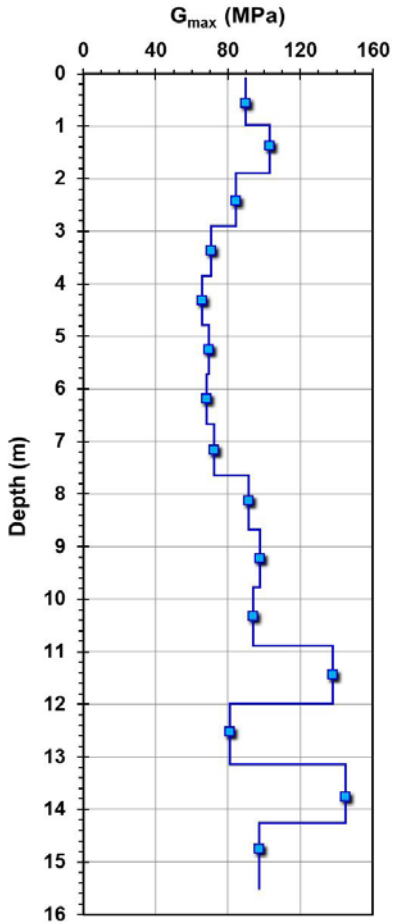

Initial shear stiffness (G_{max}) profiles from shear wave velocity (V_s) readings.

Site ID No. 59: State Road 49, Jasper County, Indiana, USA	Site ID No. 60: Texas A&M University (TAMU) NGES clay site, College Station, TX, USA	Site ID No. 61: Texas A&M University (TAMU) NGES sand site, College Station, TX, USA
Silt dominated multilayered soil	Very stiff Pleistocene clay	Medium dense sand over stiff clay
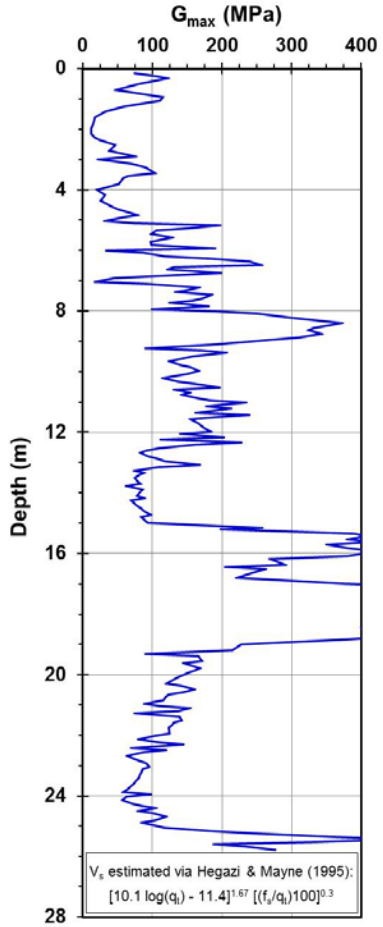	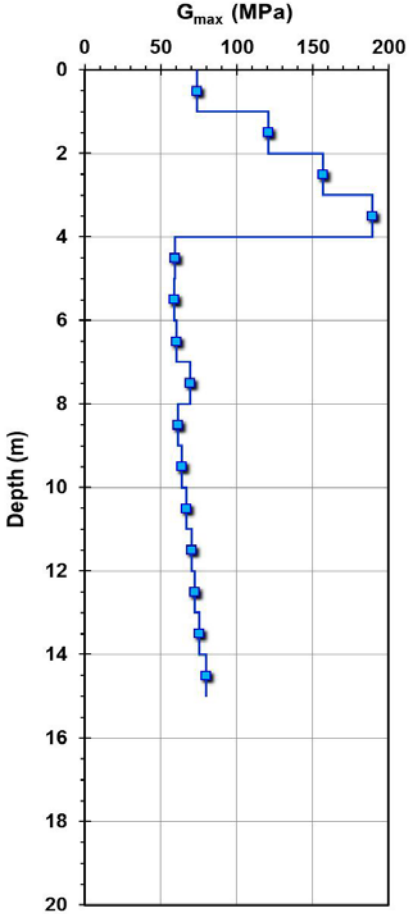	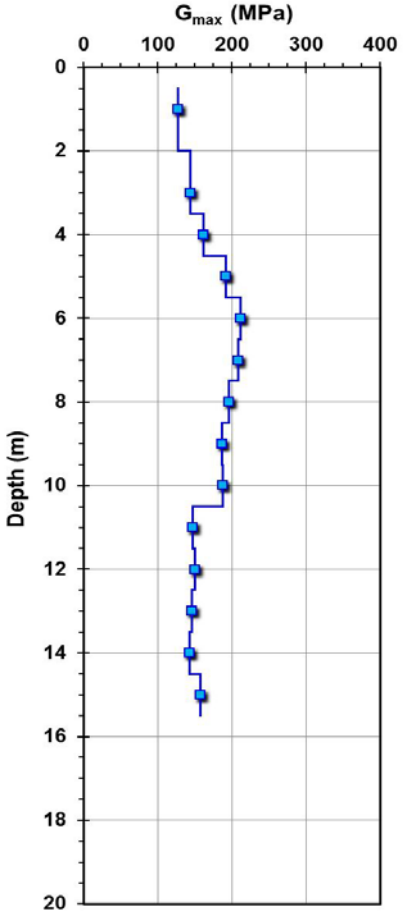

Initial shear stiffness (G_{max}) profiles from shear wave velocity (V_s) readings.

Site ID No. 62: Trunk Hwy 212 Bridge No. 10038 near Minneapolis, MN, USA	Site ID No. 63: Trunk Hwy 52 Lafayette Bridge over the Mississippi River, St. Paul, MN, USA	Site ID No. 65: University of Massachusetts-Amherst NGES, Amherst, MA, USA
Stiff clay loam glacial till over dense sand	Fine to coarse gravelly sand	Silty clay crust over soft varved clay
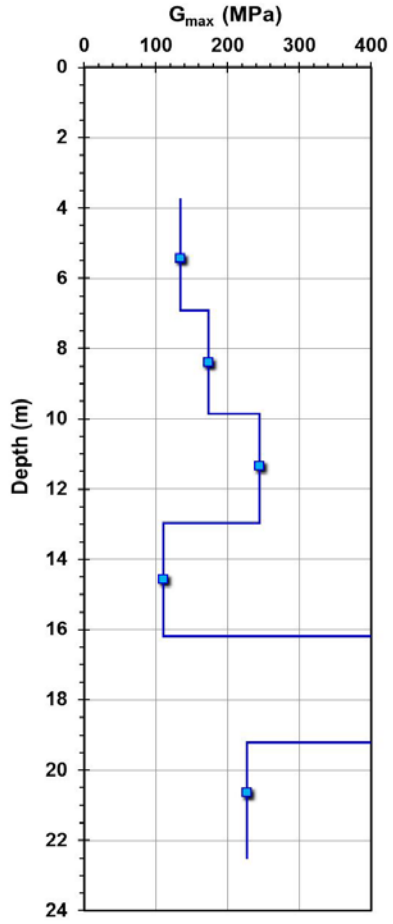	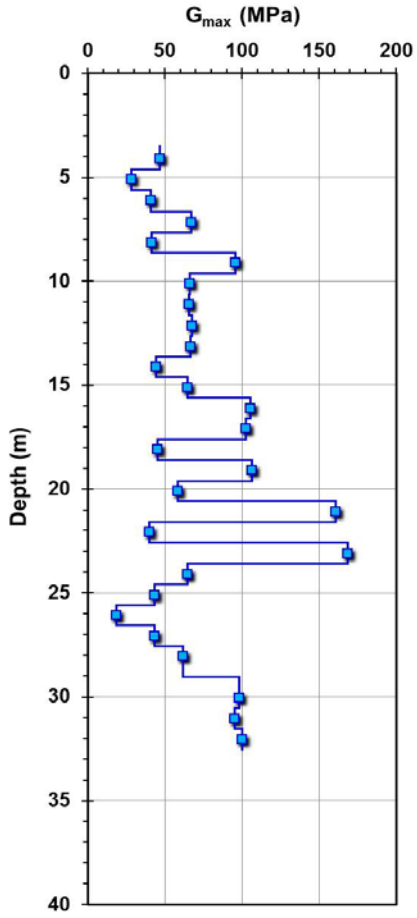	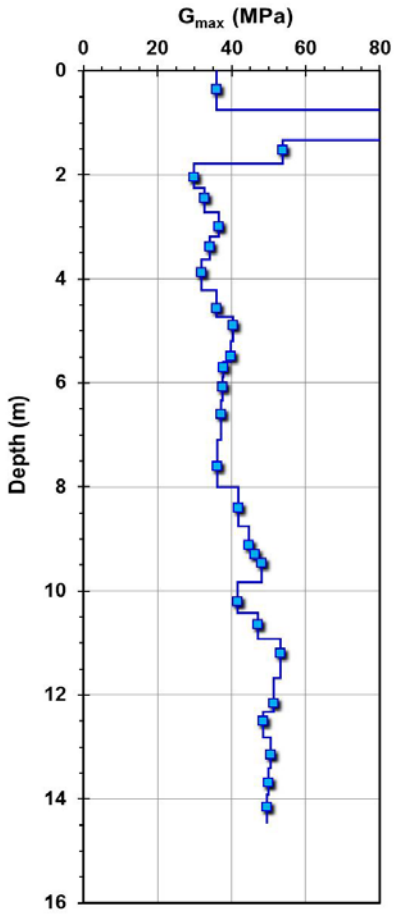

Initial shear stiffness (G_{max}) profiles from shear wave velocity (V_s) readings.

Site ID No. 66: University of Porto, Portugal (FEUP), ISC-2 experimental site	Site ID No. 67: Varina-Enon Bridge, I-295 over James River, Richmond, VA, USA	Site ID No. 68: W. R. Bennett Bridge, Okanagan Lake at Kelowna, BC, Canada
Residual silty sand	Alluvial sands, silts, and clays overlying dense sands and gravels	Loose to medium dense lacustrine silts and sandy silt overlying sand
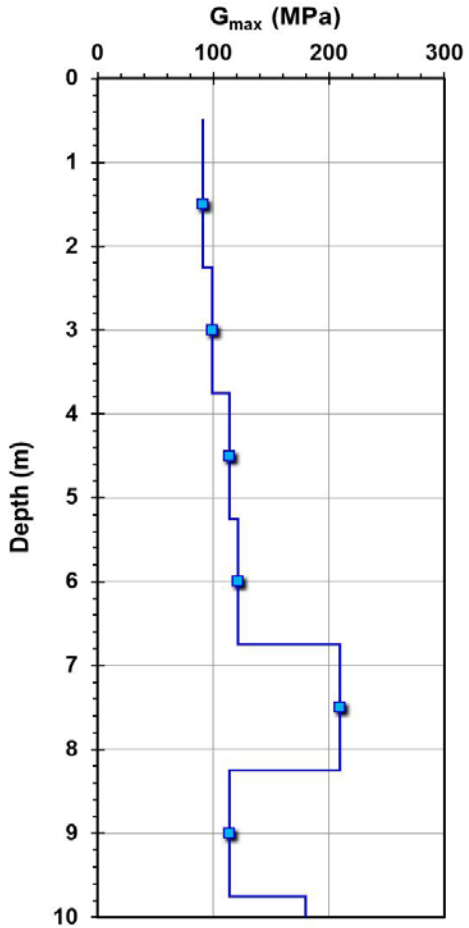	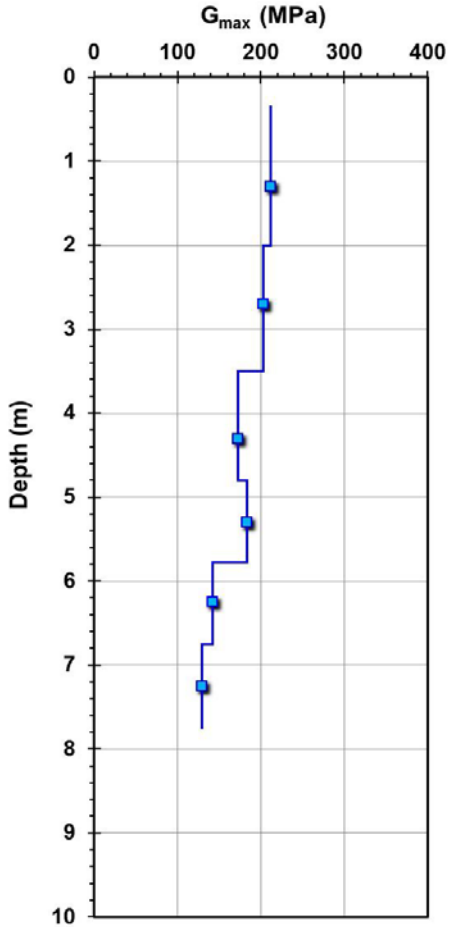	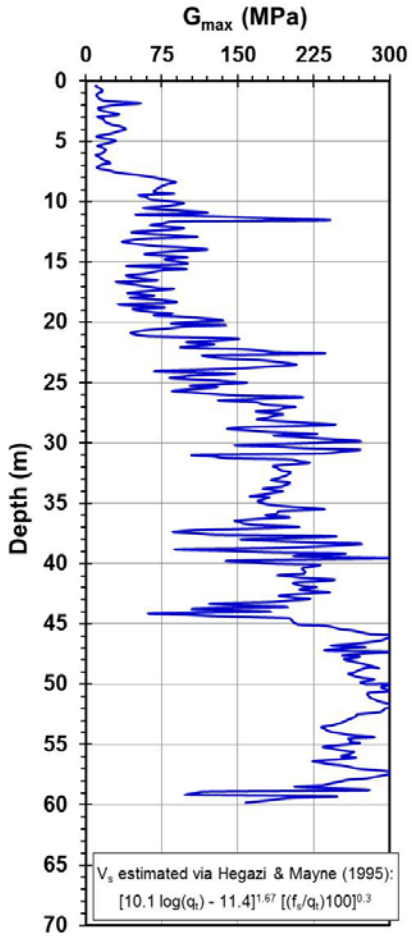

Initial shear stiffness (G_{max}) profiles from shear wave velocity (V_s) readings.

Site ID No. 69: Wakota River Bridge site (I-494 Mississippi River Bridge), MN, USA		
Sand with intermittent layers of silt and clay		
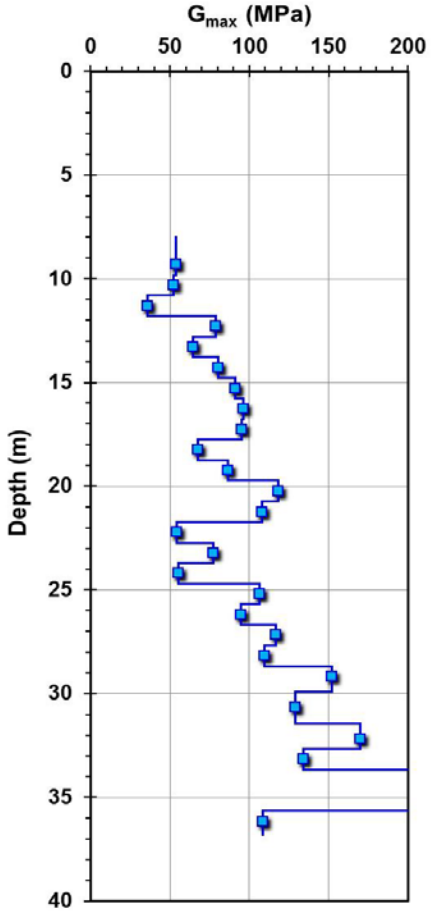		

APPENDIX I

RESULTS OF STUDY ON THE INFLUENCE OF PLASTICITY INDEX ON SHEAR MODULUS REDUCTION

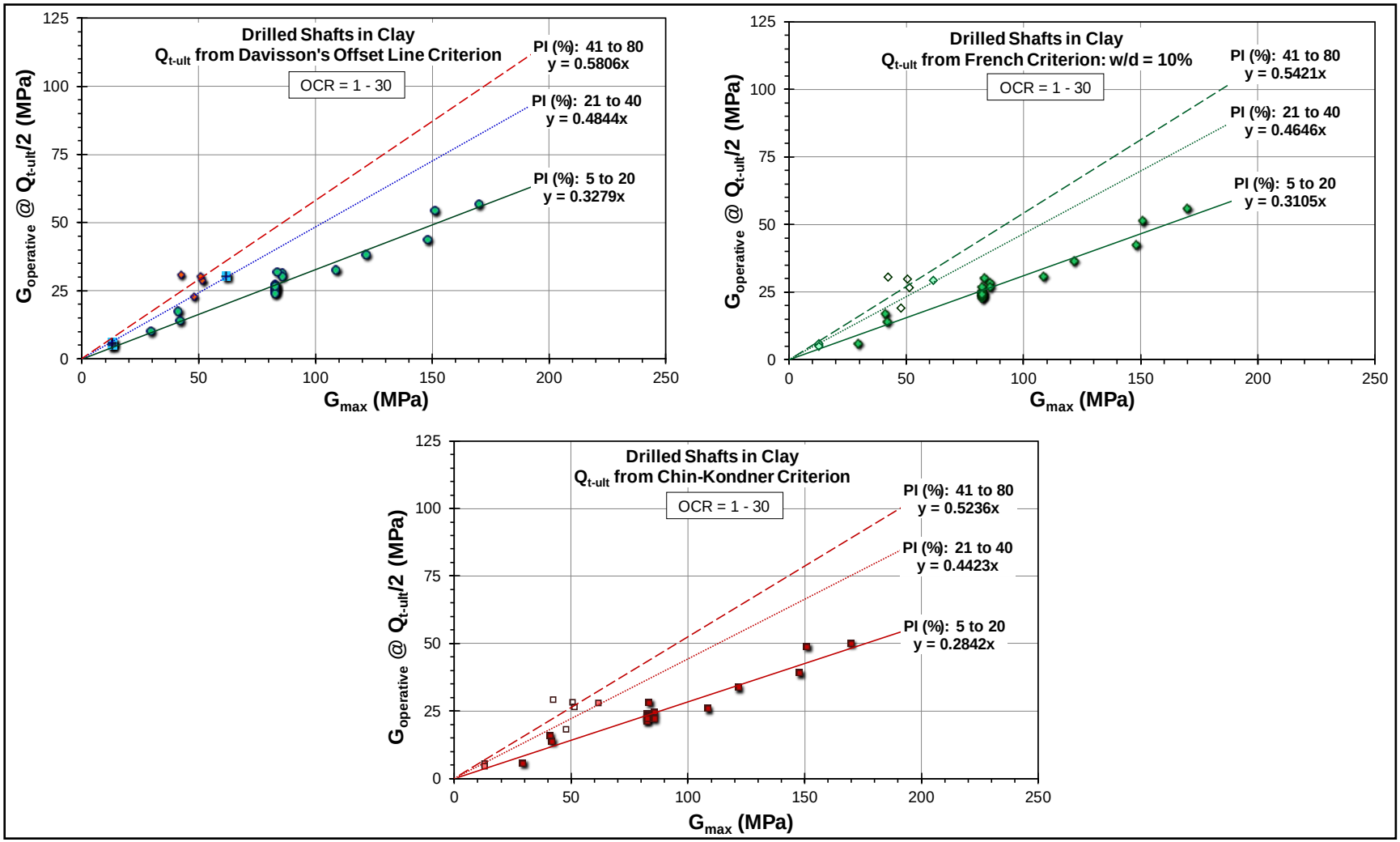

Figure. I.1. Influence of PI (%) on shear modulus reduction at $Q_t/Q_{t\text{-}ult}$ = 0.5 (drilled shafts in clay).

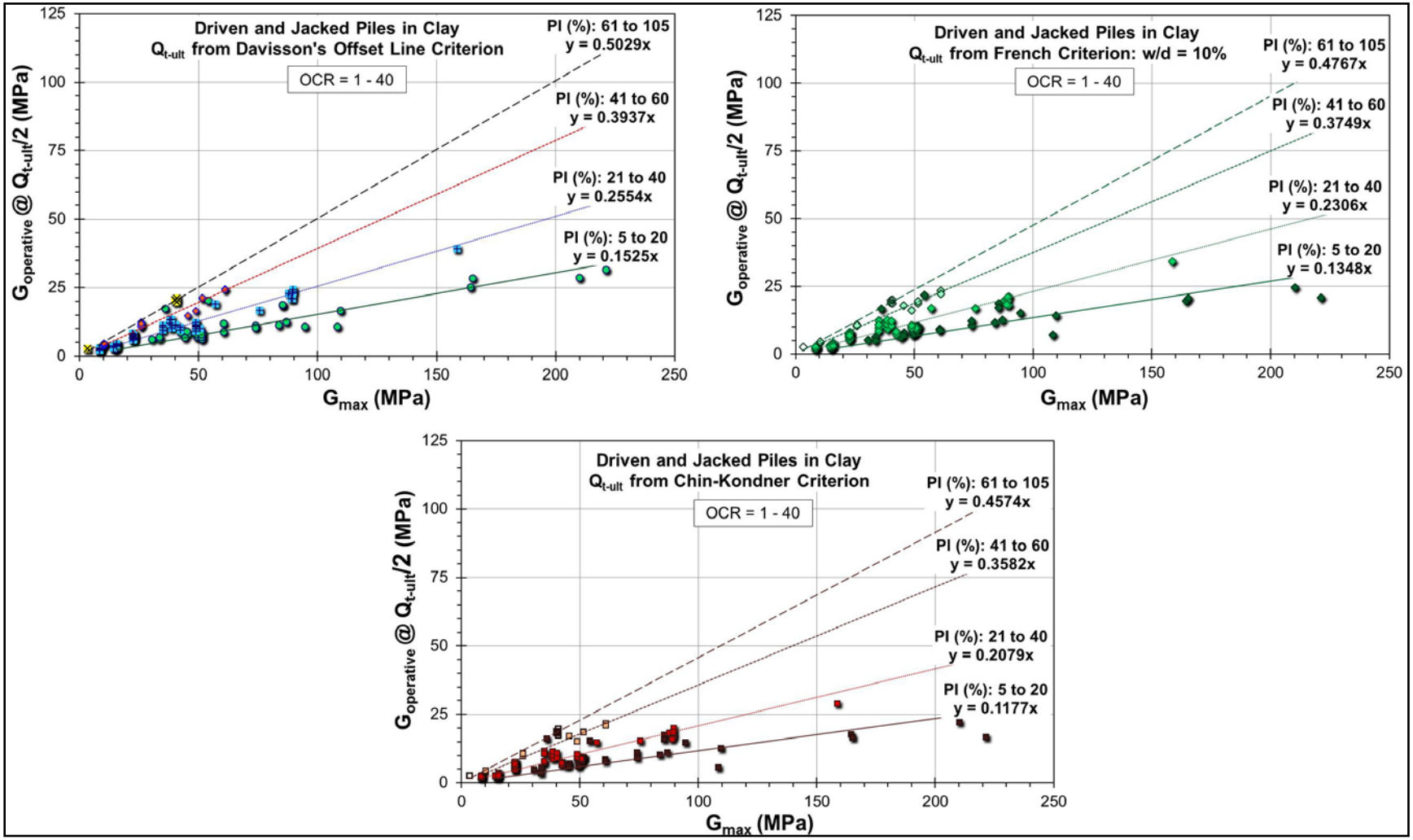

Figure. I.2. Influence of PI (%) on shear modulus reduction at $Q_t/Q_{t\text{-}ult}$ = 0.5 (driven and jacked piles).

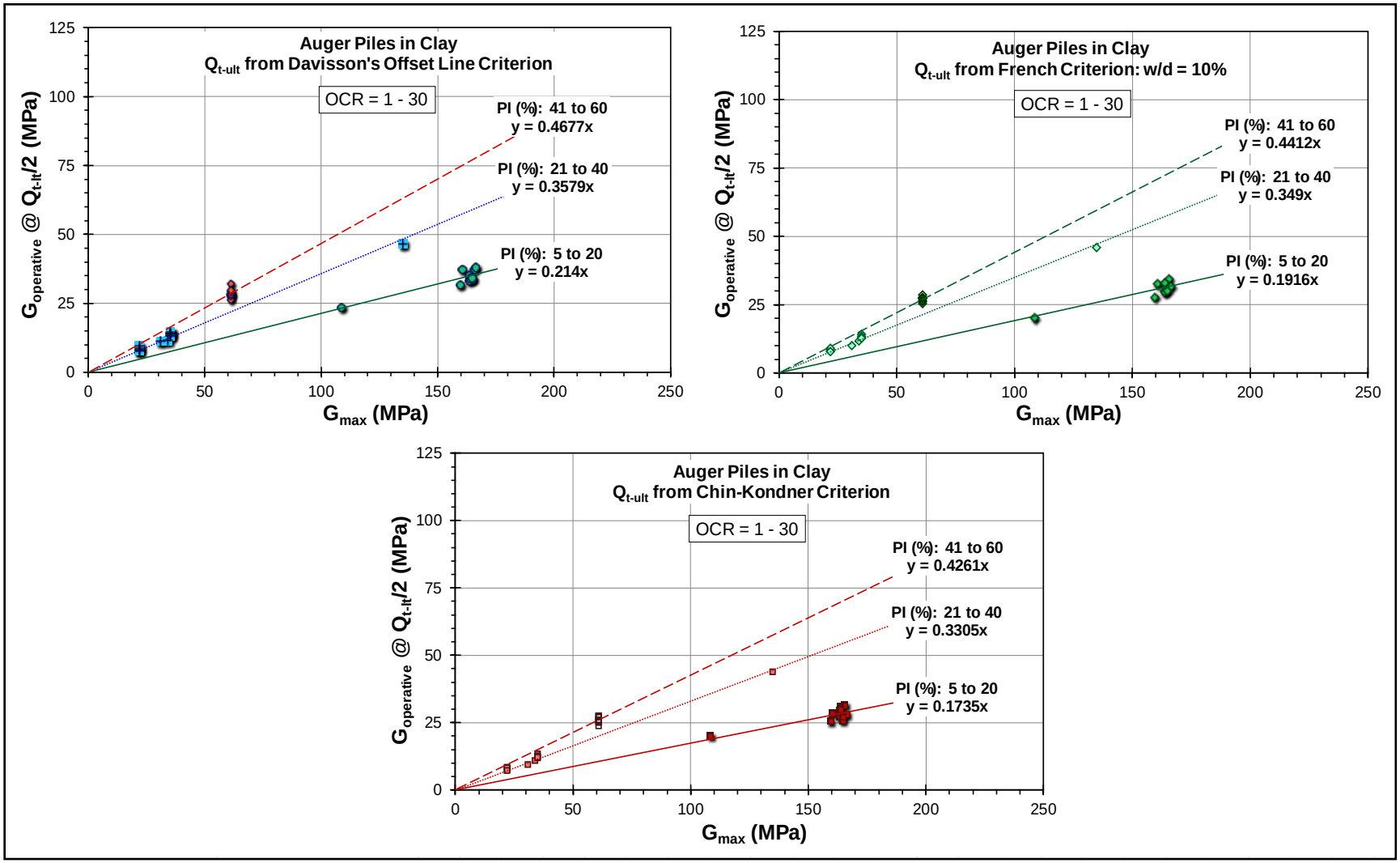

Figure. I.3. Influence of PI (%) on shear modulus reduction at $Q_t/Q_{t\text{-}ult}$ = 0.5 (auger piles in clay).

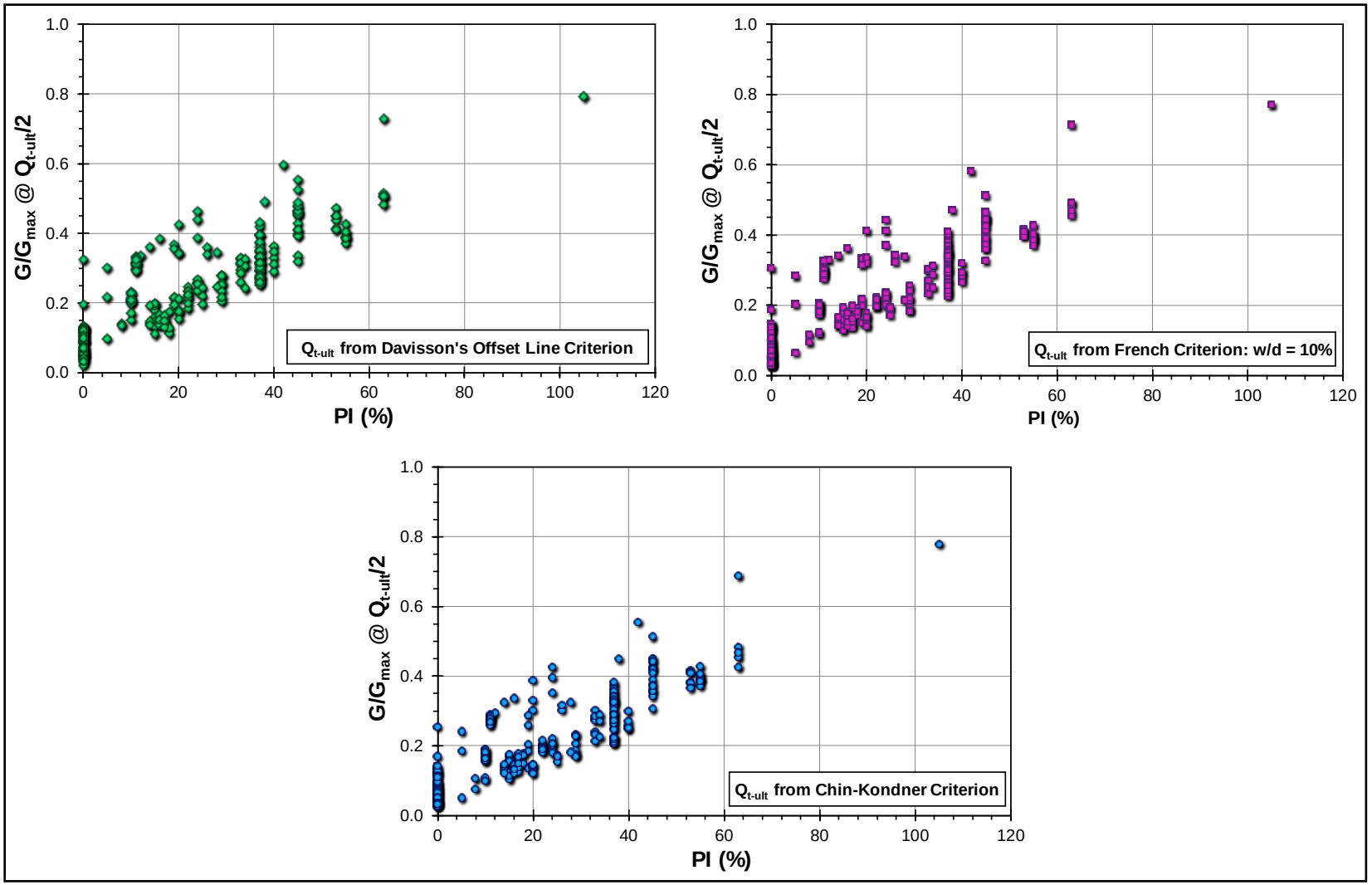

Figure I.4. Normalized operative shear stiffness at a reference rate of 0.5 · $Q_{t\text{-}ult}$ vs. percent PI: (a) $Q_{t\text{-}ult}$ estimated using Davisson's offset line criterion; (b) $Q_{t\text{-}ult}$ estimated using French criterion: w/d = 0.1; $Q_{t\text{-}ult}$ estimated using Chin-Kondner criterion.

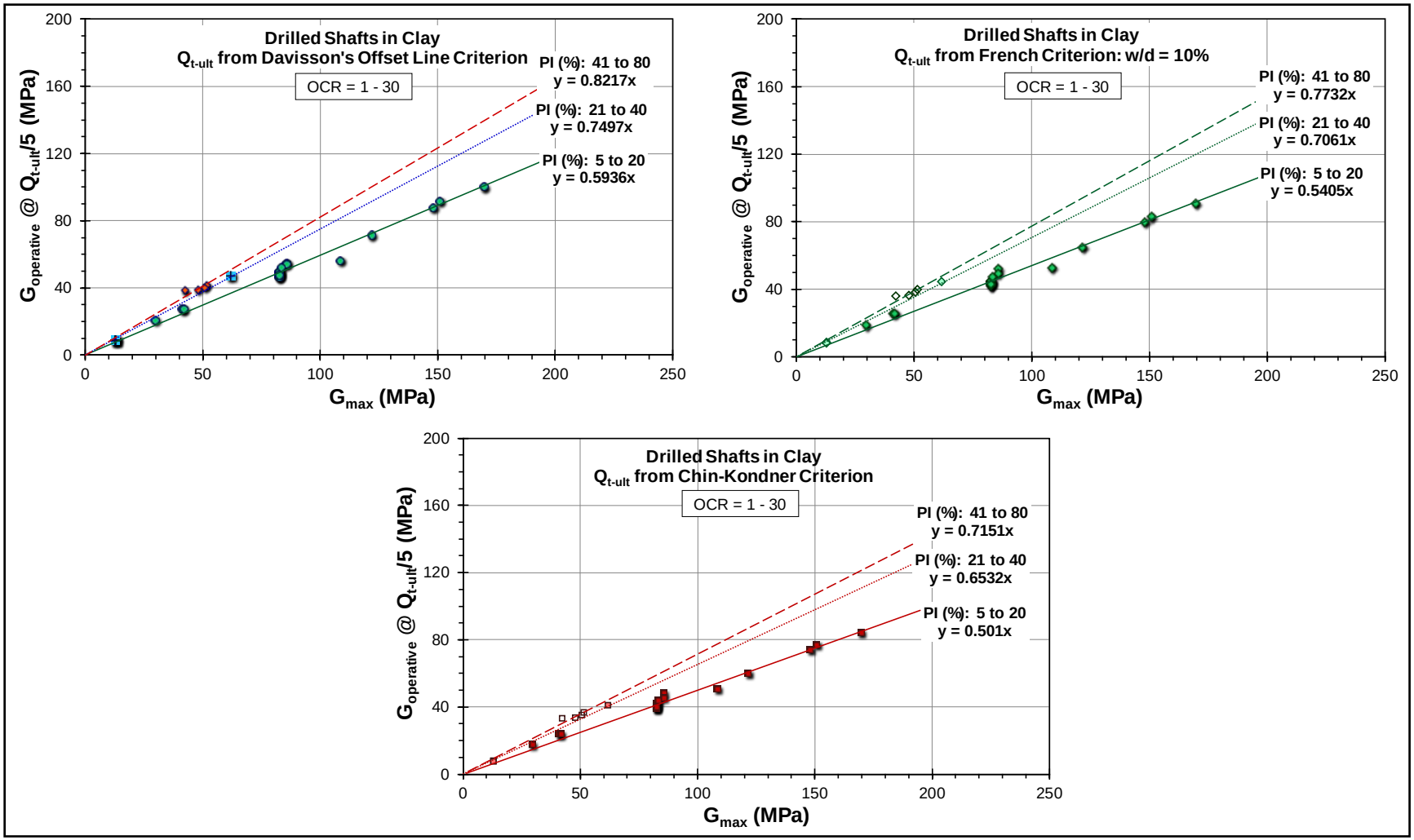

Figure. I.5. Influence of PI (%) on shear modulus reduction at $Q_t/Q_{t\text{-}ult}$ = 0.2 (drilled shafts in clay).

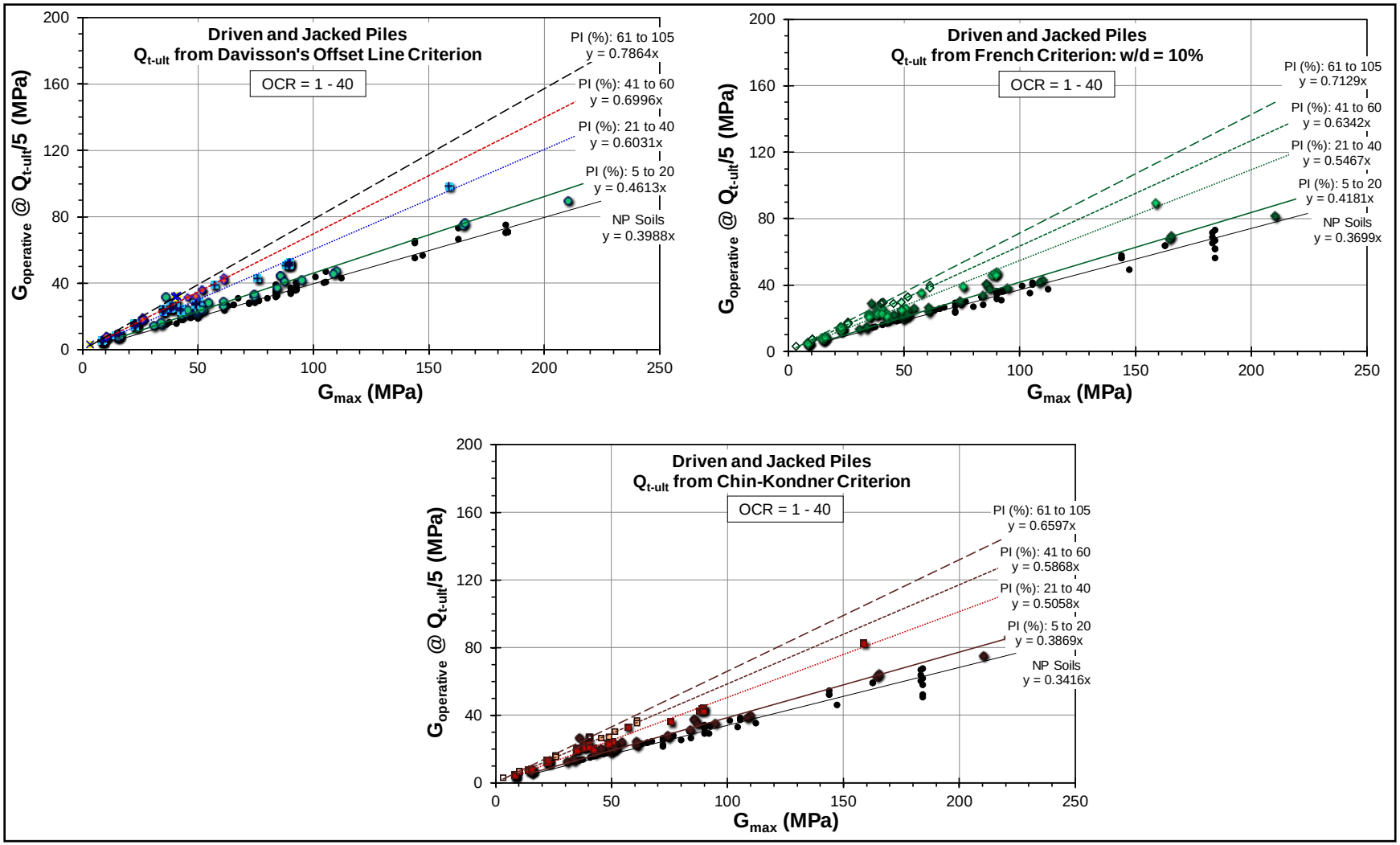

Figure. I.6. Influence of PI (%) on shear modulus reduction at $Q_t/Q_{t\text{-}ult}$ = 0.2 (driven and jacked piles).

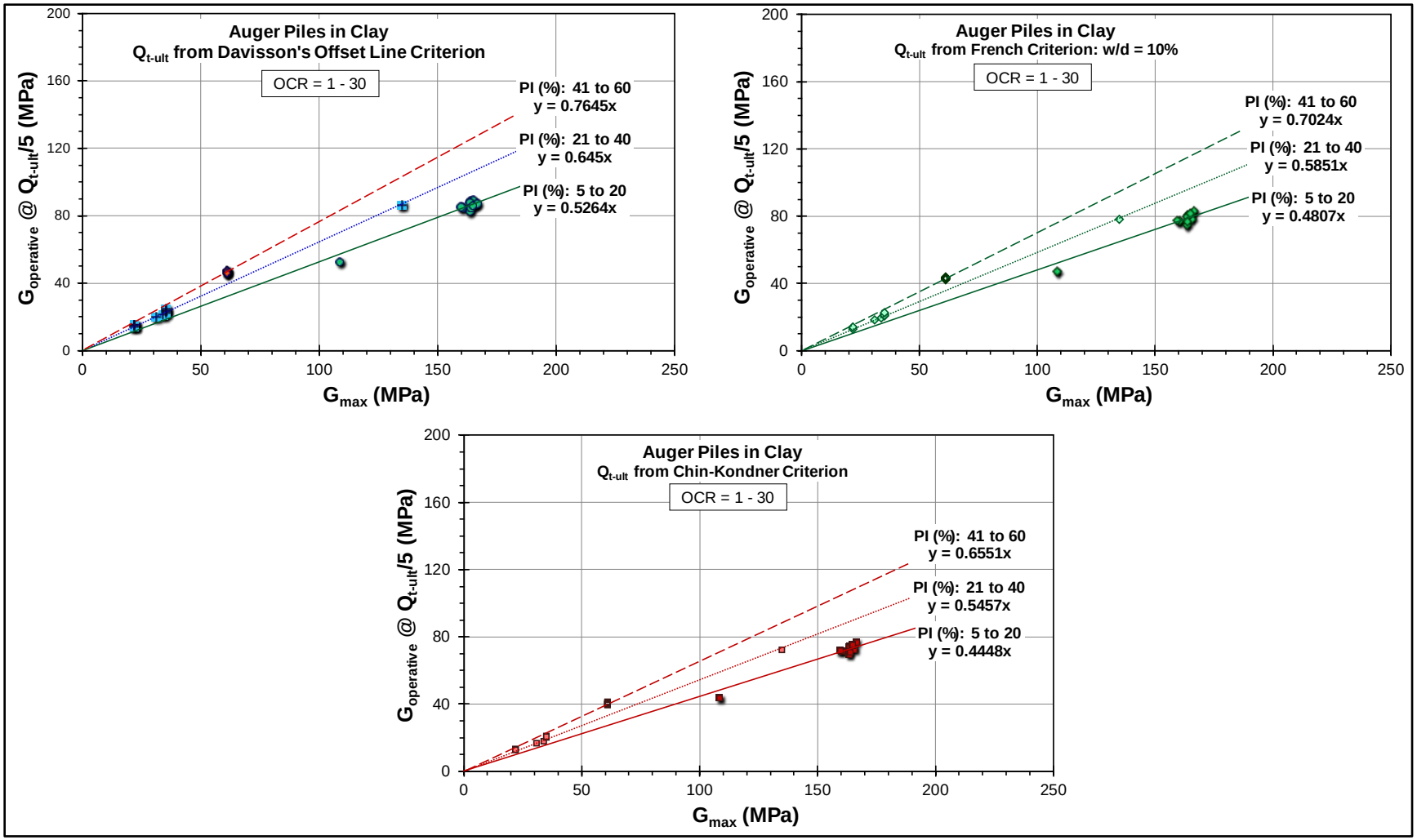

Figure. I.7. Influence of PI (%) on shear modulus reduction at $Q_t/Q_{t\text{-}ult}$ = 0.2 (auger piles in clay).

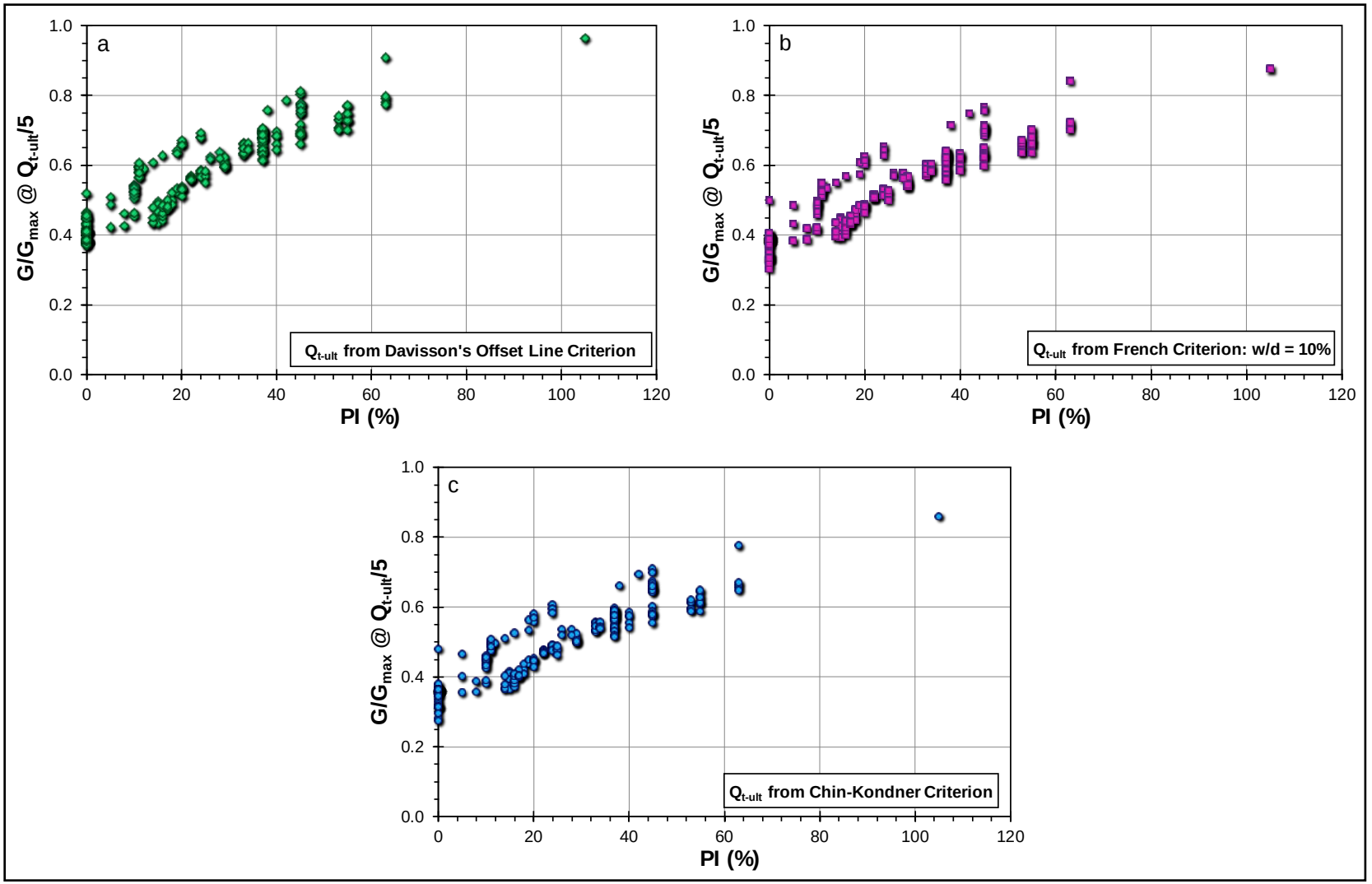

Figure I.8. Normalized operative shear stiffness at a reference rate of 0.2 · $Q_{t\text{-}ult}$ vs. percent PI: (a) $Q_{t\text{-}ult}$ estimated using Davisson's offset line criterion; (b) $Q_{t\text{-}ult}$ estimated using French criterion: w/d = 0.1; $Q_{t\text{-}ult}$ estimated using Chin-Kondner criterion.

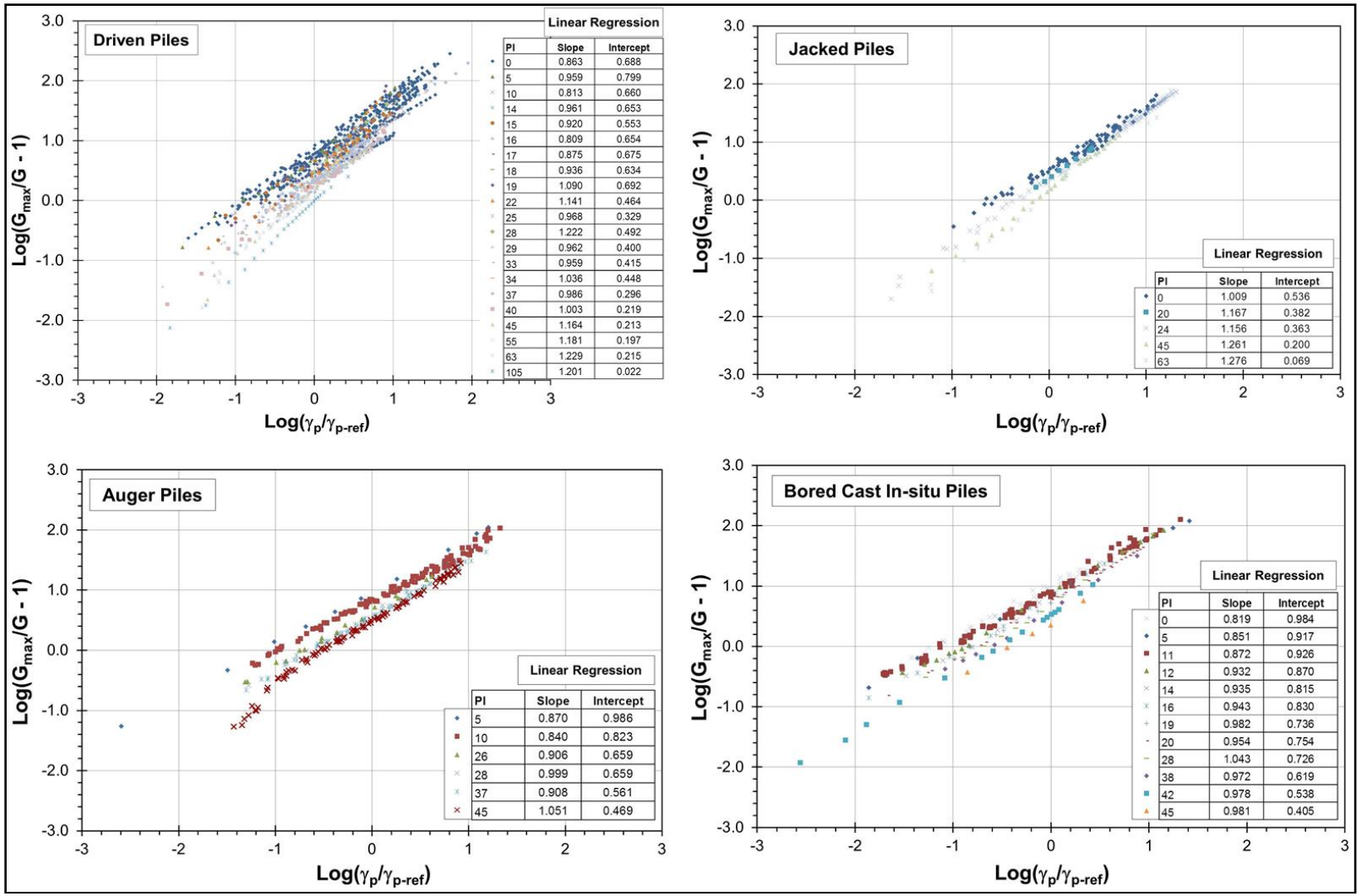

Figure I.9. Slopes and intercepts of linear regression of the transformed predictor ($\gamma_p/\gamma_{p\text{-}ref}$) and response ($G/G_{max}$) variables for different PI values for different pile categories.

APPENDIX J

APPLICATION OF ELASTIC CONTINUUM SOLUTION OF STACKED PILE MODEL FOR AXIAL LOAD DISPLACEMENT ANALYSIS

Synopsis

This appendix presents a published technical paper of a case study in which the candidate is the lead author. As part of this case study, it offers application of the stacked pile model for the load-displacement analysis within an elastic continuum solution of a bored pile, tested in a research program at Grimsby Research Site underlain by glacial till and located near Waltham, UK. The SCPTu sounding at the site enabled acquisition of the G_{max} profile from the field V_s readings and the pile capacity was determined from the cone penetrometer data. Further details of the site geotechnical conditions, testing program, and the analysis results are presented in the paper, which was published as:

Niazi, F. S., Mayne, P. W. and Woeller, D. J. (2010b). "Case history of axial pile capacity and load-settlement response by SCPTu." *Proceedings, 2nd International Symposium on Cone Penetration Testing* (CPT'10, Huntington Beach, CA), Omnipress, Vol. 3: 9 – 16. www.cpt10.com.

Case history of axial pile capacity and load-settlement response by SCPTu

F.S. Niazi & P.W. Mayne
Georgia Institute of Technology, Atlanta, Georgia, USA

D.J. Woeller
ConeTec Investigations Ltd., Richmond, British Columbia, Canada

ABSTRACT: The performance of pile foundations under axial compression loading can be rationally evaluated within an elastic continuum framework using field results from seismic piezocone tests (SCPTu). The SCPTu is an optimal means for collection of subsurface information because it captures up to 5 independent readings in one sounding: tip resistance (q_t), sleeve friction (f_s), tip or mid-face porewater pressure (u_1) and/or shoulder porewater pressure (u_2), and shear wave velocity (V_s). The measurements obtained are at opposite ends of the stress-strain-strength curves: the peak strength and stress state for capacity interpretations and the small-strain stiffness (G_{max}) for evaluating the initial deformations. Using a versatile Randolph-type elastic pile model, the approach can be applied to evaluate the axial response of pile load tests. The axial load distribution within the shaft is also evaluated. A case study is presented illustrating application of this approach on a bored cast in situ pile tested in glacial till near Grimsby, UK.

INTRODUCTION

Deep foundations in the form of driven piles and drilled shafts are commonplace for large scale projects including high-rise buildings and multi-span bridges. Conventional investigation methods for subsurface characterization of deeper soil layers affecting the performance of these foundations (boring and sampling) are time consuming and tedious. The results are constrained by the effects of sample disturbance. In-situ tests using SCPTu provide an alternate, yet quick and reliable means of obtaining soil engineering parameters of the soil layers of interested depth. For specific sites the SCPTu provides up to 5 independent readings with depth in one sounding: q_t, f_s, u_1 and/or u_2, and V_s. The recent utilization of the SCPTu offers improved interpretation procedures and correlations for the soil engineering parameters (Mayne 2005, Schnaid 2005). A multiple-readings based methodology has been devised for the analysis of pile foundations, as opposed to the older methods, many of which were based solely on q_c alone. The measured q_t is also corrected for u_2 acting behind the tip (Lunne et al. 1997). The penetrometer readings (qt, f_s, u_1 and u_2) and downhole geophysics (V_s) are at the opposite ends of the stress-strain-strength curves: the peak strength for capacity evaluation and the fundamental stiffness (G_{max} or E_{max}) for the initial soil deformations

(γ_s < 10^{-6}%). These results have been successfully applied within the elastic theory (Poulos & Davis 1980, Randolph & Wroth 1978, 1979, Fleming et al. 1992) to evaluate the entire load-displacement-capacity behavior for axial loading performance of deep foundations (e.g., Mayne & Elhakim 2002, Mayne & Zavala 2004, Mayne & Woeller 2008, Mayne & Niazi 2009).

Pile foundations analysis can be accomplished using the "rational CPT" assessments or the "direct CPT" approach, or a combination of both (Mayne 2007).

SOIL PARAMETER ASSESSMENTS BY CPT

In rational approach, the SCPTu data are used to classify the soil types, calculate soil engineering parameters, and evaluate pile capacity.

1.1 *Soil Classification*

For general use, the method based on the normalized CPTu parameters provides a soil classification index (I_c) (Jefferies & Been 2006):

$$I_c = \sqrt{\{3 - log[Q(1 - B_q) + 1]\}^2 + [1.5 + 1.3(logF)]^2} \quad (1)$$

where $Q = (q_t - \sigma_{vo})/\sigma_{vo}'$, $B_q = (u_2 - u_o)/(q_t - \sigma_{vo})$, $F = f_s \cdot 100/(q_t - \sigma_{vo})$, and σ_{vo}' is the effective overburden stress = $\sigma_{vo} - u_o$. As per Robertson (1990), the ranges of I_c values for different soil types are as follows; organic clay soils (zone 2): $I_c > 3.22$; clays (zone 3): $2.82 < I_c < 3.22$; silt mixtures (zone 4): $2.54 < I_c < 2.82$; sand mixtures (zone 5): $1.90 < I_c < 2.54$; sands (zone 6): $1.25 < I_c < 1.90$; and gravelly sands (zone 7): $I_c < 1.25$.

1.2 *Soil Engineering Parameters*

The unit weight (γ_t) of soil layers needed to calculate the overburden stress (σ_{vo}), frictional characteristics (ϕ'), shear wave velocity (V_s) for calculating fundamental stiffness (G_{max}) and the equivalent Young's Modulus (E_{max}), stress history (σ_p'), geostatic stress state ($K_o = \sigma_{ho}'/\sigma_{vo}'$), and undrained shear strength s_u of clays can be evaluated from the CPT data using the relationships already well documented (e.g., Mayne 2007; Mayne et al. 2009; and 2010).

The $(s_u / \sigma_{vo}')_{NC}$ for direct simple shear (*DSS*) mode has been shown suitable for direct use in the analysis of foundation (Ladd 1991). Values of $(s_u/\sigma_{vo}')_{OC}$ for *DSS* mode can be obtained using appropriate equations. Fissured soils exhibit half the strengths associated with those of intact clays (Mayne 2007).

G_{max} represents the elastic region of soil behavior. The value of G must be reduced corresponding to strains for the applicable loads to utilize in the elastic continuum equations. Fahey & Carter (1993) proposed the following algorithm:

$$G/G_{max} = 1 - (1 / FS)^g \quad (2)$$

where 1 / *FS* (reciprocal of factor of safety) = Q / Q_{ult} is the mobilized load level and g is a fitted exponent = 0.3 +/– 0.1 for well behaved soils (Mayne 2007).

1.3 *Capacity Evaluation*

The pile unit side resistance (f_p) and end bearing (q_b) can be obtained using relationships presented by Kulhawy et al. (1983), Lee et al. (2003), and Vesić (1977). The axial compression capacity ($Q_t = Q_{ult}$) of a circular pile foundation is calculated from:

$$Q_t = Q_s + Q_b = \Sigma(f_{pi}\, \pi d \Delta z_i) + q_b \pi d^2 / 4 - W_p \quad (3)$$

where f_{pi} is the unit side resistance at ith soil layer, $\pi d \Delta z_i$ is the shaft area of the i^{th} soil layer, and W_p = the pile weight.

DIRECT CPT METHOD

From the many available direct CPT methods, selected ones for the bored piles (relevant to the case study presented herein) are presented by Bustamante & Gianeselli (1982); Eslami & Fellenius (1997); Takesue et al. (1998); Jamiolkowski (2003) and Chen & Kulhawy (1994).

ELASTIC CONTINUUM SOLUTION

The axial load-displacement response and the fraction of load transfer to the pile base (Q_b) for top-down loading can be evaluated using an analytical closed-form elastic continuum pile solution summarized in Figure 1 (after Randolph 2003, and Fleming et al. 1992). This solution can accommodate soil models with constant G (homogeneous soils) or soils having a linearly-varying G with depth (Gibson-type soils). The pile can be either a floating-type pile ($G_{sL} = G_{sb}$) or end-bearing type where the pile base rests on a stiffer stratum ($G_{sb} > G_{sL}$). Figure 1 also presents the stacked pile model for layered soils.

PILE LOAD TEST AT GRIMSBY RESEARCH SITE, UK

The Grimsby research site was located near Waltham, Grimsby, UK, 900 m north of the nearest watercourse and 7.5 km southwest of the nearest coastline (Brown 2004). Brown et al. (2006) report the ground conditions at the site as matrix-dominant glacial till underlain by cretaceous chalk bedrock; till being cohesive, overconsolidated stiff to firm, grayish to dark brown, predominantly silty clay with cobbles, boulders and pebbles. Index properties include liquid limit: 20 – 36%, plastic limit: 12 – 18%, moisture content: 14 – 24%, specific gravity: 2.69, and clay fraction: 20 – 38%. Prior to the load test on a 12.08-m deep and 0.6-m diameter bored pile, extensive site and laboratory investigations were conducted. Of interest is a 20 m deep SCPTu sounding (see Figure 2). The measured u_1 readings were converted to u_2 via the relationship: $u_2 = 0.742 \cdot u_1$ (Chen & Mayne 1994). Brown (2004) reports of the loss of saturation of piezo-element in the upper layers for which probe was withdrawn and hole filled with water before resumption of the operation. The related effects on the u_2 profile can be observed in Figure 2. The u_2

profile has been reconstructed by averaging B_q values between 9.7 and 20 m and applying it to depths: 4.4 to 9.7 m.

The pile testing program at Grimby research site was designed to compare the results from rapid and static load tests: rapid load test (RLT) being performed first, followed by constant rate of penetration (CRP) test at 0.01 mm/s and maintained load test (MLT) (Brown et al. 2006). For this study, only the measured results of CRP test from Brown (2004) are considered, as presented in the subsequent section.

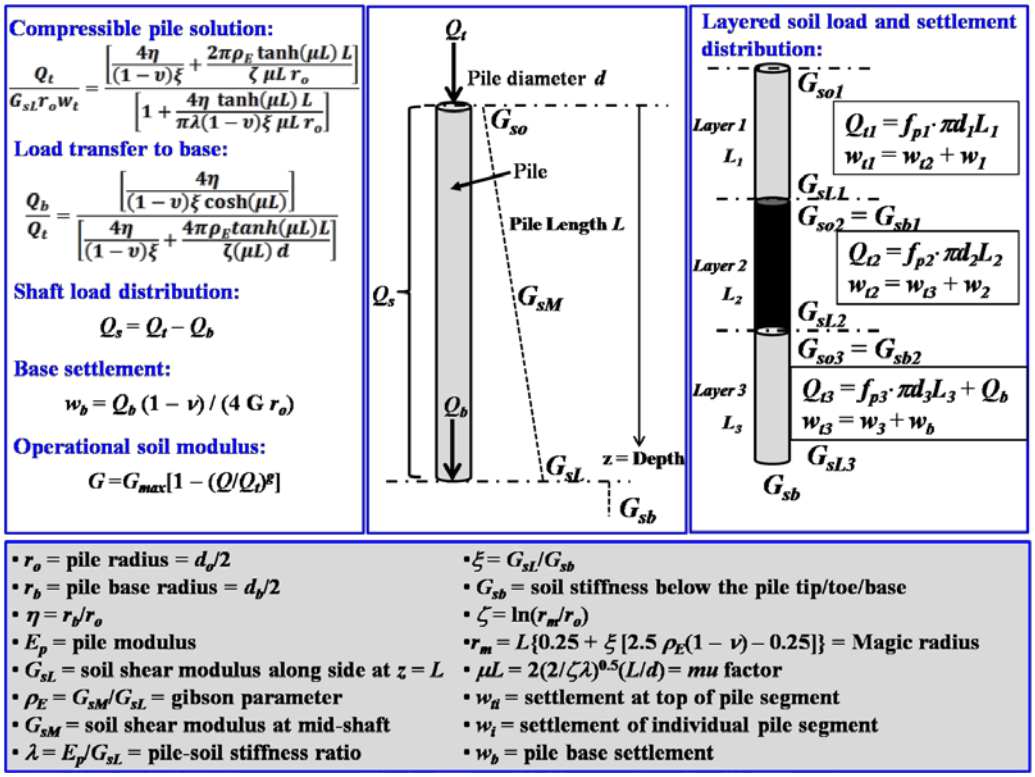

Figure 1. Elastic pile solution.

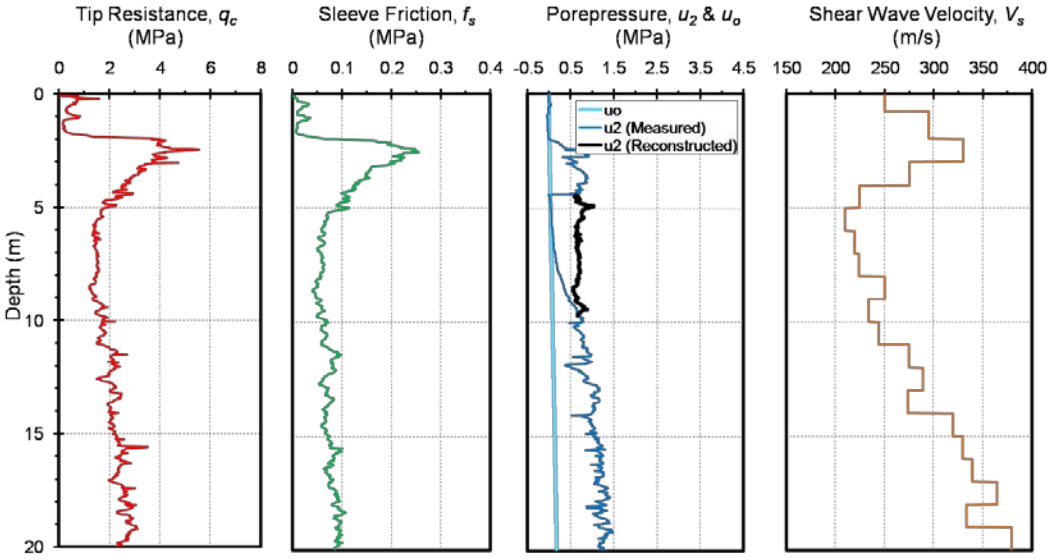

Figure 2. SCPTu sounding for pile load test at Grimsby research site, UK (after Brown 2004).

PILE RESPONSE EVALUATION

Figure 3 presents the soil classification and engineering parameters obtained by the post processing of SCPTu data using appropriate correlations. To validate the applicability of SCPTu based correlations, the measured values from Brown (2004) were also plotted. For most part, the values obtained from the correlations match closely with the measured values. Certain disagreements observed in the top layers may be attributed to the fact reported by Brown (2004) that the sounding was disrupted due to loss of saturation of the piezo-element and the final CPT data were formulated by a combination from the pre-drilled sounding (0 – 2.5 m) and the resumed operation after re-saturation. The B_q values obtained for certain depths were outside the applicable range for use in appropriate correlation for estimating ϕ ' for clays. So the ϕ ' profile was also obtained using correlation developed for sands, and the mean ratio (1.3) of the ϕ ' from the two relationships over the remaining depths was applied to obtain applicable values.

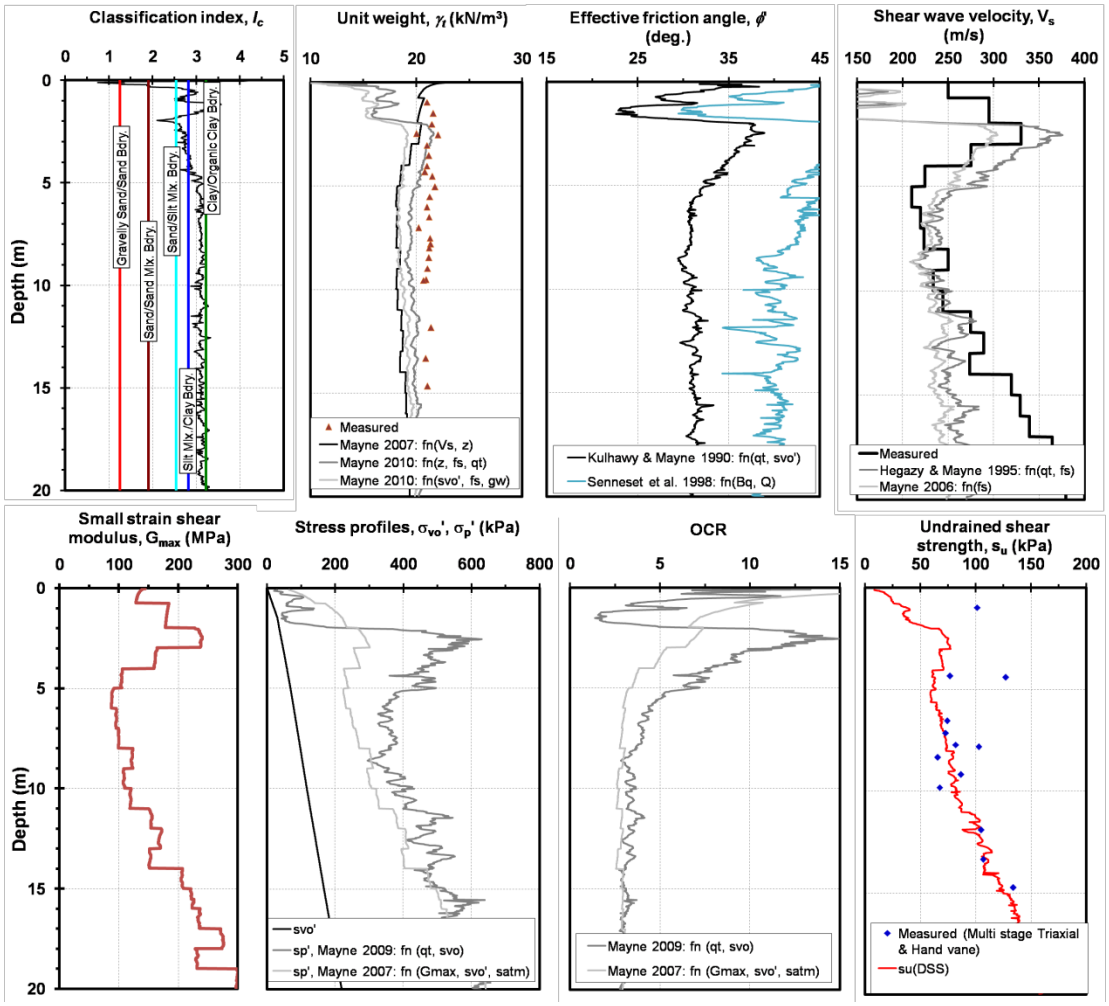

Figure 3. Soil parameters evaluation at Grimsby research site, UK.

Treating the stratum at the site as layered soil, the ultimate capacities were estimated for each layer. Figure 4 shows the individual load-settlement response based on the respective G_{max} and the capacities thus calculated. f_p and q_b for each defined layer were estimated from the various CPTu based methods. Summarized forms of the results are presented in Table 1. The KTRI method tends to overestimate Q_s, while the LCPC method yielded the least estimates for Q_s and Q_b in this case. Summation of the mean values of Q_s and Q_b found from different CPTu based methods (2386 kN) tends to match the measured Q_t. Using hyperbolic fitting model proposed by Kondner (1963), the estimated value of Q_{ult} (2372.5 kN) also goes with closely to the measured Q_t. Since Q_b values from all three methods shown in Table 1 yielded closer match, the maximum of these (307 kN) was selected. The difference of the estimated Q_{ult} from the hyperbolic fitting model and the selected Q_b was taken as the appropriate value for Q_s (2065.50 kN). Cumulative load-settlement curves (Q_t vs. w_t, Qs vs. w_t and Q_b vs. w_t) in Figure 5 shows a fine match with the measured response.

Table 1. Calculated pile capacities from direct and rational CPT methods.

Method	Tip capacity, Q_b (kN)	Shaft capacity, Q_s (kN)	Mean unit skin friction (kPa)				
			f_{p1} (0 - 0.74 m)	f_{p2} (0.74 - 1.96 m)	f_{p3} (1.96 - 2.96 m)	f_{p4} (2.96 - 4 m)	f_{p5} (4 - 12.1 m)
LCPC	264.63	711.76	12.43	13.04	35.00	35.00	34.79
Unicone	307.08	1077.6	29.27	26.40	85.9	59.58	45.79
KTRI		4875.1	11.29	13.55	448.2	473.94	199.56
Limit plasticity	299.26						
Beta		1378.33	7.30	13.53	73.3	72.68	69.36
Alpha		903.36	19.71	34.37	41.3	40.51	41.99

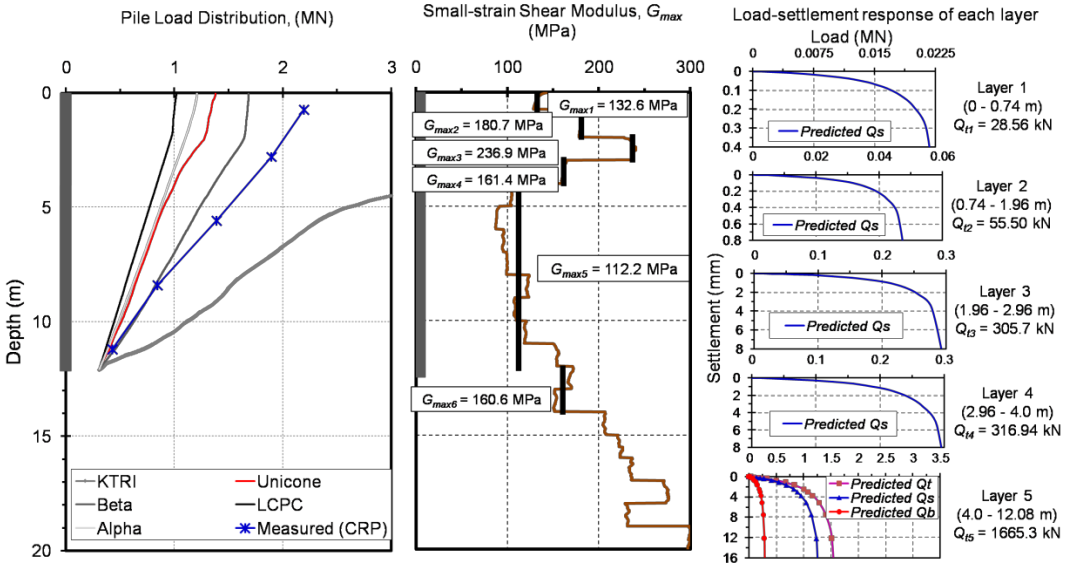

Figure 4. Pile shaft resistance and load distribution (SCPTu – based estimations vs. measured); and Load-settlement curves based on respective G_{max} and Q_t (elastic continuum solution).

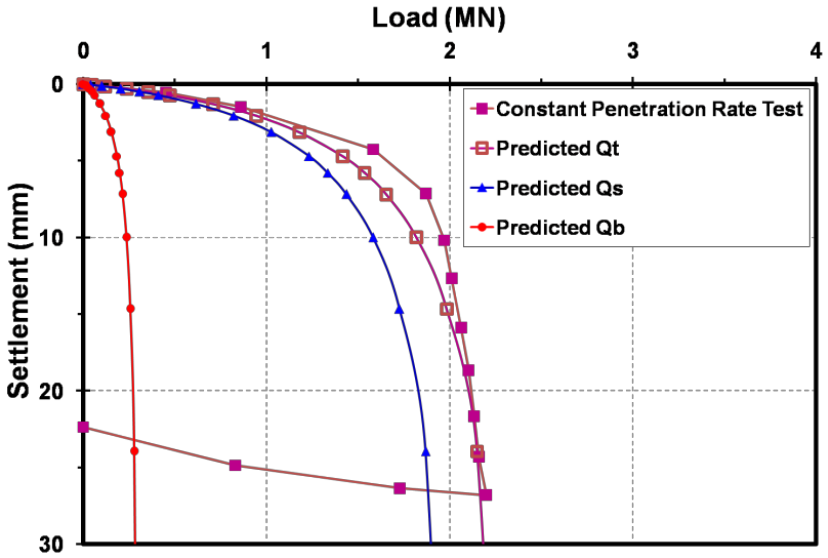

Figure 5. Load-settlement response (elastic continuum solution).

CONCLUSION

Elastic continuum solution provides a rational framework for evaluating field load test results on axially-loaded pile foundations. Various CPT based methods have been revisited, along with their application to load test on a 12.08-m deep and 0.6-m diameter bored pile in clay till at the Grimsby research site, UK. Rational CPT methods with β-analysis have shown closest agreement with the measured results. Geotechnical soil parameters for the evaluation of deep foundations are conveniently obtained from multi-independent readings (q_t, f_s, V_s, u_1, u_2) taken during SCPTu sounding conducted at the site.

ACKNOWLEDGEMENT

The authors are thankful to Dr. M. J. Brown at the Division of Civil Engineering, University of Dundee, UK for being forthcoming in providing the required data/information pertaining to the pile load test at Grimsby research site.

PREFERENCES

Brown, M.J. 2004. The rapid load testing of piles in fine grained soils. *Ph.D. Thesis*, University of Sheffield, UK: 151 – 198.

Brown, M.J., Hyde, A.F.L. & Anderson, W.F. 2006. Analysis of a rapid load test on an instrumented bored pile in clay. *Geotechnique* 56 (9): 627 – 638.

Bustamante, M., & Gianeselli, L. 1982. Pile bearing capacity predictions by means of static penetrometer CPT. *Proc., 2nd European Symp. on Penetration Testing*, Vol. 2, Amsterdam: 493–500.

Chen, B.S.Y. & Mayne, P.W. 1994. Profiling the overconsolidation ratio of clays by piezocone tests. *Report GIT-CEEGEO-94-1*, Civil Engineering, Georgia Institute of Technology, Atlanta, 280 p.

Chen, Y.J. & Kulhawy, F.H. 1994. Case history evaluation of the behavior of drilled shafts under axial and lateral loading. EPRI TR-104601, Electric Power Research Institute: 493 – 04.

Eslami, A. & Fellenius, B.H. 1997. Pile capacity by direct CPT and CPTu methods applied to 102 case histories. *Canadian Geotechnical J.*, 34 (6): 880 – 898.

Fahey, M. & Carter, J.P. 1993. A finite element study of the pressuremeter in sand using a nonlinear elastic plastic model. *Canadian Geotechnical J*. 30(2): 348 – 362.

Fleming, W.G.K., Weltman, A.J., Randolph, M.F. & Elson, W.K. 1992. *Piling Engineering*. 2nd ed., Blackie/Halsted Press, John Wiley & Sons, New York: 122 – 128.

Jamiolkowski, M. 2003. Soil parameters relevant to bored pile design from laboratory and in-situ tests. *Deep Foundations on Bored and Auger Piles*, Millpress, Rotterdam: 83 – 100.

Jefferies, M. & Been, K. 2006. *Soil Liquefaction – A Critical State Approach*. Taylor and Francis, New York, 580 p.

Kondner, R.L. 1963. Hyperbolic stress-strain response: cohesive soils. ASCE *J. of Soil Mechanics and Foundations Div*. 89 (1): 115-143.

Kulhawy, F.H., Trautmann, C.H. Beech, J.F. O'Rourke, T.D. & McGuire, W. 1983. Transmission line structure foundations for uplift-compr. loading, *Report EL-2870*, EPRI, Electric Power Research Institute, Palo Alto, California, 412 p.

Ladd, C.C. 1991. Stability evaluation during staged construction. The 22nd Terzaghi Lecture, *J. of Geotechnical Engineering* 117 (4): 540 – 615.

Lee, J., Salgado, R. & Paik, K. 2003. Estimation of load capacity of pipe piles in sand based on CPT Results. *J. of Geotechnical and Geoenvironmental Engineering*, ASCE, 129(5): 391 – 403.

Lunne, T., Robertson, P.K. & Powell, J.J.M. 1997. Cone Penetration Testing in Geotechnical Practice. Blackie Academic, EF Spon/Routledge Publishers, New York, 312 p.

Mayne, P.W. 2005. Integrated ground behavior: In-situ and laboratory tests. *Deformation Characteristics of Geomaterials*, Vol. 2 (Proc. Lyon, France), Taylor & Francis, London: 155 – 177.

Mayne, P.W. 2007. Cone penetration testing – a synthesis of highway practice. *NCHRP Synthesis 368*, Transportation Research Board, National Academies Press, Washington, DC: 117p.

Mayne, P.W. & Elhakim, A. 2002. Axial pile response evaluation by geophysical piezocone tests. *Proc. 9th International Conf. on Piling and Deep Foundations*, Nice, June 3 – 5.

Mayne, P.W. & Niazi, F.S. 2009. Evaluating axial elastic pile response from cone penetration tests (The 2009 Michael O' Neill Lecture). *The Journal of the Deep Foundations Institute*, 3(1): 3 – 12.

Mayne, P.W. & Woeller, D.J. 2008. O-cell response using elastic pile and seismic piezocone tests. *Proc. of the BGA International Conf. on Foundations*, Dundee, Scotland,24 – 27 June 2008.

Mayne, P.W. & Zavala, G. 2004. Axial shaft response from seismic piezocone tests. *Proc. GeoSupport 2004*, GSP 124, ASCE: 429 – 440.

Mayne, P.W., Coop, M., Springman, S., Huang, A.B. & Zornberg, J. 2009. Geomaterial behavior & testing. *Proc. 17th ICSMFE*, Alexandria, Millpress-IOS Press, Rotterdam.

Mayne P.W., Peuchen, J. & Bouwmeester, D. 2010. Estimation of soil unit weight from CPTs. *Proc., 2nd International Symp. on Cone Penetration Testing*, CPT'10, Huntington Beach, CA.

Randolph, M.F. 2003. PIGLET: Analysis and design of pile groups. *Users' Manual*, Ver. 4 – 2. Perth.

Poulos, H.G. & Davis, E.H. 1980. *Pile foundations analysis and design*. John Wiley & Sons, NY, 397 p.

Randolph, M.F. & Wroth, C.P. 1978. Analysis of deformation of vertically-loaded piles. ASCE *J. of the Geotechnical Engineering Div*., 104 (GT12): 1465 – 1488.

Randolph, M.F. & Wroth, C.P. 1979. A simple approach to pile design and the evaluation of pile tests. *Behavior of Deep Foundations*, STP 670, ASTM, West Conshohocken, PA: 484 – 499.

Robertson, P.K. 1990. Soil classification using the CPT. *Canadian Geotechnical J*. 27(1): 151 – 158.

Schnaid, F. 2005. Geocharacterization and engineering properties of natural soils by in-situ tests. *Proc., 16th ICSMFE* Vol. 1, Osaka, Millpress, Rotterdam: 3 – 45.

Takesue, K., Sasao, H. & Matsumoto, T. 1998. Correlation between ultimate pile skin friction and CPT data. *Geotechnical Site Characterization* (2), Rotterdam: 1177 – 1182.

Vesić, A.S. 1977. *NCHRP Synthesis of Highway Practice 42: Design of Pile Foundations*, Transportation Research Board, National Research Council, Washington, DC, 68 p.

APPENDIX K

PILES AND SOILS CHARACTERISTICS OF GROUP 3 DATASET: O-CELL LOAD TESTS

This appendix forms part of Chapter 9 and provides the characteristics of piles and soils of Group 3 dataset consisting of O-cell load tests on drilled shafts. Table K.1 provides summary of load test sites, giving details of the site locations, soil conditions, number of load tests at each site, identification references of pile load tests, and the sources of information. In Table K.2, detailed characteristics of the piles and soils in the dataset, relevant to the elastic solution are enlisted.

Table K.1. Summary of O-cell pile load test sites.

Site ID No.	Site location and pile identification	No. of tests	Soil conditions	Source
10	CNN International Blvd. Viaduct, Atlanta, GA, USA (CNN)	1	Piedmont residual silt and sand grading to partially weathered rock	Ahrens et al. (2003)
11	Cooper River Bridge on HW 17, Charleston, SC, USA (CRB-C)	4	Loose sand and soft clay overburden underlain by stiff calcareous Cooper Marl	Camp et al. (2002), Ahren et al. (2000a, b), Simpson et al. (2000a, b)
12	Cooper River Bridge on HW 17, Mt. Pleasant, SC, USA (CRB-MP)	4	Clayey sand and sandy clay over stiff calcareous Cooper Marl	Camp et al. (2002), Ahren et al. (2000c, d), Ahren and Simpson (2000a, b)
20	Foothill Medical Center, Calgary, AB, Canada (FMC)	1	Sandy clayey silt over hard silty clay till	Kort (2005)
22	Gilmerton Bridge Pier 12, Chesapeake, VA, USA (GB-P12)	1	Silty sand over Yorktown marl	Pang et al. (2010)
24	Golden Ears Bridge S. Bank, Langley, BC, Canada (GEB-S)	1	Silty sand to dense sand over soft silty clay	Amini et al. (2008), Naesgaard (2008)
49	Pinners Point Interchange, Portsmouth, VA, USA (PPI)	2	Interbedded sand and clay soils of Norfolk Formation overlying medium to dense sand of Yorktown Formation	Kort et al. (200a, b)
61	Texas A&M University NGES sand site, College Station, TX, USA (TAMU-S NGES O1)	1	Medium dense sand over stiff clay	Briaud et al. (2000), O'Neill et al. (2002)
67	University of Texas NGES, Houston, TX, USA (UH-NGES)	1	Stiff Beaumont clay over sandy clay	Ata and O'Neill (1998), O'Neill et al. (2002, 1982), Reese et al. (1976)

Table K.2. Characteristics of investigated piles, soils and O-cell load tests.

Pile ID	Levels of O-cells	Shaft segment	Shaft segment characteristics					Soil characteristics				λ_i
			L (m)	d (m)	L/d	L-ratio	E_p (MPa)	γ_T (kN/m^3)	ν_s	ξ	ρ_E	
CRB-C 1	2	Upper	30.57	2.52	12.13	1.93	49,000	18.25	0.50	0.47	0.59	290
		Middle	12.19	2.44	5.00	0.40	42,500	19.50	0.50	1.00	0.96	107
		Lower	3.65	2.44	1.50	0.085	42,500	19.50	0.50	1.00	0.99	105
CRB-C 2	2	Upper	31.39	2.52	12.46	2.12	38,200	18.25	0.50	0.47	0.59	221
		Middle	12.19	2.44	5.00	0.39	35,100	19.50	0.50	1.00	0.96	88
		Lower	2.62	2.44	1.07	0.061	35,100	19.50	0.50	1.00	0.99	87
CRB-C 3	1	Upper	29.74	2.54	11.71	12.34	29,700	18.15	0.50	0.95	0.54	83
		Lower	2.41	2.44	0.99	0.081	29,700	19.50	0.50	1.00	0.99	78
CRB-C 4	1	Upper	30.81	1.92	16.05	33.49	40,000	18.15	0.50	0.98	0.53	108
		Lower	0.92	1.83	0.51	0.030	40,000	19.50	0.50	1.00	1.00	105
CRB-MP 1	2	Upper	30.57	2.52	12.13	1.85	42,000	17.80	0.20	1.00	0.53	117
		Middle	14.02	2.44	5.75	0.46	38,800	17.50	0.50	1.00	0.98	112
		Lower	2.53	2.44	1.04	0.057	38,800	17.50	0.50	1.00	1.00	111
CRB-MP 2	2	Upper	30.93	2.54	12.18	2.05	36,700	17.80	0.20	1.00	0.53	101
		Middle	14.02	2.44	5.75	0.45	39,700	17.50	0.50	1.00	0.98	114
		Lower	1.10	2.44	0.45	0.024	39,700	17.50	0.50	1.00	1.00	113

Notes: ξ = xi factor for stiffer lower layer (= $G_{L\,max}/G_{b\,max}$); ρ_E = stiffness variation factor (= $G_{M\,max}/G_{L\,max}$) from V_s profile; λ_i = initial pile-soil stiffness ratio (= $E_p/G_{L\,max}$).

Table K.2. (continued).

Pile ID	Levels of O-cells	Shaft segment	Shaft segment characteristics					Soil characteristics				λ_i
			L (m)	d (m)	L/d	L-ratio	E_p (MPa)	γ_T (kN/m^3)	ν_s	ξ	ρ_E	
CRB-MP 3	1	Upper	30.04	2.56	11.74	22.93	38,500	17.70	0.50	1.00	0.54	110
		Lower	1.31	2.44	0.54	0.044	32,600	18.20	0.50	1.00	1.00	98
CRB-MP 4	1	Upper	31.33	2.54	12.34	22.87	36,200	17.70	0.50	1.00	0.54	99
		Lower	1.37	2.44	0.56	0.044	32,000	18.20	0.50	1.00	1.00	96
FMC	1	Upper	9.95	1.40	7.11	2.46	35,000	18.95	0.50	1.00	0.95	147
		Lower	4.05	1.40	2.89	0.41	35,000	19.30	0.50	1.00	0.98	141
GEB-S	2	Upper	44.00	2.60	16.92	1.44	35,000	20.00	0.20	1.00	0.60	247
		Middle	26.50	2.60	10.19	0.60	35,000	19.10	0.50	1.00	0.91	245
		Lower	4.00	2.60	1.54	0.06	35,000	19.10	0.50	1.00	0.90	173
TAMU-S NGES O1	1	Upper	12.20	0.92	13.34	1.32	40,000	18.40	0.20	1.00	0.94	218
		Lower	9.30	0.92	10.16	0.76	40,000	17.40	0.50	1.00	0.86	208
UH NGES O1	1	Upper	10.70	0.92	11.69	0.99	35,000	17.70	0.50	0.97	0.64	213
		Lower	10.80	0.92	11.81	1.01	35,000	17.80	0.50	1.00	0.75	105
PPI 1	2	Upper	19.89	1.53	13.05	3.20	35,100	17.80	0.35	0.16	0.98	1168
		Middle	5.34	1.53	3.50	0.27	33,300	19.20	0.25	1.00	0.91	139
		Lower	0.87	1.53	0.57	0.036	33,300	19.20	0.25	1.00	0.99	135

Notes: ξ = xi factor for stiffer lower layer (= $G_{L\,max}/G_{b\,max}$); ρ_E = stiffness variation factor (= $G_{M\,max}/G_{L\,max}$) from V_s profile; λ_i = initial pile-soil stiffness ratio (= $E_p/G_{L\,max}$).

Table K.2. (continued).

Pile ID	Levels of O-cells	Shaft segment	Shaft segment characteristics					Soil characteristics				λ_i
			L (m)	d (m)	L/d	L-ratio	E_p (MPa)	γ_T (kN/m^3)	ν_s	ξ	ρ_E	
PPI 2	2	Upper	24.40	1.53	15.95	2.29	29,400	17.80	0.35	0.15	0.99	976
		Middle	9.90	1.53	6.47	0.41	29,200	19.20	0.25	1.00	0.85	105
		Lower	0.75	1.53	0.49	0.022	29,200	19.20	0.25	1.00	0.99	119
CNN	2	Upper	14.08	1.60	8.80	2.69	24,900	18.90	0.20	1.00	0.64	98
		Middle	4.45	1.44	3.09	0.32	25,200	19.60	0.20	1.00	0.88	74
		Lower	0.78	1.44	0.54	0.042	25,200	19.80	0.20	1.00	0.97	70
GB-P12	1	Upper	24.60	1.57	15.67	32.37	33,900	18.10	0.20	1.00	0.94	348
		Lower	0.76	1.57	0.50	0.031	23,200	18.90	0.20	1.00	0.99	236

Notes: ξ = xi factor for stiffer lower layer (= $G_{L\,max}/G_{b\,max}$); ρ_E = stiffness variation factor (= $G_{M\,max}/G_{L\,max}$) from V_s profile; λ_i = initial pile-soil stiffness ratio (= $E_p/G_{L\,max}$).

APPENDIX L

INITIAL SHEAR STIFFNESS (G_{max}) PROFILES FROM SHEAR WAVE VELOCITY (V_S) READINGS: GROUP 3 DATASET

Initial shear stiffness (G_{max}) profiles from shear wave velocity (V_s) readings.

Site ID No. 10: CNN International Blvd. Viaduct, Atlanta, GA, USA	Site ID No. 11: Cooper River Bridge on HW 17, Charleston, SC, USA	Site ID No. 12: Cooper River Bridge on HW 17, MP, SC, USA
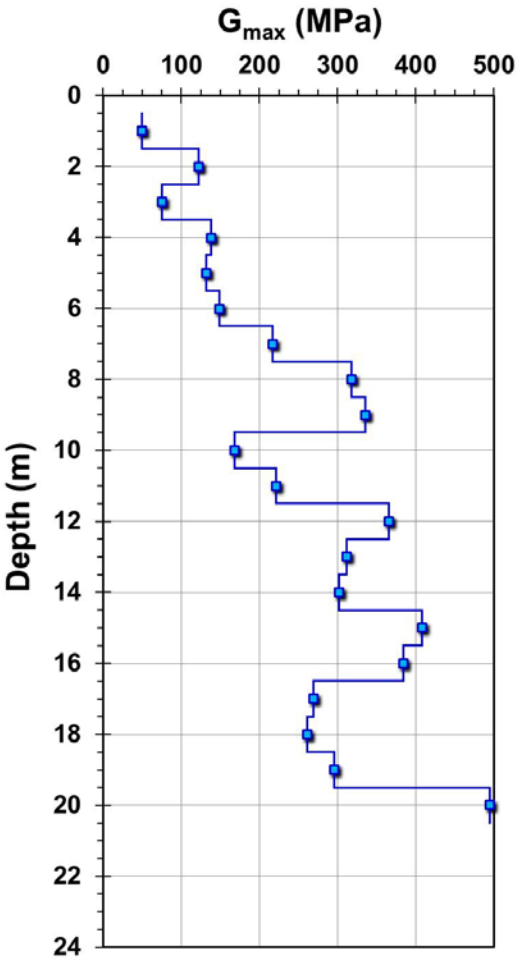	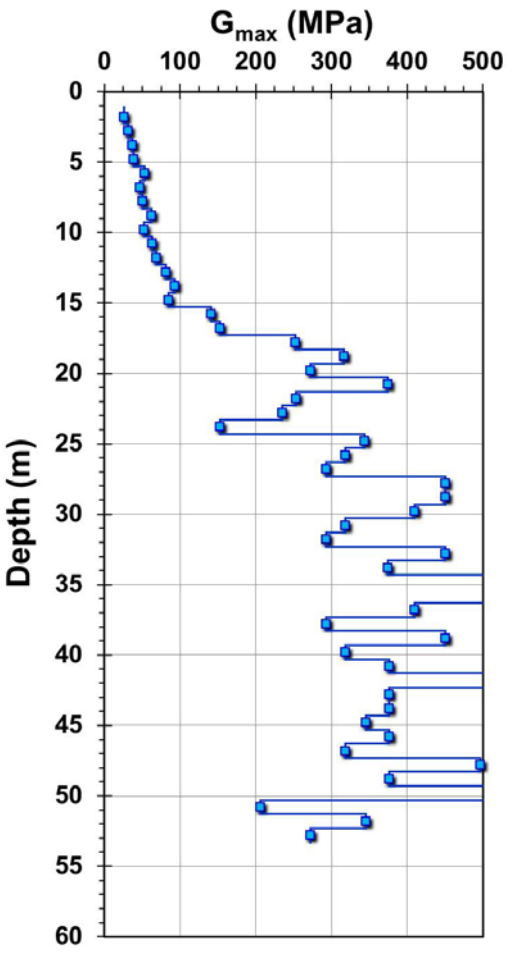	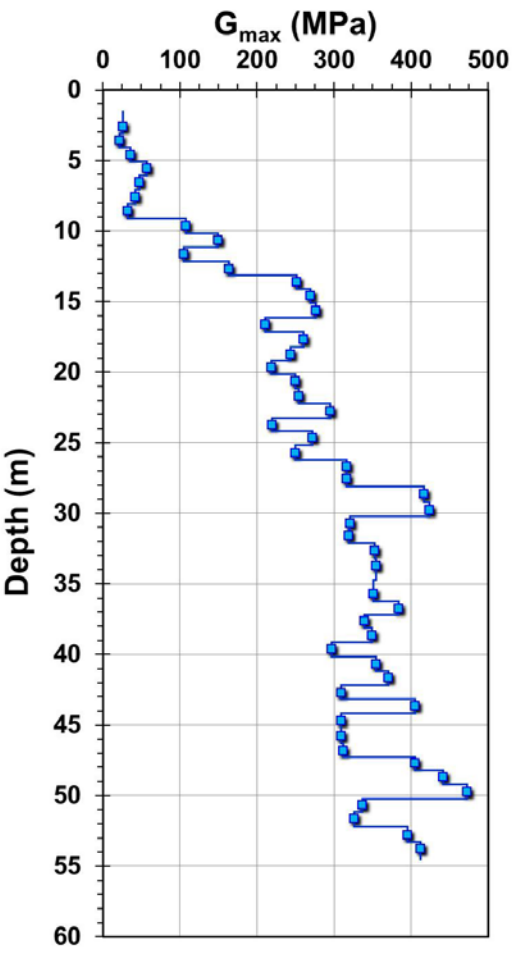

Initial shear stiffness (G_{max}) profiles from shear wave velocity (V_s) readings.

Site ID No. 20: Foothill Medical Center, Calgary, AB, Canada	Site ID No. 22: Gilmerton Bridge Pier 12, Chesapeake, VA, USA	Site ID No. 24: Golden Ears Bridge S. Bank, Langley, BC, Canada
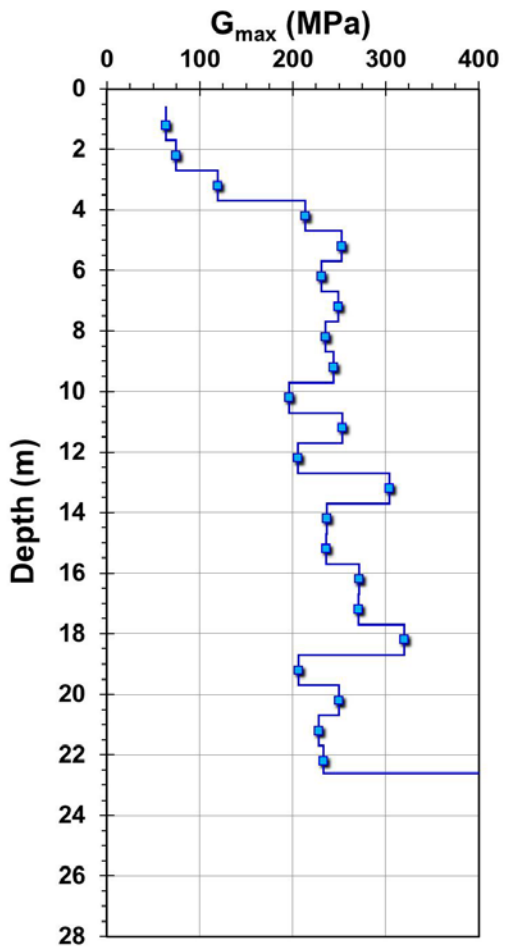	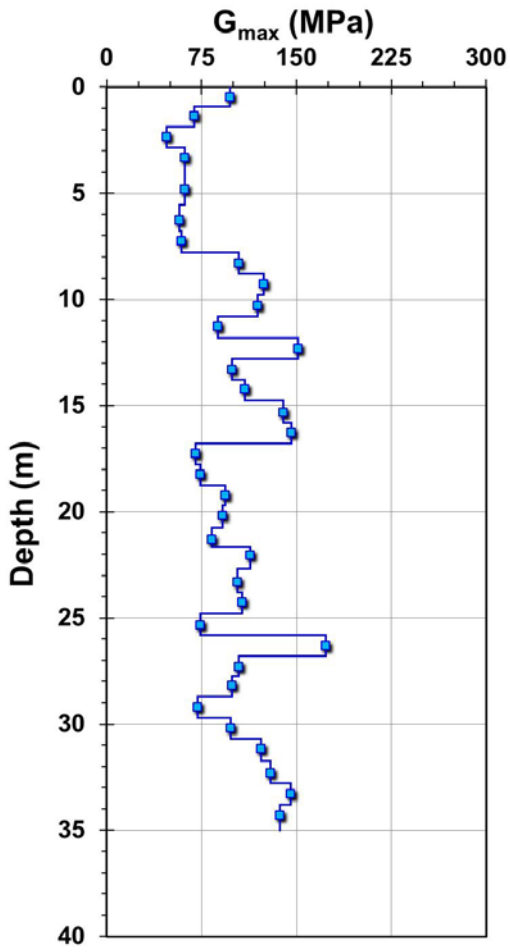	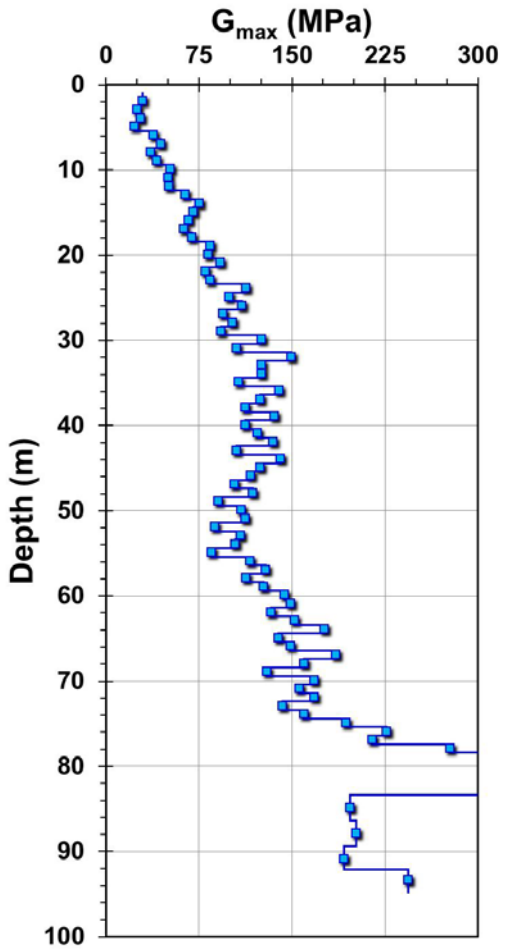

Initial shear stiffness (G_{max}) profiles from shear wave velocity (V_s) readings.

Site ID No. 49: Pinners Point Interchange, Portsmouth, VA, USA	Site ID No. 61: Texas A&M University NGES sand site, College Station, TX, USA	Site ID No. 67: University of Texas NGES, Houston, TX, USA
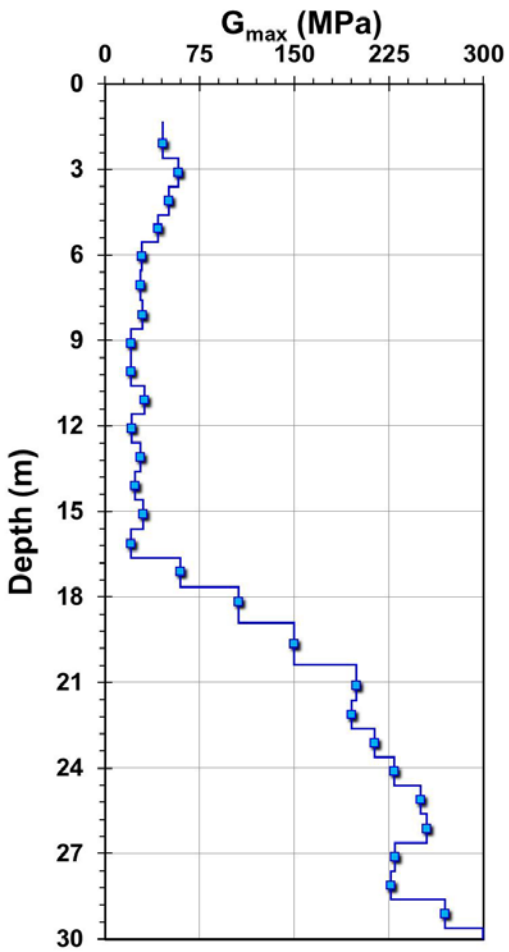	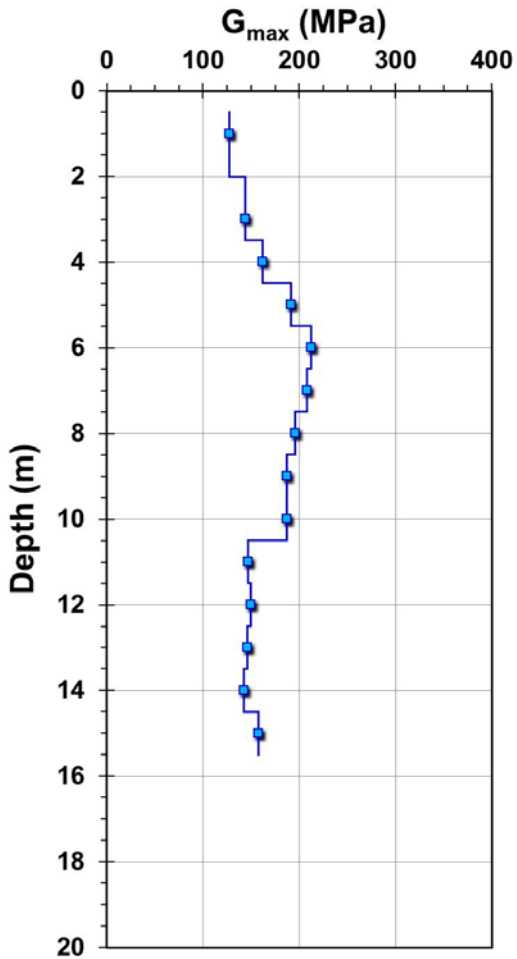	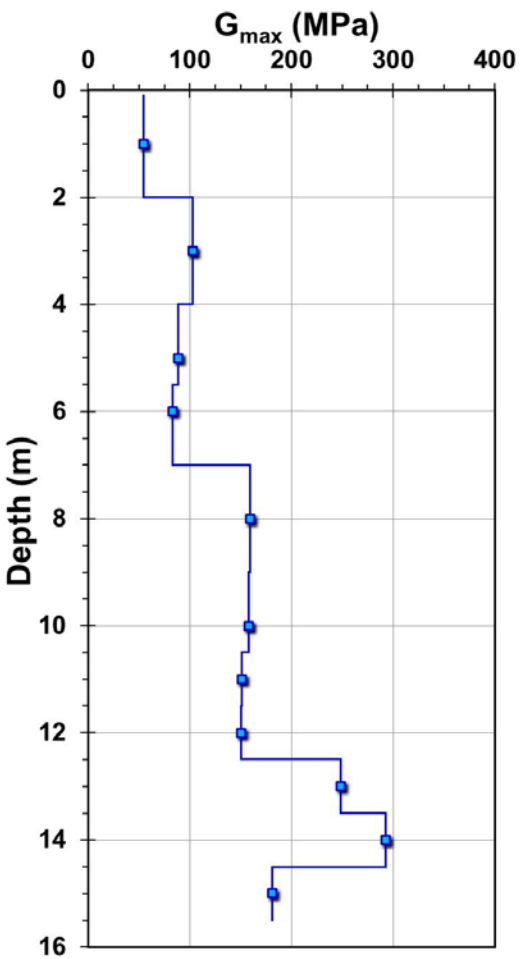

APPENDIX M

SAMPLE CALCULATIONS FROM MODIFIED ANALYTICAL SOLUTION FOR LOADS CORRESPONDING TO SELECTED DISPLACEMENTS IN MULTI STAGE O-CELL LOAD TEST AT PINNERS POINT INTERCHANGE

Stage 1: lower segment downward (measured Q_{t2} @ w_{s3} of 3.58 mm = 1,900 kN)

$L_3 = 0.87$ m

$d_{s3} = 1.524$ m

$r_{o3} = 0.762$ m

L-ratio = $L_3/(L_1 + L_2) = 0.036$

$L_3/d_{s3} = 0.57$

$E_{p3} = 33{,}300$ MPa

$G_{o\ max3} = 231.38$ MPa

$G_{L\ max3} = 238.25$ MPa

$G_{M\ max3} = 234.82$ MPa

$G_{b\ max3} = 238.25$ MPa

$\nu_{s3} = 0.25$

$\rho_{E3} = 0.99$

$\xi_3 = 1.00$

$r_{m3} = L_3 \cdot \{0.25 + \xi_3 \cdot [2.5\ \rho_{E3} \cdot (1 - \nu_{s3}) - 0.25]\} = 1.61$ m

$\zeta_3 = 0.748$

$\eta_3 = 1.00$

$w_{s3} = 3.581$ mm = 0.003581 m

γ_{p3} (%) = w_{s3}/d_{s3} (%) = 0.235

***Load calculations via operational shear stiffness Model 1*:**

$$\frac{G_{L3}}{G_{L\,max3}} = 0.032\left[\gamma_{p3}\,(\%)\right]^{-0.59}\left(\frac{L_3}{d_{s3}}\right)^{0.24}\left[L-\text{ratio}_{(\text{lower})}\right]^{0.13}(\upsilon_{s3})^{-1.06} = 0.186$$

G_{L3} = 44.32 MPa

$\lambda_3 = E_{p3}/G_{L3}$ = 751

$\mu L_3 = 2\cdot[2/(\zeta_3\lambda_3)]^{0.5}\cdot(L_3/d_{s3})$ = 0.068

$\tanh(\mu L_3)$ = 0.068

$$Q_{t2} = Q_{s3} + Q_b = \frac{w_{s3}\,G_{L3}\,r_{o3}\left[\frac{4\eta_3}{(1-\upsilon_{S3})\xi_3}+\frac{2\pi\rho_{E3}\tanh(\mu L_3)L_3}{\zeta_3\,\mu L_3\,r_{o3}}\right]}{\left[1+\frac{4\eta_3\,\tanh(\mu L_3)L_3}{\pi\lambda_3(1-\upsilon_{S3})\xi_3\,\mu L_3\,r_{o3}}\right]}$$

Q_{t2} = 1,794.10 kN

***Load calculations via operational shear stiffness Model 2* (*see Table 9.3*):**

$$\frac{G_{L3}}{G_{L\,max3}} = \frac{1}{9.0\left[\gamma_{p3}\,(\%)\right]^{0.6}+1.3\left[\gamma_{p3}\,(\%)\right]+0.88} = 0.20$$

G_{L3} = 48.03 MPa

$\lambda_3 = E_{p3}/G_{L3}$ = 693

$\mu L_3 = 2\cdot[2/(\zeta_3\lambda_3)]^{0.5}\cdot(L_3/d_{s3})$ = 0.072

$\tanh(\mu L_3)$ = 0.072

$$Q_{t2} = Q_{s3} + Q_b = \frac{w_{s3}\,G_{L3}\,r_{o3}\left[\frac{4\eta_3}{(1-\upsilon_{S3})\xi_3}+\frac{2\pi\rho_{E3}\tanh(\mu L_3)L_3}{\zeta_3\,\mu L_3\,r_{o3}}\right]}{\left[1+\frac{4\eta_3\,\tanh(\mu L_3)L_3}{\pi\lambda_3(1-\upsilon_{S3})\xi_3\,\mu L_3\,r_{o3}}\right]}$$

Q_{t2} = 1,934.54 kN

Stage 2: middle segment downward (measured Q_{s2} @ w_{s2} of 3.26 mm = 2,300 kN)

L_2 = 5.34 m

d_{s2} = 1.524 m

r_{o2} = 0.762 m

L-ratio = L_2/L_1 = 0.27

L_2/d_{s2} = 3.50

ν_{s2}= 0.25

E_{p2} = 33,300 MPa

$G_{o\ max2}$ = 189.19 MPa

$G_{L\ max2}$ = 231.38 MPa

$G_{M\ max2}$ = 210.29 MPa

$G_{b\ max2}$ = 231.38 MPa

ρ_{E2} = 0.91

ξ_2 = 1.00

$r_{m2}= L_2 \cdot \{0.25 + \xi_2 \cdot [2.5\ \rho_{E2} \cdot (1 - \nu_{s2}) - 0.25]\}$ = 9.11 m

$\zeta_2 = \ln(r_{m1}/r_{o1})$ = 2.482

w_{s2} = 3.26 mm = 0.00326 m

γ_{p2} (%) = w_{s2}/d_{s2} (%) = 0.214

***Load calculations via operational shear stiffness Model 1*:**

$$\frac{G_{L2}}{G_{L\ max2}} = 0.007\left[\gamma_{p2}\ (\%)\right]^{-0.52}\left(\frac{L_2}{d_{s2}}\right)^{1.22}\left[\mathrm{L-ratio}_{(\mathrm{middle})}\right]^{-0.98}(\upsilon_{s2})^{0.03}(\rho_{E2})^{0.5} = 0.238$$

G_{L2} = 54.97 MPa

$\lambda_2 = E_{p2}/G_{L2}$ = 605.7

$\mu L_2 = 2 \cdot [2/(\zeta_2 \lambda_2)]^{0.5} \cdot (L_2/d_{s2})$ = 0.255

$\tanh(\mu L_2)$ = 0.25

$$Q_{s2} = \frac{2\pi\, w_{s2} G_{L2}\, \rho_{E2}\, \tanh(\mu L_2) L_2}{\zeta_2\, \mu L_2}$$

Q_{s2} = 2,164.21 kN

***Load calculations via operational shear stiffness Model 2* (*see Table 9.3*):**

$$\frac{G_{L2}}{G_{L\,max2}} = \frac{1}{8.0\left[\gamma_{p2}\,(\%)\right]^{0.75} + 1.9\left[\gamma_{p2}\,(\%)\right] + 0.95} = 0.257$$

G_{L2} = 59.46 MPa

$\lambda_2 = E_{p2}/G_{L2}$ = 560

$\mu L_2 = 2\cdot[2/(\zeta_2\lambda_2)]^{0.5}\cdot(L_2/d_{s2})$ = 0.265

$\tanh(\mu L_2)$ = 0.259

$$Q_{s2} = \frac{2\pi\, w_{s2} G_{L2}\, \rho_{E2}\, \tanh(\mu L_2) L_2}{\zeta_2\, \mu L_2}$$

Q_{s2} = 2,318.84 kN

Stage 3: upper segment upward (measured Q_{t1} @ w_{s1} of 3.14 mm = 2,600 kN)

L_1 = 19.89 m

d_{s1} = 1.524 m

r_{o1} = 0.762 m

L-ratio = $L_1/(L_2 + L_3)$ = 3.20

L_1/d_{s1} = 13.05

$W_{buoyant}$ = 0.68 MN

ν_{s1}= 0.35

E_{p1} = 35,100 MPa

$G_{o\,max1}$ = 29.70 MPa

$G_{L\,max1}$ = 30.70 MPa

$G_{M\,max1}$ = 30.20 MPa

$G_{b\,max1}$ = 189.43 MPa

ρ_{E1} = 0.98

ξ_1 = 0.162

$r_{m1}= [G_{M\,max1}/G_{L\,max1}]\cdot L_1\cdot\{0.25 + \xi_1\cdot[2.5\,\rho_{E1}\cdot(1 - \nu_{s1}) - 0.25]\}$ = 9.17 m

$\zeta_1 = \ln(r_{m1}/r_{o1})$ = 2.487

w_{s1} = 3.14 mm = 0.00314 m

γ_{p1} (%) = w_{s1}/d_{s1} (%) = 0.206

***Load calculations via operational shear stiffness Model 1*:**

$$\frac{G_{L1}}{G_{L\,max1}} = 0.026\left[\gamma_{p1}\,(\%)\right]^{-0.55}\left(\frac{L_1}{d_{s1}}\right)^{0.38}\left[\text{L} - \text{ratio}_{(\text{upper})}\right]^{-0.2}(\upsilon_{s1})^{-0.18}(\xi_1)^{-0.63} = 0.496$$

G_{L1} = 15.22 MPa

$\lambda_1 = E_{p1}/G_{L1}$ = 2306

$\mu L_1 = 2\cdot[2/(\zeta_1\lambda_1)]^{0.5}\cdot(L_1/d_{s1})$ = 0.488

$\tanh(\mu L_1)$ = 0.453

$$Q_{t1} = Q_{s1} + W_{buoyant} = \frac{2\pi\, w_{s1} G_{L1}\, \rho_{E1}\, \tanh(\mu L_1) L_1}{\zeta_1\, \mu L_1} = 2{,}230 \text{ kN}$$

***Load calculations via operational shear stiffness Model 2* (*see Table 9.3*):**

$$\frac{G_{L1}}{G_{L\,max1}} = \frac{1}{1.0\left[\gamma_{p1}\,(\%)\right]^{2.0} + 2.0\left[\gamma_{p1}\,(\%)\right] + 1.18} = 0.612$$

G_{L1} = 18.78 MPa

$\lambda_1 = E_{p1}/G_{L1}$ = 1868.7

$\mu L_1 = 2\cdot[2/(\zeta_1\lambda_1)]^{0.5}\cdot(L_1/d_{s1})$ = 0.54

$\tanh(\mu L_1)$ = 0.49

$$Q_{t1} = Q_{s1} + W_{buoyant} = \frac{2\pi\, w_{s1}\, G_{L1}\, \rho_{E1}\, \tanh(\mu L_1) L_1}{\zeta_1\, \mu L_1} = 2{,}635 \text{ kN}$$

REFERENCES

Abu-Farsakh, M. Y. and Titi, H. H. (2004). "Assessment of direct cone penetration test methods for predicting the ultimate capacity of friction driven piles." *ASCE Journal of Geotechnical and Geoenvironmental Engineering*, 130(9): 935 – 944.

Ahren, M. D. and Simpson, R. C. (2000a). "Final report on drilled shaft load testing (Osterberg method), Test shaft MP-1 – Cooper River Bridge, Mt. Pleasant, SC." *Project Report* No. LT-8650-1, prepared by LoadTest Incorporated, Gainesville, FL for Trevi Icos Corporation.

Ahren, M. D. and Simpson, R. C. (2000b). "Final report on drilled shaft load testing (Osterberg method), Test shaft MP-2 – Cooper River Bridge, Mt. Pleasant, SC." *Project Report* No. LT-8650-2, prepared by LoadTest Incorporated, Gainesville, FL for Trevi Icos Corporation.

Ahren, M. D., Simpson, R. C. and Hayes, J. A. (2000a). "Final report on drilled shaft load testing (Osterberg method), Test shaft C-1 – Cooper River Bridge, Charleston, SC." *Project Report* No. LT-8650-6, prepared by LoadTest Incorporated, Gainesville, FL for Trevi Icos Corporation.

Ahren, M. D., Simpson, R. C. and Hayes, J. A. (2000a). "Final report on drilled shaft load testing (Osterberg method), Test shaft C-1 – Cooper River Bridge, Charleston, SC." Project LT-8650-6, prepared by LoadTest Incorporation for Trevi Icos Corporation.

Ahren, M. D., Simpson, R. C. and Hayes, J. A. (2000b). "Final report on drilled shaft load testing (Osterberg method), Test shaft C-2 – Cooper River Bridge, Charleston, SC." *Project Report* LT-8650-7, prepared by LoadTest Incorporated for Trevi Icos Corporation.

Ahren, M. D., Simpson, R. C. and Hayes, J. A. (2000c). "Final report on drilled shaft load testing (Osterberg method), Test shaft MP-3 – Cooper River Bridge, Mt. Pleasant, SC." *Project Report* LT-8650-3, prepared by LoadTest Incorporated for Trevi Icos Corporation.

Ahren, M. D., Simpson, R. C. and Hayes, J .A. (2000d). "Final report on drilled shaft load testing (Osterberg method), Test shaft MP-4 – Cooper River Bridge, Mt.

Pleasant, SC." *Project Report* LT-8650-4, prepared by LoadTest Incorporated for Trevi Icos Corporation.

Ahren, M. D., Simpson, R. C. and Kort, D. A. (2003). "Report on drilled shaft load testing (Osterberg method), Bent 8 W. B. test shaft, International boulevard viaduct." Atlanta, GA, *Project Report* No. LT-8862, prepared by LoadTest Incorporated, Gainesville, FL for Trevi Icos Corporation.

Ai, Z. Y. and Han, J. (2009). "Boundary element analysis of axially loaded piles embedded in a multi-layered soil." *Computers and Geotechnics*, Vol. 36: 427 – 434.

Alboom, G. V. and Whenham, V. (2003). "Soil investigation campaign at Limelette (Belgium)." *Proceedings, Second Symposium on Screw Piles – Belgian Screw Pile Technology – Design and Recent Developments*. Brussels, Balkema, Rotterdam; ISBN: 90 5809 578 9: pp. 21 – 70.

Ali, H. (2010). "Caractérisation améliorée des sols par l'essai de chargement de pointe au piézocone. Application au calcul des fondations profondes (Improved characterization of soils by the piezocone tip load stress – Application to the calculation for deep foundations)." *PhD Thesis*, Université Blaise Pascal, Clermont-Ferrand II (Blaise Pascal University), 302 p.

Almeida, M. S. S., Danziger, F. A. B. and Lunne, T. (1996). "Use of the piezocone test to predict the axial capacity of driven and jacked piles in clay." *Canadian Geotechnical Journal,* 33(1): 33 – 41.

Alsamman, O. M. (2012). "Axial load test procedures for pile foundations." Notes: *Short Course* No. G0–001, Continuing Education and Development, Incorporation, <http://www.cedengineering.com/upload/Axial Load Test for Piles.pdf> accessed electronically, July 06, 2012.

Alsamman, O. M. (1995). "The use of CPT for calculating axial capacity of drilled shafts." *PhD Thesis*, Department of Civil Engineering, University of Illinois at Urbana-Champaign: 128 – 174.

Altaee, A., Fellenius, B. H. and Evgin, E. (1992). "Axial load transfer for piles in sand. I: Tests on an instrumented precast pile." *Canadian Geotechnical Journal*, 29(1): 11–20.

Alves, A. M. L., Lopes, F. R., Randolph, M. F. and Danziger, B. R. (2009). "Investigations on the dynamic behavior of a small diameter pile driven in soft clay." *Canadian Geotechnical Journal*, 46(2): 1418 – 1430.

American Association of State Highway and Transportation Officials (1977). Standard Specifications for Highway Bridges, AASHTO, Washington, DC: 496 p.

American Society for Testing and Materials D1143M – 07 (2007). "Standard test method for deep foundations under static axial compressive load." ASTM Standards, Vol. 04.08, West Conshohocken, PA.

American Society for Testing and Materials D3689 – 07 (2007). "Standard test method for deep foundations under static axial tensile load." ASTM Standards, Vol. 04.08, West Conshohocken, PA.

Amini, A., Fellenius, B. H., Sabbagh, M., Naesgaard, E. and Buehler, M. (2008). "Pile loading tests at Golden Ears Bridge." *Proceedings, 61st Canadian Geotechnical Conference*, Edmonton, Alberta, 8p. Available from: http://www.fellenius.net/papers/283 Golden Ears Bridge Vancouver.pdf [accessed 10 March 2011].

Aoki, N. and DeAlencar, D. (1975). "An approximate method to estimate the bearing capacity of piles." *Proceedings, 5th Pan-American Conference of Soil Mechanics and Foundation Engineering*, Buenos Aires, Vol. 1: 367 – 376.

API (1969). "Recommended practice for planning, designing, and constructing fixed offshore platforms." API RP2A, 1st edition. American Petroleum Institute, Washington, DC.

API (1975). "Recommended practice for planning, designing, and constructing fixed offshore platforms." API RP2A, 6th edition. American Petroleum Institute, Washington, DC.

API (1976). "Recommended practice for planning, designing, and constructing fixed offshore platforms." API RP2A, 7th edition. American Petroleum Institute, Washington, DC.

API (1987). "Recommended practice for planning, designing, and constructing fixed offshore platforms." API RP2A, 17th edition. American Petroleum Institute, Washington, DC.

API (1993). "Recommended practice for planning, designing and constructing fixed offshore platforms – working stress design." API RP2A, 20th ed. American Petroleum Institute, Washington, DC.

Ardalan, H., Eslami, A. and Nariman-Zahed, N. (2009). "Piles shaft capacity from CPT and CPTu data by polynomial neural networks and genetic algorithms." *Computers and Geotechnics*, Vol. 36, 616 – 625.

Ata, A. A. and O'Neill, M. W. (1998). "Side-wall stability and side-shear resistance in bored piles constructed with high-molecular-weight polymer slurry." *Proceedings of the 3rd International Geotechnical Seminar on Deep Foundations on Bored and Auger Piles*, Van lmpe & Haegeman (eds.), Balkema, Rotterdam (ISBN 90-5809-022-1), pp. 111–117.

Ata, A. A. and O'Neill, M. W. (1998). "Side-wall stability and side-shear resistance in bored piles constructed with high-molecular-weight polymer slurry." *Proceedings of the 3rd International Geotechnical Seminar on Deep Foundations on Bored and Auger Piles*, Van lmpe & Haegeman (eds.), Balkema, Rotterdam (ISBN 90-5809-022-1), pp. 111–117.

Axelsson, G. (2002). "A conceptual model of pile set-up for driven piles in non-cohesive soil." *Deep Foundations 2002: An international perspective on theory, design, construction, and performance* (GSP 116), ASCE, Reston/VA: 64 – 79.

Axelsson, G. (2000). "Long-term increase in shaft capacity of non-cohesive soils." *PhD Thesis*, Royal Institute of Technology, Division of Soil and Rock Mechanics, Stockholm: 194 p.

Baaijens, A. and Kolk, H. J. (2004). "Axial pile capacity design method for offshore driven piles in sand." *Report No. P1003*, Issue 3, American Petroleum Institute, Contract No. 2003-100825, Leidschendam, The Netherlands: 122 p.

Balasubramaniam, A. S., Phienwej, N., Oh, Y. N. and Sanmugarasa, K. (2004). "Back-analysis and interpretation of driven and bored pile tests data in Bangkok sub-soils." *Proceedings, 9th Australia New Zealand Conference on Geomechanics*, Auckland, New Zealand, ISBN 0-86869-123-2. http://hdl.handle.net/10072/2207.

Baldi, G., Bellotti, R., Ghionna, V. N., Jamiolkowski, M. and LoPresti, D. C. F. (1989). "Modulus of sands from CPTs and DMTs." *Proceedings, 12th International Conference on Soil Mechanics & Foundation Engineering*, Vol. 1, Rio de Janeiro, 1989, Balkema, Rotterdam, pp. 165 – 170.

Basu, P., Prezzi, M., Salgado, R. and Chakraborty, T. (2013). "Shaft resistance and setup factors for piles jacked in clay." *Journal of Geotechnical and Geoenvironmental Engineering*, 10.1061/(ASCE)GT.1943-5606.0001018.

Basu, D., Prezzi, M., Salgado, R. and Chakraborty, T. (2008). "Settlement analysis of piles with rectangular cross-sections in multi-layered soils." *Computers and Geotechnics*, Vol. 35: 563 – 575.

Basu, P., Prezzi, M. and Basu, D. (2010). "Drilled displacement piles – current practice and design." *Deep Foundations Institute Journal*, 4(1): 3 – 20.

Begemann, H. K. S. Ph. (1963). "The use of the static penetrometer in Holland." *New Zealand Engineering*, 18(2): p. 41

Begemann, H. K. S. Ph. (1965). "The maximum pulling force on a single tension pile calculated on the basis of results of the adhesion jacket cone." *Proceedings, 6th International Conference on Soil Mechanics and Foundation Engineering*, Montreal 2: p. 229.

Begemann, H. K. S. Ph. (1969). "The Dutch static penetration test with the adhesion jacket cone." Delft Soil Mechanics and Delft Hydraulics Laboratory, XIII(1): p. 1.

Berardi, R. and Bovolenta, R. (2005). "Pile-settlement evaluation using field stiffness non-linearity." *Proceedings, Institution of Civil Engineering, Geotechnical Engineering*, 158(GE1): 35 – 44.

Berezantzev, V. G. (1970). "Computation of Foundations." Leningrad, URSS, in Russian, as referenced in Jamiolkowski (2003).

Bertok, J. and Berezowski, M. (1983). "Pile load tests for the Calgary air terminal building." *Canadian Geotechnical Journal*, 20(2): 353 – 361.

Bethlehem Steel (1979). *H-Pile Catalogue*. Bethlehem Steel Corporation, Pittsburgh, PA: 62 p.

Bishop, A. W., Collinridge, V. H. and O'Sullivan, T. P. (1948). "Driving and loading tests on six precast concrete piles in gravel." *Géotechnique*, 1(1); 49 – 58.

BOCA Basic Codes (1984). *BOCA Building Code*. 9th ed. Building Officials and Code Administrators International, Incorporation, Country Club Hill, 459 p.

Bogdanovic, L. (1961). "The use of penetration tests for determining the bearing capacity of piles." *Proceedings, 5th International Conference on Soil Mechanics and Foundation Engineering*, Paris 2: p. 17.

Bolton, M. D. (1986). "The strength and dilatancy of sands." *Géotechnique*, 36(1): 65 – 78.

Bond, A. J. and Jardine, R. J. (1991). "Effects of installing displacement piles in a high OCR clay." *Géotechnique* 41(3): 341 – 363.

Bradshaw, A. S. and Baxter, C. D. P. (2006). "Design and construction of driven pile foundations – Lessons learned on the Central Artery/Tunnel Project." *FHWA Report* No. FHWA-HRT-05-159, Federal Highway Administration, U.S. Department of Transportation, Washington DC.

Brand, E. W., Muktabhant, C. and Taechathummarak, A. (1972). "Load tests on small foundations in soft clay." *Proceedings, Specialty Conference on Performance of Earth and Earth-Supported Structures*, (Purdue University), Vol. 1, part 2, ASCE, Reston, Virginia: 903 – 928.

Briaud, J. L., Ballouz, M. and Nasr, G. (2000). "Static capacity prediction by dynamic methods for three bored piles." *ASCE Journal of Geotechnical and Geoenvironmental Engineering*, 126(7): 640–649.

Briaud, J-L. (1984). "Piles in sand: A method including residual stresses." ASCE, *Journal of Geotechnical Engineering*, 110(11): 1666 – 1680.

Brittsan, D. and Speer, D. (1993). "Pile load test results for Highway 280 pile uplift test site." *Proceedings, Caltrans Pile Load Test Results at a Deep Bay Mud Site Using Various Pile Types;* A DFI and Caltrans Specialty Seminar, September 9 and 10, 1993: 170 – 340.

Brittsan, D. and Speer, D. (2008). "Pile load test results for highway 280 pile uplift test site." In *Proceedings, Caltrans Pile Load Test Results at a Deep Bay Mud Site Using Various Pile Types* – A DFI and Caltrans Specialty Seminar, September 9 and 10, 1993: 170 – 340.

Brown, D. (2002). "Effect of construction on axial capacity of drilled foundations in piedmont soils." *Journal of Geotechnical and Geoenvironmental Engineering*, (128) 12: 967 – 973.

Brown, D. A., Turner, J. P. and Castelli, R. J. (2010). "Drilled shafts: construction procedures and LRFD design methods." *Report No. FHWA-NHI-10-016*, Federal Highway Administration, Washington, DC: 971 p.

Brown, M. J. (2004). "The rapid load testing of piles in fine grained soils." *PhD Thesis*, University of Sheffield, UK: 151 – 198.

Brown, M. J., Hyde, A. F. L. and Anderson, W.F. (2006). "Analysis of a rapid load test on an instrumented bored pile in clay." *Géotechnique*, 56 (9): 627 – 638.

Bullock, P. J., Schmertmann, J. H., McVay, M. C. and Townsend, F. C. (2005a). "Side shear setup I: Test piles driven in Florida." *Journal of Geotechnical and Geoenvironmental Engineering*, 131(3): 292 – 300.

Bullock, P. J., Schmertmann, J. H., McVay, M. C. and Townsend, F. C. (2005b). "Side shear setup II: Results from Florida test piles." *Journal of Geotechnical and Geoenvironmental Engineering*, 131(3): 301 – 310.

Burland, J. B. (1989). "Small is beautiful: The stiffness of soils at small strains." *Canadian Geotechnical Journal*, 26 (4): 499 – 516.

Burland, J. P. (1973). "Shaft friction of piles in clay – a simple fundamental approach." *Ground Engineering*, 6(3): 30 – 42.

Burland, J. P. (1993). "Closing address." *Proceedings, Recent Large-Scale Fully Instrumented Pile Tests in Clay*. Institute of Civil Engineers, London: 590 – 595.

Bustamante, M. and Frank, R. (1997). "Design of axially loaded piles—French practice." Design of axially loaded piles – European practice, *Proceedings, ERTC3 Seminar*, Brussels, Belguim, Balkema, Rotterdam, The Netherlands: 161 – 175.

Bustamante, M. and Gianeselli, L. (1982). "Pile bearing capacity predictions by means of static penetrometer CPT." *Proceedings, 2nd European Symposium on Penetration Testing* (ESOPT-II), Vol. 2, Amsterdam, 493 – 500.

Butcher, A. P. and Lord, J. A. (1993). "Engineering properties of the Gault clay in and around Cambridge, UK." *Proceedings, Geotechnical Engineering of Hard Soils – Soft Rocks*, Anagnostopoulos et al. (eds.), Balkema, Rotterdam, ISBN 90 5410 344 2: 405 – 416.

Butler, H. D. and Hoy, H. E. (1977). "User Manual for Texas Quick-Load Method for Foundation Load Testing." *Report* No. IP 77–8, Federal Highway Administration, Washington, DC: 59 p.

Butterfield, R. and Banerjee, P. K. (1971). "The elastic analysis of compressible piles and pile groups." *Géotechnique*, 21(1): 43 – 60.

Cai, G., Liu, S. and Puppala, A. J. (2012). "Reliability assessment of CPTu-based pile capacity predictions in soft clay deposits." *Engineering Geology*, Vol. 141 – 142: 84 – 91.

Cai, G., Liu, S., and A. J. Puppala. (2011). "Evaluation of pile bearing capacity from piezocone penetration test data in soft Jiangsu Quaternary clay deposits." *Marine Georesources and Geotechnology*, 29: 177 – 201.

Cai, G., Liu, S., Tong, L. and Du, G. (2009). "Assessment of direct CPT and CPTu methods for predicting the ultimate bearing capacity of single piles." *Engineering Geology* 104, 211 – 222.

Cairo, R. and Conte, E. (2006). "Settlement analysis of pile groups in layered soils." *Canadian Geotechnical Journal*, 43 (3): 788 – 801.

Camp, W. M. III. (2004). "Drilled and driven foundation behavior in a calcareous clay." *Geosupport 2004* (Proceedings ADSC-ASCE Conference, Orlando) Geotechnical Special Publication No. 124, ASCE, Reston/VA: 1 – 18.

Camp, W. M., Brown, D. A. and Mayne, P. W. (2002). "Construction method effects on axial drilled shaft performance." *ASCE Deep Foundations 2002*, Vol. 2, *Geotechnical Special Publication on Deep Foundations*, No. 116, ASCE, Reston/VA: p. 193 – 208.

Canadian Manual on Foundation Engineering (1985). *Canadian Manual on Foundation Engineering*, 2nd ed., Canadian Geotechnical Society, Technical Committee on Foundations, BiTech Publishers, Vancouver, 460 p.

Cao, Q., Chen, H. and Chen, F. (2012). "Research on application of seismic piezocone penetration tests in pile foundation." *Advanced Materials Research*, Vol. 368-373 (Advances in Civil Engineering and Architecture Innovation): 2722–2730.

Castelli, F. and Motta, E. (2003). "Settlement prevision of piles under vertical load." *Proceedings,Institution of Civil Engineers – Geotechnical Engineering*, 156(4): 183 – 191.

Chakraborty, T. Salgado, R. Basu, P. and Prezzi, M. (2013). "Shaft capacity of drilled shafts in clay." *Journal of Geotechnical and Geoenvironmental Engineering*, ASCE, 139(4): 548 – 563.

Chandler, R. J. (1968). "The shaft friction of piles in cohesive soils in terms of effective stress." *Civil Engineering and Public Works Review*, Vol. 63: 48 – 51.

Chellis, R. D. (1961). *Pile Foundations*. 2nd ed. McGraw-Hill Book Company, New York, 704 p.

Chen, B. S. Y. and Mayne, P. W. (1994). "Profiling the overconsolidation ratio of clays by piezocone tests." *Report GIT-CEEGEO-94-1*, Civil Engineering, Georgia Institute of Technology, Atlanta, 280 p.

Chen, J-J. and Zhang, L. (2013). "The effect of spatial correlation of cone tip resistance on the bearing capacity of piles." *Journal of Geotechnical and Geoenvironmental Engineering*, 139(3): 494 – 500.

Chen, Y. J. and Kulhawy, F. H. (1994). "Case history evaluation of the behavior of drilled shafts under axial and lateral loading." *EPRI Report TR-104601*, Research Project No. 1493–04, Electric Power Research Institute, Palo Alto: www.epri.com

Cheney, R. S. and Chassie, R. G. (2000). "Soils and Foundations Workshop Manual." Second Edition, Publication No. FHWA NHI-00-045, Federal Highway Administration, National Highway Institute, Washington, DC: 353 – 362.

Chin, F. K. (1970). "Estimation of the ultimate load of piles not carried to failure." *Proceedings, 2nd Southeast Asian Conference on Soil Engineering*, Singapore: 81 – 90.

Chin, J. T. and Poulos, H. G. (1991). "Axially loaded vertical piles and pile groups in layered soil." *International Journal of Numerical and Analytical Methods in Geomechanics*, 15: 497 – 511.

Chin, J. T., Chow, Y. K. and Poulos, H. G. (1990). "Numerical analysis of axially loaded vertical piles and pile groups." *Computers and Geotechnics*, 9: 273 – 290.

Chow, F. C. (1996). "Investigations into displacement pile behavior for offshore foundations." *PhD Thesis*, University of London (Imperial College), London, U.K.

Chow, Y. K. (1987). "Axial and lateral response of pile groups embedded in nonhomogeneous soils." *International Journal of Numerical and Analytical Methods in Geomechanics*, 11(6): 621 – 638.

Chow, F. C., Jardine, R. J., Brucy, F. and Nauroy, J. F. (1998). "Effects of time on capacity of pipe piles in dense marine sand." *Journal of Geotechnical and Geoenvironmental Engineering*, 124(3): 254 – 264.

City of Chicago (1982). *City of Chicago Building Code*. Index Publishing Corporation, Chicago, 1138 p.

Clausen, C. J. F., Aas, P. M. and Karlsrud, K. (2005). "Bearing capacity of driven piles in sand, the NGI approach. " *Proceedings, International Symposium on Frontiers in Offshore Geomechanics, ISFOG*, Taylor & Francis, London: 677 – 681.

Clisby, M. B., Scholtes, R. M., Corey, M. W., Cole, H. A., Teng, P. and Webb, J. D. (1978). An evaluation of pile bearing capacities, Vol. I, Final Report, Mississippi State Highway Department.

Cooke, R. W., Price, G. and Tarr, K. (1979). "Jacked piles in London Clay: a study of load transfer and settlement under working conditions." *Géotechnique*, 29(2): 113 – 147.

Cooke, R.W. 1974. "The settlement of friction pile foundations." *Proceedings, Conference on Tall Buildings*, Kuala Lumpur, Malaysia.

Coyle, H. M. and Castello, R. R. (1981). "New design correlations for piles in sand." *Journal of the Geotechnical Engineering Division*, 107(GT7): 965 – 986.

Coyle, H. M. and Reese, L. C. (1966). Load transfer for axially loaded piles in clay. *Journal of Soil Mechanics and Foundations Division*, 92(SM2): 1 – 26.

Crowthers, C. L. (1988). *Load Testing of Deep Foundations: The Planning, Design, and Conduct of Pile Load Tests*. Wiley-Interscience (ISBN: 0-471-60904-8), New York, 233 p.

Cruz, I. R., Howie, J. A., Padros, G., Papanicolas, D. and I. A. (2008). "An evaluation of pile load capacity estimates using CPTu and DMT methods in silty clay in High Prairie, Alberta." *Proceedings, 61st Canadian Geotechnical Conference* (GeoEdmonton 2008): 35 – 42.

Dasenbrock, D. D. (2006). "Assessment of pile capacity by static and dynamic methods to reconcile design predictions with observed performance." *Proceedings, University of Minnesota 54th Geotechnical Engineering Conference*, Labuz, J.F., Wachman, G.S. and Kao, C.S. (eds.), St. Paul, MN, pp 95 – 108.

Davies, M. P. (1987). "Predicting axially and laterally loaded pile behavior using in-situ testing methods." *PhD Thesis*, Dept. of Civil Engineering, The University of British Columbia, Canada: 319 p.

Davisson, M. T. (1972). "High capacity piles." *Proceedings, Lecture Series on Innovations in Foundation Construction*, ASCE Illinois Section, Chicago, Reston, VA: 81–112.

De Beer, E. E. (1963). "The scale effect in the transposition of the results of deep sounding tests on the bearing capacity of piles and caisson foundations." *Géotechnique*, 13(1): 39 – 75.

De Beer, E. E. (1970). "Experimental determination of the shape factors and the bearing capacity factors of sand." *Géotechnique* 20(4): 387 – 411.

De Nicola, A. and Randolph, M. F. (1993). "Tensile and compressive shaft capacity of piles in sand." ASCE *Journal of Geotechnical Engineering*, 119(12): 1952 – 1973.

De Nicola, A. and Randolph, M. F. (1999). "Centrifuge modelling of pipe piles in sand under axial loads." *Géotechnique* 49(3): 295 – 318.

De Ruiter, J. and Beringen, F. L. (1979). "Pile foundations for large North Sea structures." *Marine Geotechnology*, 3(3): 267 – 314.

Decourt, L. (1999). "Behavior of foundations under working load conditions." *Proceedings of the 11th Pan-American Conference on Soil Mechanics and Geotechnical Engineering*, Foz Do Iguassu, Brazil, August 1999, Vol. 4: 453 – 488.

Dennis, N. D. and Olson, R. E. (1983). "Axial capacity of steel pipe piles in clay." Proceedings, Geotechnical Practice in Offshore Engineering, Austin, Texas. Edited by Stephen Wright. ASCE, New York: 370 – 388.

Doherty, P. and Gavin, K. (2013). "Pile aging in cohesive soils." *Journal of Geotechnical and Geoenvironmental Engineering*, 139(9): 1620 – 1624.

Doherty, P. and Gavin, K. (2011a). "The shaft capacity of displacement piles in clay: a state of the art review." *Geotechnical and Geological Engineering*, 29(4): 389–410.

Doherty, P. and Gavin, K. (2011b). "The aged reloading response of piles in clay." *Proceedings, DFI 36th Annual Conference on Deep Foundations*. Boston, MA, Deep Foundations Institute: 67 – 73.

Doherty, P. and Gavin, K. (2011c). "Shaft capacity of open-ended piles in clay." *Journal of Geotechnical and Geoenvironmental Engineering*, 137(11): 1090 – 1102.

Drewry, J. M., Weidler, J. B. and Hoang, S. T. (1977). "Predicting axial pile capacities for offshore platforms." *Petroleum Engineering*: 41 – 44.

Dunham, J. W. (1957). "Pile-loading tests, Morganza floodway control structure." *Discussion, Transactions*, ASCE, Vol. 121: 577 – 578.

Eiber, R. J. (1958). "A preliminary laboratory investigation of the prediction of static pile resistances in sand." *Master's Thesis*, Department of Civil Engineering, Case Institute of Technology, Cleveland, OH.

Elhakim, A. and Mayne, P. W. (2002). "Discussion: Construction effects on drilled shaft response." *Journal of Geotechnical and Geoenvironmental Engineering*, 128(5): 448 – 450.

Elhakim, A. F. (2005). "Evaluation of shallow foundation displacements using soil small-strain stiffness." *PhD Thesis*, School of Civil and Environmental Engineering, Georgia Institute of Technology, Atlanta, Georgia.

Ellison, R. D., D' Appolonia, E. and Thiers, G. R. (1971). "Load-deformation mechanism for bored piles." *Journal of the Soil Mechanics and Foundations Division*, 97(4): 661 – 678.

England, M. (2003). "Bi-directional static load testing – state of the art.", *Proc. of the 4th Geotechnical Seminar on Deep Foundations on Bored and Augered Piles*, Ghent, Belgium, 309 – 313.

Erbland, P. and McGillivray, R. (2004). "Effects of pile setup on pile design and construction: a case history." *Current Practices and Future Trends in Deep Foundations* (GSP 125), ASCE, Reston/VA: 66 – 76.

Eslami, A. and Fellenius, B. H. (1997). "Pile capacity by direct CPT and CPTu methods applied to 102 case histories." *Canadian Geotechnical Journal*, 34(6): 880–898.

Fahey, M. and Carter, J. P. (1993). "A finite element study of the pressuremeter test in sand using a nonlinear elastic plastic model." *Canadian Geotechnical Journal*, 30(2): 348 – 362.

Fellenius, B. H. (1975). "Test Loading of Piles and New Proof Testing Procedure." *Journal of Geotechnical Engineering Division*, ASCE, 101(GT9): 855 – 869.

Fellenius, B. H. (1989). "Tangent modulus of piles determined from strain data." ASCE, Geotechnical Engineering Division, *Foundation Engineering: Current Principles and Practices*, Vol. 1 (GSP 22), ASCE, Reston, Virginia: 500 – 510.

Fellenius, B. H. (1990). "Guidelines for the interpretation and analysis of the static loading test." Sparta, NJ, Deep Foundations Institute (DFI), Continuing education short course text, 44 p.

Fellenius, B. H. (2001a). "What capacity value to choose from the results of a static loading test." Fulcrum, Deep Foundation Institute, New Jersey, 19 – 22.

Fellenius, B. H. (2001b). "Determining the true distribution of load in piles." ASCE, *International Deep Foundation Congress*, An International Perspective on

Theory, Design, Construction, and Performance, Geotechnical Special Publication No. 116, Orlando, Florida, Vol. 2: 1455 – 1470.

Fellenius, B. H. (2002a). "Determining the resistance distribution in piles. Part 1: Notes on shift of no-load reading and residual load." *Geotechnical News Magazine*, 20(2): 35 – 38.

Fellenius, B. H. (2002b). "Excerpt from Chapter 6, the red book: direct methods for estimating pile capacity." In *Background to UniCone*: www.fellenius.net.

Fellenius, B. H. (2011). *Basics of Foundation Design*. electronic edition, December 2011, <www.fellenius.net>, accessed July 25, 2012.

Fellenius, B. H. and Ochoa, M. (2009). "Testing and design of a piled foundation project. A case history." *Geotechnical Engineering, Journal of the Southeast Asian Geotechnical Society*, 40 (3): 129 – 137.

Fellenius, B. H., Harris, D. and Anderson, D. G. (2003). "Static loading test on a 45 m long pipe pile in Sandpoint, Idaho." *Canadian Geotechnical Journal*, 41(4): 613 – 628.

Fellenius, B. H., Santos, J. A. and Viana da Fonseca, A. (2007). "Analysis of piles in a residual soil—The ISC'2 prediction." *Canadian Geotechnical Journal*, 44(1): 201 – 220.

Ferber, V. and Abraham, O. (2002). "Contribution of the seismic methods to the determination of initial moduli: application on the experimental site of Merville." *Proceedings, International Symposium on Identification and Determination of Soil and Rock Parameters for Geotechnical Design* (*PARAM 2002*). Paris, 2 – 3 September, 41 – 48.

Finno, R. J. (1989). "Subsurface conditions and pile installation data: 1989 Foundation Engineering Congress Test Section." *Proceedings Symposium on Predicted and Observed Axial Behavior of Piles* (Geotechnical Special Publication No. 23), ASCE, Reston/VA: 1 – 74.

Finno, R. J., Cosmao, T. and Gitskin, B. (1989). "Results of Foundation Engineering Congress – Pile Load Tests." *Proceedings, Symposium: Predicted and Observed Axial Behavior of Piles* (Geotechnical Special Publication No. 23), ASCE, Reston, VA: 338 – 355.

Fioravante, V. (1994). "Centrifuge modeling of driven and bored piles in sand subjected to axial load." Workshop on pile foundations experimental investigation, analysis and design, Napoli: 125 – 163.

Fioravante, V., Ghionna, V. N., Jamiolkowski, M. and Pedroni, S. (1995). "Load carrying capacity of large diameter bored piles in sand and gravel." *Proceedings, 10th Asian Regional Conference on Soil Mechanics and Foundation Engineering*, Beijing, China, 1995.

Flaate, K. and Selnes, P. (1977). "Side friction of piles in clay." *Proceedings, 9th International Conference on Soil Mechanics and Foundation Engineering*, Tokyo: 517 – 522.

Fleming, W. G. K. (1992). "A new method for single pile settlement prediction and analysis." *Géotechnique*, 42(3): 411 – 425.

Fleming, W. G. K., Weltman, A. J., Randolph, M. F. and Elson, W. K. (1992). *Piling Engineering*. 2nd ed., Blackie/Halsted Press, John Wiley & Sons, New York: 390 p.

Fleming, W. G. K., Weltman, A. J., Randolph, M. F. and Elson, W.K. (2009). *Piling Engineering*. 3rd ed., Taylor & Francis, New York.

Fletcher, G. A. (1962). "Pile load tests and their evaluation." *Field Testing of Soils* (STP 322), ASTM, Philadelphia, PA: 47 – 56.

Focht, J. A. (1967). "Discussion to paper by Coyle and Reese." *Journal of Soil Mechanics and Foundations Engineering*, ASCE 93(SMl): 133 – 138.

Fragasny, R. J., Higgins, J. D. and Argo, D. E. (1988). "Comparison of methods for estimating pile capacity." *Report No*. WA-RD 163.1, Washington State Department of Transportation, 62.

Frank, R. (1975). "Etude théorique du comportement des pieux sous charge verticale." *Rapporte de Recherché No. 46*, Laboratoire Central des Ponts et Chaussées, Paris, France.

Frank, R. (1985). "Recent developments in the prediction of pile behaviour from pressuremeter results." *Proceedings of Symposium from Theory to Practice on Deep Foundations*, Porto Alegre, Brazil, Vol. 1: 69 – 99.

Fuller, F. M. and Hoy, H. E. (1970). "Pile load tests including quick load test method, conventional methods, and interpretations." *Highway Research Record 333*, Highway Research Board, Washington, DC: 74 – 86.

Garner, M. P. (2007). "Loading rate effects on axial pile capacity in clays." *Thesis*, Department of Civil and Environmental Engineering, Brigham Young University, Provo, Utah, 122 p.

Gavin, K. G. and Lehane, B. M. (2003)."The shaft capacity of pipe piles in sand." *Canadian Geotechnical Journal*, Vol. 40: 36 – 45.

Gavin, K. G. and Lehane, B. M. (2005). "Estimating the end bearing resistance of pipe piles in sand using the final filling ratio." *Proceedings*, *International Symposium on Frontiers in Offshore Geomechanics* (ISFOG 2005, Perth), Taylor and Francis Group, London: 717–723.

Gavin, K. G. and O'Kelly, B. C. (2007). "Effect of friction fatigue on pile capacity in dense sand." *Journal of Geotechnical and Geoenvironmental Engineering*, 133(1): 63 – 71.

Ghionna, V. N., Jamiolkowsi, M., Pedroni, S. and Salgado, R. (1994). "The tip displacement of drilled shafts in sands." *Vertical and Horizontal Deformations of Foundations and Embankments*, Vol. 2, GSP 40, ASCE, Reston/VA: 1039 – 1057.

Goble, G. G. and Rausche, F. (1970). "Pile load test by impact driving." Highway Research Record No. 333, Highway Research Board, Washington, DC.

Goble, G. G., Likins, G. E. and Rausche, F. (1975). "Bearing capacity of piles from dynamic measurements." *Final Report*, Department of Civil Engineering, Case Western Reserve University, Cleveland, OH, 76 p.

Goh, A. T. C., Kulhawy, F. H. and Chua, C. G. (2005). "Bayesian neural network analysis of undrained side resistance of drilled shafts." *Journal of Geotechnical and Geoenvironmental Engineering*, 131(1): 84 – 93.

Gregersen, O. S., Aas, G. and Dibiagio, E. (1973). "Load tests on friction piles in loose sand." *Proceedings, 8th International Conference of Soil Mechanics and Foundation Engineering* (ICSMFE), Moscow, Vol. 2: 109 – 117.

Guo, D. J., Tham, L. G. and Cheung, Y. K. (1987). "Infinite layer for the analysis of a single pile." *Computers and Geotechnics*, Vol. 3: 229 – 249.

Guo, W. D. (2000a). "Vertically loaded single piles in Gibson soil." *Journal of Geotechnical and Geoenvironmental Engineering*, 126(2): 189 – 193.

Guo, W. D. (2000b). "Visco-elastic load transfer models for axially loaded piles." *International Journal of Numerical and Analytical Methods in Geomechanics*, Vol. 24, 135 – 163.

Guo, W. D. and Randolph, M. F. (1997). "Vertically loaded piles in non-homogeneous media." *International Journal of Numerical and Analytical Methods in Geomechanics*, 21(8): 507 – 532.

Guo, W.D. and Randolph, M. F. (1999). "An efficient approach for settlement prediction of pile groups." *Géotechnique*, 49(2): 161 – 179.

Gwizdala, K. (1984). "Large diameter bored piles in non-cohesive soils." Swedish Geotechnical Institute, *Report* No. 26, Linkoping, Sweden.

Han, J. (1997). "An experimental and analytical study of the behavior of fiber-reinforced polymer piles and pile-sand interactions." *PhD Thesis*, Dept. of Civil and Environmental Engineering, Georgia Institute of Technology: 1 – 276.

Hanna, T. H. and Tan R. H. S. (1973). "The behavior of long piles under compressive loads in sand." *Canadian Geotechnical Journal*, 10(2): 311 – 340.

Hannigan, P. J., Goble, G. G., Thendean, G., Likins, G. E. and Rausche, F. (2006). "Design and construction of driven pile foundations." *FHWA Report* Vol. I and II, No. FHWA-NHI-05-042 and FHWA-NHI-05-043, Federal Highway Administration, U.S. Department of Transportation, Washington DC.

Hansen, J. B. (1963). Discussion: "Hyperbolic stress-strain response: cohesive soils." *ASCE Journal of the Soil Mechanics and Foundations Division*, 89(SM4): 241 – 242.

Hardin, B. O. and Drnevich, V. P. (1972). "Shear modulus and damping in soils: Design equations and curves." *Journal of Soil Mechanics and Foundations Division*, ASCE, 98(SM7): 667 – 692.

Hegazy, Y. A. and Mayne, P. W. (1995). "Statistical correlations between V_s and CPT data for different soil types." *Proceegings, International Symposium on Cone Penetration Testing*, Vol. 2, Swedish Geotechnical Society, Linköping, Sweden: 173 – 178.

Heydinger, A. G. (1982). "Analysis of axial single pile-soil interaction in clay." *PhD Dissertation*, Dept. of Civil Engineering, University of Houston, Houston, Texas.

Heydinger, A. G. and O'Neill, M. W. (1986). "Analysis of axial pile-soil interaction in clay." *International Journal of Numerical and Analytical Methods in Geomechanics*, Vol. 10: 367 – 381.

Hirany, A. and Kulhawy, F. H. (1988). "Conduct and interpretation of load tests on drilled shaft foundations." *Report EL-5915*, Vol. 1, Electric Power Research Institute, Palo Alto/CA: www.epri.com

Hirany, A. and Kulhawy, F. H. (2002). "On the interpretation of drilled foundation load test results." *Deep foundations 2002* (GSP 116), O'Neill, M. W. and Townsend, F. C., eds., ASCE, Reston, VA: 1018 – 1028.

Holloway, D. M., Clough, G. W. and Vésic A. S. (1978). "The effects of residual driving stresses on pile performance under axial load." *Proceedings of the 10th Offshore Technology Conference*, Houston, TX., Vol. 4, 2225 – 2236.

Hossain, M. S., Omelchenko, V. and Haque, M. A. (2007). "Capacity of rock socketed drilled shafts in Mid-Atlantic region." *Proceedings, Geotechnical Special Conference: Contemporary Issues in Deep Foundations*, (GSP No 157), Denver, CO, ASCE, Reston, VA: 18 – 21.

Housel, W. A. (1966). "Pile load capacity – estimates and test results." ASCE *Journal of Soil Mechanics and Foundation Engineering*, 92(SM4): 1 – 30.

Hunter, A. H. and Davisson, M. T. (1969). "Measurements of pile load transfer." *Proceedings,Symposium on Performance of Deep Foundations*, San Francisco, ASTM STP 444, 106 – 117.

Huybrechts, N. (2001). "Test campaign at Sint-Katelijne-Waver and installation techniques of screw piles." *Proceedings, Symposium on Screw Piles – Installation and Design in Stiff Clay,* Brussels. Balkema, Rotterdam, ISBN: 90 5809 192 9: pp. 151 – 204.

Huybrechts, N. and Whenham, V. (2003). "Pile testing campaign on the Limelette test site and installation techniques of screw piles." *Proceedings, Second Symposium On Screw Piles – Belgian Screw Pile Technology – Design And Recent Developments*. Brussels, Balkema, ISBN: 90 5809 578 9: 71–130.

Igoe, D. J. P. Gavin, K. G. and O'Kelly, B. C. (2011). "Shaft capacity of open-ended piles in sand." *Journal of Geotechnical and Geoenvironmental Engineering*, 137(10): 903 – 913.

Igoe, D. J. P., Gavin, K. G. and O'Kelly, B. (2010). "Field tests using an instrumented model pipe pile in sand." *Proceedings, International Conference on Physical Modelling in Geotechnical Engineering*, Springman, Laue and Seward (eds.) Zurich, Taylor and Francis Group,: 775 – 780.

Ishibashi, I. and Zhang, X. (1993). "Unified dynamic shear moduli and damping ratios of sand and clay." *Soils and Foundations*, 33(1), 182 – 191.

Iskander, M., Roy, D., Kelley S. and Ealy, C. (2003). "Drilled shaft defects: detection, and effects on capacity in varved clay." *Journal of Geotechnical and Geoenvironmental Engineering*, 129(12): 1128 – 1137.

Jamiolkowski, M. (2003). "Deep foundations on bored and auger piles." *Proceedings, 4th International Geotechnical Seminar on Deep Foundations on Bored and Auger Piles*, Ghent: 83–100.

Jamiolkowski, M., Ladd, C.C., Germaine, J.T., and Lancellotta, R. (1985). New developments in field and lab testing of soils. *Proceedings 11th International Conference on Soil Mechanics & Foundation Engineering*, Vol. 1, San Francisco: 57–154.

Jamiolkowski, M., LoPresti, D. C. F. and Manassero, M. (2001). "Evaluation of relative density and shear strength of sands from cone penetration test and flat dilatometer test." *Soil Behavior and Soft Ground Construction* (GSP 119), American Society of Civil Engineers, Reston, VA: 201 – 238.

Jardine, R. J., Bond, A. J. and Lehane, B. M. (1992). "Field experiments with instrumented piles in sand and clay." *Proceedings, Piling — European Practices and Worldwide Trends*, a conference organized by the Institution of Civil Engineers, London, April 7 – 9.

Jardine, R. J., Chow, F. C., Over, Y. R. and Standing, J. R. (2005). "ICP design methods for driven piles in sand and clays." Thomas Telford, London.

Jardine, R. J., Potts, D. M., Fourie, A. B. and Burland, J. B. (1986). "Studies of the influence of non-linear stress-strain characteristics in soil-structure interaction." *Géotechnique*, 36(3): 377 – 396.

Jardine, R., Chow, F., Overy, R. and Standing, J. (2005). *ICP Design Methods for Driven Piles in Sands and Clays*. Thomas Telford Publishing, London, 105 p.

Jefferies, M. G. and Been, K. (2006). *Soil Liquefaction – a critical state approach*. Taylor and Francis Group, London, 480 p.

Joshi, R. C. and Sharma, H. D. (1987). "Prediction of ultimate pile capacity from load tests on bored and belled, expanded base compacted and driven piles." *Proceedings, International Symposium of Prediction and Performance in Geotechnical Engineering*, Calgary, Canada: 135 – 144.

Karlsrud, K. (1988). "Design of offshore piles in clay field tests and computational modeling. Summary, interpretation and analyses of the pile load tests at the Onsøy site." *NGI Report* No. 52523-23, 15/3/88, Norwegian Geotechnical Institute, Oslo.

Karlsrud, K. (2012). "Prediction of load-displacement behavior and capacity of axially-loaded piles in clay based on analyses and interpretation of pile load test results." *PhD Dissertation*, Norwegian University of Science and Technology, Trondheim: 320 p.

Karlsrud, K., Clausen, C. J. F. and Aas, P. M. (2005). "Bearing capacity of driven piles in clay, the NGI approach." *Proceedings, Frontiers in Offshore Geotechnics*: ISFOG, Perth: 775 – 782.

Karlsrud, K., Hansen, S. B., Dyvik, R. and Kalsnes, B. (1993). "NGI's pile tests at Tilbrook and Pentre – review of testing procedures and results." *Large-Scale Pile Tests in Clay*. Thomas Telford, London: 549 – 583.

Karlsrud, K. and Haugen, T. (1985). "Axial static capacity of steel model piles in overconsolidated clay." *Proceedings, 11th International Conference on Soil Mechanics and Foundation Engineering* (San Francisco), Vol. 2, Balkema, Rotterdam: 1401 – 1406.

Kempfert, H-G., Becker, P. (2010). "Axial pile resistance of different pile types based on empirical values." *Proceedings, Geo-Shanghai 2010 Deep Foundations and Geotechnical ln-Situ Testing* (GSP 205), ASCE, Reston, Virginia: 149 – 154.

Kerisel, J. L. (1965). "Vertical and horizontal bearing capacity of deep foundations in clay." *Bearing Capacity and Settlement of Foundations*, Duke University, Durham, NC: 45 – 51.

Kim, D., Bica, A. V. D., Salgado, R., Prezzi, M. and Lee, W. (2009). "Load testing of a closed-ended pipe pile driven in multilayer soil." *Journal of Geotechnical and Geoenvironmental Engineering*, 135(4): 463 – 473.

Kim, H. and Mission, J. (2011). "Improved evaluation of equivalent top-down load-displacement curve from a bottom-up pile load test." *Journal of Geotechnical and Geoenvironmental Engineering*, 137(6): 568 – 578.

Kishida, H., Tsubakihara, Y. and Ogura, T. (1992). "Pile loading tests at Osaka amenity park project." unpublished report to Mitsubishi Co., preprint title, 7 p.

Klosinski, B. (1977). "Bearing capacity of large diameter bored piles." *Proceedings, 9th International Conference on Soil Mechanics and Foundation Engineering*, Volume 1, Tokyo: 609 – 612.

Kodikara, J. K. and Johnston, I. W. (1994). "Analysis of compressible axially loaded piles in rock." *International Journal of Numerical and Analytical Methods in Geomechanics*, 18: 427 – 37.

Kolk, H. J. and van der Velde, E. (1996). "A reliable method to determine the friction capacity of piles driven into clays." *Proceedings, 28th Annual Offshore Technology Conference*, Houston: 337 – 346.

Kolk, H. J., Baaijens, A. E. and Senders, M. (2005). "Design criteria for pipe piles in silica sands." *Proceedings, International Symposium on Frontiers in Offshore Geomechanics* (*ISFOG 2005*), Taylor and Francis Group, London: 711 – 716.

Komurka, V. E. and Grauvogl-Graham, J. L. (2010). "Pile test program report: Lafayette Bridge Replacement." *Report No. 09019* submitted to Minnesota Department of Transportation, by Wagner Komurka Geotechnical Group, Inc., Cedarburg, WI: 844 p.

Komurka, V., Winter, C. and Maxwell, S. (2005). "Applying separate safety factors to end-of-drive and set-up components of driven pile capacity." Geotechnical applications for transportation infrastructure: featuring the marquette interchange project in Milwaukee, Wisconsin (GPP 3): 65 – 80.

Kondner, R. L. (1963). "Hyperbolic stress–strain response: cohesive soil." *Journal of the Soil Mechanics and Foundations Division*, ASCE, 89(SM1): 115 – 143.

Konrad, J-M. and Roy, M. (1987). "Bearing capacity of friction piles in marine clay." *Géotechnique*, 37(2): 163 – 176.

Kort, D. A. (2005). "Report on drilled pile load testing (Osterberg method), Test pile 1, Foothills Medical Center, Calgary, Alberta." *Project Report* No. LT-9121, prepared by LoadTest Incorporated for Golder Associates.

Kort, D. A., Ahren, M. D. and Pang, S. K. (2001a). "Report on drilled shaft load testing (Osterberg method), Test shaft # 1 – Pinners Point Interchange, Portsmouth, VA." *Project Report* No. LT-8385-1, prepared by LoadTest Incorporated for Trevi Icos Corporation.

Kort, D. A., Ahren, M. D., Pang, S. K. (2001b). "Report on drilled shaft load testing (Osterberg method), Test shaft # 2 – Pinners Point Interchange, Portsmouth, VA." *Project Report* No. LT-8385-2, prepared by LoadTest Incorporated for Trevi Icos Corporation.

Kraft, L. M., Focht, J. A. and Amerasinghe, S.F. (1981a). "Friction capacity of piles driven into clay." *Journal of Geotechnical Engineering Division*, Vol. 107: 1521 – 1541.

Kraft L. M., Ray, R. P. and Kagawa, T. (1981b). "Theoretical t-z curves." *Journal of Geotechnical Engineering Divisions*, ASCE, 107(11): 1543 – 1562.

Kulhawy, F. H. (2004). "On the axial behavior of drilled foundations." *GeoSupport 2004: Drilled shafts, micropiling, deep mixing, remedial methods, and specialty foundation systems (GSP 124)*, ASCE, Reston, VA: 34 – 51.

Kulhawy, F. H. and Mayne, P. W. (1990). "Manual on estimating soil properties for foundation design." *Report EPRI EL-6800*, Electric Power Research Institute, Palo Alto, CA, 306 p.

Kulhawy, F. H. and Phoon, K. (1993). "Drilled shaft side resistance in clay soil to rock." *Design and Performance of Deep Foundations: Piles and Piers in Soil and Rock, GSP No. 38*, ASCE, Reston, VA: 172 – 183.

Kulhawy, F. H., Trautmann, C. H. Beech, J. F. O'Rourke, T. D. and McGuire, W. (1983). "Transmission line structure foundations for uplift-compression loading." *Report EL-2870*, Electric Power Research Institute, Palo Alto, CA, 412 p.

Kurian, N. P. and Shah, S. J. (2009). "Studies on the behaviour of screw piles by the finite element method." *Canadian Geotechnical Journal*, Vol. 46: 627 – 638.

Kwon, O. S., Choi, Y., Kwon, O. and Kim, M. M. (2005). "Comparison of the bidirectional load test with the top-down load test." *Transportation Research Record 1936*, Transportation Research Board, Washington, DC: 108 – 116.

Ladd, C. C. and DeGroot, D. J. (2003). "Recommended practice for soft ground site characterization." *Proceedings, 12th Pan American Conference, Soil and Rock America 2003* (MIT, Boston), Verlag Glückauf, Essen: 3 – 57.

Lee K-M. and Xiao, Z. R. (1999). "A new analytical model for settlement analysis of a single pile in multi-layered soil." *Soils and Foundations*, 39(5): 131 – 143.

Lee, C. Y. (1991). "Discrete layer analysis of axially loaded piles and pile group." *Computers and Geotechnics*, 11(4): 295 – 313.

Lee, C. Y. (1993). "Settlement of pile group-practical approach." *Journal of Geotechnical Engineering Division*, ASCE, 119(9): 1449 – 1461.

Lee, C. Y. and Small, J. C. (1991). "Finite-layer analysis of axially loaded piles." *Journal of Geotechnical Engineering*, ASCE, 117(11): 1706 – 22.

Lee, J. H. and Salgado, R. (1999). "Determination of pile base resistance in sands." *Journal of Geotechnical and Geoenvironmental Engineering*, ASCE, 125(8), 673 – 683.

Lee, J. H., Salgado, R. and Paik, K. (2003). "Estimation of load capacity of pipe piles in sand based on CPT results." *Journal of Geotechnical and Geoenvironmental Engineering*, 129(5): 391 – 403.

Lee, J. S. and Park, Y. H. (2008). "Equivalent pile load-head settlement curve using a bi-directional pile load test." *Computers and Geotechnics*, 35(2), 124–133.

Lee, K-M and Xiao, Z. R. (1999). "A new analytical model for settlement analysis of a single pile in multi-layered soil." *Soils and Foundations*, 39(5): 131 – 143.

Lee, S. and Long, J. H. (2008). "Skin friction features of drilled CIP piles in sand from pile segment analysis." *International Journal for Numerical and Analytical Methods in Geomechanics*, Vol. 32, 745 – 770.

Lefebvre, G., LeBoeuf, D., Rahhal, M. E., Lacroix, A., Warde, J. and Stokoe, K. H. (1995). "Laboratory and field determinations of small-strain shear modulus for a structured Champlain clay: Reply." *Canadian Geotechnical Journal*, 32(1): 194.

Lehane, B. (1992). "Experimental investigations of pile behavior using instrumented field piles." *PhD Thesis*, Faculty of Engineering, Imperial College, London: 615 p.

Lehane, B. M. and Cosgrove, E. (2000). "Applying triaxial compression stiffness data to settlement prediction of shallow foundations." *Geotechnical Engineering*, Vol. 142: 19 – 200.

Lehane, B. M. and Gavin, K. G. (2001). "Base resistance of jacked pipe piles in sand." *Journal of Geotechnical and Geoenvironmental Engineering*, 127(6): 473 – 480.

Lehane, B. M. and Jardine, R. J. (1994). "Displacement pile behaviour in glacial clay." *Canadian Geotechnical Journal*, 31(1): 79 – 90.

Lehane, B. M., Jardine, R. J., Bond, A. J., and Frank, R. (1993). "Mechanism of shaft friction in sand from instrumented pile tests." *Journal of Geotechnical Engineering*, 119(1): 19 – 35.

Lehane, B. M., Li, Y. and Williams, R. (2013). "Shaft capacity of displacement piles in clay using the cone penetration test." *Journal of Geotechnical and Geoenvironmental Engineering*, 139(2): 253–266.

Lehane, B. M., McCabe, B. A. and Phillips D. T. (2000). "Instrumented single and group piles in Belfast soft clay." *Australian Geomechanics*, 35(4), 33 – 45.

Lehane, B. M., Schneider, J. A. and Xu, X. (2005). "The UWA-05 method for prediction of axial capacity of driven piles in sand." *Proceedings, International Symposium on Frontiers in Offshore Geomechanics* (ISFOG, Perth), Taylor and Francis, London: 683 – 689.

Leonards, G. A. and Lovell, D. (1979). "Interpretation of load tests on high capacity driven piles." *Behavior of Deep Foundations* (STP 670), ASTM, West Conshohocken, PA: 388 – 415.

Liew S. S. and Kowng Y. W. (2005). "Design, installation and verification of driven piles in soft ground." *Proceedings, 11th International Conference on Computer Methods and Advances in Geomechanics*, Torino, Italy, Vol. 2: 491 – 498.

Liu, J., Xiao, H. B., Tang, J., Li, Q. S. (2004). "Analysis of load-transfer of single pile in layered soil." *Computers and Geotechnics*, Vol. 31, 127 – 135.

LoadTest (2012), Report, Gainesville, Florida. <http://www.loadtest.com/loadtest-usa/products/>, accessed June 10, 2012.

Long, J. H., Kerrigan, J. A. and Wysockey, M. H. (2007). "Measured time effects for axial capacity of driven piling." *Journal of the Transportation Research Board*, Vol. 1663: 8 – 15.

Lunne, T., Long, M. and Forsberg, C. F. (2003). "Characterisation and engineering properties of Onsøy clay." *Characterisation and Engineering Properties of Natural Soils* (Proceedings Singapore Workshop), Balkema, Rotterdam, pp. 395 – 428.

Lunne, T., Robertson, P. K. and Powell, J. J. M. (1997). *Cone Penetration Testing in Geotechnical Practice*, Blackie Academic/London, Routledge, New York: 312 p.

Maertens, J. and Huybrechts, N. (2003). "Results of the static pile load tests at the Limelette test site." *Proceedings, 2nd Symposium on Screw Piles – Belgian Screw Pile Technology – Design and Recent Developments*, Brussels, Balkema, ISBN: 9058095789: 167 – 214.

Mandolini, A. and Viggiani, C. (1997). "Settlement of piled foundations." *Géotechnique*, 47(4): 791 – 816.

Mansur, C. I. and Kaufman, J. M. (1956). "Pile tests, low-sill structure, Old River, Louisiana." *Journal of Soil Mechanics and Foundations Division*, ASCE, 82(SM5): 1079/1 – 1079/33.

Matsumoto, T., Michi, Y. and Hirano, T. (1995). "Performance of axially loaded steel pipe piles driven in soft rock." *Journal of Geotechnical Engineering*, 121(4): 305 – 315.

Mayne, P. W. (1994). "CPT-based prediction of footing response." *Predicted and Measured Behavior of Five Spread Footings on Sand*. Geotechnical Special Publication No. 41, ASCE, Reston, Virginia, 214 – 217.

Mayne, P.W. (1999). "Site Characterization aspects of Piedmont residual soils in Eastern U.S.", *Proceedings of the 14th International Conference on Soil Mechanics and Geotechnical Engineering*, Vol. 4, (Hamburg), Balkema, Rotterdam: 2191 – 2195.

Mayne, P.W. (2001). Invited Keynote: "Stress-Strain-Strength-Flow Parameters from Enhanced In-Situ Tests", Proceedings, International Conference on In-Situ Measurement of Soil Properties & Case Histories (In-Situ 2001), Bali, Indonesia, 27-47.

Mayne, P. W. (2002). "Seismic piezocone test and analysis: axial pile response at I-295 James River Bridge, Richmond, VA." *FHWA Report*, Ref. No. DTFH61-98-00047, Georgia Tech Report to Federal Highway Administration, McLean, VA, 26 p.

Mayne, P.W. (2005). Invited Keynote: "Integrated ground behavior: in-situ and Laboratory tests." *Proceedings, 3rd International Symposium on the Deformation Characteristics of Geomaterials*, Vol. 2 (IS Lyon'03), Taylor & Francis Group, London: 155 – 177.

Mayne, P. W. (2006). "Undisturbed sand strength from seismic cone tests." The 2nd James K. Mitchell Lecture, *Geomechanics and Geoengineering*, 1(4), 239 – 247.

Mayne, P. W. (2007). "Cone penetration testing – a synthesis of highway practice." *NCHRP Synthesis 368*, Transportation Research Board, National Academies Press, Washington, D.C., 117 p.

Mayne, P. W. and Brown, D. A. (2003). "Site characterization of Piedmont residuum of North America." *Characterization and Engineering Properties of Natural Soils*, Vol. 2 (Proc. Singapore Workshop), Swets & Zeitlinger, Lisse, 1323-1339.

Mayne, P. W. and Elhakim, A. (2002). "Axial pile response evaluation by geophysical piezocone tests." *Proceedings, 9th International Conference on Piling and Deep Foundations*, DFI, Nice, Presses de l'ecole nationale des Ponts et chaussees, 543 – 550.

Mayne, P. W. and Harris, D. E. (1993). "Axial load-displacement behavior of drilled shaft foundations in Piedmont Residuum." *Technical Report No. 41-30-2175*, submitted to Federal Highway Administration, Turner-Fairbanks Highway Research Center by Georgia Institute of Technology, 162 p.

Mayne, P. W. and Kulhawy, F. H. (1982). "K_o-OCR relationships in soil." *Journal of the Geotechnical Engineering Division*, ASCE, 108(GT6): 851 – 872.

Mayne, P. W. and Niazi, F. S. (2009). "Evaluating axial elastic pile response from cone penetration tests." (2009 Michael O'Neill Lecture), *Journal of Deep Foundations Institute*, 3(1): 3 – 12. http://www.dfi.org/toc/toc1002.pdf.

Mayne, P. W. and Poulos, H. G. (2001). "Approximate displacement influence factors for elastic shallow foundations." *ASCE Journal of Geotechnical & Geoenvironmental Engineering*, 127(1): 100 – 102.

Mayne, P. W. and Schneider, J. A. (2001). "Evaluating axial drilled shaft response by seismic cone." *Foundations and Ground Improvement.* Geotechnical Special Publication No. 113, ASCE, Reston, VA, pp. 655 – 669.

Mayne, P. W. and Woeller, D. J. (2008). "O-cell response using elastic pile and seismic piezocone tests." *Proceedings, 2nd British Geotechnical Association International Conference on Foundations* (ICOF 2008), Vol. 1, Dundee, IHS BRE Press, UK: 235 – 246.

Mayne, P. W., Coop, M. R., Springman, S. M., Huang, A. and Zornberg, J. G. (2009). "Geomaterial behavior and testing." *Proceedings, 17th International Conference*

on Soil Mechanics and Geotechnical Engineering, Vol. 4 (Alexandria, Egypt), Millpress/IOS Press, Amsterdam: 2777 – 2872.

Mayne, P. W., Niazi, F. S. and Woeller, D. J. (2010). "Drilled shaft response in Piedmont residuum using elastic continuum analysis and seismic piezocone tests." *Proceedings, GeoShanghai 2010 Deep Foundations and Geotechnical ln-Situ Testing* (GSP 205), ASCE, Reston, Virginia: 200 – 205.

Mayne, P. W., Peuchen, J. and Bouwmeester, D. (2010). "Estimation of soil unit weight from CPTs." *Proc. 2nd International Symposium on Cone Penetration Testing*, (CPT'10), Huntington Beach, CA, Vol. 2, 169 – 176.

Mazumder, N. N. and Bose, C. N. (1964). "Evaluation of safe bearing capacity of friction piles in soft clay." *Proceedings, Symposium on Bearing Capacity of Piles*, Roorkee: 43 – 50.

Mazurkiewicz, B. K. (1972). "Test loading of piles according to Polish regulations." *Report No. 35*, Commission on Pile Research, Royal Swedish Academy of Engineering Sciences, Stockholm, 20 p.

McCabe, B. A. and Lehane, B. M. (2006). "Behavior of axially loaded pile groups driven in clayey silt." *Journal of Geotechnical and Geoenvironmental Engineering*, 132(3): 401 – 410.

McClelland, B. (1974). "Design of deep penetration piles for ocean structures." *Journal of Geotechnical Engineering Division*, Vol. 100: 709 – 747.

McManus, K. J. and Kulhawy, F. H. (1994). "Cyclic axial loading of drilled shafts in cohesive soil." *Journal of Geotechnical Engineering*, 120(9): 1481 – 1497.

McVay, M. C., O'Brien, M., Townsend, F. C., Bloomquist, D. G. and Caliendo, J. A. (1989). "Numerical analysis of vertically loaded pile groups." *Foundation Engineering Congress*, Vol. II, (Proc. ASCE, GSP 22, Northwestern University), ASCE, Reston, Virginia: pp. 675 – 690.

Mendonça, A.V. and De Paiva, J. B. (2000). "Boundary element method for the static analysis of raft foundations on piles." *Engineering Analysis with Boundary Elements*, 24(3): 237 – 247.

Mengé, P. (2001). "Soil investigation results at Sint-Katelijne-Waver (Belgium)." *Proceedings, Symposium on Screw Piles – Installation and Design in Stiff Clay*, Brussels. Balkema, Rotterdam, ISBN: 90 5809 192 9: pp. 19–62.

Meyerhof, G. G. (1956). "Penetration tests and bearing capacity of cohesionless soils." *Journal of the Soil Mechanics and Foundations Division*, ASCE, Vol. 82: 866 – 1019.

Meyerhof, G. G. (1959). Compaction of sands and bearing capacity of piles. *Journal of Soil Mechanics Foundations Engineering* (ASCE), 85(SM6): l – 29.

Meyerhof, G. G. (1976). "Bearing capacity and settlement of pile foundations." *Journal of Geotechnical Engineering Division*, Vol. 102:195 – 228.

Meyerhof, G. G. (1983). "Scale effects of ultimate pile capacity." *Journal of Geotechnical Engineering*, Vol. 109: 797 – 806.

Miao, Y., Cai, G., Liu, S. and Zou, H. (2011). "Axial response analysis of single pile based on SCPTu test." *Proceedings, International Conference on Electric Technology and Civil Engineering* (*ICETCE*), pp. 2012–2015.

Miller, B. (2012). Seismic cone penetration test data at the Canadian Geotechnical Test Site, South Gloucester, ON, Canada. *Personal communication*.

Miller, G. A. and Lutenegger, A. J. (1997). "Influence of pile plugging on skin friction in overconsolidated clay." *Journal of Geotechnical and Geoenvironmental Engineering*, Vol. 123: 525 – 533.

Mindlin, R. D. (1936). "Force at a point in the interior of a semi-infinite solid." *Journal of Applied Physics*, Vol. 7: 195 – 202.

Motta, E. (1994). "Approximate elastic–plastic solution for axially loaded piles." *Journal of Geotechnical Engineering*, ASCE, 120(9): 1616 – 1624.

Mylonakis, G. (2001). "Winkler modulus for axially-loaded piles." *Géotechnique*, 51(5): 455 – 461.

Naesgaard, E., Azizian, A., Yang, D., Uthayakumar, M., Amini, A. and Byrne., P. M. (2008). "Golden Ears Bridge – geotechnical seismic design aspects." *Proceedings, 61st Canadian Geotechnical Conference*, Edmonton: 1002 – 1009.

Naesgaard, E., Uthayakumar, M., Ersoy, T. and Gillespie, D. (2006). "Pile load test for W.R. Bennett Bridge." *Proceedings, 59th Canadian Geotechnical Conference*, Canadian Geotechnical Society, Vancouver, B.C.

New York City (1981). *Building Code of the City of New York*. Gould Publications, Binghamton, 481 p.

Ng, K. W., Roling, M., AbdelSalam, S. S., Suleiman, M. T. and Sritharan, S. (2013a). "Pile setup in cohesive soils I: Experimental investigation." *Journal of Geotechnical and Geoenvironmental Engineering*, 139(2): 199 – 209.

Ng, K. W., Suleiman, M. T. and Sritharan, S. (2013b). "Pile setup in cohesive soils II: Analytical quantifications and design recommendations." *Journal of Geotechnical and Geoenvironmental Engineering*, 139(2): 210 – 222.

Niazi, F. S. and Mayne, P. W. (2010). "Evaluation of EURIPIDES pile load tests response from CPT results." *International Journal of Geoengineering Case Histories*, 1(4): 367 – 386. www.geoengineer.org

Niazi, F. S. and Mayne, P. W. (2013). "Cone penetration test based direct methods for evaluating static axial capacity of single piles: a state-of-the-art review." *Geotechnical and Geological Engineering*, Vol. 39, Springer, The Netherlands: 979–1009.

Niazi, F. S., Mayne, P. W. and Woeller, D. J. (2010a). "Drilled shaft O-Cell response at Golden Ears Bridge from seismic cone tests." *The Art of Foundation Engineering Practice*: Geotechnical Special Publication No. 198 honoring Clyde Baker, ASCE, Reston, VA: 452 – 469.

Niazi, F. S., Mayne, P. W. and Woeller, D. J. (2010b). "Case history of axial pile capacity and load-settlement response by SCPTu." *Proceedings, 2nd International Symposium on Cone Penetration Testing* (CPT'10, Huntington Beach), Vol. 3, Omnipress: 9 – 16. www.cpt10.com

Niazi, F. S., Mayne, P. W. and Woeller, D. J. (2010c). "Review of CPT-based methods for response evaluation of driven piles in dense sands." *Proceedings, International Conference on Geotechnical Engineering*, Pakistan, pp. 259 – 266.

Nordlund, R. L. (1963). "Bearing capacity of piles in cohesionless soils." ASCE, *Journal of Soil Mechanics and Foundation Engineering*, 89 (SM3): 1 – 35.

Nordlund, R. L. (1966). Personal communication as referenced by Housel (1966), 467.

Nottingham, L. C. (1975). Use of quasi-static friction cone penetrometer data to predict load capacity of displacement piles. *PhD Thesis*, Department of Civil Engineering, University of Florida, Gainesville.

O'Neill, M. W. and Reese, L. C. (1999). "Drilled shafts: Construction procedure and design methods." FHWA Report IF-99-025, U.S. Department of Transportation, Washington, DC.

O'Neill, M. W., Ata, A. A., Vipulanandan, C. and Yin, S. (2002). "Axial performance of acip piles in texas coastal soils." *Deep Foundations 2002 – An International Perspective on Theory, Design, Construction and Performance*, ASCE Geotechnical Special Publication No. 116, Vol. 2, Reston/VA: 1290 – 1304.

O'Neill, M. W., Hawkins, R. A. and Mahar, L. J. (1982). "Load transfer mechanisms in piles and pile groups." *Journal of the Geotechnical Engineering Division*, 108(GT12): 1605 – 1623.

O'Rourke, T. D. and Kulhawy, F. H. (1985). "Observations on load tests on drilled shafts." *Drilled Piers and Caissons II*, ed. Baker, C. N., ASCE, Reston, VA: 113 – 128.

Osterberg, J. O. (1989). "New device for load testing driven piles and drilled shafts separates friction and end bearing." *Proceedings, International Conference on Piling and Deep Foundations*, (IC London), A.A. Balkema, Rotterdam: 421 p.

Osterberg, J.O. (1998). "The Osterberg load test method for bored and driven piles: the first ten years." *Proceedings, 7th International Conference on Piling and Deep Foundations*. (DFI'98), Vienna, Austria, 1.28.1 – 1.28.11.

Padros, G. and Papanicolas, D. (2008). "Compressive pile load tests on continuous flight auger piles and on a driven timber pile in silty clay soils in High Prairie Alberta." *Proceedings, 61st Canadian Geotechnical Conference* (GeoEdmonton 2008): 1227 – 1230.

Pando, M. A., Fernandez, A. L. and Filz, G. M. (2004). "Pile settlement predictions using theoretical load transfer curves and seismic CPT data." *Proceedings, 2nd International Conference on Site Characterization, ISC-2: Geotechnical and Geophysical Site Characterization*, Vol. 2 (ISC-2, Porto), Millpress, Rotterdam: 1525 – 1531.

Pang S. K., Kort, D. A. and Evans, S. A, (2010). "Report on drilled shaft load testing (Osterberg method), Pier 12 shaft 5, Gilmerton Bridge, Chesapeake, VA." *Project Report LT-9577*, prepared by LoadTest Incorporated for PCL Civil Constructors Corporation.

Patel, D. C. (1989). "A case study of the shaft friction of bored piles in London clay in terms of effective stress." *Thesis*, University of London, Imperial College, as referenced in Patrizi and Burland (2001).

Patrizi, P. and Burland, J. (2001). "Development in the design of driven piles in clay in terms of effective stresses." *Rivista ltaliana di Geotecnica*, 35(3): 35 – 49.

Patton II, R. F. and Barnhill, S. A. (1988). "Pile load test, test pile and initial production pile driving, Canon manufacturing plant expansion, Newport News, Virginia." *Project Report No. NG8-1986* by Law Engineering, Inc. prepared for Citadel Corporation, Atlanta, GA. 32 p.

Peck, R. B. (1942). "Discussion: pile driving formulas." *Proceedings, Progress Report of the Committee on the Bearing Value of Pile Foundaitons*, American Society of Civil Engineers, 68(2): 905 – 909.

Peck, R. B. (1958). "A study of the comparative behavior of friction piles." *Special Report No. 36*, Highway Research Board, Washington DC.

Pelletier, J. H. and Doyle, E. H. (1982). "Tension capacity in silty clays – Beta pile tests." *Proceedings, 2nd International Conference on Numerical Methods in Offshore Piling*, Austin: 1 – 19.

Peng, L. S., Koon, A. M., Page, R. and Lee, C. W. (1999). "Osterberg cell testing of piles." *Proceedings, International Conference on Rail Transit*, Association of Consulting Engineers, Singapore.

Peuchen, J., Vanden-Berghe, J. F. and Coulais, C. (2010). "Estimation of u_1/u_2 conversion factor for piezocone." *Proceedings of the 2nd International Symposium on Cone Penetration Testing* (CPT'10, Huntington Beach, CA), Vol. 2, Omnipress. http://www.cpt10.com

Philipponnat, G. (1980). Methode pratique de calcul d'un pieu isole a l'aide du penetrometre statique. *Revue Francaise de Géotechnique*, Vol. 10, 55 – 64.

Poulos, H. G. (1979). "Settlement of single piles in nonhomogeneous soil." *Journal of Geotechnical Engineering Division*, 105(5): 627 – 641.

Poulos, H. G. (1989). "Pile behaviour: theory and applications." Rankine Lecture, *Géotechnique*, 39(3): 363 – 415.

Poulos, H. G. and Davis, E. H. (1968). "The settlement behavior of single axially loaded incompressible piles and piers." *Géotechnique*, 18(3): 351 – 371.

Poulos, H. G. and Davis, E. H. (1980). *Pile Foundation Analysis and Design*. John Wiley and Sons, New York: 397 p.

Poulos, H. G. and Mattes, N. S. (1969). "The behaviour of axially loaded end-bearing piles." *Géotechnique*, 19(2): 285 – 300.

Powell, J. J. M. and Butcher, A. P. (2003). "Characterisation of a glacial clay till at Cowden, Humberside." *Characterisation and Engineering Properties of Natural Soils*, Vol. 2 (Proc. Singapore Workshop) Balkema, Rotterdam: 983 – 1020.

Powell, J. J. M. and Lunne, T. (2005). "A comparison of different size piezocones in UK clays." *Proceedings, 16th ICSMGE*, Vol. 1, (Osaka), Millpress, Rotterdam: 729 – 734.

Powell, J. J. M. and Quarterman, R. S. T. (1988). "The interpretation of cone penetration tests in clays with particular reference to rate effects," *Penetration Testing 1988*, Vol. 2, (Orlando, Fla.), Balkema, Rotterdam, The Netherlands, 903 – 909.

Powell, J. J. M., Lunne, T. and Frank, R. (2001). "Semi-empirical design for axial pile capacity in clays." *Proceedings, 15th International Conference on Soil Mechanics and Geotechnical Engineering*, Vol. 2, (Istanbul, Turkey), Balkema, Rotterdam, The Netherlands, 991 – 994.

Powell, J. J. M., Quartermann, R. S. T. and Lunne, T. (1988). "Interpretation and use of the piezocone test in UK clays." *Proceedings, Penetration testing in the UK*, Thomas Telford, London: 151 – 156.

Prakash, S. and Sharma, H. D. (1990). *Pile Foundations in Engineering Practice*. John Wiley and Sons, New York: 634 – 676.

Premchitt, J., Gray, I. and Massey, J. B. (1988). "Initial measurements of skin friction on some driven piles in reclamation." *Hong Kong Engineer*, 16(5): 25 – 38.

Prevost, J. H. and Keane, C. M. (1990). "Shear stress-strain curve generation from simple material parameters." *Journal of Geotechnical Engineering* 116 (8): 1255 – 1263.

Price, G. and Wardle, I. F. (1982). "A comparison between cone penetration test results and the performance of small diameter instrumented piles in stiff clay." *Proceedings, 2nd European Symposium on Penetration Testing*, Amsterdam, The Netherlands. Vol. 2: 775 – 780.

Radhakrishna, H. S., Cragg, C. B. H., Tsang, R. and Bozozuk, M. (1986). "Uplift and compression behavior of drilled piers in Leda clay." *Proceedings, 39th Canadian Geotechnical Conference*, Ottawa, 123-130.

Rajapakse, R. K. N. D. (1990). "Response of an axially loaded elastic pile in a Gibson soil." *Géotechnique*, 40(2): 237 – 249.

Ramberg, W. and Osgood. W. R. (1943). "Description of stress-strain curves by three parameters." Technical Note No. 902, National Advisory Committee for Aeronautics, Washington DC.

Randolph, M. F. (2007). *Manual PIGLET: Analysis and design of pile groups*. Version 5.1, Centre for Offshore Foundation Systems, School of Civil and Resource Engineering, The University of Western Australia, Crawley, Western Australia: 35 p.

Randolph, M. F. (2003). "Science and empiricism in pile foundation design." *Géotechnique*, 53(10): 847 – 875.

Randolph, M. F. (1983). "Design considerations for offshore piles." *Proceedings, Conference on Geotechnical Practice in Offshore Engineering* (Austin), ASCE, Reston, VA: 422 – 439.

Randolph, M. F. and Murphy, B. S. (1985). "Shaft capacity of driven piles in clay." *Proceedings, 17th Annual Offshore Technology Conference*, Houston: 371 – 378.

Randolph, M. F. and Wroth, C. P. (1978). "Analysis of deformation of vertically-loaded piles." ASCE *Journal of the Geotechnical Engineering Division*, 104(GT12): 1465 – 1488.

Randolph, M. F. and Wroth, C. P. (1979). "A simple approach to pile design and the evaluation of pile tests." *Behavior of Deep Foundations*, STP 670, ASTM, West Conshohocken, PA: 484 – 499.

Randolph, M. F. and Wroth, C. P. (1982). "Recent developments in understanding the axial capacity of piles in clay." *Ground Engineering*, 15(7): 17–25.

Rausche, F., Moses, F. and Goble, G. (2004). "Soil resistance predictions from pile dynamics." *Current Practices and Future Trends in Deep Foundations* (GSP 125): 418 – 440.

Rausche, F., Thendean, G., Abou-matar, H., Likins. G. E. and Goble, G. G. (1996). "Determination of pile driveability and capacity from penetration tests." *Final Report*, U.S. Department of Transportation, Federal Highway Administration Research Contract DTFH61-91-C-00047.

Reese, L. C., and O'Neill, M. W. (1988). "Drilled shafts: construction procedures and design methods." *Report No. FHWA-HI-88-042*, Federal Highway Administration, McLean, VA, 758 p.

Reese, L. C., Touma, F. T. and O'Neill, M. W. (1976). "Behavior of drilled piers under axial loading." *Journal of Geotechnical Engineering Division* ASCE, 102(GT5): 493–510.

Reuter, G. R. (2010). "Pile capacity prediction in Minnesota soils using direct CPT and CPTu methods." *Proceedings, 2nd International Symposium on Cone Penetration Testing*. (CPT'10, Huntington Beach, CA), Omnipress, Paper Number 3-25: www.cpt10.com

Robertson, P. K. (1990). "Soil classification using the cone penetration test." *Canadian Geotechnical Journal*, 27(1): 151–158.

Robertson, P. K. (2009). "Interpretation of cone penetration tests – a unified approach." *Canadian Geotechnical Journal*, 46(11): 1337 – 1355.

Robertson, P. K. and Wride, C. E. (1998). "Evaluating cyclic liquefaction potential using the cone penetration test." *Canadian Geotechnical Journal*, 35(3): 442–459.

Rocher-Lacoste, F. (2008). "Full-scale experimental study and numerical analysis of vibratory driven piles: vibrations in the environment and bearing capacity." *PhD Thesis*, École nationale des ponts et chausses (National school of Bridges and Roads), (in French), 190p.

Rocher-Lacoste, F., Borel, S., Gianeselli, L. and Po, S. (2004). "Comparative behaviour and performances of impact and vibratory driven piles in stiff clay." *Proceedings, International Conference, Cyclic Behaviour of Soils and Liquefaction Phenomena*, Bochum, Germany, 31 March - 2 April 2004, Th. Triantafyllidis (ed.), Taylor & Francis 2004, Print ISBN: 978-90-5809-620-3, eBook ISBN: 978-1-4398-3345-2, DOI: 10.1201/9781439833452.ch64, pp. 533–540.

Russo, G., Recinto, B., Viggiani, C. and de-Sanctis, L. (2003). "A contribution to the analysis of Osterberg's cell load test." *Proceedings, Deep Foundation on Bored and Auger Piles*, Millpress, Rotterdam, The Netherlands: 331 – 338.

Said, I., De Gennaro, V. and Frank, R. (2009). "Axisymmetric finite element analysis of pile loading tests." *Computers and Geotechnics*, Vol. 36, 6 – 19.

Salgado, R. (2006). "The role of analysis in non-displacement pile design." Modern trends in geomechanics, W. Wu and H.-S. Yu, eds., Springer, New York, 521 – 540.

Salgado, R. (2008). *The Engineering of Foundations*, Mc Graw Hill, New York.

Salgado, R. (2010). "The axial resistance of nondisplacement piles." Art of foundation engineering practice, M. H. Hussein; J. B. Anderson; and W. M. Camp, eds., GeoFlorida 2010, ASCE GSP 198, 584 – 604.

Samtani, N. C. and Nowatzki, E. A. (2006). "Soils and foundations." Reference Manual. *FHWA Publication* Vol. II, No. FHWA-NHI-06-089, Federal Highway Administration, Washington, DC.

Santos, J. A. D. and Correia, A. G. (2001). "Reference threshold shear strain of soil." *Proceedings of the 15th International Conference on Soil Mechanics and Geotechnical Engineering*, Vol. 1, Istanbul, 267 – 270.

Schmertmann, J. H. (1991). "The mechanical aging of soils." *Journal of Geotechnical Engineering*, 117(9): 1288 – 1330.

Schmertmann, J. H. (1978). "Guidelines for cone penetration test, performance and design." *Report No. FHWA-TS-78-209*, Federal Highway Administration, U.S. Department of Transportation, Washington, DC,.

Schmertmann, J. H. and Hayes, J. A. (1997). "The Osterberg cell and bored pile testing – a symbiosis." *Proceedings, The 3rd International Geotechnical Engineering Conference*, Cairo University, Egypt: 139 – 167.

Schmertmann, J. H., Hayes, J. A., Molnit, T. and Osterberg, J. O. (1998). "O-cell testing case histories demonstrate the importance of bored pile (drilled shaft) construction technique." *Proceedings*: *4th International Conference on Case Histories in Geotehnical Engineering*, St. Louis, MO, 1103 – 1115.

Schneider, J. A. (2007). "Analysis of piezocone data for displacement pile design." *PhD Thesis*, Dept of Civil & Resource Engineering, University of Western Australia, Perth, Australia.

Schultze, E. (1964). "Experimental method and evaluation of some loading tests on piles." *Proceedings, Symposium on Bearing Capacity of Piles*, Roorkee: 60 – 88.

Semple, R. M. and Rigden, W. J. (1984). "Shaft capacity of driven pipe piles in clay." *Proceedings, Symposium on Analysis and Design of Deep Foundations*, (San Francisco): ASCE: 9 – 79.

Senneset, K., Sandven, R. and Janbu, N. (1989). "Evaluation of soil parameters from piezocone tests." *Transportation Research Record 1235*, National Research Council, Washington, DC: 24 – 37.

Seo, H., Yildirim, I. Z. and Prezzi, M. (2009). "Assessment of the axial load response of an H pile driven in multilayered soil." *Journal of Geotechnical and Geoenvironmental Engineering*, 135(12): 1789 – 1804.

Seo, H., Yildirim, I. Z. and Prezzi, M. (2009). "Assessment of the axial load response of an H pile driven in multilayered soil." *Journal of Geotechnical and Geoenvironmental Engineering*, 135(12): 1789–1804.

Seol, H., Jeong, S. and Kim, Y. (2009). "Load transfer analysis of rock-socketed drilled shafts by coupled soil resistance." *Computers and Geotechnics*, 36(3): 446 – 453.

Shen, W. Y., Chow, Y. K. and Yong, K. Y. (1997). "A variational approach for vertical deformation analysis of pile groups." *International Journal of Numerical and Analytical Methods in Geomechanics*, 21(11): 741 – 752.

Shen, W. Y., Chow, Y. K. and Yong, K. Y. (1999). "A variational solution for vertically loaded pile groups in an elastic half-space." *Géotechnique*, 49(2): 199 – 213.

Shen, W. Y., Chow, Y. K. and Yong, K. Y. (2000). "A variational approach for the analysis of pile group–pile cap interaction." *Géotechnique*, 50(4): 349 – 357.

Sheng, D., Eigenbrod, K. D. and Wriggers, P. (2005). "Finite element analysis of pile installation using large-slip frictional contact." *Computers and Geotechnics*, Vol. 32: 17 – 26.

Shibuya, S. and Tamrakar, S. B. (2003). "Engineering properties of Bangkok clay." *Characterization and Engineering Properties of Natural Soils*, Vol. 1 (Proceedings Singapore Workshop), Balkema, Rotterdam: pp. 645–692.

Simonini, P. (1996). "Analysis of behavior of sand surrounding pile tips." *Journal of Geotechnical Engineering*, 122(11): 897 – 905.

Simpson, R. (2011). "Gilmerton Bridge – Chesapeake, VA – Pier 9 SW R." *Report prepared for PCL on Drilled Shaft Load Testing (Osterberg Method)*, Project No. LT – 9577-2, LoadTest, Inc., Gainsesville, FL: 153 p.

Simpson, R. C., Ahren, M. D. and Hayes, J. A. (2000a). "Final report on drilled shaft load testing (Osterberg method), Test shaft C-4 – Cooper River Bridge, Charleston, SC." *Project Report* No. LT-8650-9, prepared by LoadTest Incorporated for Trevi Icos Corporation.

Simpson, R. C., Kort, D. and Hayes, J. A. (2000b). "Final data report on drilled shaft load testing (Osterberg method), Test shaft C-3 – Cooper River Bridge, Charleston, SC." *Project Report* No. LT-8650-8, prepared by LoadTest Incorporated for Trevi Icos Corporation.

Skempton, A. W. (1959). "Cast in-situ bored piles in London clay." *Géotechnique*, 9(2): 91 – 125.

Smith, I. M. (1980). "A survey of numerical methods in offshore piling." Institute of Civil Engineers, *Numerical Methods in Offshore Piling*, ICE, London, 1 – 8.

Smith, R. E. (2001). "Introduction of Michael W. O'Neill, Thirty-Fourth Terzaghi Lecturer, 1998, Boston, Massachusetts." *Journal of Geotechnical and Geoenvironmental Engineering*, 127(1): 1 – 2.

Southcott, P. H. and Small, J. C. (1996). "Finite layer analysis of vertically loaded piles and pile groups." *Computers and Geotechnics*, 18(1): 47 – 63.

Sowers, G. F. (1979). *Introductory Soil Mechanics and Foundations*. Fourth Edition, Macmillan Publishing Co., Inc., New York, 531 – 533.

Standard Building Code (1999). *Standard Building Code*. Southern Building Code Congress International, Incorporation, Birmingham, AL, 484 p.

Svinkin, M. R. and Skov, R. (2000). "Set-up effect of cohesive soils in pile capacity." *Proceedings, 6th International Conference on Application of Stress Wave Theory to Piles*, S. Niyama and J. Beim, eds., Balkema, Rotterdam, Netherlands: 107 – 111.

Swedish Pile Commission (1980). "Recommendations for pile driving tests with subsequent load testing." *Report No. 59*, Palkommissionen, Royal Swedish Academy of Engineering Sciences, Stockholm, 64 p.

Széchy, C. (1961). "A more exact evaluation of pile test loadings." *Acta Technica Academique Scientiarum Hungaricae*, 34(3–4): 445 – 451.

Takesue, K., Sasao, H. and Makihara, Y. (1996). "Cone penetration testing in volcanic soil deposits." *Proceedings, International Conference on Advances in Site Investigation Practice*, Thomas Telford, London, 452 – 463.

Takesue, K., Sasao, H. and Matsumoto, T. (1998). "Correlation between ultimate pile skin friction and CPT data." *Geotechnical Site Characterization*, Vol. 2 (Proc. ISC-1, Atlanta), Balkema, Rotterdam: 1177 – 1182.

Tan, Y. and Lin, G. (2013). "Full-scale testing of open-ended steel pipe piles in thick varved clayey silt deposit along the Delaware River in New Jersey." *Journal of Geotechnical and Geoenvironmental Engineering*, 139 (3): 518 – 524.

Tara, D. J. (2012). "Pitt River Bridge 2007 Static Pile Loading Test." *Full-Scale Testing and Foundation Design*, Geotechnical Special Publication No. 227 honoring Bengt H. Fellenius, ASCE, Reston, VA: pp. 289 – 306.

Tatsuoka, F. and Shibuya, S. (1992). *Deformation Characteristics of Soils and Rocks from Field and Laboratory Tests.* Report of the Institute of Industrial Science Vol. 37, No. 1, University of Tokyo: 136p.

Terzaghi, K. and Peck, R. B. (1967). *Soil Mechanics in Engineering Practice*. 2nd ed., John Wiley and Sons, New York, 553 p.

Timoshenko, S. P. and Goodier, J. N. (1951). *Theory of Elasticity*. McGraw-Hill Book Co., NY, 506 p.

Togliani, G. (2008). "Pile capacity prediction for in-situ tests."*Geotechnical and Geophysical Site Characterization*, CD Vol. (Proc. ISC-3, Taipei), Taylor and Francis Group, London: 1187 – 1192.

Tomlinson, M. J. (1957). "The adhesion of piles driven in clay soils." *Proceedings, 4th International Conference on Soil Mechanics and Foundation Engineering*, London, Vol. 2: 66 – 71..

Tomlinson, M. J. (1977). *Pile Design and Construction Practice*. Viewpoint Publications, London: 413 p.

Torstensson, B. A. (1982). "A combined pore pressure and point resistance probe." *Proceedings, 2nd European Symposium on Penetration Testing* (ESOPT-2), Vol. 2, Balkema, Amsterdam: 902–908.

Tosini, L., Cividini, A. and Gioda, G. (2010). "A numerical interpretation of load tests on bored piles." *Computers and Geotechnics*, Vol. 37, 425 – 430.

Trochanis, A. M., Bielak, J. and Christiano, P. (1991a). "Three-dimensional nonlinear study of piles." *Journal of Geotechnical Engineering*, 117(3): 429 – 447.

Trochanis, A. M., Bielak, J. and Christiano, P. (1991b). "Simplified model for analysis of one or two piles." *Journal of Geotechnical Engineering*, 117(3): 448 – 466.

Tucker, L. M. and Briaud, J-L. (1988). "Analysis of the pile load test program at the Lock and Dam 26 replacement project." Report to US Army Engineers District, St. Louis. (Contract No. DACW39-87-M-0752): 63 p.

Tumay, M. T. and Fakhroo, M. (1982). Friction pile capacity prediction in cohesive soils using electric quasi-static penetration tests. *Interim Research Report* No. 1, Louisiana Department of Transportation and Development, Research and Development Section, Baton Rouge, LA, 275 p.

Twine, D. (1987). "Shaft friction of bored, cast in-situ piles in stiff, overconsolidated clays in terms of effective stress." *Thesis*, University of London, Imperial College, as referenced in Patrizi and Burland (2001).

Uniform Building Code (1979). *Uniform Building Code*. International Conference of Building Officials, Whitter, 449 p.

Vallabhan, C. V. G. and Mustafa, G. (1996). "A new model for the analysis of settlement of drilled piers." *International Journal of Numerical and Analytical Methods in Geomechanics*, 20: 143 – 152.

Van der Veen, C. (1953). "The bearing capacity of a pile." *Proceedings, 3rd International Conference on Soil Mechanics and Foundation Engineering*, ISSFME, Vol. 2, Zurich: 84 – 90.

Van Dijk, B. F. J. and Kolk, H. J. (2011). "CPT-based design method for axial capacity of offshore piles in clays." *Proceedings, International Symposium on Frontiers in*

Offshore Geotechnics II, (ISFOG, Perth), Taylor and Francis Group, London: 555 – 560.

Van Impe, W. F. (1994). "Influence of screw pile installation parameters on the overall pile behaviour." *Proceedings, Workshop on Piled Foundations: full scale investigations, analysis and design*, Naples.

Vardanega, P. J. and Bolton, M. D. (2011). "Practical methods to estimate the non-linear shear stiffness of fine grained soils." *Proceedings, International Symposium on Deformation Characteristics of Geomaterials*, Seoul: 372 – 379.

Vardanega, P. J. and Bolton, M. D. (2013). "Stiffness of clays and silts: normalizing shear modulus and shear strain." *Journal of Geotechnical and Geoenvironmental Engineering*, 139 (9): 1575 – 1589.

Vesić, A. S. (1963). "Bearing capacity of deep foundations in sand." *Research Record* No. 39, Highway Research Board, Washington, 112 – 153.

Vesić, A. S. (1977). "Design of pile foundations." *NCHRP Synthesis of Highway Practice 42*, Transportation Research Board, National Research Council, Washington, D.C., 68 p.

Vesić, A. S. (1991). *Foundation Engineering Handbook*, Van Nostrand Reinhold Publishing, New York: 121 – 147.

Viana da Fonseca, A., Carvalho, J., Ferreira, C., Santos, J. A., Almeida, F., Pereira, E., Feliciano, J., Grade, J. and Oliveira, A. (2006). "Characterization of a profile of residual soil from granite combining geological, geophysical and mechanical testing techniques." *Geotechnical and Geological Engineering*, 24: 1307 – 1348.

Vijayvergiya, V. N. (1977). "Load-movement characteristic of piles." *Proceedings of the 4th Annual Symposium of the Waterways, Ports, Coastal and Ocean Division of American Society of Civil Engineers* (Port'77), New York, Vol. 2: 269 – 284.

Vijayvergiya, V. N. and Focht, J. A. (1972). "A new way to predict the capacity of piles in clay." *Proceedings, 4th Annual Offshore Techonology Conference*, Houston, 269 – 284.

Vucetic, M. and Dobry, R. (1991). "Effect of soils plasticity on cyclic response." *ASCE Journal of Geotechnical Engineering*, 117(1): 89 – 107.

Waxse, J. A., Osterberg, J. and Qudus, O. (2004). "Drilled shaft value engineering delivers success to Wahoo, Nebraska Bridge." *Proceedings, ASCE/ADSC Geo-Support 2004: International Drilled Foundation Support Specialty Conference*, ASCE, Reston, VA, 289 – 298.

Weltman, A. J. (1980). "Pile load testing procedures." *Report* PG7, Construction Industry Research and Information Association (CIRIA), London, 53 p.

White, D. J. and Bolton, M. D. (2005). "Comparing CPT and pile base resistance in sand." *Geotechnical Engineering*, 158(GE1), Institution of Civil Engineers, London: 3 – 14.

Whittle, A. J. (2003). "Settlement of single piles." In *Notes of Massachusetts Institute of Technology Course Number* 1.364 Advance Geotechnical Engineering (Fall 2003): 12.1 – 12.21. http://ocw.mit.edu/courses/civil-and-environmental-engineering/1-364-advanced-geotechnical-engineering-fall-2003 (Accessed 7 Nov, 2013). License: Creative Commons BY-NC-SA.

Whittle, A. J. and Sutabutr, T. (1999). "Prediction of pile setup in clay." *Journal of the Transportation Research Board*, Vol. 1663: 33 – 40.

Woo, S. Y., Jeong, S. S., Moon, I. S. and Lee, J. K. (2006). "Bearing capacity analysis of large diameter drilled shafts by Osterberg-cell load tests." *Proceedings, 2006 Korean Society of Civil Engineers Annual Conference*, KSCE, Seoul, 1728 – 1732.

Woodward, R. J., Lundgren, R. and Boitano, J. D. (1961). "Pile loading tests in stiff clays." *Proceedings, 6th International Conference on Soil Mechanics and Foundation Engineering*, Paris: 177 – 184.

Xiao, H. B., Luo, Q. Z., Tang, J. and Li, Q. S. (2002). "Prediction of load-settlement relationship for large-diameter piles." *Structural Design of Tall Buildings*, 11(4): 285 – 293.

Yang, L. and Liang, R. (2009). "Incorporating setup into load and resistance factor design of driven piles in sand." *Canadian Geotechnical Journal*, 46(3): 296 – 305.

Yi, L. (2004). "Finite element study on static pile load testing." *Thesis*, Department of Civil Engineering, National University of Singapore, 161 p.

Yu, F. and Yang, J. (2012). "Base capacity of open-ended steel pipe piles in sand." *Journal of Geotechnical and Geoenvironmental Engineering*, 138(9): 1116–1128.

Zhang, G., Robertson, P. K. and Brachman, R. W. I. (2002). "Estimating liquefaction-induced ground settlements from CPT for level ground." *Canadian Geotechnical Journal*, 39(5): 1168–1180.

Zhang, Q-Q. and Zhang, M-M. (2012). "Simplified calculation approach for settlement of single pile and pile groups." *Journal of Computing in Civil Engineering*, 26(6): 750– 758.

Zhang, Q-Q., Zhang, Z-M. and He, J-Y. (2010). "A simplified approach for settlement analysis of single pile and pile groups considering interaction between identical piles in multilayered soils." *Computers and Geotechnics*, Vol. 37: 969 – 976.

Zhu, H. and Chang, M-F. (2002). "Load transfer curves along bored piles considering modulus degradation." *Journal of Geotechnical and Geoenvironmental Engineering*, 128(9): 764 – 774.

Zhusupbekov, A. Zh. and Zhakulin, A. S. (2006). "Analysis of single-pile settlement in saturated soils." *Soil Mechanics and Foundation Engineering*, 43(1): 8 – 12.

Zuidberg H. M. and Vergobbi, P. (1996). "EURIPIDES, load tests on large driven piles in dense silica sands." *Proceedings 28th Offshore Technology Conference*, Houston, Texas, Vol. 1, 193 – 206.

Zuo, G., Drumm, E. C., Islam, M. Z. and Yang, M. Z. (2004). "Numerical analysis of drilled shaft O-cell testing in mica schist." *Proceedings, ASCE/ADSC Geo-Support 2004: International Drilled Foundation Support Specialty Conference*, (GSP No. 124), Orlando, ASCE, Reston, VA, 778 – 789.